ENABLING BIOMATERIALS FOR NEW BIOMEDICAL TECHNOLOGIES AND CLINICAL THERAPIES

EDITED BY: Hasan Uludag, Abhay Pandit and Liisa Kuhn
PUBLISHED IN: Frontiers in Bioengineering and Biotechnology

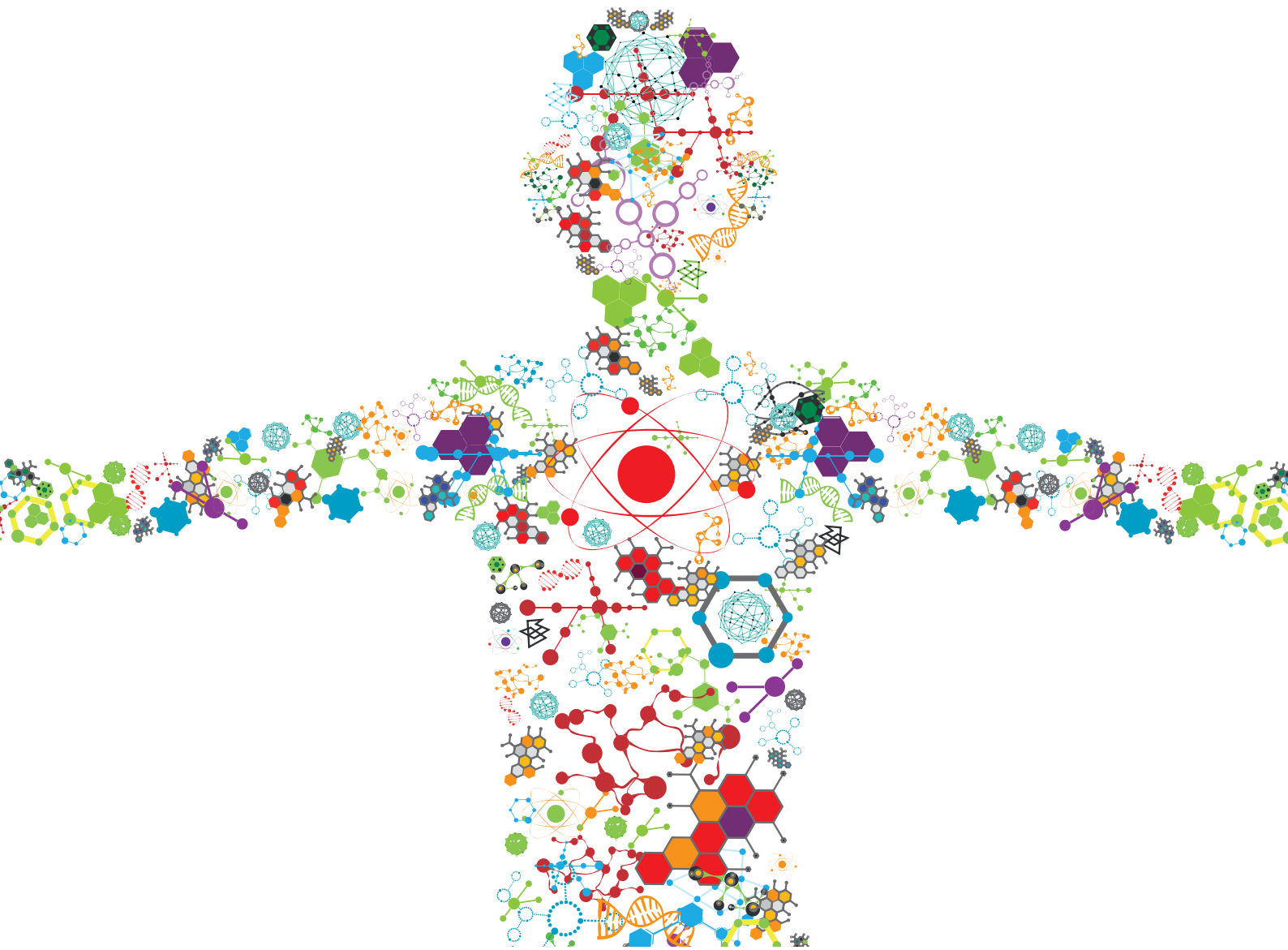

frontiers Research Topics

frontiers

ISSN 1664-8714
ISBN 978-2-88963-853-6
DOI 10.3389/978-2-88963-853-6

About Frontiers

Frontiers is more than just an open-access publisher of scholarly articles: it is a pioneering approach to the world of academia, radically improving the way scholarly research is managed. The grand vision of Frontiers is a world where all people have an equal opportunity to seek, share and generate knowledge. Frontiers provides immediate and permanent online open access to all its publications, but this alone is not enough to realize our grand goals.

Frontiers Journal Series

The Frontiers Journal Series is a multi-tier and interdisciplinary set of open-access, online journals, promising a paradigm shift from the current review, selection and dissemination processes in academic publishing. All Frontiers journals are driven by researchers for researchers; therefore, they constitute a service to the scholarly community. At the same time, the Frontiers Journal Series operates on a revolutionary invention, the tiered publishing system, initially addressing specific communities of scholars, and gradually climbing up to broader public understanding, thus serving the interests of the lay society, too.

Dedication to Quality

Each Frontiers article is a landmark of the highest quality, thanks to genuinely collaborative interactions between authors and review editors, who include some of the world's best academicians. Research must be certified by peers before entering a stream of knowledge that may eventually reach the public - and shape society; therefore, Frontiers only applies the most rigorous and unbiased reviews.
Frontiers revolutionizes research publishing by freely delivering the most outstanding research, evaluated with no bias from both the academic and social point of view. By applying the most advanced information technologies, Frontiers is catapulting scholarly publishing into a new generation.

What are Frontiers Research Topics?

Frontiers Research Topics are very popular trademarks of the Frontiers Journals Series: they are collections of at least ten articles, all centered on a particular subject. With their unique mix of varied contributions from Original Research to Review Articles, Frontiers Research Topics unify the most influential researchers, the latest key findings and historical advances in a hot research area! Find out more on how to host your own Frontiers Research Topic or contribute to one as an author by contacting the Frontiers Editorial Office: researchtopics@frontiersin.org

ENABLING BIOMATERIALS FOR NEW BIOMEDICAL TECHNOLOGIES AND CLINICAL THERAPIES

Topic Editors:
Hasan Uludag, University of Alberta, Canada
Abhay Pandit, National University of Ireland Galway, Ireland
Liisa Kuhn, University of Connecticut Health Center, United States

Citation: Uludag, H., Pandit, A., Kuhn, L., eds. (2020). Enabling Biomaterials for New Biomedical Technologies and Clinical Therapies. Lausanne: Frontiers Media SA. doi: 10.3389/978-2-88963-853-6

Table of Contents

frontiers in Bioengineering and Biotechnology

EDITORIAL
published: 05 June 2020
doi: 10.3389/fbioe.2020.00559

Editorial: Enabling Biomaterials for New Biomedical Technologies and Clinical Therapies

Hasan Uludag[1,2,3]*, *Abhay Pandit*[4] and *Liisa Kuhn*[5]

[1] Department of Chemical and Materials Engineering, University of Alberta, Edmonton, AB, Canada, [2] Faculty of Pharmacy & Pharmaceutical Sciences, Edmonton, AB, Canada, [3] Biomedical Engineering, Faculty of Medicine and Dentistry, Edmonton, AB, Canada, [4] CÚRAM, SFI Research Centre for Medical Devices, National University of Ireland Galway, Galway, Ireland, [5] Department of Biomedical Engineering, University of Connecticut Health Center, Farmington, CT, United States

Keywords: biomaterials, biocompatibility, biomaterial-host interface, regeneration, metallic implants, safety, tissue engineering, therapeutic

Editorial on the Research Topic

Enabling Biomaterials for New Biomedical Technologies and Clinical Therapies

Biomaterials have been an integral part of exciting developments in medicine. They singlehandedly enabled new therapeutic modalities and gave new life to diagnostic procedures as well as supporting innovative developments in medicine. In anticipation of the future developments in the field, we compiled this Research Topic to provide complementary perspectives from biomaterials researchers into emerging concepts in biomaterials science and engineering. The Research Topic is intended to summarize the latest biomaterials advances in emerging biomedical technologies and effective interventions promising for the clinical setting. It has the ambitious goal of broadly tackling key challenges facing biomaterials researchers. The well-established working hypothesis, that is *material chemistry influences genetic flow of information in a cell, which in turn alters cellular behavior in contact with biomaterial, leading to organ level changes*, are central in this Research Topic. Individual manuscripts in this collection represents a combination of in-depth reviews, technical studies, and perspectives from leading experts in their fields, summarizing the-state-of-the-art in critical aspects of biomaterials. The Research Topic has a relatively broad theme to allow information exchange from different aspects of the field. The experts were encouraged to highlight their recent work and identify key developments with transformative potential.

Given the central role of "biocompatibility" in the field, the hypothesis article by Williams explored the "*specifications for innovative, enabling biomaterials based on the principles of biocompatibility mechanisms.*" It has been recognized that "efficacy" and "safety" are two indispensable aspects of biomaterials (Uludag, 2014) and this article concentrates on the under-studied issue of "biocompatibility" that determines the acute and chronic interactions with the host. The article takes a case-by-case approach and explores biocompatibility in leading applications of biomaterials; some applications are relatively simple (e.g., contrast agents) while others (e.g., tissue engineering) involve complicated set of tissue events for a successful outcome. As the author rightfully calls for a clearer understanding of the mechanisms of biocompatibility pathways within the context of applications, the importance of manipulating various pathways have been emphasized to enhance the chances of designing new and improved functional biomaterials.

Eltit et al. also take on the biocompatibility challenge at the interface of hip implants, focusing on metallic implants and the mechanisms of adverse local tissue reactions. Metallic biomaterials, being as artificial as they get for organic life-forms like us, most likely elicit unique reactions in the host tissue upon corrosion and release of by-products. Alternatively, non-specific effects involving general toxicity and inflammatory reactions as a result of local host cell death may elicit a response

OPEN ACCESS

Edited and reviewed by:
Senentxu Lanceros-Mendez, Basque Center for Materials, Applications and Nanostructures, Spain

***Correspondence:**
Hasan Uludag
hasan.uludag@ualberta.ca

Specialty section:
This article was submitted to Biomaterials, a section of the journal Frontiers in Bioengineering and Biotechnology

Received: *28 April 2020*
Accepted: *11 May 2020*
Published: *05 June 2020*

Citation:
Uludag H, Pandit A and Kuhn L (2020) Editorial: Enabling Biomaterials for New Biomedical Technologies and Clinical Therapies. Front. Bioeng. Biotechnol. 8:559. doi: 10.3389/fbioe.2020.00559

common with other non-metallic biomaterials. Careful analysis of unique vs. common aspects of the adverse local tissue reactions may lend itself to not only improved metallic implants but also to implants from biomaterials beyond the metallic kind. Considering the great interest in developing metallic micro/nano-scale constructs (with elevated surface areas) in diagnostic and therapeutic utilities, the importance of metallic biocompatibility will be even greater. Focusing on the leading metallic implant, titanium, Hanawa inspects the titanium-host interfaces from the perspective of controlling the interface reaction based on engineered features. With the ultimate goal of improved osseointegration, the review lays out different approaches to achieve most desirable porous surfaces with physical, chemical and biological features to encourage integrative events and discourage inhibitory actions. As in Eltit et al. and Hanawa calls for the need for better understanding the mechanism of biocompatibility and adverse events, despite extensive medical use of titanium over the years. Key issues remain to be better clarified that will be important for future applications of this important metallic biomaterial.

The critical issue of host reaction and in particular its control for success of immune-isolation devices has been also tacked by Hu and de Vos. The authors explore the choice of polymeric coatings and crosslinking agents that induce more stable and biocompatible isolation barriers, ultimately helping to attenuate the undesirable host response. Contributions of protein adsorption on surfaces intertwined with the immune stimulation from the devices were framed with engineered interfaces to control host reactions. A perspective on cellular approaches to mediate host response could provide clues for the design of more advanced materials and immune-isolation barriers that rely on biomimicry. Bu et al. also focused on biocompatibility issues in the context of aliphatic polyesters, a class of widely used synthetic polymers that includes poly(lactide/glycolide) family of polymers with long history of medical use. Key physicochemical features of aliphatic ester surfaces are succinctly presented including surface morphology, while considerations for engineering of surfaces from chemical and physical perspective are laid out. The information from this class of popular biomaterials should guide efforts when developing novel approaches for the biomedical use of such biomaterials.

Iron oxide is another metallic biomaterial that is finding unique applications in nanoparticulate form due its inherent magnetic properties (Dadfar et al., 2019). The science and technology of iron oxide magnetic nanoparticles are presented in a review article by Xu et al. in the context of bacterial detection and eradication. Different aspects of this specific application including bacterial enrichment, bioimaging and targeted delivery of anti-bacterial drugs and hyperthermia induction are articulated. A wide range of microbial targeting agents including antibodies, molecular entities acting as antimicrobial agents, peptides, bacteriophages, and aptamers are highlighted in order to create unique technologies in the context of controlling microbial growth.

The opposite end of the biomaterial spectrum is occupied by the naturally-derived collagen that has no physical, chemical and biological similarity to metallic biomaterials. In line with the mantra of "like attracts like," Copes et al. explore the use of collagen, the ubiquitous component of the extracellular matrix, in vascular tissue-engineered grafts. The presence of inherent biological clues make collagen a no-brainer to rely on for modifying cellular activities *in situ*. The technology of collagen coatings as cell-substrates and as controlled release vehicles are explored. Industrial processing of collagen is complicated due to its heterogeneous composition (with a mix of contrasting functional groups) and excessive denaturation that may be encountered during sourcing to obtain pure formulations. Critical technological issues and limitations of collagen are carefully laid in this review, especially, when one attempts to create *de novo* vascular grafts *ex vivo*. In contrast to this philosophy, the original research article by Pohan et al. explored the synthetic polymer poly(vinyl alcohol) to create a tissue-engineered vascular graft; simple amine groups were grafted onto the luminal surface of the synthetic matrix using radio frequency glow discharge (RFGD) treatment, leading to a functional substrate for endothelial cells. Distinct differences from collagen coatings were noted in a baboon *ex vivo* shunt model, where the engineered grafts did not invoke platelet or fibrin activation in short-term studies.

Biomaterials capable to stimulating tissue repair is especially in demand for tissues with limited regenerative capacity, among which the neural tissues are most notable. Toward this goal Motamed et al. designed an RGD-bearing β-peptide hydrogel to aid the migration of neural stem cells originating from the subventricular zone within the brain tissue of an experimental model. Local delivery of Brain Derived Neurotrophic Factor (BDNF) by the hydrogels assisted with reducing the local inflammatory response, supported better host tissue-scaffold integration, and attracted astrocytes that aided with the differentiation of neuroblasts. The review article by Hosoyama et al. further explore studies focused on peptide-based approaches to create structural recognition motifs to enhance cellular attachment and induce cell signaling for functional outcomes. Current approaches to design and applications of short mimetic peptides for angiogenic, anti-inflammatory, and adhesive responses are articulated along with specific applications to better soft-tissue healing. It is evident that, starting with the simple cell-adhesive RGD technology (Huettner et al., 2018), peptide-mediated signaling is continuing to play more prominent roles in constructing functional tissues *ex vivo* and regenerative medicine *in vivo*.

Dental implantology is another area that will benefit from control of regenerative events for longer lasting interventions. Dental implants were probably the first implanted biomaterials stretching prior to recorded history, but there is still a need for novel approaches and functional biomaterials for longer lasting, more stable implants. The review article by Raddall et al. focuses on pulp-dentin interface and articulates the role of biomaterial scaffolds to support mesenchymal stem cell mediated regenerative endodontic therapy. Exploring scaffolds derived from host or exogenous sources (either synthetic or naturally derived), the article stipulates desirable features of biomaterials scaffolds and provides a glimpse of what is to come in scaffold design in endodontic repairs. The articulated ideas are likely to

be extended to regenerative events at other interfaces formed by different types of tissues (Patel et al., 2018).

Widely different and imaginative fabrication technologies are taking the field by storm. Static and dynamic constructs (so called 3D and 4D printing, respectively) are emerging fabrication techniques and Tamay et al. are providing a glimpse of the possibilities based on polymeric "printing" biomaterials. Originally rooted in manufacturing discipline, printing technology is reviewed in this article with special emphasis on the use of biologically acceptable materials and incorporating bioactive agents, including viable cells, in the printed constructs. The future of printing is going to rely on novel biomaterials with specific properties and this review provides ample avenues in the pursuit of such functional biomaterials, interwoven with specific applications that will equip the reader to match the biomaterials to applications at hand. A related bottom-up approach for tissue engineering and regenerative medicine is to deploy nanoparticles to control cellular events that was not possible in the recent past. Fathi-Achachelouei et al. describes the feasibility of spatial and temporal control of regenerative events based on nanoparticulate delivery of multiple growth factors and control of scaffold properties, along with the possibilities of diagnostic/therapeutic imaging. The spectrum of biomaterials used for nanoparticle preparation are presented, the authors emphasizing the unique features of each class of materials. Information on nanoparticle-based printing further complements the review by Tamay et al. and lays the groundwork for cost-effective therapies on the long run.

It is convenient for practitioners, albeit presumptuous, to ignore individual differences among the hosts (i.e., patients) and develop "generic" therapies with "one-size-fits-all" philosophy. However, focus on individual patients is paramount to comprehend outcomes in specific cases, and improve performance among the population while providing new approaches and mechanistic insights for novel substitutes. This is nowhere more visible than cancer therapeutics where "heterogeneity" in the disease is inherent and adaptation to intervention is the norm. The review article by Bray et al. focuses on addressing patient specificity in engineering tumor models *ex vivo*. Integrating distinct fields of cellular/molecular biology, extracellular matrix biology and scaffold design, this review summarizes exciting developments in 3D fabrication of devices to investigate fundamental issued related to tumor therapy (such as drug response and metastasis). Heterogeneity is central to this pursuit, and biomaterial scaffold-centered approaches for tissue mimics with advanced analytical tools including computational modeling and simulations will make greater impact, perhaps even obviate the animal models, before therapeutic progression to patients.

The use of bioactive glasses especially doped with strontium (Sr) has been reviewed by Kargozar et al. for bone repair. While there is an ongoing debate on the exact mechanism of beneficial effect for Sr doping, better functional outcomes on bone repair is stimulating research with these biomaterials, so that the authors provide a summary of beneficial effects of Sr-doped bioactive glasses in bone repair models along with the current state of clinical use. The review summarizes the important facets of bioactive glasses, including their synthesis and atomistic details of their structural features. The technology for fabricating different bioactive glass constructs is presented along with possible mechanism(s) of action, ultimately leading to a comprehensive glimpse into the use of this unique type of biomaterials.

Continuing with the unique applications, Mobaraki et al. summarize the recent concepts and future prospects on the use of biomaterials for corneal tissue repair and regeneration. An interwoven array of pharmacological, cellular, and biomaterial based interventions is presented, which is bound to stimulate new cross-disciplinary approaches to corneal repair. New biomaterials relying on novel mechanisms of actions may emerge in this area based on mechanistic perspective provided in this review.

Calcium/phosphate nanoparticles are attractive for patient use since their breakdown products are simple ions that can be ready metabolized with no adverse effects. To visualize them, however, is challenging given the "interference" from the mineralized tissues. To overcome this problem, Kalidoss et al. describes calcium-deficient hydroxyapatite nanoparticles with silver, gadolinium, and iron substitutions to improve contrast in computed tomography. The nanoparticles, due to strong interfacial charges, were also beneficial to deliver therapeutic agents in a sustained manner, additionally enabling therapeutic effects beyond their possible diagnostic use.

Finally, the deployment of biomaterials for development of safe and effective non-viral gene delivery is reviewed by Uludag et al., which highlighted selected aspects of gene delivery efforts where the biomaterials are making an impact. Recent understandings of how cells utilize nucleic acids has led to a review of the types of nucleic acids that can be utilized for therapy. Given the excitement with recent T-cell based therapies, biomaterial-centered approaches (instead of viral approaches) to enable more effective and safer therapy are probed in this review. Authors' perspectives on designing intelligent nanoparticles, deploying mRNA as an alternative to plasmid DNA, long-acting (integrating) expression systems, and *in vitro*/*in vivo* expansion of engineered T-cells can be found in this review.

One can easily see from the summaries of the individual contributions that the compiled articles are broad in nature, emphasizing the science and technology of the explored topics. This was the intent, again, of this Research Theme where different aspects of biomaterials science and engineering have been painted with broad brush strokes. Cross-fertilization of new ideas are likely to emanate by compiling such complementary but not necessarily overlapping articles.

AUTHOR CONTRIBUTIONS

HU drafted the manuscript. LK and AP edited and proof-read the manuscript.

REFERENCES

Dadfar, S. M., Roemhild, K., Drude, N. I., von Stillfried, S., Knüchel, R., Kiessling, F., et al. (2019). Iron oxide nanoparticles: diagnostic, therapeutic and theranostic applications. *Adv. Drug Deliv. Rev*. 138:302. doi: 10.1016/j.addr.2019.01.005

Huettner, N., Dargaville, T. R., and Forget, A. (2018). Discovering cell-adhesion peptides in tissue engineering: beyond RGD. *Trends Biotechnol*. 36:372. doi: 10.1016/j.tibtech.2018.01.008

Patel, S., Caldwell, J. M., Doty, S. B., Levine, W. N., Rodeo, S., Soslowsky, L. J., et al. (2018). Integrating soft and hard tissues via interface tissue engineering. *J. Orthop. Res*. 36:1069. doi: 10.1002/jor.23810

Uludag, H. (2014). Grand challenges in biomaterials. *Front. Bioeng. Biotechnol*. 2:43. doi: 10.3389/fbioe.2014.00043

Conflict of Interest: HU is the founder and share holder in RJH Biosciences intended to commercialize transfection reagents.

The remaining authors declare that the research was conducted in the absence of any commercial or financial relationships that could be construed as a potential conflict of interest.

frontiers in Bioengineering and Biotechnology

REVIEW
published: 03 May 2019
doi: 10.3389/fbioe.2019.00098

Surface Modification of Aliphatic Polyester to Enhance Biocompatibility

Yazhong Bu[1†], *Junxuan Ma*[2,3†], *Jianzhong Bei*[1] *and Shenguo Wang*[1*]

[1] *Beijing National Laboratory for Molecular Sciences, State Key Laboratory of Polymer Physics and Chemistry, Institute of Chemistry, Chinese Academy of Sciences, Beijing, China,* [2] *Orthopedic Research Institute, The First Affiliated Hospital of Sun Yat-sen University, Guangzhou, China,* [3] *Guangdong Provincial Key Laboratory of Orthopedics and Traumatology, Guangzhou, China*

Aliphatic polyester is a kind of biodegradable implantable polymers, which shows promise as scaffolds in tissue engineering, drug carrier, medical device, and so on. To further improve its biocompatibility and cell affinity, many techniques have been used to modify the surface of the polyester. In the present paper, the key factors of influencing biocompatibility of aliphatic polyester were illuminated, and the different surface modification methods such as physical, chemical, and plasma processing methods were also demonstrated. The advantages and disadvantages of each method were also discussed with the hope that this review can serve as a resource for selection of surface modification of aliphatic products.

Keywords: biomedical material, aliphatic polyester, biocompatibility, surface modification, tissue engineering

OPEN ACCESS

Edited by:
Anderson Oliveira Lobo,
Federal University of Piauí, Brazil

Reviewed by:
Jian Yang,
Shenzhen University, China
Saeid Kargozar,
Mashhad University of Medical Sciences, Iran

***Correspondence:**
Shenguo Wang
wangsg@iccas.ac.cn

†These authors have contributed equally to this work

Specialty section:
This article was submitted to Biomaterials, a section of the journal Frontiers in Bioengineering and Biotechnology

Received: *06 February 2019*
Accepted: *16 April 2019*
Published: *03 May 2019*

Citation:
Bu Y, Ma J, Bei J and Wang S (2019) Surface Modification of Aliphatic Polyester to Enhance Biocompatibility. Front. Bioeng. Biotechnol. 7:98. doi: 10.3389/fbioe.2019.00098

INTRODUCTION

Biodegradable polymers are defined as materials whose chemical and physical characteristics undergo deterioration and complete degradation when exposed to certain conditions, which have many important applications in medical and related fields (Rezwan et al., 2006; Nair and Laurencin, 2007). These polymers can be divided into natural biodegradable polymers and synthetic biodegradable polymers. Natural materials mainly include polysaccharides and proteins. Although they have good biocompatibility and some biofunctions, their strong immunogenic response, complex purification process and disease transmission possibility limit their applications. The synthetic biodegradable polymers can be prepared with designed routes, so they have more predictable properties and batch-to-batch uniformity. There are many synthetic biodegradable polymers, such as aliphatic polyesters, polypropylene fumarate, polyhydroxyalkanoates, and so on. Among them, aliphatic polyesters, including polyglycolide (PGA), polylactide (PLA), polycaprolactone (PCL), and their copolymers (copolylactones), are the most often used ones in tissue engineering and other bio-medical applications. Aliphatic polyesters have many advantages. Under the physiological environment, polymeric chains of the aliphatic polyesters can fracture into small pieces, with the molecular weight of the pieces decreasing from high to low. The polymeric pieces become dissolvable and finally will be absorbed or metabolized *in vivo*. In this way, not only the formation of foreign body reaction can be avoided, but also the secondary surgery for removing the foreign matter can also be avoided. Compared with the natural biodegradable polymers, aliphatic polyesters have the adjustable degradation rate, excellent processability, high mechanical strength, easiness to sterilization as well as good reproducibility and low price (Drury and Mooney, 2003). Therefore, aliphatic polyesters have become a kind of important biomedical

polymer materials and have been approved as an implantable biomaterial for using *in vivo* by Food and Drug Administration (FDA) of many countries including China, USA and European.

THE INFLUENCING FACTORS OF BIOCOMPATIBILITY OF ALIPHATIC POLYESTER

Indeed, biocompatibility includes the interactive mechanisms relating the biomaterial with its biological environment (Lotfi et al., 2013). Since the materials interact with tissues through the cell adhesion, the biocompatibility of materials is very closely related to cell adhesion (Lotfi et al., 2013). Generally, the response of cells to a surface is dictated by the interactions of the proteins and the substrate (Kasemo and Lausmaa, 1994; Anselme, 2000; Oliveira et al., 2011). Firstly, proteins adsorb onto the surface of the material, being followed by the binding of cellular membrane receptors to the chemical groups of those proteins or even directly to the substrate exposed chemical groups. The proteins adsorption is often caused by physical (Van Der Waals force) or chemical action (ionic interaction), which happens very quickly. Then, the cell attachment is caused by the interaction between cells and some bioactive molecules, such as extracellular matrix protein, membrane proteins, cytoskeleton proteins, and so on. By controlling the cell adhesion on materials, the biocompatibility of materials can be optimized (Anselme, 2000; Veiseh et al., 2015; Chaudhuri et al., 2016). Generally speaking, the aliphatic polyester is biocompatible (Rasal et al., 2010). It will not produce toxic or carcinogenic effects in local tissues. Also the degradation products will not interfere with tissue healing (Athanasiou et al., 1996). However, for some applications, the biocompatibility is still need to be improved, because polyester intrinsically is too hydrophobic and lack reactive side-chain groups (Liu et al., 2018). Given that the surface of biomaterials will contact the cells before all other parts, the properties of the surface are particularly important for the cell adhesion and later the biocompatibility and these properties are summarized as follows.

Wettability

Wettability, also known as the hydrophilicity and hydrophobicity, will influence the cell attachment and protein absorption. The cell adhesion is induced by the protein and mediated by receptors on the cell membrane. In the cell adhesion process, the proteins are firstly absorbed onto the surface of the material, after which cellular membrane receptors are bound to proteins' chemical groups or directly to the chemical groups of the substrate (Kasemo and Lausmaa, 1994). Generally, hydrophobic surfaces will display a better affinity for proteins (Lampin et al., 1997; Yousefi et al., 2018). Therefore, the surface of the material must have hydrophobicity to absorb protein to help the recognition (Hynes, 1992). However, the hydrophilic surfaces possess a higher affinity toward the cells. A number of studies have shown that enhancing the hydrophilic properties of polymers leads to increased cell spreading and adhesion (Lee and Lee, 1993; Allen et al., 2006). As a result, keeping a balance between hydrophobicity and hydrophilicity is vital to ensure the protein adsorption as well as the cell growth (Good et al., 1998; Wang Y. W. et al., 2003).

Electric Properties

The cell membrane is negative (Wen et al., 2016). So generally positive materials are good for cell adhesion and negative surface will have charge repulsion with cells (Steele et al., 1995; Hoshiba et al., 2018). However, there are reports about a newborn rat calvaria bone osteoblasts adhering in both positive and negative surface of the polystyrene ion exchange resin microspheres (Gao et al., 1998), in which protein adsorption and cell migration can be greatly enhanced. Still the data showed that different kinds of charged surfaces led to obviously different cell morphology. So, the electric properties of the materials, including the types and densities, have great influence on the cell adhesion behavior (Shirazi et al., 2016; Kuo and Rajesh, 2017).

Surface Free Energy

Surface free energy can affect polar molecules such as water and protein and high surface free energy of the material is more advantageous to cell adhesion and spreading (Vandervalk et al., 1983; Nakamura et al., 2016; Ueno et al., 2019). Nakamura et al. reported that changes in surface free energy would affect polar molecules such as water and proteins. The increase in surface free energy will improve the wettability and then accelerate the cell adhesion (Nakamura et al., 2016). The surface free energy depends on chemical composition, functional groups and electric properties of material surface. These surface properties are mainly decided by the physical and chemical properties of the materials (Vanpelt et al., 1985; Nakamura et al., 2016).

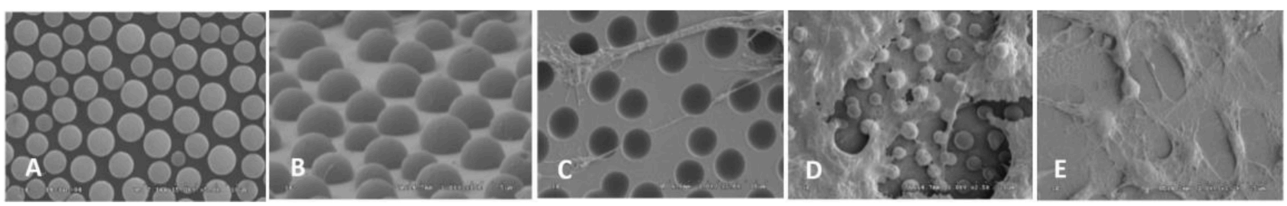

FIGURE 1 | (A) PS surface with micrometer scale pits, ×10,000; **(B)** PLLA surface with micrometer scale islands, ×10,000; OCT-1 osteoblasts on **(C)** PS surface with micrometer scale pits (×5,000), **(D)** PLLA surface with micrometer-scale islands (×2,500), and **(E)** smooth PLLA surface (×1,200) (Wan et al., 2005) [Readapted with permission from Wan et al. (2005). Copyright© 2004 Elsevier Ltd.].

Surface Morphology

Roughness

Rough surface can enhance the cell adhesion by influencing the protein adsorption and providing larger area for cell adhesion compared with smooth surface (Lampin et al., 1997). Rough surface is good for the formation and grow of biofilm (Quirynen and Bollen, 1995). Wan et al. found that although OCT-1 osteoblast could adhere to smooth, pits-patterned, and island-patterned surface of PLLA (**Figures 1A,B**), they had differences in their state of spreading. On the pits- and island-patterned surfaces (**Figures 1C,D**), the cells spread better than those on the smooth surface (**Figure 1E**). The height of cells on pit-patterned surface was obviously lower than that on the flat ones (Wan et al., 2005). It was observed that cells could adhere onto the islands and grow along the convex surface of the islands. It was also observed that the tiny pseudopodium protrusions strode from one island to another as shown in **Figure 2**. Because cells had more contact area and spread better on the rough surface than on the smooth ones, the OCT-1 cells had lower height on rough surfaces as was shown in **Figure 1**.

It could be seen that the cells could stride over the pits with 2.2 μm of radius (**Figure 3A**). The pseudopodiums of the cells could intrude inside the pits and grow along the curvature wall of the pits because the pseudopodiums of the cells had less rigidity compared to the bulk of the cells, showing "contact guidance" effects (**Figure 3B**). These pseudopodiums acted as anchoring points to pull the cell body, suggesting that cell is allowed to penetrate and proliferate on scaffolds with this pore size. Filopodia of cells would alter their original orientation to grow along the ridge of the pits when they reached the borders, which might be caused by "groove-ridge" induced "contact guidance". However, according to Wan, cells could not grow inside nano-scaled pits with the diameter to be 0.45 μm (Curtis and Wilkinson, 1997; Wan et al., 2005).

It also found that surface morphology not only affected the cell adhesion and growth, but also the adhesion efficiency. **Figure 4** demonstrated that, only around 30% of the osteoblasts could adhere on the smooth surface, while much more could adhere on rough surface (50–75%).

However, generally speaking, the response of cells to roughness is different depending on the cell type (Chang and Wang, 2011). For osteoblasts and neurons, which is large, they might need larger surface roughness (Donoso et al., 2007). For smaller cells, like human vein endothelial cells, nano-scale of roughness could enhance cell adhesion and growth (Chung et al., 2003).

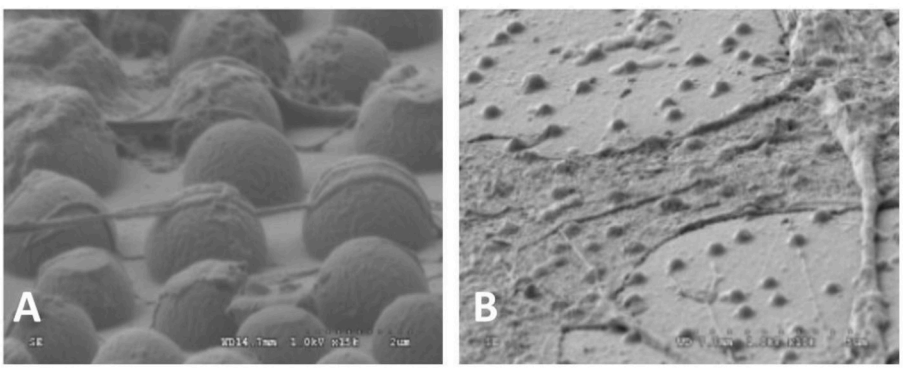

FIGURE 2 | SEM images of OCT-1 osteoblasts on PLLA surface with micro-island for 6 h: **(A)** the surface with micrometer scale islands, ×25,000; **(B)** The surface with nanometer scale islands, ×10,000 (Wan et al., 2005) [Readapted with permission from Wan et al. (2005). Copyright© 2004 Elsevier Ltd.].

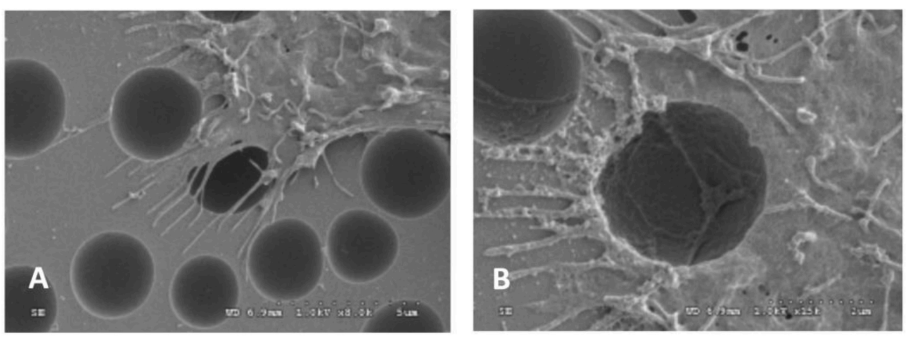

FIGURE 3 | SEM images of OCT-1 osteoblasts on PS surface with micro-pits for 6 h: **(A)** for micrometer scale pits (2.2 μm), ×8,000; **(B)** for micrometer scale pits (2.2 μm), ×15,000 (Wan et al., 2005) [Readapted with permission from Wan et al. (2005) Copyright © 2004 Elsevier Ltd.].

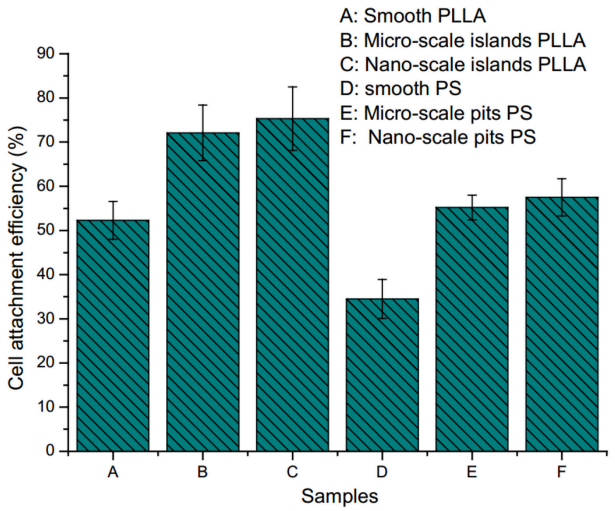

FIGURE 4 | Cell attachment efficiency on polystyrene and poly(l-lactide) surface with different sized pits and islands: **(A)** on smooth PLLA surface; **(B)** on PLLA surface with micro-scale islands; **(C)** on PLLA surface with nano-scale islands; **(D)** on smooth PS surface; **(E)** on PS surface with micro-scale pits; **(F)** on PS surface with nano-scale pits (Wan et al., 2005) [Readapted with permission from Wan et al. (2005). Copyright © 2004 Elsevier Ltd.].

Microgrooves

Some natural tissues have the parallel orientation structures such as tendon, peripheral nerve and spinal cord (**Figures 5A–C**), so the scaffolds for tissue engineering will be more promising if they can stimulate the parallel orientation structure. It was proved that by using substratum with certain shapes, alignment, or directional growth of cells in the developing brain could be induced (Hatten, 1990). By using laser ablation methods, Yao et al. fabricated micropatterned PLGA films. After being coated with collagen type I or laminin peptide (PPFLMLLKGSTR), these films showed a guidance effect on both early stage neurite outgrowth and elongation (**Figures 5D–F**) (Campbell and von Recum, 1989; Yao et al., 2009).

Surface Structure

Surface structures, such as walls, edges, or holes, influences the motility and spreading of cells and can be used to control the direction and localization of cell growth. Porous structure were reported to be conducive to the nutrients penetrate and cell metabolism, which was good for cell adhesion and growth (Kuo et al., 1997). Richter et al. reported that nylon net with smaller pores had larger specific surface area than those with larger pores and more cells grew on surface of materials with smaller pores. This was because cells could penetrate the nylon net with large pores, leading the failure of cell adhesion on the surface (Richter et al., 1996). So it is preferred that the scaffold for tissue engineering have porous structure and the cell adhesion behavior could be tuned by the size of the pores (Cai et al., 2002).

In summary, factors influencing the cellular affinity and then biocompatibility are summarized in **Table 1**. To improve the cellular affinity and biocompatibility, the modification must be used according to practical application purpose and the physical-chemical properties.

SURFACE MODIFICATION OF ALIPHATIC POLYESTER

Aiming at the above surface properties for biocompatibility, there are many ways to modify aliphatic polyester to improve the surface properties and the biocompatibility (Liu et al., 2018; Miele et al., 2018). The commonly used methods for modification are summarized in **Table 2**.

Bulk Modification—Copolymerization

By means of bulk modification, which is to copolymerize hydroxyl acid monomer with the molecules containing hydrophilic or charging groups (carboxyl group, hydroxyl group, amine group, subamine group, sulfonic group, amide group, etc.), surface properties of the polymers, such as crystallinity, hydrophilicity, the types and quantity of charging, and reactive groups, can be changed and optimized, finally enhancing the cell adhesion and cell affinity (Wang, 2002; He et al., 2004b; Cui et al., 2005; Wang S. G. et al., 2005; Shenguo and Jianzhong, 2011; Qiang et al., 2014; Amani et al., 2019). Many monomers and polymers can be used for the copolymerization. Poly(ethylene glycol) (PEG) is a highly biocompatible, nontoxic material with excellent hydrophilicity (Phelps et al., 2012; Rong et al., 2019). To enhance hydrophilicity of the poly(L-lactic acid) (PLLA), Chen et al. used poly(ethylene glycol) (PEG) macromolecular monomer to copolymerize with PLLA. With higher content of the ethylene glycol (EG) unit, water uptake ability of the PLLA-co-PEG copolymer (PLE) increased (Chen et al., 2002).

Aliphatic polyester lacks recognition sites for cells. By copolymerization of lactone monomer with other monomers containing pendant carboxyl groups and/or amino groups, it would be more easily for bioactive agents to immobilize on the material surface, enhancing the cell adhesion. He et al. used lactide to copolymerize malic acid (MA) with two carboxyl groups, and the hydrophilicity of resulting copolylactone (PLMA) could be tuned by altering the ratio of MA. With the increased amount of MA, the contact angles of the PLMA decreased (**Figure 6**) (He et al., 2003, 2004a,b). By comparing the rat 3T3 fibroblasts on the surface of PLMA with different amount of MA after 5 hours, the cells showed different morphology on the surface. PLMA (96/4) and PLMA (92/8) showed better attach efficacy than pure PLLA and PLMA (86/14) (**Figure 7**) (He et al., 2004b). One of the degradation products of PLMA, MA is a natural component of juice and also a necessary organic acid for human beings. So just like LA, MA could be metabolized and absorbed by bodies, which would not cause any side effects.

Because that the natural polymers are usually biodegradable and offer excellent biocompatibility, as well as good cell affinity, they could also be used to copolymerize with aliphatic polyesters. For example, by using the trimethylsilyl-protected (TMS) dextran as macroinitiator, Cai et al. synthesized PLA grafting dextran (PLA-g-dextran) and proved that compared PLA-g-dextran with

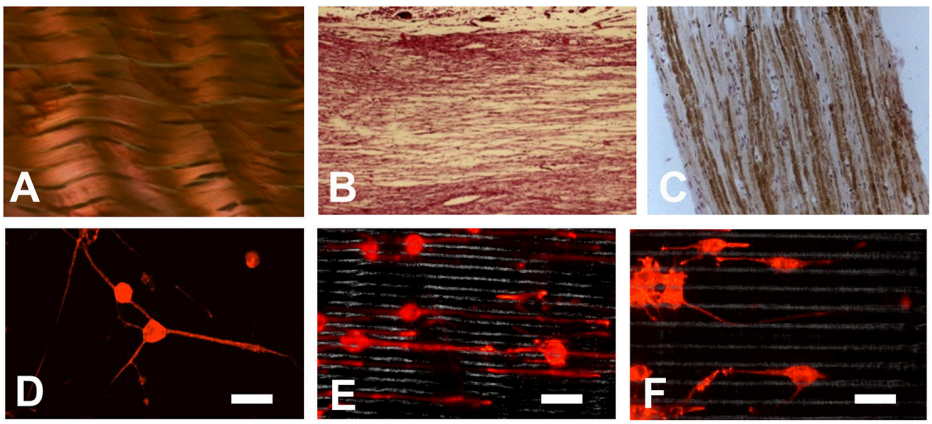

FIGURE 5 | (A–C) Some natural tissues have a parallel orientation structure: **(A)** Tendon; **(B)** Peripheral nerve; **(C)** Spinal cord; **(D–F)** Orientation of neurite growth on laminin peptide coated PLGA scaffold after 6 days culture **(D)** on smooth surface; **(E)** on scaffold with microgrooves of 5 μm; **(F)** on scaffold with microgrooves of 10 μm (Yao et al., 2009). (Bar scale, 60 μm) [Readapted with permission from Ref. (Yao et al., 2009). Copyright © 2008 Acta Materialia Inc. Published by Elsevier Ltd.].

TABLE 1 | The factors and influences of the material surface on biocompatibility and cell affinity.

Factors	Influences
Hydrophilicity/hydrophobicity (Yousefi et al., 2018)	Proper hydrophilicity is beneficial to cell adhesion and growth
Surface free energy (Nakamura et al., 2016)	High surface free energy is beneficial to cell adhesion and spread
Surface electricity (Koo et al., 2018)	Positive electricity is beneficial for attracting cells
Surface structure (Bacakova et al., 2011)	Roughness surface is beneficial for cell adhesion and biological membrane growth

TABLE 2 | The surface modification methods for polylactone-type products.

Categories	Ways	Mechanism
Chemical modification	Bulk modification (Cui et al., 2005; Phelps et al., 2012)	Copolymerization of various monomers
	Surface grafting (Lih et al., 2008)	Adding various functional groups to the surface
Physical modification	Surface coating (Yang et al., 2018)	Covering the surface with biocompatible materials
Plasma modification	Low temperature plasma treatment (Wang et al., 2004)	Changing the topological structure of surface
	Plasma treatment-biomolecule anchoring method (Shen et al., 2009, 2010)	Anchoring bioactive molecules on the surface by using the charged groups on the surface

the pure PLA, the PLA-g-dextran copolymer exhibited not only better hydrophilicity but also better cell affinity (Cai et al., 2003). Qu et al. also reported that after grafting lactic acid onto amino groups of chitosan, a novel pH-sensitive physically crosslinked hydrogels could be constructed (Qu et al., 1999).

Surface Grafting

After polymerization of glycolide, lactide, and caprolactone, there are still some functional groups at end of the polylactone chains. By using these functional groups, the hydrophilic groups and/or charged groups can be grafted onto surface of the aliphatic polyesters through chemical reaction to improve cell compatibility, blood compatibility as well as anticoagulation properties. Since the chemical bonding is strong and stable, a long-term modification effect can be realized.

Heparin is a natural anticoagulant substance. It is used to inhibit prothrombin activation, slow down and stop formation of the fibrin network. It can also prevent incidence of infection. Heparin has been also used to improve the anticoagulant properties of polyester. By using Michael-type addition between thiolated heparin and PLGA-PEG-PLGA diacrylate, Lih et al. developed novel heparin–conjugated polyester hydrogels. This hydrogel exhibited temperature dependent sol-gel transition behavior and might be used as injectable scaffold (Lih et al., 2008). Except for covalently immobilizing heparin on PLGA surface, Wang et al. also graft chitosan on the surface of PLGA using N-(3-dimethylaminopropyl)-N-ethylcarbodiimide (EDC) and N-hydroxysuccinimide (NHS). After grafting, the water contact angle of the modified film was greatly decreased and the blood and cell compatibility was improved (Wang X. H. et al., 2003). Compared with the surface coating method, surface grafting method will lead to tougher bonding between biofunctional molecules and the surface, which is expected to play a more and more important role in the field of biomedical applications.

However, it is worth noting that the aliphatic polyester is lack of functional groups, of which only the end of main chains have the functional groups. The ones exposed on surface of the aliphatic polyester are even less. Even if all these functional groups are modified, the surface modification effect is still limited. On the other hand, sometimes organic solvents might be used in the chemical modification, which might cause destruction of topology structure of the surface as well as pollution of the environment.

Surface Coating

Because the different solubility of natural polymers and the synthetic polyesters, in most cases, bulk modification was carried out using synthetic polymers, which lacked biomedical functions because of the intrinsic shortcomings of synthetic polymers. In order to add some biofunctions to the polyesters, many natural biofunctional materials such as hyaluronic acid, protein, lipid, collagen, polysaccharide, peptides, and gelatin, are coated on the surface of synthetic polymers. Generally, the coating materials are prepared in solutions and the coatings were prepared by soaking, brushing, or spraying methods. Hyaluronic acid and collagen possess excellent biocompatibility and cell affinity which are the mostly used coating materials for surface modification (Yang et al., 2018). However, although surface coating method is simple and effective, this method is still a physical treatment and the coating has bonded to the surface by Van Der Waals force, which is relatively weak. Especially in the presence of water or body fluids, the coatings are easily to dissolve and break away from the surface, shortening the duration of the surface treatment (Balaji et al., 2015). Besides, some solvents may destruct the topology of polyester, causing adverse effects on cell affinity. Some coating fluids are too viscous, which might change the topology of the original surface, and could not infiltrate into materials due to their high viscosity.

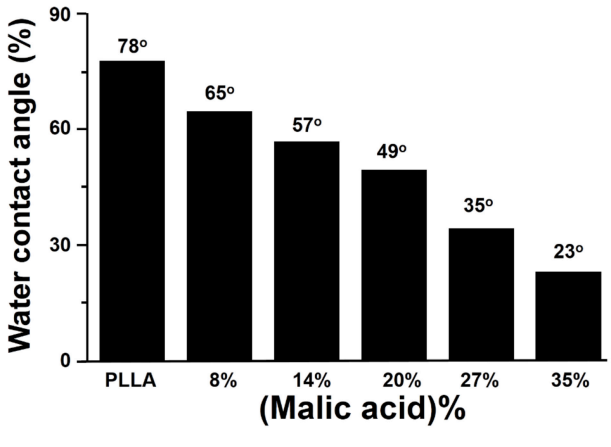

FIGURE 6 | Effect of malic acid content on water contact angle of PLMA (He et al., 2004b) [Readapted with permission from He et al. (2004b). Copyright© 2003 Elsevier Ltd.].

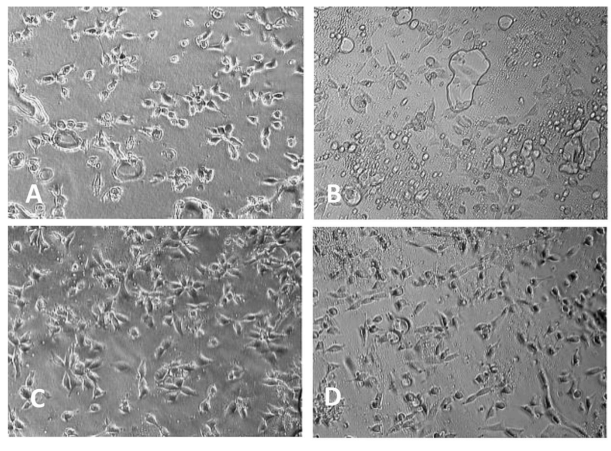

FIGURE 7 | Morphology of 3T3 mice fibroblasts cultivated on PLMA with different composition for 5 h (×150): **(A)** PLLA; **(B)** PLMA (96/4); **(C)** PLMA (92/8); **(D)** PLMA (86/14) (He et al., 2004b) [Readapted with permission from He et al. (2004b) Copyright © 2003 Elsevier Ltd.].

Plasma Modification

Plasma Modification

Plasma treatment is a straight-forward and widely used method for modifying the surface of materials to improve cell affinity of cell scaffolds (Yang et al., 2002b; Oehr, 2003). Plasma is complex system composed of neutral or excited states of atoms, molecules, free radical, electronics, ions, and radiant photon with high energy and high reactivity. It belongs to the fourth state, which is beyond the state of the solid, liquid and gas. Generally, the electromagnetic radiation, especially in ultraviolet and vacuum ultraviolet regions, is rich of plasma. By applying

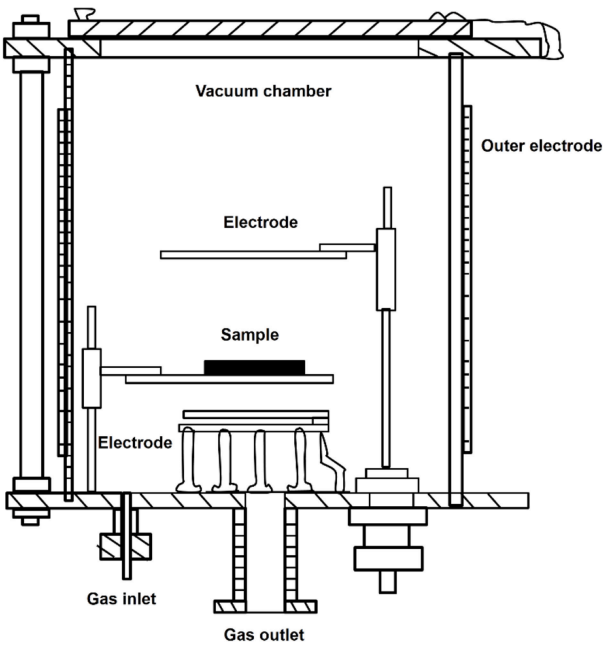

FIGURE 8 | Scheme of plasma treatment device.

the plasma generator in **Figure 8**, plasma can be obtained using radio-frequency discharge in 0.1 ∼ 100 Pa. Since surface parts of the materials are exposed to energies higher than the characteristic bonding energy of polymers, these parts undergo scission reactions and form new bonding configurations on the surface (Oehr, 2003). Functional groups such as $-NH_2$, -OH, and -COOH can be grafted by plasma treatment with non-deposition gas such as ammonia, oxygen, hydrogen oxide, and so on (Yang et al., 2002b; Oehr, 2003). Because the temperature of particles in the generator is close to or slightly higher than the room temperature, it is also called low temperature plasma.

The process for plasma treatment is relatively simple. Firstly, the generator is filled with gas that cannot be polymerized, such as methane, ammonia gas, nitrogen, oxygen, and argon. Then the sample is put into the cavity of generator; by using electrostatic field, plasma particles are generated, inducing molecular excitation, ionization, and chemical bond fracture on the surface. This method sculptures the surface in the range from dozens to thousands of Egypt to form new topology structure and will not cause the thermal decomposition or ablation of the material (Oehr, 2003).

The effect of plasma modification could be optimized by changing the gas, processing time, pressure and processing power. Different gas and pressure will result in the formation of functional groups with various types and properties. The plasma processing time and power lead to different processing depth, topology structure and densities of the formed functional groups (Favia and d'Agostino, 1998; Wang et al., 2004; Wang M. J. et al., 2005).

Under an ammonia atmosphere, some nitrogen-contained polar functional groups could be formed on the surface of polyester (**Figure 9A**). The depth of modification (**Figure 9B**) and the surface topology changed (**Figure 10**) with the increase of the plasma treatment time (Wang et al., 2004).

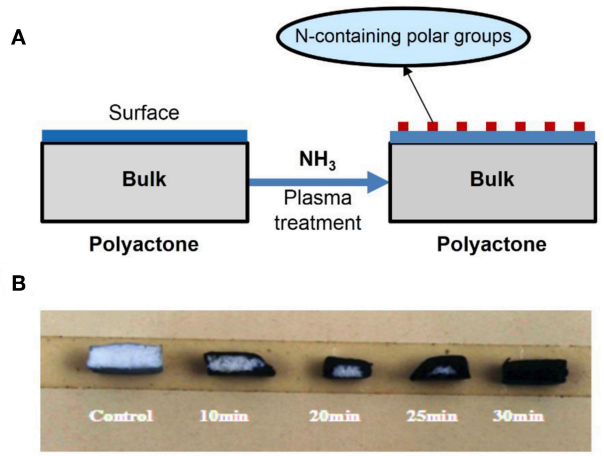

FIGURE 9 | (A) Scheme of formation of N-containing polar groups on surface of polylactone-type polymer using ammonia plasma treatment; **(B)** the influence of plasma-treating time under power 20 W and 30 Pa of NH_3 atmosphere on treated depth of PLGA scaffold.

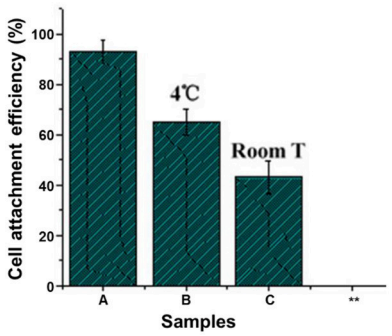

FIGURE 11 | Effect of storing temperature on adherence of mice 3T3 fibroblasts on NH_3 plasma-treated PLGA films under 20.3 N/m^2 of shear stress for 60 min (Wang et al., 2004) (Readapted with permission from Wang et al. (2004). Copyright© 2003 Elsevier Ltd.).

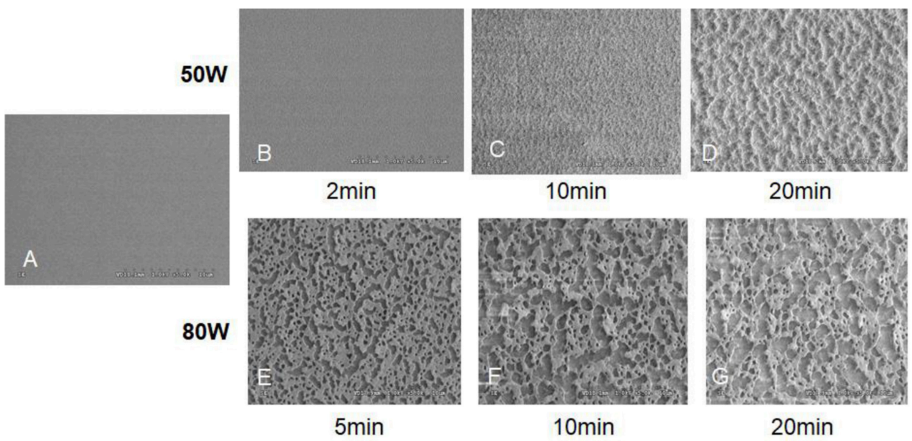

FIGURE 10 | The SEM images of control and oxygen-plasma treated PLGA surface: **(A)** Control; **(B)** 50 W, 2 min; **(C)** 50 W, 10 min; **(D)** 50 W, 20 min; **(E)** 80 W, 5 min; **(F)** 80 W, 10 min; **(G)** 80 W, 20 min (Wang et al., 2004) [Readapted with permission from Wang et al. (2004). Copyright © 2003 Elsevier Ltd.].

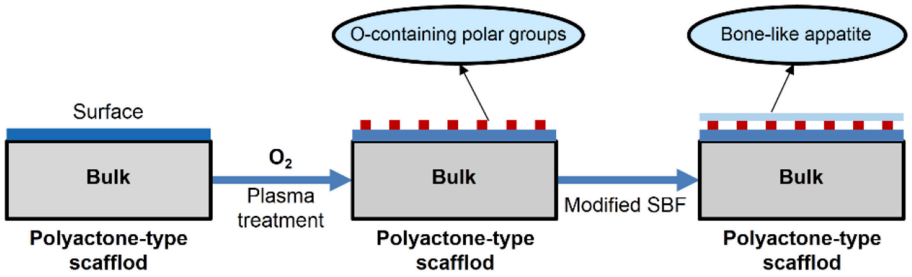

FIGURE 12 | Modification of PLGA by oxygen-plasma treatment then bone-like apatite incubation in modified SBF.

Compared with other methods, low temperature plasma is not only easier to operate but also more efficient in changing the hydrophilicity and electric properties. The method can avoid changing physical and chemical properties as well as morphology structure. It is also a green method without risk of pollution.

However, since the plasma easily moves due to the thermal action under the common temperature, the plasma on the surface would gradually migrates inside of the materials, resulting in the decreasing of functional groups on the surface and reducing attachment efficiency of the cell (**Figure 11**). To solve the problem, it is necessary to decrease storage time of the plasma treating product, and/or to keep the plasma treating product at low temperature (Wang et al., 2004).

Plasma Treatment-co-Biomolecule Anchoring Method

By using plasma treatment, functional groups with special physical and chemical properties can be generated, grafting other molecules or bioactive molecules. After the functional groups are bonded with other molecules and/or the large groups, the thermal moving of plasma will become difficult due to the increased volume, increasing the stability of the plasma treatment.

Yang et al. used nitrogen containing groups (C-N^+, -NH-) which generated under ammonia atmosphere to fix collagen. After fixing the collagen, the plasma treatment was prolonged and the biocompatibility was improved (Yang et al., 2002a,b, 2003, 2004).

Wang et al. applied oxygen plasma to modify PLGA. They found that the surface roughness was improved after modification. What's more, the formed oxygen containing functional groups on the surface could adsorb bovine serum albumin during the cell culture process and mediate cell to adhere and grow on PLGA (Wang et al., 2004).

As shown in **Figure 12**, after PLGA was performed with plasma treatment under oxygen atmosphere, a bovine serum albumin layer can be formed on the surface of PLGA. The resulting scaffold showed enhanced cell affinity with OCT-1 cells (Qu et al., 2007).

Growth factors are bio-active molecules that can influence cell growth and other functions. Growth factor was found in platelet, adult and embryonic tissues as well as many cells which differ according to types of cells. It is also one of the three main elements for Tissue Engineering. However, growth factors have poor thermal stability and easily lose biological activity at room temperature or in water (Langer and Vacanti, 1993). To keep the biological activity of the growth factor, Shen et al. fixed alkaline fibroblast growth factor (b-FGF) onto surface of the PLGA by using the plasma treatment-growth factor anchorage technique under CO_2 (Shen et al., 2008). Then they fixed rhBMP-2 onto surface of the PLGA by plasma treatment under oxygen atmosphere (Shen et al., 2009, 2010). This surface treatment technique can not only prevent the plasma from migrating inside of the scaffold, but also keep biological activity of the fixed growth factor and achieve slow release of the growth factor (Shen et al., 2007).

Plasma has good penetrability. The plasma treatment is not limited to the cell scaffolds with smooth and/or rough surface but also can be used on materials with hollows and/or porous structure. However, it must be noted that when using the plasma treatment, the special plasma generator and gas are necessary, and control equipment is also expensive. Besides, the size of the treated material is restricted by the size of the equipment chamber.

CONCLUSION

To improve biocompatibility of aliphatic polyesters, copolymerization, surface coating and grafting as well as plasma treatment can be used for the surface modification of the aliphatic polyester to optimize the properties. Chemical modification can achieve long and stable effects but is limited by the co-polymerization materials and the functional groups. Physical coating method is simple and effective, but the bonding is relatively weak, especially in water. Plasma treatment is a convenient and widely used method, but the size of the treated material is restricted. The selection of modification methods should be based on biomedical application and request.

AUTHOR CONTRIBUTIONS

YB did the literature search and paper writing. JM did literature research, data analysis and helped revise the paper. JB provided suggestion on biocompatibility. SW was responsible for the whole paper design and manuscript organization.

REFERENCES

Allen, L. T., Tosetto, M., Miller, I. S., O'Connor, D. P., Penney, S. C., Lynch, I., et al. (2006). Surface-induced changes in protein adsorption and implications for cellular phenotypic responses to surface interaction. *Biomaterials* 27, 3096–3108. doi: 10.1016/j.biomaterials.2006.01.019

Amani, A., Kabiri, T., Shafiee, S., and Hamidi, A. (2019). Preparation and characterization of PLA-PEG-PLA/PEI/DNA nanoparticles for improvement of transfection efficiency and controlled release of DNA in gene delivery systems. *Iran. J. Pharm. Res.* 18, 125–141. doi: 10.22037/ijpr.2019.2365

Anselme, K. (2000). Osteoblast adhesion on biomaterials. *Biomaterials* 21, 667–681. doi: 10.1016/S0142-9612(99)00242-2

Athanasiou, K. A., Niederauer, G. G., and Agrawal, C. M. (1996). Sterilization, toxicity, biocompatibility and clinical applications of polylactic acid/polyglycolic acid copolymers. *Biomaterials* 17, 93–102. doi: 10.1016/0142-9612(96)85754-1

Bacakova, L., Filova, E., Parizek, M., Ruml, T., and Svorcik, V. (2011). Modulation of cell adhesion, proliferation and differentiation on materials designed for body implants. *Biotechnol. Adv.* 29, 739–767. doi: 10.1016/j.biotechadv.2011.06.004

Balaji, A., Jaganathan, S. K., Vellayappan, M. V., John, A. A., Subramanian, A. P., SelvaKumar, M., et al. (2015). Prospects of common biomolecules as coating substances for polymeric biomaterials. *RSC Adv.* 5, 69660–69679. doi: 10.1039/C5RA12693B

Cai, Q., Wan, Y. Q., Bei, J. Z., and Wang, S. G. (2003). Synthesis and characterization of biodegradable polylactide-grafted dextran and its application as compatilizer. *Biomaterials* 24, 3555–3562. doi: 10.1016/S0142-9612(03)00199-6

Cai, Q., Yang, J. A., Bei, J. Z., and Wang, S. G. (2002). A novel porous cells scaffold made of polylactide-dextran blend by combining phase-separation and particle-leaching techniques. *Biomaterials* 23, 4483–4492. doi: 10.1016/S0142-9612(02)00168-0

Campbell, C. E., and von Recum, A. F. (1989). Microtopography and soft tissue response. *J. Invest. Surg.* 2, 51–74. doi: 10.3109/08941938909016503

Chang, H. I., and Wangs, Y. (2011). "Cell responses to surface and architecture of tissue engineering scaffolds," in *Regenerative Medicine and Tissue Engineering - Cells and Biomaterials*, ed D. Eberli (Rijeka: InTech), Chapter 27, 569–588. doi: 10.5772/21983

Chaudhuri, O., Gu, L., Klumpers, D., Darnell, M., Bencherif, S. A., Weaver, J. C., et al. (2016). Hydrogels with tunable stress relaxation regulate stem cell fate and activity. *Nat. Mater.* 15, 326–334. doi: 10.1038/nmat4489

Chen, W. N., Yang, J., Wang, S. G., and Bei, J. Z. (2002). Synthesis and properties of poly (L-lactide)-poly (ethylene glycol) multiblock copolymers. *Acta Polym. Sinica* 695–698.

Chung, T. W., Liu, D. Z., and Wang, S. Y., S.S. (2003). Enhancement of the growth of human endothelial cells by surface roughness at nanometer scale. *Biomaterials* 24, 4655–4661. doi: 10.1016/S0142-9612(03)00361-2

Cui, W. J., Bei, J. Z., and Wang, S. G. (2005). Research development of polylactide and its copolymers. *Polym. Bull.* 16–23.

Curtis, A., and Wilkinson, C. (1997). Topographical control of cells. *Biomaterials* 18, 1573–1583. doi: 10.1016/S0142-9612(97)00144-0

Donoso, M., Méndez-Vilas, A., Bruque, J., and González-Martin, M. L. (2007). On the relationship between common amplitude surface roughness parameters and surface area: Implications for the study of cell-material interactions. *Int. Biodeterior. Biodegradation*. 59, 245–251. doi: 10.1016/j.ibiod.2006.09.011

Drury, J. L., and Mooney, D. J. (2003). Hydrogels for tissue engineering: scaffold design variables and applications. *Biomaterials* 24, 4337–4351. doi: 10.1016/S0142-9612(03)00340-5

Favia, P., and d'Agostino, R. (1998). Plasma treatments and plasma deposition of polymers for biomedical applications. *Surf. Coat. Technol.* 98, 1102–1106. doi: 10.1016/S0257-8972(97)00285-5

Gao, C. Y., Li, A., and Feng, L. X. (1998). Polymer skeletal materials for tissue engineering. *J. Funct. Polym.* 11, 408–414.

Good, R. J., Islam, M., Baier, R. E., and Meyer, A. E. (1998). The effect of surface hydrogen bonding (acid-base interaction) on the hydrophobicity and hydrophilicity of copolymers: variation of contact angles and cell adhesion and growth with composition. *J. Dispers. Sci. Technol.* 19, 1163–1173. doi: 10.1080/01932699808913235

Hatten, M. E. (1990). Riding the glial monorail - a common mechanism for glial-guided neuronal migration in different regions of the developing mammalian. *Trends Neurosci.* 13, 179–184. doi: 10.1016/0166-2236(90)90044-B

He, B., Bei, J. Z., and Wang, S. G. (2003). Synthesis and characterization of a functionalized biodegradable copolymer: poly((L)-lactide-co-RS-beta-malic acid). *Polymer* 44, 989–994. doi: 10.1016/S0032-3861(02)00831-5

He, B., Wan, Y. Q., Bei, J. Z., and Wang, S. G. (2004a). Degradation in vitro and cell affinity of poly (L-lactide-co-beta-malic acid). *Acta Polym. Sinica* 693–399.

He, B., Wan, Y. Q., Bei, J. Z., and Wang, S. G. (2004b). Synthesis and cell affinity of functionalized poly(L-lactide-co-beta-malic acid) with high molecular weight. *Biomaterials* 25, 5239–5247. doi: 10.1016/j.biomaterials.2003.12.030

Hoshiba, T., Yoshikawa, C., and Sakakibara, K. (2018). Characterization of initial cell adhesion on charged polymer substrates in serum-containing and serum-free media. *Langmuir* 34, 4043–4051. doi: 10.1021/acs.langmuir.8b00233

Hynes, R. O. (1992). Integrins: versatility, modulation, and signaling in cell adhesion. *Cell* 69, 11–25. doi: 10.1016/0092-8674(92)90115-S

Kasemo, B., and Lausmaa, J. (1994). Material-tissue interfaces: the role of surface properties and processes. *Environ. Health Perspect.* 102, 41–45. doi: 10.1289/ehp.94102s541

Koo, M. A., Lee, M. H., Kwon, B. J., Seon, G. M., Kim, M. S., Kim, D., et al. (2018). Exogenous ROS-induced cell sheet transfer based on hematoporphyrin-polyketone film via a one-step process. *Biomaterials* 161, 47–56. doi: 10.1016/j.biomaterials.2018.01.030

Kuo, S. M., Tsai, S. W., Huang, L. H., and Wang, Y. J. (1997). Plasma-modified nylon meshes as supports for cell culturing. *Artif. Cells Blood Substit. Immobil. Biotechnol.* 25, 551–562. doi: 10.3109/10731199709117452

Kuo, Y. C., and Rajesh, R. (2017). Nerve growth factor-loaded heparinized cationic solid lipid nanoparticles for regulating membrane charge of induced pluripotent stem cells during differentiation. *Mater. Sci. Eng. C Mater. Biol. Appl.* 77, 680–689. doi: 10.1016/j.msec.2017.03.303

Lampin, M., WarocquierClerout, R., Legris, C., Degrange, M., and SigotLuizard, M. F. (1997). Correlation between substratum roughness and wettability, cell adhesion, and cell migration. *J. Biomed. Mater. Res.* 36, 99–108. doi: 10.1002/(SICI)1097-4636(199707)36:1<99::AID-JBM12>3.0.CO;2-E

Langer, R., and Vacanti, J. P. (1993). Tissue engineering. *Science* 260, 920–926. doi: 10.1126/science.8493529

Lee, J. H., and Lee, H. B. (1993). A wettability gradient as a tool to study protein adsorption and cell adhesion on polymer surfaces. *J. Biomater. Sci. Polym. Ed.* 4, 467–481. doi: 10.1163/156856293X00131

Lih, E., Joung, Y. K., Bae, J. W., and Park, K. D. (2008). An *in situ* gel-forming heparin-conjugated PLGA-PEG-PLGA copolymer. *J. Bioact. Compat. Polym.* 23, 444–457. doi: 10.1177/0883911508095245

Liu, P. M., Sun, L., Liu, P. Y., Yu, W. Q., Zhang, Q. H., Zhang, W. B., et al. (2018). Surface modification of porous PLGA scaffolds with plasma for preventing dimensional shrinkage and promoting scaffold-cell/tissue interactions. *J. Mater. Chem. B* 6, 7605–7613. doi: 10.1039/C8TB02374C

Lotfi, M., Nejib, M., and Naceur, M. (2013). "Cell adhesion to biomaterials: concept of biocompatibility," in *Advances in Biomaterials Science and Biomedical Applications,* ed. R. Pignatello (IntechOpen). doi: 10.5772/53542

Miele, D., Rossi, S., Sandri, G., Vigani, B., Sorrenti, M., Giunchedi, P., et al. (2018). Chitosan oleate salt as an amphiphilic polymer for the surface modification of poly-lactic-glycolic acid (PLGA) nanoparticles. Preliminary studies of mucoadhesion and cell interaction properties. *Mar. Drugs* 16:E447. doi: 10.3390/md16110447

Nair, L. S., and Laurencin, C. T. (2007). Biodegradable polymers as biomaterials. *Prog. Polym. Sci.* 32, 762–798. doi: 10.1016/j.progpolymsci.2007.05.017

Nakamura, M., Hori, N., Ando, H., Namba, S., Toyama, T., Nishimiya, N., et al. (2016). Surface free energy predominates in cell adhesion to hydroxyapatite through wettability. *Mater. Sci. Eng. C Mater. Biol. Appl.* 62, 283–292. doi: 10.1016/j.msec.2016.01.037

Oehr, C. (2003). Plasma surface modification of polymers for biomedical use. *Nucl. Instrum. Methods Phys. Res. B* 208, 40–47. doi: 10.1016/S0168-583X(03)00650-5

Oliveira, S. M., Song, W., Alves, N. M., and Mano, J. F. (2011). Chemical modification of bioinspired superhydrophobic polystyrene surfaces to control cell attachment/proliferation. *Soft Matter* 7, 8932–8941. doi: 10.1039/c1sm05943b

Phelps, E. A., Enemchukwu, N. O., Fiore, V. F., Sy, J. C., Murthy, N., Sulchek, T. A., et al. (2012). Maleimide cross-linked bioactive PEG hydrogel exhibits improved reaction kinetics and cross-linking for cell encapsulation and in situ delivery. *Adv. Mater*. 24, 64–70. doi: 10.1002/adma.201103574

Qiang, S., Shifang, L., Jing, J., Hengchong, S., and Jinghua, Y. (2014). Hemocompatibility of commodity polymers modified with chemical and biological method. *Mater. China* 33, 212–223. doi: 10.7502/j.issn.1674-3962.2014.04.03

Qu, X., Cui, W., Yang, F., Min, C., Shen, H., Bei, J., et al. (2007). The effect of oxygen plasma pretreatment and incubation in modified simulated body fluids on the formation of bone-like apatite on poly(lactide-co-glycolide) (70/30). *Biomaterials* 28, 9–18. doi: 10.1016/j.biomaterials.2006.08.024

Qu, X., Wirsen, A., and Albertsson, A. C. (1999). Synthesis and characterization of pH-sensitive hydrogels based on chitosan and D,L-lactic acid. *J. Appl. Polym. Sci*. 74, 3193–3202. doi: 10.1002/(SICI)1097-4628(19991220)74:13<3193::AID-APP23>3.0.CO;2-V

Quirynen, M., and Bollen, C. M. L. (1995). The influence of surface roughness and surface-free energy on supra-and subgingival plaque formation in man: a review of the literature. *J. Clin. Periodontol*. 22, 1–14. doi: 10.1111/j.1600-051X.1995.tb01765.x

Rasal, R. M., Janorkar, A. V., and Hirt, D. E. (2010). Poly(lactic acid) modifications. *Prog. Polym. Sci*. 35, 338–356. doi: 10.1016/j.progpolymsci.2009.12.003

Rezwan, K., Chen, Q. Z., Blaker, J. J., and Boccaccini, A. R. (2006). Biodegradable and bioactive porous polymer/inorganic composite scaffolds for bone tissue engineering. *Biomaterials* 27, 3413–3431. doi: 10.1016/j.biomaterials.2006.01.039

Richter, E., Fuhr, G., Muller, T., Shirley, S., Rogaschewski, S., Reimer, K., et al. (1996). Growth of anchorage-dependent mammalian cells on microstructures and microperforated silicon membranes. *J. Mater. Sci. Mater. Med*. 7, 85–97. doi: 10.1007/BF00058719

Rong, X. F., Yang, J., Ji, Y. H., Zhu, X. J., Lu, Y., and Mo, X. F. (2019). Biocompatibility and safety of insulin-loaded chitosan nanoparticles/PLGAPEG-PLGA hydrogel (ICNPH) delivered by subconjunctival injection in rats. *J. Drug Deliv. Sci. Technol*. 49, 556–562. doi: 10.1016/j.jddst.2018.12.032

Shen, H., Hu, X., Bei, J., and Wang, S. (2008). The immobilization of basic fibroblast growth factor on plasma-treated poly(lactide-co-glycolide). *Biomaterials* 29, 2388–2399. doi: 10.1016/j.biomaterials.2008.02.008

Shen, H., Hu, X., Yang, F., Bei, J., and Wang, S. (2009). The bioactivity of rhBMP-2 immobilized poly(lactide-co-glycolide) scaffolds. *Biomaterials* 30, 3150–3157. doi: 10.1016/j.biomaterials.2009.02.004

Shen, H., Hu, X., Yang, F., Bei, J., and Wang, S. (2010). An injectable scaffold: rhBMP-2-loaded poly(lactide-co-glycolide)/hydroxyapatite composite microspheres. *Acta Biomater*. 6, 455–465. doi: 10.1016/j.actbio.2009.07.016

Shen, H., Hu, X., Yang, F., Bel, J., and Wang, S. (2007). Combining oxygen plasma treatment with anchorage of cationized gelatin for enhancing cell affinity of poly(lactide-co-glycolide). *Biomaterials* 28, 4219–4230. doi: 10.1016/j.biomaterials.2007.06.004

Shenguo, W., and Jianzhong, B. (2011). Biodegradable polymer–A kind important biomaterial 2. Biocompatibility and surface modification of aliphatic polyester. *Chin. Polym. Bull*. 1–14.

Shirazi, S. F. S., Gharehkhani, S., Metselaar, H. S. C., Nasiri-Tabrizi, B., Yarmand, H., Ahmadi, M., et al. (2016). Ion size, loading, and charge determine the mechanical properties, surface apatite, and cell growth of silver and tantalum doped calcium silicate. *RSC Adv*. 6, 190–200. doi: 10.1039/C5RA17326D

Steele, J. G., Dalton, B. A., Johnson, G., and Underwood, P. A. (1995). Adsorption of fibronectin and vitronectin onto Primaria^{TM} and tissue culture polystyrene and relationship to the mechanism of initial attachment of human vein endothelial cells and BHK-21 fibroblasts. *Biomaterials* 16, 1057–1067. doi: 10.1016/0142-9612(95)98901-P

Ueno, H., Inoue, M., Okonogi, A., Kotera, H., and Suzuki, T. (2019). Correlation between Cells-on-Chips materials and cell adhesion/proliferation focused on material's surface free energy. *Colloids Surf. A Physicochem. Eng. Asp*. 565, 188–194. doi: 10.1016/j.colsurfa.2018.12.059

Vandervalk, P., Vanpelt, A. W., Busscher, H. J., Dejong, H. P., Wildevuur, C. R., Arends, J. (1983). Interaction of fibroblasts and polymer surfaces: relationship between surface free energy and fibroblast spreading. *J. Biomed. Mater. Res*. 17, 807–817. doi: 10.1002/jbm.820170508

Vanpelt, A. W. J., Busscher, H. J., Uyen, M., Weerkamp, A. H., Dejong, H. P., Arends, J., et al. (1985). Role of the surface-free energy of polymers on the adhesion of S-sanguis cells. *Caries Res*. 19, 181–181.

Veiseh, O., Doloff, J. C., Ma, M., Vegas, A. J., Tam, H. H., Bader, A. R., et al. (2015). Size- and shape-dependent foreign body immune response to materials implanted in rodents and non-human primates. *Nat. Mater*. 14, 643–651. doi: 10.1038/nmat4290

Wan, Y. Q., Wang, Y., Liu, Z. M., Qu, X., Han, B. X., Bei, J. Z., et al. (2005). Adhesion and proliferation of OCT-1 osteoblast-like cells on micro- and nano-scale topography structured poly (L-lactide). *Biomaterials* 26, 4453–4459. doi: 10.1016/j.biomaterials.2004.11.016

Wang, M. J., Chang, Y. I., and Poncin-Epaillard, F. (2005). Acid and basic functionalities of nitrogen and carbon dioxide plasma-treated polystyrene. *Surf. Interface Anal*. 37, 348–355. doi: 10.1002/sia.2029

Wang, S. G. (2002). Cells scaffold in tissue engineering. *Chin. J. Rehab. Theory Pract*. 267–269.

Wang, S. G., Cui, W. J., and Bei, J. Z. (2005). Bulk and surface modifications of polylactide. *Anal. Bioanal. Chem*. 381, 547–556. doi: 10.1007/s00216-004-2771-2

Wang, X. H., Li, D. P., Wang, W. J., Feng, Q. L., Cui, F. Z., Xu, Y. X., et al. (2003). Covalent immobilization of chitosan and heparin on PLGA surface. *Inter. J. Biol. Macromol*. 33, 95–100. doi: 10.1016/S0141-8130(03)00072-2

Wang, Y. Q., Qu, X., Lu, J., Zhu, C. F., Wan, L. J., Yang, J. L., et al. (2004). Characterization of surface property of poly(lactide-co-glycolide) after oxygen plasma treatment. *Biomaterials* 25, 4777–4783. doi: 10.1016/j.biomaterials.2003.11.051

Wang, Y. W., Wu, Q., and Chen, G. Q. (2003). Reduced mouse fibroblast cell growth by increased hydrophilicity of microbial polyhydroxyalkanoates via hyaluronan coating. *Biomaterials* 24, 4621–4629. doi: 10.1016/S0142-9612(03)00356-9

Wen, J., Weinhart, M., Lai, B., Kizhakkedathu, J., and Brooks, D. E. (2016). Reversible hemostatic properties of sulfabetaine/quaternary ammonium modified hyperbranched polyglycerol. *Biomaterials* 86, 42–55. doi: 10.1016/j.biomaterials.2016.01.067

Yang, J., Bei, J. Z., and Wang, S. G. (2002a). Enhanced cell affinity of poly (D,L-lactide) by combining plasma treatment with collagen anchorage. *Biomaterials* 23, 2607–2614. doi: 10.1016/S0142-9612(01)00400-8

Yang, J., Bei, J. Z., and Wang, S. G. (2002b). Improving cell affinity of poly(D,L-lactide) film modified by anhydrous ammonia plasma treatment. *Polym. Adv. Technol*. 13, 220–226. doi: 10.1002/pat.177

Yang, J., Bei, J. Z., and Wang, S. G. (2004). Study on improvement of cell affinity of polymer materials–modified poly (D, L-lactide) by anhydrous ammonia gaseous plasma. *Chin. J. Repar .Reconst. Surg*. 15, 269–272.

Yang, J., Wan, Y. Q., Yang, J. L., Bei, J. Z., and Wang, S. G. (2003). Plasma-treated, collagen-anchored polylactone: Its cell affinity evaluation under shear or shear-free conditions. *J. Biomed. Mater. Res. A* 67A, 1139–1147. doi: 10.1002/jbm.a.10034

Yang, X., Li, Y. Y., He, W., Huang, Q. L., Zhang, R. R., and Feng, Q. L. (2018). Hydroxyapatite/collagen coating on PLGA electrospun fibers for osteogenic differentiation of bone marrow mesenchymal stem cells. *J. Biomed. Mater .Res. A* 106, 2863–2870. doi: 10.1002/jbm.a.36475

Yao, L., Wang, S., Cui, W., Sherlock, R., O'Connell, C., Damodaran, G., et al. (2009). Effect of functionalized micropatterned PLGA on guided neurite growth. *Acta Biomater*. 5, 580–588. doi: 10.1016/j.actbio.2008.09.002

Yousefi, S. Z., Tabatabaei-Panah, P. S., and Seyfi, J. (2018). Emphasizing the role of surface chemistry on hydrophobicity and cell adhesion behavior of polydimethylsiloxane/TiO2 nanocomposite films. *Colloids Surf. B Biointerfaces* 167, 492–498. doi: 10.1016/j.colsurfb.2018.04.048

Conflict of Interest Statement: The authors declare that the research was conducted in the absence of any commercial or financial relationships that could be construed as a potential conflict of interest.

frontiers in Bioengineering and Biotechnology

ORIGINAL RESEARCH
published: 22 May 2019
doi: 10.3389/fbioe.2019.00117

Luminal Plasma Treatment for Small Diameter Polyvinyl Alcohol Tubular Scaffolds

*Grace Pohan[1], Pascale Chevallier[2], Deirdre E. J. Anderson[3], John W. Tse[1], Yuan Yao[1], Matthew W. Hagen[3], Diego Mantovani[2], Monica T. Hinds[3] and Evelyn K. F. Yim[1]**

[1] Department of Chemical Engineering, University of Waterloo, Waterloo, ON, Canada, [2] Laboratory for Biomaterials and Bioengineering, CRC-I, Department of Mining, Metallurgical and Materials Engineering, CHU de Québec Research Center, Regenerative Medicine, Laval University, Québec City, QC, Canada, [3] Department of Biomedical Engineering, Oregon Health & Science University, Portland, OR, United States

Plasma-based surface modification is recognized as an effective way to activate biomaterial surfaces, and modulate their interactions with cells, extracellular matrix proteins, and other materials. However, treatment of a luminal surface of a tubular scaffold remains non-trivial to perform in small diameter tubes. Polyvinyl alcohol (PVA) hydrogel, which has been widely used for medical applications, lacks functional groups to mediate cell attachment. This poses an issue for vascular applications, as endothelialization in a vascular graft lumen is crucial to maintain long term graft patency. In this study, a Radio Frequency Glow Discharges (RFGD) treatment in the presence of NH_3 was used to modify the luminal surface of 3-mm diameter dehydrated PVA vascular grafts. The grafted nitrogen containing functional groups demonstrated stability, and *in vitro* endothelialization was successfully maintained for at least 30 days. The plasma-modified PVA displayed a higher percentage of carbonyl groups over the untreated PVA control. Plasma treatment on PVA patterned with microtopographies was also studied, with only the concave microlenses topography demonstrating a significant increase in platelet adhesion. Thus, the study has shown the possibility of modifying a small diameter hydrogel tubular scaffold with the RFGD plasma treatment technique and demonstrated stability in ambient storage conditions for up to 30 days.

Keywords: ammonia, radio-frequency, stability, hydrogel, endothelialization

OPEN ACCESS

Edited by:
Abhay Pandit, National University of Ireland Galway, Ireland

Reviewed by:
Abbas Shafiee, Queensland University of Technology, Australia
Saeid Kargozar, Mashhad University of Medical Sciences, Iran

****Correspondence:***
Evelyn K. F. Yim
eyim@uwaterloo.ca

Specialty section:
This article was submitted to Biomaterials, a section of the journal Frontiers in Bioengineering and Biotechnology

Received: *28 February 2019*
Accepted: *07 May 2019*
Published: *22 May 2019*

Citation:
Pohan G, Chevallier P, Anderson DEJ, Tse JW, Yao Y, Hagen MW, Mantovani D, Hinds MT and Yim EKF (2019) Luminal Plasma Treatment for Small Diameter Polyvinyl Alcohol Tubular Scaffolds. Front. Bioeng. Biotechnol. 7:117. doi: 10.3389/fbioe.2019.00117

INTRODUCTION

Plasma treatment is a well-known technique for activating/functionalizing biomaterial surfaces. The exposure of these surfaces to ionized gas leads to incorporation of chemical species, which results in surface functionalization. For example, it was previously reported that the wettability of plasma treated surfaces improves after the treatment to favor either bonding of coating material or cell adhesion (Nakagawa et al., 2006; Jacobs et al., 2012; Ino et al., 2013; Liu et al., 2014; Cutiongco et al., 2016a; Recek et al., 2016; Jurney et al., 2018). Depending on the gas type and the material that is interacting with the plasma, one can introduce different surface functional groups on the biomaterial surface. For example, silanol (polar) group is formed when treating polydimethyl siloxane (PDMS) with oxygen plasma (Tan et al., 2010),

while carboxyl and thiol functional groups can be created by treating the material surface with CO_2 (Manakhov et al., 2018), and hydrogen sulfide plasma (Thiry et al., 2014), respectively. Moreover, H_2/N_2 plasma treatment demonstrated the capability to surface functionalize PVA via the introduction of amide, carboxylic acid, and OH/NH function groups (Ino et al., 2013).

Cold plasma can be generated at low temperature and pressure, and at a high voltage. Such plasma can be produced using Radio Frequency Glow Discharges (RFGD) system, which has been reported for surfaces of tubular, bar, or fibers (Blackman et al., 1994; Wade et al., 2000; Grace and Gerenser, 2003; Cao et al., 2007). To date, only few studies have investigated the effects of plasma treatment on the luminal surface of a tube with diameter smaller or equal to 3 mm (Lin and Cooper, 1995; Kaibara et al., 2000; Cao et al., 2007; Qiu et al., 2017). Kaibara et al. utilized ion coater to modify the inner surface of porous polyurethane tubes, while Qiu et al. utilized Plasma Technology Systems' low pressure plasma reactor (Kaibara et al., 2000; Qiu et al., 2017). However, both methods would require porous tubes to be successful. In contrast, Matsuzawa and Yasuda utilized a semi-continuous RFGD system and pressure difference between inner and outer tube surface to treat inner surfaces of plastic tubes (Matsuzawa and Yasuda, 1984). However, this method is not ideal for treating polymers with a certain degree of porosity. A few other groups used the back-and-forth movement of an electrode outside a plasma discharge chamber to generate uniform plasma along their tube samples (Hatada et al., 1982; Lin and Cooper, 1995; Tseng and Edelman, 1998; Cao et al., 2007). While this method successfully plasma treated tubes, Mantovani et al. reported a similar yet improved approach to perform luminal plasma treatment, as it was shown to have a greater symmetry due to the placement and the geometry of the electrodes (Mantovani et al., 1999).

Polyvinyl alcohol (PVA) is a hydrogel material rich in –OH function group and can be produced from base hydrolization of a polyvinyl acetate ester function group. It has been used in many biomedical applications (Yang et al., 1981; Wan et al., 2002; Kobayashi et al., 2005; Nugent and Higginbotham, 2007; Chaouat et al., 2008; Ding et al., 2012; Fathi et al., 2013; Cutiongco et al., 2015, 2016b) and is non-toxic, non-immunogenic, non-carcinogenic, and highly biocompatible. Importantly, PVA is non-thrombogenic as shown previously (Cutiongco et al., 2015; Anderson et al., 2019). PVA is a good material for making vascular graft as its mechanical property can be tailored to match native blood vessels. Its Young's modulus can range from 0.7 MPa (Wan et al., 2014) to 46 GPa (Peijs et al., 1995) depending on the crosslinking method and the degree of crosslinking between the polymer chains. In addition, a previous study has revealed that PVA has a suitable burst pressure and suture retention strength to withstand pulsatile flow *in vivo* (Chaouat et al., 2008). Studies have also proposed the use of PVA for making small diameter vascular grafts with diameter of <6 mm using a simple dip casting method of a cylindrical mold (Cutiongco et al., 2016a,b). Hence, PVA is a promising material for providing an off-the shelf synthetic small diameter vascular graft. The performance of small diameter vascular grafts to date has remained disappointing with high restenosis/failure rate (Tordoir et al., 1995; Tan et al., 2011). Fabricating an off-the-shelf vascular grafts can, therefore, be one of the ways to fulfill the unmet medical need.

While PVA can be fabricated into small diameter tubular graft with suitable mechanical and material properties as vascular graft, the hydrogel lacks surface functional groups that can mediate endothelialization on the inner surface of a PVA vascular graft (Ino et al., 2013; Cutiongco et al., 2016a). In native blood vessels, an endothelial cell lining functions as a barrier between blood and smooth muscle cell layers, controlling the proliferation and migration of the smooth muscle cells by secreting enzymes and inhibitors to the enzyme (Allaire and Clowes, 1997). Endothelial cells also prevent the activation of platelets and subsequent thrombogenesis. Hence, having an endothelial cell lining on the inner graft surface is crucial to attain a high graft patency rate in the long term.

Previous *in vitro* cell adhesion studies with plasma treated PVA films have shown to improve endothelial cell attachment on the PVA treated with N_2/H_2, N_2, O_2, or Ar plasma (Ino et al., 2013; Cutiongco et al., 2016a; Jurney et al., 2018). These cell adhesion studies were conducted in a short term (2–6 days), and the plasma treatments were performed on flat surfaces or on the external surface of a tube. Plasma treatment of the internal surface of a small diameter PVA vascular graft has not yet been reported before. While plasma treatment has been demonstrated to be a promising modification to enhance surface properties of PVA, performing luminal plasma treatment could be technically challenging. To obtain homogeneous plasma modification in the tube lumen, the tube would require to be completely straight. To apply plasma treatment to a hydrogel material, the scaffold would need to be dehydrated. However, an unconstrained dehydration of a hydrogel graft would often introduce curvature or deformation, which would not lead to a completely straight tube as required, depending on the wall thickness distribution along the graft and constraints applied to the graft during dehydration. Moreover, the stability of endothelial cell adhesion on plasma treated PVA hydrogel vascular grafts has not yet been reported and needs to be considered prior to performing *in vivo* work.

In this study, we demonstrated that luminal plasma treatment of PVA hydrogel grafts internal surface can be performed. We hypothesized that using the luminal RFGD plasma treatment previously reported (Mantovani et al., 1999), we would functionalize the inner surface of small diameter PVA vascular grafts (4 mm inner diameter when hydrated, and ∼3 mm inner diameter when dehydrated for plasma treatment). Moreover, it was hypothesized that the surface modification would be stable, and the surface would facilitate longer term maintenance of an endothelial cell layer without increasing platelet activation. Having stable grafted functional groups on the material surface is beneficial to achieve working off-the-shelf vascular grafts. To support clinical translatability, grafts were stored in an ambient storage condition until they were used for experiments.

MATERIALS AND METHODS

PVA Graft Fabrication

PVA crosslinking was prepared as previously published (Chaouat et al., 2008). In brief, 10% (w/v) PVA (Aldrich, USA, Mw 85,000-124,000, hydrolysis percentage 87–89%) was mixed with 15% (w/v) sodium trimetaphosphate (STMP) (Aldrich, USA) for 5–10 min until a homogeneous solution was obtained. 30% (w/v) NaOH (Sigma-Aldrich, USA) was then added into a stirring solution and the solution was mixed for an additional 5–10 min. The solution was then centrifuged to remove any bubbles.

For an unpatterned PVA tube graft, a cylindrical rod coated with crosslinking PDMS (base: crosslinker = 10:1) (Dow Corning, USA, Sylgard 184), which was cured at 60°C. The PDMS coated rod was air plasma treated (85 W, 0.8 NL/h) for 80 s and was coated with 12 layers of crosslinking PVA solution (thickness 0.95 ± 0.17 mm). The PVA coated cylindrical rod was then kept in a cabinet at a controlled temperature of 20°C and controlled humidity of 70% for 3 days. Afterwards, the PVA coated cylindrical mold was rehydrated in 10× phosphate buffered saline (PBS) (Fisher Scientific, USA) followed by 1× PBS and deionized water. The PVA grafts were subsequently demolded from the cylindrical rod.

For a PVA graft with microtopography, a thin layer of micropatterned PDMS was made by spin coating 2 g of crosslinking PDMS (base: crosslinker = 5:1) on a patterned PDMS mold at 1,500 rpm for 15 s. The thin PDMS layer was rolled around the cylindrical rod and was air plasma treated as aforementioned. The rod was kept in crosslinking PVA solution and was sonicated for 90 min at 49 kHz. The cylindrical rod was then coated with layers of crosslinking PVA and it was kept in a cabinet as before. The rehydration of the PVA patterned tubes was done in 10× PBS followed by 1× PBS and deionized water. Patterned PVA grafts were subsequently demolded from the mold.

PVA Film Fabrication

PVA crosslinking was prepared as previously described. The solution was then centrifuged to remove any bubbles and was poured into dishes. The dishes were kept in a cabinet with controlled temperature and humidity of 20°C and 70%, respectively, until the film was dried. The PVA film was then rehydrated in deionized water and demolded from the dishes.

To make a PVA film with microtopography, the crosslinking solution was poured on a dish with PDMS patterned mold. The dish was centrifuged at 600 rpm for 1.5 h and was then kept in a cabinet with controlled temperature and humidity as before until the PVA film was fully dried. The rehydration of patterned PVA film was done in 10× PBS followed by 1× PBS and deionized water.

Scanning Electron Microscopy

PVA was dehydrated and coated with gold. Scanning electron microscope images were taken with a high-resolution field-emission scanning electron microscope (Zeiss 1550, Carl Zeiss AG, Oberkochen, Germany) at accelerated voltage of 7 keV.

Luminal NH_3 Plasma Treatment

Luminal NH_3 plasma treatment with the RFGD system was performed as previously described (Mantovani et al., 1999), and the setup is shown in **Figure 1**. Thin and straight cylindrical needles with diameter at least 1.25 mm smaller than the cylindrical molds used for PVA fabrication were inserted into hydrated PVA grafts' lumen. The whole assembly was then kept in a cabinet at a controlled temperature of 20°C and controlled humidity of 70% for slow dehydration; this step is crucial as it preserves the grafts' surface topography and maintains the graft ends to remain open and the graft body to remain completely straight during dehydration process. The dehydrated PVA graft (5.5–11 cm long, ∼3 mm inner diameter) was then detached from the cylindrical needle and was inserted into a cylindrical Pyrex glass tube for luminal plasma treatment. Three capacitively coupled copper electrodes were located at the middle section of the tube for plasma generation. After pressure of $<5 \times 10^{-5}$ Torr was reached, high purity NH_3 gas was introduced into the chamber from the inlet which was 5 cm below the upper end of the tube. The NH_3 plasma ignition was initiated by a radio-frequency generator (13.56 MHz) at a power of 65 W for 45 s, and thereby modified the luminal surface of the PVA graft. To plasma treat PVA films, the hydrated films were cut into 15.6 mm diameter circles (size of wells in a 24-well plate) and dried curve on a microcentrifuge tube wall. The dried PVA films were then assembled into a 4 mm diameter straw using small pieces of double-sided tape for plasma treatment. The plasma treated samples were stored in 15 ml polypropylene centrifuge tubes (VWR, China) and were kept on a lab bench until they were used for experiments.

X-ray Photoelectron Spectroscopy (XPS) Measurement

The chemical composition of the surface was investigated by an XPS PHI 5600-ci spectrometer (Physical Electronics, Eden Prairie, MN). The main XPS chamber was maintained at a base pressure of $<8 \times 10^{-9}$ Torr. An achromatic aluminum X-ray source (1486.6 eV) was used at 300 W with a neutralizer to record the survey spectra, and a standard magnesium X-ray source (1253.6 eV) was used to record high resolution spectra of C1s and day 77 N1s, without charge neutralization. The detection angle was set at 45° with respect to the normal of the surface and the analyzed area was 0.125 mm^2. Measurements were done at equidistant positions along dehydrated PVA grafts. High resolution N1s spectra were generated with monochromated Al Kα 1486.6 eV, Thermo VG Scientific ESCALab 250 microprobe (WATLab, Waterloo) with charge compensation. The analytical chamber pressure was maintained at 2×10^{-9} mbar during measurement. The resulting high resolution N1s spectra were calibrated by 2.2 eV according to C1s spectra correction.

Fourier-Transform Infrared Spectroscopy (FTIR)

FTIR was performed using Bruker Tensor 27 equipped with liquid nitrogen cooled mercury cadmium telluride (MCT) detector. Measurement was obtained with attenuated total

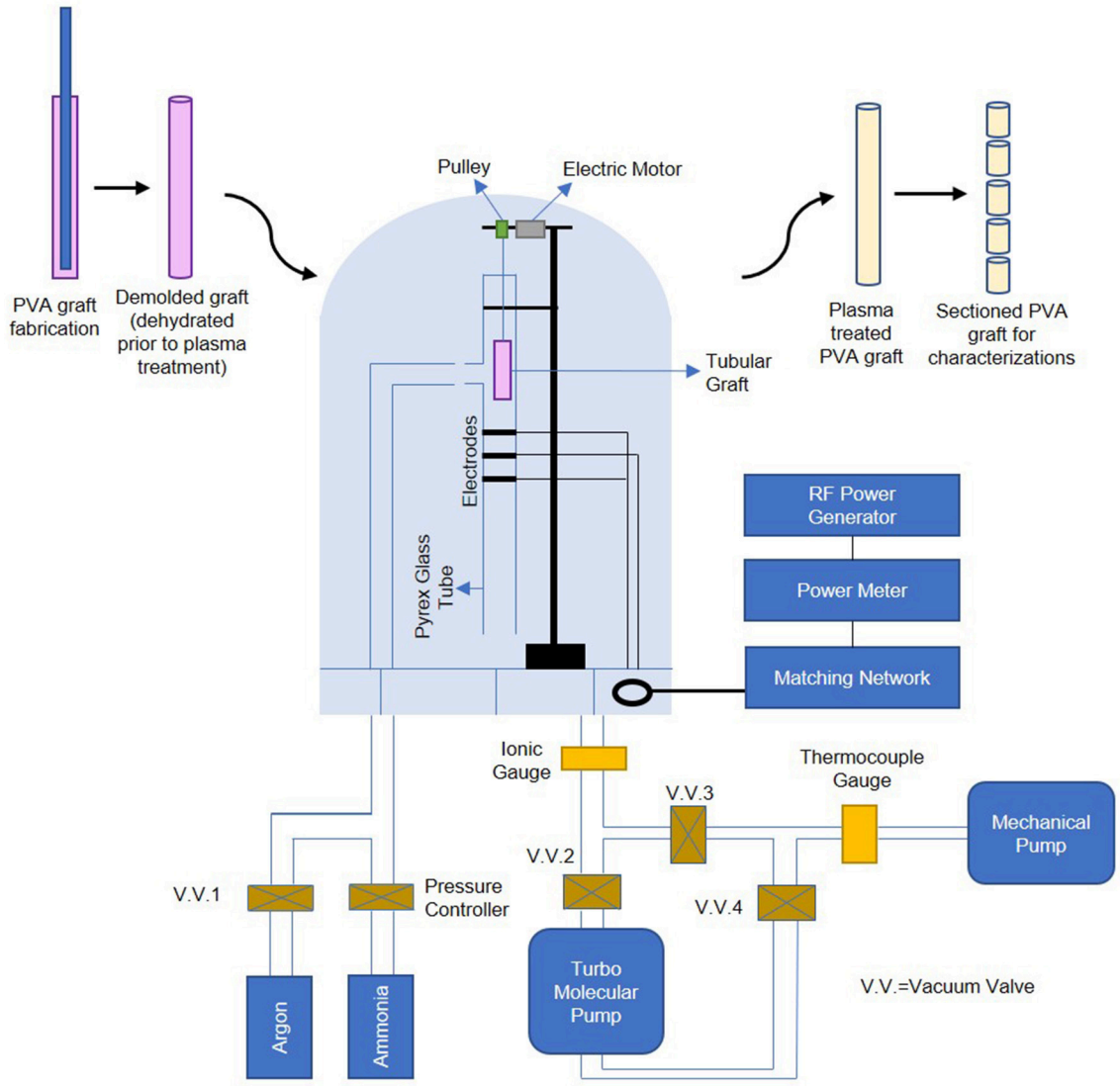

FIGURE 1 | Schematic of PVA graft plasma treatment process, plasma treatment setup is adapted by permission from Springer Nature Customer Service Center GmbH: Springer, PLASMAS AND POLYMERS, Ammonia RF-Plasma Treatment of Tubular ePTFE Vascular Prostheses, Mantovani et al. (1999).

reflection (ATR) mode with wavenumber ranges from 400 to 3,900 cm^{-1}. Sixty-four scans were acquired at a spectral resolution of 4 cm^{-1}. The depth of analysis was estimated to be 1 μm.

Water Contact Angle Measurement

Unpatterned (UP) PVA and two other topographies (2 μm linewidth × 2 μm height × 2 μm spacing gratings (2 μG) and 1.8 μm diameter × 2 μm pitch concave lenses (CCL) tubes were used in the contact angle measurement. Plasma treated films were indicated with a letter P behind the abbreviation, i.e., UPP, 2 μGP, CCLP for plasma treated unpatterned, microgratings, and concave microlenses grafts, respectively. Water contact angle was measured on PVA films using an in-house built instrument. Films were hydrated during the test, and its surface was dabbed dry prior to test. The water volume used for measurement was 3 μl and images were captured within 10 s after the water drop was on the film surface. Three samples were measured for each experimental groups and each samples were measured once.

Cell Adhesion Study

PVA grafts were cut longitudinally on one side and were exposed to UV for 20 min. Then, samples were incubated with 10% Penicillin/Streptomycin (Gibco, USA) and 1% Amphotericin-B (VWR, USA). PVA samples were then placed in 24-well plate wells with autoclaved silastic tubings (Dow Corning, USA, 0.375 inch inner diameter), yielding a seeding area of 0.7 cm^2. Samples were rinsed thoroughly with 1× PBS. Afterwards, PVA samples were incubated with fetal bovine serum (FBS) (Gibco, USA) and

were centrifuged at 1,000 rpm for 30 min. PVA was kept in 2–8°C fridge overnight or in 37°C incubator for 30 min prior to cell seeding.

EA.hy926 (ATCC, USA) and primary HUVEC (Lonza, USA) cells used at passage number 7 were cultured according to ATCC and Lonza protocols, respectively. Confluent cells were passaged with 0.05% Trypsin/EDTA (Gibco, USA) and were seeded on the PVA at a seeding density of 50,000 cells/well. The endothelial cells were seeded onto films that were stored for at least 3–30 days before cell culture. The well plate was then spun down at 100 × g for 10 min to bring the cells down closer to the PVA substrate. Cell media change was performed daily, and cells were cultured for 2, 9, 12, 14, and 30 days for EA.hy926 and for 16 days (until cell monolayer was formed) for primary HUVEC before performing subsequent cell immunofluorescence staining.

Cell Immunofluorescence Staining and Cell Number Quantification

Culture was washed with 1× DPBS buffer with calcium (Gibco) prior to fixation with 4% paraformaldehyde (PFA) (Sigma Aldrich, USA) for 15 min. The fixed samples (both cell types) were then permeabilized by incubation with 0.05% Triton X-100 (Sigma, USA) and 50 nM glycine (Aldrich, USA) for 15–20 min. Cell nuclei and F-actin staining was done with DAPI (1:5,000) and Phalloidin (1:500) (Invitrogen, USA) incubation for 30 min, respectively. The samples were imaged using Zeiss immunofluorescence microscope at 10× and 20× magnification. Brightness and contrast adjustments were performed using ImageJ version 1.50i, Java 1.8.0 (developed by Wayne Rasband). Cell number quantification was performed through manual counting of the cell number from 4 to 12 images with 20× magnification, or 3–9 images with 10× magnification of different areas on the PVA surface. The cell number was then normalized to images area to give cell density values (cells/cm^2).

Stability Study of Plasma Treated PVA Surfaces

The assessment of treatment stability was done by performing XPS measurements (high and low resolution) on day 0, day 30, and day 77, water contact angle measurements on day 7, day 23, and day 60, and a cell adhesion study for a 30-day period. The stability studies with XPS and the cell adhesion study were performed on UPP PVA grafts (plasma treated), while the contact angle measurements for stability study were done on UPP PVA films (plasma treated). Cell adhesion studies were terminated for immunofluorescence staining with DAPI and phalloidin on day 2, 9, 12, 14, and 30 of culture.

Platelet and Fibrin Accumulation Study With *ex vivo* Baboon Shunt Model

All baboons (*Papio anubis*) were housed and taken care of by Oregon National Primate Research Center (ONPRC) staff according to the "Guide to the Care and Use of Laboratory Animals." Studies were approved by ONPRC Institutional Animal Care and Use Committee (IP00000300).

The *ex vivo* shunt study was achieved as previously described (Anderson et al., 2014). Prior to experiments, baboon platelets were labeled with 111-Indium and homologous fibrinogen was labeled with 125-Iodine. The baboon femoral artery and vein were accessed and extended with silicon tubing, to which the PVA graft was attached for 60 min without anticoagulant or anti-platelet administration. The platelet accumulation was measured by gamma camera at increments of 5 min. The graft was then flushed, and fibrinogen quantification occurred after a complete decay of the 111-Indium. Data were obtained from four different animals.

Statistical Analysis

Data are presented as mean ± standard error, except for *ex vivo* shunt data, where data are presented as mean ± standard deviation. Throughout significance is defined as $p < 0.05$. In figures, * denotes statistical significance with p-value of ≤ 0.05, ** p-value ≤ 0.01, *** p-value ≤ 0.001, and **** p-value ≤ 0.0001. Number of replicates is reported in individual figure legends.

Statistical comparisons between experimental groups for surface nitrogen content, water contact angle, surface composition, and cell adhesion were completed using GraphPad Prism 6. Differences in XPS element percentages and high resolution C1s peak percentages were computed using one-way ANOVAs and Sidak analyses with 95% confidence interval, whereas differences in O/C and N/C were computed with two-sided and one-sided unpaired t-test, respectively. Differences in %N along graft surfaces to analyze surface homogeneity were computed with two-way ANOVA and Tukey's *post-hoc* analysis with 95% confidence interval. Further, differences in water contact angle and HUVEC cell number quantification were computed with one-way ANOVA and Tukey's *post-hoc* analysis with 95% confidence interval. Additionally, differences in EA.hy926 cell number on day 12 were computed with unpaired t-test (two-sided) and 95% confidence interval.

Statistical comparisons of platelet and fibrin accumulation on PVA samples in *ex vivo* shunts were calculated using R (R foundation for statistical computing, version 3.5.2) packages nlme (version 3.1–137) and multcomp (version 1.4-8). While ePTFE and collagen-coated ePTFE controls are displayed as a reference in figures, only PVA samples ($N = 6$–7 for each surface modification) were included in statistical models. Platelet and fibrin data were natural-log transformed prior to analysis in order to more closely approximate normal distributions. Transformed real-time platelet adhesion data were analyzed with a multi-way repeated measures ANOVA with factors of time, patterning, and plasma treatment over the entire 60 min time course. Transformed endpoint fibrin data were analyzed with a two-way ANOVA against patterning and plasma treatment. Patterning levels were unpatterned, gratings, and concave. Plasma levels were no plasma, fresh plasma treatment (tested 7–11 days post-treatment), and aged plasma treatment (tested 44–60 days post-treatment). Statistically significant main effects were analyzed with a Tukey's *post-hoc* as appropriate.

RESULTS

Surface Characterization of Plasma-Treated PVA Luminal Surface

The atomic percentages of C, O, and N on untreated and NH_3 plasma treated PVA grafts were shown in **Figure 2A**. The plasma surface modification inducted by NH_3 of the luminal surface of PVA successfully resulted in a significant increase in the nitrogen percentage ($p \leq 0.001$, $N = 3$ grafts for both untreated and plasma treated groups), as measured with XPS. The atomic percentages of C, O, and N on untreated PVA surfaces were 68.9 ± 1.8, 29.2 ± 1.9, and 0.0 ± 0.0%, respectively, while the atomic percentages of C, O, and N after plasma treatment were 56.3 ± 3.5, 27.9 ± 4.1, and 9.5 ± 2.5%, respectively. The significant increase in nitrogen was also shown in the N/C ratio which was calculated from the survey XPS, while there remained no significant change in O/C after plasma treatment (**Figure 2B**). The homogeneity of surface modification was further characterized by measuring the nitrogen percentages of the plasma treated PVA surface at 11 equidistant positions along the 5.5 cm long graft. There were no statistical differences found between the nitrogen percentages along the treated grafts ($N = 3$) (**Figure 2C**). The nitrogen percentage values averaged at 9.4%, while on the PVA luminal surface without plasma treatment, there was no nitrogen element detected ($N = 3$). This increase in nitrogen percentage was statistically significant with $p \leq 0.01$ compares to the untreated control. A longer (11 cm) PVA graft was also successfully plasma treated with this technique and the nitrogen atomic percentage from the graft end to 6.4 cm away from the end was shown in **Supplementary Figure 1**. In order to identify the surface functional group before and after the treatment more specifically, high-resolution XPS measurements of C1s and N1s were performed. Compared to the untreated PVA surface, the plasma treated PVA demonstrated an increase in carbonyl functional group (C=O) percentage, whereas the C-O/C-N functional group percentage was lower (**Figures 2D,E**). The overall C-C/ C-H bond percentage was also reduced due to the increase in other bond percentages. The peak percentages of the high resolution C1s spectra were calculated before and after the plasma treatment and this decrease in C-C/C-H peak was found to be statistically significant ($p \leq 0.05$, $N = 2$ grafts for both groups) as shown in **Figure 2F**. The high-resolution spectra of N1s (measured on day 16 post-plasma treatment) showed the presence of nitrogen species at 400.2 eV on the graft inner surface compared to the untreated control (**Figures 2G,H**).

To confirm the change in the surface functional group after the treatment, FTIR spectra were obtained from both treated (day 24 post-plasma treatment) and untreated PVA grafts. On the plasma treated PVA graft surface, we observed a C=O peak at wavelength 1,737 cm^{-1} which was not observed on the untreated PVA spectra (**Figure 3**). All other peaks remain the same before and after the treatment.

Changes in PVA Surface Wettability Before and After Plasma Treatment

Surface wettability can affect protein adsorption and subsequent cell attachment on a biomaterial surface; therefore, the water contact angles of the plasma treated PVA films were measured. As previous study showed the effectiveness of microgratings and concave microlenses topography in promoting improved cell attachment and alignment on the PVA surface (Cutiongco et al., 2016a), three topographies were studied: unpatterned (UP) surface (**Figure 4A**), 2 μm gratings (2 μG) topography (**Figure 4B**), and 1.8 μm concave lenses (CCL) topography (**Figure 4C**). The surfaces were characterized with SEM and were found to be in good fidelity. It was shown that the surface hydrophilicity on the plasma treated PVA surfaces was reduced. The decrease in hydrophilicity was observed on both UPP ($p \leq 0.05$ against UP control, $N = 3$) and CCLP surfaces (no significance against CCL control, $N = 3$) (**Figure 5A**). The average water contact angle of the 2 μGP topography was, however, slightly decreased after the plasma treatment and possessed a larger standard deviation compared to the 2 μG PVA. The images of water droplets on plasma treated surfaces are shown in **Figures 5B–D**.

The stability of the plasma treated surface after storage in ambient conditions was first investigated with water contact angle measurement of the UPP PVA. Water contact angle measurements were taken on day 7, 23 and 60 on plasma treated PVA films. The water contact angle was found to be lower on day 23 (33.3 ± 6.8°, $N = 3$ films) and higher on day 60 (61.6 ± 21.5°, $N = 3$ films) compared to day 7 measurements (47.4 ± 19.8°, $N = 3$ films). However, these differences were not found to be statistically significant (**Figure 5E**).

Characterization of Grafted Functional Groups up to 77 Days After Plasma Treatment

The stability study of the surface modification of samples stored in ambient conditions (25°C temperature and 60% average humidity) was examined on both plasma treated and untreated PVA surfaces. Day 0 denotes that the measurement was taken right after plasma treatment was performed. XPS measurements were taken right after graft plasma treatment, at 1- and 2-month time points after plasma treatment. A slight drop in both %N and N/C was observed in the day 77 measurement which caused a slight increase in both %O and O/C, while %C remained at 59.7% on day 30 and 59.5% on day 77 (**Figures 6A–E**). Using the curve-fit peak areas, the peak percentages of peaks at 285, 286.5, and 288.5 eV of the total C1s spectra were also measured at the three time points. The peak percentages at binding energy 285, 286.5, and 288.5 eV on day 0 were 30.79 ± 4.00%, 19.16 ± 4.40%, and 5.01 ± 1.35% ($N = 2$ grafts), respectively, while the peak percentages on day 30 were 32.85, 20.01, and 6.89% ($N = 1$ graft) as shown in **Figures 6F,G**. Additionally, the peak percentages on day 77 were 34.60, 19.95, and 4.96% ($N = 1$ graft) as shown in **Figure 6H**. While the peak percentage at 285 eV showed a slight increase on both day 30 and 77 measurements, the peak percentages at both 286.5 and 288.5 eV remained close to the day 0 measurements. Further, the high resolution N1s spectra showed the presence of nitrogen species on day 16, 31, and 77 (**Figure 6I**).

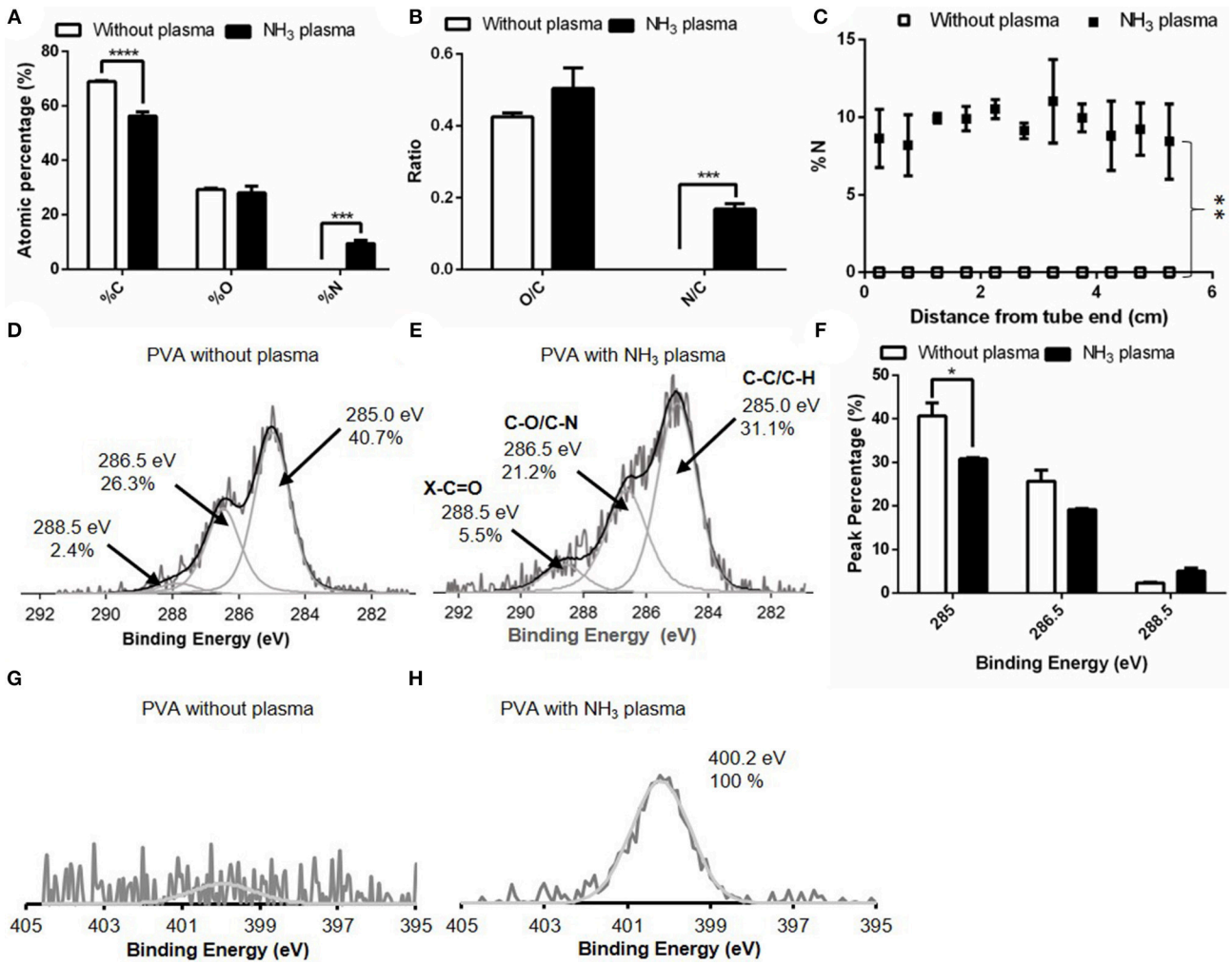

FIGURE 2 | Comparison of surface elements without and with NH_3 plasma as measured with X-ray photoelectron spectroscopy (XPS). **(A)** XPS survey for %C, %O, and %N of PVA luminal surface and **(B)** O/C and N/C ratio calculated from **(A)**. **(C)** %N as measured at 11 equidistant positions along the 5.5 cm-long grafts. $N = 3$ grafts for experimental groups in **(A–C)**. High resolution C1s spectra on PVA grafts **(D)** without plasma and **(E)** with NH_3 plasma. **(F)** Comparison of peak percentage of the C1s spectra at binding energy 285, 286.5, and 288.5 eV before and after plasma treatment. $N = 2$ grafts for both experimental groups. High resolution N1s spectra on PVA grafts **(G)** without plasma and **(H)** with NH_3 plasma. * denotes statistical significance with $p \leq 0.05$, $^{**}p \leq 0.01$, $^{***}p \leq 0.001$, and $^{****}p \leq 0.0001$.

In vitro Endothelial Cells Attachment and Cell Layer Maintenance Up to 30 Days of Culture

To assess the effectiveness of luminal NH_3 plasma treated PVA grafts in facilitating *in vitro* cell adhesion, cell adhesion studies were performed using endothelial EA.hy926 and primary HUVEC cells on 7- and 3-day old plasma treated samples, respectively, both UP and patterned surfaces with 2 μG and CCL topographies. The EA.hy926 and HUVEC cultures were maintained for 30 and 16 days, respectively, before fixing and staining (**Figures 7A,B**). Improved EA.hy926 cell attachment was observed on the plasma treated surfaces, mainly on patterned surfaces (**Figures 7A,D**, and **Supplementary Table 2**). The EA.hy926 did not show much difference in cell morphology on samples with and without plasma treatment and cells were more elongated on the 2 μG and 2 μGP topography. In contrast, HUVEC attachment improved in all the plasma treated samples, especially on the 2 μGP sample where endothelial monolayer was formed. On the plasma treated samples, HUVECs have a better cell spreading compared to the untreated controls where cells were observed to be in clumps. HUVEC cell alignment was clearly observed on the 2 μGP sample. Furthermore, EA.hy926 cells were fixed and imaged on day 2, 9, 12, 14, and 30 of culture (**Figure 7C**). The endothelial culture on the plasma treated surfaces showed improved cell attachment compared to the untreated control on day 2, 9, 12, and 14. On day 14 of culture, endothelial cells reached 90% confluency and the cell attachment was maintained up to day 30. The corresponding cell number quantification can be found in **Figure 7D** and **Supplementary Table 2**. However, there was no statistical difference between the experimental groups.

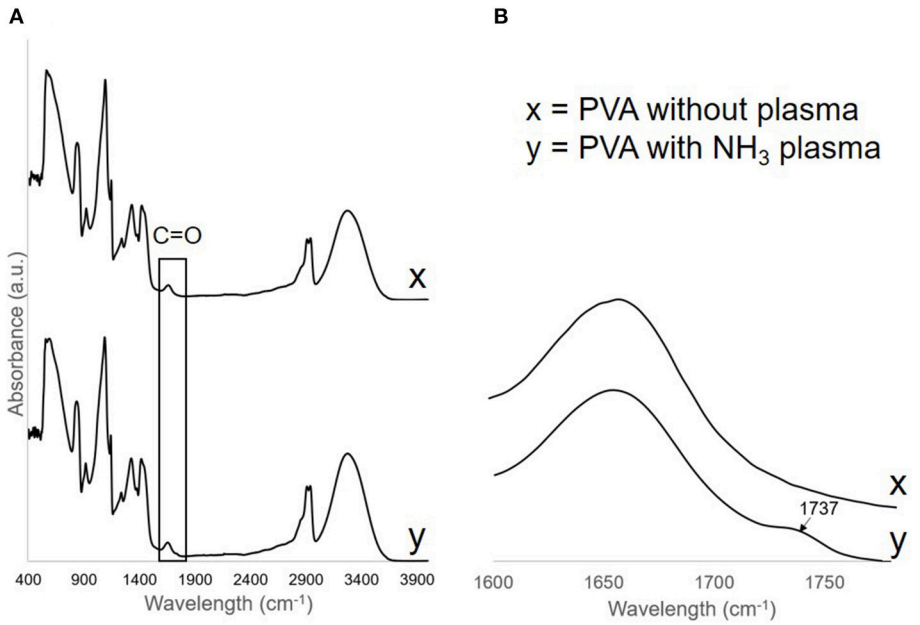

FIGURE 3 | (A) FTIR spectra of PVA without plasma, x, and PVA with NH_3 plasma, y. C=O peak was found on the PVA surface after plasma treatment and was shown more clearly in **(B)**.

Platelet and Fibrin Accumulation as Studied With *ex vivo* Baboon Shunt Models

The platelet accumulation on both plasma treated and untreated PVA grafts was measured every 5 min over 1-h duration of study (**Figure 8A**). Eight different types of vascular grafts were tested: UP, UPP, 2 μG, 2 μGP, CCL, and CCLP PVA grafts, ePTFE grafts (untreated), and collagen coated ePTFE grafts (untreated). The highest platelet accumulation was observed on the collagen coated ePTFE which served as the positive control, whereas UP and UPP, 2 μG, and CCL PVA grafts demonstrated low platelet activation.

Untransformed shunt data are shown in **Figure 8** for better biological interpretation, but statistics were performed on log-transformed data as described in the methods section. A multi-way repeated measures ANOVA found significant effects of both plasma treatment ($p = 0.004$) and material patterning ($p = 0.011$) on platelet attachment. Concave microlens patterning significantly increased platelet accumulation from unpatterned samples ($p = 0.004$), while microgratings patterning did not significantly alter platelet attachment. Fresh plasma treatments (day 7–11 samples) showed a significant increase in platelet attachment compared to no plasma treatment ($p = 0.006$); however, this was not reflected when the plasma treatment was aged (day 44–60 samples, $p = 0.195$). The change in platelet accumulation between fresh and aged plasma is shown in **Supplementary Figure 2**.

Plasma modification did not significantly alter fibrin accumulation in the two-way ANOVA ($p = 0.386$), but patterning was a significant factor ($p = 0.033$). In the *post-hoc,* concave patterning showed a significant increase in fibrin accumulation (**Figure 8B**, $p = 0.034$) compared to unpatterned samples similar to the platelet data; however, microgratings did not differ significantly from unpatterned samples ($p = 0.22$).

DISCUSSION

The challenge of plasma treating a small diameter tube structure is in achieving a sufficient amount of plasma to go through the small lumen in order to interact with the inner tube surface since plasma particles quench as they collide with the tube wall (Cao et al., 2007). A slight constriction or deformation of the tubular wall will result in plasma not being able to enter and modify the tubular structure. In this regard, care was taken when dehydrating PVA grafts prior to plasma treatment to ensure that the grafts were completely straight. A few studies have revealed that luminal plasma treatment can be accomplished (Hatada et al., 1982; Matsuzawa and Yasuda, 1984; Lin and Cooper, 1995; Kaibara et al., 2000; Cao et al., 2007; Qiu et al., 2017), and at least two studies performed the treatment for a small diameter polyethylene tubes (1–3 mm inner diameter and 46.5–60 cm long) by utilizing electrode movement outside the plasma reactor (Lin and Cooper, 1995; Cao et al., 2007). Nevertheless, none of these studies used hydrogel-based material, while hydrogel is known to have suitable mechanical properties for tissue engineering applications (Drury and Mooney, 2003; Yates et al., 2007; Abidian et al., 2012; Arslantunali et al., 2014; Cutiongco et al., 2016b). PVA hydrogel lacks surface functional groups to mediate endothelialization, while the patency rate of the currently available small diameter vascular graft (inner diameter < 6 mm) is low due to early thrombogenesis in the absence of an endothelial cell lining on the graft surface (Tordoir et al., 1995; Kirkwood et al., 2011). Therefore, this study compared the

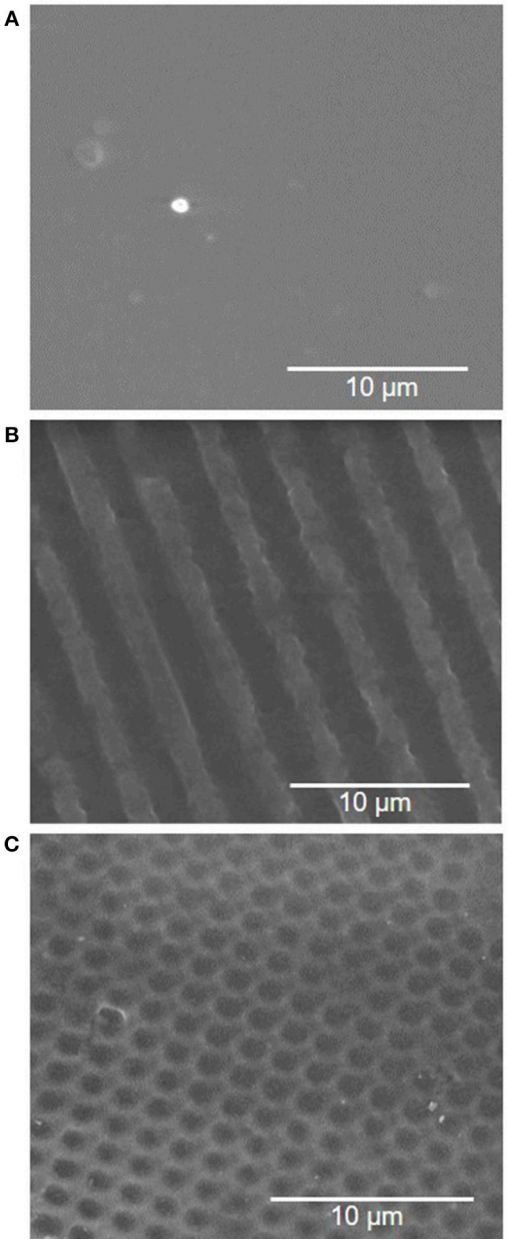

FIGURE 4 | Scanning electron microscopy (SEM) images of PVA luminal surface with **(A)** no pattern, **(B)** 2 μm gratings, and **(C)** 1.8 μm concave lenses topography.

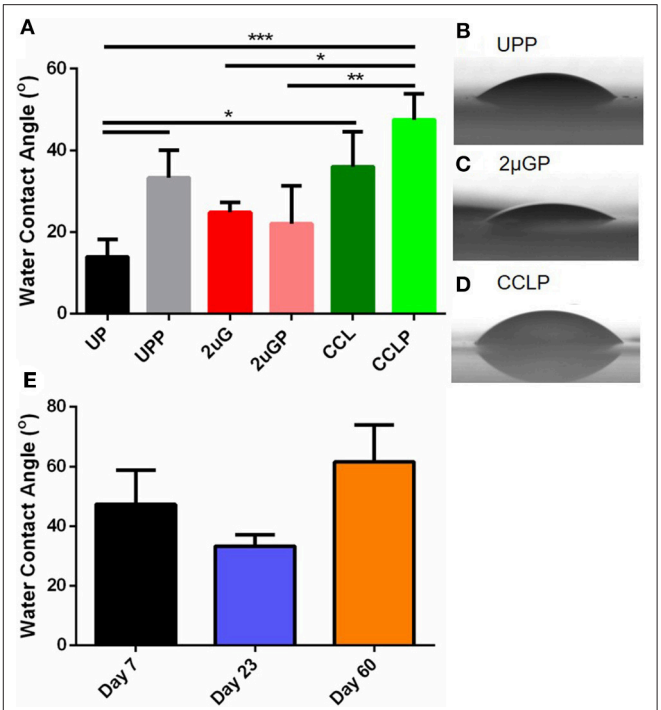

FIGURE 5 | (A) Comparison of water contact angle measurement before and after NH_3 plasma treatment on unpatterned (UP), 2 μm gratings (2 μG), and 1.8 μm concave microlenses (CCL) PVA films. Suffix *P* indicates plasma treated samples (e.g., UPP, unpatterned and plasma treated PVA). Representative images of the water droplets on plasma treated PVA surfaces were shown for **(B)** unpatterned **(C)** 2 μm gratings, and **(D)** 1.8 μm concave microlenses samples. **(E)** Water contact angle of plasma treated unpatterned PVA measured on day 7, day 23, and day 60 post-plasma treatment. $N = 3$ for all experimental groups in **(A,E)**. *Denotes statistical significance with $p \leq 0.05$, **$p \leq 0.01$, ***$p \leq 0.001$.

effects of the surface functionalization through luminal plasma treatment of small diameter PVA grafts to untreated PVA grafts and assessed the stability of the plasma treated surface.

The significant increase in atomic percentage of N as detected by the survey XPS was an indication of successful luminal plasma treatment of 3 mm dehydrated PVA grafts. In addition, the surface modification was homogeneous along 5.5 cm long grafts as there were no significant differences found between the measured *N* percentage values along the grafts, which is notable given that the grafts were made of hydrogel material. XPS results showed a significant increase in N/C ($p \leq 0.0001$) between untreated and NH_3 plasma treated samples. Further, an increase in carbonyl groups was also detected with the high resolution XPS of C1s, which could be coming from amide, ester, or carboxylic acid groups on the PVA surface. The increased ratio between C-O/C-N peak and C-C/C-H peak after the treatment could mean that amine functional groups could also be grafted on the PVA surface. However, as the nitrogen species peak binding energies are close to one another, these peaks overlap, and the differentiation of the nitrogen species cannot be easily done with XPS.

Since the grafts were stored in ambient conditions with air humidity of 50–70%, water vapor in the surrounding air can easily react with the nitrogen species such as amine to produce alkyl ammonium ion group and changing the surface composition of the treated PVA grafts. Nevertheless, on day 77, the nitrogen species was still present on the grafts as detected with XPS. Moreover, the peak percentages at 286.5 and 288.5 eV on day 30 and 77 measurements remained at similar level to day 0 measurement which indicated that the change if surface functional groups during storage, if any, was not remarkable.

While XPS could measure up to ∼5 nm depth, FTIR could analyze up to 1 μm depth. Consistent to the XPS measurement,

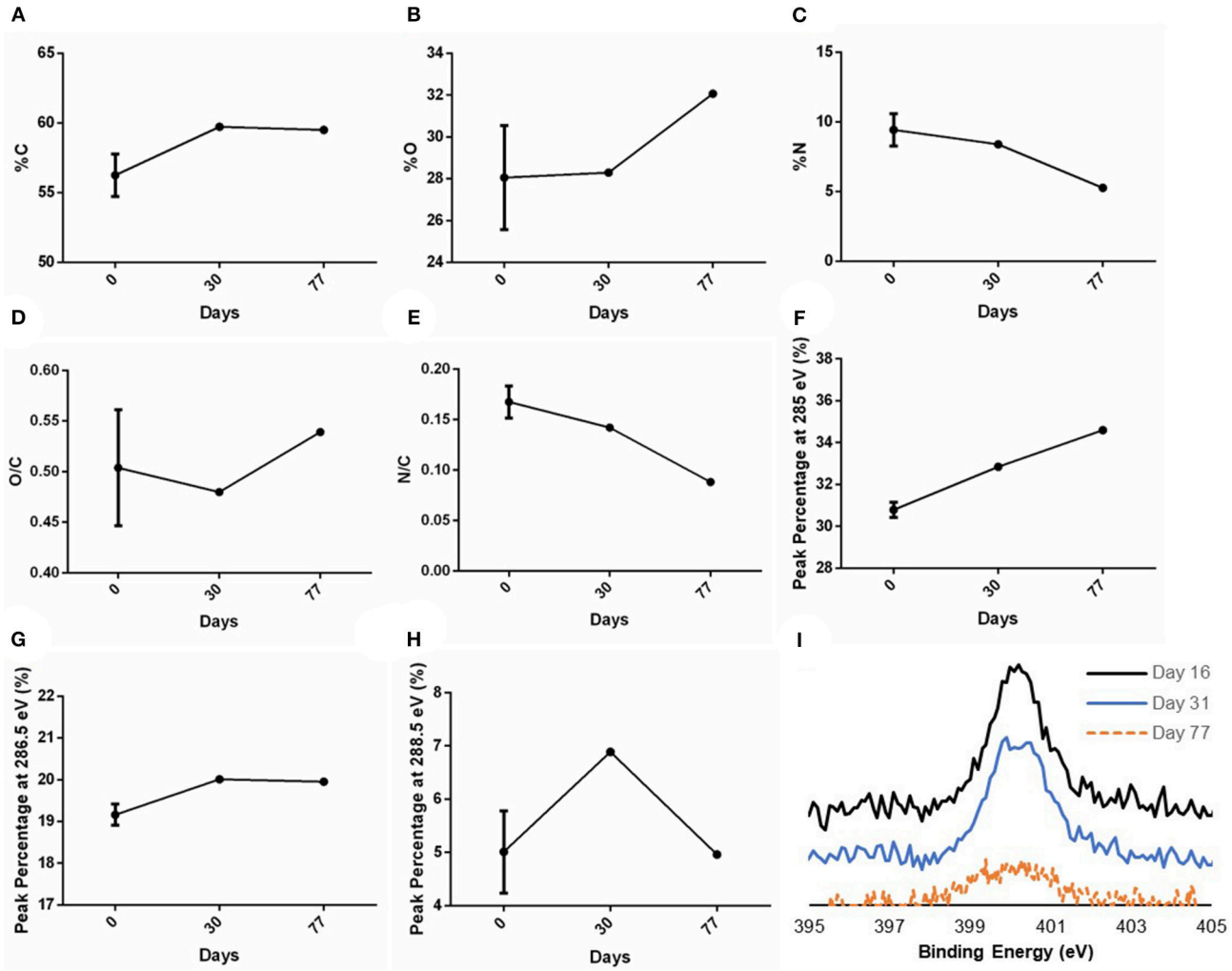

FIGURE 6 | XPS measurements of C, O, and N after graft storage in ambient conditions. XPS survey of PVA grafts performed on day 0 (right after plasma treatment), day 30 and 77 post-plasma treatment for **(A)** %C, **(B)** %O, **(C)** %N, and the calculated ratio of **(D)** O/C and **(E)** N/C based on the XPS survey. The peak percentage of the peaks at binding energy **(F)** 285 eV, **(G)** 286.5 eV, and **(H)** 288.5 eV of the high resolution C1s spectra were also measured on day 0, 30, and 77. In **(A–E)**, $N = 3$ grafts, 1 graft, and 1 graft for day 0, 30, and 77 measurements, respectively. In **(F–H)**, $N = 2$ grafts, 1 graft, and 1 graft for day 0, 30, and 77 measurements, respectively. Multiple points were measured in each sample; refer to **Supplementary Table 1** for the data for each sample. **(I)** High resolution N1s spectra measured on day 16, 31, and 77 post-plasma treatment.

a weak carbonyl (C=O) peak was found on the FTIR absorbance spectra measured on day 24 post-plasma treatment of PVA grafts, but not on the untreated grafts. However, since amide peak was not observed on the spectra, the carbonyl peak on the spectra could be mainly detected from ester or carboxylic acid groups which may be more dominant throughout the 1 μm depth of FTIR analysis. Also, the weak peak could mean that the functional groups were present mainly at the graft surface. At the depth of FTIR analysis, the plasma treatment did not seem to change the main chemical structure of the PVA hydrogel as all other absorbance peaks were present on the plasma treated PVA grafts spectra as they were on the untreated PVA grafts spectra.

Compared to microwave (MW) plasma, radio frequency (RF) plasma has an advantage of having a more controlled ion bombardment on the surface (Klemberg-Sapieha et al., 1991), and is therefore a more suitable technique for plasma treating a tube structure despite possessing a lower electron density compared to MW plasma (Moisan and Wertheimer, 1993). In this study, we observed that the N/C ratio immediately after RF NH_3 plasma treatment was significantly higher ($p \leq 0.05$) compared to the microwave N_2/H_2 plasma treatment on the flat PVA surfaces previously reported (Ino et al., 2013). Thus, the RF plasma treatment reported herein has adequately grafted nitrogen functional groups on the internal surface of PVA grafts.

The water contact angle was found to be higher on both UPP and CCLP PVA, which was likely caused by the presence of a less polar, nitrogen containing functional group on the plasma treated surfaces compared to the polar hydroxyl functional

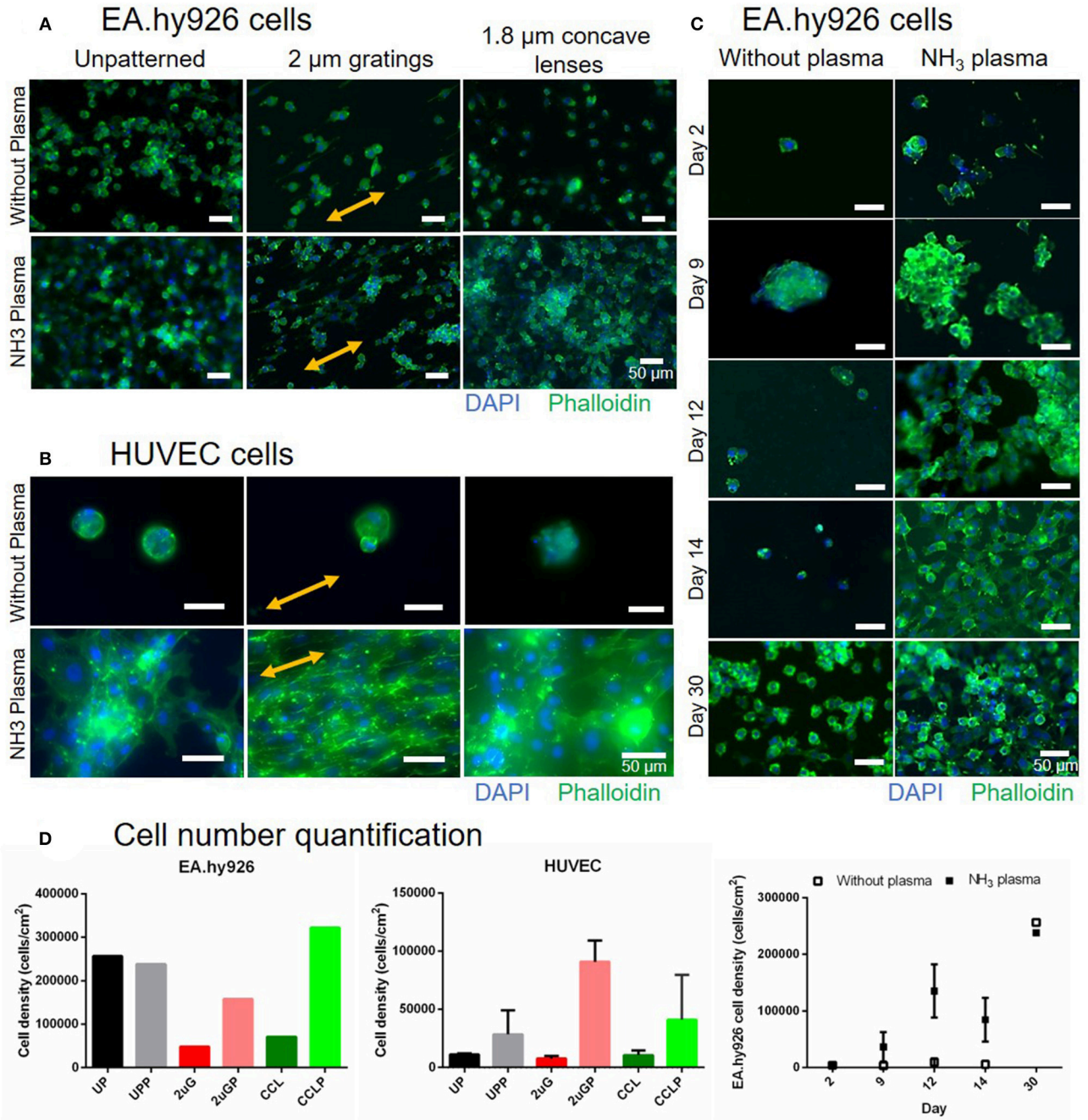

FIGURE 7 | Comparison of EA.hy926 and primary human umbilical vein endothelial cell (HUVEC) cell attachment on PVA surfaces without plasma treatment and with NH_3 plasma treatment. **(A)** Fluorescence images of EA.hy926 cells fixed on day 30 of culture and of **(B)** HUVECs fixed on day 16 of culture on unpatterned and patterned PVA. Nuclei and F-actin were stained blue and green, respectively. Double-headed arrows indicate gratings direction. **(C)** The stability of cell adhesion on the PVA surfaces with and without plasma treatment was further studied and compared on unpatterned sample up to 30 days of culture. Cells were almost confluent on day 14 on plasma treated surfaces and maintained their attachment as observed on day 30. Scale bar: 50 µm. **(D)** Cell number quantification of EA.hy926 cells (day 30, $N = 1$ for each groups), HUVECs (day 16, $N = 2$ for each groups), and stability study with EA. hy926 cells (day 2, 9, and 14, $N = 1$ and 2 for without plasma and NH_3 plasma groups, respectively; day 12, $N = 2$ and 3 for without plasma and NH_3 plasma groups, respectively; and day 30, $N = 1$ for each groups).

group. This observation agrees with Cutiongco et al. (RIE N_2 plasma on PVA) (Cutiongco et al., 2016a), but not so with Ino et al. (microwave N_2/H_2 plasma on PVA) (Ino et al., 2013), or Tusek et al. (microwave NH_3 plasma on polyamide 6 foils) (Tušek et al., 2001). As water contact angle is mostly affected by surface roughness and functional groups, the discrepancy could

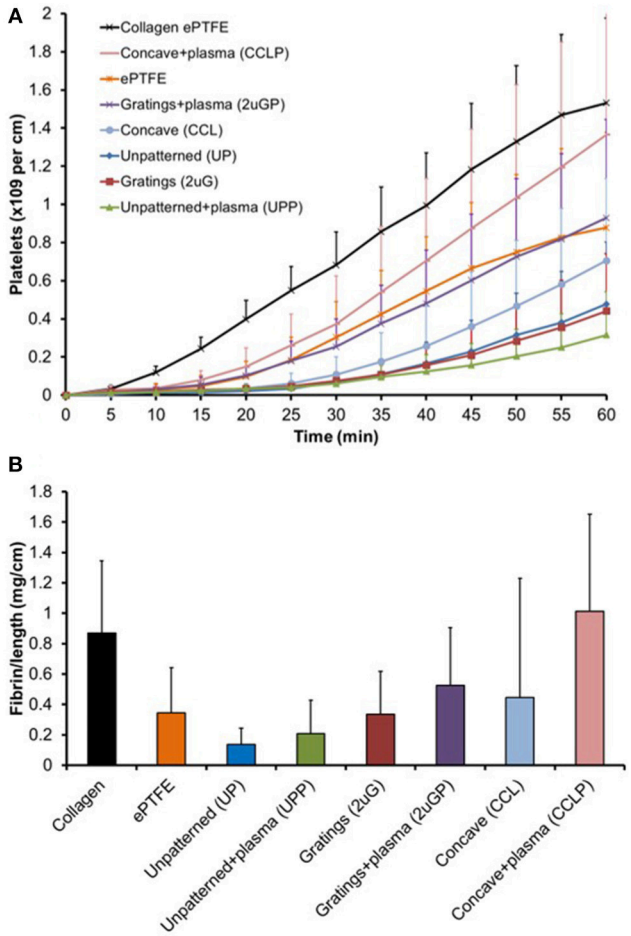

FIGURE 8 | Untransformed shunt data for biological interpretation. **(A)** Platelet accumulation on PVA graft surface after exposure to whole, flowing blood without anticoagulants in the *ex vivo* shunt model. Statistical analysis performed with repeated measures multifactor ANOVA on 5-min time point data. **(B)** Normalized fibrin accumulation amount after 60 min on PVA graft surface. Statistical analysis was performed with multi-way ANOVA with factors of time, patterning, and plasma treatment ($N = 6–7$ samples for PVA experimental groups).

be sourced from the difference in roughness of untreated PVA surfaces as well as the surface functional groups prior to the plasma treatment. In this study, the surface roughness was kept consistent by testing the contact angle of the surface that faced the PDMS mold for both UP and patterned PVA samples. We previously observed that the surfaces of PVA films that faced PDMS mold were much smoother than those that faced the air during the crosslinking process (data not shown). The average contact angle of 2 μGP PVA was slightly decreased with a larger variation in the measurements. We speculate that the plasma modification could have affected the topography sharpness which could result in a larger contact angle variation.

Cell-material interaction is facilitated by cell membrane receptors called integrins which are collectively known as focal adhesion (Kanchanawong et al., 2010). Improvement in cell adhesion on a material surface can therefore be achieved by providing ligands to the integrin which include amino and carbonyl groups on the biomaterial surface. Ammonia plasma was chosen to fulfill this role. The grafted nitrogen species on the plasma treated PVA grafts' surface, as detected by XPS and FTIR, contributed to the improved endothelial cell adhesion. In addition, because the plasma treatment caused an increase in water contact angle of the plasma treated PVA (PVA became less hydrophilic), this could create hydrophobic-hydrophobic interactions between material surface and proteins which were present in the serum during the sample serum incubation as well as in the cell media. All these factors act synergistically to result in a stable endothelial-cell lining on the plasma treated PVA surface for up to 30 days of culture. Likewise, both EA.hy926 and primary HUVEC cell attachment on patterned PVA surfaces was improved after the plasma treatment. The HUVECs on the plasma-treated PVA showed better cell-spreading compared to the untreated controls and were able to achieve monolayer formation on the 2 μGP samples. In contrast, the endothelial monolayer was unable to be formed in the case of EA.hy926 cells even after 30 days of culture. This observation agreed with a study reported before where the expression of adhesion molecule were significantly lower for the EA.hy926 cells as compared to primary HUVEC cells (Lidington et al., 1999). It was noted that the cell numbers on the day 30 untreated controls were very high compared to the untreated controls at other timepoints. Although the cause of this anomaly was still uncertain, we speculate that the highly proliferative nature of EA.hy926 cell line could contribute to the cell line survival in the absence of sufficient extracellular matrix proteins. Nevertheless, the addition of the nitrogen functional groups in the plasma treated PVA appeared to provide prolonged and more stable support of the cell adhesion on the hydrogel up to the 30-day culture period as examined in this study.

The presence of an endothelial cell lining in the graft lumen could prevent thrombosis and improve vascular graft patency. However, in *in vivo* environments, platelets' integrins may attach to the added surface functional groups and activate the platelets before an endothelial cell layer is established. Once a platelet is activated in this fashion, platelet accumulation may occur, which ultimately leads to thrombosis. In addition to platelets, fibrin is involved in the blood clot formation by forming a mesh-like structure and strengthening the clot structure. A hemocompatibility comparison was performed to characterize this phenomenon, using a well-established non-human primate model, which uses whole, flowing blood in the absence of anticoagulants (Cutiongco et al., 2015; Jurney et al., 2018). This study compared the plasma treated PVA grafts with different microtopographies, untreated PVA grafts (with and without microtopographies), and ePTFE graft controls. Studies have previously revealed that UP PVA have a relatively low platelet accumulation compared to untreated ePTFE, the gold-standard for clinical artificial material vascular grafts (Cutiongco et al., 2015; Jurney et al., 2018; Anderson et al., 2019). As measured in the shunt model, the platelet and fibrin accumulations on the CCLP PVA grafts were significantly higher than the UP PVA grafts, whereas, the 2 μGP PVA grafts did not significantly alter platelet and fibrin accumulations. This was

consistent with a previously presented lactate dehydrogenase (LDH) assay absorbance experiment that demonstrated that CCL topographies present the highest platelet activation compared to other topographies (Cutiongco et al., 2015). The CCL topography is, thus, consistently found to be a more favorable surface for platelet activation. The platelet and fibrin accumulation of the other PVA groups were lower than the collagen coated ePTFE positive control and were lower than the ePTFE clinical control grafts. A significant increase in thrombosis was also seen with fresh plasma treatments; however, aged plasma treatment did not significantly increase platelet or fibrin attachment. It is possible that the grafted nitrogen species functional groups, seen with the XPS data even at long time points, encourages platelet and cell adhesion, but the change in surface functional group composition over time during storage in ambient conditions could be reflected in the lower platelet activation on the aged plasma PVA samples (day 44–60) compared to the fresh plasma samples (day 7–11) and enhanced due to exposure of the grafts to the whole blood. Hence, in terms of hemocompatibility, the luminal NH_3 plasma treatment done between 7 and 11 days prior to graft exposure to whole blood worked well with both UPP and 2 μGP PVA, but not with CCLP PVA. The CCLP PVA had lower platelet and fibrin accumulations after the longer storage time in ambient conditions, and they were comparable to the UPP PVA. It is possible that an ideal storage range of plasma-treated PVA exists which could promote endothelialization *in vivo* without the rapid, initial thrombosis reaction, representing a promising goal for off-the-shelf vascular graft technologies that would encourage long-term clinical patency.

CONCLUSIONS

Research in plasma treatment methods has mainly focused on treating flat surfaces, and there remains a lack of studies investigating luminal plasma treatment of hydrogel-based tubular grafts. Herein, the luminal plasma treatment of small diameter PVA vascular grafts has been reported and characterized. The treatment demonstrated homogeneous luminal surface functionalization and improved endothelial cell attachment. Moreover, the grafted surface functional groups and graft endothelialization were stable up to 30 days, which proved the robustness of luminal surface functionalization. This study proved that plasma treating a tubular shape hydrogel can be done and the treatment was stable even after the hydrogel was swollen. The luminal plasma treatment technique used in this study is therefore a viable option for biomedical applications that require surface modification of tube-like structures such as vascular grafts, nerve conduits, or catheters. The NH_3-plasma treated unpatterned (UPP) and micrograting (2 μGP) surfaces were shown to not significantly invoke platelet or fibrin activation while the treatment improved PVA grafts endothelialization. Thus, this treatment technique has the potential to improve PVA vascular grafts performance and patency.

DATA AVAILABILITY

The datasets generated for this study are available on request to the corresponding author.

ETHICS STATEMENT

This study was carried out in accordance with the recommendations of Guide to the Care and Use of Laboratory Animals, Oregon National Primate Research Center (ONPRC) Institutional Animal Care and Use Committee. The protocol was approved by the ONPRC Institutional Animal Care and Use Committee (IP00000300).

AUTHOR CONTRIBUTIONS

EY, MTH, DM, and GP were responsible for conception and design of the study. GP, PC, DA, YY, and JT performed data collection. GP, PC, DA, and EY were responsible for data analysis and interpretation. GP and MWH were responsible for statistical analyses. GP was mainly responsible for writing the manuscript. All authors approve this final version of the article.

FUNDING

Financial support for this work was provided by NIH grants (R01HL130274, R01HL144113, R01DE026170), NSERC-Canada Discovery Grant (RGPIN-2016-04043), NSERC CREATE (401207296), and NSERC-CANADA.

ACKNOWLEDGMENTS

The authors would like to acknowledge Ms. Jennifer Johnson and the ONPRC staff for their assistance in the shunt studies.

SUPPLEMENTARY MATERIAL

The Supplementary Material for this article can be found online at: https://www.frontiersin.org/articles/10.3389/fbioe.2019.00117/full#supplementary-material

REFERENCES

Abidian, M. R., Daneshvar, E. D., Egeland, B. M., Kipke, D. R., Cederna, P. S., and Urbanchek, M. G. (2012). Hybrid conducting polymer-hydrogel conduits for axonal growth and neural tissue engineering. *Adv. Healthc. Mater.* 1, 762–767. doi: 10.1002/adhm.201200182

Allaire, M. D. E., and Clowes, M. D. A. W. (1997). Endothelial cell injury in cardiovascular surgery: the intimal hyperplastic response. *Ann. Thorac. Surg.* 63, 582–591. doi: 10.1016/S0003-4975(96)01045-4

Anderson, D. E., Glynn, J. J., Song, H. K., and Hinds, M. T. (2014). Engineering an endothelialized vascular graft: a rational approach to study design in a non-human primate model. *PLoS ONE* 9:e115163. doi: 10.1371/journal.pone.0115163

Anderson, D. E. J., Truong, K. P., Hagen, M. W., Yim, E. K. F., and Hinds, M. T. (2019). Biomimetic modification of poly(vinyl alcohol): encouraging endothelialization and preventing thrombosis with antiplatelet monotherapy. *Acta Biomater.* 86, 291–299. doi: 10.1016/j.actbio.2019.01.008

Arslantunali, D., Dursun, T., Yucel, D., Hasirci, N., and Hasirci, V. (2014). Peripheral nerve conduits: technology update. *Med. Devices* 7, 405–424. doi: 10.2147/MDER.S59124

Blackman, B. R. K., Kinloch, A. J., and Watts, J. F. (1994). The plasma treatment of thermoplastic fibre composites for adhesive bonding. *Composites* 25, 332–341. doi: 10.1016/S0010-4361(94)80003-0

Cao, L., Ratner, B. D., and Horbett, T. A. (2007). Plasma deposition of tetraglyme inside small diameter tubing: Optimization and characterization. *J. Biomed. Mater. Res. Part A* 81A, 12–23. doi: 10.1002/jbm.a.30906

Chaouat, M., Le Visage, C., Baille, W. E., Escoubet, B., Chaubet, F., Mateescu, M. A., et al. (2008). A novel cross-linked Poly(vinyl alcohol) (PVA) for vascular grafts. *Adv. Funct. Mater.* 18, 2855–2861. doi: 10.1002/adfm.200701261

Cutiongco, M. F., Goh, S. H., Aid-Launais, R., Le Visage, C., Low, H. Y., and Yim, E. (2016a). K. Planar and tubular patterning of micro and nano-topographies on poly(vinyl alcohol) hydrogel for improved endothelial cell responses. *Biomaterials* 84, 184–195. doi: 10.1016/j.biomaterials.2016.01.036

Cutiongco, M. F., Kukumberg, M., Peneyra, J. L., Yeo, M. S., Yao, J. Y., Rufaihah, A. J., et al. (2016b). Submillimeter diameter Poly(Vinyl Alcohol) vascular graft patency in rabbit model. *Front. Bioeng. Biotechnol.* 4:44. doi: 10.3389/fbioe.2016.00044

Cutiongco, M. F. A., Anderson, D. E. J., Hinds, M. T., and Yim, E. K. F. (2015). *In vitro* and *ex vivo* hemocompatibility of off-the-shelf modified poly(vinyl alcohol) vascular grafts. *Acta Biomater.* 25, 97–108. doi: 10.1016/j.actbio.2015.07.039

Ding, J., He, R., Zhou, G., Tang, C., and Yin, C. (2012). Multilayered mucoadhesive hydrogel films based on thiolated hyaluronic acid and polyvinylalcohol for insulin delivery. *Acta Biomater.* 8, 3643–3651. doi: 10.1016/j.actbio.2012.06.027

Drury, J. L., and Mooney, D. J. (2003). Hydrogels for tissue engineering: scaffold design variables and applications. *Biomaterials* 24, 4337–4351. doi: 10.1016/S0142-9612(03)00340-5

Fathi, E., Nassiri, S. M., Atyabi, N., Ahmadi, S. H., Imani, M., Farahzadi, R., et al. (2013). Induction of angiogenesis via topical delivery of basic-fibroblast growth factor from polyvinyl alcohol-dextran blend hydrogel in an ovine model of acute myocardial infarction. *J. Tissue Eng. Regen. Med.* 7, 697–707. doi: 10.1002/term.1460

Grace, J. M., and Gerenser, L. J. (2003). Plasma Treatment of Polymers. *J. Dispers. Sci. Technol.* 24, 305–341. doi: 10.1081/DIS-120021793

Hatada, K., Kobayashi, H., and Asai, M. (1982). The glow-discharge treatment of poly(vinyl chloride) tube. *Org. Coat. Appl. Polym. Sci. Proc.* 47, 391–396.

Ino, J. M., Chevallier, P., Letourneur, D., Mantovani, D., and Le Visage, C. (2013). Plasma functionalization of poly(vinyl alcohol) hydrogel for cell adhesion enhancement. *Biomatter* 3:e25414. doi: 10.4161/biom.25414

Jacobs, T., Morent, R., Geyter, N. D., Leys, C., Declercq, H., Cornelissen, R., et al. (2012). "Plasma surface treatment of biomedical polymers to improve cell adhesion," in *Abstracts IEEE International Conference on Plasma Science* (Edinburgh, UK). doi: 10.1109/PLASMA.2012.6384095

Jurney, P. L., Anderson, D. E. J., Pohan, G., Yim, E. K. F., and Hinds, M. T. (2018). Reactive ion plasma modification of Poly(Vinyl-Alcohol) increases primary endothelial cell affinity and reduces thrombogenicity. *Macromol. Biosci.* 18:1800132. doi: 10.1002/mabi.201800132

Kaibara, M., Takahashi, A., Kurotobi, K., and Suzuki, Y. (2000). Proliferation of endothelial cells on the plasma-treated segmented-polyurethane surface: attempt of construction of a small caliber hybrid vascular graft and antithrombogenicity. *Colloids Surfaces B Biointerfaces* 19, 209–217. doi: 10.1016/S0927-7765(00)00158-2

Kanchanawong, P., Shtengel, G., Pasapera, A. M., Ramko, E. B., Davidson, M. W., Hess, H. F., et al. (2010). Nanoscale architecture of integrin-based cell adhesions. *Nature* 468, 580–584. doi: 10.1038/nature09621

Kirkwood, M. L., Wang, G. J., Jackson, B. M., Golden, M. A., Fairman, R. M., and Woo, E. Y. (2011). Lower limb revascularization for PAD using heparin-coated PTFE conduit. *Vasc. Endovascular Surg.* 45, 329–334. doi: 10.1177/1538574411401757

Klemberg-Sapieha, J. E., Küttel, O. M., Martinu, L., and Wertheimer, M. R. (1991). Dual-frequency N2 and NH3 plasma modification of polyethylene and polyimide. *J. Vacuum Sci. Technol. A* 9, 2975–2981. doi: 10.1116/1.577158

Kobayashi, M., Chang, Y. S., and Oka, M. (2005). A two year *in vivo* study of polyvinyl alcohol-hydrogel (PVA-H) artificial meniscus. *Biomaterials* 26, 3243–3248. doi: 10.1016/j.biomaterials.2004.08.028

Lidington, E. A., Moyes, D. L., McCormack, A. M., and Rose, M. L. (1999). A comparison of primary endothelial cells and endothelial cell lines for studies of immune interactions. *Transpl. Immunol.* 7, 239–246. doi: 10.1016/S0966-3274(99)80008-2

Lin, J. C., and Cooper, S. L. (1995). Surface characterization and *ex vivo* blood compatibility study of plasma-modified small diameter tubing: effect of sulphur dioxide and hexamethyldisiloxane plasmas. *Biomaterials* 16, 1017–1023. doi: 10.1016/0142-9612(95)94910-D

Liu, W., Zhan, J., Su, Y., Wu, T., Wu, C., Ramakrishna, S., et al. (2014). Effects of plasma treatment to nanofibers on initial cell adhesion and cell morphology. *Colloids Surf B Biointerfaces* 113, 101–106. doi: 10.1016/j.colsurfb.2013.08.031

Manakhov, A., Kiryukhantsev-Korneev, P., Michlíček, M., Permyakova, E., Dvoráková, E., Polčák, J., et al. (2018). Grafting of carboxyl groups using CO2/C2H4/Ar pulsed plasma: Theoretical modeling and XPS derivatization. *Appl. Surf. Sci.* 435, 1220–1227. doi: 10.1016/j.apsusc.2017.11.174

Mantovani, D., Castonguay, M., Pageau, J. F., Fiset, M., and Laroche, G. (1999). Ammonia RF-plasma treatment of tubular ePTFE vascular prostheses. *Plasmas Polym.* 4, 207–228. doi: 10.1023/A:1021805110689

Matsuzawa, Y., and Yasuda, H. (1984). Semicontinuous plasma polymerization coating onto the inside surface of plastic tubing. *Appl Polymer Symposia* 38, 65–74.

Moisan, M., and Wertheimer, M. R. (1993). Comparison of microwave and r.f. plasmas: fundamentals and applications. *Surface Coat. Technol.* 59, 1–13. doi: 10.1016/0257-8972(93)90047-R

Nakagawa, M., Teraoka, F., Fujimoto, S., Hamada, Y., Kibayashi, H., and Takahashi, J. (2006). Improvement of cell adhesion on poly(L-lactide) by atmospheric plasma treatment. *J. Biomed. Mater. Res. A* 77, 112–118. doi: 10.1002/jbm.a.30521

Nugent, M. J., and Higginbotham, C. L. (2007). Preparation of a novel freeze thawed poly(vinyl alcohol) composite hydrogel for drug delivery applications. *Eur. J. Pharm. Biopharm.* 67, 377–386. doi: 10.1016/j.ejpb.2007.02.014

Peijs, T., van Vught, R. J. M., and Govaert, L. E. (1995). Mechanical properties of poly(vinyl alcohol) fibres and composites. *Composites* 26, 83–90. doi: 10.1016/0010-4361(95)90407-Q

Qiu, X., Lee, B. L.-P., Ning, X., Murthy, N., Dong, N., and Li, S. (2017). End-point immobilization of heparin on plasma-treated surface of electrospun polycarbonate-urethane vascular graft. *Acta Biomater.* 51, 138–147. doi: 10.1016/j.actbio.2017.01.012

Recek, N., Resnik, M., Motaln, H., Lah-Turnšek, T., Augustine, R., Kalarikkal, N., et al. (2016). Cell adhesion on polycaprolactone modified by plasma treatment. *Int. J. Polym. Sci.* 2016:7354396. doi: 10.1155/2016/7354396

Tan, S. H., Nguyen, N.-T., Chua, Y. C., and Kang, T. G. (2010). Oxygen plasma treatment for reducing hydrophobicity of a sealed polydimethylsiloxane microchannel. *Biomicrofluidics* 4, 1–8. doi: 10.1063/1.3466882

Tan, T. L., May, K. K., Robless, P. A., and Ho, P. (2011). Outcomes of endovascular intervention for salvage of failing hemodialysis access. *Ann. Vasc. Dis.* 4, 87–92. doi: 10.3400/avd.oa.10.00009

Thiry, D., Francq, R., Cossement, D., Guillaume, M., Cornil, J., and Snyders, R. (2014). A Detailed Description of the Chemistry of Thiol Supporting Plasma Polymer Films. *Plasma Process. Polymers* 11, 606–615. doi: 10.1002/ppap.201400015

Tordoir, J. H., L., H., and Leunissen, K. M., Kitslaar, P. J. (1995). Early experience with stretch polytetrafluoroethylene grafts for haemodialysis access surgery: results of a prospective randomised study. *Eur. J. Vasc. Endovasc. Surg.* 9, 305–309. doi: 10.1016/S1078-5884(05)80135-2

Tseng, D. Y., and Edelman, E. R. (1998). Effects of amide and amine plasma-treated ePTFE vascular grafts on endothelial cell lining in an artificial circulatory system. *J. Biomed. Mater. Res.* 42, 188–198.

Tušek, L., Nitschke, M., Werner, C., Stana-Kleinschek, K., and Ribitsch, V. (2001). Surface characterisation of NH3 plasma treated polyamide

6 foils. *Colloids Surfaces A* 195, 81–95. doi: 10.1016/S0927-7757(01)00831-7

Wade, G. A., Cantwell, W. J., and Pond, R. C. (2000). Plasma surface modification of glass fibre-reinforced Nylon-6,6 thermoplastic composites for improved adhesive bonding. *Interface Sci.* 8, 363–373. doi: 10.1023/A:1008779728985

Wan, W., Dawn Bannerman, A., Yang, L., and Mak, H. (2014). Poly(vinyl alcohol) cryogels for biomedical applications. *Adv. Polym. Sci.* 263, 283–316. doi: 10.1007/978-3-319-05846-7_8

Wan, W. K., Campbell, G., Zhang, Z. F., Hui, A. J., and Boughner, D. R. (2002). Optimizing the tensile properties of polyvinyl alcohol hydrogel for the construction of a bioprosthetic heart valve stent. *J. Biomed. Mater. Res.* 63, 854–861. doi: 10.1002/jbm.10333

Yang, W.-H., Smolen, V. F., and Peppas, N. A. (1981). Oxygen permeability coefficients of polymers for hard and soft contact lens applications. *J. Memb. Sci.* 9, 53–67. doi: 10.1016/S0376-7388(00)85117-0

Yates, C. C., Whaley, D., Babu, R., Zhang, J., Krishna, P., Beckman, E., et al. (2007). The effect of multifunctional polymer-based gels on wound healing in full thickness bacteria-contaminated mouse skin wound models. *Biomaterials* 28, 3977–3986. doi: 10.1016/j.biomaterials.2007.05.008

Conflict of Interest Statement: The authors declare that the research was conducted in the absence of any commercial or financial relationships that could be construed as a potential conflict of interest.

frontiers in Bioengineering and Biotechnology

REVIEW
published: 24 May 2019
doi: 10.3389/fbioe.2019.00113

Use of Nanoparticles in Tissue Engineering and Regenerative Medicine

*Milad Fathi-Achachelouei[1], Helena Knopf-Marques[2,3], Cristiane Evelise Ribeiro da Silva[4], Julien Barthès[3], Erhan Bat[1,5,6], Aysen Tezcaner[1,6,7,8] and Nihal Engin Vrana[2,3]**

[1] Department of Biomedical Engineering, Middle East Technical University, Ankara, Turkey, [2] Inserm UMR 1121, 11 rue Humann, Strasbourg, France, [3] Protip Medical, 8 Place de l'Hôpital, Strasbourg, France, [4] Department of Tests in Materials and Products, Instituto National de Tecnologia, Rio de Janeiro, Brazil, [5] Department of Chemical Engineering, Middle East Technical University, Ankara, Turkey, [6] Department of Biotechnology, Middle East Technical University, Ankara, Turkey, [7] Department of Engineering Sciences, Middle East Technical University, Ankara, Turkey, [8] BIOMATEN, METU, Center of Excellence in Biomaterials and Tissue Engineering, Ankara, Turkey

Advances in nanoparticle (NP) production and demand for control over nanoscale systems have had significant impact on tissue engineering and regenerative medicine (TERM). NPs with low toxicity, contrasting agent properties, tailorable characteristics, targeted/stimuli-response delivery potential, and precise control over behavior (via external stimuli such as magnetic fields) have made it possible their use for improving engineered tissues and overcoming obstacles in TERM. Functional tissue and organ replacements require a high degree of spatial and temporal control over the biological events and also their real-time monitoring. Presentation and local delivery of bioactive (growth factors, chemokines, inhibitors, cytokines, genes etc.) and contrast agents in a controlled manner are important implements to exert control over and monitor the engineered tissues. This need resulted in utilization of NP based systems in tissue engineering scaffolds for delivery of multiple growth factors, for providing contrast for imaging and also for controlling properties of the scaffolds. Depending on the application, materials, as polymers, metals, ceramics and their different composites can be utilized for production of NPs. In this review, we will cover the use of NP systems in TERM and also provide an outlook for future potential use of such systems.

Keywords: tissue engineering, regenerative medicine, metallic nanoparticles, ceramic nanoparticles, polymeric nanoparticles, nanoparticles in bioinks

OPEN ACCESS

Edited by:
Hasan Uludag,
University of Alberta, Canada

Reviewed by:
Jennifer Patterson,
KU Leuven, Belgium
Silvia Baiguera,
Independent Researcher, Rome, Italy

***Correspondence:**
Nihal Engin Vrana
e.vrana@protipmedical.com

Specialty section:
This article was submitted to Biomaterials, a section of the journal Frontiers in Bioengineering and Biotechnology

Received: *06 February 2019*
Accepted: *03 May 2019*
Published: *24 May 2019*

Citation:
Fathi-Achachelouei M, Knopf-Marques H, Ribeiro da Silva CE, Barthès J, Bat E, Tezcaner A and Vrana NE (2019) Use of Nanoparticles in Tissue Engineering and Regenerative Medicine. Front. Bioeng. Biotechnol. 7:113. doi: 10.3389/fbioe.2019.00113

INTRODUCTION

Due to many drawbacks of tissue and organ transplantation such as limited donor availability, the need for immunosuppression and insufficient success rate (rejection of the transplant), there is an increasing demand in tissue engineering and regenerative medicine (TERM) solutions which is a rapidly growing multidisciplinary field. It has merged the biological, material and engineering sciences to develop and manufacture artificial structures that resemble the native tissue/organ not only as implantable systems but also as model, miniaturized organs (Dvir et al., 2011; Zorlutuna et al., 2013). Mimicking the natural extracellular matrix (ECM) composition of a tissue through constructing a three dimensional (3D) scaffold for cells with appropriate mechanical strength, ease of monitoring cellular activities and delivering of bioactive agents require a nanoscale approach

rather than a macroscopic one to obtain satisfactory results. Nanoparticles (NPs) can provide high control over properties of scaffolds such as tuning their mechanical strength and providing controlled release of bioactive agents (Park et al., 2012; Pérez et al., 2013; Cheng et al., 2015; Bahal et al., 2016; Mi et al., 2016). Additionally, drawbacks and limiting factors such as low solubility, unstable bioactivity and short circulation half-life of bioactive molecules (growth factors, cytokines, inhibitors, genes, drugs etc.) and contrast agents have made the NPs as one of the most suitable candidates for bioactive agent delivery and monitoring for applications (Park et al., 2012; Pérez et al., 2013; Cheng et al., 2015; Bahal et al., 2016; Mi et al., 2016).

Nanotechnology as a processing technology includes synthesizing NPs and using them for a wide range of applications. NPs with sizes ranging from ∼ 10 to 1,000 nm can be prepared in solid and colloidal forms (Colson and Grinstaff, 2012). NPs have vast area of applications in the production of sensors, photovoltaic devices, and biomedical field such as drugs delivery and vaccine adjuvants (Saroja et al., 2011; Meng et al., 2012; Saha et al., 2012; Stratakis and Kymakis, 2013; Shang et al., 2014). The impact of nanotechnology has altered traditional and simple approaches in TERM toward more complex and efficient systems. Along NPs, other products of nanoscale technology such as nanofibers and nanopatterned surfaces have been used for directing cell behavior in TERM field. Utilizing simultaneous therapeutic and imaging systems, embedding novel biomaterials with superior spatiotemporal control within scaffolds, modulating release of multiple bioactive agents especially growth factors to direct fate of stem cells and morphogenesis, adjusting mechanical strength of scaffolds for hard tissue applications, and minimizing toxicity and increasing biocompatibility through tissue specific delivery are among various applications of NPs in TERM (**Figure 1**) (Shi et al., 2010; Colson and Grinstaff, 2012).

NPs can be prepared with various types of materials such as ceramics, metals, natural and synthetic polymers. Their compositions and characteristic advantages like high penetration ability, high surface area with tunable surface properties make them as one of the widely preferred candidates in TERM field for imaging, mechanical strength enhancement, as bioink supplements, antimicrobial, and bioactive agent carriers (**Figure 1**) (Shi et al., 2010; Colson and Grinstaff, 2012).

In this article, metallic, ceramic, and polymeric NPs with an emphasis on their TERM applications are reviewed.

METALLIC NANOPARTICLES

NPs provide a link between bulk materials and molecular or atomic structures (Salata, 2004). Metallic NPs can be manufactured and modified through utilizing different functional groups that provide conjugation of antibodies, ligands, and drugs as delivery systems (Dobson, 2006; Mody et al., 2010). This section summarizes some examples of metallic NPs with respect to biomedical applicability concerning gold and silver NPs.

Gold Nanoparticles

Gold nanoparticles (AuNPs) can be described as a colloid of nanometer sized particles of gold. Colloidal gold solutions present different properties compared to the bulk gold, for example, their optical property due to their unique interaction with light (Daniel and Astruc, 2004). Turkevich et al. synthesized monodisperse spherical gold NPs for the first time (Turkevich et al., 1951). This method was then modified by others (Frens, 1973; Kimling et al., 2006). On gold surface it is possible to conjugate various ligands including polypeptide sequences, antibodies and proteins with various moieties such as phosphines, amines, and thiols, as their strong affinity to gold is known (Alivisatos et al., 1996).

One potential use of gold NPs in the context of regenerative medicine is as a safety measure if the implanted tissue is replacing a resected tissue/organ due to tumor growth. One example is the use of AuNPs for disturbing the cancer cell division by selectively transporting the particles into affected cells' nuclei. Kang and colleagues developed polyethylene glycol (PEG) coated AuNPs (30_nm) through binding it with nuclear localization signal (NLS) peptides together with arginine—glycine—aspartic acid (RGD) (Kang et al., 2010). Human oral squamous cell carcinoma (HSC) overexpressing αvβ6 integrins and human keratinocytes (HaCat) were utilized a cancer cells and normal cells, respectively, in this study. **Figures 2A,B** shows real-time monitoring of cancer cells in the absence (control) and with 0.4 nM RGD/NLS-AuNPs. For the first case, cytokinesis of control cells started at 45 min (**Figure 2A3**). Cytoplasmic bridge connected the daughter cells and this connection was extended over time (**Figure 2A6**). Total separation of two daughter cells was observed after 2 h (**Figure 2A7**). Nevertheless, complete cell division was not observed for cells that were incubated with 0.4 nM RGD/NLS-AuNPs. Cytokinesis continued similar to the control (**Figures 2B1–4**). In contrast to control group, cytoplasmic bridge did not extend after fully contraction of cleavage furrow (**Figures 2B5–6**) and consequently, daughter cells formed a binucleated cell (**Figure 2B7**). It was concluded that cytokinesis arrest (blockage of the final step in cell division) resulted through nuclear targeting of AuNPs in cancer cells therefore preventing cells from completing cell division (Kang et al., 2010). Nuclear targeting of the cancer cells plays a crucial role in the success of the cancer treatment. Recently, it was reported that *in situ* aggregation of non near-infrared (NIR) absorbing plasmonic AuNPs took place at the nuclear region of the cells (Panikkanvalappil et al., 2017) which makes plasmonic AuNPs as a suitable candidate for NIR photoabsorber for plasmonic based photothermal therapy in cancer. By shifting significantly the absorption band to NIR range, plasmonic AuNPs they protect healthy tissue through reducing heat-induced collateral damage. In another study, it has been shown that AuNPs targeting the cell nucleus membrane has increased the overexpression of laminin A/C and mechanical stiffness of nucleus and consequently decreased the cancer cell migration (Ali et al., 2017). All these properties of AuNPs can be utilized for targeting the remaining cancer cells following tumor resection and consequently minimizing cancerous cells remaining in the healthy tissue microenvironment. Therefore,

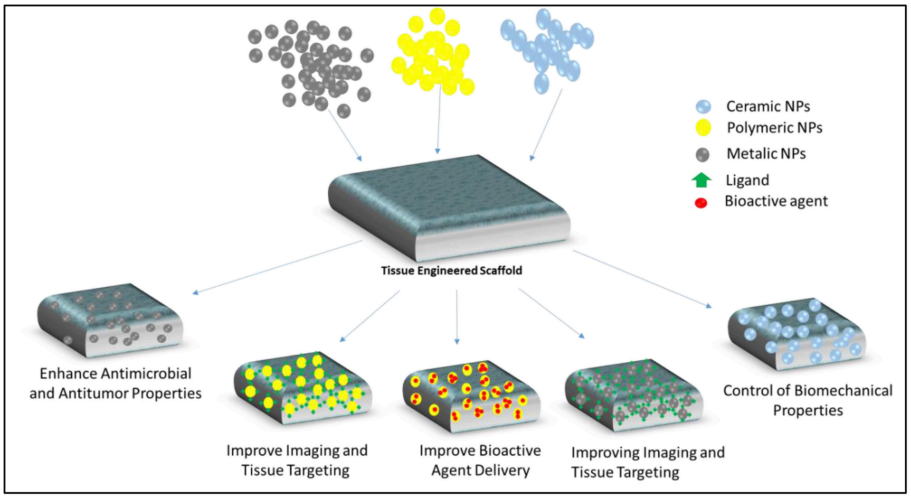

FIGURE 1 | Examples of different types (ceramic, polymeric, metallic) nanoparticles which can be utilized for various applications in TERM including tissue targeting and imaging, bioactive agent delivery, modulating mechanical properties of scaffolds, providing antimicrobial and antitumor properties.

applying AuNPs prior to implantation can provide a safety measurement toolbox to minimize the recurrence of tumor through targeted delivery to cancer cells, and consequently; increase the chance of the effective implantation for various TERM applications.

Moreover, AuNPs are widely used for drug delivery applications (Manivasagan et al., 2016; Amoli-Diva et al., 2017; Labala et al., 2017). They are also used as a probe for Raman scattering aimed for *in vivo* cell targeting. AuNPs can be conjugated to epidermal growth factor receptor (EGFR) through an antibody, for targeting tumor cells. The antibody fragment recognizes EGFR on cancer cells (Paez et al., 2004). After systemic administration, those AuNPs, were capable of intensifying the Raman scattering efficiency of adsorbed molecules nearly to 10^{15} times (Paciotti et al., 2006). Process of cell targeting is shown in **Figure 2C**. Qian et al. has prepared thiol-modified PEG coated AuNPs and compared it with AuNPs to understand their targeting efficiency using single-chain variable fragment antibodies (ScFv) as EGFR, and His-tagged green fluorescent protein (GFP) (Qian et al., 2008). PEG-coated, ScFv, and GFP bound NPs were able to directly aim biomarkers on the surface of tumor cells which were encoded with surface-enhanced reporter with a Raman reporter. Through utilization of surface-enhanced Raman scattering (SERS), recognition of human cancer cells with minimum passive aggregation and remarkably specific detection in xenograft tumors was reported by utilization of AuNPs coated with thiol-modified PEG. In the context of tissue engineering such systems can contribute to precise monitoring of potential relapse during the integration of the implanted system.

As reviewed by Vieira and colleagues, different NPs can be used for bone tissue engineering with emphasis on scaffolds' improvement and drug delivery (Vieira et al., 2017). Among NPs (organic and inorganic), AuNPs have been used in scaffolds for enhancing bone regeneration, due to their potential to promote cell differentiation (Zhang et al., 2014; Ko et al., 2015). Heo et al. presented an enhanced bone regeneration by using a complex composed of AuNPs and gelatin scaffolds (Heo et al., 2014). This combination leads to *in vitro* and *in vivo* osteogenic differentiation of adipose-derived stem cells. 2,2,6,6-Tetramethylpiperidine-N-oxyl (TEMPO) conjugated AuNPs have been reported to be efficiently uptaken by human mesenchymal stem cells (MSCs) and reduce the overproduction of reactive oxygen species in them at low dosage of TEMPO (Li J. et al., 2017). It has also enhanced osteogenic differentiation of human MSCs while suppressing the adipogenic differentiation. Consequently, it can be used for ROS-induced dysfunctions while regulating the desired differentiation type. Similarly, osteogenic differentiation of MSCs in fibrin and poly(caprolactone) (PCL)-based scaffolds containing PEGylated hollow AuNPs through increasing Runx2 gene expression has been reported (del Mar Encabo-Berzosa et al., 2017). RGD-modified AuNPs have been shown to have an effect in a ligand density dependent manner over the MSCs differentiation characteristics (Li J. et al., 2018). While high density of RGD resulted in decreased alkaline phosphatase (ALP) activity and enhanced the adipogenic marker gene expression, low density RGD caused a decrease in the oil droplet formation and adipogenic marker gene expression.

Vial and colleagues described different ways of how TERM can be affected by the use of AuNPs, as seen in **Figure 2D** (Vial et al., 2017). TERM combines the following elements: scaffold, cells, and bioactive molecules. The main objective of adding AuNPs is not only to improve scaffold structures, but also to guide cell behavior, which means enhancing cell differentiation and the intracellular delivery (Vial et al., 2017). This interaction between AuNPs and various cells could be in different aspects such as modulation of cardiomyocytes using calcium oscillation by heating AuNPs (via 532 nm picosecond pulsed laser) (Gentemann et al., 2017); stimulation of striated muscle cells with NIR using gold nanoshells as effective wireless stimulation technique for muscle tissue engineering

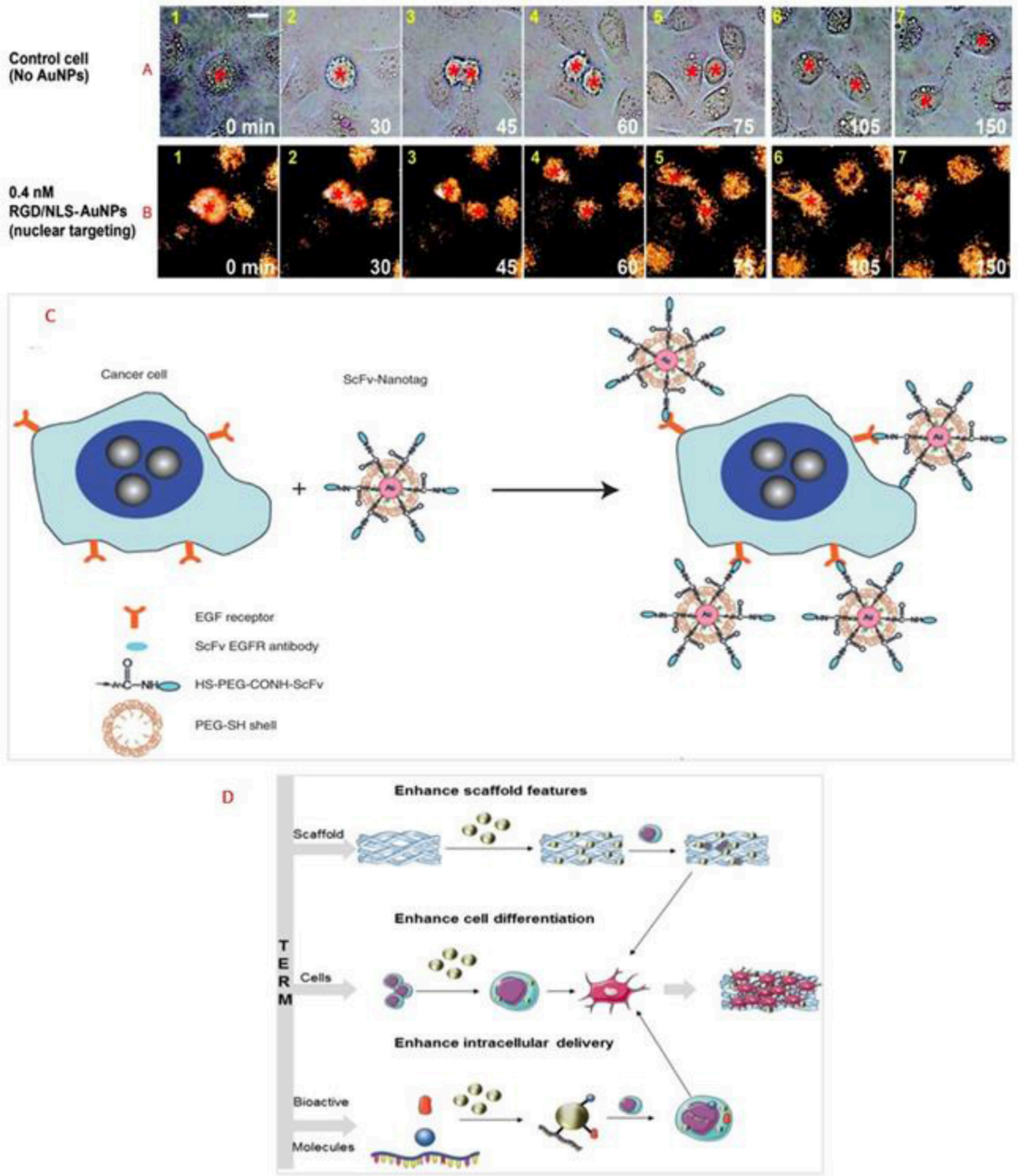

FIGURE 2 | Real-time images of cancer cell division under the following conditions: **(A)** with No AuNPs and **(B)** in the presence of 0.4 nM nuclear-targeting gold nanoparticles (RGD/NLS-AuNPs). Red stars indicate the nuclei. Scale bar: 10 μm. Reprinted from Kang et al. (2010) with permission from American Chemical Society. **(C)** Preparation of targeted surface-enhanced Raman scattering (SERS) NPs by using a mixture of SH-PEG and a hetero-functional PEG (SH-PEG-COOH). Covalent conjugation of an EGFR-antibody fragment occurs at the exposed terminal of the hetero-functional PEG. Reprinted from Qian et al. (2008) with permission from John Wiley and Sons. **(D)** Scheme representing the use of AuNPs in tissue engineering and regenerative medicine. Reprinted from Vial et al. (2017) with permission from Elsevier.

through myotube activation (Marino et al., 2017); increase in migration of pro-healing M2 macrophages and proliferation of neonatal cardiomyocytes under electrical stimulation in collagen-silver/gold NPs 3D matrix (Hosoyama et al., 2017); and enhancement in dopaminergic neural differentiation of mouse embryonic stem cells (ESCs) through mTOR/p70S6K pathway using AuNPs of around 30 nm in size (Wei et al., 2017).

Chen et al. have reported the impact of the AuNPs on MSCs for vascular tissue engineering (Chen Y.-W. et al., 2018). Incorporation of 43.5 ppm AuNPs into fibronectin (FN) coat

has decreased the elasticity of the coating of the composite material and enhanced its thermal stability. Hydrophilicity of the composite has increased compared to control groups, which would help the attachment of MSCs. FN loaded AuNPs which was coated over catheter has stable and slow degradation *in vivo*. MSCs treated with VEGF (vascular endothelial growth factor) (50 ng/ml) enhanced cell migration on the scaffold of FN-AuNPs via signaling pathway of matrix metalloproteinase (MMP)/ endothelial nitric oxide synthase (eNOS). MSCs have shown higher antithrombotic activity, better endothelialization and higher expression of CD31 and alpha-smooth muscle actin (α-SMA) with FN-AuNPs coated catheters implanted compared to control groups.

AuNPs also can be applied for wound healing applications. Akturk et al. have observed better wound closure in AuNPs containing wet electrospun silk fibroin compared to control groups (Akturk et al., 2016). Higher neovascularization and granulation tissue formation have also been observed compared to untreated skin control group.

Silver Nanoparticles

Silver nanoparticles (AgNPs) can also be described as a colloid of nanometer sized particles of silver and are one the most widely used metallic NPs in biomedical field mainly for their antimicrobial properties (Rai et al., 2009; Prabhu and Poulose, 2012). As bacterial infection is a significant risk with engineered tissues; use of AgNPs as a safety measure is a potential solution. These NPs can be produced by either physical or chemical processes (Panácek et al., 2006; Guzmán et al., 2009). The physical methods used to synthetize AgNPs are evaporation-condensation process, laser ablation of metallic bulk material, gamma irradiation or ultrasonic irradiation. Chemical methods are mostly based on the utilization of sodium borohydride or polyol as reducing agents in order to reduce silver salt solution (silver nitrate) (Frattini et al., 2005). After reduction of silver ions (Ag^{+}) into metallic silver (Ag^{0}), NPs will be formed through nucleation followed by the growth. In the past few years, biological methods using microorganisms such as bacteria or, eukaryotic fungi or plants to reduce silver ions, have emerged to synthetize AgNPs (**Figure 3A**). This method called bioreduction of silver ions is considered more eco-friendly since it does not involve the use of toxic chemicals during the process (Yasin et al., 2013; Ahmed et al., 2016). Depending on the method used (chemical or physical) and the choice of the reducing agent (weak or strong), the size of the NPs can range from few nanometers to more than 500 nm diameters. To stabilize and control the size of the particles, almost all methods comprise the use of surfactants (Iravani et al., 2014). Silver ions have been used for a long time for their antimicrobial properties toward a wide range of microorganisms. It has been shown that silver ions are able to block the microbial respiratory chain system and precipitate bacterial cellular protein (Abbasi et al., 2016). Morones et al. have studied the antimicrobial properties of AgNPs against four types of gram-negative bacteria (Morones et al., 2005). In their study they have shown that NPs in the range of 1–10 nm can act differently against Gram- bacteria by (i) attaching to cell membrane affecting permeability and respiration (ii) penetrating inside bacteria and damage them or (iii) via releasing silver ions. Gurunathan et al. have shown the antibacterial capacity of AgNPs of about 5 nm diameter against Gram- and Gram+ bacteria (Gurunathan et al., 2014).

Properties of AgNPs have also been investigated in TERM mostly for wound dressing applications. Wounds such as chronic wounds and burn wounds are highly prone to infection. Moreover, increased incidence of multi-drug resistant microbes related infections are a challenging health problem and requires the incorporation of antimicrobial components in the scaffold design for wound healing. These particles have been incorporated in scaffolds made of different materials e.g., poly(vinyl alcohol) (PVA), PCL, gelatin, chitosan-alginate and cellulose acetate scaffolds. All the resulting scaffolds exhibited strong antimicrobial activity.

NPs can be formed before the incorporation in the scaffolds and then loaded or a composite can be formed during which AgNPs are formed *in situ* in the structure using reducing agents (heat, UV, chemicals). These different scaffolds can be produced in different formats including bulk materials, electrospun fibers, fibers mats, nanofibrous or porous scaffolds (Son et al., 2004; Hong et al., 2006; Rujitanaroj et al., 2008; Augustine et al., 2016; Bhowmick and Koul, 2016; Mokhena and Luyt, 2017; Pankongadisak et al., 2017; Rosa et al., 2017; Santos et al., 2017; Venkatesan et al., 2017; Biswas et al., 2018; Mehrabani et al., 2018; Yahyaei et al., 2018). In an animal model, Tian et al. studied the impact of AgNPs treatment on burn and diabetic wounds as potential wound healing accelerator (Tian et al., 2007). They found that the delivery of AgNPs not only had an antimicrobial effect but also it has accelerated the rate of healing. Male BALB/c Mice with deep partial-thickness burn wounds normally cured after 35.4 ± 1.29 days. Wounds treatment with silver sulfadiazine (SSD) had prolonged the healing period to 37.4 ± 3.43 days. AgNPs, in contrast, have enhanced the healing process to 26.5 ± 0.93 days (**Figure 3B**). In the diabetic wounds, a similar effect has been observed and wound treated with AgNPs were healed 16 ± 0.41 days after injury, while wound treated with SSD required 18.5 ± 0.65 days for complete healing. They also have discovered that AgNPs had the ability to regulate the cytokines associated in burn wound healing. Significant decrease in neutrophils was found in wound treated with AgNPs compared to SSD groups which indicate effect of AgNPs to decrease the local and systemic inflammatory response. This effect can be complemented with hydrogels as hydrogels can prevent contraction of the wound due to high water uptake content. By Wang et al. AgNPs poly(gamma-glutamic acid) (ϒ-PGA) hydrogel copolymer has been shown to promote wound healing *in vivo* on male BALB/c mouse compared to control groups (Wang et al., 2018). Collagen deposition and intact epidermis layer formation have been observed after 14 days of impaired wound healing with histological analysis.

In the same area, AgNPs have been utilized to elaborate chitin/nanosilver composite antimicrobial scaffolds. It has been also observed that the blood clotting efficiency was increased with this scaffold due to the fact that silver can affect the pathway of coagulation by denaturing the anticoagulant proteins (Madhumathi et al., 2010). AgNPs (100 nm) have also shown

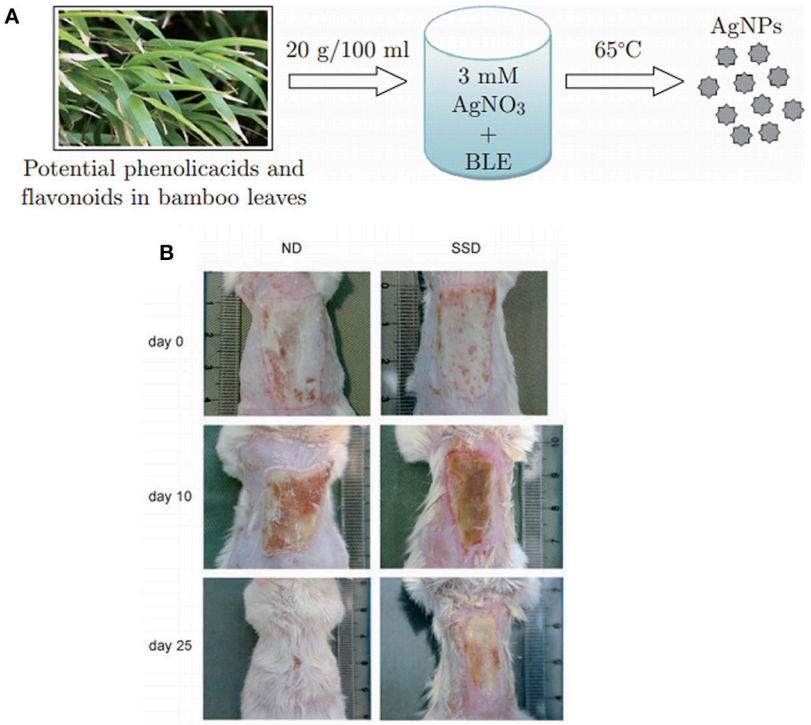

FIGURE 3 | Effect of silver nanoparticles on burn wound healing. **(A)** Synthesis mechanism of silver nanoparticles using bamboo leaves extract (BLE) to reduce silver nitrate. Reprinted with permission from Yasin et al. (2013) **(B)** Images of burn wound from mouse treated with silver nanoparticles (ND) and silver sulfadiazine (SSD) at different time point of wound healing. Reprinted from Tian et al. (2007) with permission from Springer.

to enhance the biocompatibility and structural stability of decellularized porcine liver through crosslinking (Saleh et al., 2018). Its crosslinking efficiency was appraised and compared to that of glutaraldehyde and ethyl carbodiimide hydrochloride and N-hydroxysuccinimide. Enhancement in the ultra-structure of the collagen fiber in decellularized liver and slower *in vitro* degradation have been observed compared to control groups. It is worthy to mention that AgNPs also can show cytotoxic effect over cancer cells. It was reported that a porous chitosan-alginate with biosynthesized AgNPs has been shown to have cytotoxic effects against MDA-MB-231 breast cancer cells (Venkatesan et al., 2017). These examples show the potential of AgNPs for TERM.

CERAMIC NANOPARTICLES

Ceramic nanoparticles (CNPs) are basically comprised of inorganic compounds, besides metals, metal oxides, and metal sulfides and they can be used in production of nanoscale materials of various shape, size, and porosity (Singh et al., 2016). IN general, CNPs can be classified according to their tissue response as being inert, bioactive or resorbable ceramics and magnetic NPs (Kohn, 2003).

Bioactive Glass Nanoceramics

Bioactive glass ceramic nanoparticles (n-BGC) with SiO_2-CaO–P_2O_5-Na_2O core structures were established by Larry Hench's team in 1969 (Jones, 2015). Bioglasses can be formed from various elements such as silicone, sodium, potassium, magnesium, phosphorous, oxygen, and calcium which can be absorbed by the cells (Taygun and Boccaccini, 2011). Various techniques have been developed to produce nanoscale bioactive glasses such as microemulsion, laser spinning, sol-gel, and gas-phase synthesis (Taygun and Boccaccini, 2011). nBGC can provide faster ion release compared to bulk bioactive glasses due to their improved specific surface area; consequently, enhancement of bioactivity and adsorption of proteins can be expected (Boccaccini et al., 2010). Effect of various morphologies of CaO–P_2O_5-SiO_2 based nBGC on their bioactivity was investigated through utilization of lactic acid (LA) in the sol–gel procedure through immersion in simulated body fluid (Chen et al., 2009). Addition of LA resulted in a decrease in the size of bioactive glass nanoparticles (nBGs). nBGs of either unimodal or bimodal (narrow) pore size distribution had higher bioactivity compared to the nBGs with smooth surface morphology. Wang and colleagues studied nBGs with a diameter of 12 nm (BP-12) instead of mixing conventional bioglass (diameter of 200 nm) with gelatin to manufacture a simple hydrogel for wound dressing application (Wang C. et al., 2016). Composition of gelatin with BP-12 could provide hydrogel with pronounced thixotropy (becoming less viscous) characteristic at a practically usable shear rate. Such a polymer-colloid mixture can be in a gel state, and become injectable under shear, and return to gel state as settled again; therefore, its use becomes easy for wound coverage. Fast tissue formation including regeneration of

cutaneous-tissue was observed within 7 days after implantation in rats.

Antibacterial and angiogenic properties and excellent bioactivity of nBGs have made them as a suitable candidate for dentin regeneration applications. Incorporation of boron modified nBGs in the cellulose acetate/oxidized pullulan/gelatin-based constructs has shown promising results for dentin regeneration through increase in cellular viability, Intracellular calcium deposition (ICD) and ALP activity while keeping the boron ion released below toxic level (Moonesi Rad et al., 2019). Rad et al. demonstrated that incorporation of 6.25 mg/ml boron doped nBGs into cell culture media has increased the ALP activity and ICD. The group also showed human dental pulp stem cells' odontogenic differentiation were enhanced by immunocytochemical staining of dentin sialophosphoprotein, osteopontin, and collagen I (Rad et al., 2018).

nBGs are also attractive candidates for bone tissue engineering applications. In a study by Covarrubias et al. it was reported that incorporation of dense nBGs into chitosan-gelatin polymer blend has promoted the higher activity of alkaline phosphatase compared to mesoporous bioactive glass nanosphere composites (Covarrubias et al., 2018). *In vivo* experiments have shown that in dense chitosan-gelatin hydrogels containing 5% bioactive glass nanoparticles had the highest amount of new bone formation (∼80%) in the defect area after 8 weeks of implantation compared to control groups. In another study, multifunctional poly(citrate-siloxane) (PCS) elastomer based nBGs were developed for bone tissue engineering (Li Y. et al., 2018). Hybrid material showed intrinsic biomineralization with photoluminescent properties. Addition of nBGs has increased elastomeric modulus of PCS from 20 to 200 MPa. Biodegradation and *in vivo* metabolization of the nanocomposite has been tracked through real-time monitoring through exciting with blue fluorescence at the 365 nm thanks to inherent and high photoluminescence quantum yield and lifetime of PCS. This nanocomposite had proliferative effect on osteoblasts (MC3T3-E1). Additionally, it enhanced osteoblastic differentiation of these cells and has also decreased the *in vivo* inflammatory response toward the biomaterial. Various other applications have been investigated using nBGs for bone tissue engineering including copper containing nBGs in gelatin coated scaffolds (Zheng K. et al., 2018), miRNA delivery with nBGs with ultralarge pores which leads to highly efficient miRNA loading (Xue et al., 2017), and osteogenic differentiation induction of adipose-derived stem cells using monodispersed nBGs (Guo Y. et al., 2018).

Bioresorbable Nanoceramics

Bioresorbable nanoceramics have calcium phosphate (CaP) based composition which include variety of materials such as hydroxyapatite (HAp), calcium aluminate, tricalcium phosphate, calcium phosphate dicalcium phosphate dehydrate, calcium carbonate ($CaCO_3$), calcium sulfate hemihydrate, octacalcium phosphate and biphasic calcium phosphate. HAp is major component (inorganic) of natural bone and under neutral or alkaline conditions it is the most stable form of phosphate salts. These materials have been applied in orthopedics such as bone substitutes (Yao et al., 2017). Various manufacturing processes including chemical synthesis methods have been developed for the production of HAp NPs with precise control over the nanostructure (Ferraz et al., 2004; Sadat-Shojai et al., 2013). It is difficult to synthesize highly pure HAp as calcium phosphates have variety of derivatives and reaction conditions plays crucial role in the synthesis of CaPs and their properties (Han et al., 2006). Combination of different methods can be utilized to for enhancing properties of final product (Sadat-Shojai et al., 2013). Various ions can be incorporated to the HaP lattice to modulate the characteristic features of the scaffold for desired TERM application such as degradation properties and cellular responses. Cadmium, silicon, yttrium, silver, zinc, copper, magnesium, and trace elements have been used for modifying the HaP properties (Ergun et al., 2002; Cox et al., 2014; Hidouri et al., 2018). Various single ion substitutions in HAp were reported before (Lin and Chang, 2015; Fihri et al., 2017; Kim et al., 2018; Pal et al., 2019).

Composite scaffold bearing HAp NPs have shown different mechanical properties which mainly depend on the nature of composite and preparation method. Incorporation of HAp NPs has been reported to increase modulus of compression in the porous shape memory polyurethane (Yu et al., 2018) or enhance the ultimate compressive strength in PCL/poly(lactic-co-glycolic acid) (PLGA)/HAp NPs (Li X. et al., 2017). In another study compressive modulus of gelatin HAp NPs composite hydrogel has been shown to decrease by increasing the weight percentage of HAp NPs. Such decrease was attributed to negative effect of HAp NPs on the crosslinking efficiency (Raucci et al., 2018).

HAp is commonly used in TERM applications. Combination of HAp with various from of carriers such as electrospun fibers (Cai et al., 2017; Samadian et al., 2018), porous scaffolds (Guo M. et al., 2018), and hydrogels (Ghosh et al., 2017) have been reported for preparation of nanocomposite materials to modulate the desired cellular activities. Recently, graphene oxide-incorporated silicate-doped nano-HAp composites have been used for reinforcement of fibrous scaffolds of PCL produced by wet electrospinning for bone tissue engineering (Dalgic et al., 2018). Silicate-doped nano-hydroxyapatite (10%)—graphene oxide (4%) group was reported to enhance the adhesion, spreading, proliferation and ALP activity of Saos-2 cells compared to other scaffold groups. Qian et al. compared the behavior of a biomimetic PLGA scaffold with and without HAp NPs. NPs were reported to enhance cellular activities including cell attachment, proliferation, and differentiation of pre-osteoblastic cells (Qian et al., 2014).

Multi doping may also improve the properties of HAp and such substitutions are gaining huge attention nowadays. Ba^{2+} and Ho^{3+} ions as contrast agents for computed tomography (CT) have been doped into nHAp via microwave-assisted synthesis and under various operating voltages significant enhancement in the contrast efficiency was observed (Zheng X. et al., 2018). Application of co-doped HAp NPs in bone tissue engineering has focused to enhance cellular activity including attachment, proliferation and differentiation. Alshemary et al. (2017) have successfully synthesized ferric (Fe^{3+})/selenite (Se_4^{2-}) co-doped HAp materials via microwave refluxing procedure. Degree of crystallinity was decreased and crystallite growth was inhibited by increasing the amount of Fe^{3+} doping. Acceleration in

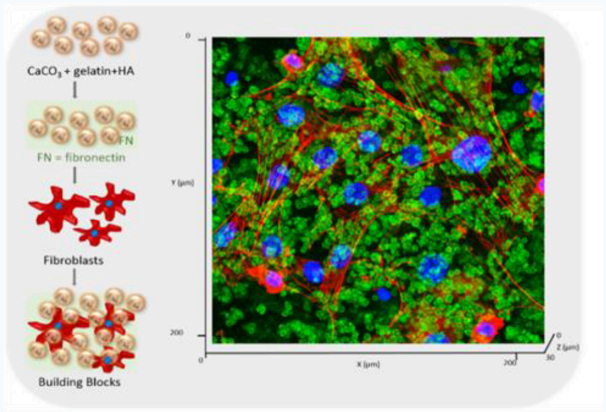

FIGURE 4 | Development of a hybrid $CaCO_3$ particular system doped with ECM components (gelatin, hyaluronic acid, fibronectin) for creating a building block strategy. Confocal images of the after 3 days of culture. The particles are labeled in green (stained by HA-FITC) and the fibroblasts were visualized with Rho-Phalloidin (red) and nuclei (blue). Reprinted with permission from Affolter-Zbaraszczuk et al. (2017).

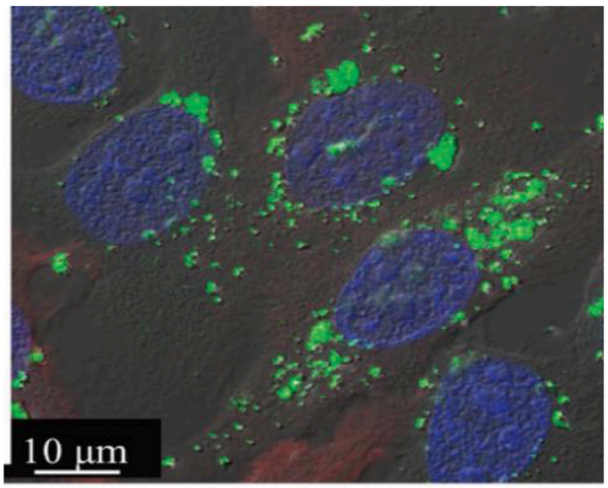

FIGURE 5 | A merged fluorescence confocal image of FMN–MTNs (green dots) in BT-20 cancer cells where the nuclei were stained with DAPI (blue spots). Reprinted from Wu et al. (2011) with permission from The Royal Society of Chemistry.

growth of apatite layer and increase in degradation rate of HAp were reported by introducing dopants. Cytocompatibility and favorable osteoblastic differentiation of stem cells were observed in Fe-SeHAp scaffolds. The group proposed Fe-SeHAp group as a suitable bioceramic for bone tissue regeneration. Recently, our group developed hybrid microspheres for constructing a $CaCO_3$ particles that are simple to administer and will allow to build-up various tissues. These particles are based on ECM factors such as fibronectin, hyaluronic acid and gelatin which can form a system for TERM applications such as wound management, as shown in **Figure 4**. Furthermore, these building blocks will provide stepwise build-up to manufacture stratified 3D cellularized scaffolds (Affolter-Zbaraszczuk et al., 2017).

CaPs have been utilized with different types of polymers to produce nanocomposite materials (Vieira et al., 2017). Advantages of these nanocomposites such as excellent mechanical characteristics could be utilized for bone tissue regeneration through enhancing scaffolds' performance (Vieira et al., 2017). Ataol et al. synthesized nano calcium phosphate particles (CaP NPs) using flame spray pyrolysis technique (Ataol et al., 2015). Urine-derived stem cells treated with the CaP NPs had shown elevated ALP activity compared to control cells, demonstrating osteogenic differentiation of these cells. From the above mentioned articles and vast number of the conducted researches in the literature it can be deduced that addition of CaP family of materials in the form of NPs can provide a better osteogenic differentiation for TERM applications.

Bioinert Nanoceramics

Bioinert nanoceramics including titanium dioxide (TiO_2), zinc oxide (ZnO) are utilized for different medical applications as they show positive interactions with body tissues. TiO_2 NPs can be synthesized with different manufacturing processes including hydrothermal, solvothermal, sol-gel process and emulsion precipitation methods (Vollath et al., 1997; Zhao et al., 2007; Gupta and Tripathi, 2011). Zhao et al. have prepared TiO_2 NPs by flame synthesis (Zhao et al., 2007). By using this method it is possible to manufacture uniformly distributed (in size) bioceramics in targeted size range. With the advancement of nanotechnology, TiO_2 nanoparticles, nanotubes or nanoprobes labeled with the fluorescent dye or magnetic resonance contrast agents have been successfully prepared for cell imaging through fluorescent analysis or magnetic resonance imaging (MRI) (Fei Yin et al., 2013). Mesoporous titania nanoparticles (MTNs) with superior biocompatibility (LC50 $\approx$ 400 $\mu g\ mL^{-1}$) and a functionalized MTNs with a phosphate-containing fluorescent molecule (flavin mononucleotide; FMN) have been recently synthesized. FMN-MTNs were used as a satisfactory intracellular bioimaging agent (Wu et al., 2011). BT-20 cells were incubated with FMN-MTNs for 4 h, and cytoplasm of cells was visualized as the FMN-MTNs emitted green fluorescence. Observing such emission indicates the presence of FMN molecules in large surface area (ca. 237.3 $m^2\ g^{-1}$), and they were further observed inside the MTNs without much leaching (**Figure 5**). The mesoporous TiO_2 have been applied with magnetic-targeting for dual-modal imaging and photodynamic therapy through combining NIR mediated photodynamic therapy, chemotherapy and gene therapy in a synergy manner for cancer treatment (Yu et al., 2017).

Various methods were developed for synthesizing nanoscale ZnO powders including precipitation, hydrothermal synthesis, spray pyrolysis, thermal decomposition and electrochemical growth (Vollath et al., 1997; Padmavathy and Vijayaraghavan, 2008). Various parameters such as type of solvent and precursor, pH and reaction temperature can affect the particle size of ZnO. Padmavathy and Vijayaraghavan used precipitation and the base hydrolysis methods for manufacturing nanosized ZnO (Padmavathy and Vijayaraghavan, 2008). Both methods yielded ZnO particles with 10–50 nm size range. Both NPs were reported

to demonstrate better antibacterial properties compared to bulk ZnO. In another study, biological technique was used for synthesis of ZnO NPs through rapid, single step and green synthesis process by utilizing *Sargassum muticum* which is a brown marine macroalga (Azizi et al., 2014). Based on the Fourier transform infrared (FTIR) spectroscopy analysis, polysaccharides in *Sargassum muticum* extracts were reported to be involved in the production of ZnO NPs.

Similar to AuNPs and AgNPs, metal oxide NPs can be utilized as antimicrobial protection agents in the context of TERM (Laurenti and Cauda, 2017). Recently, nanocomposite of chitosan/hydroxyapatite-zinc oxide (CTS/HAp-ZnO) supporting organically modified montmorillonite clay (OMMT) has been manufactured for bone tissue engineering applications (Bhowmick et al., 2018). Nanocomposite has shown strong antibacterial activities when facing Gram+ and Gram- bacteria. Mechanical properties of nanocomposite and proliferation of osteoblastic MG-63 cells on this biomaterial have shown improvement compared to control group. In another bone tissue application, a hybrid scaffold composed of polyurethane nanofibers that was reinforced with zinc oxide-functionalized multi-wall carbon nanotubes has been developed (Shrestha et al., 2017). Electrospun scaffolds with 0.2 wt% ZnO, and 0.4 wt% functionalized multi-wall carbon nanotubes were found to exhibit antibacterial activity and cytocompatibility.

Magnetic Nanoparticles

Magnetic nanoparticles (MNPs) are iron oxide NPs, (usually Fe_3O_4 or Fe_2O_3) which are widely studied in biomedical field because of their lower toxicity. Co-precipitation is used as most conventional method for synthesizing Fe_3O_4 or γ-Fe_2O_3 (Gupta and Gupta, 2005). In this method ferric and ferrous ions in highly basic solutions are mixed (1:2 molar ratio, respectively) at room temperature or at high temperatures. Similar to ZnO NPs, Fe_3O_4 NPs were reported to be synthesized from *Sargassum muticum* (Mahdavi et al., 2013). The aqueous extraction of seaweed and ferric chloride solution were mixed to produce Fe_3O_4 NPs. Xiaoming et al. reported that MNPs have been extensively utilized in MRI applications (Li et al., 2016). It consists of various applications like imaging cancer cells, pursuing stem cells *in vivo* and monitoring of transplanted tissues. In this context, they can also be used for monitoring of engineered tissues. Moreover, superparamagnetic magnetite nanocrystal clusters (SMNC) can be utilized for cell imaging. Mini emulsion/sol-gel and polyol techniques were used for synthesizing SMNCs. They were prepared by coating with polyetherimide, citric acid or silica. These SMNCs possessed very high sensitivity toward magnetic resonance, and had no adverse effect on cell viability (Li et al., 2016). It has been reported that NPs with small size (<100 nm) and narrow size distribution are suitable for both *in vitro* and *in vivo* biomedical applications (Medeiros et al., 2011). However, this optimum size can be changed depending on the applications especially for multi-functional applications including combined drug targeting and imaging. Concerning the *in vitro* and *in vivo* applications, the super paramagnetic behavior of MNPs is also of interest as they lose magnetism after removing magnetic field. Retaining of magnetism is related to the size of particles. NPs with 10–50 nm size and proper surface coating can have long circulation times, and they can also manipulated by an external magnetic field (Medeiros et al., 2011).

One of the exciting applications of TERM is the neuroregeneration and nerve tissue engineering which could improve life quality of the patients with nerve injuries. Various studies have been conducted to deliver growth factor conjugated MNPs to cells, monitoring the fate of MNPs or stimulate the cells with MNPs (Alon et al., 2015; Marcus et al., 2015; Zuidema et al., 2015; Giannaccini et al., 2017; Willmann and Dringen, 2018). Recently, superparamagnetic iron oxide (SPIO)-Au core-shell NPs decorated with nerve growth factor (NGF) with low toxicity have been developed for neuron growth and differentiation (Yuan et al., 2018). NGF functionalized NPs have provided higher neuronal growth and orientation on PC-12 cells under dynamic magnetic fields utilizing rotation have been obtained compared to static magnetic fields. Magnetic NPs also have been used for controlling collagen fiber orientation dynamically and remotely *in situ* during the gelation period through an applied external magnetic field (Chang et al., 2017). Magnetically activated 3D gels bearing neurons showed natural cellular viability and electrical activity with elongated, co-oriented morphology. The iron oxides also have the ability to pass blood brain barrier, it could be used for conjugation of various peptide and growth factors to cure and regenerate brain tissue (Pilakka-Kanthikeel et al., 2013). In a study, Fe_2O_3 was used for conjugation of peptide antisauvagine-30 (ASV-30) to reduce anxiety-like behavior of rats through binding to corticotropin releasing factor type 2 receptors (Vinzant et al., 2017). *In vivo* results demonstrated that systemic application of iron oxide+ASV-30 decreased anxiety (due to amphetamine withdrawal) with no impact on locomotion.

POLYMERIC NANOPARTICLES

For polymeric nanoparticles (PNPs), formulation, size, shape, surface chemistry and charge, porosity, mechanical strength, solubility, degradation rate and so on are among the features which can be adjusted for versatile purposes in TERM. Low cytotoxicity of PNPs, good biocompatibility, higher permeation and retention (EPR) effect, ability to deliver poorly soluble drugs and sustained release of them, retaining bioactivity of bioactive agents from enzymatic degradation for tissue engineering applications make PNPs as one of the fastest growing platform to overcome obstacles in TERM. Most of the new PNPs systems are designed to be sensitive to different physicochemical stimuli such as magnetic field, temperature, enzymes, pH, light, reducing/oxidizing agents which helps delivery or targeting systems with high specificity and efficiency for TERM applications (Cheng et al., 2013; Lale et al., 2014; Tang et al., 2016).

Composition, Manufacturing Process and Structure of Polymeric Nanoparticles

Classification of PNPs can be based on different criteria such as composition, structure and manufacturing process (**Figure 6**).

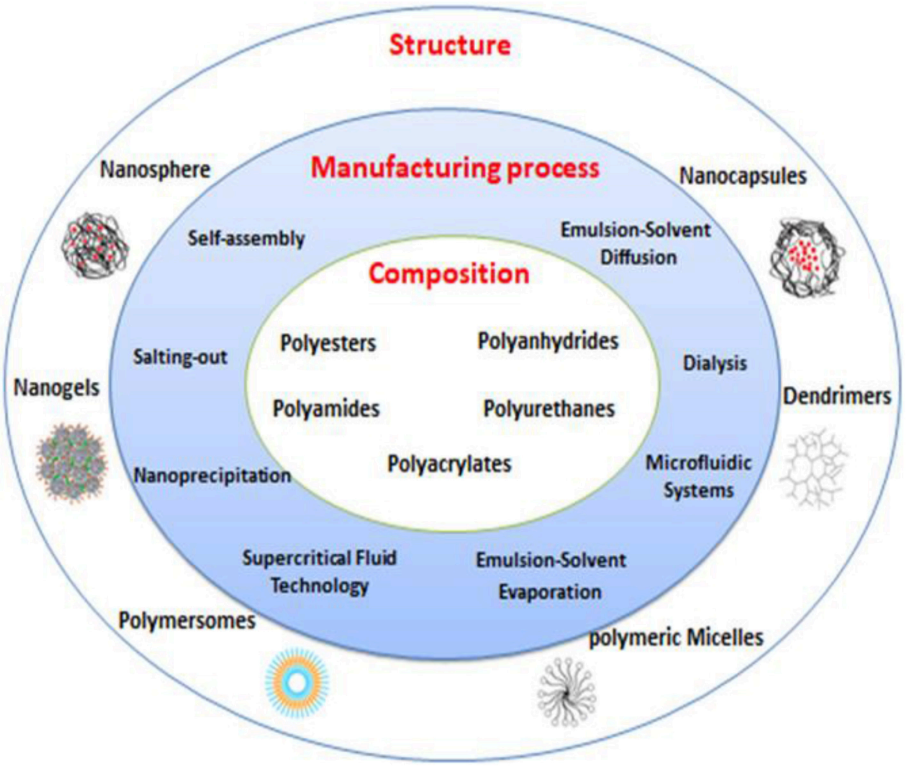

FIGURE 6 | Different polymeric nanoparticles (PNPs) based on composition, manufacturing process, and structure.

To achieve desired optimum properties, various PNPs have been designed using biodegradable and biocompatible natural and synthetic polymers. Polysaccharides (dextran, heparin, alginate, chitosan, hyaluronic acid, pullulan), proteins (albumin, gelatin, elastin, silk) and synthetic polymers such as polyesters, polyamides, polyanhydrides, polyurethanes, polyacrylates have been used alone or in conjugation with specific functional moieties or in combination with other materials to provide functionalities in TERM field (Nicolas et al., 2013; Hudson and Margaritis, 2014; Elsabahy et al., 2015; Bhatia, 2016); (Knopf-Marques et al., 2016).

PNPs can be manufactured in different shapes such as nanospheres, nanocapsules, polymersomes, dendrimers, polymeric micelles, and nanogels. Morphology of NPs will govern their macroscopic behavior; therefore, depending on the application, choosing suitable morphology is a critical point in manufacturing NPs (Nicolas et al., 2013; Bhatia, 2016); (Tang et al., 2016).

Different methods have been established for preparation of NPs such as various forms of emulsification (single and double emulsion/solvent evaporation, spontaneous emulsification, emulsion/solvent diffusion, emulsion polymerization), self-assembly, supercritical fluid (SCF) technology, nanoprecipitation, salting-out, dialysis, and microfluidic systems (Hasani-Sadrabadi et al., 2015; Bhatia, 2016; Tang et al., 2016; Herranz-Blanco et al., 2017).

Delivery of Bioactive Agents

Controlled delivery of bioactive compounds in TERM relies on the success of retention of the delivery vectors in the vicinity of regenerating tissue (Veiseh et al., 2015; Wang Q. et al., 2016). Designing a reproducible ECM which can resemble the complex nature of native tissue microenvironment with comparable mechanical strength can be obtained through choosing appropriate 3D scaffold design with incorporation of bioactive agent carriers (Barthes et al., 2015; Affolter-Zbaraszczuk et al., 2017). In recent years, to improve delivery of bioactive agents in the sense of loading, targeting, and efficacy, NP based systems have been changed from simple delivery to multifunctional responsive systems. Moreover, hybrid systems have been developed for integration of NPs within scaffolds for controlled release (Santo et al., 2010). The tailorable properties of PNPs provide versatile paths for designing NPs through applying chemical and physical techniques to optimize controlled delivery. It is crucial to control microenvironment of cells through physiochemical stimuli to anticipate and control behavior of cells in tissues. Introducing stimuli such as proteins and drugs into milieu of cells in the form of encapsulated NPs alone or embedded into delivery scaffolds such as hydrogels, fibers, foams, and so on, can provide the stable signals for cellular activities. Due to complex architecture of tissues such as different cell types and multicomponent extracellular matrix, it is inevitable to use nanoscale systems for delivering bioactive factors;

especially for multiple growth factors delivery in sequential and time dependent manner. Ability to tune release behavior from both PNPs and scaffolds through modifying composition, bulk and surface chemistry can provide delivery systems with spatiotemporal adjustable character suitable for targeted tissue (Chen et al., 2010; Jeon et al., 2013; Pérez et al., 2013); (Gaharwar et al., 2014).

Recently, plasma protein based NPs have gained attention due to their high bioavailability, non-toxicity, biodegradability, ease of manipulation, long *in vivo* half-lives and long shelf lives. There are more than 100,000 proteins in human plasma, but just a couple of these proteins have been used in TERM as a nanocarrier platform for imaging, drug delivery and tissue regeneration (Tezcaner et al., 2016). High density lipoproteins (HDL) NPs are among candidates for enhancing photodynamic therapy applications through presenting excellent tumor targeting and internalization capacity (Wang Y. et al., 2016; Raut et al., 2018). NPs from albumin, as the most abundant plasma protein, were used for bone regeneration through sustained release of bone morphogenetic protein-2 (BMP-2) (Wang Z. et al., 2016). Degeneration of the intervertebral disc (IVD) can happen due to several reasons such as enhanced local MMPs expression decreased quantities of ECM components which could lead to chronic lower back pain (Tong et al., 2017). IVD regeneration can be promoted using stem cell migration to the defect site. Zhang et al. have prepared albumin/heparin NPs as an injectable carrier for encapsulation of stromal cell-derived factor-1α (SDF-1α) as chemoattractant for the homing of bone marrow resident MSCs (Zhang et al., 2018). *In vitro* results have shown dose-dependent effect of SDF-1α over migration of the MSCs (at 50 and 100 ng/ml SDF-1α concentration, 41 and 64% MSCs migration after 24 h, respectively). Better regeneration compared to SDF-1α alone (control group) has been obtained as demonstrated by histological analysis, mRNA and protein levels for collagen type II, SOX9 and aggrecan.

Fibrin as another plasma protein has been used for encapsulation of VEGF for promoting the angiogenesis for wound healing applications (Mohandas et al., 2015). However, there are limited studies on plasma proteins. Disadvantages such as adverse immunological reaction, disease treatment, batch to batch variation or expensive isolation can be encountered in natural based materials; but plasma proteins have huge research potential as nanocarriers for TERM applications.

Bone tissue related diseases such as tumor or trauma generally are treated with bone grafts and substitutes. Nowadays TERM has provided an alternative approach for bone tissue regeneration through offering a variety form of 3D scaffolds. Bone scaffolds containing stem cells have the advantage of controlling the cellular activity such as differentiation, if appropriate bioactive agents such as drugs (e.g., dexamethasone) or growth factors [e.g., bone morphogenetic proteins (BMPs)] are incorporated in them (Basmanav et al., 2008; Santo et al., 2015; Wang et al., 2015). The ability to adjust degradation rate depends on physiological pH and intracellular drug release has led to manufacture of vast types of polymeric micelles as one of the widely used type of NPs. Santo et al. have designed a biodegradable pH responsive micelle from gelatin grafted with lactic acid oligomers and encapsulated dexamethasone (dex) for investigation the effect of intracellular release of dex for bone tissue regeneration (Santo et al., 2015). Efficient mineralized bone tissue formation was observed inside gelatin hydrogels containing dex loaded micelles seeded with pre-cultured rat bone marrow stem cells up to 4 weeks after implantation in rat ulna. In a work by Yilgor et al. how single or sequential or simultaneous growth factor delivery of BMP-2 in PLGA and BMP-7 in poly(3-hydroxybutyrate-co-3-hydroxyvalerate) (PHBV) nanocapsules in 3D chitosan and chitosan—poly(ethylene oxide) (PEO) fiber mesh constructs was studied (Yilgor et al., 2009). It was reported that rat bone marrow MSCs seeded on chitosan scaffolds which contains NPs providing sequential delivery release profile of BMP-2 (fast release) and BMP-7 (slow release), had the highest ALP activity per cell compared to those that interact with NPs loaded with one type of BMP or with those that provide the simultaneous release of two BMPs. The group reported that for sequential delivery, NPs adhered on the fibers demonstrated better than the NPs which were embedded within fiber structure.

Temperature sensitive poly(N-isopropylacrylamide) (PNIPAM) NPs have been developed for slow VEGF delivery within the collagen hydrogels (Adibfar et al., 2018). Endothelial differentiation of bone marrow derived MSCs and tube (capillary-like) formation in the hydrogels after 14 days of incubation in the osteogenic medium were observed. Expression of osteocalcin, collagen type I and runt-related transcription factor 2 as osteogenic markers besides the expressions of kinase insert domain receptor, von Willebrand factor and platelet-endothelial cell adhesion molecule-1 as angiogenic markers promoted the vasculature within bone tissue engineered constructs. Chen et al. have developed a conductive poly(aniline) NPs *in situ* in poly(L-lactide) PLLA/tetrahydrofuran through polymerization/thermal induced phase separation (TIPS) technique to produce PLLA based nanofibrous construct with conductivity feature for bone TE (Chen J. et al., 2018). Presence of well-distributed poly(aniline) NPs provided scaffolds with conductivity close to natural spongy bone. Higher proliferation, higher mineralization and osteogenic differentiation were observed on conductive scaffolds compared to control groups.

Angiogenesis as a key factor in TERM prevents cell necrosis in 3D scaffolds through providing nutrients, wastes and gas exchange. Delivery of angiogenesis triggering factors such as VEGF can enhance formation of blood vessels and promote tissue healing process. Various studies have been conducted for delivery of bioactive agents such as growth factors for promoting the neovascularization *in vitro* and *in vivo* (Lee et al., 2017; Wang B. et al., 2017). Controlled delivery of VEGF with appropriate release profile plays an important role in vascularization. VEGF loaded PCL NPs incorporated Poly(L-lysine)/hyaluronic acid polyelectrolyte multilayer film system has been reported as an approach for controlled delivery of VEGF for angiogenesis (Vrana et al., 2014). Xie et al. have embedded platelet-derived growth factor-BB (PDGF-BB) loaded PLGA NPs within VEGF loaded chitosan and PEO electrospun nanofibers for mimicking and promoting natural skin healing process (Xie et al., 2013). *In vitro* studies conducted with adult human dermal fibroblasts have shown that a fast delivery of VEGF as angiogenesis

promoter factor and PDGF-BB in delayed manner results in higher proliferation of fibroblasts. *In vivo* studies showed that use of nanoparticle/nanofiber scaffolds on rat skin resulted in faster wound healing compared to control groups due to increase in angiogenesis rate, re-epithelialization with quicker collagen deposition and earlier injury site remodeling.

Poor endothelialization and incomplete vascularization, can limit tissue-engineered scaffolds for regeneration of cardiovascular tissue damage. Tan et al. have established self-assembled NPs to accelerate vascularization of decellularized buffalo bovine jugular vein scaffolds through sustained release of VEGF (Tan et al., 2011). Low molecular weight heparin (LMWH) and N,N,N-trimethylchitosan chloride (TMC) which undergo self-assembly through non-covalent electrostatic interactions have been used to form NPs to protect bioactivity of VEGF. Results have demonstrated higher endothelial cell proliferation and new capillary formation, respectively. In another study, Izadifar et al. designed a bilayered NPs composed of PLGA as core and PLLA as shell polymers (Izadifar et al., 2016). They have used NPs of different compositions (PLGA and PLLA/PLGA bilayered) for obtaining sequential release of PDGF followed by co-release of VEGF and bFGF (basic fibroblast growth factor) as angiogenesis factors in fibrin matrix for cardiac tissue regeneration. *Ex vivo* angiogenesis using rat aortic ring assay has shown significant increase in the number of endothelial sprouts with maximum length of angiogenesis in sequential release group which was higher than that observed in simultaneous and only VEGF release groups.

Neuroregeneration through delivery of bioactive agents and stem cells has provided new opportunities for treating central and peripheral nervous systems related diseases (Liu et al., 2018). Local delivery and spatiotemporal control over the chemokine SDF-1 through various NP based delivery system has gained lots of attention as the SDF-1 can help recruitment and migration of neural stem cells (Dutta et al., 2017; Zamproni et al., 2017). Nerve growth factor loaded chitosan NPs have been used for neural differentiation of canine MSCs (Mili et al., 2018). Coupling controlled delivery with spatiotemporal control over release of nerve growth factor with SDF-1 could be an alternative way to enhance the regeneration of central and peripheral nervous systems related injuries. IVD can cause low back pain and lead to disability. Teixeira et al. have used chitosan as a natural biodegradable and biocompatible polysaccharide and ϒ-PGA as a naturally occurring peptide containing of D- and L-glutamic acids to form self-assembled NPs for encapsulation of anti-inflammatory drug, diclofenac (Df) for intervertebral disc regeneration through inhibition of inflammatory processes (Teixeira et al., 2016). Df-NPs have shown reduced proinflammatory mediators [Prostaglandin E2 (PGE2), Interleukin 6 (IL-6) and IL-8] and reduced the expression of MMP 1 and 3, while enhanced aggrecan and collagen type II in a pro-inflammatory/degenerative bovine IVD organ culture. A model for peripheral nerve injuries has been developed by Chang et al. to enhance axonal regrowth and promote nerve healing (Chang et al., 2017). Natural biodegradable multichanneled scaffolds composed of ordered electrospun nanofibers with neurotrophic gradient has been designed to control axon outgrowth. Brain derived neurotrophic factor was encapsulated in gelatin NPs and nerve growth factor has been added freely into the scaffold. Neurotrophic gradient for both growth factors have been provided using gradient maker. Gelatin-based multichanneled structure is designed to mimic the nerve fascicular structure with appropriate mechanical properties (**Figures 7A–E**). Early delivery of nerve growth factor enhanced the initial stage of axon regeneration, while delayed release of brain-derived neurotrophic factor in encapsulated gelatin NPs augmented the late stage of myelination process. Differentiated neural stem cells effectively extended their neurites along the aligned nanofibers and higher cell density was observed in regions with high NGF concentration.

Complex process of wound healing makes the full reconstruction of functional skin a challenging task after injuries. Various NP based dressings have been developed for delivering bioactive agents with spatiotemporal control for enhancing the wound healing process (Berthet et al., 2017; Ghalei et al., 2018; Follmann et al., 2019). Recently, Kheradvar et al. have designed NP based delivery system for vitamin E due to its antioxidant activity, anti-inflammatory and scar-prevention properties for wound healing applications (Kheradvar et al., 2018). To do so, core-sheath nanofibrous system composed of silk fibroin/PVA/aloe vera and vitamin E containing starch NPs prepared by electrospinning method was incorporated into this system during preparation. With encapsulation efficiency of 91.63% for vitamin E, *in vitro* results have shown that, presence of NPs and aloe vera has increased cellular viability and cell-matrix interactions. However, vitamin E was more efficient in improving antioxidant activity compared to aloe vera.

Surface features play a critical role in biocompatibility features of biomaterials and strength of host immune system reactions. In a study, polymer model based particles were manufactured from degradable mesoporous silica template and they were used to study the effect of various surface-cell interactions without substrate dependency (Song et al., 2017). Poly(N-(2 hydroxypropyl)methacrylamide) (PHPMA), PEG and poly(methacrylic acid) (PMAA) were used to produce NPs within mesoporous silica template. Residual particles were removed after template crosslinking. After crosslinking the resulted NPs, contained only interfacial polymer, each type of NPs has been evaluated *in vitro* and *in vivo* for stealth properties. PEG NPs have shown better stealth properties compared to PHPMA and PMAA. PMAA NPs has shown fast elimination from plasma and quickly absorbed by the liver and high monocyte and macrophage association *in vitro* and *ex vivo*. Aggregated levels of particles (PMA and PHPMA) in the major organs of the mononuclear phagocyte system were comparable while they were ∼2-fold higher than that of the PEG NPs. Similar systems can be applied for production of various NPs with similar structure but different type of materials and their biological response can be studied to select the most suitable candidate for various TERM applications.

Imaging and Contrast Agents

Among different diagnostic tools, imaging can visualize diseased tissues, tissue healing and stem cell fate through providing

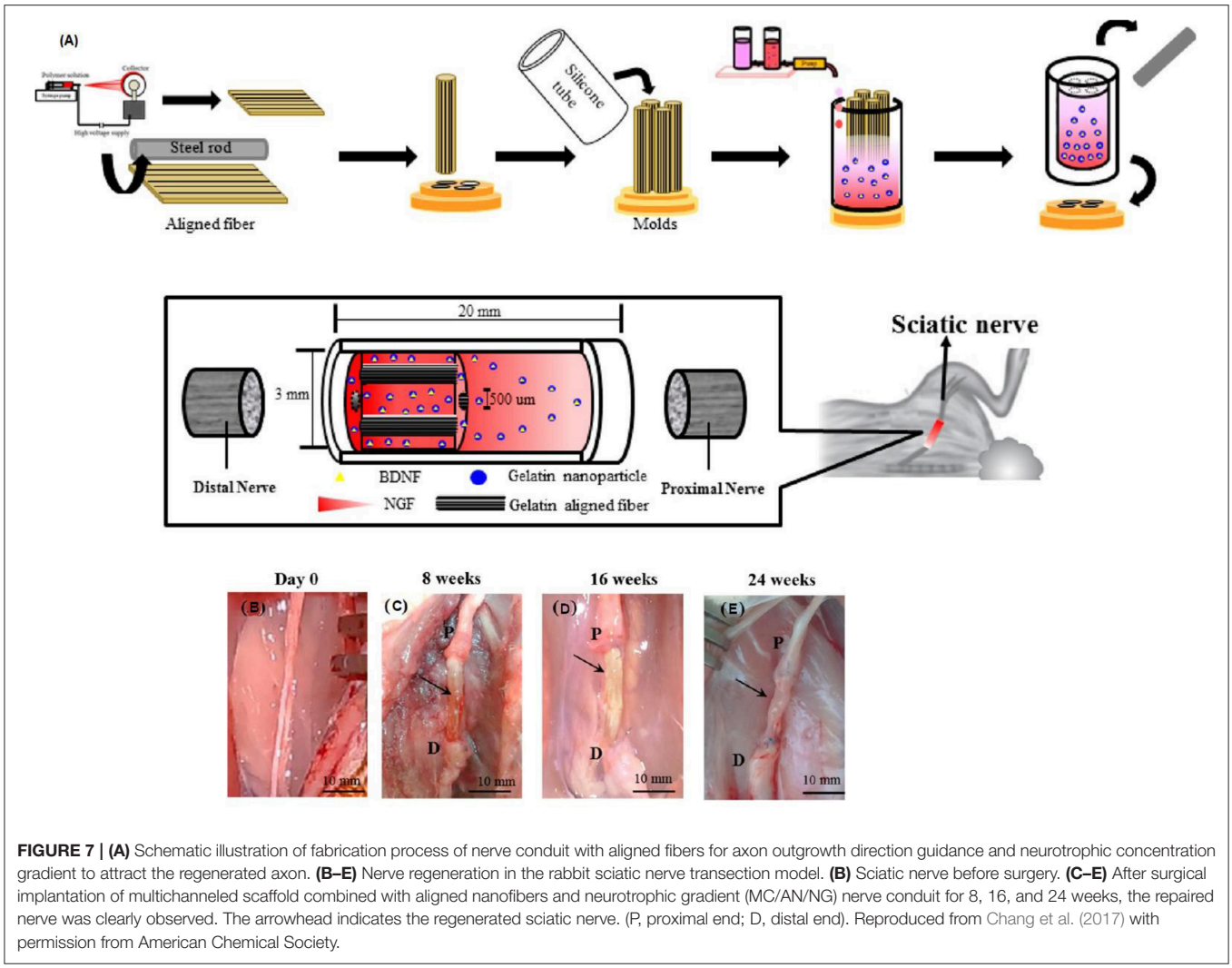

FIGURE 7 | (A) Schematic illustration of fabrication process of nerve conduit with aligned fibers for axon outgrowth direction guidance and neurotrophic concentration gradient to attract the regenerated axon. **(B–E)** Nerve regeneration in the rabbit sciatic nerve transection model. **(B)** Sciatic nerve before surgery. **(C–E)** After surgical implantation of multichanneled scaffold combined with aligned nanofibers and neurotrophic gradient (MC/AN/NG) nerve conduit for 8, 16, and 24 weeks, the repaired nerve was clearly observed. The arrowhead indicates the regenerated sciatic nerve. (P, proximal end; D, distal end). Reproduced from Chang et al. (2017) with permission from American Chemical Society.

contrast with respect to other tissues or by labeling NPs with an appropriate ligand. Fluorescent labeling, single photon emission computerized tomography (SPECT), ultrasound, MRI, NIR fluorescence imaging are among the widely used imaging techniques which alone or in conjugation with each other can provide sensitive, high resolution images from tissues through utilization of contrast agents (Harrison et al., 2014; Hong et al., 2014; Gu et al., 2017; Savla and Minko, 2017; Ekkelenkamp et al., 2018; Yan et al., 2018). Direct injection of contrast agents has poor outcomes due to short half-life, degradation, low concentration in desired tissue and toxicity at high dosages. Encapsulation of these imaging agents or attaching them on the surface of PNPs can provide longer half-life for circulation in body with efficient targeting in desired tissues.

Nowadays, most of visualizing and healing techniques have merged together for targeting the tumors by utilizing NPs with different moieties to act as both diagnostic and therapeutic tools. In TERM field it is also possible to label cells alone or within the scaffold to track the immune, differentiated and stem cells for disease treatment, tissue healing, cell migration and differentiation for monitoring applications. Molecular imprinted polymer (MIP) based NPs which are made through cell surface targeting molecular templates enable the construction of highly specific binding, 3D structures with affinity similar to antibodies for cell and tissue imaging. By mimicking glucuronic acid which is present in the form of hyaluronan on the surface of cells such as keratinocytes, Kunath et al. have imprinted glucurconic acid using (N-acrylamido) benzamidine (AAB) and methacrylamide (MAM) and polymerizable derivative of rhodamine as dye label for the detection of glycosylations on cell surface (Kunath et al., 2015). NPs applied on skin surface have shown localization of MIPs on the surface of keratinocytes without reducing cell viability. Detection of glycosylations on cell surfaces using MIP can provide a versatile synthetic tool to monitor compounds such as some glycanes which no natural receptors are available and decrease multiple labeling with various primary and secondary antibodies. Such MIPs can be also used for targeting of HA based scaffolds for monitoring scaffold behavior such as degradation.

Triggering of B cells' receptors by antigens causes priming of B and T cells and their differentiation to antibody secreting

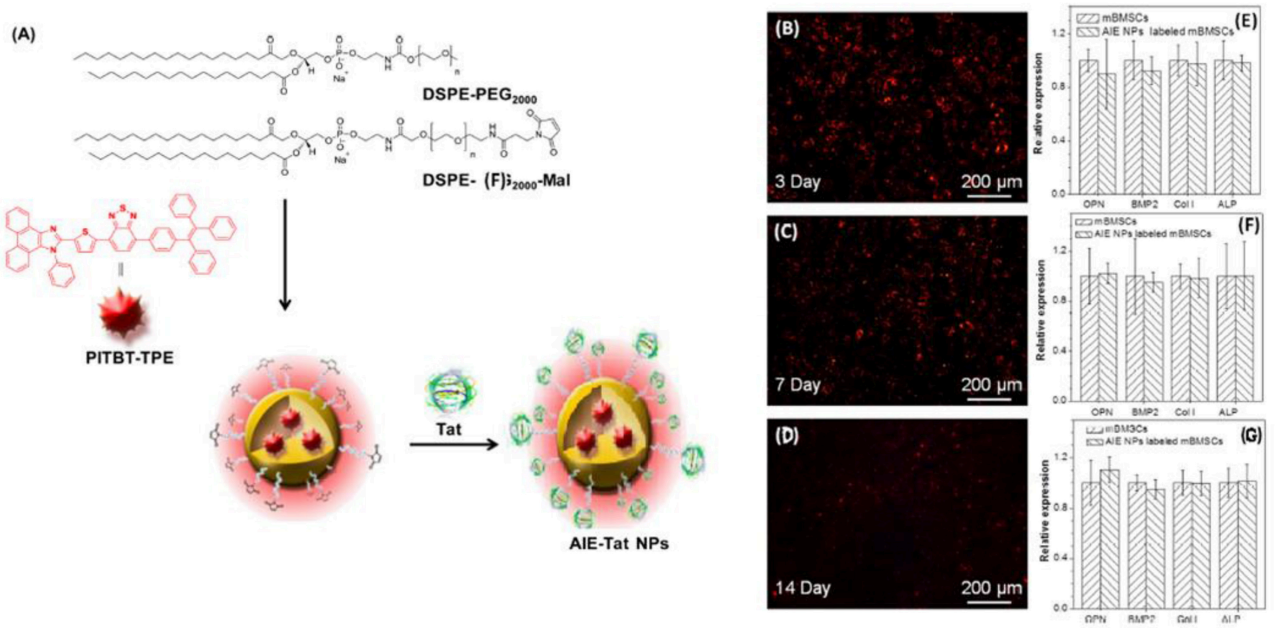

FIGURE 8 | (A) Fabrication of AIE-Tat NPs based on PITBT-TPE Fluorogen (**B–D)** Fluorescent images of mouse bone marrow MSCs grown on an HA scaffold. **(E–G)** RT-PCR results of OPN, BMP2, Col I, and ALP gene expression in AIE-Tat NP-labeled and unlabeled mouse bone marrow MSCs after osteogenic induction for 3, 7, and 14 days. Reproduced from Gao et al. (2016) with permission from American Chemical Society.

cells in the lymphoid organs. De Koker et al. have developed hydrogel NPs for antigen delivery in draining lymph nodes for immune cell subsets (De Koker et al., 2016). NPs were synthesized with infiltrating silica particles (mesoporous) with PMMA followed by disulfide-based crosslinking and Alexa Fluor 488-cadaverine (AF488) fluorescent labeling and template removal. PEGylated hydrogel NPs have shown higher lymph node targeting, consequently more dendritic and B cells turn into particle positive which followed by the priming of antigen-specific T cells. B cell activation has increased compared to non-PEGylated group. Similarly, modulating immune cells such as macrophages in TERM applications can provide more successful results through modulating immune responses such as inflammation especially for implant applications.

Stem cells can be used for treatment of various tissues such as bone, but tracking the fate of stem cells requires non-invasive labeling methods. Gao et al. have developed aggregation-induced emission (AIE) fluorogen of benzothiadiazole-based emissive aggregate, PITBT-TPE, NPs labeled with cell penetrating Tat peptides (AIE-Tat NPs) for monitoring/tracking of bone marrow MSCs in HA scaffolds for monitoring bone regeneration in mouse (Gao et al., 2016). AIE-Tat NPs treated scaffolds have shown long term internalization with bright fluorescence all along osteogenic differentiation for 2 weeks (**Figures 8A–G**). In another study conducted by Wang et al. rhodamine- conjugated core-crosslinking biodegradable elastomer poly(glycerol-co-sebacate) acrylate (PGSAR) NPs were prepared and compared with rhodamine encapsulated NPs for long term stem cell tracking (Wang L. et al., 2017). *In vivo* studies conducted with mice have shown that methyl cellulose embedded rhodamine conjugated NPs had 28.29% of its initial fluorescence signal at day 28 whereas encapsulated rhodamine NPs had undetectable fluorescent signal after 7 days.

NANOPARTICLES IN BIOINKS FOR 3D PRINTING

Currently 3D printing technologies have gained significant attraction in TERM field due to their superior control over design and manufacture of 3D scaffolds. Bioink as the main component of 3D bioprinting can be defined as a solution of one or more biomaterials which can be turned in to hydrogel form which encapsulate the required cell types. It can be stabilized or crosslinked during or after 3D printing through various mechanisms (Gungor-Ozkerim et al., 2018). Bioink based 3D printed scaffolds can provide a proper microenvironment for encapsulation of different cells within the hydrogels through modulating the biological, rheological and mechanical properties of scaffold (Gungor-Ozkerim et al., 2018). Integration of NPs within the 3D printed scaffolds can provide delivery bioactive agents for cells and tune mechanical strength of the scaffolds (Nowicki et al., 2017).

Synthetic polyurethanes (PU) have favorable mechanical properties, high biocompatibility, and tunable chemical structures which enable them to be used as 3D printing feeder for construction of custom made scaffolds. Hung et al. have used a synthetic biodegradable PU elastic NPs with hyaluronan (HA) as viscosity and cell aggregation enhancer, and Y27632 inhibitor as an alternative for transforming growth factor beta-3 (TGF-β3) for chondrogenic differentiation of MSCs as

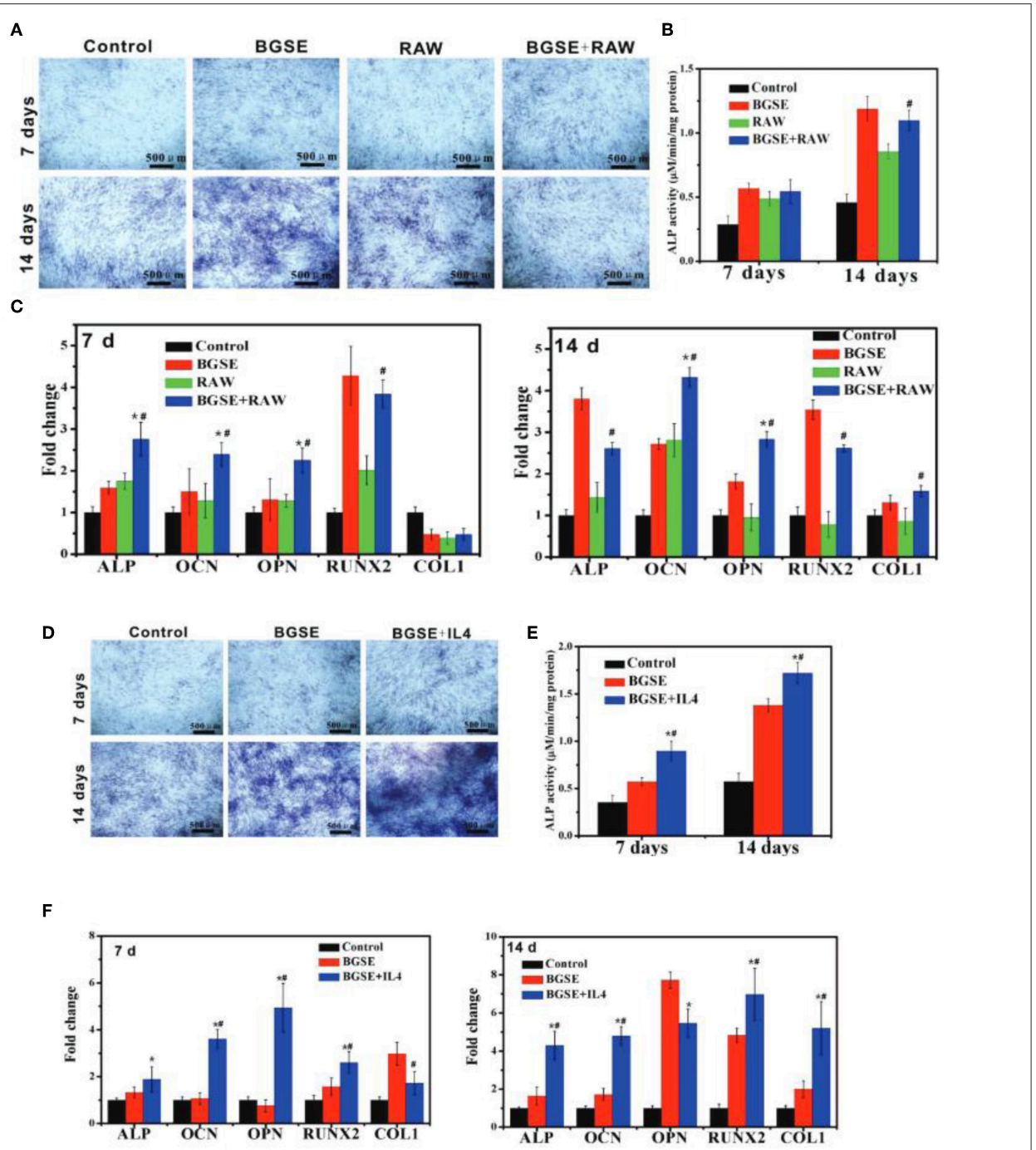

FIGURE 9 | (A-C) Osteogenic differentiation of 3T3 cells under inflammatory state. **(A)** ALP staining and **(B)** ALP quantitative assay of 3T3 cells after cultured for 7 and 14 days. **(C)** mRNA expression of osteogenesis-related genes (ALP, OCN, OPN, COL1, RUNX2) in 3T3 cells cultured for 7 and 14 days. $^{*}p < 0.05$ vs. BGSE (bioactive glass scaffolds extracts) group; $^{\#}p < 0.05$ vs. RAW (macrophage-like cell line) group. **(D–F)** Osteogenic differentiation of 3T3 cells in anti-inflammatory state. **(D)** ALP staining and **(E)** ALP quantitative assay of 3T3 cells after being treated with various samples for 7 and 14 days. **(F)** mRNA expression of osteogenesis-related genes (ALP, OCN, OPN, COL1, RUNX2) of 3T3 cells incubated with various groups for 7 and 14 days. $^{*}p < 0.05$ vs. blank control; $^{\#}p < 0.05$ vs. BGSE group. Reproduced from Zhao et al. (2018) with permission from John Wiley and Sons.

manufacture feeder materials (ink) for water based 3D printing for customized cartilage tissue engineering (Hung et al., 2016). *In vivo* implantation of scaffolds in rabbit knee with adipose-derived stem cells had resulted in better regeneration with significantly more type II collagen production compared to PU/HA—or PLGA scaffolds seeded with MSCs. In another similar study using PU NPs Lin et al. have developed thermoresponsive 3D bioink of waterborne PCL based biodegradable PU with a soft

segment replaced with 20 mol% of PLLA diol or poly(D,L-lactide) (PDLLA) diol to form two different PU NPs (Lin et al., 2016). To decrease gelation time soy protein isolate (SPI) was also blended with PU NPs. Neural stem cells (NSCs) were embedded within the ink prior to printing. The cell laden bioprinted NSCs in the PU/SPI hybrid hydrogel have shown better cell viability and proliferation than those in the PU gel. Same group has also investigated the effect of graphene on the PU hydrogels for neural tissue engineering (Huang et al., 2017). It has been reported that addition of graphene nanomaterials at very low amount (25 ppm) into the hydrogel considerably improved the oxygen metabolism (2- to 4-fold increase) along with the neural differentiation of neural stem cells in 3D printed constructs. A similar study based on dual (photo/thermo) responsive PU NPs has reported that hydrogels were developed with tunable mechanical properties upon heating the biodegradable PU NPs (Hsiao and Hsu, 2018). Cells can be easily added to the bioink prior to printing for production of cell-laden scaffolds using microextrusion-based 3D printing due to shear thinning characteristic of hydrogels at 37°C. A handable (tofu-like) and stable scaffold with inductive 3D microenvironment for differentiation of neural stem cells can be obtained using softer hydrogels with low modulus (<1 kPa).

Application of 3D printing for bone tissue applications generally requires, heating or chemical procedures during fabrication due to mechanical constraints which limits the encapsulation of cells in scaffolds. To rectify these restrictions bioink printed hydrogel scaffolds have been developed for bone grafts. These scaffolds can mimic the bone extracellular matrix for cell migration, proliferation and differentiation but lack enough mechanical strength for bone tissue application arising from nature of biomaterials used in bioink. Incorporation of nBGs and HAp NPs can increase compressive moduli of the scaffolds. Gao et al. have produced a poly(ethylene glycol) dimethacrylate (PEGDMA) 3D printed scaffold containing bioactive glass (BG) 45S5 or HAp NPs for bone marrow derived human MSCs encapsulation (Gao et al., 2014). Scaffolds containing HAp NPs have shown higher, compressive modulus, cell viability, production of collagen and ALP activity by the cells in comparison to BG 45S5 group after 21 days of culturing. In a recent study Zhao et al. have synthesized nBGs and 3D printed by mixing nBGs with PVA and investigated the effect of this structure on immunomodulation associated mechanism of osteogenesis in the extramembranous which occurs outside the cortical bone (Zhao et al., 2018). Peripheral macrophage-conditioned medium used in culturing calvaria preosteoblasts following the stimulation with nBGs. It promoted migration of preosteoblast, but osteogenic differentiation was effected restrictedly. On the other hand, the anti-inflammatory milieu and nBGs considerably increased preosteoblasts' osteogenic differentiation (**Figures 9A–F**). *In vivo* results have shown active extramembranous osteogenesis.

CONCLUSION

In vivo maturation of engineered tissues requires a well synchronized series of events involving host immune system, circulatory system and cellular component of the implanted material. Physicochemical properties of the scaffolds and the presence/immobilization of bioactive agents within the scaffolds can help in achieving a precise control over maturation. Herein, we reviewed the use of nanoscale structures with different material properties for enhancing the properties of tissue engineering scaffolds by rendering them antimicrobial, providing sequential release of several growth factors, by concentrating necessary contrasting agents for monitoring, by improving mechanical properties of bioprinted structures as bioink supplements and also by providing structural elements such a HAp in nanoscale to induce tissue specific reactions. The future tissue engineering solutions might contain multiple components for all these aspects to have higher control over integration, monitoring and long-term safety of engineered tissues. Focus of nanoscale delivery systems should not only be on manufacturing advanced delivery systems but also on also on evaluating systemic cytotoxic effect and immune responses of these systems. Such studies could provide better understanding of biocompatibility of vast numbers of nanoscale delivery systems and will direct the future studies with higher success rate in cost-effective approach. For this aim, the different nanoparticle types of different materials (metals, ceramics, magnetic/paramagnetic materials and polymers) provide a strong toolbox for tissue engineered artificial organ functionalization.

AUTHOR CONTRIBUTIONS

NV proposed the topic. MF-A, HK-M, CRdS, and JB wrote the initial and revised drafts. EB, AT, and NV provided feedback through the writing process and completed revisions based on feedback provided.

FUNDING

This work has received funding from the European Union's Seventh Framework Programme for research and technological development and demonstration (Grant number 606294, IMMODGEL) and also from the European Union's Horizon 2020 research and innovation programme under grant agreement No 760921 (PANBioRA).

REFERENCES

Abbasi, E., Milani, M., Fekri Aval, S., Kouhi, M., Akbarzadeh, A., Tayefi Nasrabadi, H., et al. (2016). Silver nanoparticles: synthesis methods, bio-applications and properties. *Crit. Rev. Microbiol.* 42, 173–180. doi: 10.3109/1040841X.2014.912200

Adibfar, A., Amoabediny, G., Eslaminejad, M. B., Mohamadi, J., Bagheri, F., and Doulabi, B. Z. (2018). VEGF delivery by smart polymeric

PNIPAM nanoparticles affects both osteogenic and angiogenic capacities of human bone marrow stem cells. *Mater. Sci. Eng. C* 93, 790–799. doi: 10.1016/j.msec.2018.08.037

Affolter-Zbaraszczuk, C., Ozcelik, H., Meyer, F., Gallet, O., Lavalle, P., Ball, V., et al. (2017). Hybrid extracellular matrix microspheres for development of complex multicellular architectures. *RSC Adv.* 7, 5528–5532. doi: 10.1039/C6RA27680F

Ahmed, S., Ahmad, M., Swami, B. L., and Ikram, S. (2016). A review on plants extract mediated synthesis of silver nanoparticles for antimicrobial applications: a green expertise. *Adv. Res.* 7, 17–28. doi: 10.1016/j.jare.2015.02.007

Akturk, O., Kismet, K., Yasti, A. C., Kuru, S., Duymus, M. E., Kaya, F., et al. (2016). Wet electrospun silk fibroin/gold nanoparticle 3D matrices for wound healing applications. *RSC Adv.* 6, 13234–13250. doi: 10.1039/C5RA24225H

Ali, M. R., Wu, Y., Ghosh, D., Do, B. H., Chen, K., Dawson, M. R., et al. (2017). Nuclear membrane-targeted gold nanoparticles inhibit cancer cell migration and invasion. *ACS Nano* 11, 3716–3726. doi: 10.1021/acsnano.6b08345

Alivisatos, A. P., Johnsson, K. P., Peng, X., Wilson, T. E., Loweth, C. J., Bruchez Jr., M. P., et al. (1996). Organization of 'nanocrystal molecules' using DNA. *Nature* 382, 609. doi: 10.1038/382609a0

Alon, N., Havdala, T., Skaat, H., Baranes, K., Marcus, M., Levy, I., et al. (2015). Magnetic micro-device for manipulating PC12 cell migration and organization. *Lab Chip* 15, 2030–2036. doi: 10.1039/C5LC00035A

Alshemary, A. Z., Engin Pazarceviren, A., Tezcaner, A., and Evis, Z. (2017). Fe3+/SeO42– dual doped nano hydroxyapatite: a novel material for biomedical applications. *J. Biomed. Mater. Res. B Appl. Biomater.* 106, 340–352. doi: 10.1002/jbm.b.33838

Amoli-Diva, M., Sadighi-Bonabi, R., and Pourghazi, K. (2017). Switchable on/off drug release from gold nanoparticles-grafted dual light- and temperature-responsive hydrogel for controlled drug delivery. *Mater. Sci. Eng. C.* 76, 242–248. doi: 10.1016/j.msec.2017.03.038

Ataol, S., Tezcaner, A., Duygulu, O., Keskin, D., and Machin, N. E. (2015). Synthesis and characterization of nanosized calcium phosphates by flame spray pyrolysis, and their effect on osteogenic differentiation of stem cells. *J. Nanopart. Res.* 17:95. doi: 10.1007/s11051-015-2901-0

Augustine, R., Kalarikkal, N., and Thomas, S. (2016). Electrospun PCL membranes incorporated with biosynthesized silver nanoparticles as antibacterial wound dressings. *Appl. Nanosci.* 6, 337–344. doi: 10.1007/s13204-015-0439-1

Azizi, S., Ahmad, M. B., Namvar, F., and Mohamad, R. (2014). Green biosynthesis and characterization of zinc oxide nanoparticles using brown marine macroalga Sargassum muticum aqueous extract. *Mater. Lett.* 116, 275–277. doi: 10.1016/j.matlet.2013.11.038

Bahal, R., Ali McNeer, N., Quijano, E., Liu, Y., Sulkowski, P., Turchick, A., et al. (2016). *In vivo* correction of anaemia in β-thalassemic mice by γPNA-mediated gene editing with nanoparticle delivery. *Nat. Commun.* 7:13304. doi: 10.1038/ncomms13304

Barthes, J., Vrana, N. E., Ozcelik, H., Gahoual, R., Francois, Y. N., Bacharouche, J., et al. (2015). Priming cells for their final destination: microenvironment controlled cell culture by a modular ECM-mimicking feeder film. *Biomater. Sci.* 3, 1302–1311. doi: 10.1039/C5BM00172B

Basmanav, F. B., Kose, G. T., and Hasirci, V. (2008). Sequential growth factor delivery from complexed microspheres for bone tissue engineering. *Biomaterials* 29, 4195–4204. doi: 10.1016/j.biomaterials.2008.07.017

Berthet, M., Gauthier, Y., Lacroix, C., Verrier, B., and Monge, C. (2017). Nanoparticle-based dressing: the future of wound treatment? *Trends Biotechnol.* 35, 770–784. doi: 10.1016/j.tibtech.2017.05.005

Bhatia, S. (2016). "Nanoparticles types, classification, characterization, fabrication methods and drug delivery applications," in *Natural Polymer Drug Delivery Systems: Nanoparticles, Plants, and Algae* (Cham: Springer International Publishing), 33–93.

Bhowmick, A., Banerjee, S. L., Pramanik, N., Jana, P., Mitra, T., Gnanamani, A., et al. (2018). Organically modified clay supported chitosan/hydroxyapatite-zinc oxide nanocomposites with enhanced mechanical and biological properties for the application in bone tissue engineering. *Int. J. Biol. Macromol.* 106, 11–19. doi: 10.1016/j.ijbiomac.2017.07.168

Bhowmick, S., and Koul, V. (2016). Assessment of PVA/silver nanocomposite hydrogel patch as antimicrobial dressing scaffold: synthesis, characterization and biological evaluation. *Mater. Sci. Eng. C.* 59, 109–119. doi: 10.1016/j.msec.2015.10.003

Biswas, D. P., O'Brien-Simpson, N. M., Reynolds, E. C., O'Connor, A. J., and Tran, P. A. (2018). Comparative study of novel *in situ* decorated porous chitosan-selenium scaffolds and porous chitosan-silver scaffolds towards antimicrobial wound dressing application. *J. Colloid Interface Sci.* 515, 78–91. doi: 10.1016/j.jcis.2018.01.007

Boccaccini, A. R., Erol, M., Stark, W. J., Mohn, D., Hong, Z., and Mano, J. F. (2010). Polymer/bioactive glass nanocomposites for biomedical applications: a review. *Compos. Sci. Technol.* 70, 1764–1776. doi: 10.1016/j.compscitech.2010.06.002

Cai, X., ten Hoopen, S., Zhang, W., Yi, C., Yang, W., Yang, F., et al. (2017). Influence of highly porous electrospun PLGA/PCL/nHA fibrous scaffolds on the differentiation of tooth bud cells *in vitro*. *J. Biomed. Mater. Res. A* 105, 2597–2607. doi: 10.1002/jbm.a.36120

Chang, Y.-C., Chen, M.-H., Liao, S.-Y., Wu, H.-C., Kuan, C.-H., Sun, J.-S., et al. (2017). Multichanneled nerve guidance conduit with spatial gradients of neurotrophic factors and oriented nanotopography for repairing the peripheral nervous system. *ACS Appl. Mater. Interfaces* 9, 37623–37636. doi: 10.1021/acsami.7b12567

Chen, F. M., Zhang, M., and Wu, Z. F. (2010). Toward delivery of multiple growth factors in tissue engineering. *Biomaterials* 31, 6279–6308. doi: 10.1016/j.biomaterials.2010.04.053

Chen, J., Yu, M., Guo, B., Ma, P. X., and Yin, Z. (2018). Conductive nanofibrous composite scaffolds based on *in-situ* formed polyaniline nanoparticle and polylactide for bone regeneration. *J. Colloid Interface Sci.* 514, 517–527. doi: 10.1016/j.jcis.2017.12.062

Chen, X., Lei, B., Wang, Y., and Zhao, N. (2009). Morphological control and *in vitro* bioactivity of nanoscale bioactive glasses. *J. Non-Cryst. Solids* 355, 791–796. doi: 10.1016/j.jnoncrysol.2009.02.005

Chen, Y.-W., Hsieh, S.-C., Yang, Y.-C., Hsu, S.-H., Kung, M.-L., Lin, P.-Y., et al. (2018). Functional engineered mesenchymal stem cells with fibronectin-gold composite coated catheters for vascular tissue regeneration. *Nanomedicine* 14, 699–711. doi: 10.1016/j.nano.2017.12.023

Cheng, C. J., Tietjen, G. T., Saucier-Sawyer, J. K., and Saltzman, W. M. (2015). A holistic approach to targeting disease with polymeric nanoparticles. *Nat. Rev. Drug Discov.* 14, 239–247. doi: 10.1038/nrd4503

Cheng, R., Meng, F., Deng, C., Klok, H.-A., and Zhong, Z. (2013). Dual and multi-stimuli responsive polymeric nanoparticles for programmed site-specific drug delivery. *Biomaterials* 34, 3647–3657. doi: 10.1016/j.biomaterials.2013.01.084

Colson, Y. L., and Grinstaff, M. W. (2012). Biologically responsive polymeric nanoparticles for drug delivery. *Adv. Mater.* 24, 3878–3886. doi: 10.1002/adma.201200420

Covarrubias, C., Cádiz, M., Maureira, M., Celhay, I., Cuadra, F., and von Marttens, A. (2018). Bionanocomposite scaffolds based on chitosan–gelatin and nanodimensional bioactive glass particles: *in vitro* properties and *in vivo* bone regeneration. *J. Biomater. Appl.* 32, 1155–1163. doi: 10.1177/0885328218759042

Cox, S. C., Jamshidi, P., Grover, L. M., and Mallick, K. K. (2014). Preparation and characterisation of nanophase Sr, Mg, and Zn substituted hydroxyapatite by aqueous precipitation. *Mater. Sci. Eng. C.* 35, 106–114. doi: 10.1016/j.msec.2013.10.015

Dalgic, A. D., Alshemary, A. Z., Tezcaner, A., Keskin, D., and Evis, Z. (2018). Silicate-doped nano-hydroxyapatite/graphene oxide composite reinforced fibrous scaffolds for bone tissue engineering. *J. Biomater. Appl.* 32, 1392–1405. doi: 10.1177/0885328218763665

Daniel, M.-C., and Astruc, D. (2004). Gold nanoparticles: assembly, supramolecular chemistry, quantum-size-related properties, and applications toward biology, catalysis, and nanotechnology. *Chem. Rev.* 104, 293–346. doi: 10.1021/cr030698+

De Koker, S., Cui, J., Vanparijs, N., Albertazzi, L., Grooten, J., Caruso, F., et al. (2016). Engineering polymer hydrogel nanoparticles for lymph node-targeted delivery. *Angew. Chem. Int. Ed. Eng.* 55, 1334–1339. doi: 10.1002/anie.201508626

del Mar Encabo-Berzosa, M., Sancho-Albero, M., Crespo, A., Andreu, V., Sebastian, V., Irusta, S., et al. (2017). The effect of PEGylated hollow gold nanoparticles on stem cell migration: potential application in tissue regeneration. *Nanoscale* 9, 9848–9858. doi: 10.1039/C7NR01853C

Dobson, J. (2006). Gene therapy progress and prospects: magnetic nanoparticle-based gene delivery. *Gene Ther.* 13:283. doi: 10.1038/sj.gt.3302720

Dutta, D., Hickey, K., Salifu, M., Fauer, C., Willingham, C., and Stabenfeldt, S. (2017). Spatiotemporal presentation of exogenous SDF-1 with PLGA

nanoparticles modulates SDF-1/CXCR4 signaling axis in the rodent cortex. *Biomater. Sci.* 5, 1640–1651. doi: 10.1039/C7BM00489C

Dvir, T., Timko, B. P., Kohane, D. S., and Langer, R. (2011). Nanotechnological strategies for engineering complex tissues. *Nat. Nano* 6, 13–22. doi: 10.1038/nnano.2010.246

Ekkelenkamp, A. E., Elzes, M. R., Engbersen, J. F., and Paulusse, J. M. (2018). Responsive crosslinked polymer nanogels for imaging and therapeutics delivery. *J. Mater. Chem. B* 6, 210–235. doi: 10.1039/C7TB02239E

Elsabahy, M., Heo, G. S., Lim, S.-M., Sun, G., and Wooley, K. L. (2015). Polymeric nanostructures for imaging and therapy. *Chem. Rev.* 115, 10967–11011. doi: 10.1021/acs.chemrev.5b00135

Ergun, C., Webster, T. J., Bizios, R., and Doremus, R. H. (2002). Hydroxylapatite with substituted magnesium, zinc, cadmium, and yttrium. I. Structure and microstructure. *J. Biomed. Mater. Res. B* 59, 305–311. doi: 10.1002/jbm.1246

Fei Yin, Z., Wu, L., Gui Yang, H., and Hua Su, Y. (2013). Recent progress in biomedical applications of titanium dioxide. *Phys. Chem. Chem. Phys.* 15, 4844–4858. doi: 10.1039/C3CP43938K

Ferraz, M. P., Monteiro, F. J., and Manuel, C. M. (2004). Hydroxyapatite nanoparticles: a review of preparation methodologies. *J. Appl. Biomater. Biomech.* 2, 74–80. doi: 10.1177/228080000400200202

Fihri, A., Len, C., Varma, R. S., and Solhy, A. (2017). Hydroxyapatite: a review of syntheses, structure and applications in heterogeneous catalysis. *Coord. Chem. Rev.* 347, 48–76. doi: 10.1016/j.ccr.2017.06.009

Follmann, H. D., Messias, I., Queiroz, M. N., Araujo, R. A., Rubira, A. F., and Silva, R. (2019). Designing hybrid materials with multifunctional interfaces for wound dressing, electrocatalysis, and chemical separation. *J. Colloid Interface Sci.* 533, 106–125. doi: 10.1016/j.jcis.2018.08.007

Frattini, A., Pellegri, N., Nicastro, D., and De Sanctis, O. (2005). Effect of amine groups in the synthesis of Ag nanoparticles using aminosilanes. *Mater. Chem. Phys.* 94, 148–152. doi: 10.1016/j.matchemphys.2005.04.023

Frens, G. (1973). Controlled nucleation for the regulation of the particle size in monodisperse gold suspensions. *Nat. Phys. Sci.* 241:20. doi: 10.1038/physci241020a0

Gaharwar, A. K., Peppas, N. A., and Khademhosseini, A. (2014). Nanocomposite hydrogels for biomedical applications. *Biotechnol. Bioeng.* 111, 441–453. doi: 10.1002/bit.25160

Gao, G., Schilling, A. F., Yonezawa, T., Wang, J., Dai, G., and Cui, X. (2014). Bioactive nanoparticles stimulate bone tissue formation in bioprinted three-dimensional scaffold and human mesenchymal stem cells. *Biotechnol. J.* 9, 1304–1311. doi: 10.1002/biot.201400305

Gao, M., Chen, J., Lin, G., Li, S., Wang, L., Qin, A., et al. (2016). Long-term tracking of the osteogenic differentiation of mouse BMSCs by aggregation-induced emission nanoparticles. *ACS Appl. Mater. Interfaces* 8, 17878–17884. doi: 10.1021/acsami.6b05471

Gentemann, L., Kalies, S., Coffee, M., Meyer, H., Ripken, T., Heisterkamp, A., et al. (2017). Modulation of cardiomyocyte activity using pulsed laser irradiated gold nanoparticles. *Biomed. Opt. Express* 8, 177–192. doi: 10.1364/BOE.8.000177

Ghalei, S., Asadi, H., and Ghalei, B. (2018). Zein nanoparticle-embedded electrospun PVA nanofibers as wound dressing for topical delivery of anti-inflammatory diclofenac. *J. Appl. Polym. Sci.* 135:46643. doi: 10.1002/app.46643

Ghosh, M., Halperin-Sternfeld, M., Grigoriants, I., Lee, J., Nam, K. T., and Adler-Abramovich, L. (2017). Arginine-presenting peptide hydrogels decorated with hydroxyapatite as biomimetic scaffolds for bone regeneration. *Biomacromolecules* 18, 3541–3550. doi: 10.1021/acs.biomac.7b00876

Giannaccini, M., Calatayud, M. P., Poggetti, A., Corbianco, S., Novelli, M., Paoli, M., et al. (2017). Magnetic nanoparticles for efficient delivery of growth factors: stimulation of peripheral nerve regeneration. *Adv. Healthc. Mater.* 6:1601429. doi: 10.1002/adhm.201601429

Gu, X., Kwok, R. T., Lam, J. W., and Tang, B. Z. (2017). AIEgens for biological process monitoring and disease theranostics. *Biomaterials* 146, 115–135. doi: 10.1016/j.biomaterials.2017.09.004

Gungor-Ozkerim, P. S., Inci, I., Zhang, Y. S., Khademhosseini, A., and Dokmeci, M. R. (2018). Bioinks for 3D bioprinting: an overview. *Biomater. Sci.* 6, 915–946. doi: 10.1039/C7BM00765E

Guo, M., Dong, Y., Xiao, J., Gu, R., Ding, M., Huang, T., et al. (2018). *In vivo* immuno-reactivity analysis of the porous three-dimensional chitosan/SiO2 and chitosan/SiO2/hydroxyapatite hybrids. *J. Biomed. Mater. Res. A* 106, 1223–1235. doi: 10.1002/jbm.a.36320

Guo, Y., Xue, Y., Niu, W., Chen, M., Wang, M., Ma, P. X., et al. (2018). Monodispersed bioactive glass nanoparticles enhance the osteogenic differentiation of adipose-derived stem cells through activating TGF-Beta/Smad3 signaling pathway. *Part. Part. Syst. Charact.* 35:1800087. doi: 10.1002/ppsc.201800087

Gupta, A. K., and Gupta, M. (2005). Synthesis and surface engineering of iron oxide nanoparticles for biomedical applications. *Biomaterials* 26, 3995–4021. doi: 10.1016/j.biomaterials.2004.10.012

Gupta, S. M., and Tripathi, M. (2011). A review of TiO2 nanoparticles. *Chin. Sci. Bull.* 56:1639. doi: 10.1007/s11434-011-4476-1

Gurunathan, S., Han, J. W., Kwon, D.-N., and Kim, J.-H. (2014). Enhanced antibacterial and anti-biofilm activities of silver nanoparticles against Gram-negative and Gram-positive bacteria. *Nanoscale Res. Lett.* 9:373. doi: 10.1186/1556-276X-9-373

Guzmán, M. G., Dille, J., and Godet, S. (2009). Synthesis of silver nanoparticles by chemical reduction method and their antibacterial activity. *Int. J. Chem. Biomol. Eng.* 2, 104–111.

Han, J.-K., Song, H.-Y., Saito, F., and Lee, B.-T. (2006). Synthesis of high purity nano-sized hydroxyapatite powder by microwave-hydrothermal method. *Mater. Chem. Phys.* 99, 235–239. doi: 10.1016/j.matchemphys.2005.10.017

Harrison, R. H., St-Pierre, J. P., and Stevens, M. M. (2014). Tissue engineering and regenerative medicine: a year in review. *Tissue Eng. Part B Rev.* 20, 1–16. doi: 10.1089/ten.TEB.2013.0668

Hasani-Sadrabadi, M. M., Pour Hajrezaei, S., Hojjati Emami, S., Bahlakeh, G., Daneshmandi, L., Dashtimoghadam, E., et al. (2015). Enhanced osteogenic differentiation of stem cells via microfluidics synthesized nanoparticles. *Nanomedicine* 11, 1809–1819. doi: 10.1016/j.nano.2015.04.005

Heo, D. N., Ko, W.-K., Bae, M. S., Lee, J. B., Lee, D.-W., Byun, W., et al. (2014). Enhanced bone regeneration with a gold nanoparticle–hydrogel complex. *J. Mater. Chem. B* 2, 1584–1593. doi: 10.1039/C3TB21246G

Herranz-Blanco, B., Ginestar, E., Zhang, H., Hirvonen, J., and Santos, H. A. (2017). Microfluidics platform for glass capillaries and its application in droplet and nanoparticle fabrication. *Int. J. Pharm.* 516, 100–105. doi: 10.1016/j.ijpharm.2016.11.024

Hidouri, M., Dorozhkin, S. V., and Albeladi, N. (2018). Thermal behavior, sintering and mechanical characterization of multiple ion-substituted hydroxyapatite bioceramics. *J. Inorg. Organomet. Polym. Mater.* 29, 87–100. doi: 10.1007/s10904-018-0969-6

Hong, G., Zou, Y., Antaris, A. L., Diao, S., Wu, D., Cheng, K., et al. (2014). Ultrafast fluorescence imaging *in vivo* with conjugated polymer fluorophores in the second near-infrared window. *Nat. Commun.* 5:4206. doi: 10.1038/ncomms5206

Hong, K. H., Park, J. L., Sul, I. H., Youk, J. H., and Kang, T. J. (2006). Preparation of antimicrobial poly (vinyl alcohol) nanofibers containing silver nanoparticles. *J. Polym. Sci. B* 44, 2468–2474. doi: 10.1002/polb.20913

Hosoyama, K., Ahumada, M., McTiernan, C., Bejjani, J., Variola, F., Ruel, M., et al. (2017). Multi-functional thermo-crosslinkable collagen-metal nanoparticle composites for tissue regeneration: nanosilver vs. *nanogold. RSC Adv.* 7, 47704–47708. doi: 10.1039/C7RA08960K

Hsiao, S.-H., and Hsu, S.-,h. (2018). Synthesis and characterization of dual stimuli-sensitive biodegradable polyurethane soft hydrogels for 3D cell-laden bioprinting. *ACS Appl. Mater. Interfaces* 10, 29273–29287. doi: 10.1021/acsami.8b08362

Huang, C.-T., Shrestha, L. K., Ariga, K., and Hsu, S.-H. (2017). A graphene–polyurethane composite hydrogel as a potential bioink for 3D bioprinting and differentiation of neural stem cells. *J. Mater. Chem. B* 5, 8854–8864. doi: 10.1039/C7TB01594A

Hudson, D., and Margaritis, A. (2014). Biopolymer nanoparticle production for controlled release of biopharmaceuticals. *Crit. Rev. Biotechnol.* 34, 161–179. doi: 10.3109/07388551.2012.743503

Hung, K. C., Tseng, C. S., Dai, L. G., and Hsu, S. H. (2016). Water-based polyurethane 3D printed scaffolds with controlled release function for customized cartilage tissue engineering. *Biomaterials* 83, 156–168. doi: 10.1016/j.biomaterials.2016.01.019

Iravani, S., Korbekandi, H., Mirmohammadi, S. V., and Zolfaghari, B. (2014). Synthesis of silver nanoparticles: chemical, physical and biological methods. *Res. Pharm. Sci.* 9, 385–406.

Izadifar, M., Kelly, M. E., and Chen, X. (2016). Regulation of sequential release of growth factors using bilayer polymeric nanoparticles for cardiac tissue engineering. *Nanomedicine* 11, 3237–3259. doi: 10.2217/nnm-2016-0220

Jeon, O., Alt, D. S., Linderman, S. W., and Alsberg, E. (2013). Biochemical and physical signal gradients in hydrogels to control stem cell behavior. *Adv. Mater.* 25, 6366–6372. doi: 10.1002/adma.201302364

Jones, J. R. (2015). Reprint of: review of bioactive glass: from hench to hybrids. *Acta Biomater.* 23, S53–S82. doi: 10.1016/j.actbio.2015.07.019

Kang, B., Mackey, M. A., and El-Sayed, M. A. (2010). Nuclear targeting of gold nanoparticles in cancer cells induces DNA damage, causing cytokinesis arrest and apoptosis. *J. Am. Chem. Soc.* 132, 1517–1519. doi: 10.1021/ja9102698

Kheradvar, S. A., Nourmohammadi, J., Tabesh, H., and Bagheri, B. (2018). Starch nanoparticle as a vitamin E-TPGS carrier loaded in silk fibroin-poly (vinyl alcohol)-Aloe vera nanofibrous dressing. *Colloids Surf. B* 166, 9–16. doi: 10.1016/j.colsurfb.2018.03.004

Kim, H., Mondal, S., Bharathiraja, S., Manivasagan, P., Moorthy, M. S., and Oh, J. (2018). Optimized Zn-doped hydroxyapatite/doxorubicin bioceramics system for efficient drug delivery and tissue engineering application. *Ceram. Int.* 44, 6062–6071. doi: 10.1016/j.ceramint.2017.12.235

Kimling, J., Maier, M., Okenve, B., Kotaidis, V., Ballot, H., and Plech, A. (2006). Turkevich method for gold nanoparticle synthesis revisited. *J. Phys. Chem. B* 110, 15700–15707. doi: 10.1021/jp061667w

Knopf-Marques, H., Pravda, M., Wolfova, L., Velebny, V., Schaaf, P., Vrana, N. E., et al. (2016). Hyaluronic acid and its derivatives in coating and delivery systems: applications in tissue engineering, regenerative medicine and immunomodulation. *Adv. Healthc. Mater.* 5, 2841–2855. doi: 10.1002/adhm.201600316

Ko, W.-K., Heo, D. N., Moon, H.-J., Lee, S. J., Bae, M. S., Lee, J. B., et al. (2015). The effect of gold nanoparticle size on osteogenic differentiation of adipose-derived stem cells. *J. Colloid Interface Sci.* 438, 68–76. doi: 10.1016/j.jcis.2014.08.058

Kohn, D. H. (2003). "Bioceramics," in *Standard Handbook of Biomedical Engineering and Design*, ed M. Kutz (New York, NY: McGraw-Hill).

Kunath, S., Panagiotopoulou, M., Maximilien, J., Marchyk, N., Sanger, J., and Haupt, K. (2015). Cell and tissue imaging with molecularly imprinted polymers as plastic antibody mimics. *Adv. Healthc. Mater.* 4, 1322–1326. doi: 10.1002/adhm.201500145

Labala, S., Jose, A., Chawla, S. R., Khan, M. S., Bhatnagar, S., Kulkarni, O. P., et al. (2017). Effective melanoma cancer suppression by iontophoretic co-delivery of STAT3 siRNA and imatinib using gold nanoparticles. *Int. J. Pharm.* 525, 407–417. doi: 10.1016/j.ijpharm.2017.03.087

Lale, S. V., R., G, A., Aravind, A., Kumar, D. S., and Koul, V. (2014). AS1411 aptamer and folic acid functionalized pH-responsive ATRP fabricated pPEGMA–PCL–pPEGMA polymeric nanoparticles for targeted drug delivery in cancer therapy. *Biomacromolecules* 15, 1737–1752. doi: 10.1021/bm5001263

Laurenti, M., and Cauda, V. (2017). ZnO nanostructures for tissue engineering applications. *Nanomaterials* 7:374. doi: 10.3390/nano7110374

Lee, M. S., Ahmad, T., Lee, J., Awada, H. K., Wang, Y., Kim, K., et al. (2017). Dual delivery of growth factors with coacervate-coated poly (lactic-co-glycolic acid) nanofiber improves neovascularization in a mouse skin flap model. *Biomaterials* 124, 65–77. doi: 10.1016/j.biomaterials.2017.01.036

Li, J., Chen, Y., Kawazoe, N., and Chen, G. (2018). Ligand density-dependent influence of arginine–glycine–aspartate functionalized gold nanoparticles on osteogenic and adipogenic differentiation of mesenchymal stem cells. *Nano Res.* 11, 1247–1261. doi: 10.1007/s12274-017-1738-5

Li, J., Zhang, J., Chen, Y., Kawazoe, N., and Chen, G. (2017). TEMPO-conjugated gold nanoparticles for reactive oxygen species scavenging and regulation of stem cell differentiation. *ACS Appl. Mater. Interfaces* 9, 35683–35692. doi: 10.1021/acsami.7b12486

Li, X., Wei, J., Aifantis, K. E., Fan, Y., Feng, Q., Cui, F. Z., et al. (2016). Current investigations into magnetic nanoparticles for biomedical applications. *J. Biomed. Mater. Res. A* 104, 1285–1296. doi: 10.1002/jbm.a.35654

Li, X., Zhang, S., Zhang, X., Xie, S., Zhao, G., and Zhang, L. (2017). Biocompatibility and physicochemical characteristics of poly(ε-caprolactone)/poly(lactide-co-glycolide)/nano-hydroxyapatite composite scaffolds for bone tissue engineering. *Mater. Des.* 114, 149–160. doi: 10.1016/j.matdes.2016.10.054

Li, Y., Guo, Y., Niu, W., Chen, M., Xue, Y., Ge, J., et al. (2018). Biodegradable multifunctional bioactive glass-based nanocomposites elastomers with controlled biomineralization activity, real-time bioimaging tracking and decreased inflammatory response. *ACS Appl. Mater. Interfaces.* 10, 17722–17731. doi: 10.1021/acsami.8b04856

Lin, H.-H., Hsieh, F.-Y., Tseng, C.-S., and Hsu, S.-H. (2016). Preparation and characterization of a biodegradable polyurethane hydrogel and the hybrid gel with soy protein for 3D cell-laden bioprinting. *J. Mater. Chem. B* 4, 6694–6705. doi: 10.1039/C6TB01501H

Lin, K., and Chang, J. (2015). "1 - Structure and properties of hydroxyapatite for biomedical applications," in *Hydroxyapatite (Hap) for Biomedical Applications*, ed M. Mucalo (Woodhead Publishing), 3–19.

Liu, X.-Y., Zhou, C.-B., and Fang, C. (2018). Nanomaterial-involved neural stem cell research: disease treatment, cell labeling, and growth regulation. *Biomed. Pharmacother.* 107, 583–597. doi: 10.1016/j.biopha.2018.08.029

Madhumathi, K., Kumar, P. S., Abhilash, S., Sreeja, V., Tamura, H., Manzoor, K., et al. (2010). Development of novel chitin/nanosilver composite scaffolds for wound dressing applications. *J. Mater. Sci. Mater. Med.* 21, 807–813. doi: 10.1007/s10856-009-3877-z

Mahdavi, M., Namvar, F., Ahmad, M., and Mohamad, R. (2013). Green biosynthesis and characterization of magnetic iron oxide (Fe3O4) nanoparticles using seaweed (Sargassum muticum) aqueous extract. *Molecules* 18, 5954–5964. doi: 10.3390/molecules18055954

Manivasagan, P., Bharathiraja, S., Bui, N. Q., Jang, B., Oh, Y.-O., Lim, I. G., et al. (2016). Doxorubicin-loaded fucoidan capped gold nanoparticles for drug delivery and photoacoustic imaging. *Int. J. Biol. Macromol.* 91, 578–588. doi: 10.1016/j.ijbiomac.2016.06.007

Marcus, M., Skaat, H., Alon, N., Margel, S., and Shefi, O. (2015). NGF-conjugated iron oxide nanoparticles promote differentiation and outgrowth of PC12 cells. *Nanoscale* 7, 1058–1066. doi: 10.1039/C4NR05193A

Marino, A., Arai, S., Hou, Y., Degl'Innocenti, A., Cappello, V., Mazzolai, B., et al. (2017). Gold nanoshell-mediated remote myotube activation. *ACS Nano* 11, 2494–2508. doi: 10.1021/acsnano.6b08202

Medeiros, S. F., Santos, A. M., Fessi, H., and Elaissari, A. (2011). Stimuli-responsive magnetic particles for biomedical applications. *Int. J. Pharm.* 403, 139–161. doi: 10.1016/j.ijpharm.2010.10.011

Mehrabani, M. G., Karimian, R., Mehramouz, B., Rahimi, M., and Kafil, H. S. (2018). Preparation of biocompatible and biodegradable silk fibroin/chitin/silver nanoparticles 3D scaffolds as a bandage for antimicrobial wound dressing. *Int. J. Biol. Macromol.* 114, 961–971. doi: 10.1016/j.ijbiomac.2018.03.128

Meng, F., Cheng, R., Deng, C., and Zhong, Z. (2012). Intracellular drug release nanosystems. *Mater. Today* 15, 436–442. doi: 10.1016/S1369-7021(12)70195-5

Mi, P., Kokuryo, D., Cabral, H., Wu, H., Terada, Y., Saga, T., et al. (2016). A pH-activatable nanoparticle with signal-amplification capabilities for non-invasive imaging of tumour malignancy. *Nat. Nanotechnol.* 11, 724–730. doi: 10.1038/nnano.2016.72

Mili, B., Das, K., Kumar, A., Saxena, A., Singh, P., Ghosh, S., et al. (2018). Preparation of NGF encapsulated chitosan nanoparticles and its evaluation on neuronal differentiation potentiality of canine mesenchymal stem cells. *J. Mater. Sci. Mater. Med.* 29:4. doi: 10.1007/s10856-017-6008-2

Mody, V. V., Siwale, R., Singh, A., and Mody, H. R. (2010). Introduction to metallic nanoparticles. *J. Pharm. Bioall. Sci.* 2:282. doi: 10.4103/0975-7406.72127

Mohandas, A., Anisha, B. S., Chennazhi, K. P., and Jayakumar, R. (2015). Chitosan–hyaluronic acid/VEGF loaded fibrin nanoparticles composite sponges for enhancing angiogenesis in wounds. *Colloids Surf. B* 127, 105–113. doi: 10.1016/j.colsurfb.2015.01.024

Mokhena, T. C., and Luyt, A. S. (2017). Electrospun alginate nanofibres impregnated with silver nanoparticles: preparation, morphology and antibacterial properties. *Carbohydr. Polym.* 165, 304–312. doi: 10.1016/j.carbpol.2017.02.068

Moonesi Rad, R., Pazarçeviren, E., Ece Akgün, E., Evis, Z., and Keskin, D., Sahin, S., et al. (2019). *In vitro* performance of a nanobiocomposite scaffold containing boron-modified bioactive glass nanoparticles for dentin regeneration. *J. Biomater. Appl.* 33, 834–853. doi: 10.1177/0885328218812487

Morones, J. R., Elechiguerra, J. L., Camacho, A., Holt, K., Kouri, J. B., Ramírez, J. T., et al. (2005). The bactericidal effect of silver nanoparticles. *Nanotechnology* 16, 2346–2653. doi: 10.1088/0957-4484/16/10/059

Nicolas, J., Mura, S., Brambilla, D., Mackiewicz, N., and Couvreur, P. (2013). Design, functionalization strategies and biomedical applications of targeted biodegradable/biocompatible polymer-based nanocarriers for drug delivery. *Chem. Soc. Rev.* 42, 1147–1235. doi: 10.1039/c2cs35265f

Nowicki, M., Castro, N. J., Rao, R., Plesniak, M., and Zhang, L. G. (2017). Integrating three-dimensional printing and nanotechnology for musculoskeletal regeneration. *Nanotechnology* 28:382001. doi: 10.1088/1361-6528/aa8351

Paciotti, G. F., Kingston, D. G., and Tamarkin, L. (2006). Colloidal gold nanoparticles: a novel nanoparticle platform for developing multifunctional tumor-targeted drug delivery vectors. *Drug Dev. Res.* 67, 47–54. doi: 10.1002/ddr.20066

Padmavathy, N., and Vijayaraghavan, R. (2008). Enhanced bioactivity of ZnO nanoparticles-an antimicrobial study. *Sci. Technol. Adv. Mater.* 9:035004. doi: 10.1088/1468-6996/9/3/035004

Paez, J. G., Jänne, P. A., Lee, J. C., Tracy, S., Greulich, H., Gabriel, S., et al. (2004). EGFR mutations in lung cancer: correlation with clinical response to gefitinib therapy. *Science* 304, 1497–1500. doi: 10.1126/science.1099314

Pal, A., Nasker, P., Paul, S., Roy Chowdhury, A., Sinha, A., and Das, M. (2019). Strontium doped hydroxyapatite from Mercenaria clam shells: synthesis, mechanical and bioactivity study. *J. Mech. Behav. Biomed. Mater.* 90, 328–336. doi: 10.1016/j.jmbbm.2018.10.027

Panácek, A., Kvitek, L., Prucek, R., Kolár, M., Vecerová, R., andPizúrová, N., et al. (2006). Silver colloid nanoparticles: synthesis, characterization, and their antibacterial activity. *J. Phys. Chem. B* 110, 16248–16253. doi: 10.1021/jp063826h

Panikkanvalappil, S. R., Hooshmand, N., and El-Sayed, M. A. (2017). Intracellular assembly of nuclear-targeted gold nanosphere enables selective plasmonic photothermal therapy of cancer by shifting their absorption wavelength toward near-infrared region. *Bioconjug. Chem.* 28, 2452–2460. doi: 10.1021/acs.bioconjchem.7b00427

Pankongadisak, P., Ruktanonchai, U. R., Supaphol, P., and Suwantong, O. (2017). Gelatin scaffolds functionalized by silver nanoparticle-containing calcium alginate beads for wound care applications. *Polym. Adv. Technol.* 28, 849–858. doi: 10.1002/pat.3988

Park, J., Wrzesinski, S. H., Stern, E., Look, M., Criscione, J., Ragheb, R., et al. (2012). Combination delivery of TGF-beta inhibitor and IL-2 by nanoscale liposomal polymeric gels enhances tumour immunotherapy. *Nat. Mater.* 11, 895–905. doi: 10.1038/nmat3355

Pérez, R. A., Won, J.-E., Knowles, J. C., and Kim, H.-W. (2013). Naturally and synthetic smart composite biomaterials for tissue regeneration. *Adv. Drug Deliv. Rev.* 65, 471–496. doi: 10.1016/j.addr.2012.03.009

Pilakka-Kanthikeel, S., Atluri, V. S. R., Sagar, V., Saxena, S. K., and Nair, M. (2013). Targeted brain derived neurotropic factors (BDNF) delivery across the blood-brain barrier for neuro-protection using magnetic nano carriers: an *in-vitro* study. *PloS ONE* 8:e62241. doi: 10.1371/journal.pone.0062241

Prabhu, S., and Poulose, E. K. (2012). Silver nanoparticles: mechanism of antimicrobial action, synthesis, medical applications, and toxicity effects. *Int. Nano Lett.* 2:32. doi: 10.1186/2228-5326-2-32

Qian, J., Xu, W., Yong, X., Jin, X., and Zhang, W. (2014). Fabrication and *in vitro* biocompatibility of biomorphic PLGA/nHA composite scaffolds for bone tissue engineering. *Mater. Sci. Eng. C.* 36, 95–101. doi: 10.1016/j.msec.2013.11.047

Qian, X., Peng, X.-H., Ansari, D. O., Yin-Goen, Q., Chen, G. Z., Shin, D. M., et al. (2008). *In vivo* tumor targeting and spectroscopic detection with surface-enhanced Raman nanoparticle tags. *Nat. Biotechnol.* 26, 83–90. doi: 10.1038/nbt1377

Rad, R. M., Alshemary, A. Z., Evis, Z., Keskin, D., Altunba,ş, K., and Tezcaner, A. (2018). Structural and biological assessment of boron doped bioactive glass nanoparticles for dental tissue applications. *Ceram. Int.* 44, 9854–9864. doi: 10.1016/j.ceramint.2018.02.230

Rai, M., Yadav, A., and Gade, A. (2009). Silver nanoparticles as a new generation of antimicrobials. *Biotech. Adv.* 27, 76–83. doi: 10.1016/j.biotechadv.2008.09.002

Raucci, M. G., Demitri, C., Soriente, A., Fasolino, I., Sannino, A., and Ambrosio, L. (2018). Gelatin/nano-hydroxyapatite hydrogel scaffold prepared by sol-gel technology as filler to repair bone defects. *J. Biomed. Mater. Res. A* 106, 2007–2019. doi: 10.1002/jbm.a.36395

Raut, S., Dasseux, J.-L., Sabnis, N. A., Mooberry, L., and Lacko, A. (2018). Lipoproteins for therapeutic delivery: recent advances and future opportunities. *Ther. Deliv.* 9, 257–268. doi: 10.4155/tde-2017-0122

Rosa, R. M., Silva, J. C., Sanches, I. S., and Henriques, C. (2017). Simultaneous photo-induced cross-linking and silver nanoparticle formation in a PVP electrospun wound dressing. *Mater. Lett.* 207, 145–148. doi: 10.1016/j.matlet.2017.07.046

Rujitanaroj, P. O., Pimpha, N., and Supaphol, P. (2008). Wound-dressing materials with antibacterial activity from electrospun gelatin fiber mats containing silver nanoparticles. *Polymer* 49, 4723–4732. doi: 10.1016/j.polymer.2008.08.021

Sadat-Shojai, M., Khorasani, M. T., Dinpanah-Khoshdargi, E., and Jamshidi, A. (2013). Synthesis methods for nanosized hydroxyapatite with diverse structures. *Acta Biomater.* 9, 7591–7621. doi: 10.1016/j.actbio.2013.04.012

Saha, K., Agasti, S. S., Kim, C., Li, X., and Rotello, V. M. (2012). Gold nanoparticles in chemical and biological sensing. *Chem. Rev.* 112, 2739–2779. doi: 10.1021/cr2001178

Salata, O. V. (2004). Applications of nanoparticles in biology and medicine. *J. Nanobiotechnol.* 2:3. doi: 10.1186/1477-3155-2-3

Saleh, T., Ahmed, E., Yu, L., Hussein, K., Park, K.-M., Lee, Y.-S., et al. (2018). Silver nanoparticles improve structural stability and biocompatibility of decellularized porcine liver. *Artif. Cells Nanomed. Biotechnol.* 46(Suppl. 2), 273–284. doi: 10.1080/21691401.2018.1457037

Samadian, H., Salehi, M., Farzamfar, S., Vaez, A., Ehterami, A., Sahrapeyma, H., et al. (2018). *In vitro* and *in vivo* evaluation of electrospun cellulose acetate/gelatin/hydroxyapatite nanocomposite mats for wound dressing applications. *Artif. Cells Nanomed. Biotechnol.* 46(Suppl. 1), 964–974. doi: 10.1080/21691401.2018.1439842

Santo, V. E., Duarte, A. R. C., Gomes, M. E., Mano, J. F., and Reis, R. L. (2010). Hybrid 3D structure of poly(d,l-lactic acid) loaded with chitosan/chondroitin sulfate nanoparticles to be used as carriers for biomacromolecules in tissue engineering. *J. Supercrit. Fluids* 54, 320–327. doi: 10.1016/j.supflu.2010.05.021

Santo, V. E., Ratanavaraporn, J., Sato, K., Gomes, M. E., Mano, J. F., Reis, R. L., et al. (2015). Cell engineering by the internalization of bioinstructive micelles for enhanced bone regeneration. *Nanomedicine* 10, 1707–1721. doi: 10.2217/nnm.15.11

Santos, F. G., Bonkovoski, L. C., Garcia, F. P., Cellet, T. S., Witt, M. A., Nakamura, C. V., et al. (2017). Antibacterial performance of a PCL–PDMAEMA Blend nanofiber-based scaffold enhanced with immobilized silver nanoparticles. *ACS Appl. Mater. Interfaces* 9, 9304–9314. doi: 10.1021/acsami.6b14411

Saroja, C., Lakshmi, P., and Bhaskaran, S. (2011). Recent trends in vaccine delivery systems: a review. *Int. J. Pharm. Investig.* 1, 64–74. doi: 10.4103/2230-973X.82384

Savla, R., and Minko, T. (2017). Nanoparticle design considerations for molecular imaging of apoptosis: diagnostic, prognostic, and therapeutic value. *Adv. Drug Deliv. Rev.* 113, 122–140. doi: 10.1016/j.addr.2016.06.016

Shang, L., Nienhaus, K., and Nienhaus, G. U. (2014). Engineered nanoparticles interacting with cells: size matters. *J. Nanobiotechnol.* 12:5. doi: 10.1186/1477-3155-12-5

Shi, J., Votruba, A. R., Farokhzad, O. C., and Langer, R. (2010). Nanotechnology in drug delivery and tissue engineering: from discovery to applications. *Nano Lett.* 10, 3223–3230. doi: 10.1021/nl102184c

Shrestha, B. K., Shrestha, S., Tiwari, A. P., Kim, J.-I., Ko, S. W., Kim, H.-J., et al. (2017). Bio-inspired hybrid scaffold of zinc oxide-functionalized multi-wall carbon nanotubes reinforced polyurethane nanofibers for bone tissue engineering. *Mater. Des.* 133, 69–81. doi: 10.1016/j.matdes.2017.07.049

Singh, D., Singh, S., Sahu, J., Srivastava, S., and Singh, M. R. (2016). Ceramic nanoparticles: recompense, cellular uptake and toxicity concerns. *Artif. Cells Nanomed. Biotechnol.* 44, 401–409. doi: 10.3109/21691401.2014.955106

Son, W. K., Youk, J. H., Lee, T. S., and Park, W. H. (2004). Preparation of antimicrobial ultrafine cellulose acetate fibers with silver nanoparticles. *Macromol. Rapid Commun.* 25, 1632–1637. doi: 10.1002/marc.200400323

Song, D., Cui, J., Sun, H., Nguyen, T.-H., Alcantara, S., De Rose, R., et al. (2017). Templated polymer replica nanoparticles to facilitate assessment of material-dependent pharmacokinetics and biodistribution. *ACS Appl. Mater. Interfaces* 9, 33683–33694. doi: 10.1021/acsami.7b11579

Stratakis, E., and Kymakis, E. (2013). Nanoparticle-based plasmonic organic photovoltaic devices. *Mater. Today* 16, 133–146. doi: 10.1016/j.mattod.2013.04.006

Tan, Q., Tang, H., Hu, J., Hu, Y., Zhou, X., Tao, Y., et al. (2011). Controlled release of chitosan/heparin nanoparticle-delivered VEGF enhances regeneration of decellularized tissue-engineered scaffolds. *Int. J. Nanomed.* 6, 929–942. doi: 10.2147/ijn.s18753

Tang, Z., He, C., Tian, H., Ding, J., Hsiao, B. S., Chu, B., et al. (2016). Polymeric nanostructured materials for biomedical applications. *Prog. Polym. Sci.* 60, 86–128. doi: 10.1016/j.progpolymsci.2016.05.005

Taygun, M. E., and Boccaccini, A. R. (2011). "Nanoscaled bioactive glass particles and nanofibers," in *Bioactive Glasses,* ed H. O. Ylanen (Cambridge: Woodhead Publishing), 235–283.

Teixeira, G. Q., Leite Pereira, C., Castro, F., Ferreira, J. R., Gomez-Lazaro, M., Aguiar, P., et al. (2016). Anti-inflammatory Chitosan/Poly-γ-glutamic acid nanoparticles control inflammation while remodeling extracellular matrix in degenerated intervertebral disc. *Acta Biomater.* 42, 168–179. doi: 10.1016/j.actbio.2016.06.013

Tezcaner, A., Erkan Türker, B., and Dilek, K. (2016). Nanoparticles based on plasma proteins for drug delivery applications. *Curr. Pharm. Des.* 22, 3445–3454. doi: 10.2174/1381612822666160209152446

Tian, J., Wong, K. K., Ho, C. M., Lok, C. N., Yu, W. Y., Che, C. M., et al. (2007). Topical delivery of silver nanoparticles promotes wound healing. *ChemMedChem* 2, 129–136. doi: 10.1002/cmdc.200600171

Tong, W., Lu, Z., Qin, L., Mauck, R. L., Smith, H. E., Smith, L. J., et al. (2017). Cell therapy for the degenerating intervertebral disc. *Transl. Res.* 181, 49–58. doi: 10.1016/j.trsl.2016.11.008

Turkevich, J., Stevenson, P. C., and Hillier, J. (1951). A study of the nucleation and growth processes in the synthesis of colloidal gold. *Faraday Soc.* 11, 55–75. doi: 10.1039/DF9511100055

Veiseh, O., Tang, B. C., Whitehead, K. A., Anderson, D. G., and Langer, R. (2015). Managing diabetes with nanomedicine: challenges and opportunities. *Nat. Rev. Drug. Discov.* 14, 45–57. doi: 10.1038/nrd4477

Venkatesan, J., Lee, J.-Y., Kang, D. S., Anil, S., Kim, S.-K., Shim, M. S., et al. (2017). Antimicrobial and anticancer activities of porous chitosan-alginate biosynthesized silver nanoparticles. *Int. J. Biol. Macromol.* 98, 515–525. doi: 10.1016/j.ijbiomac.2017.01.120

Vial, S., Reis, R. L., and Oliveira, J. M. (2017). Recent advances using gold nanoparticles as a promising multimodal tool for tissue engineering and regenerative medicine. *Curr. Opin. Solid State Mater. Sci.* 21, 92–112. doi: 10.1016/j.cossms.2016.03.006

Vieira, S., Vial, S., Reis, R. L., and Oliveira, J. M. (2017). Nanoparticles for bone tissue engineering. *Biotechnol. Progr.* 33, 590–611. doi: 10.1002/btpr.2469

Vinzant, N., Scholl, J. L., Wu, C.-M., Kindle, T., Koodali, R., and Forster, G. L. (2017). Iron oxide nanoparticle delivery of peptides to the brain: reversal of anxiety during drug withdrawal. *Front. Neurosci.* 11:608. doi: 10.3389/fnins.2017.00608

Vollath, D., Szab,ó, D. V., and Hauβelt, J. (1997). Synthesis and properties of ceramic nanoparticles and nanocomposites. *J. Eur. Ceram. Soc.* 17, 1317–1324. doi: 10.1016/S0955-2219(96)00224-5

Vrana, N. E., Erdemli, O., Francius, G., Fahs, A., Rabineau, M., Debry, C., et al. (2014). Double entrapment of growth factors by nanoparticles loaded into polyelectrolyte multilayer films. *J. Mater. Chem. B* 2, 999–1008. doi: 10.1039/C3TB21304H

Wang, B., Lv, X., Chen, S., Li, Z., Yao, J., Peng, X., et al. (2017). Bacterial cellulose/gelatin scaffold loaded with VEGF-silk fibroin nanoparticles for improving angiogenesis in tissue regeneration. *Cellulose* 24, 5013–5024. doi: 10.1007/s10570-017-1472-x

Wang, C., Zhu, F., Cui, Y., Ren, H., Xie, Y., Li, A., et al. (2016). An easy-to-use wound dressing gelatin-bioactive nanoparticle gel and its preliminary *in vivo* study. *J. Mater. Sci. Mater. Med.* 28:10. doi: 10.1007/s10856-016-5823-1

Wang, L., Xu, K., Hou, X., Han, Y., Liu, S., Wiraja, C., et al. (2017). Fluorescent poly(glycerol-co-sebacate) acrylate nanoparticles for stem cell labeling and longitudinal tracking. *ACS Appl. Mater. Interfaces* 9, 9528–9538. doi: 10.1021/acsami.7b01203

Wang, Q., Jiang, J., Chen, W., Jiang, H., Zhang, Z., and Sun, X. (2016). Targeted delivery of low-dose dexamethasone using PCL-PEG micelles for effective treatment of rheumatoid arthritis. *J. Control. Release* 230, 64–72. doi: 10.1016/j.jconrel.2016.03.035

Wang, Y., Dou, C., He, G., Ban, L., Huang, L., Li, Z., et al. (2018). Biomedical potential of ultrafine ag nanoparticles coated on poly (Gamma-Glutamic Acid) hydrogel with special reference to wound healing. *Nanomaterials* 8:324. doi: 10.3390/nano8050324

Wang, Y., Wang, C., Ding, Y., Li, J., Li, M., Liang, X., et al. (2016). Biomimetic HDL nanoparticle mediated tumor targeted delivery of indocyanine green for enhanced photodynamic therapy. *Colloids Surf. B* 148, 533–540. doi: 10.1016/j.colsurfb.2016.09.037

Wang, Z., Dong, L., Han, L., Wang, K., Lu, X., Fang, L., et al. (2016). Self-assembled biodegradable nanoparticles and polysaccharides as biomimetic ECM nanostructures for the synergistic effect of RGD and BMP-2 on bone formation. *Sci. Rep.* 6:25090. doi: 10.1038/srep25090

Wang, Z., Wang, K., Lu, X., Li, M., Liu, H., Xie, C., et al. (2015). BMP-2 encapsulated polysaccharide nanoparticle modified biphasic calcium phosphate scaffolds for bone tissue regeneration. *J. Biomed. Mater. Res. A* 103, 1520–1532. doi: 10.1002/jbm.a.35282

Wei, M., Li, S., Yang, Z., Zheng, W., and Le, W. (2017). Gold nanoparticles enhance the differentiation of embryonic stem cells into dopaminergic neurons via mTOR/p70S6K pathway. *Nanomedicine* 12, 1305–1317. doi: 10.2217/nnm-2017-0001

Willmann, W., and Dringen, R. (2018). Monitoring of the cytoskeleton-dependent intracellular trafficking of fluorescent iron oxide nanoparticles by nanoparticle pulse-chase experiments in C6 glioma cells. *Neurochem. Res.* 43:2055–2071. doi: 10.1007/s11064-018-2627-3

Wu, K. C. W., Yamauchi, Y., Hong, C.-Y., Yang, Y.-H., Liang, Y.-H., Funatsu, T., et al. (2011). Biocompatible, surface functionalized mesoporous titania nanoparticles for intracellular imaging and anticancer drug delivery. *ChemComm.* 47, 5232–5234. doi: 10.1039/C1CC10659G

Xie, Z., Paras, C. B., Weng, H., Punnakitikashem, P., Su, L.-C., Vu, K., et al. (2013). Dual growth factor releasing multi-functional nanofibers for wound healing. *Acta Biomater.* 9, 9351–9359. doi: 10.1016/j.actbio.2013.07.030

Xue, Y., Guo, Y., Yu, M., Wang, M., Ma, P. X., and Lei, B. (2017). Monodispersed bioactive glass nanoclusters with ultralarge pores and intrinsic exceptionally high miRNA loading for efficiently enhancing bone regeneration. *Adv. Healthc. Mater.* 6:1700630. doi: 10.1002/adhm.201700630

Yahyaei, B., Manafi, S., Fahimi, B., Arabzadeh, S., and Pourali, P. (2018). Production of electrospun polyvinyl alcohol/microbial synthesized silver nanoparticles scaffold for the treatment of fungating wounds. *Appl. Nanosci.* 8, 417–426. doi: 10.1007/s13204-018-0711-2

Yan, X., Remond, M., Zheng, Z., Hoibian, E., Soulage, C., Chambert, S., et al. (2018). General and scalable approach to bright, stable, and functional AIE fluorogen colloidal nanocrystals for *in vivo* imaging. *ACS Appl. Mater. Interfaces* 10, 25154–25165. doi: 10.1021/acsami.8b07859

Yao, C., Zhu, J., Xie, A., Shen, Y., Li, H., Zheng, B., et al. (2017). Graphene oxide and creatine phosphate disodium dual template-directed synthesis of GO/hydroxyapatite and its application in drug delivery. *Mater. Sci. Eng. C.* 73, 709–715. doi: 10.1016/j.msec.2016.11.083

Yasin, S., Liu, L., and Yao, J. (2013). Biosynthesis of silver nanoparticles by bamboo leaves extract and their antimicrobial activity. *J. Fiber Bioeng. Inform.* 6, 77–84. doi: 10.3993/jfbi03201307

Yilgor, P., Tuzlakoglu, K., Reis, R. L., Hasirci, N., and Hasirci, V. (2009). Incorporation of a sequential BMP-2/BMP-7 delivery system into chitosan-based scaffolds for bone tissue engineering. *Biomaterials* 30, 3551–3559. doi: 10.1016/j.biomaterials.2009.03.024

Yu, J., Xia, H., Teramoto, A., and Ni, Q. Q. (2018). The effect of hydroxyapatite nanoparticles on mechanical behavior and biological performance of porous shape memory polyurethane scaffolds. *J. Biomed. Mater. Res. A* 106, 244–254. doi: 10.1002/jbm.a.36214

Yu, Q., Sun, J., Zhu, X., Qiu, L., Xu, M., Liu, S., et al. (2017). Mesoporous titanium dioxide nanocarrier with magnetic-targeting and high loading efficiency for dual-modal imaging and photodynamic therapy. *J. Mater. Chem. B* 5, 6081–6096. doi: 10.1039/C7TB01035D

Yuan, M., Wang, Y., and Qin, Y.-X. (2018). Promoting neuroregeneration by applying dynamic magnetic fields to a novel nanomedicine: Superparamagnetic iron oxide (SPIO)-gold nanoparticles bounded with nerve growth factor (NGF). *Nanomedicine* 14, 1337–1347. doi: 10.1016/j.nano.2018.03.004

Zamproni, L. N., Mundim, M. V., Porcionatto, M. A., and des Rieux, A. (2017). Injection of SDF-1 loaded nanoparticles following traumatic brain

injury stimulates neural stem cell recruitment. *Int. J. Pharm.* 519, 323–331. doi: 10.1016/j.ijpharm.2017.01.036

Zhang, D., Liu, D., Zhang, J., Fong, C., and Yang, M. (2014). Gold nanoparticles stimulate differentiation and mineralization of primary osteoblasts through the ERK/MAPK signaling pathway. *Mater. Sci. Eng. C.* 42, 70–77. doi: 10.1016/j.msec.2014.04.042

Zhang, H., Yu, S., Zhao, X., Mao, Z., and Gao, C. (2018). Stromal cell-derived factor-1α-encapsulated albumin/heparin nanoparticles for induced stem cell migration and intervertebral disc regeneration *in vivo*. *Acta biomater.* 72, 217–227. doi: 10.1016/j.actbio.2018.03.032

Zhao, F., Xie, W., Zhang, W., Fu, X., Gao, W., Lei, B., et al. (2018). 3D Printing nanoscale bioactive glass scaffolds enhance osteoblast migration and extramembranous osteogenesis through stimulating immunomodulation. *Adv. Healthc. Mater.* 7:1800361. doi: 10.1002/adhm.201800361

Zhao, Y., Li, C., Liu, X., Gu, F., Jiang, H., Shao, W., et al. (2007). Synthesis and optical properties of TiO2 nanoparticles. *Mater. Lett.* 61, 79–83. doi: 10.1016/j.matlet.2006.04.010

Zheng, K., Wu, J., Li, W., Dippold, D., Wan, Y., and Boccaccini, A. R. (2018). Incorporation of Cu-containing bioactive glass nanoparticles in gelatin-coated scaffolds enhances bioactivity and osteogenic activity. *ACS Biomater. Sci. Eng.* 4, 1546–1557. doi: 10.1021/acsbiomaterials.8b00051

Zheng, X., Wang, S., Wu, L., and Hou, X. (2018). Microwave-assisted facile synthesisof mono-dispersed Ba/Ho co-doped nanohydroxyapatite for potential application as binary CT imaging contrast agent. *Microchem. J.* 141, 330–336. doi: 10.1016/j.microc.2018.05.044

Zorlutuna, P., Vrana, N. E., and Khademhosseini, A. (2013). The expanding world of tissue engineering: the building blocks and new applications of tissue engineered constructs. *IEEE Rev. Biomed. Eng.* 6, 47–62. doi: 10.1109/rbme.2012.2233468

Zuidema, J. M., Provenza, C., Caliendo, T., Dutz, S., and Gilbert, R. J. (2015). Magnetic NGF-releasing PLLA/iron oxide nanoparticles direct extending neurites and preferentially guide neurites along aligned electrospun microfibers. *ACS Chem. Neurosci.* 6, 1781–1788. doi: 10.1021/acschemneuro.5b00189

Conflict of Interest Statement: The authors declare that the research was conducted in the absence of any commercial or financial relationships that could be construed as a potential conflict of interest.

frontiers in Bioengineering and Biotechnology

REVIEW
published: 04 June 2019
doi: 10.3389/fbioe.2019.00134

Polymeric Approaches to Reduce Tissue Responses Against Devices Applied for Islet-Cell Encapsulation

Shuixan Hu and Paul de Vos*

Division of Medical Biology, Department of Pathology and Medical Biology, Immunoendocrinology, University of Groningen and University Medical Center Groningen, Groningen, Netherlands

Immunoisolation of pancreatic islets is a technology in which islets are encapsulated in semipermeable but immunoprotective polymeric membranes. The technology allows for successful transplantation of insulin-producing cells in the absence of immunosuppression. Different approaches of immunoisolation are currently under development. These approaches involve intravascular devices that are connected to the bloodstream and extravascular devices that can be distinguished in micro- and macrocapsules and are usually implanted in the peritoneal cavity or under the skin. The technology has been subject of intense fundamental research in the past decade. It has co-evolved with novel replenishable cell sources for cure of diseases such as Type 1 Diabetes Mellitus that need to be protected for the host immune system. Although the devices have shown significant success in animal models and even in human safety studies most technologies still suffer from undesired tissue responses in the host. Here we review the past and current approaches to modulate and reduce tissue responses against extravascular cell-containing micro- and macrocapsules with a focus on rational choices for polymer (combinations). Choices for polymers but also choices for crosslinking agents that induce more stable and biocompatible capsules are discussed. Combining beneficial properties of molecules in diblock polymers or application of these molecules or other anti-biofouling molecules have been reviewed. Emerging are also the principles of polymer brushes that prevent protein and cell-adhesion. Recently also immunomodulating biomaterials that bind to specific immune receptors have entered the field. Several natural and synthetic polymers and even combinations of these polymers have demonstrated significant improvement in outcomes of encapsulated grafts. Adequate polymeric surface properties have been shown to be essential but how the surface should be composed to avoid host responses remains to be identified. Current insight is that optimal biocompatible devices can be created which raises optimism that immunoisolating devices can be created that allows for long term survival of encapsulated replenishable insulin-producing cell sources for treatment of Type 1 Diabetes Mellitus.

Keywords: transplantation, islet, encapsulation, polymer, host response, surface properties, biocompatibility

OPEN ACCESS

Edited by:
Hasan Uludag,
University of Alberta, Canada

Reviewed by:
Pierre Gianello,
Catholic University of Louvain, Belgium
Seda Kizilel,
Koç University, Turkey

****Correspondence:***
Shuixan Hu
s.hu@umcg.nl

Specialty section:
This article was submitted to Biomaterials, a section of the journal Frontiers in Bioengineering and Biotechnology

Received: *13 February 2019*
Accepted: *20 May 2019*
Published: *04 June 2019*

Citation:
Hu S and de Vos P (2019) Polymeric Approaches to Reduce Tissue Responses Against Devices Applied for Islet-Cell Encapsulation. Front. Bioeng. Biotechnol. 7:134. doi: 10.3389/fbioe.2019.00134

INTRODUCTION

Type one diabetes mellitus (T1D) impacts 1.25 million individuals in the US alone and is associated with an annual health care cost of $9.8 billion (American Diabetes Association, 2018). These costs can be reduced by tight regulation of the blood glucose levels such as can be done with allogeneic transplantation of pancreatic islets. Up to now these islets are obtained from cadaveric donors that regulate glucose levels from a minute-to-minute level (Choby, 2017). This replaces insulin injections and prevents regular hypoglycemic events and thereby contributes to improved quality of life. The mandatory use of immunosuppression to prevent graft rejection is unfortunately an obstacle for large scale application. Application may be facilitated with effective encapsulation technologies for immunoprotection of islets that prevent graft rejection and autoimmune destruction of islets (Barkai et al., 2016). To generate immunoisolative membranes, several materials have been explored but an ongoing challenge remains prevention of too strong tissue responses that might lead to graft failure (Paredes-Juárez et al., 2014b). The tissue responses might manifest *in vivo* as immune cell adhesion and fibrotic overgrowth on the surface of micro- or macrocapsules but also strong responses in the immediate vicinity of the capsules might lead to cytokine production and death of islet-cells (de Vos, 2017; Krishnan et al., 2017). Here we review current and past approaches in which polymer engineering has been applied to improve biocompatibility of natural and synthetic polymers applied for islet micro- or macroencapsulation.

Need for Islet Transplantation in T1D

In T1D insulin-producing pancreatic β cells are destroyed by a specific autoimmune reaction resulting from a complex of environmental and genetic factors (Atkinson et al., 2014). This autoimmune destruction is irreversible, which implies lifelong insulin administration by injections to regulate homeostasis of blood glucose (Hirsch, 2009). Although this therapy is life-saving, it has a major impact on the quality of life of patients. Patients need to be taught to self-monitoring blood sugars and to adjust insulin dosing according to daily needs. Despite this intensive way of regulating glucose levels, it cannot regulate blood glucose on a minute-by-minute basis. As a consequence, of this lack of precise regulation diabetic complications may develop such as retinopathy, neuropathy, and cardiovascular disease (Choby, 2017). Also, intensive insulin therapy holds the threat of regular hypoglycemic episodes which might eventually lead to hypoglycemic unawareness (Bragd et al., 2003). Better and more precise regulation of glucose levels is highly needed to prevent diabetic complications, and for improving patient's life quality.

Ever since the groundbreaking publication of the Edmonton protocol (Shapiro et al., 2000), which reported insulin-independence in seven recipients after an average of 12 months, pancreatic-islet transplantation provides an alternative strategy to restore physiological insulin-responses to plasma glucose changes (Berney et al., 2009). Since that time 1,086 patients were transplanted with islets according to the Collaborative Islet Transplant Registry (CITR) 10th Annual Report (Collaborative Islet Transplant Registry, 2017). These patients all have a complete absence of hypoglycemia, in many cases remain insulin independent and most of them experienced an improved quality of life (Ryan et al., 2002, 2005). Despite these successes, islet transplantation is not yet a widely applied treatment for T1DM. The reason for that is the mandatory use of life-long immunosuppression of the patient to prevent graft rejection (Berney et al., 2009). Immunosuppression is associated with increased risk for serious infections and cancer (Dantal and Soulillou, 2005), as well as associated with metabolic disorders and toxicity for kidneys (Ekberg et al., 2009). Immunosuppression is therefore not considered to be an acceptable alternative for insulin therapy (Ricordi and Strom, 2004).

ISLETS ENCAPSULATION TECHNOLOGY

An advantage of islet-transplantation over whole pancreas transplantation is that islets are clumps of cells that can be packed in immunoisolating membranes. Immunoisolation is a technology that potentially allows for transplantation of islets in the absence of life long immunosuppression. Within this technology islets are encapsulated inside semi-permeable membranes that can isolate islet grafts from immune cells and antibodies of recipients while allowing ingress of nutrients, oxygen and glucose, and egress of insulin (de Vos et al., 2010). In the past three decades, three major categories of encapsulation approaches were studied for islet immunoisolation. These include intravascular macrocapsules, extravascular macrocapsules, and extravascular microcapsules (Teramura and Iwata, 2010; O'Sullivan et al., 2011). Intravascular devices are connected to the bloodstream which implies fast correction of changes in blood-glucose levels due to faster exchange of glucose and insulin (Prochorov et al., 2008). However, its clinical application was and is limited by high risks for thrombosis and infections, and the demand for major surgery for implantation. Although some groups still publish novel approaches for intravascular devices that are associated with less risks (Prochorov et al., 2008; Gmyr et al., 2017), the majority of research papers in the past decade focus on extravascular

Abbreviations: APC, activated protein C; BW, body weight; CHOPA, acrylate modified cholesterol bearing pullulan; DOPA, 3,4–dihydroxyphenethylamine; FT-IR, fourier-transform infrared spectroscopy; G, α-L-guluronic acid; GA, glutaraldehyde; HA-COL, hyaluronic acid-collagen hydrogel; Hb-C, hemoglobin; HEMA, 2-hydroxyethyl methylacrylate; IgG, immunoglobulin G; M, β-D-mannuronic acid; MAA, methacrylic acid; MGC, methacrylated glycol chitosan; MMA, methyl methacrylate; MSCs, mesenchymal stem cells; NF-κB, nuclear factor kappa-light-chain-enhancer of activated B cells; NO, nitric oxide; PAMPs, pathogen-associated molecular patterns; PAN, polyacrylonitrile; PEG, poly (ethylene glycol); PEG-4MAL, PEG-maleimide; PEG-b-PLL, poly(ethylene glycol)-block-poly(l-lysine hydrochloride; PEGDA, polyethyleneglycole diacrylate; PLGA, poly (lactic-co-glycolic acid); PLL, poly-l-lysine; PRRs, pattern-recognition receptors; PSSa, polystyrene sulfonic acid PSSa; SH, thiol; T1D, type one diabetes mellitus; Teff, T effector; TM, thrombomodulin; TM, hrombomodulin; ToF-SIMS, Time-of-Flight Secondary Ion Mass Spectrometry; Treg, T regulatory; UK, urokinase; VEGF, vascular endothelial growth; XPS, X-Ray Photoelectron Spectroscopy.

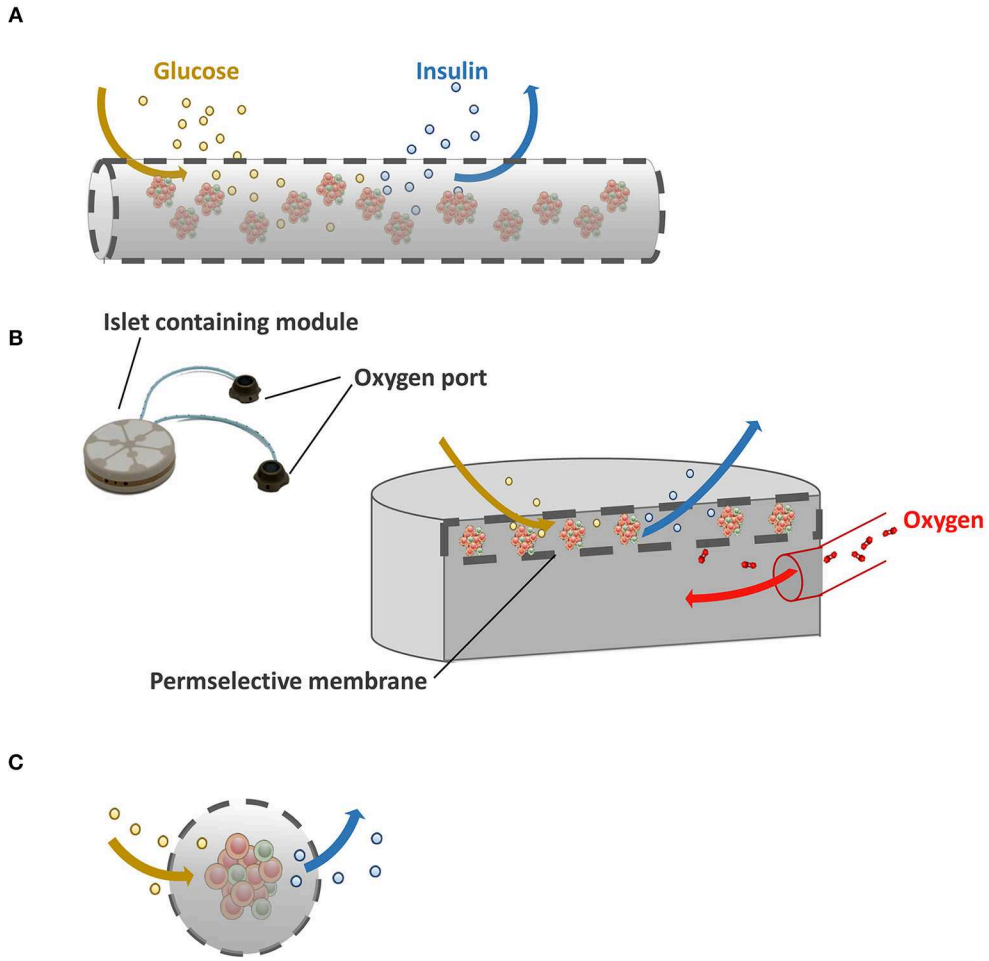

FIGURE 1 | Immunoisolating devices. **(A)** In macrocapsules, groups of islets are encapsulated in a selectively permeable membrane. Because of the unfavorable volume to surface ratio in macroencapsules insufficient supply of nutrients such as oxygen is a major issue. **(B)** Schematic illustration of Beta-O2 device. Beta-O2 is equipped with a refillable oxygen chamber that allows the diffusion of oxygen to the islet-containing chamber. **(C)** Schematic illustration of microcapsules with a better surface to volume ratio than macrocapsules which facilitates ingress of oxygen and glucose and egress of insulin.

devices. Extravascular devices are therefore the major focus of this review.

Extravascular devices can be distinguished into macro- and microcapsules. Macrodevices contain groups of islets inside the membrane (**Figure 1A**). The technique is rather simple in concept. Groups of islets are encapsulated in the devices and implanted either subcutaneously or intraperitoneally without direct connection to the blood stream. Within days blood vessels grow toward the surface for mandatory nutrient supply, but also to exchange glucose and insulin. A major issue in the field of macrocapsules, however, is the unfavorable surface to volume ratio (Orive et al., 2018). As a consequence, diffusion of essential nutrients such as oxygen is slow and islets inside the capsules compete for these nutrients. Because of this there is a limitation in seeding density that almost never exceeds 5–10% of the volume of the devices (Lacy et al., 1991).

A promising solution for this diffusion issue is the so-called Beta-O2 device (**Figure 1B**). Beta-O2 is a bioartificial pancreatic device, which is implanted under the skin or into the pre-peritoneal cavity with minimal surgery. The Beta-O2 device consists of two modules. A chamber is connected with an oxygen port that allows infusion of gas into a chamber by an injector that is operated manually. The other module is the islet graft containing capsule which is surrounded by a perm-selective membrane consisting of three layers, i.e., a polytetrafluoroethylene, a high mannuronic acid alginate gel, and a silicon rubber (Barkai et al., 2016). The multilayer membrane allows free diffusion of oxygen, glucose, and insulin and forms an effective immunoisolating membrane (Ludwig et al., 2010). Due to the presence of an oxygen supply module more islets can be encapsulated into a predefined volume without hypoxia. In the original concept of the Beta-O2 device, 2400 IEQ/device were loaded at a surface density of 1,000 IEQ/cm^2 with a refueling every 2 h with atmospheric air (Barkai et al., 2013). With this device diabetic rat recipients maintained normoglycemia through up to 240 days which was the end point of the

experiment. Also, efficacy of this approach was demonstrated in a large animal model, i.e., mini-pigs. The device with two separated islet modules attached to a gas chamber containing 6,730 ± 475 rat IEQ/kg body weight (BW) was introduced in diabetic mini-pigs. The rat islets induced normoglycemia up to 75 days without immunosuppression demonstrating efficacy and safety as well as the ability to use xenogeneic approaches with the device in larger mammals (Neufeld et al., 2013). Efficacy of xenogeneic porcine islets was recently also shown in a nonhuman primate model with T1D with 20,000 islets/kg BW (Ludwig et al., 2017). The device induced a persistent stable glycemic control even during a stepwise reduction in daily exogenous insulin dose up to 190 days after which the devices were explanted (Ludwig et al., 2017). Upon retrieval, a strongly vascularized fibrous capsule was observed around the device that according to the authors facilitates the exchange of substances in and out of the device (Ludwig et al., 2017).

Microcapsules in contrast to macrocapsules do suffer less from diffusion issues as they have a very optimal volume to surface ratio (**Figure 1C**). Other advantages are that when a minority of microcapsules are suffering from cell adhesion due to local imperfections (de Vos et al., 1996a; De Vos et al., 1996b) the grafts will not immediately fail while such a response is more deleterious for macrodevices. Additionally, microcapsules are mechanically stable and encapsulation can be done with nontoxic molecules and reagents (Bhujbal et al., 2014a). The majority of encapsulation approaches use alginate as core material followed by poly-amine thin coating to provide immunoprotection or to enhance mechanical stability (Kendall and Opara, 2017). To enhance biocompatibility many different alginates with a large variation of chemical modifications have been tested. In one of the studies, 744 alginate analogs were tested, which revealed 200 analogs associated with lower immune cell activation compared to the others (Vegas et al., 2016a). The evaluation of alginate analogs in both rodents and non-human primates identified three analogs that showed little presence of macrophages and fibroblasts on the capsule surface demonstrating that alginates are biocompatible in the correct chemical structure (Vegas et al., 2016a; Bochenek et al., 2018). A challenge in this area is however to identify and document the relationships between the surface properties and biocompatibility because even the microcapsules tested in the studies had different surface properties (Vegas et al., 2016a) and provoked different degrees of tissue responses.

Although the large surface to volume ratio of microcapsules facilitates oxygen and nutrient diffusion, the optimal size of capsules to prevent tissue responses has recently become subject of debate (Veiseh et al., 2015; de Vos, 2017). It was reported that microcapsules with a diameter of 500 μm induced significantly more macrophage and fibroblast adhesion on the surface than capsules of 1,800 μm (Veiseh et al., 2015). Remarkably, we and others using microcapsules in the 0.5 mm range (Orive et al., 2006; de Vos et al., 2009; Hall et al., 2011; Paredes-Juarez et al., 2013) never observed these responses. A possible explanation form this (de Vos, 2017) might be a variations in the level of alginate purityused by the different groups (Paredes-Juarez et al., 2013, 2014a; Paredes-Juárez et al., 2014b). Veiseh et al did not apply alginates that were purified and were free of endotoxins (Veiseh et al., 2015). These endotoxins will diffuse after capsule formation to the surface. As smaller capsules have a higher surface to volume ratio than larger capsules, more immune stimulatory endotoxins will be present on the surface of the smaller capsules, leading to stronger tissue responses (Paredes-Juarez et al., 2013, 2014a; Paredes-Juárez et al., 2014b; de Vos, 2017). It is well known that alginate which is not sufficiently purified may provoke stronger tissue responses than purified alginates (Liu et al., 2011; Fang et al., 2017b). We but also others (Tomei et al., 2014; Manzoli et al., 2017, 2018; Buchwald et al., 2018a) do not see severe responses against small capsules and also recognize that larger diameters for capsules also implies lower oxygen supply to the islets (Tomei et al., 2014; Manzoli et al., 2017; Buchwald et al., 2018a; Komatsu et al., 2018; Tomei, 2018) which unfortunately is not discussed in the Veisah study (Veiseh et al., 2015). For this reason, we prefer and keep on working on smaller capsules (Spasojevic et al., 2014a; Paredes-Juarez et al., 2015; Llacua et al., 2018a,c) which will be further discusses in the next sections.

As mentioned above a major advantage of encapsulation is the possibility to use cells from non-human sources or a replenishable cell source from animal or human origin. World-wide there is a huge gap between supply and demand for cadaveric pancreata (Robertson, 2004; Bruni et al., 2014). This might be solved by using stem cell-derived insulin-producing cells or by using islets obtained from animals (Ekser et al., 2015). Encapsulation and protection from the recipients' immune system may facilitate clinical use of these cell sources. Due to significant progress in the field of stem-cell research and creation of a replenishable insulin-producing cell source, fundamental research toward better capsule formulations has revisited. Several groups report that encapsulated porcine islets, which is considered to be a replenishable insulin-producing cell source, successfully survived in non-human primates for over 6 months with both microencapsulation (Dufrane et al., 2006) and macroencapsulation (Dufrane et al., 2006) approaches. Another study with microencapsulated porcine islets reported up to 70 days survival in non-human primates which might be improved by enhancing oxygen supply (Safley et al., 2018). Successes also have been shown in human patients transplanted with microencapsulated porcine islets (Omami et al., 2017). A clinical study has reported improved HbA1c levels and reduced hypoglycemic episodes for more than 600 days (Matsumoto et al., 2016). Living Cell Technologies has performed a larger clinical study using Diabecell®, which is a commercial microencapsulated porcine islet graft which in humans resulted in a reduction in exogenous insulin use (Tan, 2010; Hillberg et al., 2013). Also, with stem-cells the usefulness of encapsulation technologies has been demonstrated. Pagliuca et al. (2014) transplanted alginate microencapsulated glucose-responsive stem-cell-derived β cells without any immunosuppression into T1D mice models which induced normoglycemia until their removal at 174 days after implantation (Vegas et al., 2016b). More recently, the maturation of human stem-cell-derived β cells was stimulated by forming islet-sized enriched β-clusters that responded to glucose stimulation as early as 3 days after transplant (Nair

et al., 2019). This, however, is not the only development in replenishable cell sources in which cell-encapsulation is instrumental. Genome-editing techniques have been creating a novel field that might lead to new insulin-producing cell sources (Cooper et al., 2016).

Despite its revisiting and promising application, cell encapsulation in extravascular systems still suffer from a common issue which is host responses against the capsules. These responses might ultimately lead to adhesion of inflammatory cells, fibroblast, collagen deposits that interfere with nutrition of the cells in the devices (Krishnan et al., 2017). Some groups report more and stronger host responses than others (Orive et al., 2018) with seemingly similar approaches. In this review we discuss progress made in the field and novel approaches to reduce or delete these responses on extravascular devices. This involves choice of type of polymer, the absence of proinflammatory residues or contaminants in the devices or polymers, insights in chemical conformation of surfaces to reduce host responses but also novel approaches for biofouling or immunomodulating biomaterials and application of polymers that form polymer brushes. In addition, we discuss possible beneficial effects of local release of immunomodulation molecules or inclusion and/or co-encapsulation of immunomodulatory cells.

ATTENUATE HOST RESPONSES BY RATIONAL CHOICES FOR POLYMERS

The original promise of the islet encapsulation technology is to hide islets from the host immune system and to make them untouchable (de Vos and Marchetti, 2002). This is still the basis of many membranes that have been developed over the past decade (Paredes-Juarez et al., 2013; Paredes-Juárez et al., 2014b; Paredes-Juarez et al., 2015; Llacua et al., 2016). Another pertinent aim is to use and design encapsulation materials that are biocompatibility and are having a permeability that guarantees protection against larger immune mediators such as immunoglobulins and complement factors but at the same time allowing exchange of essential nutrients in and out of capsules (Grace et al., 2016). The polymers that have been tested are derived from both natural sources or synthetic. There are different classes of natural polymers i.e., polysaccharides, polypeptide, and polynucleotides, of which polysaccharides are the most commonly used in cell encapsulation. They offer several advantages over the other two natural sources. They can provide cells with a membrane in a relatively mild fashion and generally without application of toxic solvents (de Vos et al., 2014). Furthermore, the majority of polysaccharides form hydrogels that are as flexible as natural tissue, mechanically stable (Li, 1998), and reportedly associated with minor host responses (Cieslinski and David Humes, 1994). Synthetic polymers are also widely investigated. Theoretically synthetic polymers can be reproducibly be produced without batch-to-batch variation. Another relevant advantage is that synthetic polymers can be tailor-made to improve biocompatibility or to induce other desired properties (Miura et al., 2006; Najjar et al., 2015; Pham et al., 2018).

Alginate

The most commonly applied and detailed studied polymer in encapsulation is alginate and applied in both macro- and microencapsulation approaches (Wang et al., 2011; Cañibano-Hernández et al., 2019). Alginate can be extracted from several organisms including *Azotobacter vinelandii*, several *Pseudomonas* species, and a variety of algae (Wee and Gombotz, 1998). Alginate is a natural anionic linear polysaccharide consisting of 1,4′-linked β-D-mannuronic acid (M) and α-L-guluronic acid (G) in different sequences or blocks, namely G-G blocks, G-M blocks, and M-M blocks (de Vos et al., 2014). The ratio and molecular weight of the blocks depends on the applied natural raw material for alginate extraction and is used to form capsules with different physical and chemical properties (Ostgaard et al., 1993; de Vos et al., 2014). Alginate capsules are usually formed by collecting cell-containing alginate droplets in a solution with a high concentration of cations. The cations in the solution bind to uronic acid blocks in alginate according a so-called egg-box model (**Figure 2**) (Li et al., 2007). The pliability and rigidity of alginate capsules depends on both the type of alginate and type of cation applied. Ca^{2+}, Sr^{2+}, and Ba^{2+} are having a high affinity and are in the concentration and duration of exposure not toxic for cells (Stokke et al., 1991). Gels generated from alginates with a high guluronic acid (High-G) content also form stronger gels (Uludag et al., 2000; de Vos et al., 2004; Bhujbal et al., 2014a). It was reported that the proinflammatory properties of alginate also depends on alginate types (Grace et al., 2016). Intermediate-G alginate provoked a lower immune response than low- and high-G alginate (Paredes-Juarez et al., 2013). This however can be changed by varying the cation types. Eg using barium instead of calcium in high-M alginates results in stable and biocompatible capsules. Barium in contrast to calcium can bind to both G-G and M-M and produces capsules with completely different properties. Duvivier-Kali et al. demonstrated with this approach survival of islet grafts in diabetic BALB/c and NOD mice for more than 350 days (Duvivier-Kali et al., 2001).

Other Natural Polymers

In addition to alginate, there are many other natural polymers used in encapsulation, which have received less attention than alginate but have shown some success. These include agarose, chitosan, cellulose, and collagen (de Vos et al., 2014).

Agarose is produced from agar and associated with minimal immune responses (Fernández-Cossío et al., 2007; Takemoto et al., 2015). Some successes have been shown in diabetic dogs with allogeneic islets in agarose microcapsules inducing normoglycemia for up to 49 days without significant accumulation of inflammatory cells and fibroblasts around the capsules (Tashiro et al., 1997). In diabetic Balb/c mice agarose microencapsulated mouse islets induced normoglycemia for up to 56 days without inflammatory cell infiltration (Agudelo et al., 2009). Also, agarose macrocapsules have been tested in diabetic mice (Iwata et al., 1994) and pancreatectomized dogs (Gazda et al., 2014). The main challenge with agarose is to create a gel with sufficient immunoprotection as it does not block diffusion of cytotoxic immunoglobulin G (IgG) (Iwata et al., 1992a,b). In principle, the immunoprotective properties of agarose gels are

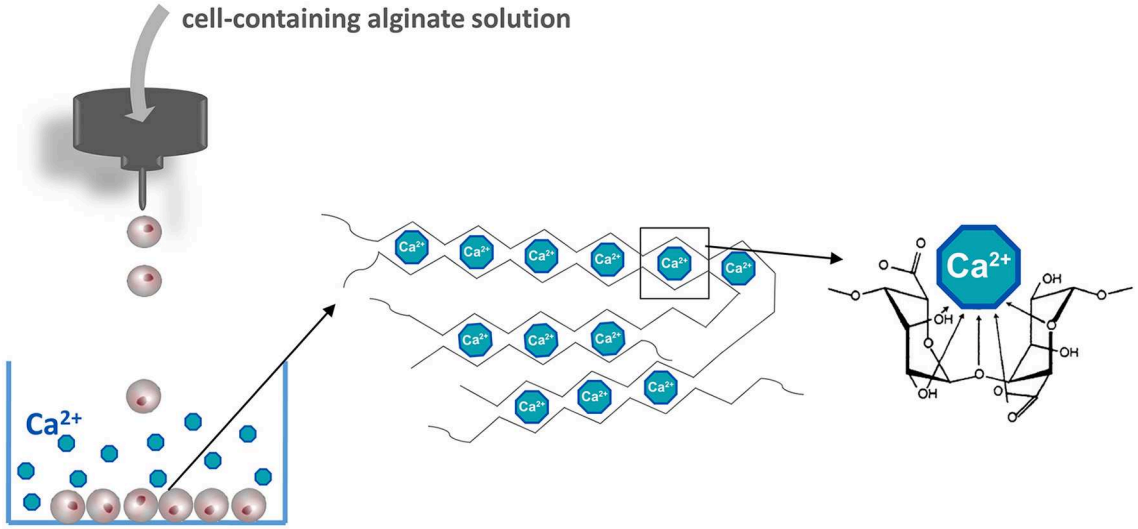

FIGURE 2 | Manufacturing islet-containing alginate-based microcapsules. Islets are suspended in an alginate solution solved in a balanced physiological salt solution in the absence of calcium. Alginate containing islet droplets are formed by an air- or electrostatic driven droplet generator. Droplets are collected in a $CaCl_2$ solution to form microcapsules. The basis of the gel formation is calcium crosslinking constitutive alginate molecules according to the egg-box model.

determined by the concentration of agar solution to form perm-selective membranes. Usually 5% agarose is used to generate immunoprotective capsules (Kobayashi et al., 2003). However, to enhance immunoprotection in *in vivo* studies, the agarose concentration was raised to 7.5–10% (Iwata et al., 1994). Another approach to enhance immunoprotection has been coating of agarose microcapsules with poly-acrylamide, which successfully prevented the entry of antibodies but provoked major host responses (Dupuy et al., 1990). To overcome the host responses more complex three layer agarose-based immunoisolation systems were introduced (Tun et al., 1996). To improve immunoprotection and mechanical stability, 5% polystyrene sulfonic acid (PSSa) was added together with 5% agarose to form the core of microcapsules. A polybrene layer coating was applied to prevent the leakage of PSSa that may stimulate host responses. Another layer of carboxylmethyl cellulose as the outermost shell offered biocompatibility of microcapsules (Tun et al., 1996). In addition to fine tuning permeability to enhance immunoprotection, researchers also investigated the possibility to combine local immunosuppression by co-encapsulating SEK-1005. SEK-1005 is an anti-inflammatory agent (Kuriyama et al., 2000). The rod was explanted 10 days after implantation leaving a subcutaneous transplant site that was surrounded by highly vascularized granulomatous tissue (Kuwabara et al., 2018). Islet transplanted in the site survived more than 100 days without immunosuppression owning to regulatory T cells in the granulomatous tissue that regulated immune reactions against islet grafts (Takemoto et al., 2015).

Also chitosan has been proposed as alternative for alginate. Several groups have shown success with chitosan as a coating layer for alginate-based microcapsule to reduce pericapsular fibrosis (Yang et al., 2016). Chitosan-alginate complexes have been suggested to improve long-term mechanical stability (Baruch and Machluf, 2006). However, the application of chitosan in islet encapsulation is somewhat limited due to low solubility of chitosan under physiological pH (Kubota et al., 2000; Ruel-Gariépy et al., 2002; Yang et al., 2010). PH values as low as four are needed to solve the polymer. Islets are very sensitive for low pH. Significant attempts have been made to modify chitosan as such that it is soluble under more physiological pH. Novel water-soluble chitosan derivatives have been developed (Sobol et al., 2013) that can be dissolved at pH 7.0. These novel formulations are obtained from oligochitosan and different aliphatic amines. When applied as membrane for alginate/calcium beads, no negative effects were observed (Sobol et al., 2013). Another study focusing on chitosan derivatives synthesized methacrylated glycol chitosan (MGC) in a saline solution at pH 9. These MGC membranes on the outside of alginate capsules enhanced mechanical stability and were associated with less fibroblast overgrowth than alginate/poly-L-ornithine/alginate capsules (Hillberg et al., 2015). Another approach to generate chitosan hydrogel that allow capsule formation at physiological pH values is adding glycerol 2-phosphate disodium salt hydrate into acetic chitosan solution (Yang et al., 2010). Rat islets macroencapsulated in this hydrogel reversed hyperglycemia in diabetic mice with a progressive increase in body weight as a consequence (Yang et al., 2010).

Cellulose is also proposed for cell encapsulation but a poorly soluble polysaccharide and has been chemically modified to hydroxypropyl cellulose (Heng and Wan, 1997), carboxymethyl cellulose (Tun et al., 1996), and ethylcellulose (Wandrey et al., 2010) for better solubility facilitating application in cell-encapsulation processes. Cellulose has been applied as encapsulation material with rat (Wang et al., 1997), porcine (Schaffellner et al., 2005) and mouse islets (Risbud et al., 2003). A pertinent issue with cellulose derivates is controversies about its

biocompatibility. Some groups report absence of host reactions to cellulose-based capsules (Pelegrin et al., 1998; Schneider et al., 2001), whereas other authors report visible tissue reactions involving immune infiltrates and fibrous capsular formation *in vivo* (Risbud et al., 2003). Another issue is that in contrast to alginate-based membranes, cellulose molecules can arrange closely together and form rigid structures which impact the permeability of the membranes. It has been shown that cellulose membranes prevent contact between activated complement proteins and the encapsulated islets (Risbud and Bhonde, 2001), but the low-permeability also delays insulin responses (Risbud et al., 2003).

Collagen is also able to form microcapsules for cell encapsulation. An advantage is that collagens are associated with minimal host responses (Yin et al., 2003). Although there are five major types of collagens, collagen type I is the most commonly applied polymer and also the most abundant type in the human body (Ramachandran, 1963; Lee et al., 2001). However, application of collagen in capsule manufacturing was limited by short-term mechanical stability and unstable permeability due to rapid enzymatic degradation post-transplantation (Szymanska and Winnicka, 2015). An enzyme resistant outer shell is required to maintain the integrity of the inner collagen core. A tetrapolymer of 2-hydroxyethyl methylacrylate—methacrylic acid—methyl methacrylate (HEMA– MAA–MMA) has been tested for this purpose (Chia et al., 2002; Yin et al., 2003). The capsules showed enhanced mechanical stability, a smoother surface and absence of protruding cells resulting in enhanced cell survival and function (Lahooti and Sefton, 2000; Chia et al., 2002). Other approaches involve application of crosslinkers to achieve long-term stability (Jorge-Herrero et al., 1999). Glutaradehyde was used as crosslinker to increase collagen stability but experiments were limited to *in vitro* studies due to severe host immune reactions (Marinucci et al., 2003). Success has been shown in reversing hyperglycemia in a diabetic rat model with hyaluronic acid-collagen hydrogel (HA-COL) encapsulated rat islets. These collagen based capsules were functional for up to 80 weeks with minimal fibrotic overgrowth or cellular rejection (Harrington et al., 2017). This might be due to more durable covalent crosslinks between HA and COL.

Synthetic Polymers

Compared with natural polymers, synthetic materials do not suffer from batch-to-batch variations and can be chemically modified to achieve different physical, chemical and biological properties (Pişkin, 1995). However, toxic conditions such as non-physiological pH or temperature, UV illumination or harsh solvents needed during manufacturing of immunoisolating devices might compromise cell viability and function of cells in synthetic polymer-based capsules (Young et al., 2012; Headen et al., 2014; Esfahani et al., 2017). This is the reason why in the majority of studies with synthetic molecules focus on macrocapsules which can be manufactured in absence of islets. With macrocapsules in contrast to microcapsules membranes are first produced and islets loaded later when all solvents are washed out. This is more difficult with microcapsules were islets have to be packed in the capsules and polymerization has to occur when islets are embedded in the polymers.

Poly (ethylene glycol) (PEG) is one of the most versatile synthetic polymer and also the most commonly applied synthetic molecule for encapsulation of pancreatic islets (Hill et al., 1997; Cruise et al., 1999) and coating microcapsules (Villa et al., 2017). PEG is a water-soluble polymer, which allows application in microencapsulation in absence of too harsh solvents. Several groups have shown success with PEG as an immunoprotective membrane to prolong islet functional survival (Weber et al., 2009; Knobeloch et al., 2017). In contrast to most synthetic polymers, PEG forms hydrogels with a high water content that offers a mild microenvironment (Lutolf and Hubbell, 2005; Nuttelman et al., 2008) for encapsulated cells inside and a protein-resistant surface outside (Andrade and Hlady, 1987). Although without harsh solvents, a threat to islet survival still exists during the photopolymerization crosslinking process (Nguyen and West, 2002; Lin et al., 2009), which is associated with free radical generation and, consequently, functional cell loss (Sabnis et al., 2009). However, novel approaches have emerged. A microfluidic strategy for generation of PEG-maleimide (PEG-4MAL) was developed (Phelps et al., 2013). PEG-4MAL showed minimal toxicity to islets and inflammation *in vivo*. The PEG-4MAL microcapsule was generated by enveloping cells in the core of the PEG-4MAL solution and subsequently rapid crosslinking the droplets with dithiothreitol, which was associated with short residence time, minimal cell stress in absence of generation of free radicals. The system is still versatile as the network structure of PEG-4MAL can be tuned by applying PEG of different molecular weights to fine-tune molecular weight cut-off (Headen et al., 2014) Recently, an innovative four-arm PEG-4MAL polymer carrying vascular endothelial growth factor (VEGF) has been introduced for coating macrocapsules in order to accelerate device vascularization post-transplantation (Weaver et al., 2018).

Aliphatic polyesters have also been proposed for cell encapsulation (Cameron and Shaver, 2011) but its mechanical instability and difficult to tune permeability due to its biodegradability (Buchholz et al., 2016) has limited its application. Poly (lactic-co-glycolic acid) (PLGA) is a linear, polymerized aliphatic polyester that may overcome some issues as it possesses better biostability (Angelova and Hunkeler, 1999). However, PLGA still undergoes hydrolysis under physiological conditions and produces lactic acid and glycolic acid (Ding and Schwendeman, 2008) but these two monomers are non-toxic at normal physiological dose. It has been reported however that the degradation of PLGA lowered the surrounding pH and subsequently created an autocatalytic environment for proteins (van de Weert et al., 2000). The low pH in the microenvironment may influence the release of insulin and may even evoke host responses (Jiskoot et al., 2009). PLGA microencapsulated porcine islets have been xenotransplanted into diabetic rats and reduced hyperglycemia significantly, but hyperglycemia could be completely reversed (Abalovich et al., 2001). The PLGA encapsulated islets release less insulin than islets placed in diffusion chambers *in vitro*, which might illustrate a negative impact of PLGA degradation products on islet function or insulin releasing capacity (Abalovich et al., 2001). If the degradation of

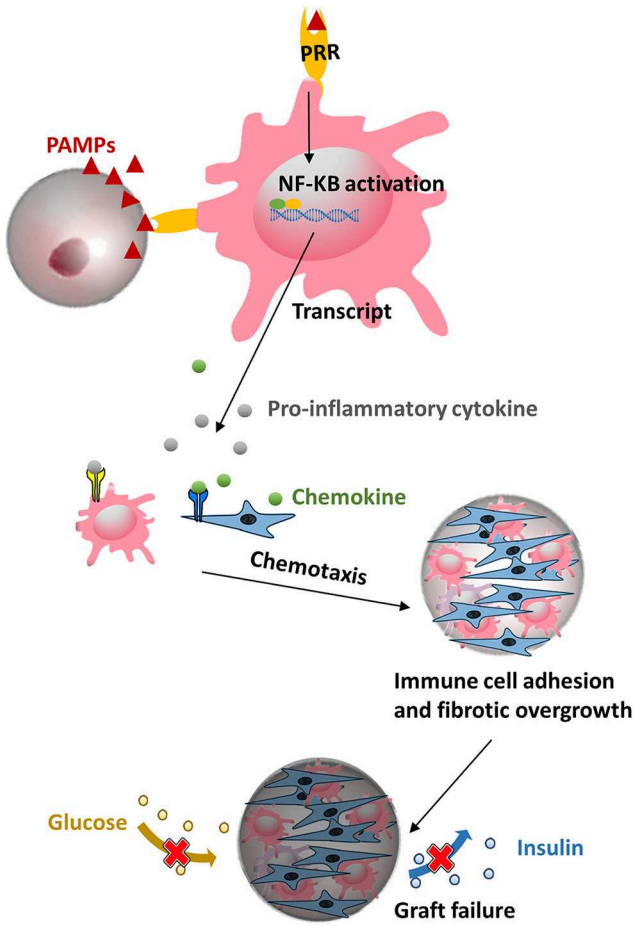

FIGURE 3 | Microcapsule made from polymers might contain pathogen associated molecular patterns (PAMPs) that can be recognized by pattern-recognition receptors (PRRs) on macrophage and evoke subsequent a cascade of proinflammatory responses, ultimately leading to a pericapsular fibrotic overgrowth of capsules and necrosis of the islets.

PLGA can be inhibited by modifying its structure, or its degree of crystallinity or amount of residual monomer (Xu et al., 2017) it still is a promising material for cell encapsulation because of its biocompatibility.

Another synthetic polymer that has been tested for cell-encapsulation is polyacrylate. This has been applied for both microencapsulation and macroencapsulation of pancreatic islets (Ronel et al., 1983; Sugamori and Sefton, 1989). Initial formulations of polyacrylate-based capsules had insufficient membrane permeability for water-soluble nutrients (Lahooti and Sefton, 1999). A modification that enhanced its applicability in cell encapsulation was that polyacrylate can be copolymerized with different acrylate units to tailor capsules with optimal biocompatibility and permeability (Stevenson and Sefton, 1987). To get an optimal rigidity and permeability, the hydrogel poly (2-hydroxyethyl methylacrylate) (HEMA) was copolymerized with the glassy poly (methyl methacrylate) (MMA) to manufacture the copolymer HEMA-MMA that can form flexible hydrogels for microcapsule generation (Babensee et al., 1992). A comparison of permeability between EUDRAGIT® RL (a commercially available copolymer of ethyl acrylate, methyl methacrylate, and methacrylic acid ester) and HEMA-MMA indicated sufficient permeability offered by both of the two materials to insulin and glucose (Douglas and Sefton, 1990). However, it was too porous to protect enveloped cells for immunity and consequently only postponed graft destruction (Surzyn et al., 2009). The molecular weight cut-off of HEMA-MMA is around 100 kDa (Crooks et al., 1990), which cannot protect for escape of antigens and subsequent T cell activation (Surzyn et al., 2009). The application of HEMA-MMA microcapsules needs a novel approach to reduce and fine-tune permeability.

As a derivative of polyacrylate, polyacrylonitrile (PAN) was copolymerized with methallylsulfonate to produce AN69 (polyacrylonitrile-sodium methallylsulfonate) (Honiger et al., 1994). AN69 has been applied in macrocapsules (Kessler et al., 1991, 1992; Honiger et al., 1994; Colton, 1996). The AN69 membrane possesses optimal immunoisolation ability and is permeable to small molecular water-soluble substances (Sevastianov et al., 1984). However, the *in vivo* studies of AN69-based macrocapsules showed a reduced permeability for nutrients and insulin (Kessler et al., 1992), as a consequence of extreme protein adsorption (Silva et al., 2006).

Current challenges in application of many synthetic polymers for cell encapsulation are overcoming the use of hazardous solvents (Olabisi, 2015), reducing strong host responses (i.e., polyurethane and polypropylene) (George et al., 2002; Kawiak et al., 2003), or preventing fibrotic overgrowth (i.e., polyvinyl alcohol and polypropylene). Probably because of these issues combinations of natural and synthetic materials have attracted much attention from researchers. Several new concepts and multilayer encapsulation systems have emerged, which are discussed in following sections. However, first a common issue in application of synthetic and natural polymers needs to be discussed which is possible contaminations with endotoxins or better, pathogen-associated molecular patterns needs to be discussed.

Pathogen-Associated Molecular Patterns (PAMPs) in Polymers

A still ongoing and pertinent consideration in application of any polymer in cell-encapsulation is the need to use the polymers as pure as possible. Taking the most widely used natural polymer alginate as an example, all commercially available crude alginate contain proinflammatory PAMPs, including flagellin, lipopolysaccharide, peptidoglycan, lipoteichoic acid, and polyphenols (Paredes-Juárez et al., 2014b). Also other sources such as synthetic molecules i.e., polyethylene glycol was found in our assays to contain PAMPs. All of the above mentioned contaminants will play a negative role in host responses against capsules (Krishnan et al., 2017). During recent years it has been shown that these PAMPs (Paredes-Juarez et al., 2013, 2014a; Paredes-Juárez et al., 2014b) induce inflammatory responses in recipients either by diffusing out of the capsules or by being present at the capsule surface.

This happens primarily via pattern-recognition receptors (PRRs) (**Figure 3**). After activation of PRRs on immune cells a cascade of intracellular signaling pathways are activated, leading to translocation of nuclear factor kappa-light-chain-enhancer of activated B cells (NF-κB) inducing inflammatory cytokine secretion, ultimately resulting in overgrowth of the capsules by immune-cells and fibroblasts (Kendall et al., 2004; Tam et al., 2006; Ménard et al., 2010; Paredes-Juárez et al., 2014b). Because fibrosis of the surface obstructs the ingress of nutrient and egress of waste, effective regulation of hyperglycemia is restricted to a limited period (de Vos et al., 1994, 2002b, 2012). Notably, apart from contaminants, it has been reported that uncrosslinked mannuronic acid polymers can trigger immune activation (Flo et al., 2002). For all these reasons, it is mandatory to apply purification procedures and quality assessment systems for purity of alginate (Paredes-Juarez et al., 2014a; de Vos, 2017; Orive et al., 2018).

There are a number of purification strategies published that obtain relatively endotoxin-free alginate. There are three mainstream classic "in-house" purification approaches (Klöck et al., 1994; De Vos et al., 1997b; Prokop and Wang, 1997). The protocol of de Vos starts with protein extraction with chloroform/butanol mixtures under acidic and neutral pH conditions (De Vos et al., 1997b). Prokop purified alginate by charcoal treatment and dialysis (Prokop and Wang, 1997), whereas the processes of forming, washing and dissolving alginate Ba^{2+} beads are applied in Klöck's protocol (Klöck et al., 1994). Purification procedures can reduce endotoxin, polyphenols, and proteins, but the final product differs greatly in degree of purity (Dusseault et al., 2006). In 2016 a novel purification strategy was added to the list of methods. This method is based on activated charcoal treatment, hydrophobic membrane filtration and dialysis (Sondermeijer et al., 2016). Using this approach, purified alginate was created that induced minimal foreign body reactions up to 1 month after implantation. In addition to purification a fast and efficient platform is needed to test the efficacy of purification. Paredes-Juarez et al. have published a platform that allows for identification of PRR activating capacity of polymers and finally identification of the type of contaminant in the polymers (Paredes-Juarez et al., 2014a). This eventually can lead to strategies to remove the contaminants. Despite the availability of several methods to purify alginates and to identify contaminants in polymers, it is still rarely used. This is however highly recommended as there are several lines of evidence that even polymers sold as ultrapure (Paredes-Juarez et al., 2013; Paredes-Juárez et al., 2014b) still contain endotoxins that might be responsible for inflammatory responses after implantation.

POLYMERIC ENGINEERING APPROACHES TO REDUCE TISSUE RESPONSES

Multilayer Capsules

Due to shortcoming of some of the above discussed available polymers, the majority of researchers choose to produce microcapsule with application of combinations of molecules. Often these are applied in layer-by-layer systems (Tun et al., 1996; Schneider et al., 2001; Chia et al., 2002; Park et al., 2017). Alginate, as the most commonly used encapsulation materials, was in some confirmations, too porous to prevent penetration of IgG (Dembczynski and Jankowski, 2001) and some formulations were associated with low mechanical stability and higher surface roughness caused by cell protrusions after long term culture. Cationic polymers from chemical synthesis procedures were used to coat alginate-based capsules and overcome these issues. Commonly used examples are alginate coated with poly-l-lysine (PLL) (de Vos et al., 2002b), poly-L-Ornithine (Darrabie et al., 2005), PEG (Park et al., 2017), chitosan or agarose.

PLL was originally applied to decrease the pore size of alginate membranes and to enhance mechanical stability (De Vos et al., 1997a; Kendall and Opara, 2017). For many years, application of PLL was reported to be associated with enhanced immune responses against capsules. However, systemic studies with application of, for the field new, physics and chemical technologies such as Fourier-transform infrared spectroscopy (FT-IR), X-Ray Photoelectron Spectroscopy (XPS), and Time-of-Flight Secondary Ion Mass Spectrometry (ToF-SIMS) has revealed that PLL should be forced in a specific conformation to avoid responses. Any PLL that is not in the structure will bind cells in the vicinity of the capsules and provoke tissue responses. The following steps are essential to generate capsules with PLL that do not provoke responses. First, after gelification in a calcium solution alginate-based capsules have to be suspended in a low calcium high sodium buffer. During this step calcium on the surface of capsules is displaced by sodium that has lower affinity for alginate than PLL. This has to happen in the first few microns of the surface. Sodium will subsequently be substituted by PLL in a PLL-solution that lacks divalent cations. This process is temperature sensitive and should always be done in a consistent way. If done correctly, it creates a calcium alginate system that is composed of two layers, namely an alginate core and a layer of PLL-alginate complexes. There are three different binding modes in the outer layer, including (i) random coil formation between alginate and PLL, (ii) α-helicoidal structure between amide groups of PLL, and (iii) antiparallel β-sheet structure between amide groups of PLL (de Vos et al., 2002a; van Hoogmoed et al., 2003; Paredes-Juárez et al., 2014b). All PLL should be in this network which can be documented by FT-IR. By a stepwise approach and repeated implantations in mice it has been demonstrated that optimal biocompatible alginate-PLL capsules can be created as long as the PLL is in these confirmations (Juste et al., 2005). The PLL also improved the mechanical stability and permeability of alginate-based capsules (van Hoogmoed et al., 2003; Bhujbal et al., 2014b).

Conformal Coating

As outlines in section Islets Encapsulation Technology many groups prefer to encapsulate islets in the smallest capsule possible to guarantee optimal nutritional supply to the enveloped islets (Orive et al., 2006; de Vos et al., 2009; Hall et al., 2011; Paredes-Juarez et al., 2013; Villa et al., 2017; Buchwald et al., 2018a). A recent study even suggest that the distance between islet-and surrounding fluid should be below 100 μm to allow optimal

supply of nutrients (Iwata et al., 2018). These type of distances can be achieved with a technology called conformal coating (Tomei et al., 2014; Manzoli et al., 2017, 2018; Buchwald et al., 2018a). In addition to improving oxygen and nutrient transport conformal coating strategies also reduce the total transplant volume allowing implantation in other sites than the traditionally applied peritoneal cavity (Tomei et al., 2014; Buchwald et al., 2018b; Ernst et al., 2019). As this review does focus on polymers and tissue responses, we will discuss this subject in view of polymers applied and not current developments with this technology. Islet conformal coating approaches typically apply polyelectrolytes or complementary materials which are coated on a surface of cells or cell aggregates via intermolecular forces, i.e., electrostatic forces, hydrogen-bonds, or covalent linkages (Borges and Mano, 2014; Yamamoto et al., 2016). PEG was one of the first and still commonly applied polymers in islet conformal coating technologies. PEG is used in conformal coating techniques with photopolymerization (Cruise et al., 1999) microfluidic approaches (Tomei et al., 2014), via ester-bonding (Lazarjani et al., 2010), and via hydrogen-bonds (Wilson et al., 2010). In order to regulate permeability, multiple-arm PEG was developed. Islets conformally coated with this technique successfully corrected hyperglycemia for more than 100 days in mice (Rengifo et al., 2014; Giraldo et al., 2017). More recently, a heparin functionalized, 8-arm PEG was synthesized to coat islets with nanoscale barriers. This enhanced survival as it inhibited islet-cell apoptosis and promoted neovascularization *in vitro* (Lou et al., 2017). However, the potential anti-inflammatory effects of incorporated heparin, which is a well-known effect of heparin (Mao et al., 2017), was not discussed in this study.

During recent years the lay-by-layer (LBL) assembly with PEG has emerged as another promising alternative strategy (Ryan et al., 2017) to conformally coat islets. Theoretically this should overcome some limitation of the single-layer-PEG approach and in particular the potential harmful effects of PEG conformal coating techniques (Miura et al., 2006; Wilson et al., 2010; Chen et al., 2011) on mechanical instability (Itagaki et al., 2015; Yamamoto et al., 2016), and on sometimes inadequate immune-protection (Teramura et al., 2007). Polyelectrolytes applied in LBL coating can both be synthetic and natural polyelectrolytes (Granicka, 2014). In a recent study, acrylate modified cholesterol bearing pullulan (CHOPA) was employed to create a multilayer coating on β cell aggregates under mild polymerization conditions (Bal et al., 2018). In these CHOPA nanogels, pullulan can form immunologically inert gels without the use of toxic cations or other chemicals. In this system cholesterol units provide hydrophobic crosslinking points that promote self-assembly of polymeric particles (Bal et al., 2018). To reach an optimal equilibrium point of diffusion and immunoisolation, oppositely charged polymers (positively charged chitosan and negatively charged PSS) was applied in 9 layers on human islets (Syed et al., 2018). This system could induce normoglycemia for up to 180 days in a model of human to mice xenotransplantation with minimal immunocyte infiltration on the capsules (Syed et al., 2018). Also linear or star-shaped PEG derivatives are intensively studied for application in layer-by-layer approaches (Ryan et al., 2017; Perez-Basterrechea et al., 2018). Haque et al has built an coating layer with thiol-6-arm-PEG-lipid (SH-6-arm-PEG-lipid) and with gelatin-catechol to provide islets with a substitute for the extracellular matrix of islets and added three other coatings with 6-arm-PEG-SH, 6-arm-PEG-catechol, and linear PEG-SH respectively to provide immunoprotection (Haque et al., 2016). The multi-layer system preserved islet cell viability but the polymers showed minimal adsorption of human serum albumin, fibronectin, and immunoglobulin G. The system induced prolonged graft survival in a xenogeneic porcine-to-mouse model, which was further enhanced by applying an immunosuppressive cocktail (Haque et al., 2016). There is even efficacy shown in a xenogeneic monkey-to-mouse model in which 100% of the grafts survived for more than 150 days. After this period minimal or no immunocyte infiltration was observed (Haque et al., 2017). Given the potential severe side effects of generalized immunosuppression, a more recent study developed a controlled immunosuppressant FK506 release nanoparticle system using 3,4–dihydroxyphenethylamine (DOPA) conjugated PLGA–PEG to coat islet surfaces and to provide local immunosuppression (Pham et al., 2018). This study illustrates the potential of using layer-by-layer assembly as both barrier and carrier system for graft-survival promoting molecules.

Anti-biofouling

In the post-transplantation period the host response starts with nonspecific protein adsorption and subsequent adhesion of immune cells and fibroblasts onto the capsule surface, a process termed "biofouling" (Harding and Reynolds, 2014). Several approaches have been explored to inhibit this issue with an approach called anti-biofouling which involves application of molecules on the surface of capsules to reduce protein adsorption. Most-studied strategies are based on application of low-biofouling polymers. Coated with hydrophilic polymeric materials the capsule surface is covered by a layer of water molecules, providing a highly resistant surface to protein adsorption (Kingshott and Griesser, 1999).

One of the most commonly applied molecules for anti-biofouling is PEG. PEG matrices can induce low protein adsorption but efficacy depends on chain density, length, and conformation (Michel et al., 2005; Unsworth et al., 2008). The protein resistance of a PEG surface proportionally increases with higher polymerization degrees and denser brush bristles on the surface (Andrade and Hlady, 1987; Cruje and Chithrani, 2014). PEG has been applied to coat alginate capsules to lower permeability and enhance mechanical stability but also served as anti-biofouling layer (Chen et al., 1998; Park et al., 2017). To coat alginate-based microcapsules, the PEG backbone was charged with added amine groups (NHs^{+}), which can interact with naturally negatively charged alginate (Chen et al., 1998). In this way, PEG-amines can stably crosslink with alginate as a coating layer (Chen et al., 1998). Another group of investigators used mild glutaraldehyde (GA) treatment which increased the capsule strength, flexibility, and biocompatibility (Chandy et al., 1999). PEG coating brought many beneficial properties for cell encapsulation, including prevention of fibrotic overgrowth on the capsule surface

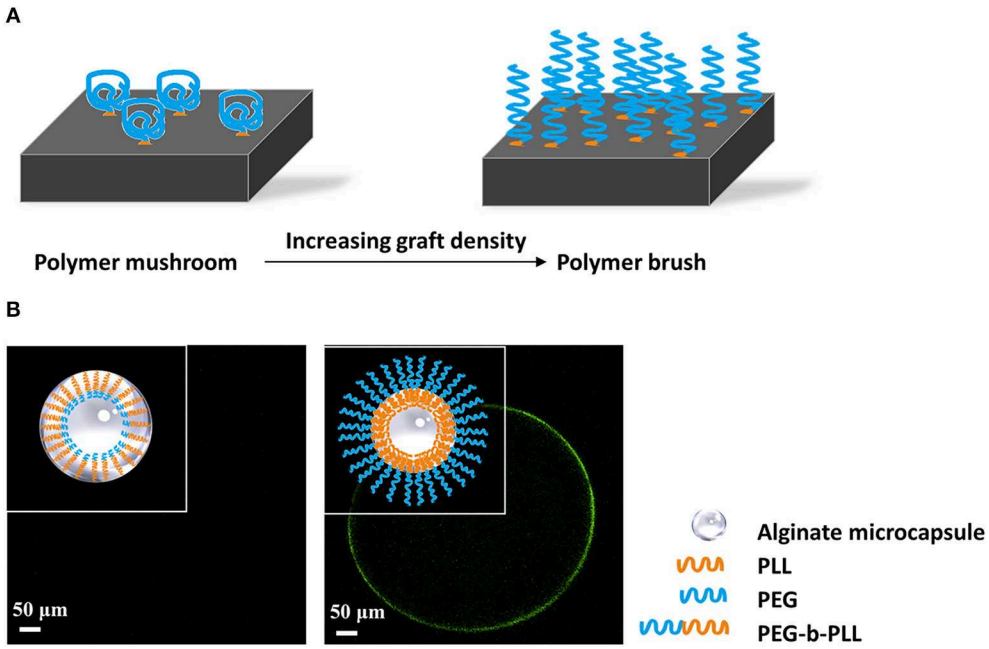

FIGURE 4 | (A) Principle of formation of polymer brushes. At low grafting density polymers will have a mushroom conformation at the surface of capsules. When the grafting density increases and space becomes limited, the polymers will stretch and form a polymer brush that does not allow for protein and cell adhesion. **(B)** Schematic illustration of antibiofouling polymer brush surface formatted from PEG-b-PLL. PEG has to be long to prevent penetration into the alginate network and to stimulate stretching of the molecules on the surface (Spasojevic et al., 2014b). The outer PEG layer blocks shed unbound cytotoxic PLL and simultaneously provides a protein resistant surface, which showed antibiofouling properties *in vivo* studies.

(Chen et al., 1998). However, still tissue responses may occur which was further reduced by introducing immunosuppressive agents. In one of these approaches, rapamycin-PEG-coated alginate microcapsules inhibited non-specific binding and proliferation of macrophages *in vitro* and decreased fibrosis of capsules with more than 50% in a xenogeneic islet transplantation model (Park et al., 2017). Another approach using the protein-resistant property of PEG was by application of copolymers with PEG. Poly(ethylene glycol)-block-poly(l-lysine hydrochloride) (PEG-b-PLL) was coated on top of a proinflammatory, but immunoisolating, perm-selective alginate-PLL membrane (Spasojevic et al., 2014b). The diblock copolymer masked proinflammatory PLL and built an anti-fouling outer layer and successfully ameliorate host responses. A more recent study present a novel macroencapsulation strategy (Marchioli et al., 2017) that possibly induces anti-biofouling but also supports neovascularization while minimizing fibroblast adhesion. The technology applies two layers made of an anti-biofouling polyethyleneglycole diacrylate (PEGDA), and two pro-angiogenic growth factors conjugated to PEGDA. These two layers were covalently crosslinked and induced controlled release of basic fibroblast growth factor (bFGF) and vascular endothelial growth factor (VEGF) for up to 14 days (Marchioli et al., 2017) stimulating neovascularization.

Polymer Brushes

An emerging new approach to reduce protein adsorption and cell-adhesion is application of polymer brushes. Polymer brushes consist of polymer chains that are densely tethered with other polymer chains on a surface (**Figure 4A**) (Feng and Huang, 2018). Polymer brushes form an ultrathin, solid coating (Kim and Jung, 2016).The polymer brush coating not only significantly changes the surface properties but also gives the surface new functionalities (Barbey et al., 2009). Spasojevic and colleagues showed a novel strategy combining the benefits of PLL and PEG by creating diblock co-polymers of poly(ethylene glycol)-block-poly(l-lysine hydrochloride) (PEG_{454}-b-PLL_{100}) (Spasojevic et al., 2014a). The copolymers bind with alginate with its positive charged PLL tail. PEG has to be long to prevent penetration into the alginate network and to stimulate stretching of the molecules on the surface (**Figure 4B**). The outer PEG layer blocks shed unbound cytotoxic PLL and simultaneously provides a biocompatible surface. Subsequent *in vivo* study proved the microcapsules have better biocompatibility illustrated by an absence of cell adherence (Spasojevic et al., 2014b).

Also other polymer brushes have been investigated recently. One of the studies coated soft chitosan surfaces with polymer brushes of oligo(ethylene glycol) methyl ether methacrylate and 2-hydroxyethyl methacrylate by photopolymerization (Buzzacchera et al., 2017). The novel polymer brush surface was reported to reduce protein adhesion and eliminated platelet activation and leukocyte adhesion (de los Santos Pereira et al., 2016; Buzzacchera et al., 2017). The application of diblock polymers is to our opinion a promising approach to combine advantages of different polymers but needs a multidisciplinary approach as in our hands uniform and complete coverage of the capsules surface with a brush was challenging.

ACCESSORY CELL STRATEGIES TO REDUCE TISSUE RESPONSES

Often polymeric approaches are combined with pharmaceutical approaches to reduce tissue responses but during recent years a new emerging trend of applying and co-encapsulating "immunosuppressive" cells has shown some success. One of these immunosuppressive cell-types are T regulatory (Treg) cells. Tregs have been successfully immobilized on islet surfaces through streptavidin-biotin interactions (Gołab et al., 2014). This was done by first incubating the islets with a Biotin-PEG-succinimidyl valeric acid ester followed by an incubation with streptavidin. Subsequently, Treg cells were brought onto the islets (Gołab et al., 2014; Gliwinski et al., 2017). The islets coated with Treg-cells showed a lower glucose-stimulated insulin release than controls (Gołab et al., 2014). Although efficacy *in vivo* is not reported yet, this approach holds some promises as recruiting Treg cells by intramuscular co-transplantation of islets with a plasmid encoding Treg cell specific chemokine CCL22 was efficacious in preventing graft rejection (Vågesjö et al., 2015). Some success has also been shown in xenotransplantation with blockade of the costimulatory pathway of CD40/CD154, which inhibited T cell and B cell signaling (Ock et al., 2018; Do et al., 2019). In mice treated with this approach, increased numbers of Treg cells and an elevated anti-inflammatory cytokine profile was found around a porcine islet grafts (Wu et al., 2017). More recently, it was shown that Jagged-1, i.e., a potent immunomodulatory factor, immobilized on PEG-coated islet surfaces induced an increased population of Treg cells and a decreased level of proinflammatory cytokines *in vitro*, and an improved blood glucose control *in vivo* (Izadi et al., 2018). However, instead of enhancing the population of Treg cells, a recent study induced downregulation of proinflammatory T effector (Teff) cells by co-transplanting microgels conjugated with Fas-ligand on their surface (Headen et al., 2018). Fas, as a death receptor on the surface of T effector cells, can be activated by Fas-ligand resulting in an increased ratio of Treg to Teff (Headen et al., 2018). This system induced normoglycemia for more than 200 days in mice (Headen et al., 2018). The results show that a combination of polymeric encapsulation with recruitment of immune regulating cells might provide improved islet survival.

In addition to application of T-cells to regulate tissue responses, various endothelial cell types have been applied for co-encapsulation to promote survival of encapsulated cells (Ernst et al., 2019). Endothelial cells might have some benefits for islets as they have been shown to resist and neutralize reactive oxygen species, inhibit thrombogenesis, promote revascularization, and form extracellular matrices (Staels et al., 2016; Karimian et al., 2017). Co-transplanting these cells with islets has successfully promoted graft revascularization and promoted survival in several micro-and macroencapsulation approaches (Gupta and Sefton, 2011; Buitinga et al., 2016; Li et al., 2017). One study reports successful and expedited islet cell engraftment by coating islets with vascular endothelial cells (Barba-Gutierrez et al., 2016). During the last decade, also the application and co-encapsulated mesenchymal stem cells (MSCs) has been intensively studied in islet transplantation (Ben Nasr et al., 2015; Hirabaru et al., 2015; Unsal et al., 2015; Yoshimatsu et al., 2015; Cao et al., 2016). MSCs theoretically support angiogenesis and produces immunomodulatory molecules (Kim et al., 2019; Laporte et al., 2019), when co-transplanted with islets. Indeed co-encapsulation of MSCs have been shown to increase neovascularization and reduce islet cell death in both micro- and macroencapsulation approaches (Vériter et al., 2014; Borg et al., 2016; Buitinga et al., 2016; Bal et al., 2017; Hamilton et al., 2017) and might hold promises for improving graft survival.

IMMUNOMODULATORY MATERIALS

During recent years novel biomaterials have been designed that eventually might serve as immunomodulating polymers to reduce or prevent host reactions to encapsulated cell systems. One such an approach is application of Staudinger ligation chemistry to link immunomodulatory proteins with PEG. Staudinger chemistry, based on the specific crosslinking reaction between azide- and phosphine-labeled molecules, was successfully applied for conjugating different polymers (Hall et al., 2011) or bio-functional molecules with encapsulation polymers (Chen et al., 2011). Specifically, an amide bond was generated from an azide on protein and a specifically functionalized phosphine on triphenylphosphine-PEG. By this approach, thrombomodulin (TM) was bound with PEG, subsequently being immobilized on islet surfaces through streptavidin-biotin interactions. TM catalyzes the generation of activated protein C (APC) (Esmon, 2004), which possesses potent anti-inflammatory activity by inhibiting proinflammatory cytokines production in macrophages (Grey et al., 1994; Esmon, 2004). Co-immobilized TM induced protein C activation, which was similar to the activated protein C level catalyzed by endogenous TM in mouse pancreatic islets indicated reduction of inflammatory processes (Wilson et al., 2010). Chen and colleagues reported a different method to co-immobilized urokinase (UK) and TM on islet surfaces by PEG-conjugated phospholipids (Chen et al., 2011). Maleimide–PEG–lipid-anchored to the lipid bilayer membrane through hydrophobic interactions. Thiol (SH) groups on the SH-UK and SH-TM replaced maleimide groups and conjugated at the end of PEG chains on the cell membrane (Chen et al., 2011). The surface of islets coated with these membranes increased APC generation and released functional UK and TM, which reduced the instant blood-mediated inflammatory reactions after implantation and prolonged graft survival (Korsgren et al., 2008). In another approach to immunomodulate, hemoglobin (Hb-C) was crosslinked with PEG to scavenge nitric oxide (NO) and limit NO's negative biological actions (Han et al., 2002; Chae et al., 2004). Because of constraints that not every immunomodulator can be conjugated with polymers, an alternative strategy involves simple mixing immunomodulatory substances with polymers. Rapamycin has been trapped into PEG microcapsules and successfully prevented foreign body responses against capsules containing porcine islets (Park et al., 2017).

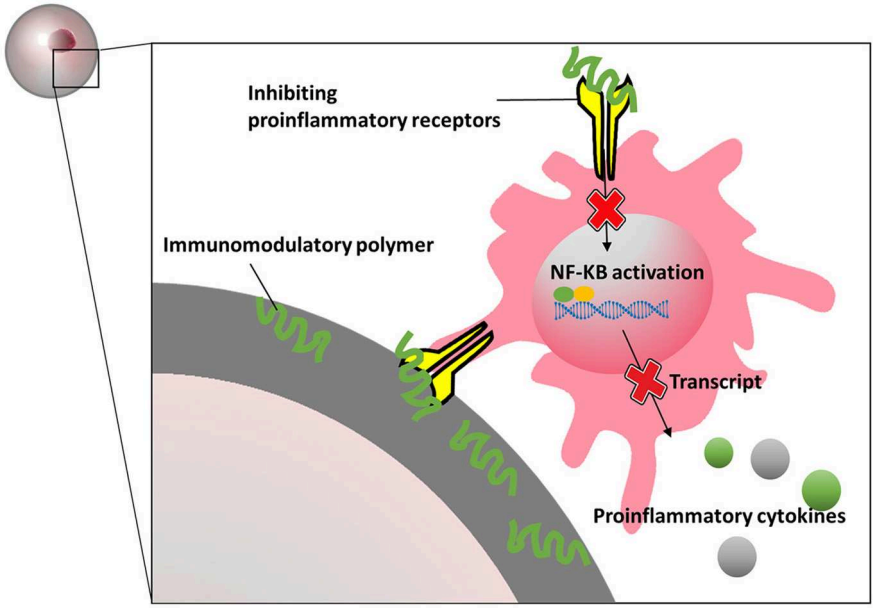

FIGURE 5 | Schematics presentation of how immunomodulatory polymers block proinflammatory receptors and inhibit inflammatory signal pathways.

Also silk hydrogels have been shown to have immunomodulatory effects on macroencapsulated rat islets (Hamilton et al., 2017). Islets were seeded on silk scaffold and subsequently encapsulated in an alginate-Ba^{2+} network. An additional alginate-layer was added and cross-linked on the periphery of the scaffolds for immunoisolation (Kumar et al., 2017). The results indicate that blended silk hydrogel not only influenced islet viability, insulin secretion and endothelial cell maintenance, but also decreased production of proinflammatory cytokines *in vitro*. After injected with interleukin-4 (IL-4) and dexamethasone-loaded hydrogels, the silk macrocapsules showed a strong macrophage polarization toward a M2 phenotype which might provide an immunopermissive environment for the implants. A more recent study demonstrate that 2-aminoethyl methacrylate hydrochloride coupled to alginate can reduce tissue responses (Somo et al., 2018). By ionic crosslinking followed by exposure to ultraviolet light, 2-aminoethyl methacrylate hydrochloride modified alginate can be formed. The capsules were reportedly more mechanical stable than the alginate-beads and showed less inflammation on the surface of the beads after 3 weeks in LPS-stimulated rats (Somo et al., 2018). Meanwhile, in the field of intestinal immunity and bromatology, several heteropolysaccharides have been reported to possess immunomodulatory properties. Polysaccharide extracted from *Morinda citrifolia Linn* (Sousa et al., 2018), *Lentinula edodes* (Ren et al., 2018), *Schizophyllum commune* (Du et al., 2017), and lemon showed immunomodulatory effects. Most of these molecules bind to specific pro-inflammatory immune receptors which to our opinion might be a valuable approach to create immunomodulating capsules surfaces (**Figure 5**).

CONCLUDING REMARKS AND FUTURE PERSPECTIVES

Although encapsulation in permselective membranes is a field that is around for more than three decades, important new polymeric approaches have emerged during recent years that create optimism that a technology can be developed that provokes minimal tissue responses and allows long term survival of encapsulated cells. The technology has revisited together with new approaches for creating a replenishable cell sources for curing endocrine diseases such as T1D. Some of these sources involve the use of xenogeneic tissue which might be particularly challenging in an encapsulation setting as indirect antigen presentation might be involved (Shin et al., 2014, 2015). Conceivable approaches to overcome influences of indirect antigen presentation might be application of the discussed polymer brushes and immunomodulating materials. With this approach either effector arms of the immune response can be blocked or adsorption of essential molecules to full-fill the response can be prevented. Also, lowering the permeability may be a suitable approach. The Beta-O2 device applied in pigs was having an Mw cutoff of about 80 kDa which might have been enough to prevent antigens responsible for indirect presentation to leak out (Neufeld et al., 2013). As such this review has attempted to demonstrate that rational choices for polymers and surface modification to modulate tissue responses and to prolong graft survival.

In addition to novel polymers to reduce tissue responses also other approaches have emerged. Some promising approaches are coating or co-encapsulation of nanoparticles for targeted and local drug delivery without systemical side-effects (Fang et al.,

2014, 2017a, 2018; Dehaini et al., 2017; Zhang et al., 2017). Also approaches in which immune regulatory cells are applied in combination with encapsulation show promise although convincing *in vivo* results are not yet available. Apart from impact of polymers and tissue responses, long-term maintenance of islet cell viability is an important issue that requires much more attention by the scientific community. This is essential for graft function but also for reducing tissue responses as dead cells release danger-associated molecular patterns that provoke local tissue responses (Paredes-Juarez et al., 2015). A possible approach to prevent or reduce cell-death is by including extracellular matrix molecules (ECM) (Llacua et al., 2018b) in encapsulation systems (Del Guerra et al., 2001; Llacua et al., 2018a,c). ECM is damaged during islet isolation and has an enormous impact on survival of islets in encapsulated islet grafts (de Vos et al., 2016). ECM can stimulate cell proliferation, and eliminate known adverse factors.

Overall, current insight points to several potential successful strategies to reduce tissue responses against encapsulated islets grafts. This include novel or improved polymers but possibly also immune modulatory molecules or cells to allow long-term survival of encapsulated islet grafts. Although many long-term successes have been shown in several animal models there is consensus among insurance companies that 1-year survival is required with possibility to retrieve the graft before human application can be considered. To achieve this with in this review discussed approaches is to our opinion a realistic goal.

AUTHOR CONTRIBUTIONS

All authors listed have made a substantial, direct and intellectual contribution to the work, and approved it for publication.

REFERENCES

Abalovich, A., Jatimliansky, C., Diegex, E., Arias, M., Altamirano, A., Amorena, C., et al. (2001). Pancreatic islets microencapsulation with polylactide-co-glycolide. *Transplant. Proc.* 33, 1977–1979. doi: 10.1016/S0041-1345(01)01918-2

Agudelo, C. A., Teramura, Y., and Iwata, H. (2009). Cryopreserved agarose-encapsulated islets as bioartificial pancreas: a feasibility study. *Transplantation* 87, 29–34. doi: 10.1097/TP.0b013e318191b24b

American Diabetes Association (2018). Economic costs of diabetes in the U.S. in 2017. *Diabetes Care* 41, 917–928. doi: 10.2337/dci18-0007

Andrade, J. D., and Hlady, V. (1987). Plasma protein adsorption: the big twelvea. *Ann. N. Y. Acad. Sci.* 516, 158–172. doi: 10.1111/j.1749-6632.1987.tb33038.x

Angelova, N., and Hunkeler, D. (1999). Rationalizing the design of polymeric biomaterials. *Trends Biotechnol.* 17, 409–421. doi: 10.1016/S0167-7799(99)01356-6

Atkinson, M. A., Eisenbarth, G. S., and Michels, A. W. (2014). Type 1 diabetes. *Lancet* 383, 69–82. doi: 10.1016/S0140-6736(13)60591-7

Babensee, J. E., De Boni, U., and Sefton, M. V. (1992). Morphological assessment of hepatoma cells (HepG2) microencapsulated in a HEMA-MMA copolymer with and without Matrigel. *J. Biomed. Mater. Res.* 26, 1401–1418. doi: 10.1002/jbm.820261102

Bal, T., Nazli, C., Okcu, A., Duruksu, G., Karaöz, E., and Kizilel, S. (2017). Mesenchymal stem cells and ligand incorporation in biomimetic poly(ethylene glycol) hydrogels significantly improve insulin secretion from pancreatic islets. *J. Tissue Eng. Regen. Med.* 11, 694–703. doi: 10.1002/term.1965

Bal, T., Oran, D. C., Sasaki, Y., Akiyoshi, K., and Kizilel, S. (2018). Sequential coating of insulin secreting beta cells within multilayers of polysaccharide nanogels. *Macromol. Biosci.* 18:e1800001. doi: 10.1002/mabi.201800001

Barba-Gutierrez, D. A., Daneri-Navarro, A., Villagomez-Mendez, J. J., Kanamune, J., Robles-Murillo, A. K., Sanchez-Enriquez, S., et al. (2016). Facilitated engraftment of isolated islets coated with expanded vascular endothelial cells for islet transplantation. *Transplant. Proc.* 48, 669–672. doi: 10.1016/j.transproceed.2016.02.036

Barbey, R., Lavanant, L., Paripovic, D., Schüwer, N., Sugnaux, C., Tugulu, S., et al. (2009). Polymer brushes via surface-initiated controlled radical polymerization: synthesis, characterization, properties, and applications. *Chem. Rev.* 109, 5437–5527. doi: 10.1021/cr900045a

Barkai, U., Rotem, A., and de Vos, P. (2016). Survival of encapsulated islets: more than a membrane story. *World J. Transplant.* 6, 69–90. doi: 10.5500/wjt.v6.i1.69

Barkai, U., Weir, G. C., Colton, C. K., Ludwig, B., Bornstein, S. R., Brendel, M. D., et al. (2013). Enhanced oxygen supply improves islet viability in a new bioartificial pancreas. *Cell Transplant.* 22, 1463–1476. doi: 10.3727/096368912X657341

Baruch, L., and Machluf, M. (2006). Alginate–chitosan complex coacervation for cell encapsulation: Effect on mechanical properties and on long-term viability. *Biopolymers* 82, 570–579. doi: 10.1002/bip.20509

Ben Nasr, M., Vergani, A., Avruch, J., Liu, L., Kefaloyianni, E., D'Addio, F., et al. (2015). Co-transplantation of autologous MSCs delays islet allograft rejection and generates a local immunoprivileged site. *Acta Diabetol.* 52, 917–927. doi: 10.1007/s00592-015-0735-y

Berney, T., Ferrari-Lacraz, S., Bühler, L., Oberholzer, J., Marangon, N., Philippe, J., et al. (2009). Long-term insulin-independence after allogeneic islet transplantation for type 1 diabetes: over the 10-year mark. *Am. J. Transplant.* 9, 419–423. doi: 10.1111/j.1600-6143.2008.02481.x

Bhujbal, S. V., de Haan, B., Niclou, S. P., and de Vos, P. (2014b). A novel multilayer immunoisolating encapsulation system overcoming protrusion of cells. *Sci. Rep.* 4:6856. doi: 10.1038/srep06856

Bhujbal, S. V., Paredes-Juarez, G. A., Niclou, S. p., and de Vos, P. (2014a). Factors influencing the mechanical stability of alginate beads applicable for immunoisolation of mammalian cells. *J. Mech. Behav. Biomed. Mater.* 37, 196–208. doi: 10.1016/j.jmbbm.2014.05.020

Bochenek, M. A., Veiseh, O., Vegas, A. J., McGarrigle, J. J., Qi, M., Marchese, E., et al. (2018). Alginate encapsulation as long-term immune protection of allogeneic pancreatic islet cells transplanted into the omental bursa of macaques. *Nat. Biomed. Eng.* 2, 810–821. doi: 10.1038/s41551-018-0275-1

Borg, D. J., Welzel, P. B., Grimmer, M., Friedrichs, J., Weigelt, M., Wilhelm, C., et al. (2016). Macroporous biohybrid cryogels for co-housing pancreatic islets with mesenchymal stromal cells. *Acta Biomater.* 44, 178–187. doi: 10.1016/j.actbio.2016.08.007

Borges, J., and Mano, J. F. (2014). Molecular interactions driving the layer-by-layer assembly of multilayers. *Chem. Rev.* 114, 8883–8942. doi: 10.1021/cr400531v

Bragd, J., Adamson, U., Lins, P. E., Wredling, R., and Oskarsson, P. (2003). A repeated cross-sectional survey of severe hypoglycaemia in 178 Type 1 diabetes mellitus patients performed in 1984 and 1998. *Diabet. Med.* 20, 216–219. doi: 10.1046/j.1464-5491.2003.00902.x

Bruni, A., Gala-Lopez, B., Pepper, A. R., Abualhassan, N. S., and Shapiro, A. J. (2014). Islet cell transplantation for the treatment of type 1 diabetes: recent advances and future challenges. *Diabetes Metab. Syndr. Obes.* 7, 211–223. doi: 10.2147/DMSO.S50789

Buchholz, V., Agarwal, S., and Greiner, A. (2016). Synthesis and enzymatic degradation of soft aliphatic polyesters. *Macromol. Biosci.* 16, 207–213. doi: 10.1002/mabi.201500279

Buchwald, P., Tamayo-Garcia, A., Manzoli, V., Tomei, A. A., and Stabler, C. L. (2018a). Glucose-stimulated insulin release: parallel perifusion studies of free and hydrogel encapsulated human pancreatic islets. *Biotechnol. Bioeng.* 115, 232–245. doi: 10.1002/bit.26442

Buchwald, P., Tomei, A. A., and Stabler, C. L. (2018b). Predicting insulin secretion profiles for immunoisolating devices with transplanted islets. *Diabetes* 67(Suppl. 1):27-OR. doi: 10.2337/db18-27-OR

Buitinga, M., Janeczek Portalska, K., Cornelissen, D. J., Plass, J., Hanegraaf, M., Carlotti, F., et al. (2016). Coculturing human islets with proangiogenic support cells to improve islet revascularization at the subcutaneous transplantation site. *Tissue Eng. Part A* 22, 375–385. doi: 10.1089/ten.tea.2015.0317

Buzzacchera, I., Vorobii, M., Kostina, N. Y., de los Santos Pereira, A., Riedel, T., Bruns, M., et al. (2017). Polymer brush-functionalized chitosan hydrogels as antifouling implant coatings. *Biomacromolecules* 18, 1983–1992. doi: 10.1021/acs.biomac.7b00516

Cameron, D. J., and Shaver, M. P. (2011). Aliphatic polyester polymer stars: synthesis, properties and applications in biomedicine and nanotechnology. *Chem. Soc. Rev.* 40, 1761–1776. doi: 10.1039/C0CS00091D

Cañibano-Hernández, A., Saenz Del Burgo, L., Espona-Noguera, A., Orive, G., Hernández, R. M., Ciriza, J., et al. (2019). Hyaluronic acid enhances cell survival of encapsulated insulin-producing cells in alginate-based microcapsules. *Int. J. Pharm.* 557, 192–198. doi: 10.1016/j.ijpharm.2018.12.062

Cao, X. K., Li, R., Sun, W., Ge, Y., and Liu, B. L. (2016). Co-combination of islets with bone marrow mesenchymal stem cells promotes angiogenesis. *Biomed. Pharmacother.* 78, 156–164. doi: 10.1016/j.biopha.2016.01.007

Chae, S. Y., Lee, M., Kim, S. W., and Bae, Y. H. (2004). Protection of insulin secreting cells from nitric oxide induced cellular damage by crosslinked hemoglobin. *Biomaterials* 25, 843–850. doi: 10.1016/S0142-9612(03)00605-7

Chandy, T., Mooradian, D. L., and Rao, G. H. (1999). Evaluation of modified alginate-chitosan-polyethylene glycol microcapsules for cell encapsulation. *Artif. Organs* 23, 894–903. doi: 10.1046/j.1525-1594.1999.06244.x

Chen, H., Teramura, Y., and Iwata, H. (2011). Co-immobilization of urokinase and thrombomodulin on islet surfaces by poly(ethylene glycol)-conjugated phospholipid. *J. Control. Release* 150, 229–234. doi: 10.1016/j.jconrel.2010.11.011

Chen, J.-P., Chu, I. M., Shiao, M.-Y., Hsu, B.R.-S., and Fu, S.-H. (1998). Microencapsulation of islets in PEG-amine modified alginate-poly(l-lysine)-alginate microcapsules for constructing bioartificial pancreas. *J. Ferment. Bioeng.* 86, 185–190. doi: 10.1016/S0922-338X(98)80059-7

Chia, S. M., Wan, A. C., Quek, C. H., Mao, H. Q., Xu, X., Shen, L., et al. (2002). Multi-layered microcapsules for cell encapsulation. *Biomaterials* 23, 849–856. doi: 10.1016/S0142-9612(01)00191-0

Cruje, C., and Chithrani, D. B. (2014). Polyethylene glycol density and length affects nanoparticle uptake by cancer cells. *J. Nanomed. Res.* 1:00006. doi: 10.15406/jnmr.2014.01.00006

Choby, B. (2017). Diabetes update: prevention and management of diabetes complications. *FP Essent* 456, 36–40.

Cieslinski, D. A., and David Humes, H. (1994). Tissue engineering of a bioartificial kidney. *Biotechnol. Bioeng.* 43, 678–681. doi: 10.1002/bit.260430718

Collaborative Islet Transplant Registry (2017). *10th Annual Report*. Rockville, MD: The Emmes Corporation.

Colton, C. K. (1996). Engineering challenges in cellencapsulation technology. *Trends Biotechnol.* 14, 158–162. doi: 10.1016/0167-7799(96)10021-4

Cooper, D. K., Matsumoto, S., Abalovich, A., Itoh, T., Mourad, N. I., Gianello, P. R., et al. (2016). Progress in clinical encapsulated islet xenotransplantation. *Transplantation* 100, 2301–2308. doi: 10.1097/TP.0000000000001371

Crooks, C. A., Douglas, J. A., Broughton, R. L., and Sefton, M. V. (1990). Microencapsulation of mammalian cells in a HEMA-MMA copolymer: effects on capsule morphology and permeability. *J. Biomed. Mater. Res.* 24, 1241–1262. doi: 10.1002/jbm.820240908

Cruise, G. M., Hegre, O. D., Lamberti, F. V., Hager, S. R., Hill, R., Scharp, D. S., et al. (1999). *In vitro* and *in vivo* performance of porcine islets encapsulated in interfacially photopolymerized poly(ethylene glycol) diacrylate membranes. *Cell Transplant.* 8, 293–306. doi: 10.1177/096368979900800310

Dantal, J., and Soulillou, J. P. (2005). Immunosuppressive drugs and the risk of cancer after organ transplantation. *N. Engl. J. Med.* 352, 1371–1373. doi: 10.1056/NEJMe058018

Darrabie, M. D., Kendall, W. F. Jr., and Opara, E. C. (2005). Characteristics of Poly-L-Ornithine-coated alginate microcapsules. *Biomaterials* 26, 6846–6852. doi: 10.1016/j.biomaterials.2005.05.009

de los Santos Pereira, A., Sheikh, S., Blaszykowski, C., Pop-Georgievski, O., Fedorov, K., Thompson, M., et al. (2016). Antifouling polymer brushes displaying antithrombogenic surface properties. *Biomacromolecules* 17, 1179–1185. doi: 10.1021/acs.biomac.6b00019

de Vos, P. (2017). Historical perspectives and current challenges in cell microencapsulation. *Methods Mol. Biol.* 1479, 3–21. doi: 10.1007/978-1-4939-6364-5_1

de Vos, P., de Haan, B., Pater, J., and Van Schilfgaarde, R. (1996a). Association between capsule diameter, adequacy of encapsulation, and survival of microencapsulated rat islet allografts. *Transplantation* 62, 893–899. doi: 10.1097/00007890-199610150-00004

De Vos, P., De Haan, B., and Van Schilfgaarde, R. (1997a). Effect of the alginate composition on the biocompatibility of alginate-polylysine microcapsules. *Biomaterials* 18, 273–278. doi: 10.1016/S0142-9612(96)00135-4

De Vos, P., De Haan, B., Wolters, G. H., and Van Schilfgaarde, R. (1996b). Factors influencing the adequacy of microencapsulation of rat pancreatic islets. *Transplantation* 62, 888–893. doi: 10.1097/00007890-199610150-00003

de Vos, P., de Haan, B. J., de Haan, A., van Zanten, J., and Faas, M. M. (2004). Factors influencing functional survival of microencapsulated islet grafts. *Cell Transplant.* 13, 515–524. doi: 10.3727/000000004783983738

De Vos, P., De Haan, B. J., Wolters, G. H., Strubbe, J. H., and Van Schilfgaarde, R. (1997b). Improved biocompatibility but limited graft survival after purification of alginate for microencapsulation of pancreatic islets. *Diabetologia* 40, 262–270. doi: 10.1007/s001250050673

de Vos, P., Hoogmoed, C. G., and Busscher, H. J. (2002a). Chemistry and biocompatibility of alginate-PLL capsules for immunoprotection of mammalian cells. *J. Biomed. Mater. Res.* 60, 252–259. doi: 10.1002/jbm.10060

de Vos, P., Lazarjani, H. A., Poncelet, D., and Faas, M. M. (2014). Polymers in cell encapsulation from an enveloped cell perspective. *Adv. Drug Deliv. Rev.* 67–68, 15–34. doi: 10.1016/j.addr.2013.11.005

de Vos, P., and Marchetti, P. (2002). Encapsulation of pancreatic islets for transplantation in diabetes: the untouchable islets. *Trends Mol. Med.* 8, 363–366. doi: 10.1016/S1471-4914(02)02381-X

de Vos, P., Smink, A. M., Paredes, G., Lakey, J. R., Kuipers, J., Giepmans, B. N., et al. (2016). Enzymes for pancreatic islet isolation impact chemokine-production and polarization of insulin-producing beta-cells with reduced functional survival of immunoisolated rat islet-allografts as a consequence. *PLoS ONE* 11:e0147992. doi: 10.1371/journal.pone.0147992

de Vos, P., Spasojevic, M., de Haan, B. J., and Faas, M. M. (2012). The association between *in vivo* physicochemical changes and inflammatory responses against alginate based microcapsules. *Biomaterials* 33, 5552–5559. doi: 10.1016/j.biomaterials.2012.04.039

de Vos, P., Spasojevic, M., and Faas, M. M. (2010). Treatment of diabetes with encapsulated islets. *Adv. Exp. Med. Biol.* 670, 38–53. doi: 10.1007/978-1-4419-5786-3_5

de Vos, P., van Hoogmoed, C. G., de Haan, B. J., and Busscher, H. J. (2002b). Tissue responses against immunoisolating alginate-PLL capsules in the immediate posttransplant period. *J. Biomed. Mater. Res.* 62, 430–437. doi: 10.1002/jbm.10345

de Vos, P., Wolters, G. H., and van Schilfgaarde, R. (1994). Possible relationship between fibrotic overgrowth of alginate-polylysine-alginate microencapsulated pancreatic islets and the microcapsule integrity. *Transplant. Proc.* 26, 782–783.

de Vos, P.,Bucko, M., Gemeiner, P., Navrátil, M., Svitel, J., Faas, M., et al. (2009). Multiscale requirements for bioencapsulation in medicine and biotechnology. *Biomaterials* 30, 2559–2570. doi: 10.1016/j.biomaterials.2009.01.014

Dehaini, D., Wei, X., Fang, R. H., Masson, S., Angsantikul, P., Luk, B. T., et al. (2017). Erythrocyte–platelet hybrid membrane coating for enhanced nanoparticle functionalization. *Adv. Mater.* 29:1606209. doi: 10.1002/adma.201606209

Del Guerra, S., Bracci, C., Nilsson, K., Belcourt, A., Kessler, L., Lupi, R., et al. (2001). Entrapment of dispersed pancreatic islet cells in CultiSpher-S macroporous gelatin microcarriers: preparation, *in vitro* characterization, and microencapsulation. *Biotechnol. Bioeng.* 75, 741–744. doi: 10.1002/bit.10053

Dembczynski, R., and Jankowski, T. (2001). Determination of pore diameter and molecular weight cut-off of hydrogel-membrane liquid-core capsules for immunoisolation. *J. Biomater. Sci. Polym. Ed.* 12, 1051–1058. doi: 10.1163/156856201753252552

Ding, A. G., and Schwendeman, S. P. (2008). Acidic microclimate pH distribution in PLGA microspheres monitored by confocal laser scanning microscopy. *Pharm. Res.* 25, 2041–2052. doi: 10.1007/s11095-008-9594-3

Do, P., Beckwith, K. A., Cheney, C., Tran, M., Beaver, L., Griffin, B. G., et al. (2019). Leukemic B cell CTLA-4 suppresses costimulation of T cells. *J. Immunol.* 202, 2806–2816. doi: 10.4049/jimmunol.1801359

Douglas, J. A., and Sefton, M. V. (1990). The permeability of EUDRAGIT RL and HEMA–MMA microcapsules to glucose and inulin. *Biotechnol. Bioeng.* 36, 653–664. doi: 10.1002/bit.260360702

Du, B., Yang, Y., Bian, Z., and Xu, B. (2017). Characterization and anti-inflammatory potential of an exopolysaccharide from submerged mycelial culture of schizophyllum commune. *Front Pharmacol.* 8, 252–252. doi: 10.3389/fphar.2017.00252

Dufrane, D., Goebbels, R. M., Saliez, A., Guiot, Y., and Gianello, P. (2006). Six-month survival of microencapsulated pig islets and alginate biocompatibility in primates: proof of concept. *Transplantation* 81, 1345–1353. doi: 10.1097/01.tp.0000208610.75997.20

Dupuy, B., Baquey, A., Baquey, C., and Ducassou, D. (1990). Lack of responsiveness to glucose of microencapsulated islets of Langerhans after three weeks' implantation in the rat—influence of the complement AU - Gin, H. *J. Microencapsul.* 7, 341–346. doi: 10.3109/02652049009021844

Dusseault, J., Tam, S. K., Ménard, M., Polizu, S., Jourdan, G., Yahia, L., et al. (2006). Evaluation of alginate purification methods: effect on polyphenol, endotoxin, and protein contamination. *J. Biomed. Mater. Res. A* 76, 243–251. doi: 10.1002/jbm.a.30541

Duvivier-Kali, V. F., Omer, A., Parent, R. J., O'Neil, J. J., and Weir, G. C. (2001). Complete protection of islets against allorejection and autoimmunity by a simple barium-alginate membrane. *Diabetes* 50, 1698–1705. doi: 10.2337/diabetes.50.8.1698

Ekberg, H., Bernasconi, C., Tedesco-Silva, H., Vitko, S., Hugo, C., Demirbas, A., et al. (2009). Calcineurin inhibitor minimization in the Symphony study: observational results 3 years after transplantation. *Am. J. Transplant.* 9, 1876–1885. doi: 10.1111/j.1600-6143.2009.02726.x

Ekser, B., Cooper, D. K. C., and Tector, A. J. (2015). The need for xenotransplantation as a source of organs and cells for clinical transplantation. *Int. J. Surg.* 23(Pt B), 199–204. doi: 10.1016/j.ijsu.2015.06.066

Ernst, A. U., Bowers, D. T., Wang, L. H., Shariati, K., Plesser, M. D., Brown, N. K., et al. (2019). Nanotechnology in cell replacement therapies for type 1 diabetes. *Adv. Drug Deliv. Rev.* doi: 10.1016/j.addr.2019.01.013

Esfahani, R. R., Jun, H., Rahmani, S., Miller, A., and Lahann, J. (2017). Microencapsulation of live cells in synthetic polymer capsules. *ACS Omega* 2, 2839–2847. doi: 10.1021/acsomega.7b00570

Esmon, C. T. (2004). Crosstalk between inflammation and thrombosis. *Maturitas* 47, 305–314. doi: 10.1016/j.maturitas.2003.10.015

Fang, R. H., Hu, C. M. , Luk, B. T., Gao, W., Copp, J. A., Tai, Y., et al. (2014). Cancer cell membrane-coated nanoparticles for anticancer vaccination and drug delivery. *Nano Lett.* 14, 2181–2188. doi: 10.1021/nl500618u

Fang, R. H., Jiang, Y., Fang, J. C., and Zhang, L. (2017a). Cell membrane-derived nanomaterials for biomedical applications. *Biomaterials* 128, 69–83. doi: 10.1016/j.biomaterials.2017.02.041

Fang, R. H., Kroll, A. V., Gao, W., and Zhang, L. (2018). Cell membrane coating nanotechnology. *Adv. Mater.* 30:e1706759. doi: 10.1002/adma.201706759

Fang, W., Bi, D., Zheng, R., Cai, N., Xu, H., Zhou, R., et al. (2017b). Identification and activation of TLR4-mediated signalling pathways by alginate-derived guluronate oligosaccharide in RAW264.7 macrophages. *Sci. Rep.* 7, 1663–1663. doi: 10.1038/s41598-017-01868-0

Feng, C., and Huang, X. (2018). Polymer brushes: efficient synthesis and applications. *Acc. Chem. Res.* 51, 2314–2323. doi: 10.1021/acs.accounts.8b00307

Fernández-Cossío, S., León-Mateos, A., Sampedro, F. G., and Oreja, M. T. (2007). Biocompatibility of agarose gel as a dermal filler: histologic evaluation of subcutaneous implants. *Plast. Reconstr. Surg.* 120, 1161–1169. doi: 10.1097/01.prs.0000279475.99934.71

Flo, T. H., Ryan, L., Latz, E., Takeuchi, O., Monks, B. G., Lien, E., et al. (2002). Involvement of toll-like receptor (TLR) 2 and TLR4 in cell activation by mannuronic acid polymers. *J. Biol. Chem.* 277, 35489–35495. doi: 10.1074/jbc.M201366200

Gazda, L. S., Vinerean, H. V., Laramore, M. A., Hall, R. D., Carraway, J. W., and Smith, B. H. (2014). Pravastatin improves glucose regulation and biocompatibility of agarose encapsulated porcine islets following transplantation into pancreatectomized dogs. *J. Diabetes Res.* 2014:405362. doi: 10.1155/2014/405362

George, S., Nair, P. D., Risbud, M. V., and Bhonde, R. R. (2002). Nonporous polyurethane membranes as islet immunoisolation matrices – biocompatibility studies. *J. Biomater. Appl.* 16, 327–340. doi: 10.1106/088532802024249

Giraldo, J. A., Molano, R. D., Rengifo, H. R., Fotino, C., Gattás-Asfura, K. M., Pileggi, A., et al. (2017). The impact of cell surface PEGylation and short-course immunotherapy on islet graft survival in an allogeneic murine model. *Acta Biomater.* 49, 272–283. doi: 10.1016/j.actbio.2016.11.060

Gliwinski, M., Iwaszkiewicz-Grześ, D., and Trzonkowski, P. (2017). Cell-based therapies with T regulatory cells. *BioDrugs Clin. Immunother. Biopharm. Gene Ther.* 31, 335–347. doi: 10.1007/s40259-017-0228-3

Gmyr, V., Bonner, C., Moerman, E., Tournoys, A., Delalleau, N., Quenon, A., et al. (2017). Human recombinant antithrombin (ATryn((R))) administration improves survival and prevents intravascular coagulation after intraportal islet transplantation in a piglet model. *Cell Transplant.* 26, 309–317. doi: 10.3727/096368916X693554

Gołab, K., Kizilel, S., Bal, T., Hara, M., Zielinski, M., Grose, R., et al. (2014). Improved coating of pancreatic islets with regulatory T cells to create local immunosuppression by using the biotin-polyethylene glycol-succinimidyl valeric acid ester molecule. *Transplant. Proc.* 46, 1967–1971. doi: 10.1016/j.transproceed.2014.05.075

Grace, K., Arjun, N., Shu-Meng, K., Rahul, K., So-Ra, L., Michael, A., et al. (2016). "Alginate composition, temperature, and presence of islet tissue influence microcapsule permeability," in *Frontiers in Bioengineering and Biotechnology 10th World Biomaterials Congress, Vol.* 4 (Montréal, QC). doi: 10.3389/conf.FBIOE.2016.01.03002

Granicka, L. H. (2014). Nanoencapsulation of cells within multilayer shells for biomedical applications. *J. Nanosci. Nanotechnol.* 14, 705–716. doi: 10.1166/jnn.2014.9106

Grey, S. T., Tsuchida, A., Hau, H., Orthner, C. L., Salem, H. H., and Hancock, W. W. (1994). Selective inhibitory effects of the anticoagulant activated protein C on the responses of human mononuclear phagocytes to LPS, IFN-gamma, or phorbol ester. *J. Immunol.* 153, 3664–3672.

Gupta, R., and Sefton, M. V. (2011). Application of an endothelialized modular construct for islet transplantation in syngeneic and allogeneic immunosuppressed rat models. *Tissue Eng. Part A* 17, 2005–2015. doi: 10.1089/ten.tea.2010.0542

Hall, K. K., Gattás-Asfura, K. M., and Stabler, C. L. (2011). Microencapsulation of islets within alginate/poly(ethylene glycol) gels cross-linked via Staudinger ligation. *Acta Biomater.* 7, 614–624. doi: 10.1016/j.actbio.2010.07.016

Hamilton, D. C., Shih, H. H., Schubert, R. A., Michie, S. A., Staats, P. N., Kaplan, D. L., et al. (2017). A silk-based encapsulation platform for pancreatic islet transplantation improves islet function *in vivo*. *J. Tissue Eng. Regen. Med.* 11, 887–895. doi: 10.1002/term.1990

Han, T. H., Hyduke, D. R., Vaughn, M. W., Fukuto, J. M., and Liao, J. C. (2002). Nitric oxide reaction with red blood cells and hemoglobin under heterogeneous conditions. *Proc. Natl. Acad. Sci. U.S.A.* 99, 7763–7768. doi: 10.1073/pnas.122118299

Haque, M. R., Jeong, J. H., and Byun, Y. (2016). Combination strategy of multi-layered surface camouflage using hyperbranched polyethylene glycol and immunosuppressive drugs for the prevention of immune reactions against transplanted porcine islets. *Biomaterials* 84, 144–156. doi: 10.1016/j.biomaterials.2016.01.039

Haque, M. R., Kim, J., Park, H., Lee, H. S., Lee, K. W., Al-Hilal, T. A., et al. (2017). Xenotransplantation of layer-by-layer encapsulated non-human primate islets with a specified immunosuppressive drug protocol. *J. Control. Release* 258, 10–21. doi: 10.1016/j.jconrel.2017.04.021

Harding, J. L., and Reynolds, M. M. (2014). Combating medical device fouling. *Trends Biotechnol.* 32, 140–146. doi: 10.1016/j.tibtech.2013.12.004

Harrington, S., Williams, J., Rawal, S., Ramachandran, K., and Stehno-Bittel, L. (2017). Hyaluronic acid/collagen hydrogel as an alternative to alginate for long-term immunoprotected islet transplantation. *Tissue Eng. Part A* 23, 1088–1099. doi: 10.1089/ten.tea.2016.0477

Headen, D. M., Aubry, G., Lu, H., and García, A. J. (2014). Microfluidic-based generation of size-controlled, biofunctionalized synthetic

polymer microgels for cell encapsulation. *Adv. Mater.* 26, 3003–3008. doi: 10.1002/adma.201304880

Headen, D. M., Woodward, K. B., Coronel, M. M., Shrestha, P., Weaver, J. D., Zhao, H., et al. (2018). Local immunomodulation with Fas ligand-engineered biomaterials achieves allogeneic islet graft acceptance. *Nat. Mater.* 17, 732–739. doi: 10.1038/s41563-018-0099-0

Heng, W. S., and Wan, L. S. C. (1997). Effect of cellulose derivatives on alginate micro spherespreprared by emulsification AU - Chanp, L. *W. J. Microencapsul.* 14, 545–555. doi: 10.3109/02652049709006808

Hill, R. S., Cruise, G. M., Hager, S. R., Lamberti, F. V., Yu, X., Garufis, C. L., et al. (1997). Immunoisolation of adult porcine islets for the treatment of diabetes mellitus. The use of photopolymerizable polyethylene glycol in the conformal coating of mass-isolated porcine islets. *Ann. N. Y. Acad. Sci.* 831, 332–343. doi: 10.1111/j.1749-6632.1997.tb52208.x

Hillberg, A. L., Kathirgamanathan, K., Lam, J. B., Law, L. Y., Garkavenko, O., and Elliott, R. B. (2013). Improving alginate-poly-L-ornithine-alginate capsule biocompatibility through genipin crosslinking. *J. Biomed. Mater. Res. B Appl. Biomater.* 101, 258–268. doi: 10.1002/jbm.b.32835

Hillberg, A. L., Oudshoorn, M., Lam, J. B., and Kathirgamanathan, K. (2015). Encapsulation of porcine pancreatic islets within an immunoprotective capsule comprising methacrylated glycol chitosan and alginate. *J. Biomed. Mater. Res. Part B Appl. Biomater.* 103, 503–518. doi: 10.1002/jbm.b.33185

Hirabaru, M., Kuroki, T., Adachi, T., Kitasato, A., Ono, S., Tanaka, T., et al. (2015). A method for performing islet transplantation using tissue-engineered sheets of islets and mesenchymal stem cells. *Tissue Eng. Part C Methods* 21, 1205–1215. doi: 10.1089/ten.tec.2015.0035

Hirsch, I. B. (2009). Realistic expectations and practical use of continuous glucose monitoring for the endocrinologist. *J. Clin. Endocrinol. Metab.* 94, 2232–2238. doi: 10.1210/jc.2008-2625

Honiger, J., Darquy, S., Reach, G., Muscat, E., Thomas, M., and Collier, C. (1994). Preliminary report on cell encapsulation in a hydrogel made of a biocompatible material, AN69, for the development of a bioartificial pancreas. *Int. J. Artif. Organs* 17, 46–52. doi: 10.1177/039139889401700108

Itagaki, T., Arima, Y., Kuwabara, R., Kitamura, N., and Iwata, H. (2015). Interaction between cells and poly(ethylene glycol)-lipid conjugates. *Colloids Surfaces B Biointerfaces* 135, 765–773. doi: 10.1016/j.colsurfb.2015.08.014

Iwata, H., Arima, Y., and Tsutsui, Y. (2018). Design of bioartificial pancreases from the standpoint of oxygen supply. *Artif. Organs* 42, E168–E185. doi: 10.1111/aor.13106

Iwata, H., Kobayashi, K., Takagi, T., Oka, T., Yang, H., Amemiya, H., et al. (1994). Feasibility of agarose microbeads with xenogeneic islets as a bioartificial pancreas. *J. Biomed. Mater. Res.* 28, 1003–1011. doi: 10.1002/jbm.820280905

Iwata, H., Takagi, T., and Amemiya, H. (1992a). Agarose microcapsule applied in islet xenografts (hamster to mouse). *Transplant. Proc.* 24, 952.

Iwata, H., Takagi, T., Amemiya, H., Shimizu, H., Yamashita, K., Kobayashi, K., et al. (1992b). Agarose for a bioartificial pancreas. *J. Biomed. Mater. Res.* 26, 967–977. doi: 10.1002/jbm.820260711

Izadi, Z., Hajizadeh-Saffar, E., Hadjati, J., Habibi-Anbouhi, M., Ghanian, M. H., Sadeghi-Abandansari, H., et al. (2018). Tolerance induction by surface immobilization of Jagged-1 for immunoprotection of pancreatic islets. *Biomaterials* 182, 191–201. doi: 10.1016/j.biomaterials.2018.08.017

Jiskoot, W., van Schie, R. M., Carstens, M. G., and Schellekens, H. (2009). Immunological risk of injectable drug delivery systems. *Pharm. Res.* 26, 1303–1314. doi: 10.1007/s11095-009-9855-9

Jorge-Herrero, E., Fernández, P., Turnay, J., Olmo, N., Calero, P., García R, et al. (1999). Influence of different chemical cross-linking treatments on the properties of bovine pericardium and collagen. *Biomaterials* 20, 539–545. doi: 10.1016/S0142-9612(98)90205-8

Juste, S., Lessard, M., Henley, N., Ménard, M., and Hallé, J. P. (2005). Effect of poly-L-lysine coating on macrophage activation by alginate-based microcapsules: assessment using a new *in vitro* method. *J. Biomed. Mater. Res. A* 72, 389–398. doi: 10.1002/jbm.a.30254

Karimian, M. S., Pirro, M., Johnston, T. P., Majeed, M., and Sahebkar, A. (2017). Curcumin and endothelial function: evidence and mechanisms of protective effects. *Curr. Pharm. Des.* 23, 2462–2473. doi: 10.2174/1381612823666170222122822

Kawiak, J., Snochowski, M., Wójcicki, J. M., Sabalinska, S., and Werynski, A. (2003). Polypropylene hollow fiber for cells isolation: methods for evaluation of diffusive transport and quality of cells encapsulation AU - Granicka, Ludomira, H. *Arti. Cells Blood Substit. Biotechnol.* 31, 249–262. doi: 10.1081/BIO-120023156

Kendall, W. F. , Darrabie, M. D., El-Shewy, H. M., and Opara, E. C. (2004). Effect of alginate composition and purity on alginate microspheres. *J. Microencapsul.* 21, 821–828. doi: 10.1080/02652040400015452

Kendall, W. F., and Opara, E. C. (2017). Polymeric materials for perm-selective coating of alginate microbeads. *Methods Mol. Biol.* 1479, 95–109. doi: 10.1007/978-1-4939-6364-5_7

Kessler, L., Aprahamian, M., Keipes, M., Damgé, C., Pinget, M., and Poinsot, D. (1992). Diffusion properties of an artificial membrane used for Langerhans islets encapsulation: an *in vitro* test. *Biomaterials* 13, 44–49. doi: 10.1016/0142-9612(92)90094-5

Kessler, L., Pinget, M., Aprahamian, M., Dejardin, P., and Damgé, C. (1991). *In vitro* and *in vivo* studies of the properties of an artificial membrane for pancreatic islet encapsulation. *Horm. Metab. Res.* 23, 312–317. doi: 10.1055/s-2007-1003685

Kim, J.-S., Jung, Y., Kim, S. H., Shin, J.-S., Kim, S. H., and Park, C.-G. (2019). Vascularization of PLGA-based bio-artificial beds by hypoxia-preconditioned mesenchymal stem cells for subcutaneous xenogeneic islet transplantation. *Xenotransplantation* 26:e12441. doi: 10.1111/xen.12441

Kim, W., and Jung, J. (2016). Polymer brush: a promising grafting approach to scaffolds for tissue engineering. *BMB Rep.* 49, 655–661. doi: 10.5483/BMBRep.2016.49.12.166

Kingshott, P., and Griesser, H. J. (1999). Surfaces that resist bioadhesion. *Curr. Opin. Solid State Mater. Sci.* 4, 403–412. doi: 10.1016/S1359-0286(99)00018-2

Klöck, G., Frank, H., Houben, R., Zekorn, T., Horcher, A., Siebers, U., et al. (1994). Production of purified alginates suitable for use in immunoisolated transplantation. *Appl. Microbiol. Biotechnol.* 40, 638–643. doi: 10.1007/BF00173321

Knobeloch, T., Abadi, S. E. M., Bruns, J., Zustiak, S. P., and Kwon, G. (2017). Injectable polyethylene glycol hydrogel for islet encapsulation: an *in vitro* and *in vivo* characterization. *Biomed. Phys. Eng. Express* 3:035022. doi: 10.1088/2057-1976/aa742b

Kobayashi, T., Aomatsu, Y., Iwata, H., Kin, T., Kanehiro, H., Hisanaga, M., et al. (2003). Indefinite islet protection from autoimmune destruction in nonobese diabetic mice by agarose microencapsulation without immunosuppression1. *Transplantation* 75, 619–625. doi: 10.1097/01.TP.0000053749.36365.7E

Komatsu, H., Kandeel, F., and Mullen, Y. (2018). Impact of oxygen on pancreatic islet survival. *Pancreas* 47, 533–543. doi: 10.1097/MPA.0000000000001050

Korsgren, O., Lundgren, T., Felldin, M., Foss, A., Isaksson, B., Permert, J., et al. (2008). Optimising islet engraftment is critical for successful clinical islet transplantation. *Diabetologia* 51, 227–232. doi: 10.1007/s00125-007-0868-9

Krishnan, R., Ko, D., Foster, C. E. III., Liu, W., Smink, A. M., de Haan, B., et al. (2017). Immunological challenges facing translation of alginate encapsulated porcine islet xenotransplantation to human clinical trials. *Methods Mol. Biol.* 1479, 305–333. doi: 10.1007/978-1-4939-6364-5_24

Kubota, N., Tatsumoto, N., Sano, T., and Toya, K. (2000). A simple preparation of half N-acetylated chitosan highly soluble in water and aqueous organic solvents. *Carbohydr. Res.* 324, 268–274. doi: 10.1016/S0008-6215(99)00263-3

Kumar, M., Nandi, S. K., Kaplan, D. L., and Mandal, B. B. (2017). Localized immunomodulatory silk macrocapsules for islet-like spheroid formation and sustained insulin production. *ACS Biomater. Sci. Eng.* 3, 2443–2456. doi: 10.1021/acsbiomaterials.7b00218

Kuriyama, K., Fujiwara, A., Inagaki, K., and Abe, Y. (2000). Anti-inflammatory action of a novel peptide, SEK-1005, isolated from a Streptomyces. *Eur. J. Pharmacol.* 390, 223–228. doi: 10.1016/S0014-2999(00)00017-0

Kuwabara, R., Hamaguchi, M., Fukuda, T., Sakai, H., Inui, M., Sakaguchi, S., et al. (2018). Long-term functioning of allogeneic islets in subcutaneous tissue pretreated with a novel cyclic peptide without immunosuppressive medication. *Transplantation* 102, 417–425. doi: 10.1097/TP.0000000000001923

Lacy, P. E., Hegre, O. D., Gerasimidi-Vazeou, A., Gentile, F. T., and Dionne, K. E. (1991). Maintenance of normoglycemia in diabetic mice by subcutaneous xenografts of encapsulated islets. *Science* 254, 1782–1784. doi: 10.1126/science.1763328

Lahooti, S., and Sefton, M. V. (1999). Methods for microencapsulation with HEMA-MMA. *Tissue Eng. Methods Protoc.* 18, 331–348. doi: 10.1385/0-89603-516-6:331

Lahooti, S., and Sefton, M. V. (2000). Effect of an immobilization matrix and capsule membrane permeability on the viability of encapsulated HEK cells. *Biomaterials* 21, 987–995. doi: 10.1016/S0142-9612(99)00251-3

Laporte, C., Tubbs, E., Cristante, J., Gauchez, A.-S., Pesenti, S., Lamarche, F., et al. (2019). Human mesenchymal stem cells improve rat islet functionality under cytokine stress with combined upregulation of heme oxygenase-1 and ferritin. *Stem Cell Res. Ther.* 10, 85–85. doi: 10.1186/s13287-019-1190-4

Lazarjani, H. A., Vasheghani-Farahani, E., Barani, L., Hashemi-Najafabadi, S., Shojaosadati, S. A., Zahediasl, S., et al. (2010). Effect of polymer concentration on camouflaging of pancreatic islets with mPEG-succinimidyl carbonate. *Arti. Cells Blood Substit. Biotechnol.* 38, 250–258. doi: 10.3109/10731199.2010.488634

Lee, C. H., Singla, A., and Lee, Y. (2001). Biomedical applications of collagen. *Int. J. Pharm.* 221, 1–22. doi: 10.1016/S0378-5173(01)00691-3

Li, L., Fang, Y., Vreeker, R., Appelqvist, I., and Mendes, E. (2007). Reexamining the egg-box model in calcium–alginate gels with X-ray diffraction. *Biomacromolecules* 8, 464–468. doi: 10.1021/bm060550a

Li, R. H. (1998). Materials for immunoisolated cell transplantation. *Adv Drug Deliv Rev* 33, 87–109. doi: 10.1016/S0169-409X(98)00022-2

Li, Y., Fan, P., Ding, X.-M., Tian, X.-H., Feng, X.-S., Yan, H., et al. (2017). Polyglycolic acid fibrous scaffold improving endothelial cell coating and vascularization of islet. *Chin. Med. J.* 130, 832–839. doi: 10.4103/0366-6999.202730

Lin, C.-C., Metters, A. T., and Anseth, K. S. (2009). Functional PEG–peptide hydrogels to modulate local inflammation inducedby the pro-inflammatory cytokine TNFα. *Biomaterials* 30, 4907–4914. doi: 10.1016/j.biomaterials.2009.05.083

Liu, W. F., Ma, M., Bratlie, K. M., Dang, T. T., Langer, R., and Anderson, D. G. (2011). Real-time in vivo detection of biomaterial-induced reactive oxygen species. *Biomaterials* 32, 1796–1801. doi: 10.1016/j.biomaterials.2010.11.029

Llacua, A., de Haan, B. J., Smink, S. A., and de Vos, P. (2016). Extracellular matrix components supporting human islet function in alginate-based immunoprotective microcapsules for treatment of diabetes. *J. Biomed. Mater. Res. A* 104, 1788–1796. doi: 10.1002/jbm.a.35706

Llacua, L. A., de Haan, B. J., and de Vos, P. (2018a). Laminin and collagen IV inclusion in immunoisolating microcapsules reduces cytokine-mediated cell death in human pancreatic islets. *J. Tissue Eng. Regen. Med.* 12, 460–467. doi: 10.1002/term.2472

Llacua, L. A., Faas, M. M., and de Vos, P. (2018b). Extracellular matrix molecules and their potential contribution to the function of transplanted pancreatic islets. *Diabetologia* 61, 1261–1272. doi: 10.1007/s00125-017-4524-8

Llacua, L. A., Hoek, A., de Haan, B. J., and de Vos, P. (2018c). Collagen type VI interaction improves human islet survival in immunoisolating microcapsules for treatment of diabetes. *Islets* 10, 60–68. doi: 10.1080/19382014.2017.1420449

Lou, S., Zhang, X., Zhang, J., Deng, J., Kong, D., and Li, C. (2017). Pancreatic islet surface bioengineering with a heparin-incorporated starPEG nanofilm. *Mater. Sci. Eng. C* 78, 24–31. doi: 10.1016/j.msec.2017.03.295

Ludwig, B., Ludwig, S., Steffen, A., Knauf, Y., Zimerman, B., Heinke, S., et al. (2017). Favorable outcome of experimental islet xenotransplantation without immunosuppression in a nonhuman primate model of diabetes. *Proc. Natl. Acad. Sci. U.S.A.* 114, 11745–11750. doi: 10.1073/pnas.1708420114

Ludwig, B., Zimerman, B., Steffen, A., Yavriants, K., Azarov, D., Reichel, A., et al. (2010). A novel device for islet transplantation providing immune protection and oxygen supply. *Horm. Metab. Res.* 42, 918–922. doi: 10.1055/s-0030-1267916

Lutolf, M. P., and Hubbell, J. A. (2005). Synthetic biomaterials as instructive extracellular microenvironments for morphogenesis in tissue engineering. *Nat. Biotechnol.* 23, 47–55. doi: 10.1038/nbt1055

Manzoli, V., Colter, D. C., Dhanaraj, S., Fornoni, A., Ricordi, C., Pileggi, A., et al. (2017). Engineering human renal epithelial cells for transplantation in regenerative medicine. *Med. Eng. Phys.* 48, 3–13. doi: 10.1016/j.medengphy.2017.03.009

Manzoli, V., Villa, C., Bayer, A. L., Morales, L. C., Molano, R. D., Torrente, Y., et al. (2018). Immunoisolation of murine islet allografts in vascularized sites through conformal coating with polyethylene glycol. *Am. J. Transplant.* 18, 590–603. doi: 10.1111/ajt.14547

Mao, D., Zhu, M., Zhang, X., Ma, R., Yang, X., Ke, T., et al. (2017). A macroporous heparin-releasing silk fibroin scaffold improves islet transplantation outcome by promoting islet revascularisation and survival. *Acta Biomater.* 59, 210–220. doi: 10.1016/j.actbio.2017.06.039

Marchioli, G., Zellner, L., Oliveira, C., Engelse, M., Koning, E., Mano, J., et al. (2017). Layered PEGDA hydrogel for islet of Langerhans encapsulation and improvement of vascularization. *J. Mater. Sci. Mater. Med.* 28, 195–195. doi: 10.1007/s10856-017-6004-6

Marinucci, L., Lilli, C., Guerra, M., Belcastro, S., Becchetti, E., Stabellini, G., et al. (2003). Biocompatibility of collagen membranes crosslinked with glutaraldehyde or diphenylphosphoryl azide: an *in vitro* study. *J. Biomed. Mater. Res. Part A* 67A, 504–509. doi: 10.1002/jbm.a.10082

Matsumoto, S., Abalovich, A., Wechsler, C., Wynyard, S., and Elliott, R. B. (2016). Clinical benefit of islet xenotransplantation for the treatment of type 1 diabetes. *EBioMedicine* 12, 255–262. doi: 10.1016/j.ebiom.2016.08.034

Ménard, M., Dusseault, J., Langlois, G., Baille, W. E., Tam, S. K., Yahia, L., et al. (2010). Role of protein contaminants in the immunogenicity of alginates. *J. Biomed. Mater. Res. B Appl. Biomater.* 93, 333–340. doi: 10.1002/jbm.b.31570

Michel, R., Pasche, S., Textor, M., and Castner, D. G. (2005). Influence of PEG architecture on protein adsorption and conformation. *Langmuir* 21, 12327–12332. doi: 10.1021/la051726h

Miura, S., Teramura, Y., and Iwata, H. (2006). Encapsulation of islets with ultra-thin polyion complex membrane through poly(ethylene glycol)-phospholipids anchored to cell membrane. *Biomaterials* 27, 5828–5835. doi: 10.1016/j.biomaterials.2006.07.039

Nair, G. G., Liu, J. S., Russ, H. A., Tran, S., Saxton, M. S., Chen, R., et al. (2019). Recapitulating endocrine cell clustering in culture promotes maturation of human stem-cell-derived β cells. *Nat. Cell Biol.* 21, 263–274. doi: 10.1038/s41556-018-0271-4

Najjar, M., Manzoli, V., Abreu, M., Villa, C., Martino, M. M., Molano, R. D., et al. (2015). Fibrin gels engineered with pro-angiogenic growth factors promote engraftment of pancreatic islets in extrahepatic sites in mice. *Biotechnol. Bioeng.* 112, 1916–1926. doi: 10.1002/bit.25589

Neufeld, T., Ludwig, B., Barkai, U., Weir, G. C., Colton, C. K., Evron, Y., et al. (2013). The efficacy of an immunoisolating membrane system for islet xenotransplantation in minipigs. *PLoS ONE* 8:e70150. doi: 10.1371/journal.pone.0070150

Nguyen, K. T., and West, J. L. (2002). Photopolymerizable hydrogels for tissue engineering applications. *Biomaterials* 23, 4307–4314. doi: 10.1016/S0142-9612(02)00175-8

Nuttelman, C. R., Rice, M. A., Rydholm, A. E., Salinas, C. N., Shah, D. N., and Anseth, K. S. (2008). Macromolecular monomers for the synthesis of hydrogel niches and their application in cell encapsulation and tissue engineering. *Prog. Polym. Sci.* 33, 167–179. doi: 10.1016/j.progpolymsci.2007.09.006

Ock, S. A., Oh, K. B., Hwang, S., Yun, I. J., Ahn, C., Chee, H. K., et al. (2018). Immune molecular profiling of whole blood drawn from a non-human primate cardiac xenograft model treated with anti-CD154 monoclonal antibodies. *Xenotransplantation* 25:e12392. doi: 10.1111/xen.12392

Olabisi, R. M. (2015). Cell microencapsulation with synthetic polymers. *J. Biomed. Mater. Res. A* 103, 846–859. doi: 10.1002/jbm.a.35205

Omami, M., McGarrigle, J. J., Reedy, M., Isa, D., Ghani, S., Marchese, E., et al. (2017). Islet microencapsulation: strategies and clinical status in diabetes. *Curr. Diab. Rep.* 17:47. doi: 10.1007/s11892-017-0877-0

Orive, G., Emerich, D., Khademhosseini, A., Matsumoto, S., Hernández, R. M., Pedraz, J. L., et al. (2018). Engineering a clinically translatable bioartificial pancreas to treat type I diabetes. *Trends Biotechnol.* 36, 445–456. doi: 10.1016/j.tibtech.2018.01.007

Orive, G., Tam, S. K., Pedraz, J. L., and Hallé, J.-P. (2006). Biocompatibility of alginate–poly-l-lysine microcapsules for cell therapy. *Biomaterials* 27, 3691–3700. doi: 10.1016/j.biomaterials.2006.02.048

Ostgaard, K., Knutsen, S. H., Dyrset, N., and Aasen, I. M. (1993). Production and characterization of guluronate lyase from *Klebsiella pneumoniae* for applications in seaweed biotechnology. *Enzyme Microb. Technol.* 15, 756–763. doi: 10.1016/0141-0229(93)90006-N

O'Sullivan, E. S., Vegas, A., Anderson, D. G., and Weir, G. C. (2011). Islets transplanted in immunoisolation devices: a review of the progress and the challenges that remain. *Endocr. Rev.* 32, 827–844. doi: 10.1210/er.2010-0026

Pagliuca, F. W., Millman, J. R., Gürtler, M., Segel, M., Van Dervort, A., Ryu, J. H., et al. (2014). Generation of functional human pancreatic beta cells *in vitro*. *Cell* 159, 428–439. doi: 10.1016/j.cell.2014.09.040

Paredes-Juarez, A. G., de Haan, J. B., Faas, M. M., and de Vos, P. (2014a). A technology platform to test the efficacy of purification of alginate. *Materials* 7, 2087–2103. doi: 10.3390/ma7032087

Paredes-Juarez, G. A., de Haan, B. J., Faas, M. M., and de Vos, P. (2013). The role of pathogen-associated molecular patterns in inflammatory responses against alginate based microcapsules. *J. Control. Release Official J. Control. Release Soc.* 172, 983–992. doi: 10.1016/j.jconrel.2013.09.009

Paredes-Juarez, G. A., Sahasrabudhe, N. M., Tjoelker, R. S., de Haan, B. J., Engelse, M. A., de Koning, E. J., et al. (2015). DAMP production by human islets under low oxygen and nutrients in the presence or absence of an immunoisolating-capsule and necrostatin-1. *Sci. Rep.* 5:14623. doi: 10.1038/srep14623

Paredes-Juárez, G. A., Spasojevic, M., Faas, M. M., and de Vos, P. (2014b). Immunological and technical considerations in application of alginate-based microencapsulation systems. *Front Bioeng Biotechnol* 2:26. doi: 10.3389/fbioe.2014.00026

Park, H.-S., Kim, J.-W., Lee, S.-H., Yang, H. K., Ham, D.-S., Sun, C.-L., et al. (2017). Antifibrotic effect of rapamycin containing polyethylene glycol-coated alginate microcapsule in islet xenotransplantation. *J. Tissue Eng. Regen. Med.* 11, 1274–1284. doi: 10.1002/term.2029

Pelegrin, M., Marin, M., Noël, D., Del Rio, M., Saller, R., Stange, J., et al. (1998). Systemic long-term delivery of antibodies in immunocompetent animals using cellulose sulphate capsules containing antibody-producing cells. *Gene Ther.* 5, 828–834. doi: 10.1038/sj.gt.3300632

Perez-Basterrechea, M., Esteban, M. M., Vega, J. A., and Obaya, A. J. (2018). Tissue-engineering approaches in pancreatic islet transplantation. *Biotechnol. Bioeng.* 115, 3009–3029. doi: 10.1002/bit.26821

Pham, T. T., Nguyen, T. T., Pathak, S., Regmi, S., Nguyen, H. T., Tran, T. H., et al. (2018). Tissue adhesive FK506–loaded polymeric nanoparticles for multi–layered nano–shielding of pancreatic islets to enhance xenograft survival in a diabetic mouse model. *Biomaterials* 154, 182–196. doi: 10.1016/j.biomaterials.2017.10.049

Phelps, E. A., Headen, D. M., Taylor, W. R., Thulé, P. M., and García, A. J. (2013). Vasculogenic bio-synthetic hydrogel for enhancement of pancreatic islet engraftment and function in type 1 diabetes. *Biomaterials* 34, 4602–4611. doi: 10.1016/j.biomaterials.2013.03.012

Pişkin, E. (1995). Biodegradable polymers as biomaterials. *J. Biomater. Sci. Polym. Ed.* 6, 775–795. doi: 10.1163/156856295X00175

Prochorov, A. V., Tretjak, S. I., Goranov, V. A., Glinnik, A. A., and Goltsev, M. V. (2008). Treatment of insulin dependent diabetes mellitus with intravascular transplantation of pancreatic islet cells without immunosuppressive therapy. *Adv. Med. Sci.* 53, 240–244. doi: 10.2478/v10039-008-0045-5

Prokop, A., and Wang, T. G. (1997). Purification of polymers used for fabrication of an immunoisolation barrier. *Ann. N. Y. Acad. Sci.* 831, 223–231. doi: 10.1111/j.1749-6632.1997.tb52197.x

Ramachandran, G. N. (1963). Molecular structure of collagen. *Int. Rev. Connect. Tissue Res.* 1, 127–182. doi: 10.1016/B978-1-4831-6755-8.50009-7

Ren, Z., Liu, W., Song, X., Qi, Y., Zhang, C., Gao, Z., et al. (2018). Antioxidant and anti-inflammation of enzymatic-hydrolysis residue polysaccharides by Lentinula edodes. *Int. J. Biol. Macromol.* 120, 811–822. doi: 10.1016/j.ijbiomac.2018.08.114

Rengifo, H. R., Giraldo, J. A., Labrada, I., and Stabler, C. L. (2014). Long-term survival of allograft murine islets coated via covalently stabilized polymers. *Adv. Healthcare Mater.* 3, 1061–1070. doi: 10.1002/adhm.201300573

Ricordi, C., and Strom, T. B. (2004). Clinical islet transplantation: advances and immunological challenges. *Nat. Rev. Immunol.* 4, 259–268. doi: 10.1038/nri1332

Risbud, M. V., Bhargava, S., and Bhonde, R. R. (2003). *In vivo* biocompatibility evaluation of cellulose macrocapsules for islet immunoisolation: implications of low molecular weight cut-off. *J. Biomed. Mater. Res. Part A* 66A, 86–92. doi: 10.1002/jbm.a.10522

Risbud, M. V., and Bhonde, R. R. (2001). Suitability of cellulose molecular dialysis membrane for bioartificial pancreas: *in vitro* biocompatibility studies. *J. Biomed. Mater. Res.* 54, 436–444. doi: 10.1002/1097-4636(20010305)54:3<436::AID-JBM180>3.0.CO;2-8

Robertson, R. P. (2004). Islet transplantation as a treatment for diabetes - a work in progress. *N. Engl. J. Med.* 350, 694–705. doi: 10.1056/NEJMra032425

Ronel, S. H., D'Andrea, M. J., Hashiguchi, H., Klomp, G. F., and Dobelle, W. H. (1983). Macroporous hydrogel membranes for a hybrid artificial pancreas. I. Synthesis and chamber fabrication. *J. Biomed. Mater. Res.* 17, 855–864. doi: 10.1002/jbm.820170512

Ruel-Gariépy, E., Leclair, G., Hildgen, P., Gupta, A., and Leroux, J. C. (2002). Thermosensitive chitosan-based hydrogel containing liposomes for the delivery of hydrophilic molecules. *J. Control. Release* 82, 373–383. doi: 10.1016/S0168-3659(02)00146-3

Ryan, A. J., O'Neill, H. S., Duffy, G. P., and O'Brien, F. J. (2017). Advances in polymeric islet cell encapsulation technologies to limit the foreign body response and provide immunoisolation. *Curr. Opin. Pharmacol.* 36, 66–71. doi: 10.1016/j.coph.2017.07.013

Ryan, E. A., Lakey, J. R. T., Paty, B. W., Imes, S., Korbutt, G. S., Kneteman, N. M., et al. (2002). Successful islet transplantation continued insulin reserve provides long-term glycemic control. *Diabetes* 51, 2148–2157. doi: 10.2337/diabetes.51.7.2148

Ryan, E. A., Paty, B. W., Senior, P. A., Bigam, D., Alfadhli, E., Kneteman, N. M., et al. (2005). Five-year follow-up after clinical islet transplantation. *Diabetes* 54, 2060–2069. doi: 10.2337/diabetes.54.7.2060

Sabnis, A., Rahimi, M., Chapman, C., and Nguyen, K. T. (2009). Cytocompatibility studies of an *in situ* photopolymerized thermoresponsive hydrogel nanoparticle system using human aortic smooth muscle cells. *J. Biomed. Mater. Res. Part A* 91A, 52–59. doi: 10.1002/jbm.a.32194

Safley, S. A., Kenyon, N. S., Berman, D. M., Barber, G. F., Willman, M., Duncanson, S., et al. (2018). Microencapsulated adult porcine islets transplanted intraperitoneally in streptozotocin-diabetic non-human primates. *Xenotransplantation* 25:e12450. doi: 10.1111/xen.12450

Schaffellner, S., Stadlbauer, V., Stiegler, P., Hauser, O., Halwachs, G., Lackner, C., et al. (2005). Porcine islet cells microencapsulated in sodium cellulose sulfate. *Transplant. Proc.* 37, 248–252. doi: 10.1016/j.transproceed.2005.01.042

Schneider, S., Feilen, P. J., Slotty, V., Kampfner, D., Preuss, S., Berger, S., et al. (2001). Multilayer capsules: a promising microencapsulation system for transplantation of pancreatic islets. *Biomaterials* 22, 1961–1970. doi: 10.1016/S0142-9612(00)00380-X

Sevastianov, V. I., Tseytlina, E. A., Volkov, A. V., and Shumakov, V. I. (1984). Importance of adsorption-desorption processes of plasma proteins in biomaterials hemocompatibility. *ASAIO J.* 30, 137–142.

Shapiro, A. M., Lakey, J. R., Ryan, E. A., Korbutt, G. S., Toth, E., Warnock, G. L., et al. (2000). Islet transplantation in seven patients with type 1 diabetes mellitus using a glucocorticoid-free immunosuppressive regimen. *N. Engl. J. Med.* 343, 230–238. doi: 10.1056/NEJM200007273430401

Shin, J. S., Kim, J. M., Kim, J. S., Min, B. H., Kim, Y. H., Kim, H. J., et al. (2015). Long-term control of diabetes in immunosuppressed nonhuman primates (NHP) by the transplantation of adult porcine islets. *Am. J. Transplant.* 15, 2837–2850. doi: 10.1111/ajt.13345

Shin, J. S., Kim, J. S., Kim, J. M., Jang, J. Y., Kim, Y. H., Kim, H. J., et al. (2014). Minimizing immunosuppression in islet xenotransplantation. *Immunotherapy* 6, 419–430. doi: 10.2217/imt.14.14

Silva, A. I., de Matos, A. N., Brons, I. G., and Mateus, M. (2006). An overview on the development of a bio-artificial pancreas as a treatment of insulin-dependent diabetes mellitus. *Med. Res. Rev.* 26, 181–222. doi: 10.1002/med.20047

Sobol, M., Bartkowiak, A., de Haan, B., and de Vos, P. (2013). Cytotoxicity study of novel water-soluble chitosan derivatives applied as membrane material of alginate microcapsules. *J. Biomed. Mater. Res. Part A* 101A, 1907–1914. doi: 10.1002/jbm.a.34500

Somo, S. I., Langert, K., Yang, C.-Y., Vaicik, M. K., Ibarra, V., Appel, A. A., et al. (2018). Synthesis and evaluation of dual crosslinked alginate microbeads. *Acta Biomater.* 65, 53–65. doi: 10.1016/j.actbio.2017.10.046

Sondermeijer, H. P., Witkowski, P., Woodland, D., Seki, T., Aangenendt, F. J., van der Laarse, A., et al. (2016). Optimization of alginate purification using

polyvinylidene difluoride membrane filtration: effects on immunogenicity and biocompatibility of three-dimensional alginate scaffolds. *J. Biomater. Appl.* 31, 510–520. doi: 10.1177/0885328216645952

Sousa, S. G., Oliveira, L. A., de Aguiar Magalhães, D., de Brito, T. V., Batista, J. A., Pereira, C. M. C., et al. (2018). Chemical structure and anti-inflammatory effect of polysaccharide extracted from *Morinda citrifolia* Linn (Noni). *Carbohydr. Polym.* 197, 515–523. doi: 10.1016/j.carbpol.2018.06.042

Spasojevic, M., Bhujbal, S., Paredes, G., de Haan, B. J., Schouten, A. J., and de Vos, P. (2014a). Considerations in binding diblock copolymers on hydrophilic alginate beads for providing an immunoprotective membrane. *J. Biomed. Mater. Res. A* 102, 1887–1896. doi: 10.1002/jbm.a.34863

Spasojevic, M., Paredes-Juarez, G. A., Vorenkamp, J., de Haan, B., Schouten, A. J., and de Vos, P. (2014b). Reduction of the inflammatory responses against alginate-poly-L-lysine microcapsules by anti-biofouling surfaces of PEG-b-PLL diblock copolymers. *PLoS ONE* 9:e109837. doi: 10.1371/journal.pone.0109837

Staels, W., De Groef, S., Heremans, Y., Coppens, V., Van Gassen, N., Leuckx, G., et al. (2016). Accessory cells for β-cell transplantation. *Diabetes Obes. Metab.* 18, 115–124. doi: 10.1111/dom.12556

Stevenson, W. T., and Sefton, M. V. (1987). Graft copolymer emulsions of sodium alginate with hydroxyallsyl methacrylates for microencapsulation. *Biomaterials* 8, 449–457. doi: 10.1016/0142-9612(87)90081-0

Stokke, B. T., Smidsroed, O., Bruheim, P., and Skjaak-Braek, G. (1991). Distribution of uronate residues in alginate chains in relation to alginate gelling properties. *Macromolecules* 24, 4637–4645. doi: 10.1021/ma00016a026

Sugamori, M. E., and Sefton, M. V. (1989). Microencapsulation of pancreatic islets in a water insoluble polyacrylate. *ASAIO Trans.* 35, 791–799.

Surzyn, M., Symes, J., Medin, J. A., and Sefton, M. V. (2009). IL-10 secretion increases signal persistence of HEMA-MMA-microencapsulated luciferase-modified CHO fibroblasts in mice. *Tissue Eng. Part A* 15, 127–136. doi: 10.1089/ten.tea.2008.0028

Syed, F., Bugliani, M., Novelli, M., Olimpico, F., Suleiman, M., Marselli, L., et al. (2018). Conformal coating by multilayer nano-encapsulation for the protection of human pancreatic islets: *in-vitro* and *in-vivo* studies. *Nanomed. Nanotechnol. Biol. Med.* 14, 2191–2203. doi: 10.1016/j.nano.2018.06.013

Szymanska, E., and Winnicka, K. (2015). Stability of chitosan-a challenge for pharmaceutical and biomedical applications. *Marine Drugs* 13, 1819–1846. doi: 10.3390/md13041819

Takemoto, N., Konagaya, S., Kuwabara, R., and Iwata, H. (2015). Coaggregates of regulatory T cells and islet cells allow long-term graft survival in liver without immunosuppression. *Transplantation* 99, 942–947. doi: 10.1097/TP.0000000000000579

Tam, S. K., Dusseault, J., Polizu, S., Ménard, M., Hallé, J. P., and Yahia, L. (2006). Impact of residual contamination on the biofunctional properties of purified alginates used for cell encapsulation. *Biomaterials* 27, 1296–1305. doi: 10.1016/j.biomaterials.2005.08.027

Tan, P. L. (2010). Company profile: tissue regeneration for diabetes and neurological diseases at Living Cell Technologies. *Regen. Med.* 5, 181–187. doi: 10.2217/rme.10.4

Tashiro, H., Iwata, H., Warnock, G. L., Takagi, T., Machida, H., Ikada, Y., et al. (1997). Characterization and transplantation of agarose microencapsulated canine islets of Langerhans. *Ann. Transplant.* 2, 33–39. doi: 10.1016/S0041-1345(97)01369-9

Teramura, Y., and Iwata, H. (2010). Bioartificial pancreas: Microencapsulation and conformal coating of islet of Langerhans. *Adv. Drug Delivery Rev.* 62, 827–840. doi: 10.1016/j.addr.2010.01.005

Teramura, Y., Kaneda, Y., and Iwata, H. (2007). Islet-encapsulation in ultra-thin layer-by-layer membranes of poly(vinyl alcohol) anchored to poly(ethylene glycol)–lipids in the cell membrane. *Biomaterials* 28, 4818–4825. doi: 10.1016/j.biomaterials.2007.07.050

Tomei, A. A. (2018). Engineering confined and prevascularized sites for islet transplantation. *Transplantation* 102, 1793–1794. doi: 10.1097/TP.0000000000002290

Tomei, A. A., Manzoli, V., Fraker, C. A., Giraldo, J., Velluto, D., Najjar, M., et al. (2014). Device design and materials optimization of conformal coating for islets of Langerhans. *Proc. Natl. Acad. Sci. U.S.A.* 111, 10514–10519. doi: 10.1073/pnas.1402216111

Tun, T., Inoue, K., Hayashi, H., Aung, T., Gu, Y. J., Doi, R., et al. (1996). A newly developed three-layer agarose microcapsule for a promising biohybrid artificial pancreas: rat to mouse xenotransplantation. *Cell Transplant.* 5(5, Suppl. 1), S59–S63. doi: 10.1016/0963-6897(96)00042-5

Uludag, H., De Vos, P., and Tresco, P. A. (2000). Technology of mammalian cell encapsulation. *Adv Drug Deliv Rev* 42, 29–64. doi: 10.1016/S0169-409X(00)00053-3

Unsal, I. O., Ginis, Z., Pinarli, F. A., Albayrak, A., Cakal, E., Sahin, M., et al. (2015). Comparison of therapeutic characteristics of islet cell transplantation simultaneous with pancreatic mesenchymal stem cell transplantation in rats with type 1 diabetes mellitus. *Stem Cell Rev. Rep.* 11, 526–532. doi: 10.1007/s12015-014-9563-7

Unsworth, L. D., Sheardown, H., and Brash, J. L. (2008). Protein-resistant poly(ethylene oxide)-grafted surfaces: chain density-dependent multiple mechanisms of action. *Langmuir* 24, 1924–1929. doi: 10.1021/la702310t

Vågesjö, E., Christoffersson, G., Waldén, T. B., Carlsson, P.-O., Essand, M., Korsgren, O., et al. (2015). Immunological shielding by induced recruitment of regulatory T-lymphocytes delays rejection of islets transplanted in muscle. *Cell Transplant.* 24, 263–276. doi: 10.3727/096368914X678535

van de Weert, M., Hennink, W. E., and Jiskoot, W. (2000). Protein instability in poly(lactic-co-glycolic acid) microparticles. *Pharm. Res.* 17, 1159–1167. doi: 10.1023/A:1026498209874

van Hoogmoed, C. G., Busscher, H. J., and de Vos, P. (2003). Fourier transform infrared spectroscopy studies of alginate-PLL capsules with varying compositions. *J. Biomed. Mater. Res. A* 67, 172–178. doi: 10.1002/jbm.a.10086

Vegas, A. J., Veiseh, O., Doloff, J. C., Ma, M., Tam, H. H., Bratlie, K., et al. (2016a). Combinatorial hydrogel library enables identification of materials that mitigate the foreign body response in primates. *Nat. Biotechnol.* 34, 345–352. doi: 10.1038/nbt.3462

Vegas, A. J., Veiseh, O., Gurtler, M., Millman, J. R., Pagliuca, F. W., Bader, A. R., et al. (2016b). Long-term glycemic control using polymer-encapsulated human stem cell-derived beta cells in immune-competent mice. *Nat. Med.* 22, 306–311. doi: 10.1038/nm.4030

Veiseh, O., Doloff, J. C., Ma, M., Vegas, A. J., Tam, H. H., Bader, A. R., et al. (2015). Size- and shape-dependent foreign body immune response to materials implanted in rodents and non-human primates. *Nat. Mater.* 14, 643–651. doi: 10.1038/nmat4290

Vériter, S., Gianello, P., Igarashi, Y., Beaurin, G., Ghyselinck, A., Aouassar, N., et al. (2014). Improvement of subcutaneous bioartificial pancreas vascularization and function by coencapsulation of pig islets and mesenchymal stem cells in primates. *Cell Transplant.* 23, 1349–1364. doi: 10.3727/096368913X663550

Villa, C., Manzoli, V., Abreu, M. M., Verheyen, C. A., Seskin, M., Najjar, M., et al. (2017). Effects of composition of alginate-polyethylene glycol microcapsules and transplant site on encapsulated islet graft outcomes in mice. *Transplantation* 101, 1025–1035. doi: 10.1097/TP.0000000000001454

Wandrey, C., Bartkowiak, A., and Harding, S. E. (2010). "Materials for encapsulation," in *Encapsulation Technologies for Active Food Ingredients and Food Processing*, eds N. Zuidam and V. Nedovic (New York, NY: Springer), 31–100. doi: 10.1007/978-1-4419-1008-0_3

Wang, J. P., Zhang, X. X., and Wang, X. C. (2011). Preparation, characterization and permeation kinetics description of calcium alginate macro-capsules containing shape-stabilize phase change materials. *Renew. Energy* 36, 2984–2991. doi: 10.1016/j.renene.2011.03.039

Wang, T., Lacík, I., Brissová, M., Anilkumar, A. V., Prokop, A., Hunkeler, D., et al. (1997). An encapsulation system for the immunoisolation of pancreatic islets. *Nat. Biotechnol.* 15, 358–362. doi: 10.1038/nbt0497-358

Weaver, J. D., Headen, D. M., Hunckler, M. D., Coronel, M. M., Stabler, C. L., and García, A. J. (2018). Design of a vascularized synthetic poly(ethylene glycol) macroencapsulation device for islet transplantation. *Biomaterials* 172, 54–65. doi: 10.1016/j.biomaterials.2018.04.047

Weber, L. M., Lopez, C. G., and Anseth, K. S. (2009). Effects of PEG hydrogel crosslinking density on protein diffusion and encapsulated islet survival and function. *J. Biomed. Mater. Res. A* 90, 720–729. doi: 10.1002/jbm.a.32134

Wee, S., and Gombotz, W. R. (1998). Protein release from alginate matrices. *Adv. Drug Deliv. Rev.* 31, 267–285. doi: 10.1016/S0169-409X(97)00124-5

Wilson, J. T., Haller, C. A., Qu, Z., Cui, W., Urlam, M. K., and Chaikof, E. L. (2010). Biomolecular surface engineering of pancreatic islets with thrombomodulin. *Acta Biomater.* 6, 1895–1903. doi: 10.1016/j.actbio.2010.01.027

Wu, J., Hu, M., Qian, Y. W., Hawthorne, W. J., Burns, H., Liuwantara, D., et al. (2017). *In vivo* costimulation blockade-induced regulatory T cells demonstrate dominant and specific tolerance to porcine islet xenografts. *Transplantation* 101, 1587–1599. doi: 10.1097/TP.0000000000001482

Xu, Y., Kim, C. S., Saylor, D. M., and Koo, D. (2017). Polymer degradation and drug delivery in PLGA-based drug-polymer applications: a review of experiments and theories. *J. Biomed. Mater. Res. B Appl. Biomater.* 105, 1692–1716. doi: 10.1002/jbm.b.33648

Yamamoto, T., Teramura, Y., Itagaki, T., Arima, Y., and Iwata, H. (2016). Interaction of poly(ethylene glycol)-conjugated phospholipids with supported lipid membranes and their influence on protein adsorption. *Sci. Technol. Adv. Mater.* 17, 677–684. doi: 10.1080/14686996.2016.1240006

Yang, H. K., Ham, D.-S., Park, H.-S., Rhee, M., You, Y. H., Kim, M. J., et al. (2016). Long-term efficacy and biocompatibility of encapsulated islet transplantation with chitosan-coated alginate capsules in mice and canine models of diabetes. *Transplantation* 100, 334–343. doi: 10.1097/TP.0000000000000927

Yang, K. C., Qi, Z., Wu, C. C., Shirouza, Y., Lin, F. H., Yanai, G., et al. (2010). The cytoprotection of chitosan based hydrogels in xenogeneic islet transplantation: An in vivo study in streptozotocin-induced diabetic mouse. *Biochem. Biophys. Res. Commun.* 393, 818–823. doi: 10.1016/j.bbrc.2010.02.089

Yin, C., Mien Chia, S., Hoon Quek, C., Yu, H., Zhuo, R.-X., Leong, K. W., et al. (2003). Microcapsules with improved mechanical stability for hepatocyte culture. *Biomaterials* 24, 1771–1780. doi: 10.1016/S0142-9612(02)00580-X

Yoshimatsu, G., Sakata, N., Tsuchiya, H., Minowa, T., Takemura, T., Morita, H., et al. (2015). The co-transplantation of bone marrow derived mesenchymal stem cells reduced inflammation in intramuscular islet transplantation. *PLoS ONE* 10:e0117561. doi: 10.1371/journal.pone.0117561

Young, C. J., Poole-Warren, L. A., and Martens, P. J. (2012). Combining submerged electrospray and UV photopolymerization for production of synthetic hydrogel microspheres for cell encapsulation. *Biotechnol. Bioeng.* 109, 1561–1570. doi: 10.1002/bit.24430

Zhang, Y., Gao, W., Chen, Y., Escajadillo, T., Ungerleider, J., Fang, R. H., et al. (2017). Self-assembled colloidal gel using cell membrane-coated nanosponges as building blocks. *ACS Nano* 11, 11923–11930. doi: 10.1021/acsnano.7b06968

Conflict of Interest Statement: The authors declare that the research was conducted in the absence of any commercial or financial relationships that could be construed as a potential conflict of interest.

frontiers in Bioengineering and Biotechnology

ORIGINAL RESEARCH
published: 04 June 2019
doi: 10.3389/fbioe.2019.00126

Theranostic Calcium Phosphate Nanoparticles With Potential for Multimodal Imaging and Drug Delivery

Madhumathi Kalidoss[1], *Rubaiya Yunus Basha*[2], *Mukesh Doble*[2] *and T. S. Sampath Kumar*[1]*

[1] *Medical Materials Laboratory, Department of Metallurgical and Materials Engineering, Indian Institute of Technology Madras, Chennai, India,* [2] *Department of Biotechnology, Indian Institute of Technology Madras, Chennai, India*

Calcium phosphate (CaP) bioceramics closely resemble the natural human bone, which is a main reason for their popularity as bone substitutes. However, this compositional similarity makes it difficult to distinguish CaPs, especially in particulate form, from native bone by imaging modalities such as X-ray radiography, computed tomography (CT), and magnetic resonance imaging (MRI) to monitor the healing progress. External contrast agents can improve the imaging contrast of CaPs but can affect their physicochemical properties and can produce artifacts. In this work, we have attempted to improve the contrast of CaP nanoparticles *via* ion substitutions for multimodal imaging. Calcium-deficient hydroxyapatite (CDHA) nanoparticles with silver (Ag), gadolinium (Gd), and iron (Fe) substitution were prepared by a microwave-accelerated wet chemical process to improve the contrast in CT, T1 (spin–lattice), and T2 (spin–spin) MRI relaxation modes, respectively. Ag, Gd, and Fe were substituted at 0.25, 0.5, and 0.25 at.%, respectively. The ion-substituted CDHA (ICDHA) was found to be phase pure by X-ray diffraction (XRD) and Fourier transform infrared spectroscopy (FT-IR). Transmission electron microscopy (TEM) images showed that the ICDHA nanoparticles were platelet shaped and of 52 ± 2 nm length and 6 ± 1 nm width. The ICDHA showed high contrast in X-ray and CT compared to CDHA. The vibrating sample magnetometry (VSM) studies showed the ICDHA to exhibit paramagnetic behavior compared to diamagnetic CDHA, which was further confirmed by improved contrast in T1 and T2 MRI mode. In addition, the *in vitro* tetracycline drug loading and release was studied to investigate the capability of these nanoparticles for antibiotic drug delivery. It was found that a burst release profile was observed for 24 h with 47–52% tetracycline drug release. The ICDHA nanoparticles also showed *in vitro* antibacterial activity against *Staphylococcus aureus* and *Escherichia coli* due to Ag, which was further enhanced by antibiotic loading. *In vitro* biocompatibility studies showed that the triple-ion-substituted ICDHA nanoparticles were cytocompatible. Thus, the ion-substituted CDHA nanoparticles can have potential theranostic applications due to their multimodal image contrast, antibacterial activity, and drug delivery potential. Future work will be conducted with actual bone samples *in vitro* or in animal models.

Keywords: multimodal imaging, calcium phosphate nanoparticles, drug delivery, antibacterial, image contrast, ion substitution, bone substitute, theranostics

OPEN ACCESS

Edited by:
Hasan Uludag,
University of Alberta, Canada

Reviewed by:
Jonathan F. Lovell,
University at Buffalo, United States
Sergey V. Dorozhkin,
Independent Researcher, Moscow, Russia

***Correspondence:**
T. S. Sampath Kumar
tssk@iitm.ac.in

Specialty section:
This article was submitted to Biomaterials, a section of the journal Frontiers in Bioengineering and Biotechnology

Received: *13 February 2019*
Accepted: *09 May 2019*
Published: *04 June 2019*

Citation:
Kalidoss M, Yunus Basha R, Doble M and Sampath Kumar TS (2019) Theranostic Calcium Phosphate Nanoparticles With Potential for Multimodal Imaging and Drug Delivery. Front. Bioeng. Biotechnol. 7:126. doi: 10.3389/fbioe.2019.00126

INTRODUCTION

Calcium phosphate (CaP) bioceramics are one of the most commonly studied bone substitutes used for the repair of bony defects and alveolar ridge augmentation, as ear implants and as bone graft extender in spinal fusion surgery (Vallet-Regi and Gonzalez-Calbet, 2004; Habraken et al., 2016). Their popularity in bone therapeutic application is due to their compositional similarity to bone mineral as well as excellent biocompatibility and bioactivity (Sampath Kumar and Madhumathi, 2016b). CaP has also been used as delivery carriers for antibiotics, anti-inflammatory agents, anticancer drugs, growth factors, proteins, and DNA for bone tissue engineering due to its high drug loading ability (Uskokovic and Uskokovic, 2011). Hydroxyapatite (HA), calcium-deficient hydroxyapatite (CDHA), tricalcium phosphate (TCP), and biphasic calcium phosphate (BCP) are some of the popularly used CaPs.

A major drawback of CaPs, especially in nanoparticulate forms, is the difficulty in differentiating them from native bone tissue by imaging modalities such as X-ray radiography and computed tomography (CT) (Ramanathan and Ackerman, 1999; Ventura et al., 2014). It is essential to follow the stability of the implanted biomaterial, its infiltration by bone cells, the new bone formation and bone remodeling to optimize the performance of such bone substitutes. Imaging offers a non-destructive way of quantitative and longitudinal analysis of the above parameters. CaPs have nearly the same X-ray absorption as natural bone due to their compositional similarity to bone mineral. Other imaging modes such as magnetic resonance imaging (MRI) have not been utilized to image hard tissue like bone and synthetic CaPs, as it is exceedingly difficult to obtain MR signals due to the short spin–spin relaxation times of the nuclei (Wu et al., 1999). It has been observed that even at a high resolution, there is lack of contrast between surrounding bone and synthetic CaP bone substitute (Beaman et al., 2006). In order to enhance the imaging contrast of CaP bioceramics, addition of contrast agents has been proposed. They include barium sulfate, tantalum oxide, strontium carbonate, gold, etc., for X-ray/CT imaging (Wang et al., 2007; Hoekstra et al., 2014; Mastrogiacomo et al., 2017) and gadolinium, iron, perfluorocarbon-based contrast agents, etc., for MR imaging (Wichlas et al., 2012; Mastrogiacomo et al., 2017; Nakamura et al., 2018). There are certain drawbacks associated with addition of such external contrast agents. For example, it has been shown that addition of CT and MRI contrast agents affects the setting time and mechanical properties of CaP and other bone cements (Tanomaru-Filho et al., 2012; Sun et al., 2013). Similarly, addition of external magnetic contrast agents like super paramagnetic iron oxide nanoparticles (SPIONS) can cause artifacts like blooming effects (Ventura et al., 2014).

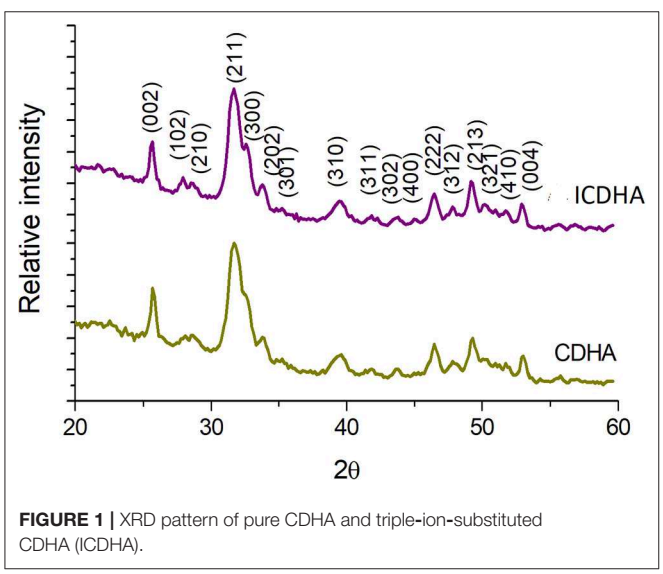

FIGURE 1 | XRD pattern of pure CDHA and triple-ion-substituted CDHA (ICDHA).

Efforts toward improving the imaging of CaPs are currently focused on refining the current diagnostic techniques for better imaging and improving the inherent contrast of CaP bioceramics. Recent advancements in MRI are an example of the former approach. The development of ultra-short echo time and zero echo time techniques has made high-resolution bone imaging possible (Ventura et al., 2013; Dou et al., 2018). HA and other CaPs are highly amenable to functional modifications *via* ionic substitutions. Hence, toward the latter approach, contrast-enhanced CaPs have been developed by ionic substitutions (Qi et al., 2018). Since MRI and CT are two of the most common methods of imaging that, when combined together, can image both soft and hard tissues, it is very prudent to develop multimodal CT/MR contrast-enhanced CaP bioceramics.

Multimodal imaging refers to combining several imaging techniques by developing multifunctional contrast agents. Due to their multiple binding sites and functional groups, CaPs, in nanoparticulate form especially, have been widely tried as multimodal contrast agents for simultaneous diagnosis and therapeutic applications (nanotheranosis) (Qi et al., 2018). CaP nanoparticles have been used as contrast agents by conjugating with or encapsulating organic fluorophores, encapsulating gold nanoclusters, doping with elements [e.g., europium (Eu^{3+}), manganese (Mn^{2+}), gadolinium (Gd^{3+}), iron (Fe^{3+}), neodymium (Nd^{3+}), terbium (Tb^{3+}), dysprosium (Dy^{3+}), etc.], conjugating with quantum dots, radiolabeling with samarium (^{153}Sm), indium (^{111}In), lutherium (^{177}Lu), technetium (^{99m}Tc), etc., for imaging modalities including fluorescence, CT, MR, and nuclear imaging (Qi et al., 2018). HA nanoparticles exhibiting paramagnetism, near-infrared (NIR)

TABLE 1 | List of cell parameters, cell volume, and crystallite size obtained from XRD and TEM results.

Samples	Ion substitution (at.%)	Cell parameters (Å)		Cell volume $(Å)^3$	Crystallite size (nm)	
		a	*c*		XRD	TEM (L*W)
CDHA	–	9.371	6.862	505	31	(40 ± 3)*(5 ± 3)
ICDHA	0.25 Ag 0.5 Gd 0.25 Fe	9.470	6.860	533	49	(52 ± 2)*(6 ± 1)

fluorescence, and X-ray absorption by Eu^{3+} and Gd^{3+} doping have been developed by Ashokan et al. (2010). They had also developed CaP nanoparticles doped with both indocyanine green (ICG) and gadolinium (Gd^{3+}), and labeled with ^{99m}Tc-MDP for combined optical, magnetic, and nuclear imaging (Ashokan et al., 2013). The synthesis of Gd^{3+}-doped HA labeled with ^{153}Sm for serving as a dual-modal probe for SPECT and MRI is another example for multimodal imaging using CaPs (Liu et al., 2014). Modified CaPs with therapeutic agents can be used to achieve disease diagnosis by enhancing the imaging contrasts combined with chemotherapy/gene therapy/hyperthermia therapy (HTT)/photodynamic therapy (PDT)/radiation therapy (RT), etc. (Qi et al., 2018). For example, Eu^{3+}/Gd^{3+} dual-doped HA have been used for simultaneous photoluminescent and magnetic imaging along with drug delivery application (Chen et al., 2011). Folic-acid-functionalized, Gd^{3+}-doped HA that functions as a theranostic system with MR imaging and production of HA-^{159}Gd-^{32}P radioisotope by neutron activation for active targeting of osteosarcomas has been developed (Cipreste et al., 2016). Similarly, HA doped with both Fe^{2+} and Fe^{3+} ions has been developed for theranostic applications (Tampieri et al., 2012). The Fe-doped HA exhibited intrinsic magnetization and can be used for multiple applications including hyperthermia treatment as well to develop new magnetic ceramics for enhanced bone regeneration. Tseng et al. (2014) have reported that ^{111}In-labeled lipid CaP nanoparticles preferentially accumulated in the lymph nodes *via* lymphatic drainage, which were used for SPECT/CT imaging-guided lymphatic gene delivery.

In the current work, a multimodal CaP drug delivery system with intrinsic antibacterial activity and enhanced contrast for CT/MR imaging modalities has been attempted by ion substitution. The CDHA of Ca/P ratio 1.61 was chosen for triple ion substitutions based on our previous results where it was found to be superior to HA as a drug-releasing resorbable bone substitute for the prevention and treatment of bone infections (Madhumathi and Sampath Kumar, 2014). Our preliminary work has shown that silver and gadolinium substitution into the HA crystal structure has resulted in significant CT and T1 MR contrast (Madhumathi et al., 2014). Iron (Fe^{3+}) with its large magnetic moments is used as a contrast agent in T2 relaxation mode of MRI (Chandra et al., 2012). Hence, the substitution of Fe along with Ag and Gd in CDHA for the additional T2 MR contrast will be studied. The contrast enhancement provided by the triple-ion-substituted CDHA nanoparticles will be characterized through X-ray, CT imaging, and MR imaging modes. In addition, the *in vitro* tetracycline loading and release profile, antibacterial activity, and biocompatibility of the substituted CDHA nanoparticles will also be evaluated.

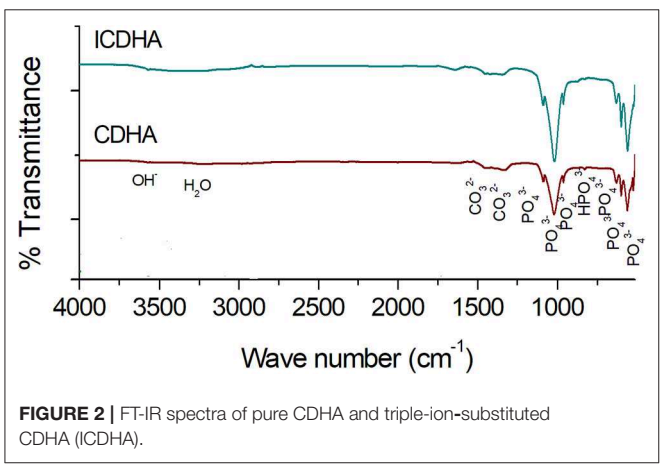

FIGURE 2 | FT-IR spectra of pure CDHA and triple-ion-substituted CDHA (ICDHA).

MATERIALS AND METHODS

Materials

Analytical grade calcium nitrate $Ca(NO_3)_2{\cdot}4H_2O$, diammonium hydrogen phosphate $(NH_4)_2HPO_4$, silver nitrate $Ag(NO_3)$, gadolinium oxide Gd_2O_3, ferric nitrate nonahydrate $Fe(NO_3)_3{\cdot}9H_2O$, and ammonia (30% GR) were purchased from MERCK, India. The drug tetracycline was purchased from Sigma Aldrich, India.

Synthesis of Pure CDHA Nanocarriers

Pure CDHA of Ca/P ratio 1.61 was prepared as reported earlier through a microwave-accelerated wet chemical reaction using $Ca(NO_3)_2{\cdot}4H_2O$ and $(NH_4)_2HPO_4$ as precursors (Siddharthan et al., 2004). The reaction was carried out at pH 10 using ammonia with stirring. The precipitate formed was subjected to microwave irradiation in a microwave oven (BPL India, 2.45 GHz, 800 W power) for 20 min, after which it was washed with distilled water and dried. The dried samples were then powdered using an agate mortar and pestle.

Synthesis of Triple-Ion-Substituted ICDHA Nanocarriers

The triple-ion-substituted CDHA was prepared by adding Ag, Gd, and Fe precursors along with $Ca(NO_3)_24H_2O$ and $(NH_4)_2HPO_4$ using the same microwave-accelerated wet chemical method mentioned in the section Synthesis of Pure CDHA Nanocarriers. The amount of precursors was calculated by fixing Ag^+ concentration at 0.25 at.%, Fe^{3+} at 0.25 at.%, and Gd^{3+} at 0.5 at.%, restricting the total substitution to 1 at.%. The (Ca+Ag+Gd+Fe)/P ratios were maintained at 1.61. The sample was labeled as ICDHA.

Material Characterization

The phase and crystallinity of the nanocarriers were characterized by X-ray diffraction method (XRD, Bruker D8 DISCOVER, USA) using Cu Kα radiation ($\lambda = 1.54$ Å). The diffraction patterns were recorded at a scanning rate of 1 step/s with a step size of 0.1°/step. The functional groups present in the CDHA and ICDHA nanocarriers were analyzed by Fourier transform infrared spectroscopy (FT-IR, Perkin-Elmer Spectrum Two, Germany) in the attenuated total internal reflectance (ATR) mode. The FT-IR spectra were collected from the range 4,000–510 cm^{-1}. The elemental composition of ICDHA was studied by scanning electron microscopy (SEM, FEI Quanta 200, Netherlands) using energy dispersive X-ray (EDS) analysis. The

particles were dispersed in distilled water and ultrasonicated for 5 min. The dispersed nanoparticles were then sprayed on a cylindrical metal stub using an adhesive carbon tape. The surface was then dried and coated using gold for 2 min to improve the conductivity of the sample. Transmission electron microscopy (TEM, Philips CM20, Netherlands) was used to identify the size and morphology of the prepared nanocarriers. For TEM analysis, the apatite particles were dispersed in ethanol and ultrasonicated for 15 min. The dispersed samples were coated on carbon-coated copper grids, dried, and examined under TEM operated at 120 kV. The surface area measurements of the samples were obtained at the temperature of liquid nitrogen using the Brunauer–Emmett–Teller (BET) N_2 adsorption/desorption isotherm method (Sorptomatic 1990, USA). The magnetic properties of the nanocarriers were evaluated using vibrating sample magnetometry (VSM) at room temperature in an applied magnetic field of ± 1.5 T (Lakeshore VSM 7410, USA).

In vitro Imaging Studies

The image contrast properties of the ion-substituted samples were studied using radiography (X-ray) and CT imaging. The powder samples were weighed and compressed into pellets of equal weight (200 mg) and 1 cm diameter. The X-ray radiographs were taken in a high-frequency X-ray generator (Siemens Multiphos 15, USA) along with aluminum standards of 1–5 mm thickness to differentiate the contrast. For CT scan, the pellets were placed inside a phantom model and imaged using a six-slice spiral CT (Philips Ingenuity Core128, USA) in a coronal section. For MR imaging, the nanocarriers were dispersed in distilled water. The MRI studies of triple-ion-substituted CDHAs were carried out by dispersing them in distilled H_2O at different concentrations (10–200 mM) and imaged in both T1 and T2 mode using a preclinical MR system (Bruker Biospec, France) of 4.7 T.

Drug Loading and Release

The drug loading and release studies were carried out from the ion-substituted samples using tetracycline following the procedure described earlier (Madhumathi and Sampath Kumar, 2014). About 5 mg of the drug was dispersed in 50 ml of suitable medium like ethanol or phosphate buffer solution (PBS). The CDHA and ICDHA nanocarriers (50 mg) were added to the drug-dispersed solution and placed in a constant temperature water bath at 37°C for 24 h. After 24 h, 2 ml of supernatant was removed

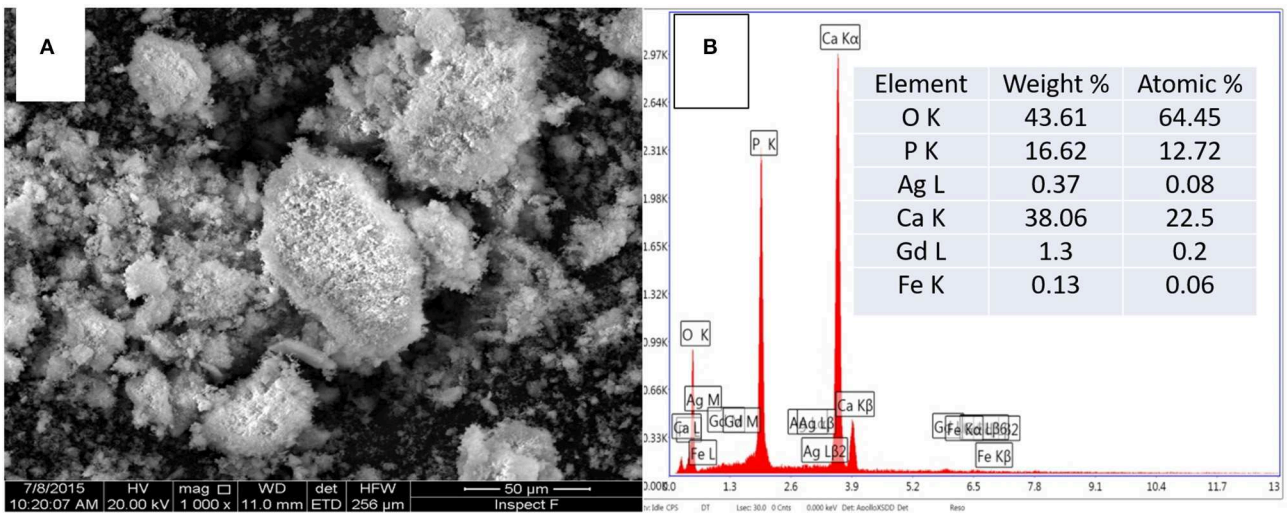

FIGURE 3 | (A) SEM image and **(B)** corresponding EDS spectra of ICDHA.

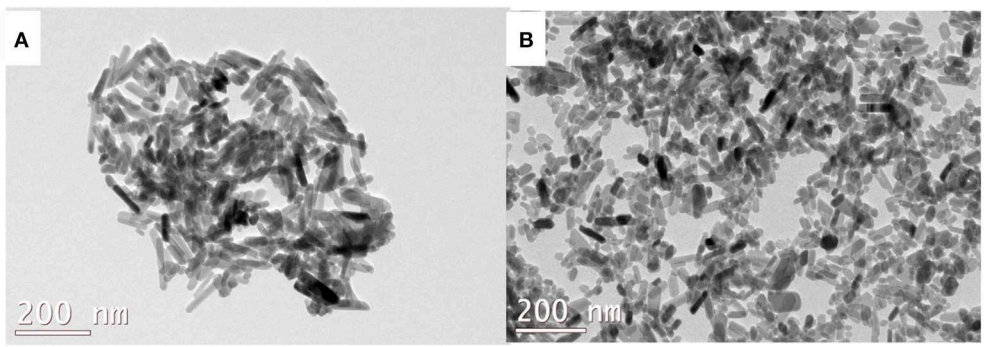

FIGURE 4 | TEM image of **(A)** CDHA and **(B)** ICDHA.

for estimation of drug concentration using UV–Vis spectroscopy (Lambda 35, Perkin-Elmer, USA). The samples were centrifuged, filtered, and dried at room temperature for 24 h.

The amount of drug loaded onto the carriers was determined by the following equation:

$$\text{Drug loading \%} = (\text{Ic} - \text{Fc}) \div \text{Ic} \times 100 \quad (1)$$

Where Ic and Fc are the initial and final concentration of drug in PBS.

The release study was performed by dispersing 10 mg of drug-loaded carriers in 10 ml of PBS of pH 7.4. The samples were placed in a constant temperature water bath at 37°C. The concentration of drug released was estimated by removing 2 ml of supernatant and replaced by fresh PBS at various time intervals. The drug release profile was determined by measuring the absorbance values at different time intervals (Fc) from the initial loaded concentration (Ic). All the experiments were performed in triplicate.

In vitro Antibacterial Studies

The drug-loaded CDHA and ICDHA samples (10 mg) were added to 9 ml of nutrient broth. Pure and ion-substituted samples without drug were taken as controls. The suspensions were then inoculated with 1 ml of *Staphylococcus aureus* and *Escherichia coli* bacterial cultures and incubated at 37°C for 24 h with shaking. The antibacterial efficacy of the samples was determined from the optical density (OD) of the cultures at 600 nm using the following equation:

$$\text{Bacterial reduction \%} = \{1 - (\text{sample OD} \div \text{control OD}) \times 100\} \quad (2)$$

In vitro Biocompatibility Studies

The biocompatibility of the drug-loaded triple-ion-substituted nanoparticulate system was tested against Swiss 3T3 fibroblast cells (NCCS, Pune) by the colorimetric MTT [3-(4, 5-181dimethylthiazole-2-yl)-2,5-diphenyl tetrazolium bromide] assay for 48 h. The Swiss 3T3 fibroblast cells were grown to confluence with Dulbecco's modified Eagle's medium (DMEM) supplemented with 10% fetal bovine serum (FBS) and 1% 100× antibiotic–antimycotic liquid and incubated at 37°C with 5% carbon dioxide in a CO_2 incubator (Astec, Japan). The cells were then trypsinized and counted with a hemocytometer (Marienfeld, Germany). They were then diluted at 5,000 cells per well, seeded in 96-well plates, and cultured for 24 h. Ten milligrams of the samples was suspended in 1 ml of DMEM and incubated at 37°C for 24 h. The media in the 96-well plates was then replaced with 100 µl of the supernatant from the CDHA samples and again incubated for 24 h. Twenty microliters of 5 mg/ml MTT was added to each well and incubated for 4 h. The purple formazan precipitate formed selectively by live cells was solubilized in dimethyl sulfoxide (DMSO), and the absorbance was measured at 570 nm using a multimode plate reader (EnSpire, Perkin-Elmer, Singapore). The percentage of viable cells was calculated as the percentage relative to the control (standard polystyrene tissue culture plates) using the following equation:

$$\text{Cell viability \%} = (\text{Sample OD} \div \text{Control OD}) \times 100 \quad (3)$$

Statistical Analysis

The values are expressed as mean ± SD. Statistical analysis was performed using one- and two-way ANOVA wherever applicable with a p-value < 0.05 considered statistically significant.

RESULTS

Material Characterization

The XRD pattern of pure CDHA and ICDHA is shown in **Figure 1**. The ion-substituted samples exhibit peaks similar to pure HA (JCPDS 09-432) and also revealed no secondary phases other than that of HA, suggesting ionic substitution in CDHA lattice. The cell parameters and cell volume calculated using "Unitcell" software and the crystallite size calculated using Scherrer's formula from XRD spectra are listed in **Table 1**. The ICDHA sample also showed larger cell parameters and a crystallite size of 49 nm when compared to pure CDHA with a crystallite size of 31 nm.

The FT-IR spectra of pure and triple-ion-substituted CDHA are shown in **Figure 2**. All the vibration bands of ion-substituted CDHA correspond to that of the characteristic bands of pure CDHA. The peaks observed include lattice OH (3,573 cm^{-c}); vibrational OH (634 cm^{-v}); phosphate bands at 470, 565, 603, 962, 1,035, and 1,090 cm^{-c}; carbonate (1,457 and 1,423 cm^{-c}); and lattice water (3,422 cm^{-c}). Additional HPO_4^{2-} peak at 874 cm^{-p} was also observed from ion-substituted CDHA samples.

Figure 3 shows the SEM image and corresponding EDS spectra of ICDHA. It can be seen that ICDHAs appear as micron-sized aggregates in **Figure 3A**. The EDS spectra show the presence of Ag, Gd, and Fe in the samples in addition to Ca and P. The typical TEM images of triple-ion-substituted

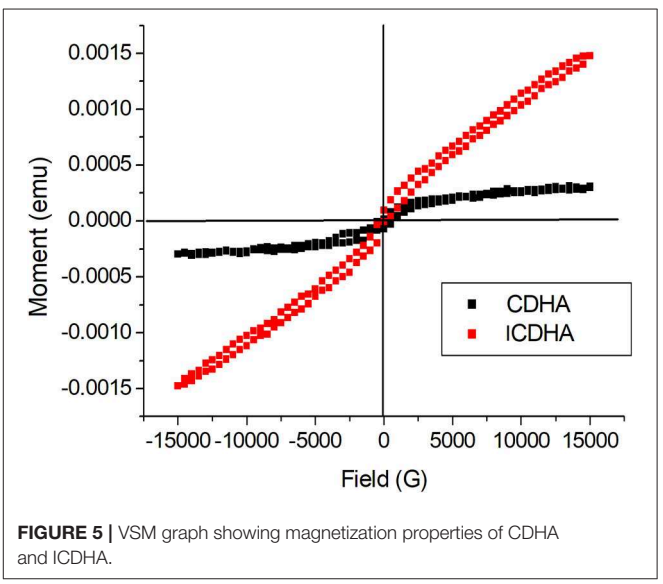

FIGURE 5 | VSM graph showing magnetization properties of CDHA and ICDHA.

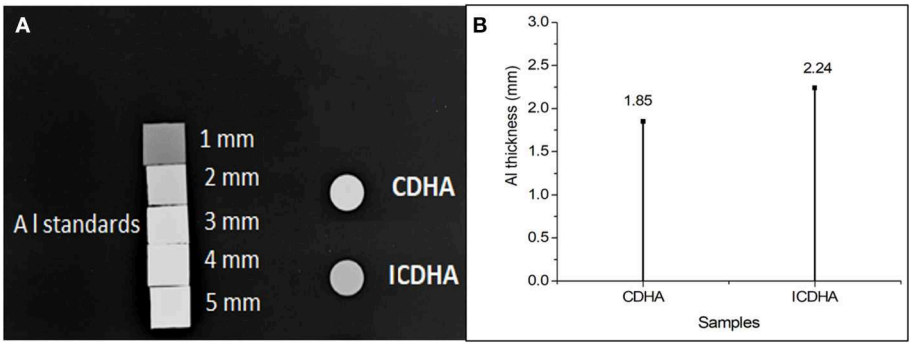

FIGURE 6 | (A) X-ray and **(B)** grayscale value graph of CDHA and ICDHA.

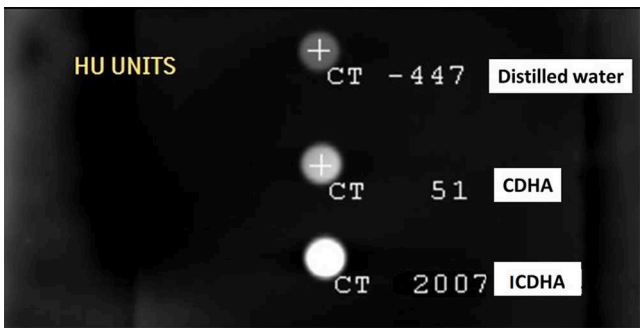

FIGURE 7 | CT contrast of ICDHA samples compared with CDHA in HU (Hounsfield Units).

samples can be seen in **Figure 4**. The TEM image of ICDHA samples showed large nanoparticles with acicular morphology. The particle sizes calculated from TEM micrographs using ImageJ image analysis software are listed in **Table 1**. The surface areas of CDHA and ICDHA samples from BET studies were 58 and 45 m^2/g, respectively. **Figure 5** shows the results of VSM studies presenting the magnetization properties before and after ion substitutions in CDHA nanocarriers. It can very well be seen that the diamagnetic CDHA nanoparticles showed paramagnetic behavior on ion substitution.

X-ray, CT, and MR Imaging Studies

The X-ray radiographical image of the pellets of ICDHA in comparison to CDHA is shown in **Figure 6A**. It can be seen that the ICDHA pellet exhibited visibly higher contrast than pure CDHA. To further quantify the contrast (grayscale value), the pellets of the samples were compared along with aluminum (Al) standards of varying thickness (1–5 mm) as can be seen in **Figure 6A**. ImageJ software was used to quantify the grayscale value. **Figure 6B** shows the grayscale value graph corresponding to the X-ray image. The graph was obtained by plotting the contrast of the pellets (*x*-axis) with respect to the contrast of Al standards (*y*-axis). The graph shows that the contrast of ICDHA is comparable to that of 2.24 mm Al thickness while that of CDHA can be compared to 1.8-mm Al thickness. The substitution of elements with high density like Ag^{+} (10.49 g/cm^3), Gd^{3+} (7.90 g/cm^3), and Fe^{3+} (7.86 g/cm^3) greatly increased the radiopacity of ICDHA compared to CDHA. The CT scan radiograph with ICDHA and CDHA samples is shown in **Figure 7**. The contrast values in CT are quantified in Hounsfield Units (HU). While both CDHA and ICDHA showed greater contrast than distilled water (control), ICDHA (2007 HU) exhibited much superior contrast than CDHA (51 HU).

The MR contrast images of ICDHA in T1 and T2 mode are shown in **Figure 8**. As observed in **Figure 8A**, the T1 MR contrast increased for the ICDHA samples with increasing concentrations. The color bar adjacent to the MR image shows the color change from bottom to top according to increase in contrast. Significant T1 contrast was observed at a concentration of 50 μg/ml and increased up to the concentration of 200 μg/ml. **Figure 8B** shows the concentration vs. longitudinal relaxivity (r1) plot for ICDHA samples. The r1 was calculated according to the equation:

$$(1 \div T_1)_{obs} = (1 \div T_1)_{dia} + r1M \quad (4)$$

where $(1/T_1)_{obs}$ is the observed relaxation rate in the presence of ICDHA, $(1/T_1)_{dia}$ is the diamagnetic relaxation rate in the absence of nanoparticles, and M is the molar concentration (Ashokan et al., 2010). The T1 relaxivity increased with an increase in the ICDHA nanocarrier concentration. The maximum r1 observed for ICDHA nanocarriers was 0.61 mM^{-1} s^{-1} for 200 μg/ml.

Figure 9 shows the T2 MR contrast for different concentrations of the ICDHA samples (10–200 μg/ml). The T2 images were obtained by pulse sequence spin-echo technique with TR/TE = 4,000/60 ms and FOV as 8 × 8 cm^2. Mild T2 contrast was observed at 10 μg/ml concentration and increased for up 75 μg/ml concentration with no further increase. The contrast obtained in T2 mode was much lower than that of the T1 mode, and so the T2 relaxivity graph was not plotted.

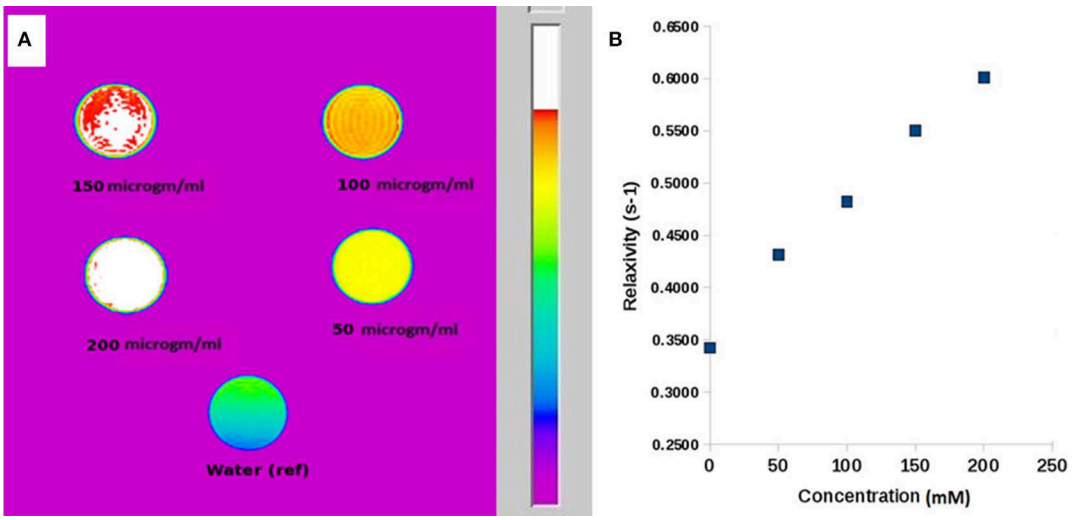

FIGURE 8 | (A) T1-weighted MR image of ICDHA substituted samples dispersed at different concentrations in distilled water and **(B)** longitudinal relaxivity vs. concentration graph of ICDHA.

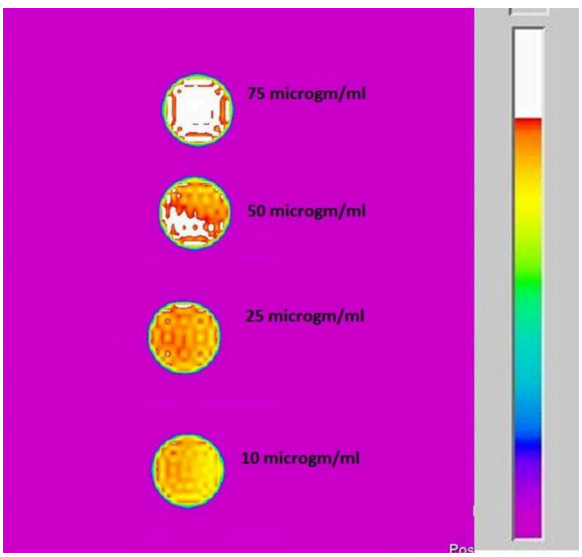

FIGURE 9 | T2-weighted MR image of ICDHA substituted samples dispersed at different concentrations in distilled water.

Drug Loading and Release Studies

The drug loading and release studies were carried out using the tetracycline antibiotic. **Figure 10** shows the drug loading percentage of ion-substituted apatites compared with pure samples. ICDHA showed a lower antibiotic loading (∼40–55%) compared to CDHA (65–70%). This may be attributed to the lower surface area of ICDHA as well as due to the replacement of Ca^{2+} ions with other ions that might affect the drug binding.

The drug release profile of tetracycline from CDHA and ICDHA, however, looks similar (**Figure 11**). The ion substitutions caused a minor change in the drug release profiles. The ICDHA samples showed a burst release of tetracycline with maximum release at 24 h, and the maximum release was lower than CDHA, which can be related to the changes in particle size as well as the non-stoichiometric nature of ion-substituted apatites.

In vitro Antibacterial Studies

The results of the antibacterial studies of ion-substituted apatites against *S. aureus* and *E. coli* are shown in **Figure 12**. Although pure CDHA was not antibacterial, the ICDHA showed antibacterial activity between 20 and 25%, which can be attributed to the presence of Ag^{+}. The antibacterial activity further increased with tetracycline loading as expected. All tetracycline-loaded samples showed >90% activity against both bacterial strains. The ion-substituted tetracycline-loaded ICDHA showed the highest antimicrobial activity against *S. aureus*, which is known to cause osteomyelitis and prosthetic joint infection when introduced through trauma, surgery, direct colonization from a proximal infection, or systemic circulation (Sampath Kumar and Madhumathi, 2016a).

In vitro Biocompatibility Studies

The MTT assay results of pure and drug-loaded ICDHA apatites on Swiss 3T3 fibroblast cells are shown in **Figure 13**. It can be seen that all samples including the antibiotic-loaded CDHA and ICDHA samples showed 80–100% cell viability on Day 1 and 75–85% cell viability on Day 2. The high cell viability in ion-substituted samples may be due to the low total ionic substitution of ∼1%.

DISCUSSION

Regeneration and healing of bone tissue post trauma, surgery, or infection often require the implantation of a natural bone graft or synthetic bone substitute. While the ability to aid and promote new bone formation is the main emphasis in developing such

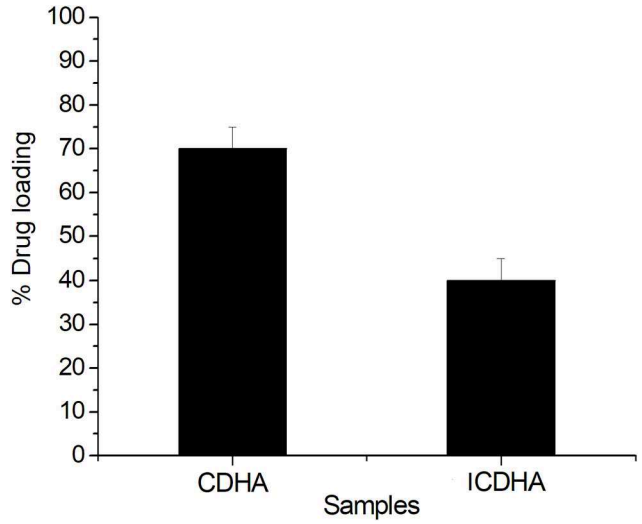

FIGURE 10 | Loading profile of tetracycline from ion-substituted CDHA (ICDHA) compared to pure CDHA ($n = 3$; data shown as mean ± SD; $p < 0.05$, one-way ANOVA).

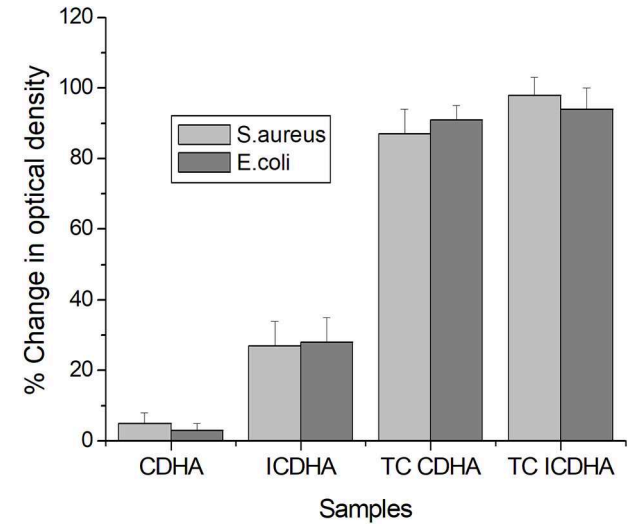

FIGURE 12 | Antibacterial activity of pure and tetracycline-loaded CDHA and ICDHA ($n = 3$; data shown as mean ± SD; $p < 0.05$, one-way ANOVA).

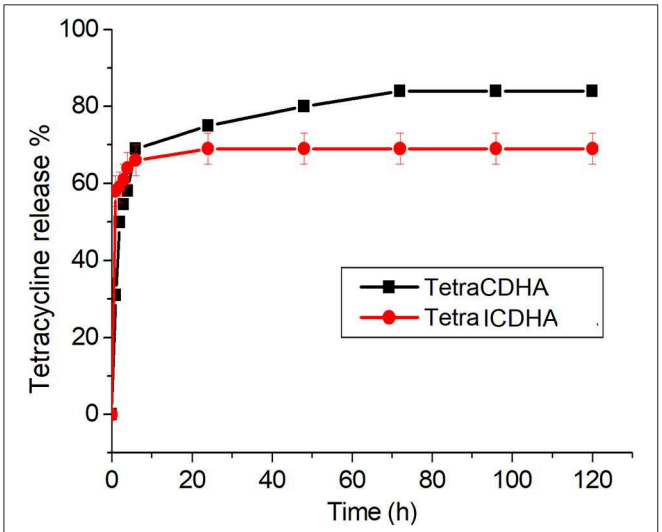

FIGURE 11 | Tetracycline release profile from ICDHA compared to that of CDHA ($n = 3$; data shown as mean ± SD; $p < 0.05$, one-way ANOVA).

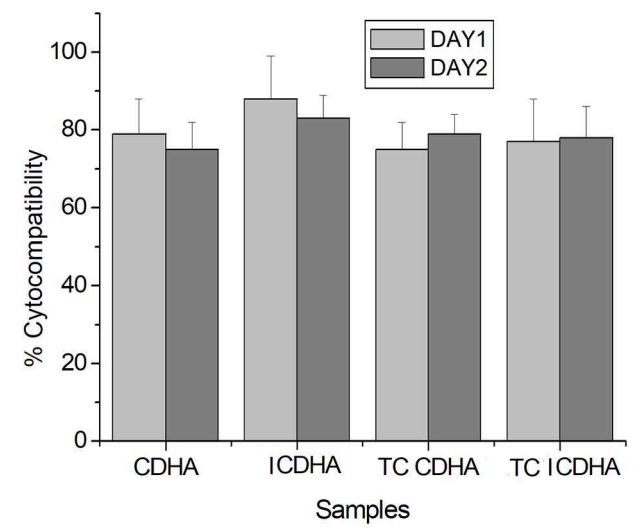

FIGURE 13 | Biocompatibility of pure and tetracycline-loaded samples against Swiss 3T3 fibroblast cells by MTT assay for 24 and 48 h; TC, tetracycline ($n = 3$; data shown as mean ± SD; $p < 0.05$, two-way ANOVA).

bone substitutes, it is also desirable to focus on other beneficial properties such as drug delivery ability, antibacterial activity, and optimal image contrast. In our previous studies, nanoparticulate bone substitutes with the abovementioned properties have been developed through approaches of drug loading and/or ion substitutions (Madhumathi and Sampath Kumar, 2014; Sampath Kumar et al., 2015). It was found that the substitution of ions such as Ag^{+}, Gd^{3+}, etc. imparted antibacterial activity and greater image contrast in CT and T1 MR modes.

Conventional MRI contrast agents enhance contrast either in T1 mode (bright signal) or T2 mode (dark signal). Recent research in the field of MR imaging focuses on the challenge to develop contrast agents that enhance both dual T1 and T2 MRI contrast. These T1/T2 contrast agents are designed for a single instrument and assumed to have advantages such as signal reliability and lack of image mismatch, which can occur when using different contrast agents or different instruments (Shin et al., 2015). An overlay of the T1 and T2 signals can help distinguish the targets from the surroundings. Dual T1/T2 imaging has been achieved through complex routes such as conjugation of T1 and T2 elements [e.g., covalently attaching Gd-DTPA with dopamine-coated iron oxide nanoparticles *via* isothiourea linkage, manganese (Mn)-embedded iron oxide

nanoparticles, etc.] and magnetically decoupled T1–T2 dual mode contrast agents [e.g., Mn-doped iron oxide ($MnFe_2O_4$) nanoparticles as the core T2 contrast material and $Gd_2O(CO_3)_2$ as the shell T1 contrast material separated by non-magnetic silica layer] (Bae et al., 2010; Choi et al., 2010; Huang et al., 2014). Since the apatitic structure allows for flexible ion substitution, we aimed to develop CDHA nanoparticles capable of simultaneous T1 and T2 MR contrast along with CT by substituting both Gd^{3+} and Fe^{3+} ions. One of the main criteria in deciding the percentage of Ag^{+}, Gd^{3+}, and Fe^{3+} ion substitutions in CDHA was biocompatibility, and the total ion substitution was restricted to 1 at.%. Previous reports have shown that the Ag^{+} and Gd^{3+} ion substitutions in HA have been found to be biocompatible at up to 0.5 and 4.4 at.%, respectively (Ramesh babu et al., 2007; Getman et al., 2010). Hence, the silver concentration was fixed at 0.25 at.%, the Gd^{3+} concentration was restricted to 0.50 at.% allowing Fe^{3+} substitution of 0.25 at.%, and the maximum combined substitution was restricted to 1 at.%.

The synthesized ICDHA samples were found to be phase pure as observed from XRD pattern and FT-IR spectra. The EDS spectra showed the presence of Ca, P, Ag, Gd, and Fe ions in the ICDHA samples. TEM image of ICDHA samples showed them to be of similar morphology but larger sized compared to CDHA. The ICDHA samples showed a greater X-ray and CT contrast than CDHA. ICDHA also showed a greater magnetic moment in VSM than pure CDHA. A dual T1/T2 imaging ability was observed with the ICDHA, although the contrast enhancement obtained in T1 mode was much higher than that in T2 mode. The relaxivity plot for the T2 mode was not obtained due to the low T2 contrast probably owing to the low at.% of Fe^{3+} substitution compared to Gd^{3+}. However, a dual T1/T2 contrast using very low ionic substitution was demonstrated. Drug delivery studies using tetracycline were performed to observe any modification in the antibiotic binding and release kinetics due to ion substitution in ICDHA. The studies showed a distinct reduction in the loading and a tendency toward burst release for these samples compared to pure CDHA. While the low loading may be attributed to the lower surface area of ion-substituted apatites and loss of Ca^{2+} binding sites, the burst release in ICDHA can be attributed to the release of drugs adsorbed on the surface. The antibacterial studies on *S. aureus* and *E. coli* showed a significant antibacterial activity of ICDHA due to Ag^{+} even without antibiotic loading. With antibiotic binding, the antibacterial activity increased to >95%. Due to the low total ionic substitution of 1 at.%, both samples showed high biocompatibility for up to 48 h even with drug loading. Further *in vivo* studies can validate the above observations, suggesting that ICDHA samples can act as biodegradable theranostic nanocarriers of antibiotics with inherent CT/T1/T2 MR contrast and antibacterial activity.

CONCLUSION

In the present study, ion-substituted CDHA nanoparticles with antibacterial activity and enhanced CT/T1/T2 MR image contrast for theranostic applications were developed. Ions such as Ag^{+}, Gd^{3+}, and Fe^{3+}, which enhance contrast in CT, T1, and T2 MR modes, respectively, were substituted into the CDHA apatitic crystal structure. Preliminary results showed that the contrast enhancement in CT/T1/T2 MR modes was significant for a low amount of ionic substitution (0.25 at.% Ag^{+}, 0.5 at.% Gd^{3+}, and 0.25 at.% Fe^{3+}). These multifunctional CDHA nanoparticles were inherently antibacterial due to Ag^{+} substitution and also showed predominantly burst release of tetracycline antibiotic. The ion-substituted CDHA nanocarriers were also biocompatible due to the total ionic substitution of 1 at.%. The antibiotic-loaded triple-ion-substituted CDHA nanoparticles with antibacterial activity and multimodal image contrast are highly suitable for clinical orthopedic applications.

DATA AVAILABILITY

All datasets generated for this study are included in the manuscript and/or the supplementary files.

AUTHOR CONTRIBUTIONS

TS and MK conceived the idea. MK performed the material synthesis, characterization, drug release, and imaging experiments. RY planned and carried out the antibacterial and biocompatibility studies under the guidance of MD.

FUNDING

The study is funded by Department of Biotechnology, Govt. of India.

ACKNOWLEDGMENTS

We thank the Institute Hospital, Indian Institute of Technology Madras for providing the X-ray facility. We also thank Prof. N. Chandrakumar and Dr. Abhishek Banerjee of MRI-MRS Center, Department of Chemistry, Indian Institute of Technology Madras for help with the MR imaging.

REFERENCES

Ashokan, A., Gowda, G. S., Somasundaram, V. H., Bhupathi, A., Peethambaran, R., Unni, A. K. K., et al. (2013). Multifunctional calcium phosphate nano-contrast agent for combined nuclear, magnetic and near-infrared *in vivo* imaging. *Biomaterials* 34, 7143–7157. doi: 10.1016/j.biomaterials.2013.05.077

Ashokan, A., Menon, D., Nair, S., and Koyakutty, M. (2010). A molecular receptor targeted, hydroxyapatite nanocrystal based multi-modal contrast agent. *Biomaterials* 31, 2606–2616. doi: 10.1016/j.biomaterials.2009.11.113

Bae, K. H., Kim, Y. B., Lee, Y., Hwang, J., Park, H., and Park, T. J. (2010). Bio inspired synthesis and characterization of gadolinium labelled magnetite nanoparticles for dual contrast T1 and T2 weighted magnetic resonance imaging. *Bioconjugate Chem.* 21, 505–512. doi: 10.1021/bc900424u

Beaman, F. D., Bancroft, L. W., Peterson, J. J., Kransdorf, M. J., Menke, D. M., and DeOrio, J. K. (2006). Imaging characteristics of bone graft materials. *Radiographics* 26, 373–388. doi: 10.1148/rg.262055039

Chandra, V. S., Baskar, G., Suganthi, R. V., Elayaraja, K., Joshy, M. I. A., Beaula, W. S., et al. (2012). Blood compatibility of iron-doped nanosize hydroxyapatite and its drug release. *ACS Appl. Mater. Interfaces* 4, 1200–1210. doi: 10.1021/am300140q

Chen, F., Huang, P., Zhu, Y. J., Wu, J., Zhang, C. L., and Cui, D. X. (2011). The photoluminescence, drug delivery and imaging properties of multifunctional Eu3+/Gd3+ dual-doped hydroxyapatite nanorods. *Biomaterials* 32, 9031–9039. doi: 10.1016/j.biomaterials.2011.08.032

Choi, J. S., Lee, J. H., Shin, T. H., Song, H. T., Kim, E. Y., and Cheon, J. (2010). Self-confirming "AND" logic nanoparticles for fault-free MRI. *J. Am. Chem. Soc.* 132, 11015–11017. doi: 10.1021/ja104503g

Cipreste, M. F., Peres, A. M., Cotta, A. A. C., Aragon, F. H., Antunes, A. M., Leal, A. S., et al. (2016). Synthesis and characterization of 159Gd-doped hydroxyapatite nanorods for bioapplications as theranostic systems. *Mater. Chem. Phy.* 181, 301–311. doi: 10.1016/j.matchemphys.2016.06.063

Dou, W., Mastrogiacomo, S., Veltien, A., Alghamdi, H. S., Walboomers, X. F., and Heerschap, A. (2018). Visualization of calcium phosphate cement in teeth by zero echo time 1H MRI at high field. *NMR Biomed.* 31, 3859–3871. doi: 10.1002/nbm.3859

Getman, E. I., Loboda, S. N., Kachenko, T. V., Yablochkova, N. V., and Chebyshev, K. A. (2010). Isomorphous substitution of samarium and gadolinium for calcium in hydroxyapatite structure. *Russ. J. Inorg. Chem.* 55, 333–338. doi: 10.1134/S0036023610030058

Habraken, W., Habibovic, P., Epple, M., and Bohner, M. (2016). Calcium phosphates in biomedical applications: Materials for the future? *Mat. Today* 19, 69–87. doi: 10.1016/j.mattod.2015.10.008

Hoekstra, J. W., Van den Beucken, J. J., Leeuwenburgh, S. C., Bronkhorst, E. M., Meijer, G. J., and Jansen, J. A. (2014). Tantalum oxide and barium sulfate as radiopacifiers in injectable calcium phosphate-poly (lactic-co-glycolic acid) cements for monitoring *in vivo* degradation. *J. Biomed. Mater. Res. A.* 102, 141–149. doi: 10.1002/jbm.a.34677

Huang, G., Li, H., Chen, J., Zhao, Z., Yang, L., Chi, X., et al. (2014). Tunable T1 and T2 contrast abilities of manganese engineered iron oxide nanoparticles through size control. *Nanoscale* 6, 10404–10412. doi: 10.1039/C4NR02680B

Liu, Y., Sun, Y., Cao, C., Yang, Y., Wu, Y., Ju, D., et al. (2014). Long term biodistribution *in vivo* and toxicity of radioactive/magnetic hydroxyapatite nanorods. *Biomaterials* 35, 3348–3355. doi: 10.1016/j.biomaterials.2013.12.064

Madhumathi, K., and Sampath Kumar, T. S. (2014). Regenerative potential and anti-bacterial activity of tetracycline loaded apatitic nanocarriers for the treatment of periodontitis. *Biomed. Mater.* 9:035002. doi: 10.1088/1748-6041/9/3/035002

Madhumathi, K., Sampath Kumar, T. S., Mohammed Sanjeed, T., Sabik Muhammed, A., Nazrudeen, S., and Sharanya, D. (2014). Silver and gadolinium ions co-substituted hydroxyapatite nanoparticles as bimodal contrast agent for medical imaging. *Bioceram. Dev. Appl.* 4, 1–4. doi: 10.4172/2090-5025.1000079

Mastrogiacomo, S., Dou, W., Koshkina, O., Boerman, O. C., Jansen, J. A., Heerschap, A., et al. (2017). Perfluorocarbon/gold loading for noninvasive *in vivo* assessment of bone fillers using ^{19}F magnetic resonance imaging and computed tomography. *ACS Appl. Mater. Interfaces* 9, 22149–22159. doi: 10.1021/acsami.7b04075

Nakamura, M., Oyane, A., Kuroiwa, K., Shimizu, Y., Pyatenko, A., Misawa, M., et al. (2018). Facile one-pot fabrication of calcium phosphate-based composite nanoparticles as delivery and MRI contrast agents for macrophages. *Colloids Surf. B Biointerfaces* 162, 135–145. doi: 10.1016/j.colsurfb.2017.11.034

Qi, C., Lin, J., Fu, L. H., and Huang, P. (2018). Calcium-based biomaterials for diagnosis, treatment, and theranostics. *Chem. Soc. Rev.* 47, 357–403. doi: 10.1039/C6CS00746E

Ramanathan, C., and Ackerman, J. L. (1999). Quantitative solid-state NMR imaging of synthetic calcium phosphate implants. *Mag. Reson. Med.* 41, 1214–1220. doi: 10.1002/(SICI)1522-2594(199906)41:6<1214::AID-MRM18>3.0.CO;2-H

Ramesh babu, N., Sampath Kumar, T. S., Prabhakar, T. G., Sastry, V. S., and Murthy, K. V. (2007). Antibacterial nanosized silver substituted hydroxyapatite: Synthesis and characterization. *J. Biomed. Mater. Res. A* 80, 581–591. doi: 10.1002/jbm.a.30958

Sampath Kumar, T. S., and Madhumathi, K. (2016a). "Antibacterial potential of bioceramics used as nanocarriers," in *Handbook of Bioceramics and Biocomposites*, ed I. V. Antoniac (Cham: Springer), 1333–1373. doi: 10.1007/978-3-319-12460-5_58

Sampath Kumar, T. S., and Madhumathi, K. (2016b). Antibiotic delivery by nanobioceramics. *Ther. Deliv.* 7, 573–588. doi: 10.4155/tde-2016-0025

Sampath Kumar, T. S., Madhumathi, K., Rubaiya, Y., and Doble, M. (2015). Dual mode antibacterial activity of ion substituted calcium phosphate nanocarriers for bone infections. *Front. Bioeng. Biotechnol.* 3:59. doi: 10.3389/fbioe.2015.00059

Shin, T. H., Choi, Y., Kim, S., and Cheon, J. (2015). Recent advances in magnetic nanoparticle-based multi-modal imaging. *Chem. Soc. Rev.* 44, 4501–4516. doi: 10.1039/C4CS00345D

Siddharthan, A., Seshadri, S. K., and Sampath Kumar, T. S. (2004). Microwave accelerated synthesis of nanosized calcium deficient hydroxyapatite. *J. Mater. Sci. Mater. Med.* 15, 1279–1284. doi: 10.1007/s10856-004-5735-3

Sun, Y., Ventura, M., Oosterwijk, E., Jansen, J. A., Walboomers, X. F., and Heerschap, A. (2013). Zero echo time magnetic resonance imaging of contrast-agent-enhanced calcium phosphate bone defect fillers. *Tissue Eng. Part C Methods* 19, 281–287. doi: 10.1089/ten.tec.2011.0745

Tampieri, A., D'Alessandro, T., Sandri, M., Sprio, S., Landi, E., Bertinetti, L., et al. (2012). Intrinsic magnetism and hyperthermia in bioactive Fe-doped hydroxyapatite. *Acta Biomater.* 8, 843–851. doi: 10.1016/j.actbio.2011.09.032

Tanomaru-Filho, M., Morales, V., Da Silva, G. F., Bosso, R., Reis, J. M. S. N., Duarte, M. A. H., et al. (2012). Compressive strength and setting time of MTA and Portland cement associated with different radiopacifying agents. *ISRN Dent.* 2012, 898051–898055. doi: 10.5402/2012/898051

Tseng, Y. C., Xu, Z., Guley, K., Yuan, H., and Huang, L. (2014). Lipid-calcium phosphate nanoparticles for delivery to the lymphatic system and SPECT/CT imaging of lymph node metastases. *Biomaterials* 35, 4688–4698. doi: 10.1016/j.biomaterials.2014.02.030

Uskokovic, V., and Uskokovic, D. P. (2011). Nanosized hydroxyapatite and other calcium phosphates: Chemistry of formation and application as drug and gene delivery agents. *J. Biomed. Mater. Res. Appl. Biomater.* 96B, 152–191. doi: 10.1002/jbm.b.31746

Vallet-Regi, M., and Gonzalez-Calbet, J. M. (2004). Calcium phosphates as substitution of bone tissues. *Prog. Solid State Chem.* 32, 1–31. doi: 10.1016/j.progsolidstchem.2004.07.001

Ventura, M., Sun, Y., Cremers, S., Borm, P., Birgani, Z. T., Habibovic, P., et al. (2014). A theranostic agent to enhance osteogenic and magnetic resonance imaging properties of calcium phosphate cements. *Biomaterials* 35, 2227–2233. doi: 10.1016/j.biomaterials.2013.11.084

Ventura, M., Sun, Y., Rusu, V., Laverman, P., Borm, P., Heerschap, A., et al. (2013). Dual contrast agent for computed tomography and magnetic resonance hard tissue imaging. *Tissue Eng. C* 19 , 405–416. doi: 10.1089/ten.tec.2012.0007

Wang, X., Ye, J., and Wang, Y. (2007). Influence of a novel radiopacifier on the properties of an injectable calcium phosphate cement. *Acta Biomater.* 3, 757–763. doi: 10.1016/j.actbio.2007.01.004

Wichlas, F., Seebauer, C. J., Schilling, R., Rump, J., Chopra, S. S., Walter, T., et al. (2012). A signal-inducing bone cement for magnetic resonance imaging-guided spinal surgery based on hydroxyapatite and polymethylmethacrylate. *Cardiovasc. Intervent. Radiol.* 35, 661–667. doi: 10.1007/s00270-011-0192-0

Wu, Y., Chesler, D. A., Glimcher, M. J., Garrido, L., Wang, J., Jiang, H. J., et al. (1999). Multinuclear solid-state three-dimensional MRI of bone and synthetic calcium phosphates. *Proc. Natl. Acad. Sci. U.S.A.* 96, 1574–1578. doi: 10.1073/pnas.96.4.1574

Conflict of Interest Statement: The authors declare that the research was conducted in the absence of any commercial or financial relationships that could be construed as a potential conflict of interest.

frontiers in Bioengineering and Biotechnology

REVIEW
published: 04 June 2019
doi: 10.3389/fbioe.2019.00131

At the Intersection of Biomaterials and Gene Therapy: Progress in Non-viral Delivery of Nucleic Acids

Hasan Uludag[1,2,3]*, *Anyeld Ubeda*[2] *and Aysha Ansari*[1]

[1] Department of Chemical and Materinals Engineering, University of Alberta, Edmonton, AB, Canada, [2] Department of Biomedical Engineering, University of Alberta, Edmonton, AB, Canada, [3] Faculty of Pharmacy and Pharmaceutical Sciences, University of Alberta, Edmonton, AB, Canada

Biomaterials play a critical role in technologies intended to deliver therapeutic agents in clinical settings. Recent explosion of our understanding of how cells utilize nucleic acids has garnered excitement to develop a range of older (e.g., antisense oligonucleotides, plasmid DNA and transposons) and emerging (e.g., short interfering RNA, messenger RNA and non-coding RNAs) nucleic acid agents for therapy of a wide range of diseases. This review will summarize biomaterials-centered advances to undertake effective utilization of nucleic acids for therapeutic purposes. We first review various types of nucleic acids and their unique abilities to deliver a range of clinical outcomes. Using recent advances in T-cell based therapy as a case in point, we summarize various possibilities for utilizing biomaterials to make an impact in this exciting therapeutic intervention technology, with the belief that this modality will serve as a therapeutic paradigm for other types of cellular therapies in the near future. We subsequently focus on contributions of biomaterials in emerging nucleic acid technologies, specifically focusing on the design of intelligent nanoparticles, deployment of mRNA as an alternative to plasmid DNA, long-acting (integrating) expression systems, and *in vitro*/*in vivo* expansion of engineered T-cells. We articulate the role of biomaterials in these emerging nucleic acid technologies in order to enhance the clinical impact of nucleic acids in the near future.

Keywords: biomaterials, gene medicine, nucleic acid delivery, nanoparticle, siRNA, mRNA, pDNA delivery, T-cell therapy

OPEN ACCESS

Edited by:
Francesca Taraballi, Houston Methodist Research Institute, United States

Reviewed by:
Masoud Mozafari, Materials and Energy Research Center, Iran
Evan Alexander Scott, Northwestern University, United States

***Correspondence:**
Hasan Uludag
hasan.uludag@ualberta.ca

Specialty section:
This article was submitted to Biomaterials, a section of the journal Frontiers in Bioengineering and Biotechnology

Received: *20 March 2019*
Accepted: *15 May 2019*
Published: *04 June 2019*

Citation:
Uludag H, Ubeda A and Ansari A (2019) At the Intersection of Biomaterials and Gene Therapy: Progress in Non-viral Delivery of Nucleic Acids. Front. Bioeng. Biotechnol. 7:131. doi: 10.3389/fbioe.2019.00131

INTRODUCTION

Synthetic and naturally derived biomaterials have been firmly entrenched in technologies intended to deliver therapeutic and diagnostic agents in a clinical setting. Biomaterials typically package the agents in a form that effectively deliver them to desired sites of actions without being impeded by physiological clearance mechanisms. They could additionally provide stability to agents in the physiological milieu as well as incorporate elements that can respond to physiological stimuli to enhance the functionality of delivered agents. Their ability to incorporate therapeutic and diagnostic agents is nowhere more demanding than the attempts to employ nucleic acid-based agents, so called *gene medicines*. Nucleic acids provide seemingly infinite opportunities to undertake molecular therapy and remedy the abnormal physiology, and furthermore "personalize" the intervention with the knowledge of patient-specific complementary information. Ever since the recombinant technology has been advanced to produce natural and engineered proteins en mass (Gräslund et al., 2008), various possibilities with gene medicines have excited clinicians that are eager to replace the

conventional small molecular drugs that are prone to non-specific effects on a multitude of cellular systems, and face resistance once the innate physiological mechanisms are induced by the rogue cells in order to overcome the drug effects. The recent explosion of molecular understanding of the participation of deoxyribonucleic acid (DNA) and ribonucleic acid (RNA) biomolecules in control of the cell physiology has further garnered excitement in the field to commercialize a range of older nucleic acids (e.g., antisense oligonucleotides, plasmid DNA, etc.) and emerging agents such as short interfering RNA (siRNA), non-coding microRNAs (miRs), and messenger RNA (mRNA). The latter has particularly garnered exuberant interest from the business community with the largest biotech US IPO of 2018 being undertaken by Moderna Therapeutics that focusses on development of mRNA therapeutics.

In this review article, we will summarize recent exciting developments in gene medicines, knowledge gaps in the literature and outline future avenues of fruitful activity that will enable biomaterials to "propel" DNA and RNA based agents into the clinical realm. The range of promising nucleic acids is initially summarized providing the reader with a glimpse of clinical possibilities with them. The potential impact of different nucleic acids is presented and their perceived advantages and limitations are summarized when deployed in a clinical setting. Using the T-cell therapy paradigm, we will explore the possible impact of biomaterials in implementing this mode of therapy as a representative case for an emerging, broad-impact technology. We anticipate similar technology platforms based on *ex vivo* modified/expanded cells to find clinical validation in the treatment of an increasing number of diseases. Finally, we articulate emerging areas in nucleic acid therapeutics that will be impacted by employment of biomaterials, concentrating on intelligent nanoparticles (NPs), *ex vivo* cell expansion, mRNA delivery, and long-term transgene expression. This review will primarily focus on (i) therapeutic (rather than diagnostic) modalities, and (ii) non-viral, biomaterials-centered methods to undertake effective delivery of nucleic acids. The authors acknowledge that exciting developments are taking place in viral design and engineering to undertake clinical therapy, but we refer the reader to other sources on recent developments on this front (Schott et al., 2016; Lundstrom, 2018).

SPECTRUM OF NUCLEIC ACIDS FOR CLINICAL UTILITY

The crux of gene medicine relies on the ability of nucleic acids to alter the physiology of a target cell. It is critical to understand the properties and physiological functions of different nucleic acids, especially at their site of action, to select the appropriate biomaterials carrier for effective transfection (**Figure 1**). The transient nature of the functional effects achieved with most nucleic acids forces the practitioners to choose the right target for an effective therapy. Targets whose silencing temporarily halts or simply slows down the pathological changes will not be desirable; oncogenes whose silencing lead to irreversible processes such as apoptosis induction, or targets that can sensitize the cells to deadly drug action subsequently are more desirable for effective outcomes. Below we inspect various types of nucleic acids based on their ability to derive distinct types of functional outcomes.

Transgene Expression

In the original gene therapy approach, a gene of interest was introduced into the cells to tap into the native machinery to produce the therapeutic protein, in order to replace a defective version (such as a mutated, non-functional protein) or supplement an additional capability such as morphogen-induced tissue regeneration. The use of viruses has been favored to ensure effective (increased uptake) and long-lasting (chromosomal integration) transgene expression, but using plasmid DNA (pDNA) and other naked nucleic acids eliminates several undesirable viral effects, as long as the delivery is effective. It has been possible to design tissue-specific, inducible, minimally-recognizable and "mini" pDNAs to overcome various limitations of the initial pDNA configurations. In addition to circular pDNA, it is possible to rely on other configurations of functional genes; the expression cassettes may come in various molecular weights, conformation and topologies (Sum et al., 2014). Lower molecular weight mini pDNA vectors, both linear and circular conformations, show better cytoplasmic diffusion compared to their parental plasmid precursors. Ministring DNA vectors, which are mini linear covalently closed DNA vectors, demonstrate improved cellular uptake, transfection efficiency, and target gene expression in comparison to isogenic minicircle DNA, which are mini circular covalently closed DNA vectors, of the same size and structure as the ministring DNA (Nafissi et al., 2014). Simultaneous delivery of two pDNAs is employed in the *sleeping beauty* (SB) transposon system, wherein one pDNA carries the SB transposase gene while the other pDNA carries the gene of interest flanked by the transposase recognizable terminal inverted repeats (TIRs). The capability of the transposon system to permanently insert transgene constructs in the host genome and relatively superior biosafety profile, makes the SB approach advantageous over non-integrating non-viral vectors and viruses, respectively (Kebriaei et al., 2017; Tipanee et al., 2017a). We (Hsu and Uludag, 2008) and others (Dhanoya et al., 2011) have previously shown that polymeric gene carriers can condense and deliver widely different DNA molecules. How cells process different DNA molecules is an understudied area with important implications in transgene expression efficiency; comparative assessment of uptake of nucleic acid complexes (Hsu and Uludag, 2008; Symens et al., 2013; Levacic et al., 2017), nuclear localization (Dhanoya et al., 2011), intracellular diffusion, and increased propensity for dissociation and/or endosomal release (Ribeiro et al., 2012) remains to be fully investigated

Abbreviations: DNA, deoxyribonucleic acid; RNA, ribonucleic acid; siRNA, small interfering RNA; shRNA, short hairpin RNA; mRNA, messenger RNA; miR, microRNA; pDNA, plasmid DNA; SB, sleeping beauty; TIR, Terminal Inverted Repeat; ASO, Antisense oligonucleotide; RNAi, RNA interference; lncRNA, Long non-coding RNAs; circRNA, circular RNA; gRNA, guide RNA; PEG, polyethyleneglycol; PEI, polyethyleneimine; mAb, monoclonal antibody; CAR, Chimeric Antigen Receptor; APC, Antigen presenting cell; GAM, Gene Activated Matrix; TAM, Transcript Activated Matrix; TCR, T-cell Receptor; NP, nanoparticle; PLGA, polylactide-co-glycolide; CRISPR, Clustered Regularly Interspaced Short Palindromic Repeat.

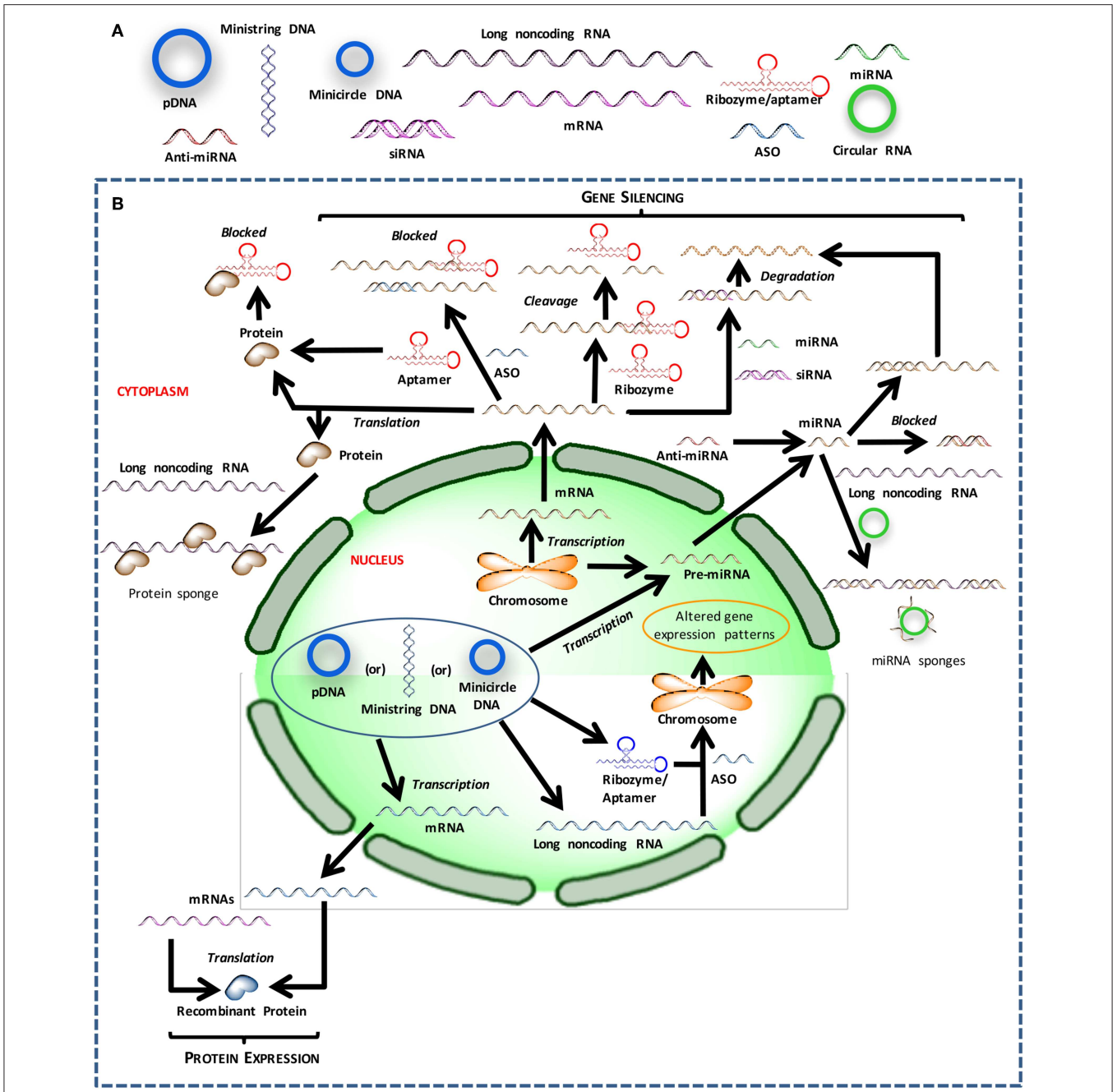

FIGURE 1 | Different nucleic acids that could be used to derive therapeutic outcomes. **(A)** Major types of nucleic acids used to modulate cell behavior and could serve as therapeutic agents. **(B)** Intracellular trafficking and site of action for intervention with different types of nucleic acids.

especially in clinically relevant cells, but the ease of industrial expansion favors pDNA of various configurations for large scale applications. To overcome any transcriptional barriers (such as nuclear targeting and recognition by transcription factors), recent attempts have focused on delivering mRNA that can remain in cytoplasm and access the translational machinery readily (see section mRNA Delivery to Replace pDNA Therapy for more details on mRNA delivery).

Gene Silencing

In order to silence unwanted or undesirable genes, antisense oligonucleotides (ASO; 16–20 nucleotide long single-stranded DNAs) that "neutralize" and block translation of target mRNAs were initially pursued that rely on *ex vivo* chemical synthesis and delivery. Apart from silencing defective genes, ASOs are finding applications in restoring the correct splicing patterns of pre-mRNAs that possess aberrant sequence elements involved in

splicing or aberrant splice sites, as well as in altering expression levels of splice variants to affect a change in the function of a gene. This is executed by designing ASOs complementary to specific splice sites, thus blocking spliceosome assembly at the targeted splice site, which thereby leads to a shift of the splicing machinery to another splice site. The ASOs are expected to be capable of entering the cell nucleus, which is the site for pre-mRNA splicing. This is achieved by employing nucleotide bases, sugars and internucleotide linkages with modified chemistries (Kole and Sazani, 2001). A notable example of utilizing ASOs in this modality is the development of exon skipping therapy, wherein ASOs are used to restore the reading frame by skipping an exon or exons containing disease-driving mutations. Exon skipping therapy has been well-explored clinically in the context of Duchenne Muscular Dystrophy (Cirak et al., 2011; Goemans et al., 2016; Mendell et al., 2016; Aartsma-Rus et al., 2017), with an ASO drug receiving FDA approval in 2016 (Sarepta Therapeutics)[1].

The endogenous RNA interference (RNAi) mechanism has been adopted for therapy by silencing genes based on blockage and/or degradation of corresponding mRNAs. RNAi can be implemented with synthetic short interfering RNAs (siRNAs; 19–27 nucleotide long double-stranded RNAs), as well as *in situ* production of silencer molecules (short hairpin RNAs; shRNAs) through typical pDNA-based expression vectors. While the latter relies on nuclear targeting for efficient expression, siRNAs can be delivered to the cytoplasmic space to engage the RNA-induced silencing complex (RISC) directly with minimal processing by host cells. To achieve sustained silencing of gene expression, siRNA needs to be continually supplied exogenously, or stable integration and expression is required in the case of shRNAs. The exciting possibilities with RNAi was recently (2018) confirmed with the FDA approval of the first siRNA based drug (Patisiran by Alnylam) to treat the nerve damage caused by the rare disease hereditary transthyretin-mediated amyloidosis (hATTR) in adults. To further regulate gene expression, endogenous miRs, the non-coding single stranded RNAs with 19 to 25 nucleotides and mis-matched base pairing, can be introduced into host cells either to augment or "mimic" a particular miR. In cases where the elevated miRs themselves are the cause of underlying pathophysiology and need to be down-regulated, single stranded RNA molecules with sequence complementary to a target miR, an anti-miR, could be deployed.

Gene suppression can also be executed by utilizing a subset of RNAs, called ribozymes or catalytic RNAs, that possess enzymatic action and can cleave target mRNA with high specificity to prevent protein translation (Abera et al., 2012). Besides utilizing artificially engineered ribozymes exogenously, significant efforts have been directed toward intracellular expression of these molecules. Expression cassettes with different kinds of promoters (e.g., long-acting, cell-specific, inducible, etc.) have been explored to optimize activity of the expressed ribozyme *in vivo*. To enhance stability and ensure proper folding into its active structure, ribozymes are expressed as part of a larger transcript, called carrier RNA, the sequence of which is carefully chosen so that the resulting transcript not only adopts a secondary structure that does not impede ribozyme activity but is also stable (Cagnon et al., 1995; Good et al., 1997; Prislei et al., 1997). Apart from downregulation of aberrant genes by *trans*-cleaving ribozymes, pathogenic genes can be repaired and/or reprogrammed by another subset called *trans*-splicing ribozymes. In the repair modality, mutated genes are cleaved and replaced by wild-type RNA sequences to yield properly functioning genes while maintaining the spatial and temporal gene expression patterns in cells and tissues (Byun et al., 2003; Shin et al., 2004). In malignancies and pathological tissue induction, where multiple pathways are dysregulated, repairing a single gene may not be sufficiently effective and hence require expression of multiple therapeutic genes. *Trans*-splicing ribozymes with reprogramming capabilities have been developed that not only remove viral transcripts and tumor-related genes but also induce cell death leading to elimination of virus-infected and cancer cells (Won and Lee, 2012; Carter et al., 2014; Kim et al., 2017). Since reprogramming genes comes with a great risk of unconstrained expression and unintended gene removal, it is paramount to introduce elements that maintain a check on the activity of *trans*-splicing ribozymes. This has been achieved by incorporating miR target sites or hypoxia-inducible elements in ribozymes to regulate their activity in a miR expression status-dependent manner or the ambient cellular environment, respectively. The potential of *trans*-splicing ribozymes in gene therapy and as anti-viral and anti-cancer tools has been reviewed elsewhere (Lee et al., 2018).

"Sponging" Nucleic Acids

Long non-coding RNAs (lncRNA) have been recently identified whose sole function seem to sequester and alleviate the effects of intracellular molecules responsible for undesirable changes. It may be possible to alter the activity of specific DNA, RNA, and protein targets by deploying lncRNAs 'sponges.' Sponging may be additionally undertaken by so called circular RNAs (circRNAs) distinct from linear lncRNAs and miRs, featuring higher cellular stability due to the absence of free ends and resistance to exonucleolytic degradation. CircRNAs may harbor one or more binding sites for a single miR or possess binding sites for multiple miRs, thereby regulating entire miR families (Panda et al., 2016; Chen et al., 2017; Hsiao et al., 2017). Besides miR sponges, circRNAs harboring a high density of binding sites for one or more RNA-binding proteins, serve as protein sponges, thereby modulating levels of target proteins which leads to changes in downstream intracellular events (Ashwal-Fluss et al., 2014; Abdelmohsen et al., 2017). Alternatively, they may operate as protein scaffolds facilitating contact between two or more proteins when they possess binding sites for enzymes and their substrates (Du et al., 2017). Their sponging capacity can be harnessed by engineering them to include combinations of miR and protein binding sites to target specific disease profiles. Since they can also serve as templates for protein expression in the presence of appropriate translation signals (Legnini et al., 2017; Pamudurti et al., 2017; Yang et al., 2017), expression cassettes

[1]FDA letter to Sarepta Therapeutics Inc. on eteplirsen approval. Available online at https://www.accessdata.fda.gov/drugsatfda_docs/nda/2016/206488_summary%20review_Redacted.pdf

for therapeutic proteins can be incorporated into circRNAs for gene therapy. Research on the practical implementation of therapeutic circRNAs is still in its infancy, with significant room for exploratory studies to realize their therapeutic potential.

Other nucleic acids that can affect cellular events by sequestering biomolecules are DNA and RNA aptamers. They are 56–120 nucleotides long, single-stranded synthetic oligonucleotides that can bind to various targets including small organic compounds and proteins, both intracellular and extracellular, with high affinity and specificity. They can fold into three-dimensional (3D) structures for binding to their target proteins through structural recognition and inhibit their interactions with other molecules in a manner similar to protein antagonists and antibodies, thereby serving as decoys. Their ability to recognize and bind highly structured nucleic acid targets lends them a unique functionality that may be more advantageous over previously mentioned agents (i.e., ASOs, siRNAs, miRs, ribozymes etc.). While extracellular molecules can be targeted by exogenous aptamers with relative ease, *in situ* production of aptamers through expression vectors has been explored for more efficient targeting of intracellular molecules (aptly known as "intramers") (Chaloin et al., 2002; Choi et al., 2006; Mi et al., 2006). Many different promoter systems and expression cassettes have been designed to obtain high intracellular levels and sustained expression of aptamers. The functionality of endogenously expressed RNA aptamers can be impaired by flanking sequences in the RNA aptamer transcript, as interaction with them can hamper proper folding and render them inert (Sullenger et al., 1990; Blind et al., 1999; Martell et al., 2002). To overcome this limitation, sequences coding for ribozymes have been incorporated into the vector, which upon expression cleaves the aptamer from the nascent RNA transcript (Joshi and Prasad, 2002; Nishikawa et al., 2003). A strategy to direct intramers to extra-nuclear compartments and localize them close to their target(s) is to include nuclear export signal sequences, which enable translocation of expressed aptamers through nuclear pore complex (Grimm et al., 1997; Hamm and Fornerod, 2000). Control over intramer activity can be attained by employing a bi-aptamer construct where one aptamer serves as a sensor for the biological trigger and the other aptamer exerts inhibitory action. The expression cassette for these trigger-inducible systems include a connection sequence between the two aptamer sequences, resulting in a functional fusion product (Ausländer et al., 2011). In a separate avenue of exploration, the capacity of aptamers to bind a diverse range of targets has been extensively exploited for derivatization of NP delivery systems for site- or target-specific delivery. The success of this strategy is evident by numerous therapeutic RNA aptamers undergoing clinical trials (Sundaram et al., 2013; Sridharan and Gogtay, 2016).

Gene Editing

Recent advances in gene editing technology based on clustered regularly interspaced short palindromic repeat (CRISPR)/Cas9 nuclease is providing exciting possibilities but also raising the bar for biomaterial-mediated delivery. The CRISPR/Cas9 system requires a single guide RNA (gRNA) and the Cas9 nuclease to undertake gene editing. For practical implementation, alongside the gRNA, the Cas9 nuclease may be delivered directly as a protein, as a pDNA cassette for protein expression in host cell, or as a "translatable" mRNA (Lino et al., 2018; Wang et al., 2018). Co-delivery of different cargoes presents a great challenge in designing an optimal delivery vehicle due to differences in physical structure and chemical properties of the different types of cargo. For instance, in contrast to anionic nucleic acids, the Cas9 protein is cationic (Sun et al., 2015), so that biomaterials have to accommodate the contrasting features of the cargo during the packaging and delivery. Biomaterials capable of optimally complexing long-string like transposase mRNA will be different from carriers that optimally interact with gRNA, so that mutually compatible carriers are likely to require concerted efforts. The situation is analogous to the SB transposon system, where supplying transposase from *in situ* translated mRNA (preferable to avoid the risk of chromosomal integration) (Wiehe et al., 2007; Holstein et al., 2018) instead of pDNA expression cassette will require distinct optimization of the biomaterial carrier to accomodate both types of cargo. We had previously articulated on the importance of delivering multiple agents as being the preferred approach in the case of most pathophysiologies (e.g., cancers where the internal physiology is altered in several respects) (KC et al., 2017). Deploying a single agent, while convenient for pharmacological development, may not be as effective in controlling the disease in these cases. Augmenting a defective gene may need to be undertaken while suppressing other mediators or augmenting other genes and miRs, for which combinatorial delivery of different nucleic acids will be needed (KC et al., 2017). In attempts to co-deliver a pDNA and siRNA, for example, one is faced with the delivery of a long flexible DNA molecule (>3000 bp) and a short rigid RNA molecule (<30 bp). Composite materials or chemically-distinct delivery vehicles capable of self-assembling into functional structures with different nucleic acids are needed to this end. While technically challenging, undertaking combinatorial delivery may offer the advantage of enhancing the biosafety and toxicity of certain vectors given the improvements in efficacy and the need to deploy a lower dose of the therapeutic agents.

"Hybrid" Nucleic Acids for Responsive Systems

The simplicity of the four-nucleotide chemistry and Watson-Crick base pairing provides significant room for flexibility, as a consequence of which generation of different combinations of polynucleotides has been feasible. Chimeric constructs developed by combining different types of nucleic acids allows us to benefit from their respective desirable characteristics and diverse functionalities. The targeting capability of aptamers has been harnessed by conjugating them with ASOs, siRNAs, shRNAs, and miRs for cell-specific delivery and subsequent gene silencing (Soldevilla et al., 2018). Additionally, the unique binding capability of aptamers to small molecules has been employed to generate RNA-based regulators that integrate sensing functions and endogenous gene regulation, through ligand-responsive aptamer-miR chimeras (Beisel et al., 2011).

Molecular switches that turn on/off a certain function contingent upon a physiological signal has been manifested by integrating aptamers with ribozymes, known as aptazymes. It has been shown that target interaction with aptamer induces adaptive folding around the bound target leading to adoption of a distinct conformation as well as further stabilization of adjacent helical domains. This stabilization affects the conformation of the attached ribozyme leading to a switch in its activity (Famulok et al., 2007). These triggerable systems, once optimized, permit better control over relatively complicated therapeutic strategies that target regulatory networks or genome reprogramming, as reported in a study where an aptazyme was embedded within the gRNA of a CRISPR/Cas9 system (Tang et al., 2017). By inserting multiple aptamer sequences harboring specificities for different ligands, it may be possible to obtain more precise control over genome editing and subsequently over spatial and temporal gene expression patterns to rectify diseased states.

Apart from aptamers, DNA could also serve as a delivery vehicle when folded into nanostructures through the scaffolding DNA origami technique, as demonstrated by successful *in vivo* delivery of siRNA by a DNA tetrahedron (Lee et al., 2012). Although the added functionality imparted by hybridizing different nucleic acids has a great appeal, especially in the context of gene therapy, it is critical to ensure that integration does not hamper the biological activity of either molecule. Other practical considerations such as synthesis cost:yield ratio, benefit:cost ratio, suitability and need for the intended application should also be evaluated during design and creation of these types of hybrid constructs.

Nucleic Acids Without Carriers

Finally, we note that numerous clinical studies are underway where new generation of nucleic acids are being deployed without the use of a carrier (**Table 1**). Presumably, the rationale behind this approach is to avoid the introduction of synthetic carrier materials which may not be degraded at times and hence may accumulate leading to adverse effects. Carrier-free delivery eliminates the process of development and optimization of a delivery vehicle, but however poses its own set of challenges. Several factors such as poor permeability to cell membranes due to their anionic nature, rapid clearance owing to their small size, and susceptibility to degradation by ubiquitous nucleases, render the nucleic acids unfavorable in their native form. To overcome these physiological barriers, chemical modifications have been incorporated in their sugar-phosphate backbones as well as sugar and base moieties. While these modifications confer desirable attributes such as enhanced stability, nuclease resistance, target binding affinity, and reduced immune stimulation, it is crucial to include them in a balanced proportion to circumvent loss of potency. Besides chemical modifications, nucleic acids are conjugated with lipid moieties or polyethylene glycol (PEG) or small cationic proteins to aid in increasing their size, traversing the complex physiological milieu, enhancing circulation half-life, and eventually potentiating their therapeutic efficacy. Practically, utilization of naked nucleic acids seems most appropriate for localized treatment strategies, as is evident from **Table 1**, where ∼60% of the indicated clinical studies employ subcutaneous, intramuscular, intravitreal or other localized routes of administration. In these modes, they are challenged with relatively less physiological hurdles to reach their site of action and carry out their activity. Accordingly, carrier-free nucleic acid therapeutics are suitable for external and/or easily accessible tissues such as ocular, epidermal, pancreatic, pulmonary, and colonic tissues. The route of administration has a significant influence on drug biodistribution, bioavailability, and eventually its therapeutic efficacy, so that initial focus on the development of nucleic acid therapeutics for ailments of the eye, skin, and muscle are understandable. Local administration also allows for implementing gene medicines by patients through eye drops and nasal sprays. However, for more deep-seated maladies, naked nucleic acids may not be satisfactory as in this case they need to be administered systemically and are required to seek out the diseased tissue in the complex *in vivo* environment to be effective. For this, they need to be equipped with the right elements to identify target tissues and evade degradation, while still be biologically active. Incorporating chemical modifications can adversely effect potency, making it incumbent to utilize carriers for nucleic acid therapeutics intended for these applications. While viruses are efficient and effective carriers, significant effort has been invested in developing safer, less immunogenic non-viral techniques and biomaterials for delivering nucleic acid therapeutics in hematological malignancies, as reviewed elsewhere (Ansari et al., 2017).

TECHNOLOGY FOR CELLULAR ENGINEERING: T-CELL THERAPY AS A CASE IN POINT

The exciting developments in T-cell therapies are providing opportunities for biomaterials to implement a new type of gene medicine. T-lymphocytes are essential for adaptive immunity as they acquire T-cell receptors (TCRs) in the thymus to recognize foreign antigens from infectious pathogens as well as tumor antigens (Mitchison, 1955; Jorgensen et al., 1992; Park and Renier, 2010). Since 1980s, *ex-vivo* expanded T-cells have been used for treatment of diseases such as melanoma, cytomegalovirus and HIV (Rosenberg et al., 1988; Riddell et al., 1992; Levine et al., 2002). The initial deployment of T-cells required sorting and expansion of allogeneic or autologous lymphocytes for their reintroduction into patients, yet generation of disease-specific T-cells is cumbersome as patients usually express limited numbers of cells that are reactive against the specific target (Sadelain et al., 2003; Park and Renier, 2010). Using allogeneic T-cells and in some cases autologous T-cells led to high risks of developing graft-vs.-host disease and rejection of infused T-cells. Relying on naturally expressed TCRs requires tumor antigens to be presented by specific major histocompatibility complexes (MHC), which are usually down-regulated or dysfunctional in many tumors besides being very specific to each patient (Hicklin et al., 1999; Khong and Restifo, 2002; Park and Renier, 2010).

Engineered T-cells have emerged to better control the safety and effectiveness of T-cell therapies particularly controlling antigen targeting and T-cell function (Sadelain et al., 2003).

TABLE 1 | Carrier-free nucleic acid therapeutics in clinical trials.

Drug	Nucleic acid	Target	Route of administration	Indication
SYL1001	siRNA	TRPV1	Ophthalmic drops	Dry eye syndrome
ALN-GO1 (Lumasiran)	GalNAc-siRNA	HAO1	Subcutaneous	Primary hyperoxaluria type I
Bevasiranib	siRNA	VEGF	Intravitreal injection	AMD/DME
SYL040012	siRNA	ADRB2	Ophthalmic drops	Intraocular pressure
PF-655	siRNA	RTP801	Intravitreal injection	AMD/DME
I5NP (QPI-1002)	siRNA	P53	Intravenous	AKI and DGF
DCR-HBVS	GalNAc-siRNA	HBV	Subcutaneous	Chronic hepatitis B
DCR-PHXC	GalNAc-siRNA	LDHA	Subcutaneous	Primary hyperoxaluria
BMT101	Lipophilic compound-siRNA	CTGF	Intradermal injection	Hypertrophic scars
QPI-1007	siRNA	Caspase 2	Intravitreal injection	NAION
AGN-745	siRNA	VEGFR-1	Intravitreal injection	AMD
TD101	siRNA	KRT6A	Intralesional injection	Pachyonychia congenita
ALN-RSV01	siRNA	RSV nucleocapsid	Nebulization or intranasal	RSV infection
SRP-4053	ASO	Exon 53 skipping in dystrophin gene	Intravenous	DMD
GTI-2040	ASO	RNR	Intravenous	Leukemia, MDS, solid tumors
NS-065/NCNP-01	ASO	Exon 53 skipping in dystrophin gene	Intravenous	DMD
EZN-2968	ASO	HIF-1α	Intravenous	Advanced solid tumors and lymphoma
TPI ASM8	Two ASOs	CCR3 and β chain of IL3, IL5, and GM-CSF receptors	Inhalation	Asthma
ISIS 104838	ASO	TNF-α	Subcutaneous	Rheumatoid arthritis
OGX-427 (Apatorsen)	ASO	Hsp27	Intravenous	Prostate, ovarian, breast, bladder cancer, and SCLC
G3139 (Oblimersen)	ASO	Bcl-2	Intravenous or subcutaneous	Solid tumors, multiple myeloma, DLBCL and CLL
AZD4785	ASO	KRAS	Intravenous	Advanced solid tumors
AZD5312	ASO	Androgen receptor	Intravenous	Advanced solid tumors
ISIS 5132	ASO	c-Raf kinase	Intravenous	Metastatic breast cancer
ISIS 3521	ASO	PKC α	Intravenous	Metastatic breast cancer
AZD9150	ASO	STAT3	Intravenous	Gastrointestinal, ovarian cancer, hepatocellular carcinoma, and DLBCL
ISIS 183750	ASO	eIF4E	Intravenous	Colorectal cancer
DS-5141b	ASO	Exon 45 skipping in dystrophin gene	Subcutaneous	DMD
AVI-4658	ASO	Exon 51 skipping in dystrophin gene	Intramuscular	DMD
EZN-4176	ASO	Androgen receptor	Intravenous	Prostate cancer
ISTH0036	ASO	TGF-β2	Intravitreal injection	Glaucoma
AEG35156	ASO	XIAP	Intravenous	Pancreatic and breast cancer
RG6042	ASO	Huntingtin	Intrathecal injection	Huntington's disease
WVE-120102	ASO	Huntingtin	Intrathecal injection	Huntington's disease
WVE-210201	ASO	Exon 51 skipping in dystrophin gene	Intravenous	DMD
OGX-011 (Custirsen)	ASO	Clusterin	Intravenous	Solid tumors
RO7070179	ASO	HIF-1α	Intravenous	Hepatocellular carcinoma
ISIS 396443 (Nusinersen)	ASO	SMN2	Intrathecal injection	Spinal muscular atrophy

(Continued)

TABLE 1 | Continued

Drug	Nucleic acid	Target	Route of administration	Indication
Kynamro* (Mipomersen)	ASO	ApoB	Subcutaneous	Homozygous familial hypercholesterolemia
ISIS 420915	ASO	Transthyretin	Subcutaneous	Cardiac amyloidosis
ISIS 113715	ASO	PTP-1B	Subcutaneous	Type 2 diabetes mellitus
ISIS 2302	ASO	ICAM-1	Intravenous	Crohn's disease
Cenersen	ASO	P53	Intravenous	MDS
IONIS-STAT3Rx	ASO	STAT3	Intravenous	DLBCL and advanced lymphoma
IONIS-ENaCRx	ASO	ENaC	Inhalation	Healthy volunteers
IONIS FXI-LRx	ASO	Factor XI	Subcutaneous	Healthy volunteers
IONIS PKK-LRx	ASO	PKK	Subcutaneous	Healthy volunteers
IONIS APOC-III-LRx	GalNAc3-ASO	ApoC-III	Subcutaneous	Elevated triglycerides
SB101	DNAzyme	GATA-3 transcription factor	Inhalation	Asthma
SB012	DNAzyme	GATA-3 transcription factor	Rectal route	Ulcerative colitis
MRG-201	miR mimic	miR-29b	Intradermal	Pathologic fibrosis, keloids
SPC3649	AntimiR	miR-122	Subcutaneous	Hepatitis C
CV9104	50% free mRNA + 50% protamine/mRNA (2:1 w/w)	PSA, PSMA, PSCA, STEAP1, PAP, MUC1	Intradermal	Prostate cancer
CV9201	50% free mRNA + 50% protamine/mRNA (2:1 w/w)	NY-ESO1, MAGE-C1, MAGE-C2, survivin, 5T4	Intradermal	NSCLC
CV7201	Free and protamine/mRNA	Rabies virus glycoprotein	Intradermal or intramuscular	Rabies vaccine
iHIVARNA-01	mRNA	CD40L, CD70, caTLR4, HIV immunogen	Intranodal injection	HIV-1 infection
Tumor mRNA vaccine	mRNA	Melan A, MAGE A1, MAGE A3, survivin, gp100, tyrosinase	Intradermal or subcutaneous	Malignant melanoma
QR-421a	RNA-based oligonucleotide	Exon 13 skipping in USH2A gene	Intravitreal injection	Retinitis Pigmentosa
QR-110	RNA-based ASO	CEP290	Intravitreal injection	Leber's Congenital Amaurosis
QR-010	RNA-based ASO	CFTR	Intranasal	Cystic fibrosis
REG1	RNA aptamer and a PEG-RNA aptamer	Factor IXa	Intravenous	Acute coronary syndrome, coronary artery disease, PCI
AS1411	PEG-DNA aptamer	Nucleolin	Intravenous	AML and solid tumors
ARC1799	PEG-DNA aptamer	Von Willebrand factor	Intravenous	Von Willebrand disease, purpura, thrombotic thrombocytopenia, PCI, AMI, and thrombosis
NOX-E36	PEG-RNA aptamer	CCL2	Intravenous or subcutaneous	Chronic inflammatory diseases, type 2 diabetes mellitus, and SLE
NOX-A12	PEG-RNA aptamer	CXCL12	Intravenous	Stem cell transplantation, multiple myeloma, CLL, NHL, colorectal and pancreatic cancer
E10030	PEG-DNA aptamer	PDGF	Intravitreal injection	AMD and Von Hippel-Lindau Syndrome
ARC1905	PEG-RNA aptamer	Complement 5	Intravitreal injection	AMD and idiopathic polypoidal choroidal vasculopathy
NU172	DNA aptamer	Thrombin	Intravenous	Thrombosis
Macugen* (Pegaptanib)	PEG-RNA aptamer	VEGF	Intravitreal injection	AMD/DME
ARC19499	PEG-RNA aptamer	TFP1	Intravenous or subcutaneous	Hemophilia
NOX-H94	PEG-RNA aptamer	Hepcidin peptide hormone	Intravenous	Anemia of chronic disease and end stage renal disease

(Continued)

TABLE 1 | Continued

Drug	Nucleic acid	Target	Route of administration	Indication
Angiozyme	Ribozyme	VEGFR-1	Subcutaneous	Renal cancer
Heptazyme	Ribozyme	HCV IRES	Subcutaneous	Hepatitis C

The data is compiled from www.ClinicalTrials.gov based on nucleic acid keyword search and choosing the trials where no obvious carrier was used. FDA approved drugs are indicated with an.*

TRPV1, Capsaicin receptor; GalNAc, N-acetylgalactosamine; HAO1, Hydroxyacid oxidase; VEGF, Vascular endothelial growth factor; AMD, Age related macular degeneration; DME, Diabetic macular edema; ADRB2, Beta-2 adrenergic receptor; RTP801, Pro-angiogenic factor; AKI, Acute kidney injury; DGF, Delayed graft function; HBV, Hepatitis B virus; LDHA, Lactate dehydrogenase A; CTGF, Connective tissue growth factor; NAION, Non-arteritic anterior ischemic optic neuropathy; VEGFR-1, Vascular endothelial growth factor receptor-1; KRT6A, Keratin 6a; RSV, Respiratory syncytial virus; DMD, Duchenne muscular dystrophy; RNR, Ribonucleotide reductase; MDS, Myelodysplastic syndrome; CCR3, Eotaxin receptor; IL, Interleukin; GM-CSF, Granulocyte-macrophage colony-stimulating factor; TNF-α, Tumor necrosis factor- α Hsp27, Heat shock protein 27; SCLC, Squamous cell lung cancer; Bcl-2, B-cell lymphoma 2; DLBCL, Diffuse large B-cell lymphoma; CLL, Chronic lymphocytic leukemia; CML, Chronic myeloid leukemia; KRAS - Ki-ras2 Kirsten rat sarcoma viral oncogene homolog; PKC α, Protein kinase C α; TGF-β2, Transforming growth factor-β2; HIF-1α, Hypoxia inducible factor-1α; XIAP, X-linked inhibitor of apoptosis; SMN2, Survival motor neuron 2; ApoB, Apolipoprotein B; PTP-1B, Protein tyrosine phosphatase 1B; ICAM-1, Intercellular adhesion molecule 1; STAT3, Signal transducer and activator of transcription 3; ENaC, Epithelial sodium channel; PKK, Protein kinase C-associated kinase; ApoC-III, Apolipoprotein C3; eIF4E, Eukaryotic translation initiation factor 4E; GATA-3, GATA binding protein 3; PSA, Prostate-specific antigen; PSMA, Prostate-specific membrane antigen; PSCA, Prostate stem cell antigen; STEAP1, Six transmembrane epithelial antigen of the prostate 1; PAP, Prostatic acid phosphatase; MUC1, Mucin 1; NY-ESO1, New York esophageal squamous cell carcinoma; MAGE, Melanoma antigen family; 5T4, Trophoblast glycoprotein; NSCLC, Non-small cell lung cancer; CD, Cluster of differentiation; TLR, Toll-like receptor; HIV, Human immunodeficiency virus; Gp100, Glycoprotein 100; USH2A, Usher syndrome type IIa; CEP290, Centrosomal protein 290; CFTR, Cystic fibrosis transmembrane conductance regulator; PCI, Percutaneous coronary intervention; AMI, Acute myocardial infarction; AML, Acute myeloid leukemia; CCL2, Chemokine (C-C motif) ligand 2; SLE, Systemic lupus erythematosus; CXCL12, C-X-C motif chemokine 12; NHL, Non-Hodgkin's lymphoma; PDGF, Platelet-derived growth factor; TFP1, Tissue factor pathway inhibitor; HCV IRES, Hepatitis C virus internal ribosome entry site.

They represent one of the most advanced therapeutic options as they are a "living drug" which combine major advances in antibody engineering, vaccination and transplantation (Lim and June, 2017). Two T-cell based therapies recently approved by the FDA (National Cancer Institute, 2017), axicabtagene ciloleucel (Yescarta™)[2] and tisagenlecleucel (Kymriah™)[3], are genetically modified cells to express Chimeric Antigen Receptors (CARs) against CD19, an antigen present throughout the B-cell lineage and one of the first targets for development of monoclonal antibodies (mAb) for B-cell malignancies (Engel et al., 1995; Katz and Herishanu, 2014; Park et al., 2016). Along with targeting "liquid" cancers, they are now being explored to target 'solid' cancers, as well as infectious diseases or undesired immune responses with >250 ongoing clinical trials (Scholler et al., 2012; American Association for Cancer Research, 2017; Maldini et al., 2018).

T-cells have been primarily modified to express CARs by viral gene transfer; in cases of Yescarta™ and Kymriah™, replication-defective gammaretrovirus and lentivirus vectors, respectively, were used for gene transfer (Hu and Pathak, 2000; Sadelain, 2017; Zhang et al., 2017), which enabled permanent transgene insertion into the genome (Hu and Pathak, 2000). However, retroviral gene transfer has been associated with high risk of insertional mutagenesis in the past, especially when vectors get inserted close to growth-control genes, leading to oncogenesis, immune reactions, and other toxicities (Hacein-Bey-Abina et al., 2008; Wang et al., 2008, 2015). The production of viral vectors is also laborious, with production times ranging from 2 weeks to 6 months and differences in batches or sources making it difficult to compare and replicate (Przybylowski et al., 2005; Ivics et al., 2009; Levine et al., 2016; Kebriaei et al., 2017; Zhang et al., 2017). As a result of these drawbacks, non-viral vectors that are easier to synthesize, cheaper, less toxic and more consistent to produce are being constantly developed to match the effectiveness of viral vectors (**Table 2**). SB transposons, just as retroviral vectors, can integrate themselves in the genome and address the issue of longevity of expression (Ivics et al., 2009). The SB transposon system was the first one to be effective in vertebrate cells and since then other transposons that are more active in some cell lines, such as the piggyback transposon, have been investigated (Wu et al., 2006; Muñoz-López and García-Pérez, 2010). Transposons rely on TIRs that are recognized by transposases to "cut" and "paste" the gene at desired destinations. Thus, a transposon vector with the gene of interest with the TIRs and a transposase-coding pDNA or mRNA need to be delivered to target cells (Yant et al., 2000; Wu et al., 2006). While transposon systems could be simpler and more predictable with lower risk of immunogenicity (Walisko et al., 2008), transposable elements are not free of risks of genotoxicity and they still rely on carriers for transport through the cell membrane. Viral vectors are still being used for transposons with the same challenges discussed before (Doudna and Charpentier, 2014; Boehme et al., 2016; Richter et al., 2016). Other gene editing technologies include designer nucleases, including zinc finger nucleases (ZFN), transcription activator-like effector nucleases (TALEN) and CRISPR/Cas9 system which induce double strand breaks in a target site followed by the addition of a gene of interest (Urnov et al., 2010; Gaj et al., 2013; Jung and Lee, 2018). The CRISPR/Cas9 system is already being tested in clinical trials in China and CAR T-cell engineering in the US (Svoboda et al., 2018). The designer nucleases depend on cellular enzymes for gene insertion that require dividing cells in contrast to some integrating viruses and transposon systems that can also target non-dividing cells (Di Stasi et al., 2011).

[2]Yescarta™ (axicabtagene ciloleucel) suspension for intravenous infusion Initial U.S. Approval: 2017. Available online at: https://www.fda.gov/files/vaccines%2C%20blood%20%26%20biologics/published/Package-Insert---YESCARTA.pdf

[3]Kymriah™ *(tisagenlecleucel), first-in-class CAR-T therapy from Novartis, receives second FDA approval to treat appropriate r/r patients with large B-cell lymphoma (2018).* Available online at: https://www.novartis.com/news/media-releases/kymriahr-tisagenlecleucel-first-class-car-t-therapy-from-novartis-receives-second-fda-approval-treat-appropriate-rr-patients-large-b-cell-lymphoma

TABLE 2 | Broad comparison of viral and non-viral transfection vectors.

Criteria	Viral	Non-viral
Immunogenicity, Inflammation	High-medium risk	Medium-low risk
Mutagenesis	High-medium risk	Medium-low risk
Vector production	Laborious, batch to batch variability	Ranges in difficulty
Transfection efficiency	High efficiency	Medium-low efficiency
Duration of gene expression	Long term	Medium, transient

One of the main challenges associated with shifting to non-viral methods for transfection of T-cells is the inability of non-viral systems to match the efficiency of viral systems, especially in terms of longevity of gene expression. However, the transient expression by non-viral vectors may be advantageous as it may lead to reduced side effects and complications for patients (Hardee et al., 2017). Another challenge for non-viral vectors in T-cell engineering is less than optimal *in vivo* targeting and continuous stimulation that must be provided by the material to the cells, which is inherently difficult to achieve as these cells are present in suspension, are constantly dividing and usually exist in an immunosuppressive environment (Zheng et al., 2013; Ansari et al., 2017). Thus, innovative biomaterials that find solutions to these two challenges are of paramount importance in the field and can also serve as a point of reference for biomaterials targeting various cells besides T-cells. The alternative to viral modification of T-cells is commonly based on membrane pore-inducing electroporation/nucleofection without any carriers. Ramanayake et al. recently compared the average costs of viral delivery ($3-500,000) with an electroporation/transposon approach ($6,000) to produce CAR T-cells under GMP conditions. By optimizing electroporation conditions, modified CAR T-cells persisted in the peripheral blood for >3 weeks and transgene expression was >50% (Wells, 2004). A safety guard included in their transposon sequence was the inducible caspase 9 suicide gene, which directs targeted elimination of engineered T-cells by administration of a small molecule (Wang et al., 2017). Some drawbacks of electroporation, however, are toxicity and difficulty for *in vivo* applications due to limited access to target sites (Holstein et al., 2018). Longer *ex vivo* expansion might be required to allow cells to recover from undesirable consequences of electroporation, since grafting nucleofected hematopoietic cells in a preclinical model was improved with longer culture times (Holstein et al., 2018). An alternative approach to electroporation is "cell squeezing" using microfluidic devices that rely on rapid mechanical deformation of cells to passively introduce genes and materials of interest (Sharei et al., 2013a,b).

In a similar manner, as more precise control is desired for immunomodulation of T-cells, diverse biomaterials and nanotechnologies have emerged as platforms to address major stages and challenges of CAR T-cell development, namely *ex vivo* and *in vivo* expansion of cells and CAR gene delivery (**Table 2**). The majority of T-cell therapies involve *ex vivo* expansion of modified/to be modified cells but not all expanded T-cells have the same therapeutic efficacy (Fraietta et al., 2018). T-cell expansion most commonly employs commercially available polystyrene microbeads (Dynabeads) that aim to simulate the action of antigen presenting cells (APCs) targeting T-cell activation through CD3 and CD28 stimulus and IL-2 supplementation (Kalamasz et al., 2004; Hollyman et al., 2009; Li and Kurlander, 2010). However, these non-degradable beads need to be separated prior to cell delivery to patients and they also dysregulate some T-cell functions as their mode of action is not as close as APC activation. Other alternatives to naturally derived APCs include poly(lactide-co-glycolide) (PLGA) microparticles (Steenblock and Fahmy, 2008), phosphatidylcholine and cholesterol liposomal systems (Prakken et al., 2000), paramagnetic iron-dextran NPs (Perica et al., 2014), polydimethylsiloxane (PDMS) microbeads (Lambert et al., 2017) and carbon nanotubes composites with PLGA NPs (Fadel et al., 2014), highlighting the compatibility of various systems with T-cell stimulation and also how different physiochemical properties of the particles may have different efficiencies on T-cell expansion. Besides the use of NP systems, 3D scaffolds have also been developed which can be used as implants at tumor sites. These systems have included commercial Matrigel and polystyrene scaffolds (Pérez Del Río et al., 2018), mesoporous silica microrods with supported lipid bilayer composites (Cheung et al., 2018), 3D-printed polycaprolactone lattices (Delalat et al., 2017), alginate scaffolds (Stephan et al., 2014) and injectable polyisocyanopeptide and PEGylated chitosan hydrogels (Tsao et al., 2014; Weiden et al., 2018a). With such broad possibilities, the versatility of biomaterials to design biomimetic systems to effectively expand T-cells is evident. Scaffolds have also been used as *in vivo* immunomodulation niches promoting sustained release and expansion of T-cells directly at tumor sites. For example, an alginate scaffold was reported that delivered T-cells and a STING (Stimulator of Interferon Genes) agonist, serving as a vaccine in pancreatic and melanoma mice models (Smith et al., 2017a). Co-delivery of T-cells and STING agonist not only eradicated the tumors in some mice, but also enabled the cured mice to develop a systemic antitumor immune response and resistance to metastasis when re-challenged with pancreatic tumor cells (Kim et al., 2014). One of the limitations of implantable scaffolds is that they require surgery to be introduced to desired sites, but to address this, injectable formulations that form scaffolds *in situ* are being developed. Injectable mesoporous silica rods were able to spontaneously form scaffolds, recruit APCs and subsequently elicit specific T-cell responses (Kim et al., 2014).

To deliver the CAR genes, synthetic carriers have also been developed (**Table 3**) with the aim of reducing viral-induced reactions, while increasing delivery loads and ease of manufacture (Zhou et al., 2017). Synthetic carriers may need to be modified with targeting antibodies, peptides or recombinant molecules that augment their transfection specificity in hard-to-transfect cells growing in suspension (Liu et al., 2018). So far, lipid (Moon et al., 2011) and polymeric (Smith et al., 2017b; Olden et al., 2018) delivery systems have been used for generating CAR T-cells with targeting capacity inducing tumor regression in a mouse model (Smith et al., 2017b). To our knowledge

only two groups have reported *in vivo* generation of CAR T-cells, the Buchholz group at the Paul-Ehrlich-Institut and the Stephan group at the Fred Hutchinson Cancer Research Center. The Buchholz group reported a lentiviral approach targeting CD8 receptors and the Stephan group utilized poly(β-amino ester) NPs, both successfully generating CD19-CAR T cells *in vivo* (Smith et al., 2017b; Pfeiffer et al., 2018). Comparing the two approaches, the lentiviral approach allowed for greater percentage of CAR T-cell generation of up to 35% in blood and the synthetic NPs reported up to ∼20% transfection. In addition, both studies compared their *in vivo* targeting systems to infusions with conventionally generated CAR T-cells *ex-vivo* and did not find significant differences between the two treatments. This opens up a new avenue to increase the efficiency of CAR T-cell engineering and avoid the cumbersome *ex vivo* expansion and reprogramming steps. It is to be noted, however, that even though both approaches established significant advances in the efficiency of CAR T-cell generation, they still encountered some of the main challenges of the therapy including B-cell depletion and signs of cytokine release syndrome with the use of lentivirus. B-cell depletion arises since CD-19 is not only present in leukemic cells but also in non-leukemic B-cells, highlighting the hurdle of finding the right antigen to target.

As more advances are reported for CAR T-cell technologies, some common challenges have emerged. The treatment of solid tumors is one such major challenge, as the tumor microenvironment is highly immunosuppressive due to combination of down-regulated tumor antigens and T-cell suppression (Joyce and Fearon, 2015; Cheung et al., 2018). However, the *in situ* scaffold approaches aim to reverse the immunosuppressive environment by sustained release of cytokines for recruitment of immune cells at tumor sites. Once the cells are transferred to patients, T-cells act autonomously and so far it is very difficult to control their actions and unwanted side effects *in-situ* [e.g., cytokine release syndrome, neurotoxicity or B-cell aplasia (Yant et al., 2000)], so that feedback systems are needed to better control the therapy (Lim and June, 2017). As CAR T-cell technologies continue to progress, an inter-disciplinary effort must be made to address some of the pressing challenges that include their mode of delivery and expansion, migration, and mechanism of action so as to exert their action on tumor cells while sparing the normal cells.

BIOMATERIALS AND EMERGING NUCLEIC ACID TECHNOLOGIES

Biomaterials have been an integral part of emerging cell and gene based technologies over the years. Early work on skin substitutes, for example, laid the foundation for the tissue engineering field by relying on biomaterials to create the right milieu to allow tissue-like organization of seeded (*ex vivo*) or invading (*in vivo*) cells (Bell et al., 1979; Yannas, 1992), while separate efforts were being undertaken to devise ingenious ways to transfer foreign genes into tissues by using projectiles to penetrate the skin (Williams et al., 1991). The amalgamation of separate approaches allowed biomaterials to support tissue organization *ex vivo* and to implement new gene transfer techniques, resulting in *ex vivo* construction of devices from gene-modified cells for transplantation (Tai and Sun, 1993). From these beginnings, biomaterials have evolved to now enable several key technologies at the center of nucleic acid-based therapies. Below we summarize the impact of biomaterials in key areas important for the future of nucleic acid therapeutics.

More Intelligent NPs (Figure 2)

Increasing complexity (i.e., functionalization) in nucleic acid bearing NPs will be the way forward to realize more effective therapeutic outcomes from nucleic acids. Despite emergence of a wide range of synthetic, "intelligent" materials for NP fabrication in the last decade, there is still a need to create new functional NPs for hard-to-transfect cell types. Using commercial and in-house developed non-viral reagents, the authors frequently encounter cell types (e.g., leukemic stem cell lines and certain mesenchymal stem cells) that are exceptionally difficult to transfect. Patient-derived cells in particular have shown variable results in our hands for siRNA-mediated silencing of therapeutic targets, with significant fraction of cells either not responding or responding weakly to nucleic acid treatments (unpublished observations, and Gul-Uludag et al., 2014; Landry et al., 2016; Valencia-Serna et al., 2019). We recognize that increasing complexity in NP design, while improving performance, places extra burden on manufacturing processes, so that new design features amenable for scale-up will be especially critical for clinical translation.

Packaging nucleic acids with a combination of cationic and lipidic biomaterials have been recognized to improve delivery as compared to either moiety alone (Incani et al., 2010; Liu et al., 2010). Additional functionalization of NPs has been possible with antibodies (Kedmi et al., 2018) and other ligands (Guan et al., 2019) using lipidic anchors, and peptides/proteins by electrostatic anchors on self-assembled systems (Dong et al., 2018). Excessive cationic charge density, a recognized limitation of NPs, could be altered by incorporating anionic macromolecules into NPs. We incorporated anionic hyaluronic acid into NPs, either as a surface coating or additive into the core, that controlled the ζ-potential of NPs in a predictable way as well as increased the propensity of NPs for dissociation that was beneficial for both pDNA (Remant Bahadur et al., 2015) and siRNA delivery (Parmar et al., 2018). Another benefit was improved stability of NPs (Rose et al., 2013), with direct implications for *in vivo* administration. This benefit was not unique for multivalent polymeric carriers, but even liposomal systems such as the commercially available Fugene^{TM} which derived a beneficial effect from the additives in complexes (Nakamura et al., 2015); the additives in this case were hydrophilic/uncharged PEG and anionic tRNA that were widely different in molecular features, yet they were both able to enhance the transcriptional activity of a minimal PCR-amplified DNA expression cassette in the robust HEK293 cells (Nakamura et al., 2015). Different mechanisms might therefore be responsible (or effective) to weaken nucleic acid binding just enough to enhance the availability of nucleic acids intracellularly. Alternatively, the cationic charge density initially required for nucleic acid complexation could be removed by a controlled

TABLE 3 | Emergent biomaterial approaches for T-cell therapies.

Material	Approach	References
***ANTIGEN PRESENTING* PARTICLES FOR EXPANSION OF T-CELLS**		
Superparamagnetic beads (Dynabeads)	Conjugated to anti-CD3 and anti-CD28 to stimulate antigen specific T-cell expansion *ex-vivo*	Kalamasz et al., 2004
PLGA microparticles	Sustained IL-2 release to stimulate CD8+ T-cell expansion	Steenblock and Fahmy, 2008
Phosphatidylcholine liposome	Incorporated MHC II and highlighted how a synthetic system could mimic APC and T-cell interactions	Prakken et al., 2000
Iron dextran NPs	Utilized an external magnetic field to drive particle aggregation and enhance T-cell activation	Perica et al., 2014
PDMS microbeads	Soft elastomer formulation conjugated to anti-CD3 and anti-CD28	Lambert et al., 2017
Carbon nanotubes and PLGA composite	Composite system to cluster antigen presentation and release IL-2	Fadel et al., 2014
SCAFFOLDS FOR EXPANSION OF T-CELLS		
3D Polystyrene and Matrigel scaffolds	3D culture with polystyrene or Matrigel sustained superior proliferation of T-cells than suspension systems	Pérez Del Río et al., 2018
Fluid lipid bilayer on mesoporous silica rods	Combined fluidity of lipids on a solid platform that could present surface and soluble stimulus to T-cells	Cheung et al., 2018
3D printed polycaprolactone lattices	Printed scaffold with high reproducibility and scalability; superior than nanoparticle T-cell expansion	Delalat et al., 2017
Alginate scaffold modified with collagen-mimetic peptide	Introduced T-cells into mice tumor models using the alginate scaffold and prevented tumor relapse	Stephan et al., 2014
Polyisocyanopeptide hydrogel	Injectable thermo-responsive scaffolds that allowed *in-vivo* T-cell survival and migration	Weiden et al., 2018a
PEG-g-Chitosan Hydrogel (PCgel)	PCgel was compared to Matrigel and allowed for enhanced migration of T-cells targeting glioblastoma	Tsao et al., 2014
Alginate scaffold with collagen-mimetic peptide and adjuvant silica microparticles	Combined the release of T-cells with adjuvant compounds to elicit a local and systemic response	Smith et al., 2017a
Mesoporous silica rod assembled scaffold	Macroporous scaffold formed *in situ* recruited and modulated immune cells *in vivo*	Kim et al., 2014
BIOMATERIALS FOR GENETIC MODIFICATION OF T-CELLS		
Cationic pHEMA-g-pDMAEMA polymer	Highlighted different architectures of polymeric delivery systems achieving maximum transfection with comb and sunflower shaped polymers in primary T cells	Olden et al., 2018
Poly(B-amino) ester polymer	First time CAR T-cells developed *in vivo* by a nanoparticle system. Targeting ligands allowed for comparable survival improvement to conventional T-cell adoptive transfer.	Smith et al., 2017b

chemical cleavage (Jiang et al., 2019), while the NPs are retained in place by covalent linkages or possibly by other affinity interactions such as the hydrophobic domains. Improved toxicity was reported against a well-recognized liposomal formulation as a result of charge reduction, but systematic studies on the beneficial effect of reducing cationic charge density remains to be reported (Jiang et al., 2019).

Self-assembly has been favored in the hands of most researchers due to its convenience to create NPs at the time and site of application, in addition to the possibility of seamlessly incorporating additional functional molecules into the NPs. However, pre-manufactured NPs that bear nucleic acids may reduce variability associated with "on-the-spot" NP preparations and improve stability during the delivery. Nanogels, physically or chemically crosslinked polymeric networks with high water content, are emerging as leading candidates in this regard (Zilkowski et al., 2019). Nanogels with targeting ligands can entrap nucleic acids by electrostatic interactions or "irreversible" covalent linkages. Cargo can be loaded during synthesis or post-synthesis. Compared to conventional hydrolytically-degrading NPs, nanogels offer the possibility of more robust degradation under defined redox, pH and microenvironmental conditions, leaving behind a smaller footprint. To create a biomimetic means to shield the excess cationic charge of nanogels, they have been decorated with "recognizable" polysaccharide chains in a way replacing the synthetic PEG decoration. Polysaccharide chains can undergo degradation at sites of specific enzymatic activity (Nishimura et al., 2017), so that cellular uptake is facilitated at these sites, preventing non-specific interactions caused by the cationic charge in other (especially serum) sites. Recently, NPs prepared with adenosine-5′-triphosphate (ATP) responsive phenylboronic acid (PBA) bearing polymers (Naito et al., 2012) or ATP-responsive aptamers (Mo et al., 2015) are providing new ways of releasing the cargo intracellularly in response to high cellular ATP concentration that is typically absent in the extracellular space. The ATP-triggered release is reminiscent of the glutathione (GSH)-sensitive disulfide linkages, an earlier approach for intracellular cargo release

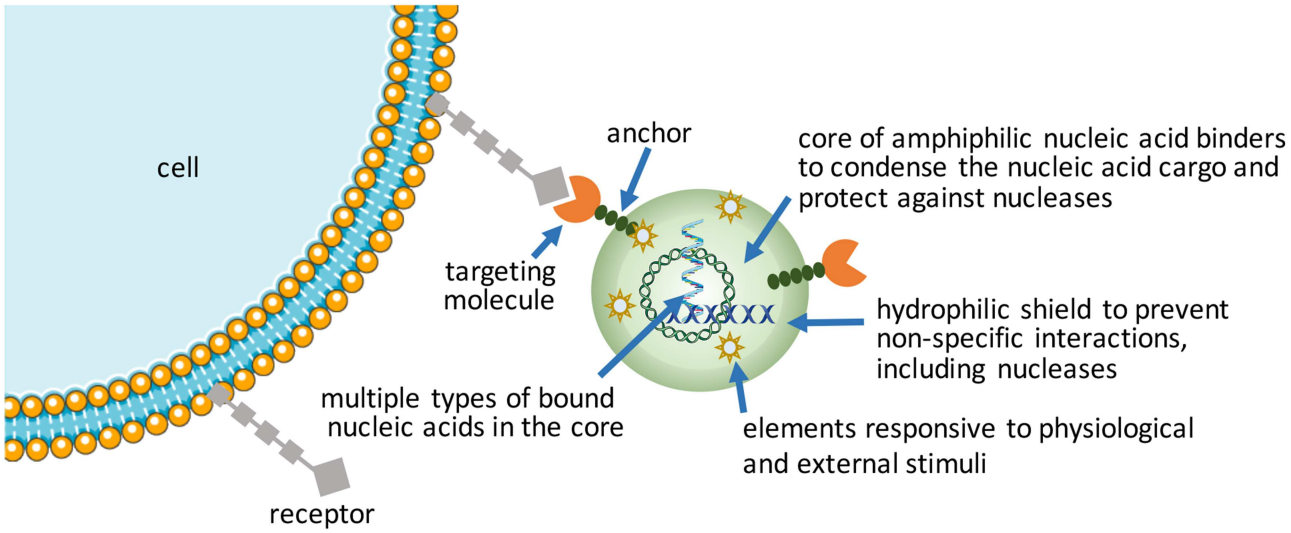

FIGURE 2 | Design of intelligent NPs for delivery of nucleic acids.

triggered by the severe GSH gradient between the intracellular and extracellular compartments. The latter approach seems simpler to implement but the relative efficiency of intracellular vs. extracellular cleavage rates under physiological conditions for the two approaches remains to be thoroughly compared. Both of these approaches rely on physiological stimuli to execute the cargo release. If one wishes to rely on an external trigger for cargo release, analogous to inducer-activated gene expression or silencing, Khan et al. have recently reported an externally activated approach to nucleic acid release (Khan et al., 2017), whereby the small molecule tetrazine was capable of breaking the trans-cyclooctene linkages holding onto siRNAs in a NP. The relative stability of the trans-cyclooctene linkage and its specificity to tetrazine cleavage was proposed as a superior 'on-demand' release of nucleic acids, where the proof-of-principle studies were reported in cell culture conditions.

Finally, another approach to intelligent NPs proposed by Mirkin group is to create spherical nucleic acids (SNAs) assembled on NP cores; they were shown to effectively penetrate the blood-brain-barrier as well as the blood-tumor-barrier and implement the RNAi silencing pathway (Cutler et al., 2012; Young et al., 2012; Jensen et al., 2013; Li et al., 2018). This seems to be possible with clustering of polynucleotides (which by themselves do not effectively cross cell membrane), perhaps due to an increased fluid phase uptake of the NP configuration and/or the lipophilic NP core.

mRNA Delivery to Replace pDNA Therapy

mRNA delivery has been pursued for some time now with successful mRNA transfer by lipidic carriers reported as early as 1989 (Malone et al., 1989). Recent efforts to modify the nucleic acid for improved stability, better translation and lower immunogenicity are opening up new possibilities for its broader deployment (Kormann et al., 2011). Given the wealth of already developed carriers for other types of nucleic acids, a critical issue is whether we need new carriers for mRNA delivery or are the previous carriers sufficient to deploy this particular nucleic acid. While debatable, new carriers that rely on charge alteration to reduce/eliminate the electrostatic binding to mRNA and making mRNA freely available to translation machinery have been reported (McKinlay et al., 2017). Even with these apparently effective carriers, the outcome from *in vivo* mRNA administration is short-lived, with expression levels returning to baseline levels within ~48 h time frame. Some studies indicate that carriers previously developed for other nucleic acids can be employed, and in head-to-head comparisons, optimized pDNA delivery could be even superior to mRNA delivery in some cases, for example with human bronchial epithelial cells and lung delivery *in vivo* (Guan et al., 2019). Other studies reported the opposite; when comparing mRNA vs. pDNA delivery, biomaterial scaffolds were reported to display superior mRNA-induced transgene expression for a longer duration *in vitro* (Elangovan et al., 2015; Balmayor et al., 2016). The nature of the delivered gene and its regulation, the nature of the carrier (i.e., its influence on intracellular pharmacokinetics of the cargo) as well as the specific cellular system (i.e., in particular endocytosis efficiency against different cargos and ability for nuclear import) could be the reason(s) for the observed differences. It is likely that minicircle pDNA (that bear no non-essential genetic elements) with improved design over the traditional pDNA could be superior over the mRNA based gene expression, while mRNA could be superior over the traditional pDNAs. On the other hand, optimization of terminal repeats and/or incorporated modified bases make significant differences in mRNA performance, so that the effectiveness of mRNA over conventional pDNAs may be variable in different systems and this may take some time to clarify. Our own experience indicates that relative performance of pDNA vs. mRNA is cell-line dependent, and that some cells display better transgene expression from mRNA polyplexes, while others provide more robust expression from pDNA

(unpublished). This observation possibly reflects the nuclear import capability of the cells, their proliferation rate and/or the capability of the carrier to deliver the pDNA to the nucleus.

Vaccination seems to be an especially appropriate area for mRNA administration where the adjuvant ability of mRNA may be additionally beneficial for a strong transient response. Implants where the biomaterials act as a local matrix (scaffold) to modulate the release of mRNA are an effective approach to vaccination (Chen et al., 2018), especially if prolonged local presence and/or controlled release is optimal. Scaffolds could be viewed as passive carriers of mRNA particles; transfection reagents are usually designed to transfect cells with no specific consideration to scaffolds (Steinle et al., 2018). The avidity (i.e., overall strength) between the nucleic acid and the complexing biomaterial has been shown to control mRNA release from NP formulations (Lallana et al., 2017) and it is likely that such a relationship will hold true for macroscopic scaffolds as well. In a presumably continuous scaffold, this will require control over the density of charges if no other "binders" are considered. The relatively weak immune-adjuvant features of mRNA could be further improved by employing double stranded mRNAs that are highly recognized by pattern recognition receptors (PRRs); in this case, an optimal length of double strands was needed to balance the immunostimulation with translational activity (Uchida et al., 2018). Alternatively, polymer-condensed mRNA could be entrapped in lipidic envelopes to enhance uptake and adjuvant activity (Persano et al., 2017).

Bone induction by mRNA translation is another indication where transient transgene expression might be sufficient for clinical success. Morphogens such as Bone Morphogenetic Proteins (BMPs) are known to "kick-start" the osteogenesis process beyond a critical concentration and their continued presence might not be required to sustain tissue induction and repair. The precise design of mRNA with particular chemical and end-group modifications are critical for effective translation, but several successful configurations have emerged for relatively long term protein production indicating some flexibility in the mRNA design. A longer sustained expression was noted when a BMP-2 morphogen was delivered with mRNA in scaffolds, presumably reflecting favorable pharmacokinetics and cell exposure (i.e., gradual vs. bolus) (Balmayor et al., 2017; Guan et al., 2019). Recent studies led by Balmayor et al. (2017), Badieyan et al. (2016) and Zhang et al. (2019) employed small animal models to assess the potential of mRNA-based bone repair, with so called "transcript activated matrices" (TAMs). A range of cells including easy-to-transfect cell lines and primary cells derived from adipose tissue and bone marrow were effectively induced for mRNA translation and significant secretion of therapeutic proteins (Badieyan et al., 2016; Balmayor et al., 2017; Zhang et al., 2019). It appears that robust effects were obtained even though the scaffolds were not optimized for bone repair (Elangovan et al., 2015). The elimination of the additional nuclear import barrier in primary cells, which is the limiting step for pDNA delivery, is an important advantage for deploying mRNA and makes this nucleic acid the preferred agent for delivery. Older studies, however, also showed some bone repair with pDNA based systems (so called "gene activated matrices," GAMs) in similar preclinical models (Ono et al., 2004; Huang et al., 2005; Zhang et al., 2009; Qiao et al., 2013). Limited regeneration was noted in early investigations with BMP-4 pDNA/PEI25 (25 kDa branched PEI) implants around defect edges (Huang et al., 2005) potentially due to toxicities of high pDNA/PEI25 dose (200 μg of pDNA and likely >200 μg of PEI25) (Plonka et al., 2017; Khorsand et al., 2019). Ono et al. employed a hydroxyapatite scaffold to deliver cationic liposome condensed pDNA in a rabbit cranial defect, where the BMP-2 pDNA induced new bone tissue had penetrated halfway into the defect after 9 weeks (Ono et al., 2004). Qiao *et al.* employed PLGA particles containing BMP-2 pDNA/PEI25 and gelatin sponges in a calvarial defect model; bone formation was stimulated by BMP-2 gene delivery at defect edges (Qiao et al., 2013). More recently, in a head-to-head comparison, a GAM with pDNA and a TAM with mRNA for BMP-9 expression were found to be equivalent for bone induction *in vivo* (Khorsand et al., 2019), again suggesting no clear impediment to pDNA based GAMs in tissue induction. While difficult to compare these independent studies, the authors believe that mRNA may provide more robust osteogenic transformation *in vivo* (given the lower dose of mRNA in implants vs. pDNA), leading to comparatively better results in certain animal models. Lower doses of nucleic acids/synthetic carriers may minimize adverse inflammatory/immune reactions that may impede new tissue induction. The delivery system used in mRNA delivery were not particularly tailored in these early studies (i.e., PEI and a cationic lipid), so that improved carriers are bound to further improve regeneration with reduced doses. Collectively, these studies indicate that a robust translation of mRNA for ∼10 days *in vitro* appears to be sufficient for effective tissue induction in small animal models. Investigations in larger animals, however, will be required to truly assess clinical potential. Considering that μg quantities of BMP proteins are needed for effective regeneration in small animals and that clinical therapy in the past relied on 10–20 mg of the protein *in situ*, it will be important to determine the functional mRNA doses in larger preclinical models to better assess its potential for clinical translation.

Long-Acting Gene Expression With Non-viral Systems

The emerging T-cell therapy has again shined a light on the need for long-term gene expression with non-viral approaches. Transposons have emerged as a viable alternative to integrating viruses to this end whose utility is now being tested in clinical studies (Kebriaei et al., 2016; Tipanee et al., 2017b). The SB system relies on integration-enabling transposases, which can be delivered in protein form, in an expression plasmid, including the minicircle approach (Holstein et al., 2018) or more recently with mRNA (Monjezi et al., 2017). The latter approach obviates the need for nuclear delivery and may be a superior alternative due to transient induction of a transposase that will limit long-term transposition and hence unpredictable events. The current process of transposon delivery operates with nucleofection, which is a special form of electroporation with "facilitating"

buffers. Although effective, nucleofection process is associated with loss of viability in a significant proportion of treated cells, so that it hampers *ex vivo* expansion efforts and prolongs attainment of critical mass of cells needed for transplantation. With an optimized combination of expression/integration system, 25–35% of cells were shown to retain the transgene expression in hard to transfect CD34+ hematopoietic stem and progenitor cells (HSPCs) (Holstein et al., 2018), based on the assessment of transgene expression in HSPC colonies or vector copy integrated/diploid genome. From a safety perspective, integration profiles of the transgene were favorable for the SB system over lentiviral vectors in human HSPCs, leading to random integration away from transcriptional regulatory elements of active genes and other "hotspots." However, with integrating vectors, a finite risk of long-term adverse effects is present and should be considered in the face of benefit to be derived (Moffett et al., 2018).

Implementing transposon-based long-term gene expression *in vivo* will be desirable but also particularly challenging. Toward this goal, a NP system was described that were deigned to transfect T-cells (functionalized with an anti-CD3e f(ab')2 fragment) in a murine model (Smith et al., 2017b); *in vitro* results indicated a relatively low level of transfection (∼4% of population), but this was sufficient for target cell killing and matched the performance of lentiviral-modified T-cells. The low levels of transfection will translate into benefit in terms of lower non-specific binding (and modification) of non-target cells. The extent of *in vivo* modification was similar with ∼5% of circulating T-cells displaying transgene expression after 6 days, but the cells expanded with increasing population of cells displaying CAR expression (∼20% after day 12), that was dependent on transposase delivery. In the absence of transposase delivery, no effective anti-tumor response was seen, clearly indicating the beneficial effect of vector integration. A similar delivery system was used for transiently transfecting T-cells with mRNA, whose biocompatibility was compared to electroporation modified cells (Weiden et al., 2018a); the modification with the non-viral system was implemented with lower adverse effects on cells, as evident in subsequent expansion rate *ex vivo*. It was interesting to note that this study also used a transiently expressed transcription factor Foxo1 (from mRNA whose expression lasted for ∼5 days) that favors the expansion of desirable population of T-cells, that may provide a superior alternative to transient delivery systems towards the ultimate goal of integrated (long-acting) vectors (Broderick and Humeau, 2017).

Expanding Genetically Modified Cells

Irrespective of the modification approach, CAR and other genetically modified cells may need to be expanded to provide them with a survival advantage when grafted into a host. This has been implemented in the past by using soluble cytokines, intracellular expressed factors (Weiden et al., 2018a) and immobilized ligands on tissue culture surfaces. The "Dynabead" system with immobilized CD3/CD28 antibodies on microparticles has been commercialized towards this end. Alternatively, one can employ biomaterials scaffold-conjugated ligands to enhance stimulation over that of soluble cytokines, and avoid additional manipulation of cells for transcription factor

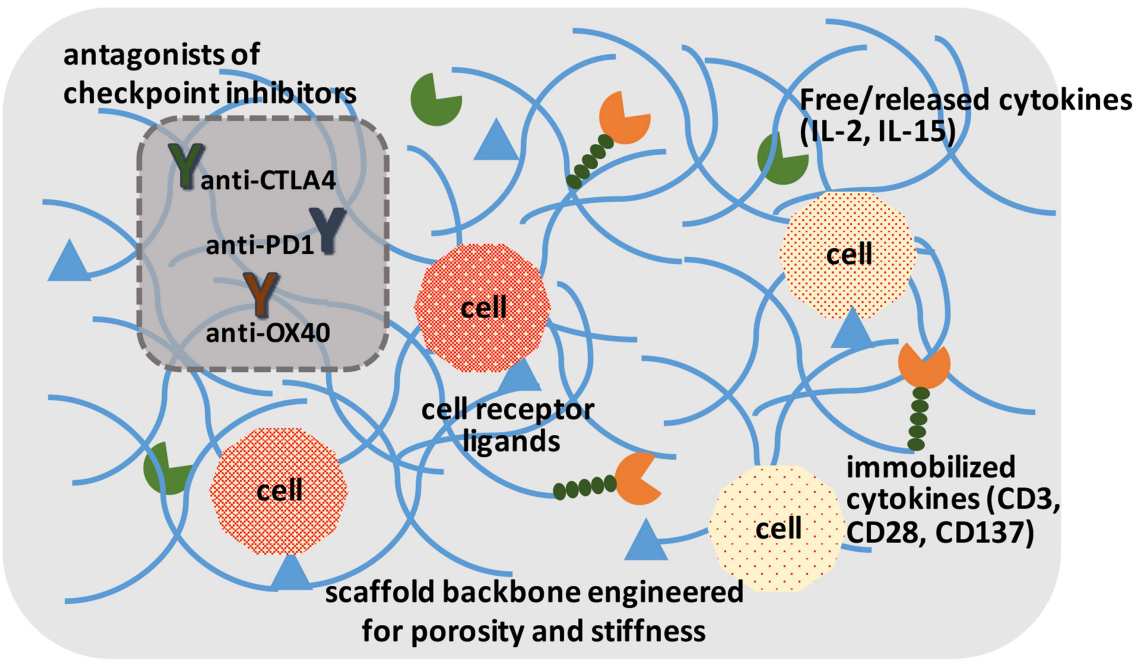

FIGURE 3 | A schematic of ideal scaffolds to expand and/or activate T-cells for disease management. A sophisticated scaffold could be designed to support cell survival and expansion based on cell-attachment ligands, free/released cytokines, and immobilized ligands to promote cell proliferation. The cells could be activated with local presentation of antagonists of checkpoint inhibitors. The scaffolds could serve for *ex vivo* expansion of T-cells, as well as *in vivo* activation of T-cells.

expression. Hydrogels derivatized with $\alpha_2\beta_1$ collagen receptor binding GFOGER peptide or multiple integrin-binding RGD motif have been described that support T-cell expansion *in vitro* and housing after grafting the cells *in vivo* (Cheung et al., 2018; Weiden et al., 2018b). The hydrogels could immobilize ligands or provide local release of cytokines important for cell expansion (**Figure 3**), which may be difficult to implement with systemically administered agents. Infiltrating cells can be stimulated and expanded within designer niches (Ren and Lim, 2018). Delivering anti-CTLA-4 and anti-OX40 mAbs has been described to stimulate tumor-infiltrating killer T-cells with scaffolds in the vicinity of resected tumors (Wang et al., 2016). It has been possible to create scaffolds from nucleic acids (DNA-based) to release immune stimulatory PD-1 blocking agents (Lynn et al., 2019). The importance of size, architecture and ligand density, among others, are beginning to be elucidated for *in vivo* expansion of T-cells (Liu et al., 2018), while a similar approach is implemented for *ex vivo* expansion. It has been recognized for some time that immobilized antibodies are more potent in stimulating T-cell expansion compared to soluble ligands, and a mechanosensor receptor (Piezo1) was recently identified as a mediator of TCR activation (Zhang et al., 2018). This provides a mechanistic link on how mechanical properties of a scaffold could affect T-cell stimulation and expansion directly, and may provide a more rational design of the biomaterials scaffold to optimize TCR activation and T-cell expansion.

Vaccination with pDNA is continuing to be explored with biomaterial-based delivery and adjuvant systems (Zhang et al., 2018), with muscle and skin sites (by electroporation) popularly used for *in situ* expression of tumor antigens from pDNA directly (Amante et al., 2015; Broderick and Humeau, 2017). Inhibition of immune checkpoints CTLA-4 and PD-1 is making inroads to enhance the anti-tumor response with *in situ* expressed tumor antigens (Lopes et al., 2018). Simple injection of pDNA without the use of electroporation has been made effective with the use of a combination of cationic lipid formulations, where the 2-dis-tearoyl-sn-glycero-3-phosphoethanolamine-N-[methoxy(PEG-2000)] was critical in supporting expression of antigens and long-term antibody response (Ho et al., 2018). Hydrolytically-cleaving polyesters have also been shown to successfully elicit effective antibody response against pDNA-coded antigens, with a lipid-modifed PEI (PEI1.8-deoxycholic acid) facilitating local transfection and antigen expression (Giang Phan et al., 2019).

CONCLUDING REMARKS ON FUTURE NUCLEIC ACID THERAPIES

Synthetic, precisely engineered biomaterials and self-assembled systems from such biomaterials are leading the way to enable a diverse array of therapeutic modalities that rely on nucleic acids. The prospect of improved clinical safety of the biomaterial-based delivery is driving this endeavor and significant efforts are in place now to enhance the effectiveness of the delivery, while allowing a high degree of modification of "hard-to-transfect" cells and realizing permanent modification (whether it may be transgene expression or silencing). Nucleic acids themselves derived from DNA and RNA molecules have the potential to replace synthetic biomaterials and act as carriers for nucleic acid agents (Hu et al., 2018). It has been possible to create responsive systems to release different effector molecules from a scaffold of nucleic acids with precise controlled features. One can envision delivering CpG oligodeoxynucleotides, that bind TLR9, from DNA scaffolds effortlessly to stimulate dendritic cells against tumors (Bourquin et al., 2008). The possibilities are diverse, but whether they can be produced in economical terms, their *in vivo* stability be controlled and adverse reactions *in situ* be minimized remains to be seen for such nucleic acid scaffolds. While delivery with biomaterials for therapeutic purposes has been the main focus, one can envision relying on nucleic acids for "preventative" medicine as well; with the identification of aberrant genes and/or miRs before manifestation of clinical symptoms, one has the opportunity to employ nucleic acids before disease development. One can envision deleting "aberrant" cells or restoring normal physiology ahead of detectable symptoms. Perhaps our next generation of "vitamins" will be based on nucleic acids as preventative remedies; nevertheless, the functional use of nucleic acids will rely on designer biomaterials and nano-engineered systems in order to present the nucleic acids to the appropriate cells in the appropriate manner.

AUTHOR CONTRIBUTIONS

All authors contributed to the conceptualization, literature search/review, and writing of the article. Final editing was undertaken by HU.

FUNDING

The gene therapy and nucleic acid studies in the authors lab have been supported by operating grants from Canadian Institutes of Health Research (CIHR), Canadian Breast Cancer Foundation (CBCF), Natural Sciences and Engineering Council of Canada (NSERC), Women and Children Health Research Institute (University of Alberta), Alberta Innovates (AI), and the University of Alberta Office of Research. Past infrastructure support was provided by AI, Edmonton Civic Employees and Canadian Foundation for Innovation (CFI). We thank numerous current and past trainees, and collaborators for contributing to the evolution of our ideas on this review topic.

REFERENCES

Aartsma-Rus, A., Straub, V., Hemmings, R., Haas, M., Schlosser-Weber, G., Stoyanova-Beninska, V., et al. (2017). Development of exon skipping therapies for Duchenne Muscular Dystrophy: a critical review and a perspective on the outstanding issues. *Nucleic Acid Ther.* 27, 251–259. doi: 10.1089/nat.2017.0682

Abdelmohsen, K., Panda, A. C., Munk, R., Grammatikakis, I., Dudekula, D. B., De, S., et al. (2017). Identification of HuR target circular RNAs uncovers

suppression of PABPN1 translation by CircPABPN1. *RNA Biol*. 14, 361–369. doi: 10.1080/15476286.2017.1279788

Abera, G., Berhanu, G., and Tekewe, A. (2012). Ribozymes: nucleic acid enzymes with potential pharmaceutical applications: a review. *Pharmacophore* 3, 164–178.

Amante, D. H., Smith, T. R., Mendoza, J. M., Schultheis, K., McCoy, J. R., Khan, A. S., et al. (2015). Skin transfection patterns and expression kinetics of electroporation-enhanced plasmid delivery using the CELLECTRA-3P, a portable next-generation dermal electroporation device. *Hum. Gene Ther. Methods* 26, 134–146. doi: 10.1089/hgtb.2015.020

American Association for Cancer Research (2017). Engineering CAR T cells with biomaterials. *Cancer Discov.* 7, 656–657. doi: 10.1158/2159-8290.CD-NB2017-068

Ansari, A. S., Santerre, P. J., and Uludag, H. (2017). Biomaterials for polynucleotide delivery to anchorage-independent cells. *J. Mater. Chem. B* 5, 7238–7261. doi: 10.1039/C7TB01833A

Ashwal-Fluss, R., Meyer, M., Pamudurti, N. R., Ivanov, A., Bartok, O., Hanan, M., et al. (2014). circRNA biogenesis competes with pre-mRNA splicing. *Mol. Cell* 56, 55–66. doi: 10.1016/j.molcel.2014.08.019

Ausländer, D., Wieland, M., Ausländer, S., Tigges, M., and Fussenegger, M. (2011). Rational design of a small molecule-responsive intramer controlling transgene expression in mammalian cells. *Nucleic Acids Res*. 39:e155. doi: 10.1093/nar/gkr829

Badieyan, Z. S., Berezhanskyy, T., Utzinger, M., Aneja, M. K., Emrich, D., Erben, R., et al. (2016). Transcript-activated collagen matrix as sustained mRNA delivery system for bone regeneration. *J. Control. Rel*. 239, 137–148. doi: 10.1016/j.jconrel.2016.08.037

Balmayor, E. R., Geiger, J. P., Aneja, M. K., Berezhanskyy, T., Utzinger, M., Mykhaylyk, O., et al. (2016). Chemically modified RNA induces osteogenesis of stem cells and human tissue explants as well as accelerates bone healing in rats. *Biomaterials* 87, 131–146. doi: 10.1016/j.biomaterials.2016.02.018

Balmayor, E. R., Geiger, J. P., Koch, C., Aneja, M. K., van Griensven, M., Rudolph, C., et al. (2017). Modified mRNA for BMP-2 in combination with biomaterials serves as a transcript-activated matrix for effectively inducing osteogenic pathways in stem cells. *Stem Cells Dev*. 26, 25–34. doi: 10.1089/scd.2016.0171

Beisel, C. L., Chen, Y. Y., Culler, S. J., Hoff, K. G., and Smolke, C. D. (2011). Design of small molecule-responsive microRNAs based on structural requirements for Drosha processing. *Nucleic Acids Res*. 39, 2981–2994. doi: 10.1093/nar/gkq954

Bell, E., Ivarsson, B., and Merrill, C. (1979). Production of a tissue-like structure by contraction of collagen lattices by human fibroblasts of different proliferative potential *in vitro*. *Proc. Natl. Acad. Sci. U.S.A*. 76, 1274–1278. doi: 10.1073/pnas.76.3.1274

Blind, M., Kolanus, W., and Famulok, M. (1999). Cytoplasmic RNA modulators of an inside-out signal-transduction cascade. *Proc. Natl. Acad. Sci. U.S.A*. 96, 3606–3610. doi: 10.1073/pnas.96.7.3606

Boehme, P., Zhang, W., Solanki, M., Ehrke-Schulz, E., and Ehrhardt, A. (2016). A high-capacity adenoviral hybrid vector system utilizing the hyperactive sleeping beauty transposase SB100X for enhanced integration. *Mol. Ther. Nucleic Acids* 5:e337. doi: 10.1038/mtna.2016.44

Bourquin, C., Anz, D., Zwiorek, K., Lanz, A. L., Fuchs, S., Weigel, S., et al. (2008). Targeting CpG oligonucleotides to the lymph node by nanoparticles elicits efficient antitumoral immunity. *J Immunol*. 181, 2990–2998. doi: 10.4049/jimmunol.181.5.2990

Broderick, K. E., and Humeau, L. M. (2017). Enhanced delivery of DNA or RNA vaccines by electroporation. *Methods Mol. Biol*. 1499, 193–200. doi: 10.1007/978-1-4939-6481-9_12

Byun, J., Lan, N., Long, M., and Sullenger, B. A. (2003). Efficient and specific repair of sickle beta-globin RNA by trans-splicing ribozymes. *RNA* 9, 1254–1263. doi: 10.1261/rna.5450203

Cagnon, L., Cucchiarini, M., Lefebvre, J. C., and Doglio, A. (1995). Protection of a T-cell line from human immunodeficiency virus replication by the stable expression of a short antisense RNA sequence carried by a shuttle RNA molecule. *J. Acquir. Immune Defic. Syndr. Hum. Retrovirol*. 9, 349–358. doi: 10.1097/00042560-199508000-00004

Carter, J. R., Keith, J. H., Fraser, T. S., Dawson, J. L., Kucharski, C. A., Horne, K. M., et al. (2014). Effective suppression of dengue virus using a novel group-I intron that induces apoptotic cell death upon infection through conditional expression of the Bax C-terminal domain. *Virol. J*. 11:111. doi: 10.1186/1743-422X-11-111

Chaloin, L., Lehmann, M. J., Sczakiel, G., and Restle, T. (2002). Endogenous expression of a high-affinity pseudoknot RNA aptamer suppresses replication of HIV-1. *Nucleic Acids Res*. 30, 4001–4008. doi: 10.1093/nar/gkf522

Chen, J., Li, Y., Zheng, Q., Bao, C., He, J., Chen, B., et al. (2017). Circular RNA profile identifies circPVT1 as a proliferative factor and prognostic marker in gastric cancer. *Cancer Lett*. 388, 208–219. doi: 10.1016/j.canlet.2016.12.006

Chen, R., Zhang, H., Yan, J., and Bryers, J. D. (2018). Scaffold-mediated delivery for non-viral mRNA vaccines. *Gene Ther*. 25, 556–567. doi: 10.1038/s41434-018-0040-9

Cheung, A. S., Zhang, D., Koshy, S. T., and Mooney, D. J. (2018). Scaffolds that mimic antigen-presenting cells enable *ex vivo* expansion of primary T cells. *Nat. Biotech.* 36, 160–169. doi: 10.1038/nbt.4047

Choi, K. H., Park, M. W., Lee, S. Y., Jeon, M. Y., Kim, M. Y., Lee, H. K., et al. (2006). Intracellular expression of the T-cell factor-1 RNA aptamer as an intramer. *Mol. Cancer Ther*. 5, 2428–2434. doi: 10.1158/1535-7163.MCT-05-0204

Cirak, S., Arechavala-Gomeza, V., Guglieri, M., Feng, L., Torelli, S., Anthony, K., et al. (2011). Exon skipping and dystrophin restoration in patients with Duchenne muscular dystrophy after systemic phosphorodiamidate morpholino oligomer treatment: an open-label, phase 2, dose-escalation study. *Lancet* 378, 595–605. doi: 10.1016/S0140-6736(11)60756-3

Cutler, I. J., Auyeung, E., and Mirkin, C. A. (2012). Spherical nucleic acids. *J. Am. Chem. Soc*. 134, 1376–1391. doi: 10.1021/ja209351u

Delalat, B., Harding, F., Gundsambuu, B., De-Juan-Pardo, E. M., Wunner, F. M., Wille, M., et al. (2017). 3D printed lattices as an activation and expansion platform for T-cell therapy. *Biomaterials* 140, 58–68. doi: 10.1016/j.biomaterials.2017.05.009

Dhanoya, A., Chain, B. M., and Keshavarz-Moore, E. (2011). The impact of DNA topology on polyplex uptake and transfection efficiency in mammalian cells. *J. Biotechnol*. 155, 377–386. doi: 10.1016/j.jbiotec.2011.07.023

Di Stasi, A., Tey, S. K., Dotti, G., Fujita, Y., Kennedy-Nasser, A., Martinez, C., et al. (2011). Inducible apoptosis as a safety switch for adoptive cell therapy. *N. Enn. J. Med.* 365, 1673–1683. doi: 10.1056/NEJMoa1106152

Dong, Y., Yu, T., Ding, L., Laurin,i, E., and Huang, Y., Zhang, M., et al. (2018). A dual targeting dendrimer-mediated siRNA delivery system for effective gene silencing in cancer therapy. *J. Am. Chem. Soc*. 140, 16264–16274. doi: 10.1021/jacs.8b10021

Doudna, J. A., and Charpentier, E. (2014). Genome editing. The new frontier of genome engineering with CRISPR-Cas9. *Science* 346:1258096. doi: 10.1126/science.1258096

Du, W. W., Fang, L., Yang, W., Wu, N., Awan, F. M., Yang, Z., et al. (2017). Induction of tumor apoptosis through a circular RNA enhancing Foxo3 activity. *Cell Death Differ*. 24, 357–370. doi: 10.1038/cdd.2016.133

Elangovan, S., Khorsand, B., Do, A. V., Hong, L., Dewerth, A., Kormann, M., et al. (2015). Chemically modified RNA activated matrices enhance bone regeneration. *J. Control. Rel*. 218, 22–28. doi: 10.1016/j.jconrel.2015.09.050

Engel, P., Zhou, L. J., Ord, D. C., Sato, S., Koller, B., and Tedder, T. F. (1995). Abnormal B lymphocyte development, activation, and differentiation in mice that lack or overexpress the CD19 signal transduction molecule. *Immunity* 3, 39–50. doi: 10.1016/1074-7613(95)90157-4

Fadel, T. R., Sharp, F. A., Vudattu, N., Ragheb, R., Garyu, J., Kim, D., et al. (2014). A carbon nanotube–polymer composite for T-cell therapy. *Nat. Nanotech.* 9, 639–647. doi: 10.1038/nnano.2014.154

Famulok, M., Hartig, J. S., and Mayer, G. (2007). Functional aptamers and aptazymes in biotechnology, diagnostics, and therapy. *Chem. Rev*. 107, 3715–3743. doi: 10.1021/cr0306743

Fraietta, J. A., Lacey, S. F., Orlando, E. J., Pruteanu-Malinici, I., Gohil, M., Lundh, S., et al. (2018). Determinants of response and resistance to CD19 chimeric antigen receptor (CAR) T cell therapy of chronic lymphocytic leukemia. *Nat. Med*. 24, 563–571. doi: 10.1038/s41591-018-0010-1

Gaj, T., Gersbach, C. A., and Barbas, C. F. (2013). ZFN, TALEN, and CRISPR/Cas-based methods for genome engineering. *Trends Biotech*. 31, 397–405. doi: 10.1016/j.tibtech.2013.04.004

Giang Phan, V. H., Duong, H. T. T., Thambi, T., Nguyen, T. L., Turabee, M. H., Yin, Y., et al. (2019). Modularly engineered injectable hybrid hydrogels based on protein-polymer network as potent immunologic adjuvant *in vivo*. *Biomaterials* 195, 100–110. doi: 10.1016/j.biomaterials.2018.12.034

Goemans, N. M., Tulinius, M., van den Hauwe, M., Kroksmark, A. K., Buyse, G., Wilson, R. J., et al. (2016). Long-term efficacy, safety, and pharmacokinetics

of drisapersen in duchenne muscular dystrophy: results from an open-label extension study. *PLoS ONE* 11:e0161955. doi: 10.1371/journal.pone.0161955

Good, P. D., Krikos, A. J., Li, S. X., Bertrand, E., Lee, N. S., Giver, L., et al. (1997). Expression of small, therapeutic RNAs in human cell nuclei. *Gene Ther*. 4, 45–54. doi: 10.1038/sj.gt.3300354

Gräslund, S., Nordlund, P., Weigelt, J., Hallberg, B. M., Bray, J., Gileadi, O., et al. (2008). Protein production and purification. *Nat. Methods* 5, 135–146. doi: 10.1038/nmeth.f.202

Grimm, C., Lund, E., and Dahlberg, J. E. (1997). Selection and nuclear immobilization of exportable RNAs. *Proc. Natl. Acad. Sci. U.S.A.* 94, 10122–10127. doi: 10.1073/pnas.94.19.10122

Guan, S., Munder, A., Hedtfeld, S., Braubach, P., Glage, S., Zhang, L., et al. (2019). Self-assembled peptide-poloxamine nanoparticles enable *in vitro* and *in vivo* genome restoration for cystic fibrosis. *J. Nat. Nanotechnol*. 14, 287–297. doi: 10.1038/s41565-018-0358-x

Gul-Uludag, H., Valencia-Serna, J., Kucharski, C., Marquez-Curtis, L. A., Jiang, X., Larratt, L., et al. (2014). Nanoparticle-mediated silencing of CD44 receptor in CD34+ acute myeloid leukemia blasts. *Leukemia Res.* 38, 1299–1308. doi: 10.1016/j.leukres.2014.08.008

Hacein-Bey-Abina, S., Garrigue, A., Wang, G. P., Soulier, J., Lim, A., Morillon, E., et al. (2008). Insertional oncogenesis in 4 patients after retrovirus-mediated gene therapy of SCID-X1. *J. Clin. Invest.* 118, 3132–3142. doi: 10.1172/JCI35700

Hamm, J., and Fornerod, M. (2000). Anti-idiotype RNAs that mimic the leucine-rich nuclear export signal and specifically bind to CRM1/exportin1. *Chem. Biol.* 7, 345–354. doi: 10.1016/S1074-5521(00)00112-5

Hardee, C. L., Arévalo-Soliz, L. M., Hornstein, B. D., and Zechiedrich, L. (2017). Advances in non-viral DNA vectors for gene therapy. *Genes* 8:65. doi: 10.3390/genes8020065

Hicklin, D. J., Marincola, F. M., and Ferrone, S. (1999). HLA class I antigen down regulation in human cancers: T-cell immunotherapy revives an old story. *Mol. Med. Today* 5,178–186. doi: 10.1016/S1357-4310(99)01451-3

Ho, J. K., White, P. J., and Pouton, C. W. (2018). Self-crosslinking lipopeptide/DNA/PEGylated particles: a new platform for DNA vaccination designed for assembly in aqueous solution. *Mol. Ther. Nucleic Acids* 12, 504–517. doi: 10.1016/j.omtn.2018.05.025

Hollyman, D., Stefanski, J., Przybylowski, M., Bartido, S., Borquez-Ojeda, O., Taylor, C., et al. (2009). Manufacturing validation of biologically functional T cells targeted to CD19 antigen for autologous adoptive cell therapy. *J. Immunother.* 32,169–180. doi: 10.1097/CJI.0b013e318194a6e8

Holstein, M., Mesa-Nuñez, C., Miskey, C., Almarza, E., Poletti, V., Schmeer, M., et al. (2018). Efficient non-viral gene delivery into human hematopoietic stem cells by minicircle sleeping beauty transposon vectors. *Mol. Ther*. 26, 1137–1153. doi: 10.1016/j.ymthe.2018.01.012

Hsiao, K. Y., Lin, Y. C., Gupta, S. K., Chang, N., Yen, L., Sun, H. S., et al. (2017). Noncoding effects of circular RNA CCDC66 promote colon cancer growth and metastasis. *Cancer Res*. 77, 2339–2350. doi: 10.1158/0008-5472.CAN-16-1883

Hsu, C. Y., and Uludag, H. (2008). Effects of size and topology of DNA molecules on intracellular delivery with non-viral gene carriers. *BMC Biotechnol*. 8:23. doi: 10.1186/1472-6750-8-23

Hu, Q., Wang, S., Wang, L., Gu, H., and Fan, C. (2018). DNA nanostructure-based systems for intelligent delivery of therapeutic oligonucleotides. *Adv. Healthcare Mater*. 7:1701153. doi: 10.1002/adhm.201701153

Hu, W., and Pathak, V. K. (2000). Design of retroviral vectors and helper cells for gene therapy. *Pharmacol. Rev.* 52, 493–512.

Huang, Y. C., Simmons, C., Kaigler, D., Rice, H. G., and Mooney, D. J. (2005). Bone regeneration in a rat cranial defect with delivery of PEI-condensed plasmid DNA encoding for bone morphogenetic protein-4 (BMP-4). *Gene Ther*. 12, 418–426. doi: 10.1038/sj.gt.3302439

Incani, V., Lavasanifar, A., and Uludag, H. (2010). Hydrophobic modification of cationic polymers on route to superior gene carriers. *Soft Matter* 6, 2124–2138. doi: 10.1039/b916362j

Ivics, Z., Li, M. A., Mátés, L., Boeke, J. D., Nagy, A., Bradley, A., et al. (2009). Transposon-mediated genome manipulation in vertebrates. *Nat. Methods* 6, 415–422. doi: 10.1038/nmeth.1332

Jensen, S. A., Day, E. S., Ko, C. H., Hurley, L. A., Luciano, J. P., Kouri, F. M., et al. (2013). Spherical nucleic acid nanoparticle conjugates as an RNAi-based therapy for glioblastoma. *Sci. Transl. Med.* 5:209ra152. doi: 10.1126/scitranslmed.3006839

Jiang, Z., Cui, W., Prasad, P., Touve, M. A., Gianneschi, N. C., Mager, J., et al. (2019). Bait-and-switch supramolecular strategy to generate noncationic RNA–polymer complexes for RNA delivery. *Biomacromol*. 20, 435–442. doi: 10.1021/acs.biomac.8b01321

Jorgensen, J. L., Reay, P. A., Ehrich, E. W., and Davis, M. M. (1992). Molecular components of T-cell recognition. *Annu. Rev. Immunol*. 10, 835–873. doi: 10.1146/annurev.iy.10.040192.004155

Joshi, P., and Prasad, V. R. (2002). Potent inhibition of human immunodeficiency virus type I replication by template analog reverse transcriptase inhibitors derived by SELEX (systematic evolution of ligands by exponential enrichment). *J. Virol*. 76, 6545–6557. doi: 10.1128/JVI.76.13.6545-6557.2002

Joyce, J. A., and Fearon, D. T. (2015). T cell exclusion, immune privilege, and the tumor microenvironment. *Science* 348, 74–80. doi: 10.1126/science.aaa6204

Jung, I. Y., and Lee, J. (2018). Unleashing the therapeutic potential of CAR-T cell therapy using gene-editing technologies. *Mol. Cells* 41, 717–723. doi: 10.14348/molcells.2018.0242

Kalamasz, D., Long, S. A., Taniguchi, R., Buckner, J. H., Berenson, R. J., and Bonyhadi, M. (2004). Optimization of human T-cell expansion *ex vivo* using magnetic beads conjugated with anti-CD3 and Anti-CD28 antibodies. *J. Immunother*. 27, 405–418. doi: 10.1097/00002371-200409000-00010

Katz, B. Z., and Herishanu, Y. (2014). Therapeutic targeting of CD19 in hematological malignancies: past, present, future and beyond. *Leuk. Lymph*. 55, 999–1006. doi: 10.3109/10428194.2013.828354

KC, R. B., Thapa, B., Valencia-Serna, J., Aliabadi, H. M., and Uludag, H. (2017). Nucleic acid combinations: a new frontier for cancer treatment. *J. Control. Release* 256, 153–169. doi: 10.1016/j.jconrel.2017.04.029

Kebriaei, P., Izsvák, Z., Narayanavari, S. A., Singh, H., and Ivics, Z. (2017). Gene therapy with the sleeping beauty transposon system. *Trends Genet.* 33, 852–870. doi: 10.1016/j.tig.2017.08.008

Kebriaei, P., Singh, H., Huls, M. H., Figliola, M. J., Bassett, R., Olivares, S., et al. (2016). Phase I trials using sleeping beauty to generate CD19-specific CAR T cells. *J. Clin. Invest*. 126, 3363–3376. doi: 10.1172/JCI86721

Kedmi, R., Veiga, N., Ramishetti, S., Goldsmith, M., Rosenblum, D., Dammes, N., et al. (2018). A modular platform for targeted RNAi therapeutics. *Nat. Nanotechnol*. 13, 214–219. doi: 10.1038/s41565-017-0043-5

Khan, I., Seebald, L. M., Robertson, N. M., Yigit, M. V., and Royzen, M. (2017). Controlled in-cell activation of RNA therapeutics using bond-cleaving bio-orthogonal chemistry. *Chem Sci*. 8, 5705–5712. doi: 10.1039/C7SC01380A

Khong, H. T., and Restifo, N. P. (2002). Natural selection of tumor variants in the generation of "tumor escape" phenotypes. *Nat. Immunol*. 3, 999–1005. doi: 10.1038/ni1102-999

Khorsand, B., Elangovan, S., Hong, L., Kormann, M. S. D., and Salem, A. K. (2019). A bioactive collagen membrane that enhances bone regeneration. *J. Biomed. Mat. Res. Appl. Biomater*. doi: 10.1002/jbm.b.34275 [Epub ahead of print].

Kim, J., Li, W. A., Choi, Y., Lewin, S. A., Verbeke, C. S., Dranoff, G., et al. (2014). Injectable, spontaneously assembling, inorganic scaffolds modulate immune cells *in vivo* and increase vaccine efficacy. *Nat. Biotech* 33, 64–72. doi: 10.1038/nbt.3071

Kim, S. J., Kim, J. H., Yang, B., Jeong, J. S., and Lee, S. W. (2017). Specific and efficient regression of cancers harboring KRAS mutation by targeted RNA replacement. *Mol. Ther*. 25, 356–367. doi: 10.1016/j.ymthe.2016.11.005

Kole, R., and Sazani, P. (2001). Antisense effects in the cell nucleus: Modification of splicing. *Curr. Opin. Mol. Ther*. 3, 229–234.

Kormann, M. S., Hasenpusch, G., Aneja, M. K., Nica, G., Flemmer, A. W., Herber-Jonat, S., et al. (2011). Expression of therapeutic proteins after delivery of chemically modified mRNA in mice. *Nat. Biotechnol*. 29, 154–157. doi: 10.1038/nbt.1733

Lallana, E., Rios de la Rosa, J. M., Tirella, A., Pelliccia, M., Gennari, A., Stratford, I. J., et al. (2017). Chitosan/hyaluronic acid nanoparticles: rational design revisited for RNA delivery. *Mol. Pharm*. 14, 2422–2436. doi: 10.1021/acs.molpharmaceut.7b00320

Lambert, L. H., Goebrecht, G. K., De Leo, S. E., O'Connor, R. S., Nunez-Cruz, S., Li, T. D., et al. (2017). Improving T cell expansion with a soft touch. *Nano Lett.* 17, 821–826. doi: 10.1021/acs.nanolett.6b04071

Landry, B., Gül-Uludag, H., Plianwong, S., Kucharski, C., Zak, Z., Parmar, M. B., et al. (2016). Targeting CXCR4/SDF-1 axis by lipopolymer complexes of siRNA in acute myeloid leukemia. *J. Control. Rel.* 224, 8–21. doi: 10.1016/j.jconrel.2015.12.052

Lee, C. H., Han, S. R., and Lee, S. W. (2018). Therapeutic applications of group I intron-based trans-splicing ribozymes. *Wiley Interdiscip. Rev. RNA* 9:e1466. doi: 10.1002/wrna.1466

Lee, H., Lytton-Jean, A. K., Chen, Y., Love, K. T., Park, A. I., Karagiannis, E. D., et al. (2012). Molecularly self-assembled nucleic acid nanoparticles for targeted *in vivo* siRNA delivery. *Nat. Nanotechnol.* 7, 389–393. doi: 10.1038/nnano.2012.73

Legnini, I., Di Timoteo, G., Rossi, F., Morlando, M., Briganti, F., Sthandier, O., et al. (2017). Circ-ZNF609 is a circular RNA that can be translated and functions in myogenesis. *Mol. Cell* 66, 22–37. doi: 10.1016/j.molcel.2017.02.017

Levacic, A. K., Morys, S., Kempter, S., Lächelt, U., and Wagner, E. (2017). Minicircle versus plasmid DNA delivery by receptor-targeted polyplexes. *Hum. Gene Ther.* 28, 862–874. doi: 10.1089/hum.2017.123

Levine, B. L., Bernstein, N. E., Aronson, K., Schlienger, J., Cotte, S., Perfetto, M. J., et al. (2002). Adoptive transfer of costimulated CD4+ T cells induces expansion of peripheral T cells and decreased CCR5 expression in HIV infection. *Nat. Med.* 8, 47–53. doi: 10.1038/nm0102-47

Levine, B. L., Miskin, J., Wonnacott, K., and Keir, C. (2016). Global manufacturing of CAR T cell therapy. *Mol. Ther. Meth. Clin. Develop.* 4, 92–101. doi: 10.1016/j.omtm.2016.12.006

Li, H., Zhang, B., Lu, X., Tan, X., Jia, F., Xiao, Y., et al. (2018). Molecular spherical nucleic acids. *Proc. Natl. Acad. Sci. U.S.A.* 115, 4340–4344. doi: 10.1073/pnas.1801836115

Li, Y., and Kurlander, R. J. (2010). Comparison of anti-CD3 and anti-CD28-coated beads with soluble anti-CD3 for expanding human T cells: differing impact on CD8 T cell phenotype and responsiveness to restimulation. *J. Transl. Med.* 8:104. doi: 10.1186/1479-5876-8-104

Lim, W. A., and June, C. H. (2017). The principles of engineering immune cells to treat cancer. *Cell.* 16, 724–740. doi: 10.1016/j.cell.2017.01.016

Lino, C. A., Harper, J. C., Carney, J. P., and Timlin, J. A. (2018). Delivering CRISPR: a review of the challenges and approaches. *Drug Deliv.* 25, 1234–1257. doi: 10.1080/10717544.2018.1474964

Liu, C. S. C., Raychaudhuri, D., Paul, B., Chakrabarty, Y., Ghosh, A. R., Rahaman, O., et al. (2018). Piezo1 mechanosensors optimize human T cell activation. *J. Immunol.* 200, 1255–1260. doi: 10.4049/jimmunol.1701118

Liu, Z., Jiang, W., Nam, J., Moon, J. J., and Kim, B. (2018). Immunomodulating nanomedicine for cancer therapy. *Nano Lett.* 18, 6655–6659. doi: 10.1021/acs.nanolett.8b02340

Liu, Z., Zhang, Z., Zhou, C., and Jiao, Y. (2010). Hydrophobic modifications of cationic polymers for gene delivery. *Prog. Poly. Sci.* 35, 1144–1162. doi: 10.1016/j.progpolymsci.2010.04.007

Lopes, A., Vanvarenberg, K., Kos, Š., Lucas, S., Colau, D., Van den Eynde, B., et al. (2018). Combination of immune checkpoint blockade with DNA cancer vaccine induces potent antitumor immunity against P815 mastocytoma. *Sci. Rep.* 8:15732. doi: 10.1038/s41598-018-33933-7

Lundstrom, K. (2018). Viral vectors in gene therapy. *Diseases* 6:E42. doi: 10.3390/diseases6020042

Lynn, G. M., Chytil. P., Francica, J. R., Lagová, A., Kueberuwa, G., Ishizuka, A. S., et al. (2019). Impact of polymer-TLR-7/8 agonist (adjuvant) morphology on the potency and mechanism of CD8 T cell induction. *Biomacromolecules* 20, 854–870. doi: 10.1021/acs.biomac.8b01473

Maldini, C. R., Ellis, G. I., and Riley, J. L. (2018). CAR T cells for infection, autoimmunity and allotransplantation. *Nat. Rev. Immunol.* 18, 605–616. doi: 10.1038/s41577-018-0042-2

Malone, R. W., Felgner, P. L., and Verma, I. M. (1989). Cationic liposome-mediated RNA transfection. *Proc. Natl. Acad. Sci. U.S.A.* 86, 6077–6081. doi: 10.1073/pnas.86.16.6077

Martell, R. E., Nevins, J. R., and Sullenger, B. A. (2002). Optimizing aptamer activity for gene therapy applications using expression cassette SELEX. *Mol. Ther.* 6, 30–34. doi: 10.1006/mthe.2002.0624

McKinlay, C. J., Vargas, J. R., Blake, T. R., Hardy, J. W., Kanada, M., Contag, C. H., et al. (2017). Charge-altering releasable transporters (CARTs) for the delivery and release of mRNA in living animals. *Proc. Natl. Acad. Sci. U.S.A.* 114, E448–E456. doi: 10.1073/pnas.1614193114

Mendell, J. R., Goemans, N., Lowes, L. P., Alfano, L. N., Berry, K., Shao, J., et al. (2016). Longitudinal effect of eteplirsen versus historical control on ambulation in Duchenne Muscular Dystrophy. *Ann. Neurol.* 79, 257–271. doi: 10.1002/ana.24555

Mi, J., Zhang, X., Rabbani, Z. N., Liu, Y., Su, Z., Vujaskovic, Z., et al. (2006). H1 RNA polymerase III promoter-driven expression of an RNA aptamer leads to high-level inhibition of intracellular protein activity. *Nucleic Acids Res.* 34, 3577–3584. doi: 10.1093/nar/gkl482

Mitchison, N. A. (1955). Studies on the immunological response to foreign tumor transplants in the mouse. I The role of lymph node cells in conferring immunity by adoptive transfer. *J. Exp. Med.* 102, 157–177. doi: 10.1084/jem.102.2.157

Mo, R., Jiang, T., Sun, W., and Gu, Z. (2015). ATP-responsive DNA-graphene hybrid nanoaggregates for anticancer drug delivery. *Biomaterials* 50, 67–74. doi: 10.1016/j.biomaterials.2015.01.053

Moffett, F., Coon, M. E., Radtke, S., Stephan, S. B., McKnight, L., Lambert, A., et al. (2018). Hit-and-run programming of therapeutic cytoreagents using mRNA nanocarriers. *Nat. Commun.* 8:389. doi: 10.1038/s41467-017-00505-8

Monjezi, R., Miskey, C., Gogishvili, T., Schleef, M., Schmeer, M., Einsele, H., et al. (2017). Enhanced CAR T-cell engineering using non-viral sleeping beauty transposition from minicircle vectors. *Leukemia* 31, 186–194. doi: 10.1038/leu.2016.180

Moon, J. J., Suh, H., Bershteyn, A., Stephan, M. T., Liu, H., Huang, B., et al. (2011). Interbilayer-crosslinked multilamellar vesicles as synthetic vaccines for potent humoral and cellular immune responses. *Nat. Mat.* 10, 243–251. doi: 10.1038/nmat2960

Muñoz-López, M., and García-Pérez, J. L. (2010). DNA transposons: nature and applications in genomics. *Curr. Genomics* 11, 115–128. doi: 10.2174/138920210790886871

Nafissi, N., Alqawlaq, S., Lee, E. A., Foldvari, M., Spagnuolo, P. A., and Slavcev, R. A. (2014). DNA ministrings: highly safe and effective gene delivery vectors. *Mol. Ther. Nucleic Acids* 3:e165. doi: 10.1038/mtna.2014.16

Naito, M., Ishii, T., Matsumoto, A., Miyata, K., Miyahara, Y., and Kataoka, K. (2012). A phenylboronate-functionalized polyion complex micelle for ATP-triggered release of siRNA. *Angew. Chem. Int. Ed.* 51, 10751–10755. doi: 10.1002/anie.201203360

Nakamura, M., Suzuki, A., Akada, J., Yarimizu, T., Iwakiri, R., Hoshida, H., et al. (2015). A novel terminator primer and enhancer reagents for direct expression of PCR-amplified genes in mammalian cells. *Mol. Biotech.* 57, 767–780. doi: 10.1007/s12033-015-9870-5

National Cancer Institute (2017). *CAR T Cells: Engineering Patients' Immune Cells to Treat Their Cancers*. Retrieved from: https://www.cancer.gov/about-cancer/treatment/research/car-t-cells (accessed March 18, 2019).

Nishikawa, F., Kakiuchi, N., Funaji, K., Fukuda, K., Sekiya, S., and Nishikawa, S. (2003). Inhibition of HCV NS3 protease by RNA aptamers in cells. *Nucleic Acids Res.* 31, 1935–1943. doi: 10.1093/nar/gkg291

Nishimura, T., Yamada, A., Umezaki, K., Sawada, S. I., Mukai, S. A., Sasaki, Y., et al. (2017). Self-assembled polypeptide nanogels with enzymatically transformable surface as a small interfering RNA delivery platform. *Biomacromol.* 18, 3913–3923. doi: 10.1021/acs.biomac.7b00937

Olden, B. R., Cheng, Y., Yu, J. L., and Pun, S. H. (2018). Cationic polymers for non-viral gene delivery to human T cells. *J. Contr. Rel.* 282, 140–147. doi: 10.1016/j.jconrel.2018.02.043

Ono, I., Yamashita, T., Jin, H. Y., Ito, Y., Hamada, H., Akasaka, Y., et al. (2004). Combination of porous hydroxyapatite and cationic liposomes as a vector for BMP-2 gene therapy. *Biomaterials* 25, 4709–4718. doi: 10.1016/j.biomaterials.2003.11.038

Pamudurti, N. R., Bartok, O., Jens, M., Ashwal-Fluss, R., Stottmeister, C., Ruhe, L., et al. (2017). Translation of CircRNAs. *Mol. Cell* 66, 9-21. e7. doi: 10.1016/j.molcel.2017.02.021

Panda, A. C., Grammatikakis, I., Kim, K. M., De, S., Martindale, J. L., Munk, R., et al. (2016). Identification of senescence-associated circular RNAs (SAC-RNAs) reveals senescence suppressor CircPVT1. *Nucleic Acids Res.* 45, 4021–4035. doi: 10.1093/nar/gkw1201

Park, J. H., Geyer, M. B., and Brentjens, R. J. (2016). CD19-targeted CAR T-cell therapeutics for hematologic malignancies: interpreting clinical outcomes to date. *Blood* 127, 3312–3320. doi: 10.1182/blood-2016-02-629063

Park, J. H., and Renier, J. B. (2010). Adoptive immunotherapy for B-cell malignancies with autologous chimeric antigen receptor modified tumor targeted T cells. *Dis. Med.* 9, 277–288.

Parmar, M. B., KC, R., Löebenberg, R., and Uludag, H. (2018). Additive polyplexes to undertake siRNA therapy against CDC20 and survivin in breast cancer cells. *Biomacromol.* 19, 4193–4206. doi: 10.1021/acs.biomac.8b00918

Pérez Del Río, E., Martinez Miguel, M., Veciana, J., Ratera, I., and Guasch, J. (2018). Artificial 3D culture systems for T-cell expansion. *ACS Omega* 3, 5273–5280. doi: 10.1021/acsomega.8b00521

Perica, K., Tu, A., Richter, A., Bieler, J. G., Edidin, M., and Schneck, J. P. (2014). Magnetic field-induced T cell receptor clustering by nanoparticles enhances T cell activation and stimulates antitumor activity. *ACS Nano* 8, 2252–2260. doi: 10.1021/nn405520d

Persano, S., Guevara, M. L., Li, Z., Mai, J., Ferrari, M., Pompa, P. P., et al. (2017). Lipopolyplex potentiates anti-tumor immunity of mRNA-based vaccination. *Biomaterials* 125, 81–89. doi: 10.1016/j.biomaterials.2017.02.019

Pfeiffer, A., Thalheimer, F. B., Hartmann, S., Frank, A. M., Bender, R. R., Danisch, S., et al. (2018). *In vivo* generation of human CD19-CAR T cells results in B-cell depletion and signs of cytokine release syndrome. *EMBO Mol. Med.* 10:e9158. doi: 10.15252/emmm.201809158

Plonka, A. B., Khorsand, B., Yu, N., Sugai, J. V., Salem, A. K., Giannobile, W. V., et al. (2017). Effect of sustained PDGF nonviral gene delivery on repair of tooth-supporting bone defects. *Gene Ther.* 24, 31–39. doi: 10.1038/gt.2016.73

Prakken, B., Wauben, M., Genini, D., Samodal, R., Barnett, J., Mendivil, A., et al. (2000). Artificial antigen-presenting cells as a tool to exploit the immune 'synapse'. *Nat. Med.* 6:1406. doi: 10.1038/82231

Prislei, S., Buonomo, S. B., Michienzi, A., and Bozzoni, I. (1997). Use of adenoviral VAI small RNA as a carrier for cytoplasmic delivery of ribozymes. *RNA* 3, 677–687.

Przybylowski, M., Hakakha, A., Stefanski, J., Hodges, J., Sadelain, M., and Rivière, I. (2005). Production scale-up and validation of packaging cell clearance of clinical-grade retroviral vector stocks produced in cell factories. *Gene Ther.* 13, 95–100. doi: 10.1038/sj.gt.3302648

Qiao, C., Zhang, K., Jin, H., Miao, L., Shi, C., Liu, X., et al. (2013). Using poly(lactic-co-glycolic acid) microspheres to encapsulate plasmid of bone morphogenetic protein 2/polyethylenimine nanoparticles to promote bone formation *in vitro* and *in vivo*. *Int. J. Nanomed.* 8, 2985–2995. doi: 10.2147/IJN.S45184

Remant Bahadur, K. C., Kucharski, C., and Uludag, H. (2015). Additive nanocomplexes of cationic lipopolymers for improved non-viral gene delivery to mesenchymal stem cells. *J. Mat. Chem. B* 3, 3972–3982. doi: 10.1039/C4TB02101K

Ren, L., and Lim, Y. T. (2018). Degradation-regulatable architectured implantable macroporous scaffold for the spatiotemporal modulation of immunosuppressive microenvironment and enhanced combination cancer immunotherapy. *Adv. Funct. Mat.* 28:1804490. doi: 10.1002/adfm.201804490

Ribeiro, S., Mairhofer, J., Madeira, C., Diogo, M. M., Lobato da Silva, C., Monteiro, G., et al. (2012). Plasmid DNA size does affect nonviral gene delivery efficiency in stem cells. *Cell Reprogram.* 14, 130–137. doi: 10.1089/cell.2011.0093

Richter, M., Saydaminova, K., Yumul, R., Krishnan, R., Liu, J., Nagy, E. E., et al. (2016). *In vivo* transduction of primitive mobilized hematopoietic stem cells after intravenous injection of integrating adenovirus vectors. *Blood* 128, 2206–2217. doi: 10.1182/blood-2016-04-711580

Riddell, S. R., Watanabe, K. S., Goodrich, J. M., Li, C. R., Agha, M. E., and Greenberg, P. D. (1992). Restoration of viral immunity in immunodeficient humans by the adoptive transfer of T cell clones. *Science* 257, 238–241. doi: 10.1126/science.1352912

Rose, L., Kucharski, C., Aliabadi, H. M., and Uluda,g, H. (2013). Gelatin coating to stabilize the transfection ability of nucleic acid polyplexes. *Acta Biomaterial.* 9, 7429–7438. doi: 10.1016/j.actbio.2013.03.029

Rosenberg, S. A., Packard, B. S., Aebersold, P. M., Solomon, D., Topalian, S. L., Toy, S. T., et al. (1988). Use of tumor infiltrating lymphocytes and interleukin-2 in the immunotherapy of patients with metastatic melanoma. A preliminary report. *N. Engl. J. Med.* 319, 1676–1680. doi: 10.1056/NEJM198812223192527

Sadelain, M. (2017). CD19 CAR T cells. *Cell* 171:1471. doi: 10.1016/j.cell.2017.12.002

Sadelain, M., Rivière, I., and Brentjens, R. (2003). Targeting tumours with genetically enhanced T lymphocytes. *Nat. Rev. Cancer* 3, 35–45. doi: 10.1038/nrc971

Scholler, J., Brady, T. L., Binder-Scholl, G., Hwang, W. T., Plesa, G., and Hege, K. M. (2012). Decade-long safety and function of retroviral-modified chimeric antigen receptor T cells. *Sci. Transl. Med.* 4:132ra53. doi: 10.1126/scitranslmed.3003761

Schott, J. W., Morgan, M., Galla, M., and Schambach, A. (2016). Viral and synthetic RNA vector technologies and applications. *Mol. Ther.* 24, 1513–1527. doi: 10.1038/mt.2016.143

Sharei, A., Cho, N., Mao, S., Jackson, E., Poceviciute, R., Adamo, A., et al. (2013a). Cell squeezing as a robust, microfluidic intracellular delivery platform. *J. Vis. Exp.* 81:e50980. doi: 10.3791/50980

Sharei, A., Zoldan, J., Adamo, A., Sim, W. Y., Cho, N., and Jackson, E. (2013b). A vector-free microfluidic platform for intracellular delivery. *Proc. Natl. Acad. Sci. U.S.A.* 110, 2082–2087. doi: 10.1073/pnas.1218705110

Shin, K. S., Sullenger, B. A., and Lee, S. W. (2004). Ribozyme-mediated induction of apoptosis in human cancer cells by targeted repair of mutant p53 RNA. *Mol. Ther.* 10, 365–372. doi: 10.1016/j.ymthe.2004.05.007

Smith, T. T., Moffett, H. F., Stephan, S. B., Opel, C. F., Dumigan, A. G., Jiang, X., et al. (2017a). Biopolymers codelivering engineered T cells and STING agonists can eliminate heterogeneous tumors. *J. Clin. Invest.* 127, 2176–2191. doi: 10.1172/JCI87624

Smith, T. T., Stephan, S. B., Moffett, H. F., McKnight, L. E., Ji, W., Reiman, D., et al. (2017b). *In situ* programming of leukaemia-specific T cells using synthetic DNA nanocarriers. *Nat. Nanotech.* 12, 813–820. doi: 10.1038/nnano.2017.57

Soldevilla, M. M., Meraviglia-Crivelli de Caso, D., Menon, A. P., and Pastor, F. (2018). Aptamer-iRNAs as therapeutics for cancer treatment. *Pharmaceuticals.* 11:108. doi: 10.3390/ph11040108

Sridharan, K., and Gogtay, N. J. (2016). Therapeutic nucleic acids: current clinical status. *Br. J. Clin. Pharmocol.* 82, 659–672. doi: 10.1111/bcp.12987

Steenblock, E. R., and Fahmy, T. M. (2008). A comprehensive platform for *ex vivo* T-cell expansion based on biodegradable polymeric artificial antigen-presenting cells. *Mol. Ther.* 16, 765–772. doi: 10.1038/mt.2008.11

Steinle, H., Ionescu, T. M., Schenk, S., Golombek, S., and Kunnakattu, S. J., Özbek, M. T., et al. (2018). Incorporation of synthetic mRNA in injectable chitosan-alginate hybrid hydrogels for local and sustained expression of exogenous proteins in cells. *Int. J. Mol. Sci.* 19:1313. doi: 10.3390/ijms19051313

Stephan, S. B., Taber, A. M., Jileaeva, I., Pegues, E. P., Sentman, C. L., and Stephan, M. T. (2014). Biopolymer implants enhance the efficacy of adoptive T-cell therapy. *Nat. Biotech.* 33, 97–101. doi: 10.1038/nbt.3104

Sullenger, B. A., Gallardo, H. F., Ungers, G. E., and Gilboa, E. (1990). Overexpression of TAR sequences renders cells resistant to human immunodeficiency virus replication. *Cell* 63, 601–608. doi: 10.1016/0092-8674(90)90455-N

Sum, C. H., Wetting, S., and Slavcev, R. A. (2014). Impact of DNA vector topology on non-viral gene therapeutic safety and efficacy. *Curr. Gene Ther.* 14, 309–329. doi: 10.2174/1566523214666140612154929

Sun, W., Ji, W., Hall, J. M., Hu, Q., Wang, C., Beisel, C. L., et al. (2015). Self-assembled DNA nanoclews for the efficient delivery of CRISPR-Cas9 for genome editing. *Angew. Chem. Int. Ed. Engl.* 54, 12029–12033. doi: 10.1002/anie.201506030

Sundaram, P., Kurniawan, H., Byrne, M. E., and Wower, J. (2013). Therapeutic RNA aptamers in clinical trials. *Eur. J. Pharm. Sci.* 48, 259–271. doi: 10.1016/j.ejps.2012.10.014

Svoboda, J., Rheingold, S. R., Gill, S. I., Grupp, S. A., Lacey, S. F., Kulikovskaya, I., et al. (2018). Nonviral RNA chimeric antigen receptor–modified T cells in patients with Hodgkin lymphoma. *Blood* 132, 1022–1026. doi: 10.1182/blood-2018-03-837609

Symens, N., Rejman, J., Lucas, B., Demeester, J., De Smedt, S. C., and Remaut, K. (2013). Noncoding DNA in lipofection of HeLa cells – a few insights. *Mol. Pharm.* 10, 1070–1079. doi: 10.1021/mp300569j

Tai, I. T., and Sun, A. M. (1993). Microencapsulation of recombinant cells: a new delivery system for gene therapy. *FASEB J.* 7, 1061–1069. doi: 10.1096/fasebj.7.11.8370477

Tang, W., Hu, J. H., and Liu, D. R. (2017). Aptazyme-embedded guide RNAs enable ligand-responsive genome editing and transcriptional activation. *Nat. Commun*. 8:15939. doi: 10.1038/ncomms15939

Tipanee, J., Chai, Y. C., VandenDriessche, T., and Chuah, M. K. (2017a). Preclinical and clinical advances in transposon-based gene therapy. *Biosci. Rep.* 37:BSR20160614. doi: 10.1042/BSR20160614

Tipanee, J., VandenDriessche, T., and Chuah, M. K. (2017b). Transposons: moving forward from preclinical studies to clinical trials. *Hum. Gene Ther*. 28, 1087–1104. doi: 10.1089/hum.2017.128

Tsao, C. T., Kievit, F. M., Ravanpay, A., Erickson, A. E., Jensen, M. C., Ellenbogen, R. G., et al. (2014). Thermoreversible poly(ethylene glycol)-g-chitosan hydrogel as a therapeutic T lymphocyte depot for localized glioblastoma immunotherapy. *Biomacromolecules* 15, 2656–2662. doi: 10.1021/bm500502n

Uchida, S., Yoshinaga, N., Yanagihara, K., Yuba, E., Kataoka, K., and Itaka, K. (2018). Designing immunostimulatory double stranded messenger RNA with maintained translational activity through hybridization with poly A sequences for effective vaccination. *Biomaterials* 150, 162–170. doi: 10.1016/j.biomaterials.2017.09.033

Urnov, F. D., Rebar, E. J., Holmes, M. C., Zhang, H. S., and Gregory, P. D. (2010). Genome editing with engineered zinc finger nucleases. *Nat. Rev. Genet.* 11, 636–646. doi: 10.1038/nrg2842

Valencia-Serna, J., Kucharski, C., Chen, M., K.C., R., Jiang, X., et al. (2019). siRNA-mediated BCR-ABL silencing in primary chronic myeloid leukemia cells with lipopolymers. Submitted to J. Controlled Release.

Walisko, O., Schorn, A., Rolfs, F., Devaraj, A., Miskey, C., Izsvák, Z., et al. (2008). Transcriptional activities of the sleeping beauty transposon and shielding its genetic cargo with insulators. *Mol. Ther.* 16, 359–369. doi: 10.1038/sj.mt.6300366

Wang, C., Sun, W., Wright, G., Wang, A. Z., and Gu, Z. (2016). Inflammation-triggered cancer immunotherapy by programmed delivery of CpG and anti-PD1 antibody. *Adv. Mater.* 28, 8912–8920. doi: 10.1002/adma.201506312

Wang, G. P., Garrigue, A., Ciuffi, A., Ronen, K., Leipzig, J., Berry, C., et al. (2008). DNA bar coding and pyrosequencing to analyze adverse events in therapeutic gene transfer. *Nucleic Acids Res.* 36:e49. doi: 10.1093/nar/gkn125

Wang, H., Li, M., Lee, C. M., Chakraborty, S., Kim, H., Bao, G., et al. (2017). CRISPR/Cas9-based genome editing for disease modeling and therapy: challenges and opportunities for nonviral delivery. *Chem. Rev.* 117, 9874–9906. doi: 10.1021/acs.chemrev.6b00799

Wang, H. X., Song, Z., Lao, Y. H., Xu, X., Gong, J., Cheng, D., et al. (2018). Nonviral gene editing via CRISPR/Cas9 delivery by membrane-disruptive and endosomolytic helical polypeptide. *Proc. Natl. Acad. Sci. U.S.A.* 115, 4903–4908. doi: 10.1073/pnas.1712963115

Wang, X., Olszewska, M., Qu, J., Wasielewska, T., Bartido, S., Hermetet, G., et al. (2015). Large-scale clinical-grade retroviral vector production in a fixed-bed bioreactor. *J. Immunother.* 38, 127–135. doi: 10.1097/CJI.0000000000000072

Weiden, J., Tel, J., and Figdor, C. G. (2018b). Synthetic immune niches for cancer immunotherapy. *Nat. Rev. Immunol.* 18, 212–219. doi: 10.1038/nri.2017.89

Weiden, J., Voerman, D., Dölen, Y., Das, R. K., van Duffelen, A., Hammink, R., et al. (2018a). Injectable biomimetic hydrogels as tools for efficient T cell expansion and delivery. *Front. Immunol.* 9:2798. doi: 10.3389/fimmu.2018.02798

Wells, D. J. (2004). Gene therapy progress and prospects: electroporation and other physical methods. *Gene Ther.* 11, 1363–1369. doi: 10.1038/sj.gt.3302337

Wiehe, J. M., Ponsaerts, P., Rojewski, M. T., Homann, J. M., Greiner, J., Kronawitter, D., et al. (2007). mRNA-mediated gene delivery into human progenitor cells promotes highly efficient protein expression. *J. Cell. Mol. Med.* 11, 521–530. doi: 10.1111/j.1582-4934.2007.00038.x

Williams, R. S., Johnston, S. A., Riedy, M., DeVit, M. J., McElligott, S. G., and Sanford, J. C. (1991). Introduction of foreign genes into tissues of living mice by DNA-coated microprojectiles. *Proc. Natl. Acad. Sci. U.S.A.* 88, 2726–2730. doi: 10.1073/pnas.88.7.2726

Won, Y. S., and Lee, S. W. (2012). Selective regression of cancer cells expressing a splicing variant of AIMP2 through targeted RNA replacement by trans-splicing ribozyme. *J. Biotechnol.* 158, 44–49. doi: 10.1016/j.jbiotec.2012.01.006

Wu, S. C., Meir, Y. J., Coates, C. J., Handler, A. M., Pelczar, P., Moisyadi, S., et al. (2006). piggyBac is a flexible and highly active transposon as compared to sleeping beauty, Tol2, and Mos1 in mammalian cells. *Proc. Natl. Acad. Sci. U.S.A.* 103, 15008–15013. doi: 10.1073/pnas.0606979103

Yang, Y., Fan, X., Mao, M., Song, X., Wu, P., Zhang, Y., et al. (2017). Extensive translation of circular RNAs driven by N^6-methyladenosine. *Cell Res.* 27, 626–641. doi: 10.1038/cr.2017.31

Yannas, I. V. (1992). Tissue regeneration by use of collagen-glycosaminoglycan copolymers. *Clin. Mater.* 9, 179–187. doi: 10.1016/0267-6605(92)90098-E

Yant, S. R., Meuse, L., Chiu, W., Ivics, Z., Izsvak, Z., and Kay, M. A. (2000). Somatic integration and long-term transgene expression in normal and haemophilic mice using a DNA transposon system. *Nat Genet.* 25, 35–41. doi: 10.1038/75568

Young, K. L., Scot, A. W., Hao, L., Mirkin, S. E., Liu, G., and Mirkin, C. A. (2012). Hollow spherical nucleic acids for intracellular gene regulation. *Nano Lett.* 12, 3867–3871. doi: 10.1021/nl3020846

Zhang, C., Liu, J., Zhong, J. F., and Zhang, X. (2017). Engineering CAR-T cells. *Biomarker Res.* 5:22. doi: 10.1186/s40364-017-0102-y

Zhang, R., Billingsley, M. M., and Mitchell, M. J. (2018). Biomaterials for vaccine-based cancer immunotherapy. *J. Cont. Rel.* 292, 256–276. doi: 10.1016/j.jconrel.2018.10.008

Zhang, S., Doschak, M., and Uludag, H. (2009). Pharmacokinetics and bone formation by BMP-2 entrapped in polyethylenimine-coated albumin nanoparticles. *Biomaterials* 30, 5143–5155. doi: 10.1016/j.biomaterials.2009.05.060

Zhang, W., De La Vega, R. E., Coenen, M. J., Müller, S. A., Peniche Silva, C. J., Aneja, M. K., et al. (2019). An improved, chemically modified RNA encoding BMP-2 enhances osteogenesis *in vitro* and *in vivo*. *Tissue Eng A*. 25, 131–144. doi: 10.1089/ten.tea.2018.0112

Zheng, Y., Stephan, M. T., Gai, S. A., Abraham, W., Shearer, A., and Irvine, D. J. (2013). *In vivo* targeting of adoptively transferred T-cells with antibody- and cytokine-conjugated liposomes. *J. Control. Release* 172, 426–435. doi: 10.1016/j.jconrel.2013.05.037

Zhou, Z., Liu, X., Zhu, D., Wang, Y., Zhang, Z., Zhou, X., et al. (2017). Nonviral cancer gene therapy: delivery cascade and vector nanoproperty integration. *Adv. Drug Del. Rev.* 115, 115–154. doi: 10.1016/j.addr.2017.07.021

Zilkowski, I., Ziouti, F., Schulze, A., Hauck, S., Schmidt, S., Mainz, L., et al. (2019). Nanogels enable efficient miRNA delivery and target gene downregulation in transfection-resistant multiple myeloma cells. *Biomacromolecules* 20, 916–926. doi: 10.1021/acs.biomac.8b01553

Conflict of Interest Statement: HU is a founder and share holder in a private company (RJH Biosciences Inc.) intended to develop nucleic acid based therapies and declares conflict of interest.

The remaining authors declare that the research was conducted in the absence of any commercial or financial relationships that could be construed as a potential conflict of interest.

frontiers in Bioengineering and Biotechnology

REVIEW
published: 11 June 2019
doi: 10.3389/fbioe.2019.00135

Corneal Repair and Regeneration: Current Concepts and Future Directions

*Mohammadmahdi Mobaraki[1], Reza Abbasi[1], Sajjad Omidian Vandchali[1], Maryam Ghaffari[1], Fathollah Moztarzadeh[1] and Masoud Mozafari[2]**

[1] Biomaterials Group, Department of Biomedical Engineering, Amirkabir University of Technology, Tehran, Iran, [2] Department of Tissue Engineering and Regenerative Medicine, Faculty of Advanced Technologies in Medicine, Iran University of Medical Sciences, Tehran, Iran

The cornea is a unique tissue and the most powerful focusing element of the eye, known as a window to the eye. Infectious or non-infectious diseases might cause severe visual impairments that need medical intervention to restore patients' vision. The most prominent characteristics of the cornea are its mechanical strength and transparency, which are indeed the most important criteria considerations when reconstructing the injured cornea. Corneal strength comes from about 200 collagen lamellae which criss-cross the cornea in different directions and comprise nearly 90% of the thickness of the cornea. Regarding corneal transparency, the specific characteristics of the cornea include its immune and angiogenic privilege besides its limbus zone. On the other hand, angiogenic privilege involves several active cascades in which anti-angiogenic factors are produced to compensate for the enhanced production of proangiogenic factors after wound healing. Limbus of the cornea forms a border between the corneal and conjunctival epithelium, and its limbal stem cells (LSCs) are essential in maintenance and repair of the adult cornea through its support of corneal epithelial tissue repair and regeneration. As a result, the main factors which threaten the corneal clarity are inflammatory reactions, neovascularization, and limbal deficiency. In fact, the influx of inflammatory cells causes scar formation and destruction of the limbus zone. Current studies about wound healing treatment focus on corneal characteristics such as the immune response, angiogenesis, and cell signaling. In this review, studied topics related to wound healing and new approaches in cornea regeneration, which are mostly related to the criteria mentioned above, will be discussed.

Keywords: cornea, tissue engineering, wound healing, regenerative medicine, biomaterials, immune privilege, angiogenesis, limbus

OPEN ACCESS

Edited by:
Hasan Uludag,
University of Alberta, Canada

Reviewed by:
Julien Georges Didier Barthès,
Protip Medical, France
Emilio Isaac Alarcon,
University of Ottawa, Canada

***Correspondence:**
Masoud Mozafari
mozafari.masoud@gmail.com

Specialty section:
This article was submitted to Biomaterials, a section of the journal Frontiers in Bioengineering and Biotechnology

Received: *14 December 2018*
Accepted: *20 May 2019*
Published: *11 June 2019*

Citation:
Mobaraki M, Abbasi R, Omidian Vandchali S, Ghaffari M, Moztarzadeh F and Mozafari M (2019) Corneal Repair and Regeneration: Current Concepts and Future Directions. Front. Bioeng. Biotechnol. 7:135. doi: 10.3389/fbioe.2019.00135

INTRODUCTION

Diseases affecting the cornea can be either infectious or non-infectious, and both may cause severe visual impairments requiring intervention. Trachoma, onchocerciasis, corneal ulceration, corneal dystrophies, and xerophthalmia are some of the major causes of blindness worldwide (Sommer, 1982). However, the prevalence and epidemiology of corneal diseases varies from region to region.

From the use of traditional eye medicines (which is now considered a significant risk factor for corneal ulceration) to collagen cross-linking, which has recently been approved by the US FDA to strengthen the cornea, the ultimate goal in corneal treatment is to employ minimally invasive procedures that can restore or preserve vision (Jeng et al., 2016). Stimulating the body's repair mechanisms is now considered to be the gold standard for the functional healing of damaged tissues and organs (Khadem et al., 2000, 2004; Zarrintaj et al., 2017). This approach is typified by corneal transplantation and tissue engineering.

The most striking advance in the medical treatment of corneal diseases over recent decades has been corneal transplantation and, nowadays, the cornea is the most commonly transplanted tissue worldwide. Corneal transplantations are divided into two main categories based upon the amount of surgically replaced tissue. In penetrating keratoplasty, the entire cornea is replaced with a donor tissue. However, in a newer procedure called lamellar keratoplasty, only the damaged layers are replaced with a donor graft, and the healthy part of the cornea is left intact. In lamellar keratoplasty, the integrity of the cornea and the surrounding tissues are preserved; as a result, better visual improvement is usually achieved. Unfortunately, there are sometimes poor outcomes because of graft rejection or late graft failure. Furthermore, according to a World Health Organization (WHO) report, 15–20% of patients who need corneal transplantation remain untreated because of the shortage of corneal donors (Whitcher et al., 2001). Over the last few decades, the shortage of donor tissues, beside fears of transmissible diseases, has accelerated studies on finding an alternative treatment to transplantation, and an artificial cornea or keratoprosthesis has been suggested as an option. Historically, Guillaume Pellier de Quengsy Jr. was the first person who proposed a thin silver-rimmed convex glass disc as an artificial cornea, as long ago as 1789 (Mannis and Mannis, 1999). At that time, the first priority was to choose transparent and non-irritating materials, but as time went by other researchers concentrated on designing an artificial cornea which was able to promote better incorporation with the host tissue. Glass and quartz were the choices for the transparent part of the prosthesis and natural polymers like gutta-percha and casein were added to the artificial cornea design. Later, gold rings and platinum rings were used to achieve better incorporation with the host cornea. Further studies on artificial corneas resulted in replacing glass and quartz with lighter materials. At the beginning of the twentieth century, attention was diverted from artificial corneas to transplantation of donor corneal after the first successful keratoplasty (Zirm, 1989). Nevertheless, studies on artificial corneas have never ceased. Today there are four types of keratoprostheses, which are in commercial use. In the following section, these keratoprostheses will be further discussed. Despite some clinical success in using artificial corneas, the host rejection is still relatively high. The presence of corneal epithelial stem cells, which are located in the basal epithelial layer of the corneal limbus (the border between the cornea and the sclera), has given some hope for better healing and integration. Therefore, many researchers have focused on employing new biomaterials to mimic the corneal architecture, which would allow better corneal self-repair. This review will discuss recent advances in repairing damaged corneas, focusing on new concepts and biomaterials (**Figure 1**; Muijzer et al., 2019).

CORNEA STRUCTURE AND TRANSPARENCY

The human cornea is a unique tissue with two critical functions. On the one hand, the cornea forms the anterior portion of the outer casing of the eye and protects the inner portion of the eye from the external environment. On the other hand, it is the single most powerful focusing element of the eye. It provides about 80% refractive power of the eye and it is roughly twice as powerful as the lens. Because of these functions, the cornea is both mechanically strong and transparent. Its strength comes from about 200 collagen lamellae, which criss-cross the cornea in different directions. This collagen-rich layer of the cornea comprises nearly 90% of the thickness of the cornea and is called the "stroma proper layer." In fact, the human cornea is composed of five primary layers—epithelium, Bowman's layer, stroma proper, Descemet's membrane, and endothelium. This hierarchical structure can be described as a fibril-reinforced laminate biocomposite, which provides an excellent compromise between stiffness, strength, toughness, and extensibility. In **Figure 2** the hierarchical structure of the cornea, with macroscopic, microscopic, and nanoscopic features, is shown (Kaufman et al., 2011). As noted earlier, the cornea is transparent; however, the hierarchical structure and the presence of interfaces between the different layers, each with its own index of refraction, seem to be in contradiction with its clarity. There have been lots of studies attempting to explain the transparency of the cornea. The first explanations in the nineteenth century emphasized the homogeneity of the cornea and the fact that the collagen fibrils had the same refractive index. After about a century, Dr. Maurice (1957) tried to explain the optical structure of the cornea considering its geometric form, dimensions and the refractive indices of its components. He suggested that the scattered waves from collagen fibrils interfered with each other in such a way that they canceled out each other in all directions, except the forward direction. Meanwhile, Miller and Benedek (1973) in 1973 showed that the gaps between the interfaces were smaller than one-half the wavelength of visible light; and as a result, the cornea is crystal clear. Recently Meek and Knupp (2015) have reviewed the current state of knowledge about the corneal architecture and its optical transparency. These authors outlined the general basis and molecular mechanisms of corneal transparency. Maurice's suggestion regarding the interaction of the incoming electromagnetic waves with the collagen fibrils was proved to be correct by new imaging technologies (Quantock et al., 2015).

CORNEAL REPLACEMENTS

Boston Keratoprosthesis (B-KPro), Osteo-Odonto-Keratoprosthesis (OOKP), AlphaCor, and the KeraKlear Artificial Cornea are the four types of keratoprostheses which

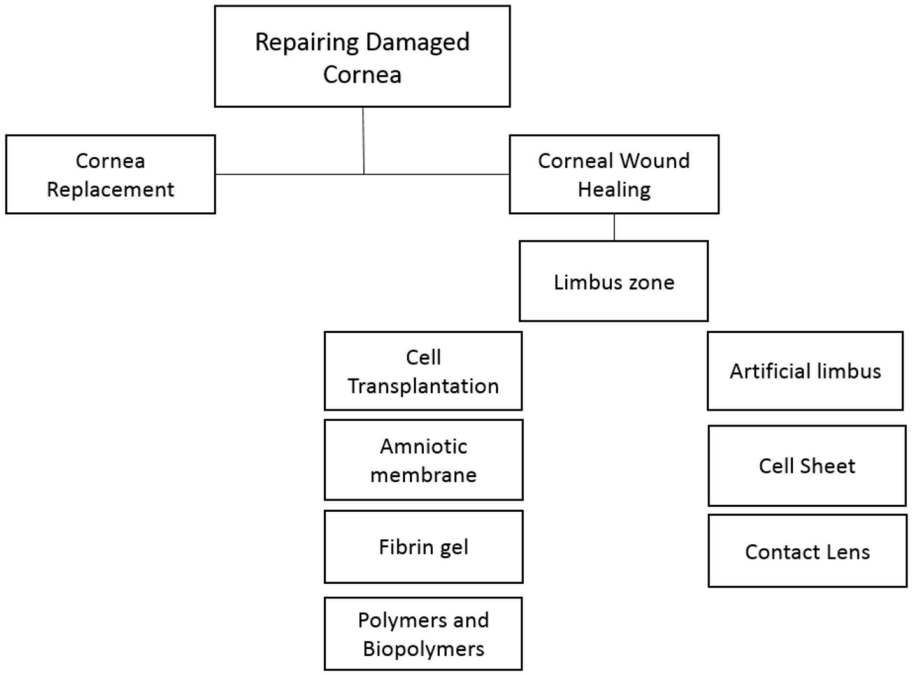

FIGURE 1 | Current strategies for the repair and regeneration of damaged cornea.

have, so far, been commercialized. Over the last decade, implantation of artificial corneas has been dramatically increased. For instance, fewer than 50 units of B-KPro were implanted before 2002, while more than 9,000 implantations were carried out in 2014. In this section, recent advances in the design of artificial corneas will be discussed with regard to the type of materials employed.

The B-KPro is the most widely implanted artificial cornea and was developed at the Massachusetts Eye and Ear Infirmary. There are two types of B-KPro each with different indications. The B-KPro type I is commonly used in patients with a non-cicatrizing disease such as repeated allograft failure, corneal opacity with extensive neovascularization, aniridia, trauma, etc. In contrast, B-KPro type II is used in cicatrizing diseases and severe dry eye conditions, such as severe autoimmune ocular diseases. Both types of B-KPro have similar compartments but are different in some details. They have a front plate and a back plate, which act to sandwich a fresh donor cornea; a titanium locking-ring is used to secure the plates. Medical grade polymethyl methacrylate (PMMA) with the ability to block UVA/UVB is used for the front and back plates. The idea of using PMMA was conceived due to its ability to induce only minimal inflammatory responses in the eye (Griffith et al., 2016). PMMA is a transparent thermoplastic polymer, also known as acrylic glass, which can be modified to achieve desired mechanical properties, like toughness and stiffness. On the other hand, modifying the PMMA polymer with nano-dimensional TiO2, SiO2, ZnO, ZrO2, Al2O3, CNT, and graphene has been investigated for electromagnetic shielding, thermal insulation, antiglare resistance, scratch resistance, and also resistance against UV radiation (Pandey et al., 2010; Cano et al., 2013; Soumya et al., 2014). The apparent success of PMMA in keratoprostheses has been plagued by numerous complications like tissue necrosis, retroprosthetic membrane formation, vitreous opacities, etc. The main reasons for these shortcomings include poor adhesion between the PMMA and the host corneal collagen at the PMMA-host interface and fibrous membrane formation due to fibroblast attachment onto the inner surface of PMMA. Therefore, there have been ongoing research efforts to overcome these drawbacks. In the first attempts, PMMA surfaces were modified with polyethylene glycol (PEG) or extracellular matrix molecules to block cell adhesion (Kim et al., 2001; Aucoin et al., 2002). The results were promising in terms of preserving the inner surface of PMMA but, at the external PMMA-host interface, the reduction in cell attachment resulted in endophthalmitis and extrusion of the implant. Endophthalmitis is an internal inflammation of the eye, which is a possible complication of B-KPro, arising because of inadequate integration of PMMA with the host corneal tissue allowing penetration of microorganisms. Suggested ways to reduce this drawback include using of daily antibiotics and modifying the B-KPro surface. Using antibiotics is out of the scope of this paper, so only surface modification of PMMA will be discussed.

Surface modifications of PMMA have been studied using two approaches. One of them focuses on improving cell attachment at the PMMA-corneal tissue interface to prevent the penetration of microorganisms into the internal part of the eye. In this context, Patel et al. (2006) studied the region-specific control of cell adhesion by grafting di-amino-PEG onto the surface of PMMA which could be used to improve cell adhesion and spatially control cell attachment onto the PMMA. Recently the

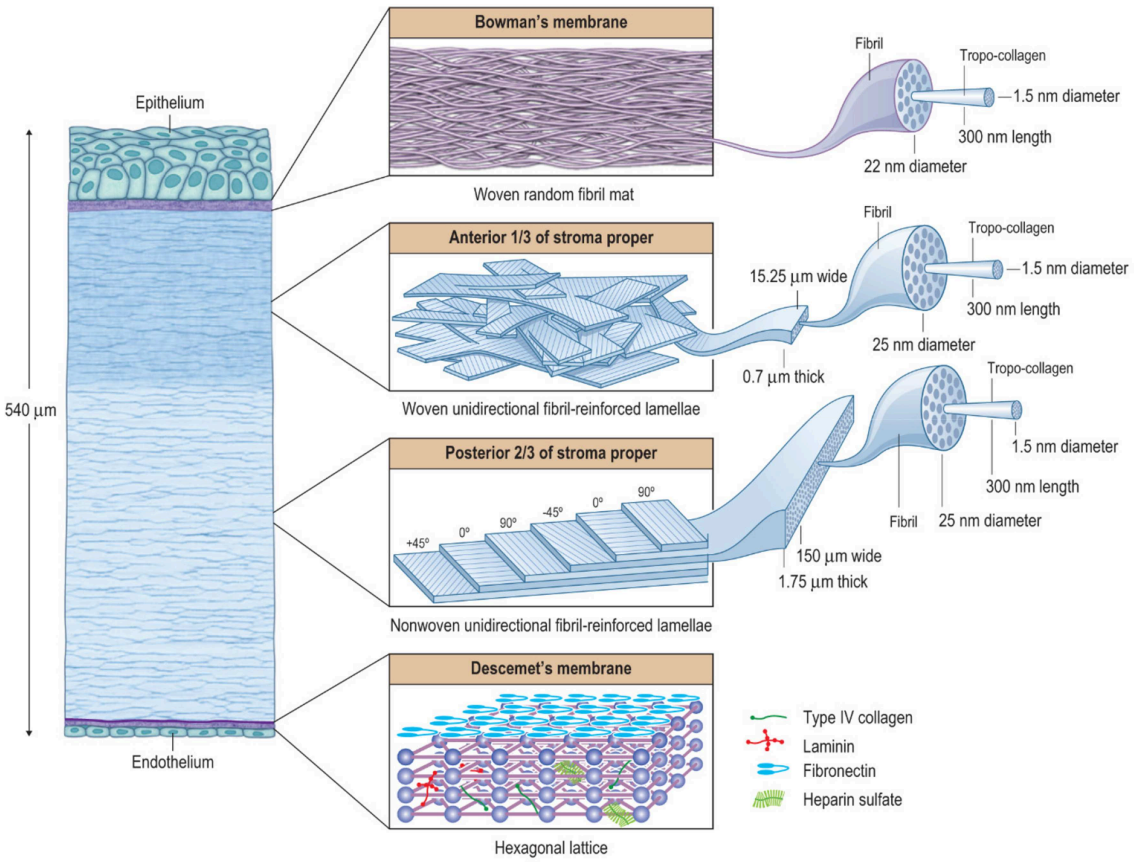

FIGURE 2 | The hierarchical structure of the cornea showing that it is basically composed of three composite regions. A fourth composite region, Descemet's membrane, is included for completion. The macroscopic, microscopic, and nanoscopic features are emphasized (from left to right) to help illustrate the various interactions between the tissue components. Bowman's layer is essentially a random fibril, woven-mat composite, which maximizes multi-axial stiffness and strength. The underlying anterior third of the stroma proper is a lamellar interwoven fabric composed of unidirectionally (UD) fibril-reinforced lamellae. This architectural hierarchy is more rigid against z-axis deformations compared to non-woven UD-laminates. In the human body, the corneal structure is most similar to that of the pericardium, which serves to mechanically prevent the formation of aneurysms in the heart. The posterior two-thirds of the stroma is essentially a non-woven, UD-fibril-reinforced lamellar composite, which maximizes longitudinal x- and y-axis stiffness and strength, but has only weak transverse z-axis stiffness and strength. In the human body, its structure is most similar to that of the annulus fibrosis of the intervertebral disk, which functions efficiently as a cushioning mechanism for the spine, but is prone to chronic biomechanical failure. The UD-orientation of collagen fibrils in each lamella is vital because this arrangement prevents fibril undulation and thus maximizes the initial axial tensile strength of each fibril. Descemet's membrane forms a hexagonal lattice. Taken together these composite-like regions are responsible for the overall stiffness, strength, extensibility, and toughness of the cornea. They also help explain how the cornea behaves biomechanically after surgery, disease, or injury. Reprinted with permission (Kaufman et al., 2011).

stability and biocompatibility of poly (2-hydroxyl methacrylate)-polymethyl methacrylate (PHEMA-PMMA) has been studied and has shown promising optical transparency, flexibility, and good mechanical properties. Nevertheless, its stability and biocompatibility still need further research (Hwang and Kim, 2016). The second approach is to fabricate a PMMA polymer with antibacterial properties. Examples of these antibacterial coatings are titanium dioxide (TiO2) (Riau et al., 2016) and silver nanocluster (Baino et al., 2016). For instance, Salvador-Culla et al. showed that a TiO2 coating on PMMA enhanced keratocyte cell integration and attachment, while at the same time demonstrated antibacterial properties (Salvador-Culla et al., 2016). In another attempt, researchers at the University of California, Irvine (UC Irvine) mimicked the surface of insect wings to make an antibacterial PMMA for using in an artificial cornea (Kowalski, 2016).

In the presence of severe ocular surface inflammation like chemical burns, end-stage Stevens-Johnson syndrome, ocular cicatricial pemphigoid, multiple failed penetrating keratoplasties, and trachoma, the use of the Osteo-Odonto-Keratoprosthesis (OOKP) is an alternative approach. Multiple efforts in using more biologically compatible substances resulted in the introduction of OOKP in 1963 by Strampelli (Han et al., 2015b). In this kind of artificial cornea, an autologous tooth was cut horizontally (OOKP) or longitudinally (MOOKP) to allow an optical cylinder made of PMMA to be introduced inside it. MOOKP is a modified OOKP introduced by Falcinelli et al. (1987). Tibia KPro is another type of biological keratoprosthesis

in which a fragment of the autologous tibia was used to allow anatomical retention for an extended period of time. The biological parts of OOKP and MOOKP are known as a "keratoprosthesis skirt" and various studies have suggested that the use of living materials results in lowering the risk of extrusion and infection (Falcinelli et al., 2005). Beside the biological parts of OOKP and MOOKP, two other types of synthetic materials are used in these implants. These are (a) the transparent material, which is used in the optical cylinder, and (b) the adhesive, which is used to bond the optical cylinder to the biological parts. PMMA is a gold standard transparent, water-resistant, and durable material for the optical cylinder. However, as mentioned before, there are ongoing studies toward improving its characteristics. Acrylic bone cement is a standard dental adhesive, which is commonly used, and its suitability has never been seriously challenged. Yet, studies on other dental adhesives like glass ionomer and universal resin cement have been conducted (Weisshuhn et al., 2014; Alarcon et al., 2016).

In comparison with B-KPo, MOOKP is cheaper and does not require a viable donor cornea. However, there are some obstacles and controversial issues related to the use of OOKP and MOOKP. For instance, two fundamental surgical procedures need to be performed to implant the biological keratoprosthesis, and there is a 3-month interval between these procedures. This requirement complicates the surgery and reduces patient satisfaction. As a result, in the last decade, research on OOKP and MOOKP has focused on replacing the biological skirt with a synthetic skirt that enables it to biointegrate with the surrounding corneal tissue. Synthetic skirts have shown better mechanical biocompatibility with the sclera, in addition to more comfortable fabrication and better handling during the surgery. AlphaCor is one of the commercially available artificial corneas with a synthetic skirt. This kind of keratoprosthesis has been studied and developed in the Lion Eye Institute of Western Australia since 1989. AlphaCor is a one-piece device with two concentric regions that made from poly-(2-hydroxyethyl-methacrylate) (PHEMA). The central core of the device is a transparent PHEMA cylinder, and the skirt is a porous PHEMA material to improve biointegration with the surrounding corneal stromal tissue. Nevertheless, the rejection rates of the synthetic skirt is much higher than the biological skirts discussed above (Polisetti et al., 2013). Thus, improving the biointegration of the synthetic skirt is an important objective in recent studies. In this regard, Pino et al. (2008) attempted to increase the bioactivity of various synthetic polymers using biomimetic coatings. They suggested that growing a bioactive apatite layer on the surface of the polymers would provide well *in vivo* biointegration. Another approach to enhancing the bioactivity of the skirt is to modify the surface of the skirt with extracellular matrix proteins like fibronectin, laminin, and collagen (Xie et al., 1997). Moreover, replacing the polymers with bioactive materials like bioglass has also been investigated (Laattala et al., 2011). Accordingly, Huhtinen et al. (2013) replaced the polymeric skirt of the keratoprosthesis with bioactive glass. They claimed that the porous bioglass had a capacity to induce and support tissue ingrowth, resulting in better biointegration. Similar investigations using other innovative materials have been proposed by other research groups. Recently, Tan et al. (2015) assessed the potential of two-dimensional graphene film and 3D graphene foam as a next-generation biomaterial for the synthetic keratoprosthesis skirt.

Considering the advantages and disadvantages of the three commercial keratoprosthesis which have been discussed above, KeraMed Inc. (Sunnyvale, California) has introduced a newer design to address the limitations of previous keratoprostheses while retaining their advantages. KeraKlear Artificial Cornea is a one-piece keratoprosthesis without any need for a donor cornea. Moreover, using only acrylic material allows KeraKlear to be foldable and injectable. However, its implantation is technically challenging, and further investigations are needed to overcome these challenges (Pineda, 2015). Besides, KeraKlear is a new product, and more clinical evaluation is necessary to ensure its safety and efficacy. To summarize the above discussions, the keratoprostheses are compared with two other recently introduced artificial corneas in **Table 1** and **Figure 3**.

CORNEAL WOUND HEALING

Corneal wound healing, like wound healing in general, is a complex and dynamic process which is divided into four phases: the hemostasis, inflammation, cell proliferation, and remodeling phases. In fact, wound healing involves the interaction of various different cell lineages and a choreographed series of cellular events resulting in the replacement of the missing tissue or cellular structures. The cornea has special characteristics, which are important to consider in choosing a treatment strategy for wound healing. The most prominent characteristics of the cornea include its limbus zone, its lack of blood vessels, and its immune privilege (see **Figure 4**). As a result, current studies in corneal wound healing treatment have focused on a corneal characteristic like an immune response, avoiding angiogenesis and modulating cell signaling. In this section, topics related to angiogenesis and immune privilege, such as blocking immune signaling pathways, exosomes, biopolymers, growth factors, and use of amniotic membrane, will be discussed. New approaches to corneal wound healing related to the limbus zone will be reviewed in the following section (Simpson et al., 2019).

Corneal Immune Privilege and Avoidance of Angiogenesis

Generally, the transparency and avascularity of the cornea are essential for proper vision. The main factors, which are threatening the corneal clarity are inflammatory reactions, neovascularization, and limbal deficiency. As a result, avoiding angiogenesis, maintaining immune privilege, and supporting the limbus zone are strategies that have been investigated to combat processes that endanger corneal transparency. Immune privilege describes the natural lack of inflammation in the cornea, but when wound healing is taking place, the immune response needs to be modulated and limited. The influx of inflammatory cells causes scar formation and destruction of the limbus zone. Since there is a naturally enhanced production of proangiogenic factors during wound healing (Cursiefen, 2007; Ellenberg et al., 2010),

TABLE 1 | Comparison of major clinically used keratorostheses.

	Core material	Skirt material	Surgery stages	Further studies on	References
B-KPro	Donor cornea with PMMA	Titanium	1 stages	Improve adhesion between the cornea and the prosthesis	Lee et al., 2017
OOKP	PMMA	Tooth, Tibia	2-3 stages	Replace the biological part	Hille, 2018
Alphacor	PHEMA	Porous PHEMA	2 stages	Improve adhesion between the cornea and the prosthesis	Jirásková et al., 2011
KeraKlear®	Hydrophilic acrylic polymer	Hydrophilic acrylic material	1 stages	Improve adhesion between the cornea and the prosthesis (biointegration)	Pineda, 2015
MICOF*	PMMA	Titanium	2 stages	Improve adhesion between the cornea and the prosthesis (biointegration)	Wang et al., 2015; Ma et al., 2017
Miro Cornea®	Hydrophobic acrylic polymer	Hydrophobic acrylic polymer	1 stages	Improve adhesion between the cornea and the prosthesis (biointegration)	Schrage et al., 2014

**Moscow eye microsurgery complex in Russia.*

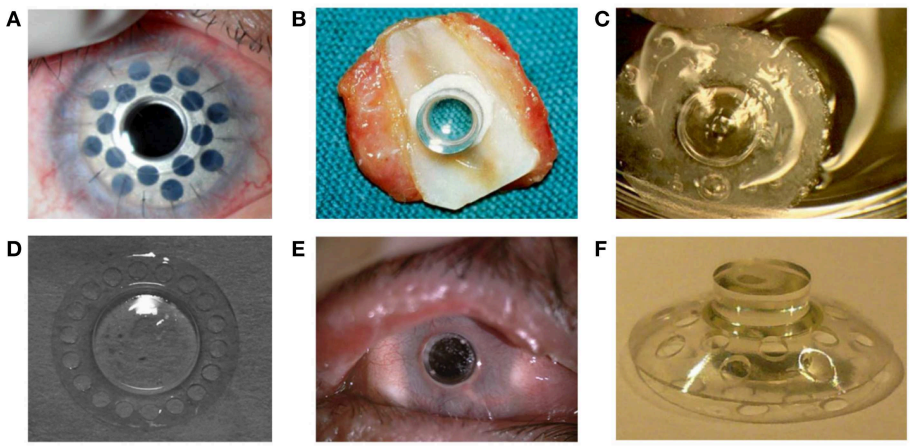

FIGURE 3 | (A) Boston keratoprosthesis Type I with titanium back plate. Reprinted with permission from Dohlman et al. (2014). **(B)** Osteodental-acrylic complex with polymethyl methacrylate optical cylinder. **(C)** Both core and skirt are shown in this picture. The skirt is white due to collagen incorporated in the pores. The clear ring between the center and the skirt shows interdigitation between the two components. **(D)** Front profile of the KeraKlear keratoprosthesis demonstrating the 18-hole peripheral design with 4.0 mm central optic. Reprinted with permission from Cortina and De La Cruz (2015). **(E)** MICOF KPro is composed of two parts: a titanium frame and a central PMMA cylinder. Reprinted with permission from Huang et al. (2012). **(F)** MiroCornea UR keratoprosthesis. Reprinted with permission from Duncker et al. (2014).

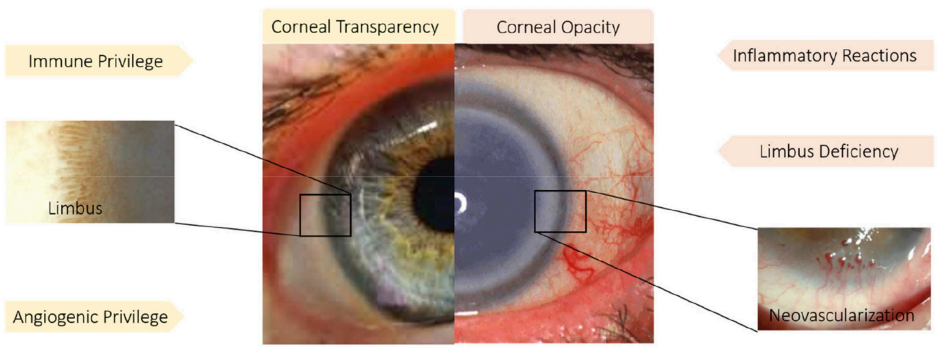

FIGURE 4 | Immune and angiogenic privilege besides limbus structure play a pivotal role in corneal transparency. While inflammatory reaction, neovascularization and limbus deficiency endanger corneal transparency. Reprinted with permission from Ellenberg et al. (2010) and Haagdorens et al. (2016).

actions need to be taken to restrict the undesirable growth of blood vessels into the cornea. In the following section, recent studies on this issue will be discussed.

Blocking Immune Signaling Pathways

Aggressive inflammatory responses following ocular injuries often tend to impair corneal re-epithelization which results in loss of corneal transparency and impairment of vision. Immune responses in cornea have been studied extensively in the context of the role of epithelial cells and immune signaling pathways that are involved. One of the most recognized immune signaling pathways is the inflammasome pathway which is activated in the wound healing response (Schroder and Tschopp, 2010). Recently, Bian et al. described a novel inflammasome signaling pathway which is activated in damaged corneal epithelial cells. They also suggested that blocking this pathway could result in a reduced inflammation which would improve the wound healing and the corneal transparency (Bian et al., 2017).

Exosome

Corneal epithelial cells (besides their ability to renew themselves) play a pivotal role in wound healing by carrying out intercellular signaling and communication with stromal cells. Exosomes are cell-derived nanoscale vesicles containing bioactive molecules, which mediate intracellular signaling (Cocucci et al., 2009; Han et al., 2015a). Han et al. have focused on the role of exosomes in corneal wound healing. In their recent study (Han et al., 2017), they characterized corneal epithelial cell-derived exosomes. Their findings indicate the role of exosomes derived from corneal epithelial cells in mediating the intercellular communication between the epithelium and the stroma during corneal wound healing. These exosomes may serve as a therapeutic strategy for the corneal repair.

Biopolymers

Common treatments for corneal epithelial defects include artificial tears and lubricants which reduce the mechanical stress and inflammatory cytokines. Inhibiting the inflammatory responses may result in the acceleration of corneal wound healing (Zarrintaj et al., 2018d). Inasmuch as biopolymers have shown promising results in tissue engineering and wound healing, their deployment in corneal wound healing has attracted lots of attention (Gholipourmalekabadi et al., 2018; Zarrintaj et al., 2018c). Chitosan, hyaluronic acid, silk fibroin, and polyarginine are among the most studied biopolymers for corneal wound healing. Chitosan and its derivatives have a large number of applications in the human body in various forms, such as scaffolds, drug carriers, and wound dressings (Dai et al., 2011; St. Denis et al., 2012; Oryan and Sahvieh, 2017; Sigroha and Khatkar, 2017). In regard to corneal wound healing, Cui et al. (2017) recently have reported a mechanism by which chitosan could promote corneal wound healing. Their findings showed that the chitosan-stimulated epithelial wound healing was partially mediated through the activation of the extracellular signal-regulated kinase (ERK) pathway. ERK signaling plays a pivotal role in cell proliferation, migration, and differentiation. Chitosan and its derivatives have also been studied as a drug carrier in ocular wound healing (Schmidl et al., 2017; Rahmati and Mozafari, 2019a). Fischak et al. (2017) studied the effects of chitosan-N-acetylcysteine (C-NAC), a new biopolymer, on corneal wound healing. The results showed a faster wound healing due to the specific chemical and biological properties of C-NAC. Other chitosan compositions which have been investigated for corneal wound healing are chitosan-based hydrogels. These hydrogels may either serve as drug carriers (Tsai et al., 2016) or as tissue adhesive materials for hemostasis or wound healing (Deng et al., 2010; Lih et al., 2012; Wicklein et al., 2019).

Hyaluronic acid is one of the abundant polysaccharides in the human body and plays a significant role in corneal wound healing. *In vitro* and *in vivo* studies have confirmed the ability of hyaluronic acid to promote wound healing (Neuman et al., 2015). Zhong et al. (2016) studied the mechanism by which exogenous hyaluronic acid promotes corneal wound healing. They studied the expression level of cytokines like Cluster of differentiation (CD44), interferon (IFN), interleukin 1 beta (IL-1β), and matrix metallopeptidase 9 (MMP-9). Hyaluronic acid down-regulates the expression of inflammatory cytokines and up-regulates the expression of anti-inflammatory cytokines associated with the tissue repair and healing. Though, despite the confirmed effects of hyaluronic acid on promoting corneal wound healing, Gronkiewicz et al. (2017) reported that the topical addition of hyaluronic acid, in combination with standard medical management of corneal ulcers, did not accelerate wound healing.

Fibroin is an insoluble protein derived from the fibers of silk. Hydrophobic domains in the primary sequence of amino acids in fibroin generally result in this protein adopting a β-sheet structure (Vepari and Kaplan, 2007; Mohammadi et al., 2017; Rahmati and Mozafari, 2018). Lui et al. studied fibroin as a 2D and 3D-scaffold for corneal stromal engineering applications (Liu et al., 2012) and as a carrier for exogenous application of corneal epithelial cell sheets (Lawrence et al., 2009). Recently, Abdel-Naby et al. (2017) evaluated the influence of fibroin on epithelial cell migration, proliferation, and adhesion. Their results indicated that fibroin might directly enhance wound healing by both stimulating epithelial proliferation and positively impacting the cell migration rate.

Polyarginine is a short cationic polypeptide, which can translocate through cell membranes; as a result, it has attracted much attention as a drug carrier. Some studies have shown that the presence of guanidinium moieties in the backbone of polyarginine, which interacts with anionic groups on the cell membrane through hydrogen bonds and hydrophobic forces, results in the cell-penetrating property of polyarginine (Takechi et al., 2012). Studies of polyarginine as a nanocarrier have significantly increased in recent years, and it has emerged as a new strategy to accelerate wound healing (Gonzalez-Paredes et al., 2017). Reimondez-Troitiño et al. (2016) designed and evaluated polyarginine nanocapsules to improve corneal wound healing. Their findings showed that polyarginine had an intrinsic capacity to promote corneal wound healing through the transforming growth factor beta /SMAD (TGF-β/SMAD) signaling pathway.

Amniotic Membrane (AM)

Both fresh and preserved human amniotic membranes have been investigated as naturally occurring biomaterials in tissue reconstruction, especially for the ocular surface. AM is one of the thickest basement membranes that exists in the human body, with the ability to promote epithelial cell healing, besides inhibiting fibroblast proliferation and myofibroblast differentiation. In addition, it contains several anti-angiogenic, anti-inflammatory, and neurotrophic factors (Ramachandran et al., 2019). At present, AM transplantation has been used for various indications including repairing persistent epithelial defects and treating corneal ulceration, limbal stem cell deficiency, acute Stevens Johnson Syndrome (SJS), chemical and thermal burns, infectious keratitis, and after refractive surgery (St. Denis et al., 2012; Manolova et al., 2017; Prabhasawat, 2017; Westekemper et al., 2017). Despite the fact that during the last decades, AM transplantation has been a gold standard for the treatment of a variety of ocular surface diseases, AM transplantation still has several disadvantages. Therefore, multiple efforts have been made to address these downsides. One of the disadvantages is related to the surgical procedure that has several problems. The precise conditions, under which the AM is prepared, affects its biomedical applications (Islam et al., 2018). Wu et al. (2017) analyzed the effect of two different methods of preparations of AM on human corneal epithelial cell (HCEC) viability, migration, and proliferation *in vitro*. Their study showed that biochemical factors (Keratinocyte growth factor (KGF), Fibroblast growth factor-basic (FGFb), Hepatocyte growth factor (HGF), and TGF-β1) released from the AM preparation had a complex, possibly non-linear effects, on HCECs. In another study Ogawa et al. identified an active matrix component [Heavy chain-hyaluronan/pentraxin3 (HC-HA/PTX3)] that was shown to exert the anti-inflammatory and anti-scarring effects of AM. Their studies revealed that subcutaneous and subconjunctival injection of HC-HA/PTX3 might be a novel approach in the treatment of ocular disease (He et al., 2017a; Ogawa et al., 2017). Recently, this group developed eye drops containing morselized and cryopreserved AM, and also an umbilical cord preparation to understand their therapeutic potential in promoting corneal re-epithelization and restoring the regularity of the corneal surface (Tighe et al., 2017).

Pharmaceutical Agents

Pathological angiogenesis that occurs in the proliferative phase of corneal wound healing leads to a reduced corneal transparency and loss of vision via lipid deposition and scar formation. Neovascularization is closely related to the angiogenic signaling pathway, which is initiated by the infiltration into the cornea of large numbers of neutrophils and macrophages. Several studies have shown the potential benefit of using anti-angiogenic agents to inhibit corneal neovascularization. Different methods have been suggested to inhibit the development of corneal neovascularization like genetic ablation of the chemokine receptor CCR2 (Ambati et al., 2003) and to control pro-angiogenic factors (Baradaran-Rafii et al., 2017). Zerumbone is a cyclic terpene which is isolated from the rhizomes of wild ginger. Presently, zerumbone has been extensively studied for its antitumor, anti-inflammatory, antimicrobial, and anti-angiogenic activities (Rahman et al., 2014). Kim et al. (2017b) recently examined the effects of zerumbone on chemokine-related macrophage infiltration in the corneal wound healing process. Their results indicated that zerumbone prevented angiogenesis and fibrosis through the inhibition of inflammatory cells activation.

Anti-inflammatory agents like corticosteroids have long been topically applied for the treatment of ocular inflammation. However, they show a low therapeutic efficacy in the treatment of neovascularization, because of their poor corneal permeability, and lack of bioavailability (Mozafari, 2014). Various drug delivery systems like viscous solutions, nanoparticles, carbon nanotubes, micelles, liposomes, and hydrogels have been proposed to overcome the aforementioned problems (Karimi et al., 2015a,b, 2016a,b,c; Weng et al., 2017). Recently, Nagai et al. (2017) designed a new type of solid nanoparticles based on zirconia beads containing dexamethasone, to improve drug permeability through the cornea. These solid nanoparticles facilitated topical passage of dexamethasone through the barriers of the eye. With the goal of combining the prevention of neovascularization and reduction of inflammation, Huang et al. (2017) designed a supramolecular hydrogel for co-delivery of dexamethasone sodium phosphate and Avastin® (an antiangiogenic agent). The supramolecular hydrogel was composed of MPEEG-PCL micelles and α-cyclodextrin (an oligosaccharide cage). The *in vivo* studies showed that this supramolecular hydrogel significantly attenuated the inflammatory response and inhibited neovascularization through downregulation of the vascular endothelial growth factor (VEGF), CD31, and alpha-smooth muscle actin (α-SMA) expression.

Natural tears have trophic effects on epithelial cells because they contain vitamins, immunoglobulins, proteins, growth factors, and electrolytes (Grigoryeva et al., 2013). "Autologous serum eye drops" contain several essential nutrients like growth factors, vitamins, cytokines, proteins, and lipids that may assist in corneal re-epithelization. In addition to autologous serum, bandage-type contact lenses have been studied for repairing the corneal epithelial defect. Bandage contact lenses prevent the mechanical tension associated with blinking, therefore reducing necrosis and desquamation of the corneal epithelium (Ho and Mathews, 2017). Several studies have been done to combine the therapeutic effects of autologous serum and bandage contact lenses (Schrader et al., 2006; Choi and Chung, 2011). In a recent study, Wang et al. (2017) described the therapeutic outcomes of a combination of a topical 20% autologous serum and a silicone hydrogel contact lens in 12 patients during a 3-month follow-up period. All patients suffering from post-infection corneal epithelial defects were successfully treated; "corneal melting" during acute disease was successfully prevented. Studies have shown that breast milk performs similarly to autologous serum and natural tears. Thus, breast milk may accelerate epithelial wound healing because it contains anti-infection agents and growth factors. In one study, Asena et al. (2017) compared human breast milk with autologous serum and artificial tears in corneal epithelial wound healing. Their results showed that the presence of growth factors like TGF-β, insulin-like growth

factor-1 (IGF-1), lipids, and vitamins in breast milk played important roles in epithelial and stromal wound healing in the cornea.

A novel therapeutic approach, described by Bazen and his colleague at Louisiana University, employed a neurotrophic and anti-angiogenic factors (pigment epithelium-derived factor [PEDF]) combined with an essential fatty acid (docosahexaenoic acid, DHA] stimulated nerve regeneration in diabetic keratopathy (Bazan et al., 2014; He et al., 2015). In their recent study, they evaluated the therapeutic effects of topical application of PEDF and DHA over 2 weeks on the regeneration of the corneal sensory nerve in both wounded and unwounded diabetic corneas. They proposed some possible mechanisms for their results including neuroprotective and anti-oxidant actions of the PEDF+DHA, neurotrophic function, and the anti-inflammatory activity of this treatment. **Figure 5** shows promoted wound healing on days one and two after injuries in the PEDF+DHA treated corneas (He et al., 2017b).

Another pharmaceutical agent, which has recently gained much attention, is a new type of extracellular matrix agent called ReGeneraTingAgent or RGTA (Arvola et al., 2016; Chappelet et al., 2017; Robciuc et al., 2018). This approach consists of engineered polymers designed to protect and replace cellular signaling proteins of the extracellular matrix (ECM), such as heparan sulfate. This unique property encourages the reconstruction of the ECM; therefore facilitating tissue wound healing (Barritault et al., 2017). Recently Gumus et al. (2017) investigated the topical effects of a biodegradable nanopolymer (alpha 1-6 polycarboxymethyl-sulfate) to mimic heparan sulfate in order to accelerate corneal re-epithelization and stromal healing, after epi-off corneal cross-linking technique. In fact, RGTAs were engineered to bind to heparan sulfate binding sites on proteins of the ECM. These agents are large enough to bridge between neighboring matrix proteins and recreate a cellular microenvironment and a microniche, where cells can respond appropriately to the cascade of signals involved in the wound healing process.

Many investigations have emphasized the role of several growth factors like platelet-derived growth factor (PDGF), VEGF, TGF-β, HGF, and tumor necrosis factor-beta (TNF-β) in the wound healing process. Among these growth factors, PDGF, TGF-β, and HGF played a pivotal role in modulating cell proliferation and myofibroblast differentiation. There is extensive literature available concerning the role of growth factors in corneal wound healing (Gallego-Muñoz et al., 2017; Sriram et al., 2017). In fact, a better understanding of the role of growth factors in corneal wound healing would likely lead to the development of new treatments. In one of the corresponding studies, Omoto et al. (2017) reported the effects of topical administration of HGF on inflammation of corneal epithelial cells. Their results demonstrated that topical application of HGF promoted corneal epithelial cell proliferation which was revealed by higher expression of the Ki-67 and p63 proliferation markers in HGF-treated mice. In addition, HGF treatment reversed the anti-proliferative effect of IL-1β *in vitro*, indicating that HGF actively suppressed the inflammatory environment in the corneal epithelium. On the other hand, HGF significantly reduced the infiltration of CD45+ inflammatory cells in the cornea (see **Figure 6**).

Limbus Zone

The limbus of the cornea forms a border between the corneal and conjunctival epithelium and its limbal stem cells (LSCs) are essential in the maintenance and repair of the adult cornea as they support the repair and regeneration of corneal epithelial tissue. In fact, this undulated limbal region is considered to be a niche for LSCs, which play a critical role in the corneal wound healing process. In limbal tissue engineering, like the other tissues, three factors affect the regeneration of injured tissues: cell availability, suitable and biocompatible scaffolds, and the presence of growth factors. In corneal disorders, depletion or the absence of LSCs results in impairment of the corneal wound healing process. Regarding tissue engineering, there are three approaches to remedy this deficiency. The first approach is cell transplantation using the desired cell population obtained in tissue culture. This approach has been considered as a type of corneal transplantation that was briefly discussed in the previous section. The second approach is cell transplantation using cells such as corneal epithelial, where stem cells are dissociated, cultivated on a supportive matrix (biosynthetic scaffold) like an amniotic membrane, fibrin gel or polymers, and then injected into the desired location in the cornea. The main problem in the last approach is the lack of stem cell enrichment because the stem cells which are used for transplantation contain heterogeneous cell populations. This deficiency might result in a graft failure (Rajendran et al., 2017). As an alternative solution, a few groups have recently focused on a new approach by mimicking the LSC microenvironment (niche) in which the LSCs live. In this section, new progress and emerging alternatives related to the second and third approaches will be discussed. Moreover, in order to get a broad overview of the subject, **Figure 7** covers the evolutionary pathway of limbus regeneration over the past four decades.

Cell Transplantation

Using the bioengineered cornea is an alternative approach to addressing the aforementioned restrictions of corneal transplantation and artificial corneas. In most articles, tissue engineering of the outermost layer of the eye is known as ocular surface regeneration. In this approach, the optical and biomechanical characteristics of the tissue-engineered cornea are essential. For instance, tissue engineered cornea must be transparent and withstand about 10–20 mm Hg of intraocular pressure. Therefore, biomaterial selection to produce appropriate scaffolds is an ongoing subject of investigation due to the emergence of tissue engineering. The main approaches in corneal tissue engineering to repair corneal defects can be divided into full thickness, stromal, epithelial, and endothelial types of regeneration. All of them involve the aid of a scaffold in combination with different cell types. Recent advances in corneal tissue engineering have been reviewed by Ghezzi et al. (2015). Meanwhile, the most studied biomaterials are amniotic membrane, collagen matrix, hydrogels, and other natural and synthetic polymers. After choosing the necessary materials, the physical, chemical, and biochemical modification

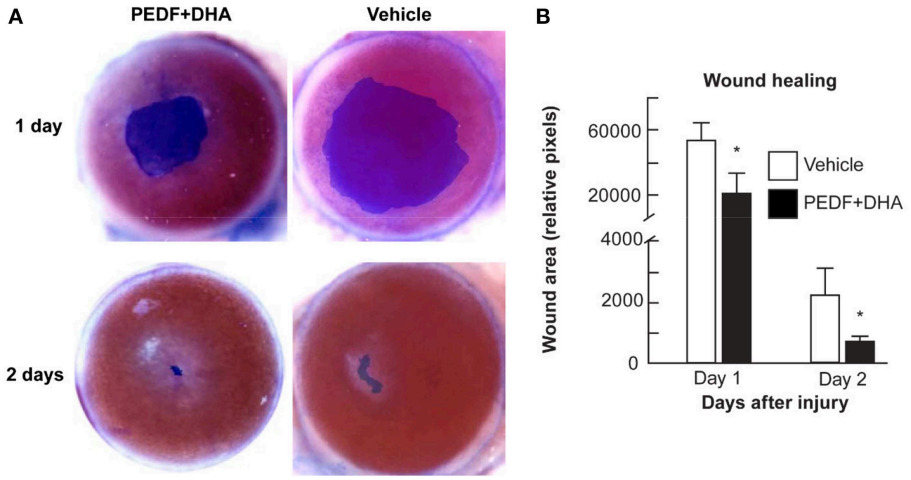

FIGURE 5 | Effect of PEDF+DHA treatment on wound healing in diabetic corneas. The right eyes of 16 mice with hyperglycemia for 10 weeks were injured and divided randomly into two groups and treated for 1 or 2 days with PEDF+DHA or vehicle. **(A)** The wounded corneas were stained with 0.5% methylene blue and photographed with a surgical microscopy through an attached digital camera. **(B)** Wounded area. Data is expressed as mean ± SD (*$p < 0.05$, $n = 4$ mice/group). Reprinted with permission from He et al. (2017b).

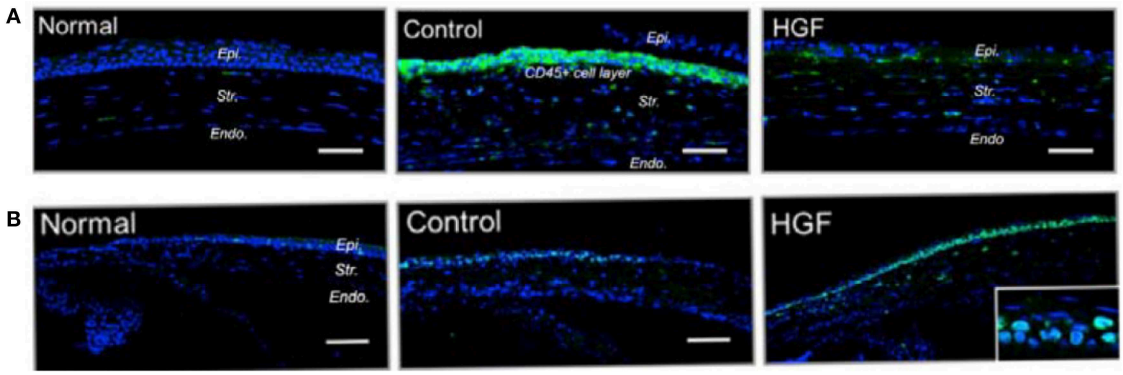

FIGURE 6 | Mechanical injury was induced in murine corneas by scraping the epithelium and either topical recombinant hepatocyte growth factor (HGF) was applied twice daily. Normal corneas without injury or injured corneas receiving MSA served as controls. Corneas were harvested at day 3 after injury. **(A)** Representative immunofluorescent images of sections of mouse cornea stained for Ki-67 (green) showing proliferating cells (scale bar, 100 mm). **(B)** Representative immunofluorescence images of corneal cross sections showing higher expression of CD45 (green) in MSA-treated controls, compared to HGF-treated eyes (scale bar, 50 mm). Reprinted with permission from Omoto et al. (2017).

of these materials play a pivotal role in the results. In this section, we have tried to review these modifications (Ismail et al., 2019; Wijnholds, 2019).

Amniotic membrane (AM)

Due to the specific characteristics which were described in detail in the last section, the gold standard substrate for the *ex vivo* expansion of LSCs remains AM. In recent years, different studies have focused on AM as a biological carrier in *ex vivo* reconstruction and transplantation of tissue engineered corneal epithelium (Sabater and Perez, 2017). Various aspects of this strategy have been investigated. One of these aspects is the relative transparency of the AM. In fact, AM features lower clarity than human cornea, and this lack of transparency restricts the use of AM as a carrier in corneal epithelial tissue engineering. Zhang et al. (2016) proposed a thinning protocol for the generation of ultra-thin amniotic membrane. The prepared AM was transparent and composed of a compact transparent layer which made it an ideal carrier for the construction of tissue engineered corneal epithelium (see **Figure 8**). Another challenge in using the AM is its potential to transmit infectious disease. Decellularization processes have been applied to various types of tissue for laboratory investigations and clinical applications. The most important aspects of any tissue decellularization protocol are to eliminate the risk of immune rejection and disease transmission, while at the same time retaining the underlying ECM structure. In this regard, Figueiredo et al. (2017) studied the potential use of decellularized human amniotic membrane

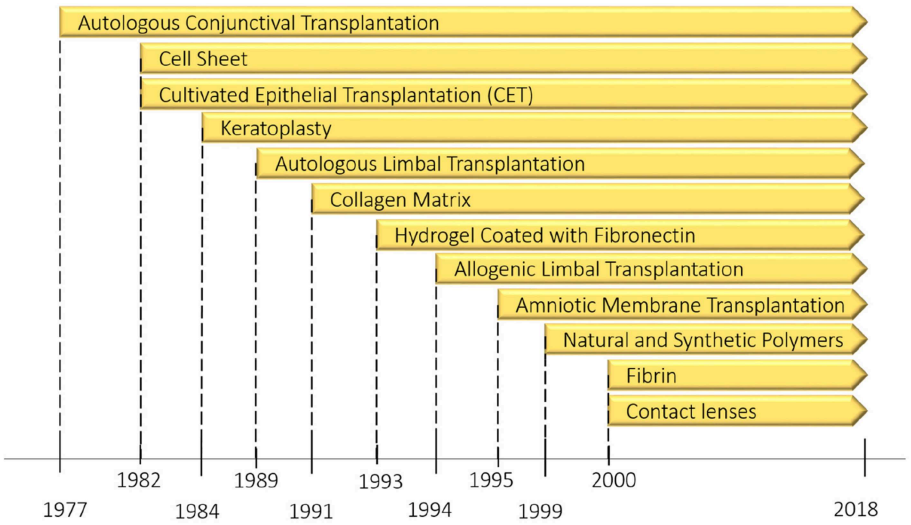

FIGURE 7 | The evolution pathway of ocular surface reconstruction investigations which started with autologous conjunctival transplantation in a patient with bilateral alkali burn in 1977 and have been continued with other methods specially limbus regeneration over the past four decades. Partially reprinted with permission from Nakamura et al. (2016).

for the *ex vivo* expansion of LSCs. They also evaluated, using gamma irradiation as a final sterilization step, the potential minimization of risk regarding disease transmission. Their results showed that *ex vivo* expansion of LSCs using an explant culture system occurred at a faster rate on decellularized human AM in comparison with fresh human AM. Human amniotic membrane is in clinical trials for corneal wound healing (Zakaria et al., 2014).

Fibrin gel

Fibrin was first introduced for wound healing applications in the form of tissue glue or engineered sheets. Fibrin is a natural protein involved in blood coagulation and, because of its biocompatibility, biodegradability, and its potential in wound healing, has attracted much interest in corneal wound healing (Ronfard et al., 1991; Pellegrini et al., 1999). In corneal surface reconstruction fibrin has been used as a glue for tissue adhesion or as a fibrin gel acting as a carrier of LSCs. The first studies on fibrin gel were carried out in early 2000s by Rama et al. (2001), Ronfard et al. (2000), Duchesne et al. (2001), and Han et al. (2002). Among these groups, Rama et al. published a long term follow-up (up to 10 years) in 2010, and their results showed that the renewal of corneal epithelium was attained in 76.6% of 112 patient eyes (Rama et al., 2010). Rama et al. also studied the 3T3 cell line cultured on fibrin matrix as a feeder-layer which could supply metabolites to the LSCs. Recently, Lužnik et al. (2017) have studied the possibility of omitting the feeder-layer to achieve the xeno-free scaffold. Fibrin gel is in the clinical trial to investigate the cultivated oral mucosal epithelial cell sheet transplantation (COMET) of substrate-free cell sheets on reconstructing the ocular surface. In the study, fibrin-coated dishes with proteins inhibitor was used to adjust the degree of fibrin degradation (Hirayama et al., 2012). Nevertheless, studies on fibrin as a matrix have been overshadowed by other types of natural and synthetic polymers.

Natural and synthetic polymers

Natural and synthetic polymers have been the subject of several studies aiming to find a suitable carrier for the transfer of stem cells. In this regard, various polymers like hydrogels, self-assembling peptide nanofibers, collagen matrix, conductive polymers, and thermosensitive polymers have been studied (Deng et al., 2010; Zarrintaj et al., 2018a,b). Mechanical strength and transparency are the most important considerations in order to reconstruct the injured cornea (Fagerholm et al., 2010; Mozafari et al., 2019; Wicklein et al., 2019). In **Table 2** pioneering studies on polymers as a substrate for corneal tissue engineering are summarized.

Contact lens

Despite the promising clinical outcomes of AM and fibrin gel, the study of other transplantation procedures has been continued. Among them, the carrier-free transfer method (cell sheets), and the use of a contact lens have gained more attention as they reduce the risk of xenobiotic infections and side effects from using non-Food and Drug Administration (FDA) approved biomaterials. Girolamo's group developed a novel autologous technique by using an FDA-approved soft contact lens as a carrier and bandage to protect the eye during LSC transplantation, thereby promoting corneal repair and regeneration (Di Girolamo et al., 2009). Their cell-laden siloxane-hydrogel contact lens was successful in reconstituting a healthy ocular surface in 16 patients with limbal stem cell deficiency (LSCD) (Bobba et al., 2015). Studies by several groups have reported attempts to modify the tissue adherence to the carrier, and to vary the stem cell type in order to improve the efficiency of the explant culture

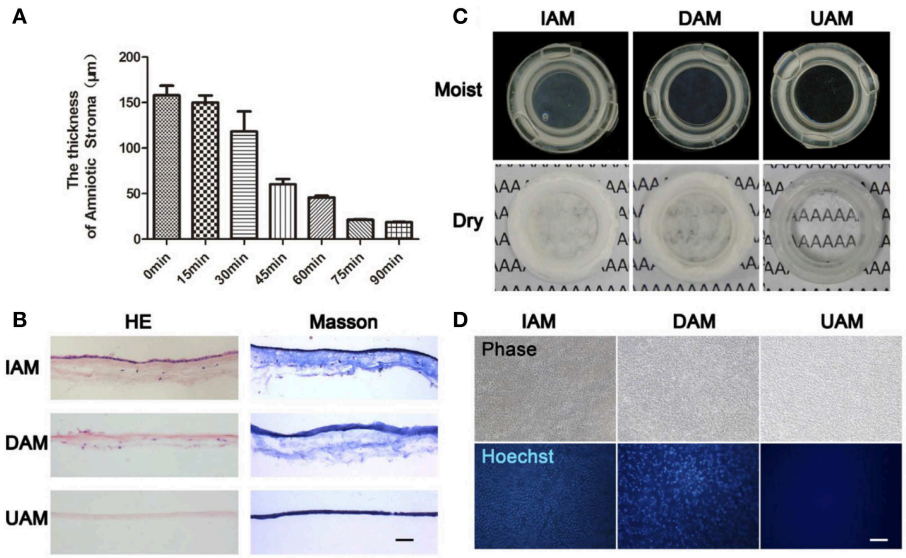

FIGURE 8 | The characteristics of ultra-thin amniotic membrane. **(A)** The thickness change of amniotic membrane after digestion with collagenase type IV for different time durations. **(B)** HandE and Masson trichrome staining of IAM, DAM, and UAM tissues (Bar: 100 μ m). **(C)** Macroscopic views of IAM, DAM, and UAM were evaluated by photography scanning in moist form and light microscope in freeze dry form. **(D)** Hoechst whole mount staining of IAM, DAM, and UAM (Bar: 100 μ m). Reprinted with permission from Zakaria et al. (2014).

system. Tóth et al. (2017) tested several methods for affixing the cells to prevent them from "floating off" the contact lens. Their results showed that in comparison with cyanoacrylate, silicon, and fibrin glue, suturing was the most efficient method to improve tissue adherence. In treating bilateral LSCD, the oral mucosal epithelium was shown to be a suitable autologous stem cell source. Accordingly, Zsebik et al. (2017) cultured human oral mucosal epithelium as a source for cell expansion on a lotrafilcon (a contact lens). They claimed that they established a xenobiotic-free culture system from human oral mucosal explants on the contact lens surface.

Cell sheet

Over the past 30 years, conventional tissue engineering approaches (like the use of biodegradable scaffolds and/or injection of isolated cell suspensions) have been successful in the regeneration of different tissues (Koizumi and Okumura, 2019). However, these tissue engineering approaches still face some obstacles when applied for reconstruction of the ocular surface. There is a significant risk of infection when biological materials are employed, the attachment to the replacement site can be insufficient and can lead to degradation and loss of optical transparency. Sheet-like cell assemblies were introduced as a method to address these limitations (Green et al., 1979; Fagerholm et al., 2014). In this cell sheet technology, the desired cells are grown on a particular cell culture surface which allows reversal of cell adhesion, so an intact cell sheet can be transplanted to the host tissue without using scaffolds. In cell sheet technology several external stimuli have been applied to facilitate cell detachment like specific enzymes, temperature variation, magnetic force, electrochemical polarization, pH variation, polyelectrolytes, and illumination (Owaki et al., 2014). The cell sheet technique needs further study to become standardized before it can be used in routine clinical practices. One of the obstacles in this method is to find the optimal preservation medium to maintain the viability of the reconstructed tissue. Recently, Katori et al. (2016) introduced a new preservation medium for cell sheets (containing the antioxidant ebselen) derived from human corneal tissue and human oral mucosal epithelium. Another attempt to improve this technique was reported by Syed-Picard et al. (2018). They designed a highly organized structure with aligned microgrooves which directed parallel cell alignment, and allowed matrix organization, similar to that of native corneal stromal lamella (Buznyk et al., 2015). As a result, after transplantation of the engineered corneal tissues, the tissue sheets were incorporated into surrounding tissues and became transparent. A research group led by Okano at Tokyo University has studied the production of cell sheets from the corneal epithelium. They used a temperature responsive polymer to generate multilayered corneal epithelial sheets (Nishida et al., 2004a). Clinical results in four patients with the use of cultured autologous oral mucosal epithelial cell sheets showed that corneal transparency was restored, along with remarkable improvements in postoperative visual acuity (Nishida et al., 2004b). Recently they tried to optimize the cell sheet fabrication process in order to improve cell sheet quality and decrease risk of biological contamination. They developed a "cell cartridge" which acted as a closed culture system for regenerative medicine (Kobayashi et al., 2013; Nakajima et al., 2015). Self-lifting analogous tissue equivalent (SLATE) is a bio-fabricated, scaffold-free system which has been recently used in corneal tissue engineering. Peptide amphiphile used as

TABLE 2 | Natural and synthetic polymers used for corneal wound healing.

Carrier	Novelty	Target tissue	results	References
Gelatin/ascorbic acid (AA) cryogel	Using antioxidant molecule-mediated structure	Corneal stroma tissue engineering	Low-to-moderate AA loading demonstrated better capability to enhance tissue matrix regeneration and transparency maintenance in animal model.	Luo et al., 2018
Plastic compressed collagen gel/electrospun poly(lactic-co-glycolide) (PLGA) mats	Laser-perforating sandwich-like hybrid construct	Corneal epithelial and stroma tissue engineering	Co-culture of two kinds of cells for corneal tissue reconstruction	Kong et al., 2017
Aligned silk membrane	Multi-layered silk membrane with neuropeptide substrate	Corneal stroma tissue engineering	Differentiating periodontal ligament stem cells (PDLSCs) toward keratocytes	Chen et al., 2017
Silk/polyurethane hybrid nanofibrous	Using conjunctiva derived mesenchymal stem cell(CJMSCs) as a new source for differentiation	Corneal epithelial tissue engineering	Interconnected pore to accelerate nutrient diffusion with sufficient mechanical properties	Soleimanifar et al., 2017
Thermosensitive chitosan-gelatin hydrogel	Human stromal cell-derived factor-1 alpha (SDF-1 alpha) loaded	Corneal epithelial tissue engineering	Exogenous SDF-1 alpha promotes corneal epithelium reconstruction through increase local expression of other growth factor	Tang et al., 2017
Collagen type-I coated poly(lactic-co-glycolic acid) film	Using hybrid graft	Corneal endothelial tissue engineering	Limiting the probability of non-specific interaction between the construct and the biological environment	Kim et al., 2017a
Hyaluronic acid/pluronic hydrogel	Injectable hydrogel with porcine platelet rich plasma(P-PRP)	Corneal endothelial tissue engineering	Limiting hydrogel-induced cell death	Lin et al., 2017
Silk fibroin	Developing artificial endothelial graft	Corneal endothelial tissue engineering	Appropriate biological properties beside mechanical properties that allowed its use in a Descemet membrane endothelial keratoplasty	Vázquez et al., 2017
Poly(glycerol sebacate)PGS-poly (ε-caprolactone) PCL nanofibrous	Elastomeric biodegradable scaffold	Corneal endothelial tissue engineering	Semi-transparent and highly elastic aligned nanofibrous PGS-PCL blended scaffold	Salehi et al., 2017
Sequential hybrid crosslinking gelatin methacrylate	Hydrogel patterning with Nanoscale resolution	Corneal endothelial tissue engineering	Increased mechanical strength, transparent and provide adequate nutrient transport	Rizwan et al., 2017
Gelatin microcarriers Functionalized with oxidized hyaluronic acid	Using cell-containing microcarriers	Corneal stromal tissue engineering	Microcarriers well tolerated and can be degraded by endogenous enzymes following intracameral implantation	Lai and Ma, 2017
Short collagen-like peptides conjugated to polyethylene glycol	Using synthetic and customizable analogs	Corneal endothelial tissue engineering	Promoting corneal regeneration through stimulation of extracellular vesicle production by endogenous host cells that migrate into the scaffold	Jangamreddy et al., 2018

a surface template provides a platform to control the structural, mechanical, and biofunctional properties of the SLATE to replace damaged corneal tissue. In this study, SLATEs were implanted in a rabbit corneal. After a 9-months follow-up, SLATE was well integrated with surrounding hot tissue without a sign of rejection and provoking inflammation (Gouveia et al., 2017).

Artificial Limbus

"Form follows function" is a well-known concept accepted as a principle in the field of modernist architecture; although it is also universally observed throughout the nature. According to this principle, the shape of an object should be predominantly based upon its intended function or purpose (Griffith and Harkin, 2014; Ghaffari et al., 2016). The application of this principle in the engineering of limbus tissue can be translated into mimicking the three-dimensional morphological structure of tissues in order to provide a specific niche to support stem cells. In the last decade, an emphasis on the importance of architectural features in tissues is a sign that attention is being paid to this principle. Meanwhile, the study of the stem cell microenvironment (niche) and its highly regulated and specific structure has attracted more attention (Rahmati and Mozafari, 2019b). Stem cells are defined by their ability to self-renew and to participate in the regeneration of damaged tissues, and their niche exhibits distinct anatomical and biochemical features in comparison with their surrounding tissue. On the other hand, some studies have shown niche morphology was altered in limbal stem cell deficiency, caused by disease or increased age (Zheng and Xu, 2008; Lagali et al., 2013). Researchers have attempted to characterize and quantify the stem cell niche by various visualization methods, and to utilize these data to fabricate artificial niches for stem cells. Several techniques are now under investigation in order to mimic the niche structure for corneal repair (Ortega et al., 2012). In a recent study, Claeyssens et al. focused on the characterization and evaluation of the impact of the "Palisades of Vogt" structure on the function of limbal stem cells.

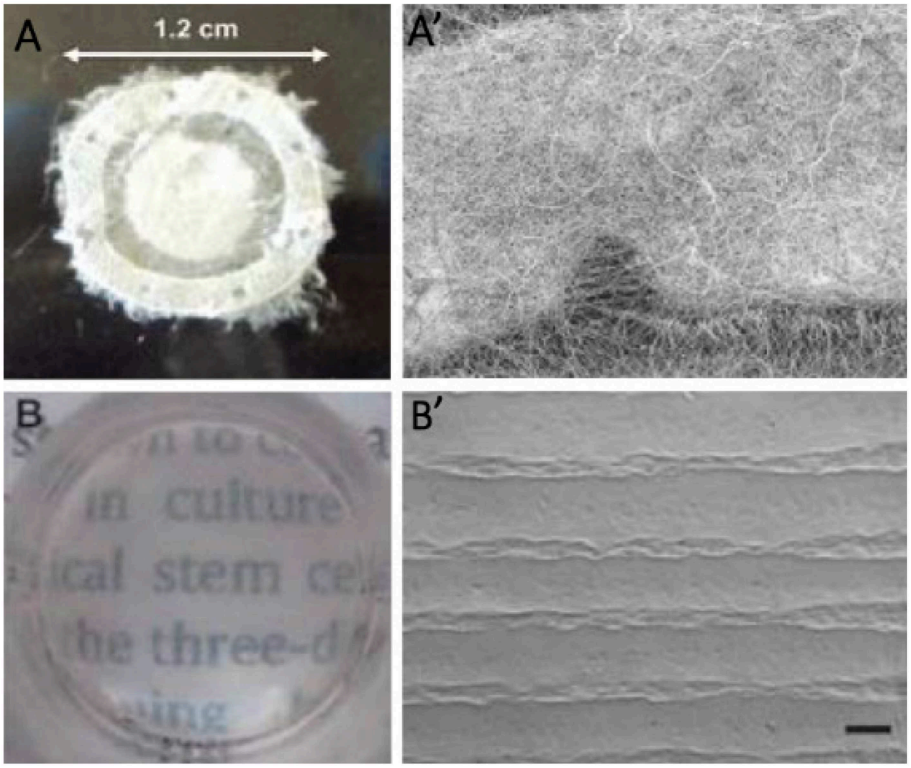

FIGURE 9 | (A) Detail of electrospun outer ring with 1.2 cm of diameter, **(A′)** SEM micrograph of a section of the electrospun scaffold showing a horseshoe electrospun micropocket. **(B)** Stability and transparency of cultured RAFT (Ortega et al., 2013b). **(B′)** SEM image of bioengineered limbal crypts on the RAFT surface. Scale bar 200 μm. Reprinted with permission from Levis and Daniels (2016).

They combined micro-stereolithography and electrospinning to fabricate PLGA rings containing microfabricated pockets. In this study, they reported the physical and protective properties of the niche. Their results showed that micropockets of the PLGA ring played a pivotal role in cell migration and directionality (Ortega et al., 2013b, 2014a,b). They also studied the fabrication of polyethylene glycol diacrylate rings containing microfeatures, which were modified by biotinylated fibronectin. In their study, the use of ECM proteins stimulated limbal cell outgrowth and migration (Ortega et al., 2013a). Levis group at UCL Institute of Ophthalmology have developed a method to create bioengineered limbal crypts with a functional 3D niche architecture (Levis et al., 2013). This novel process for production was referred to as "Real Architecture For 3D Tissue" or RAFT^{TM}. **Figure 9** illustrates two kinds of cultured RAFT limbal crypts. This new 3D cell culture system uses physiologically relevant concentrations of collagen to create the most natural environment for cells. The custom molded micro-ridges on the surface of the thin collagen resembles the dimensions of the stromal crypts in the human limbus. They also studied the effect of the 3D topography and ECM markers on the human limbal epithelium. The bioengineered limbal crypts expressed putative limbal epithelial stem cell markers like ΔNp63a and BMi1 and also produced basement membrane proteins like laminin-β1 and laminin-γ3 (Massie et al., 2014; Levis and Daniels, 2016).

CONCLUSION AND FUTURE OUTLOOK

From the earliest concepts such as replacement of the opaque cornea, to cornea wound healing and regeneration, ophthalmologists, and material scientists worldwide have faced a variety of challenges. Advances in visualization techniques and histology have made significant progress in the fundamental understanding of cornea structure and its microenvironment. Due to this valuable information and nanotechnology advances, therapeutic strategies in devastating corneal diseases have turned from corneal replacement into corneal wound healing and regeneration (Kargozar and Mozafari, 2018). Consequently, studies on the limbus zone and immune and angiogenic privilege have attracted more attention. In addition, the exploration of cell signaling in the natural process of wound healing and the attempts to mimic this process have opened new horizons in corneal disease treatment.

Most of the suggested treatments have shown promising results for wound healing at the ocular surface, and entire thickness dystrophies were neglected. While, in order to reduce transplantation of a donor cornea, tissue engineering of the whole thickness of the cornea must be considered. Corneal stromal and endothelium tissue engineering have recently shown noticeable progress (Matthyssen et al., 2018). However, more focus is needed on biomimetic strategies, like employing a combination of cell

signaling agents with tissue engineering. Rho-kinase (ROCK) inhibitor is a serine/threonine protein kinase that participates in regulating cell signaling pathway. Recently ROCK has been introduced as an innovative therapeutic agent for corneal endothelial dystrophy (Han et al., 2018). The compilation of these approaches can be a promising method for visual rehabilitation in patients suffering from corneal dystrophies.

Until now, most studies have worked on introducing new materials and biochemical approaches in cornea wound healing and regeneration; while paying attention to physical properties of these approaches might be a leap in this area. For instance Long et al. have tried to use a cross-linking agent in collagen membrane to regulate collagen fibril spacing and therefore improve optical clarity of collagen and increase permeability of neurites (Long et al., 2018). Hence, advances in visualization techniques will help to improve corneal physical structure identification that, in combination with material science, will lead to new sights in the typical treatment approaches. Slip-lamp biomacroscopy, optical coherence tomography (OCT), *in vivo* confocal fluorescence microscopy, and full-field optical microscopy are part of visualization techniques which help to quantify corneal architecture (Grieve et al., 2015; Werkmeister et al., 2017). According to previous studies, investigation on visualization methods would boost corneal medical treatments.

Considering the remarkable role of stem cells in tissue regeneration, a large part of future studies is expected to focus on the deployment of stem cells on cornea wound healing and regeneration (Rahmati et al., 2018). Several studies have been done to isolate and characterize multipotent stem cells from various tissues in order to use their great potential in regenerative medicine. Bone marrow-derived mesenchymal stem cells (Islam et al., 2018), human umbilical cord mesenchymal stem cells (Yamashita et al., 2018), postnatal periodontal ligament (Yam et al., 2018), and limbal stem cells (Inatomi et al., 2018; Sasamoto et al., 2018) are recently studied stem cells sources in corneal wound healing and regeneration. Saghizadeh et al. (2017) have recently reviewed all major stem cells usage in corneal wound healing. On the other hand, developing innovative methods to produce 3D tissue-like architecture has allowed mimicking the microarchitecture and physiology of the native cornea. In this regards 3D microfabrication methods are promising approaches in designing cornea substitutes (Prina et al., 2017; Ludwig et al., 2018). Among additive manufacturing methods, study on bioprinting and the development of bioinks provides great promise regarding the fabrication of human corneal substitutes that mimic the structure of native corneal tissues (Isaacson et al., 2018; Sorkio et al., 2018).

AUTHOR CONTRIBUTIONS

MoM and RA wrote the first draft. SO and MG wrote the first draft and analyzed the data. FM and MaM, created the idea, managed the team, and finalized the draft.

REFERENCES

Abdel-Naby, W., Cole, B., Liu, A., Liu, J., Wan, P., Guaiquil, V. H., et al. (2017). Silk-derived protein enhances corneal epithelial migration, adhesion, and proliferation. *Invest. Ophthalmol. Visual Sci.* 58, 1425–1433. doi: 10.1167/iovs.16-19957

Alarcon, E., Vulesevic, B., Argawal, A., Ross, A., Bejjani, P., Podrebarac, J., et al. (2016). Coloured cornea replacements with anti-infective properties: expanding the safe use of silver nanoparticles in regenerative medicine. *Nanoscale* 8, 6484–6489. doi: 10.1039/C6NR01339B

Ambati, B. K., Joussen, A. M., Kuziel, W. A., Adamis, A. P., and Ambati, J. (2003). Inhibition of corneal neovascularization by genetic ablation of CCR2. *Cornea* 22, 465–467. doi: 10.1097/00003226-200307000-00013

Arvola, R. P., Robciuc, A., and Holopainen, J. M. (2016). Matrix regeneration therapy: a case series of corneal neurotrophic ulcers. *Cornea* 35, 451–455. doi: 10.1097/ICO.0000000000000759

Asena, L., Suveren, E. H., Karabay, G., and Dursun Altinors, D. (2017). Human breast milk drops promote corneal epithelial wound healing. *Curr. Eye Res.* 42, 506–512. doi: 10.1080/02713683.2016.1223318

Aucoin, L., Griffith, C. M., Pleizier, G., Deslandes, Y., and Sheardown, H. (2002). Interactions of corneal epithelial cells and surfaces modified with cell adhesion peptide combinations. *J. Biomater. Sci.* 13, 447–462. doi: 10.1163/156856202320253956

Baino, F., Ferraris, S., Miola, M., Perero, S., Verné, E., Coggiola, A., et al. (2016). Novel antibacterial ocular prostheses: proof of concept and physico-chemical characterization. *Mater. Sci. Eng. C* 60, 467–474. doi: 10.1016/j.msec.2015.11.075

Baradaran-Rafii, A., Eslani, M., Haq, Z., Shirzadeh, E., Huvard, M. J., and Djalilian, A. R. (2017). Current and upcoming therapies for ocular surface chemical injuries. *Ocular Surf.* 15, 48–64. doi: 10.1016/j.jtos.2016.09.002

Barritault, D., Gilbert-Sirieix, M., Rice, K. L., Siñeriz, F., Papy-Garcia, D., Baudouin, C., et al. (2017). RGTA® or ReGeneraTing Agents mimic heparan sulfate in regenerative medicine: from concept to curing patients. *Glycoconjugate J.* 34, 325–338. doi: 10.1007/s10719-016-9744-5

Bazan, H. E., He, J., Kakazu, A. H., Cortina, M. S., Musarrat, F., and Neumann, D. (2014). Treatment with pigment epithelial-derived factor (PEDF) plus docosahexaenoic acid (DHA) increases corneal sensitivity and reduces inflammatory response after HSV-1 infection. *Invest. Ophthalmol. Visual Sci.* 55, 1467–1467. doi: 10.1016/j.exer.2017.06.015

Bian, F., Xiao, Y., Zaheer, M., Volpe, E. A., Pflugfelder, S. C., Li, D. Q., et al. (2017). Inhibition of NLRP3 inflammasome pathway by butyrate improves corneal wound healing in corneal alkali burn. *Int. J. Mol. Sci.* 18:562. doi: 10.3390/ijms18030562

Bobba, S., Chow, S., Watson, S., and Di Girolamo, N. (2015). Clinical outcomes of xeno-free expansion and transplantation of autologous ocular surface epithelial stem cells via contact lens delivery: a prospective case series. *Stem Cell Res. Ther.* 6:23. doi: 10.1186/s13287-015-0009-1

Buznyk, O., Pasyechnikova, N., Islam, M. M., Iakymenko, S., Fagerholm, P., and Griffith, M. (2015). Bioengineered corneas grafted as alternatives to human donor corneas in three high-risk patients. *Clin. Transl. Sci.* 8, 558–562. doi: 10.1111/cts.12293

Cano, L., Gutierrez, J., and Tercjak, A. (2013). Rutile TiO2 nanoparticles dispersed in a self-assembled polystyrene-block-polymethyl methacrylate diblock copolymer template. *J. Phys. Chem. C* 117, 1151–1156. doi: 10.1021/jp309335x

Chappelet, M. A., Bernheim, D., Chiquet, C., and Aptel, F. (2017). Effect of a new matrix therapy agent in persistent epithelial defects after bacterial keratitis treated with topical fortified antibiotics. *Cornea* 36, 1061–1068. doi: 10.1097/ICO.0000000000001261

Chen, J., Zhang, W., Kelk, P., Backman, L. J., and Danielson, P. (2017). Substance P and patterned silk biomaterial stimulate periodontal ligament stem cells to form corneal stroma in a bioengineered three-dimensional model. *Stem Cell Res. Ther.* 8:260. doi: 10.1186/s13287-017-0715-y

Choi, J. A., and Chung, S. H. (2011). Combined application of autologous serum eye drops and silicone hydrogel lenses for the treatment of persistent epithelial defects. *Eye Contact Lens* 37, 370–373. doi: 10.1097/ICL.0b013e318233c9bb

Cocucci, E., Racchetti, G., and Meldolesi, J. (2009). Shedding microvesicles: artefacts no more. *Trends Cell Biol.* 19, 43–51. doi: 10.1016/j.tcb.2008.11.003

Cortina, M. S., and De La Cruz, J. (2015). *Keratoprostheses and Artificial Corneas: Fundamentals Surgical Applications*. Heidelberg: Springer. doi: 10.1007/978-3-642-55179-6

Cui, R., Lu, Q., Teng, Y., Li, K., and Li, N. (2017). Chitosan promoted the Corneal epithelial wound healing via activation of ERK pathway. *Curr. Eye Res.* 42, 21–27. doi: 10.3109/02713683.2016.1145235

Cursiefen, C. (2007). "Immune privilege and angiogenic privilege of the cornea," in *Immune Response and the Eye*, eds J. Y. Niederkorn and H. J. Kaplan (Basel: Karger Publishers), 50–57. doi: 10.1159/000099253

Dai, T., Tanaka, M., Huang, Y. Y., and Hamblin, M. R. (2011). Chitosan preparations for wounds and burns: antimicrobial and wound-healing effects. *Expert Rev. Anti-Infect. Ther.* 9, 857–879. doi: 10.1586/eri.11.59

Deng, C., Li, F., Hackett, J. M., Chaudhry, S. H., Toll, F. N., Toye, B., et al. (2010). Collagen and glycopolymer based hydrogel for potential corneal application. *Acta Biomater.* 6, 187–194. doi: 10.1016/j.actbio.2009.07.027

Di Girolamo, N., Bosch, M., Zamora, K., Coroneo, M. T., Wakefield, D., and Watson, S. L. (2009). A contact lens-based technique for expansion and transplantation of autologous epithelial progenitors for ocular surface reconstruction. *Transplantation* 87, 1571–1578. doi: 10.1097/TP.0b013e3181a4bbf2

Dohlman, C. H., Cruzat, A., and White, M. (2014). The Boston keratoprosthesis 2014: a step in the evolution of artificial corneas. *Spektrum der Augenheilkunde* 28, 226–233. doi: 10.1007/s00717-014-0240-7

Duchesne, B., Tahi, H., and Galand, A. (2001). Use of human fibrin glue and amniotic membrane transplant in corneal perforation. *Cornea* 20, 230–232. doi: 10.1097/00003226-200103000-00027

Duncker, G. I., Storsberg, J., and Müller-Lierheim, W. G. (2014). The fully synthetic, bio-coated MIRO® CORNEA UR keratoprosthesis: development, preclinical testing, and first clinical results. *Spektrum der Augenheilkunde* 28, 250–260. doi: 10.1007/s00717-014-0243-4

Ellenberg, D., Azar, D. T., Hallak, J. A., Tobaigy, F., Han, K. Y., Jain, S., et al. (2010). Novel aspects of corneal angiogenic and lymphangiogenic privilege. *Prog. Retinal Eye Res.* 29, 208–248. doi: 10.1016/j.preteyeres.2010.01.002

Fagerholm, P., Lagali, N. S., Merrett, K., Jackson, W. B., Munger, R., Liu, Y., et al. (2010). A biosynthetic alternative to human donor tissue for inducing corneal regeneration: 24-month follow-up of a phase 1 clinical study. *Sci. Trans. Med.* 2:46ra61. doi: 10.1126/scitranslmed.3001022

Fagerholm, P., Lagali, N. S., Ong, J. A., Merrett, K., Jackson, W. B., Polarek, J. W., et al. (2014). Stable corneal regeneration four years after implantation of a cell-free recombinant human collagen scaffold. *Biomaterials* 35, 2420–2427. doi: 10.1016/j.biomaterials.2013.11.079

Falcinelli, G., Falsini, B., Taloni, M., Colliardo, P., and Falcinelli, G. (2005). Modified osteo-odonto-keratoprosthesis for treatment of corneal blindness: long-term anatomical and functional outcomes in 181 cases. *Arch. Ophthalmol.* 123, 1319–1329. doi: 10.1001/archopht.123.10.1319

Falcinelli, G., Missiroli, A., Petitti, V., and Pinna, C. (1987). Osteo odonto keratoprosthesis up to date. *Acta XXV Concilium Ophthalmol. Milan* 2, 2772–2776.

Figueiredo, G., Bojic, S., Rooney, P., Wilshaw, S.-P., Connon, C., Gouveia, R., et al. (2017). Gamma-irradiated human amniotic membrane decellularised with sodium dodecyl sulfate is a more efficient substrate for the *ex vivo* expansion of limbal stem cells. *Acta Biomater.* 61, 124–133. doi: 10.1016/j.actbio.2017.07.041

Fischak, C., Klaus, R., Werkmeister, R. M., Hohenadl, C., Prinz, M., Schmetterer, L., et al. (2017). Effect of topically administered chitosan-N-acetylcysteine on corneal wound healing in a rabbit model. *J. Ophthalmol.* 2017:5192924. doi: 10.1155/2017/5192924

Gallego-Muñoz, P., Ibares-Frías, L., Valsero-Blanco, M. C., Cantalapiedra-Rodriguez, R., Merayo-Lloves, J., and Martínez-García, M. C. (2017). Effects of TGFβ1, PDGF-BB, and bFGF, on human corneal fibroblasts proliferation and differentiation during stromal repair. *Cytokine* 96, 94–101. doi: 10.1016/j.cyto.2017.03.011

Ghaffari, M., Moztarzadeh, S., Rahmanian, F., Yazdanpanah, A., Ramedani, A., Mills, D. K., et al. (2016). "Nanobiomaterials for bionic eye: vision of the future," in *Engineering of Nanobiomaterials,* ed A. Grumezescu (Amsterdam: Elsevier), 257–285. doi: 10.1016/B978-0-323-41532-3.00008-7

Ghezzi, C. E., Rnjak-Kovacina, J., and Kaplan, D. L. (2015). Corneal tissue engineering: recent advances and future perspectives. *Tissue Eng. Part B Rev.* 21, 278–287. doi: 10.1089/ten.teb.2014.0397

Gholipourmalekabadi, M., Samadikuchaksaraei, A., Seifalian, A. M., Urbanska, A. M., Ghanbarian, H., Hardy, J. G., et al. (2018). Silk fibroin/amniotic membrane 3D bi-layered artificial skin. *Biomed. Mater.* 13:035003. doi: 10.1088/1748-605X/aa999b

Gonzalez-Paredes, A., Torres, D., and Alonso, M. J. (2017). Polyarginine nanocapsules: a versatile nanocarrier with potential in transmucosal drug delivery. *Int. J. Pharma.* 529, 474–485. doi: 10.1016/j.ijpharm.2017.07.001

Gouveia, R. M., González-Andrades, E., Cardona, J. C., González-Gallardo, C., Ionescu, A. M., Garzon, I., et al. (2017). Controlling the 3D architecture of Self-Lifting Auto-generated Tissue Equivalents (SLATEs) for optimized corneal graft composition and stability. *Biomaterials* 121, 205–219. doi: 10.1016/j.biomaterials.2016.12.023

Green, H., Kehinde, O., and Thomas, J. (1979). Growth of cultured human epidermal cells into multiple epithelia suitable for grafting. *Proc. Natl. Acad. Sci.* 76, 5665–5668. doi: 10.1073/pnas.76.11.5665

Grieve, K., Ghoubay, D., Georgeon, C., Thouvenin, O., Bouheraoua, N., Paques, M., et al. (2015). Three-dimensional structure of the mammalian limbal stem cell niche. *Exp. Eye Res.* 140, 75–84. doi: 10.1016/j.exer.2015.08.003

Griffith, M., Alarcon, E. I., and Brunette, I. (2016). Regenerative approaches for the cornea. *J. Intern. Med.* 280, 276–286. doi: 10.1111/joim.12502

Griffith, M., and Harkin, D. G. (2014). Recent advances in the design of artificial corneas. *Curr. Opin. Ophthalmol.* 25, 240–247. doi: 10.1097/ICU.0000000000000049

Grigoryeva, A., Eremina, A., Druzhinin, I., Chernykh, D., Varvarinsky, E., and Ryabchikova, E. (2013). Diagnostic potential of the electron microscopic analysis of human lacrimal fluid. *Oftal'mokhirurgiya* 4, 104–107.

Gronkiewicz, K. M., Giuliano, E. A., Sharma, A., and Mohan, R. R. (2017). Effects of topical hyaluronic acid on corneal wound healing in dogs: a pilot study. *Veter. Ophthalmol.* 20, 123–130. doi: 10.1111/vop.12379

Gumus, K., Guerra, M. G., de Melo Marques, S. H., Karaküçük, S., and Barritault, D. (2017). A new matrix therapy agent for faster corneal healing and less ocular discomfort following epi-off accelerated corneal cross-linking in progressive keratoconus. *J. Refract. Surg.* 33, 163–170. doi: 10.3928/1081597X-20161206-07

Haagdorens, M., Van Acker, S. I., Van Gerwen, V., N.í, Dhubhghaill, S., and Koppen, C., Tassignon, M.-J., et al. (2016). Limbal stem cell deficiency: current treatment options and emerging therapies. *Stem Cells Int.* 2016:9798374. doi: 10.1155/2016/9798374

Han, B., Schwab, I. R., Madsen, T. K., and Isseroff, R. R. (2002). A fibrin-based bioengineered ocular surface with human corneal epithelial stem cells. *Cornea* 21, 505–510. doi: 10.1097/00003226-200207000-00013

Han, K. Y., Dugas-Ford, J., Seiki, M., Chang, J. H., and Azar, D. T. (2015a). Evidence for the involvement of MMP14 in MMP2 processing and recruitment in exosomes of corneal fibroblasts. *Invest. Ophthalmol. Visual Sci.* 56, 5323–5329. doi: 10.1167/iovs.14-14417

Han, K. Y., Tran, J. A., Chang, J. H., Azar, D. T., and Zieske, J. D. (2017). Potential role of corneal epithelial cell-derived exosomes in corneal wound healing and neovascularization. *Sci. Rep.* 7:40548. doi: 10.1038/srep40548

Han, S. B., Dunlap, K., and Akpek, E. K. (2015b). "Boston KPro type I in the pediatric age group," in *Keratoprostheses and Artificial Corneas,* eds M. Soledad Cortina and J. de la Cruz (New York, NY: Springer), 145–152. doi: 10.1007/978-3-642-55179-6_17

Han, S. B., Liu, Y. C., Mohamed-Noriega, K., and Mehta, J. S. (2018). Application of novel drugs for corneal cell regeneration. *J. Ophthalmol.* 2018:1215868. doi: 10.1155/2018/1215868

He, H., Kuriyan, A. E., Su, C. W., Mahabole, M., Zhang, Y., Zhu, Y. T., et al. (2017a). Inhibition of proliferation and epithelial mesenchymal transition in retinal pigment epithelial cells by heavy chain-hyaluronan/pentraxin 3. *Sci. Rep.* 7:43736. doi: 10.1038/srep43736

He, J., Cortina, M. S., Kakazu, A., and Bazan, H. E. (2015). The PEDF neuroprotective domain plus DHA induces corneal nerve regeneration after experimental surgery. *Invest. Ophthalmol. Visual Sci.* 56, 3505–3513. doi: 10.1167/iovs.15-16755

He, J., Pham, T. L., Kakazu, A., and Bazan, H. E. (2017b). Recovery of corneal sensitivity and increase in nerve density and wound healing in diabetic mice after PEDF plus DHA treatment. *Diabetes* 2017:170249. doi: 10.2337/db17-0249

Hille, K. (2018). Long-term outcome of keratoprosthesis with biological support. *Der Ophthalmol.* 115, 5–11. doi: 10.1007/s00347-017-0503-1

Hirayama, M., Satake, Y., Higa, K., Yamaguchi, T., and Shimazaki, J. (2012). Transplantation of cultivated oral mucosal epithelium prepared in fibrin-coated culture dishes. *Invest. Ophthalmol. Visual Sci.* 53, 1602–1609. doi: 10.1167/iovs.11-7847

Ho, D. K., and Mathews, J. P. (2017). Folded bandage contact lens retention in a patient with bilateral dry eye symptoms: a case report. *BMC Ophthalmol.* 17:116. doi: 10.1186/s12886-017-0505-4

Huang, J., Wang, W., Yu, J., Yu, X., Zheng, Q., Peng, F., et al. (2017). Combination of dexamethasone and Avastin® by supramolecular hydrogel attenuates the inflammatory corneal neovascularization in rat alkali burn model. *Colloids Surfaces B Biointerfaces* 159, 241–250. doi: 10.1016/j.colsurfb.2017.07.057

Huang, Y., Dong, Y., Wang, L., Du, G., Yu, J., Song, J., et al. (2012). Long-term outcomes of MICOF keratoprosthesis in the end stage of autoimmune dry eyes: an experience in China. *Br. J. Ophthalmol.* 96, 28–33. doi: 10.1136/bjo.2010.193029

Huhtinen, R., Sandeman, S., Rose, S., Fok, E., Howell, C., Fröberg, L., et al. (2013). Examining porous bio-active glass as a potential osteo-odonto-keratoprosthetic skirt material. *J. Mater. Sci.* 24, 1217–1227. doi: 10.1007/s10856-013-4881-x

Hwang, Y., and Kim, G. (2016). Evaluation of stability and biocompatibility of PHEMA-PMMA keratoprosthesis by penetrating keratoplasty in rabbits. *Lab. Anim. Res.* 32, 181–186. doi: 10.5625/lar.2016.32.4.181

Inatomi, T., Nakamura, T., Koizumi, N., Sotozono, C., and Kinoshita, S. (2018). "Ocular surface reconstruction using cultivated corneal and oral mucosal epithelial transplantation," in *Ocular Surface Disease,* ed A. R. Djalilian (New York, NY: Springer), 349–361. doi: 10.1007/978-3-319-15823-5_23

Isaacson, A., Swioklo, S., and Connon, C. (2018). 3D bioprinting of a corneal stroma equivalent. *Exp. Eye Res.* 173, 188–193. doi: 10.1016/j.exer.2018.05.010

Islam, M. M., Buznyk, O., Reddy, J. C., Pasyechnikova, N., Alarcon, E. I., Hayes, S., et al. (2018). Biomaterials-enabled cornea regeneration in patients at high risk for rejection of donor tissue transplantation. *NPJ Regenerat. Med.* 3:2. doi: 10.1038/s41536-017-0038-8

Ismail, S., McGhee, J. J., Li, Y., Mathan, J. J., Yoon, J. J., Wadhwa, H., et al. (2019). "Stem cell spheres for corneal regeneration," in *Corneal Regeneration : Therapy and Surgery,* eds J. L. Alió, J. L. Alió del Barrio, and F. Arnalich-Montiel (Cham: Springer International Publishing), 299–316.

Jangamreddy, J. R., Haagdorens, M. K. C., Islam, M., Lewis, P., Samanta, A., Fagerholm, P., et al. (2018). Short peptide analogs as alternatives to collagen in pro-regenerative corneal implants. *Acta Biomater.* 69, 120–130. doi: 10.1016/j.actbio.2018.01.011

Jeng, B. H., Farid, M., Patel, S. V., and Schwab, I. R. (2016). Corneal cross-linking for Keratoconus: a look at the data, the Food and Drug Administration, and the future. *Ophthalmology* 123, 2270–2272. doi: 10.1016/j.ophtha.2016.08.006

Jirásková, N., Rozsival, P., Burova, M., and Kalfertova, M. (2011). AlphaCor artificial cornea: clinical outcome. *Eye* 25, 1138–1146. doi: 10.1038/eye.2011.122

Kargozar, S., and Mozafari, M. (2018). Nanotechnology and nanomedicine: start small, think big. *Mater. Today Proc.* 5, 15492–15500. doi: 10.1016/j.matpr.2018.04.155

Karimi, M., Bahrami, S., Ravari, S. B., Zangabad, P. S., Mirshekari, H., Bozorgomid, M., et al. (2016a). Albumin nanostructures as advanced drug delivery systems. *Expert Opin. Drug Delivery* 13, 1609–1623. doi: 10.1080/17425247.2016.1193149

Karimi, M., Ghasemi, A., Zangabad, P., Rahighi, R., Basri, S. M., Mirshekari, H., et al. (2016b). Smart micro/nanoparticles in stimulus-responsive drug/gene delivery systems. *Chem. Soc. Rev.* 45, 1457–1501. doi: 10.1039/C5CS00798D

Karimi, M., Mirshekari, H., Aliakbari, M., Sahandi-Zangabad, P., and Hamblin, M. R. (2016c). Smart mesoporous silica nanoparticles for controlled-release drug delivery. *Nanotechnol. Rev.* 5, 195–207. doi: 10.1515/ntrev-2015-0057

Karimi, M., Solati, N., Amiri, M., Mirshekari, H., Mohamed, E., Taheri, M., et al. (2015a). Carbon nanotubes part I: preparation of a novel and versatile drug-delivery vehicle. *Expert Opin. Drug Delivery* 12, 1071–1087. doi: 10.1517/17425247.2015.1003806

Karimi, M., Solati, N., Ghasemi, A., Estiar, M. A., Hashemkhani, M., Kiani, P., et al. (2015b). Carbon nanotubes part II: a remarkable carrier for drug and gene delivery. *Expert Opin. Drug Delivery* 12, 1089–1105. doi: 10.1517/17425247.2015.1004309

Katori, R., Hayashi, R., Kobayashi, Y., Kobayashi, E., and Nishida, K. (2016). Ebselen preserves tissue-engineered cell sheets and their stem cells in hypothermic conditions. *Sci. Rep.* 6:38987. doi: 10.1038/srep38987

Kaufman, P. L., Levin, L. A., Adler, F. H., and Alm, A. (2011). *Adler's Physiology of the Eye.* Amsterdam: Elsevier Health Sciences.

Khadem, J., Martino, M., Anatelli, F., Dana, M. R., and Hamblin, M. R. (2004). Healing of perforating rat corneal incisions closed with photodynamic laser-activated tissue glue. *Lasers Surg. Med.* 35, 304–311. doi: 10.1002/lsm.20099

Khadem, J., Tsao, K., Hamblin, M., Goslee, M., Tolentino, F., and Dana, M. (2000). "Photodynamic biologic tissue glue in perforating rabbit corneal wounds," in *Investigative Ophthalmology and Visual Science* (Bethesda, MD: Assoc Research Vision Ophthalmology Inc.), S700–S700.

Kim, E. Y., Tripathy, N., Cho, S. A., Lee, D., and Khang, G. (2017a). Collagen type I–PLGA film as an efficient substratum for corneal endothelial cells regeneration. *J. Tissue Eng. Regenerat. Med.* 11, 2471–2478. doi: 10.1002/term.2145

Kim, J. W., Jeong, H., Yang, M. S., Lim, C. W., and Kim, B. (2017b). Therapeutic effects of zerumbone in an alkali-burned corneal wound healing model. *Int. Immunopharmacol.* 48, 126–134. doi: 10.1016/j.intimp.2017.05.005

Kim, M. K., Park, I. S., Dal Park, H., Wee, W. R., Lee, J. H., Park, K. D., et al. (2001). Effect of poly (ethylene glycol) graft polymerization of poly (methyl methacrylate) on cell adhesion: *in vitro* and *in vivo* study. *J. Cataract Refract. Surg.* 27, 766–774. doi: 10.1016/S0886-3350(00)00701-X

Kobayashi, T., Kan, K., Nishida, K., Yamato, M., and Okano, T. (2013). Corneal regeneration by transplantation of corneal epithelial cell sheets fabricated with automated cell culture system in rabbit model. *Biomaterials* 34, 9010–9017. doi: 10.1016/j.biomaterials.2013.07.065

Koizumi, N., and Okumura, N. (2019). "Cell based therapy for corneal endothelial regeneration," in *Corneal Regeneration : Therapy and Surgery*, eds J. L. Alió, J. L. Alió del Barrio, and F. Arnalich-Montiel (Cham: Springer International Publishing), 455–462.

Kong, B., Sun, W., Chen, G., Tang, S., Li, M., Shao, Z., et al. (2017). Tissue-engineered cornea constructed with compressed collagen and laser-perforated electrospun mat. *Sci. Rep.* 7:970. doi: 10.1038/s41598-017-01072-0

Kowalski, K. (2016). "Plastic that mimics insect wings kills bacteria the curved plastic may one day be used as an artificial cornea," in *ScienceNewsforStudents*. Available online at: https://www.sciencenewsforstudents.org/article/plastic-mimics-insect-wings-kills-bacteria

Laattala, K., Huhtinen, R., Puska, M., Arstila, H., Hupa, L., Kellomäki, M., et al. (2011). Bioactive composite for keratoprosthesis skirt. *J. Mech. Behav. Biomed. Mater.* 4, 1700–1708. doi: 10.1016/j.jmbbm.2011.05.025

Lagali, N., Edén, U., Utheim, T. P., Chen, X., Riise, R., Dellby, A., et al. (2013). In vivo morphology of the limbal palisades of vogt correlates with progressive stem cell deficiency in aniridia-related keratopathy. *Invest. Ophthalmol. Visual Sci.* 54, 5333–5342. doi: 10.1167/iovs.13-11780

Lai, J. Y., and Ma, D. H. (2017). Ocular biocompatibility of gelatin microcarriers functionalized with oxidized hyaluronic acid. *Mater. Sci. Eng. C* 72, 150–159. doi: 10.1016/j.msec.2016.11.067

Lawrence, B. D., Marchant, J. K., Pindrus, M. A., Omenetto, F. G., and Kaplan, D. L. (2009). Silk film biomaterials for cornea tissue engineering. *Biomaterials* 30, 1299–1308. doi: 10.1016/j.biomaterials.2008.11.018

Lee, R., Khoueir, Z., Tsikata, E., Chodosh, J., Dohlman, C. H., and Chen, T. C. (2017). Long-term visual outcomes and complications of Boston keratoprosthesis type II implantation. *Ophthalmology* 124, 27–35. doi: 10.1016/j.ophtha.2016.07.011

Levis, H. J., and Daniels, J. T. (2016). Recreating the human limbal epithelial stem cell niche with bioengineered limbal crypts. *Curr. Eye Res.* 41, 1153–1160. doi: 10.3109/02713683.2015.1095932

Levis, H. J., Massie, I., Dziasko, M. A., Kaasi, A., and Daniels, J. T. (2013). Rapid tissue engineering of biomimetic human corneal

limbal crypts with 3D niche architecture. *Biomaterials* 34, 8860–8868. doi: 10.1016/j.biomaterials.2013.08.002

Lih, E., Lee, J. S., Park, K. M., and Park, K. D. (2012). Rapidly curable chitosan–PEG hydrogels as tissue adhesives for hemostasis and wound healing. *Acta Biomater.* 8, 3261–3269. doi: 10.1016/j.actbio.2012.05.001

Lin, Y.-K., Sharma, R., Ma, H., Chen, W.-S., and Yao, C.-L. (2017). In situ polymerizable hydrogel incorporated with specific pathogen-free porcine platelet-rich plasma for the reconstruction of the corneal endothelium. *J. Taiwan Institute Chem. Eng.* 78, 65–74. doi: 10.1016/j.jtice.2017.06.006

Liu, J., Lawrence, B. D., Liu, A., Schwab, I. R., Oliveira, L. A., and Rosenblatt, M. I. (2012). Silk fibroin as a biomaterial substrate for corneal epithelial cell sheet generation. *Invest. Ophthalmol. Visual Sci.* 53, 4130–4138. doi: 10.1167/iovs.12-9876

Long, Y., Zhao, X., Liu, S., Chen, M., Liu, B., Ge, J., et al. (2018). Collagen–hydroxypropyl methylcellulose membranes for corneal regeneration. *ACS Omega* 3, 1269–1275. doi: 10.1021/acsomega.7b01511

Ludwig, P. E., Huff, T. J., and Zuniga, J. M. (2018). The potential role of bioengineering and three-dimensional printing in curing global corneal blindness. *J. Tissue Eng.* 9:2041731418769863. doi: 10.1177/2041731418769863

Luo, L. J., Lai, J. Y., Chou, S. F., Hsueh, Y. J., and Ma, D. H. (2018). Development of gelatin/ascorbic acid cryogels for potential use in corneal stromal tissue engineering. *Acta Biomater.* 65, 123–136. doi: 10.1016/j.actbio.2017.11.018

Lužnik, Z., Breda, C., Barbaro, V., Ferrari, S., Migliorati, A., Di Iorio, E., et al. (2017). Towards xeno-free cultures of human limbal stem cells for ocular surface reconstruction. *Cell Tissue Banking* 18, 461–474. doi: 10.1007/s10561-017-9632-7

Ma, X., Xiang, R., Meng, X., Qin, L., Wu, Y., Tain, L., et al. (2017). Russian keratoprosthesis in stevens–johnson syndrome. *Cornea* 36, 304–309. doi: 10.1097/ICO.0000000000001094

Mannis, M. J., and Mannis, A. A. (1999). *Corneal Transplantation: A History in Profiles.* Oostende: JP Wayenborgh.

Manolova, Y., Stoycheva, Z., Yordanov, Y., and Grupcheva, C. (2017). Amniotic membrane transplantation–Analysis of structural characteristics in amniotic membrane transplant and corneal ulcers. *Scripta Sci. Med.* 49, 12–20. doi: 10.14748/ssm.v49i1.2060

Massie, I., Levis, H. J., and Daniels, J. T. (2014). Response of human limbal epithelial cells to wounding on 3D RAFT tissue equivalents: effect of airlifting and human limbal fibroblasts. *Exp. Eye Res.* 127, 196–205. doi: 10.1016/j.exer.2014.07.024

Matthyssen, S., Van den Bogerd, B., Dhubhghaill, S. N., Koppen, C., and Zakaria, N. (2018). Corneal regeneration: a review of stromal replacements. *Acta Biomater.* 69, 31–41. doi: 10.1016/j.actbio.2018.01.023

Maurice, D. M. (1957). The structure and transparency of the cornea. *J. Physiol.* 136, 263–286. doi: 10.1113/jphysiol.1957.sp005758

Meek, K. M., and Knupp, C. (2015). Corneal structure and transparency. *Prog. Retinal Eye Res.* 49, 1–16. doi: 10.1016/j.preteyeres.2015.07.001

Miller, D., and Benedek, G. (1973). *Intraocular Light Scattering: Theory and Clinical Application*. Charles City, IA: Thomas Publisher. doi: 10.1097/00006324-197312000-00019

Mohammadi, M. R., Nojoomi, A., Mozafari, M., Dubnika, A., Inayathullah, M., and Rajadas, J. (2017). Nanomaterials engineering for drug delivery: a hybridization approach. *J. Mater. Chem. B* 5, 3995–4018. doi: 10.1039/C6TB03247H

Mozafari, M. (2014). The critical impact of controlled drug delivery in the future of tissue engineering. *Trends Biomater. Artif. Organs* 28, 124–126. Available online at: https://web.a.ebscohost.com/abstract?direct=true&profile=ehost&scope=site&authtype=crawler&jrnl=09711198&AN=111415494&h=Lx8yPqvR3v22gqn82gz3O%2fxlskO6fvyL9LRiTDXlHKpjDUKnuEk10FiOvQRFUcEbstQSYWjQmaXS9NxGA93QbA%3d%3d&crl=c&resultNs=AdminWebAuth&resultLocal=ErrCrlNotAuth&crlhashurl=login.aspx%3fdirect%3dtrue%26profile%3dehost%26scope%3dsite%26authtype%3dcrawler%26jrnl%3d09711198%26AN%3d111415494

Mozafari, M., Rajadas, J., and Kaplan, D. (2019). *Nanoengineered Biomaterials for Regenerative Medicine.* Amsterdam: Elsevier. doi: 10.1016/B978-0-12-813355-2.00001-6

Muijzer, M. B., van Luijk, C. M., van den Bogaerdt, A. J., Kruit, P. J., Groeneveld-van Beek, E., Melles, G. R. J., et al. (2019). Prospective evaluation of clinical outcomes between pre-cut corneal grafts prepared using a manual or automated technique: with one-year follow-up. *Acta Ophthalmol.* doi: 10.1111/aos.14074. [Epub ahead of print].

Nagai, N., Nakazawa, Y., Ito, Y., Kanai, K., Okamoto, N., and Shimomura, Y. (2017). A nanoparticle-based ophthalmic formulation of dexamethasone enhances corneal permeability of the drug and prolongs its corneal residence time. *Biol. Pharma. Bull.* 40, 1055–1062. doi: 10.1248/bpb.b17-00137

Nakajima, R., Kobayashi, T., Moriya, N., Mizutani, M., Kan, K., Nozaki, T., et al. (2015). A novel closed cell culture device for fabrication of corneal epithelial cell sheets. *J. Tissue Eng. Regenerat. Med.* 9, 1259–1267. doi: 10.1002/term.1639

Nakamura, T., Inatomi, T., Sotozono, C., Koizumi, N., and Kinoshita, S. (2016). Ocular surface reconstruction using stem cell and tissue engineering. *Prog. Retinal Eye Res.* 51, 187–207. doi: 10.1016/j.preteyeres.2015.07.003

Neuman, M. G., Nanau, R. M., Oruña-Sanchez, L., and Coto, G. (2015). Hyaluronic acid and wound healing. *J. Pharmacy Pharma. Sci.* 18, 53–60. doi: 10.18433/J3K89D

Nishida, K., Yamato, M., Hayashida, Y., Watanabe, K., Maeda, N., Watanabe, H., et al. (2004a). Functional bioengineered corneal epithelial sheet grafts from corneal stem cells expanded *ex vivo* on a temperature-responsive cell culture surface. *Transplantation* 77, 379–385. doi: 10.1097/01.TP.0000110320.45678.30

Nishida, K., Yamato, M., Hayashida, Y., Watanabe, K., Yamamoto, K., Adachi, E., et al. (2004b). Corneal reconstruction with tissue-engineered cell sheets composed of autologous oral mucosal epithelium. *N. Engl. J. Med.* 351, 1187–1196. doi: 10.1056/NEJMoa040455

Ogawa, Y., He, H., Mukai, S., Imada, T., Nakamura, S., Su, C. W., et al. (2017). Heavy chain-hyaluronan/pentraxin 3 from amniotic membrane suppresses inflammation and scarring in murine lacrimal gland and conjunctiva of chronic graft-versus-host disease. *Sci. Rep.* 7:42195. doi: 10.1038/srep42195

Omoto, M., Suri, K., Amouzegar, A., Li, M., Katikireddy, K. R., Mittal, S. K., et al. (2017). Hepatocyte growth factor suppresses inflammation and promotes epithelium repair in corneal injury. *Mol. Ther.* 25, 1881–1888. doi: 10.1016/j.ymthe.2017.04.020

Ortega, Í., Deshpande, P., Gill, A. A., MacNeil, S., and Claeyssens, F. (2013a). Development of a microfabricated artificial limbus with micropockets for cell delivery to the cornea. *Biofabrication* 5:025008. doi: 10.1088/1758-5082/5/2/025008

Ortega, I., McKean, R., Ryan, A. J., MacNeil, S., and Claeyssens, F. (2014a). Characterisation and evaluation of the impact of microfabricated pockets on the performance of limbal epithelial stem cells in biodegradable PLGA membranes for corneal regeneration. *Biomater. Sci.* 2, 723–734. doi: 10.1039/C3BM60268K

Ortega, I., Ryan, A., MacNeil, S., and Claeyssens, F. (2012). Development of tissue engineered stem cell niches for corneal repair", in *Journal of Tissue Engineering and Regenerative Medicine* (Hoboken, NJ: Wiley-Blackwell), 137–137.

Ortega, Í., Ryan, A. J., Deshpande, P., MacNeil, S., and Claeyssens, F. (2013b). Combined microfabrication and electrospinning to produce 3-D architectures for corneal repair. *Acta Biomater.* 9, 5511–5520. doi: 10.1016/j.actbio.2012.10.039

Ortega, Í., Sefat, F., Deshpande, P., Paterson, T., Ramachandran, C., Ryan, A. J., et al. (2014b). Combination of microstereolithography and electrospinning to produce membranes equipped with niches for corneal regeneration. *J. Visual. Exp.* 91:51826. doi: 10.3791/51826

Oryan, A., and Sahvieh, S. (2017). Effectiveness of chitosan scaffold in skin, bone and cartilage healing. *Int. J. Biol. Macromolecules* 104, 1003–1011. doi: 10.1016/j.ijbiomac.2017.06.124

Owaki, T., Shimizu, T., Yamato, M., and Okano, T. (2014). Cell sheet engineering for regenerative medicine: current challenges and strategies. *Biotechnol. J.* 9, 904–914. doi: 10.1002/biot.201300432

Pandey, A., Prasad, A., Moscatello, J. P., and Yap, Y. K. (2010). Stable electron field emission from PMMA– CNT Matrices. *Acs Nano* 4, 6760–6766. doi: 10.1021/nn100925g

Patel, S., Thakar, R. G., Wong, J., McLeod, S. D., and Li, S. (2006). Control of cell adhesion on poly (methyl methacrylate). *Biomaterials* 27, 2890–2897. doi: 10.1016/j.biomaterials.2005.12.009

Pellegrini, G., Ranno, R., Stracuzzi, G., Bondanza, S., Guerra, L., Zambruno, G., et al. (1999). The control of epidermal stem cells (holoclones) in the treatment of massive full-thickness burns with autologous keratinocytes cultured on fibrin1. *Transplantation* 68, 868–879. doi: 10.1097/00007890-199909270-00021

Pineda, R. (2015). "The keraklear artificial cornea," in *Keratoprostheses and Artificial Corneas*, eds M. Cortina and J. de la Cruz (New York, NY: Springer), 213–219. doi: 10.1007/978-3-642-55179-6_23

Pino, M., Stingelin, N., and Tanner, K. E. (2008). Nucleation and growth of apatite on NaOH-treated PEEK, HDPE and UHMWPE for artificial cornea materials. *Acta Biomater.* 4, 1827–1836. doi: 10.1016/j.actbio.2008.05.004

Polisetti, N., McLaughlin, C. R., Vemuganti, G. K., and Griffith, M. (2013). "Biomaterials-enabled regenerative medicine in corneal applications," in *Regenerative Medicine: From Protocol to Patient,* ed G. Steinhoff. (Dordrecht: Springer Netherlands), 557–580. doi: 10.1007/978-94-007-5690-8_22

Prabhasawat, P. (2017). Amniotic membrane: a treatment for prevention of blindness from various ocular diseases. *Siriraj Med. J.* 59, 139–141. Available online at: http://www.smj.si.mahidol.ac.th/sirirajmedj/index.php/smj/article/viewFile/641/653

Prina, E., Mistry, P., Sidney, L. E., Yang, J., Wildman, R. D., Bertolin, M., et al. (2017). 3D microfabricated scaffolds and microfluidic devices for ocular surface replacement: a review. *Stem Cell Rev. Rep.* 13, 430–441. doi: 10.1007/s12015-017-9740-6

Quantock, A. J., Winkler, M., Parfitt, G. J., Young, R. D., Brown, D. J., Boote, C., et al. (2015). From nano to macro: studying the hierarchical structure of the corneal extracellular matrix. *Exp. Eye Res.* 133, 81–99. doi: 10.1016/j.exer.2014.07.018

Rahman, H. S., Rasedee, A., Yeap, S. K., Othman, H. H., Chartrand, M. S., Namvar, F., et al. (2014). Biomedical properties of a natural dietary plant metabolite, zerumbone, in cancer therapy and chemoprevention trials. *BioMed Res. Int.* 2014:920742. doi: 10.1155/2014/920742

Rahmati, M., and Mozafari, M. (2018). Protein adsorption on polymers. *Mater. Today Commun.* 17, 527–540. doi: 10.1016/j.mtcomm.2018.10.024

Rahmati, M., and Mozafari, M. (2019a). Biological response to carbon-family nanomaterials: interactions at the nano-bio interface. *Front. Bioeng. Biotechnol.* 7:4. doi: 10.3389/fbioe.2019.00004

Rahmati, M., and Mozafari, M. (2019b). Nano-immunoengineering: opportunities and challenges. *Curr. Opin. Biomed. Eng.* 10, 51–59. doi: 10.1016/j.cobme.2019.02.001

Rahmati, M., Pennisi, C. P., Mobasheri, A., and Mozafari, M. (2018). Bioengineered scaffolds for stem cell applications in tissue engineering and regenerative medicine. *Adv. Exp. Med. Biol.* 1107, 73–89. doi: 10.1007/5584_2018_215

Rajendran, V., Netuková, M., Griffith, M., Forrester, J. V., and Kuffová, L. (2017). Mesenchymal stem cell therapy for retro-corneal membrane – a clinical challenge in full-thickness transplantation of biosynthetic corneal equivalents. *Acta Biomater.* 64, 346–356. doi: 10.1016/j.actbio.2017.10.011

Rama, P., Bonini, S., Lambiase, A., Golisano, O., Paterna, P., De Luca, M., et al. (2001). Autologous fibrin-cultured limbal stem cells permanently restore the corneal surface of patients with total limbal stem cell deficiency1. *Transplantation* 72, 1478–1485. doi: 10.1097/00007890-200111150-00002

Rama, P., Matuska, S., Paganoni, G., Spinelli, A., De Luca, M., and Pellegrini, G. (2010). Limbal stem-cell therapy and long-term corneal regeneration. *N. Engl. J. Med.* 363, 147–155. doi: 10.1056/NEJMoa0905955

Ramachandran, C., Sangwan, V. S., Ortega, I., Bhatnagar, U., Mulla, S. M. A., McKean, R., et al. (2019). Synthetic biodegradable alternatives to the use of the amniotic membrane for corneal regeneration: assessment of local and systemic toxicity in rabbits. *Br. J. Ophthalmol.* 103, 286–292. doi: 10.1136/bjophthalmol-2018-312055

Reimondez-Troitiño, S., Alcalde, I., Csaba, N., Íñigo-Portugués, A., de la Fuente, M., Bech, F., et al. (2016). Polymeric nanocapsules: a potential new therapy for corneal wound healing. *Drug Deliver. Trans. Res.* 6, 708–721. doi: 10.1007/s13346-016-0312-0

Riau, A. K., Mondal, D., Setiawan, M., Palaniappan, A., Yam, G. H., Liedberg, B., et al. (2016). Functionalization of the polymeric surface with bioceramic nanoparticles via a novel, nonthermal dip coating method. *ACS Appl. Mater. Interfaces* 8, 35565–35577. doi: 10.1021/acsami.6b12371

Rizwan, M., Peh, G. S. L, Ang, H. P., Lwin, N. C., Adnan, K., Mehta, J. S., et al. (2017). Sequentially-crosslinked bioactive hydrogels as nano-patterned substrates with customizable stiffness and degradation for corneal tissue engineering applications. *Biomaterials* 120, 139–154. doi: 10.1016/j.biomaterials.2016.12.026

Robciuc, A., Arvola, R. P. J., Jauhiainen, M., and Holopainen, J. M. (2018). Matrix regeneration agents improve wound healing in non-stressed human corneal epithelial cells. *Eye* 32:813. doi: 10.1038/eye.2017.277

Ronfard, V., Broly, H., Mitchell, V., Galizia, J. P., Hochart, D., Chambon, E., et al. (1991). Use of human keratinocytes cultured on fibrin glue in the treatment of burn wounds. *Burns* 17, 181–184. doi: 10.1016/0305-4179(91)90099-3

Ronfard, V., Rives, J.-M., Neveux, Y., Carsin, H., and Barrandon, Y. (2000). Long-term regeneration of human epidermis on third degree burns transplanted with autologous cultured epithelium grown on a fibrin matrix1, 2. *Transplantation* 70, 1588–1598. doi: 10.1097/00007890-200012150-00009

Sabater, A. L., and Perez, V. L. (2017). Amniotic membrane use for management of corneal limbal stem cell deficiency. *Curr. Opin. Ophthalmol.* 28, 363–369. doi: 10.1097/ICU.0000000000000386

Saghizadeh, M., Kramerov, A. A., Svendsen, C. N., and Ljubimov, A. V. (2017). Concise review: stem cells for corneal wound healing. *Stem Cells* 35, 2105–2114. doi: 10.1002/stem.2667

Salehi, S., Czugala, M., Stafiej, P., Fathi, M., Bahners, T., Gutmann, J. S., et al. (2017). Poly (glycerol sebacate)-poly (ε-caprolactone) blend nanofibrous scaffold as intrinsic bio-and immunocompatible system for corneal repair. *Acta Biomater.* 50, 370–380. doi: 10.1016/j.actbio.2017.01.013

Salvador-Culla, B., Jeong, K. J., Kolovou, P. E., Chiang, H. H., Chodosh, J., Dohlman, C. H., et al. (2016). Titanium coating of the Boston keratoprosthesis. *Trans. Vis. Sci. Technol.* 5:17. doi: 10.1167/tvst.5.2.17

Sasamoto, Y., Ksander, B. R., Frank, M. H., and Frank, N. Y. (2018). Repairing the corneal epithelium using limbal stem cells or alternative cell-based therapies. *Expert Opin. Biol. Ther.* 18, 505–513. doi: 10.1080/14712598.2018.1443442

Schmidl, D., Werkmeister, R., Kaya, S., Unterhuber, A., Witkowska, K. J., Baumgartner, R., et al. (2017). A controlled, randomized double-blind study to evaluate the safety and efficacy of chitosan-N-acetylcysteine for the treatment of dry eye syndrome. *J. Ocular Pharmacol. Ther.* 33, 375–382. doi: 10.1089/jop.2016.0123

Schrader, S., Wedel, T., Moll, R., and Geerling, G. (2006). Combination of serum eye drops with hydrogel bandage contact lenses in the treatment of persistent epithelial defects. *Graefe's Arch. Clin. Exp. Ophthalmol.* 244, 1345–1349. doi: 10.1007/s00417-006-0257-y

Schrage, N., Hille, K., and Cursiefen, C. (2014). Current treatment options with artificial corneas: boston Kpro, Osteo-odontokeratoprosthesis, Miro Cornea® and KeraKlear®. *Der Ophthalmol.* 111, 1010–1018. doi: 10.1007/s00347-013-3009-5

Schroder, K., and Tschopp, J. (2010). The inflammasomes. *Cell* 140, 821–832. doi: 10.1016/j.cell.2010.01.040

Sigroha, S., and Khatkar, A. (2017). Chitosan-A naturally derived antioxidant polymer with diverse applications. *Curr. Organic Chem.* 21, 333–341. doi: 10.2174/1385272820666161018130542

Simpson, F., Alarcon, E. I., Hilborn, J., Brunette, I., and Griffith, M. (2019). "Regenerative medicine in the cornea," in *Principles of Regenerative Medicine*, eds A. Atala, R. Lanza, T. Mikos, and R. Nerem (Amsterdam: Elsevier), 1115–1129. doi: 10.1016/B978-0-12-809880-6.00063-1

Soleimanifar, F., Mortazavi, Y., Nadri, S., and Soleimani, M. (2017). Conjunctiva derived mesenchymal stem cell (CJMSCs) as a potential platform for differentiation into corneal epithelial cells on bioengineered electrospun scaffolds. *J. Biomed. Mater. Res. A* 105, 2703–2711. doi: 10.1002/jbm.a.36123

Sommer, A. (1982). *Nutritional Blindness. Xerophthalmia and Keratomalacia*. New York, NY; Oxford University Press. doi: 10.1001/archopht.1982.01030030401002

Sorkio, A., Koch, L., Koivusalo, L., Deiwick, A., Miettinen, S., Chichkov, B., et al. (2018). Human stem cell based corneal tissue mimicking structures using laser-assisted 3D bioprinting and functional bioinks. *Biomaterials* 171, 57–71. doi: 10.1016/j.biomaterials.2018.04.034

Soumya, S., Mohamed, A. P., Paul, L., Mohan, K., and Ananthakumar, S. (2014). Near IR reflectance characteristics of PMMA/ZnO nanocomposites for solar thermal control interface films. *Solar Energy Mater. Solar Cells* 125, 102–112. doi: 10.1016/j.solmat.2014.02.033

Sriram, S., Tran, J. A., Guo, X., Hutcheon, A. E. K., Kazlauskas, A., and Zieske, J. D. (2017). development of wound healing models to study Tgfβ3's effect on Sma. *Exp. Eye Res.* 161, 52–60. doi: 10.1016/j.exer.2017.06.005

St. Denis, T. G., Dai, T., Huang, Y. Y., and Hamblin, M. R. (2012). "Wound-healing properties of chitosan and its use in wound dressing biopharmaceuticals," in *Chitosan-Based Systems for Biopharmaceuticals: Delivery, Targeting Polymer Therapeutics*, eds B. Sarmento and J. das Neves, 429–450. doi: 10.1002/9781119962977.ch22. [Epub ahead of print].

Syed-Picard, F. N., Du, Y., Hertsenberg, A. J., Palchesko, R., Funderburgh, M. L., Feinberg, A. W., et al. (2018). Scaffold-free tissue engineering of functional corneal stromal tissue. *J. Tissue Eng. Regenerat. Med.* 12, 59–69. doi: 10.1002/term.2363

Takechi, Y., Tanaka, H., Kitayama, H., Yoshii, H., Tanaka, M., and Saito, H. (2012). Comparative study on the interaction of cell-penetrating polycationic polymers with lipid membranes. *Chem. Phys. Lipids* 165, 51–58. doi: 10.1016/j.chemphyslip.2011.11.002

Tan, X. W., Thompson, B., Konstantopoulos, A., Goh, T. W., Setiawan, M., Yam, G. H., et al. (2015). Application of graphene as candidate biomaterial for synthetic keratoprosthesis skirt. *Invest. Ophthalmol. Visual Sci.* 56, 6605–6611. doi: 10.1167/iovs.15-17306

Tang, Q., Luo, C., Lu, B., Fu, Q., Yin, H., Qin, Z., et al. (2017). Thermosensitive chitosan-based hydrogels releasing stromal cell derived factor-1 alpha recruit MSC for corneal epithelium regeneration. *Acta Biomater.* 61, 101–113. doi: 10.1016/j.actbio.2017.08.001

Tighe, S., Moein, H. R., Chua, L., Cheng, A., Hamrah, P., and Tseng, S. C. (2017). Topical cryopreserved amniotic membrane and umbilical cord eye drops promote re-epithelialization in a murine corneal abrasion model. *Invest. Ophthalmol. Visual Sci.* 58, 1586–1593. doi: 10.1167/iovs.16-20834

Tóth, E., Beyer, D., Zsebik, B., Vereb, G., and Takács, L. (2017). Limbal and conjunctival epithelial cell cultivation on contact lenses—different affixing techniques and the effect of feeder cells. *Eye Contact Lens* 43, 162–167. doi: 10.1097/ICL.0000000000000259

Tsai, C. Y., Woung, L. C., Yen, J. C., Tseng, P. C., Chiou, S. H., Sung, Y. J., et al. (2016). Thermosensitive chitosan-based hydrogels for sustained release of ferulic acid on corneal wound healing. *Carbohydrate Polymers* 135, 308–315. doi: 10.1016/j.carbpol.2015.08.098

Vázquez, N., Rodríguez-Barrientos, C. A., Aznar-Cervantes, S. D., Chacón, M., Cenis, J. L., Riestra, A. C., et al. (2017). Silk fibroin films for corneal endothelial regeneration: transplant in a rabbit descemet membrane endothelial keratoplasty. *Invest. Ophthalmol. Visual Sci.* 58, 3357–3365. doi: 10.1167/iovs.17-21797

Vepari, C., and Kaplan, D. L. (2007). Silk as a biomaterial. *Prog. Polymer Sci.* 32, 991–1007. doi: 10.1016/j.progpolymsci.2007.05.013

Wang, L., Huang, Y., Du, G., Dong, Y., Guo, H., Wang, D., et al. (2015). Long-term outcomes and complications of Moscow Eye Microsurgery Complex in Russia (MICOF) keratoprosthesis following ocular surface burns: clinical experience in China. *Br. J. Ophthalmol.* 99:12. doi: 10.1136/bjophthalmol-2014-306115

Wang, W. Y., Lee, Y. K., Tsai, S. H., Lin, Y. C., and Chen, Y. M. (2017). Autologous serum eye drops combined with silicone hydrogen lenses for the treatment of postinfectious corneal persistent epithelial defects. *Eye Contact Lens* 43, 225–229. doi: 10.1097/ICL.0000000000000261

Weisshuhn, K., Berg, I., Tinner, D., Kunz, C., Bornstein, M. M., Steineck, M., et al. (2014). Osteo-odonto-keratoprosthesis (OOKP) and the testing of three different adhesives for bonding bovine teeth with optical poly-(methyl methacrylate)(PMMA) cylinder. *Br. J. Ophthalmol.* 98, 980–983. doi: 10.1136/bjophthalmol-2013-303141

Weng, Y., Liu, J., Jin, S., Guo, W., Liang, X., and Hu, Z. (2017). Nanotechnology-based strategies for treatment of ocular disease. *Acta Pharma. Sin. B* 7, 281–291. doi: 10.1016/j.apsb.2016.09.001

Werkmeister, R. M., Sapeta, S., Schmidl, D., Garhöfer, G., Schmidinger, G., dos Santos, V., et al. (2017). Ultrahigh-resolution OCT imaging of the human cornea. *Biomed. Optics Express* 8, 1221–1239. doi: 10.1364/BOE.8.001221

Westekemper, H., Figueiredo, F. C., Siah, W. F., Wagner, N., Steuhl, K. P., and Meller, D. (2017). Clinical outcomes of amniotic membrane transplantation in the management of acute ocular chemical injury. *Br. J. Ophthalmol.* 101, 103–107. doi: 10.1136/bjophthalmol-2015-308037

Whitcher, J. P., Srinivasan, M., and Upadhyay, M. P. (2001). Corneal blindness: a global perspective. *Bull. World Health Organ.* 79, 214–221. Available online at: http://www.who.int/iris/handle/10665/58078

Wicklein, V. J., Singer, B. B., Scheibel, T., and Salehi, S. (2019). "Nanoengineered biomaterials for corneal regeneration," in *Nanoengineered Biomaterials for Regenerative Medicine*, eds M. Mozafari, J. Rajadas, and D. Kaplan (Amsterdam: Elsevier), 379–415. doi: 10.1016/B978-0-12-813355-2.00017-X

Wijnholds, J. (2019). "Basal cell migration" in regeneration of the corneal wound-bed. *Stem Cell Rep.* 12, 3–5. doi: 10.1016/j.stemcr.2018.12.009

Wu, M. F., Stachon, T., Langenbucher, A., Seitz, B., and Szentmáry, N. (2017). Effect of amniotic membrane suspension (AMS) and amniotic membrane homogenate (AMH) on human corneal epithelial cell viability, migration and proliferation *in vitro*. *Curr. Eye Res.* 42, 351–357. doi: 10.1080/02713683.2016.1192193

Xie, R. Z., Sweeney, D. F., Beumer, G. J., Johnson, G., Griesser, H. J., and Steele, J. G. (1997). Effects of biologically modified surfaces of synthetic lenticules on corneal epithelialization *in vivo*. *Austr. N. Zeal. J. Ophthalmol.* 25, 46–49. doi: 10.1111/j.1442-9071.1997.tb01755.x

Yam, G. H., Teo, E. P., Setiawan, M., Lovatt, M. J., Yusoff, N. Z. B. M., Fuest, M., et al. (2018). Postnatal periodontal ligament as a novel adult stem cell source for regenerative corneal cell therapy. *J. Cell. Mol. Med.* 22, 3119–3132. doi: 10.1111/jcmm.13589

Yamashita, K., Inagaki, E., Hatou, S., Higa, K., Ogawa, A., Miyashita, H., et al. (2018). Corneal endothelial regeneration using mesenchymal stem cell derived from human umbilical cord. *Stem Cells Dev.* 27:16. doi: 10.1089/scd.2017.0297

Zakaria, N., Possemiers, T., Dhubhghaill, S. N., Leysen, I., Rozema, J., Koppen, C., et al. (2014). Results of a phase I/II clinical trial: standardized, non-xenogenic, cultivated limbal stem cell transplantation. *J. Trans. Med.* 12:58. doi: 10.1186/1479-5876-12-58

Zarrintaj, P., Ahmadi, Z., Saeb, M. R., and Mozafari, M. (2018a). Poloxamer-based stimuli-responsive biomaterials. *Mater. Today Proc.* 5, 15516–15523. doi: 10.1016/j.matpr.2018.04.158

Zarrintaj, P., Bakhshandeh, B., Saeb, M. R., Sefat, F., Rezaeian, I., Ganjali, M. R., et al. (2018b). Oligoaniline-based conductive biomaterials for tissue engineering. *Acta Biomater.* 27, 16–34. doi: 10.1016/j.actbio.2018.03.042

Zarrintaj, P., Manouchehri, S., Ahmadi, Z., Saeb, M. R., Urbanska, A. M., Kaplan, D. L., et al. (2018c). Agarose-based biomaterials for tissue engineering. *Carbohydrate Polymers* 187, 66–84. doi: 10.1016/j.carbpol.2018.01.060

Zarrintaj, P., Moghaddam, A. S., Manouchehri, S., Atoufi, Z., Amiri, A., Amirkhani, M. A., et al. (2017). Can regenerative medicine and nanotechnology combine to heal wounds? The search for the ideal wound dressing. *Nanomedicine* 12, 2403–2422. doi: 10.2217/nnm-2017-0173

Zarrintaj, P., Saeb, M. R., Ramakrishna, S., and Mozafari, M. (2018d). Biomaterials selection for neuroprosthetics. *Curr. Opin. Biomed. Eng.* 6, 99–109. doi: 10.1016/j.cobme.2018.05.003

Zhang, L., Zou, D., Li, S., Wang, J., Qu, Y., Ou, S., et al. (2016). An ultra-thin amniotic membrane as carrier in corneal epithelium tissue-engineering. *Sci. Rep.* 6:21021. doi: 10.1038/srep21021

Zheng, T., and Xu, J. (2008). Age-related changes of human limbus on *in vivo* confocal microscopy. *Cornea* 27, 782–786. doi: 10.1097/ICO.0b013e31816f5ec3

Zhong, J., Deng, Y., Tian, B., Wang, B., Sun, Y., Huang, H., et al. (2016). Hyaluronate acid-dependent protection and enhanced corneal wound healing against oxidative damage in corneal epithelial cells. *J. Ophthalmol.* 2016:6538051. doi: 10.1155/2016/6538051

Zirm, E. K. (1989). Eine erfolgreiche totale Keratoplastik (A successful total keratoplasty). *J. Refract. Surg.* 5, 258–261.

Zsebik, B., Ujlaky-Nagy, L., Losonczy, G., Vereb, G., and Takács, L. (2017). Cultivation of human oral mucosal explants on contact lenses. *Curr. Eye Res.* 42, 1094–1099. doi: 10.1080/02713683.2017.1279635

Conflict of Interest Statement: The authors declare that the research was conducted in the absence of any commercial or financial relationships that could be construed as a potential conflict of interest.

frontiers in Bioengineering and Biotechnology

REVIEW
published: 18 June 2019
doi: 10.3389/fbioe.2019.00141

Applications of Iron Oxide-Based Magnetic Nanoparticles in the Diagnosis and Treatment of Bacterial Infections

Chen Xu[1,2,3], *Ozioma Udochukwu Akakuru*[1], *Jianjun Zheng*[4]* *and Aiguo Wu*[1]*

[1] *Cixi Institute of Biomedical Engineering, Chinese Academy of Science (CAS) Key Laboratory of Magnetic Materials and Devices & Key Laboratory of Additive Manufacturing Materials of Zhejiang Province, Ningbo Institute of Materials Technology and Engineering, Chinese Academy of Sciences, Ningbo, China,* [2] *Department of Experimental Medical Science, Hwa Mei Hospital, University of Chinese Academy of Sciences, Ningbo, China,* [3] *Key Laboratory of Diagnosis and Treatment of Digestive System Tumors of Zhejiang Province, Ningbo, China,* [4] *Department of Radiology, Hwa Mei Hospital, University of Chinese Academy of Sciences, Ningbo, China*

OPEN ACCESS

Edited by:
Hasan Uludag,
University of Alberta, Canada

Reviewed by:
Rajendra K. Singh,
Institute of Tissue Regeneration Engineering (ITREN), South Korea
Steve Meikle,
Independent Researcher, United Kingdom

***Correspondence:**
Jianjun Zheng
zhjjnb2@163.com
Aiguo Wu
aiguo@nimte.ac.cn

Specialty section:
This article was submitted to Biomaterials, a section of the journal Frontiers in Bioengineering and Biotechnology

Received: *24 March 2019*
Accepted: *28 May 2019*
Published: *18 June 2019*

Citation:
Xu C, Akakuru OU, Zheng J and Wu A (2019) Applications of Iron Oxide-Based Magnetic Nanoparticles in the Diagnosis and Treatment of Bacterial Infections. Front. Bioeng. Biotechnol. 7:141. doi: 10.3389/fbioe.2019.00141

Diseases caused by bacterial infections, especially drug-resistant bacteria have seriously threatened human health throughout the world. It has been predicted that antimicrobial resistance alone will cause 10 million deaths per year and that early diagnosis and therapy will efficiently decrease the mortality rate caused by bacterial infections. Considering this severity, it is urgent to develop effective methods for the early detection, prevention and treatment of these infections. Until now, numerous efforts based on nanoparticles have been made to detect and kill pathogenic bacteria. Iron oxide-based magnetic nanoparticles (MNPs), as potential platforms for bacteria detection and therapy, have drawn great attention owing to their magnetic property. These MNPs have also been broadly used as bioimaging contrast agents and drug delivery and magnetic hyperthermia agents to diagnose and treat bacterial infections. This review therefore overviews the recent progress on MNPs for bacterial detection and therapy, including bacterial separation and enrichment *in vitro*, bacterial infection imaging *in vivo*, and their therapeutic activities on pathogenic bacteria. Furthermore, some bacterial-specific targeting agents, used to selectively target the pathogenic bacteria, are also introduced. In addition, the challenges and future perspective of MNPs for bacterial diagnosis and therapy are given at the end of this review. It is expected that this review will provide a better understanding toward the applications of MNPs in the detection and therapy of bacterial infections.

Keywords: magnetic nanoparticles, bacterial infection, bacterial target molecules, detection, therapy

INTRODUCTION

Diseases caused by bacterial infections have raised worldwide concern and the early diagnosis of such bacterial infections is of great significance for diseases therapy in the clinic (Váradi et al., 2017). The conventional diagnosis method to discriminate bacterial pathogens in the clinic often depends on the cultivation of bacteria, which is acknowledged as the "gold standard" in the clinical diagnosis of bacterial diseases (Pazos-Perez et al., 2016; Wohlwend et al., 2016; Xu et al., 2018). However, the

traditional detection method consisting of cultivation, selective enrichment and conformation, is a tedious and time-consuming process; it takes up to 3 to 7 or more days to complete the biochemical testing process, delaying feedback to patients (Law et al., 2015; Váradi et al., 2017). To shorten the detection time and to acquire more accurate information about the bacteria, many more advanced methods including enzyme-linked immunoassays (Liu et al., 2017), western blotting (Liana et al., 2017), polymerase chain reaction (PCR) (Nguyen et al., 2017; Váradi et al., 2017), and whole genome sequencing (Ellington et al., 2017; Váradi et al., 2017), have been developed. The deficiencies of these modern methods are that they not only need precise and expensive instruments but also demand a lot from the operators (Sheikhzadeh et al., 2016; Wang et al., 2018a), consequently hindering their extensive use in the clinic.

For the past few years, iron oxide-based magnetic nanoparticles (MNPs) have extensively been studied as useful bacterial detection platforms due to their magnetic property (Shen et al., 2016; Suaifan et al., 2017; Yang et al., 2017; Wang et al., 2018b). Additionally, these MNPs have been widely used as bacterial separation agents (Shen et al., 2016; Xu et al., 2018), drug delivery (Bhattacharya and Neogi, 2017; Tokajuk et al., 2017; Wang et al., 2018c), bioimaging contrast agents (Lefevre et al., 2011; Li et al., 2017b) and magnetic hyperthermia agents (Ribeiro et al., 2018; Wang et al., 2018c) to diagnose and treat bacterial infections. For example, MNPs can be functionalized with target molecules such as various antibodies, antibiotics, antimicrobial peptides, bacteriophages and aptamers for bacterial separation and concentration (Chen et al., 2017). On the basis of the surface modification, MNPs conjugated with different metals allow the development of various methods for bacterial detection, including colorimetric, fluorescent, and surface-enhanced Raman detections (Yuan et al., 2018b). Apart from the *in vitro* detection methods, superparamagnetic iron oxide-based NPs have also been demonstrated as magnetic resonance imaging (MRI) contrast agents for *in vivo* bacterial imaging (Li et al., 2017b). Furthermore, MNPs with unique magnetic properties and high specific surface area have shown great promise in antibacterial applications (Lai and Chen, 2013; Ribeiro et al., 2018).

The diagnosis and treatment of bacterial diseases are of great concern for the prevention and control of bacterial infections. Figuring out the role of MNPs on bacterial diagnosis and treatment might have a guiding significance in designing and constructing MNPs-based materials for the detection and therapy of bacterial infections. This review therefore summarizes some recent progress on MNPs-based materials for bacterial detection and therapy, including bacterial detection *in vitro*, *in vivo* bacterial infection imaging, and their therapeutic activities on pathogenic bacteria (**Scheme 1**). First, target molecules for bacteria are listed, and their detection sensitivities as well as bacterial selectivity are summarized. Second, we present the available methods based on MNPs for *in vitro* and *in vivo* bacterial detection. Third, MNPs used as antibiotic delivery and magnetic hyperthermia agents for bacteria therapy are discussed. Lastly, the challenges and outlook of MNPs for bacterial diagnosis and treatment are put forward.

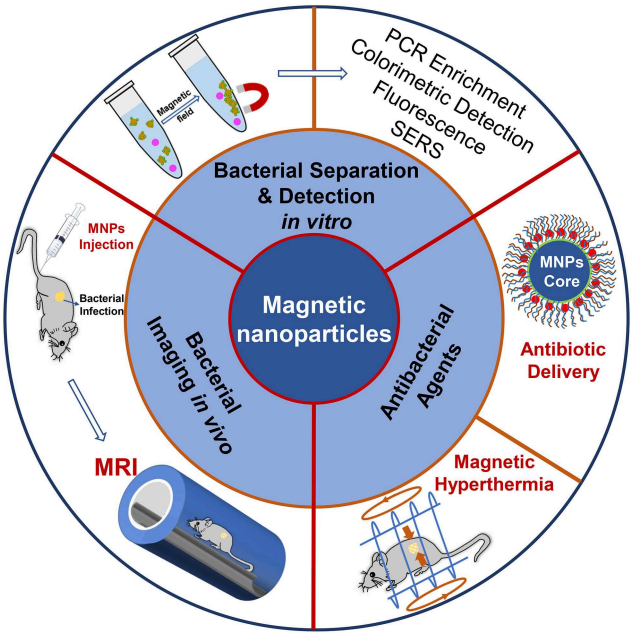

SCHEME 1 | MNPs based nanoparticles for bacterial detection and therapy.

BACTERIAL TARGET MOLECULES FOR BACTERIAL SEPARATION AND ENRICHMENT

It was reported that centrifugation and filtration are commonly used for rapid bacterial separation and concentration (Liébana et al., 2013). Compared to the nonspecific methods, MNPs modified with bacteria-specific target molecules are quite suitable for bacterial separation and concentration because they can selectively target specific bacteria and can be controlled easily by an external magnetic field (Zhu et al., 2015). These emphasize their potential use in the rapid, efficient, specific capture, and enrichment of targeted bacteria from complex samples. The success of the separation and enrichment of designated bacteria by MNPs depends on the selection of target molecules. Previous studies have reported that various antibodies, antibiotics, antimicrobial peptides, bacteriophages as well as aptamers, which can be used as target molecules for bacteria, have been modified on the surface of MNPs for bacteria labeling and separation under a magnetic field (Chen et al., 2017). The representative target molecules for bacterial detection are listed in **Table 1**.

Antibodies

Many studies have proven that antibodies specific to different bacteria can be conjugated on the surfaces of MNPs for the selective targeting and separation of bacteria. For instance, MNPs have been modified with H- or O-antibodies for the separation of *Salmonella typhimurium* (*S. typhimurium*), since the H- or O-antigens are recognized as the two typical surface structures of the *Salmonella* (Kuang et al., 2013; Sakudo et al., 2015; Kim et al., 2016). The H-antigen is the antigenic type

TABLE 1 | Examples of bacterial target molecules conjugated MNPs for bacterial detection.

Target agent	Materials	Detected bacteria	Sample	Method	Detection limit	References
Antibodies	Anti-*E. coli* antibody conjugated MNPs	*E. coli*	Bacterial suspension	Fluorescence	10 CFU/mL	Park et al., 2017
	monoclonal antibody (MAb)-conjugated MNPs	*S. typhimurium*	Bacterial suspension	Colorimetric detection	2 × 10 cells	Shim et al., 2014b
	monoclonal antibodies (mAbs)-conjugated magnetic beads	*E. coli* and *F. tularensis*	Bacterial suspension	SERS and fluorescence	10^2 cells/mL	Jang et al., 2016
Vancomycin	Fe_3O_4/Van/PEG magnetic nanocarrier; Van-PEG-PLL-MNPs	*L. monocytogenes*	Mixed solutions	PCR	10 CFU/mL	Zhu et al., 2015; Yang et al., 2017
	Van-PEGylated-MNPs	*L. monocytogenes*	Bacterial suspension	PCR	30 CFU/mL	Meng et al., 2017
	Fe_3O_4@Ag-Van MNPs and Au@Ag NPs	Broad range of Gram-positive and Gram-negative bacteria	Bacterial suspension	SERS	5 × 10^2 cells/mL	Wang et al., 2018a
Vancomycin and ALP-IgG	ALP-IgG-Van- magnetic beads	*S. aureus*	Water/milk/urine and saliva	Fluorescence	3.3 CFU/mL	Yang et al., 2016
Streptavidin	MNP@Strep/Ag	*S. aureus* and *S. pyogenes*	knee joint fluid	SERS	–	Fargašová et al., 2017
Amoxicillin	Amoxicillin-conjugated Fe_3O_4	*S. aureus*/ *E. coli*	Mixed solutions	MALDI MS	10^3 CFU/mL	Hasan et al., 2016
Antimicrobial peptide	AMP modified Fe_3O_4 NPs and 4-MPBA modified Au@Ag-GO nanocomposites	*E. coli*, *S. aureus* and *P. aeruginosa*	Whole blood	SERS	10 CFU/mL	Yuan et al., 2018a
T4 bacteriophage	T4 bacteriophage modified Fe_3O_4	*E. coli*	Bacterial suspension	–	–	Liana et al., 2017
T7 bacteriophage	T7 bacteriophage-conjugated magnetic beads	*E. coli*	Drinking water	Colorimetric detection	10 CFU/mL	Chen et al., 2015a
PAP1 bacteriophage	PAP1-functionalized magnetic beads	*P. aeruginosa*	Bacterial suspension	Colorimetric detection	2 × 10^2 CFU/mL	He et al., 2017
E. coli specific DNAzyme	MNP-DNAzyme-AChE (MDA) complex and DNA-templated fluorescent silver nanoclusters	*E. coli*	Bacterial suspension	Fluorescence	60 CFU/mL	Zheng et al., 2018
Aptamers	Fe_3O_4-Ce6-Aptamer	*S. aureus*/ *E. coli*	Blood samples from mice	Fluorescence	10 CFU/mL	Wang et al., 2018b
	Aptamer modified Fe_3O_4 NPs and Co^{2+} enhanced N-(aminobutyl)-N-(ethylisoluminol) (ABEI) functional flowerlike gold nanoparticles	*S. typhimurium*	*In vitro*	Fluorescence	32 CFU/mL	Hao et al., 2017
	Aptamer-functionalized Fe_3O_4@silica	*S. aureus*	Whole blood	Fluorescence	682 CFU	Borsa et al., 2016

of bacterial flagella while the O-antigen is a glycan polymer comprising lipopolysaccharides (LPS). The detection method for *S. typhimurium* was rapid and specific with neither the requirement of harmful reagents nor laborious pretreatments.

To enhance the antibody immobilization at conjugation sites, MNPs clusters developed by the microemulsion method were used to highly select and rapidly separate *S. typhimurium* (Kim et al., 2016). As illustrated in **Figure 1A**, the MNPs coated with oleic acid were used as the precursor to form magnetic nanoclusters. Owing to the exposed carboxyl groups around the nanoclusters, they provided more conjugation sites for the immobilization of H- and O-antibodies. Consequently, the MNPs nanoclusters had the ability to effectively capture *S. typhimurium*. A difference in the cell separation efficiency was observed between the two antibodies-decorated nanoclusters, with a capture efficiency of about 99 and 57% for the O- and H-antibody-modified nanoclusters, respectively (Kim et al., 2016). Transmission electron microscopic analysis (**Figure 1B**) confirmed that the two different types of antibody-modified nanoclusters accumulated in different spatial locations of the bacteria according to the different antibody-antigen interactions. The H-antibody-modified nanoclusters accumulated in the bacterial flagella (**Figure 1Ba**), while the O-antibody-coated nanoclusters accumulated on the bacterial cell wall (**Figure 1Bb**).

To explain the difference in the capture efficiencies, the authors put forward several potential reasons: on one hand, the mobility of the flagella as well as its easy detachment from the bacterial body hindered the binding interaction between the H-antibody and the corresponding antigen. On the other hand, the magnetic nanoclusters demonstrated a tendency to be adsorbed on biofilm containing polysaccharides and cellulose. As a type of glycan polymer, O-antigen on the cell wall membrane can capture more nanoclusters than that of the H-antigen. Accordingly, the O-antibody-coated nanoclusters showed high capture efficiency toward *S. typhimurium* (Kim et al., 2016). Therefore, the combined antibodies and MNPs-based nanoclusters led to a synergistic effect on the efficient and rapid detection of bacterial pathogens. The material design shows an inspiring strategy to improve bacterial capture efficiency by decorating MNPs with optimal types of antibodies. However, at very low concentrations of the detecting bacteria, the magnetic separation method still requires several hours to complete the enrichment steps.

A 3D microfluidic magnetic preconcentrator, in which an antibody was conjugated to the target molecule was fabricated to preconcentrate enterohemorrhagic *Escherichia coli* (*E. coli*) within 1 h (Park et al., 2017). By comparison, it can preconcentrate bacterial cells in large-volume samples. In general, antibody modified MNPs show potential as tools to capture, concentrate and discriminate different strains of bacteria. However, the high-cost and poor stability in severe environments remain the major drawbacks for the utility of antibodies.

Antibiotics

Various antibiotics, including vancomycin, amoxicillin, streptavidin etc., have been extensively applied as agents for targeting bacteria. Vancomycin, which can bind to the bacterial cell wall of both Gram-negative and Gram-positive bacteria, was recognized as a target molecule for specific bacterial detection (Wang et al., 2014). As a glycopeptide antibiotic, vancomycin can recognize bacteria because of its ability to interact with the peptidoglycans on the bacterial cell wall. For Gram-positive bacteria, vancomycin can bind onto D-alanyl-D-alanine—the terminal residues of mucopeptides on the bacterial cell wall (Batchelor et al., 2010; Wang et al., 2014). For Gram-negative bacteria, vancomycin can bind with the L-lysin-D-alanine residues of peptidoglycans expressed on the outer membrane of bacterial cells (Kell et al., 2008; Wang et al., 2014). Thus, MNPs functionalized with vancomycin have been considered as an attractive type of capturing agent to effectively concentrate multiple strains of bacteria, such as *Staphylococcus aureus* (*S. aureus*) (Yang et al., 2016), *Bacillus subtilis* (*B. subtilis*) (Yang et al., 2016), and *Lister monocytogenes* (*L. monocytogenes*) (Wang et al., 2014, 2018a; Zhu et al., 2015; Yang et al., 2017). However, it is not efficient for the capture of vancomycin-resistant bacteria because of its poor affinity for the cell wall. Another antibiotic amoxicillin, which is a β-lactam antibiotic, can be attached to bacteria though penicillin binding proteins (PBPs). Thus, amoxicillin modified MNPs can also be used for the separation of bacteria (Hasan et al., 2016). The selective affinity of amoxicillin-functionalized MNPs toward bacteria mainly depends on the affinity of the β-lactam of amoxicillin with PBPs on the bacteria. Based on the binding mechanism, the amoxicillin modified MNPs were successfully applied to separate *S. aureus* and *E. coli*. The advantages of antibiotics are that they are highly stable, inexpensive and highly specific for most bacteria. Even so, it is generally thought that antibiotics are often small molecules and as such cannot provide a proper number of binding sites for bacterial identification. Ulteriorly, bacteria resistance issues have increased in recent years, necessitating the need to provide routes that avoids abusing antibiotics in bacteria detection.

Antimicrobial Peptides

Antimicrobial peptides (AMP) enable the inactivation of different bacteria, viruses and fungi, making them remarkable as therapeutic agents for diseases. On account of the terrible increase of drug-resistant bacteria, the use of both synthetic and natural antimicrobial peptides has been explored for bacteria separation and detection (Da Costa et al., 2015). It has been demonstrated that antimicrobial peptides, such as bacitracin A- (Yuan et al., 2018a), pediocin- (Adhikari et al., 2014), cecropin- (Baek et al., 2016) functionalized MNPs can be applied as probes for bacteria capture, isolation and enrichment. Yuan et al. developed bacitracin A-modified MNPs and observed no change in the recognition site of the bacitracin A for bacteria, irrespective of its modification with MNPs. Owing to the direct interaction between bacitracin A and lipid, and indirect interactions mediated by Zn^{2+} and Na^{+}, bacitracin A was tightly wrapped around the lipid pyrophosphate before and after the modification with MNPs, resulting in a strong interaction between bacitracin A and the bacteria. Thus, MNPs-bacitracin A conjugates would be attached to the bacteria, and the complexes would be easily separated under an external magnetic field (Yuan et al., 2018a). When applied as the bacteria capture element, antimicrobial peptides have several attractive advantages over antibodies: they are cost effective, possess better stability in harsh environments, and have long peptide chains, leading to a higher density of recognition sites for bacteria capture.

Bacteriophages

Bacteriophages, which can specifically target bacteria without particular affinity for human host cells, have gained increased attention as an alternative to bacterial separation and detection. On the basis of the targeting and infectivity toward designated bacteria, bacteriophages have been used as recognition agents for bacterial detection. In this regard, T4 and T7 bacteriophages, which can infect *E. coli*, have been widely used to decorate MNPs for capturing *E. coli* (Chen et al., 2015a,b; Liana et al., 2017). Additionally, PAP1, a bacteriophage with high specificity for *Pseudomonas aeruginosa* (*P. aeruginosa*), was used to functionalize MNPs in order to establish a bacteriophage-affinity strategy for the separation and detection of *P. aeruginosa* (He et al., 2017). The PAP1-modified MNPs showed very high specificity toward *P. aeruginosa* without any response to the other interfering bacteria. The entire bacterial separation and detection process, including bacteria capture, PAP1 replication and bacteria lysis could be completed within 2 h (He et al., 2017). Interestingly, MNPs modified with bacteriophages can also be used to exclude

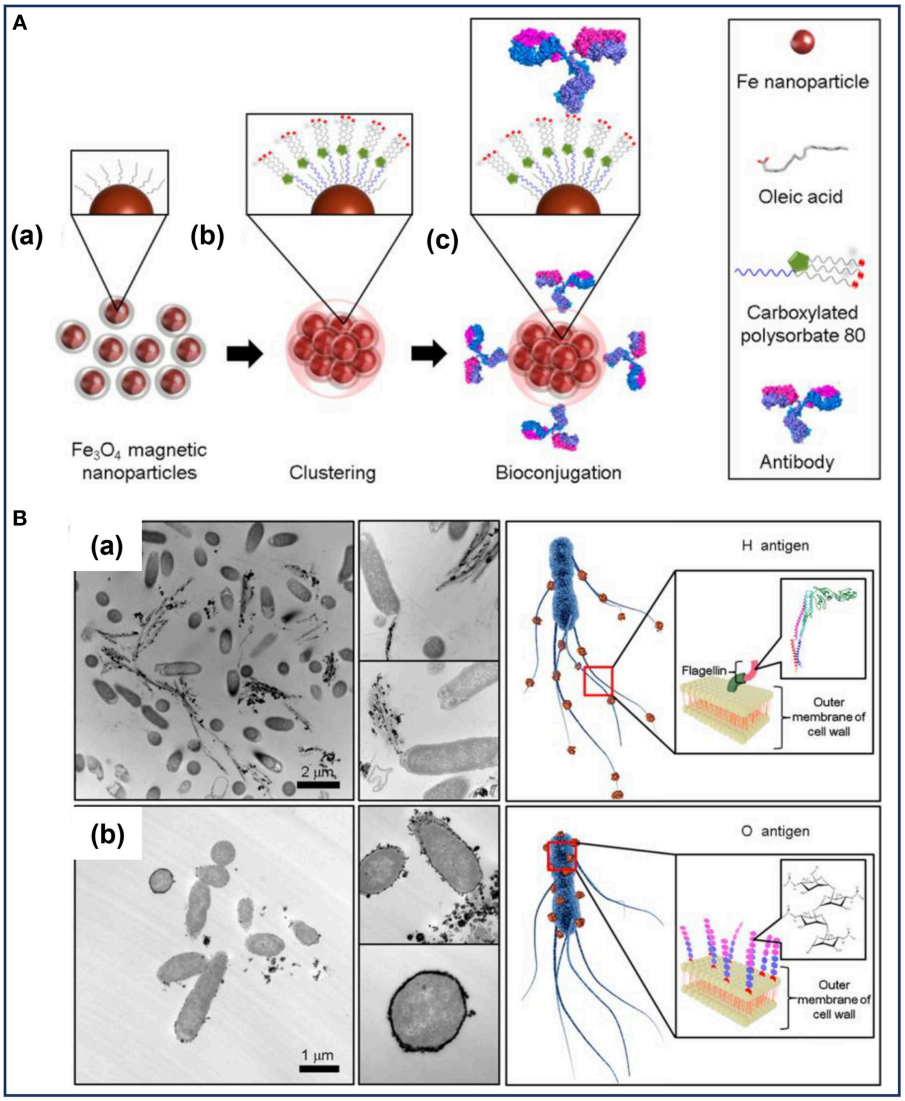

FIGURE 1 | (A) Illustration of the preparation of the bioconjugated magnetic clusters with antibodies and **(B)** the different selective targets of *Salmonella typhimurium* for different antigens. Reprinted with permission from Kim et al. (2016). Copyright (2016) American Chemical Society.

the interference of inactive bacteria, since the bacteriophages only replicate in active bacterial cells (Chen et al., 2017; He et al., 2017). Furthermore, these kinds of MNPs modified with bacteriophages could be extensively used for the detection of other bacterial pathogens by utilizing virulent bacteriophages specific to target bacteria. Considering the relatively inexpensive and easy solution to obtain bacteriophages for different strains of bacteria, bacteriophages offer significant advantages for bacterial detection.

Aptamers

As single stranded nucleic acids (DNA or RNA), aptamers have shown great potential in constructing recognition probes for bacterial detection. To sensitively detect the pathogenic bacteria, aptamers can be integrated with MNPs to construct a simple capture platform for bacteria (Shen et al., 2016; Wang et al., 2018b). When exposed to target bacteria, the corresponding aptamer will attach on the bacterial cells with high affinity and selectivity, and in contrast to antibodies, they can be exposed to elevated temperatures without being irreversibly denatured. Afterwards, the bacterial pathogens can be separated and further concentrated from their bloodstreams by an external magnetic field. It is worth noting that MNPs modified with different aptamers can be used to separate and concentrate different bacteria or other biomarkers. For instance, Wang and co-researchers reported a nanosystem based on aptamer functionalized MNPs for early diagnosis of blood disinfection (Wang et al., 2018b). Based on the nanoparticles, the multiple strains of bacteria could be successfully diagnosed, and bacterial strains identification and enrichment could be achieved in a

single step. Aptamer-based capture platform (denoted as Apt-Fe_3O_4@$mTiO_2$) has been constructed for the sensitive detection of *S. aureus* in bloodstream infections (Shen et al., 2016). The bacterial-capture efficiency of the Apt-Fe_3O_4@$mTiO_2$ platform within 2 h was up to 80% even at low infectious doses. After the application of an external magnetic field, the *S. aureus* in the complexes could be selectively separated for further detection. It was demonstrated that MNPs conjugated with different aptamers could provide a feasibility for sensitive and specific detection of bacterial pathogens.

MNPs-BASED COMPOSITES FOR BACTERIAL DETECTION *IN VITRO*

The ease of utilizing magnetic fields to control the location of MNPs-based composites after their conjugation with different bacterial target molecules has been explored for bacterial separation, enrichment, and discrimination. Thus, MNPs assisted with different detection methods, such as polymerase chain reaction (PCR), colorimetric detection, fluorescent detection, and surface-enhanced Raman detection (Yuan et al., 2018b) have been used to design various platforms for bacterial detection.

PCR Enrichment

PCR is considered as one of the most promising alternatives to conventional methods of molecular diagnostics. However, it requires onerous steps and excessive labor for preconcentrating a relatively small number of bacterial cells from a liquid sample. To reduce the preconcentration time and extra steps, MNPs conjugated with different bacterial target molecules can enable bacterial cells to be concentrated prior to PCR in an integrated microfluidic PCR system, taking about 2 h or less to complete the preconcentration process and PCR steps (Ganesh et al., 2016). The system shows potential for an application as a platform for the rapid and specific detection of bacteria. To enhance the detection sensitivity of bacterial pathogens, Fe_3O_4@SiO_2-based MNPs conjugated with *Pseudomonas aeruginos*a (*P. aeruginos*a) Genomic DNA (Tang et al., 2013), amino-rich silica-coated MNPs (Bai et al., 2016), MNPs conjugated with different antibodies for *S. aureus* and *Salmonella enteritidis* (*S. enteritidis*) (Houhoula et al., 2017), and MNPs functionalized with vancomycin (Meng et al., 2017) were used directly in the PCR enrichment procedure for bacterial pathogen enrichment. These studies demonstrated that the MNPs-based composites showed great potential for highly efficient enrichment of bacterial pathogens without time-consuming and onerous steps in the PCR procedure.

Colorimetric Detection

Colorimetric detection is a qualitative analysis, which is based on bacteria-induced color changes which are visible to the naked eye. MNPs-based platforms have been developed for colorimetric detection of bacteria. Previous studies have reported that MNPs modified with monoclonal antibodies (mAb) were directly used to rapidly and sensitively detect *Salmonella typhimurium* (*S. typhimurium*) (Shim et al., 2014b) and *Listeria monocytogenes* (*L. monocytogenes*) (Shim et al., 2014a) based on color changes, which arose from MNPs aggregates through the filtration process. First, MNPs conjugated with the antibody were used to concentrate and purify the target bacterium under magnetic fields. After filtering through a membrane, the MNPs conjugates bound or unbound to bacteria can be easily separated by vacuum pressure, and the changes of color signals caused by the remaining MNPs reflected the amount of bacteria as shown in **Figure 2** (Kim et al., 2018). For the *L. monocytogenes*, the capture efficiency of the conjugates ranged from 48 to 89% for solutions with bacterial cells from 2×10^3 to 2×10^1, and the results can be concluded within 35 min (Shim et al., 2014a). The efficiencies gradually decreased with an increase in the concentration of *L. monocytogenes*, which might be because of the limited addition of mAb-MNPs. It was observed that the bacterial capture efficiency would increase significantly, if more mAb-MNPs were used to test the bacterial solutions.

Gold (Au) NPs, which have distinct color changes caused by NPs aggregation, are the most common noble metal NPs to be used in colorimetric detection (Yuan et al., 2018b). As a consequence, MNPs-Au conjugates are promising platforms for bacterial detection. For example, Alhogail and others designed MNPs-coated Au conjugates for the detection of *L. monocytogenes*. After the surface modification of the gold sensor, the black MNPs covered up the color of the gold NPs. Upon cleavage of the peptide sequence by *Listeria* protease, the color of the conjugates changed from black to gold (Alhogail et al., 2016). Colorimetric method is very convenient and does not require any complicated equipment, and therefore could be used as a rapid, sensitive, and cost-effective tool for bacterial detection.

Fluorescent Detection

Fluorescent detection is more sensitive and offers a higher detection limit than colorimetric methods. As a result of its low background, high sensitivity, high specificity, and the ease for quantitative analysis, fluorescent detection has been widely combined with MNPs for bacterial detection, since it is an emerging trend for the development of efficient biosensors for clinical use (Kwon et al., 2013; Tang et al., 2013; Chen et al., 2015c; Qin et al., 2016). MNPs with different fluorescent labels, such as Au (Kwon et al., 2013), rare earth-doped upconversion NPs (Qin et al., 2016), and the other labels (Jang et al., 2016; Shelby et al., 2017; Gontero et al., 2018) were conjugated with antibody or other target molecules for the detection of pathogenic bacteria. In these composite NPs, MNPs were used to capture and separate bacteria. Kwon et al. prepared Au-coated MNPs for the detection of *S. typhimurium* with the help of magnetophoretic separation (Kwon et al., 2013). The absorption of visible light could be observed after coating with Au NPs, indicating an enhanced sensitivity of the light absorption (**Figure 3Aa**). It was observed that after co-culturing with *S. typhimurium*, the Au-coated MNPs tended to accumulate around the bacteria (**Figure 3Ab**). As shown in **Figure 3B**, Au-coated MNPs-bacteria complex separated from the free Au-coated MNPs could move under an external magnetic field. The isolated Au-coated MNPs-bacteria complex at the bottom of each tube could be dispersed for further measurement by UV-vis spectrometer. This detection method based on magnetophoretic chromatography provided a detection limit of 100 CFU/mL for *S. typhimurium*.

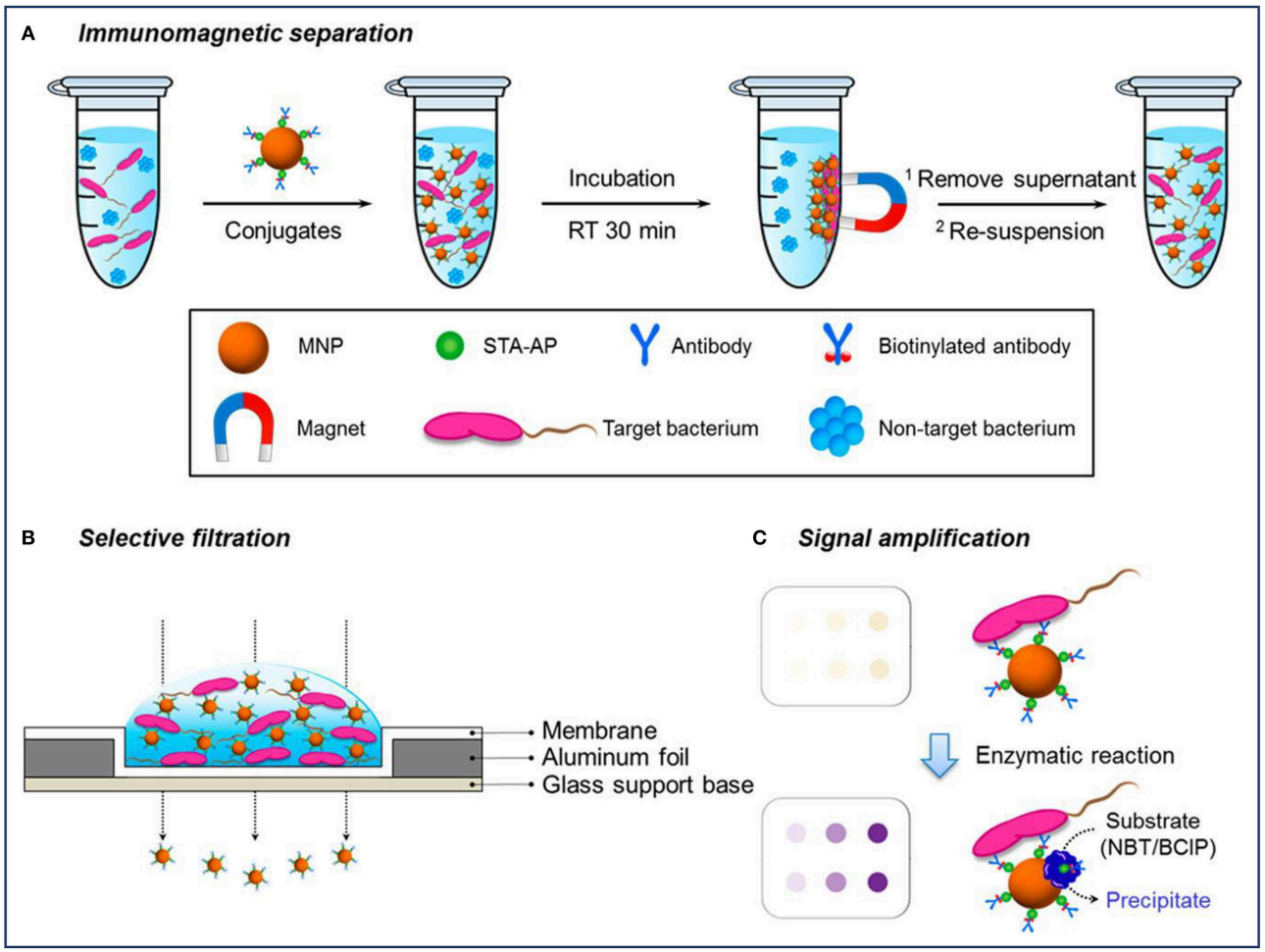

FIGURE 2 | Schematic diagram of a selective filtration method for the colorimetric detection of *Escherichia coli*. Reprinted with permission from Kim et al. (2018). Copyright (2018) American Chemical Society. **(A)** Immunomagnetic separation for target bacteria using MNP conjugates; **(B)** selective filtration of target bacteria-conjugates complexes, and **(C)** colored spots on the filter membrane by target bacteria-conjugates (upper) and enhanced colorimetric spots by enzymatic amplification with precipitation on the bacteria-conjugate surfaces (lower).

Furthermore, the detection sensitivity can be improved by doping with other fluorescent labels (Kwon et al., 2013). Rare earth-doped upconversion NPs (UCNs) can also be used as the luminescence labels to detect bacterial pathogens since they have many attractive properties such as superior photostability, sharp emission lines and lack of autofluorescence. Consequently, MNPs have been combined with UCNs to construct a specific and sensitive platform to combine magnetic capture with fluorescent identification for the detection of *Porphyromonas gingivalis* (*P. gingivalis*) (Qin et al., 2016). The results showed that the platform, which comprised of magnetic and fluorescent modalities, allowed for the quantitative detection of pathogens in a wide range of concentrations.

Surface-Enhanced Raman Detection

Surface-enhanced Raman spectroscopy (SERS) detection for bacteria can avoid the lengthy time for sample preparation and has been exploited for bacterial detection owing to the tremendous enhancement of Raman signal. In order to make the most of SERS for bacterial detection and monitoring, it is desirable to combine MNPs with SERS to construct a method for bacteria capture and detection (Liu et al., 2011). Recently, Fe_3O_4@Ag (Fargašová et al., 2017; Wang et al., 2018a) and Ag@Fe_3O_4 (Li et al., 2017a) composite MNPs have been constructed and modified with different target molecules such as vancomycin for a wide range of bacteria, biotinylated antibodies for both *S. aureus,* and *Streptococcus pyogenes* (*S. pyogenes*), for pathogenic bacteria separation and detection. Wang and co-researchers presented a sensitive MNPs-assisted SERS biosensor based on Fe_3O_4@Ag MNPs and Au@Ag NPs to effectively capture and discriminate bacteria. The Fe_3O_4@Ag MNPs were used as multifunctional platforms for bacteria capture and enrichment, as well as SERS substrates to enhance the signals of captured bacteria. An additional amount of the Au@Ag NPs was also introduced to further improve the SERS detection sensitivity. Since vancomycin has been reported to have a strong affinity for a broad range of Gram-positive and Gram-negative bacteria, this combined platform based on vancomycin modified

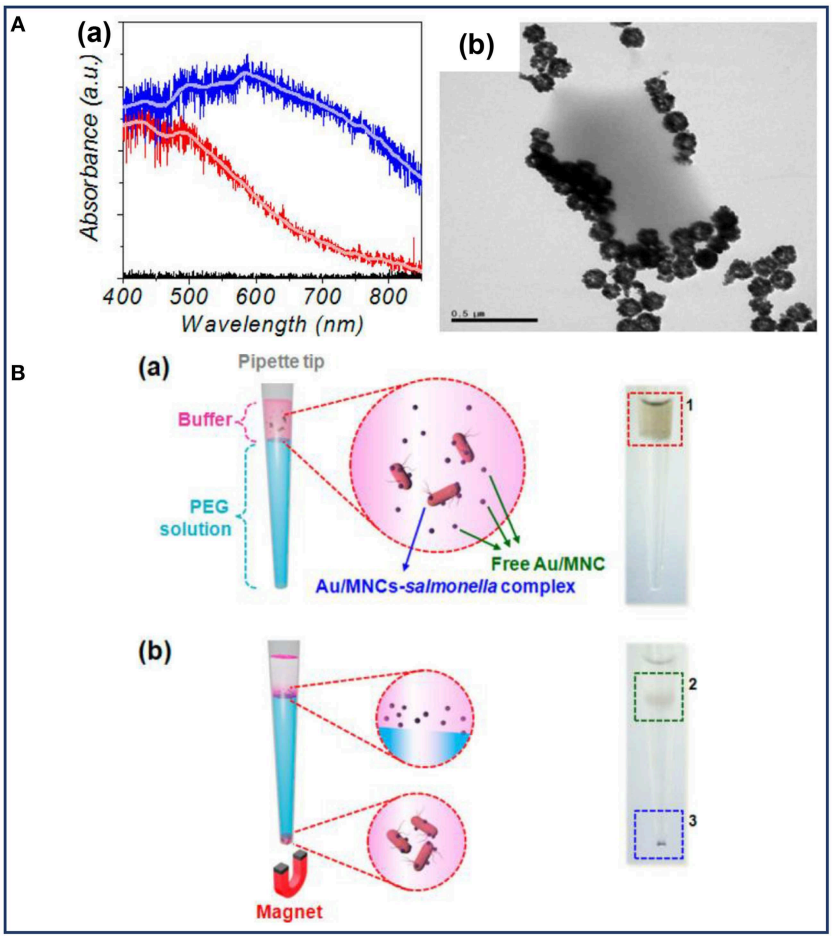

FIGURE 3 | (A) Characterization of the Au-coated MNPs: (a) absorption spectra of MNPs (red line) and Au-coated MNPs (blue line), (b) TEM image of Au-coated MNPs bound with *Salmonella typhimurium*; **(B)** schematic illustration and the corresponding optical images before (a) and after (b) magnetophoretic chromatography. Reprinted with permission from Kwon et al. (2013). Copyright (2013) American Chemical Society.

Fe_3O_4@Ag MNPs and Au@Ag NPs could be applied for the detection of various strains of bacteria. It was demonstrated that both *E. coli* and methicillin-resistance *S. aureus* (MRSA) could be effectively captured by vancomycin-modified Fe_3O_4@Ag MNPs. Upon separating and rinsing the bacteria, the MNPs and Au@Ag NPs constructed a very large number of hot spots on the bacteria cells synergistically, leading to an ultrasensitive SERS detection with a low detection limit of 5×10^2 cells/mL. More importantly, different bacteria such as *S. aureus*, *E. coli,* and MRSA could be sensitively and specifically discriminated according to different SERS spectra, and the results were further verified by the principal component analysis (PCA).

Previous studies have demonstrated that bacterial Raman spectra is directly related to bacterial cell wall components. Therefore, the differences in bacterial cell wall components make the SERS signals unique for different strains of bacteria. Based on these, the combined system shows great potential for the detection of bacterial infections. Furthermore, it was reported that the SERS intensity could also reflect the concentration of bacteria (Wang et al., 2016). As shown in **Figure 4A**, Au-coated core/shell magnetic NPs (AuMNPs) were designed, and further modified with *S. aureus* antibody and SERS tag for *S. aureus* capture, separation and detection (**Figure 4B**). The magnetic core endowed the nanocomposites with superior magnetic property for bacteria separation, and the outer Au shell provided high SERS activity for bacteria detection. According to the SERS spectra corresponding to different concentrations of *S. aureus*, several strong Raman bands of the SERS tag were observed (**Figure 4C**). It was obvious that with the help of SERS tag, *S. aureus* was detected with a detection limit of 10 cells/mL. Moreover, the main Raman peak (1331 cm^{-1}) exhibited a linear relationship with the logarithm of bacteria concentrations ranging from 10^1 to 10^5 cells/mL (**Figure 4D**).

MAGNETIC NANOPARTICLES AS MRI CONTRAST AGENTS FOR BACTERIAL DETECTION *IN VIVO*

The common *in vivo* imaging methods for bacterial infections based on fluorophores, radioisotopes and microbubbles cannot

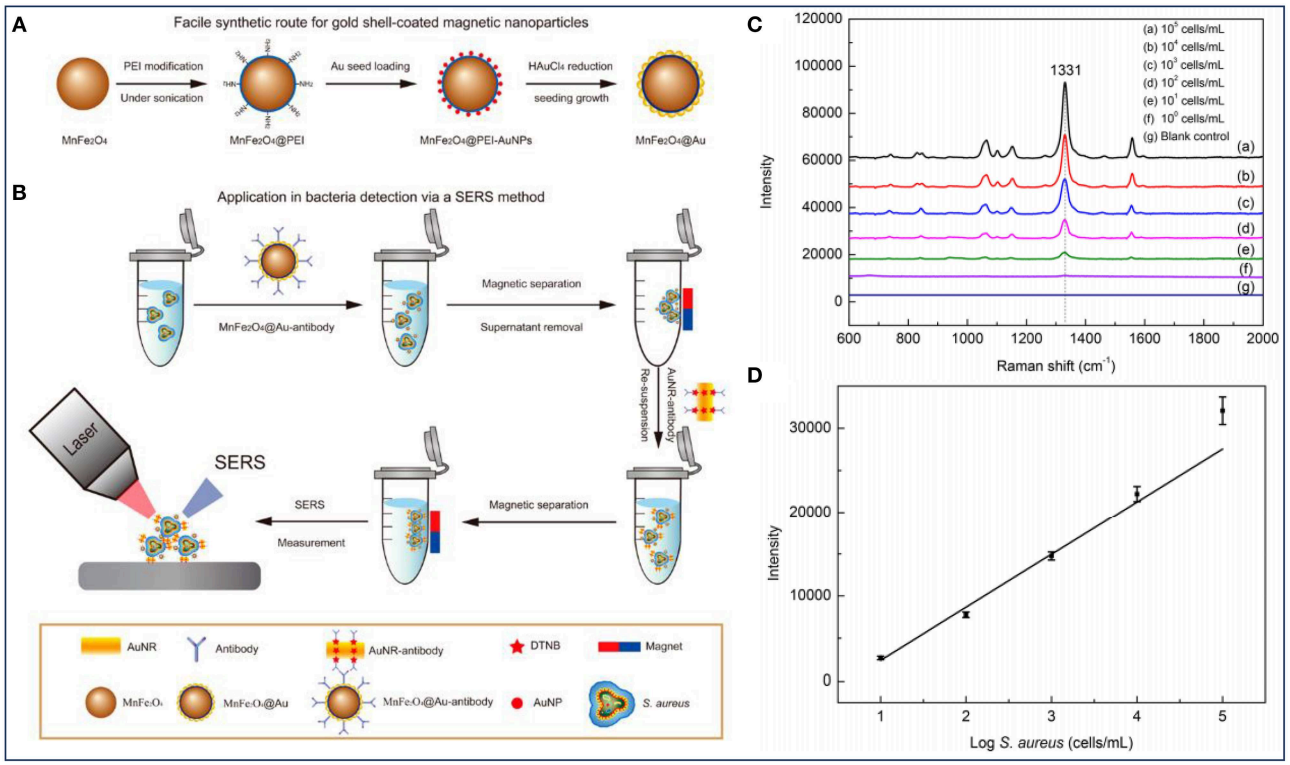

FIGURE 4 | Au-coated magnetic NPs (AuMNPs) for *Staphylococcus aureus* capture, separation and detection. **(A)** Illustration of synthetic route of AuMNPs, **(B)** illustration of the detection procedures for *S. aureus* via a SERS method, **(C)** SERS spectra with various concentrations of *S. aureus* (from 10^1 to10^5 cells/mL), and **(D)** calibration curve for *S. aureus* at a concentration ranging from 10^1 to 10^5 cells/mL obtained by using SERS intensity at 1,077 cm^{-1}. Reprinted with permission from Wang et al. (2016). Copyright (2016) American Chemical Society.

provide enough information about the lesion site. Various studies have reported MRI as an alternative imaging modality for visualizing bacterial infection *in vivo* without ionizing radiation and invasion, since ^1H is the most abundant magnetic nucleus in humans and is the most commonly investigated subject in MRI. This is complemented by the capacity of MRI to image the abnormal structures in a three-dimensional tomographic manner with a high spatial resolution. Previous studies reported that MNPs with superparamagnetism could shorten the longitudinal or transverse relaxation time of water protons nearby, thus MNPs-based contrast agents have been used to enhance the signal of the abnormal anatomy for the detection and monitoring of infectious diseases (Lefevre et al., 2011; Chen et al., 2016a). Particularly, MRI has been explored to noninvasively track bacteria and monitor antibiotic therapy of bacterial infection by using MNPs-based contrast agents (Lefevre et al., 2011; Hoerr et al., 2013).

To investigate the infection biology of clinically relevant bacteria, Hoerr and others established an imaging platform for *S. aureus* tracking *in vivo* by MRI. They constructed subcutaneous and systemic mouse infection models by the direct injection of MNPs-labeled or unlabeled *S. aureus*. After 24 h, MRI images showed a high resolution in both systemic and subcutaneous mouse infection model, which allowed for bacterial cells tracking and afforded information on the organ's morphology as well as the inflammatory response (Hoerr et al., 2013). By labeling different bacteria with MNPs, the established bacterial labeling strategy for MRI can also be applied for tracking the other infectious diseases to investigate infection biology.

Furthermore, MNPs for contrast-enhanced macrophage MRI *in vivo* have been used for the assessment of antibiotic therapy. In contrast to the conventional extracellular contrast agents such as gadoterate dimeglumine, the MNPs-based contrast agents undergo macrophage phagocytosis, which would bring a visible signal intensity change during the acute period and after antibiotic treatment (Lefevre et al., 2011). On the other hand, MNPs-based contrast agents provided an ultrasensitive imaging in *Mycobacterium tuberculosis* (*M. tuberculosis*) (Lee et al., 2012) and *Helicobacter pylori* (*H. pylori*) (Li et al., 2017b) infection. Li et al. illustrated this strategy for the specific capture of *H. pylori* in the gastric environment for the first time (Li et al., 2017b). By reversibly binding with peptidoglycan on the bacterial cell wall, the crab-like MNPs allowed for an accelerated aggregation of magnetic graphitic nanocapsules (MGNs), which allowed an easier capture of *H. pylori*. For the *in vivo* study, mice were treated with MGN and MGN@B-PEG, respectively, by intragastric administration. When the MNPs were intravenously injected into

infectious mice model, the signal intensity in the granulomatous site showed an enhancement on the T_2-weighted MRI images. Obviously, it was observed that *H. pylori* was difficult to be detected after MGNs injection because of the rapid elimination of the NPs. On the contrary, MGN@B-PEG was aggregated and retained in the mice abdomen for a prolonged period, thus enabling a stable T_2-weighted imaging of gastric mucosa infected with *H. pylori* (Li et al., 2017b). Taken together, MNPs-based contrast agents might serve as promising diagnostic and bioimaging platforms for the *in vivo* detection and tracking of bacterial infections.

MAGNETIC NANOPARTICLES AS ANTIBACTERIAL AGENTS

MNPs have been used in medical and pharmaceutical areas as drug delivery and hyperthermia agents for bacteria killing since the late 1970s (Sica de Toledo et al., 2018). Different nanostructures of MNPs have been reported as antibacterial agents to kill a range spectrum of bacteria species, including multidrug-resistant bacteria and bacterial biofilms with less damage to the human host cells (Sica de Toledo et al., 2018), and their minimum inhibitory concentrations (MIC) toward different bacteria or biofilms in previous studies have been summarized in **Table 2**.

Upon conjugating with different antibiotics such as vancomycin (Lai and Chen, 2013), gentamicin (Bhattacharya and Neogi, 2017), methicillin (Geilich et al., 2017) and cephalexin (Rayegan et al., 2018), MNPs and their derivatives (Au coated, Ag coated, Co doped, or cationic polymer modified) have been widely investigated for their potential to penetrate into bacteria cells and biofilm mass, which may inactivate bacteria and antibiotic-resistant bacteria (Niemirowicz et al., 2014, 2015; Venkatesan et al., 2015; Chen et al., 2016b; Pu et al., 2016; Zomorodian et al., 2018). Geilich et al. established highly organized methicillin-resistant biofilms on glass coverslips, and subsequently treated them with MNPs with and without an external magnetic field. After incubation for 24 h, the MNPs could penetrate into the robust biofilms in the presence of a magnet, while minimal iron penetration was observed in the absence of any magnetic field (Geilich et al., 2017). Furthermore, they demonstrated the penetration depth and antibacterial property of the MNPs loaded with methicillin. By using laser scanning confocal microscopy of the bacterial biofilms stained with Live/Dead Biofilm Viability kit, it was verified that the antibiotic delivery system constructed with MNPs could deepen the drug penetration as well as deliver high concentrations of antibiotics into the multiple layers of the biofilms, while the antibiotic alone could only control the planktonic bacteria without the ability to penetrate biofilms (Geilich et al., 2017). Consequently, the MNPs delivery system showed great potential as magnetic drug delivery system, which can control the movement and location of antibiotics, resulting in a rapid, and efficient treatment of biofilms.

Wang et al. also conducted the antibiofilm activity assay by treating the biofilms with MNPs, and similar results have been obtained. To further understand the behaviors of biofilms treated with the nanocarrier, the authors presented a probable mechanism, collected and analyzed the CLSM 3D images of the biofilms. As illustrated in **Figure 5**, a powerful nanocarrier based on MNPs for antibiotics and Ag NPs delivery could be guided to penetrate into *S. aureus* biofilm and significantly enhance the biofilm disruption (Wang et al., 2018d). When there was no external magnetic field, the intact and dense biofilm hindered the nanocarrier from penetrating into the biofilm, resulting in an insufficient antibiofilm efficiency (**Figure 5A**). It can be observed in **Figure 5B** that the number of dead bacteria increased significantly after treatment with the nanocarrier. However, the structure of the biofilm seemed to be compact and high amounts of live bacteria were protected by the extracellular polymeric substances (EPS) of bacteria. In contrast, the presence of an external magnetic field facilitated a deeper penetration of the nanocarrier into the established biofilms of *S. aureus*. It was illustrated in **Figure 5A** that under the acid environment caused by *S. aureus*, the nanocarrier was degraded and allowed the release of the antibiotics and Ag ions to the surrounding. Subsequently, the Ag ions also induced the production of intracellular reactive oxygen species (ROS), which accelerated the decomposition of EPS and further promoted the penetration of antibiotics into the biofilms. Notably, it can be seen in **Figure 5B**, after treatment with the nanocarrier under an external magnetic field, the number of live bacteria decreased dramatically and the thickness of biofilm also decreased compared with that of untreated group as well as the treated group without magnetic fields (Wang et al., 2018d).

Recently, MNPs were used as hyperthermia agents to treat bacterial infections which show more temperature susceptibility than human healthy host cells (Sica de Toledo et al., 2018). When placed under an alternating magnetic field with high frequency and amplitude, MNPs would absorb electromagnetic radiation and subsequently convert the magnetic energy to localized heat. Conjugated with different bacterial target molecules, these MNPs can specifically target the bacteria site and homogenous heat under alternating magnetic fields. The magnetic hyperthermia process will result in an enhanced membrane permeability and antibacterial property, since most bacterial pathogens will become vulnerable at an environmental temperature around 45°C or higher (Ibelli et al., 2018). It was also confirmed by Rodrigues and others that the bacterial morphology, viability and mechanical properties of *Pseudomonas fluorescens* (*P. fluorescens*) could be affected significantly by temperatures above 45°C. In order to study the effect of the magnetic heating on cell viability, planktonic *P. fluorescens* cells and biofilms were cultured on silicone coupons, and then were transferred to the hyperthermia equipment. After exposure to an external alternating magnetic field, the viability of both planktonic and biofilm cells decreased with the increasing temperature. According to CLSM and SEM, an increasing amount of dead bacterial cells was observed as the temperature increased, and most of the dead cells in the biofilm tended to be planktonic. Additionally, compared with the same direct heating

TABLE 2 | The minimum inhibitory concentrations (MIC) of various MNPs toward different bacteria of biofilms.

Materials	Particle size (nm)	MIC (μg/mL)	Bacteria	Method	Antibiotic	References
Fe_3O_4	4–10	10	*E. coli* biofilm	–	–	Thukkaram et al., 2014
			S. aureus biofilm			
			P. aeruginosa biofilm			
Fe_3O_4	≤ 18	100	*S. epidermidis*	–	–	Taylor and Webster, 2009
Ag/Fe_3O_4	20	3	*E. coli*	–	–	Ghaseminezhad and Shojaosadati, 2016
Fe_3O_4	10	9.2				
Fe_3O_4@PEG-Ag	20–25	16	*E. coli*	–	–	Zomorodian et al., 2018
			S. aureus			
Fe_3O_4@PAA	10 ± 2	8000	*P. fluorescens*	Magnetic hyperthermia	–	Rodrigues et al., 2013
Fe_3O_4@APTES	17	100	*B. subtilis* biofilm	–	–	Ranmadugala et al., 2017
$CoFe_2O_4$	16 ± 5	50	*E. coli*	–	–	Venkatesan et al., 2015
Fe_3O_4-TiO_2	–	12.5	*E. coli*	Simulated solar irradiation	–	Ma et al., 2015
			S. aureus			
MNP-CSA-13	14 ± 2	1	*P. aeruginosa*	–	–	Niemirowicz et al., 2015
VancomycinPEG-chitosan-$MnFe_2O_4$	25	0.61	*S. epidermitis*	–	Vancomycin	Esmaeili and Ghobadianpour, 2016
		0.78	*S. aureus*			
		0.78	*B. subtilis*			
		0.98	*MRSA*			
		39.06	*E. coli*			
		78.12	*P. aeroginosa*			
MNPs@Ag@HA	∼40	200	*S. aureus* biofilm	Magnetic field	Gentamicin	Wang et al., 2018d
$MnFe_2O_4$@PrBrT	10	8	*E. coli*	Magnetic hyperthermia	–	Pu et al., 2016
		8	*S. aureus*			

temperatures, magnetic hyperthermia caused by MNPs resulted to a greater destruction of the bacterial biofilms (Rodrigues et al., 2013). Kim et al. further verified the antimicrobial efficacy of the magnetic hyperthermia in a mouse infection model caused by *S. aureus* (Kim et al., 2013). The MNPs-based hyperthermia agent was prepared by conjugating MNPs with biotinylated anti-protein A mAb for targeting *S. aureus in vivo*. After the injection of the MNPs conjugates, the infected mouse was placed under an alternating magnetic field with high frequency and amplitude. Subsequently, the remaining *S. aureus* was monitored by a luminescence method. The results showed that antibody modified MNPs had an enhanced antibacterial efficiency of about 80% against *S. aureus* under the alternating magnetic field. Therefore, MNPs based hyperthermia agents can be used as a kind of efficient antibacterial agents for the treatment of bacteria and biofilms.

Furthermore, the antimicrobial activity caused by magnetic hyperthermia can be improved by modifying MNPs with cationic polymers (Pu et al., 2016) or antibiotics (Nguyen et al., 2015; Wang et al., 2018c; Zomorodian et al., 2018). The probable direct reason is that the modification leads to a stronger interaction between the MNPs and the bacterial surface. When grafted with "soft" polycarbonate as the shell, the "hard" superparamagnetic core was afforded with greater charge density, leading to a stronger interaction between the MNPs and bacteria. As such, more bacterial cell membranes could be disrupted with the effect of magnetic hyperthermia under an external magnetic field. Thus, the structural integration of MNPs with cationic polymers brought about a synergistic destructive effect on bacterial cells (Pu et al., 2016). Fang and co-researchers combined magnetic hyperthermia with vancomycin to treat peri-implant osteomyelitis in rats' infection model (Fang et al., 2017). After the establishment of osteomyelitis model in rats, vancomycin and MNPs were injected intramuscularly, and the therapeutic effect was evaluated by incubating the specimens from the subcutaneous tissue and the implant site. Under an external magnetic field, MNPs conjugates could be heated up to 75°C. This high temperature enhanced the bacterial killing efficiency of vancomycin against methicillin-sensitive *Staphylococcus aureus* (MSSA). Meanwhile, the magnetic hyperthermia could also destroy the protection effect of biofilm on bacteria, leading to a deeper antibiotic penetration into the mature biofilm and an effective antibiotic delivery for the eradication of MSSA (Fang et al., 2017). Consequently,

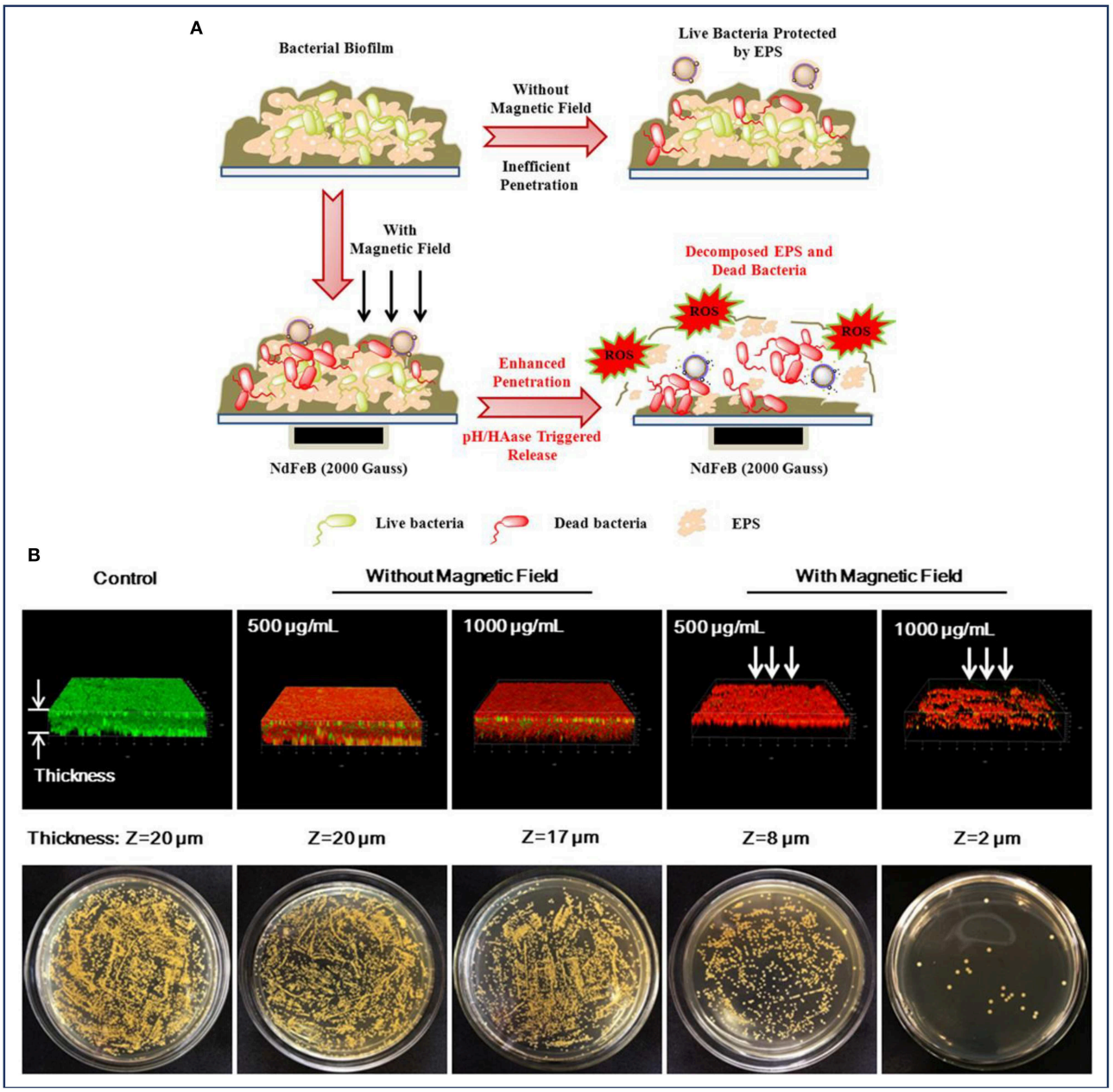

FIGURE 5 | MNPs for enhanced biofilm distribution under magnetic field. **(A)** Illustration of MNPs based antibiotic and Ag delivery for inactivating the embedded bacteria with or without an external magnetic field, and **(B)** Live/dead staining of 3D reconstructions of *S. aureus* biofilm and bacterial colonies of surviving *S. aureus* in biofilms after treatment without and with an applied magnetic field, respectively. Reprinted with permission from Wang et al. (2018d). Copyright (2018) American Chemical Society.

MNPs can be applied as drug delivery systems as well as magnetic hyperthermia agents for the synergistic therapy of bacterial infection.

CONCLUSION AND OUTLOOK

In this review, MNPs were showcased as potential platforms to detect and treat bacterial infections. Upon the conjugation of different bacterial target molecules with MNPs, the conjugates demonstrate the ability to selectively attach on the surface of bacterial pathogens, showing their great potential as bioimaging contrast agents, drug delivery and hyperthermia agents for bacterial detection and therapy. However, several challenges still need to be overcome. For *in vitro* bacterial detection, most bacterial target molecules such as antibodies and bacteriophages are specific to one

or some types of designated bacterium strains. If there are several different and uncertain bacteria strains to be tested, it is difficult to choose accurate target molecules to discriminate the different bacteria strains simultaneously. Thus, the detection selectivity needs to be further improved through different modification strategies. Additionally, most of the *in vitro* bacterial detection experiments were carried out and verified in simplified bacterial fluids, and further experiments should be conducted in complex biological fluids to demonstrate their sensitivity, specificity, and validity. For bacterial imaging *in vivo*, how to endow the NPs with the ability to discriminate infections caused by different bacteria strains remains a big challenge. Finally, there are few studies on MNPs with both detection and therapeutic features for bacterial infections, necessitating more research into the construction of multifunctional MNPs with the utility of imaging-guided treatment of bacterial infection since they have both imaging and therapeutic properties.

AUTHOR CONTRIBUTIONS

JZ and AW conceived the review paper proposal. CX wrote the manuscript draft. OA improved the quality of language. All authors revised the manuscript.

ACKNOWLEDGMENTS

This work was supported by the National Key R & D Program of China (2018YFC0910601), the National Natural Science Foundation of China (U1432114), Zhejiang Province Financial Support (2017C03042, LGF18H180017, LY18H180011), The Science & Technology Bureau of Ningbo City (2015B11002, 2017C110022). Furthermore, the authors also acknowledge Shanghai Synchrotron Radiation Facility at Line BL15U (No. h15sr0021) used for X-ray fluorescence imaging and the National Synchrotron Radiation Laboratory in Hefei used for soft X-ray imaging (No. 2016-HLS-PT-002193).

REFERENCES

Adhikari, M. D., Mukherjee, S., Saikia, J., Das, G., and Ramesh, A. (2014). Magnetic nanoparticles for selective capture and purification of an antimicrobial peptide secreted by food-grade lactic acid bacteria. *J. Mater. Chem. B* 2, 1432–1438. doi: 10.1039/c3tb21735c

Alhogail, S., Suaifan, G. A. R. Y., and Zourob, M. (2016). Rapid colorimetric sensing platform for the detection of *Listeria monocytogenes* foodborne pathogen. *Biosens. Bioelectron.* 86, 1061–1066. doi: 10.1016/j.bios.2016.07.043

Baek, M. H., Kamiya, M., Kushibiki, T., Nakazumi, T., Tomisawa, S., Abe, C., et al. (2016). Lipopolysaccharide-bound structure of the antimicrobial peptide cecropin P1 determined by nuclear magnetic resonance spectroscopy. *J. Peptide Sci.* 22, 214–221. doi: 10.1002/psc.2865

Bai, Y., Cui, Y., Paoli, G. C., Shi, C., Wang, D., Zhou, M., et al. (2016). Synthesis of amino-rich silica-coated magnetic nanoparticles for the efficient capture of DNA for PCR. *Colloids Surfaces B-Biointerf.* 145, 257–266. doi: 10.1016/j.colsurfb.2016.05.003

Batchelor, M., Zhou, D., Cooper, M. A., Abell, C., and Rayment, T. (2010). Vancomycin dimer formation between analogues of bacterial peptidoglycan surfaces probed by force spectroscopy. *Organ. Biomol. Chem.* 8, 1142–1148. doi: 10.1039/b919347b

Bhattacharya, P., and Neogi, S. (2017). Gentamicin coated iron oxide nanoparticles as novel antibacterial agents. *Mater. Res. Express* 4:095005. doi: 10.1088/2053-1591/aa8652

Borsa, B. A., Tuna, B. G., Hernandez, F. J., Hernandez, L. I., Bayramoglu, G., Arica, M. Y., et al. (2016). *Staphylococcus aureus* detection in blood samples by silica nanoparticle-oligonucleotides conjugates. *Biosens. Bioelectron.* 86, 27–32. doi: 10.1016/j.bios.2016.06.023

Chen, C., Wang, S., Li, L., Wang, P., Chen, C., Sun, Z., et al. (2016a). Bacterial magnetic nanoparticles for photothermal therapy of cancer under the guidance of MRI. *Biomaterials* 104, 352–360. doi: 10.1016/j.biomaterials.2016.07.030

Chen, J., Alcaine, S. D., Jiang, Z., Rotello, V. M., and Nugen, S. R., (2015a). Detection of Escherichia coli in drinking water using T7 bacteriophage-conjugated magnetic probe. *Anal. Chem.* 87, 8977–8984. doi: 10.1021/acs.analchem.5b02175

Chen, J., Andler, S. M., Goddard, J. M., Nugen, S. R., and Rotello, V. M. (2017). Integrating recognition elements with nanomaterials for bacteria sensing. *Chem. Soc. Rev.* 46, 1272–1283. doi: 10.1039/c6cs00313c

Chen, J., Duncan, B., Wang, Z., Wang, L. S., Rotello, V. M., and Nugen, S. R. (2015b). Bacteriophage-based nanoprobes for rapid bacteria separation. *Nanoscale* 7, 16230–16236. doi: 10.1039/c5nr03779d

Chen, Q., Li, Z., Liu, B., He, B., Wei, X., Du, J., et al. (2015c). Highly sensitive detection of mycobacterium tuberculosis for the diagnosis of osteoarticular tuberculosis based on magnetic nanoparticles and chemiluminescence. *J. Biomater. Tissue Eng.* 5, 241–245. doi: 10.1166/jbt.2015.1287

Chen, X., Hu, B., Xiang, Q., Yong, C., Liu, Z., and Xing, X. (2016b). Magnetic nanoparticles modified with quaternarized N-halamine based polymer and their antibacterial properties. *J. Biomater. Sci. Polymer Ed.* 27, 1187–1199. doi: 10.1080/09205063.2016.1188471

Da Costa, J. P., Cova, M., Ferreira, R., and Vitorino, R. (2015). Antimicrobial peptides: an alternative for innovative medicines? *Appl. Microbiol. Biotechnol.* 99, 2023–2040. doi: 10.1007/s00253-015-6375-x

Ellington, M. J., Ekelund, O., Aarestrup, F. M., Canton, R., Doumith, M., Giske, C., et al. (2017). The role of whole genome sequencing in antimicrobial susceptibility testing of bacteria: report from the EUCAST Subcommittee. *Clin. Microbiol. Infect.* 23, 2–22. doi: 10.1016/j.cmi.2016.11.012

Esmaeili, A., and Ghobadianpour, S. (2016). Vancomycin loaded superparamagnetic $MnFe_2O_4$ nanoparticles coated with PEGylated chitosan to enhance antibacterial activity. *Int. J. Pharma.* 501, 326–330. doi: 10.1016/j.ijpharm.2016.02.013

Fang, C. H., Tsai, P. I., Huang, S. W., Sun, J. S., Chang, J. Z., Shen, H. H., et al. (2017). Magnetic hyperthermia enhance the treatment efficacy of peri-implant osteomyelitis. *BMC Infect. Dis.* 17:516. doi: 10.1186/s12879-017-2621-4

Fargašová, A., Balzerová, A., Prucek, R., Sedláková, M. H., Bogdanová, K., Gallo, J., et al. (2017). Detection of prosthetic joint infection based on magnetically assisted surface enhanced raman spectroscopy. *Anal. Chem.* 89, 6598–6607. doi: 10.1021/acs.analchem.7b00759

Ganesh, I., Buu Minh, T., Kim, Y., Kim, J., Cheng, H., Lee, N. Y., et al. (2016). An integrated microfluidic PCR system with immunomagnetic nanoparticles for the detection of bacterial pathogens. *Biomed. Microdev.* 18:6. doi: 10.1007/s10544-016-0139-y

Geilich, B. M., Gelfat, I., Sridhar, S., van de Ven, A. L., and Webster, T. J. (2017). Superparamagnetic iron oxide-encapsulating polymersome nanocarriers for biofilm eradication. *Biomaterials* 119, 78–85. doi: 10.1016/j.biomaterials.2016.12.011

Ghaseminezhad, S. M., and Shojaosadati, S. A. (2016). Evaluation of the antibacterial activity of Ag/Fe_3O_4 nanocomposites synthesized using starch. *Carbohydrate Polymers* 144, 454–463. doi: 10.1016/j.carbpol.2016.03.007

Gontero, D., Veglia, A. V., Boudreau, D., and Guillermo Bracamonte, A. (2018). Ultraluminescent gold core-shell nanoparticles applied to individual bacterial detection based on metal-enhanced fluorescence nanoimaging. *J. Nanophotonics* 12:012505. doi: 10.1117/1.jnp.12.012505

Hao, L., Gu, H., Duan, N., Wu, S., Ma, X., Xia, Y., et al. (2017). A chemiluminescent aptasensor based on rolling circle amplification

and Co^{2+}/N-(aminobut3r1)-N-(ethylisolumino1) functional flowerlike gold nanoparticles for *Salmonella typhimurium* detection. *Talanta* 164, 275–282. doi: 10.1016/j.talanta.2016.11.053

Hasan, N., Guo, Z., and Wu, H. F. (2016). Large protein analysis of *Staphylococcus aureus* and Escherichia coli by MALDI TOF mass spectrometry using amoxicillin functionalized magnetic nanoparticles. *Anal. Bioanaly. Chem.* 408, 6269–6281. doi: 10.1007/s00216-016-9730-6

He, Y., Wang, M., Fan, E., Ouyang, H., Yue, H., Su, X., et al. (2017). Highly specific bacteriophage-affinity strategy for rapid separation and sensitive detection of viable *pseudomonas aeruginosa*. *Anal. Chem.* 89, 1916–1921. doi: 10.1021/acs.analchem.6b04389

Hoerr, V., Tuchscherr, L., Hüve, J., Nippe, N., Loser, K., Glyvuk, N., et al. (2013). Bacteria tracking by *in vivo* magnetic resonance imaging. *BMC Biology* 11:63. doi: 10.1186/1741-7007-11-63

Houhoula, D., Papaparaskevas, J., Zatsou, K., Nikolaras, N., Malkawi, H. I., Mingeot-Leclercq, M. sP., et al. (2017). Magnetic nanoparticle-enhanced PCR for the detection and identification of *Staphylococcus aureus* and *Salmonella enteritidis*. *N. Microbiol.* 40, 165–169. Available online at: http://www.newmicrobiologica.org/PUB/allegati_pdf/2017/3/165.pdf

Ibelli, T., Templeton, S., and Levi-Polyachenko, N. (2018). Progress on utilizing hyperthermia for mitigating bacterial infections. *Int. J. Hyperthermia* 34, 144–156. doi: 10.1080/02656736.2017.1369173

Jang, H., Hwang, E. Y., Kim, Y., Choo, J., Jeong, J., and Lim, D. W. (2016). Surface-enhanced raman scattering and fluorescence-based dual nanoprobes for multiplexed detection of bacterial pathogens. *J. Biomed. Nanotechnol.* 12, 1938–1951. doi: 10.1166/jbn.2016.2309

Kell, A. J., Stewart, G., Ryan, S., Peytavi, R., Boissinot, M., Huletsky, A., et al. (2008). Vancomycin-modified nanoparticles for efficient targeting and preconcentration of Gram-positive and Gram-negative bacteria. *Acs Nano* 2, 1777–1788. doi: 10.1021/nn700183g

Kim, M. H., Yamayoshi, I., Mathew, S., Lin, H., Nayfach, J., and Simon, S. I. (2013). Magnetic nanoparticle targeted hyperthermia of cutaneous *Staphylococcus aureus* infection. *Anna. Biomed. Eng.* 41, 598–609. doi: 10.1007/s10439-012-0698-x

Kim, S. U., Jo, E. J., Mun, H., Noh, Y., and Kim, M. G. (2018). Ultrasensitive detection of escherichia coli o157:h7 by immunomagnetic separation and selective filtration with nitroblue tetrazolium/5-bromo-4-chloro-3-indolyl phosphate signal amplification. *J. Agri. Food Chem.* 66, 4941–4947. doi: 10.1021/acs.jafc.8b00973

Kim, Y. T., Kim, K. H., Kang, E. S., Jo, G., Ahn, S. Y., Park, S. H., et al. (2016). Synergistic effect of detection and separation for pathogen using magnetic clusters. *Bioconjugate Chem.* 27, 59–65. doi: 10.1021/acs.bioconjchem.5b00681

Kuang, H., Cui, G., Chen, X., Yin, H., Yong, Q., Xu, L., et al. (2013). A one-step homogeneous sandwich immunosensor for Salmonella detection based on magnetic nanoparticles (MNPs) and quantum dots (QDs). *Int. J. Mol. Sci.* 14, 8603–8610. doi: 10.3390/ijms14048603

Kwon, D., Joo, J., Lee, J., Park, K. H., and Jeon, S. (2013). Magnetophoretic chromatography for the detection of pathogenic bacteria with the naked eye. *Anal. Chem.* 85, 7594–7598. doi: 10.1021/ac401717f

Lai, B. H., and Chen, D. H. (2013). Vancomycin-modified LaB6@SiO_2/Fe_3O_4 composite nanoparticles for near-infrared photothermal ablation of bacteria. *Acta Biomateri.* 9, 7573–7579. doi: 10.1016/j.actbio.2013.03.023

Law, J. W., Ab Mutalib, N. S., Chan, K. G., and Lee, L. H. (2015). Rapid methods for the detection of foodborne bacterial pathogens: principles, applications, advantages and limitations. *Front. Microbiol.* 5:770. doi: 10.3389/fmicb.2014.00770

Lee, C. N., Wang, Y. M., Lai, W. F., Chen, T. J., Yu, M. C., Fang, C. L., et al. (2012). Super-paramagnetic iron oxide nanoparticles for use in extrapulmonary tuberculosis diagnosis. *Clin. Microbiol. Infect.* 18, E149–E157. doi: 10.1111/j.1469-0691.2012.03809.x

Lefevre, S., Ruimy, D., Jehl, F., Neuville, A., Robert, P., Sordet, C., et al. (2011). Septic arthritis: monitoring with USPIO-enhanced macrophage MR imaging. *Radiology* 258, 722–728. doi: 10.1148/radiol.10101272

Li, H., Li, C., Martin, F. L., and Zhang, D. (2017a). Diagnose pathogens in drinking water via magnetic surface-enhanced raman scattering (SERS) assay. *Mater. Today-Proc.* 4, 25–31. doi: 10.1016/j.matpr.2017.01.189

Li, Y., Hu, X., Ding, D., Zou, Y., Xu, Y., Wang, X., et al. (2017b). *In situ* targeted MRI detection of Helicobacter pylori with stable magnetic graphitic nanocapsules. *Nat. Commun.* 8:15653. doi: 10.1038/ncomms15653

Liana, A. E., Marquis, C. P., Gunawan, C., Gooding, J. J., and Amal, R. (2017). T4 bacteriophage conjugated magnetic particles for *E. coli* capturing: influence of bacteriophage loading, temperature and tryptone. *Colloids Surfaces B-Biointerf.* 151, 47–57. doi: 10.1016/j.colsurfb.2016.12.009

Liébana, S., Spricigo, D. A., Cortés, M. P., Barbé, J., Llagostera, M and., Alegret, S. (2013). Phagomagnetic separation and electrochemical magneto-genosensing of pathogenic bacteria. *Anal. Chem.* 85, 3079–3086. doi: 10.1021/ac3024944

Liu, C. Y., Weng, C. C., Lin, C. H., Yang, C. Y., Mong, K. T., and Li, Y. K. (2017). Development of a novel engineered antibody targeting Neisseria species. *Biotechnol. Lett.* 39, 407–413. doi: 10.1007/s10529-016-2258-1

Liu, T. Y., Tsai, K. T., Wang, H. H., Chen, Y., Chen, Y. H., Chao, Y. C., et al. (2011). Functionalized arrays of Raman-enhancing nanoparticles for capture and culture-free analysis of bacteria in human blood. *Nat. Commun.* 2:538. doi: 10.1038/ncomms1546

Ma, S., Zhan, S., Jia, Y., and Zhou, Q. (2015). Superior antibacterial activity of Fe_3O_4-TiO_2 nanosheets under solar light. *Acs Appl. Mater. Interfaces* 7, 21875–21883. doi: 10.1021/acsami.5b06264

Meng, X., Li, F., Li, F., Xiong, Y., and Xu, H. (2017). Vancomycin modified PEGylated-magnetic nanoparticles combined with PCR for efficient enrichment and detection of *Listeria monocytogenes*. *Sens. Actuators B-Chem.* 247, 546–555. doi: 10.1016/j.snb.2017.03.079

Nguyen, T. K., Duong, H. T., Selvanayagam, R., Boyer, C., and Barraud, N. (2015). Iron oxide nanoparticle-mediated hyperthermia stimulates dispersal in bacterial biofilms and enhances antibiotic efficacy. *Sci. Rep.* 5:18385. doi: 10.1038/srep18385

Nguyen, T. T., Trinh, K. T. L., Yoon, W. J., Lee, N. Y., and Ju, H. (2017). Integration of a microfluidic polymerase chain reaction device and surface plasmon resonance fiber sensor into an inline all-in-one platform for pathogenic bacteria detection. *Sens. Actuat. B: Chem.* 242, 1–8. doi: 10.1016/j.snb.2016.10.137

Niemirowicz, K., Surel, U., Wilczewska, A. Z., Mystkowska, J., Piktel, E., Gu, X., et al. (2015). Bactericidal activity and biocompatibility of ceragenin-coated magnetic nanoparticles. *J. Nanobiotechnol.* 13:32. doi: 10.1186/s12951-015-0093-5

Niemirowicz, K., Swiecicka, I., Wilczewska, A. Z., Misztalewska, I., Kalska-Szostko, B., Bienias, K., et al. (2014). Gold-functionalized magnetic nanoparticles restrict growth of *Pseudomonas aeruginosa*. *Int. J. Nanomed.* 9, 2217–2224. doi: 10.2147/ijn.s56588

Park, C., Lee, J., Kim, Y., Kim, J., Lee, J., and Park, S. (2017). 3D-printed microfluidic magnetic preconcentrator for the detection of bacterial pathogen using an ATP luminometer and antibody-conjugated magnetic nanoparticles. *J. Microbiol. Methods* 132, 128–133. doi: 10.1016/j.mimet.2016.12.001

Pazos-Perez, N., Pazos, E., Catala, C., Mir-Simon, B., Gómez-de Pedro, S., Sagales, J., et al. (2016). Ultrasensitive multiplex optical quantification of bacteria in large samples of biofluids. *Sci. Rep.* 6:29014. doi: 10.1038/srep29014

Pu, L., Xu, J., Sun, Y., Fang, Z., Chan-Park, M. B., and Duan, H. (2016). Cationic polycarbonate-grafted superparamagnetic nanoparticles with synergistic dual-modality antimicrobial activity. *Biomater. Sci.* 4, 871–879. doi: 10.1039/c5bm00545k

Qin, W., Zheng, B., Yuan, Y., Li, M., Bai, Y., Chang, J., et al. (2016). Sensitive detection of Porphyromonas gingivalis based on magnetic capture and upconversion fluorescent identification with multifunctional nanospheres. *Eur. J. Oral Sci.* 124, 334–342. doi: 10.1111/eos.12286

Ranmadugala, D., Ebrahiminezhad, A., Manley-Harris, M., Ghasemi, Y., and Berenjian, A. (2017). The effect of iron oxide nanoparticles on *Bacillus subtilis* biofilm, growth and viability. *Process Biochem.* 62, 231–240. doi: 10.1016/j.procbio.2017.07.003

Rayegan, A., Allafchian, A., Sarsari, I. A., and Kameli, P. (2018). Synthesis and characterization of basil seed mucilage coated Fe3O4 magnetic nanoparticles as a drug carrier for the controlled delivery of cephalexin. *Int. J. Biol. Macromol.* 113, 317–328. doi: 10.1016/j.ijbiomac.2018.02.134

Ribeiro, K. L., Frías, I. A. M., Franco, O. L., Dias, S. C., Sousa-Junior, A. A., Silva, O. N., et al. (2018). Clavanin A-bioconjugated Fe_3O_4/Silane core-shell nanoparticles for thermal ablation of bacterial biofilms. *Colloids Surf. B: Biointer.* 169, 72–81. doi: 10.1016/j.colsurfb.2018.04.055

Rodrigues, D., Bañobre-López, M., Espiña, B., Rivas, J., and Azeredo, J. (2013). Effect of magnetic hyperthermia on the structure of biofilm and cellular viability of a food spoilage bacterium. *Biofouling* 29, 1225–1232. doi: 10.1080/08927014.2013.834893

Sakudo, A., Chou, H., and Nagatsu, M. (2015). Antibody-integrated and functionalized graphite-encapsulated magnetic beads, produced using ammonia gas plasma technology, for capturing Salmonella. *Bioorgan. Med. Chem. Lett.* 25, 1012–1016. doi: 10.1016/j.bmcl.2015.01.031

Sheikhzadeh, E., Chamsaz, M., Turner, A. P. F., Jager, E. W. H., and Beni, V. (2016). Label-free impedimetric biosensor for *Salmonella Typhimurium* detection based on poly [pyrrole-co-3-carboxyl-pyrrole] copolymer supported aptamer. *Biosens. Bioelectron.* 80, 194–200. doi: 10.1016/j.bios.2016.01.057

Shelby, T., Sulthana, S., McAfee, J., Banerjee, T., and Santra, S. (2017). Foodborne pathogen screening using magneto-fluorescent nanosensor: Rapid detection of *E. Coli* O157:H7. *Jove-J. Visual. Experi.* 127:e55821. doi: 10.3791/55821

Shen, H., Wang, J., Liu, H., Li, Z., Jiang, F., Wang, F. B., et al. (2016). Rapid and selective detection of pathogenic bacteria in bloodstream infections with aptamer-based recognition. *Acs Appl. Mater. Interf.* 8, 19371–19378. doi: 10.1021/acsami.6b06671

Shim, W.-B., Song, J.-E., Mun, H., Chung, D.-H., and Kim, M.-G. (2014b). Rapid colorimetric detection of *Salmonella typhimurium* using a selective filtration technique combined with antibody-magnetic nanoparticle nanocomposites. *Anal. Bioanal. Chem.* 406, 859–866. doi: 10.1007/s00216-013-7497-6

Shim, W. B., Lee, C. W., Kim, M. G., and Chung, D.-H. (2014a). An antibody-magnetic nanoparticle conjugate-based selective filtration method for the rapid colorimetric detection of *Listeria monocytogenes*. *Anal. Methods* 6, 9129–9135. doi: 10.1039/c4ay01313a

Sica de Toledo, L. D. A., Rosseto, H. C., and Bruschi, M. L. (2018). Iron oxide magnetic nanoparticles as antimicrobials for therapeutics. *Pharmaceut. Dev. Technol.* 23, 316–323. doi: 10.1080/10837450.2017.1337793

Suaifan, G. A. R. Y., Alhogail, S., and Zourob, M. (2017). Paper-based magnetic nanoparticle-peptide probe for rapid and quantitative colorimetric detection of *E. coli* O157:H7. *Biosensors Bioelectron.* 92, 702–708. doi: 10.1016/j.bios.2016.10.023

Tang, Y., Zou, J., Ma, C., Ali, Z., Li, Z., Li, X., et al. (2013). Highly sensitive and rapid detection of *Pseudomonas aeruginosa* based on magnetic enrichment and magnetic separation. *Theranostics* 3, 85–92. doi: 10.7150/thno.5588

Taylor, E. N., Webster, T. J. (2009). The use of superparamagnetic nanoparticles for prosthetic biofilm prevention. *Int. J. Nanomed.* 4, 145–152. doi: 10.2147/IJN.S5976

Thukkaram, M., Sitaram, S., Kannaiyan, S. K., and Subbiahdoss, G. (2014). Antibacterial efficacy of iron-oxide nanoparticles against biofilms on different biomaterial surfaces. *Int. J. Biomater.* 2014:716080. doi: 10.1155/2014/716080

Tokajuk, G., Niemirowicz, K., Deptuła, P., Piktel, E., Cieśluk, M., Wilczewska, A. Z., et al. (2017). Use of magnetic nanoparticles as a drug delivery system to improve chlorhexidine antimicrobial activity. *Int. J. Nanomed.* 12, 7833–7846. doi: 10.2147/IJN.S140661

Váradi, L., Luo, J. L., Hibbs, D. E., Perry, J. D., Anderson, R. J., Orenga, S., et al. (2017). Methods for the detection and identification of pathogenic bacteria: past, present, and future. *Chem. Soc. Rev.* 46, 4818–4832. doi: 10.1039/c6cs00693k

Venkatesan, K., Rajan Babu, D., Kavya Bai, M. P., Supriya, R., Vidya, R., Madeswaran, S., et al. (2015). Structural and magnetic properties of cobalt-doped iron oxide nanoparticles prepared by solution combustion method for biomedical applications. *Int. J. Nanomed. 10* (Suppl. 1), 189–198. doi: 10.2147/ijn.s82210

Wang, C., Gu, B., Liu, Q., Pang, Y., Xiao, R., and Wang, S. (2018a). Combined use of vancomycin-modified Ag-coated magnetic nanoparticles and secondary enhanced nanoparticles for rapid surface-enhanced Raman scattering detection of bacteria. *Int. J. Nanomed.* 13, 1159–1178. doi: 10.2147/ijn.s150336

Wang, C. H., Chang, C. J., Wu, J. J., and Lee, G. B. (2014). An integrated microfluidic device utilizing vancomycin conjugated magnetic beads and nanogold-labeled specific nucleotide probes for rapid pathogen diagnosis. *Nanomed. Nanotechnol. Biol. Med.* 10, 809–818. doi: 10.1016/j.nano.2013.10.013

Wang, J., Wu, H., Yang, Y., Yan, R., Zhao, Y., Wang, Y., et al. (2018b). Bacterial species-identifiable magnetic nanosystems for early sepsis diagnosis and extracorporeal photodynamic blood disinfection. *Nanoscale* 10, 132–141. doi: 10.1039/c7nr06373c

Wang, J., Wu, X., Wang, C., Rong, Z., Ding, H., Li, H., et al. (2016). Facile synthesis of Au-coated magnetic nanoparticles and their application in bacteria detection via a SERS method. *ACS Appl. Mater. Interf.* 8, 19958–19967. doi: 10.1021/acsami.6b07528

Wang, X., Deng, A., Cao, W., Li, Q., Wang, L., Zhou, J., et al. (2018c). Synthesis of chitosan/poly (ethylene glycol)-modified magnetic nanoparticles for antibiotic delivery and their enhanced anti-biofilm activity in the presence of magnetic field. *J. Mater. Sci.* 53, 6433–6449. doi: 10.1007/s10853-018-1998-9

Wang, X., Wu, J., Li, P., Wang, L., Zhou, J., Zhang, G., et al. (2018d). Microenvironment-responsive magnetic nanocomposites based on silver nanoparticles/gentamicin for enhanced biofilm disruption by magnetic field. *ACS Appl. Mater. Interf.* 10, 34905–34915. doi: 10.1021/acsami.8b10972

Wohlwend, N., Tiermann, S., Risch, L., Risch, M., and Bodmer, T. (2016). Evaluation of a multiplex real-time PCR assay for detecting major bacterial enteric pathogens in fecal specimens: intestinal inflammation and bacterial load are correlated in campylobacter infections. *J. Clin. Microbiol.* 54, 2262–2266. doi: 10.1128/jcm.00558-16

Xu, Y., Wang, H., Luan, C., Liu, Y., Chen, B., and Zhao, Y. (2018). Aptamer-based hydrogel barcodes for the capture and detection of multiple types of pathogenic bacteria. *Biosen. Bioelectron.* 100, 404–410. doi: 10.1016/j.bios.2017.09.032

Yang, S., Hui, O., Su, X., Gao, H., Kong, W., Wang, M., et al. (2016). Dual-recognition detection of *Staphylococcus aureus* using vancomycin-functionalized magnetic beads as concentration carriers. *Biosens. Bioelectron.* 78, 174–180. doi: 10.1016/j.bios.2015.11.041

Yang, X., Zhou, X., Zhu, M., and Xing, D. (2017). Sensitive detection of *Listeria monocytogenes* based on highly efficient enrichment with vancomycin-conjugated brush-like magnetic nano-platforms. *Biosens. Bioelectron.* 91, 238–245. doi: 10.1016/j.bios.2016.11.044

Yuan, K., Mei, Q., Guo, X., Xu, Y., Yang, D., Sánchez, B. J., et al. (2018a). Antimicrobial peptide based magnetic recognition elements and Au@Ag-GO SERS tags with stable internal standards: a three in one biosensor for isolation, discrimination and killing of multiple bacteria in whole blood. *Chem. Sci.* 9, 8781–8795. doi: 10.1039/c8sc04637a

Yuan, P., Ding, X., Yang, Y. Y., and Xu, Q. H. (2018b). Metal nanoparticles for diagnosis and therapy of bacterial infection. *Adv. Healthcare Mater.* 7:1701392. doi: 10.1002/adhm.201701392

Zheng, L., Qi, P., and Zhang, D. (2018). DNA-templated fluorescent silver nanoclusters for sensitive detection of pathogenic bacteria based on MNP-DNAzyme-AChE complex. *Sens. Actuat. B-Chem.* 276, 42–47. doi: 10.1016/j.snb.2018.08.078

Zhu, M., Liu, W., Liu, H., Liao, Y., Wei, J., Zhou, X., et al. (2015). Construction of Fe_3O_4/vancomycin/PEG magnetic nanocarrier for highly efficient pathogen enrichment and gene sensing. *Acs Appl. Mater. Interf.* 7, 12873–12881. doi: 10.1021/acsami.5b02374

Zomorodian, K., Veisi, H., Mousavi, S. M., Ataabadi, M. S., Yazdanpanah, S., Bagheri, J., et al. (2018). Modified magnetic nanoparticles by PEG-400-immobilized Ag nanoparticles (Fe_3O_4@PEG-Ag) as a core/shell nanocomposite and evaluation of its antimicrobial activity. *Int. J. Nanomed.* 13, 3965–3973. doi: 10.2147/ijn.s161002

Conflict of Interest Statement: The authors declare that the research was conducted in the absence of any commercial or financial relationships that could be construed as a potential conflict of interest.

frontiers in Bioengineering and Biotechnology

REVIEW
published: 05 July 2019
doi: 10.3389/fbioe.2019.00161

Multiple and Promising Applications of Strontium (Sr)-Containing Bioactive Glasses in Bone Tissue Engineering

Saeid Kargozar[1], Maziar Montazerian[2], Elisa Fiume[3] and Francesco Baino[3,4]**

[1] Tissue Engineering Research Group (TERG), Department of Anatomy and Cell Biology, School of Medicine, Mashhad University of Medical Sciences, Mashhad, Iran, [2] Center for Research, Technology and Education in Vitreous Materials, Federal University of São Carlos, São Carlos, Brazil, [3] Department of Applied Science and Technology, Institute of Materials Physics and Engineering, Politecnico di Torino, Turin, Italy, [4] Interuniversity Center for the Promotion of the 3Rs Principles in Teaching and Research, Italy

Improving and accelerating bone repair still are partially unmet needs in bone regenerative therapies. In this regard, strontium (Sr)-containing bioactive glasses (BGs) are highly-promising materials to tackle this challenge. The positive impacts of Sr on the osteogenesis makes it routinely used in the form of strontium ranelate (SR) in the clinical setting, especially for patients suffering from osteoporosis. Therefore, a large number of silicate-, borate-, and phosphate-based BGs doped with Sr and produced in different shapes have been developed and characterized, in order to be used in the most advanced therapeutic strategies designed for the management of bone defects and injuries. Although the influence of Sr incorporation in the glass is debated regarding the obtained physicochemical and mechanical properties, the biological improvements have been found to be substantial both *in vitro* and *in vivo*. In the present study, we provide a comprehensive overview of Sr-containing glasses along with the current state of their clinical use. For this purpose, different types of Sr-doped BG systems are described, including composites, coatings and porous scaffolds, and their applications are discussed in the light of existing experimental data along with the significant challenges ahead.

Keywords: bioactive glasses, strontium, cement, coating, scaffold, osteogenesis, tissue engineering

OPEN ACCESS

Edited by:
Hasan Uludag,
University of Alberta, Canada

Reviewed by:
Natalia Karpukhina,
Queen Mary University of London, United Kingdom
Jonathan Lao,
Université Clermont Auvergne, France

****Correspondence:***
Saeid Kargozar
kargozarsaeid@gmail.com
Francesco Baino
francesco.baino@polito.it

Specialty section:
This article was submitted to Biomaterials, a section of the journal Frontiers in Bioengineering and Biotechnology

Received: *11 February 2019*
Accepted: *20 June 2019*
Published: *05 July 2019*

Citation:
Kargozar S, Montazerian M, Fiume E and Baino F (2019) Multiple and Promising Applications of Strontium (Sr)-Containing Bioactive Glasses in Bone Tissue Engineering. Front. Bioeng. Biotechnol. 7:161. doi: 10.3389/fbioe.2019.00161

INTRODUCTION

Bioactive glasses (BGs) are currently used as implantable materials for the management of various types of bone disorders and diseases (Baino et al., 2018,a; Kargozar et al., 2019a; Miola et al., 2019). After five decades from the invention of Hench's 45S5 formulation, numerous commercially- produced BGs are being now used as effective substitute materials for hard tissue engineering. A few key advantages have been counted for BGs regarding their application in bone regeneration including the ability to bond to the living tissues and to improve the growth and proliferation of osteoblasts, the stimulation of osteogenesis and angiogenesis, and the local induction of antibacterial and antifungal effects (Kargozar et al., 2017, 2018a, 2019b,c; Mozafari et al., 2019). The main reason for these abilities is related to the release of various metallic ions

(e.g., silicate ions, Cu^{2+}) from the glass structure into the surrounding biological environment (Kargozar et al., 2018b). Therefore, the researchers incorporate different ions into the glass structure in order to obtain favorable biological effects. Indeed, the ionic dissolution products of BGs stimulate the expression and secretion of biochemical markers involved in the repair and regeneration of bone such as osteocalcin (OCN), osteopontin (OPN), and vascular endothelial growth factor (VEGF) (Jell and Stevens, 2006; Johari et al., 2016; Kargozar et al., 2019d).

Among the different therapeutic elements, increasing attention has been paid to add Sr^{2+} ions to silicate-based glasses for bone reconstruction application. Strontium (Sr) is an alkaline earth metal, which normally exists in the human skeleton (Hodges et al., 1950). This element can be substituted in the calcium (Ca) positions of apatite with a strong bone-seeking property (Vaughan, 1975). Sr in the form of strontium ranelate (SrR) has been used for the treatment of a common bone disease, i.e., osteoporosis, over the last decades (O'Donnell et al., 2006). Strontium has also been used in toothpaste to repair decayed teeth due to its restorative capability (Huang et al., 2016). Sr^{2+} ions via improving osteoblast activity and inhibiting osteoclast function can enhance the density of the bone tissue, resulting in a significant reduction in fracture risk in mammals (Bonnelye et al., 2008). This increase is supposed to be connected with the potential of Sr^{2+} ions to enhance the expression and activity of osteogenesis-related genes and proteins [e.g., Runx2 and alkaline phosphatase (ALP)] through the activation of a couple of cellular signaling pathways (Hurtel-Lemaire et al., 2009; Peng et al., 2009). Moreover, some researchers have proposed the immunomodulatory effects of Sr element, which provides an appropriate environment for enhancing bone regeneration (Zhang et al., 2016). It was reported that Sr^{2+} ions might have antibacterial property when released from different product formulations (Li et al., 2016; Liu et al., 2016). Having the above-mentioned characteristics, Sr is being currently used in various types of glasses (melt-derived and sol-gel) for bone tissue engineering applications. Moreover, there are several studies in which Sr-doped BGs have been added to polymeric matrices for the development of osteoinductive composites in order to accelerate the bone tissue reconstruction (Kargozar et al., 2018c).

Several formulations of glasses have been developed in which Ca is partially substituted by Sr. These formulations are presented as silicate-, phosphate- and borosilicate-based glasses (Lao et al., 2008; Abou Neel et al., 2009; Pan et al., 2009; Sriranganathan et al., 2016), which can be produced as fine powders, granules, fibers, and three-dimensional (3D) scaffolds (Ren et al., 2014; Kargozar et al., 2016; Yin et al., 2018; Baino et al., 2019).

In the present study, we aim to cover the main aspects around Sr-containing glass-derived biomaterials that are relevant to their application in bone tissue engineering strategies. The basic properties of Sr-doped glasses, such as their physicochemical characteristics and reactivity upon contact with biological fluids, are discussed and critically compared in section Sr-containing BGs: an overview. The use of these materials to prepare cements, coatings, and composites is described in section Cements, composites, coatings, and glass-ceramics based on Sr-doped BGs, while section Three-dimensional (3D) scaffolds is focused on Sr-based bioactive glass porous scaffolds. The results of *in vitro* and *in vivo* experiments are discussed in section Biological functions of strontium to show the great importance of Sr as a therapeutic ion for bone repair and regeneration. In this regard, Sr-regulated cell signaling pathways involved in osteogenesis induction, osteoclastogenesis, and bacterial inhibition are presented in detail to provide a comprehensive picture of the biological significance of Sr-doped BGs. A concise forecast for future research is then exposed in section Conclusions and outlook, just before the Conclusions. In summary, the present study aims to show a comprehensive view of synthesis methods, structure and reactivity, and biological outputs of this type of materials as an updated and focused study for researchers working in the field. While some general reviews have previously been published on bioactive glasses, including some contributions oriented to clinical applications and commercial products (Jones et al., 2016; Baino, 2017), to the best of the authors' knowledge this is the first review paper dealing specifically with Sr-doped BGs and related biomaterials.

SR-CONTAINING BGs: AN OVERVIEW

Sr-containing BGs have recently attracted much interest among researchers and scientists due to the positive effects of Sr on bone metabolism by preventing bone resorption and enhancing new tissue growth, both *in vitro* and *in vivo* (Hoppe et al., 2011). All these aspects, combined with the well-known features of BGs (Rahaman et al., 2011), make Sr-containing BGs highly appealing in the treatment of degenerative bone pathologies (e.g., osteoporosis) (Wei et al., 2014; Mao et al., 2017).

Synthesis Methods: Melt-Derived and Sol-Gel Glasses

According to the specific needs related to the final clinical application, BGs can be produced either by traditional melt-quenching route or by sol-gel method, which can confer specific physical and chemical properties to the material, regardless of the composition (Fiume et al., 2018). In the past, the sol-gel route was demonstrated to allow better structural control and homogeneity of the final material compared to traditional melt-derived glasses. Moreover, the possibility to obtain a mesoporous structure often represents an advantage in bone tissue engineering applications because of the higher specific surface area of the final product (Zhang et al., 2016), which induces an acceleration of the hydroxyapatite (HA) formation kinetics on the surface of the glass by providing more reaction sites for the nucleation of the crystals (Baino et al., 2018,a).

In a typical melt-quenching approach, the melting of the reagents is carried out at high temperatures (in the typical range of 1,300 to 1,550°C) in electrical furnaces. Adequate processing parameters (i.e., heating rate and melting time) are fundamental to obtain a homogeneous and bubble-free melt, thus guarantying the high quality of the final product. According to the different desired applications, the melt could be cast

into molds, quenched in water ("frit") or drawn into fibers (Ylanen, 2011; Fagerlund and Hupa, 2016).

Sol-gel process is defined as a chemical-based processing technique for the production of ceramic materials at noticeably lower processing temperatures since the polymerization reaction of a solution containing precursors occurs at room temperature resulting in the formation of the 3D network, which are properly chosen in order to tailor the final composition of the system to the intended purpose (Hench and West, 1990). Briefly, sol-gel synthesis allows the production of ceramic materials by three steps: (i) preparation of the precursor solution (sol), (ii) gelation process of the prepared sol, and (iii) removal of the solvent by thermal treatments. Doping glasses by the introduction of trace elements in the sol is relatively easier compared to the traditional melt-quenching route and allows preserving the bioactivity of the system while providing a specific therapeutic effect upon ion release (e.g., angiogenesis, antibacterial and antioxidant properties) (Owens et al., 2016).

As almost all the BGs compositions, also Sr-doped BGs can be produced either by melt-quenching route or sol-gel process, using, respectively, strontium carbonate or strontium nitrate as a precursor of SrO. Carbonates, in fact, are not of common usage in the sol-gel process since the temperatures used to stabilize the network (calcination process) would not be high enough for allowing the complete removal of undesired carbon residues.

The final products obtained by sol-gel method, including monoliths, porous scaffolds, fibers, coatings, and granules, are all characterized by the presence of a mesoporous texture, which is inherent of sol-gel materials (Owens et al., 2016; Baino et al., 2018). It is worth mentioning that sol-gel process was also widely used to synthesize spherical nanoparticles (Kargozar and Mozafari, 2018; Leite et al., 2018) to be used as nanocarriers for controlled drug release for the treatment of bone pathologies, such as osteoporosis (Fiorilli et al., 2018).

Figure 1 provides a schematic representation of the two synthesis approaches previously described together with some examples of final products that could be obtained.

Thermal Properties, Crystallization, and Sintering Behavior of Sr-doped Bioactive Glasses

One of the major issues concerning the processing of BGs to obtain, for example, porous scaffolds, or coatings is the devitrification, which occurs upon the sintering treatments required for the densification of the structure. This is an aspect of concern in tissue engineering applications because the nucleation of crystalline phases, as well as the specific surface area, are directly linked to the reactivity of the surface itself and, thus, to the capability of the material to bond to the host tissue.

As a result, understanding the sintering conditions of glass powders and how the introduction of modifier cations in the glass network could affect the thermal properties and crystallization of the materials are among the key aspects to be considered when choosing a BG to fabricate sintered products for tissue engineering applications.

When introduced within the glassy matrix as a network modifier, SrO was found to affect the thermal behavior, sintering ability, microstructure and crystallization of the system, depending on both on the synthesis method and on the composition.

During the last decade, the thermal properties of Sr-doped bioactive glasses, together with crystallization kinetics and sinterability have been the object of study of several research groups.

Sr^{2+} is often introduced in the glass network as a modifier cation by partially replacing CaO with SrO. Due to the similar chemical role played by the two oxides, no significant structural alterations of the network (Network Connectivity - NC) were reported, with predominant Q^2 silicate structure (**Figure 2**).

The very similar field strength of Ca^{2+} and Sr^{2+} ions resulted in no significant shielding/de-shielding of the ^{29}Si nuclei (Fredholm et al., 2010). Anyway, the larger size of the Sr^{2+} ion compared to that of Ca^{2+} was found to expand and weaken the network, thus leading to a modification of the thermal properties of the glass (Lotfibakhshaiesh et al., 2010; Goel et al., 2011; Hasan et al., 2015; Li et al., 2015; Bellucci et al., 2017).

A careful analysis of the currently-available literature suggests that the effect of the inclusion of Sr on the structural alterations of BGs is strongly affected by the use of mole or weight percent in the compositional design. When weight percentage (wt %) is used, the higher molecular weight (mol%) of SrO compared to CaO can determine an increase of silica content in mole percentage, thereby resulting in higher network connectivity. On the contrary, when the mole percentage is used, the opposite effect could be observed in melt-derived glasses (O'donnell and Hill, 2010).

Several thermal studies performed on melt-derived Sr-doped BGs revealed the possibility to enhance the densification of the structure upon sintering by increasing the SrO/CaO molar ratio while preserving the amorphous nature of the system.

DTA analyses performed by Goel et al., for example, reported no alterations in the glass transition temperature (T_g) and increased values of the crystallization onset (T_c) and the crystallization peak (T_p) as a result of the increase in the Sr content up to 8 mol%, resulting in a significantly wider processing window (PW) of the glass, defined as the difference between the T_c and the T_g (Goel et al., 2011).

The complete thermal behavior and sintering ability of CaO-rich silica-based BGs modified by the replacement of CaO (10 mol%) with MgO, SrO or both in a 1:1 ratio was recently reported by Bellucci et al. (2017). Interestingly, DTA curves showed lower T_g of the modified glasses compared to that of the original composition (Bellucci et al., 2017). A similar outcome was found in another study by Lotfibakhshaiesh et al. (2010), who attributed the decrease of the T_g to the expansion of the glass network resulting from the replacement of Ca with Sr.

On the other hand, the substitution of Sr^{2+} for Na^+, was found to induce an increase of the T_g from 591 to 760°C with (Li et al., 2015), despite no significant changes of the glass structure were detected by X-ray photoelectron spectroscopy (XPS), Raman Spectroscopy and MAS-NMR. In fact, even if both

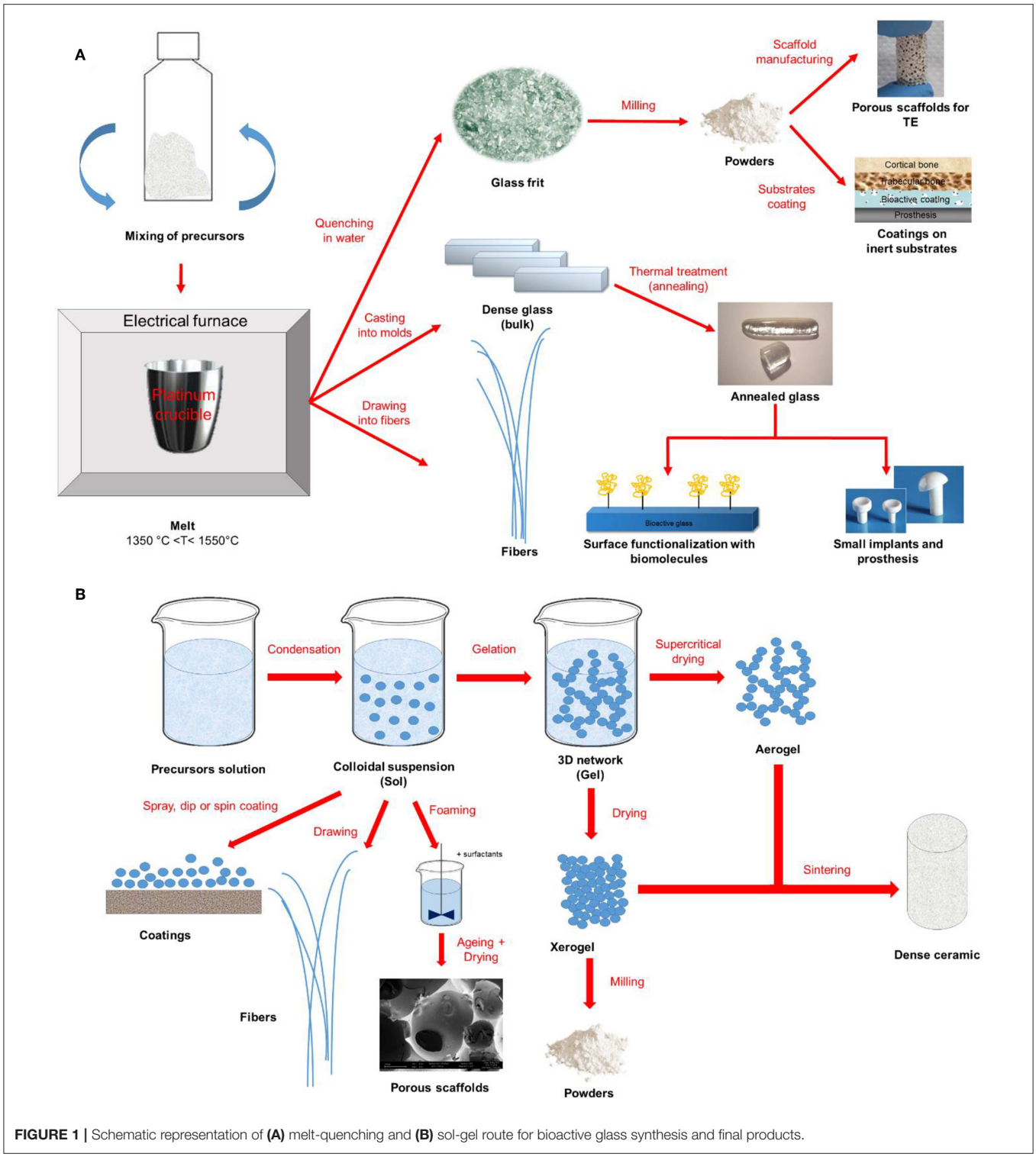

FIGURE 1 | Schematic representation of **(A)** melt-quenching and **(B)** sol-gel route for bioactive glass synthesis and final products.

Sr^{2+} and Na^{+} ions act as network modifiers, the increase in the T_g could be attributed to the different valence of the two ions. In fact, while Na^{+} can compensate just one non-bonding oxygen NBO^{-}, bivalent Sr^{2+}, can charge compensate $2NBO^{-}$ at the same time.

One of the major differences between Sr-doped sol-gel and melt-derived glasses concerns the possibility to retain the amorphous structure of the material upon sintering. In sol-gel BGs, XRD analyses revealed that, as the Sr^{2+} increased within the composition, the tendency toward crystallization

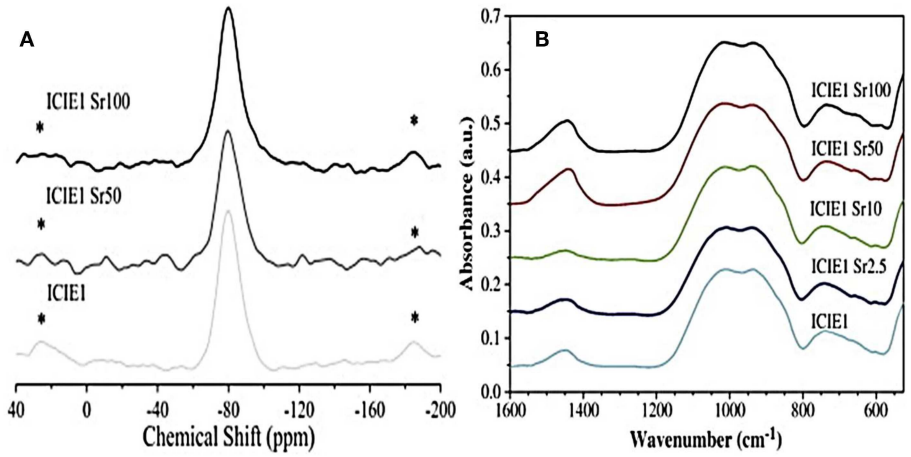

FIGURE 2 | ^{29}Si MAS-NMR **(A)** and FTIR **(B)** spectra related to glasses with various calcium-to-strontium substitutions. The results reveal no significant effects on structural properties and network connectivity (Fredholm et al., 2010). *represents spinning sideband.

was more pronounced. In particular, a complete crystalline structure was observed when CaO was totally substituted by SrO, with diffraction peaks associated with the Sr_2SiO_4 phase (Taherkhani and Moztarzadeh, 2016). The presence of Sr-containing crystalline phases in sol-gel materials was already reported by Solgi and coworkers (Solgi et al., 2017), while no crystallization was observed in melt-derived glasses as a result of the increase in Sr content (Hill et al., 2004; Fredholm et al., 2010; Kargozar et al., 2016). In fact, most of the XRD patterns in melt-derived systems (Hill et al., 2004; Kargozar et al., 2016) revealed just a slight shift in the amorphous scattering maxima to lower 2θ-values as a result of the replacement of Ca^{2+} with Sr^{2+} ions because of the larger size of the Sr^{2+} ions than Ca^{2+} ions (Kargozar et al., 2016).

However, Massera et al. reported DTA analyses on phosphate melt-derived glasses (Massera et al., 2013), showed a shift of the main crystallization peak toward lower temperatures as a result of the increase of SrO within the composition up to 5 mol%. For SrO amounts higher than 10 mol%, however, a shift toward higher temperatures could be observed, and a second crystallization peak could appear (Massera et al., 2013; Dessou et al., 2017).

Even if a direct comparison between these studies is difficult to establish due to the different compositions of the systems investigated, it can be stated that synthesis method indeed plays a crucial role in defining the physical and thermal properties of Sr-doped BGs. It is believed that further studies focused on the direct comparison of equivalent compositions produced by the traditional melt-quenching route and sol-gel chemical synthesis would provide a valuable contribution in shedding light on these peculiar aspects.

Structure and Reactivity of Sr-Doped Silicate, Borate, and Phosphate Glasses

Achieving highly-controlled ion release from biomaterials is one of the most important challenges in bone regeneration (Hoppe et al., 2011). In the last years, BGs have received much attention because of their interesting capability to promote cell attachment, proliferation, and differentiation thanks to their dissolution in a physiological environment based on an ion-release mechanism (Fiume et al., 2018).

The bioactivity mechanism, proposed for the first time by Larry Hench, is still accepted for silica-based BGs (Hench, 2006). Upon contact with biological fluids, the formation of a hydroxycarbonate apatite (HCA) layer is observed on the material surface, following the crystallization of the amorphous calcium phosphate film; at the same time, the ionic dissolution products released from the glass surface (basically calcium and silicate ions) confers osteogenetic properties to the material, stimulating the beneficial response of the surrounding tissue, which culminates in the mineralization of the newly-synthesized extracellular matrix (ECM) (Hench, 2006; Rahaman et al., 2011; Jones, 2015).

Probably, one of the most attractive aspects of BGs is the possibility to tailor their properties by introducing selected cations able to play a specific functional and/or biological role. In fact, it has been demonstrated that the addition of such cations, e.g., Sr^{2+}, into the glass network, affect crystallization kinetics, crystallinity, and thermal stability of the system to devitrification, as already discussed in the previous section. Moreover, the formation of the surface HCA layer, observed during the bioactive mechanism of glass dissolution, and the osteogenetic properties were found to be deeply related both to the type of former oxides and to the presence of dopants.

According to the final application of the material, either slow or fast dissolution rates might be required. In fact, while higher dissolution rates are usually associated with high reactivity and enhanced capability to bond to the host tissue providing early-stage stability of the implant, it should be pointed out that having slow dissolution rates of the material could represent an advantage in those bone-repair applications characterized by weak metabolic activity typical of some pathologies, as slower reaction kinetics would be more suitable in order to match the physiological healing time of the tissue.

In the present section, the effect of Sr incorporation within the glass network of silicate, borate and phosphate glasses will be discussed by focusing the attention on the structure modification and the influence on the mechanism of reactivity with biological fluids (Oudadesse et al., 2011; Li et al., 2014).

Silicate Sr-doped BGs

As regards silicate Sr-doped bioactive glasses, several studies confirmed that the introduction of Sr as a network modifier was able to induce important modifications in the bioactivity rate based on both the composition design (O'donnell and Hill, 2010) and the synthesis method. pH measurements during bioactivity tests in SBF and XRD patterns revealed that Sr for Ca substitution in molar proportions in melt-derived systems was able to increase both the degradation rate and the apatite-forming ability of the system because of the expansion of the glass network determined by the larger dimensions of the Sr^{2+} ion compared to Ca one (Fredholm et al., 2011). In particular, Ca release was found to follow a linear trend for Sr substitution $\leq$10 mol%, but an increase of Ca release was observed for Sr substitution of 2.5 mol% because of the larger ionic radius of Sr element (1.16 A) in comparison to Ca (0.94 A), which expands the glass network. XRD pattern was characterized by the presence of apatite nucleation peaks that become more pronounced as the Sr content increases, while in the Sr-free control no apatite peaks were detected (Fredholm et al., 2011).

Interestingly, an opposite behavior was observed in sol-gel glasses, where the replacement of Sr with Ca in the glass composition was proved to slow down the formation of the apatite layer on to the glass surface (Hesaraki et al., 2010a; Lao et al., 2013). A similar trend was found in sol-gel derived Sr-containing 13–93 nanoparticles doped with different amounts of Sr (Hoppe et al., 2014). Interestingly, at the nanoscale, an inhibitory effect of Sr-doping on the crystallization of the deposited calcium phosphate layer with respect to the Sr-free 13–93 nano-BG was observed because of the incorporation of Sr in the HA layer. This can be supported by Aina et al. (2013) study, showing a decrease in crystallite size and degree of crystallinity after introducing Sr into HA due to the larger size of Sr^{2+} ion in comparison to Ca, which causes an increase in d-spacing and crystal cell unit parameters. Therefore, the high local release of Sr^{2+} ions facilitated by the high surface area of sol-gel materials might have led to inhibited HA crystallization. These outcomes are in line with Rokidi and Koutsoukos's findings (Rokidi and Koutsoukos, 2012), showing that the presence of strontium in supersaturated solutions of calcium phosphate retarded the crystal growth of both octacalcium phosphate and HA.

Anyway, despite the dissolution rate and HA nucleation kinetics could be delayed as a result of the increase in Sr content which can increase the chemical stability of the glass, all the studies proved the possibility to retain the bioactive potential of the systems upon Sr-doping in different amounts.

Borate Sr-Doped BGs

Besides silicate BGs, borate systems recently gained increased scientific interest as attractive materials for several biomedical applications. Unlike the case of silicon, the coordination number of boron does not allow the formation of fully three-dimensional structures, which results, from a chemical viewpoint, in a lower resistance of network interconnection and hence in higher degradation rates during contact with body fluids (Wright et al., 2010). As a result, the cytotoxicity deriving from the rapid release of boron in the physiological environment has to be carefully controlled (Balasubramanian et al., 2018). The incorporation of Sr and other modifiers within the network of borate BGs seems to be one of the most effective strategies used to face this issue. The effect of different bivalent modifier oxides (i.e., BaO, SrO, ZnO, and MgO) on melt-derived borate-based glasses was recently investigated in a study by Kumari et al. (2017). MgO, SrO and BaO are conventional modifiers that enter the glass network by disrupting B–O–B, P–O–P and B–O–P bonds. In particular, the addition of modifying oxides in borate glasses can augment the network via the following events: (i) breaking of B–O–B bonds with the contiguous creation of non-bridging oxygens; (ii) increasing the oxygen coordination of boron; and (iii) combining both mechanisms mentioned above (Hasan et al., 2015).

In borosilicate and borate glasses, a slower release of boron was observed as a result of the increase in strontium content. The ion movements within the network are, in fact, partially inhibited by the expansion of the network caused by the larger size of Sr^{2+} ion (Pan et al., 2009). Moreover, while Na and B are easily released into the external environment, SrO uses to form $Sr(OH)_2$ species, which are chemically more resistant and difficult to dissolve (Hasan et al., 2015).

Phosphate Sr-doped BGs

Phosphate-based BGs are typically used in those clinical applications which require high dissolution rates of the implant (Brow, 2000).

In 2017, Patel and coworkers used Sr/Ca substitution to control and tune the dissolution behavior of melt-derived phosphate glasses in the $40P_2O_5-(16-x)CaO-20Na_2O-24$ MgO–x SrO system (x = 0, 4, 8, 12, 16 mol%) in order to achieve an accurate control on the rate of release of therapeutic ions included within the glass composition. The initial addition of SrO into the glass composition (up to 4 mol%) resulted in a decrease of the dissolution rate of the glass, thus suggesting an increase of the cross-linking between phosphate chains (Patel et al., 2017).

Kapoor and coworkers studied the structure-properties relationships in different melt-derived alkali-free phospho-silicate glass compositions co-doped with Zn^{2+} and Sr^{2+} ions (Kapoor et al., 2014). In particular, the attention was focused on the co-doping effects of Sr and Zn on the chemical dissolution behavior and bioactive mechanism in SBF. No effect of the Zn/Mg and Ca/Sr substitution was observed on the NC, which remained constant at about 1.95. Despite the lower NC compared to that of commercial 45S5 Bioglass®, the system showed lower solubility as a result of the ionic field strength associated with its constituent ions. There was a significant difference in the leaching of Zn^{2+} and Sr^{2+} ions in SBF and Tris-HCl despite equimolar ZnO, and SrO concentrations were incorporated, with a higher rate of release for Sr (Kapoor et al., 2014).

Phosphate glass properties make them very appealing as basic materials for the production of resorbable implants. In

TABLE 1 | Comparison among the Sr-doped glass systems discussed in the section Sr-containing BGs: an overview.

Glass system	Synthesis method/ former oxide	The object of the study	Thermal and structural properties	Bioactivity tests	References
$Na_2O/K_2O/MgO/CaO/B_2O_3$ $SiO_2/P_2O_5/SrO$	M/B	Controlled release of borate and Sr^{2+} ions for new bone formation	-No crystallization upon doping -No changes in the glass structure	-Complete conversion to apatite -Controlled degradation and ion release below the cytotoxic level	Li et al., 2016
$CaO/SrO/SiO_2/MgO/P_2O_5$ $/CaF_2$	M/S	Effect of Sr for Ca substitution on structural features, sintering behavior, and apatite-forming ability	- No changes in the glass structure - Wider PW up to 10 SrO mol%	-Lower apatite-forming ability in SBF - Lower chemical degradation in TRIS-HCl -Ion release within therapeutically effective range	Kargozar et al., 2016
$Na_2O/SrO/SiO_2/TiO_2/CaO$	M/S	Influence of Na^+ and Sr^{2+} on solubility	- No changes in the glass structure - Higher T_g	- Lower ion release rates	Ren et al., 2014
$B_2O_3/SrO/TiO2$ $B_2O_3/SrO/Na_2O/TiO_2$	M/B	Production of a borate glass system without the addition of other network formers; assessment of the physical, structural, thermal, and biological properties	-Higher T_g -Higher glass density	- SrO content influences degradation rate and ion release -Sr concentration above cytotoxicity levels	Yin et al., 2018
$CaO/SrO/SiO_2/P_2O_5/Na_2O$	M/S	Influence of Sr for Ca substitution on physical properties	- No changes in the glass structure - Higher glass density - Lower oxygen density (network expansion) - Lower dilatometric softening point - Higher thermal expansion coefficient - Lower T_g	_	Baino et al., 2019
CaO/ SrO-MgO/SiO_2/Na_2O K_2O/P_2O_5	M/S	Combination of the thermal behavior of Ca-rich silicate glasses with an improvement in biological results of MgO- and SrO-modified glasses	- Improved thermal stability - Improved mechanical properties	- Strong apatite-forming ability	Jones et al., 2016
$CaO/SrO/SiO_2/MgO/Na_2O$ $K_2O/ZnO/P_2O_5$	M/S	Influence of Sr/Ca substitution on the sintering behavior	- Lower T_g - Higher T_c - Wider PW	_	Baino, 2017
$SiO_2/CaO/SrO$	SG/S	Development of Sr-delivering glasses	- No alterations in the mesoporous texture	- Enhanced bioactivity - Increased reaction kinetic	Wei et al., 2014
$SiO_2/CaO/MgO/SrO$	SG/S	Synthesis, characterization, and investigation of the apatite-forming ability in SBF	- Crystalline phases (calcium and strontium silicates)	- Good apatite-forming ability - Apatite layer after 3-5 days immersion in SBF	Fiume et al., 2018
$CaO/SrO/P_2O_5/$ $Na_2/CaO/SrO$	M/P	Glass fiber production	- Higher thermal stability - Wider PW	Reduced phosphate ions release - Formation of the apatite layer - SrO and MgO embedded in the apatite layer - Improved chemical stability	Baino et al., 2018,a
$P_2O_5/CaO/SrO/Na_2O/MgO$ SrO	M/P	Investigation of phosphate glass formulation for controlled Sr release	- Lower T_g and T_m - Broadening of the main crystallization peak - No changes in the glass structure	- Higher chemical durability - Lower dissolution rates	Hench, 2006
$SiO_2/P_2O_5/CaO/SrO$	SG/S-P	Production and characterization of Sr-doped silico-phosphate glasses	- Higher T_p - Nucleation of new crystalline phases - Increase in the gel viscosity	- Higher biodegradation rate	Hesaraki et al., 2010b

M, Melt-quenching route; SG, Sol-gel route; S, Silicate glasses; B, Borate glasses; P, Phosphate glasses; PW, Processing Window; T_g, Glass transition temperature; T_c, Crystallization onset temperature; T_p, Maximum rate of crystallization temperature; T_m, Melting temperature; SBF, Simulated body fluid. All the results are referred to the doped system, compared to the undoped one. If the effect of SrO replacement for another oxide is specifically investigated, the oxide couple (e.g., SrO/CaO) is indicated in the column "Glass system."

this attempt, melt-derived Sr-containing polyphosphate glasses doped with Mg and Ti were investigated by Weiss et al. (2014). The inclusion of Mg and Ti was found to increase the bonding strength between phosphate chains resulting in a higher glass stiffness, better mechanical properties, and lower degradation rates in Tris-HCl solution. The HA layer observed after 15 days of immersion in SBF was thicker and denser for the doped systems, thus suggesting a stimulatory and synergic effect of multiple ions on the bioactivity mechanism of the glass (Weiss et al., 2014).

Interestingly, some studies demonstrated that the improvement in the chemical stability of phosphate glasses seems to be not affected by the thermal properties (Hesaraki et al., 2010b; Stefanic et al., 2018).

Stefanic et al. investigated the effect of Sr substitution in $40P_2O_5$-25CaO−$5Na_2O$–(30 – x) MgO–xSrO systems (x= 0, 1, 5, 10 mol%). FTIR analysis revealed no significant structural modifications with no variations in the O/P ratio and the Q speciation. However, phosphate bands shifted toward lower wavenumbers as the Sr content increased from 1 to 10 mol%. This shift could be attributed to the lower field strength of Sr^{2+} ions, which have higher atomic number compared to that of Mg^{2+} ions, as the total divalent cation-to-phosphate ratio did not change within all the glasses investigated. Despite the higher thermal stability of the Sr-free system, the chemical durability of these melt-derived glasses in water was found to decrease with decreasing Sr content, and it was characterized by linear degradation and highly controllable profiles (Stefanic et al., 2018).

Comparative Remarks

Table 1 provides a summary of the literature results discussed in the previous sections and relates thermal and structural properties to the bioactive potential of the systems analyzed. In summary, it can be stated that there is a strong dependence on the basic compositional system, and some peculiar trends can be observed. While Sr doping in silicate glasses was found to enhance the mechanism of bioactivity and accelerate the ion release rates, the increase of SrO in borate and phosphate systems typically led to improved chemical stability of the material. However, it is worth pointing out the presence of some exceptional cases (reported in Table E1) that suggest caution in generalizing the results. In fact, a direct comparison between different systems is hard to carry out since all the properties of glasses are affected by multiple factors that simultaneously contribute to the final and complete behavior of the examined material.

Atomistic Simulations

Understanding the relationship that exists between glass structure and functional properties is not always immediate, especially when the design of the glass composition becomes complex and rich of different elements whose effects are the result of the interaction of multiple factors.

In this section, atomistic simulations will be presented as a valuable instrument aimed at rationally designing glass compositions in order to define, investigate and better understand the structure, dissolution, and bioactivity mechanisms of glasses used in biomedical applications thanks to the rapid increase in computing power and development of new algorithms and methodologies (Tilocca, 2010; Xiang and Du, 2011; Du and Xiang, 2012).

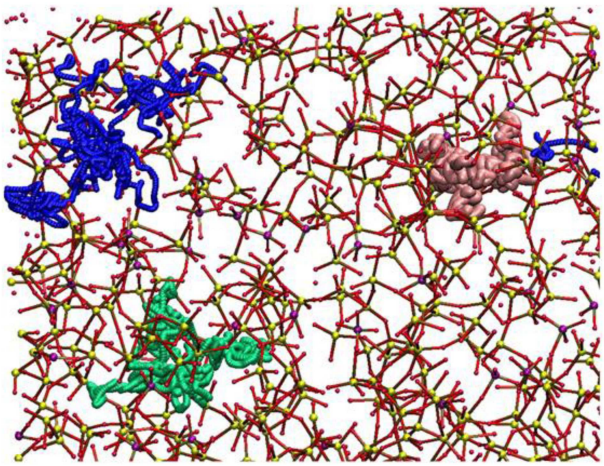

FIGURE 3 | Diffusion pathways suggested for atoms of Na (green ball), Ca (blue ball), and Sr (pink ball). The other elements are depicted as Si (small yellow ball), P (small purple ball), O (small red ball) (Du and Xiang, 2012).

Molecular dynamics (MD) simulations are currently the most widely used method that allows very accurate and reliable glass structural models to be generated. Experimental studies showed that Sr-containing BGs, especially in the case of SrO/CaO substitution, did not exhibit very large modifications in terms of glass structure because of the similarity of Sr^{2+} and Ca^{2+} ions from a chemical viewpoint. Apart from these preliminary considerations, MD simulations were indeed useful to define the local environment and the diffusion behavior of SrO containing BGs (Xiang and Du, 2011; Du and Xiang, 2012; Xiang et al., 2013). The effects of SrO/CaO substitution on glass diffusion and bioactivity was deeply investigated by Du and Xiang (2012), Du and Xiang (2016) on three different compositions characterized by a silica content ranging from 46 to 65 mol% to cover multiple bioactivity levels (Du and Xiang, 2016). The local environment around modifiers cations, as well as network connectivity, were determined as a function of the glass composition. **Figure 3** shows the diffusion pathways of Na, Ca, and Sr obtained by MD simulations.

Sodium ions were found to have a higher diffusion coefficient and lower energy barriers compared to Ca^{2+} and Sr^{2+} ions. Interestingly, an increase in silica content led to a decrease in the diffusion coefficient of the modifiers cations.

Because of the similarities of the self-diffusion coefficients and energy barriers of Sr^{2+} and Ca^{2+}, Du and Xiang suggested that it is actually possible to maintain almost unaltered the basic physicochemical properties of the starting glass composition while enhancing tissue growth due to the release of Sr^{2+} ions (Du and Xiang, 2016).

While in classical MD simulations the interatomic forces are approximated by an empirical potential, easier to compute but affected by the introduction of approximations and loss

of information on the electronic structure, in a recent study (Christie and de Leeuw, 2017). They investigated the effect of Sr addition on the bioactivity of phosphate glasses by developing a new interatomic potential able to consider the polarizability of oxygen ions in order to investigate the medium-range structure, which is responsible for the bioactivity mechanism. Several Sr-containing glass compositions were simulated by both classical and first-principle MD. In general, it was confirmed that Sr incorporation caused minimal changes in the dissolution of the glass, and the bioactivity remains preserved. The NC and Q^n distribution were shown to be essentially unaffected by the incorporation of Sr. The first result was to be expected, as the network connectivity depends on the ratio of the number of oxygen atoms to the number of phosphorus atoms, which does not change for SrO/CaO or SrO/Na_2O substitutions. The Q^n distribution might change, but the amounts of Sr incorporated in the studied compositions were relatively small (10 mol% max.) and, thus, the associated change was small, too (Christie and de Leeuw, 2017).

CEMENTS, COMPOSITES, COATINGS, AND GLASS-CERAMICS BASED ON SR-DOPED BGS

The majority of the BGs form a strong interfacial bond with the bone (Hench, 2013). An initial investigation by Piotrowski et al. (1975) proved that the interfacial bond between 45S5 Bioglass® and cortical bone in rat and monkey models is equal to or even higher than the strength of the host bone (Piotrowski et al., 1975), and this finding was eventually confirmed clinically (Montazerian and Zanotto, 2017a). As summarized in the previous section, many Sr-doped BGs have excellent biochemical compatibility; however, they have some limitations from a biomechanical viewpoint. The bending strength and fracture toughness of most of the compositions discussed above are in the range of 40–60 MPa and 0.5–1 MPa $m^{1/2}$, respectively. These values are <50–150 MPa and 2–12 MPa $m^{1/2}$, which are the typical ranges of cortical bone (Hench, 1991), and thus make Sr-doped BGs inappropriate for load-bearing applications. However, for some applications, low strength and fracture toughness are offset by the low elastic modulus of the glass (30–35 GPa), which is close to that of cortical bone (7–30 GPa). Therefore, the low strength does not question the usefulness of Sr-doped BGs for several important applications like cements, composites, and coatings. Low strength also does not affect the application of BGs as buried, low-loaded and compressively loaded implants, or in the form of powders and a bioactive phase in bone cements. Thus, several Sr-doped BGs were considered for the development of coating or composite to expand their range of applications. Furthermore, the development of glass-ceramics (GCs) provides another option for improving the mechanical properties of BGs.

Bone Cements

Conventional polymeric bone cements like poly(methyl methacrylate) (PMMA) and glass ionomer cements are among the most used materials in dentistry and orthopedics, but they have numerous drawbacks. They commonly show poor bonding with bone, a high exothermic reaction *in situ*, low mechanical reliability, and inadequate radiopacity. Moreover, the high-temperature or elaborated processing techniques, slow degradation rate, and low strength are other limitations of commercial ceramic bone cements such as calcium phosphate cement (CPC) and HA (Kenny and Buggy, 2003). Therefore, the objective of numerous studies was to develop and characterize bone cements composed of reinforcing components like Sr-doped BG particles that serve as the reinforcing and radiopaque phase in polymers or sintering aid in ceramics. In addition, the Sr-doped BGs are usually selected due to their outstanding characteristics, including bioactivity, osteogenic potential, and the capability of the controlled release of Sr^{2+} ions.

A Sr-doped HA bone cement was prepared to enhance bioactivity and biocompatibility. The release of Sr^{2+} ions was supposed to the main reason for promoted osteoblast proliferation, which could facilitate the precipitation of newly-formed HA and resulting in the enhanced strength of the bone-cement interface (Cheung et al., 2005; Ni et al., 2006).

The preparation of an injectable Sr-containing CPC has been successfully reported with promising properties, including setting time, compressive strength, and radiopacity (Yu et al., 2009). This cement could improve the proliferation and differentiation of both osteoblastic cells and human bone marrow mesenchymal stem cells (hBMSCs) *in vitro* (Kuang et al., 2012; Schumacher et al., 2013) and the new bone formation was accelerated at the bone-cement interface, as well as in the entire metaphyseal fracture defect site in ovariectomized rats (Thormann et al., 2013).

Sr-BGs in Ionomer Cements

Starting from 2008, glass polyalkenoate cements (GPCs), used for restorative purposes in dentistry and orthopedics, were the subject of extensive research by Boyd et al. (2008), Wren et al. (2008), Clarkin et al. (2009), Wren et al. (2010), Wren et al. (2013). They employed new SiO_2-ZnO–CaO–SrO glasses instead of the commercial fluoro-aluminosilicate glass. The glass usually reacts with an aqueous portion of the cement such as polyacrylic acid (PAA). The degradation of the glass structure is regulated by PAA, leading to the release of metallic cations into the aqueous phase of the setting cement. The carboxylate groups cross-link these cations on the PAA chains; embedding reacted and unreacted glass particles in a hydrated polysalt matrix of the cement (Boyd et al., 2008; Wren et al., 2008, 2010, 2013; Clarkin et al., 2009).

Different from aluminum as a neurotoxin, zinc is expected to inference positively the proper functioning of the immune system and to impart antibacterial properties to the cement (Kargozar et al., 2018a). Sr^{2+} ions were substituted with Ca^{2+} in the glass because their ionic radii are similar. Furthermore, strontium was known to have a lot of beneficial effects on bone, to share some of the same physiological pathways as Ca and to improve the radiopacity.

Boyd et al. (2008) produced GPCs from $48SiO_2-36ZnO-(16-x)CaO-xSrO$ (x = 0, 4, 8, and 12 mol%) glasses and PAA.

Glass frits were prepared via the conventional method of melting-quenching in water. They prepared the cements by thoroughly mixing 2 g of glass (particle sizes $< 45\,\mu m$) with 0.6 g of PAA powders and 0.9 mL of distilled water on a glass plate. Thorough mixing of cements was undertaken during 30 s. The results reported in this research indicated that the replacement of Ca with Sr in the glasses has no significant influence on the structure of the studied glasses, as proved by the trivial effect that the replacement had on T_g and NMR-derived Q^n distributions of each glass. Nonetheless, it was stated that increasing substitution of Ca with Sr increased the setting times, which was ascribable to the higher basicity of SrO over CaO. Wren et al. (2008) reported 29 and 110 s as the maximum working time and setting time, respectively; which was inadequate for clinical procedures. Sufficient working and setting times were expected to reach 6–10 and 15 min, respectively. However, the optimum biaxial flexural and compressive strength reached 34 and 75 MPa, respectively, proving that these materials could be potentially used in load-bearing applications. The *in vitro* evaluation in SBF showed that all the prepared cements could promote the development of amorphous calcium phosphate at their surface after 1 day of incubation. This event became more apparent (increased density and coverage) over time, representing that these cements could bond to bone directly (Wren et al., 2008).

In line with these researches, Clarkin et al. (2009), Clarkin et al. (2010) employed $4SrO-12CaO-36ZnO-48SiO_2$ (mol%) glass, low molecular weight PAA and a modifying agent, trisodium citrate dihydrate (TSC), to optimize working and setting times which were too short for invasive surgical procedures, including bone fracture fixation and void filling. In their study, the newly-formulated GPC was compared with Hydroset^{TM}, a commercial self-setting CPC. They compared compressive strength, flexural strength, Young's modulus, working and setting times, and injectability. The formulation had higher mechanical strength (39 MPa in compression) than both vertebral bone (18.4 MPa) and Hydroset^{TM} (14 MPa). However, the working time (2 min compared to ∼4 min for Hydroset^{TM}) and rheological properties of the cement, although improved, still required further modifications before their application in minimally invasive surgery, e.g., vertebroplasty or luting applications (Clarkin et al., 2009, 2010).

In their endeavor to adjust the working and setting times of their promising cementitious composites, Wren et al. (2010) added some naturally-derived proteins/polymers to the zinc-containing glass polyalkenoate cements (GPCs). The authors used chitin (Chi.), collagen (Col.), cysteine (Cys.), and keratin (Ker.). They concluded that the addition of these proteins/polymers could lead to little change to the working and setting times, and even the compressive strength was found to decrease slightly. No significant difference was observed in the flexural test. The same GPC containing $4SrO-12CaO-36ZnO-48SiO_2$ (mol%) glass, named Zn-GPC, was compared to commercial materials (Fuji IX and Ketac Molar) which have setting chemistry comparable to Zn-GPCs. Working and setting times (handling properties) for Zn-GPCs were shorter than the commercial materials. Zn-GPCs also had a higher setting exotherm (34°C) than the commercial products (29°C). The maximum compressive strength for Zn-GPC, Ketac Molar and Fuji IX was 75, 216, and 238 MPa, and biaxial flexural strength was 34, 62, and 54 MPa, respectively. Based on the results of compressive strength test, Zn-GPCs have appeared to be more appropriate for spinal applications in comparison to commercial GPCs but the characteristic times for surgical handling still need optimization (Clarkin et al., 2010; Wren et al., 2013).

Sr-BGs in Calcium Phosphate Cements (CPCs)

In 2016, Kent et al. (2016) developed a kind of CPCs by reacting BGs with $Ca(H_2PO_4)_2$ to form cement. They found that a P_2O_5 content of 4 mol% or greater is required in $SiO_2-P_2O_5-CaO-Na_2O$ glass to produce cement. The phases formed depend on glass composition; brushite ($CaHPO_4{\cdot}2H_2O$) and octacalcium phosphate ($Ca_8H_2(PO_4)_6{\cdot}5H_2O$, OCP) form first with 6 mol% P_2O_5 in the glass. Brushite dissolves, reforms as OCP and then transforms to apatite. These new cements offer a new route to forming CPCs that combine *in situ* setting and injectability of "conventional" CPCs with resorbability and bioactivity of BGs. D'Onofrio et al. (2016) designed and synthesized a series of Sr-doped BGs to add them in a range of CPCs. They aimed to synthesize, as the final product of the cement, Sr-containing HA and investigated the effects of Sr^{2+} ions on the physicochemical properties of the cement. Glasses in the $42SiO_2-4P_2O_5-(39-x)CaO-15Na_2O-xSrO$ (mol%) system were synthesized by progressively replacement of Sr with Ca (x = 1.95, 3.90, 9.75, 19.5, 29.25, 39%). Sr-doped CPCs were developed by mixing the glass and $Ca(H_2PO_4)_2$ powders with a 2.5% solution of Na_2HPO_4. Setting time and compressive strength were measured at 1 h, 1 day, 7 and 28 days post-incubation in Tris buffer solution. XRD, FTIR, and radiopacity were measured, too, and crystal morphology was assessed by SEM. Sr substitution in the glass increased setting time up to 25%, while its higher substitutions acted oppositely and resulted in a decrease in the setting time. Compressive strength reached 12.5 MPa because of the interlocking morphology of the crystals. XRD showed that Sr influenced the type of crystal phases formed. Octacalcium phosphate was the main phase present after 1 h and 1 day while after 28 days OCP was completely transformed to Sr-containing HA ($Sr_xCa(10-x)(PO_4)_6(OH)_2$, Sr-HA). Radiopacity enhanced proportionally to Sr substitution in the glass network. This study introduces a novel method regarding the development of a bone graft forming *in vitro* Sr-HA as a final product by applying a Sr-BG as a precursor, and the authors claimed that the prepared injectable cements are promising candidates for orthopedic and dental applications.

Sr-doped BGs in Polymeric Cements

Sr-doped BG particles are added in polymeric cements as a bioactive, reinforcing or radiopaque phase. In this regard, Zhang et al. (2015) proposed a new injectable cement composed of Sr-doped borate BG particles ($5.5Na_2O-7.34K_2O-7.34MgO-20.18CaO-49.54B_2O_3-1.83P_2O_5-8.27SrO$ in mol%) and a chitosan-based bonding phase. The glass was prepared by the conventional melt-quenching route and ground to form particles of $<40\,\mu m$. The authors prepared the hardening phase via mixing chitosan with a

β-glycerophosphate at a ratio of 7:1 by volume. In addition, they prepared the cement paste by mixing the glass particles with the hardening liquid at a ratio of 2.0 g/mL. The BGs stimulated the bioactivity, conversion to HA, and the ability to encourage osteogenesis, whereas the chitosan provided an interconnected biodegradable and biocompatible bonding component. The cement set *in situ* after the initial setting time of 11.6 ± 1.2 min) and represented a compressive strength of 19 ± 1 MPa. The proliferation and differentiation of hBMSCs treated with the cement were significantly higher than the cells incubated with a similar cement made of chitosan-bonded Sr-free borate BG particles. The osteogenic capacity of the cement was shown by micro-computed tomography (micro-CT) and histology of the samples obtained from critical-sized rabbit femoral condyle defects treated with the material. The results showed newly-formed bone at different distances from the implants after 8 weeks. Moreover, the index of bone-implant contact was considerably higher for the implant containing Sr-doped glass compared to the implant with Sr-free glass particles. Overall, the results indicated that this Sr-containing cement could be considered as a promising substitute for the repair and regeneration of irregularly-shaped bone defects with the use of minimally invasive surgery (Zhang et al., 2015).

Cui et al. (2017) added another Sr-containing borate BG as the reinforcing and bioactive filler to PMMA cement. The PMMA cement and Sr-BG/PMMA composites were prepared by mixing solid and liquid components at particular solid-to-liquid ratios. The solid part of composite cement contained Sr-doped BG (10–50 μm) and PMMA (10–80 μm) particles. The glass composition was $6Na_2O-8K_2O-8MgO-16CaO-6SrO-27B_2O_3-27SiO_2-2P_2O_5$ (mol%) and prepared by the melting-casting method. The glass and PMMA solid powders were mixed with the liquid component containing 3 mL of MMA monomer and 0.14 μl DMPT accelerator. Detailed compositions of the PMMA cement and Sr-BG/PMMA composite cements are summarized in **Table 2** (Cui et al., 2017). **Figure 4** shows the microstructure of the PMMA cement and 10Sr-BG/PMMA and 30Sr-BG/PMMA composite cements. The Sr-doped glass powders adhered to the PMMA matrix (**Figures 4B,C**), and there were some pores within the Sr-BG/PMMA composite cements. Elemental mapping by energy dispersive spectroscopy (EDS) (**Figures 4D,E**) revealed a homogeneous distribution of silicon and calcium – and hence of glass particles – within the PMMA matrix (Cui et al., 2017).

The exothermic polymerization temperature significantly decreased after using Sr-BG/PMMA composite cements compared with BG-free PMMA while the suitable setting time and high mechanical strength were retained. The Sr-BG/PMMA composites were bioactive *in vitro* and released B, Ca, and P ions into SBF. The addition of Sr-doped BG promoted the adhesion, proliferation, migration, and collagen secretion of MC3T3-E1 cells *in vitro*. Moreover, *in vivo* investigation revealed that Sr-BG/PMMA composite cements were better osseointegrated than BG-free PMMA bone cement. Sr-doped BG in the composite cement could enhance new bone formation in rat tibia defects around the cement-bone interface after 8 and 12 weeks post-implantation (**Figure 5**), while conventional PMMA could only stimulate the formation of an intervening connective tissue layer. As a result, the Sr-BG/PMMA composite cement was recommended as a substitute to PMMA bone cement in clinical orthopedic applications and minimally invasive surgery (Cui et al., 2017).

TABLE 2 | Compositions of PMMA cement and related Sr-BG/PMMA cements (Cui et al., 2017).

Cements	Filler loading (wt%)	Solid parts (g)		Liquid parts (mL)	S/L (S = PMMA + SrBG)
		PMMA powder (g)	Sr-BG (g)		
Control (PMMA)	0	2	0	1	2: 1
10Sr-BG/PMMA	10	2	0.2	1	2.2: 1
20Sr-BG/PMMA	20	2	0.4	1	2.4: 1
30Sr-BG/PMMA	30	2	0.6	1	2.6: 1

In order to improve visualization by radiography during surgery, radiopacifying agents such as barium sulfate (Ba_2SO_4) or zirconium dioxide (ZrO_2) are added to cements. These materials may deteriorate the biocompatibility of the cements or have detrimental influences, such as bone resorption, and degradation of mechanical properties (Bhambri and Gilbertson, 1995; Sabokbar et al., 1997; Demian and McDermott, 1998; Wang et al., 2005). However, incorporating bioactive and biocompatibility radiopacifier agents would have beneficial effects. Bioactive radiopaque glasses containing heavy elements such as Sr (Boyd et al., 2009), niobium (Nb) (Bauer et al., 2016), and zirconium (Zr) (Tallia et al., 2014; Montazerian et al., 2015; Montazerian and Zanotto, 2016), known to have positive and therapeutic influences on bone, have attracted the attention of the researchers nowadays. Therefore, O'Brien et al. (2010) incrementally replaced Ba_2SO_4 in the commercial Spineplex® cement with a Sr-containing radiopaque glass composition ($40SiO_2-30Na_2O-20SrO-10CaO$ in mol%). The substitution increased the setting time from 13.1 min for Spineplex® to 16.6–18.3 min for the new cements. A reduction in the peak exotherm during curing (23°C) was observed for Spineplex® in comparison to the fully replaced cement, demonstrating that reduced thermal necrosis in the *in vivo* setting is achievable using these materials. No significant deterioration was recorded regarding Young's modulus and compressive strength of each formulation due to the addition of Sr-doped BG. Although the radiopacity of the new cements was decreased up to 18% relative to the control, but still maintained radiopacity equal to several millimeters of aluminum (O'Brien et al., 2010).

More recently, Goñi et al. (2018) prepared different composite bone cements comprising PMMA beads and particles of gel-derived SiO_2-CaO–P_2O_5 BGs with 0-20 wt% of CaO substituted with SrO (Mendez et al., 2004). The difference between the

Cements	Filler loading (wt%)	Solid parts (g)		Liquid parts (mL)	S/L (S=PMMA+SrBG)
		PMMA powder (g)	Sr-BG (g)		
30Sr-BG/PMMA	30	2	0.6	1	2.6 : 1

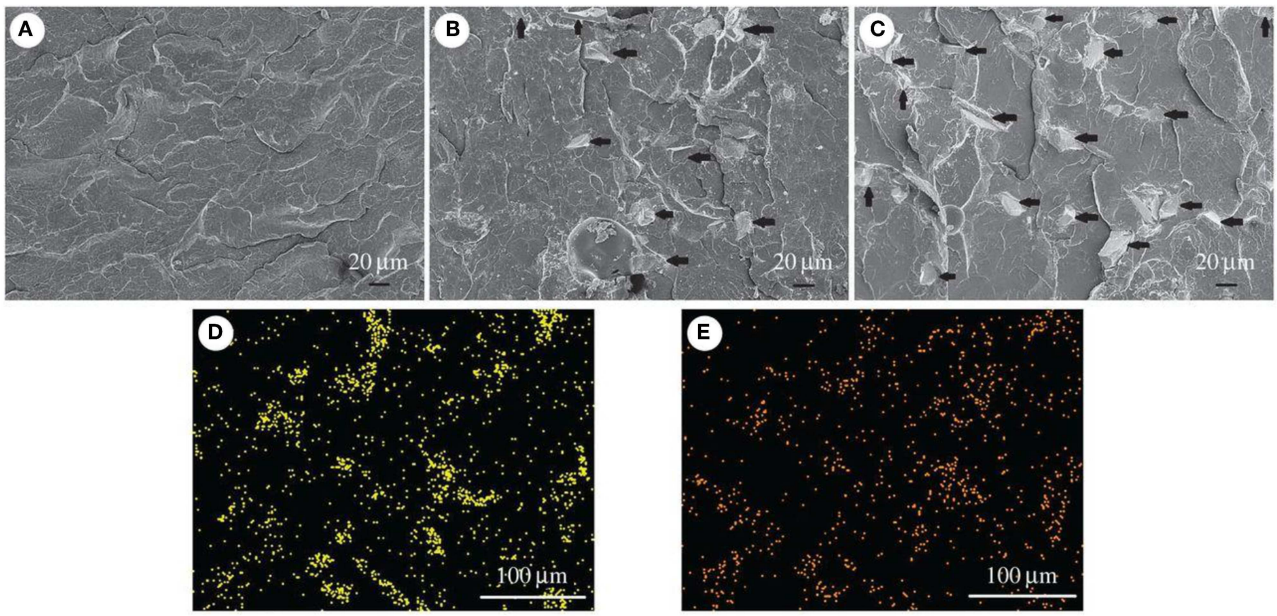

FIGURE 4 | The microstructure of **(A)** PMMA bone cement, **(B)** 10Sr-BG/PMMA and **(C)** 30Sr-BG/PMMA composite cements (the black arrows indicate the Sr-doped BG particles). EDS mapping of the elements **(D)** Si and **(E)** Ca shows that Sr-BG particles are well-dispersed in the 30Sr-BG/PMMA composite cement [Adapted from Cui et al. (2017) with permission from The Royal Society].

cementitious materials was in the Sr content of BG and relative amounts of the solid phase. The aim was to determine the effect of the mixture of solid phase constituents on maximum exothermic temperature, setting time, and injectability. Regarding the obtained results, they stated that composite formulations have improved performance than that of PMMA the reference (PMMA), with lower exotherm temperature and setting time and higher injectability. The same authors showed that incorporation of Sr-substituted BGs into these materials conferred bioactive properties linked to the role of Sr in bone formation, introducing some composite cements that may be appropriate for application in percutaneous vertebroplasty (Goñi et al., 2018).

Bone Graft Ceramic/Polymeric Composites

Calcium phosphate-based ceramics, e.g., HA and β-tricalcium phosphate (β-TCP), have been extensively using in dental and orthopedic applications since the 1980s (Bohner, 2000), primarily due to their similarity (crystal and chemical properties) to the mineral component of the bone tissue. The supportive role of calcium phosphates regarding adhesion, proliferation, and the differentiation of MSCs and osteoblasts is previously well-documented (Kamitakahara et al., 2008). HA and TCP are both highly osteoconductive and biocompatible. Although HA and TCP are recognized as biocompatible and osteoconductive materials, they suffer from some limitations, such as brittleness and poor mechanical properties. Therefore, a large number of attempts have been made to enhance their mechanical strength, like the addition of a sintering aid to increase the density and minimize the residual porosity of the system. Most of these studies employed BGs and, in particular, 45S5 Bioglass® (Goller et al., 2003) and a CaO-rich BG formulation ($2.3K_2O-2.3Na_2O-45.6CaO-2.6P_2O_5-47.3SiO_2$ in mol%) that is reluctant to crystallization (Bellucci et al., 2014). Additionally, there is proof of the positive effects of the presence of Sr in these materials. To test the influence of the addition of Sr-doped BGs to produce composites, Hesaraki et al. (2012) added different amounts of sol-gel derived Sr-containing BG nano-powders ($26CaO-5SrO-5P_2O_5-64SiO_2$ wt.%) to HA with a mean particle size of 0.5 µm to improve its mechanical properties after sintering. The samples were sintered at 1,000–1,200°C. A couple of physicochemical and biological assays, including XRD,

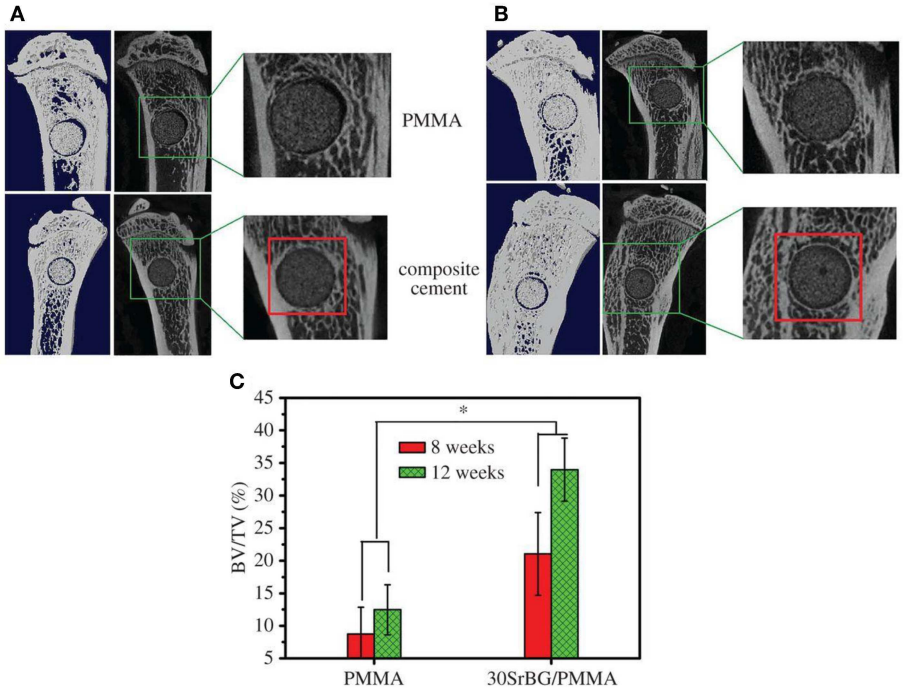

FIGURE 5 | Micro-CT evaluation of bone regeneration in the rat tibia defects after implantation of PMMA and 30Sr-BG/PMMA composite cements. The 3D reconstructed sagittal images of the area surrounding the cement implants show new bone formation around the cement-host bone interface at **(A)** 8 and **(B)** 12 weeks (area outlined in red); **(C)** BV/TV (bone volume/total volume) in the defects implanted with 30SrBG/PMMA composite cement for different post-implantation times. Values are presented as mean ± s.d.; $n = 3$. *Significant difference between groups ($p < 0.05$) [Adapted from Cui et al. (2017) with permission from The Royal Society].

SEM, microindentation, MTT, and ALP assay were carried out by the authors to characterize the samples. The obtained results showed that the inclusion of 1–10% of BG nano-powder led to the formation of β-TCP phase, the content of which increased with increasing the amount of Sr-BG and temperature. In addition to β-TCP, α-TCP, and calcium phosphate silicate were also found in the composition of HA sintered with 10% glass. After sintering at 1,200°C, bending strength (∼70 MPa), microhardness (∼300 HV) and fracture toughness (∼1.2 MPa.$m^{1/2}$) improved by adding 1–5% Sr-BGs, whereas these mechanical properties decreased when 10% glass was added. The addition of nano-sized Sr-BGs did not alter the rate of cell proliferation but increased the level of ALP produced (Hesaraki et al., 2012). The same gel-derived Sr-BG was added to biphasic calcium phosphate (BCP) by Nezafati et al. (2014), who sintered the mixture at 1,100, 1,200, and 1,300°C. The maximum bending strength (45 MPa) was achieved when BCP was added with 3 wt% Sr-BGs and sintered at 1,200°C. The addition of Sr-BGs did not affect the phase composition of BCP when it was treated at 1,200°C, and the composite supported the adhesion and expansion of rat calvarium-derived osteoblasts.

Sr-containing phosphate-based glass ($45P_2O_5-32SrO-23Na_2O$ in wt%) was also used as a sintering aid for β-TCP, which was heat-treated at 1,250°C (He and Tian, 2018). The results showed that the glass addition allowed liquid-phase sintering of β-TCP with the noticeable promotion of densification (He and Tian, 2018). In the sintering process, the Sr-doped BG reacted with β-TCP, and the Sr^{+2} ions replaced Ca^{2+} ions of β-TCP. Furthermore, the glass addition efficiently hindered the transformation of β-TCP to α-TCP. The compressive strength of these porous β-TCP-based bioceramics was improved from 7 to 11 MPa by introducing 10 wt% Sr-doped BGs.

It has also been proved in several other studies that Sr-substituted TCP and HA cements/ceramics show promise for use in orthopedic, e.g., in filling bone defects (Kim et al., 2004; Saint-Jean et al., 2005; Pina et al., 2010). More recently, Kuda et al. (2018) have prepared composite materials by adding 1 wt% SrO to biogenic HA (BHA) and sodium borosilicate glass in a ratio of 50/50 by weight. The composites were sintered at 780°C for 1 h. The BG addition improved the sinterability, while the crystal lattice constant of biogenic HA decreased. It was also found that such BHA/glass/SrO composite possessed a higher porosity and rate of dissolution in a physiologic solution, which make it highly attractive for use in the replacement of defective areas of bone (Kuda et al., 2018).

Other promising applications of Sr-doped BGs are addressed to the repair of alveolar bone in dentistry. Polymeric membranes are one of the extensively used materials in periodontology and dental implantology, which improve the bone healing process in the method of guided bone regeneration (GBR) (Misra et al., 2006). The standard rule of this treatment is to physically provide

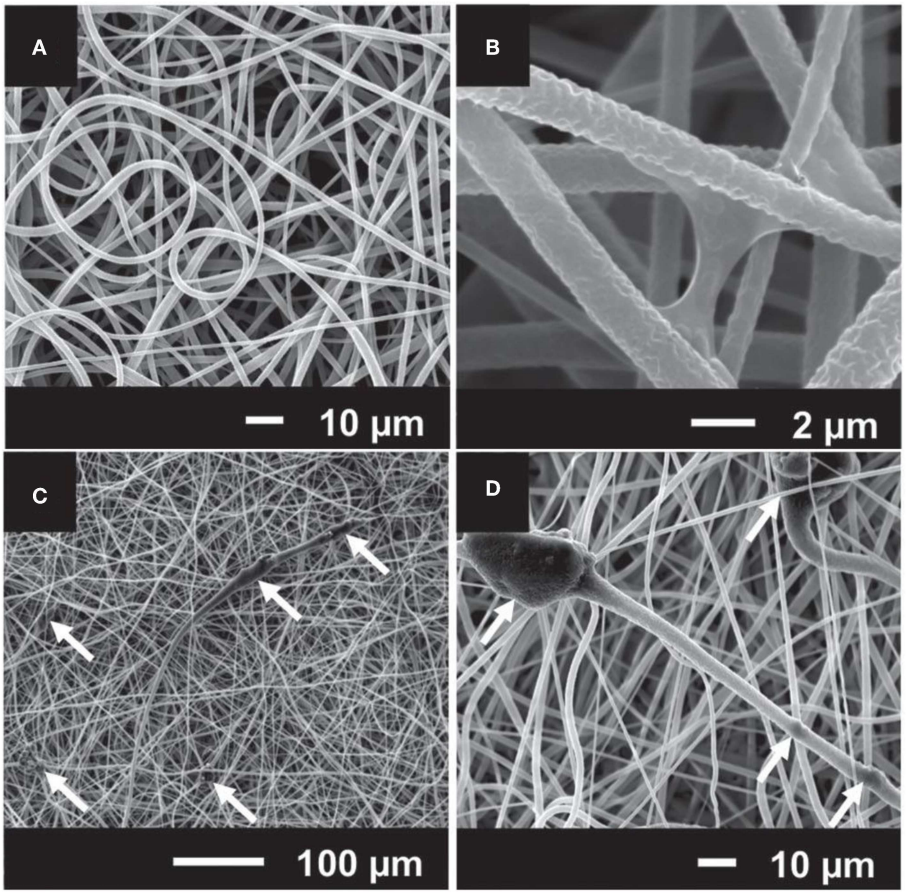

FIGURE 6 | SEM micrographs of electrospun composites made of **(A)** and **(B)** poly(caprolactone) (PCL); **(C)** and **(D)** PCL and particles of Sr-containing BG. The white arrows indicate that BG particles are embedded in the polymeric electrospun fibers [Adapted from Santocildes-Romero et al. (2016), after permission by Wiley and Sons].

a relatively remote environment where bone can repair via keeping out local soft tissues from a defect site. An ideal barrier membrane should resorb and stimulate bone tissue regeneration within the defect (Misra et al., 2006). The prospective of electrospinning (Agarwal et al., 2008) and advantages of Sr-substituted BGs have been discussed for this purpose, and it is expected that the combination of these two approaches results in the fabrication of potent membranes in terms of bone tissue regeneration. Ren et al. (2014) combined melt-electrospun polycaprolactone (PCL) with Sr-containing 45S5 BG to prepare composite scaffolds. They did not include 45S5 BG as reference material, so it was uncertain whether the final device benefitted from the substitution of Ca with Sr. Furthermore, Ren et al. (2014) reported the diameter of the fibers in the range of several tens of micrometers as a result of electrospinning of melt. It has been stated that fibers with smaller diameters (a few micrometers to hundreds of nanometers) are more favored for bone tissue engineering strategies due to their close similarity in size with bone tissue's collagen fibrils (Holzwarth and Ma, 2011); this outcome may be achieved through solution-electrospinning. Therefore, Santocildes-Romero et al. (2016) developed composite electrospun membranes made of a bioresorbable PCL and particles of Sr-substituted BG, which demonstrated osteogenic potential (Santocildes-Romero et al., 2015), and assessed their potential for bone tissue regeneration. The electrospun fibers exhibited porous surfaces and some regions of increased diameter where the particles were accumulated; interestingly, the Sr-doped BG particles were observed both inside and on the surface of the fibers (**Figure 6**). The glass dissolved after immersion in water, releasing alkaline ions that are related to increased pH. Further evidence suggested that pH changes is controlled or even reduced due to the accelerated polymer degradation, which offsets the pH variation after glass dissolution. All compositions were biocompatible *in vitro* after being tested with rat osteosarcoma cells, except for the membranes with more than 50 µg of glass on their surface (Santocildes-Romero et al., 2016).

In another novel research, Fernandes et al. (2016) fabricated a composite membrane by combining poly-L-lactic acid (PLLA) with 10 wt% Sr-doped borosilicate BG ($0.05Na_2O$–xMgO–yCaO– (0.35-x-y)SrO$-0.20B_2O_3-0.40SiO_2$ in molar ratio, where x, y = 0.35 or 0.00, and x ≠ y) using

electrospinning. Smooth and uniform fibers (1–3 μm in width) with a homogeneous distribution of Sr-doped BG microparticles (sizes < 45 μm) were obtained. Degradation studies, performed in phosphate buffered saline, revealed that the inclusion of Sr-doped BG particles into the PLLA membranes accelerated the degradability and enhanced the water uptake; furthermore, a continuous release of cations from the glass was observed. The addition of glass particles increased the mechanical properties of the membranes: specifically, Young's modulus and tensile strength increased by about 69 and 36 %, respectively. Additionally, cellular *in vitro* evaluation confirmed that the membranes enhanced the osteogenic differentiation of BMSCs as verified by increased ALP activity and up-regulated osteogenic gene expression (Alpl, Sp7, and Bglap) in comparison to PLLA alone. This study further suggests that such composites have great potential as effective biomaterials capable of promoting bone regeneration (Fernandes et al., 2016).

Coatings

One approach for solving the mechanical restrictions of BGs for load-bearing applications is to apply them as a coating on a mechanically strong and tough substrate. BG coatings for biomedical applications were the subject of many studies and have been comprehensively reviewed by Rawlings (1993), Niinomi (2010), Cao and Hench (1996), Verné (2012), Xuereb et al. (2015), Marghussian (2015), and Montazerian and Zanotto (2016). Many promising BGs including Sr-doped BGs have been studied to coat Ti, ZrO_2, Al_2O_3, stainless steel, and glass-ceramic implants. Many methods, such as enameling, sputtering, flame spraying, laser deposition, plasma spraying, and electrophoretic deposition (EPD), have been attempted for application of "perfect" coatings (Verné, 2012). Sr-containing glasses have also been utilized to develop coatings over implants. For example, Lotfibakhshaiesh et al. (2010) were interested in determining how SrO substitution for CaO (0, 10, 25, 50, 75, and 100%) affects sintering and crystallization of $49.96SiO_2-7.25MgO-3.30Na_2O-3.30K_2O-3.00ZnO-1.07P_2O_5-32.62CaO$ (mol%) glass (Gentleman et al., 2010) coating. Amorphous coatings on Ti-6Al-4V alloy produced by enameling showed good adhesion to the substrate except for the 100% Sr-substituted coating. Substituting Sr for Ca reduced the glass transition temperature and increased the onset temperature of crystallization. The mixed Ca/Sr glasses exhibited a larger sintering range (i.e., the temperature range between glass transition and crystallization), which favors glass processing without crystallization and obtaining amorphous well-sintered coatings. On the other hand, complete substitution led to crystallization and reduced the temperature range for sintering (Lotfibakhshaiesh et al., 2010). One of these resistant-to-crystallization glasses, having thermal expansion coefficient (TEC) similar to HA, was employed by Newman et al. (2014) for *in vivo* investigations, too. The coating was applied to roughened Ti-6Al-4V, and it produced no unfavorable tissue reaction following implantation into the distal femur and proximal tibia of twenty-seven New Zealand White rabbits for 6, 12, or 24 weeks. In this research, the glass dissolved over 6 weeks, stimulating enhanced peri-implant bone formation compared with HA-coated implants in the contralateral limb used as controls. Moreover, superior mechanical fixation was reported in the Sr-doped BG group after 24 weeks of implantation (Newman et al., 2014).

Miola et al. (2015) modified the original 45S5 BG composition by introducing 6 mol% of ZnO and/or SrO in place of CaO. SEM and XRD analyses proved that Zr and Sr addition did not significantly modify the glass structure while EDS analysis verified the presence of these elements in the glass composition. Sr-containing glasses were mixed with chitosan to synthesize organic-inorganic composite coatings on stainless steel (AISI 316L) by EPD. Tape and bending tests revealed a good coating-substrate adhesion for coatings made from Sr-doped 45S5 and Zn/Sr-codoped 45S5 glasses, whereas the adherence to the substrate decreased by using Zn-doped 45S5 glass. Microstructural analyses showed the composite character of coatings and indicated that the glass particles were well-embedded into the polymeric matrix, and the coatings were relatively uniform and crack-free. Although the bioactive behavior of the Sr-containing coating was confirmed after

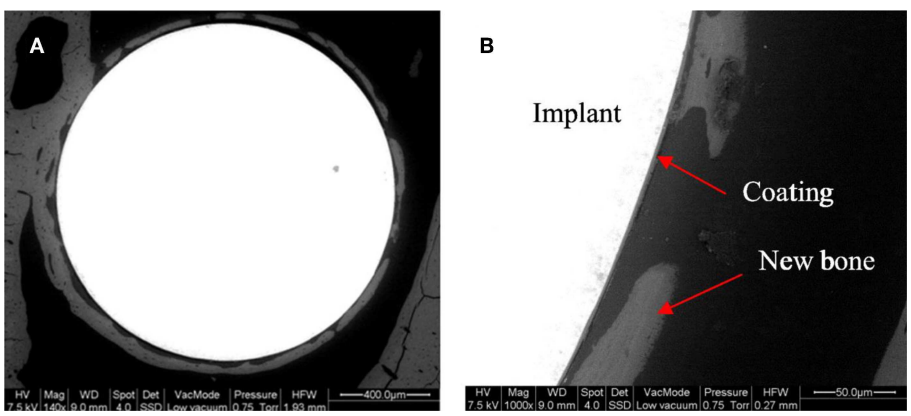

FIGURE 7 | Backscattering SEM images of a Sr-doped 45S5 glass coating after 4 weeks of implantation in the rat femur **(A)**. A detail of the different portions of the system is shown with arrows **(B)** [Adapted from Omar et al. (2015), after permission by Elsevier].

immersion in SBF, the coatings containing Zn exhibited no bioactivity.

Later, Omar et al. (2015) utilized another organic-inorganic composite coating to protect the stainless-steel implant and generate a barrier for metallic ion dissolution by using the potential of BG particles. The composite was made by a sol-gel method containing TEOS, methyl-triethoxysilane (MTES), colloidal silica nanoparticles, and 45S5 BG particles in which 2 mol% of CaO was substituted with SrO. The corrosion resistance and bioactivity of the stainless steel coated with this composite were evaluated *in vitro* and *in vivo* to analyze bone formation. The coating system provided outstanding protection against aggressive fluids. The formation of HA was observed after 30 days of immersion in SBF. *In vivo* tests in Wistar–Hokkaido rat femur after 4 or 8 weeks showed minor differences in the thickness of newly formed bone observed by SEM and noteworthy changes in bone quality. The *in vivo* reaction of the coatings containing Sr-doped BG was successful in the early stages of implantation regarding the bone morphology and quality (**Figure 7**) (Omar et al., 2015).

More recently, Molino et al. (2017) developed a hierarchical scaffold with a trabecular architecture mimicking that of cancellous bone via EPD of Sr-doped mesoporous BG (MBG) particles on the surface of sponge replicated strong but inert glass-ceramic scaffold. The spherical particles of mesoporous $SiO_2-CaO-SrO$ glass was synthesized by aerosol-assisted spray drying that, after being deposited on the glass-ceramic scaffold walls, stimulated a fast apatite-forming ability. Such a meso-macroporous hierarchical implant was suggested as a bioactive and mechanically strong implant for potential applications in bone tissue engineering.

Glass-Ceramics

It is known that bioactive GCs are designed for at least two main objectives: (i) improving the mechanical properties of glasses or (ii) benefiting from a particular characteristic of crystals (Montazerian and Zanotto, 2016). For example, needle-like apatite in many GCs improves mechanical properties, resembles the biological apatite in bone, and enhances the aesthetic features of dental GCs (Montazerian and Zanotto, 2017b). In this regard, the conversion of Sr-containing glasses into glass-ceramic in which different type of crystals, e.g., Sr-doped phases, are crystallized would have some beneficial effects. Therefore, (Topalović et al., 2017) have developed glass-ceramics in the $42P_2O_5-40CaO-5SrO-10Na_2O-3TiO_2$ (mol%) system through the sintering of melt-quenched glassy frits. They neither detected a phase containing Sr nor measured mechanical properties. However, they observed the formation of HA on the glass-ceramic surface immersion of the GCs for 21 days in SBF solution (Topalović et al., 2017). Dessou *et al.* have also reported no adverse influence on the bioactivity mechanism after increasing Sr content which leads to the formation of strontium silicate and Sr-doped diopside ($MgCaSi_2O_6$) in the thermally treated gel-derived BG powder discussed in section Sr-containing BGs: an overview (Dessou et al., 2017). We agree with them that the new glass-ceramic can be employed for the synthesis of Sr-containing/releasing scaffolds for bone tissue repair or engineering. Nevertheless, to examine the kinetics of Sr release and to provide insights into its beneficial effect on cell attachment, proliferation differentiation, and also mechanical properties, further work should be conducted.

Additionally, Kapoor et al. (2013) have studied the influence of SrO and ZnO co-dopants on thermo-mechanical behavior of alkali-free bioactive glass-ceramics of $(36.07\text{-}x)CaO–xSrO–(19.24\text{-}y)MgO–y\,ZnO-5.61P_2O_5-38.49SiO_2-0.59CaF_2$ ($x = 2–10$, $y = 2–10$) (mol%). They could sinter the glass powders before the onset of crystallization, leading to well-sintered and mechanically strong glasses/glass-ceramics after heat treating for 1 h at 800, 850, and 900°C. The crystalline phases of diopside and fluorapatite [$Ca_5(PO_4)_3F$] with partial replacement of Ca for Sr with increasing strontium contents were detected in the densified specimens (Kapoor et al., 2013). The substitution of SrO with CaO led to the partial replacement of Ca^{2+} by Sr^{2+} in the fluorapatite and diopside crystal structures. The maximum flexural strength of ∼150 MPa and Weibull modulus of ∼19 were recorded for the samples sintered at 850°C. In another research, Cai et al. (2011) have sintered Sr and Mg co-doped calcium phosphate gel-glasses to prepare GCs. XRD data revealed the presence of $Ca_4P_6O_{19}$ and β-$Ca_2P_2O_7$ for all heat-treated samples, and amorphous glass decreased with the increase of the heat treatment temperature. A fast release of Mg^{2+} ions from the residual glass was documented in the case of the glass-ceramics obtained by heat treatment at 700°C. This event supports the formation of amorphous apatite deposition. Although, the presence of Mg^{2+} ions in the solution resulted in a delay in the crystallization of apatite layer, and induced dissolution/precipitation dynamic processes on the glass-ceramic surface and an unstable surface that had a detrimental effect on cell attachment and proliferation during *in vitro* cell culture procedure. On the contrary, less glassy phase, and a stable apatite layer were observed in the samples heat-treated at 760 and 780°C, resulting in creating a proper surface for cell growth and differentiation. Sr element, preliminary existed in the glassy phase, was later detected in all the deposited apatite particles on sample surface immersed in SBF, indicating that the incorporated Sr was capable of substituting into the apatite nuclei and favoring its crystallization. It seems that the release of Sr^{2+} ions from glassy phase or Sr-doped crystals, e.g., $Ca_4P_6O_{19}$, in GCs offer an insight into the choice of a sintered Sr-containing GCs for the development of three-dimensional porous scaffolds for bone tissue engineering. However, further focus on the effect of these crystals on the biological and mechanical properties of GCs are required. **Table 3** summarizes different characteristics of Sr-doped or Sr-BGs containing materials described in section Bone cements.

THREE-DIMENSIONAL (3D) SCAFFOLDS

Sr-doped BGs have also been processed to acquire a porous structure at different size scales (from macro- to meso-range), thus obtaining tissue engineering 3D scaffolds allowing bone ingrowth and regeneration.

TABLE 3 | Physical, chemical, and biological properties of some Sr-doped or Sr-BGs containing materials described in section Bone cements.

Material type and composition	Physical properties*	Mechanical properties*	*In vitro* / *In vivo* properties	References
Sr-doped hydroxyapatite (HA)	Final setting time: 15–18 min Setting temperature: max. 58°C	Compressive strength: ~41 MPa Bending strength: ~31 MPa Elasticity modulus: ~1.5 GPa	Improving the osteoblast adhesion and mineralization *in vitro* and bone growth and osseointegration *in vivo*	Cheung et al., 2005; Ni et al., 2006
Sr-doped calcium phosphate-based cement (CPC)	Initial and final setting of 8–10 min and ~15 min, respectively	Compressive strength: ~12 MPa	Promoting cell proliferation and ALP activity of MG-63 cells cultured on the cement doped with Sr	Kuang et al., 2012
Series of ionomer cements containing SiO_2-ZnO–CaO–SrO based BGs	Working and setting time still have to be adjusted	Compressive strength: 39–75 MPa Flexural strength: 34–62 MPa	Have to be evaluated after optimizing physical and mechanical properties	Boyd et al., 2008; Wren et al., 2008, 2010, 2013; Clarkin et al., 2009
CPC containing $42SiO_2$-$4P_2O_5$-(39-x)CaO−$15Na_2O$–xSrO (in mol%, x=1.95, 3.90, 9.75, 19.5, 29.25, 39)	Final setting time: 20-40 min	Max. ompressive strength: 12.5 MPa	Forming *in vitro* Sr-doped HA	D'Onofrio et al., 2016
Chitosan-based cement containing $5.5Na_2O$−$7.34K_2O$−7.34MgO−20.18 CaO−$49.54B_2O_3$−$1.83P_2O_5$−8.27SrO in mol% borate BGs	Initial setting time: 12 min	Max. compressive strength of 19 MPa	Enhancing the proliferation and osteogenic differentiation of hBMSCs *in vitro* New bone in rat tibia after 8 weeks	Zhang et al., 2015
PMMA-based cement containing $6Na_2O$−$8K_2O$−8MgO−16CaO−6SrO −$27B_2O_3$−$27SiO_2$−$2P_2O_5$ (mol%) in mol% borosilicate BGs	Final setting time: 8–12 min	Max. compressive strength of 78–88 MPa Flexural strength: 50–60 MPa Elasticity modulus: ~2.5–2.7 GPa	Promoting the adhesion, migration, proliferation, and collagen secretion of MC3T3-E1 cells *in vitro* New bone formation in rat tibia after 8–12 weeks	Cui et al., 2017
PMMA-based cement (Spineple®) containing $40SiO_2$-$30Na_2O$−20SrO−10 CaO in mol% BGs	Setting time: 16–18 min Setting temperature: 50–75°C	Max. compressive strength of 75–100 MPa Elasticity modulus: ~2.5–2.7 GPa	–	O'Brien et al., 2010
PMMA-based cement (Spineple®) containing SiO_2-CaO–P_2O_5-SrO gel-derived BGs	Setting time: 16–20 min Setting temperature: ~34–45°C	Max. compressive strength: ~100 MPa Elasticity modulus: ~1.5–2.5 GPa	–	Goñi et al., 2018

** Minimum requirement set by ISO 5833 for polymeric cements:*
Max. peak temperature:: 908°C.
Setting times for operation in a surgical room 6–15 min.
Compressive strength > 70 MPa.
Flexural strength > 50 MPa.
Elasticity modulus > 1.8 GPa.

Sr-containing BG scaffolds were first prepared by two independent research groups from China Zhu et al. (2011) and Japan Wang et al. (2011) in 2011 by using MBGs as starting materials. Specifically, CaO-SrO-SiO_2-P_2O_5 MBG scaffolds were fabricated by the combination of polyurethane foam and block copolymer $EO_{20}PO_{70}EO_{20}$ (P123) as co-templates and evaporation-induced self-assembly (EISA) process, according to a strategy pioneered in 2007 by Li et al. (2007) for the production of macro-mesoporous hierarchical scaffolds. These Sr-doped MBG scaffolds exhibited an interconnected macroporous 3D network with a pore diameter in the range of 100 to 400 μm, which closely mimicked the trabecular architecture of cancellous bone and mesoporous walls with mesopore size of 4–5 nm. They showed no significant difference in terms of phase composition (being amorphous), macroporous structure, and textural characteristics compared to the Sr-free scaffolds used as a reference. The release of Sr^{2+} ions into the culture medium was reported to enhance the proliferation and ALP activity of mesenchymal stem cells (MSCs)(Wang et al., 2011) as well as the osteogenic expression of MC3T3-E1 osteoblast-like cells (Li et al., 2007).

Interestingly, the osteogenesis/cementogenesis-related gene expression of periodontal ligaments cells (harvested from human patients) was also observed to be stimulated by increasing concentrations of Sr released by MBG foams, thus suggesting the suitability of these materials for periodontal tissue engineering applications (Wu et al., 2012). This early *in vitro* evidence was further corroborated by the results from a study in an osteoporotic animal model of bilaterally ovariectomized rats (Zhang et al., 2014a). Specifically, Sr-doped MBG scaffolds were reported to significantly increase alveolar bone regeneration in the periodontium of osteoporotic rats at 1 month after surgery (bone formation: 46.67%) as compared to the Sr-free MBG group (39.33%) and unfilled controls (17.50%). Furthermore, osteoclasts were significantly reduced in defects receiving Sr-MBG scaffolds, as expected from the ability of Sr to halt bone resorption. Analogous results about the ability of Sr-doped MBG scaffolds to promote bone formation and reduce osteoclast activity were reported after implanting the graft in critical-size defects created in the femur of ovariectomized rats (osteopenic animal model) (Zhang et al., 2013; Wei et al., 2014).

Despite the attractive textural and biological properties, MBG foams produced by co-templating (polymeric sponge + EISA) often suffer from a major limitation, namely high brittleness (compressive strength about 50–250 kPa (Wu et al., 2010, 2011, 2013), which make them difficult to easily handle by surgeons and to easily apply in clinics. Therefore, other processing routes have been experimented to increase the mechanical properties of MBG scaffolds to more acceptable levels for bone repair applications. Zhang et al. (2014b) first reported the use of 3D printing to fabricate hierarchical Sr-doped MBG scaffolds by extruding and depositing filaments of glass powders bound together with poly(vinyl alcohol) gel according to a layer-wise approach (**Figure 8**). These scaffolds, retaining the mesoporous texture in the glass walls along with a grid-like macroporous structure, exhibited a compressive strength (8–9 MPa) that was about 170 times higher than that of sponge-templated MBGs, and an excellent apatite-forming ability in SBF. Furthermore, the fabricated samples could promote the proliferation and differentiation of osteoblastic cells *in vitro* and showed attractive properties for sustained drug release (model drug: dexamethasone) for use in local drug delivery therapy, due to their inherent mesoporous structure. After being implanted in critical-size calvarial defects of rats, these 3D-printed Sr-doped MBG scaffolds revealed superior osteoinductive properties and pro-angiogenic ability to enhance bone formation compared to Sr-free MBG controls (Zhao et al., 2015). On the other hand, major general drawbacks of 3D-printed MBG scaffolds compared to sponge-replicated ones include higher manufacturing cost and loss of the typical bone-like trabecular architecture, which is replaced by a more simplified grid-like array of micro-sized channels (Baino et al., 2016).

Instead of using sol-gel MBGs, Erol et al. (2012) fabricated macroporous SiO_2-CaO-P_2O_5-SrO glass scaffolds by sponge replication starting from melt-derived glass powder. These scaffolds were bioactive, as demonstrated by the formation of a surface HA layer after immersion in SBF, and able to act as vehicles for the local release of therapeutic Sr^{2+} ions. However, the kinetics of both apatite formation and Sr delivery were significantly lower and less finely controllable compared to Sr-doped MBGs, due to the absence of a mesoporous texture—and hence a lower specific surface area (Izquierdo-Barba and Vallet-Regí, 2015)—in melt-quenched materials. Furthermore, the compressive strength of these Sr-containing BG foams (0.1 MPa) was one order of magnitude lower than that of cancellous bone; some improvements (1.4 MPa) were obtained by the coating of the scaffold struts with gelatin, which performed a crack-bridging action. Özarslan and Yücel, 2016) produced Sr-doped glass scaffolds by the same method using rice hull ash as a sustainable source for SiO_2 and obtained analogous results to Erol et al. (2012).

Given its importance in the context of bone tissue engineering scaffolds, the bioactivity mechanism of Sr-containing melt-derived BGs was studied by Sriranganathan et al. in detail (Sriranganathan et al., 2016). It was observed that Ca replacement with Sr in the glass composition could retard the formation of a HA-like phase. It was proposed that the formation of apatite happens through an octa-calcium phosphate precursor phase, which subsequently transforms to HA. However, the equivalent octa-Sr phosphate does not exist, and hence, in the absence of Ca, apatite formation does not occur.

A few studies have recently dealt with the incorporation of Sr-doped BG particles in polymeric matrices to obtain composite scaffolds, such as electrospun polycaprolactone fibrous meshes (Ren et al., 2014), gelatin-based freeze-dried bone grafts (Jalise et al., 2018; Zhao et al., 2018), and acrylic gel (Zhang et al., 2017). In general, all these studies have emphasized the role of Sr-containing glass inclusions to impart osteogenic and angiogenic properties to the non-bioactive polymeric matrix. Early extrusion tests were also performed to produce composite scaffolds by 3D printing of type I collagen gel enriched with spray-dried SiO_2-CaO-SrO MBG submicronic spheres (Montalbano et al., 2018).

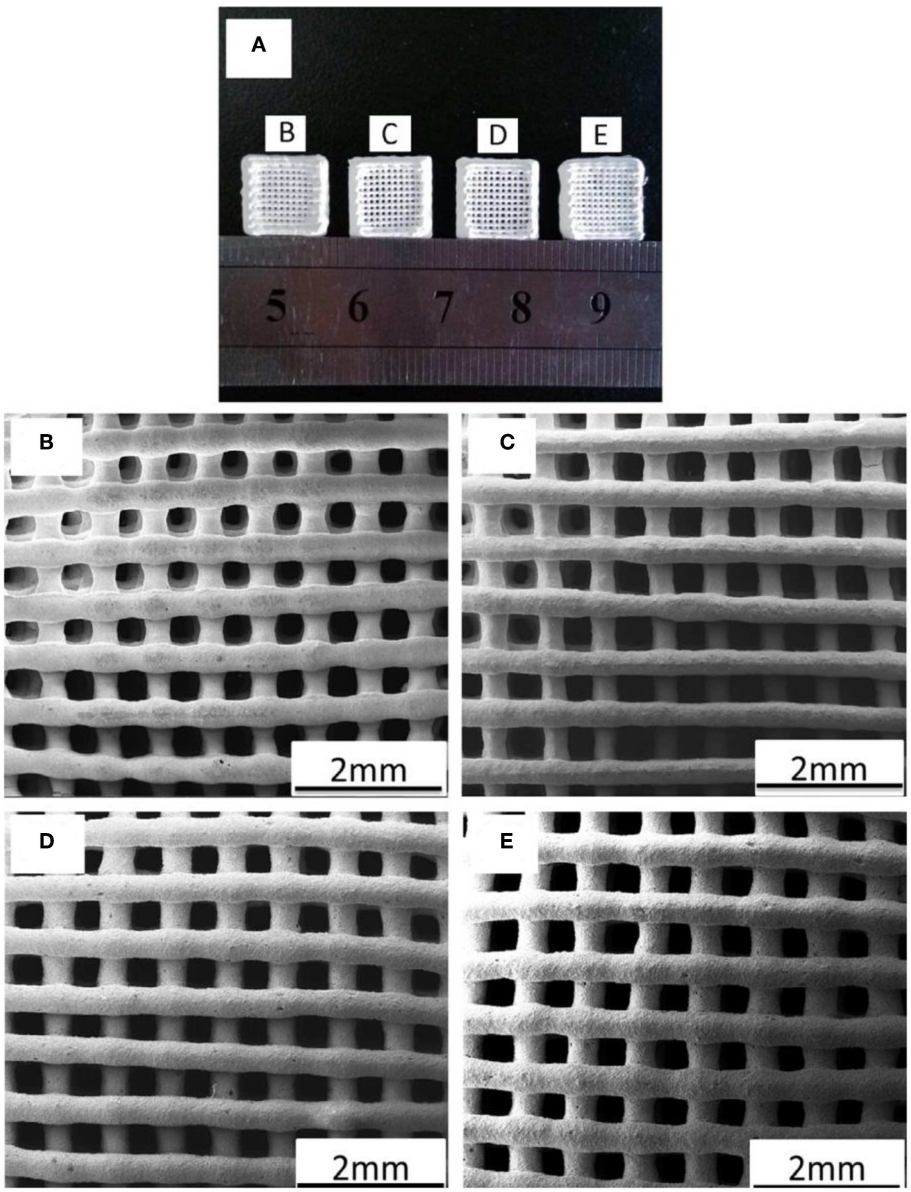

FIGURE 8 | 3D printing of Sr-doped MBGs: **(A)** photograph of 3D-printed scaffolds; SEM images of the MBG scaffolds doped with **(B)** 0 (control), **(C)** 5, **(D)** 10, and **(E)** 20 mol% of Sr. Images adapted from Zhang et al. (2014b).

In a very interesting study, Zhang et al. (2017) fabricated 3D-printed polycaprolactone/Sr-doped MBG composite scaffolds and tackled the ambitious challenge of finding a correlation between macroporous characteristics of the implant and biological response of bone cells. For this purpose, three batches of composite scaffolds were prepared in which the angles between the latitudes and longitudes of printed filaments were set to 45, 60 and 90°, and then the proliferation and ALP activity of MC3T3-E1 cells were tested to assess any difference due to macropore geometry. It was shown that the cell proliferation rate on the 45°-oriented scaffolds was slightly higher than that on the other types after 1 and 4 days, but there was a significant increase at 1 week. Furthermore, the 45°-oriented scaffolds were associated with a significant increase in ALP activity of cells compared to the other groups after 2 weeks. These early results, suggesting that an orientation of 45° among the scaffold struts could be more favorable to promote cell proliferation and osteogenic differentiation, represent an important step toward the development of optimal scaffold design and motivate further investigation on this topic.

Most of the available studies focus on Sr-doped silicate glasses, produced by either melting or sol-gel-like strategies (MBGs); however, Yin et al. (2018) recently reported the fabrication of sponge-templated scaffolds using melt-derived borosilicate

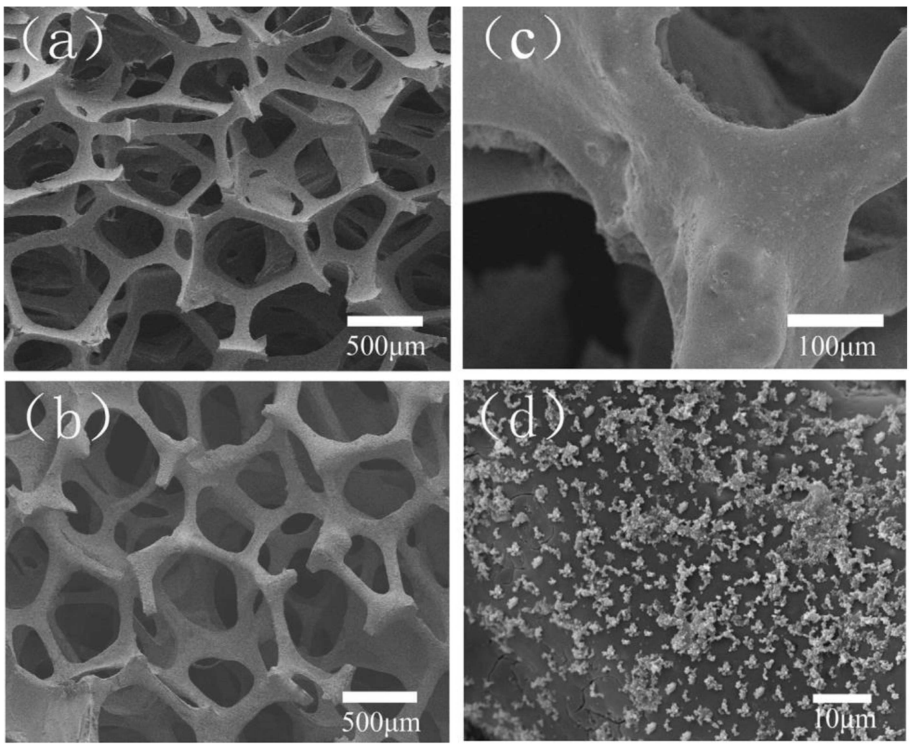

FIGURE 9 | Borosilicate 13-93B2 glass foam doped with 6 mol% of Sr: **(a)** polyurethane foam used as a template; **(b,c)** foam-replicated scaffold; **(d)** apatite agglomerates formed on the surface of the scaffold after immersion in SBF for 5 days. Images adapted from Yin et al. (2018) with permission.

glasses with high B_2O_3 content (13-93B2 basic composition ($18SiO_2$–$36B_2O_3$–$22CaO$–$6Na_2O$–$8K_2O$–$8MgO$–$2P_2O_5$ mol%) doped with 3, 6, and 9 mol% SrO). Borosilicate glasses are attractive for tissue engineering applications being characterized by higher reactivity with biological fluids—and hence faster apatite-forming kinetics—compared to silicate glasses, but high amounts of boron ions can be toxic to cells (Balasubramanian et al., 2018). It was reported that Sr-doped 13-93B2 glass scaffolds were bioactive and had suitable features for bone repair (bone-like trabecular structure, porosity 80 vol.%, pore size 200–500 μm, compressive strength 11 MPa) (**Figure 9**); moreover, very interestingly, the increase of Sr concentration in the glass formulation accelerated the release of silicate and Ca^{2+} ions, known for having a stimulatory effect on osteogenesis (Hench, 2009) and angiogenesis (Kargozar et al., 2018d), and significantly reduced the release of boron ions in some extent. Therefore, doping with particular proportions of SrO was suggested as a mean to decrease or even suppress the rapid release of boron, thus minimizing its cytotoxicity.

BIOLOGICAL FUNCTIONS OF STRONTIUM

Osteogenesis Induction

The main concept behind adding Sr to BG structure is related to its potential of improving the proliferation and the differentiation of pre-osteoblastic cells into osteoblasts via the activation of various cell signaling pathways such as Ras-mitogen-activated protein kinase (Ras/MAPK) (Peng et al., 2009). Sr can bond to the calcium-sensing receptor (CaRS) and, thereby, activates Ras/MAPK resulting in the up-regulation of genes involved in osteogenesis (e.g., Runx2) (Schindeler and Little, 2006). The activation of the NFATc1 signaling pathway is another mechanism by which Sr^{2+} ions can promote osteogenesis. This signaling pathway can up-regulate Wnt3A mRNA expression and trigger β-catenin dependent Wnt/β-catenin signaling pathway in MSCs (Yang et al., 2011). It has been previously shown that Wnt/β-catenin signaling plays an important role in bone development and homeostasis as well as regulation of the commitment of the differentiation of stem cells into osteoblastic lineages during fracture healing (Chen et al., 2007). Furthermore, Sr may activate the osteogenic differentiation of MSCs through the production of cyclo-oxygenase 2 (COX-2)-mediated prostaglandin E2 (PGE2) (Marie, 2007). Regarding the mentioned data, several researchers worldwide investigated the potential of Sr-containing glasses to accelerate bone repair and regeneration. As an illustration, Santocildes-Romero et al. prepared a series of 45S5 BGs in which Ca was partially (50%) or fully (100%) substituted by Sr (named as Sr50 and Sr100, respectively) and evaluated the osteogenic effects of the materials produced (Santocildes-Romero et al., 2015). The results of real-time PCR showed that the incubation of MSCs with 13.3 mg/mL of Sr50 and ≥6.7 mg/mL of Sr100 actually resulted in up-regulation of some specific bone-related genes like Alpl and OCN. In another study, Lao et al. using

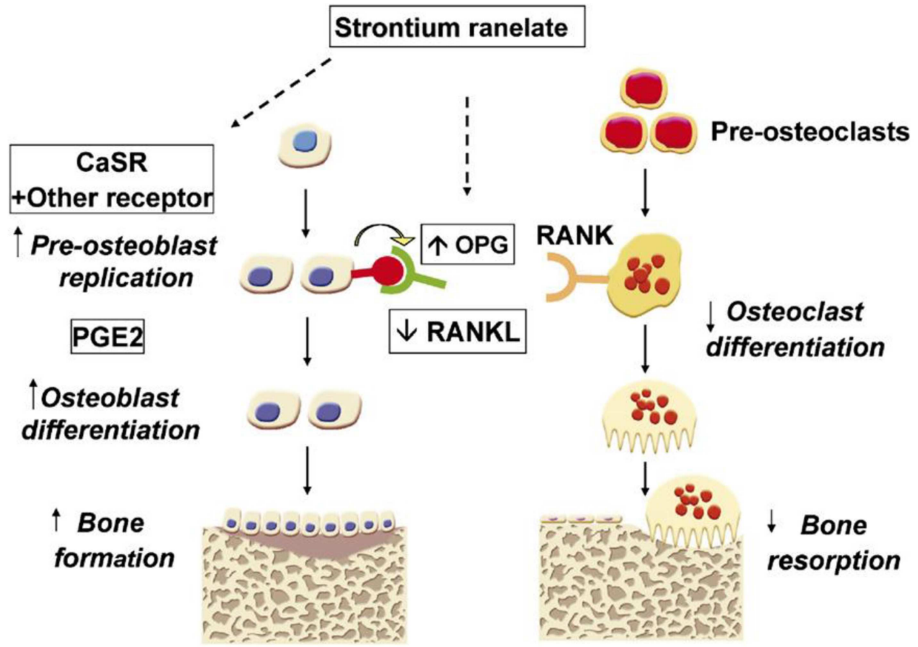

FIGURE 10 | The mechanisms proposed for the action of strontium ranelate (SrR) on the bone cells. SrR can stimulate bone formation through activating some well-known receptors such as the calcium-sensing receptor (CaSR) and increasing prostaglandin E2 (PE2) production by osteoblasts. In contrast, SrR can inhibit bone resorption via increasing osteoprotegerin and decreasing receptor activator of nuclear factor kappa B ligand (RANK) expression by osteoblasts. Adapted from Marie (2007) with permission.

particle-induced X-ray emission (PIXE) technique showed that biomineralization in the defect sites of the distal epiphysis of the femur of adult male New Zealand White rabbit implanted with 5 wt.% Sr-containing sol-gel BGs is significantly higher than Sr-free glasses (Lao et al., 2013). The authors concluded that this event could be correlated with the delivery of Sr^{2+} ions up to several ten microns around the implanted Sr-doped glass particles.

It is noteworthy that the osteogenic effect of Sr is dose-dependent (Verberckmoes et al., 2003). It has been shown that Sr at low concentrations (25–500 μM) promotes the osteogenic differentiation of cells, while it has an inverse effect on the differentiation at high concentrations (1,000–3,000 μM). In fact, Sr at higher doses induces apoptosis via the phosphorylation of ERK1/2 signaling molecules followed by the downregulation of Bcl-2 and increasing the phosphorylation of BAX (Aimaiti et al., 2017).

Osteoclastogenesis Inhibition

In addition to osteoblastogenesis, Sr plays a significant role in the osteoclastogenesis (see **Figure 10**). In fact, Sr is known to reduce osteoclast differentiation, activity, and bone resorption (Baron and Tsouderos, 2002).

Receptor activator of nuclear factor kappa-B ligand (RANKL) is a molecule with the ability to affect bone regeneration and remodeling. This molecule can bind to RANK on cells of the myeloid lineages (e.g., osteoclast precursor cells) and act as a major factor for improving the differentiation and activation of osteoclasts (Boyle et al., 2003). Strontium causes a reduced pre-osteoclast differentiation into osteoclasts via down-regulating the RANKL expression and also up-regulating its antagonist, i.e., osteoprotegerin (OPG), Saidak and Marie (2012). Moreover, it has been documented that Sr (as SrR formulation) at high concentrations can stimulate apoptosis in osteoclasts through the PKC βII pathway (Hurtel-Lemaire et al., 2009). With respect to this evidence, (Gentleman et al., 2010) evaluated the effects of Sr-substituted BGs on osteoblasts and osteoclasts *in vitro* (Gentleman et al., 2010). They developed a series of BGs based on $SiO_2-P_2O_5-Na2O-CaO$ formulation in which 0–100% of the CaO was substituted by SrO. Their results revealed that the release of Sr^{2+} ions from the glasses into cell culture medium enhances metabolic activity in osteoblasts, whereas the activity of osteoclasts inhibits (RAW264.7 monocytes). The last event is approved through the reduction of tartrate-resistant acid phosphatase activity and the inhibition of resorption of calcium phosphate films in a dose-dependent manner. The authors stated that the inhibition of osteoclast differentiation and disruption of cytoskeletal elements are the two main reasons by which the Sr-substituted glasses act.

Antibacterial Properties

The antibacterial effect of Sr has not been well-understood and is an open issue of research. Some researchers have reported that Sr has an inhibitory effect on various strains such as *Escherichia Coli* (E. coli) and *Porphyromonas gingivalis* (P. gingivalis) (Zhang et al., 2014c; Liu et al., 2016). For instance, Brauer et al. showed

that the bactericidal action of injectable bone cements based on BGs could be increased via Sr substitution (Brauer et al., 2012). They reported that the samples containing small amounts of Sr (2.5 mol%) reduce the number of bacteria *(Streptococcus faecalis)* up to one order of magnitude as compared to Sr-free samples. However, the concentrations above 0.16 mmol/L (14 ppm) exhibited no further bactericidal action. One of the mechanisms by which Sr elicits its antibacterial activity may be attributed to its potential to depress intracellular polysaccharide (IPS) accumulation in bacteria such as *Streptococcus mutans* (Wegman et al., 1984). It has been shown that IPS plays an important role in the persistence of bacteria in excess sugar environments (Busuioc et al., 2009). Another proposed mechanism for the antibacterial effect of Sr is related to its intervention to bacterial metabolism at concentrations above 180 mM since Sr^{2+} ions can act as a competitor to iron for specific binding sites in iron-sensing proteins (Brown et al., 2006). In contrast to the studies mentioned above, other scientists showed that the release of increased levels of Sr^{2+} has no positive effect on the bacteria inhibition (Dabsie et al., 2009; Li et al., 2016). On this matter, Dabsie et al. showed that Sr^{2+} ions have no significant antibacterial effect at the concentrations of 0.19, 0.37, 0.74, and 1.11 mol/L. However, they suggested that Sr^{2+} ions could have a synergistic effect with F^{-} ions in promoting the antibacterial activity.

In vitro Behavior of Sr-Containing Glasses

The biological properties of bivalent cation-doped BGs were reviewed in details elsewhere (Cacciotti, 2017). Regardless of the former oxides used for the design of the glass network, several studies demonstrated that the addition of Sr into the glass composition could promote osteoblast activity and inhibit osteoclasts *in vitro* (Gentleman et al., 2010). It was shown that Sr^{2+} concentrations ranging between 8.7 and 87.6 ppm could induce a positive response of osteoblastic phenotypes (Murphy et al., 2009). Enhanced ALP activity (Hesaraki et al., 2010a), together with higher mineralization (Kargozar et al., 2017) and production of ECM were also reported (Bonnelye et al., 2008; Gentleman et al., 2010; Hesaraki et al., 2010b; Bellucci and Cannillo, 2018). Some other studies pointed out the beneficial effects of Sr release on cellular attachment, proliferation (O'donnell et al., 2010) and differentiation (Isaac et al., 2011; Strobel et al., 2013; Santocildes-Romero et al., 2015; Stefanic et al., 2018).

It was reported that the substitution of Ca with Sr in the 45S5 glass composition led to an altered biological response *in vitro*, as a result of the modifications of the physical and chemical properties (density and solubility). Cellular metabolic activity was critically inhibited by totally replacing Ca with Sr, but a positive effect on mesenchymal stromal cells derived from rat bone marrow was observed in the glass with a molar SrO/CaO substitution of 50% (Santocildes-Romero et al., 2015).

In another study, *in vitro* experiments with osteosarcoma cells revealed that 5 mol% was the optimal Sr concentration in sol-gel BGs for stimulating bone cell production of ALP (Solgi et al., 2017).

The cytocompatibility of $CaO–SrO–Na_2O–ZnO–SiO_2$ glass systems was compared to that of commercial Novabone® (i.e., 45S5 Bioglass®), used as the control in order to evaluate their potential as synthetic bone grafts. Cell viability assays revealed no significantly increased cell viability when compared to commercial control. Sr^{2+} concentration was found to range between 0.8 and 38 ppm, actually in the active stimulatory range for biomedical applications. Interestingly, it was observed that the beneficial effect on cells was the result of a synergistic combination of the ions dissolved in the culture medium (Murphy et al., 2010), as enhanced proliferation was also observed with otherwise-inactive concentrations of Ca^{2+} and silicate ions only in Sr-doped systems, coherently with another previous study (Wu et al., 2007). Comparable results in terms of cellular proliferation were reported by Hesaraki et al., who observed that the inclusion of SrO within the glass network of silicophosphate glasses promoted cell proliferation and ALP activity depending on time (Hesaraki et al., 2010b).

Naruphontjirakul et al. recently investigated the response of MC3T3-E1 cells to BG nanoparticles (diameter 80-100 nm) doped with different SrO amounts (Naruphontjirakul et al., 2018). No negative effects on *in vitro* cell viability were observed with up to 250 μg/mL of glass, and the ionic dissolution products were non-toxic, regardless of the concentrations. However, concentrations of Sr-doped nanoparticles at or above 500 μg/mL led to cellular death after 3 days when the direct contact testing method was used (Naruphontjirakul et al., 2018). This study interestingly demonstrated that the concentration of glass nanoparticles is potentially able to affect both the mineralization mechanism and the synthesis of new extracellular matrix; enhanced protein expression (ALP, OSC, and OSP) and collagen production were also observed as Sr increased both in the nanoparticle composition and the dissolution products (Naruphontjirakul et al., 2018).

Cytotoxicity evaluation performed by Oudadesse et al. on both Sr-doped and Sr-free glasses revealed no differences related to the Sr addition within the network and its subsequent release in contact with the biological environment (Oudadesse et al., 2011). Inhibition of the pro-inflammatory response was also observed in direct contact testing mode by exposing murine macrophages to 1 mg/mL Sr-doped MBG particles, with a significant reduction of IL6 and IL1β expressions in MBG containing 2 mol% of Sr (Fiorilli et al., 2018).

In vivo Evaluations of Sr-Containing Glasses

The *in vivo* effects of Sr-doped biomaterials in bone formation and remodeling was exhaustively reported by Neves et al. (2017). The *in vivo* bone response to Sr-containing SiO_2-$CaO–Na_2O–P_2O_5$ glass particles was first reported by Gorustovich et al. in 2009 (Gorustovich et al., 2010). This study revealed no remarkable differences in terms of osteoconductivity with respect to the 45S5 glass control system. In fact, the amount of Sr detected at the interface did not alter the osteoconductive properties, and Sr was not found in the newly-formed bone tissue.

In the same year, Boyd et al. (2009) designed a bone graft with composition $28SrO–32ZnO–40SiO_2$ (mol%) and implanted it in a standard rat femur model using healthy Wistar rats. No

inflammatory response was detected, and the same material was then implanted into ovariectomized rats in order to evaluate the therapeutic potential in osteoporotic bone. The performance of the material was found to be almost the same both in healthy and osteoporotic bone, which was encouraging as a bone response to implants is usually diminished in ovariectomized rats and, therefore, suggested the great potential of such material in the treatment of osteoporosis.

Antioxidant properties and regenerative bone capacity were also investigated by Jebahi et al. *in vivo*. Sr-doped glasses were implanted in the femoral condyles of Wistar rats; experimental results showed a remarkable improvement in cell proliferation and antioxidant properties against reactive oxygen species (ROSs) due to three different mechanisms: (i) physiological bone remodeling enhanced by the ions released which supported cells to restore their physiological functionality and enhancement of osteoblastic activity, responsible for the production antioxidant species (GPx); (ii) Sr support in the elimination of oxidative radicals, thus protecting the surrounding tissue against damage; (iii) combined action of Sr and other ions released from the material which contributed to restore a balanced oxidative status (Jebahi et al., 2012).

Zhang et al. showed that Sr-incorporated MBGs scaffolds could stimulate *in vivo* regeneration of osteoporotic bone defects (Zhang et al., 2013). They implanted the scaffolds in critical-sized femur defects in ovariectomized rats and evaluated the bone regeneration process at time points 2, 4, and 8 weeks post-implantation. The results revealed an enhanced new bone formation in the animals treated with Sr-MBG scaffolds in comparison to those treated with MBG scaffolds alone (See **Figure 11**). The authors stated that Sr-MBG scaffolds could be a promising candidate for regenerating osteoporosis-related injuries. Moreover, O'Connell et al. (2017) observed a reduction in the inflammatory cell infiltration, but no significant differences in terms of neovascularization and fibrosis. These results indicate that Sr has no effects on the normal healing process, thus confirming the enormous potential of Sr-doped materials in biomedical applications such as bone augmentation. However, it is worth underlying that recent studies concern about cardiac safety of Sr, for example, in the form of SR used currently as a treatment for patients with osteoporosis (Donneau and Reginster, 2014; Reginster, 2014). Although the increased risk for cardiac events with SR was detected in randomized controlled trials (RCTs), the situation does not appear in real life, and Sr remains a beneficial therapeutic alternative in patients suffering severe osteoporosis without cardiovascular contraindications, who cannot receive another osteoporosis treatment.

CONCLUSIONS AND OUTLOOK

Using therapeutic elements released from implantable biomaterials to efficiently and locally treat various diseases is arising as one of the major challenges of modern bioengineering and regenerative medicine. Sr is known to be beneficial to patients who suffer from osteoporosis due to its capability of promoting osteoblast function and inhibiting osteoclast activity. Therefore, Sr incorporation in BGs may be a valuable strategy to deliver a steady supply of Sr^{2+} ions to osseous defect sites in the elderly. However, too much osteoclast inhibition may delay bone remodeling and, hence, tissue regeneration in osteoporotic patients. BG composition, amount of Sr incorporated and form of application (e.g., granules, injectable cements, porous scaffolds) are all key factors that dictate the release kinetics of Sr^{2+} ions and should be taken into account while developing

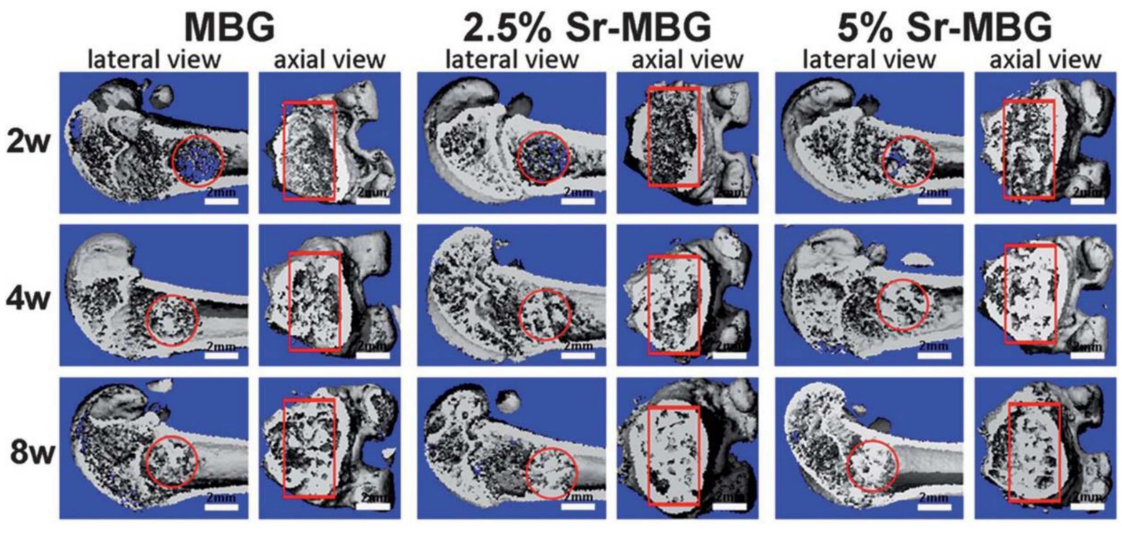

FIGURE 11 | Micro-CT images from implantation of MBGs doped with 2.5 and 5% Sr in the critical femoral defect of ovariectomized rats at two, four, and 8 weeks post-surgery. The red circle and rectangle show the boundary of the defected sites. As shown, a little new bone is present in the defects at 2 weeks, while abundant new bone is observed at the other time points (four and 8 weeks) which depicted visible difference among the groups. Scale bar 2 mm. Adapted from Zhang et al. (2013) with permission by The Royal Society.

potentially suitable biomaterials for the advanced treatment of osteoporosis.

To the best of the authors' knowledge, only one Sr-containing glass (melt-derived Stronbone^{TM}, $44.5SiO_2-4Na_2O-4K_2O-7.5MgO-17.8CaO-4.4P_2O_5-17.8SrO$ mol%) achieved the market as well as clinical applications in the form of particles and granules for dental applications (periodontal defect filler and toothpastes) (Hill and Stevens, 2009). More recently, it was shown that Sr could be easily incorporated in sol-gel systems, too. In this regard, MBGs might represent the future of Sr-doped glass-based biomaterials being able to allow the finely-controlled release of various therapeutic metallic elements (Kargozar et al., 2018a), including Sr. Compared to melt-derived glasses, these sol-gel materials potentially exhibit higher versatility in terms of ion release rate, which could ideally be tailored according to the needs of each patient, or clinical case.

Furthermore, there is early evidence suggesting the antibacterial potential of Sr^{2+} ions. The molecular mechanisms behind the antiseptic activity of Sr should still be well-elucidated, but this could open new horizons toward the development of multifunctional Sr-releasing BGs able to promote bone regeneration and prevent infections, thus significantly accelerating the healing of bone injuries.

AUTHOR CONTRIBUTIONS

SK, MM, EF, and FB: wrote the first draft. SK, MM, and FB: prepared the revisions.

ACKNOWLEDGMENTS

MM is grateful to the São Paulo Research Foundation (FAPESP) for the post-doctoral fellowship granted to him (# 2015/13314-9).

REFERENCES

Abou Neel, E. A., Chrzanowski, W., Pickup, D. M., O'Dell, L. A., Mordan, N. J., Newport, M. E., et al. (2009). Structure and properties of strontium-doped phosphate-based glasses. *J. Royal Soc. Interface* 6, 435–446. doi: 10.1098/rsif.2008.0348

Agarwal, S., Wendorff, J., H., and Greiner, A. (2008). Use of electrospinning technique for biomedical applications. *Polymer* 49, 5603–5621. doi: 10.1016/j.polymer.2008.09.014

Aimaiti, A., Maimaitiyiming, A., Boyong, X., Aji, K., Li, C., and Cui, L. (2017). Low-dose strontium stimulates osteogenesis but high-dose doses cause apoptosis in human adipose-derived stem cells via regulation of the ERK1/2 signaling pathway. *Stem Cell Res. Ther.* 8:282. doi: 10.1186/s13287-017-0726-8

Aina, V., Bergandi, L., Lusvardi, G., Malavasi, G., Imrie, F. E., Gibson, G., et al. (2013). Sr-containing hydroxyapatite: morphologies of HA crystals and bioactivity on osteoblast cells. *Mater. Sci. Eng.* 33, 1132–1142. doi: 10.1016/j.msec.2012.12.005

Baino, F. (2017). "Ceramics for bone replacement: commercial products, and clinical use," in *Advances in Ceramic Biomaterials,* eds P. Palmero, F. Cambier, and E. De Barra (Cambridge: Elsevier), 249–278. doi: 10.1016/B978-0-08-100881-2.00007-5

Baino, F., Fiorilli, S., and Vitale-Brovarone, C. (2016). Bioactive glass-based materials with hierarchical porosity for medical applications: review of recent advances. *Acta Biomater.* 42, 18–32. doi: 10.1016/j.actbio.2016.06.033

Baino, F., Fiume, E., Barberi, J., Kargozar, S., Marchi, J., Massera, J., et al. (2019). Processing methods for making porous bioactive glass-based scaffolds—A state-of-the-art review. *Int. J. Appl. Ceramic Technol.* doi: 10.1111/ijac.13195. [Epub ahead of print].

Baino, F., Fiume, E., Miola, M., and Verné, E. (2018). Bioactive sol-gel glasses: processing, properties, and applications. *Int. J. Appl. Ceramic Technol.* 15, 841–860. doi: 10.1111/ijac.12873

Baino, F., Hamzehlou, S., and Kargozar, S. (2018a). Bioactive glasses: where are we and where are we going? *J. Funct. Biomater.* 9:25. doi: 10.3390/jfb9010025

Balasubramanian, P., Buettner, T., Pacheco, V. M., and Boccaccini, A. R. (2018). Boron-containing bioactive glasses in bone and soft tissue engineering. *J. Eur. Ceramic Soc.* 38, 855–869. doi: 10.1016/j.jeurceramsoc.2017.11.001

Baron, R., and Tsouderos, Y. (2002). *In vitro* effects of S12911-2 on osteoclast function and bone marrow macrophage differentiation. *Eur. J. Pharmacol.* 450, 11–17. doi: 10.1016/S0014-2999(02)02040-X

Bauer, J., Carvalho, E. M., Carvalho, C. N., Meier, M. M., de Souza, J. P., de Carvalho, R. M., et al. (2016). Development of a simplified etch-and-rinse adhesive containing niobiophosphate bioactive glass. *Int. J. Adh. Adhes.* 69, 110–114. doi: 10.1016/j.ijadhadh.2016.03.015

Bellucci, D., and Cannillo, V. (2018). A novel bioactive glass containing strontium and magnesium with ultra-high crystallization temperature. *Mater. Lett.* 213, 67–70. doi: 10.1016/j.matlet.2017.11.020

Bellucci, D., Sola, A., Cacciotti, I., Bartoli, C., Gazzarri, M., Bianco, A., et al. (2014). Mg-and/or Sr-doped tricalcium phosphate/bioactive glass composites: Synthesis, microstructure and biological responsiveness. *Mater. Sci. Eng. C* 42, 312–324. doi: 10.1016/j.msec.2014.05.047

Bellucci, D., Sola, A., Salvatori, R., Anesi, A., Chiarini, L., and Cannillo, V. (2017). Role of magnesium oxide and strontium oxide as modifiers in silicate-based bioactive glasses: effects on thermal behaviour, mechanical properties and *in-vitro* bioactivity. *Mater. Sci. Eng. C* 72, 566–575. doi: 10.1016/j.msec.2016.11.110

Bhambri, S. K., and Gilbertson, L. N. (1995). Micromechanisms of fatigue crack initiation and propagation in bone cements. *J. Biomed. Mater. Res.* 29, 233–237. doi: 10.1002/jbm.820290214

Bohner, M. (2000). Calcium orthophosphates in medicine: from ceramics to calcium phosphate cements, *Injury* 31, D37–D47. doi: 10.1016/S0020-1383(00)80022-4

Bonnelye, E., Chabadel, A., Saltel, F., and Jurdic, P. (2008). Dual effect of strontium ranelate: stimulation of osteoblast differentiation and inhibition of osteoclast formation and resorption *in vitro*. *Bone* 42, 129–138. doi: 10.1016/j.bone.2007.08.043

Boyd, D., Carroll, G., Towler, M., Freeman, C., Farthing, P., and Brook, I. (2009). Preliminary investigation of novel bone graft substitutes based on strontium–calcium–zinc–silicate glasses. *J. Mater. Sci.* 20, 413–420. doi: 10.1007/s10856-008-3569-0

Boyd, D., Towler, M. R., Watts, S., Hill, R. G., Wren, A. W., and Clarkin, O. M. (2008). The role of Sr 2+ on the structure and reactivity of SrO–CaO–ZnO–SiO 2 ionomer glasses. *J. Mater. Sci.* 19, 953–957. doi: 10.1007/s10856-006-0060-7

Boyle, W. J., Simonet, W. S., and Lacey, D. L. (2003). Osteoclast differentiation and activation. *Nature* 423, 337–342. doi: 10.1038/nature01658

Brauer, D. S., Karpukhina, N., Kedia, G., Bhat, A., Law, R. V., Radecka, I., et al. (2012). Bactericidal strontium-releasing injectable bone cements based on bioactive glasses. *J. R. Soc. Interface* 10:rsif20120647. doi: 10.1098/rsif.2012.0647

Brow, R. K. (2000). The structure of simple phosphate glasses. *J. Non-Crystal. Solids* 263, 1–28. doi: 10.1016/S0022-3093(99)00620-1

Brown, S. D., Martin, M., Deshpande, S., Seal, S., Huang, K., Alm, E., et al. (2006). Cellular response of Shewanella oneidensis to strontium stress. *Appl. Environ. Microbiol.* 72, 890–900. doi: 10.1128/AEM.72.1.890-900.2006

Busuioc, M., Mackiewicz, K., Buttaro, B. A., and Piggot, P. J. (2009). Role of Intracellular Polysaccharide in Persistence of Streptococcus mutans. *J. Bacteriol.* 191, 7315–7322. doi: 10.1128/JB.00425-09

Cacciotti, I. (2017). Bivalent cationic ions doped bioactive glasses: the influence of magnesium, zinc, strontium and copper on the physical and biological properties. *J. Mater. Sci.* 52, 8812–8831. doi: 10.1007/s10853-017-1010-0

Cai, S., Li, J., Xu, G., Li, X., Ye, X., and Jiang, W. (2011). *In vitro* solubility and bioactivity of Sr and Mg co-doped calcium phosphate glass-ceramics derived from different heat-treatment temperatures. *Mater. Chem. Phys.* 131, 462–470. doi: 10.1016/j.matchemphys.2011.10.005

Cao, W., and Hench, L. L. (1996). Bioactive materials. *Ceram. Int.* 22, 493–507. doi: 10.1016/0272-8842(95)00126-3

Chen, Y., Whetstone, H. C., Lin, A. C., Nadesan, P., Wei, Q., Poon, R., et al. (2007). Beta-catenin signaling plays a disparate role in different phases of fracture repair: implications for therapy to improve bone healing. *PLoS Med.* 4:e249. doi: 10.1371/journal.pmed.0040249

Cheung, K. M., Lu, W. W., Luk, K. D., Wong, C. T., Chan, D., Shen, X., et al. (2005). Vertebroplasty by use of a strontium-containing bioactive bone cement. *Spine* 30, S84–S91. doi: 10.1097/01.brs.0000175183.57733.e5

Christie, J. K., and de Leeuw, N. H. (2017). Effect of strontium inclusion on the bioactivity of phosphate-based glasses. *J. Mater. Sci.* 52, 9014–9022. doi: 10.1007/s10853-017-1155-x

Clarkin, O., Boyd, D., Madigan, S., and Towler, M. (2009). Comparison of an experimental bone cement with a commercial control, Hydroset^{TM}. *J. Mater. Sci.* 20, 1563–1570. doi: 10.1007/s10856-009-3701-9

Clarkin, O., Boyd, D., and Towler, M. (2010). Strontium-based glass polyalkenoate cements for luting applications in the skeleton. *J. Biomater. Appl.* 24, 483–502. doi: 10.1177/0885328208099085

Cui, X., Huang, C., Zhang, M., Ruan, C., Peng, S., Li, L., et al. (2017). Enhanced osteointegration of poly (methylmethacrylate) bone cements by incorporating strontium-containing borate bioactive glass. *J. R. Soc. Interface* 14:20161057. doi: 10.1098/rsif.2016.1057

Dabsie, F., Gregoire, G., Sixou, M., and Sharrock, P. (2009). Does strontium play a role in the cariostatic activity of glass ionomer? strontium diffusion and antibacterial activity. *J. Dentistry* 37, 554–559. doi: 10.1016/j.jdent.2009.03.013

Demian, H. W., and McDermott, K. (1998). Regulatory perspective on characterization and testing of orthopedic bone cements. *Biomaterials* 19, 1607–1618. doi: 10.1016/S0142-9612(97)00122-1

Dessou, N., Theodorou, G., Kantiranis, N., Papadopoulou, L., Zorba, T., Patsiaoura, D., et al. (2017). Influence of strontium for calcium substitution on the glass–ceramic network and biomimetic behavior in the ternary system SiO 2–CaO–MgO. *J. Mater. Sci.* 52, 8871–8885. doi: 10.1007/s10853-017-0914-z

Donneau, A.-F., and Reginster, J.-Y. (2014). Cardiovascular safety of strontium ranelate: real-life assessment in clinical practice. *Osteoporos Int*. 25, 397–398. doi: 10.1007/s00198-013-2583-3

D'Onofrio, A., Kent, N., Shahdad, S., and Hill, R. (2016). Development of novel strontium containing bioactive glass based calcium phosphate cement. *Dental Mater.* 32, 703–712. doi: 10.1016/j.dental.2016.03.006

Du, J., and Xiang, Y. (2012). Effect of strontium substitution on the structure, ionic diffusion and dynamic properties of 45S5 bioactive glasses. *J. Non-Crystal. Solids* 358, 1059–1071. doi: 10.1016/j.jnoncrysol.2011.12.114

Du, J., and Xiang, Y. (2016). Investigating the structure–diffusion–bioactivity relationship of strontium containing bioactive glasses using molecular dynamics based computer simulations. *J. Non Crystalline Solids*. 432, 35–40. doi: 10.1016/j.jnoncrysol.2015.03.015

Erol, M., Özyuguran, A., Özarpat, Ö., and Küçükbayrak, S. (2012). 3D Composite scaffolds using strontium containing bioactive glasses. *J. Eur. Ceram. Soc.* 32, 2747–2755. doi: 10.1016/j.jeurceramsoc.2012.01.015

Fagerlund, S., Hupa, L. (2016). "Melt-derived bioactive silicate glasses," in *Bioactive Glasses*, eds A. R. Boccaccini, D. S. Brauer, and L. Hupa (Cambridge: Royal Society of Chemistry), 1–26.

Fernandes, J. S., Gentile, P., Martins, M., Neves, N. M., Miller, Crawford, A., et al. (2016). Reinforcement of poly-l-lactic acid electrospun membranes with strontium borosilicate bioactive glasses for bone tissue engineering. *Acta Biomater.* 44, 168–177. doi: 10.1016/j.actbio.2016.08.042

Fiorilli, S., Molino, G., Pontremoli, C., Iviglia, G., Torre, E., Cassinelli, C., et al. (2018). The incorporation of strontium to improve bone-regeneration ability of mesoporous bioactive glasses. *Materials* 11:E678. doi: 10.3390/ma11050678

Fiume, E., Barberi, J., Verné, E., and Baino, F. (2018). Bioactive glasses: from parent 45S5 composition to scaffold-assisted tissue-healing therapies. *J. Funct. Biomater.* 9:24. doi: 10.3390/jfb9010024

Fredholm, Y. C., Karpukhina, N., Brauer, D. S., Jones, J. R., Law, R. V., and Hill, R. G. (2011). Influence of strontium for calcium substitution in bioactive glasses on degradation, ion release and apatite formation. *J. R. Soc. Interface* 9, 880–889. doi: 10.1098/rsif.2011.0387

Fredholm, Y. C., Karpukhina, N., Law, R. V., and Hill, R. G. (2010). Strontium containing bioactive glasses: glass structure and physical properties. *J. Non-Cryst. Solids* 356, 2546–2551. doi: 10.1016/j.jnoncrysol.2010.06.078

Gentleman, E., Fredholm, Y. C., Jell, G., Lotfibakhshaiesh, N., O'Donnell, M. D., Hill, R. G., et al. (2010). The effects of strontium-substituted bioactive glasses on osteoblasts and osteoclasts in vitro. *Biomaterials* 31, 3949–3956. doi: 10.1016/j.biomaterials.2010.01.121

Goel, A., Rajagopal, R. R., and Ferreira, J. M. (2011). Influence of strontium on structure, sintering and biodegradation behaviour of CaO–MgO–SrO–SiO2–P2O5–CaF2 glasses. *Acta Biomater.* 7, 4071–4080. doi: 10.1016/j.actbio.2011.06.047

Goller, G., Demirkiran, H., Oktar, F., N., and Demirkesen, E. (2003). Processing and characterization of bioglass reinforced hydroxyapatite composites. *Ceram. Int.* 29, 721–724. doi: 10.1016/S0272-8842(02)00223-7

Goñi, I., Rodríguez, R., García-Arnáez, I., Parra, J., and Gurruchaga, M. (2018). Preparation and characterization of injectable PMMA-strontium-substituted bioactive glass bone cement composites. *J. Biomed. Mater. Res. B Appl. Biomater.* 106, 1245–1257. doi: 10.1002/jbm.b.33935

Gorustovich, A. A., Steimetz, T., Cabrini, R. L., and Porto López, J. M. (2010). Osteoconductivity of strontium-doped bioactive glass particles: A histomorphometric study in rats. *J. Biomed. Mat. Res. A* 92, 232–237. doi: 10.1002/jbm.a.32355

Hasan, M. S., Werner-Zwanziger, U., and Boyd, D. (2015). Composition-structure-properties relationship of strontium borate glasses for medical applications. *J. Biomed. Mater. Res. Part A*, 103, 2344–2354. doi: 10.1002/jbm.a.35361

He, F., and Tian, Y. (2018). Improvements in phase stability and densification of β-tricalcium phosphate bioceramics by strontium-containing phosphate-based glass additive. *Ceram. Int.* 44, 11622–11627. doi: 10.1016/j.ceramint.2018.03.236

Hench, L. L. (1991). Bioceramics: from concept to clinic. *J. Am. Ceram. Soc.* 74, 1487–510. doi: 10.1111/j.1151-2916.1991.tb07132.x

Hench, L. L. (2006). The story of bioglass®. *J. Mater. Sci.* 17, 967–978. doi: 10.1007/s10856-006-0432-z

Hench, L. L. (2009). Genetic design of bioactive glass. *J. Eur. Ceram. Soc.* 29, 1257–1265. doi: 10.1016/j.jeurceramsoc.2008.08.002

Hench, L. L. (2013). *An Introduction to Bioceramics, 2nd Edn.* (London: Imperial College Press).

Hench, L. L., and West, J. K. (1990). The sol-gel process. *Chem. Rev.* 90, 33–72. doi: 10.1021/cr00099a003

Hesaraki, S., Alizadeh, M., Nazarian, H., and Sharifi, D. (2010b). Physico-chemical and *in vitro* biological evaluation of strontium/calcium silicophosphate glass. *J. Mater. Sci.* 21, 695–705. doi: 10.1007/s10856-009-3920-0

Hesaraki, S., Gholami, M., Vazehrad, S., and Shahrabi, S. (2010a). The effect of Sr concentration on bioactivity and biocompatibility of sol–gel derived glasses based on CaO–SrO–SiO2–P2O5 quaternary system. *Mat. Sci. Eng.* 30, 383–390. doi: 10.1016/j.msec.2009.12.001

Hesaraki, S., Hasan Barounian, M., Farhangdoust, S., Khorami, M., Zamanian, A., and Borhan, S. (2012). Mechanical and *in vitro* biological properties of hydroxyapatite bioceramics reinforced with strontium-containing nano-bioactive glass. *Curr. Nanosci.* 8, 612–622. doi: 10.2174/157341312801784285

Hill, R., Stamboulis, A., Law, R., Clifford, A., Towler, M., and Crowley, C. (2004). The influence of strontium substitution in fluorapatite glasses and glass-ceramics. *J. Non Crystal. Solids* 336, 223–229. doi: 10.1016/j.jnoncrysol.2004.02.005

Hill, R. G., and Stevens, M. M. (2009). "Bioactive Glass." in *Google Patents*.

Hodges, R. M., MacDonald, N. S., Nusbaum, R., Stearns, R., Ezmirlian, F., Spain, P., et al. (1950). The strontium content of human bones. *J. Biol. Chem.* 185, 519–524.

Holzwarth, J. M., and Ma, P. X. (2011). Biomimetic nanofibrous scaffolds for bone tissue engineering. *Biomaterials* 32, 9622–9629. doi: 10.1016/j.biomaterials.2011.09.009

Hoppe, A., Güldal, N. S., and Boccaccini, A. R. (2011). A review of the biological response to ionic dissolution products from bioactive glasses and glass-ceramics. *Biomaterials* 32, 2757–2774. doi: 10.1016/j.biomaterials.2011.01.004

Hoppe, A., Sarker, B., Detsch, R., Hild, N., Mohn, D., Stark, W., et al. (2014). *In vitro* reactivity of Sr-containing bioactive glass (type 1393) nanoparticles. *J. Non Crystal. Solids* 387, 41–46. doi: 10.1016/j.jnoncrysol.2013.12.010

Huang, M., Hill, R., G., and Rawlinson, S., C. (2016). Strontium (Sr) elicits odontogenic differentiation of human dental pulp stem cells (hDPSCs): a therapeutic role for Sr in dentine repair? *Acta Biomater.* 38, 201–211. doi: 10.1016/j.actbio.2016.04.037

Hurtel-Lemaire, A. S., Mentaverri, R., Caudrillier, A., Cournarie, F., Wattel, A., Kamel, S., et al. (2009). The calcium-sensing receptor is involved in strontium ranelate-induced osteoclast apoptosis new insights into the associated signaling pathways. *J. Biol. Chem.* 284, 575–584. doi: 10.1074/jbc.M801668200

Isaac, J., Nohra, J., Lao, J., Jallot, E., Nedelec, J.-M., Berdal, A., et al. (2011). Effects of strontium-doped bioactive glass on the differentiation of cultured osteogenic cells. *Eur. Cell Mater.* 21, 130–43. doi: 10.22203/eCM.v021a11

Izquierdo-Barba, I., and Vallet-Regí, M. (2015). Mesoporous bioactive glasses: relevance of their porous structure compared to that of classical bioglasses. *Biomed. Glasses* 1, 140–150. doi: 10.1515/bglass-2015-0014

Jalise, S. Z., Baheiraei, N., and Bagheri, F. (2018). The effects of strontium incorporation on a novel gelatin/bioactive glass bone graft: *in vitro* and *in vivo* characterization. *Ceram. Int.* 44, 14217–14227. doi: 10.1016/j.ceramint.2018.05.025

Jebahi, S., Oudadesse, H., El Feki, H., Rebai, T., Keskes, H., Pellen, P., et al. (2012). Antioxidative/oxidative effects of strontium-doped bioactive glass as bone graft. *In vivo* assays in ovariectomised rats. *J. Appl. Biomed.* 10, 195–209. doi: 10.2478/v10136-012-0009-8

Jell, G., and Stevens, M. M. (2006). Gene activation by bioactive glasses. *J. Mater. Sci.* 17, 997–1002. doi: 10.1007/s10856-006-0435-9

Johari, B., Kadivar, M., Lak, S., Gholipourmalekabadi, M., Urbanska, A. M., Mozafari, M., et al. (2016). Osteoblast–seeded bioglass/gelatin nanocomposite: a promising bone substitute in critical-size calvarial defect repair in rat. *Int. J. Artif. Organs* 39, 524–533. doi: 10.5301/ijao.5000533

Jones, J. R. (2015). Reprint of: review of bioactive glass: from Hench to hybrids. *Acta Biomater.* 23, S53–82. doi: 10.1016/j.actbio.2015.07.019

Jones, J. R., Brauer, D. S., Hupa, L., and Greenspan, D. C. (2016). Bioglass and bioactive glasses and their impact on healthcare. *Int. J. Appl. Glass Sci.* 7, 423–434. doi: 10.1111/ijag.12252

Kamitakahara, M., Ohtsuki, C., and Miyazaki, T. (2008). Behavior of ceramic biomaterials derived from tricalcium phosphate in physiological condition. *J. Biomater. Applic.* 23, 197–212. doi: 10.1177/0885328208096798

Kapoor, S., Goel, A., Pascual, M. J., and Ferreira, J. M. (2013). Thermo-mechanical behaviour of alkali free bioactive glass-ceramics co-doped with strontium and zinc. *J. Non Crystall. Solids* 375, 74–82. doi: 10.1016/j.jnoncrysol.2013.05.007

Kapoor, S., Goel, A., Tilocca, A., Dhuna, V., Bhatia, G., Dhuna, K., et al. M. (2014). Role of glass structure in defining the chemical dissolution behavior, bioactivity and antioxidant properties of zinc and strontium co-doped alkali-free phosphosilicate glasses. *Acta Biomater.* 10, 3264–3278. doi: 10.1016/j.actbio.2014.03.033

Kargozar, S., Baino, F., Hamzehlou, S., Hill, R. G., and Mozafari, M. (2018b). Bioactive glasses entering the mainstream. *Drug Discov. Today*, 23, 1700–1704. doi: 10.1016/j.drudis.2018.05.027

Kargozar, S., Baino, F., Hamzehlou, S., Hill, R. G., and Mozafari, M. (2018d). Bioactive glasses: Sprouting angiogenesis in tissue engineering. *Trends Biotechnol.* 36, 430–444. doi: 10.1016/j.tibtech.2017.12.003

Kargozar, S., Hamzehlou, S., and Baino, F. (2019b). Can bioactive glasses be useful to accelerate the healing of epithelial tissues? *Mater. Sci. Eng. C* 97, 1009–1020. doi: 10.1016/j.msec.2019.01.028

Kargozar, S., Lotfibakhshaiesh, N., Ai, J., Mozafari, M., Milan, P., B., Hamzehlou, S., et al. (2017). Strontium-and cobalt-substituted bioactive glasses seeded with human umbilical cord perivascular cells to promote bone regeneration via enhanced osteogenic, and angiogenic activities. *Acta Biomater.* 58, 502–514. doi: 10.1016/j.actbio.2017.06.021

Kargozar, S., Lotfibakhshaiesh, N., Ai, J., Samadikuchaksaraie, A., Hill, R. G., Shah, P. A., et al. (2016). Synthesis, physico-chemical and biological characterization of strontium and cobalt substituted bioactive glasses for bone tissue engineering. *J. Non-Cryst. Solids* 449, 133–140. doi: 10.1016/j.jnoncrysol.2016.07.025

Kargozar, S., Montazerian, M., Hamzehlou, S., Kim, H.-W., and Baino, F. (2018a). Mesoporous bioactive glasses: Promising platforms for antibacterial strategies. *Acta Biomater.* 81, 1–19. doi: 10.1016/j.actbio.2018.09.052

Kargozar, S., and Mozafari, M. (2018). Nanotechnology and Nanomedicine: start small, think big. *Mater. Today 5* (7 *Part* 3), 15492–15500. doi: 10.1016/j.matpr.2018.04.155

Kargozar, S., Mozafari, M., Hamzehlou, S., and Baino, F. (2019c). Using bioactive glasses in the management of burns. *Front. Bioeng. Biotechnol.* 7:62. doi: 10.3389/fbioe.2019.00062

Kargozar, S., Mozafari, M., Hamzehlou, S., Brouki Milan, P.-H., Kim, W., and Baino, F. (2019d). Bone tissue engineering using human cells: a comprehensive review on recent trends, current prospects, and recommendations. *Appl. Sci.* 9:174. doi: 10.3390/app9010174

Kargozar, S., Mozafari, M., Hamzehlou, S.-H., Kim, W., and Baino, F. (2019a). Mesoporous bioactive glasses (MBGs) in cancer therapy: full of hope and promise. *Mater. Lett.* 251, 241–246. doi: 10.1016/j.matlet.2019.05.019

Kargozar, S., Mozafari, M., Hill, R. G., Brouki Milan, P., Taghi Joghataei, M., Hamzehlou, S., et al. (2018c). Synergistic combination of bioactive glasses and polymers for enhanced bone tissue regeneration. *Mater. Today 5 (7, Part* 3), 15532–15539. doi: 10.1016/j.matpr.2018.04.160

Kenny, S., and Buggy, M. (2003). Bone cements and fillers: a review. *J. Mater. Sci.* 14, 923–938. doi: 10.1023/A:1026394530192

Kent, N. W., Hill, R. G., and Karpukhina, N. (2016). A new way of forming a calcium phosphate cement using bioactive glasses as a reactive precursor. *Mater. Lett.* 162, 32–36. doi: 10.1016/j.matlet.2015.09.099

Kim, H.-W., Koh, Y.-H., Kong, Y.-M., Kang, J.-G., and Kim, H.-E. (2004). Strontium substituted calcium phosphate biphasic ceramics obtained by a powder precipitation method. *J. Mater. Sci.* 15, 1129–1134. doi: 10.1023/B:JMSM.0000046395.76435.60

Kuang, G. M., Yau, W., Lam, W., Wu, J., Chiu, K., Lu, W. W. et al. (2012). An effective approach by a chelate reaction in optimizing the setting process of strontium-incorporated calcium phosphate bone cement. *J. Biomed. Mater. Res. Part B.* 100, 778–787. doi: 10.1002/jbm.b.32511

Kuda, O., Pinchuk, N., Bykov, O., Tomila, T., Olifan, O., and Golovkova, M. (2018). Development and characterization of Sr-containing glass-ceramic composites based on biogenic hydroxyapatite. *Nanoscale Res. Lett.* 13l:155. doi: 10.1186/s11671-018-2550-1

Kumari, C. V., Sobhanachalam, P., Jayasankar, C. K., Veeraiah, N., and Kumar, V. R. (2017). Bioactive properties of CuO doped CaF2–CaO–B2O3–P2O5–MO(M=Ba, Sr, Zn, Mg) glasses. *Ceram. Int.* 43, 4335–4343. doi: 10.1016/j.ceramint.2016.12.078

Lao, J., Jallot, E., and Nedelec, J.-M. (2008). Strontium-delivering glasses with enhanced bioactivity: a new biomaterial for antiosteoporotic applications? *Chem. Mater.* 20, 4969–4973. doi: 10.1021/cm800993s

Lao, J., Lacroix, J., Nohra, J., Naaman, N., and Sautier, J. (2013). Bioavailability of strontium ions from bioactive glasses *in vivo*: a micro-PIXE study of trace elements at the bone interface. *Bioceram. Dev. Appl.* 1:1–3. doi: 10.4172/2090-5025.S1-004

Leite, A. J., Gonçalves, A. I., Rodrigues, M. T., Gomes, M. E., and Mano, J. F. (2018). Strontium-doped bioactive glass nanoparticles in osteogenic commitment. *ACS Appl. Mater. Interfaces* 10, 23311–23320. doi: 10.1021/acsami.8b06154

Li, X., Wang, X., Chen, H., Jiang, P., Dong, X., and Shi, J. (2007). Hierarchically porous bioactive glass scaffolds synthesized with a PUF and P123 cotemplated approach. *Chem. Mater.* 19, 4322–4326. doi: 10.1021/cm0708564

Li, Y., Coughlan, A., and Wren, A. W. (2014). Investigating the surface reactivity of SiO 2–TiO 2–CaO–Na 2 O/SrO bioceramics as a function of structure and incubation time in simulated body fluid. *J. Mater. Sci.* 25, 1853–1864. doi: 10.1007/s10856-014-5229-x

Li, Y., Placek, L., Coughlan, A., Laffir, F., Pradhan, D., Mellott, N., et al. (2015). Investigating the influence of Na+ and Sr 2+ on the structure and solubility of SiO 2–TiO 2–CaO–Na 2 O/SrO bioactive glass. *J. Mater. Sci.* 26:85. doi: 10.1007/s10856-015-5415-5

Li, Y., Stone, W., Schemitsch, E., H., Zalzal, P., Papini, M., Waldman, S. D., et al. (2016). Antibacterial and osteo-stimulatory effects of a borate-based glass series doped with strontium ions. *J. Biomater. Applicat.* 31, 674–683. doi: 10.1177/0885328216672088

Liu, J., Rawlinson, S. C., Hill, R. G., and Fortune, F. (2016). Strontium-substituted bioactive glasses *in vitro* osteogenic and antibacterial effects. *Dental Mater.* 32, 412–422. doi: 10.1016/j.dental.2015.12.013

Lotfibakhshaiesh, N., Brauer, D. S., and Hill, R. G. (2010). Bioactive glass engineered coatings for Ti6Al4V alloys: influence of strontium substitution for calcium on sintering behaviour. *J. Non Crystal. Solids* 356, 2583–2590. doi: 10.1016/j.jnoncrysol.2010.05.017

Mao, L., Xia, L., Chang, J., Liu, J., Jiang, L., Wu, C., et al. (2017). The synergistic effects of Sr and Si bioactive ions on osteogenesis, osteoclastogenesis and angiogenesis for osteoporotic bone regeneration. *Acta Biomater.* 61, 217–232. doi: 10.1016/j.actbio.2017.08.015

Marghussian, V. (2015). *Nano-Glass Ceramics: Processing, Properties and Applications* (Oxford: Elsevier).

Marie, P. J. (2007). Strontium ranelate: new insights into its dual mode of action. *Bone* 40, S5–S8. doi: 10.1016/j.bone.2007.02.003

Massera, J., Petit, L., Cardinal, T., J.-,Videau, J., Hupa, M., and Hupa, L. (2013). Thermal properties and surface reactivity in simulated body fluid of new strontium ion-containing phosphate glasses. *J. Mater. Sci.* 24, 1407–1416. doi: 10.1007/s10856-013-4910-9

Mendez, J., Fernández, M., Gonzalez-Corchon, A., Salvado, M., Collia, F., De Pedro, J., et al. (2004). Injectable self-curing bioactive acrylic-glass composites charged with specific anti-inflammatory/analgesic agent, *Biomaterials* 25, 2381–2392. doi: 10.1016/j.biomaterials.2003.09.004

Miola, M., Pakzad, Y., Banijamali, S., Kargozar, S., Vitale-Brovarone, C., Yazdanpanah, A., et al. (2019). Glass-ceramics for cancer treatment: So close, or yet so far? *Acta Biomater.* 83, 55–70. doi: 10.1016/j.actbio.2018.11.013

Miola, M., Verné, E., Ciraldo, F. E., Cordero-Arias, L., and Boccaccini, A. R. (2015). Electrophoretic deposition of chitosan/45S5 bioactive glass composite coatings doped with Zn and Sr. *Front. Bioeng. Biotechnol.* 3:159. doi: 10.3389/fbioe.2015.00159

Misra, S. K., Valappil, S. P., Roy, I., and Boccaccini, A., R. (2006). Polyhydroxyalkanoate (PHA)/inorganic phase composites for tissue engineering applications. *Biomacromolecules* 7, 2249–2258. doi: 10.1021/bm060317c

Molino, G., Bari, A., Baino, F., Fiorilli, S., and Vitale-Brovarone, C. (2017). Electrophoretic deposition of spray-dried Sr-containing mesoporous bioactive glass spheres on glass–ceramic scaffolds for bone tissue regeneration. *J. Mater. Sci.* 52, 9103–9114. doi: 10.1007/s10853-017-1026-5

Montalbano, G., Fiorilli, S., Caneschi, A., and Vitale-Brovarone, C. (2018). Type I collagen and strontium-containing mesoporous glass particles as hybrid material for 3D printing of bone-like materials. *Materials* 11:E700. doi: 10.3390/ma11050700

Montazerian, M., Yekta, B. E., Marghussian, V. K., Bellani, C. F., Siqueira, R, L., and Zanotto, E. D. (2015). Bioactivity and cell proliferation in radiopaque gel-derived CaO–P 2 O 5–SiO 2–ZrO 2 glass and glass–ceramic powders. *Mater. Sci. Eng.* 55, 436–447. doi: 10.1016/j.msec.2015.05.065

Montazerian, M., and Zanotto, D. (2016). History, and trends of bioactive glass-ceramics. *J. Biomed. Mater. Res. A* 104, 1231–1249. doi: 10.1002/jbm.a.35639

Montazerian, M., and Zanotto, E. D. (2016). Bioactive glass-ceramics: processing, properties and applications. *Bioactive Glasses* 27–33. doi: 10.1039/9781782622017-00027

Montazerian, M., and Zanotto, E. D. (2017a). A guided walk through Larry Hench's monumental discoveries. *J. Mater. Sci.* 52, 8695–8732. doi: 10.1007/s10853-017-0804-4

Montazerian, M., and Zanotto, E. D. (2017b). Bioactive and inert dental glass-ceramics. *J. Biomed. Mater. Res. A* 105, 619–639. doi: 10.1002/jbm.a.35923

Mozafari, M., Banijamali, S., Baino, F., Kargozar, S., and Hill, R. G. (2019). Calcium carbonate: adored and ignored in bioactivity assessment. *Acta Biomater.* 91, 35–47. doi: 10.1016/j.actbio.2019.04.039

Murphy, S., Boyd, D., Moane, S., and Bennett, M. (2009). The effect of composition on ion release from Ca–Sr–Na–Zn–Si glass bone grafts. *J. Mater. Sci.* 20, 2207. doi: 10.1007/s10856-009-3789-y

Murphy, S., Wren, A., Towler, M., and Boyd, D. (2010). The effect of ionic dissolution products of Ca–Sr–Na–Zn–Si bioactive glass on *in vitro* cytocompatibility. *J. Mater. Sci.* 21, 2827–2834. doi: 10.1007/s10856-010-4139-9

Naruphontjirakul, P., Porter, A. E., and Jones, J. R. (2018). *In vitro* osteogenesis by intracellular uptake of strontium containing bioactive glass nanoparticles. *Acta Biomater.* 66, 67–80. doi: 10.1016/j.actbio.2017.11.008

Neves, N., Linhares, D., Costa, G., Ribeiro, C., and Barbosa, M. (2017). *In vivo* and clinical application of strontium-enriched biomaterials for bone regeneration: a systematic review. *Bone Joint Res.* 6, 366–375. doi: 10.1302/2046-3758.66.BJR-2016-0311.R1

Newman, S. D., Lotfibakhshaiesh, N., O'Donnell, M., Walboomers, X., F., Horwood, N., Jansen, J. A., et al. (2014). Enhanced osseous implant fixation with strontium-substituted bioactive glass coating. *Tissue Eng. A* 20, 1850–1857. doi: 10.1089/ten.tea.2013.0304

Nezafati, N., Hesaraki, S., and Badr-Mohammadi, M.-R. (2014). Synthesis, characterization and *in vitro* evaluation of strontium-containing sol-gel derived bioactive glass/biphasic calcium phosphate nanocomposite. *Appl. Mech. Mater.* 467, 64–69. doi: 10.4028/www.scientific.net/AMM.467.64

Ni, G., Lu, W., Chiu, K., Li, Z., Fong, D., and Luk, K. (2006). Strontium-containing hydroxyapatite (Sr-HA) bioactive cement for primary hip replacement: an *in vivo* study. *J. Biomed. Mater. Res. Part B.* 77, 409–415. doi: 10.1002/jbm.b.30417

Niinomi, M. (2010). *Metals for Biomedical Devices* (Cambridge: Elsevier). doi: 10.1533/9781845699246

O'Brien, D., Boyd, D., Madigan, S., and Murphy, S. (2010). Evaluation of a novel radiopacifiying agent on the physical properties of surgical spineplex®. *J Mat Sci.* 21, 53–58. doi: 10.1007/s10856-009-3844-8

O'Connell, K., Pierlot, C., O'Shea, H., Beaudry, D., Chagnon, M., Assad, M., et al. (2017). Host responses to a strontium releasing high boron glass using a rabbit bilateral femoral defect model. *J. Biomed. Mater. Res. B* 105, 1818–1827. doi: 10.1002/jbm.b.33694

O'donnell, M., Candarlioglu, P., Miller, C., Gentleman, E., and Stevens, M. (2010). Materials characterisation and cytotoxic assessment of strontium-substituted bioactive glasses for bone regeneration. *J. Mater. Chem.* 20, 8934–8941. doi: 10.1039/c0jm01139h

O'donnell, M., and Hill, R. (2010). Influence of strontium and the importance of glass chemistry and structure when designing bioactive glasses for bone regeneration. *Acta Biomater.* 6, 2382–2385. doi: 10.1016/j.actbio.2010.01.006

O'Donnell, S., Cranney, A., Wells, G. A., Adachi, J., D., and Reginster, J., Y. (2006). Strontium ranelate for preventing and treating postmenopausal osteoporosis. *Cochr. Database Syst. Rev.* doi: 10.1002/14651858.CD005326.pub2

Omar, S., Repp, F., Desimone, P. M., Weinkamer, R., Wagermaier, W., Ceré, S., et al. (2015). Sol–gel hybrid coatings with strontium-doped 45S5 glass particles for enhancing the performance of stainless steel implants: electrochemical, bioactive and *in vivo* response. *J. Non Crystall. Solids* 425, 1–10. doi: 10.1016/j.jnoncrysol.2015.05.024

Oudadesse, H., Dietrich, E., Bui, X. V., Le Gal, Y., Pellen, P., and Cathelineau, G. (2011). Enhancement of cells proliferation and control of bioactivity of strontium doped glass. *Appl. Surf. Sci.* 257, 8587–8593. doi: 10.1016/j.apsusc.2011.05.022

Owens, G. J., Singh, R. K., Foroutan, F., Alqaysi, M., Han, C.-M., Mahapatra, C., et al. (2016). Sol–gel based materials for biomedical applications. *Progr. Mater. Sci.* 77, 1–79. doi: 10.1016/j.pmatsci.2015.12.001

Özarslan, A. C., and Yücel, S. (2016). Fabrication, and characterization of strontium incorporated 3-D bioactive glass scaffolds for bone tissue from biosilica. *Mater. Sci. Eng. C* 68, 350–357. doi: 10.1016/j.msec.2016.06.004

Pan, H., Zhao, X., Zhang, X., Zhang, K., Li, L., Li, Z., et al. (2009). Strontium borate glass: potential biomaterial for bone regeneration. *J. R. Soc. Interface 7:rsif* 20090504. doi: 10.1098/rsif.2009.0504

Patel, U., Moss, R., Hossain, K. M. Z., Kennedy, A. R., Barney, E. R., Hannon, A. C., et al. (2017). Structural and physico-chemical analysis of calcium/strontium substituted, near-invert phosphate based glasses for biomedical applications. *Acta Biomater.* 60, 109–127. doi: 10.1016/j.actbio.2017.07.002

Peng, S., Zhou, G., Luk, K. D., Cheung, K. M., Li, Z., Lam, Z., et al. (2009). Strontium promotes osteogenic differentiation of mesenchymal stem cells through the Ras/MAPK signaling pathway. *Cell. Physiol. Biochem.* 23, 165–174. doi: 10.1159/000204105

Pina, S., Torres, P., Goetz-Neunhoeffer, F., Neubauer, J., and Ferreira, J. (2010). Newly developed Sr-substituted α-TCP bone cements. *Acta Biomater.* 6, 928–935. doi: 10.1016/j.actbio.2009.09.001

Piotrowski, G., Hench, L., Allen, W., and Miller, G. (1975). Mechanical studies of the bone bioglass interfacial bond. *J. Biomed. Mater. Res.* 9, 47–61. doi: 10.1002/jbm.820090408

Rahaman, M. N., Day, D. E., Bal, B. S., Fu, Q., Jung, S. B., Bonewald, L. F., et al. (2011). Bioactive glass in tissue engineering. *Acta Biomater.* 7, 2355–2373. doi: 10.1016/j.actbio.2011.03.016

Rawlings, R. D. (1993). Bioactive glasses, and glass-ceramics. *Clin. Mater.* 14, 155–179. doi: 10.1016/0267-6605(93)90038-9

Reginster, J.-Y. (2014). Cardiac concerns associated with strontium ranelate. *Expert Opin. Drug Safety* 13, 1209–1213. doi: 10.1517/14740338.2014.939169

Ren, J., Blackwood, K. A., Doustgani, A., Poh, P. P., Steck, R., Stevens, M. M., et al. (2014). Melt-electrospun polycaprolactone strontium-substituted bioactive glass scaffolds for bone regeneration. *J. Biomed. Mater. Res. A* 102, 3140–3153. doi: 10.1002/jbm.a.34985

Rokidi, S., and Koutsoukos, P. G. (2012). Crystal growth of calcium phosphates from aqueous solutions in the presence of strontium. *Chem. Eng. Sci.* 77, 157–164. doi: 10.1016/j.ces.2012.02.049

Sabokbar, A., Fujikawa, Y., Murray, D. W., and Athanasou, N. A. (1997). Radio-opaque agents in bone cement increase bone resorption. *J. Bone Joint Surg.* 79, 129–134. doi: 10.1302/0301-620X.79B1.6966

Saidak, Z., and Marie, P. J. (2012). Strontium signaling: molecular mechanisms and therapeutic implications in osteoporosis. *Pharmacol. Ther.* 136, 216–226. doi: 10.1016/j.pharmthera.2012.07.009

Saint-Jean, S. J., Camire, C., Nevsten, P., Hansen, S., and Ginebra, M. (2005). Study of the reactivity and *in vitro* bioactivity of Sr-substituted α-TCP cements. *J. Mater. Sci.* 16, 993–1001. doi: 10.1007/s10856-005-4754-z

Santocildes-Romero, M. E., Crawford, A., Hatton, P., V., Goodchild, R. L., Reaney, I. M., and Miller, C. A. (2015). The osteogenic response of mesenchymal stromal cells to strontium-substituted bioactive glasses. *J. Tissue Eng. Regenerat. Med.* 9, 619–631. doi: 10.1002/term.2003

Santocildes-Romero, M. E., Goodchild, R. L., Hatton, P. V., Crawford, A., Reaney, I. M., and Miller, C. A. (2016). Preparation of composite electrospun membranes containing strontium-substituted bioactive glasses for bone tissue regeneration. *Macromol. Mater. Eng.* 301, 972–981. doi: 10.1002/mame.201600018

Schindeler, A., and Little, D. G. (2006). Ras-MAPK signaling in osteogenic differentiation: friend or foe? *J. Bone Min. Res.* 21, 1331–1338. doi: 10.1359/jbmr.060603

Schumacher, M., Lode, A., Helth, A., and Gelinsky, M. (2013). A novel strontium(II)-modified calcium phosphate bone cement stimulates human-bone-marrow-derived mesenchymal stem cell proliferation and osteogenic differentiation *in vitro*. *Acta Biomater.* 9, 9547–9557. doi: 10.1016/j.actbio.2013.07.027

Solgi, S., Khakbiz, M., Shahrezaee, M., Zamanian, A., Tahriri, M., Keshtkari, S., et al. (2017). Synthesis, characterization and *in vitro* biological evaluation of Sol-gel derived Sr-containing nano bioactive glass. *Silicon* 9, 535–542. doi: 10.1007/s12633-015-9291-x

Sriranganathan, D., Kanwal, N., Hing, K. A., and Hill, R. G. (2016). Strontium substituted bioactive glasses for tissue engineered scaffolds: the importance of octacalcium phosphate. *J. Mater. Sci.* 27:39. doi: 10.1007/s10856-015-5653-6

Stefanic, M., Peroglio, M., Stanciuc, A.-M., Machado, G., Campbell, I., KrŽmanc, M. M., et al. (2018). The influence of strontium release rate from bioactive phosphate glasses on osteogenic differentiation of human mesenchymal stem cells. *J. Eur. Ceram. Soc.* 38, 887–897. doi: 10.1016/j.jeurceramsoc.2017.08.005

Strobel, L., Hild, N., Mohn, D., Stark, W. J., Hoppe, A., Gbureck, U., et al. (2013). Novel strontium-doped bioactive glass nanoparticles enhance proliferation and osteogenic differentiation of human bone marrow stromal cells. *J. Nanoparticle Res.* 15:1780. doi: 10.1007/s11051-013-1780-5

Taherkhani, S., and Moztarzadeh, F. (2016). Influence of strontium on the structure and biological properties of sol–gel-derived mesoporous bioactive glass (MBG) powder. *J. Sol Gel Sci. Technol.* 78, 539–549. doi: 10.1007/s10971-016-3995-2

Tallia, F., Gallo, M., Pontiroli, L., Baino, F., Fiorilli, S., Onida, B., et al. (2014). Vitale-Brovarone: zirconia-containing radiopaque mesoporous bioactive glasses. *Mater. Lett.* 130, 281–284. doi: 10.1016/j.matlet.2014.05.062

Thormann, U., Ray, S., Sommer, U., ElKhassawna, T., Rehling, T., Hundgeburth, M., Henß, A., et al. (2013). Bone formation induced by strontium modified calcium phosphate cement in critical-size metaphyseal fracture defects in ovariectomized rats. *Biomaterials* 34, 8589–8598. doi: 10.1016/j.biomaterials.2013.07.036

Tilocca, A. (2010). Models of structure, dynamics and reactivity of bioglasses: a review. *J. Mater. Chem.* 20, 6848–6858. doi: 10.1039/c0jm01081b

Topalović, V. S., Grujić, S. R., Živanović, V. D., Matijašević, S. D., Nikolić, J. D., Stojanović, J. N., et al. (2017) Bioactive glass-ceramics prepared by powder sintering and crystallization of polyphosphate glass containing strontium. *Ceram. Int,* 43, 12061–12069. doi: 10.1016/j.ceramint.2017.06.061

Vaughan, J. M. (1975). *The Physiology of Bone.* Oxford University Press.

Verberckmoes, S. C., De Broe, M. E., and D'Haese, P. C. (2003). Dose-dependent effects of strontium on osteoblast function, and mineralization. *Kidney Int.* 64, 534–543. doi: 10.1046/j.1523-1755.2003.00123.x

Verné, E. (2012). "Bioactive glass, and glass-ceramic, coatings," in *Bio-Glasses: An Introduction,* eds J. R. Jones and A. G. Clare (West Sussex: John Wiley & Sons), 107–119. doi: 10.1002/9781118346457.ch8

Wang, J.-S., Diaz, J., Sabokbar, A., Athanasou, N., Kjellson, F., Tanner, K., et al. (2005). *In vitro* and *in vivo* biological responses to a novel radiopacifying agent for bone cement. *J. R. Soc. Interface* 2, 71–78. doi: 10.1098/rsif.2004.0009

Wang, X., Li, X., Ito, A., and Sogo, Y. (2011). Synthesis and characterization of hierarchically macroporous and mesoporous CaO–MO–SiO2–P2O5 (M= Mg, Zn, Sr) bioactive glass scaffolds. *Acta Biomater.* 7, 3638–3644. doi: 10.1016/j.actbio.2011.06.029

Wegman, M., Eisenberg, A., Curzon, M., and Handelman, S. (1984). Effects of fluoride, lithium, and strontium on intracellular polysaccharide accumulation in *S. mutans* and *A. viscosus*. *J. Dent. Res.* 63, 1126–1129. doi: 10.1177/00220345840630090601

Wei, L., Ke, J., Prasadam, I., Miron, R. J., Lin, S., Xiao, J., et al. (2014). A comparative study of Sr-incorporated mesoporous bioactive glass scaffolds for regeneration of osteopenic bone defects. *Osteop. Int.* 25, 2089–2096. doi: 10.1007/s00198-014-2735-0

Weiss, D., Torres, R., Buchner, S., Blunk, S., and Soares, P. (2014). Effect of Ti and Mg dopants on the mechanical properties, solubility, and bioactivity *in vitro* of a Sr-containing phosphate based glass. *J. Non-Crystal. Solids* 386, 34–38. doi: 10.1016/j.jnoncrysol.2013.11.036

Wren, A., Boyd, D., and Towler, M. (2008). The processing, mechanical properties and bioactivity of strontium based glass polyalkenoate cements. *J. Mater. Sci.* 19, 1737–1743. doi: 10.1007/s10856-007-3287-z

Wren, A., Coughlan, A., Hall, M., German, M., and Towler, M. (2013). Comparison of a SiO 2–CaO–ZnO–SrO glass polyalkenoate cement to commercial dental materials: ion release, biocompatibility and antibacterial properties. *J. Mater. Sci.* 24, 2255–2264. doi: 10.1007/s10856-013-4974-6

Wren, A., Cummins, N. M., Coughlan, A., and Towler, M. (2010). The effect of adding organic polymers on the handling properties, strengths and bioactivity of a Ca–Sr–Zn–Si glass polyalkenoate cement. *J. Mater. Sci.* 45, 3554–3562. doi: 10.1007/s10853-010-4398-3

Wright, A. C., Dalba, G., Rocca, F., and Vedishcheva, N. M. (2010). Borate versus silicate glasses: why are they so different? *Phys. Chem. Glasses-Eur. J. Glass Sci. Technol. Part B*, 51, 233–265.

Wu, C., Fan, W., Zhu, Y., Gelinsky, M., Chang, J., Cuniberti, G., et al. (2011). Multifunctional magnetic mesoporous bioactive glass scaffolds with a hierarchical pore structure. *Acta Biomater.* 7, 3563–3572. doi: 10.1016/j.actbio.2011.06.028

Wu, C., Ramaswamy, Y., Kwik, D., and Zreiqat, H. (2007). The effect of strontium incorporation into CaSiO3 ceramics on their physical and biological properties. *Biomaterials* 28, 3171–3181. doi: 10.1016/j.biomaterials.2007.04.002

Wu, C., Zhang, Y., Zhu, Y., Friis, T., and Xiao, Y. (2010). Structure–property relationships of silk-modified mesoporous bioglass scaffolds. *Biomaterials* 31, 3429–3438. doi: 10.1016/j.biomaterials.2010.01.061

Wu, C., Zhou, Y., Lin, C., Chang, J., and Xiao, Y. (2012). Strontium-containing mesoporous bioactive glass scaffolds with improved osteogenic/cementogenic differentiation of periodontal ligament cells for periodontal tissue engineering. *Acta Biomater.* 8, 3805–3815. doi: 10.1016/j.actbio.2012.06.023

Wu, C., Zhou, Y., Xu, M., Han, P., Chen, L., Chang, J., et al. (2013). Copper-containing mesoporous bioactive glass scaffolds with multifunctional

properties of angiogenesis capacity, osteostimulation and antibacterial activity. *Biomaterials* 34, 422–433. doi: 10.1016/j.biomaterials.2012.09.066

Xiang, Y., and Du, J. (2011). Effect of strontium substitution on the structure of 45S5 bioglasses. *Chem. Mater.* 23, 2703–2717. doi: 10.1021/cm102889q

Xiang, Y., Du, J., Skinner, L. B., Benmore, C. J., Wren, A. W., Boyd, D. J., et al. (2013). Structure and diffusion of ZnO–SrO–CaO–Na2O–SiO2 bioactive glasses: a combined high energy X-ray diffraction and molecular dynamics simulations study. *RSC Adv.* 3, 5966–5978. doi: 10.1039/c3ra23231j

Xuereb, M., Camilleri, J., and Attard, N., J. (2015). Systematic review of current dental implant coating materials and novel coating techniques. *Int. J. Prosthodont.* 28, 51–9. doi: 10.11607/ijp.4124

Yang, F., Yang, D., Tu, J., Zheng, Q., Cai, L., and Wang, L. (2011). Strontium enhances osteogenic differentiation of mesenchymal stem cells and *in vivo* bone formation by activating Wnt/catenin signaling. *Stem Cells* 29, 981–991. doi: 10.1002/stem.646

Yin, H., Yang, C., Gao, Y., Wang, C., Li, M., Guo, H., et al. (2018). Fabrication and characterization of strontium-doped borate-based bioactive glass scaffolds for bone tissue engineering. *J. Alloys Comp.* 743, 564–569. doi: 10.1016/j.jallcom.2018.01.099

Ylanen, H. O. (2011). Bioactive glasses: materials, properties, and applications. *Addit. Manufactur.* 24, 647–657.doi: 10.1533/9780857093318

Yu, T., Ye, J., and Wang, Y. (2009). Preparation and characterization of a novel strontium-containing calcium phosphate cement with the two-step hydration process. *Acta Biomater.* 5, 2717–2727. doi: 10.1016/j.actbio.2009.03.015

Zhang, J., Zhao, S., Zhu, Y., Huang, Y., Zhu, M., Tao, C., et al. (2014b). Three-dimensional printing of strontium-containing mesoporous bioactive glass scaffolds for bone regeneration. *Acta Biomater.* 10, 2269–2281. doi: 10.1016/j.actbio.2014.01.001

Zhang, L., Tan, P. Y., Chow, C. L., Lim, C. K., Tan, O. K., Tse, M. S., et al. (2014c). Antibacterial activities of mechanochemically synthesized perovskite strontium titanate ferrite metal oxide. *Colloids Surfaces A* 456, 169–175. doi: 10.1016/j.colsurfa.2014.05.032

Zhang, Q., Chen, X., Geng, S., Wei, L., Miron, R. J., Zhao, Y., et al. (2017). Nanogel-based scaffolds fabricated for bone regeneration with mesoporous bioactive glass and strontium: *in vitro* and *in vivo* characterization. *J. Biomed. Mat. Res. A* 105, 1175–1183. doi: 10.1002/jbm.a.35980

Zhang, W., Zhao, F., Huang, D., Fu, X., Li, X., and Chen, X. (2016). Strontium-substituted submicrometer bioactive glasses modulate macrophage responses for improved bone regeneration. *ACS Appl. Mater. Interfaces* 8, 30747–30758. doi: 10.1021/acsami.6b10378

Zhang, X., Lianghao, W., Dejian, L., Rongguang, A., Chen, F., Bin, Y., et al. (2017). Three-dimensional printing of strontium-containing mesoporous bioactive glass scaffolds with varied macropore morphologies: an *in vitro* cytological experiment. *Chin. J. Tissue Eng. Res.* 21, 2858–2863. doi: 10.3969/j.issn.2095-4344.2017.18.012

Zhang, Y., Cui, X., Zhao, S., Wang, H., Rahaman, M. N., Liu, Z., et al. (2015). Evaluation of injectable strontium-containing borate bioactive glass cement with enhanced osteogenic capacity in a critical-sized rabbit femoral condyle defect model. *ACS Appl. Mater. Interfaces* 7, 2393–2403. doi: 10.1021/am507008z

Zhang, Y., Wei, L., Chang, J., Miron, R. J., Shi, B., Yi, S., et al. (2013). Strontium-incorporated mesoporous bioactive glass scaffolds stimulating *in vitro* proliferation and differentiation of bone marrow stromal cells and in vivo regeneration of osteoporotic bone defects. *J. Mater. Chem. B* 1, 5711–5722. doi: 10.1039/C3TB21047B

Zhang, Y., Wei, L., Wu, C., and Miron, R. J. (2014a). Periodontal regeneration using strontium-loaded mesoporous bioactive glass scaffolds in osteoporotic rats. *PLoS ONE* 9:e104527. doi: 10.1371/journal.pone.0104527

Zhao, F., Lei, B., Li, X., Mo, Y., Wang, R., Chen, D., et al. (2018). Promoting *in vivo* early angiogenesis with sub-micrometer strontium-contained bioactive microspheres through modulating macrophage phenotypes. *Biomaterials* 178, 36–47. doi: 10.1016/j.biomaterials.2018.06.004

Zhao, S., Zhang, J., Zhu, M., Zhang, Y., Liu, Z., Tao, C., et al. (2015). Three-dimensional printed strontium-containing mesoporous bioactive glass scaffolds for repairing rat critical-sized calvarial defects. *Acta Biomater.* 12, 270–280. doi: 10.1016/j.actbio.2014.10.015

Zhu, Y., Li, X., Yang, J., Wang, S., Gao, H., and Hanagata, N. (2011). Composition–structure–property relationships of the CaO–M x O y–SiO 2–P 2 O 5 (M= Zr, Mg, Sr) mesoporous bioactive glass (MBG) scaffolds. *J. Mater. Chem.* 21, 9208–9218. doi: 10.1039/c1jm10838g

Conflict of Interest Statement: The authors declare that the research was conducted in the absence of any commercial or financial relationships that could be construed as a potential conflict of interest.

frontiers in Bioengineering and Biotechnology

REVIEW
published: 09 July 2019
doi: 10.3389/fbioe.2019.00164

3D and 4D Printing of Polymers for Tissue Engineering Applications

Dilara Goksu Tamay[1,2†], *Tugba Dursun Usal*[1,2,3†], *Ayse Selcen Alagoz*[1†], *Deniz Yucel*[1,4], *Nesrin Hasirci*[1,2,5,6] *and Vasif Hasirci*[1,2,3,7*]

[1] BIOMATEN, Center of Excellence in Biomaterials and Tissue Engineering, Middle East Technical University, Ankara, Turkey, [2] Department of Biotechnology, Middle East Technical University, Ankara, Turkey, [3] Department of Biological Sciences, Middle East Technical University, Ankara, Turkey, [4] Department of Histology and Embryology, School of Medicine, Acıbadem Mehmet Ali Aydinlar University, Istanbul, Turkey, [5] Department of Biomedical Engineering, Middle East Technical University, Ankara, Turkey, [6] Department of Chemistry, Middle East Technical University, Ankara, Turkey, [7] Department of Medical Engineering, School of Engineering, Acıbadem Mehmet Ali Aydinlar University, Istanbul, Turkey

Three-dimensional (3D) and Four-dimensional (4D) printing emerged as the next generation of fabrication techniques, spanning across various research areas, such as engineering, chemistry, biology, computer science, and materials science. Three-dimensional printing enables the fabrication of complex forms with high precision, through a layer-by-layer addition of different materials. Use of intelligent materials which change shape or color, produce an electrical current, become bioactive, or perform an intended function in response to an external stimulus, paves the way for the production of dynamic 3D structures, which is now called 4D printing. 3D and 4D printing techniques have great potential in the production of scaffolds to be applied in tissue engineering, especially in constructing patient specific scaffolds. Furthermore, physical and chemical guidance cues can be printed with these methods to improve the extent and rate of targeted tissue regeneration. This review presents a comprehensive survey of 3D and 4D printing methods, and the advantage of their use in tissue regeneration over other scaffold production approaches.

Keywords: 3D printing, 4D printing, tissue engineering, smart materials, bioprinting, bioinks, scaffold

OPEN ACCESS

Edited by:
Hasan Uludag,
University of Alberta, Canada

Reviewed by:
Justin Lee Brown,
Pennsylvania State University, United States
Eunsoo Yoo,
Texas A&M University, United States

***Correspondence:**
Vasif Hasirci
vasif.hasirci@acibadem.edu.tr

†These authors have contributed equally to this work

Specialty section:
This article was submitted to Biomaterials, a section of the journal Frontiers in Bioengineering and Biotechnology

Received: *12 February 2019*
Accepted: *21 June 2019*
Published: *09 July 2019*

Citation:
Tamay DG, Dursun Usal T, Alagoz AS, Yucel D, Hasirci N and Hasirci V (2019) 3D and 4D Printing of Polymers for Tissue Engineering Applications. Front. Bioeng. Biotechnol. 7:164. doi: 10.3389/fbioe.2019.00164

INTRODUCTION

Tissues are dynamic structures constituted by multiple cell types, an extracellular matrix (ECM) and a variety of signaling molecules. The extracellular matrix (ECM) is a crucial component of the cellular microenvironment and forms a complex three-dimensional network (Marchand et al., 2018). ECM, with various architectural forms and compositions in different tissues, is a complex 3D network consisting of mainly collagen and elastic fibers, which also contain proteoglycans, multiadhesive proteins (e.g., fibronectin, laminin), and glycosaminoglycans (e.g., hyaluronan). ECM structurally supports and helps the spatial organization of tissues and also serves as the site for cell anchorage. In addition, ECM is a dynamic system that transmits biochemical and mechanical signals from the microenvironment into the cells and affects cell behavior. The development of tissue specific scaffolds that possess the complex hierarchy of natural tissues remains deficient in tissue engineering applications. Three-dimensional printing (additive manufacturing) is achieved by adding materials layer by layer to form the final shape and is a valuable tool in the fabrication of biomimetic scaffolds with desired properties and well-controlled spatial chemistry and architecture. Three-dimensional printing mainly involves the use of 3D software to establish a model; the model

is imported into slicing software, and a 3D printer is used to print the model (Bhushan and Caspers, 2017). These 3D constructs, with microporous structures, can be produced through a computer controlled, layer-by-layer process. The conventional production of scaffolds in a sponge or mesh form are achieved by lyophilization, salt leaching, wet spinning and electrospinning. However, it is difficult to obtain pre-determined, well-defined architectures in a controlled manner using these techniques. In addition, cells are seeded onto these scaffolds after fabrication and may not penetrate the depths of the structure; therefore, cells may not be homogeneously distributed within the scaffold. Three-dimensional printing technology overcomes these limitations of conventional scaffold fabrication techniques. The main advantage of 3D printing is the production of patient-specific scaffolds. Four-dimensional printing is an emerging field in tissue engineering, where the scaffolds are fabricated using smart materials that enable the scaffolds to mimic the dynamic nature of tissues to a very large extent. Thus, besides having the advantages of 3D printing, such as the production of scaffolds with well-defined internal organization, 4D printing benefits from the property of smart materials to closely imitate the dynamic responses of tissues against natural stimuli. Four-dimensional printing is an invasive and robust technique that enables users to design the modeled simple shapes to transform to complex designs over time through a programming phase which is distinctly different than 3D printing (Rastogi and Kandasubramanian, 2019). The smart materials used to make the 4D scaffolds respond to a range of stimuli and adapt to the microenvironment by changing their conformation or other properties. The details of 3D and 4D scaffold preparation techniques and the types of stimuli they respond to are presented in this review.

3D PRINTING

Three-dimensional (3D) printing, also known as additive manufacturing or rapid prototyping, plays an important role in tissue engineering applications where the goal is to produce scaffolds to repair or replace damaged tissues and organs. Three-dimensional printing uses a bottom-up approach. Production is guided by a computer model which uses cross-sectional data obtained by slicing magnetic resonance (MR) or digital image of the defect area. Thus, production in a layer-by-layer fashion is possible using this technique, with high structural complexity, especially for patient-specific implants (Peltola et al., 2008). The main 3D printing categories that use solid polymers for product formation are; fused deposition modeling (FDM), selective laser sintering (SLS), and stereolithography (SLA). Bioprinting which uses polymeric hydrogels loaded with cells constitutes another category. The principles of these techniques are presented below.

3D Printing Techniques Using Polymers

Fused Deposition Modeling (FDM)

Fused deposition modeling (FDM) was developed and patented by Scott Crump in the late 1980s and is one of the most commonly used rapid prototyping techniques. This technology has been used in a broad range of applications including automotive, aerospace, model production for visualization, design verification, and biomedicine (Casavola et al., 2016). FDM is based on heating a thermoplastic polymer introduced to the device (in the form of a filament or powder), in the heating chamber, to a molten state which is then extruded through a nozzle onto the platform where it is deposited layer-by-layer in order to construct a 3D form. During the fabrication process, the position of the nozzle is controlled by a computer program and moves in x-y plane in order to create the desired pattern. Once a layer is completed, the nozzle moves upwards along the z-axis, a predefined distance to print the next layer. This process continues until the desired form is created (Xu et al., 2014). The components of FDM are shown in **Figure 1A**. The resolution of the details of the product is defined by the nozzle diameter, print speed, the angle and the distance between fibers of the subsequent layers, and the number of layers (Yuan et al., 2017).

The key advantage of FDM is the possibility of multiple extrusions with different materials. In the process, nozzles containing different thermoplastic materials are controlled by the system where they extrude sequentially, and the total form composed of the varied properties can be obtained. Other advantages of the FDM are simplicity, cost effectiveness and high speed (Wang et al., 2017). This method is solvent-free, therefore, an organic solvent (e.g., chloroform, acetone) which may be toxic or damaging for the cells is avoided (Thavornyutikarn et al., 2014). The disadvantage of the technique is the limited number of usable thermoplastic materials; as medical grade, biocompatible materials are not abundant. Additionally, it is difficult to find materials with the proper melt viscosity, which should be high enough to deposit and low enough to extrude (Chia and Wu, 2015).

Selective Laser Sintering (SLS)

Selective laser sintering (SLS) is an additive manufacturing (AM) technique which was developed and patented by Carl Deckard and Joe Beaman in 1989 (Deckard, 1989). In this technique, a laser beam is used as the energy source which melts a thin layer of powder material (ceramics, metals, and thermoplastic polymers) spread in the form of a powder bed. The beam heats the material and fuses them together to draw the 2D shape according to the computer program. After a layer is produced, the built platform moves down one-layer of thickness, and a new layer of powder is spread on the surface of the platform by a piston to sinter on the next layer. This process is repeated until the final structure is built (Mazzoli et al., 2015) (**Figure 1B**). After the fabrication is completed, excess powder is removed either by brushing or application of compressed air (Mazzoli, 2013).

SLS offers the advantage of fabricating large and complex scaffolds. Another advantage is that SLS does not require any support structures during the production process, since the sintered object is located in a solid powder bed and a sacrificial layer is not needed (Bai et al., 2015). SLS is a solvent-free fabrication method (like the FDM) thus the printed product does not have traces of the remaining solvent. The main disadvantage of SLS is that the product surface is not smooth and needs polishing because the product, and naturally its surface, is created

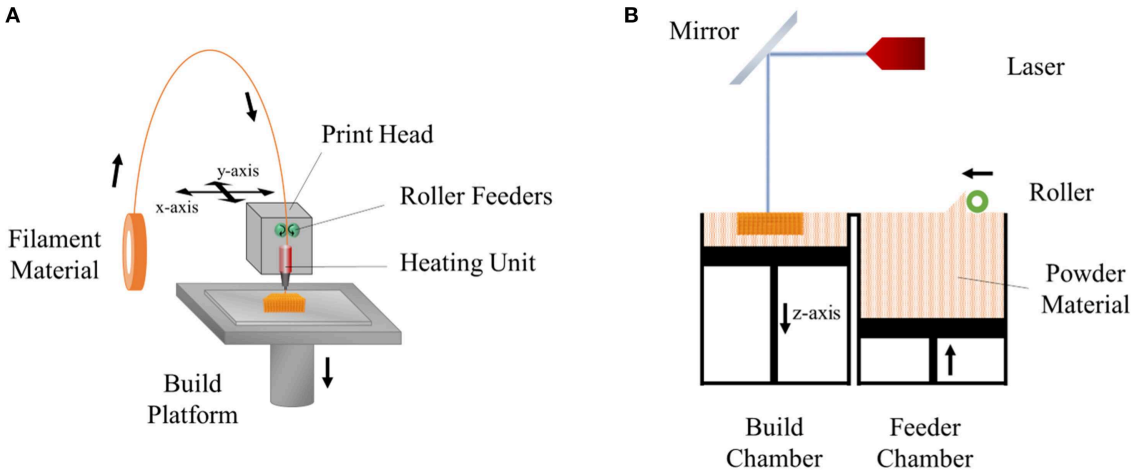

FIGURE 1 | Schemes of **(A)** fused deposition modeling (FDM) and **(B)** selective laser sintering (SLS) techniques.

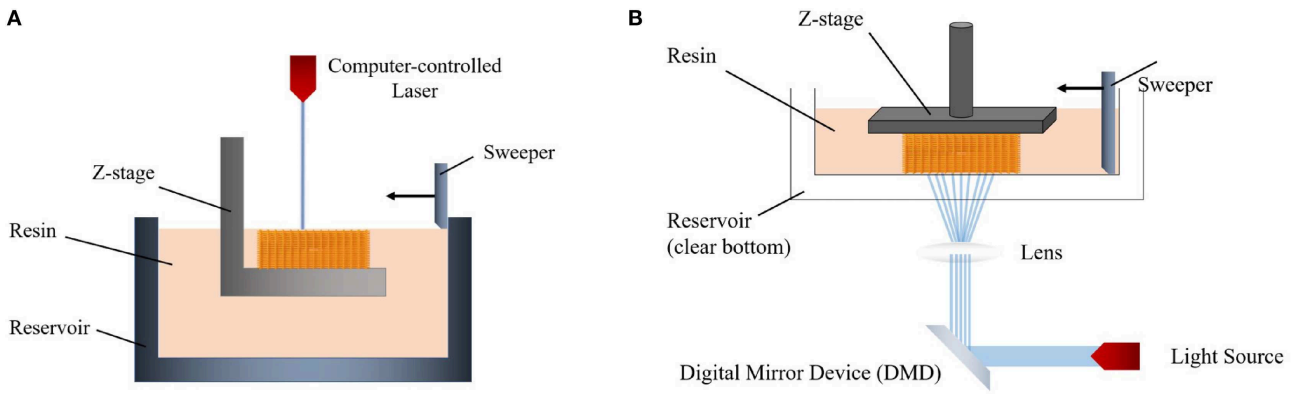

FIGURE 2 | Schemes of **(A)** laser-based stereolithography and **(B)** digital light projection (DLP) system.

by fusing spherical particles which introduce a certain degree of roughness (Mazzoli, 2013).

Stereolithography (SLA)

Stereolithography (SLA) is based on selective polymerization of a liquid, photosensitive resin by a light source, such as UV light or a laser (Mondschein et al., 2017). In the early 1980s, the first study on the fabrication of the 3D structure, through the photopolymerization of the liquid-based resin utilizing UV light, was achieved by Kodama, who developed two approaches, one utilizing a mask for each layer to do the exposure through, and the other using an optical fiber to cure the photopolymer selectively (Kodama, 1981). A predefined design was created by controlling the fiber movement along the x and y axes. Hull (1986) contributed to this by the addition of movement along the z-axis to produce 3D scaffolds in a layer-by-layer approach via UV light (Zorlutuna et al., 2013; Du, 2018).

In essence, stereolithography is a dynamic version of photolithography and uses a narrow beam of light to cure the polymer to produce the desired pattern, unlike photolithography which uses a static photomask to build a micropattern (Cha et al., 2014). In this system, light selectively polymerizes the resin according to a computer aided design (CAD) model. After the formation of the first layer, the platform is lowered, and a fresh resin material is added to polymerize and to create the second layer. It can also be achieved by moving the product in the z-direction after dipping into the liquid medium. Finally, uncrosslinked resin between the layers is washed, the construct is post-cured with UV in order to complete the polymerization reactions and increase the stability of the product (Melchels et al., 2010).

In order to cure the resin of the two different irradiation approaches, laser-based stereolithography and digital light projection (DLP) can be used. In the laser-based method, a laser beam which is controlled by a computer directly writes an object in a bottom-up way (**Figure 2A**) (Skoog et al., 2014). The required light intensity for printing is controlled by a digital micro-mirror device (DMD) which

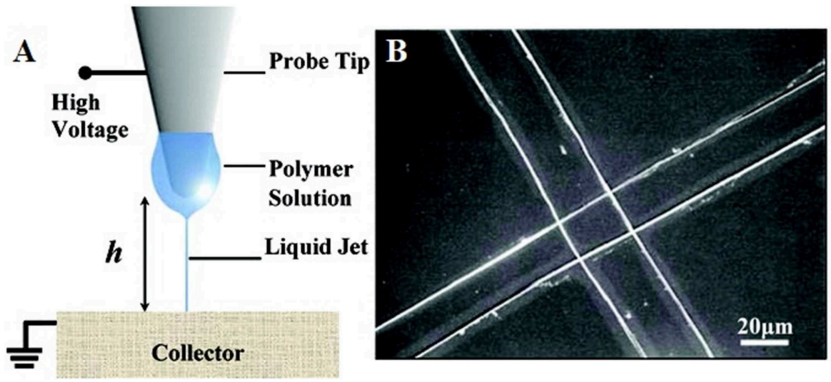

FIGURE 3 | (A) Schematic representation of NFES system and **(B)** perpendicular fibers deposited using the NFES system (adapted with permission from Sun et al., 2006. Copyright 2019 American Chemical Society).

TABLE 1 | Comparative analysis of traditional electrospinning (TES) and near-field electrospinning (NFES) (adapted with permission from He et al., 2017. Copyright 2019 American Chemical Society).

Method	Forms	Working distance (cm)	Voltage applied (kV)	Collector type	Fiber diameter (μm)	Advantages	Disadvantages
TES	Solution	5–50	10–30	Static	0.01–1	Device simplicity	Random fiber deposition
	Melt			Dynamic		Variety of usable materials	High voltage
						Large-scale production	
NFES	Solution	0.05–5	0.2–12	Static	0.05–30	Controlled fiber deposition	Immature mechanism
	Melt			Dynamic		Low voltage	Larger fiber diameter
						Precision in structures built	Small-scale production

uses microscale mirrors aligned in an array (**Figure 2B**). Each mirror can be rotated independently in this array to on-and-off states. Thus, only the desired area is exposed to light and polymerized (Lee et al., 2015).

SLA offers many advantages over the other techniques. First, each layer is printed at the same time when multiple objects are being printed, and total printing time is only based on the structure thickness. This significantly decreases printing time (Wang Z. et al., 2015). Also, external geometry and internal architecture of the scaffold can be precisely controlled by SLA due to a high resolution advantage of accuracy at 20 μm, due to the width of the light source being very small and highly controlled (Ji et al., 2018). Thus, the complex scaffold can be easily fabricated. The main disadvantage is that only a few biocompatible materials are available to be used in SLA to produce tissue engineering scaffolds (Colasante et al., 2016).

Near-Field Electrospinning (NFES)

Electrospinning (ES), a traditional scaffold production technique frequently adopted in tissue engineering applications, is based on the uniaxial elongation of a viscoelastic jet of a polymer solution or melt under high voltage (Li and Xia, 2004). Although it is an advantageous method of building micro and nano fibers and structures due to its simplicity, efficiency, and variety in applicable materials and fields, it lacks the precision that some areas, such as microelectromechanical systems (MEMS) and tissue engineering require. Near-field electrospinning (NFES), introduced first by Sun et al. (2006), applies the same principle as traditional electrospinning (TES) but with low voltage and reduced working distance to achieve controlled deposition of fibers and precision in the spun structures (**Figure 3**). With the reduced working distance, bending instability that arises in TES is significantly restrained, so that the fibers can be deposited as straight lines rather than randomized chaotic patterns. The collector, unlike in TES, is placed on a platform that moves along the x and y-axes, and this movement is precisely controlled by a computer program that enables laying fibers down in a predetermined path to obtain a desired pattern or shape in 2D, or 3D by depositing fibers layer by layer. Similar to TES, NFES also work with polymer solutions and melts. **Table 1** summarizes the differences between TES and NFES.

NFES has some trade-offs between the controllability of fibers and the morphology of the structure (He et al., 2017). The shortened distance between the tip and the collector enables accurate fiber deposition while limiting the stretching and thinning of fibers, resulting in fiber diameters larger than those observed in TES. Some research shows that this issue can be improved by introducing minor modifications in solution concentrations, spinning voltage and distance, and collector speed. Also, in contrast to TES where the polymer solution can be deposited continuously from a syringe pump, NFES requires dipping of a probe tip intermittently into the polymer solution, which hinders the continuous large-scale production of micro and nano fibers.

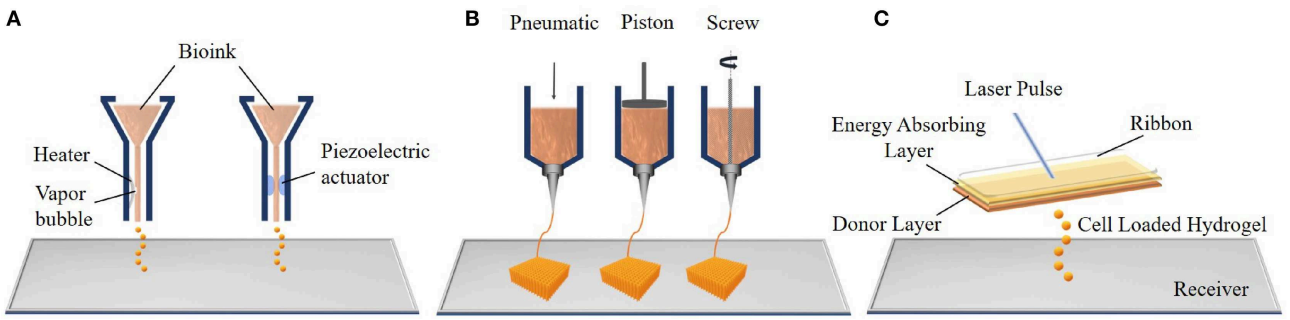

FIGURE 4 | Components of the three main bioprinting techniques: **(A)** inkjet bioprinting, **(B)** extrusion bioprinting, and **(C)** laser assisted bioprinting (LAB).

Bioprinting

Bioprinting is another 3D fabrication technique which prints complex tissue constructs using hydrogels that are loaded with cells to print. This technology has the potential to generate a variety of transplantable soft tissues, including skin, bone and cartilage (Mandrycky et al., 2016). Bioprinting has three major process approaches: inkjet, extrusion, and laser-assisted bioprinting (**Figure 4**) which are described below.

Inkjet Bioprinting

The Inkjet was the first bioprinting technology of additive manufacturing and was developed by the Hewlett-Packard Company in the 1970s as a 2D printing method. Then, an elevator platform which can move along the z-axis and a chamber were added to this system in 1992 and a 3D bioprinting system was developed (Huang et al., 2017). Thermal and piezoelectric inkjet bioprinters are more frequently used for tissue engineering applications. In thermal inkjet bioprinting, a prepolymer solution which can contain cells, known as the bioink, is loaded in an ink cartridge. The cartridge is placed in the printer head which is controlled by a computer and small droplets of ink are ejected by the help of small air bubbles created by heat in the printing head. The size of droplets can be changed with ink viscosity, the frequency of the current pulse and the gradient of applied temperature (Cui et al., 2012). The working principle of the piezoelectric inkjet bioprinter is based on applying different potentials to the piezoelectric crystal in the bioprinter, and this generates the pressure needed to eject the bioink droplets from the nozzle. The major advantages of inkjet bioprinting are its fast fabrication and the affordability of the device (Murphy and Atala, 2014).

Extrusion Bioprinting

Extrusion bioprinting, an advanced version of inkjet bioprinting, dispenses bioink using pneumatic (air pressure) or mechanical (screw or piston) systems. In the pneumatic system, bioink is extruded from the nozzle or needle as an uninterrupted cylindrical filament by applying continuous air pressure instead of single droplets. This provides high structural integrity to the product (Knowlton et al., 2018). The mechanical system enables a more direct control over the flow of bioink because of the screw extruding the material. Extrusion bioprinting can print tissues using a variety of bioinks, such as cell-carrying hydrogels, micro-carriers and cell aggregates (Ozbolat and Hospodiuk, 2016). However, the cells are subjected to high mechanical stresses during extrusion which may decrease the cell viability (Mandrycky et al., 2016). In addition, the main problems of both inkjet and extrusion bioprinting are clogging of the nozzle due to cell aggregation, high viscosity of the ink or drying of the injected material within the nozzle.

Laser-Assisted Bioprinting (LAB)

Laser-assisted bioprinting (LAB) is another bioprinting system which consists of a pulsed laser source, a donor layer, and a receiving substrate. The principle of LAB is that, bioink is placed below a ribbon which also contains a thin, energy absorbing layer. The ribbon is placed parallel to the receiver. The pulsed laser source is focused on the laser absorbing-layer and this generates a vapor bubble. This bubble creates a pressure to deform the bioink and forms droplets. These cell loaded hydrogel droplets are propelled toward the receiver where they are collected and crosslinked (Gruene et al., 2011). LAB offers certain advantages including not clogging due to the absence of a nozzle and not causing any mechanical stress on the cells because of its non-contact printing approach. All of these increase the cell viability. However, the LAB system is more expensive compared to other bioprinters (Mandrycky et al., 2016).

Materials Used in 3D Printing

A variety of biomaterials are used in additive manufacturing to form the desired, complex-shaped products with different sizes and stiffness. Polymeric materials are generally preferred because of their easy processability, biodegradability, biocompatibility, and low cost. These materials are used in the form of filaments and powders in FDM and SLS, and as bioinks for SLA and bioprinting. In this section, properties of materials used in 3D printing and bioprinting are discussed.

Fibrous Materials

Fiber-based thermoplastic polymeric materials are commonly employed in fused deposition modeling (FDM), also known as fused filament fabrication (FFF), and is the simplest 3D printing method. Polymeric filaments must have a certain diameter to fit the heating and extruding head of the printer. Quite a

number of commercial filaments, such as acrylonitrile butadiene styrene (ABS), and poly(lactic acid) (PLA) are available on the market. ABS is the most preferred 3D printing material for FDM applications because of its relatively low glass transition temperature and absence of crystallites due to it being an amorphous polymer. These properties enhance accuracy in printing and dimensional stability of the product because the shrinkage ratio during the cooling step is very small. However, the use of ABS filaments in tissue engineering is limited due to its non-biodegradable and non-biocompatible nature (Rosenzweig et al., 2015). A PLA filament is another material used because of properties similar to that of ABS. PLA is an environmentally friendly material that can be produced using natural sources, such as beets and corn. Its biodegradability and biocompatibility make it a good alternative to petroleum-based materials like ABS. It can generally print at temperatures between 200 and 230°C (Guvendiren et al., 2016).

A major disadvantage of the commercial filaments is that their composition is unknown. Therefore, their biocompatibility is not certain and medical use is not possible (Ravi et al., 2017). Extensive cytotoxicity and other biocompatibility tests are needed for these materials prior to any biomedical application. To overcome the biocompatibility problem and unknown ingredients, some researchers fabricated filaments from PCL and PLA pellets using an extruder (Hutmacher et al., 2001; Senatov et al., 2016a).

Powder Materials

The majority of the powder-based materials used in additive manufacturing systems are polymers. The techniques generally applied are fused deposition modeling (FDM) and selective laser sintering (SLS).

Poly(caprolactone) (PCL) is a common polymeric material utilized by FDM and SLS for tissue engineering applications because of its low melting temperature (55–60°C), excellent viscoelastic and rheological properties in addition to its a biodegradability and biocompatibility. It is approved by the FDA (Food and Drug Administration of USA) for certain medical applications (Brunello et al., 2016). It is also a stable material in the human body; it can stay for more than 6 months without significant degradation and its complete degradation could take around 2 years. However, the molecular weight, form, porosity and surface area of the material can change this duration significantly. The degradation profile and high stiffness of PCL make it a good molecule particularly for bone tissue engineering. PCL blended with hydroxyapatite (HAP) and tricalcium phosphate (TCP) is also used as printing material for bone tissue engineering where HAP serves to promote osteoinductive and osteoconductive properties of the printed scaffolds (Eosoly et al., 2010; Park et al., 2011; Mota et al., 2015).

Poly(D,L-lactic acid-co-glycolic acid) is one of several commonly used PLGA copolymers and is another synthetic thermoplastic polymer approved by the FDA for clinical use. It was used in FDM applications to fabricate scaffolds due to its processability and high mechanical strength (Do et al., 2015). Nevertheless, the high glass transition temperature of PLGA necessitates high temperatures to create the required flow viscosity for extrusion from the nozzle (Maniruzzaman, 2019).

The powders of block copolymers of polyethylene oxide terephthalate (PEOT) and polybutylene terephthalate (PBT), are thermoplastic elastomers employed in FDM applications. These block copolymers display excellent properties, such as toughness and elasticity, biocompatibility and easy processability. However, PEOT/PBT has been less studied compared to PCL and PLA because it requires an extremely high melting point (225°C) (Moroni et al., 2005).

Polyether ether ketone (PEEK) is a semi-crystalline thermoplastic polymer which has extensively been utilized in SLS. PEEK has a high elastic modulus similar to cortical bone, making it a good alternative to metal implants (Mazzoli, 2013). It is also biocompatible, bioinert, and heat resistant but not degradable, thus not suitable for tissue engineering. PEEK can only be processed by SLS technique due to its very high melting point (350°C) (Schmidt et al., 2007). Sintered PEEK and PEEK/HA have been employed for various orthopedic applications (e.g., joints) (Kurtz and Devine, 2007).

Poly(vinyl alcohol) (PVA), and blends of PVA and HAP have been studied as other powder-based materials for SLS for use in cartilage and bone tissue engineering (Chua et al., 2004; Shuai et al., 2013). PVA is a semi crystalline copolymer composed of vinyl alcohol and vinyl acetate units. It is bioinert, biocompatible, biodegradable and can be sintered at a low temperature (65°C) (Wiria et al., 2008).

Types of powder-based polymers used to produce scaffolds by FDM and SLS are summarized in **Table 2**.

Bioinks

Bioinks are the main constituents of bioprinting and stereolithography which are important for the printing of 3D tissues and organs. Bioinks should have certain characteristics to serve as printing materials. They should be biocompatible (not cause any immune or undesirable response after implantation), printable (as printing materials), and robust (resist physical forces of the environment) (Mosadegh et al., 2015). Today, hydrogels are the most commonly used bioinks and they can easily be loaded with cells. They are preferable because of their printable, cross-linkable, biocompatible nature and high swelling capacity. Hydrogel sources can be natural or synthetic (Mandrycky et al., 2016).

Natural hydrogels are mainly polysaccharides (e.g., chitosan, alginate, agarose) and components of the extracellular matrix (ECM) (e.g., collagen, gelatin, fibronectin, and laminin) (Zorlutuna et al., 2013). Alginate is a natural linear polysaccharide obtained from the wall of brown algae. It is widely used in 3D bioprinting applications due to its biocompatibility, promotion of cell proliferation, low price and the ability of fast gelation in calcium ion containing solutions. The major limitation of alginate derived hydrogels is mechanical stiffness for 3D bioprinting (Du, 2018). Agarose is another linear polysaccharide which is in gel form at room temperature when hydrated, but it can revert to solution form when the temperature is raised above 37°C. Chitin is a major constituent of crustaceous animals and chitosan is a linear polysaccharide that is obtained

TABLE 2 | Summary of commonly used fiber and powder-based polymers for 3D printing and their advantages and disadvantages.

Polymer	State of starting material	Technique	Advantage	Disadvantage	References
ABS	Filament	FDM	Low T_g	Non-biodegradable	Rosenzweig et al., 2015
			Easy processability	Non-biocompatible	
PLA	Filament	FDM	Flexibility	High melting point (200–230°C)	Guvendiren et al., 2016
			High mechanical properties		
PCL	Powder	FDM, SLS	Low melting temperature (55–60°C)	Slow degradation	Ravi et al., 2017
PCL/HAP PCL/TCP			Excellent viscoelastic and rheological properties		Hutmacher et al., 2001; Brunello et al., 2016; Senatov et al., 2016b
PLGA	Powder	FDM	Higher processability and mechanical strength	High T_g	Eosoly et al., 2010; Park et al., 2011
PEOT/PBT	Powder	FDM	High toughness and elasticity	High melting point (225°C)	Mota et al., 2015
			Easy processability		
PEEK	Powder	SLS	High elastic modulus	High melting point (350°C)	Do et al., 2015; Maniruzzaman, 2019
			Heat resistance		
			Bioinert		
PVA	Powder	SLS	Bioinert	Low mechanical properties	Moroni et al., 2005; Mazzoli, 2013
PVA/HAP					Schmidt et al., 2007

by deacetylation of chitin. However, it is not suitable to print large scale scaffolds due to its low mechanical strength and low gelation speed. Gelatin and collagen are highly biocompatible materials and enhance cell proliferation. The methacrylated form of gelatin (GelMA) can be easily printed by bioprinters and then stabilized by exposure to UV irradiation (Zhang X.-F. et al., 2017).

Synthetic hydrogels are produced chemically in the laboratory; thus, their mechanical and chemical properties can be controlled by the route or the conditions of the preparation process. Photosensitive synthetic hydrogels, such as polyethylene glycol diacrylate (PEGDA) are generally used as resins in stereolithography (SLA) (Du, 2018). PEG is chemically modified with acrylate groups to form the photopolymerizable polyethylene glycol diacrylate (PEGDA) in which cells can be entrapped in Skardal and Atala (2015). The major limitation of hydrogels is that the bioprinted structure tends to collapse because of low viscosity and low mechanical strength (Billiet et al., 2012).

Poly(propylene fumarate) (PPF) is also a photo-crosslinkable polymer utilized in stereolithography and overcomes some limitations of synthetic hydrogels, such as lower mechanical strength and a lack of biodegradability. PPF polymer is generally mixed with a photoinitiator and a solvent like diethyl fumarate (DEF). Printability and mechanical properties of the scaffold depend on the PPF/DEF ratio (Lee et al., 2015).

4D PRINTING

Additive manufactured structures using smart (intelligent) materials are able to self-transform into a predefined shape or exert a predefined function depending on the stimuli present in the microenvironment; these processes are regarded as "4D printing" (Tibbits, 2013, 2014; Pei, 2014; Choi et al., 2015). Four-dimensional printing utilizes the same additive manufacturing techniques and devices discussed above in the 3D printing section. What constitutes the main difference between 3D and 4D printing is the nature of the materials used. For a 3D printed product to be considered 4D printed, it should exhibit at least one type of smart behavior, such as "shape memory" or "self-actuation" (**Table 3**) (Li X. et al., 2016). Four-dimensional printing has several advantages over 3D printing (**Table 4**). Introduction of the fourth dimension, time, in addition to the 3D arrangement gives both spatial and temporal control over the fabricated product. Therefore, 4D printing overcomes one of the major drawbacks of 3D printing and produces structures that are dynamic and animate. Smart materials are most commonly referred to as "materials that exhibit changes in physical or chemical properties in a controlled and functional manner upon exposure to an external stimulus, such as heat, moisture, light, magnetic field or pH." Thus, a 4D printed product can change its shape, color, function or other physical or chemical properties in response to the aforementioned stimuli types. Programmability of the state and function of the 4D printed product as a result of the smartness of the material eliminates the need for external devices or methods for post-processing, and reduce the production duration, and in some cases may also aid in the application process (Tibbits, 2014). For example, shape changing smart scaffolds that exhibit compactness prior to *in vivo* application could be used in minimally invasive procedures and self-assembly to the required complex shape due to dynamic response upon implantation (Miao et al., 2016a).

Factors Influencing 4D Printing

Five main factors influence the process of 4D printing: (i) type of additive manufacturing process, (ii) type of responsive material, (iii) type of stimulus, (iv) interaction mechanism between

TABLE 3 | Types of smart behavior observed in responsive materials.

Smart behavior	Description	Examples	References
Shape memory	Material changes into a predefined shape in response to an external stimulus	Poly(ε-caprolactone) dimethacrylate (PCLDMA)	Neuss et al., 2009
		Poly(ether urethane)	Cui et al., 2011
		Polyimide	Zhang and Ionov, 2014
Self-assembly	Exposure to external stimulus induces folding of chains and assembly into a preprogrammed shape	4,4′-diglycidyloxyazobenzene polymerized with sebacic acid	Li Y. et al., 2016
Self-actuating	Automated actuation of material upon exposure to an external stimulus	*N*-isopropylacrylamide (NIPAM) and ruthenium(II) tris-(2,2′-bipyridine) copolymer	Tabata et al., 2002
Self-sensing	Material detects and quantifies the exerted external stimuli	Mechanophore crosslinked poly(methyl acrylate) and poly(methyl methacrylate)	Davis et al., 2009
Self-healing	Damage caused in the structure is repaired without any external intervention	Microencapsulated dicyclopentadiene (DCPD)-Grubbs' catalyst embedded in epoxy matrix	White et al., 2001
		Poly(ethylene-co-methacrylic acid) copolymers and ionomers	Kalista and Ward, 2006; Kalista et al., 2007

TABLE 4 | Comparison of 3D printing and 4D printing.

Property	3D printing	4D printing
Manufacturing process	2D sections of a 3D structure (with respect to the z-axis) are built layer-by-layer from top to bottom or from bottom to top	Produced in the same way as 3D printed products, but changes shape or function after manufacturing, upon exposure to a specific stimulus
Materials used	Thermoplastic polymers, ceramics, metals, biomaterials, and their composites	Smart materials (polymers, ceramics, metals, biomaterials, and composites) that undergo a change in property or function over time in response to a specific stimulus
Material programmability	Not possible	Material properties and functions are programmable with a specific exposure sequence and time of stimulus, and the spatial organization of material in desired final product
Object shape/function	Stable over time	Object shape or function changes over time when structure is exposed to a specific external stimulus
Application areas	Fields including but not limited to medical, engineering, dentistry, automotive, jewelry etc.	All 3D print application areas where a dynamic change in configuration is required or beneficial.

stimulus and the material, and (v) mathematical modeling of the material transformation.

Additive manufacturing process, as in 3D printing, realizes the spatial geometry provided by the digital information produced in computer aided design/manufacturing (CAD/CAM) programs. Many additive manufacturing processes that are commonly used, such as fused deposition modeling (FDM) (Hendrikson et al., 2017) and stereolithography (SLA) (Miao et al., 2018) are also suitable for 4D printing applications. Stimuli responsive material and additive manufacturing processes should be compatible with each other in 4D printing, as in the material selection process in 3D printing applications. In the case of multi-material structures where the difference in material properties (swelling, thermal expansion, etc.) drive the transformation of the shape or function, the additive manufacturing process selected should support the homogeneous distribution of the material and produce a single printed structure.

The most important element of 4D printing is the responsive material, since it is the material which introduces the fourth dimension into the process. The time-dependent change observed in the responsive material upon exposure to a stimulus can be physical or chemical. Some responses include folding, curling, twisting, expansion, contraction, color change, and degradation (Li Y. C. et al., 2016).

The stimulus enforces the transformation of shape or function of the responsive material, thus the 4D printed structure is manipulated over time, after the manufacturing process. Types of stimuli that act on responsive materials can be physical, chemical or biological. Physical stimuli include temperature, light, and magnetic field, whereas humidity, and pH are examples of chemical stimuli (**Figure 5**). Some smart materials have multi-functionality and respond to two or more signals simultaneously (Zhang et al., 2015).

Types of stimuli to be exerted, and thus the smart material, should be selected with care, taking into consideration the requirements and constraints of the specific application area, and the relevance of the interaction mechanism to the selected application. Interaction mechanism refers to the process of application of stimulus to the responsive material. In some applications, transformations require additional processes prior to application of the stimulus, rather than simple exposure of the material, to obtain a response and the desired outcome. For example, in the case of constrained-thermomechanics, the smart material exhibits a shape memory effect upon being exposed to heat. In order to achieve the shape memory function, however, the material is first subjected to an external load at a high temperature and deformed. Then temperature is lowered while the structure is still under load. The load is removed at low

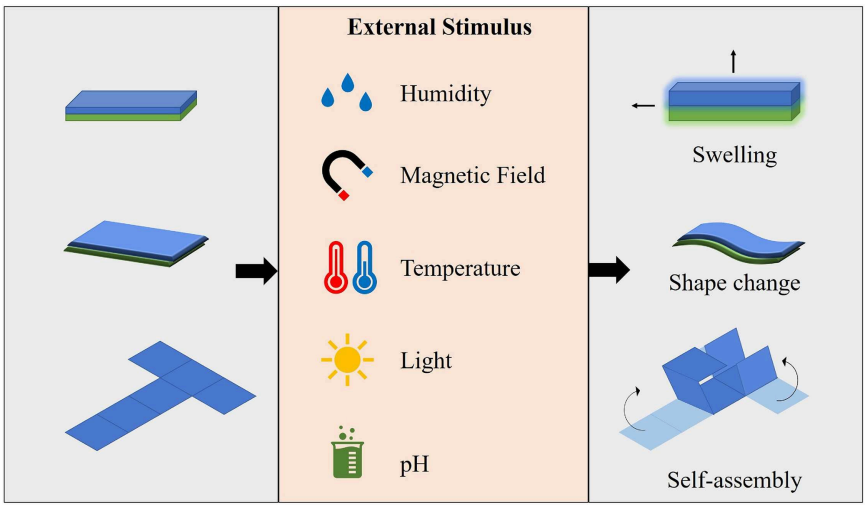

FIGURE 5 | Types of stimuli, and responses observed in smart materials.

temperature and the material is molded in this predetermined shape. When heat is applied as the stimulus, the earlier form is regained.

In order to achieve a successfully programmed and controlled 4D effect for a specific application, theoretical and numerical models are generally utilized. These models aid in predicting the appropriate exposure sequence of stimuli, and time required for the structure to reflect the desired behavior by establishing connections between material and stimulus properties, structure, and the desired final shape. The targeted 3D spatial orientation and material distribution in structure, and the estimation of system behavior with different material properties and geometries are tested with these models through a finite-element analysis (FEA).

An ongoing debate about 4D printing is whether gradual degradation of 3D printed constructs can be categorized as a time-dependent 4D effect (Choi et al., 2015; Zhou et al., 2015). Scaffolds manufactured from biodegradable biomaterials and the sustained release of therapeutic agents from such scaffolds would have to be included in 4D printing applications if the biodegradation process is a strictly programmable, time-dependent phenomenon. While biodegradability is a desired material property in the field of tissue engineering, an important requirement of the transformation through the 4D process is that the structure must display a minimum of two stable configurations or shapes before and after the triggering stimulus is applied, because the responses to the stimuli should be reversible (Zhou et al., 2015). Thus, 3D structures based on self-degrading polymers are not regarded as having a 4D effect.

Smart Polymers for 4D Printing in Tissue Engineering Applications

Tissue engineering and regenerative medicine have -to some extent- overcome the challenge of fabricating complex tissue/organ geometries and controlling the tissue microarchitecture with the aid of 3D printing. Recently, tissue mimics and scaffolds that are capable of sensing the dynamic tissue microenvironment and adapting their shape or chemistry are also in increasing demand. Such products fabricated by combining stimuli responsive materials and 3D printing are expected to improve responses to pathology (Morrison et al., 2015), and allow application of minimally invasive surgical procedures (Javaid and Haleem, 2018) and insertion of implants to sites that are otherwise not accessible (Zarek et al., 2016a).

Stimuli responsive polymers, as explained previously, undergo physical or chemical changes when exposed to appropriate stimuli. The cause of this responsiveness is the presence of certain functional groups along the polymer backbone that are sensitive to a change in state, such as charge or polarity. The resulting changes in chemical structure lead to the macroscopic level transformations i.e., changes in chain dimensions and size, secondary structure, solubility, degree of intermolecular association, sol-gel transition, and even chain breakage (Aguilar and San Román, 2014).

An important aspect of some stimuli responsive polymers is the reversibility of the response; meaning that the material is able to return to its original state upon removal of the stimulus. A natural example of this would be the hygroscopic folding and unfolding of pinecone scales, in response to the level of humidity. The scales contract upon increase of humidity and expand when the humidity level is low, scattering the seeds they hold inside (Song et al., 2015). This reversibility of response introduces some drawbacks to the utilization of the said polymers in 4D printing processes; impaired printability of the material, and reproducibility of the desired 4D effect in the product (Lee A. Y. et al., 2017). To overcome these issues, stimuli responsive polymers can be used in combination with other polymers or ceramics where the non-responsive component may serve as a biological or mechanical property enhancer (Senatov et al., 2016b, 2017), or a processing aid.

The mechanisms behind responsiveness to various stimuli exhibited by smart polymers are summarized in this section,

along with some examples that have been utilized in 3D printed tissue engineering applications. Responsiveness of polymers are categorized into two classes; responsiveness to (i) physical stimuli and (ii) chemical stimuli. Temperature responsive, photo responsive, and magneto-responsive polymers fall under those that respond to physical stimuli, while pH and humidity responsive polymers are classified under responsiveness to chemical stimuli.

Responsiveness to Physical Stimuli

Temperature responsive polymers

Temperature responsive polymers are among the most frequently used materials in 4D printing applications especially in the tissue engineering field where a change in temperature can be easily controlled and applied in a non-invasive manner. Many applications exploit the human body temperature, 37°C, to trigger the desired response of some materials. The two most common classes of temperature responsive polymers used in 4D printing applications are (i) shape memory polymers, and (ii) responsive polymer solutions (Hoogenboom, 2014).

Shape memory polymers (SMP) that have temperature responsiveness are thermoplastic elastomers consisting of two distinct components, one is the elastic segment with a high glass transition temperature ($T_{g,1}$) and the other is the switching segment with intermediate glass transition temperature ($T_{g,2}$) or melting temperature (T_m) (**Figure 6**). When deformed at a temperature above the highest T_g, these materials obtain their permanent shape. At a temperature between the two glass transition temperatures, the switching segment becomes soft and pliable while the elastic segment resists the applied constraint, such as stretching or compressing. After deformation at this state, if the polymer is cooled below the glass transition temperature of the switching segment ($T_{g,2}$), a temporary shape is formed. At this stage the elastic segment cannot return to its original form even after the removal of applied constraints. The driving energy for the shape change effect of the polymer is the elastic spring energy contained within this segment. When the polymer is heated above $T_{g,2}$ again, the elastic segment is able to drive the shape change effect that transforms the polymer back to the original permanent shape (Sun et al., 2012).

Shape memory polymers have some advantages and drawbacks compared to their metal and ceramic counterparts. The advantages include low density, low cost, ease of shape manipulation and good control over recovery temperature, high strain recovery, and physical and chemical modification ability to achieve desired properties (e.g., biodegradability). As drawbacks compared to metals and ceramics they have lower strength, elastic modulus and processing temperatures.

Some examples of shape memory polymers used in 4D printed tissue engineering applications are poly(ε-caprolactone) dimethacrylate (PCLDMA) (Neuss et al., 2009), soybean oil epoxidized acrylate (Miao et al., 2016b, 2018), polycaprolactone triol (Ptriol) (Miao et al., 2016a), poly(ether urethane) (PEU) (Cui et al., 2011), and poly(lactic acid) (Senatov et al., 2016b, 2017).

Responsive polymer solutions are generally copolymers that have a critical solution temperature that affect the hydrophilic and hydrophobic interactions between polymer chains and the solvent (Hasirci and Hasirci, 2018). A change in temperature disrupts these interactions, leading to intra- and intermolecular interactions that result in the precipitation of the polymer, or in the case of a hydrogel, to a shrinkage or expansion (due to chain collapse and chain expansion, respectively). Polymer solutions that have an upper critical solution temperature (UCST) exhibit monophasic behavior above this temperature and undergo phase separation below UCST. Inversely, polymer solutions that have a lower critical solution temperature (LCST) undergo phase separation above this temperature and exhibit monophasic behavior below it. For example, a shrunken hydrogel with UCST of 25°C would swell and expand when introduced to the human body (37°C). These materials are widely utilized in drug delivery applications and tissue engineering applications, such as cell sheet engineering. Some examples are poly(*N*-isopropylacrylamide) (PNIPAM) (Ozturk et al., 2009), poly(*N*-vinylcaprolactam) (PNVC) (Haq et al., 2017), gelatin and GelMA (Kolesky et al., 2014), collagen and ColMA, methylcellulose, agarose, pluronic (Fedorovich et al., 2009), and poly(ethylene glycol) based block polymers (Suntornnond et al., 2017).

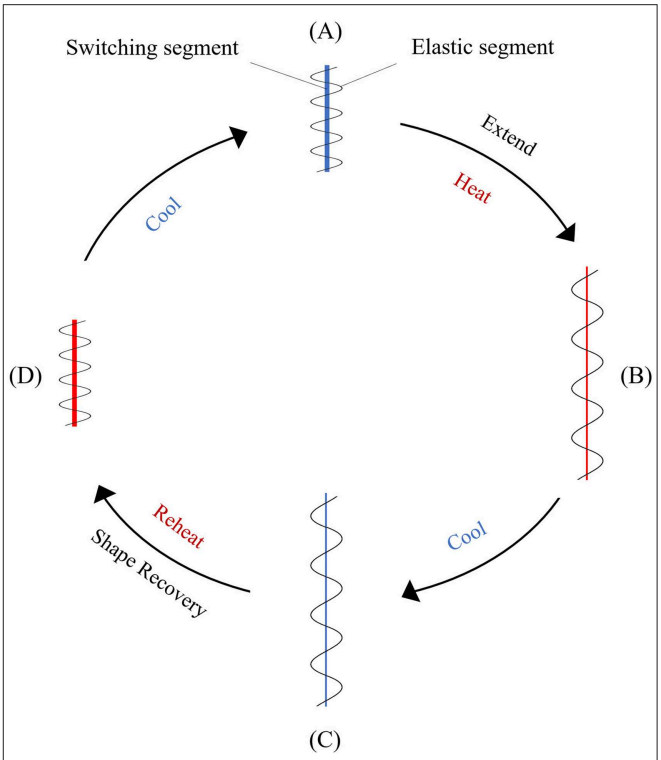

FIGURE 6 | Schematic representation of the mechanism in a temperature responsive SMP. **(A)** Original conformation where the elastic and the switching segments are entangled; **(B)** upon stretching at high temperatures the switching segment becomes soft and is deformed, and the elastic segment is extended; **(C)** when the temperature is lowered, the switching segment hardens, preventing the recovery of the elastic segment; **(D)** after reheating, the original shape is recovered because of the softening of the switching segment and the release of the elastic energy from the pre-deformed elastic segment.

Photo responsive polymers

Photo responsive polymers undergo physical or chemical transformation upon exposure to light. Photo-stimulation can induce changes, such as conformation, polarity, hydrophilicity, charge, or bond strength which is translated to changes in the wettability, solubility, optical properties, and degradability of the material (Cabane et al., 2012). It has advantages, such as remote application with zero contact and ease of dose adjustment to control response strength (Cui and Del Campo, 2014). The photo responsiveness is due to presence of photosensitive side groups (chromophores) on the polymer backbone. Azobenzenes, spiropyrans, spirooxazines, diarylethenes, and fulgides are families of these side groups commonly found in photosensitive polymeric systems (Ercole et al., 2010). Depending on the type of chromophore present, the response induced can be reversible or irreversible. Irreversible photo responsive polymers are generally photodegradable polymers that are utilized in the development of drug delivery systems. For tissue engineering applications, 4D printing of hydrogels that swell or shrink or self-assemble upon photo-stimulation is an area waiting to be explored. Examples of such systems are poly(N-isopropylacrylamide) (PNIPAM) functionalized with spirobenzopyran (Sumaru et al., 2006), and a hydrogel system consisting of 4,4′-azodibenzoic acid (ADA), α-cyclodextrin, and dodecyl (C_{12})-modified poly(acrylic acid) (PAA) (Tomatsu et al., 2005).

Magneto-responsive polymers

Magneto-responsive polymeric systems are, in general, polymer networks physically or chemically functionalized with magnetic nanoparticles (MNP) which consist of magnetic elements, such as iron (Fe), cobalt (Co), nickel (Ni), or their oxides (Montero et al., 2019). When physically entrapped (by blending, *in situ* precipitation, or dip coating methods) or covalently immobilized, these magnetic nanoparticles introduce responsiveness to a magnetic field (Adedoyin and Ekenseair, 2018). This responsiveness results in a spatio-temporal control over the physical, structural, and mechanical properties of the polymeric scaffold. The degree and uniformity of the response depends on the types of the polymers and MNPs and their ratio, along with the distribution of MNPs within the matrix.

The potential of magneto-responsive materials in biomedical applications, has been demonstrated in many targeted drug delivery applications, where they offer minimally invasive, locally effective, and controlled therapeutic action (Chang et al., 2011; Peters et al., 2016; Casolaro and Casolaro, 2017). From a tissue engineering perspective, manipulations on the direction and strength of the magnetic field will result in specific alterations of scaffold morphology and geometry, and this can be used in certain tissue regeneration applications that require structural alignment (Xu et al., 2011; Panseri et al., 2012; Kokkinis et al., 2015), mechanical stimulation (Sapir-Lekhovitser et al., 2016), and stem cell differentiation (Fuhrer et al., 2013).

The disadvantage of using magnetic nanoparticles in living systems is that when leached from the matrix, MNPs smaller than 50 nm are able to cross biological membranes and adversely affect the function of the tissues by inducing inflammation, generating reactive oxygen species, impeding DNA function, and driving cells to apoptosis (Adedoyin and Ekenseair, 2018). Thus, the biocompatibility of any given magneto-responsive polymer is directly related to the type of MNPs used and the method of their incorporation into the polymeric network. Furthermore, the behavior of magneto-responsive materials under *in vivo* conditions should be estimated prior to application, using proper models that consider the magnetic field strength, the amount of MNPs used, and the responsiveness of these MNPs to the applied magnetic field, in order to achieve a controlled and successful therapeutic action (Pernal et al., 2018). These models would provide information on the appropriate manner and amount of magnetic stimulation required to induce tissue regeneration. This information is crucial, especially for vascular and osteochondral tissue applications where mechanotransduction plays an important role in induction of regeneration.

Examples of 3D printed polymeric magneto-responsive systems used in tissue engineering applications are iron(III)oxide (Fe_3O_4) nanoparticles containing mesoporous bioactive glass/poly(ε-caprolactone) (Fe_3O_4/MBG/PCL) (Zhang et al., 2014), magnetic nanocomposite scaffolds consisting of iron(III)oxide/PCL and iron(III)oxide/poly(ethylene glycol diacrylate) (PEGDA) (De Santis et al., 2015), and PCL/iron-doped hydroxyapatite (PCL/FeHA) nanocomposite scaffolds (D'Amora et al., 2017).

Responsiveness to Chemical Stimuli

pH responsive polymers

pH responsive polymers are polyelectrolytes that bear weak acidic or basic groups in their structure that accept or release protons in response to environmental pH changes. Carboxyl, pyridine, sulfonic, phosphate, and tertiary amine groups in polymers ionize with changes in pH which results in structural or property changes, such as solubility, degradability, configuration, chain conformation swelling, surface activity, and self-assembly (Reyes-Ortega, 2014). pH responsive polymer systems have been utilized in several biomedical applications, such as drug delivery (Bagherifam et al., 2015), gene delivery, and glucose sensors due to their unique properties.

In pH responsive systems, polymers of basic monomers act as cationic polymers under acidic conditions and polymers of acidic monomers behave as anionic polymers under basic conditions. One of the two types of polymers or a combination of the two can be implemented in a stimuli responsive system depending on the application. The origin of pH responsive polymers can be natural or synthetic. Poly(L-glutamic acid) (PGA), poly(histidine) (PHIS), poly(acrylic acid) (PAA) (Dutta and Cohn, 2017), and poly(aspartic acid) (PASA) are examples of synthetic pH responsive polymers which are biocompatible and biodegradable [except for poly(acrylic acid)], while chitosan, hyaluronic acid, gelatin, alginic acid, and dextran are examples of pH responsive polymers of natural origin (Kocak et al., 2017). pH differences are observed in many compartments of the human body (acidic environment in the stomach and basic environments of the intestines along the gastrointestinal tract, or the hypoxic nature of tumor tissue microenvironment), and

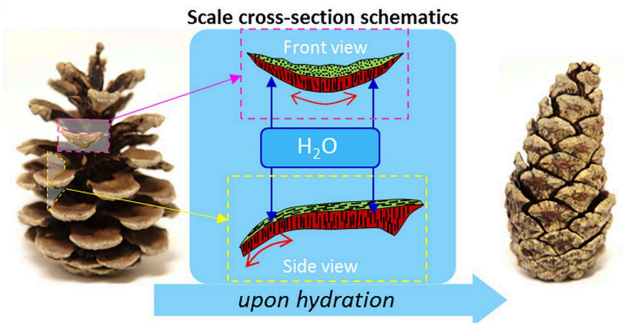

FIGURE 7 | Stimulus responsiveness of pinecones. (Left) Dehydrated open pinecone; (Right) hydrated closed pinecone. Differences in the cellulose fibril winding angles in the top and bottom layers of the cells (sclereids in red and sclerenchyma in green) controls the expansion of these cells during hydration/dehydration. The cooperative anisotropic expansion of these differentiated cells results in the opening and closing of pinecone scales in response to hydration (adapted from Mulakkal et al., 2018).

the responsiveness of these materials can be exploited in tissue engineering applications.

Humidity responsive polymers

Humidity responsiveness is a phenomenon that has many examples in nature. One such example is the movement of pinecone scales to preserve or dispense the seeds in response to the level of environmental humidity (**Figure 7**). The scales contract upon the increase of humidity and expand when the humidity level is low, scattering the seeds they hold inside (Song et al., 2015). These biological systems inspired the development of humidity responsive materials that release or absorb moisture in response to changes in humidity of the environment (Li Y. C. et al., 2016). Systems composed of these materials are able to transform the sorption or desorption of moisture into driving forces for movement. Poly(ethylene glycol) diacrylate (PEGDA) (Lv et al., 2018), cellulose (Mulakkal et al., 2018), and polyurethane copolymers (Jung et al., 2006) are some examples of humidity responsive materials that have been studied.

3D PRINTING APPLICATIONS

Providing extreme control over the shape and architecture of the scaffolds makes 3D printing very attractive for the fabrication of the tissue engineering products. In this section, 3D printing applications for different types of tissues, such as bone, skin, nerve, vasculature, and other tissues are presented.

Bone Tissue Engineering Applications

Bone is a mineralized tissue which has a high mechanical strength. Therefore, the mechanical properties of the printed polymers should be enhanced to match the properties of the bone tissue. There are many studies in the literature presenting the fabrication of 3D printed scaffolds for bone tissue engineering (Lee et al., 2011; Kao et al., 2015; Petrochenko et al., 2015; Saito et al., 2015; Wang et al., 2016). To strengthen the products, minerals, such as hydroxyapatite (HAP) and tricalcium phosphate (TCP) are blended with the polymers and then printed (Eosoly et al., 2012; Buyuksungur et al., 2017). Poly(ε-caprolactone) (PCL) is the most commonly used polymer for 3D printing of scaffold for bone tissue (Liao et al., 2011; Wang M. O. et al., 2015). PCL is a biodegradable, biocompatible and FDA approved polymer for certain medical applications. One of the main reasons for using this polymer is its relatively low T_g (~60°C) and T_m which makes it a very good compound for fused deposition modeling (Lee et al., 2016). However, PCL is a hydrophobic polymer and does not have any cell attractive moieties. In one report, it was blended with poly(propylene fumarate) (PPF) to increase the hydrophilicity of the 3D printed PCL scaffolds (Buyuksungur et al., 2017). Other materials, such as graphene and bioactive borate glass were also added for the production of composite scaffolds with PCL in order to improve the properties of the printed constructs (Wang et al., 2016; Murphy et al., 2017). Bone morphogenic protein (BMP) is another substance incorporated in 3D printed scaffolds either as is or in microparticles to increase the healing rate of the bone tissue, because a large number of studies showed the positive effect of BMPs on bone regeneration (Huang et al., 2005; Yilgor et al., 2009; Liu et al., 2013).

Different types of cells are used in bone tissue engineering applications. Among them, mesenchymal stem cells (MSCs) isolated from bone marrow or adipose tissue are the most frequently used ones (Duarte Campos et al., 2016; Cunniffe et al., 2017). Their high capacity to differentiate into bone cells makes them an ideal cell type to study and achieve bone regeneration. Some researchers added human umbilical vein endothelial cells (HUVECs) on the 3D printed scaffolds to achieve vascularization at the defect site (H. Cui et al., 2016). These cells were seeded to produce a tissue engineered bone tissue. However, recent studies focus on printing the cells together with the scaffold (Bendtsen et al., 2017; Keriquel et al., 2017; Wenz et al., 2017). For these applications, agarose, alginate, collagen, GelMA, methacrylated hyaluronic acid (HAMA), and PEG dimethacrylate (PEGDMA) hydrogels were used as bioinks. Nano HAP is also blended with these hydrogels in order to improve the mechanical properties of the printed constructs (Bendtsen et al., 2017; Cunniffe et al., 2017; Keriquel et al., 2017). MC3T3, which is an osteoblast precursor cell line was also commonly used in bioprinting applications (Lee et al., 2011; Eosoly et al., 2012).

Three-dimensional printed tissue engineered products were implanted *in vivo* at the defect site in order to study their effect on bone regeneration (Lee et al., 2011; Loozen et al., 2013; Saito et al., 2015; Buyuksungur et al., 2017; Keriquel et al., 2017). MSCs are incorporated with the PCL based scaffolds, and are reported to improve the bone regeneration when applied to rabbit femurs (Buyuksungur et al., 2017). Bone tissue engineering applications of 3D printing discussed here are summarized in **Table 5**.

Skin Tissue Engineering Applications

Skin is a soft tissue; therefore, hydrogels are commonly used in 3D printing of skin substitutes. Many of the 3D printing

TABLE 5 | 3D printing of polymers for tissue engineering applications.

Target tissue	Printing method	Printing material	*In vitro* study	*In vivo* study	References
Bone	FDM	PCL, HAP, PPF	Rabbit bone marrow stem cells (BMSCs)	Femurs of rabbits	Buyuksungur et al., 2017
Bone	Continuous digital light processing	PPF	Angiogenesis modeling (representing endothelial cells)	Rat subcutaneous implantation	Wang M. O. et al., 2015
Bone	FDM	PCL	Pre-osteoblast MC3T3-E1	–	Lee et al., 2016
Bone	Extrusion based AM	PCL, graphene	Human adipose derived MSCs	–	Wang et al., 2016
Bone	SLS	PCL	Porcine adipose derived stem cells	–	Liao et al., 2011
Bone	SLS	PCL, HAP	Osteoblast-like cells MC 3T3	–	Eosoly et al., 2012
Bone	SLA	PPF/diethyl fumarate (DEF)	Pre-osteoblast MC3T3-E1	Cranial bone defect in rat	Lee et al., 2011
Bone	SLA	PLA coated with PDA	Human adipose derived stem cells	–	Kao et al., 2015
Bone	RP	PLLA, PCL	Human gingival fibroblasts	Subcutaneous implantation in mice	Saito et al., 2015
Bone	Two-photon polymerization	Urethane, acrylate based photo elastomer	Human BMSCs	–	Petrochenko et al., 2015
Bone	Bioprinting	PCL/bioactive borate glass	Human adipose stem cells	–	Murphy et al., 2017
Bone	Bioprinting	Alginate	Multipotent stromal cells	Subcutaneous implantation in nude mice	Loozen et al., 2013
Bone	Bioprinting	Alginate/PVA/HAP hydrogel	Mouse calvaria 3T3-E1 (MC3T3)	–	Bendtsen et al., 2017
Bone	LAB	Collagen, nano-HAP	Mouse MSCs	Calvaria defect model in mice	Keriquel et al., 2017
Bone	Bioprinting	PLGA, PEG	Immortalized human MSCs	–	Sawkins et al., 2015
Bone-Cartilage	Inkjet bioprinting	PEGDMA, GelMA	Human MSCs	–	Gao et al., 2015
Bone	Bioprinting	Collagen type I, agarose hydrogel	Human bone marrow derived MSCs	–	Duarte Campos et al., 2016
Bone	Bioprinting	Agarose hydrogel	3T3 murine embryonic fibroblasts	–	Carlier et al., 2016
Bone	Dual 3D bioprinting	PLA fibers, GelMA	hMSCs and HUVECs	–	Cui et al., 2016
Bone	Bioprinting/FDM	PCL, alginate and nano-HAP	Bone marrow derived MSCs	–	Cunniffe et al., 2017
Bone	Bioprinting	GelMA, HAMA, HAP	Human adipose derived stem cells	–	Wenz et al., 2017
Skin	Extrusion based printing	Silk sericin (SS), GelMA	L929, HaCaT and HSF cells	Mouse subcutaneous implantation	Chen et al., 2018
Skin	LAB	Collagen	NIH-3T3 and HaCaT	–	Koch et al., 2012
Skin	Extrusion based bioprinting	Chitosan, gelatin	HFF-1 cells	–	Ng et al., 2016
Skin	Free-form fabrication (FFF)	Fibrin	hFBs and hKCs	Immunodeficient athymic mice	Cubo et al., 2016
Skin	Bioprinting	Gelatin, alginate, fibrinogen	Human dermal fibroblasts (HDFs)	–	Pourchet et al., 2017
Skin	LAB	Matriderm	Fibroblasts and keratinocytes	Dorsal skin fold chamber in nude mice	Michael et al., 2013
Skin	Extrusion and inkjet printing	Skin-derived extracellular matrix (S-dECM)	HDFs, human epidermal keratinocyte (HEK), human adipose derived MSCs, EPCs	Dorsal wound of BALB/cA-nu/nu mice	Kim et al., 2018

(Continued)

TABLE 5 | Continued

Target tissue	Printing method	Printing material	*In vitro* study	*In vivo* study	References
Nerve	Inkjet printing	Fibrin	Primary embryonic hippocampal, cortical neurons	–	Xu et al., 2006
Nerve	Direct inkjet printing	Collagen	Rat embryonic astrocytes, neurons	–	Lee et al., 2009
Nerve	Direct inkjet printing	Collagen, fibrin VEGF release	Murine neural stem cells (C17.2)	–	Lee et al., 2010
Nerve	Two-photon polymerization	Photopolymerizable PLA	SH-SY5Y human neuronal cell line, rat SCs	–	Koroleva et al., 2012
Nerve	Bioprinting	Agarose rods as supports, scaffold-free	Mouse BMSCs, SCs	Rat sciatic nerve injury model	Owens et al., 2013
Nerve	Piezoelectric inkjet printing	–	Adult rat retinal ganglion cells, retinal glia	–	Lorber et al., 2014
Nerve	Bioprinting	Gellan gum-RGD	Primary cortical neurons	–	Lozano et al., 2015
Nerve	FDM, bioprinting	Polyurethane	NSCs	Zebrafish embryo neural injury model	Hsieh et al., 2015
Nerve	Microextrusion bioprinting	Alginate, carboxymethyl-chitosan, agarose	Cortical human NSCs	–	Gu et al., 2016
Nerve	SLA-Low-level light therapy	GelMA and PEGDA	Mouse NSCs	–	Zhu et al., 2017
Nerve	SLA	PEGDA	NSCs	–	Lee S.-J. et al., 2017
Vascular	Digital light processing SLA	PPF	HUVECs, human umbilical vein SMCs	Mice animal model	Melchiorri et al., 2016
Vascular	E-jet 3D printing	PCL	HUVECs	Segment of the abdominal artery in rats	Huang et al., 2018
Vascular	Bioprinting	Multicellular spheroids, scaffold-free	HUVECs, HASMCs, human normal dermal fibroblasts (HNDFB)	Implantation in nude rats	Itoh et al., 2015
Vascular	RP bioprinting	Multicellular spheroids, scaffold-free	Smooth muscle cells, fibroblasts	–	Norotte et al., 2009
Cardiovascular	3D cell printing	MSCs-laden heart tissue-derived decellularized ECM	Human c-kit + cardiac progenitor cells (hCPCs)	Subcutaneous implantation in nude mice/rat myocardial infarction model	Jang et al., 2017
Vascular	Bioprinting	MEF cell aggregates	Mouse embryonic fibroblast (MEFs)	–	Kucukgul et al., 2015
Vascularization	Bioprinting	Matrigel/alginate	Endothelial progenitor cells (EPCs)	Subcutaneous implantation in nude mice	Poldervaart et al., 2014
Cartilage	SLS	PCL, collagen hydrogel	Chondrocytes	Dorsal area of 6-weeks-old male nude mice	Chen et al., 2014
Cartilage	Inkjet bioprinting	Nanocellulose, alginate	Human chondrocytes	–	Markstedt et al., 2015
Cartilage	Low-temperature FDM	Polyurethane	MSCs	Rabbit osteochondral defect	Hung et al., 2016
Cartilage	Electromagnetic jet technology	Nanofibrillated cellulose and alginate	Human nasal chondrocytes (hNC)	–	Martínez Ávila et al., 2016
Cartilage	Extrusion based bioprinting	Collagen, alginate, agarose	Primary rat chondrocytes	–	Yang et al., 2018
Meniscus	SLA	GelMA	Human avascular zone meniscus cells	Meniscus defect in an explant organ culture model	Grogan et al., 2013

(Continued)

TABLE 5 | Continued

Target tissue	Printing method	Printing material	*In vitro* study	*In vivo* study	References
Meniscus	FDM	PCL	–	–	Cengiz et al., 2016
Meniscus	FDM	PCL	–	–	Szojka et al., 2017
Meniscus	FDM	PCL	Porcine fibrochondrocytes	–	Bahcecioglu et al., 2018
Meniscus	FDM	PCL	Porcine fibrochondrocytes	–	Bahcecioglu et al., 2019
Cornea	Extrusion based bioprinting	Collagen, alginate	Corneal keratocytes	–	Isaacson et al., 2018
Cornea	LAB	Recombinant human laminin and collagen	Human ESC derived limbal epithelial stem cells, hASCs	Porcine organ culture	Sorkio et al., 2018
Urethra	Bioprinting	PCL, PLCL	Urothelial cells (UCs), SMCs	–	Zhang K. et al., 2017

technologies, such as extrusion-based printing and laser-assisted bioprinting are used to fabricate skin constructs (Koch et al., 2012). Tissue engineering is also used in the production of whole skin constructs to treat burns or chronic wounds. Collagen-based materials are used in most of the printing studies, as collagen is the main component of native skin. However, collagen has poor printability and a long crosslinking time (Ng et al., 2016). Chitosan is preferred over collagen for wound healing applications due to its antimicrobial properties and ability to trigger hemostasis. Alginate (Pourchet et al., 2017), gelatin (Ng et al., 2016), GelMA (Chen et al., 2018), and fibrin (Cubo et al., 2016) are also used to print skin constructs.

In most studies, bioprinting of skin grafts is achieved with the use of both hydrogels and skin cells (Vijayavenkataraman et al., 2016). Fibroblasts (NIH-3T3) and keratinocytes (HaCaT) are widely used because they are the main cell types in the skin tissue (Michael et al., 2013). Different types of skin cells should be placed in a skin mimicking organization within a 3D printed construct in order to create native human skin (Ng et al., 2015). Some of the 3D printed skin grafts were tested *in vivo* and achieved regeneration of the tissue at the injury site (Cubo et al., 2016; Kim et al., 2018). Skin tissue engineering applications of 3D printing are summarized in **Table 5**.

Nerve Tissue Engineering Applications

Nerve tissue has a directional (uniaxial) organization due to the anisotropic orientation of the nerve fibers. Nerve guides are used to bring the proximal and the distal ends of a damaged nerve after an injury occurs. They can also be fabricated by 3D printing to provide patient-specific constructs with a complex inner architecture. Various types of additive manufacturing (AM), such as ink jet printing, stereolithography (SLA), fused deposition modeling (FDM) and bioprinting are frequently used in order to produce nerve tissue engineering products. Fibrin (Xu et al., 2006), collagen (Lee et al., 2009), PLA (Koroleva et al., 2012), gellan gum (Lozano et al., 2015), carboxymethyl chitosan (Gu et al., 2016), agarose (Owens et al., 2013), polyurethane (Hsieh et al., 2015), GelMA (Zhu et al., 2017) and PEGDA (Lee S.-J. et al., 2017) were also used to print constructs for nerve tissue engineering applications.

Mostly neural stem cells (NSCs) are incorporated into the constructs, however, glial cells, primary cortical neurons, astrocytes, Schwann cells (SCs), bone marrow stem cells (BMSCs), and retinal ganglion cells (RGCs) were also used in nerve regeneration studies (Zhu et al., 2017). The nervous system is composed of different types of cells, such as neurons, glial cells, and SCs, and therefore, many studies have concentrated on printing these cell combinations to obtain a whole nerve tissue construct (Koroleva et al., 2012). The orientation of these cells is also important because the nerve tissue is anisotropic. Bioprinting provides a very good solution to this problem since cells can be printed within hydrogel tubes or on fibers in a specific orientation, using this technique (Hsieh et al., 2015). Molecules of biochemical importance can also be added into the 3D printed structures. For example, vascular endothelial growth factor (VEGF) was incorporated into fibrin gel, and murine neural stem cells were shown to migrate toward this gel and exhibit an elongated shape with neurite-like extensions (Lee et al., 2010).

The number of *in vivo* studies is relatively few when compared with other tissues, mostly due to the complexity of the nervous system. In an *in vivo* study in rats, a mainly cellular nerve graft, composed of mouse bone marrow stem cells (BMSCs) and Schwann cells (SCs), was printed and tested in a sciatic nerve injury model (Owens et al., 2013). Tubular structures loaded with spheroids were deposited layer-by-layer into the agarose hydrogel. Extensive axonal regrowth across the biofabricated grafts was observed. In another study, 3D-printed NSC-loaded polyurethane (PU) constructs were tested in a zebra fish embryo neural injury model (Hsieh et al., 2015). After creating a defect in the nervous system, PU dispersions and NSCs were mixed, or only NSC suspensions were printed and implanted at the defect site. The adult zebra fish with a traumatic brain injury recovered after implantation of 3D printed NSC carrying PU constructs. Embryos injected with only NSCs showed low cell survival and the NSCs were not distributed in an aligned fashion.

3D printing was also combined with other techniques to enhance the properties of the nerve tissue constructs. For example, electrospinning together with printing was tested to increase the mechanical properties of the scaffolds (Lee S.-J. et al., 2017). PEGDA scaffolds were printed on electrospun PCL or PCL/gelatin fibers. Scaffolds with PCL/gelatin fibers had more neural stem cells that adhered, the average neurite length increased and directed neurite extension of primary cortical

neurons was observed along the fibers. Nerve tissue engineering applications of 3D printing are also summarized in **Table 5**.

Vascular Tissue Engineering Applications

Vascularization is one of the most important aspects of tissue regeneration, therefore, 3D printing introduces vascularization strategies and adds its advantages to create vasculature and therefore, healthy vascularized constructs (Duan, 2017). Even though stereolithography and ink-jet printing are used to print PCL and PPF products, most of the applications nowadays focus on bioprinting (Melchiorri et al., 2016; Huang et al., 2018). HUVECs are the most preferred cell type in cell printing studies to achieve vascularization (Itoh et al., 2015). Smooth muscle cells (SMCs) and fibroblasts are also incorporated into the construct structure. In some studies, scaffold-free constructs composed of multicellular aggregates, spheroids were printed (Norotte et al., 2009). Three-dimensional printed vascular grafts made of Matrigel and endothelial progenitor cells (EPCs) were tested on mice (Poldervaart et al., 2014). MSC-loaded heart tissue-derived ECM were also implanted in rats (Jang et al., 2017). All these studies showed promising vascularization results. Vascular tissue engineering applications of 3D printing are also summarized in **Table 5**.

Other Tissue Engineering Applications

Three-dimensional printing has been employed in cartilage, meniscus, cornea, and urethra tissue engineering applications. For example, for cartilage tissue engineering, SLS (Chen et al., 2014), ink-jet bioprinting (Markstedt et al., 2015), and extrusion-based bioprinting (Yang et al., 2018) were used. Nanocellulose, alginate, polyurethane (PU), collagen, and agarose are used as the printing polymers. Chondrocytes are the most frequently used cells in cartilage regeneration (Martínez Ávila et al., 2016). In a study, a bioactive molecule, TGF β3, was incorporated into 3D printed PU constructs to achieve cartilage regeneration (Hung et al., 2016). The scaffolds promoted self-aggregation of MSCs with a controlled release of the bioactive ingredients and when implanted into rabbit osteochondral defects, they showed cartilage regeneration at the defect site.

Three-dimensional printing techniques are also used in meniscus tissue engineering applications. In a study, GelMA scaffolds printed with SLA were implanted into a meniscus defect in an explant organ culture model (Grogan et al., 2013). Results demonstrated that micropatterned GelMA scaffolds produce cellular alignment and promoted meniscus-like tissue formation. PCL is one of the most commonly used polymers for cartilage tissue engineering applications (Cengiz et al., 2016; Szojka et al., 2017). An artificial meniscus shaped PCL scaffold was printed with cartilage-like inside and fibrocartilage-like outer component (Bahcecioglu et al., 2018). In that study, agarose (Ag) and GelMA hydrogels were added onto PCL as the inner and outer regions, respectively. Ag increased glycosaminoglycan (GAG) production 4-fold, while GelMA enhanced collagen production ca. 50-fold after being seeded with porcine fibrochondrocytes. In a related study, porcine fibrochondrocyte-seeded hydrogels, such as agarose, GelMA, HAMA, and GelMA-HAMA were combined with 3D printed PCL scaffolds and evaluated under static and dynamic compression conditions (Bahcecioglu et al., 2019). After 35 days, cell carrying hydrogels produced higher levels of ECM components than the 3D printed PCL control.

TABLE 6 | 4D printing of polymers for tissue engineering applications.

Application	Technique	External stimulus	Polymer type	Cells used	References
Fabrication of 3D tissue constructs	Extrusion based bioprinting	Biological (Cell-laid mineralized ECM)	PCL, PLGA, β-TCP	Human nasal inferior turbinate tissue derived MSCs	Pati et al., 2015
Materials for self-evolving deformation	Inkjet printing	Humidity	Vinyl Caprolactam, Polyethylene	–	Raviv et al., 2014
Tissue engineering	Extrusion based AM	Humidity	Nanofibrillated cellulose	–	Gladman et al., 2016
Optogenetic muscle ring-powered biobots	SLA	Light	PEGDA	C2C12 murine myoblasts	Raman et al., 2016
Bone tissue engineering	FDM	Magnetic	Fe_3O_4/MBG/PCL	Human BMSCs	Zhang et al., 2014
Tissue engineering scaffolds	FDM and SLA	Magnetic	PCL/Fe_3O_4	Human MSCs	De Santis et al., 2015
			PEGDA/Fe_3O_4		
Bone tissue engineering	FDM	Magnetic	PCL/iron-doped HAP	Human MSCs	D'Amora et al., 2017
Endoluminal medical devices	UV-LED SLA	Temperature	Methacrylated polycaprolactone	–	Zarek et al., 2016b
Biomedical scaffolds	SLA	Temperature	Soybean oil epoxidized acrylate	Human bone marrow MSCs	Miao et al., 2016b
Tissue engineering scaffolds	FDM	Temperature	Polycaprolactone triol	Primary human bone marrow MSCs	Miao et al., 2016a
Cardiac regeneration	Photolithographic SLA-tandem strategy	Temperature	Soybean oil epoxidized acrylate	hMSCs	Miao et al., 2018
Soft robotic and surgical application	Photolithography	Temperature and Magnetic	Poly(*N*-isopropylacrylamide-*co*-acrylic acid)	L929	Breger et al., 2015

A limited numbers of studies were reported for 3D printing of corneal tissues. Collagen-based 3D bioprinted scaffolds containing corneal keratocytes were studied and keratocytes exhibited high cell viability on days 1 (>90%) and 7 (83%) in the culture medium (Isaacson et al., 2018). In a different study, 3D cornea mimicking tissues were constructed by laser assisted bioprinting (LAB) using human embryonic stem cell derived limbal epithelial stem cells (hESC-LESC) and human adipose tissue derived stem cells (hADSCs) (Sorkio et al., 2018). The structure of the 3D bioprinted stroma showed that the hADSCs aligned horizontally and also demonstrated expression of collagen type I. They attached to the host tissue with hADSCs migration from the printed structure after 7 days in porcine organ cultures.

Zhang et al. printed cell-loaded urethra in order to mimic the structure and mechanical properties of the natural urethra of rabbits (Zhang K. et al., 2017). The tubular scaffold was fabricated using an integrated bioprinting system, with urothelial cells (UCs) and smooth muscle cells (SMCs). Results showed that mechanical properties of the polycaprolactone (PCL)/poly(lactide-co-caprolactone) (PLCL) (50:50) spiral scaffold were equivalent to the native urethra in the rabbit. Both UCs and SMCs maintained more than 80% viability 7 days after printing and expressed specific biomarkers in the cell-loaded hydrogel.

In some studies, 3D printing techniques are combined with near field electrospinning (NFES) to introduce highly aligned and reproducible fibrous structures into the 3D printed scaffolds. NFES technology provides precise control over the orientation of the fibers. Therefore, it is generally used in the development of anisotropic tissues, such as the nerve, cornea, and muscle (He et al., 2017). In this study, melt near field electrospinning was used in a direct writing mode onto a rotating cylindrical collector (drum) to fabricate tubular scaffolds (Brown et al., 2012). Primary human osteoblasts (hOB), mouse osteoblasts (mOB), and human mesothelial cells infiltrated into the fibrillar scaffolds, and the resultant architecture produced by the application of these processes was found to be supportive of cells spanning between adjacent fibers. Yan et al. (2014) also printed chitosan-gelatin composite scaffolds, and chitosan-PVA fibers produced by NFES were integrated with this 3D printed structure. This macro/micro-controlled tissue engineering scaffold had proper porosity (55%) and mechanical strength (modulus of elasticity of 288 MPa). In another study, poly(methyl methacrylate) (PMMA) fibers were printed in between 3D collagen gels loaded with hMSCs to create an anisotropic platform for cell growth and proliferation (Fattahi et al., 2017). Aligned PMMA fibers supported hMSCs growth, aligned them within the gels, and increased the anisotropic properties of gels.

4D PRINTING APPLICATIONS

Four-dimensional printing includes groups of programmable responsive self-assembly, self-folding or self-accommodating technologies (An et al., 2016). Programmable design, the 3D printing process, and triggering by external stimuli, such as temperature and light are the three main components of 4D printing. Smart materials which have the ability to change their properties under the influence of external signals are the basis of 4D printing applications (Khoo et al., 2015).

Like in 3D printing applications, SLA (Raman et al., 2016), AM (Hendrikson et al., 2017), FDM (Miao et al., 2016b), and bioprinting (Pati et al., 2015) techniques are employed in 4D printing applications. Four-dimensional bioprinting is used in tissue engineering applications because it is possible to fabricate sensitive and complex structures by 4D printing (Gao et al., 2016). Responsive materials, such as poly(N-isopropylacrylamide-co-acrylic acid) (pNIPAM-AAc) (Breger et al., 2015), methacrylated polycaprolactone (Zarek et al., 2016b), polycaprolactone triol (Miao et al., 2016a), nanofibrillated cellulose (Gladman et al., 2016), soybean oil epoxidized acrylate (Miao et al., 2018), iron(III)oxide (Fe_3O_4) nanoparticles containing mesoporous bioactive glass/poly(ε-caprolactone) (Fe_3O_4/MBG/PCL) (Zhang et al., 2014), magnetic nanocomposite scaffolds consisting of PCL/Fe_3O_4 and poly(ethylene glycol diacrylate) (PEGDA)/Fe_3O_4 (De Santis et al., 2015), and PCL/iron-doped hydroxyapatite (PCL/FeHA) nanocomposite scaffolds (D'Amora et al., 2017) are used as printing materials for 4D printing. They respond to temperature, light, magnetic field, humidity, and change their properties, but mainly the shape. Mostly mesenchymal stem cells (MSCs) are utilized in *in vitro* studies of the 4D printed scaffolds (Pati et al., 2015). There are limited number of *in vivo* studies since it is a relatively new technique. Tissue engineering applications of 4D printing are summarized in **Table 6**.

CONCLUSION AND FUTURE PERSPECTIVES

Three-dimensional printing is becoming an indispensable tool in the production of devices and systems in biomaterials and tissue engineering areas. It changed the face of the biomaterials world with the production of patient specific devices that have the required shape and organization. Stimuli responsive materials, such as metals and polymers have been in use in the biomedical field, and the combination of material and responsiveness in a biomedical device creates 4D printing which introduces highly useful, viable, dynamic, and responsive systems in tissue engineering applications. As it is, 3D and 4D printing methods is still keeping researchers busy in their quest for producing novel biomaterials and biomedical devices. The current types of stimuli to which the materials are responsive to are quite well-known but is, unfortunately, limited. So, the development of different materials with multi-sensitivities for use in the enhancement of the dynamic nature of devices is still a challenging issue.

AUTHOR CONTRIBUTIONS

DT, TD, and AA wrote the first draft. DY, NH, and VH edited, revised, and finalized the text.

REFERENCES

Adedoyin, A. A., and Ekenseair, A. K. (2018). Biomedical applications of magneto-responsive scaffolds. *Nano Res.* 11, 5049–5064. doi: 10.1007/s12274-018-2198-2

Aguilar, M. R., and San Román, J. (2014). "Introduction to smart polymers and their applications," in *Smart Polymers and their Applications*, eds M. R. Aguilar and J. San Román (Cambridge: Woodhead Publishing), 1–11. doi: 10.1533/9780857097026.1

An, J., Chua, C. K., and Mironov, V. (2016). A Perspective on 4D Bioprinting. *Int. J. Bioprint.* 2, 3–5. doi: 10.18063/IJB.2016.01.003

Bagherifam, S., Skjeldal, F. M., Griffiths, G., Mælandsmo, G. M., Engebråten, O., Nyström, B., et al. (2015). pH-responsive nano carriers for doxorubicin delivery. *Pharm. Res.* 32, 1249–1263. doi: 10.1007/s11095-014-1530-0

Bahcecioglu, G., Hasirci, N., Bilgen, B., and Hasirci, V. (2018). A 3D printed PCL/hydrogel construct with zone-specific biochemical composition mimicking that of the meniscus. *Biofabrication* 11:2. doi: 10.1088/1758-5090/aaf707

Bahcecioglu, G., Hasirci, N., Bilgen, B., and Hasirci, V. (2019). Hydrogels of agarose, and methacrylated gelatin and hyaluronic acid are more supportive for *in vitro* meniscus regeneration than three dimensional printed polycaprolactone scaffolds. *Int. J. Biol. Macromol.* 122, 1152–1162. doi: 10.1016/J.IJBIOMAC.2018.09.065

Bai, J., Goodridge, R. D., Yuan, S., Zhou, K., Chua, C. K., and Wei, J. (2015). Thermal influence of CNT on the polyamide 12 nanocomposite for selective laser sintering. *Molecules* 20, 19041–19050. doi: 10.3390/molecules201019041

Bendtsen, S. T., Quinnell, S. P., and Wei, M. (2017). Development of a novel alginate-polyvinyl alcohol-hydroxyapatite hydrogel for 3D bioprinting bone tissue engineered scaffolds. *J. Biomed. Mater. Res. A* 105, 1457–1468. doi: 10.1002/jbm.a.36036

Bhushan, B., and Caspers, M. (2017). An overview of additive manufacturing (3D printing) for microfabrication. *Microsyst. Technol.* 23, 1117–1124. doi: 10.1007/s00542-017-3342-8

Billiet, T., Vandenhaute, M., Schelfhout, J., Van Vlierberghe, S., and Dubruel, P. (2012). A review of trends and limitations in hydrogel-rapid prototyping for tissue engineering. *Biomaterials* 33, 6020–6604. doi: 10.1016/j.biomaterials.2012.04.050

Breger, J. C., Yoon, C., Xiao, R., Kwag, H. R., Wang, M. O., Fisher, J. P., et al. (2015). Self-folding thermo-magnetically responsive soft microgrippers. *ACS Appl. Mater. Interfaces* 7, 3398–3405. doi: 10.1021/am508621s

Brown, T. D., Slotosch, A., Thibaudeau, L., Taubenberger, A., Loessner, D., Vaquette, C., et al. (2012). Design and fabrication of tubular scaffolds via direct writing in a melt electrospinning mode. *Biointerphases* 7, 1–16. doi: 10.1007/s13758-011-0013-7

Brunello, G., Sivolella, S., Meneghello, R., Ferroni, L., Gardin, C., Piattelli, A., et al. (2016). Powder-based 3D printing for bone tissue engineering. *Biotechnol. Adv.* 34, 740–753. doi: 10.1016/j.biotechadv.2016.03.009

Buyuksungur, S., Endogan Tanir, T., Buyuksungur, A., Bektas, E. I., Torun Kose, G., Yucel, D., et al. (2017). 3D printed poly(ε-caprolactone) scaffolds modified with hydroxyapatite and poly(propylene fumarate) and their effects on the healing of rabbit femur defects. *Biomater. Sci.* 5, 2144–2158. doi: 10.1039/C7BM00514H

Cabane, E., Zhang, X., Langowska, K., Palivan, C. G., and Meier, W. (2012). Stimuli-responsive polymers and their applications in nanomedicine. *Biointerphases* 7:9. doi: 10.1007/s13758-011-0009-3

Carlier, A., Skvortsov, G. A., Hafezi, F., Ferraris, E., Patterson, J., Koç, B., et al. (2016). Computational model-informed design and bioprinting of cell-patterned constructs for bone tissue engineering. *Biofabrication* 8:025009. doi: 10.1088/1758-5090/8/2/025009

Casavola, C., Cazzato, A., Moramarco, V., and Pappalettere, C. (2016). Orthotropic mechanical properties of fused deposition modelling parts described by classical laminate theory. *Mater. Des.* 90, 453–458. doi: 10.1016/j.matdes.2015.11.009

Casolaro, M., and Casolaro, I. (2017). Pulsed release of antidepressants from nanocomposite hydrogels. *Biol. Eng. Med.* 2, 1–8. doi: 10.15761/BEM.1000132

Cengiz, I. F., Pitikakis, M., Cesario, L., Parascandolo, P., Vosilla, L., Viano, G., et al. (2016). Building the basis for patient-specific meniscal scaffolds: from human knee MRI to fabrication of 3D printed scaffolds. *Bioprinting* 1, 1–10. doi: 10.1016/j.bprint.2016.05.001

Cha, C., Piraino, F., and Khademhosseini, A. (2014). "Microfabrication technology in tissue engineering," in *Tissue Engineering*, eds A. Clemens, B. Van, and D. Jan (London: Academic Press), 283–310. doi: 10.1016/B978-0-12-420145-3.00009-2

Chang, B., Sha, X., Guo, J., Jiao, Y., Wang, C., and Yang, W. (2011). Thermo and pH dual responsive, polymer shell coated, magnetic mesoporous silica nanoparticles for controlled drug release. *J. Mater. Chem.* 21, 9239–9247. doi: 10.1039/C1JM10631G

Chen, C.-H., Shyu, V. B.-H., Chen, J.-P., and Lee, M.-Y. (2014). Selective laser sintered poly-ε-caprolactone scaffold hybridized with collagen hydrogel for cartilage tissue engineering. *Biofabrication* 6:015004. doi: 10.1088/1758-5082/6/1/015004

Chen, C.-S., Zeng, F., Xiao, X., Wang, Z., Li, X.-L., Tan, R.-W., et al. (2018). Three-dimensionally printed silk-sericin-based hydrogel scaffold: a promising visualized dressing material for real-time monitoring of wounds. *ACS Appl. Mater. Interfaces* 10, 33879–33890. doi: 10.1021/acsami.8b10072

Chia, H. N., and Wu, B. M. (2015). Recent advances in 3D printing of biomaterials. *J. Biol. Eng.* 9:4. doi: 10.1186/s13036-015-0001-4

Choi, J., Kwon, O. C., Jo, W., Lee, H. J., and Moon, M. W. (2015). 4D printing technology: a review. *3D Print. Addit. Manuf.* 2, 159–167. doi: 10.1089/3dp.2015.0039

Chua, C. K., Leong, K. F., Tan, K. H., Wiria, F. E., and Cheah, C. M. (2004). Development of tissue scaffolds using selective laser sintering of polyvinyl alcohol/hydroxyapatite biocomposite for craniofacial and joint defects. *J. Mater. Sci. Mater. Med.* 15, 1113–1121. doi: 10.1023/B:JMSM.0000046393.81449.a5

Colasante, C., Sanford, Z., Garfein, E., and Tepper, O. (2016). Current trends in 3D printing, bioprosthetics, and tissue engineering in plastic and reconstructive surgery. *Curr. Surg. Rep.* 4:6. doi: 10.1007/s40137-016-0127-4

Cubo, N., Garcia, M., del Cañizo, J. F., Velasco, D., and Jorcano, J. L. (2016). 3D bioprinting of functional human skin: production and *in vivo* analysis. *Biofabrication* 9:015006. doi: 10.1088/1758-5090/9/1/015006

Cui, H., Zhu, W., Nowicki, M., Zhou, X., Khademhosseini, A., and Zhang, L. G. (2016). Hierarchical fabrication of engineered vascularized bone biphasic constructs via dual 3D bioprinting: integrating regional bioactive factors into architectural design. *Adv. Healthc. Mater.* 5, 2174–2181. doi: 10.1002/adhm.201600505

Cui, J., and Del Campo, A. (2014). "Photo-responsive polymers: properties, synthesis and applications," in *Smart Polymers and Their Applications*, eds M. R. Aguilar and J. San Román (Cambridge: Woodhead Publishing), 93–133. doi: 10.1533/9780857097026.1.93

Cui, J., Kratz, K., Heuchel, M., Hiebl, B., and Lendlein, A. (2011). Mechanically active scaffolds from radio-opaque shape-memory polymer-based composites. *Polym. Adv. Technol.* 22, 180–189. doi: 10.1002/pat.1733

Cui, X., Boland, T., D'Lima, D. D., and Lotz, M. K. (2012). Thermal inkjet printing in tissue engineering and regenerative medicine. *Recent. Pat. Drug. Deliv. Formul.* 6, 149–155. doi: 10.2174/187221128006729 49

Cunniffe, G. M., Gonzalez-Fernandez, T., Daly, A., Sathy, B. N., Jeon, O., Alsberg, E., et al. (2017). Three-dimensional bioprinting of polycaprolactone reinforced gene activated bioinks for bone tissue engineering. *Tissue Eng. Part A* 23, 891–900. doi: 10.1089/ten.tea.2016.0498

D'Amora, U., Russo, T., Gloria, A., Rivieccio, V., D'Antò, V., Negri, G., et al. (2017). 3D additive-manufactured nanocomposite magnetic scaffolds: effect of the application mode of a time-dependent magnetic field on hMSCs behavior. *Bioact. Mater.* 2, 138–145. doi: 10.1016/J.BIOACTMAT.2017.04.003

Davis, D. A., Hamilton, A., Yang, J., Cremar, L. D., Van Gough, D., Potisek, S. L., et al. (2009). Force-induced activation of covalent bonds in mechanoresponsive polymeric materials. *Nature* 459, 68–72. doi: 10.1038/nature07970

De Santis, R., D'Amora, U., Russo, T., Ronca, A., Gloria, A., and Ambrosio, L. (2015). 3D fibre deposition and stereolithography techniques for the design of multifunctional nanocomposite magnetic scaffolds. *J. Mater. Sci. Mater. Med.* 26:250. doi: 10.1007/s10856-015-5582-4

Deckard, C. R. (1989). *Method and Apparatus for Producing Parts by Selective Sintering*. U.S. Patent No. 4,863,538. Washington, DC: U.S. Patent and Trademark Office.

Do, A. V., Khorsand, B., Geary, S. M., and Salem, A. K. (2015). 3D printing of scaffolds for tissue regeneration applications. *Adv. Healthc. Mat.* 4, 1742–1762. doi: 10.1002/adhm.201500168

Du, X. (2018). 3D bio-printing review. *IOP Conf. Ser. Mater. Sci. Eng.* 301:012023. doi: 10.1088/1757-899X/301/1/012023

Duan, B. (2017). State-of-the-art review of 3D bioprinting for cardiovascular tissue engineering. *Ann. Biomed. Eng.* 45, 195–209. doi: 10.1007/s10439-016-1607-5

Duarte Campos, D. F., Blaeser, A., Buellesbach, K., Sen, K. S., Xun, W., Tillmann, W., et al. (2016). Bioprinting organotypic hydrogels with improved mesenchymal stem cell remodeling and mineralization properties for bone tissue engineering. *Adv. Healthc. Mater.* 5, 1336–1345. doi: 10.1002/adhm.201501033

Dutta, S., and Cohn, D. (2017). Temperature and pH responsive 3D printed scaffolds. *J. Mater. Chem. B* 5, 9514–9521. doi: 10.1039/C7TB02368E

Eosoly, S., Brabazon, D., Lohfeld, S., and Looney, L. (2010). Selective laser sintering of hydroxyapatite/poly-ε-caprolactone scaffolds. *Acta Biomater.* 6, 2511–2517. doi: 10.1016/j.actbio.2009.07.018

Eosoly, S., Vrana, N. E., Lohfeld, S., Hindie, M., and Looney, L. (2012). Interaction of cell culture with composition effects on the mechanical properties of polycaprolactone-hydroxyapatite scaffolds fabricated via selective laser sintering (SLS). *Mat. Sci. Eng. C* 32, 2250–2257. doi: 10.1016/J.MSEC.2012.06.011

Ercole, F., Davis, T. P., and Evans, R. A. (2010). Photo-responsive systems and biomaterials: photochromic polymers, light-triggered self-assembly, surface modification, fluorescence modulation and beyond. *Polym. Chem.* 1, 37–54. doi: 10.1039/B9PY00300B

Fattahi, P., Dover, J. T., and Brown, J. L. (2017). 3D near-field electrospinning of biomaterial microfibers with potential for blended microfiber-cell-loaded gel composite structures. *Adv. Healthc. Mat.* 6, 1–9. doi: 10.1002/adhm.201700456

Fedorovich, N. E., Swennen, I., Girones, J., Moroni, L., Van Blitterswijk, C. A., Schacht, E., et al. (2009). Evaluation of photocrosslinked lutrol hydrogel for tissue printing applications. *Biomacromolecules* 10, 1689–1696. doi: 10.1021/bm801463q

Fuhrer, R., Hofmann, S., Hild, N., Vetsch, J. R., Herrmann, I. K., Grass, R. N., et al. (2013). Pressureless mechanical induction of stem cell differentiation is dose and frequency dependent. *PLoS ONE* 8:e81362. doi: 10.1371/journal.pone.0081362

Gao, B., Yang, Q., Zhao, X., Jin, G., Ma, Y., and Xu, F. (2016). 4D bioprinting for biomedical applications. *Trends Biotechnol.* 34, 746–756. doi: 10.1016/J.TIBTECH.2016.03.004

Gao, G., Schilling, A. F., Hubbell, K., Yonezawa, T., Truong, D., Hong, Y., et al. (2015). Improved properties of bone and cartilage tissue from 3D inkjet-bioprinted human mesenchymal stem cells by simultaneous deposition and photocrosslinking in PEG-GelMA. *Biotechnol. Lett.* 37, 2349–2355. doi: 10.1007/s10529-015-1921-2

Gladman, A. S., Matsumoto, E. A., Nuzzo, R. G., Mahadevan, L., and Lewis, J. A. (2016). Biomimetic 4D printing. *Nat. Mater.* 15, 413–418. doi: 10.1016/j.proeng.2018.01.056

Grogan, S. P., Chung, P. H., Soman, P., Chen, P., Lotz, M. K., Chen, S., et al. (2013). Digital micromirror device projection printing system for meniscus tissue engineering. *Acta Biomater.* 9, 7218–7226. doi: 10.1016/j.actbio.2013.03.020

Gruene, M., Unger, C., Koch, L., Deiwick, A., and Chichkov, B. (2011). Dispensing pico to nanolitre of a natural hydrogel by laser-assisted bioprinting. *Biomed. Eng. Online* 10:19. doi: 10.1186/1475-925X-10-19

Gu, Q., Tomaskovic-Crook, E., Lozano, R., Chen, Y., Kapsa, R. M., Zhou, Q., et al. (2016). Functional 3D neural mini-tissues from printed gel-based bioink and human neural stem cells. *Adv. Healthc. Mater.* 5, 1429–1438. doi: 10.1002/adhm.201600095

Guvendiren, M., Molde, J., Soares, R. M., and Kohn, J. (2016). Designing biomaterials for 3D printing. *ACS Biomater Sci. Eng.* 2, 1679–1693. doi: 10.1021/acsbiomaterials.6b00121

Haq, M. A., Su, Y., and Wang, D. (2017). Mechanical properties of PNIPAM based hydrogels: a review. *Mater. Sci. Eng. C* 70, 842–855. doi: 10.1016/j.msec.2016.09.081

Hasirci, V., and Hasirci, N. (2018). "Controlled release systems," in *Fundamentals of Biomaterials* (New York, NY: Springer), 257–279. doi: 10.1007/978-1-4939-8856-3

He, X. X., Zheng, J., Yu, G. F., You, M. H., Yu, M., Ning, X., et al. (2017). Near-field electrospinning: progress and applications. *J. Phys. Chem. C* 121, 8663–8678. doi: 10.1021/acs.jpcc.6b12783

Hendrikson, W. J., Rouwkema, J., Clementi, F., Van Blitterswijk, C. A., Farè, S., and Moroni, L. (2017). Towards 4D printed scaffolds for tissue engineering: exploiting 3D shape memory polymers to deliver time-controlled stimulus on cultured cells. *Biofabrication* 9:031001. doi: 10.1088/1758-5090/aa8114

Hoogenboom, R. (2014). "Temperature-responsive polymers: properties, synthesis and applications," in *Smart Polymers and Their Applications*, eds M. R. Aguilar and J. San Román (Cambridge: Woodhead Publishing), 15–44. doi: 10.1533/9780857097026.1.15

Hsieh, F.-Y., Lin, H.-H., and Hsu, S. H. (2015). 3D bioprinting of neural stem cell-laden thermoresponsive biodegradable polyurethane hydrogel and potential in central nervous system repair. *Biomaterials* 71, 48–57. doi: 10.1016/J.BIOMATERIALS.2015.08.028

Huang, R., Gao, X., Wang, J., Chen, H., Tong, C., Tan, Y., et al. (2018). Triple-layer vascular grafts fabricated by combined E-jet 3D printing and electrospinning. *Ann. Biomed. Eng.* 46, 1254–1266. doi: 10.1007/s10439-018-2065-z

Huang, Y., Zhang, X. F., Gao, G., Yonezawa, T., and Cui, X. (2017). 3D bioprinting and the current applications in tissue engineering. *Biotechnol. J.* 12:1600734. doi: 10.1002/biot.201600734

Huang, Y.-C., Simmons, C., Kaigler, D., Rice, K. G., and Mooney, D. J. (2005). Bone regeneration in a rat cranial defect with delivery of PEI-condensed plasmid DNA encoding for bone morphogenetic protein-4 (BMP-4). *Gene Ther.* 12, 418–426. doi: 10.1038/sj.gt.3302439

Hull, C. W. (1986). *Patent: Apparatus for Production of Three-Dimensional Objects by Stereolithography*. U.S. Patent No. 4,575,330. Washington, DC: U.S. Patent and Trademark Office.

Hung, K.-C., Tseng, C.-S., Dai, L.-G., and Hsu, S. H. (2016). Water-based polyurethane 3D printed scaffolds with controlled release function for customized cartilage tissue engineering. *Biomaterials* 83, 156–168. doi: 10.1016/J.BIOMATERIALS.2016.01.019

Hutmacher, D. W., Schantz, T., Zein, I., Ng, K. W., Teoh, S. H., and Tan, K. C. (2001). Mechanical properties and cell cultural response of polycaprolactone scaffolds designed and fabricated via fused deposition modeling. *J. Biomed. Mater. Res. A* 55, 203–216. doi: 10.1002/1097-4636(200105)55:2<203::AID-JBM1007>3.0.CO;2-7

Isaacson, A., Swioklo, S., and Connon, C. J. (2018). 3D bioprinting of a corneal stroma equivalent. *Exp. Eye Res.* 173, 188–193. doi: 10.1016/j.exer.2018.05.010

Itoh, M., Nakayama, K., Noguchi, R., Kamohara, K., Furukawa, K., Uchihashi, K., et al. (2015). Scaffold-free tubular tissues created by a Bio-3D printer undergo remodeling and endothelialization when implanted in rat aortae. *PLoS ONE* 10:e0136681. doi: 10.1371/journal.pone.0136681

Jang, J., Park, H.-J., Kim, S.-W., Kim, H., Park, J. Y., Na, S. J., et al. (2017). 3D printed complex tissue construct using stem cell-laden decellularized extracellular matrix bioinks for cardiac repair. *Biomaterials* 112, 264–274. doi: 10.1016/J.BIOMATERIALS.2016.10.026

Javaid, M., and Haleem, A. (2018). 4D printing applications in medical field: a brief review. *Clin. Epidemiol. Glob. Health* doi: 10.1016/j.cegh.2018.09.007. [Epub ahead of print].

Ji, K., Wang, Y., Wei, Q., Zhang, K., Jiang, A., Rao, Y., et al. (2018). Application of 3D printing technology in bone tissue engineering. *Biodes. Manuf.* 1, 203–210. doi: 10.1007/s42242-018-0021-2

Jung, C. Y., So, H. H., and Cho, W. J. (2006). Water-responsive shape memory polyurethane block copolymer modified with polyhedral oligomeric silsesquioxane. *J. Macromol. Sci. B.* 45, 453–461. doi: 10.1080/00222340600767513

Kalista S. J. Jr., and Ward, T. C. (2006). Thermal characteristics of the self-healing response in poly(ethylene-co-methacrylic acid) copolymers. *J. R. Soc. Interface* 4, 405–411. doi: 10.1098/rsif.2006.0169

Kalista, S. J. Jr., Ward, T. C., and Oyetunji, Z. (2007). Self-healing of poly(ethylene-co-methacrylic acid) copolymers following projectile puncture. *Mech. Adv. Mater. Struc.* 14, 391–397. doi: 10.1080/15376490701298819

Kao, C.-T., Lin, C.-C., Chen, Y.-W., Yeh, C.-H., Fang, H.-Y., and Shie, M.-Y. (2015). Poly(dopamine) coating of 3D printed poly(lactic acid) scaffolds for bone tissue engineering. *Mater. Sci. Eng. C* 56, 165–173. doi: 10.1016/J.MSEC.2015.06.028

Keriquel, V., Oliveira, H., Rémy, M., Ziane, S., Delmond, S., Rousseau, B., et al. (2017). *In situ* printing of mesenchymal stromal cells, by laser-assisted bioprinting, for *in vivo* bone regeneration applications. *Sci. Rep.* 7:1778. doi: 10.1038/s41598-017-01914-x

Khoo, Z. X., Teoh, J. E. M., Liu, Y., Chua, C. K., Yang, S., An, J., et al. (2015). 3D printing of smart materials: a review on recent progresses in 4D printing. *Virtual Phys. Prototyp.* 10, 103–122. doi: 10.1080/17452759.2015.1097054

Kim, B. S., Kwon, Y. W., Kong, J.-S., Park, G. T., Gao, G., Han, W., et al. (2018). 3D cell printing of *in vitro* stabilized skin model and *in vivo* pre-vascularized skin patch using tissue-specific extracellular matrix bioink: a

step towards advanced skin tissue engineering. *Biomaterials* 168, 38–53. doi: 10.1016/J.BIOMATERIALS.2018.03.040

Knowlton, S., Anand, S., Shah, T., and Tasoglu, S. (2018). Bioprinting for neural tissue engineering. *Trends Neurosci.* 41, 31–46. doi: 10.1016/j.tins.2017.11.001

Kocak, G., Tuncer, C., and Butun, V. (2017). pH-Responsive polymers. *Polym. Chem.* 8, 144–176. doi: 10.1039/C6PY01872F

Koch, L., Deiwick, A., Schlie, S., Michael, S., Gruene, M., Coger, V., et al. (2012). Skin tissue generation by laser cell printing. *Biotechnol. Bioeng.* 109, 1855–1863. doi: 10.1002/bit.24455

Kodama, H. (1981). Automatic method for fabricating a three-dimensional plastic model with photo-hardening polymer. *Rev. Sci. Instrum.* 52, 1770–1773. doi: 10.1063/1.1136492

Kokkinis, D., Schaffner, M., and Studart, A. R. (2015). Multimaterial magnetically assisted 3D printing of composite materials. *Nat. Commun.* 6:8643. doi: 10.1038/ncomms9643

Kolesky, D. B., Truby, R. L., Gladman, A. S., Busbee, T. A., Homan, K. A., and Lewis, J. A. (2014). 3D bioprinting of vascularized, heterogeneous cell-laden tissue constructs. *Adv. Mater.* 26, 3124–3130. doi: 10.1002/adma.201305506

Koroleva, A., Gill, A. A., Ortega, I., Haycock, J. W., Schlie, S., Gittard, S. D., et al. (2012). Two-photon polymerization-generated and micromolding-replicated 3D scaffolds for peripheral neural tissue engineering applications. *Biofabrication* 4:025005. doi: 10.1088/1758-5082/4/2/025005

Kucukgul, C., Ozler, S. B., Inci, I., Karakas, E., Irmak, S., Gozuacik, D., et al. (2015). 3D bioprinting of biomimetic aortic vascular constructs with self-supporting cells. *Biotechnol. Bioeng.* 112, 811–821. doi: 10.1002/bit.25493

Kurtz, S. M., and Devine, J. N. (2007). PEEK biomaterials in trauma, orthopedic, and spinal implants. *Biomaterials* 28, 4845–4869. doi: 10.1016/j.biomaterials.2007.07.013

Lee, A. Y., An, J., and Chua, C. K. (2017). Two-way 4D printing: a review on the reversibility of 3D-printed shape memory materials. *Engineering* 3, 663–674. doi: 10.1016/J.ENG.2017.05.014

Lee, J. W., Kang, K. S., Lee, S. H., Kim, J.-Y., Lee, B.-K., and Cho, D.-W. (2011). Bone regeneration using a microstereolithography-produced customized poly(propylene fumarate)/diethyl fumarate photopolymer 3D scaffold incorporating BMP-2 loaded PLGA microspheres. *Biomaterials* 32, 744–752. doi: 10.1016/j.biomaterials.2010.09.035

Lee, M. P., Cooper, G. J., Hinkley, T., Gibson, G. M., Padgett, M. J., and Cronin, L. (2015). Development of a 3D printer using scanning projection stereolithography. *Sci. Rep.* 5:9875. doi: 10.1038/srep09875

Lee, S.-J., Nowicki, M., Harris, B., and Zhang, L. G. (2017). Fabrication of a highly aligned neural scaffold via a table top stereolithography 3D printing and electrospinning. *Tissue Eng. Part A* 23, 491–502. doi: 10.1089/ten.tea.2016.0353

Lee, S. J., Lee, D., Yoon, T. R., Kim, H. K., Jo, H. H., Park, J. S., et al. (2016). Surface modification of 3D-printed porous scaffolds via mussel-inspired polydopamine and effective immobilization of rhBMP-2 to promote osteogenic differentiation for bone tissue engineering. *Acta Biomater.* 40, 182–191. doi: 10.1016/J.ACTBIO.2016.02.006

Lee, W., Pinckney, J., Lee, V., Lee, J. H., Fischer, K., Polio, S., et al. (2009). Three-dimensional bioprinting of rat embryonic neural cells. *Neuroreport* 20, 798–803. doi: 10.1097/WNR.0b013e32832b8be4

Lee, Y. B., Polio, S., Lee, W., Dai, G., Menon, L., Carroll, R. S., et al. (2010). Bio-printing of collagen and VEGF-releasing fibrin gel scaffolds for neural stem cell culture. *Exp. Neurol.* 223, 645–652. doi: 10.1016/j.expneurol.2010.02.014

Li, D., and Xia, Y. (2004). Electrospinning of nanofibers: reinventing the wheel? *Adv. Mater.* 16, 1151–1170. doi: 10.1002/adma.200400719

Li, X., Shang, J., and Wang, Z. (2016). Intelligent materials: a review of applications in 4D printing. *Assembly Autom.* 37, 170–185. doi: 10.1108/AA-11-2015-093

Li, Y., Rios, O., Keum, J. K., Chen, J., and Kessler, M. R. (2016). Photoresponsive liquid crystalline epoxy networks with shape memory behavior and dynamic ester bonds. *ACS Appl. Mater. Interfaces* 8, 15750–15757. doi: 10.1021/acsami.6b04374

Li, Y. C., Zhang, Y. S., Akpek, A., Shin, S. R., and Khademhosseini, A. (2016). 4D bioprinting: the next-generation technology for biofabrication enabled by stimuli-responsive materials. *Biofabrication* 9:012001. doi: 10.1088/1758-5090/9/1/012001

Liao, H.-T., Chang, K.-H., Jiang, Y., Chen, J.-P., and Lee, M.-Y. (2011). Fabrication of tissue engineered PCL scaffold by selective laser-sintered machine for osteogeneisis of adipose-derived stem cells. *Virtual Phys. Prototyp.* 6, 57–60. doi: 10.1080/17452759.2011.559742

Liu, H., Peng, H., Wu, Y., Zhang, C., Cai, Y., Xu, G., et al. (2013). The promotion of bone regeneration by nanofibrous hydroxyapatite/chitosan scaffolds by effects on integrin-BMP/Smad signaling pathway in BMSCs. *Biomaterials* 34, 4404–4417. doi: 10.1016/J.BIOMATERIALS.2013.02.048

Loozen, L. D., Wegman, F., Öner, F. C., Dhert, W. J. A., and Alblas, J. (2013). Porous bioprinted constructs in BMP-2 non-viral gene therapy for bone tissue engineering. *J. Mater. Chem. B* 1, 6619–6626. doi: 10.1039/c3tb21093f

Lorber, B., Hsiao, W. K., Hutchings, I. M., and Martin, K. R. (2014). Adult rat retinal ganglion cells and glia can be printed by piezoelectric inkjet printing. *Biofabrication* 6:015001. doi: 10.1088/1758-5082/6/1/015001

Lozano, R., Stevens, L., Thompson, B. C., Gilmore, K. J., Gorkin, R., Stewart, E. M., et al. (2015). 3D printing of layered brain-like structures using peptide modified gellan gum substrates. *Biomaterials* 67, 264–273. doi: 10.1016/j.biomaterials.2015.07.022

Lv, C., Sun, X. C., Xia, H., Yu, Y. H., Wang, G., Cao, X. W., et al. (2018). Humidity-responsive actuation of programmable hydrogel microstructures based on 3D printing. *Sens. Actuators B Chem.* 259, 736–744. doi: 10.1016/j.snb.2017.12.053

Mandrycky, C., Wang, Z., Kim, K., and Kim, D. H. (2016). 3D bioprinting for engineering complex tissues. *Biotechnol. Adv.* 34, 422–434. doi: 10.1016/j.biotechadv.2015.12.011

Maniruzzaman, M. (Ed). (2019). *3D and 4D Printing in Biomedical Applications: Process Engineering and Additive Manufacturing*. Brighton: Wiley-VCH.

Marchand, M., Monnot, C., Muller, L., and Germain, S. (2018). Extracellular matrix scaffolding in angiogenesis and capillary homeostasis. *Semin. Cell Dev. Biol.* 89, 147–156. doi: 10.1016/j.semcdb.2018.08.007

Markstedt, K., Mantas, A., Tournier, I., Martínez Ávila, H., Hägg, D., and Gatenholm, P. (2015). 3D bioprinting human chondrocytes with nanocellulose–alginate bioink for cartilage tissue engineering applications. *Biomacromolecules* 16, 1489–1496. doi: 10.1021/acs.biomac.5b00188

Martínez Ávila, H., Schwarz, S., Rotter, N., and Gatenholm, P. (2016). 3D bioprinting of human chondrocyte-laden nanocellulose hydrogels for patient-specific auricular cartilage regeneration. *Bioprinting* 1, 22–35. doi: 10.1016/j.bprint.2016.08.003

Mazzoli, A. (2013). Selective laser sintering in biomedical engineering. *Med. Biol. Eng. Comput.* 51, 245–256. doi: 10.1007/s11517-012-1001-x

Mazzoli, A., Ferretti, C., Gigante, A., Salvolini, E., and Mattioli-Belmonte, M. (2015). Selective laser sintering manufacturing of polycaprolactone bone scaffolds for applications in bone tissue engineering. *Rapid. Prototyp. J.* 21, 386–392. doi: 10.1108/RPJ-04-2013-0040

Melchels, F. P., Feijen, J., and Grijpma, D. W. (2010). A review on stereolithography and its applications in biomedical engineering. *Biomaterials* 31, 6121–6130. doi: 10.1016/j.biomaterials.2010.04.050

Melchiorri, A. J., Hibino, N., Best, C. A., Yi, T., Lee, Y. U., Kraynak, C. A., et al. (2016). 3D-printed biodegradable polymeric vascular grafts. *Adv. Healthc. Mater.* 5, 319–325. doi: 10.1002/adhm.201500725

Miao, S., Cui, H., Nowicki, M., Lee, S. J., Almeida, J., Zhou, X., et al. (2018). Photolithographic-stereolithographic-tandem fabrication of 4D smart scaffolds for improved stem cell cardiomyogenic differentiation. *Biofabrication* 10:035007. doi: 10.1088/1758-5090/aabe0b

Miao, S., Zhu, W., Castro, N. J., Leng, J., and Zhang, L. G. (2016a). Four-dimensional printing hierarchy scaffolds with highly biocompatible smart polymers for tissue engineering applications. *Tissue Eng. Part C Methods* 22, 952–963. doi: 10.1089/ten.tec.2015.0542

Miao, S., Zhu, W., Castro, N. J., Nowicki, M., Zhou, X., Cui, H., et al. (2016b). 4D printing smart biomedical scaffolds with novel soybean oil epoxidized acrylate. *Sci. Rep.* 6:27226. doi: 10.1038/srep27226

Michael, S., Sorg, H., Peck, C.-T., Koch, L., Deiwick, A., Chichkov, B., et al. (2013). Tissue engineered skin substitutes created by laser-assisted bioprinting form skin-like structures in the dorsal skin fold chamber in mice. *PLoS ONE* 8:e57741. doi: 10.1371/journal.pone.0057741

Mondschein, R. J., Kanitkar, A., Williams, C. B., Verbridge, S. S., and Long, T. E. (2017). Polymer structure-property requirements for stereolithographic 3D printing of soft tissue engineering scaffolds. *Biomaterials* 140, 170–188. doi: 10.1016/j.biomaterials.2017.06.005

Montero, A., Valencia, L., Corrales, R., Jorcano, J. L., and Velasco, D. (2019). "Smart polymer gels: properties, synthesis, and applications," in

Smart Polymers and Their Applications, 2nd Edn., eds M. R. Aguilar and J. San Román (Cambridge: Woodhead Publishing), 279–321. doi: 10.1016/B978-0-08-102416-4.09992-0

Moroni, L., De Wijn, J. R., and Van Blitterswijk, C. A. (2005). Three-dimensional fiber-deposited PEOT/PBT copolymer scaffolds for tissue engineering: influence of porosity, molecular network mesh size, and swelling in aqueous media on dynamic mechanical properties. *J. Biomed. Mater. Res. A* 75, 957–965. doi: 10.1002/jbm.a.30499

Morrison, R. J., Hollister, S. J., Niedner, M. F., Mahani, M. G., Park, A. H., Mehta, D. K., et al. (2015). Mitigation of tracheobronchomalacia with 3D-printed personalized medical devices in pediatric patients. *Sci. Transl. Med.* 7:285ra64. doi: 10.1126/scitranslmed.3010825

Mosadegh, B., Xiong, G., Dunham, S., and Min, J. K. (2015). Current progress in 3D printing for cardiovascular tissue engineering. *Biomed. Mater.* 10:034002. doi: 10.1088/1748-6041/10/3/034002

Mota, C., Puppi, D., Chiellini, F., and Chiellini, E. (2015). Additive manufacturing techniques for the production of tissue engineering constructs. *J. Tissue. Eng. Regen. Med.* 9, 174–190. doi: 10.1002/term.1635

Mulakkal, M. C., Trask, R. S., Ting, V. P., and Seddon, A. M. (2018). Responsive cellulose-hydrogel composite ink for 4D printing. *Mater. Des.* 160, 108–118. doi: 10.1016/j.matdes.2018.09.009

Murphy, C., Kolan, K., Li, W., Semon, J., Day, D., and Leu, M. (2017). 3D bioprinting of stem cells and polymer/bioactive glass composite scaffolds for tissue engineering. *Int. J. Bioprint.* 3:1. doi: 10.18063/IJB.2017.01.005

Murphy, S. V., and Atala, A. (2014). 3D bioprinting of tissues and organs. *Nat. Biotechnol.* 32:773. doi: 10.1038/nbt.2958

Neuss, S., Blomenkamp, I., Stainforth, R., Boltersdorf, D., Jansen, M., Butz, N., et al. (2009). The use of a shape-memory poly (ε-caprolactone) dimethacrylate network as a tissue engineering scaffold. *Biomaterials* 30, 1697–1705. doi: 10.1016/j.biomaterials.2008.12.027

Ng, W. L., Yeong, W. Y., and Naing, M. W. (2015). Cellular approaches to tissue-engineering of skin: a review. *J. Tissue Sci. Eng.* 6, 1–9. doi: 10.4172/2157-7552.1000150

Ng, W. L., Yeong, W. Y., and Naing, M. W. (2016). Polyelectrolyte gelatin-chitosan hydrogel optimized for 3D bioprinting in skin tissue engineering. *Int. J. Bioprint.* 2, 53–62. doi: 10.18063/IJB.2016.01.009

Norotte, C., Marga, F. S., Niklason, L. E., and Forgacs, G. (2009). Scaffold-free vascular tissue engineering using bioprinting. *Biomaterials* 30, 5910–5917. doi: 10.1016/j.biomaterials.2009.06.034

Owens, C. M., Marga, F., Forgacs, G., and Heesch, C. M. (2013). Biofabrication and testing of a fully cellular nerve graft. *Biofabrication* 5:045007. doi: 10.1088/1758-5082/5/4/045007

Ozbolat, I. T., and Hospodiuk, M. (2016). Current advances and future perspectives in extrusion-based bioprinting. *Biomaterials* 76, 321–343. doi: 10.1016/j.biomaterials.2015.10.076

Ozturk, N., Girotti, A., Kose, G. T., Rodríguez-Cabello, J. C., and Hasirci, V. (2009). Dynamic cell culturing and its application to micropatterned, elastin-like protein-modified poly (N-isopropylacrylamide) scaffolds. *Biomaterials* 30, 5417–5426. doi: 10.1016/j.biomaterials.2009.06.044

Panseri, S., Russo, A., Giavaresi, G., Sartori, M., Veronesi, F., Fini, M., et al. (2012). Innovative magnetic scaffolds for orthopedic tissue engineering. *J. Biomed. Mater. Res. A* 100, 2278–2286. doi: 10.1002/jbm.a.34167

Park, S. A., Lee, S. H., and Kim, W. D. (2011). Fabrication of porous polycaprolactone/hydroxyapatite (PCL/HA) blend scaffolds using a 3D plotting system for bone tissue engineering. *Bioproc. Biosyst. Eng.* 34, 505–513. doi: 10.1007/s00449-010-0499-2

Pati, F., Song, T.-H., Rijal, G., Jang, J., Kim, S. W., and Cho, D.-W. (2015). Ornamenting 3D printed scaffolds with cell-laid extracellular matrix for bone tissue regeneration. *Biomaterials* 37, 230–241. doi: 10.1016/J.BIOMATERIALS.2014.10.012

Pei, E. (2014). 4D Printing: dawn of an emerging technology cycle. *Assembly Autom.* 34, 310–314. doi: 10.1108/AA-07-2014-062

Peltola, S. M., Melchels, F. P., Grijpma, D. W., and Kellomäki, M. (2008). A review of rapid prototyping techniques for tissue engineering purposes. *Ann. Med.* 40, 268–280. doi: 10.1080/07853890701881788

Pernal, S. P., Willis, A. J., and Engelhard, H. H. (2018). Magnetic nanoparticles (MNPs) for cancer drug delivery: the value of *in vitro* modeling. *Cancer Res.* 78:4661. doi: 10.1158/1538-7445.AM2018-4661

Peters, C., Hoop, M., Pané, S., Nelson, B. J., and Hierold, C. (2016). Degradable magnetic composites for minimally invasive interventions: device fabrication, targeted drug delivery, and cytotoxicity tests. *Adv. Mater.* 28, 533–538. doi: 10.1002/adma.201503112

Petrochenko, P. E., Torgersen, J., Gruber, P., Hicks, L. A., Zheng, J., Kumar, G., et al. (2015). Laser 3D printing with sub-microscale resolution of porous elastomeric scaffolds for supporting human bone stem cells. *Adv. Healthc. Mater.* 4, 739–747. doi: 10.1002/adhm.201400442

Poldervaart, M. T., Gremmels, H., van Deventer, K., Fledderus, J. O., Oner, F. C., Verhaar, M. C., et al. (2014). Prolonged presence of VEGF promotes vascularization in 3D bioprinted scaffolds with defined architecture. *J. Control. Release.* 184, 58–66. doi: 10.1016/j.jconrel.2014.04.007

Pourchet, L. J., Thepot, A., Albouy, M., Courtial, E. J., Boher, A., Blum, L. J., et al. (2017). Human skin 3D bioprinting using scaffold-free approach. *Adv. Healthc. Mater.* 6:1601101. doi: 10.1002/adhm.201601101

Raman, R., Cvetkovic, C., Uzel, S. G., Platt, R. J., Sengupta, P., Kamm, R. D., et al. (2016). Optogenetic skeletal muscle-powered adaptive biological machines. *Proc. Natl. Acad. Sci. U.S.A.* 113, 3497–3502. doi: 10.1073/pnas.1516139113

Rastogi, P., and Kandasubramanian, B. (2019). Breakthrough in the printing tactics for stimuli-responsive materials: 4D printing. *Chem. Eng. J.* 366, 264–304. doi: 10.1016/j.cej.2019.02.085

Ravi, P., Shiakolas, P. S., and Welch, T. R. (2017). Poly-l-lactic acid: pellets to fiber to fused filament fabricated scaffolds, and scaffold weight loss study. *Add. Manuf.* 16, 167–176. doi: 10.1016/j.addma.2017.06.002

Raviv, D., Zhao, W., Mcknelly, C., Papadopoulou, A., Kadambi, A., Shi, B., et al. (2014). Active printed materials for complex self-evolving deformations. *Sci. Rep.* 4, 1–9. doi: 10.1038/srep07422

Reyes-Ortega, F. (2014). "pH-responsive polymers: properties, synthesis and applications," in *Smart Polymers and Their Applications*, eds M. R. Aguilar and J. San Román (Cambridge: Woodhead Publishing), 45–92. doi: 10.1533/9780857097026.1.45

Rosenzweig, D. H., Carelli, E., Steffen, T., Jarzem, P., and Haglund, L. (2015). 3D-printed ABS and PLA scaffolds for cartilage and nucleus pulposus tissue regeneration. *Int. J. Mol. Sci.* 16, 15118–15135. doi: 10.3390/ijms160715118

Saito, E., Suarez-Gonzalez, D., Murphy, W. L., and Hollister, S. J. (2015). Biomineral coating increases bone formation by *ex vivo* BMP-7 gene therapy in rapid prototyped poly(l-lactic acid) (PLLA) and poly(ε-caprolactone) (PCL) porous scaffolds. *Adv. Healthc. Mater.* 4, 621–632. doi: 10.1002/adhm.201400424

Sapir-Lekhovitser, Y., Rotenberg, M. Y., Jopp, J., Friedman, G., Polyak, B., and Cohen, S. (2016). Magnetically actuated tissue engineered scaffold: Insights into mechanism of physical stimulation. *Nanoscale* 8, 3386–3399. doi: 10.1039/C5NR05500H

Sawkins, M. J., Mistry, P., Brown, B. N., Shakesheff, K. M., Bonassar, L. J., and Yang, J. (2015). Cell and protein compatible 3D bioprinting of mechanically strong constructs for bone repair. *Biofabrication* 7:035004. doi: 10.1088/1758-5090/7/3/035004

Schmidt, M., Pohle, D., and Rechtenwald, T. (2007). Selective laser sintering of PEEK. *CIRP Ann. Manuf. Technol.* 56, 205–208. doi: 10.1016/j.cirp.2007.05.097

Senatov, F. S., Niaza, K. V., Stepashkin, A. A., and Kaloshkin, S. D. (2016a). Low-cycle fatigue behavior of 3d-printed PLA-based porous scaffolds. *Compos. Part B Eng.* 97, 193–200. doi: 10.1016/j.compositesb.2016.04.067

Senatov, F. S., Niaza, K. V., Zadorozhnyy, M. Y., Maksimkin, A. V., Kaloshkin, S. D., and Estrin, Y. Z. (2016b). Mechanical properties and shape memory effect of 3D-printed PLA-based porous scaffolds. *J. Mech. Behav. Biomed. Mater.* 57, 139–148. doi: 10.1016/j.jmbbm.2015.11.036

Senatov, F. S., Zadorozhnyy, M. Y., Niaza, K. V., Medvedev, V. V., Kaloshkin, S. D., Anisimova, N. Y., et al. (2017). Shape memory effect in 3D-printed scaffolds for self-fitting implants. *Eur. Polym. J.* 93, 222–231. doi: 10.1016/j.eurpolymj.2017.06.011

Shuai, C., Mao, Z., Lu, H., Nie, Y., Hu, H., and Peng, S. (2013). Fabrication of porous polyvinyl alcohol scaffold for bone tissue engineering via selective laser sintering. *Biofabrication.* 5:015014. doi: 10.1088/1758-5082/5/1/015014

Skardal, A., and Atala, A. (2015). Biomaterials for integration with 3-D bioprinting. *Ann. Biomed. Eng.* 43, 730–746. doi: 10.1007/s10439-014-1207-1

Skoog, S. A., Goering, P. L., and Narayan, R. J. (2014). Stereolithography in tissue engineering. *J. Mater. Sci. Mater. Med.* 25, 845–856. doi: 10.1007/s10856-013-5107-y

Song, K., Yeom, E., Seo, S. J., Kim, K., Kim, H., Lim, J. H., et al. (2015). Journey of water in pine cones. *Sci. Rep.* 5:9963. doi: 10.1038/srep09963

Sorkio, A., Koch, L., Koivusalo, L., Deiwick, A., Miettinen, S., Chichkov, B., et al. (2018). Human stem cell based corneal tissue mimicking structures using laser-assisted 3D bioprinting and functional bioinks. *Biomaterials* 171, 57–71. doi: 10.1016/J.BIOMATERIALS.2018.04.034

Sumaru, K., Ohi, K., Takagi, T., Kanamori, T., and Shinbo, T. (2006). Photoresponsive properties of poly (N-isopropylacrylamide) hydrogel partly modified with spirobenzopyran. *Langmuir* 22, 4353–4356. doi: 10.1021/la052899+

Sun, D., Chang, C., Li, S., and Lin, L. (2006). Near-field electrospinning. *Nano Lett.* 6, 839–842. doi: 10.1021/nl0602701

Sun, L., Huang, W. M., Ding, Z., Zhao, Y., Wang, C. C., Purnawali, H., et al. (2012). Stimulus-responsive shape memory materials: a review. *Mater. Des.* 33, 577–640. doi: 10.1016/j.matdes.2011.04.065

Suntornnond, R., An, J., and Chua, C. K. (2017). Bioprinting of thermoresponsive hydrogels for next generation tissue engineering: a review. *Macromol. Mater. Eng.* 302:1600266. doi: 10.1002/mame.201600266

Szojka, A., Lalh, K., Andrews, S. H. J., Jomha, N. M., Osswald, M., and Adesida, A. B. (2017). Biomimetic 3D printed scaffolds for meniscus tissue engineering. *Bioprinting* 8, 1–7. doi: 10.1016/j.bprint.2017.08.001

Tabata, O., Hirasawa, H., Aoki, S., Yoshida, R., and Kokufuta, E. (2002). Ciliary motion actuator using self-oscillating gel. *Sens. Actuators A Phys.* 95, 234–238. doi: 10.1016/S0924-4247(01)00731-2

Thavornyutikarn, B., Chantarapanich, N., Sitthiseripratip, K., Thouas, G. A., and Chen, Q. (2014). Bone tissue engineering scaffolding: computer-aided scaffolding techniques. *Prog. Biomater.* 3, 61–102. doi: 10.1007/s40204-014-0026-7

Tibbits, S. (2013). *Skylar Tibbits: The Emergence of "4D printing"*. Retrieved from: https://www.ted.com/talks/skylar_tibbits_the_emergence_of_4d_printing/up-next

Tibbits, S. (2014). 4D printing: multi-material shape change. *Arch. Design*. 84, 116–121. doi: 10.1002/ad.1710

Tomatsu, I., Hashidzume, A., and Harada, A. (2005). Photoresponsive hydrogel system using molecular recognition of α-cyclodextrin. *Macromolecules* 38, 5223–5227. doi: 10.1021/ma050670v

Vijayavenkataraman, S., Lu, W. F., and Fuh, J. Y. (2016). 3D bioprinting of skin: a state-of-the-art review on modelling, materials, and processes. *Biofabrication.* 8:032001. doi: 10.1088/1758-5090/8/3/032001

Wang, M. O., Vorwald, C. E., Dreher, M. L., Mott, E. J., Cheng, M.-H., Cinar, A., et al. (2015). Evaluating 3D-printed biomaterials as scaffolds for vascularized bone tissue engineering. *Adv. Mater.* 27, 138–144. doi: 10.1002/adma.201403943

Wang, W., Caetano, G., Ambler, W. S., Blaker, J. J., Frade, M. A., Mandal, P., et al. (2016). Enhancing the hydrophilicity and cell attachment of 3D printed PCL/graphene scaffolds for bone tissue engineering. *Materials* 9:992. doi: 10.3390/ma9120992

Wang, X., Jiang, M., Zhou, Z., Gou, J., and Hui, D. (2017). 3D printing of polymer matrix composites: a review and prospective. *Compos. Part B Eng.* 110, 442–458. doi: 10.1016/j.compositesb.2016.11.034

Wang, Z., Abdulla, R., Parker, B., Samanipour, R., Ghosh, S., and Kim, K. (2015). A simple and high-resolution stereolithography-based 3D bioprinting system using visible light crosslinkable bioinks. *Biofabrication.* 7:045009. doi: 10.1088/1758-5090/7/4/045009

Wenz, A., Borchers, K., Tovar, G. E. M., and Kluger, P. J. (2017). Bone matrix production in hydroxyapatite-modified hydrogels suitable for bone bioprinting. *Biofabrication.* 9:044103. doi: 10.1088/1758-5090/aa91ec

White, S. R., Sottos, N. R., Geubelle, P. H., Moore, J. S., Kessler, M. S., Sriram, S. R., et al. (2001). Autonomic healing of polymer composites. *Nature.* 409, 794–797. doi: 10.1038/35057232

Wiria, F. E., Chua, C. K., Leong, K. F., Quah, Z. Y., Chandrasekaran, M., and Lee, M. W. (2008). Improved biocomposite development of poly (vinyl alcohol) and hydroxyapatite for tissue engineering scaffold fabrication using selective laser sintering. *J. Mater. Sci. Mater. Med.* 19, 989–996. doi: 10.1007/s10856-007-3176-5

Xu, F., Wu, C. A., Rengarajan, V., Finley, T. D., Keles, H. O., Sung, Y., et al. (2011). Three-dimensional magnetic assembly of microscale hydrogels. *Adv. Mater.* 23, 4254–4260. doi: 10.1002/adma.201101962

Xu, N., Ye, X., Wei, D., Zhong, J., Chen, Y., Xu, G., et al. (2014). 3D artificial bones for bone repair prepared by computed tomography-guided fused deposition modeling for bone repair. *ACS Appl. Mater. Interfaces.* 6, 14952–14963. doi: 10.1021/am502716t

Xu, T., Gregory, C. A., Molnar, P., Cui, X., Jalota, S., Bhaduri, S. B., et al. (2006). Viability and electrophysiology of neural cell structures generated by the inkjet printing method. *Biomaterials* 27, 3580–3588. doi: 10.1016/j.biomaterials.2006.01.048

Yan, F., Liu, Y., Chen, H., Zhang, F., Zheng, L., and Hu, Q. (2014). A multi-scale controlled tissue engineering scaffold prepared by 3D printing and NFES technology. *AIP Adv.* 4:3. doi: 10.1063/1.4867959

Yang, X., Lu, Z., Wu, H., Li, W., Zheng, L., and Zhao, J. (2018). Collagen-alginate as bioink for three-dimensional (3D) cell printing based cartilage tissue engineering. *Mater. Sci. Eng. C* 83, 195–201. doi: 10.1016/j.msec.2017.09.002

Yilgor, P., Tuzlakoglu, K., Reis, R. L., Hasirci, N., and Hasirci, V. (2009). Incorporation of a sequential BMP-2/BMP-7 delivery system into chitosan-based scaffolds for bone tissue engineering. *Biomaterials* 30, 3551–3559. doi: 10.1016/J.BIOMATERIALS.2009.03.024

Yuan, B., Zhou, S. Y., and Chen, X. S. (2017). Rapid prototyping technology and its application in bone tissue engineering. *J. Zhejiang Univ. Sci. B* 18, 303–315. doi: 10.1631/jzus.B1600118

Zarek, M., Layani, M., Cooperstein, I., Sachyani, E., Cohn, D., and Magdassi, S. (2016a). 3D printing of shape memory polymers for flexible electronic devices. *Adv. Mater.* 28, 4449–4454. doi: 10.1002/adma.201503132

Zarek, M., Mansour, N., Shapira, S., and Cohn, D. (2016b). 4D printing of shape memory-based personalized endoluminal medical devices. *Macromol. Rapid Commun.* 38:1600628. doi: 10.1002/marc.201600628

Zhang, J., Zhao, S., Zhu, M., Zhu, Y., Zhang, Y., Liu, Z., et al. (2014). 3D-printed magnetic Fe_3O_4/MBG/PCL composite scaffolds with multifunctionality of bone regeneration, local anticancer drug delivery and hyperthermia. *J. Mater. Chem. B* 2, 7583–7595. doi: 10.1039/C4TB01063A

Zhang, K., Fu, Q., Yoo, J., Chen, X., Chandra, P., Mo, X., et al. (2017). 3D bioprinting of urethra with PCL/PLCL blend and dual autologous cells in fibrin hydrogel: an *in vitro* evaluation of biomimetic mechanical property and cell growth environment. *Acta Biomater.* 50, 154–164. doi: 10.1016/J.ACTBIO.2016.12.008

Zhang, M., Vora, A., Han, W., Wojtecki, R. J., Maune, H., Le, A. B., et al. (2015). Dual-responsive hydrogels for direct-write 3D printing. *Macromolecules* 48, 6482–6488. doi: 10.1021/acs.macromol.5b01550

Zhang, X.-F., Huang, Y., Gao, G., and Cui, X. (2017). "Current progress in bioprinting," in *Advances in Biomaterials for Biomedical Applications*, eds A. Tripathi and J. S. Melo (Singapore: Springer), 227–259. doi: 10.1007/978-981-10-3328-5

Zhang, Y., and Ionov, L. (2014). Actuating porous polyimide films. *ACS Appl. Mater. Interfaces* 6, 10072–10077. doi: 10.1021/am502492u

Zhou, Y., Huang, W. M., Kang, S. F., Wu, X. L., Lu, H. B., Fu, J., et al. (2015). From 3D to 4D printing: approaches and typical applications. *J. Mech. Sci. Technol.* 29, 4281–4288. doi: 10.1007/s12206-015-0925-0

Zhu, W., George, J. K., Sorger, V. J., and Grace Zhang, L. (2017). 3D printing scaffold coupled with low level light therapy for neural tissue regeneration. *Biofabrication* 9:025002. doi: 10.1088/1758-5090/aa6999

Zorlutuna, P., Vrana, N. E., and Khademhosseini, A. (2013). The expanding world of tissue engineering: the building blocks and new applications of tissue engineered constructs. *IEEE Rev. Biomed. Eng.* 6, 47–62. doi: 10.1109/RBME.2012.2233468

Conflict of Interest Statement: The authors declare that the research was conducted in the absence of any commercial or financial relationships that could be construed as a potential conflict of interest.

frontiers in Bioengineering and Biotechnology

REVIEW
published: 12 July 2019
doi: 10.3389/fbioe.2019.00166

Collagen-Based Tissue Engineering Strategies for Vascular Medicine

Francesco Copes[1,2], *Nele Pien*[1,3], *Sandra Van Vlierberghe*[3], *Francesca Boccafoschi*[1,2] *and Diego Mantovani*[1]*

[1] *Laboratory for Biomaterials and Bioengineering, Canada Research Chair Tier I for the Innovation in Surgery, Department of Min-Met-Materials Engineering & Regenerative Medicine, CHU de Quebec Research Center, Laval University, Quebec City, QC, Canada,* [2] *Laboratory of Human Anatomy, Department of Health Sciences, University of Piemonte Orientale, Novara, Italy,* [3] *Polymer Chemistry & Biomaterials Group, Department of Organic and Macromolecular Chemistry, Centre of Macromolecular Chemistry, Ghent University, Ghent, Belgium*

Cardiovascular diseases (CVDs) account for the 31% of total death per year, making them the first cause of death in the world. Atherosclerosis is at the root of the most life-threatening CVDs. Vascular bypass/replacement surgery is the primary therapy for patients with atherosclerosis. The use of polymeric grafts for this application is still burdened by high-rate failure, mostly caused by thrombosis and neointima hyperplasia at the implantation site. As a solution for these problems, the fast re-establishment of a functional endothelial cell (EC) layer has been proposed, representing a strategy of crucial importance to reduce these adverse outcomes. Implant modifications using molecules and growth factors with the aim of speeding up the re-endothelialization process has been proposed over the last years. Collagen, by virtue of several favorable properties, has been widely studied for its application in vascular graft enrichment, mainly as a coating for vascular graft luminal surface and as a drug delivery system for the release of pro-endothelialization factors. Collagen coatings provide receptor–ligand binding sites for ECs on the graft surface and, at the same time, act as biological sealants, effectively reducing graft porosity. The development of collagen-based drug delivery systems, in which small-molecule and protein-based drugs are immobilized within a collagen scaffold in order to control their release for biomedical applications, has been widely explored. These systems help in protecting the biological activity of the loaded molecules while slowing their diffusion from collagen scaffolds, providing optimal effects on the targeted vascular cells. Moreover, collagen-based vascular tissue engineering substitutes, despite not showing yet optimal mechanical properties for their use in the therapy, have shown a high potential as physiologically relevant models for the study of cardiovascular therapeutic drugs and diseases. In this review, the current state of the art about the use of collagen-based strategies, mainly as a coating material for the functionalization of vascular graft luminal surface, as a drug delivery system for the release of pro-endothelialization factors, and as physiologically relevant *in vitro* vascular models, and the future trend in this field of research will be presented and discussed.

Keywords: collagen, tissue engineering, cardiovascular, coating, drug delivery system, vascular model

OPEN ACCESS

Edited by:
Hasan Uludag,
University of Alberta, Canada

Reviewed by:
John Law Brash,
McMaster University, Canada
Dimitrios I. Zeugolis,
National University of Ireland Galway, Ireland

***Correspondence:**
Diego Mantovani
diego.mantovani@gmn.ulaval.ca

Specialty section:
This article was submitted to Biomaterials, a section of the journal Frontiers in Bioengineering and Biotechnology

Received: *13 February 2019*
Accepted: *24 June 2019*
Published: *12 July 2019*

Citation:
Copes F, Pien N, Van Vlierberghe S, Boccafoschi F and Mantovani D (2019) Collagen-Based Tissue Engineering Strategies for Vascular Medicine. Front. Bioeng. Biotechnol. 7:166. doi: 10.3389/fbioe.2019.00166

INTRODUCTION AND SHORT HISTORICAL PERSPECTIVE

Cardiovascular diseases (CVDs) account for 17.9 million deaths each year, making them the leading cause of death in the world (WHO[1]). Heart attacks and strokes account for 85% of these deaths. Most often, atherosclerosis is at the basis of these two pathologies. Atherosclerosis is a pathological progressive condition in which plaques, mainly due to the accumulation of lipids, cholesterol, foamy cells, and cellular debris, progressively grow inside the lumens, thus leading to the partial or complete obstruction of blood flow, and leading to severe medical conditions and, ultimately, to death. The increase of risk factors associated with the pathology (obesity, diabetes, hypertension, and smoking), coupled with the increase in average life expectancy, has led to the urgent search for durable and effective solutions. Vascular bypass/substitution surgery represents the most common, ultimate clinical treatment of occlusive CVDs. Autologous blood vessels, such as saphenous veins or radial arteries, that present the best structural, mechanical, and biological properties are the gold standard for this kind of application. However, the use of these substitutes is not always possible, due to the multiple surgical procedures required, or the poor general health conditions of patients. Some of the limiting factors for the use of autografts include the typical old age of the patients needing treatments, vascular diseases preventing the use of autologous vessels, and/or previous harvesting for other surgical treatments. In this light, the need for other sources of vascular substitutes is critically urgent. Synthetic prostheses development started in the 1950s and opened a therapeutic alternative for the replacement of injured arterial segments. The first synthetic vascular bypass has been performed in 1952 with the implantation of a porous textile prosthesis made of polyethylene terephthalate (PET), also known as Dacron® (Voorhees et al., 1952; Kannan et al., 2005). Prostheses made of Dacron® are usually applied for the replacement of vessels of large caliber (>10 mm in diameter). Then, in 1976, the first use of expanded polytetrafluoroethylene (ePTFE), also known as Teflon®, was reported (Kannan et al., 2005; Chlupac et al., 2009). These prostheses are applied in the replacement of medium-sized vessels, between 6 and 10 mm in diameter. No studies show the superiority of PET compared to ePTFE (Roll et al., 2008). Since their introduction in cardiovascular medicine, a number of improvements have been made to enhance the performance of the synthetic vascular substitutes (SVS). Nevertheless, their low patency owing to short- and intermediate-term failure still limits their clinical application. Two of the main causes of SVS failure are thrombosis and intima hyperplasia. In-graft thrombosis is the result of a perturbation of the hemostatic balance, usually maintained by a series of anti-coagulation reactions involving both physical–mechanical and biological factors, acting on the inhibition of the coagulation process (Edelberg et al., 2001). Among the different factors acting in this complex balance, the intima layer, composed of endothelial cells (ECs), greatly contributes to the maintenance of the hemostatic balance by producing several antithrombotic molecules. The disruption of the endothelial layer or its absence greatly compromises the antithrombotic environment of healthy blood vessels. Intimal hyperplasia, especially at the anastomotic sites, results in the abnormal migration and proliferation of vascular smooth muscle cells (SMCs) with associated deposition of extracellular connective tissue matrix and is thought to be due to a variety of injuries that always involve some endothelial damage (Clowes, 1993). Intima hyperplasia is composed of about 20% of vascular SMCs that have migrated from the media to the intima and have proliferated and deposited extracellular matrix (ECM), which comprises most (60–80%) of the intimal area. Normal endothelium produces factors that inhibit SMC proliferation. A damage of the endothelium layer decreases the production of growth-inhibiting factors and increases the expression of growth-stimulating factors, shifting the balance toward SMC proliferation and migration toward the intima.

As previously described, both these adverse outcomes have a common basis in the lack or uncomplete endothelialization of the implanted substitutes. Therefore, the rapid establishment of a complete and functional ECs layer on the luminal surface of SVS would be beneficial to prevent failures and for ensuring the long-term patency of the implanted substitutes.

Tissue engineering is a multidisciplinary domain aimed to develop biologically based tissues that can be used in the clinical treatments of diseases. Tissue engineering products have already shown to be effective in different applications, ranging from burn treatment to osteo-regeneration. The success obtained by this approach in other medical fields has opened the door for its use in vascular reconstruction. The use of scaffolding systems based on natural polymers is one of the strategies used in vascular tissue engineering (vTE) to promote cellular integration and proliferation. The ideal scaffold should be able to mimic the native vascular ECM and the highly complex organization of the arterial wall, showing important biological and mechanical characteristics, such as non-thrombogenicity, hemocompatibility, biocompatibility (low cytotoxicity, optimal cell adhesion, bioresorbable), and non-immunogenicity, along with tensile strength and viscoelasticity.

Among the natural polymers currently used for vTE, collagen is the most used one. Collagen is one of the main components of the vascular ECM. Its main function is to subdue constraints imposed by elongation under pressure in large vessels while providing attachment for vascular cells [12].

In this review, the main properties of the collagen molecule, along with the different types, will be presented. Moreover, collagen-based coatings will be detailed mainly in the context of vascular substitutes, and the use of collagen for the development of drug delivery systems (DDS) (with a focus on the ones with vascular applications) will be discussed. Finally, the development of *in vitro* physiologically relevant artery models based on collagen scaffolds for the study and validation of drugs and cardiovascular devices will be overviewed (**Figure 1**).

[1]World Health Organization. *Top 10 Causes of Death*. Available online at: http://www.who.int/gho/mortality_burden_disease/causes_death/top_10/en/ (accessed January 28, 2019).

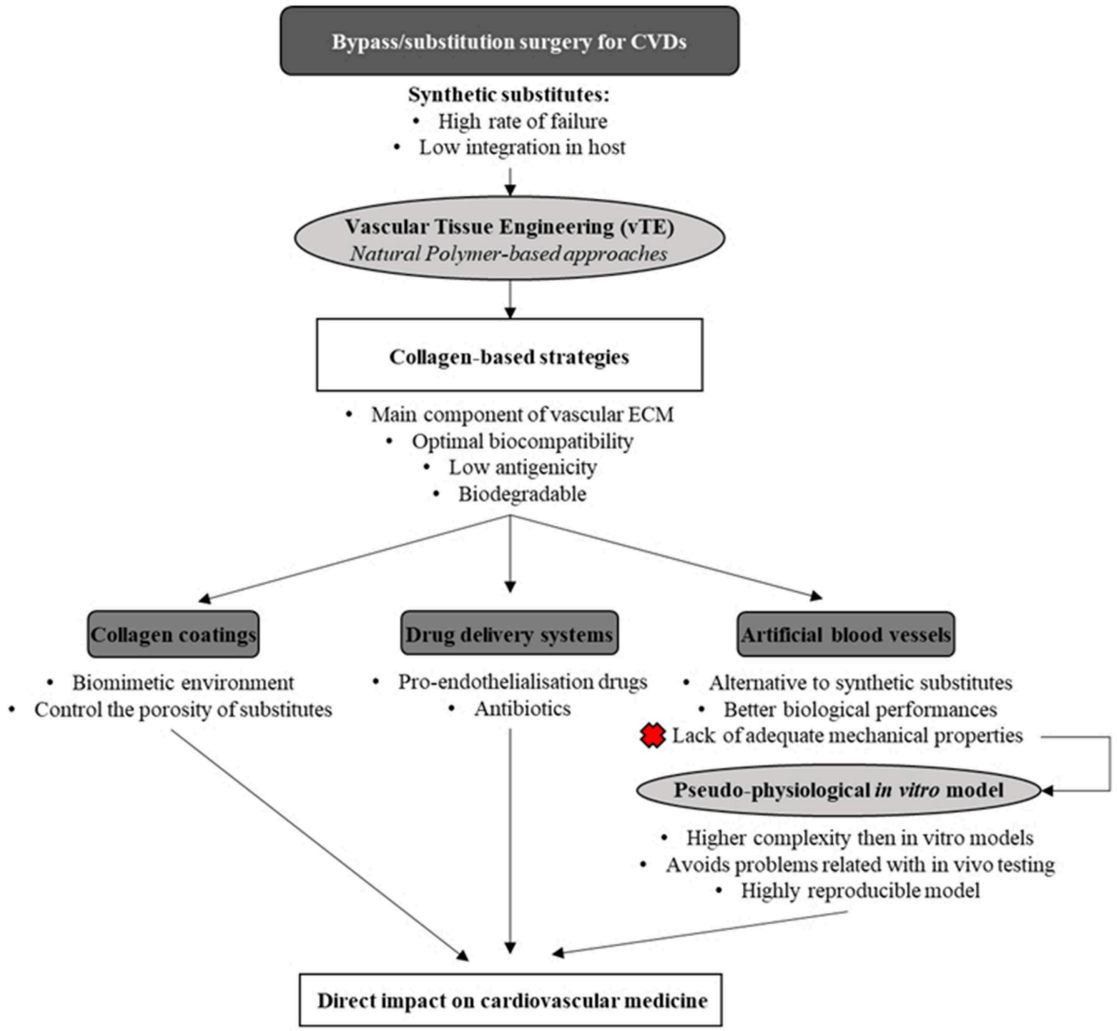

FIGURE 1 | Schematic view of the layout of this review.

COLLAGEN

Structure and Biosynthesis

Collagen is the most abundant protein in animals, including the human body (Shoulders and Raines, 2009). It accounts for one third of the total protein content, and it constitutes the main component of the ECM. To date, 28 different collagen types have been identified in vertebrates, and the discovery of collagen in dinosaur bone fossils make it the oldest protein ever detected (Exposito et al., 2002; Schweitzer et al., 2007). Collagens can be divided into two main categories: fibrillar and non-fibrillar. Fibrillar collagens form elongated fibril structures, which are known for their structural role in mechanical support for most animal tissues (Hulmes, 2002; Jenkins et al., 2005; Exposito et al., 2010). Non-fibrillar collagens can be divided in sub-categories, such as network-forming collagens (collagen types IV and VII), fibril-associated collagens with interrupted triple helices (FACITs, collagen types IX and XII), and membrane-associated collagens with interrupted triple helices (MACITs). The main types of collagens, along with their distribution and composition, are listed in **Table 1**.

All collagens, fibrillar or not, are characterized by the same molecular structure, which is composed of three α chains. These chains can either be identical, thus originating a homotrimer, or be a combination of two or three distinct α chains forming a heterotrimer. Each α chain contains three basic amino acids, which are glycine, proline, and hydroxyproline, and is characterized by the presence of at least one collagenous domain, consisting of a repeating Gly-Xaa-Yaa triplet (Brazel et al., 1987), where Xaa is usually a proline and Yaa is a hydroxyproline. However, both Xaa and Yaa can be any amino acid, conferring specific functions for the collagen (**Figure 2**).

Fibrillar collagens are the most used in the production of collagen-based biomaterials, with type I being the most

TABLE 1 | Main collagen types and their distribution in the human body.

Structure	Type	Composition	Chains	Distribution
Fibrillar Collagens	I	Heterotrimer	$[\alpha1(I)]_2\alpha2(I)$	Skin, cornea, blood vessels, bone, ligaments, and tendons
	II	Homotrimer	$[\alpha1(II)]_3$	Cartilage, intervertebral discs
	III	Homotrimer	$[\alpha1(III)]_3$	Skin, blood vessels
	V	Heterotrimer	$[\alpha1(V)]_2\alpha2(V)$ or $\alpha1(V)\alpha2(V)\alpha3(V)$	Skin, cornea, blood vessels, bone, ligaments, and tendons
	XI	Heterotrimer	$\alpha1(XI)\alpha2(XI)\alpha3(XI)$	Cartilage, intervertebral discs
FACITs	IX	Heterotrimer	$\alpha1(IX)\alpha2(IX)\alpha3(IX)$	Cartilage
	XII	Homotrimer	$[\alpha1(XII)]_3$	Ligaments and tendons
Network Forming	IV	Heterotrimer	$[\alpha1(IV)]_2\alpha2(IV)$	Basal lamina
	VI	Heterotrimer	$\alpha1(VI)\alpha2(VI)\alpha3(VI)$ or $\alpha1(VI)\alpha2(VI)\alpha4(VI)$	Bone, cartilage, cornea, dermis
	VII	Homotrimer	$[\alpha1(VII)]_3$	Under stratified epithelium
MACITs	XIII	—	—	Endothelial cells, dermis, eye, heart

Modified from Shoulders and Raines (2009). FACITs, fibril-associated collagens with interrupted triple helices; MACITs, membrane-associated collagens with interrupted triple helices.

abundant collagen type in the human body (Di Lullo et al., 2002). During the synthesis of fibrillar collagen molecules, alpha chains are formed by ribosomes present on the surface of rough endoplasmic reticulum (RER). These chains present registration peptides and a signal peptide that, once released in the lumen of the RER, is cleaved to form pro-collagen chains (Ishikawa and Bachinger, 2013). At this point, the pro-collagens go through several modifications (mainly hydroxylation of the lysine and proline residues and glycosylation of specific hydroxylysines) and they are finally assembled in triple helical structures. These pro-collagen triple helices are then transferred to the Golgi apparatus to be encapsulated and secreted by exocytosis. Once in the extracellular environment, the registration peptides present on the pro-collagen are cleaved and tropo-collagen is formed. Through cross-linking, several tropo-collagen molecules are assembled to produce collagen fibrils. In turn, collagen fibrils assemble to form collagen fibers (Bella and Hulmes, 2017).

Collagen as a Biomaterial

Collagen is the most used natural polymer for tissue engineering applications due to its presence in the ECM of almost every human tissue. The use of collagen as a biomaterial dates back to the early decades of the twentieth century, when the first characterization of the interaction between cells and extracted collagen was studied (Huzella and Lengyel, 1932; Ehrmann and Gey, 1956). The use of collagen is prompted by several characteristics that make it a good material for biomedical applications: Weak antigenicity and robust biocompatibility (Schmitt et al., 1964; Furthmayr and Timpl, 1976; Lee et al., 2001; Lynn et al., 2004), promotion of cell adhesion through cell receptors that recognize a specific peptide sequence within collagen molecules (Gullberg et al., 1992; Smethurst et al., 2007; Konitsiotis et al., 2008), and biodegradability (Chiang et al., 1978; Postlethwaite et al., 1978; Yannas et al., 1982). As an added value, collagen can be isolated from several sources, being one of the most abundant and best conserved proteins among vertebrates. Usual sources for collagen extractions are bovine skin and tendons (Rodrigues et al., 2003), porcine acellular bladder collagen (Chen et al., 1999), porcine collagen type I (Salamanca et al., 2018), and rat tail tendons (Ehrmann and Gey, 1956; Chandrakasan et al., 1976; Habermehl et al., 2005), but collagen has also been extracted from other organisms, such as sponges (Exposito et al., 1991), fishes (Sugiura et al., 2009), kangaroos (Johnson et al., 1999), and alligators (Wood et al., 2008), making it a cost-effective solution for scaffold-based tissue engineering.

Collagen-based biomaterials are mainly used for the treatment of burns and as wound dressing (Chattopadhyay and Raines, 2014). Due to their structure, porosity and surface properties, collagen sponges have long been used for wound dressing applications (Abramo and Viola, 1992; Fleck and Simman, 2010). Moreover, they can be loaded with therapeutic agents, such as growth factors (Lee, 2005) or antibiotics (Sripriya et al., 2004) that greatly improve the healing process once implanted. Another common application for collagen products is as an osteogenic scaffold and filling material in orthopedy (Matassi et al., 2011; Zhang et al., 2018). Collagen type I scaffolds modified with hydroxyapatite have been used as an osteochondral scaffold to improve bone and cartilage regeneration (Kon et al., 2011). Collagen scaffolds can also be used as injectable mineralized bone substitutes (Stephan et al., 2000). Next to this, collagen has been widely used for dentistry applications, such as for the production of membranes for periodontal and implant therapy to improve cell proliferation (Patino et al., 2002). Another field of application for collagen is in ophthalmology as corneal shield (Willoughby et al., 2002; Eshar et al., 2011) and as eye implants for post-operative recovery (Delarive et al., 2003) and corneal implantation (Liu et al., 2006). Finally, the use of collagen as a scaffold for the development of a DDS has attracted the attention of many researchers all over the world (Wallace and Rosenblatt, 2003) for several applications, such as bone regeneration, eye, cardiac, and brain medicine (Lucas et al., 1989; Kaufman et al., 1994; Chiu et al., 2010; Chan et al., 2017) since the 1970s (Bradley and Wilkes, 1977).

Functionalization of Collagen for Tissue Engineering Applications

One of the most important limitations in using collagen-based materials in regenerative medicine applications remains their mechanical properties, which are often limited, especially at the viscoelastic level, specifically, for vTE, mechanical properties related to the high pressures and stresses encountered in the blood vessel (Achilli et al., 2010; Meghezi et al., 2015). Research has therefore focused on various ways of enhancing and controlling the polymerization, the stability in solutions, reducing enzymatic sensitivity, and controlling the pore size, in an attempt to increase mechanical strength. An

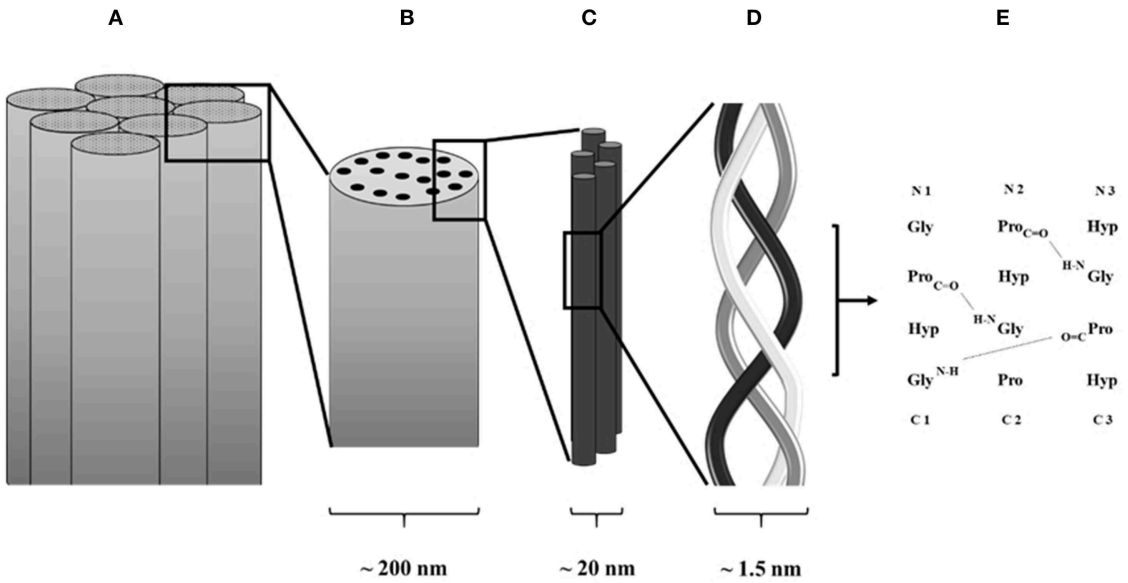

FIGURE 2 | Schematic collagen structure. **(A)** Collagen fiber formed by assembled collagen fibrils. **(B)** Collagen fibrils. **(C)** Assembled tropocollagen. **(D)** Collagen triple helix. **(E)** Hydrogen bond in between collagen α chains.

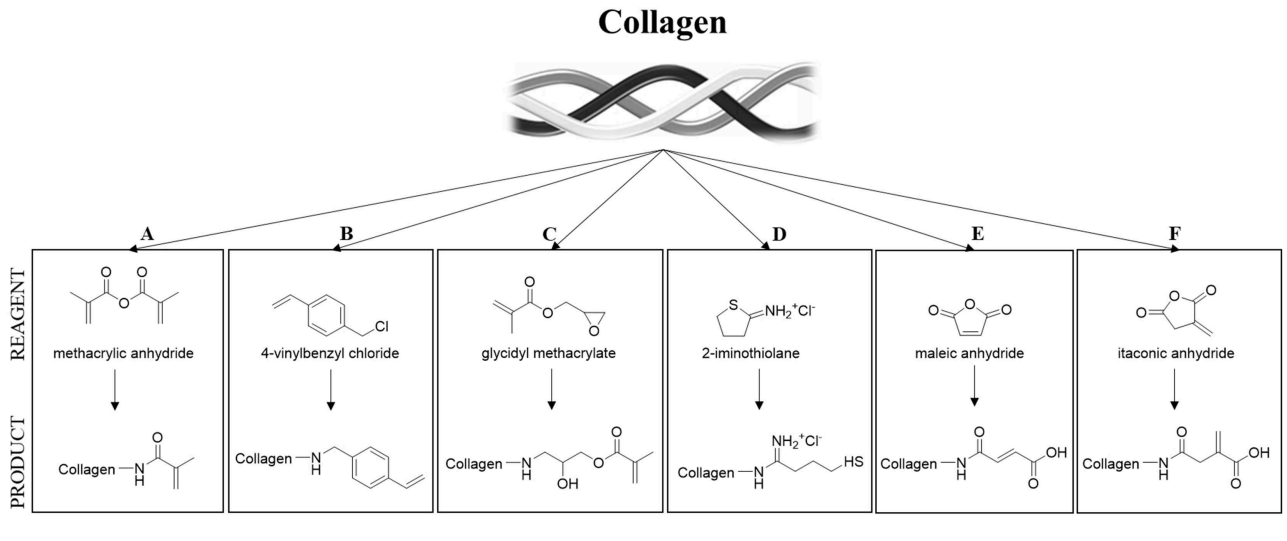

FIGURE 3 | Strategies for collagen functionalization. **(A)** Methacrylic anhydride (Gaudet and Shreiber, 2012; Pupkaite et al., 2017); **(B)** 4-vinylbenzylchloride and **(C)** glycidyl methacrylate (Tronci et al., 2013); **(D)** thiol-functionalization (Holmes et al., 2017) and **(E,F)** unsaturated cyclic anhydrides (Potorac et al., 2014).

interesting approach to maintain the structural integrity of a scaffold is to chemically, physically, or enzymatically cross-link the biopolymer (Davidenko et al., 2015; Liu et al., 2019). However, collagen has a limited number of functional groups (i.e., amine and carboxylic acids) that can enable cross-linking (Gallop and Paz, 1975; Rýglová et al., 2017). For this reason, cross-linkable modifications have been introduced on the protein structure (Ravichandran et al., 2016) (**Figure 3**). An overview of various types of modified collagen is shown in **Table 2**.

COLLAGEN IN vTE

Collagen Coatings for Vascular Substitutes

One of the main complications related to the use of synthetic vascular grafts, and especially with the ones made of PET (Dacron), is linked to their high porosity and low elasticity. While porosity allows tissue ingrowth, ensuring a physiological integration of the implanted grafts, and a faster healing, it also causes excessive bleeding, inducing potential serious complications for the patients. Thus, the walls of the grafts must

TABLE 2 | Overview on various functional groups that have been introduced on the collagen backbone.

Material	Functional group	Aim of the modification	Figure	References
Collagen Type I	Methacrylate	Sutureless wound closure	A	Pupkaite et al., 2017
Collagen Type I	Methacrylate	Mechanically heterogeneous environments	A	Gaudet and Shreiber, 2012
Collagen Type I	4-vinylbenzyl chloride (4VBC) and glycidyl methacrylate (GMA)	Programmable macroscopic properties	B, C	Tronci et al., 2013
Collagen Type I	8-arm poly (ethylene glycol) norbornene-terminated (PEG-NB)	Injectable regenerative hydrogels	D	Holmes et al., 2017
Collagen Type I + III	Cyclic anhydrides	Mechanical performance enhancement	E, F	Potorac et al., 2014

be rendered impermeable in order to avoid this outcome. For this reason, pre-clotting is a mandatory clinical step prior to the implantation of a Dacron (PET knitted or woven) graft. This technique consists in the conversion of the porous wall of the prosthesis into one that has been rendered impervious by reaction with blood (Yates et al., 1978). Despite helping in limiting bleeding, this technique is hampered by several disadvantages, such as the increase of the roughness of the luminal surface of the implanted grafts. This rougher surface increases the occurrence of turbulent blood flow and thrombus formation, and the increase in the rigidity of the graft straightforwardly diminishes their pliability.

The impregnation of porous Dacron vascular grafts with collagen was first proposed in the early 1960s (Humphries et al., 1961) as an alternative to pre-clotting. Striking improvements were obtained years later by Scott and colleagues in 1987 (Scott et al., 1987). Their bovine collagen-coated grafts did not require pre-clotting or special preparation and did not bleed once implanted in a canine model. The luminal surface of the grafts showed neointima formation, and the collagen coating was completely resorbed and substituted by native tissue after 3 months of implantation. Moreover, the collagen was non-thrombogenic or antigenic. That opened the door for the use of collagen-impregnated vascular grafts in the surgical treatment of aneurysms and for arterial bypass (Reigel et al., 1988; Freischlag and Moore, 1990; Noishiki et al., 1996), proving to be a viable alternative to the previously used pre-clotting technique, being able to compete equally against other proposed techniques and materials (Prager et al., 2003).

Nonetheless, these collagen-coated grafts have been demonstrated over the years not to be free from complications: Variable inflammatory response and tissue adhesion (Jonas et al., 1987), need of sustained chest drainage (Suehiro et al., 2003), and initiation of the immune response (Kobayashi et al., 1993) in the treated patients. Moreover, they showed no added value for the replacement of small-caliber arteries (Guidoin et al., 1996). However, the performances of the collagen-coated vascular grafts have stood the test of time, resulting in being one of the most used vascular grafts for medium- and large-diameter arteries substitution nowadays.

Collagen-Based DDS

Biological signaling represents an important point in cell-driven tissue regeneration and providing signaling molecules greatly improves this process. However, when administering molecules and drugs, it is of crucial importance to reach the appropriate dose at a specific site and for the necessary period of time, in order to accomplish the desired effects. Thus, there is a need to release these molecules in a controlled way.

The development of collagen-based DDS for the release of pro-angiogenetic factors for wound healing applications and pro-endothelialization factors for vascular implant functionalization is highly sought after. Collagen has been widely studied as a biomaterial for DDS (Friess, 1998) and has found several uses in a variety of applications (**Table 3**).

The use of collagen-based DDS for vascular applications has been explored in recent years. Most of the studies performed aimed to increase the affinity for the collagen scaffolds toward ECs. The enrichment of collagen matrices with several pro-angiogenetic growth factors, such as vascular endothelial growth factor (VEGF) (Steffens et al., 2004; Koch et al., 2006; He et al., 2011), stromal derived factor-1 alpha (SDF-1α) (Laiva et al., 2018), and basic fibroblast growth factor (bFGF) (Hao et al., 2018), has shown promising results in terms of controlling the release of the loaded molecules and the angiogenesis induction, which in turn results in compelling effects during wound repair and for tissue engineering applications.

As mentioned in the Introduction, the use of synthetic vascular grafts for the treatment of occlusive vascular diseases is still a burden by grafts failure, mainly caused by thrombosis and neointima hyperplasia. Implants modifications using pro-endothelialization molecules and growth factors with the aim of speeding up the re-endothelialization process have been proposed over the last years to guide the optimal integration of the grafts and to overcome the aforementioned problems. The use of vascular graft enrichment has also been investigated. In their work from 2000, Wissink et al. developed a heparinized, cross-linked collagen matrix for the controlled release of bFGF to improve the endothelialization of vascular grafts (Wissink et al., 2000). They were able to improve the binding of the loaded bFGF to the heparinized cross-linked matrix and to release it in a controlled way over time, leading to an improvement in the proliferation of treated EC *in vitro*.

The occurrence of infections in newly implanted synthetic vascular grafts is one of the complications that may arise, hampering the functionality of the prosthesis. Conventional treatments of vascular graft infections consist in the excision of the infected graft with extra anatomic bypass grafting (Yeager et al., 1999). To avoid the need of another surgical operation to treat the infected grafts, the use of DDS has

TABLE 3 | Collagen-based drug delivery systems.

	Scaffold structure	Medical application	Biomolecule used	Cells seeded	References
Growth factors/Drugs	Collagen sponges	Wound healing	VEGF	/	Schroeder et al., 2007
	Collagen sponges	Tissue regeneration	bFGF, HGF, PDGF-BB, VEGF, IGF-1, HB-EGF	/	Kanematsu et al., 2004
		Antibacterial	Gentamicin	/	Ivester et al., 2006
Genes	Collagen gels	Skin wound repair	PDGF A and B (genes)	/	Chandler et al., 2000
Cells	Electrospun collagen	Bone	/	BM-MSC	Shih et al., 2006
	Collagen–glycosaminoglycans scaffold	Cardiovascular	/	BM-MSC	Xiang et al., 2006
	Collagen sponges	Brain	/	NSC	Yu et al., 2010
	Collagen sponges and hydrogels	Intervertebral discs	/	Human intervertebral disc cells	Gruber et al., 2004, 2006

bFGF, basic fibroblast growth factor; VEGF, vascular endothelial growth factor; HGF, hepatocyte growth factor; PDGF-BB, platelet-derived growth factor-BB; IGF-1, insulin-like growth factor-1; HB-EGF, heparin binding epidermal growth factor-like growth factor; BM-MSC, bone marrow mesenchymal stem cells; NSC, neural stem cells.

been proposed. In particular, collagen-based matrices have been demonstrated to be effective in delivering antibiotic agents to limit and treat bacterial infections in implanted synthetic vascular grafts (Chervu et al., 1991; Batt et al., 2003; Schneider et al., 2008; Herten et al., 2017), avoiding the need for subsequent surgical interventions.

Collagen Scaffolds for Vascularization and Artificial Blood Vessel Development

Over the years, collagen has been used as a pro-vascularization scaffold for several applications. In fact, the ability of collagen scaffolds to support angiogenesis and the formation of neo-vasculature has been demonstrated (Nicosia et al., 1991). Collagen scaffolds have been first used as an *in vitro* model for the study of the angiogenetic process (Vernon et al., 1995), but their use has been shortly translated to the clinic (Abraham et al., 2000) for several applications. In 2008, Shen et al. showed how a VEGF-modified collagen scaffold was able to efficiently promote penetration, proliferation, and assembly of ECs in the scaffold (Shen et al., 2008). In 2016, Chan and colleagues developed a 3D scaffold from bovine collagen type I able to support capillary formation *in vivo* and vascularization once implanted in animal models (Chan et al., 2016). Similarly, other groups demonstrated how implanted collagen scaffolds were able to promote EC infiltration and vascularization (Cherubino et al., 2016; Wahl et al., 2016). Interestingly, the joint use of other ECM components along collagen, like elastin or glycosaminoglycans, has been shown to exert different effects on the vascularization of collagen scaffolds (Schmidt et al., 2017).

Collagen is one of the most abundant proteins in the vascular ECM. There, collagen fibers limit the distension of the vessel and provide attachment for SMCs, allowing them to transmit circumferential forces to the vessel wall, ultimately conferring excellent mechanical support to the blood vessel wall (Bou-Gharios et al., 2004). Therefore, the use of collagen, in particular type I, as a scaffold in the development of tissue-engineered vascular substitutes has been largely explored. The first use of collagen gels to manufacture a vascular substitute dates back to 1986, when Weinberg and Bell attempted to reconstitute a blood vessel (Weinberg and Bell, 1986). Their method consisted in the production of a multilayered tubular construct made of collagen seeded with SMCs and fibroblasts and of the endothelialization of its lumen. Despite showing very low mechanical properties and the impossibility to be used for clinical purposes, this work marked a major advance in the field of vTE, with several groups following in the footsteps (Hirai et al., 1994; Seliktar et al., 2000; Boccafoschi et al., 2007) and trying to improve the system. One of the main problems related to this kind of construct is its mechanical properties. Different variants of the methodology from Weinberg and Bell, such as winding leaflets around a mandrel to promote compaction of collagen (L'Heureux et al., 1993), magnetic pre-alignment of collagen fibers to increase tensile strength (Tranquillo et al., 1996), cross-linking of collagen scaffolds by glycation (Girton et al., 2000), or ultraviolet radiation (Charulatha and Rajaram, 2003) have been developed to improve the mechanical properties of the substitutes. However, the extent of these improvements still does not allow the implantation and, thus, the use in the medical practice of these grafts. The seeded cells play an important role too: SMCs have been demonstrated to actively influence the compaction of the collagen scaffold (Berglund et al., 2003; Meghezi et al., 2015) and to align along the direction of the collagen fibers (Hirai et al., 1994), helping in increasing the mechanical properties of the substitutes. The biological properties have also been studied. Different molecules have been used to modulate the cellular response toward these scaffolds. The addition of insulin and growth factors, such as TGF-β makes it possible to increase collagen production by the seeded cells (Long and Tranquillo, 2003), and the addition of dermatan sulfate has been able to increase the endothelialization of the lumen and, as a result, to reduce platelet adhesion and activation (Matsuda et al., 1988). In recent years, hybrid collagen vascular substitutes containing both synthetic (He et al., 2005; Stitzel et al., 2006; Jeong et al., 2007) and natural polymers, such as fibrin (Cummings et al., 2004) and elastin in particular (Berglund et al., 2004; Koens et al., 2010,

2015), have been developed to further increase the mechanical and biological properties of the collagen-based vascular grafts, aiming to obtain an artificial vessel as close as possible to the natural ones.

Pre-clinical and Clinical Studies of Collagen for vTE Applications

As of today, the main use of collagen for clinical applications is as replacement scaffolds (i.e., tissue fillers) and as support matrices (i.e., matrix rich tissues). Collagen scaffolds used in clinical practice primarily include skin substitutes and dermal fillers. However, the use of collagen for other applications, including vascular applications, is increasing. In fact, a number of positive factors indicate that the use of a collagen-based product is becoming an attracting prospective for vTE purposes (Dogan et al., 2017). **Table 4** shows some of the pre-clinical studies conducted on collagen-based vTE products. It can be observed that collagen-based materials for vascular applications, especially for vascular grafts, are successfully used in pre-clinical studies involving *in vivo* testing and, therefore, physiological stimulation. It can be concluded that research in the field is moving toward the achievement of those optimal properties needed for the clinical translation.

COLLAGEN-BASED PSEUDO-PHYSIOLOGICAL MODELS FOR CARDIOVASCULAR THERAPY DEVELOPMENT

Development of 3D *in vitro* Models for Cardiovascular Research

Although tissue-engineered blood vessels as living arterial substitutes have been studied extensively in the last 25 years, clinical translation has not yet happened (Zhang et al., 2007; Nemeno-Guanzoni et al., 2012). The mechanism by which these grafts integrate into the host's circulatory system and remodel into functional blood vessels remains unclear (Pashneh-Tala et al., 2016). Despite this drawback, the vTE grafts can be used as an advanced model of the vascular wall for the *in vitro* testing of drugs and devices. In fact, currently used *in vitro* pre-clinical models represent an overly simplified vascular environment, not able to reproduce the complex cell–cell and cell–environment interactions taking place *in vivo*. On the other hand, *in vivo* animal models currently used for the development of medical drugs and devices show limitations and disadvantages, such as animal-to-human variations in anatomy, physiology, and functions together with high costs and ethical burden (Byrom et al., 2010; Swartz and Andreadis, 2013). The four main factors to consider in order to develop a successful *in vitro* vascular wall model are as follows: (i) a scaffold that can support cell growth, (ii) an appropriate cell population, (iii) the right biological (use of biomolecules, such as growth factors), and (iv) mechanical stimuli to influence the proper development of the construct (Fortunato et al., 2017). Different research groups have been working with the final aim to develop *in vitro* models able to finely mimic the wall structure of a healthy human artery. Some examples of the development in *in vitro* models, based on different approaches, can be found in **Table 5**.

Collagen is widely used for the development of physiologically relevant *in vitro* models (Boccafoschi et al., 2005; Seifu et al., 2013; Pawelec et al., 2016). One of the main challenges in developing an *in vitro* vascular wall model is the interaction between the different populations of cells (Battiston et al., 2014). Loy et al. (2016, 2018) developed an *in vitro* model of the vascular wall based on collagen gels cellularized with SMCs, fibroblasts, and ECs. In this study, the importance of co-culturing these three vascular cell types in order to promote cell–matrix remodeling and to obtain an early expression of elastic fiber-related proteins was stressed. Furthermore, it was shown that the use of a tri-culture model resulted in cell–cell interactions similar to *in vivo* conditions. Another challenge in the development of advanced *in vitro* vascular models, as for vTE grafts, is the improvement of mechanical properties (i.e., compliance, burst pressure, and elasticity) and an increase in complexity of the model. Pezzoli et al. (2018) developed a collagen-based *in vitro* model that was supplemented with human plasma fibronectin. This resulted in an increase in elastin deposition by SMCs, as well as an increase in the expression levels of several proteins required for elastogenesis (i.e., fibrillin-1, lysyl oxidase, fibulin-4, and latent TGF-β binding protein-4). The study showed how fibronectin plays a crucial role in the production of physiological-like, elastin-containing collagen matrices displaying superior mechanical properties compared to the currently used models. It has been shown that *in vitro* simulation of physiological biochemical and biomechanical conditions plays a crucial role in the development of a physiologically relevant model of the vascular wall. To achieve this, research has focused on different strategies, including the use of bioreactors (Bono et al., 2017; Tresoldi et al., 2017). Bioreactors have gained large interest because they provide the possibility to mimic a physiological environment similar to the human *in vivo* situation, allowing the improvement of both mechanical and biological properties of *in vitro* models (Arslan-Yildiz et al., 2016; Tresoldi et al., 2017; Loy et al., 2018). The physiological-like mechanical stimulation is of utmost importance in the development of an engineered model of the vascular wall. The applied hemodynamic forces can lead to improvements in the structural and mechanical properties of the engineered construct. This is mainly due to an increased circumferential orientation of the SMCs and the alignment of the ECs along the flow direction, leading to a higher yield stress, ultimate stress, and elastic modulus (Ziegler et al., 1995; Tresoldi et al., 2017). Moreover, the simulation of physiological pulsatile perfusion improves not only the artificial vascular development in terms of cell alignment and organization (Houtchens et al., 2008; Lesman et al., 2016; Asano et al., 2018), but also the cell differentiation and phenotypic maintenance (Cevallos et al., 2006; Li and Xu, 2007; Qiu et al., 2014), ECM production (Stanley et al., 2000; Halka et al., 2008), vascular tone (Garoffolo et al., 2018), and mechanical properties (Seliktar et al., 2000) of the engineered construct (Meghezi et al., 2012; Wissing et al., 2017; Colunga and Dalton, 2018).

TABLE 4 | Pre-clinical and clinical studies on collagen-based vascular tissue engineering products.

Material	Structure	Application	Implanted in	References
Bovine collagen type I	Porous collagen scaffolds	Tissue vascularization	Murine model (C57B/L6 mice)	Chan et al., 2016
Rat tail type I collagen	Dense gel tubes	Small-diameter vascular grafts	Murine model (Sprague–Dawley rats)	Li et al., 2017
Autologous collagen matrix	*in vivo* tissue-engineered autologous vascular graft	Pediatric pulmonary artery augmentation	Human model (2-years-old girl with pulmonary atresia)	Kato et al., 2016
Collagen type I and type III	Porous collagen membranes	Myocardial ischemia repair	Rabbit model	Gao et al., 2011

TABLE 5 | Vascular tissue-engineered *in vitro* models and strategies used.

Developed model	Strategy	References
Planar vessel wall model	Collagen type I hydrogel	Loy et al., 2016
Tissue-engineered vascular equivalent	Polyglycolic-acid (PGA) meshes	Robert et al., 2013
Tubular vascular model for inflammatory response analysis	Collagen type I Scaffold	Chen et al., 2018
Micro-vascular networks	3-D printing approach	Schoneberg et al., 2018

Currently Used Collagen-Based *in vitro* Models for CVDs and Drug Development Studies

Medical drugs that contribute to blood pressure elevation or reduction can have a great efficacy in reducing cardiovascular risks (Cameron et al., 2016). Vasodilation and vasoconstriction directly affect the blood vessel diameter and thus an increased or decreased blood flow; therefore, they have an immediate impact on the blood pressure (Toda et al., 2013). More than 80% of currently proposed pharmaceutical drug candidates that enter clinical trials fail due to concerns with human efficacy and toxicity (Fernandez et al., 2016). Animal responses to drugs exhibit differences in toxic doses and drug metabolism. Therefore, the development of *in vitro* models that accurately mimic specific biological interactions, particularly relevant to diseases, using human cells to be able to predict local responses to administered drugs is of critical importance (Truskey and Fernandez, 2015; Fernandez et al., 2016; Ronaldson-Bouchard and Vunjak-Novakovic, 2018). For example, it is known that the SMCs in the media layer of the vascular wall are fundamental for the regulation of the vascular tone, being a key factor in the contractile portion of the vascular wall (Wolf et al., 2016). Next to this, the ECs layer exerts important effects on the vascular tone too, mainly through the release of vasoconstrictor and vasodilator molecules (Toda et al., 2013). Vaso-activity, being the vascular activity involving the effect of either increasing or decreasing blood pressure and/or heart rate, is considered an important feature and a desirable characteristic for a tissue-engineered model. It is influenced by many factors including cell phenotype and cell–matrix interactions. Different models have been developed over the years. The group of Laflamme (Laflamme et al., 2005) made use of a simple SMC-based media layer for studying the vaso-reactive properties, whereas Fernandez et al. (2016) and Niklason et al. (1999) fabricated a model based on a media layer combined with an EC layer to mimic the vessel intima layer.

Fernandez et al. (2016) validated the use of non-destructive monitoring strategies on collagen-based vascular constructs. This strategy helped in discovering that acetylcholine, which stimulates the release of nitric oxide, prostacyclin, and endothelium-derived hyperpolarization factor in vessels with a healthy and intact endothelium, is an important vasodilator in coronary arteries, enabling the quantification of endothelium-dependent vasodilation. On the other hand, phenylephrine enables the non-destructive measure of endothelium-independent vasoconstriction. The group of Schutte has studied the functionality of collagen-based engineered vascular media layers by looking at a large panel of vasoactive agents that consists of drugs from both intrinsic and extrinsic pathways (Schutte et al., 2010b). The study has shown that the collagen-based models were capable of generating a measurable response to several different vasoconstrictors and vasodilators. They highlighted the importance of vaso-activity and the functionality of developed models, as well as the choice of a large panel of drugs to test both features. In their work from 2016, Wolf et al. gave an overview on different engineered vascular constructs studied for pharmacological studies (Wolf et al., 2016). These studies demonstrate that TE vascular constructs can be used as *in vitro* models to investigate pharmacologically induced responses. However, these studies have currently been done on simplified models of the vascular wall using only the media and intima layer. Further research on the evaluation of the effects of vaso-reactive stimuli on a more advanced, complex, and physiologically relevant model of the vascular wall is yet to be studied. It can be concluded that *in vitro* models of the vascular wall show great potential and importance in the study of CVD and treatment, both at pre-clinical and clinical stages.

DISCUSSION

Strengths, Weaknesses, Opportunities, and Threats of Collagen as a Biomaterial for vTE

Despite the multiple beneficial properties and the variety of proposed applications in vTE described in this review, the use of collagen in vascular medicine is still hampered by some problems. The strength, weaknesses, opportunities, and threats (SWOT)

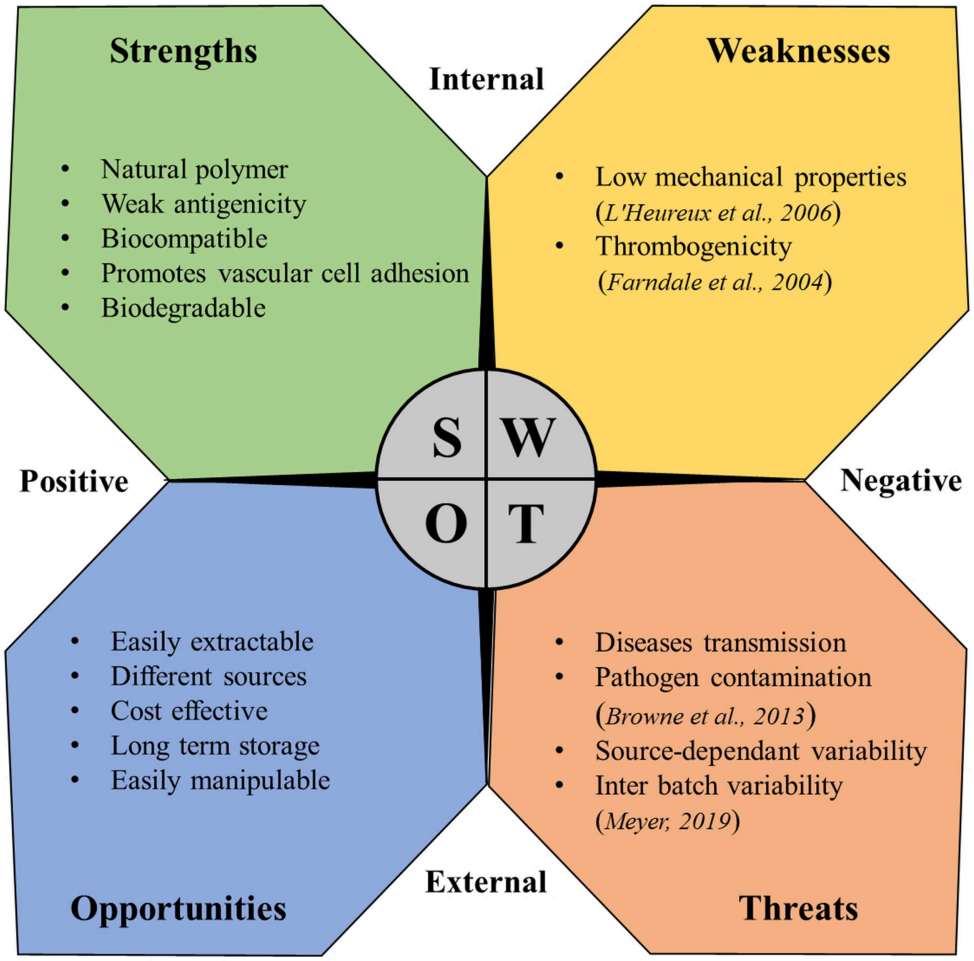

FIGURE 4 | SWOT analysis for collagen as a material for vascular tissue engineering (Farndale et al., 2004; L'Heureux et al., 2006; Browne et al., 2013; Meyer, 2019).

analysis represented in **Figure 4** summarizes the benefits and the main problems and concerns related to the use of collagen in this field.

Limits of Collagen

As mentioned in the SWOT analysis, two main limits heavily hamper the use of collagen in vTE: collagen thrombogenicity and its poor mechanical properties. Especially for applications where blood contact plays a major role like in vTE, collagen intrinsic thrombogenicity represents a major limitation. In fact, collagen is known to be one of the major activators of platelet response, being able to trigger and support both platelet adhesion and activation (Farndale et al., 2004), thus impacting the thrombogenicity of vascular devices. Thrombogenic potential, especially for vascular graft, is a major issue, being responsible for earlier graft occlusion (Sarkar et al., 2007). Thus, the use of collagen has been addressed for these reasons (Guidoin et al., 1996). Modification of the collagen through bonding of antithrombotic agents, such as heparin has been proposed over the years (Keuren et al., 2004; Scharn et al., 2006; Al Meslmani et al., 2014), partially solving the issue but leaving an open problem. Collagen plays a major role for *in vivo* vascular stiffness, conferring mechanical resistance along with the other molecules of the vascular ECM. However, extraction processes critically compromised the mechanical strength of collagen. As a consequence, low mechanical properties are reported as one of the main problems related to collagen for vTE (L'Heureux et al., 2006), thus limiting its clinical application. Over the years, improvements have been shown through dynamic conditioning (Seliktar et al., 2000; Buttafoco et al., 2006; Schutte et al., 2010a) or enhanced cross-linking techniques (Brinkman et al., 2003). Unfortunately, although these are promising techniques, all reported cases in the literature show ultimate mechanical properties significantly below those of native blood vessels (Pashneh-Tala et al., 2016), once again showing the difficulties in the clinical translation.

CONCLUSIONS AND OUTLOOK

Collagen-based scaffolds have been proven to be a versatile biomaterial for vascular applications, gaining great achievements in vTE. Although collagen is complex by nature, its use allowed

great developments in implants and drug delivery and offers great opportunities in several fields of tissue engineering, for dermal, cardiovascular, and connective applications. From a scientific point of view, the open challenge remains to be able to reproduce the hierarchically complex nature of tissues starting from collagen. In fact, in living tissue, a number of biologically active molecules, proteins, and cells work together in a very dynamic environment continuously orchestrating regeneration. From an industrial point of view, although some companies are now able to extract, sterilize, de-immunize, neutralize, and finally provide different types of collagen in a reproducible manner, its cost remains prohibitive and seriously limits studies and developments in the field. Therefore, the open challenges remain to find alternative sources and to optimize processes and protocols for reliable, reproducible, safe, and low-cost collagen. Finally, accreditation and regulatory bodies are the missed elements in this complex equation. The idea to synthesize collagen in laboratory is an idea worthy to be further explored and that will also facilitate the regulation concerning the collagen structures, in the interest of the patients, and for the benefit of the society.

AUTHOR CONTRIBUTIONS

FC and DM conceived the layout, the rationale, and the plan of this manuscript. FC and NP wrote the first draft of the manuscript that was iteratively improved by SV, FB, and DM.

REFERENCES

Abraham, G. A., Murray, J., Billiar, K., and Sullivan, S. J. (2000). Evaluation of the porcine intestinal collagen layer as a biomaterial. *J. Biomed. Mater. Res.* 51, 442–452. doi: 10.1002/1097-4636(20000905)51:3<442::AID-JBM19>3.0.CO;2-4

Abramo, A. C., and Viola, J. C. (1992). Heterologous collagen matrix sponge: histologic and clinical response to its implantation in third-degree burn injuries. *Br. J. Plast. Surg.* 45, 117–122. doi: 10.1016/0007-1226(92)90170-3

Achilli, M., Lagueux, J., and Mantovani, D. (2010). On the effects of UV-C and pH on the mechanical behavior, molecular conformation and cell viability of collagen-based scaffold for vascular tissue engineering. *Macromol. Biosci.* 10, 307–316. doi: 10.1002/mabi.200900248

Al Meslmani, B., Mahmoud, G., Strehlow, B., Mohr, E., Leichtweiss, T., and Bakowsky, U. (2014). Development of thrombus-resistant and cell compatible crimped polyethylene terephthalate cardiovascular grafts using surface co-immobilized heparin and collagen. *Mater. Sci. Eng. C. Mater. Biol. Appl.* 43, 538–546. doi: 10.1016/j.msec.2014.07.059

Arslan-Yildiz, A., El Assal, R., Chen, P., Guven, S., Inci, F., and Demirci, U. (2016). Towards artificial tissue models: past, present, and future of 3D bioprinting. *Biofabrication* 8:014103. doi: 10.1088/1758-5090/8/1/014103

Asano, S., Ito, S., Morosawa, M., Furuya, K., Naruse, K., Sokabe, M., et al. (2018). Cyclic stretch enhances reorientation and differentiation of 3-D culture model of human airway smooth muscle. *Biochem. Biophys. Rep.* 16, 32–38. doi: 10.1016/j.bbrep.2018.09.003

Batt, M., Magne, J. L., Alric, P., Muzj, A., Ruotolo, C., Ljungstrom, K. G., et al. (2003). *In situ* revascularization with silver-coated polyester grafts to treat aortic infection: early and midterm results. *J. Vasc. Surg.* 38, 983–989. doi: 10.1016/S0741-5214(03)00554-8

Battiston, K. G., Cheung, J. W., Jain, D., and Santerre, J. P. (2014). Biomaterials in co-culture systems: towards optimizing tissue integration and cell signaling within scaffolds. *Biomaterials* 35, 4465–4476. doi: 10.1016/j.biomaterials.2014.02.023

Bella, J., and Hulmes, D. J. (2017). Fibrillar collagens. *Subcell. Biochem.* 82, 457–490. doi: 10.1007/978-3-319-49674-0_14

Berglund, J. D., Mohseni, M. M., Nerem, R. M., and Sambanis, A. (2003). A biological hybrid model for collagen-based tissue engineered vascular constructs. *Biomaterials* 24, 1241–1254. doi: 10.1016/S0142-9612(02)00506-9

Berglund, J. D., Nerem, R. M., and Sambanis, A. (2004). Incorporation of intact elastin scaffolds in tissue-engineered collagen-based vascular grafts. *Tissue Eng.* 10, 1526–1535. doi: 10.1089/ten.2004.10.1526

Boccafoschi, F., Habermehl, J., Vesentini, S., and Mantovani, D. (2005). Biological performances of collagen-based scaffolds for vascular tissue engineering. *Biomaterials* 26, 7410–7417. doi: 10.1016/j.biomaterials.2005.05.052

Boccafoschi, F., Rajan, N., Habermehl, J., and Mantovani, D. (2007). Preparation and characterization of a scaffold for vascular tissue engineering by direct-assembling of collagen and cells in a cylindrical geometry. *Macromol. Biosci.* 7, 719–726. doi: 10.1002/mabi.200600242

Bono, N., Meghezi, S., Soncini, M., Piola, M., Mantovani, D., and Fiore, G. B. (2017). A dual-mode bioreactor system for tissue engineered vascular models. *Ann. Biomed. Eng.* 45, 1496–1510. doi: 10.1007/s10439-017-1813-9

Bou-Gharios, G., Ponticos, M., Rajkumar, V., and Abraham, D. (2004). Extra-cellular matrix in vascular networks. *Cell Prolif.* 37, 207–220. doi: 10.1111/j.1365-2184.2004.00306.x

Bradley, W. G., and Wilkes, G. L. (1977). Some mechanical property considerations of reconstituted collagen for drug release supports. *Biomater. Med. Devices Artif. Organs* 5, 159–175. doi: 10.3109/10731197709118671

Brazel, D., Oberbaumer, I., Dieringer, H., Babel, W., Glanville, R. W., Deutzmann, R., et al. (1987). Completion of the amino acid sequence of the alpha 1 chain of human basement membrane collagen (type IV) reveals 21 non-triplet interruptions located within the collagenous domain. *Eur. J. Biochem.* 168, 529–536. doi: 10.1111/j.1432-1033.1987.tb13450.x

Brinkman, W. T., Nagapudi, K., Thomas, B. S., and Chaikof, E. L. (2003). Photo-cross-linking of type I collagen gels in the presence of smooth muscle cells: mechanical properties, cell viability, and function. *Biomacromolecules* 4, 890–895. doi: 10.1021/bm0257412

Browne, S., Zeugolis, D. I., and Pandit, A. (2013). Collagen: finding a solution for the source. *Tissue Eng. Part A* 19, 1491–1494. doi: 10.1089/ten.tea.2012.0721

Buttafoco, L., Engbers-Buijtenhuijs, P., Poot, A. A., Dijkstra, P. J., Vermes, I., and Feijen, J. (2006). Physical characterization of vascular grafts cultured in a bioreactor. *Biomaterials* 27, 2380–2389. doi: 10.1016/j.biomaterials.2005.10.017

Byrom, M. J., Bannon, P. G., White, G. H., and Ng, M. K. (2010). Animal models for the assessment of novel vascular conduits. *J. Vasc. Surg.* 52, 176–195. doi: 10.1016/j.jvs.2009.10.080

Cameron, A. C., Lang, N. N., and Touyz, R. M. (2016). Drug treatment of hypertension: focus on vascular health. *Drugs* 76, 1529–1550. doi: 10.1007/s40265-016-0642-8

Cevallos, M., Riha, G. M., Wang, X., Yang, H., Yan, S., Li, M., et al. (2006). Cyclic strain induces expression of specific smooth muscle cell markers in human endothelial cells. *Differentiation* 74, 552–561. doi: 10.1111/j.1432-0436.2006.00089.x

Chan, E. C., Kuo, S. M., Kong, A. M., Morrison, W. A., Dusting, G. J., Mitchell, G. M., et al. (2016). Three dimensional collagen scaffold promotes intrinsic vascularisation for tissue engineering applications. *PLoS ONE* 11:e0149799. doi: 10.1371/journal.pone.0149799

Chan, S. J., Love, C., Spector, M., Cool, S. M., Nurcombe, V., and Lo, E. H. (2017). Endogenous regeneration: Engineering growth factors for stroke. *Neurochem. Int.* 107, 57–65. doi: 10.1016/j.neuint.2017.03.024

Chandler, L. A., Gu, D. L., Ma, C., Gonzalez, A. M., Doukas, J., Nguyen, T., et al. (2000). Matrix-enabled gene transfer for cutaneous wound repair. *Wound Repair Regen.* 8, 473–479. doi: 10.1046/j.1524-475x.2000.00473.x

Chandrakasan, G., Torchia, D. A., and Piez, K. A. (1976). Preparation of intact monomeric collagen from rat tail tendon and skin and the structure of the nonhelical ends in solution. *J. Biol. Chem.* 251, 6062–6067.

Charulatha, V., and Rajaram, A. (2003). Influence of different crosslinking treatments on the physical properties of collagen

membranes. *Biomaterials* 24, 759–767. doi: 10.1016/S0142-9612(02)00412-X

Chattopadhyay, S., and Raines, R. T. (2014). Review collagen-based biomaterials for wound healing. *Biopolymers* 101, 821–833. doi: 10.1002/bip.22486

Chen, F., Yoo, J. J., and Atala, A. (1999). Acellular collagen matrix as a possible "off the shelf" biomaterial for urethral repair. *Urology* 54, 407–410. doi: 10.1016/S0090-4295(99)00179-X

Chen, Z., Tang, M., Huang, D., Jiang, W., Li, M., Ji, H., et al. (2018). Real-time observation of leukocyte–endothelium interactions in tissue-engineered blood vessel. *Lab Chip* 18, 2047–2054. doi: 10.1039/C8LC00202A

Cherubino, M., Valdatta, L., Balzaretti, R., Pellegatta, I., Rossi, F., Protasoni, M., et al. (2016). Human adipose-derived stem cells promote vascularization of collagen-based scaffolds transplanted into nude mice. *Regen. Med.* 11, 261–271. doi: 10.2217/rme-2015-0010

Chervu, A., Moore, W. S., Chvapil, M., and Henderson, T. (1991). Efficacy and duration of antistaphylococcal activity comparing three antibiotics bonded to Dacron vascular grafts with a collagen release system. *J. Vasc. Surg.* 13, 897–901. doi: 10.1016/0741-5214(91)90057-2

Chiang, T. M., Postlethwaite, A. E., Beachey, E. H., Seyer, J. M., and Kang, A. H. (1978). Binding of chemotactic collagen-derived peptides to fibroblasts. The relationship to fibroblast chemotaxis. *J. Clin. Invest.* 62, 916–922. doi: 10.1172/JCI109219

Chiu, L. L., Radisic, M., and Vunjak-Novakovic, G. (2010). Bioactive scaffolds for engineering vascularized cardiac tissues. *Macromol. Biosci.* 10, 1286–1301. doi: 10.1002/mabi.201000202

Chlupac, J., Filova, E., and Bacakova, L. (2009). Blood vessel replacement: 50 years of development and tissue engineering paradigms in vascular surgery. *Physiol. Res.* 58, S119–S139.

Clowes, A. W. (1993). Intimal hyperplasia and graft failure. *Cardiovasc. Pathol.* 2, 179–186. doi: 10.1016/1054-8807(93)90058-A

Colunga, T., and Dalton, S. (2018). Building blood vessels with vascular progenitor cells. *Trends Mol. Med.* 24, 630–641. doi: 10.1016/j.molmed.2018.05.002

Cummings, C. L., Gawlitta, D., Nerem, R. M., and Stegemann, J. P. (2004). Properties of engineered vascular constructs made from collagen, fibrin, and collagen-fibrin mixtures. *Biomaterials* 25, 3699–3706. doi: 10.1016/j.biomaterials.2003.10.073

Davidenko, N., Schuster, C. F., Bax, D. V., Raynal, N., Farndale, R. W., Best, S. M., et al. (2015). Control of crosslinking for tailoring collagen-based scaffolds stability and mechanics. *Acta Biomater.* 25, 131–142. doi: 10.1016/j.actbio.2015.07.034

Delarive, T., Rossier, A., Rossier, S., Ravinet, E., Shaarawy, T., and Mermoud, A. (2003). Aqueous dynamic and histological findings after deep sclerectomy with collagen implant in an animal model. *Br. J. Ophthalmol.* 87, 1340–1344. doi: 10.1136/bjo.87.11.1340

Di Lullo, G. A., Sweeney, S. M., Korkko, J., Ala-Kokko, L., and San Antonio, J. D. (2002). Mapping the ligand-binding sites and disease-associated mutations on the most abundant protein in the human, type I collagen. *J. Biol. Chem.* 277, 4223–4231. doi: 10.1074/jbc.M110709200

Dogan, A., Elcin, A. E., and Elcin, Y. M. (2017). Translational applications of tissue engineering in cardiovascular medicine. *Curr. Pharm. Des.* 23, 903–914. doi: 10.2174/1381612823666161111141954

Edelberg, J. M., Christie, P. D., and Rosenberg, R. D. (2001). Regulation of vascular bed-specific prothrombotic potential. *Circ Res.* 89, 117–124. doi: 10.1161/hh1401.093954

Ehrmann, R. L., and Gey, G. O. (1956). The growth of cells on a transparent gel of reconstituted rat-tail collagen. *J. Natl. Cancer Inst.* 16, 1375–1403.

Eshar, D., Wyre, N. R., and Schoster, J. V. (2011). Use of collagen shields for treatment of chronic bilateral corneal ulcers in a pet rabbit. *J. Small Anim. Pract.* 52, 380–383. doi: 10.1111/j.1748-5827.2011.01077.x

Exposito, J. Y., Cluzel, C., Garrone, R., and Lethias, C. (2002). Evolution of collagens. *Anat. Rec.* 268, 302–316. doi: 10.1002/ar.10162

Exposito, J. Y., Le Guellec, D., Lu, Q., and Garrone, R. (1991). Short chain collagens in sponges are encoded by a family of closely related genes. *J. Biol. Chem.* 266, 21923–21928.

Exposito, J. Y., Valcourt, U., Cluzel, C., and Lethias, C. (2010). The fibrillar collagen family. *Int. J. Mol. Sci.* 11, 407–426. doi: 10.3390/ijms11020407

Farndale, R. W., Sixma, J. J., Barnes, M. J., and de Groot, P. G. (2004). The role of collagen in thrombosis and hemostasis. *J. Thromb. Haemost.* 2, 561–573. doi: 10.1111/j.1538-7836.2004.00665.x

Fernandez, C. E., Yen, R. W., Perez, S. M., Bedell, H. W., Povsic, T. J., Reichert, W. M., et al. (2016). Human vascular microphysiological system for *in vitro* drug screening. *Sci. Rep.* 6:21579. doi: 10.1038/srep21579

Fleck, C. A., and Simman, R. (2010). Modern collagen wound dressings: function and purpose. *J. Am. Col. Certif. Wound Spec.* 2, 50–54. doi: 10.1016/j.jcws.2010.12.003

Fortunato, T. M., De Bank, P. A., and Pula, G. (2017). Vascular regenerative surgery: promised land for tissue engineers? *Int. J. Stem Cell Res. Transplant.* 5, 268–276. doi: 10.19070/2328-3548-1700041

Freischlag, J. A., and Moore, W. S. (1990). Clinical experience with a collagen-impregnated knitted Dacron vascular graft. *Ann. Vasc. Surg.* 4, 449–454. doi: 10.1016/S0890-5096(07)60069-7

Friess, W. (1998). Collagen—biomaterial for drug delivery. *Eur. J. Pharm. Biopharm.* 45, 113–136. doi: 10.1016/S0939-6411(98)00017-4

Furthmayr, H., and Timpl, R. (1976). Immunochemistry of collagens and procollagens. *Int. Rev. Connect Tissue Res.* 7, 61–99. doi: 10.1016/B978-0-12-363707-9.50008-3

Gallop, P. M., and Paz, M. A. (1975). Posttranslational protein modifications, with special attention to collagen and elastin. *Physiol. Rev.* 55, 418–487. doi: 10.1152/physrev.1975.55.3.418

Gao, J., Liu, J., Gao, Y., Wang, C., Zhao, Y., Chen, B., et al. (2011). A myocardial patch made of collagen membranes loaded with collagen-binding human vascular endothelial growth factor accelerates healing of the injured rabbit heart. *Tissue Eng. Part A* 17, 2739–2747. doi: 10.1089/ten.tea.2011.0105

Garoffolo, G., Madonna, R., de Caterina, R., and Pesce, M. (2018). Cell based mechanosensing in vascular patho-biology: more than a simple go-with the flow. *Vascul. Pharmacol.* 111, 7–14. doi: 10.1016/j.vph.2018.06.013

Gaudet, I. D., and Shreiber, D. I. (2012). Characterization of methacrylated type-I collagen as a dynamic, photoactive hydrogel. *Biointerphases* 7:25. doi: 10.1007/s13758-012-0025-y

Girton, T. S., Oegema, T. R., Grassl, E. D., Isenberg, B. C., and Tranquillo, R. T. (2000). Mechanisms of stiffening and strengthening in media-equivalents fabricated using glycation. *J. Biomech. Eng.* 122, 216–223. doi: 10.1115/1.429652

Gruber, H. E., Hoelscher, G. L., Leslie, K., Ingram, J. A., and Hanley, E. N., Jr. (2006). Three-dimensional culture of human disc cells within agarose or a collagen sponge: assessment of proteoglycan production. *Biomaterials* 27, 371–376. doi: 10.1016/j.biomaterials.2005.06.032

Gruber, H. E., Leslie, K., Ingram, J., Norton, H. J., and Hanley, E. N. (2004). Cell-based tissue engineering for the intervertebral disc: *in vitro* studies of human disc cell gene expression and matrix production within selected cell carriers. *Spine J.* 4, 44–55. doi: 10.1016/S1529-9430(03)00425-X

Guidoin, R., Marois, Y., Deng, X., Chakfe, N., Marois, M., Roy, R., et al. (1996). Can collagen impregnated polyester arterial prostheses be recommended as small diameter blood conduits? *ASAIO J.* 42, 974–983. doi: 10.1097/00002480-199642060-00010

Gullberg, D., Gehlsen, K. R., Turner, D. C., Ahlen, K., Zijenah, L. S., Barnes, M. J., et al. (1992). Analysis of alpha 1 beta 1, alpha 2 beta 1 and alpha 3 beta 1 integrins in cell–collagen interactions: identification of conformation dependent alpha 1 beta 1 binding sites in collagen type I. *EMBO J.* 11, 3865–3873. doi: 10.1002/j.1460-2075.1992.tb05479.x

Habermehl, J., Skopinska, J., Boccafoschi, F., Sionkowska, A., Kaczmarek, H., Laroche, G., et al. (2005). Preparation of ready-to-use, stockable and reconstituted collagen. *Macromol. Biosci.* 5, 821–828. doi: 10.1002/mabi.200500102

Halka, A. T., Turner, N. J., Carter, A., Ghosh, J., Murphy, M. O., Kirton, J. P., et al. (2008). The effects of stretch on vascular smooth muscle cell phenotype *in vitro*. *Cardiovasc. Pathol.* 17, 98–102. doi: 10.1016/j.carpath.2007.03.001

Hao, W., Han, J., Chu, Y., Huang, L., Zhuang, Y., Sun, J., et al. (2018). Collagen/heparin bi-affinity multilayer modified collagen scaffolds for controlled bFGF release to improve angiogenesis *in vivo*. *Macromol. Biosci.* 18:e1800086. doi: 10.1002/mabi.201870028

He, Q., Zhao, Y., Chen, B., Xiao, Z., Zhang, J., Chen, L., et al. (2011). Improved cellularization and angiogenesis using collagen scaffolds chemically conjugated with vascular endothelial growth factor. *Acta Biomater.* 7, 1084–1093. doi: 10.1016/j.actbio.2010.10.022

He, W., Yong, T., Teo, W. E., Ma, Z., and Ramakrishna, S. (2005). Fabrication and endothelialization of collagen-blended biodegradable polymer nanofibers: potential vascular graft for blood vessel tissue engineering. *Tissue Eng.* 11, 1574–1588. doi: 10.1089/ten.2005.11.1574

Herten, M., Idelevich, E. A., Sielker, S., Becker, K., Scherzinger, A. S., Osada, N., et al. (2017). Vascular graft impregnation with antibiotics: the influence of high concentrations of rifampin, vancomycin, daptomycin, and bacteriophage endolysin HY-133 on viability of vascular cells. *Med. Sci. Monit. Basic Res.* 23, 250–257. doi: 10.12659/MSMBR.902879

Hirai, J., Kanda, K., Oka, T., and Matsuda, T. (1994). Highly oriented, tubular hybrid vascular tissue for a low pressure circulatory system. *ASAIO J.* 40, M383–M388. doi: 10.1097/00002480-199407000-00027

Holmes, R., Yang, X. B., Dunne, A., Florea, L., Wood, D., and Tronci, G. (2017). Thiol-ene photo-click collagen-PEG hydrogels: impact of water-soluble photoinitiators on cell viability, gelation kinetics and rheological properties. *Polymers* 9:226. doi: 10.3390/polym9060226

Houtchens, G. R., Foster, M. D., Desai, T. A., Morgan, E. F., and Wong, J. Y. (2008). Combined effects of microtopography and cyclic strain on vascular smooth muscle cell orientation. *J. Biomech.* 41, 762–769. doi: 10.1016/j.jbiomech.2007.11.027

Hulmes, D. J. (2002). Building collagen molecules, fibrils, and suprafibrillar structures. *J. Struct. Biol.* 137, 2–10. doi: 10.1006/jsbi.2002.4450

Humphries, A. W., Hawk, W. A., and Cuthbertson, A. M. (1961). Arterial prosthesis of collagen-impregnated Dacron tulle. *Surgery* 50, 947–954.

Huzella, T., and Lengyel, J. (1932). Orientation de la croissance des cultures de tissus sur la trame fibrillaire artificielle coagulée de la solution de "collagène A" (Nageotte) par les forces de la cristallisation. *Compt. Rend. Soc. Biol.* 109, 515–518.

Ishikawa, Y., and Bachinger, H. P. (2013). A molecular ensemble in the rER for procollagen maturation. *Biochim. Biophys. Acta* 1833, 2479–2491. doi: 10.1016/j.bbamcr.2013.04.008

Ivester, K. M., Adams, S. B., Moore, G. E., Van Sickle, D. C., and Lescun, T. B. (2006). Gentamicin concentrations in synovial fluid obtained from the tarsocrural joints of horses after implantation of gentamicin-impregnated collagen sponges. *Am. J. Vet. Res.* 67, 1519–1526. doi: 10.2460/ajvr.67.9.1519

Jenkins, E., Moss, J. B., Pace, J. M., and Bridgewater, L. C. (2005). The new collagen gene COL27A1 contains SOX9-responsive enhancer elements. *Matrix Biol.* 24, 177–184. doi: 10.1016/j.matbio.2005.02.004

Jeong, S. I., Kim, S. Y., Cho, S. K., Chong, M. S., Kim, K. S., Kim, H., et al. (2007). Tissue-engineered vascular grafts composed of marine collagen and PLGA fibers using pulsatile perfusion bioreactors. *Biomaterials* 28, 1115–1122. doi: 10.1016/j.biomaterials.2006.10.025

Johnson, K. A., Rogers, G. J., Roe, S. C., Howlett, C. R., Clayton, M. K., Milthorpe, B. K., et al. (1999). Nitrous acid pretreatment of tendon xenografts cross-linked with glutaraldehyde and sterilized with gamma irradiation. *Biomaterials* 20, 1003–1015. doi: 10.1016/S0142-9612(98)90187-9

Jonas, R. A., Schoen, F. J., Ziemer, G., Britton, L., and Castaneda, A. R. (1987). Biological sealants and knitted Dacron conduits: comparison of collagen and fibrin glue pretreatments in circulatory models. *Ann. Thorac. Surg.* 44, 283–290. doi: 10.1016/S0003-4975(10)62075-9

Kanematsu, A., Yamamoto, S., Ozeki, M., Noguchi, T., Kanatani, I., Ogawa, O., et al. (2004). Collagenous matrices as release carriers of exogenous growth factors. *Biomaterials* 25, 4513–4520. doi: 10.1016/j.biomaterials.2003.11.035

Kannan, R. Y., Salacinski, H. J., Butler, P. E., Hamilton, G., and Seifalian, A. M. (2005). Current status of prosthetic bypass grafts: a review. *J. Biomed. Mater. Res. B Appl. Biomater.* 74, 570–581. doi: 10.1002/jbm.b.30247

Kato, N., Yamagishi, M., Kanda, K., Miyazaki, T., Maeda, Y., Yamanami, M., et al. (2016). First successful clinical application of the *in vivo* tissue-engineered autologous vascular graft. *Ann. Thorac. Surg.* 102, 1387–1390. doi: 10.1016/j.athoracsur.2016.06.095

Kaufman, H. E., Steinemann, T. L., Lehman, E., Thompson, H. W., Varnell, E. D., Jacob-LaBarre, J. T., et al. (1994). Collagen-based drug delivery and artificial tears. *J. Ocul. Pharmacol.* 10, 17–27. doi: 10.1089/jop.1994.10.17

Keuren, J. F., Wielders, S. J., Driessen, A., Verhoeven, M., Hendriks, M., and Lindhout, T. (2004). Covalently-bound heparin makes collagen thromboresistant. *Arterioscler. Thromb. Vasc. Biol.* 24, 613–617. doi: 10.1161/01.ATV.0000116026.18945.66

Kobayashi, J., Backer, C. L., Zales, V. R., Crawford, S. E., Muster, A. J., and Mavroudis, C. (1993). Failure of the Hemashield extension in right ventricle-to-pulmonary artery conduits. *Ann. Thorac. Surg.* 56, 277–281. doi: 10.1016/0003-4975(93)91159-K

Koch, S., Yao, C., Grieb, G., Prevel, P., Noah, E. M., and Steffens, G. C. (2006). Enhancing angiogenesis in collagen matrices by covalent incorporation of VEGF. *J. Mater. Sci. Mater. Med.* 17, 735–741. doi: 10.1007/s10856-006-9684-x

Koens, M. J., Faraj, K. A., Wismans, R. G., van der Vliet, J. A., Krasznai, A. G., Cuijpers, V. M., et al. (2010). Controlled fabrication of triple layered and molecularly defined collagen/elastin vascular grafts resembling the native blood vessel. *Acta Biomater.* 6, 4666–4674. doi: 10.1016/j.actbio.2010.06.038

Koens, M. J., Krasznai, A. G., Hanssen, A. E., Hendriks, T., Praster, R., Daamen, W. F., et al. (2015). Vascular replacement using a layered elastin-collagen vascular graft in a porcine model: one week patency versus one month occlusion. *Organogenesis* 11, 105–121. doi: 10.1080/15476278.2015.1038448

Kon, E., Delcogliano, M., Filardo, G., Busacca, M., Di Martino, A., and Marcacci, M. (2011). Novel nano-composite multilayered biomaterial for osteochondral regeneration: a pilot clinical trial. *Am. J. Sports Med.* 39, 1180–1190. doi: 10.1177/0363546510392711

Konitsiotis, A. D., Raynal, N., Bihan, D., Hohenester, E., Farndale, R. W., and Leitinger, B. (2008). Characterization of high affinity binding motifs for the discoidin domain receptor DDR2 in collagen. *J. Biol. Chem.* 283, 6861–6868. doi: 10.1074/jbc.M709290200

Laflamme, K., Roberge, C. J., Labonte, J., Pouliot, S., D'Orleans-Juste, P., Auger, F. A., et al. (2005). Tissue-engineered human vascular media with a functional endothelin system. *Circulation* 111, 459–464. doi: 10.1161/01.CIR.0000153850.53419.50

Laiva, A. L., Raftery, R. M., Keogh, M. B., and O'Brien, F. J. (2018). Pro-angiogenic impact of SDF-1alpha gene-activated collagen-based scaffolds in stem cell driven angiogenesis. *Int. J. Pharm.* 544, 372–379. doi: 10.1016/j.ijpharm.2018.03.032

Lee, A. R. (2005). Enhancing dermal matrix regeneration and biomechanical properties of 2nd degree-burn wounds by EGF-impregnated collagen sponge dressing. *Arch. Pharm. Res.* 28, 1311–1316. doi: 10.1007/BF02978217

Lee, C. H., Singla, A., and Lee, Y. (2001). Biomedical applications of collagen. *Int. J. Pharm.* 221, 1–22. doi: 10.1016/S0378-5173(01)00691-3

Lesman, A., Rosenfeld, D., Landau, S., and Levenberg, S. (2016). Mechanical regulation of vascular network formation in engineered matrices. *Adv. Drug Deliv. Rev.* 96, 176–182. doi: 10.1016/j.addr.2015.07.005

L'Heureux, N., Dusserre, N., Konig, G., Victor, B., Keire, P., Wight, T. N., et al. (2006). Human tissue-engineered blood vessels for adult arterial revascularization. *Nat. Med.* 12, 361–365. doi: 10.1038/nm1364

L'Heureux, N., Germain, L., Labbe, R., and Auger, F. A. (1993). *In vitro* construction of a human blood vessel from cultured vascular cells: a morphologic study. *J. Vasc. Surg.* 17, 499–509. doi: 10.1016/0741-5214(93)90150-K

Li, C., and Xu, Q. (2007). Mechanical stress-initiated signal transduction in vascular smooth muscle cells *in vitro* and *in vivo*. *Cell Signal* 19, 881–891. doi: 10.1016/j.cellsig.2007.01.004

Li, X., Xu, J., Nicolescu, C. T., Marinelli, J. T., and Tien, J. (2017). Generation, endothelialization, and microsurgical suture anastomosis of strong 1-mm-diameter collagen tubes. *Tissue Eng. Part A* 23, 335–344. doi: 10.1089/ten.tea.2016.0339

Liu, X., Zheng, C., Luo, X., Wang, X., and Jiang, H. (2019). Recent advances of collagen-based biomaterials: multi-hierarchical structure, modification and biomedical applications. *Mater. Sci. Eng. C. Mater. Biol. Appl.* 99, 1509–1522. doi: 10.1016/j.msec.2019.02.070

Liu, Y., Gan, L., Carlsson, D. J., Fagerholm, P., Lagali, N., Watsky, M. A., et al. (2006). A simple, cross-linked collagen tissue substitute for corneal implantation. *Invest. Ophthalmol. Vis. Sci.* 47, 1869–1875. doi: 10.1167/iovs.05-1339

Long, J. L., and Tranquillo, R. T. (2003). Elastic fiber production in cardiovascular tissue-equivalents. *Matrix Biol.* 22, 339–350. doi: 10.1016/S0945-053X(03)00052-0

Loy, C., Meghezi, S., Levesque, L., Pezzoli, D., Kumra, H., Reinhardt, D., et al. (2016). A planar model of the vessel wall from cellularized-collagen scaffolds: focus on cell–matrix interactions in mono-, bi- and tri-culture models. *Biomater. Sci.* 5, 153–162. doi: 10.1039/C6BM00643D

Loy, C., Pezzoli, D., Candiani, G., and Mantovani, D. (2018). A cost-effective culture system for the *in vitro* assembly, maturation, and stimulation of advanced multilayered multiculture tubular tissue models. *Biotechnol. J.* 13. doi: 10.1002/biot.201700359

Lucas, P. A., Syftestad, G. T., Goldberg, V. M., and Caplan, A. I. (1989). Ectopic induction of cartilage and bone by water-soluble proteins from bovine bone using a collagenous delivery vehicle. *J. Biomed. Mater. Res.* 23, 23–39. doi: 10.1002/jbm.820231306

Lynn, A. K., Yannas, I. V., and Bonfield, W. (2004). Antigenicity and immunogenicity of collagen. *J. Biomed. Mater. Res. B Appl. Biomater.* 71, 343–354. doi: 10.1002/jbm.b.30096

Matassi, F., Nistri, L., Chicon Paez, D., and Innocenti, M. (2011). New biomaterials for bone regeneration. *Clin. Cases Miner. Bone Metab.* 8, 21–24.

Matsuda, T., Kitamura, T., Iwata, H., Takano, H., and Akutsu, T. (1988). A hybrid artificial vascular graft based upon an organ reconstruction model. Significance and design criteria of an artificial basement membrane. *ASAIO Trans.* 34, 640–643.

Meghezi, S., Couet, F., Chevallier, P., and Mantovani, D. (2012). Effects of a pseudophysiological environment on the elastic and viscoelastic properties of collagen gels. *Int. J. Biomater.* 2012:319290. doi: 10.1155/2012/319290

Meghezi, S., Seifu, D. G., Bono, N., Unsworth, L., Mequanint, K., and Mantovani, D. (2015). Engineering 3D cellularized collagen gels for vascular tissue regeneration. *J. Vis. Exp.* e52812. doi: 10.3791/52812

Meyer, M. (2019). Processing of collagen based biomaterials and the resulting materials properties. *Biomed. Eng. Online* 18:24. doi: 10.1186/s12938-019-0647-0

Nemeno-Guanzoni, J. G., Lee, S., Berg, J. R., Jo, Y. H., Yeo, J. E., Nam, B. M., et al. (2012). Trends in tissue engineering for blood vessels. *J. Biomed. Biotechnol.* 2012:956345. doi: 10.1155/2012/956345

Nicosia, R. F., Belser, P., Bonanno, E., and Diven, J. (1991). Regulation of angiogenesis *in vitro* by collagen metabolism. *In Vitro Cell Dev. Biol.* 27A, 961–966. doi: 10.1007/BF02631124

Niklason, L. E., Gao, J., Abbott, W. M., Hirschi, K. K., Houser, S., Marini, R., et al. (1999). Functional arteries grown *in vitro*. *Science* 284, 489–493. doi: 10.1126/science.284.5413.489

Noishiki, Y., Marat, D., Yamane, Y., Satoh, S., Ma, X. H., Iwai, Y., et al. (1996). A collagen coated fabric vascular prosthesis as a punctureable A-V shunt. *ASAIO J.* 42, M687–M693. doi: 10.1097/00002480-199609000-00075

Pashneh-Tala, S., MacNeil, S., and Claeyssens, F. (2016). The tissue-engineered vascular graft—past, present, and future. *Tissue Eng. Part B Rev.* 22, 68–100. doi: 10.1089/ten.teb.2015.0100

Patino, M. G., Neiders, M. E., Andreana, S., Noble, B., and Cohen, R. E. (2002). Collagen as an implantable material in medicine and dentistry. *J. Oral Implantol.* 28, 220–225. doi: 10.1563/1548-1336(2002)028<0220:CAAIMI>2.3.CO;2

Pawelec, K. M., Best, S. M., and Cameron, R. E. (2016). Collagen: a network for regenerative medicine. *J. Mater. Chem. B* 4, 6484–6496. doi: 10.1039/C6TB00807K

Pezzoli, D., Di Paolo, J., Kumra, H., Fois, G., Candiani, G., Reinhardt, D. P., et al. (2018). Fibronectin promotes elastin deposition, elasticity and mechanical strength in cellularised collagen-based scaffolds. *Biomaterials* 180, 130–142. doi: 10.1016/j.biomaterials.2018.07.013

Postlethwaite, A. E., Seyer, J. M., and Kang, A. H. (1978). Chemotactic attraction of human fibroblasts to type I, II, and III collagens and collagen-derived peptides. *Proc. Natl. Acad. Sci U.S.A.* 75, 871–875. doi: 10.1073/pnas.75.2.871

Potorac, S., Popa, M., Picton, L., Dulong, V., Verestiuc, L., and Le Cerf, D. (2014). Collagen functionalized with unsaturated cyclic anhydrides—interactions in solution and solid state. *Biopolymers.* 101, 228–236. doi: 10.1002/bip.22319

Prager, M. R., Hoblaj, T., Nanobashvili, J., Sporn, E., Polterauer, P., Wagner, O., et al. (2003). Collagen-versus gelatine-coated Dacron versus stretch PTFE bifurcation grafts for aortoiliac occlusive disease: long-term results of a prospective, randomized multicenter trial. *Surgery* 134, 80–85. doi: 10.1067/msy.2003.179

Pupkaite, J., Ahumada, M., McLaughlin, S., Temkit, M., Alaziz, S., Seymour, R., et al. (2017). Collagen-based photoactive agent for tissue bonding. *ACS Appl. Mater. Interfaces* 9, 9265–9270. doi: 10.1021/acsami.7b01984

Qiu, J., Zheng, Y., Hu, J., Liao, D., Gregersen, H., Deng, X., et al. (2014). Biomechanical regulation of vascular smooth muscle cell functions: from *in vitro* to *in vivo* understanding. *J. R. Soc. Interface* 11:20130852. doi: 10.1098/rsif.2013.0852

Ravichandran, R., Islam, M. M., Alarcon, E. I., Samanta, A., Wang, S., Lundström, P., et al. (2016). Functionalised type-I collagen as a hydrogel building block for bio-orthogonal tissue engineering applications. *J. Mat. Chem. B* 4, 318–326. doi: 10.1039/C5TB02035B

Reigel, M. M., Hollier, L. H., Pairolero, P. C., and Hallett, J. W. Jr. (1988). Early experience with a new collagen-impregnated aortic graft. *Am. Surg.* 54, 134–136.

Robert, J., Weber, B., Frese, L., Emmert, M. Y., Schmidt, D., von Eckardstein, A., et al. (2013). A three-dimensional engineered artery model for *in vitro* atherosclerosis research. *PLoS ONE* 8:e79821. doi: 10.1371/journal.pone.0079821

Rodrigues, C. V., Serricella, P., Linhares, A. B., Guerdes, R. M., Borojevic, R., Rossi, M. A., et al. (2003). Characterization of a bovine collagen-hydroxyapatite composite scaffold for bone tissue engineering. *Biomaterials* 24, 4987–4997. doi: 10.1016/S0142-9612(03)00410-1

Roll, S., Muller-Nordhorn, J., Keil, T., Scholz, H., Eidt, D., Greiner, W., et al. (2008). Dacron vs. PTFE as bypass materials in peripheral vascular surgery—systematic review and meta-analysis. *BMC Surg.* 8:22. doi: 10.1186/1471-2482-8-22

Ronaldson-Bouchard, K., and Vunjak-Novakovic, G. (2018). Organs-on-a-chip: a fast track for engineered human tissues in drug development. *Cell Stem Cell* 22, 310–324. doi: 10.1016/j.stem.2018.02.011

Rýglová, Š., Braun, M., and Suchý, T. (2017). Collagen and its modifications—crucial aspects with concern to its processing and analysis. *Macromol. Mater. Eng.* 302:1600460. doi: 10.1002/mame.201600460

Salamanca, E., Hsu, C. C., Huang, H. M., Teng, N. C., Lin, C. T., Pan, Y. H., et al. (2018). Bone regeneration using a porcine bone substitute collagen composite *in vitro* and *in vivo*. *Sci. Rep.* 8:984. doi: 10.1038/s41598-018-19629-y

Sarkar, S., Sales, K. M., Hamilton, G., and Seifalian, A. M. (2007). Addressing thrombogenicity in vascular graft construction. *J. Biomed. Mater. Res. B Appl. Biomater.* 82, 100–108. doi: 10.1002/jbm.b.30710

Scharn, D. M., Oyen, W. J., Klemm, P. L., Verhofstad, A. A., and van der Vliet, J. A. (2006). Thrombogenicity and related biological properties of heparin bonded collagen coated polyester and human umbilical vein prosthetic vascular grafts. *J. Surg. Res.* 134, 182–189. doi: 10.1016/j.jss.2006.01.025

Schmidt, V. J., Wietbrock, J. O., Leibig, N., Gloe, T., Henn, D., Hernekamp, J. F., et al. (2017). Collagen-elastin and collagen-glycosaminoglycan scaffolds promote distinct patterns of matrix maturation and axial vascularization in arteriovenous loop-based soft tissue flaps. *Ann. Plast. Surg.* 79, 92–100. doi: 10.1097/SAP.0000000000001096

Schmitt, F. O., Levine, L., Drake, M. P., Rubin, A. L., Pfahl, D., and Davison, P. F. (1964). The antigenicity of tropocollagen. *Proc. Natl. Acad. Sci. U.S.A.* 51, 493–497. doi: 10.1073/pnas.51.3.493

Schneider, F., O'Connor, S., and Becquemin, J. P. (2008). Efficacy of collagen silver-coated polyester and rifampin-soaked vascular grafts to resist infection from MRSA and Escherichia coli in a dog model. *Ann. Vasc. Surg.* 22, 815–821. doi: 10.1016/j.avsg.2008.06.011

Schoneberg, J., De Lorenzi, F., Theek, B., Blaeser, A., Rommel, D., Kuehne, A. J. C., et al. (2018). Engineering biofunctional *in vitro* vessel models using a multilayer bioprinting technique. *Sci. Rep.* 8:10430. doi: 10.1038/s41598-018-28715-0

Schroeder, J. W. Jr., Rastatter, J. C., and Walner, D. L. (2007). Effect of vascular endothelial growth factor on laryngeal wound healing in rabbits. *Otolaryngol. Head Neck Surg.* 137, 465–470. doi: 10.1016/j.otohns.2007.04.027

Schutte, S. C., Chen, Z., Brockbank, K. G., and Nerem, R. M. (2010a). Cyclic strain improves strength and function of a collagen-based tissue-engineered vascular media. *Tissue Eng. Part A* 16, 3149–3157. doi: 10.1089/ten.tea.2010.0009

Schutte, S. C., Chen, Z., Brockbank, K. G., and Nerem, R. M. (2010b). Tissue engineering of a collagen-based vascular media: Demonstration of functionality. *Organogenesis* 6, 204–211. doi: 10.4161/org.6.4.12651

Schweitzer, M. H., Suo, Z., Avci, R., Asara, J. M., Allen, M. A., Arce, F. T., et al. (2007). Analyses of soft tissue from *Tyrannosaurus rex* suggest the presence of protein. *Science* 316, 277–280. doi: 10.1126/science.1138709

Scott, S. M., Gaddy, L. R., Sahmel, R., and Hoffman, H. (1987). A collagen coated vascular prosthesis. *J. Cardiovasc. Surg.* 28, 498–504.

Seifu, D. G., Purnama, A., Mequanint, K., and Mantovani, D. (2013). Small-diameter vascular tissue engineering. *Nat. Rev. Cardiol.* 10, 410–421. doi: 10.1038/nrcardio.2013.77

Seliktar, D., Black, R. A., Vito, R. P., and Nerem, R. M. (2000). Dynamic mechanical conditioning of collagen-gel blood vessel constructs induces remodeling *in vitro*. *Ann. Biomed. Eng.* 28, 351–362. doi: 10.1114/1.275

Shen, Y. H., Shoichet, M. S., and Radisic, M. (2008). Vascular endothelial growth factor immobilized in collagen scaffold promotes penetration and proliferation of endothelial cells. *Acta Biomater.* 4, 477–489. doi: 10.1016/j.actbio.2007.12.011

Shih, Y. R., Chen, C. N., Tsai, S. W., Wang, Y. J., and Lee, O. K. (2006). Growth of mesenchymal stem cells on electrospun type I collagen nanofibers. *Stem Cells* 24, 2391–2397. doi: 10.1634/stemcells.2006-0253

Shoulders, M. D., and Raines, R. T. (2009). Collagen structure and stability. *Annu. Rev. Biochem.* 78, 929–958. doi: 10.1146/annurev.biochem.77.032207.120833

Smethurst, P. A., Onley, D. J., Jarvis, G. E., O'Connor, M. N., Knight, C. G., Herr, A. B., et al. (2007). Structural basis for the platelet–collagen interaction: the smallest motif within collagen that recognizes and activates platelet glycoprotein VI contains two glycine-proline-hydroxyproline triplets. *J. Biol. Chem.* 282, 1296–1304. doi: 10.1074/jbc.M606479200

Sripriya, R., Kumar, M. S., and Sehgal, P. K. (2004). Improved collagen bilayer dressing for the controlled release of drugs. *J. Biomed. Mater. Res. B Appl. Biomater.* 70, 389–396. doi: 10.1002/jbm.b.30051

Stanley, A. G., Patel, H., Knight, A. L., and Williams, B. (2000). Mechanical strain-induced human vascular matrix synthesis: the role of angiotensin II. *J. Renin. Angiotensin Aldosterone Syst.* 1, 32–35. doi: 10.3317/jraas.2000.007

Steffens, G. C., Yao, C., Prevel, P., Markowicz, M., Schenck, P., Noah, E. M., et al. (2004). Modulation of angiogenic potential of collagen matrices by covalent incorporation of heparin and loading with vascular endothelial growth factor. *Tissue Eng.* 10, 1502–1509. doi: 10.1089/ten.2004.10.1502

Stephan, E. B., Renjen, R., Lynch, S. E., and Dziak, R. (2000). Platelet-derived growth factor enhancement of a mineral-collagen bone substitute. *J. Periodontol.* 71, 1887–1892. doi: 10.1902/jop.2000.71.12.1887

Stitzel, J., Liu, J., Lee, S. J., Komura, M., Berry, J., Soker, S., et al. (2006). Controlled fabrication of a biological vascular substitute. *Biomaterials* 27, 1088–1094. doi: 10.1016/j.biomaterials.2005.07.048

Suehiro, K., Hata, T., Yoshitaka, H., Tsushima, Y., Matsumoto, M., Ohtani, S., et al. (2003). Impact of collagen-coated and gelatine-impregnated woven Dacron branched grafts on the early postoperative period. *Jpn. J. Thorac. Cardiovasc. Surg.* 51, 641–645. doi: 10.1007/s11748-003-0001-z

Sugiura, H., Yunoki, S., Kondo, E., Ikoma, T., Tanaka, J., and Yasuda, K. (2009). *In vivo* biological responses and bioresorption of tilapia scale collagen as a potential biomaterial. *J. Biomater. Sci. Polym. Ed.* 20, 1353–1368. doi: 10.1163/092050609X12457418396658

Swartz, D. D., and Andreadis, S. T. (2013). Animal models for vascular tissue-engineering. *Curr. Opin. Biotechnol.* 24, 916–925. doi: 10.1016/j.copbio.2013.05.005

Toda, N., Nakanishi, S., and Tanabe, S. (2013). Aldosterone affects blood flow and vascular tone regulated by endothelium-derived NO: therapeutic implications. *Br. J. Pharmacol.* 168, 519–533. doi: 10.1111/j.1476-5381.2012.02194.x

Tranquillo, R. T., Girton, T. S., Bromberek, B. A., Triebes, T. G., and Mooradian, D. L. (1996). Magnetically orientated tissue-equivalent tubes: application to a circumferentially orientated media-equivalent. *Biomaterials* 17, 349–357. doi: 10.1016/0142-9612(96)85573-6

Tresoldi, C., Bianchi, E., Pellegata, A. F., Dubini, G., and Mantero, S. (2017). Estimation of the physiological mechanical conditioning in vascular tissue engineering by a predictive fluid-structure interaction approach. *Comput. Methods Biomech. Biomed. Eng.* 20, 1077–1088. doi: 10.1080/10255842.2017.1332192

Tronci, G., Russell, S. J., and Wood, D. J. (2013). Photo-active collagen systems with controlled triple helix architecture. *J. Mater. Chem. B* 1, 3705–3715. doi: 10.1039/c3tb20720j

Truskey, G. A., and Fernandez, C. E. (2015). Tissue-engineered blood vessels as promising tools for testing drug toxicity. *Expert Opin. Drug Metab. Toxicol.* 11, 1021–1024. doi: 10.1517/17425255.2015.1047342

Vernon, R. B., Lara, S. L., Drake, C. J., Iruela-Arispe, M. L., Angello, J. C., Little, C. D., et al. (1995). Organized type I collagen influences endothelial patterns during "spontaneous angiogenesis *in vitro*": planar cultures as models of vascular development. *In Vitro Cell Dev. Biol. Anim.* 31, 120–131. doi: 10.1007/BF02633972

Voorhees, A. B. Jr., Jaretzki, A., and Blakemore, A. H. (1952). The use of tubes constructed from vinyon "N" cloth in bridging arterial defects. *Ann. Surg.* 135, 332–336. doi: 10.1097/00000658-195203000-00006

Wahl, E. A., Schenck, T. L., Machens, H. G., and Balmayor, E. R. (2016). VEGF released by deferoxamine preconditioned mesenchymal stem cells seeded on collagen-GAG substrates enhances neovascularization. *Sci. Rep.* 6:36879. doi: 10.1038/srep36879

Wallace, D. G., and Rosenblatt, J. (2003). Collagen gel systems for sustained delivery and tissue engineering. *Adv. Drug Deliv. Rev.* 55, 1631–1649. doi: 10.1016/j.addr.2003.08.004

Weinberg, C. B., and Bell, E. (1986). A blood vessel model constructed from collagen and cultured vascular cells. *Science* 231, 397–400. doi: 10.1126/science.2934816

Willoughby, C. E., Batterbury, M., and Kaye, S. B. (2002). Collagen corneal shields. *Surv. Ophthalmol.* 47, 174–182. doi: 10.1016/S0039-6257(01)00304-6

Wissing, T. B., Bonito, V., Bouten, C. V. C., and Smits, A. (2017). Biomaterial-driven *in situ* cardiovascular tissue engineering–a multi-disciplinary perspective. *NPJ Regen. Med.* 2:18. doi: 10.1038/s41536-017-0023-2

Wissink, M. J., Beernink, R., Poot, A. A., Engbers, G. H., Beugeling, T., van Aken, W. G., et al. (2000). Improved endothelialization of vascular grafts by local release of growth factor from heparinized collagen matrices. *J. Control Release* 64, 103–114. doi: 10.1016/S0168-3659(99)00145-5

Wolf, F., Vogt, F., Schmitz-Rode, T., Jockenhoevel, S., and Mela, P. (2016). Bioengineered vascular constructs as living models for *in vitro* cardiovascular research. *Drug Discov. Today* 21, 1446–1455. doi: 10.1016/j.drudis.2016.04.017

Wood, A., Ogawa, M., Portier, R. J., Schexnayder, M., Shirley, M., and Losso, J. N. (2008). Biochemical properties of alligator (*Alligator mississippiensis*) bone collagen. *Comp. Biochem. Physiol. B Biochem. Mol. Biol.* 151, 246–249. doi: 10.1016/j.cbpb.2008.05.015

Xiang, Z., Liao, R., Kelly, M. S., and Spector, M. (2006). Collagen-GAG scaffolds grafted onto myocardial infarcts in a rat model: a delivery vehicle for mesenchymal stem cells. *Tissue Eng.* 12, 2467–2478. doi: 10.1089/ten.2006.12.2467

Yannas, I. V., Burke, J. F., Orgill, D. P., and Skrabut, E. M. (1982). Wound tissue can utilize a polymeric template to synthesize a functional extension of skin. *Science* 215, 174–176. doi: 10.1126/science.7031899

Yates, S. G., Barros D'Sa, A. A., Berger, K., Fernandez, L. G., Wood, S. J., Rittenhouse, E. A., et al. (1978). The preclotting of porous arterial prostheses. *Ann. Surg.* 188, 611–622. doi: 10.1097/00000658-197811000-00005

Yeager, R. A., Taylor, L. M., Jr., Moneta, G. L., Edwards, J. M., Nicoloff, A. D., et al. (1999). Improved results with conventional management of infrarenal aortic infection. *J. Vasc. Surg.* 30, 76–83. doi: 10.1016/S0741-5214(99)70178-3

Yu, H., Cao, B., Feng, M., Zhou, Q., Sun, X., Wu, S., et al. (2010). Combinated transplantation of neural stem cells and collagen type I promote functional recovery after cerebral ischemia in rats. *Anat. Rec. (Hoboken)* 293, 911–917. doi: 10.1002/ar.20941

Zhang, D., Wu, X., Chen, J., and Lin, K. (2018). The development of collagen based composite scaffolds for bone regeneration. *Bioact. Mater.* 3, 129–138. doi: 10.1016/j.bioactmat.2017.08.004

Zhang, W. J., Liu, W., Cui, L., and Cao, Y. (2007). Tissue engineering of blood vessel. *J. Cell. Mol. Med.* 11, 945–957. doi: 10.1111/j.1582-4934.2007.00099.x

Ziegler, T., Alexander, R. W., and Nerem, R. M. (1995). An endothelial cell-smooth muscle cell co-culture model for use in the investigation of flow effects on vascular biology. *Ann. Biomed. Eng.* 23, 216–225. doi: 10.1007/BF02584424

Conflict of Interest Statement: The authors declare that the research was conducted in the absence of any commercial or financial relationships that could be construed as a potential conflict of interest.

frontiers in Bioengineering and Biotechnology

REVIEW
published: 17 July 2019
doi: 10.3389/fbioe.2019.00170

Titanium–Tissue Interface Reaction and Its Control With Surface Treatment

*Takao Hanawa**

Department of Metallic Biomaterials, Institute of Biomaterials and Bioengineering, Tokyo Medical and Dental University, Tokyo, Japan

Titanium (Ti) and its alloys are widely used for medical and dental implant devices—artificial joints, bone fixators, spinal fixators, dental implant, etc. —because they show excellent corrosion resistance and good hard-tissue compatibility (bone formation and bone bonding ability). Osseointegration is the first requirement of the interface structure between titanium and bone tissue. This concept of osseointegration was immediately spread to dental-materials researchers worldwide to show the advantages of titanium as an implant material compared with other metals. Since the concept of osseointegration was developed, the cause of osseointegration has been actively investigated. The surface chemical state, adsorption characteristics of protein, and bone tissue formation process have also been evaluated. To accelerate osseointegration, roughened and porous surfaces are effective. HA and TiO_2 coatings prepared by plasma spray and an electrochemical technique, as well as alkalinization of the surface, are also effective to improve hard-tissue compatibility. Various immobilization techniques for biofunctional molecules have been developed for bone formation and prevention of platelet and bacteria adhesion. These techniques make it possible to apply Ti to a scaffold of tissue engineering. The elucidation of the mechanism of the excellent biocompatibility of Ti can provide a shorter way to develop optimal surfaces. This review should enhance the understanding of the properties and biocompatibility of Ti and highlight the significance of surface treatment.

Keywords: titanium, titanium alloy, biocompatibility, biofunction, bone formation, bone bonding, surface treatment, surface morphology

OPEN ACCESS

Edited by:
Hasan Uludag,
University of Alberta, Canada

Reviewed by:
Kathryn Grandfield,
McMaster University, Canada
Diego Mantovani,
Laval University, Canada

***Correspondence:**
Takao Hanawa
hanawa.met@tmd.ac.jp

Specialty section:
This article was submitted to Biomaterials, a section of the journal Frontiers in Bioengineering and Biotechnology

Received: *12 February 2019*
Accepted: *03 July 2019*
Published: *17 July 2019*

Citation:
Hanawa T (2019) Titanium–Tissue Interface Reaction and Its Control With Surface Treatment. Front. Bioeng. Biotechnol. 7:170. doi: 10.3389/fbioe.2019.00170

INTRODUCTION

Many medical devices made of metals have been substituted by those made of ceramics and polymers during the past half century because of innovation in ceramics and polymers and their excellent biocompatibility and biofunction, as shown in **Figure 1**. Despite this situation, more than 70% of surgical implant devices, especially more than 95% of orthopedic implants (calculated based on statics from the Ministry of Health, Labor and Welfare, Japan), still consist of metals because of the large fracture toughness and durability of metals. In particular, titanium (Ti) materials, such as commercially pure titanium (CP Ti) and Ti alloys are widely used in medicine and dentistry because of their large corrosion resistance, large specific strength, and high performance in medicine and dentistry (Brunette et al., 2001). Their good interfacial and chemical compatibility against tissues are well-known based on substantial evidence from basic research and high clinical performances. However, the mechanism of the excellent biocompatibility of Ti among metals is not completely

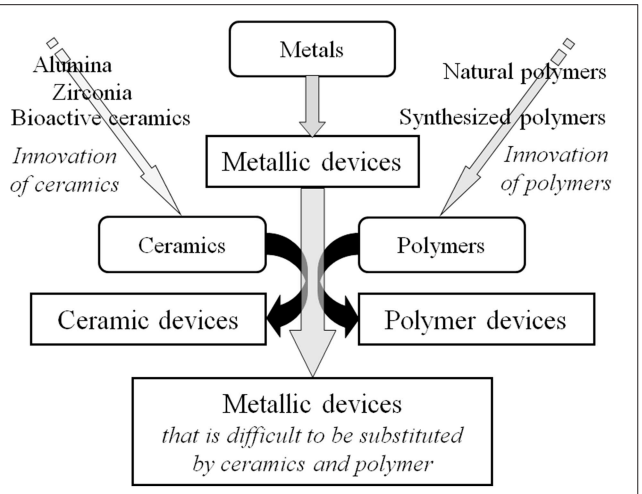

FIGURE 1 | Substitution of metallic devices by ceramic devices and polymer devices due to innovation of ceramics and polymers.

understood. After a metallic material is implanted into a human body, a reaction immediately occurs between the living tissue and the material surface. In other words, the first reaction at the interface directly influences the material's biocompatibility. The Young's modulus of α + β-type Ti alloy (100–111 GPa) is half those of type 316L stainless steel (200 GPa) and Cobalt (Co)–chromium (Cr)–molybdenum (Mo) alloy (∼220 GPa), which is a large advantage to prevent stress shielding in bone plates and stems of artificial hip joints in orthopedics. In addition, the magnetic susceptibilities of Ti (31.9×10^{-9} m^3 kg^{-1}) and Ti−6Al−4V ELI alloy (39.8×10^{-9} m^3 kg^{-1}) are much smaller than that of Co–Cr–Mo alloy (94.5×10^{-9} m^3 kg^{-1}), as well as stainless steels, decreasing the influences of magnetic resonance imaging (MRI), such as motion, attraction force, torque, heat generation, and artifacts. This property is significant, because MRI is commonly used for medical examination.

A disadvantage of metals for use as biomaterials is that they are artificial materials, and metals do not have biofunction. To promote biocompatibility and add biofunction to metals, surface modification or surface treatment is necessary, because biocompatibility is not promoted and biofunction is not added through conventional manufacturing processes, such as melting, casting, forging, and heat treatment. Surface treatment is a process that changes surface morphology, structure, and composition, leaving the bulk mechanical properties. In orthopedics, bone bonding is required in the stem and acetabular cup of artificial hip joints. In the case of dentistry, hard-tissue compatibility for bone formation and bone bonding, soft-tissue compatibility for adhesion of gingival epithelium, and an antibacterial property for the inhibition of bacterial invasion are required in dental implants. For these purposes, a variety of surface treatment techniques have been investigated at the research level, and some of them have been commercialized.

In this overview, a brief history of CP Ti and Ti alloys, the application of Ti to medical devices (including dental devices), their use and tasks in medicine, proposed mechanisms of excellent biocompatibility of Ti, and surface treatment to improve biocompatibility and to add biofunction are reviewed. This review is intended to enhance the understanding of the properties and biocompatibility of Ti and the significance of surface treatment, including surface-morphological alteration.

HISTORY OF APPLICATION TO MEDICINE

The history of the application of CP Ti and Ti alloys to medicine and dentistry is summarized in **Table 1**. The first report on CP Ti for medicine was appeared in 1940, and excellent bone compatibility was found based on an animal test (Bothe et al., 1940). Thereafter, the compatibility to bone and soft tissue of rabbits (Leventhal, 1951), its non-cytotoxicity due to excellent corrosion resistance in biological environments (Beder et al., 1957), and excellent biocompatibility in dogs were reported. The large-scale industrial manufacturing process for Ti achieved in the last half 1940s made it possible to conduct many studies for medical applications, revealing excellent biocompatibility in long-term animal testing (Williams, 1982a). Thereafter, the usefulness of CP Ti was widely recognized by the last half 1960s through clinical evaluation (Pillar and Weatherly, 1982; Williams, 1982a,b).

However, to avoid the fracture of CP Ti in the human body, an aerospace Ti−6Al−4V alloy was diverted to artificial joints and bone fixators (Pillar and Weatherly, 1982; Williams, 1982a,b). Thereafter, vanadium (V)- and/or aluminum (Al)-free α + β-type Ti alloys and β-type Ti alloys with low Young's modulus have been developed. V that creates the cytotoxicity of Ti−6Al−4V alloy was replaced by niobium (Nb), which is a safe element, to develop a new α + β-type Ti−6Al−7Nb alloy (Semlitsch and Staub, 1985; Li et al., 2010). Other α + β-type alloys, Ti−6Al−2.5iron (Fe) alloy and Ti−6Al−2Nb−1 tantalum (Ta)−0.8Mo alloy, were developed in 1970s (Rao and Houska, 1979; Anon, 1994).

On the other hand, β-type Ti alloys for medical use have been developed. Ti−13zirconium (Zr)−13Ta alloy (nearly β) has been developed in the United States. Various β-type alloys, Ti−12Mo−6Zr−2Fe alloys (Wang et al., 1993), T−15Mo (Zardiackas et al., 1996), and Ti−15Mo−2.8Nb−0.2silicon (Si)−0.28oxygen (O) (Fanning, 1996), have been developed in the United States. Ti−15Mo−5Zr and Ti−15Mo−5Zr−3Al alloys (Rao and Houska, 1979; Matsuda et al., 1997) and Ti−15Zr−4Nb−4Ta alloy (Okazaki, 2001) have been developed in Japan. The history of the development of β-type Ti alloys is well-summarized elsewhere (Niinomi, 2019). Young's modulus could decrease to 40–60 GPa in a β-type alloy.

Since 2000, a new wave of the development of Ti alloys has been generated. The design of Ti alloys through twinning-induced plasticity (TWIP) and transformation-induced plasticity (TRIP) has been attempted, making it possible to develop novel β-metastable Ti alloys (Marteleur et al., 2012; Ahmed et al., 2016: Brozek et al., 2016; Zhan et al., 2016; Zhang et al., 2017; Lai et al., 2018). The TRIP and TWIP concepts were first invented in the field of steels and applied to Ti alloys through Ti–nickel (Ni) shape memory alloy. It is possible that this design will be applied to biomedical alloys in the near future.

TABLE 1 | History of titanium application to medicine and development of titanium alloys.

Year	Material	Circumstance	References
1940	Ti	Confirmation of equivalent biocompatibility as stainless steel and cobalt-chromium alloy with animal test	Bothe et al., 1940
1940	Ti	Success of smelting by Kroll process	Kroll, 1940
1948	Ti	Launching industrial production	
1951	Ti	Confirmation of both soft and hard tissues compatibility with animal test	Leventhal, 1951
1957	Ti	Confirmation of non-toxicity with long-term implantation	Beder et al., 1957
1959	Ti–Ni	Development of shape memory alloy in USA	Buehler et al., 1963; Wang et al., 1965
1960	Ti	Excellent results in artificial joints	Williams, 1982a
1960's	Ti	Marketing as surgical implants in UK and USA	
1970's	Ti−6Al−4V	Diverting aircraft material to orthopedic implants	
1978	Ti–Cu–Ni	Trial of dental casting	Waterstrat et al., 1978
1980	Ti−5Al−2.5Fe	Development in Europe	
1982	Ti	Development of investment material and casting machine for dental casting	Miura and Ida, 1988
1985	Ti−6Al−7Nb	Development in Switzerland	Semlitsch and Staub, 1985
1993	Ti−13Nb−13Zr	Development in USA	
1993	Ti−12Mo−6Zr−2Fe	Development in USA	Wang et al., 1993
1996	Ti−15Mo	Development in USA	Zardiackas et al., 1996
1988	Ti−29Nb−13Ta−4.6Zr	Development in Japan	Kuroda et al., 1988
Around 2000	Ti−15Mo−5Zr−3Al	Development in Japan	Rao and Houska, 1979; Matsuda et al., 1997
Around 2000	Ti−6Al−2Nb−1Ta−0.8Mo	Development in Japan	Okazaki, 2001
2004	Ti−15Zr−4Nb−4Ta	Development in Japan	Ozaki et al., 2004
After 2000	β-metastable alloys based on TRIP and TWIP	Development in mainly China	Marteleur et al., 2012; Ahmed et al., 2016: Brozek et al., 2016; Zhan et al., 2016; Zhang et al., 2017; Lai et al., 2018

In dentistry, CP Ti has been successfully used for dental implants since 1965 (Waterstrat et al., 1978), and the excellent hard-tissue compatibility is well-known. A magnesia-system investment material and argon-arc casting machine were developed in 1982, followed by the development of various dental casting systems for dental restoratives (Miura and Ida, 1988).

The development of new Ti alloys for medical devices continuously challenges by researchers, and new designs have been attempted based on d-electron alloy design theory (Kuroda et al., 1988) and the TRIP and TWIP concept.

MEDICAL APPLICATION AND TASKS OF TITANIUM

Because of the excellent properties of CP Ti and Ti alloy as biomaterials, they are used for devices requiring strength, elongation, and long-term bone bonding in orthopedics, cardiovascular medicine, dentistry, etc. The specifications of Ti alloys used for medicine are listed in **Table 2**. Medical devices and CP Ti and Ti alloys are listed in **Table 3**, and problems of CP Ti and Ti alloys in medicine are summarized in **Table 4**.

Ti alloys are used in orthopedics for artificial joints, bone fixators, spinal fixators, etc., receiving large mechanical stress. Bone absorption caused by stress shielding sometimes appears in bone fixators and artificial hip joints. Because load is mainly applied to the metal plate and stem, less load is applied to cortical bone by the difference in Young's modulus between metal and cortical bone (Gefen, 2002). If the Young's modulus of the metal plate is similar to that of cortical bone, load is equally applied to both metal and bone to prevent bone absorption. In this sense, β-type Ti alloys showing a lower Young's modulus are more suitable than α + β-type alloys. Therefore, β-type Ti alloys consisting of Group 4 and 5 elements in the periodic table have continued to be designed and developed.

However, bone screws and bone nails made of Ti alloys form calluses and assimilate to bone tissue, forming calluses, during implantation, so bone is sometimes refractured when the devices are retrieved (Sanderson et al., 1992). Therefore, when the devices must be retrieved after healing, devices made of 316L-type stainless steel are selected. This assimilation occurs because of the excellent hard-tissue compatibility of Ti alloys. A proper surface treatment may inhibit bone formation and bonding of Ti alloys contacting bone tissue.

In spinal surgery and maxillofacial surgery, the rod and plate of Ti alloys are sometimes bent by medical doctors in the operation room. These operations sometimes generate crack or fracture of Ti alloys, because the elongation to fracture of α + β-type Ti alloy (10% of Ti−6Al−4V ELI; Brunette et al., 2001) is much smaller than that of 316L-type stainless steel (40%; ASTM

TABLE 2 | Specification of titanium alloys for medical use.

Composition (mass%)	Type	ASTM	ISO	JIS
Ti–5Al–2.5Fe	α + β	–	ISO 5832-10	
Ti–6Al–4V	α + β	F1108 (Cast) F1472 (Wrought)	ISO 5832-3	T7401-2
Ti–6Al–4V ELI	α + β	F136 (Wrought)	ISO 5832-3	–
Ti–6Al–2Nb–1Ta	α + β	–	–	T7401-3
T–15Zr–4Nb–4Ta	α + β	–	–	T7401-4
Ti–6Al–7Nb	α + β	F1295	ISO 5832-11	T7401-5
Ti–3Al–2.5V	α + β	F2146		
Ti–6Al–2Nb–1Ta–0.8Mo	α + β	F136	ISO 5832-14	
Ti–13Nb–13Zr	Near β	F1713	–	
Ti–15Mo	β	F2066	–	
Ti–12Mo–6Zr–2Fe	β	F1813	–	
Ti–15Mo–5Zr–3Al	β	F136	ISO 5832-14	T7401-6
Ti–55.8Ni	Intermetallic compound	ASTM F 2063		T7404

A240). Therefore, the strengthening of α + β-type Ti alloy while maintaining elongation is required.

Ti–Ni alloy is used as guidewires and self-expanding stents. However, 37.2% (45 of 121 cases) of Ti–Ni stents are fractured in 10.7 months of service (Scheinert et al., 2005). Corrosion may be related to the fracture, while the main cause is fatigue. In the case of stent grafts of Ti–Ni, severe pitting and crevice corrosion appears by the acceleration of corrosion due to the crevice between Ti–Ni alloy and a polymer as an artificial blood vessel (Heintz et al., 2001). Therefore, Ni-free Ti-based superelastic alloys have been researched (Shinohara et al., 2015).

In dentistry, the fixture part of dental implants consists of CP Ti and Ti alloys to bond alveolar bone. A Ti–Ni superelastic alloy and a Ti–Mo alloy are used as orthodontic arch wire. In particular, Ti–Ni alloy is widely used, because proper and continuous orthodontic force remains for a long time. Ti–Ni alloy is suitable for reamers and files for endodontics for bending tooth roots, while the alloy sometimes fractures from an overload with dental engines.

Corrosion of metallic implant devices implanted into the human body has been studied (Nakayama et al., 1989; Brunette et al., 2001; Alves et al., 2009; Asri et al., 2017; Manam et al., 2017; Eliaz, 2019), because the corrosion is related to toxicity and fracture, whereas examples of corrosion-fracture of metal implants are few. The reason is because the retrieval case of implants is limited, and surgeons are rarely interested in corroded retrieved implants. In particular, severe corrosion cases of CP Ti and Ti alloys are rare. However, Ti used as dental restoratives is corroded by fluorine compounds contained in mouthwashes and dental pastes (Nakagawa et al., 1999). Microbial corrosion of Ti in the oral cavity has also been studied (Fukushima et al., 2014). The corrosion phenomena of metallic biomaterials including Ti alloys are reviewed (Manam et al., 2017; Eliaz, 2019), while the case of Ti alloys is rare.

As described above, CP Ti and Ti alloys are widely used in medicine and dentistry because of their lightness, high corrosion resistance, and excellent biocompatibility compared with other metals.

TABLE 3 | Medical devices consisting of titanium and titanium alloys.

Clinical department	Medical device	CP Ti and Ti alloy
Orthopedics	Spinal fixator	CP Ti; Ti–6Al–4V; Ti–6Al–7Nb
	Bone fixator (bone plate, screw, wire, bone nail, mini palate, etc.)	CP Ti; Ti–6Al–4V; Ti–6Al–7Nb
	Artificial joint; artificial head	Ti–6Al–4V; Ti–6Al–7Nb; Ti–15Mo–5Zr–3Al; Ti–6Al–2Nb–1Ta–0.8Mo
	Spinal spacer	Ti–6Al–4V; Ti–6Al–7Nb
Cardiovascular department	Implantable artificial heart (housing)	CP Ti
	Heart pacemaker (case) (electrode) (terminal)	CP Ti; Ti–6Al–4V CP Ti CP Ti
	Artificial valve (flame)	Ti–6Al–4V
	Vascular stent	Ti–Ni
	Guide wire	Ti–Ni
	Cerebral aneurysm clip	CP Ti; Ti–6Al–4V
Dentistry	Inlay; crown; bridge; clasp; denture base	CP Ti; Ti–6Al–7Nb
	Dental implant	CP Ti; Ti–6Al–4V; Ti–6Al–7Nb
	Orthodontic wire	Ti–Ni; Ti–Mo
General surgery	Surgical instrument (scalpel; tweezer; scissor; drill)	CP Ti
	Catheter	Ti–Ni

TABLE 4 | Problem to be solved in titanium and titanium alloys for medical use.

Problem	Material	Medical device
Stress shielding	α+β type Ti alloy	Bone plate; stem of artificial hip joint
Adhesion to bone	Whole Ti alloy	Bone screw; bone nail
Cracking and fracture by excessive deformation	CP Ti, α+β type Ti alloy	Spinal rod; maxillofacial plate
Crevice corrosion; pitting	Ti–Ni alloy	Stent graft
Fracture	Ti–Ni alloy	Endodontic file
Corrosion with fluoride	CP Ti; whole Ti alloy	Dental restorative
Cytotoxicity	CP Ti; whole Ti alloy	All devices
Peri-implantitis	CP Ti; whole Ti alloy	Abutment of dental implant; orthodontic implant anchor; percutaneous device; screw of external bone fixator

BIOCOMPATIBILITY OF TITANIUM

Biocompatibility is defined as "the ability of a material to perform with an appropriate host response in a specific application" (William, 1987). The biocompatibility of a material is governed by initial and continuous reactions between the material and host body: adsorption of molecules, protein adsorption, cell adhesion, bacterial adhesion, activation of macrophage, formation of

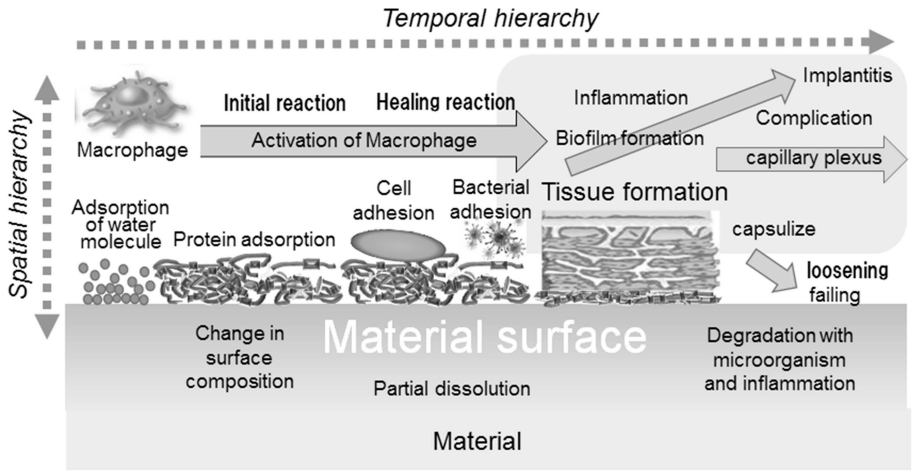

FIGURE 2 | Interfacial reactions of materials and the host body.

tissues, inflammation, etc. In addition, the reaction occurs with a temporal and spatial hierarchy, as illustrated in **Figure 2**.

CP Ti shows a unique property, "osseointegration," among metals. Osseointegration is defined as follows. It is the "formation of a direct interface between an implant and bone, without intervening soft tissue. No scar tissue, cartilage or ligament fibers are present between the bone and implant surface. The direct contact of bone and implant surface can be verified microscopically" (Brånemark et al., 1977). Osseointegration shows the excellent hard-tissue property of Ti. This concept, osseointegration, in dental implants generated and explosively accelerated studies on the reaction between hard tissue (bone and tooth) and Ti, followed by studies on surface treatment.

Extensive research on the hard-tissue compatibility of Ti has been reported; it is impossible to introduce everything here, so we advise referring to a book in which it is reviewed (Brunette et al., 2001). Excellent hard-tissue compatibility of Ti was confirmed by studies on calcium phosphate formation ability in simulated body fluids; evaluation of osteoblast activity and calcification; histological and molecular-biological evaluation of Ti implanted in animals, such as bone formation, bone contacting rate, and bone bonding strength; and clinical results. The above results revealed that, when Ti is implanted in bone, the surrounding tissue contacts Ti in an early stage, and the bone bonding strength is large. Important factors governing hard-tissue compatibility are the adhesion and proliferation of osteogenic cells because of the surface morphology (roughness), wettability, etc. Bone formation occurs through the inflammatory response period, osteoblast induction period, and bone formation period. The surfaces of Ti implant and Ti–bone interface reaction have been characterized to explain the importance of surface morphology, wettability, and energy for osseointegration (Rupp et al., 2018; Shah et al., 2018, 2019). The surface of Ti implants stored for a long time after manufacturing becomes contaminated, and the bone conduction ability is depressed during storage (Art et al., 2009).

Bonding between metals and soft tissue is also important in abutments of dental implants, orthodontic implant anchors, transdermal devices, and screws of external fixators. In these devices, metals penetrate from the inside to the outside of tissues. Therefore, insufficient bonding of soft tissue makes the invasion of bacteria that generates inflammation possible, followed by loosening, movement, and falling out of the implant. In the case of dental implants, these events are known as peri-implantitis. Other medical devices completely implanted in tissues may be covered by fibrous tissue unless enough soft-tissue compatibility is shown. It is well-known that Ti shows good soft-tissue compatibility only in the case of complete implantation, while chemical bonding of soft tissue to Ti is not observed. In particular, despite the significance of the adhesion of junctional epithelium to Ti in dental implants, this subject is still unresolved. Bonding of junctional epithelium to Ti is attempted by a mechanical anchoring with rough or grooved Ti surfaces at present, because chemical adhesion of soft tissue to metals is difficult (Williams, 2011).

A platelet adhesion test with human blood revealed that platelets easily adhered and a fibrin network formed on Ti (Tanaka et al., 2009; Ratner et al., 2013). Ti may form a thrombus easily and show low blood compatibility. Probably for this reason, bare Ti and Ti alloys except Ti-Ni alloy are not used for devices contacting blood.

MECHANISM OF BIOCOMPATIBILITY OF TITANIUM

Response of the Host Body

The interface between Ti and bone tissue has been observed from early on at a micrometer and nanometer scale (Albrektsson and Hansson, 1986; Davies et al., 1990; Listgarten et al., 1992; Sennerby et al., 1993; Murai et al., 1996; Branemark et al., 1998; Sundell et al., 2017). Metal Ti substrate is covered by titanium oxide (a few nanometers in thickness), an amorphous layer containing proteoglycans (20–50 nm in thickness), a slender

cell layer, a weakly calcified region, and bone tissue, in that order. Endeavors to observe a structure near the Ti surface have continued to elucidate the mechanism of osseointegration (Palmquist et al., 2010; Goriainov et al., 2014).

Recently, red-blood-cell and platelet interactions (Park and Davies, 2000), wettability and hydrophilicity (Gittens et al., 2014; Albrektsson and Wennerberg, 2019), increase in osteogenesis-, angiogenesis-, and neurogenesis-associated gene expression (Salvi et al., 2015), healing- and immune-modulating effect (Trindade et al., 2016), immune osteocyte-related molecular signaling mechanisms (Shah et al., 2018), and inflammation-immunological balance (Trindade et al., 2018; Albrektsson et al., 2019) have been considered as factors of osseointegration.

However, the focus of the research moved to surface treatments to accelerate bone formation and bone bonding. The reaction mechanism is usually investigated to explain the effect of the treatments. The above phenomena are caused by the surface properties of Ti and situational evidence; the surface properties causing the above phenomena must be understood. Properties of the Ti surface that may cause osseointegration are explained in the following subsections.

Corrosion Resistance

Ti shows excellent corrosion resistance compared with other metals (Nakayama et al., 1989; Brunette et al., 2001; Asri et al., 2017; Manam et al., 2017; Eliaz, 2019), inducing low toxicity (**Figure 3**). One of the reasons for the excellent biocompatibility of Ti is caused by the excellent corrosion resistance, while the corrosion resistance is not sufficient condition for the biocompatibility. Even the best corrosion-resistant metal, Au, is inferior in tissue compatibility. In addition, electric plating of Pt to Ti increases the corrosion resistance but depletes bone formation (Itakura et al., 1989), because a property of Ti is shielded, and the bone formation ability is prevented. These results reveal that hard-tissue compatibility is not induced only by the corrosion resistance. In other words, the corrosion resistance is a necessary condition but not a sufficient condition for biocompatibility; there are other factors that contribute to biocompatibility. This concept is illustrated in **Figure 4.**

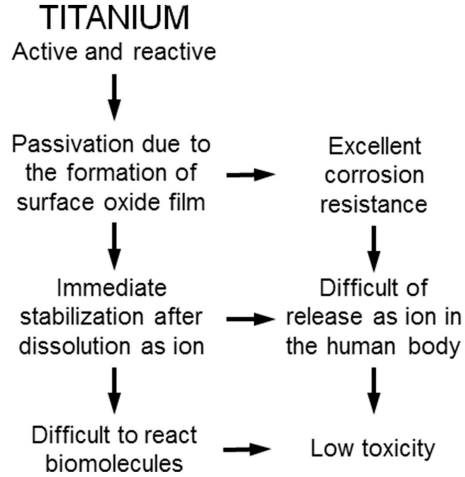

FIGURE 3 | Excellent corrosion resistance and low toxicity of titanium based on its high activity.

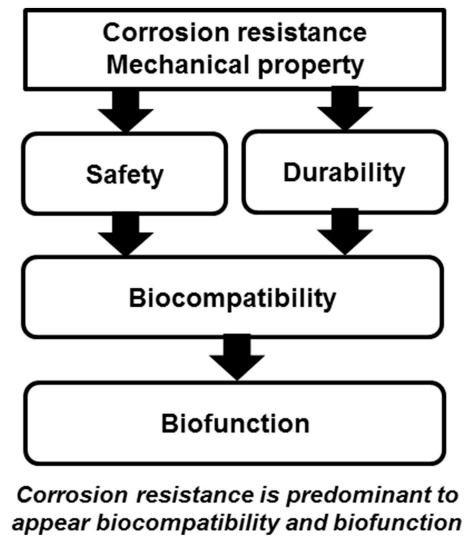

FIGURE 4 | Biocompatibility and biofunction based on corrosion resistance and mechanical property.

Surface Hydroxyl Groups

The interface reaction between Ti and living tissue is governed by the property of surface oxide film (passive film) covering the Ti substrate. This surface oxide film forms hydroxyl groups on itself because of a reaction with moisture in the air (Boehm, 1966). These hydroxyl groups dissociate in aqueous solutions, such as body fluid, to form electric charges (Boehm, 1966, 1971; Parfitt, 1976). The electric charge depends on the pH of the surrounding solution, and it becomes zero at a certain pH. This pH is defined as the point of zero charge (p.z.c.) (**Figure 5**). The p.z.c. is a unique value depending on each oxide and an indicator to show an acid or basic property. In the case of TiO_2, the p.z.c. of rutile is 5.3, and that of anatase is 6.2 (Parfitt, 1976); therefore, TiO_2 does not show an outstanding acid or basic property but shows almost a neutral property. The concentration of surface hydroxyl groups on TiO_2 is relatively large—4.9–12.5 nm^{-2} (Boehm, 1971; Westall and Hohl, 1980). After immersion in aqueous solution, this concentration or wettability increases. This large concentration promotes the adsorption of proteins, such as integrin and cytokine.

Protein Adsorption

The conformation of proteins is changed by the adsorption to the metal surface, because proteins are charged objects. The electrostatic force of proteins to a metal surface is governed by the relative permittivity of the surface oxide film: the larger the relative permittivity, the smaller the electrostatic force. The relative permittivity of TiO_2 is much larger than those of other oxides, 82.1, and similar to that of water (80.0) (Lide, 2006). Therefore, the conformational change of protein adsorbed on TiO_2 is possibly small (**Figure 6**). The adsorption layer of

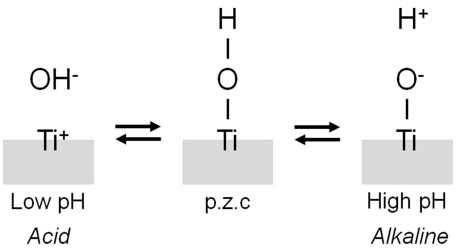

FIGURE 5 | Dissociation of surface hydroxyl group on metal.

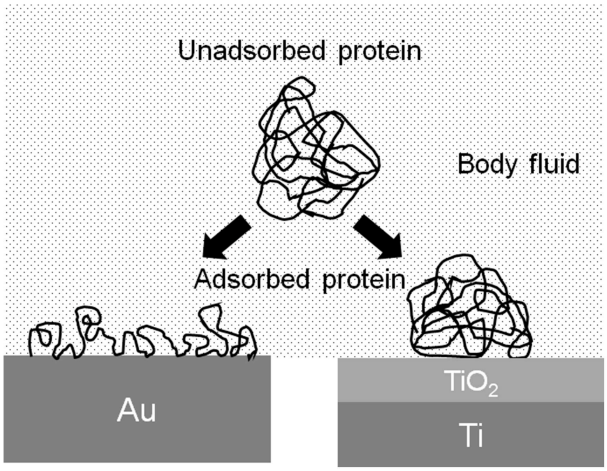

FIGURE 6 | Schematic model of change in the conformation of protein adsorbed on Au and Ti.

fibrinogen is thicker, but the adsorption amount is smaller on Ti than on Au in aqueous solution (Sundgren et al., 1986a). The electrostatic force on Ti is small, but on Au is large, because Ti is covered by TiO_2 and Au metal exposes without surface oxide. The change in the conformation of proteins on Ti is smaller than that on Au. Proteins adsorbed on Ti are less susceptible.

Formation of Calcium Phosphate

The composition and chemical state of surface oxide film vary according to the surrounding environment; while the film is macroscopically stable. A passive film maintains a continuous process of partial dissolution and reprecipitation in the electrolyte from the microscopic viewpoint. In this sense, the surface composition is always changing according to the environment (Kelly, 1982). Ti and Ti alloys easily form calcium phosphates on themselves in a biological environment, and form sulfite and sulfide, especially under cell culture (Hanawa and Ota, 1991, 1992; Healy and Ducheyne, 1992; Serro et al., 1997; Hiromoto et al., 2004). Ti is stabilized after the formation of calcium phosphate in Hanks' solution (Tsutsumi et al., 2009). In addition, calcium and phosphorus are detected at the interface between Ti and bone tissue (Sundgren et al., 1986b; Esposito et al., 1999; Sundell et al., 2017). One of the reasons for the excellent hard-tissue compatibility in Ti is its ability to form calcium phosphate.

SURFACE TREATMENT OF TITANIUM

Category

To promote the biocompatibility of Ti and to add biofunction to Ti while retaining the advantage of its mechanical property, surface treatment is necessary. Surface treatment techniques for Ti continue to be reviewed (Brunette et al., 2001; Hanawa, 2009, 2017; Williams, 2011; Ratner et al., 2013; Civantos et al., 2017). Surface treatment techniques for medical applications are categorized in **Figure 7**, and most of them are commercially viable in the engineering field. However, some of them were originally developed for medical devices. In addition, the major purpose of surface treatments is to accelerate bone formation and bonding. Another category of surface finishing and surface treatment of implants is summarized in **Figure 8**. Recently, immunomodulatory applications to regenerate tissues have attracted the attention of biomaterials researchers (Lee et al., 2019). As shown in **Figure 8**, surface treatments and their effects are summarized in the following subsections.

Control of Surface Morphology and Porous Surface

Surface roughness influences the healing and remodeling process of tissues. Osteoblastic cells adhere well to rough metal surfaces *in vitro* (Rautray et al., 2011). Surface roughness also plays an important role for the differentiation of cells. For example, osteoblast accelerates collagen production and calcification on rough surfaces rather than on smooth surfaces (Keller et al., 1994). The shear bonding force increases with increasing roughness. Influence of surface topography on osseointegration has been studied (Albrektsson and Wennerberg, 2004; Wennerberg and Albrektsson, 2010; Nagasawa et al., 2016; Rupp et al., 2018). The surface roughness of a material is an important factor for bonding of tissues. Mechanical anchoring results from the ingrowth of bone tissue into pores. Even in the case where surface treatment improves the chemical composition, the effects of not only the chemical composition but also the roughness produced simultaneously by the treatment appear in most cases to accelerate bone formation and bone bonding.

The first surface treatment for biomaterials was the control of surface morphology—that is, the formation of macroscopic grooves or grids. Living tissues become ingrown in holes or pores, and mechanical anchoring is achieved. Plasma spray of Ti and hydroxyapatite (HA) on the stem of artificial joints made of Ti alloys and blast and acid etching in dental implants have been commercialized. Micro-arc oxidation (MAO) or plasma electrolytic oxidation (PEO) to form a connective porous TiO_2 layer have also been commercialized in dental implants. Bone tissue grows into pores to achieve bonding. A scanning electron micrograph of porous TiO_2 oxide formed on Ti by MAO is shown in **Figure 9**.

In the advanced morphology surface fabrication in **Figure 8**, an evolutional technique of surface morphological control is the formation of TiO_2 nanotubes promoting cell adhesion and bone formation because of the effect of the nanometer size (Allam et al., 2008; Brammer et al., 2012; Narayanan et al., 2014;

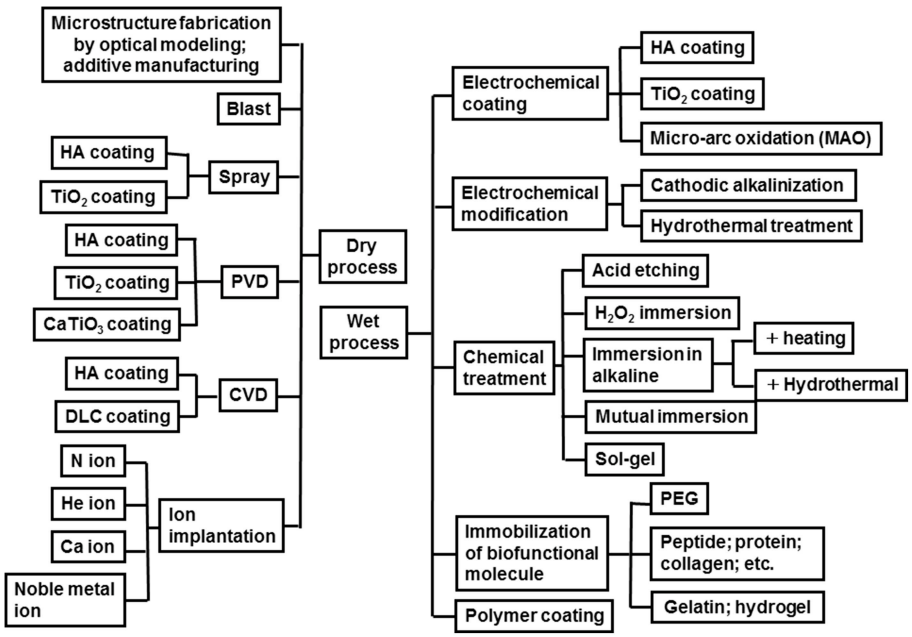

FIGURE 7 | Category of surface finishing and surface treatment of Ti to accelerate bone formation, bone bonding, soft tissue adhesion, wear resistance, antibacterial property and blood compatibility.

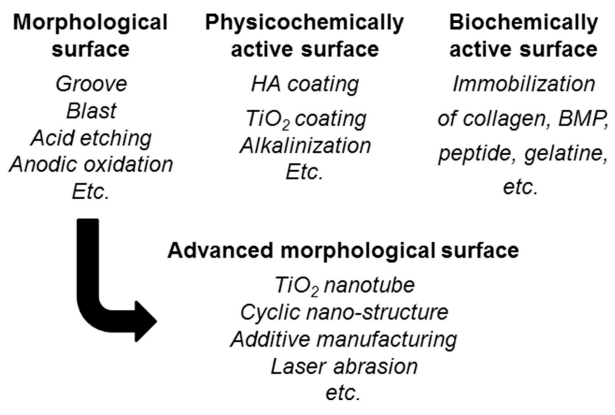

FIGURE 8 | Surface finishing and surface treatment of Ti to accelerate bone formation and bone bonding.

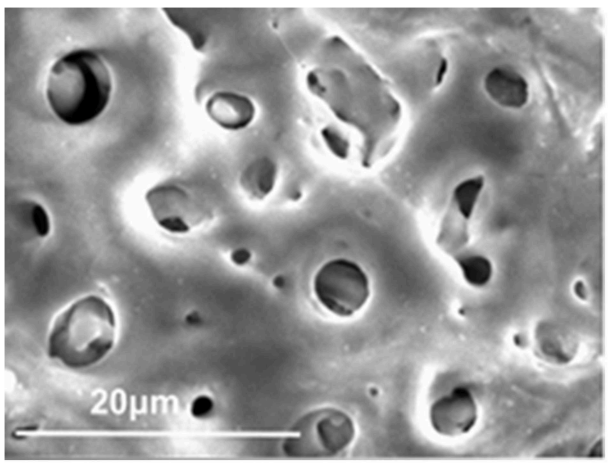

FIGURE 9 | Porous TiO_2 oxide layer formed on Ti by micro-arc oxidation.

Awad et al., 2017). On the other hand, a cyclic nanometer-level structure accelerates bone formation (Shinonaga et al., 2014; Matsugaki et al., 2015). In addition, this structure also accelerates the adhesion and differentiation of a stem cell (Olivares-Navarrete et al., 2010; Chen et al., 2017, 2018). Bone quality is governed not only by bone density but also bone structure orientation (Ishimoto et al., 2013). Grooves oriented to a main stress vector have been designed that control the orientation of the bone structure (Noyama et al., 2013). This technique has been commercialized in a dental implant. Recently, studies to control bacterial adhesion by a cyclic structure at a micrometer level have been increasing in number (Anselme et al., 2010). Nanotopographies have been applied to form antibacterial surfaces (Orapiriyakul et al., 2018; Mas-Moruno et al., 2019).

Three-dimensional additive manufacturing is an effective tool to form the above surface morphology (Wang et al., 2016). Additive-manufactured implants have been clinically applied, and effective ingrowth of bone to porous implants has been observed (Wang et al., 2017; Gao et al., 2018).

Hydroxyapatite and Oxide Coatings

To form a physicochemical active surface, HA is a main inorganic component of tooth and bone, so a coating of HA has been popular for accelerating bone formation and increasing resistance (Harun et al., 2018). The first technique was plasma spray (Ong and Lucas, 1994), which has been applied to various

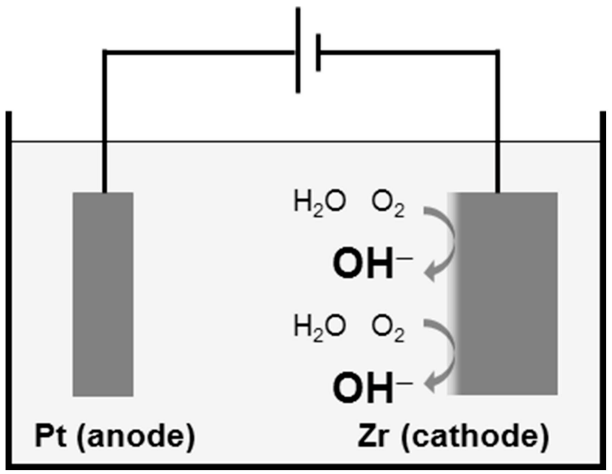

FIGURE 10 | Local alkalinization of Zr surface by cathodic polarization in a supporting electrolyte solution.

products. Thereafter, other coating techniques to form HA have been developed. Physical vapor deposition (PVD) in dry processes and electrochemical formation in wet processes are predominant, while a sol-gel technique (Li et al., 1996) and alternate immersion technique (Taguchi et al., 1999) have been developed. In addition, coatings of bioactive glass, tricalcium phosphate (Kitsugi et al., 1996), carbonate apatite (Yamaguchi et al., 2010), and octacalcium phosphate (Lin et al., 2003) with a bone formation ability larger than that of HA have been studied and developed. On the other hand, TiO_2 and other oxides have been coated on Ti (Umetsu et al., 2013). The surface is simultaneously roughened with a spray coating.

Surface Modification Layer Formation

Another technique to form a physicochemical active surface has been developed. The Ti surface is activated without coatings of HA and calcium phosphate. This surface is expected to form HA in bone tissue spontaneously. The oldest technique is calcium ion implantation (Hanawa et al., 1993, 1997). On the other hand, when Ti is immersed in an alkaline solution, such as NaOH and KOH, and heated, the surface is alkalinized, and the alkaline component is released to body fluid, followed by HA formation to form bone (Kim et al., 1996). This technique has been commercialized in an artificial hip joint. However, this technique is not effective for Zr, which does not form calcium phosphate on itself. Thus, Zr is cathodically polarized, and the surface of Zr is locally alkalinized, as shown in **Figure 10** (Tsutsumi et al., 2010).

Immobilization of Biofunctional Molecules and Biomolecules

The ideas of improvement of bone formation and of bone bonding by the immobilization of biomolecules involved in bone formation to a metal surface are logical. Such biomolecules as peptides, gelatins, and bone morphogenetic protein (BMP) are immobilized on the Ti surface (Hanawa, 2013). Immobilization of Type I collagen (Morra et al., 2011), fibronectin (Pegueroles et al., 2011), Arg-Gly-Asp (RGD) array peptide (Yamamichi et al., 2008), and BMP (Schliephake et al., 2012) is effective to promote cell spreading and bone formation. Immobilization of biomolecules has also been applied to create antibacterial surfaces (Qin et al., 2018). In the case of electrodeposition of poly(ethylene glycol) (PEG), the PEG-immobilized Ti inhibits protein adsorption, platelet adhesion (Tanaka et al., 2010a), and bacteria (Tanaka et al., 2010b).

The idea that the bone formation of a material's surface becomes active by the immobilization of biomolecules in bone formation is reasonable, and many studies have been conducted. However, to popularize the immobilization of biofunctional molecules widely, it is necessary to ensure the safety, maintenance of quality during storage, and dry-conditioned durability of the immobilized layer. It is difficult for manufacturers to commercialize this technique unless they see value in commercialization. There are many problems with commercializing the immobilized materials, although it is easy to show good results in basic research.

Cleaning and Hydrophilic Treatment

Surface contamination prevents bone formation and bone bonding in dental implants (Ueno et al., 2012). Instruments for optical activation treatments, such as ultraviolet irradiation and plasma irradiation, are available. Surface contamination is removed, and surface hydroxyl groups appear on the Ti surface in these optical activation treatments. The bone formation ability of a material is related to its wettability (Yamamoto et al., 2012). Surface characteristics of Ti implant have been reviewed elsewhere (Rupp et al., 2018).

SUMMARY AND PERSPECTIVE

Ti is the most biocompatible material among metals. Unfortunately, the underlying mechanism still has not been elucidated completely. Research and development have been focused on surface treatments to improve bone formation and bone bonding, leaving behind the understanding of the mechanism. However, the mechanism of the biocompatibility of Ti is gradually being understood with the research on surface-treated materials. Ti is the most bioactive material among metals, but it is less active than bioactive ceramics. The elucidation of the relevant mechanism can accelerate the development of optimal surfaces. The surface treatment techniques introduced in this review make it possible to apply metals to a scaffold in regenerative medicine or tissue engineering.

AUTHOR CONTRIBUTIONS

The author confirms being the sole contributor of this work and has approved it for publication.

ACKNOWLEDGMENTS

This work was supported by Creation of Life Innovation Materials for Interdisciplinary and International Researcher Development Project and Biable Materials Project, Ministry of Education, Culture, Sports, Science and Technology (MEXT), Japan.

REFERENCES

Ahmed, M., Wexler, D., Castillas, G., Savvakin, D. G., and Pereloma, E. V. (2016). Strain rate dependence of deformation-induced transformation and twinning in a metastable titanium alloy. *Acta Mater.* 104, 190–200. doi: 10.1016/j.actamat.2015.11.026

Albrektsson, T., and Hansson, H. A. (1986). An ultrastructural characterization of the interface between bone and sputtered titanium or stainless steel surfaces. *Biomaterials* 7, 201–205. doi: 10.1016/0142-9612(86)90103-1

Albrektsson, T., Jemt, T., Molne, J., Tengvall, P., and Wennerberg, A. (2019). On inflammation-immunological balance theory-A critical apprehension of disease concepts around implants: mucositis and marginal bone loss may represent normal conditions and not necessarily a state of disease. *Clin. Implant. Dent. Relat. Res.* 21, 183–189. doi: 10.1111/cid.12711

Albrektsson, T., and Wennerberg, A. (2004). Oral implant surfaces: part 1 - review focusing on topographic and chemical properties of different surfaces and *in vivo* responses to them. *Int. J. Prosthodont.* 17, 536–543.

Albrektsson, T., and Wennerberg, A. (2019). On osseointegration in relation to implant surfaces. *Clin. Implant. Dent. Relat. Res.* 21, 4–7. doi: 10.1111/cid.12742

Allam, N. K., Shankar, K., and Grimes, C. A. (2008). A general method for the anodic formation of crystalline metal oxide nanotube arrays without the use of thermal annealing. *Adv. Mater.* 20, 3942–3946. doi: 10.1002/adma.200800815

Alves, V. A., Reis, R. Q., Santos, I. C. B., Souza, D. G., Goncalves, T. D., Pereira-da-Silva, M. A., et al. (2009). *In situ* impedance spectroscopy study of the electrochemical corrosion of Ti and Ti-6Al-4V in simulated body fluid at 25 degrees C and 37 degrees C. *Corros. Sci.* 51, 2473–2482. doi: 10.1016/j.corsci.2009.06.035

Anon (1994). "Ti-6Al-2Nb-lTa-0.8Mo(Ti-6211)," in *Materials Properties Handbook*, eds R. Boyer, G. Welsch, and E. W. Collings (Phoenix, AZ: ASM International), 321–336.

Anselme, K., Davidson, P., Popa, A. M., Giazzon, M., Liley, M., and Ploux, I. (2010). The interaction of cells and bacteria with surfaces structured at the nanometre scale. *Acta Biomater.* 6, 3824–3846. doi: 10.1016/j.actbio.2010.04.001

Art, W., Hori, N., Takeuchi, M., Ouyang, J., Yang, Y., Anpo, M., et al. (2009). Time- dependent degradation of titanium osteoconductivity: an implication of biological aging of implant materials. *Biomaterials* 30, 5352–5363. doi: 10.1016/j.biomaterials.2009.06.040

Asri, R. I. M., Harun, W. S. W., Samykano, M., Lah, N. A. C., Ghani, S. A. C., Tarlochan, F., et al. (2017). Corrosion and surface modification on biocompatible metals: a review. *Mater. Sci. Eng. C* 77, 1261–1274. doi: 10.1016/j.msec.2017.04.102

Awad, N. K., Edwards, S. L., and Morsi, Y. S. (2017). A review of TiO_2 NTs on Ti metal: electrochemical synthesis, functionalization and potential use as bone implants. *Mater. Sci. Eng. C* 76, 1401–1412. doi: 10.1016/j.msec.2017.02.150

Beder, O. E., Stevenson, J. K., and Jones, T. W. (1957). A further investigation of the surgical application of titanium metal in dogs. *Surgery* 41, 1012–1015.

Boehm, H. P. (1966). Functional groups on the surfaces of solids. *Angew. Chem.* 5, 533–544. doi: 10.1002/anie.196605331

Boehm, H. P. (1971). Acidic and basic properties of hydroxylated metal oxide surfaces. *Discuss. Faraday Soc.* 52, 264–289. doi: 10.1039/DF9715200264

Bothe, R. T., Beaton, L. E., and Davenport, H. A. (1940). Reaction of bone to multiple metallic implants. *Surg. Gynec. Obsbtet.* 71, 598–602.

Brånemark, P.-I., Hansson, B. O., Adell, R., Breine, U., Lindström, J., Hallén, O., et al. (1977). Osseointegrated implants in the treatment of the edentulous jaw. Experience from a 10-year period. *Scand. J. Plastic Reconstruct. Surg. Hand Surg.* 11(Suppl. 16), 1–132.

Brammer, K. S., Frandsen, C. J., and Jin, S. (2012). TiO_2 nanotubes for bone regeneration. *Trend. Biotechnol.* 30, 315–322. doi: 10.1016/j.tibtech.2012.02.005

Branemark, R., Ohrnell, L. O., Skalak, R., Carlsson, L., and Brånemark, P.-I. (1998). Biomechanical characterization of osseointegration: an experimental *in vivo* investigation in the beagle dog. *J. Orthop. Res.* 16, 61–69. doi: 10.1002/jor.1100160111

Brozek, C., Sun, F., Vermaut, P., Millet, Y., Lenain, A., Embury, D., et al. (2016). A β-type alloy with extra high strain-hardening rate: design and mechanical properties. *Scr. Mater.* 114, 60–64. doi: 10.1016/j-scriptamat.2015.11.020

Brunette, D. M., Tenvall, P., Textor, M., and Thomsen, P. (2001). *Titanium in Medicine*. Berlin: Springer.

Buehler, W. J., Gilfrich, J. W., and Wiley, R. C. (1963). Effects of low-temperature phase changes on the mechanical properties of alloys near composition TiNi. *J. Appl. Phys.* 34, 1475–1477. doi: 10.1063/1.1729603

Chen, P., Aso, T., Sasaki, R., Ashida, M., Tsutsumi, Y., Doi, H., et al. (2018). Adhesion and differentiation behaviors of mesenchymal stem cells on titanium with micrometer and nanometer-scale grid patterns produced by femtosecond laser irradiation, *J. Biomed. Mater. Res. Part A* 106, 2736–2743. doi: 10.1002/jbm.a.36503

Chen, P., Aso, T., Sasaki, R., Tsutsumi, Y., Ashida, M., Doi, H., et al. (2017). Micron/submicron hybrid topography of titanium surfaces influences adhesion and differentiation behaviors of the mesenchymal stem cells. *J. Biomed. Nanotechnol.* 13, 324–336. doi: 10.1166/jbn.2017.2335

Civantos, A., Martinez-Campos, E., Ramos, V., Elvira, C., Gallardo, A., and Abarrategi, A. (2017). Titanium coatings and surface modifications: toward clinically useful bioactive implants. *ACS Biomater.* 3, 1245–1261. doi: 10.1021/acsbiomaterials.6b00604

Davies, J. E., Lowenberg, B., and Shiga, A. (1990). The bone titanium interface *in vitro*. *J. Biomed. Mater. Res.* 24, 1289–1306. doi: 10.1002/jbm.820241003

Eliaz, N. (2019). Corrosion of metallic biomaterials: a review. *Materials* 12:407. doi: 10.3390/ma12030407

Esposito, M., Lausmaa, J., Hirsch, J. M., and Thomsen, P. (1999). Surface analysis of failed oral titanium implants. *J. Biomed. Mater. Res.* 48, 559–568.

Fanning, J. C. (1996). "Properties and processing of a new metastable beta titanium alloy for surgical implant applications," in *Titanium'95: Science and Technology*, eds P. A. Blenkinsop, W. J. Evans, and H. Flower (Cambridge: The University Press), 1800–1807.

Fukushima, A., Mayanagi, G., Nakajo, K., Sasaki, K., and Takahashi, N. (2014). Microbiologically induced corrosive properties of the titanium surface. *J. Dent. Res.* 93, 525–529. doi: 10.1177/0022034514524782

Gao, C., Wang, C., Jin, H., Wang, Z., Li, Z., Shi, C., et al. (2018). Additive manufacturing technique-designed metallic porous implants for clinical application in orthopedics. *RSC Adv.* 8:25210. doi: 10.1039/c8ra04815k

Gefen, A. (2002). Computational simulations of stress shielding and bone resorption around existing and computer-designed orthopaedic screws. *Med. Bio. Eng. Comp.* 40, 311–322. doi: 10.1007/BF02344213

Gittens, R. A., Scheideler, L., Rupp, F., Hyzy, S. L., Geis-Gerstorfer, J., Schwartz, Z., et al. (2014). A review on the wettability of dental implant surfaces II: biological and clinical aspects. *Acta Biomater.* 10, 2907–2918. doi: 10.1016/j.actbio.2014.03.032

Goriainov, V., Cook, R., Latham, J. M., Dunlop, D. G., and Oreffo, R. O. C. (2014). Bone and metal: an orthopaedic perspective on osseointegration of metals. *Acta Biomater.* 10, 4043–4057. doi: 10.1016/j.actbio.2014.06.004

Hanawa, T. (2009). An overview of biofunctionalisation of metals in Japan. *J. R. Soc. Interface* 6, S361–S369. doi: 10.1098/rsif.2008.0427.focus

Hanawa, T. (2013). "Metal–polymer composite biomaterial," *Polymeric Biomaterials: Structure and Function, Volume 1*, eds S. Dumitriu and V. Popa (Boca Raton, FL: CRC Press), 343.

Hanawa, T. (2017). "Transition of surface modification of titanium for medical and dental use," *Titanium in Medical and Dental Applications*, eds F. H. Froes and M. Qian (Cambridge, UK: Woodhead Publishing), 95–114.

Hanawa, T., Kamiura, Y., Yamamoto, S., Kohgo, T., Amemiya, A., Ukai, H., et al. (1997). Early bone formation around calcium-ion-implanted titanium inserted into rat tibia. *J. Biomed. Mater. Res.* 36, 131–136.

Hanawa, T., and Ota, M. (1991). Calcium phosphate naturally formed on titanium in electrolyte solution. *Biomaterials* 12, 767–774. doi: 10.1016/0142-9612(91)90028-9

Hanawa, T., and Ota, M. (1992). Characterization of surface-film formed on titanium in electrolyte using XPS. *Appl. Surf. Sci.* 55, 269–276. doi: 10.1016/0169-4332(92)90178-Z

Hanawa, T., Ukai, H., and Murakami, K. (1993). X-ray photoelectron spectroscopy of calcium-ion-implanted titanium. *J. Electron Spectros. Relat. Phenomena* 63, 347–354. doi: 10.1016/0368-2048(93)80032-H

Harun, W. S. W., Asri, R. I. M., Alias, J., Zulkifli, F. H., Kadirgama, K., Ghani, S. A. C., et al. (2018). A comprehensive review of hydroxyapatite-based coatings adhesion on metallic biomaterials. *Ceram. Int.* 44, 1250–1268. doi: 10.1016/j.ceramint.2017.10.162

Healy, K. E., and Ducheyne, P. (1992). The mechanisms of passive dissolution of titanium in a model physiological environment. *J. Biomed. Mater. Res.* 26, 319–338. doi: 10.1002/jbm.820260305

Heintz, C., Riepe, G., Birken, L., Kaiser, E., Chakfe, N., Morlock, M., et al. (2001). Corroded nitinol wires in explanted aortic endografts: an important mechanism of failure? *J. Endovasc. Ther.* 8, 248–253. doi: 10.1177/152660280100800303

Hiromoto, S., Hanawa, T., and Asami, K. (2004). Composition of surface oxide film of titanium with culturing murine fibroblasts L929. *Biomaterials* 25, 979–986. doi: 10.1016/S0142-9612(03)00620-3

Ishimoto, T., Nakano, T., Umakosh, Y., Yamamoto, M., and Tabata, Y. (2013). Degree of biological apatite c-axis orientation rather than bone mineral density controls mechanical function in bone regenerated using recombinant bone morphogenetic protein-2. *J. Bone Miner. Res.* 28, 1170–1179. doi: 10.1002/jbmr.1825

Itakura, Y., Tajima, T., Ohoke, S., Matsuzawa, J., Sudo, H., and Yamamoto, S. (1989). Osteocompatibility of platinum-plated titanium assessed *in vitro*. *Biomaterials* 10, 489–493. doi: 10.1016/0142-9612(89)90091-4

Keller, J. C., Stanford, C. M., Wightman, J. P., Draughn, R. A., and Zaharias, R. (1994). Characterizations of titanium implant surfaces. *III. J. Biomed. Mater. Res.* 28:939. doi: 10.1002/jbm.820280813

Kelly, E. J. (1982). Electrochemical behavior of titanium. *Mod. Aspect. Electrochem.* 14, 319–424.

Kim, H. M., Miyaji, F., Kokubo, T., and Nakamura, T. (1996). Preparation of bioactive Ti and its alloys via simple chemical surface treatment. *J. Biomed. Mater. Res.* 32, 409–417.

Kitsugi, T., Nakamura, T., Oka, M., Senaha, Y., Goto, T., and Shibuya, T. (1996). Bone-bonding behavior of plasma-sprayed coatings of Bioglass(R), AW-glass ceramic, and tricalcium phosphate on titanium alloy. *J. Biomed. Mater. Res.* 30, 261–269.

Kroll, W. J. (1940). The production of ductile titanium. *Trans. Electrochem. Soc.* 78, 35–47. doi: 10.1149/1.3071290

Kuroda, D., Niinomi, M., Morinaga, M., Kato, Y. T., and Yashiro, T. (1988). Design and mechanical properties of new β type titanium alloys for implant materials. *Mater. Sci. Eng. A* 243, 244–249. doi: 10.1016/S0921-5093(97)00808-3

Lai, M. J., Li, T., and Raabe, D. (2018). ω phase acts as a switch between dislocation channeling and joint twinning- and transformation-induced plasticity in a metastable β titanium alloy. *Acta Mater.* 151, 67–77. doi: 10.1016/j.actamat.2018.03.053

Lee, J., Byun, H., Perikamana, S. K. M., Lee, S., and Shin, H. (2019). Current advances in immunolomodulatory biomaterials for bone regeneration. *Adv. Healthcare Mater.* 8:1801106. doi: 10.1002/adhm.201801106

Leventhal, G. S. (1951). Titanium, a metal for surgery. *J. Bone Joint Surg. Am.* 33A, 473–474. doi: 10.2106/00004623-195133020-00021

Li, P., deGroot, K., and Kokubo, T. (1996). Bioactive $Ca_{10}(PO_4)_6(OH)_2$-TiO_2 composite coating prepared by sol-gel process. *J. Sol Gel Sci. Technol.* 7, 27–34. doi: 10.1007/BF00401880

Li, Y., Wong, C., Xiong, J., Hodgson, P., and Wen, C. (2010). Cytotoxicity of titanium and titanium alloying elements. *J. Dent. Res.* 89, 493–497. doi: 10.1177/0022034510363675

Lide, D. R. (ed.). (2006). *CRC Handbook of Chemistry and Physics*, 87th Edn. Boca Raton, FL: CRC Press.

Lin, S. J., LeGeros, R. Z., and LeGeros, J. P. (2003). Adherent octacalcium phosphate coating on titanium alloy using modulated electrochemical deposition method, *J. Biomed. Mater. Res.* 66A, 819–828. doi: 10.1002/jbm.a.10072

Listgarten, M. A., Buser, D., Steinemann, S. G., Donath, K., Lang, N. P., and Weber, H. P. (1992). Light and transmission electron microscopy of the intact interfaces between non-submerged titanium-coated epoxy resin implants and bone or gingiva. *J. Dent. Res.* 71, 364–371. doi: 10.1177/00220345920710020401

Manam, N. S., Harum, W. S. W., Shri, D. N. A., Ghani, S. A. C., Kurniawan, T., and Ismail, M. H. (2017). Study of corrosion in biocompatible metals for implants: a review. *J. Alloy. Compound.* 701, 698–715. doi: 10.1016/j.allcom.2017.01.196

Marteleur, M., Sun, F., Gloriant, T., Vermaut, P., Jacques, P. J., and Prima, F. (2012). On the design of new n-metastable titanium alloys with improved work hardening rate thanks to simultaneous TRIP and TWIP effects. *Scr. Mater.* 66, 794–752. doi: 10.1016/j-scriptamat.2012.01.049

Mas-Moruno, C., Su, B., and Dalby, M. J. (2019). Multifunctional coatings and nanotopographies: toward cell instructive and antibacterial implants. *Adv. Healthcare Mater.* 8:1801103. doi: 10.1002/adhm.201801103

Matsuda,. Y., Nakamura, T., Ido, K., Oka, M., Okumura, H., and Matsushita, T. (1997). Femoral component made of Ti-15Mo-5Zr-3Al alloy in total hip arthroplasty. *J. Orthop. Sci.* 2, 166–170.

Matsugaki, A., Aramoto, G., Ninomiya, T., Sawada, H., Hata, S., and Nakano, T. (2015). Abnormal arrangement of a collagen/apatite extracellular matrix orthogonal to osteoblast alignment is constructed by a nanoscale periodic surface structure. *Biomaterials* 37, 134–143. doi: 10.1016/j.biomaterials.2014.10.025

Miura, I., and Ida, K. (Eds.). (1988). *Titanium in Dentistry*. Tokyo: Quintessence.

Morra, M., Cassinelli, C., Cascardo, G., Bollati, D., and Rodriguezy Baena, R. (2011). Collagen I-coated titanium surfaces: mesenchymal cell adhesion and *in vivo* evaluation in trabecular bone implants. *J. Biomed. Mater. Res.* 96A, 449–458. doi: 10.1002/jbm.a.30783

Murai, K., Takeshita, F., Ayukawa, Y., Kiyoshima, T., Suetsugu, T., and Tanaka, T. (1996). Light and electron microscopic studies of bone-titanium interface in the tibiae of young and mature rats. *J. Biomed. Mater. Res.* 30, 523–533.

Nagasawa, M., Cooper, L. F., Ogino, Y., Mendonca, D., Liang, R., Yang, S., et al. (2016). Topography influences adherent cell regulation of osteoclastogenesis. *J. Dent. Res.* 95, 319–326. doi: 10.1177/0022034515616760

Nakagawa, M., Matsuya, S., Shiraishi, T., and Ohta, M. (1999). Effect of fluoride concentration and pH on corrosion behavior of titanium for dental use. *J. Dent. Res.* 78, 1568–1572. doi: 10.1177/00220345990780091201

Nakayama, Y., Yamamuro, T., Kotoura, Y., and Oka, M. (1989). *In vivo* measurement of anodic polarization of orthopaedic implant alloys: comparative study of *in vivo* and *in vitro* experiments. *Biomaterials* 10, 420–414. doi: 10.1016/0142-9612(89)90134-8

Narayanan, R., Kwon, T. W., and Kim, K. H. (2014). TiO_2 nanotubes from stirred glycerol/NH_4F electrolyte: roughness, wetting behavior and adhesion for implant applications. *Mater. Chem. Phys.* 117, 460–464. doi: 10.1016/j.matchemphys.2009.06.023

Niinomi, M. (2019). Design and development of metallic biomaterials with biological and mechanical biocompatibility. *J. Biomed. Mater. Res. Part A* 107A, 944–954. doi: 10.1022/jbm.a.36667

Noyama, Y., Nakano, T., Ishimoto, T., Sakai, T., and Yoshikawa, H. (2013). Design and optimization of the oriented groove on the hip implant surface to promote bone microstructure integrity. *Bone* 52, 659–667. doi: 10.1016/j.bone.2012.11.005

Okazaki, Y. (2001). A New Ti−15Zr−4Nb−4Ta alloy for medical applications. *Curr. Opin. Solid State Mater. Sci.* 5, 45–53. doi: 10.1016/S1359-0286(00)00025-5

Olivares-Navarrete, R., Hyzy, S. L., Hutton, D. L., Erdman, C. P., Wieland, M., Boyan, B. D., et al. (2010). Direct and indirect effects of microstructured titanium substrates on the induction of mesenchymal stem cell differentiation towards the osteoblast lineage. *Biomaterials* 31, 2728–2735. doi: 10.1016/j.biomaterials.2009.12.029

Ong, J. L., and Lucas, L. C. (1994). Postdeposition heat-treatments for ion-beam sputter-deposited calcium-phosphate coatings. *Biomaterials* 15, 337–341. doi: 10.1016/0142-9612(94)90245-3

Orapiriyakul, W., Young, P. S., Damiati, L., and Tsimbouri, P. M. (2018). Antibacterial surface modification of titanium implants in orthopaedics. *J. Tissue Eng.* 9, 1–16. doi: 10.1177/2041731418789838

Ozaki, T., Matsumoto, H., Watanabe, S., and Hanada, S. (2004). Beta Ti alloys with low Young's modulus. *Mater. Trans.* 45, 2776–2779. doi: 10.2320/matertrans.45.2776

Palmquist, A., Omar, O. M., Esposito, M., Lausmaa, J., and Thomsen, P. (2010). Titanium oral implants: surface characteristics, interface biology and clinical outcome. *J. R. Soc. Interface* 7, S515–S527. doi: 10.1098/rsif.2010.0118.focus

Parfitt, G. D. (1976). The surface of titanium dioxide. *Prog. Surf. Membr. Sci.* 11, 181–226.

Park, J. Y., and Davies, J. E. (2000). Red blood cell and platelet interactions with titanium implant surfaces. *Clin. Oral Implant. Res.* 11, 530–539. doi: 10.1034/j.1600-0501.2000.011006530.x

Pegueroles, M., Aguirre, A., Engel, E., Pavon, G., Gil, F. J., Planell, J. A., et al. (2011). Effect of blasting treatment and Fn coating on MG63 adhesion and

differentiation on titanium: a gene expression study using real-time RT-PCR. *J. Mater. Sci. Mater. Med.* 22, 617–627. doi: 10.1007/s10856-011-4229-3

Pillar, R. M., and Weatherly, G. C. (1982). "Development in implant alloys" in *Clinical Reviews in Biocompatibility,* Vol. 1, ed D. F. Williams (Boca Raton, FL: CRC Press), 371–473.

Qin, S., Xu, K., Nie, B., Ji, F., and Zhang, H. (2018). Approaches based on passive and active antibacterial coating on titanium to achieve antibacterial activity. *J. Biomed. Mater. Res. Part A* 106A, 2531–2539. doi: 10.1002/jbm.a.36413

Rao, V. B., and Houska, C. R. (1979). Kinetics of the phase-transformation in a Ti-15Mo-5Zr-3Al alloy as studied by X-ray-diffraction. *Metal. Trans. A* 10, 355–358. doi: 10.1007/BF02658345

Ratner, B. D., Hoffman, A. S., Schoen, F. J., and Lemons, J. E. (Eds.). (2013). *Biomaterials Science-An Introduction to Materials in Medicine*, 3rd Edn. Oxford, UK: Academic Press.

Rautray, T. R., Narayanan, R., Kwon, T. Y., and Kim, K. H. (2011). Ion implantation of titanium based biomaterials. *Prog. Mater. Sci.* 56, 1137–1177. doi: 10.1016/j.pmatsci. 2011.03.002

Rupp, F., Liang, L., Geis-Gerstorfer, J., Scheideler, L., and Hüttig, F. (2018). Surface characteristics of dental implants: a review. *Dent. Mater.* 34, 40–57. doi: 10.1016/j.dental.2017.09.007

Salvi, G. E., Bosshardt, D. D., Lang, N. P., Abrahamsson, I., Berglundh, T., Lindhe, J., et al. (2015). Temporal sequence of hard and soft tissue healing around titanium dental implants. *Periodontology* 68, 135–152. doi: 10.1111/prd.12054

Sanderson, L., Ryan, W., and Turner, P. G. (1992). Complications of metalwork removal injury. *Injury* 23, 29–30. doi: 10.1016/0020-1383(92)90121-8

Scheinert, D., Scheinert, S., Sax, J., Piorkowski, C., Braunlich, S., Ulrich, M., et al. (2005). Prevalence and clinical impact of stent fractures after femoropopliteal stenting. *J. Am. Coll. Cardiol.* 45, 312–315. doi: 10.1016/j.jacc.2004.11.026

Schliephake, H., Boetel, C., Foerster, A., Schwenzer, B., and Reichert, J. (2012). Effect of oligonucleotide mediated immobilization of bone morphogenic proteins on titanium surfaces. *Biomaterials* 33, 1315–1322. doi: 10.1016/j.biomaterials.2011.10.027

Semlitsch, M., and Staub, F. H. W. (1985). Titanium-aluminium-niobium alloy development for biocompatible, high strength surgical implants. *Biomed. Tech.* 30, 334–339.

Sennerby, L., Thomsen, P., and Ericson, L. E. (1993). Early tissue response to titanium implants inserted in rabbit cortical bone. *J. Mater. Sci. Mater. Med.* 4, 494–502. doi: 10.1007/BF00120129

Serro, A. P., Fernandes, A. C., Saramago, B., Lima, J., and Barbosa, M. A. (1997). Apatite desorption on titanium surfaces – the role of albumin adsorption. *Biomaterials* 18, 963–968. doi: 10.1016/S0142-9612(97)00031-8

Shah, F. A., Thomsen, P., and Palmquist, A. (2018). A review of the impact of implant biomaterials on osteocytes. *J. Dent. Res.* 97, 977–986. doi: 10.1177/0022034518778033

Shah, F. A., Thomsen, P., and Palmquist, A. (2019). Osseointegration and current interpretations of bone-implant interface. *Acta Biomater.* 84, 1–15. doi: 10.1016/j.actbio.2018.11.018

Shinohara, Y., Tahara, M., Inamura, T., Miyazaki, S., and Hosoda, H. (2015). Effect of annealing temperature on microstructure and superelastic properties of Ti-Au-Cr-Zr alloy. *Mater. Trans.* 56, 404–409. doi: 10.2320/matertrans.M2014439

Shinonaga, T., Tsukamoto, M., Nagai, A., Yamashiata, K., Hanawa, T., Matsushita, N., et al. (2014). Cell spreading on titanium dioxide film formed and modified with aerosol beam and femtosecond laser. *Appl. Surf. Sci.* 288, 649–653. doi: 10.1016/j.apsusc.2013.10.090

Sundell, G., Dahlin, C., Andersson, M., and Thuvander, M. (2017). The bone-implant interface of dental implants in humans on the atomic scale. *Acta Biomater.* 48, 445–450. doi: 10.1016/j.actbio.2016.11.044

Sundgren, J.-E., Bodö, P., Ivarsson, B., and Lundström, I. (1986a). Adsorption of fibrinogen on titanium and gold surfaces studied by esca and ellipsometry. *J. Colloid Interface Sci.* 113, 530–543.

Sundgren, J. E., Bodo, P., and Lundstrom, I. (1986b). Auger electron spectroscopic studies of the interface between human tissue and implants of titanium and stainless steel. *J. Colloid Interface Sci.* 110, 9–20. doi: 10.1016/0021-9797(86)90348-6

Taguchi, T., Kishida, A., and Akashi, M. (1999). Apatite formation on/in hydrogel matrices using an alternate soaking process (III): effect of physico-chemical factors on apatite formation on/in poly(vinyl alcohol) hydrogel matrices. *J. Biomater. Sci. Polymer Ed.* 10, 795–804. doi: 10.1163/156856299X00883

Tanaka, Y., Kurashima, K., Saito, H., Nagai, A., Tsutsumi, Y., Doi, H., et al. (2009). *In vitro* short term platelet adhesion on various metals. *J. Artf. Org.* 12, 182–186. doi: 10.1007/s10047-009-0468-1

Tanaka, Y., Matin, K., Gyo, M., Okada, A., Tsutsumi, Y., Doi, H., et al. (2010b). Effects of electrodeposited poly(ethylene glycol) on biofilm adherence to titanium. *J. Biomed. Mater. Res. Part A* 95A, 1105–1113. doi: 10.1002/jbm.a.32932

Tanaka, Y., Matsuo, Y., Komiya, T., Tsutsumi, Y., Doi, H., Yoneyama, T., et al. (2010a). Characterization of the spatial immobilization manner of poly(ethylene glycol) to a titanium surface with immersion and electrodeposition and its effects on platelet adhesion. *J. Biomed. Mater. Res. Part A* 92A, 350–358. doi: 10.1002/jbm.a.32375

Trindade, R., Albrektsson, T., Galli, S., Prgomet, Z., Tengvall, P., and Wennerberg, A. (2018). Osseointegration and foreign body reaction: titanium implants activate the immune system and suppress bone resorption during the first 4 weeks after implantation. *Clin. Implant Dent. Relat. Res.* 20, 82–91. doi: 10.1111/cid.12578

Trindade, R., Albrektsson, T., Tengvall, P., and Wennerberg, A. (2016). Foreign body reaction to biomaterials: on mechanisms for buildup and breakdown of osseointegration. *Clin. Implant Dent. Relat. Res.* 18, 192–203. doi: 10.1111/cid.12274

Tsutsumi, Y., Nishimura, D., Doi, H., Nomura, N., and Hanawa, T. (2009). Calcium phosphate formation on titanium and zirconium and its application to medical devices. *Mater. Sci. Eng.* C29, 1702–1708. doi: 10.4303/bda/D110119

Tsutsumi, Y., Nishimura, D., Doi, H., Nomura, N., and Hanawa, T. (2010). Cathodic alkaline treatment of zirconium to give the ability to form calcium phosphate. *Acta Biomater.* 6, 4161–4166. doi: 10.1016/j.actbio.2010.05.010

Ueno, T., Takeuchi, M., Hori, N., Iwasa, F., Minamikawa, H., Igarashi, Y., et al. (2012). Gamma ray treatment enhances bioactivity and osseointegration capability of titanium. *J. Biomed. Mater. Res. Appl. Biomater.* 100B, 2279–2287. doi: 10.1002/jbm.b.32799

Umetsu, N., Sado, S., Ueda, K., Tajima, K., and Narushima, T. (2013). Formation of anatase on commercially pure Ti by two-step thermal oxidation using N_2-CO gas. *Mater. Trans.* 54, 1302–1307. doi: 10.2320/matertrans.ME201315

Wang, F. E., Buehler, W. J., and Pickart, S. J. (1965). Crystal structure and a unique martensitic transition of TiNi. *J. Appl. Phys.* 36, 3232–3239. doi: 10.1063/1.1702955

Wang, K., Gustavson, L., and Dumbleton, J. (1993). "Low modulus, high strength, biocompatible titanium alloy for medical implants, in *Titanium'92: Science and Technology,* eds F. H. Froes and H. L. Caplan (Warrenda, PA: TMS), 2697–2704.

Wang, X., Xu, S., Zhou, S., Xu, W., Leary, M., Choong, P., et al. (2016). Topological design and additive manufacturing of porous metals for bone scaffolds and orthopaedic implants: a review. *Biomaterials* 83, 127–141. doi: 10.1016/j.biomaterials.2016.01.012

Wang, Z., Wang, C., Li, C., Qin, Y., Zhong, L., Chen, B., et al. (2017). Analysis of factors influencing bone ingrowth into three-dimensional printed porous metal scaffolds: a review. *J. Alloy. Comp.* 717, 271–285. doi: 10. 1016/j.jallcom.2017.05.079

Waterstrat, R. M., Rupp, N. W., and Franklin, O. (1978). Production of a cast titanium-base partial denture. *J. Dent. Res.* 57:254.

Wennerberg, A., and Albrektsson, T. (2010). On implant surfaces: a review of current knowledge and opinions. *Int. J. Oral Maxillofac Implant.* 25, 63–74.

Westall, J., and Hohl, H. (1980). A comparison of electrostatic models for the oxide/solution interface. *Adv. Colloid Interface Sci.* 12, 265–294. doi: 10.1016/0001-8686(80)80012-1

William, D. F. (1987). "Definitions in biomaterials," in *Proceedings of a Consensus Conference of the European Society for Biomaterials,* Vol. 4 (Chester; New York, NY: Elsevier).

Williams, D. F. (1982a). "Titanium and titanium alloys," in *Biocompatibility of Clinical Implant Materials*, eds D. F. Williams (Boca Raton, FL: CRC Press), 10–44.

Williams, D. F. (1982b). "Biological effects of titanium," in *Systematic Aspects of Biocompatibility*, ed D. F. Williams (Boca Raton, FL: CRC Press), 170–177.

Williams, R. (ed.). (2011). *Surface Modification of Biomaterials*. Cambridge, UK: Woodhead Publishing.

Yamaguchi, Y., Adachi, M., Iijima, M., Wakamatsu, N., Kamemizu, H., Omoto, S., et al. (2010). Thin carbonate apatite layer biomimetically-coated on SAM-Ti substrate surfaces. *J. Ceram. Soc. Jpn.* 118, 458–461. doi: 10.2109/jcersj2.118.458

Yamamichi, N., Pugdee, K., Chang, W., Lee, S., and Yoshinari, M. (2008). Gene expression monitoring in osteoblasts on titanium coated with fibronectin-derived peptide. *Dent. Mater. J.* 27, 744–750. doi: 10.4012/dmj.27.744

Yamamoto, D., Iida, T., Arii, K., Kuroda, K., Ichino, R., Okido, M., et al. (2012). Surface hydrophilicity and osteoconductivity of anodized Ti in aqueous solutions with various solute ions. *Mater. Trans.* 53, 1956–1961. doi: 10.2320/matertrans.M2012082

Zardiackas, L. D., Mitchell, D. W., and Disegi, J. A. (1996). "Characterization of Ti-15Mo beta titanium alloy for orthopaedic implant applications," in *Medical Applications of Titanium and Its Alloys*, eds S. A. Browns and J. E. Lemons (West Conshohoken, PA: ASTM), 60–75.

Zhan, H., Wang, G., Kent, D., and Dargusch, M. (2016). The dynamic response of metastable β Ti-Nb alloy to high strain rates at room and elevated temperatures. *Acta Mater.* 105, 104–113. doi: 10.1016/j.actamat.2015.11.056

Zhang, J. Y., Li, J. S., Chen, Z., Meng, Q. K., Sun, F., and Shen, B. L. (2017). Microstructural evolution of a ductile metastable b titanium alloy with combined TRIP/TWIP effects. *J. Alloys Compd.* 699,775–782. doi: 10.1016/j.jallcom.201612.394

Conflict of Interest Statement: The author declares that the research was conducted in the absence of any commercial or financial relationships that could be construed as a potential conflict of interest.

frontiers in Bioengineering and Biotechnology

REVIEW
published: 30 July 2019
doi: 10.3389/fbioe.2019.00176

Mechanisms of Adverse Local Tissue Reactions to Hip Implants

Felipe Eltit[1,2,3], *Qiong Wang*[1,2,3] *and Rizhi Wang*[1,2,3]*

[1] Department of Materials Engineering, University of British Columba, Vancouver, BC, Canada, [2] School of Biomedical Engineering, University of British Columba, Vancouver, BC, Canada, [3] Centre for Hip Health and Mobility, Vancouver, BC, Canada

Adverse Local Tissue Reactions (ALTRs) are one of the main causes of hip implant failures. Although the metal release from the implants is considered as a main etiology, the mechanisms, and the roles of the released products are topics of ongoing research. The alloys used in the hip implants are considered biocompatible and show negligible corrosion in the body environment under static conditions. However, modularity and its associated mechanically assisted corrosion have been shown to release metal species into the body fluids. ALTRs associated with metal release have been observed in hip implants with metal-on-metal articulation initially, and later with metal-on-polyethylene articulation, the most commonly used design in current hip replacement. The etiological factors in ALTRs have been the topics of many studies. One commonly accepted theory is that the interactions between the metal species and body proteins and cells generate a delayed type IV hypersensitivity reaction leading to ALTRs. However, lymphocyte reactions are not always observed in ALTRS, and the molecular mechanisms have not been clearly demonstrated. A more accepted mechanism is that cell damage generated by metal ions may trigger the secretion of cytokines leading to the inflammatory reactions observed in ALTRs. In this inflammatory environment, some patients would develop hypersensitivity that is associated with poor outcomes. Concerns over ALTRS have brought significant impact to both the clinical selection and development of hip implants. This review is focused on the mechanisms of ALTRs, specifically, the metal release process and the roles of the metal species released in the etiology and pathogenesis of the disease. Hopefully, our presentation and discussion of this biological process from a material perspective could improve our current understanding on the ALTRs and provide useful guidance in developing preventive solutions.

Keywords: pseudotumors, corrosion, mitochondrial stress, tribocorrosion, fretting corrosion, metal hypersensitivity, total hip implants, adverse local tissue reactions

OPEN ACCESS

Edited by:
Hasan Uludag,
University of Alberta, Canada

Reviewed by:
Joanna Mystkowska,
Białystok Technical University, Poland
Steve Meikle,
Independent Researcher, Eastbourne, United Kingdom

***Correspondence:**
Rizhi Wang
rzwang@mail.ubc.ca

Specialty section:
This article was submitted to Biomaterials, a section of the journal Frontiers in Bioengineering and Biotechnology

Received: *04 March 2019*
Accepted: *08 July 2019*
Published: *30 July 2019*

Citation:
Eltit F, Wang Q and Wang R (2019) Mechanisms of Adverse Local Tissue Reactions to Hip Implants. Front. Bioeng. Biotechnol. 7:176. doi: 10.3389/fbioe.2019.00176

INTRODUCTION

Over one million people receive hip replacements every year to relieve pain and restore hip functions from osteoarthritis, a degenerative disease that affects most people in their seventh decade of life (RIPO, 2014; The Canadian Joint Replacement Registry, 2015). Although hip arthroplasty is generally a successful procedure, adverse local tissue reactions (ALTRs) can develop to the materials used in hip implants, affecting patients' health and decreasing their quality of life. ALTRs affect at least 10% of patients with Metal-on-Metal (MoM) hip implants as well as a lower but significant

number of patients with Metal-on-Polyethylene (MoP) hip implants, the most commonly used system in total hip replacements (Matharu et al., 2016a).

The main symptoms of ALTRs are pain and swelling. They can generate extensive destruction to the soft tissues of the hip, challenging the prognosis of further clinical solutions (Williams et al., 2011; Almousa et al., 2013). The exact etiology of ALTRs is not clear. But their exclusive development after hip replacement suggests a link with the metal components of the hip implants (Cooper et al., 2013). It has been widely accepted that metal release can affect the periprosthetic tissues, leading to development of ALTRs. In order to guide clinical selection of orthopedic implants and facilitate the development of new implant technologies, there is a need to critically review current progress and clarify the mechanisms responsible for the development of ALTRs. In the following sections, we will start with corrosion and wear mechanisms from a material perspective, and then discuss the biological and immunological processes that led to the development of ALTRs.

MATERIALS AND DESIGNS IN HIP REPLACEMENTS

Metals have been commonly used in hip implants because of their excellent mechanical properties. Since the introduction of the highly biocompatible titanium alloys in 1970s (Albrektsson et al., 1981; Brånemark, 1983), a typical total hip replacement (THR) system is generally composed of a titanium femoral stem, a CoCrMo femoral head articulating with a polyethylene liner, supported by a titanium acetabular shell (**Figure 1C**). However, polyethylene wear debris generated in articulation against CoCrMo femoral head trigger osteolytic lesions, inducing inflammation and bone resorption (Ormsby et al., 2019). To minimize the wear of polyethylene in articulation, second-generation MoM articulation was developed in the 1990s (**Figure 1A**). The CoCrMo alloy used in articulating surfaces of MoM implants is composed of 60–65% cobalt, 27–30% chromium, 5–7% molybdenum, and 2–5% other trace elements as manganese, silicon, iron, nickel, and carbon (Schmidt et al., 1996). Through advanced technologies, it was possible to obtain smoother surfaces which theoretically would reduce wear and friction (Dowson, 2006). The assumption of lower wear was later demonstrated "*in vitro*" (Anissian et al., 1999; Clarke et al., 2000). Positive clinical outcomes were observed at that time (van der Bracht et al., 2011). Cr and Co ions levels in most of the patients' serum were considered acceptable, and there was no higher risk of cancer in patients with MoM compared to the general population (Mathiesen et al., 1995; Keegan et al., 2008; Makela et al., 2012; Lalmohamed et al., 2013). Due to these observations, MoM implants were considered safe to humans. The FDA approved the MoM systems for clinical use through the 510 K or "substantial equivalence" to previously cleared devices (Ardaugh et al., 2013).

To avoid dislocation, a common clinical complication, large femoral heads were introduced in the second-generation MoM hip implants in order to increase range of motion and joint stability (Kostensalo et al., 2012; Dargel et al., 2014). Tribological analyses demonstrated that there was no significant increase in friction between larger contact surfaces if the clearance between the surfaces was decreased (Rieker et al., 2005; Dowson, 2006). The possibility of having a metal femoral head, articulating directly over the metal acetabular cup, prompts the development of hip resurfacing (**Figure 1B**), a surgical procedure in MoM hip replacements that involves minimal bone removal on the femoral head. This design was especially effective for young and active patients, with good outcomes after 5 years follow-up, and a lower hospital stay (2.3 days) compared with total hip replacement (4.1 days) (Ward et al., 2011; Jameson et al., 2012; RIPO, 2014). Due to those advantages, 35% of THA performed between 1998 and 2008 in the US and Europe were MoM implants (Meier, 2010; Liao et al., 2013). Unfortunately, adverse reactions due to metals release started to be reported in 10–30% of the patients (Langton et al., 2011b; Smith et al., 2012; Almousa et al., 2013). They were clinically characterized by pain, rash, and the development of a local benign fibroma described as pseudotumor (Pandit et al., 2008; Mahendra et al., 2009). Subsequently most manufacturers have halted the production of MoM implants (Cohen, 2011).

Another technological improvement to hip prostheses was the development of modularity of the femoral components (**Figure 1**). The modularity allows surgeons to select the components independently to best fit patient's anatomy. It reduces the inventory in hospitals and manufacturers, and simplifies revisions procedure if needed (Srinivasan et al., 2012). However, the modular junctions between components experience corrosion due to fretting, which can be a source of metal particles or ions release responsible for the development of ALTRs (Fricker and Shivanatil, 1990; Brown et al., 1995; Kawalec et al., 1995; Kop et al., 2012; Wang et al., 2016).

MECHANISMS OF IMPLANT DEGRADATION

The metal alloys used in hip replacements are considered to be corrosion resistant, mostly due to the protection provided by a dense 2–4 nm-thick passive oxide layer formed on their surfaces. Laboratory studies showed that Ti6Al4V and CoCrMo alloys would not experience significant corrosion when they contact each other under simulated physiological conditions in static environment (Lucas et al., 1981; Griffin et al., 1983). However, the presence of corrosion products at the modular junction of the retrieved implants, and elevated metal ions in the serum of patients have been widely reported since 1990s (Collier et al., 1990, 1992; Mathiesen et al., 1991). This corrosion process is attributed to the disruption of the passive film caused by mechanical wear (Brown et al., 1995; Jacobs et al., 1998). There are two possible locations where this mechanically assisted corrosion is likely to happen: (i) the articulating surfaces, where the friction between the moving femoral head and acetabular components generates wear on the surfaces and accelerates corrosion. This material degradation process is often referred as tribocorrosion. (ii) the modular junction of the implants, in which the cyclic load generates micromotion (fretting) at

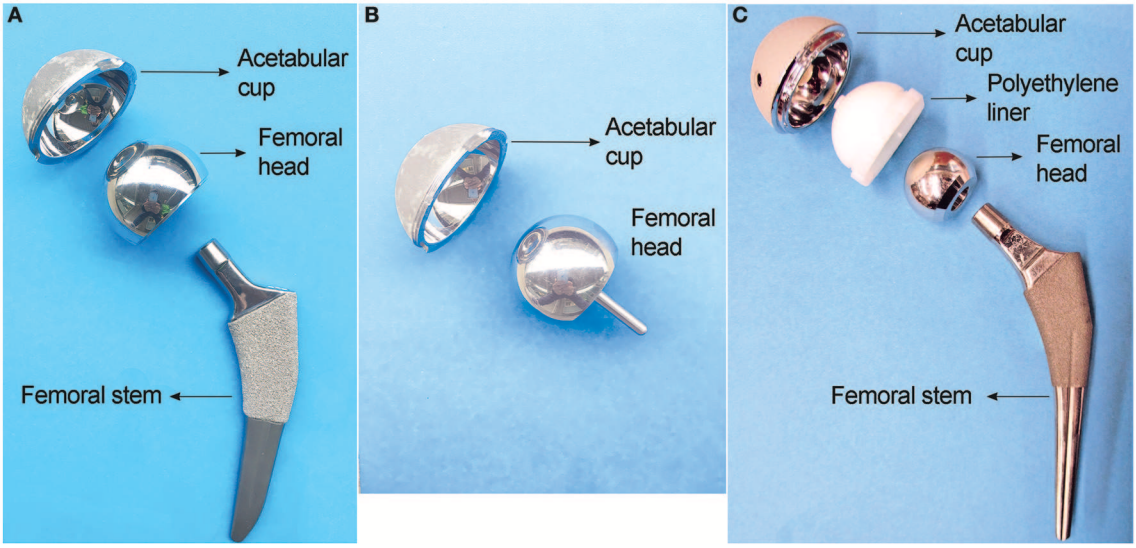

FIGURE 1 | Three main types of hip implants. **(A)** Large head metal-on-metal (MoM) total hip implant. **(B)** MoM hip resurfacing. **(C)** Metal-on-polyethylene (MoP) total hip implant.

the interface of the components, causing destruction of the passive layers on both surfaces and subsequent corrosion of the underlying metals. This fretting corrosion at the modular junction is enhanced by the presence of crevice corrosion, which is characteristic in confined space of the tapper junctions of modular implants (**Figure 2**). The reactions that occurs inside the crevice are initiated by the mechanical removal of the passive layer (fretting corrosion). Subsequently, the surfaces re-passivate, consuming oxygen in the reaction. After each cycle and due to the confined space, oxygen is depleted, which further retard the formation of a new passive layer and increase corrosion rate (Jacobs et al., 1998).

Mechanically assisted corrosion of metal alloys in hip implants releases solid particles as well as metal ions into the peri-implant environment. It is generally accepted that those released metal species would trigger adverse tissue reactions which ultimately require revision surgery. It is thus necessary to first discuss our current understanding on the *in vivo* metal release process and the nature of the degradation products in terms of morphology, composition, crystallinity, and concentration.

Another important factor regarding the corrosion of hip implants is the presence of biological products interacting with the implants' surfaces. The effects of biological elements on the degradation of materials is referred as biocorrosion (Cadosch et al., 2009). The articulating surfaces and modular junctions of the hip implants are surrounded by the synovial fluid, which constitutes a relatively mild environment of buffered solution at around pH of 7.4 with temperature of 37°C (Hanawa, 2004). However, there are some specific bio-corrosive elements such as ions, proteins, proteoglycans, biologically induced pH changes, and oxidizers, that may affect its physicochemical behavior (Talha et al., 2019). The presence of proteins in the physiological environment may affect the corrosion of metallic materials by changing the mechanics and kinetics of the corrosion

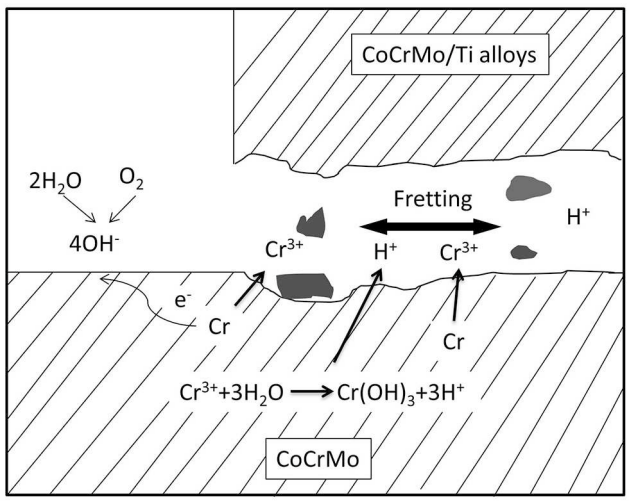

FIGURE 2 | Illustration of fretting corrosion between two metallic components. Fretting corrosion is complexed by crevice corrosion that results in oxygen depletion and reduced pH in the crevice where fretting happens.

reactions on the surface (Goldberg and Gilbert, 1997; Hallab et al., 2003; Okazaki and Gotoh, 2005; Valero Vidal et al., 2010; Igual Munoz et al., 2015). A decrease in the pH is usually a consequence of inflammation or hypoxia, produced by the enhanced glycolytic pathways and subsequent increase in the production of lactate or pyruvate. This decrease in pH could theoretically enhance corrosion of the implants alloys; Additionally, active oxygen species released by immunological cells such as macrophages when responding to a foreign body or during inflammation are potential oxidizers that could enhance the corrosion process (Hanawa, 2004; Gilbert et al., 2015; Liu and Gilbert, 2017).

TABLE 1 | Summary of reported corrosion debris from CoCrMo hip implants.

Locations	Corrosion debris and representative reports
Head-neck junction	**Inside:** crystalline metal oxides containing Cr, Mo with depleted Co (Urban et al., 1994, 1997)
	At the opening: amorphous chromium (III) phosphate hydrate (Urban et al., 1994, 1997)
Peri-implant tissues	**MoM implants:** oxide particles containing Cr^{3+} (Catelas et al., 2004, 2006; Goode et al., 2012);
	Nano-sized metallic particles (Doorn et al., 1998; Catelas et al., 2004, 2006; Goode et al., 2012; Topolovec et al., 2013; Bitounis et al., 2016);
	Chromium (III) phosphate (Huber et al., 2009; Hart et al., 2010, 2012).
	MoP implants: oxide particles containing Cr with low Co and sub-micron metallic particles (Shahgaldi et al., 1995; Urban et al., 2000; Topolovec et al., 2013); chromium phosphate (Clarke et al., 2003; Illgen et al., 2008).

Particles Release From Tribocorrosion at the Articulating Surfaces

Tribocorrosion at the articulating surfaces has been studied both through retrieval analyses and *"in vitro"* laboratory wear tests by using hip simulator in simulated body fluid (**Table 1**). Material release from implants depends on the design and material composition. In general, the size of particles generated is on average 300 nm for polyethylene, 30 nm for metal and 9 nm for ceramic (Tipper et al., 2001). Although the volumetric wear in MoM articulations is about one tenth of the polyethylene wear observed in zirconia on polyethylene or MoP implants, the nature of the particles released presents a higher risk for the development of adverse local tissue reactions (Goldsmith et al., 2000). Analyses on articulating surfaces of MoM implants have proposed that wear (tribocorrosion) on CoCrMo alloys may be responsible for hip implant failure (Campbell et al., 2006; Matthies et al., 2011; Al-Hajjar et al., 2013).

Hip simulation studies showed that CoCrMo metallic particles and chromium oxide nanoparticles are the main particles released as a consequence of tribocorrosion in Metal-on-Metal articulation (**Figures 3A,B**; Firkins et al., 2001; Catelas et al., 2003). The generation of wear particles is also affected by loading conditions. Under edge-loading, CoCrMo nanoparticles generated were relatively larger; while under normal loading, most particles generated are smaller chromium oxide nanoparticles (Kovochich et al., 2018).

The particles released *"in vivo"* from the articulating surfaces by tribocorrosion are not retained to the surface of implants. Since there are no modular junctions in MoM hip resurfacing system (**Figure 1B**), tribocorrosion at the articulating surface is the sole source of metal release. Analysis of corrosion products in synovial fluid and tissues from MoM hip resurfacing offer insights on particles associated with tribocorrosion at the metal bearing surfaces. By use of *SEM-EDX* analysis, three types of particles have been observed in tissues surrounding MoM hip resurfacing: chromium oxide, CoCrMo metal, and chromium phosphate particles (Doorn et al., 1998; Hart et al., 2010; Goode et al., 2012). The oxidation state of these particles is Cr (III) (Hart et al., 2010; Goode et al., 2012). Compared to laboratory studies, *"in vivo"* studies revealed another type of particle—chromium phosphate particles. Similar chromium phosphate compound was also commonly observed in the tissues from MoM THR and MoP THR. The formation of this type particles is speculated to be the reaction product of Cr ions with the body fluid containing phosphate ions.

Particles Released From Fretting Corrosion at the Modular Junctions

Fretting corrosion has been demonstrated to affect modular interfaces of implants composed of similar or different alloys, as observed in systematic analysis of retrieved implants (**Table 1**) (Gilbert et al., 1993). But limited experimental studies have analyzed variables such as materials, electrolytes and load to explain the mechanisms associated with these variables (Swaminathan and Gilbert, 2012).

An early *"ex-vivo"* study led by Jacobs et al. (1995), analyzed the morphology and the chemical compositions of corrosion products at the modular interfaces of retrieved femoral heads. The study concluded that the composition of corrosion compounds varies along the topographical locations. Chromium oxides and chlorides existed inside the tapper junction, in the contact area between head and neck, but chromium orthophosphate was found mainly at the rim of the head bore and, on the neck surface distal to the head-neck junction (Jacobs et al., 1995). Another study from the same group in 1997 described that at the contact area, the products corresponded to mixed crystalline oxides of Cr, Mo, and Ti, while in the open crevice, the products were mostly amorphous hydrated chromium orthophosphate. Interestingly, minimal cobalt was found in the corrosion particles on the implant surfaces (Mathiesen et al., 1991; Urban et al., 1997). These observations were later confirmed by other researchers (Huber et al., 2009; Chana et al., 2012; Baleani et al., 2017). The Cr-rich fretting corrosion products with low or depleted Co indicated that Co was released in the form of soluble species.

Since MoM THR consists of articulating surfaces as well as the head-neck junction, the presence of solid particles in periprosthetic tissues can be associated with both tribocorrosion at the articulating surfaces and fretting corrosion at head-neck junction (**Figures 3**, **4**). In tissues and synovial fluid surrounding MoM THRs, oxide particles containing Cr as well metallic nanoparticles were observed (Doorn et al., 1998; Catelas et al., 2004, 2006; Ward et al., 2010; Topolovec et al., 2013); corrosion particles rich in chromium and phosphate were also observed (Huber et al., 2009; Xia et al., 2017).

In MoP hip implants, most studies assumed negligible wear on metal head because of the relatively low wear resistance of polyethylene. It was commonly accepted that particles observed in tissues surrounding MoP hip implants were mainly associated with fretting corrosion at the head-neck interface. Chromium and phosphate rich particles were the primary debris detected in the tissues surrounding MoP hip implants (Cooper et al., 2013). However, we recently observed the presence of extensive

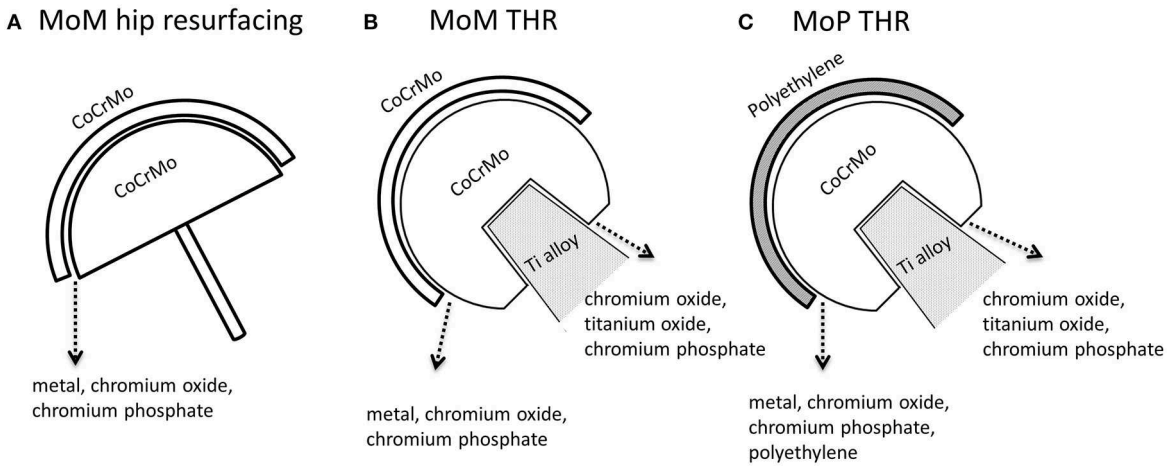

FIGURE 3 | Types of particles released from the femoral head-cup articulation and head-neck junction of CoCrMo based hip implants. **(A)** MoM hip resurfacing. **(B)** MoM total hip implant. **(C)** MoP total hip implant. In addition to polyethylene (PE) and titanium oxide particles, metal particles are particles with similar chemical composition to the alloy CoCrMo; chromium oxide is a type of particles containing Cr, O with low or depleted Co; chromium phosphate particles contain Cr, O, P, Ca with low or depleted Co in EDS spectrum.

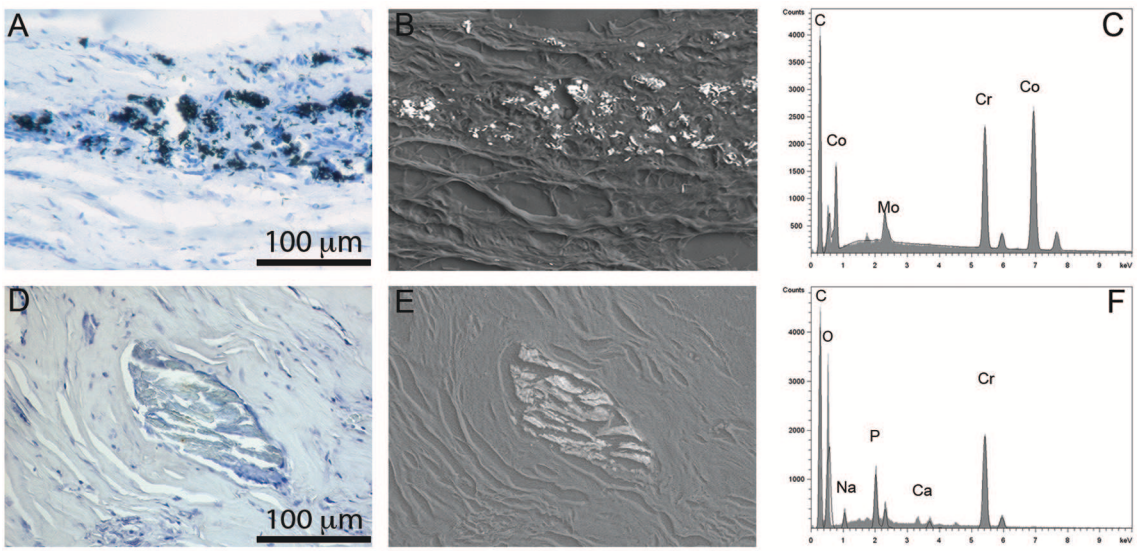

FIGURE 4 | Particles observed in periprosthetic tissues. **(A–C)** CoCrMo metal particles of sub-micron size group in leukocyte infiltrated areas **(A)**; they show a high contrast in back-scattered electron image due to their high density **(B)**; the EDS spectrum shows peaks of Co, Cr, and Mo **(C)**. **(D–F)** chromium phosphate particles, tens to hundreds of microns in size usually surrounded by a collagenous capsule **(D)**, showing low density in back scattered electron image **(E)**, and peaks in Cr, O, and P in EDS spectrum **(F)**.

wear on the articular surfaces of CoCrMo femoral heads in MoP hip implants, which demonstrated that tribocorrosion could also result in significant metal release in MoP hip implants.

Metal Ions Release From Metal Implants

The presence of elevated metal ions in serum and synovial fluid have been associated with the development of ALTRs (Amstutz and Le Duff, 2017). Monitoring Co and Cr levels in serum or whole blood is the current clinical predictor of hip implants malfunction and provides alert to the development of ALTRs. The metal release is directly associated with mechanically assisted corrosion, such as tribocorrosion and fretting. Mechanically assisted corrosion not only releases solid particles, but also has a tremendous impact on metal ions release. Especially, the metal ions are released by multiple mechanisms. The wear disrupts the passive layer on the implant surface, re-passivates and releases metal ions. The nano- and micron-sized particles generated by wear may further release ions when exposed to body fluids due to their large surface areas. Cell reactions to the particles generate an oxidizing environment. It has been observed that phagocyted metal particles by tissue macrophages are processed in lysosomes, which are known to be highly oxidative structures, capable of

increasing the release of metal ions from the phagocyted particles (Park, 2003; Billi and Campbell, 2010).

Cobalt (Co) is preferentially released as Co^{2+} during the formation of the passive film (mainly chromium oxide) on the implant surfaces (Li et al., 1999; Milošev and Strehblow, 2003; Hanawa, 2004). Cobalt salts are highly soluble, and do not tend to precipitate in solution (Foote, 1923). A immersion study of CoCrMo alloy in phosphate buffered solution (PBS) demonstrated that Co^{2+} was the most abundant ion released from the alloy with a ratio Co:Cr:Mo = 13:2:1 (Hedberg and Odnevall Wallinder, 2014). Interestingly in the same study it was observed that cobalt release rate was higher in PBS enriched with albumin, which suggests a cobalt-protein interaction that affects the electrochemical reaction of Co. This enhanced effect was not observed in Cr or Mo.

Chromium (Cr) is the major elemental component in the passive layer formed on the CoCrMo surfaces. It is released from the implants as Cr^{3+} at extremely low rate in static immersion tests compared with Co^{2+} and Mo (Metikos-Huković et al., 2006). However, after long-term implantation of CoCrMo alloys, elevated levels of Cr^{3+} ions were observed in blood and urine of patients with metal hip replacements (Lhotka et al., 2003). This release of chromium is believed to be associated with disruption of passive film due to mechanical wear. Chromium compounds are believed to be formed rapidly after ion release, by reaction with phosphate in the synovial fluid and formation of highly insoluble precipitates (Ness et al., 1952; Rai et al., 1987).

Molybdenum (Mo) is rarely studied in the research associated to ALTRs. However, the lack of studies in synovial fluid does not exclude the possible adverse effects of Mo on the periprosthetic tissues. Molybdenum species are stable in passivity at low pH, but a pH higher than 7.0 is thermodynamically favorable for Mo dissolution (Martin et al., 2013). Moreover, molybdenum oxides formed on the metal surfaces exposed to air, disappeared quickly after immersion in 0.15 M NaCl (Li et al., 1999). Although traditionally it was not considered an important factor, its interaction with proteins recently revealed an important role in the dynamics of molybdenum release. A study using Electrochemical Quartz Crystal Microbalance reported that protein deposition occurs preferentially on Mo surfaces (Martin et al., 2013). Furthermore, by improving protocol for metal ion measurement with use of extended centrifugation and ultrafiltration, researchers revealed an accelerated release of molybdenum ion from CoCrMo particles in the presence of bovine serum albumin compared to PBS alone (Simoes et al., 2016).

Co and Cr concentrations in blood have been often monitored to evaluate the performance of hip implants. Comparison studies revealed that Co and Cr ions in the blood of patients with ALTRs were significantly higher than the control group without ALTRs (Kwon et al., 2011; McGrory et al., 2017). Concerns over metal over release in patients with MoM hip replacements were raised shortly after the introduction of the second generation MoM implants (Savarino et al., 2002). In 2015, UK Medicines and Healthcare Regulatory Agency (MHRA) issued a blood cobalt and chromium guidance value of 7 μg/L to identify MoM hip implant patients who may need further surveillance on excessive implant wear (archived in 2017) (Medicines Healthcare products Regulatory Agency, 2015). Similarly, the American Association of Hip and Knee Surgeons, the American Academy of Orthopedic Surgeons, and the Hip Society recommends a systematic evaluation of patients with dual modular neck systems, to include the analysis of serum ions levels to optimize the management of these patients (Kwon et al., 2014). Although cobalt and chromium in serum have been proposed as a monitoring tool for the performance of CoCrMo hip implants, it has been demonstrated that their analysis only has a modest sensitivity and specificity (60%) in identifying patients with ALTRs in MoM hip implants (Malek et al., 2012; Matharu et al., 2016b).

Despite the challenges to define thresholds of Co or Cr ion concentration in serum as predictors of ALTRs, the relative Cr/Co in serum provide insights on the releasing mechanisms. Most reports revealed a higher Cr/Co in serum from patients with MoM hip resurfacing (without head-neck junction) than patients with MoM total hip replacement. One study revealed 1.73 and 2.15 of mean Cr/Co in serum from total 160 cases of two types of hip resurfacings (Langton et al., 2009), much higher than 0.67 of mean Cr/Co from 17 patients with MoM total hip replacement (Eltit et al., 2017). This is consistent with the direct comparison showing the higher Cr/Co in serum from hip resurfacings than MoM total hip replacements (Garbuz et al., 2010). Another report also supported a much higher Cr/Co (0.91) in blood in hip resurfacing group than in total hip replacement group (0.53) (Matharu et al., 2017). These reports suggested that Cr in serum was preferably released from tribocorrosion at the bearing surface rather than fretting corrosion at the head-neck junction.

Compared to MoM hip implants, concentrations of Co and Cr ions in serum of patients with MoP total hip implants were far less studied. Metal ions in patients with well-functioning MoP total hip implants are usually analyzed as the control to compare with patients with MoM hip implants (Savarino et al., 2002; Cobb and Schmalzreid, 2006). To the best of our knowledge, there are no alerts regarding metal or serum ion levels in MoP systems, but a recent study proposed a threshold of 1 μg/L as cutoff for identification of ALTRs in patients with MoP hip implants (Fillingham et al., 2017). Our study revealed increased Co and Cr ions in serum of patients with ALTRs in MoP compared to ones without ALTRs (Eltit et al., 2017). These results indicated metal species released from CoCrMo implants were the stimuli responsible for developing ALTRs in patients with MoP total hip implants. Our latest results on metal ions measurement combined with wear analysis showed elevated Cr ion in serum with increasing roughness of CoCrMo femoral head in retrieved MoP hip implants. It indicated that Cr ions in serum were mainly attributed to the tribocorrosion at the articulating surface. In addition, we also showed that accelerated tribocorrosion also resulted in high level of Co ions in serum of patients with MoP hip implants.

Compared to metal ions in blood, far fewer studies had been reported on metal ions in synovial fluid. Hip implants are exposed to the joint fluid, a viscous fluid produced by the synovial membrane. It contains hydrophilic molecules such as hyaluronic acid that increase its viscosity and reduce friction. The

concentration of Co and Cr ions in the synovial fluid of patients without implants is around 1 μg/L and 4 μg/L, respectively. These numbers could increase to a range between 50 and 100 μg/L in patients with well-functioning implants and could reach between 500 and 10,000 μg/L in patients with failed implants (Lass et al., 2014; Eltit et al., submitted). Compared to serum, it has been observed that the Co and Cr ions concentrations in synovial fluid have greater variations and are relatively higher (De Smet et al., 2008; Davda et al., 2011; Eltit et al., 2017).

ALTRs

Definition and Nomenclature

Adverse Local Tissue Reactions (ALTRs) have been histologically described as the growth of cystic or solid fibrotic masses originating in the synovial membrane of patients with hip implants (Doorn et al., 1996; Mahendra et al., 2009; Natu et al., 2012; Perino et al., 2014; Matharu et al., 2016a). ALTRs generate pain and discomfort, as well as pressure on vein and nerves, but some can also be asymptomatic (Maurer-Ertl et al., 2011; Konan et al., 2017).

Different terms have been used to describe lesions associated with hip replacements. The clinical name "Pseudotumor" was used in the 1980s to describe soft tissue growth around hip implants (Griffiths et al., 1987), it was thought to be a reaction to the acrylic cement of the femoral components but was later observed in non-cemented systems (Svensson and Mathiesen, 1988). The same term was reincorporated for the lesions found in second generation MoM implants in the study of Pandit et al. (2008). Pseudotumor refers to the Greek "pseudo" for false and the Latin "tumor" for increase in volume. The actual pathology observed surrounding the implants corresponds to a true volume increase, but since the term "tumor" has been associated with neoplasms, the prefix pseudo was added to reduce concerns over the malignancy of these inflammatory lesions. Pseudotumor then, corresponds to a clinical and imaging description of a benign volume growth associated with a hip replacement system. Aseptic Lymphocyte-dominated Vasculitis-Associated Lesion, was introduced by Willert et al. (2005). Although the acronym ALVAL was used for the first time by Campbell et al. (2010) who also introduced a method of quantifying the severity of the lesions based on the histological observations (ALVAL score), which is now been used in most of the studies to describe the severity of the lesions around hip implants (Campbell et al., 2010). The term ALVAL corresponds to the histological description of the lesions that are found in the clinically described "pseudotumors." Adverse Reaction to Metal Debris (ARMD) was introduced by Langton et al. (2010). ARMD is used to define the pathology associated with MoM implants which suggests that the failure is due to the presence of wear debris (Langton et al., 2010), which was supported by an increased wear rate in failed implants (Langton et al., 2011a). However, it indicates that metal debris are the main cause of the adverse reactions, which is still under investigation. Adverse Local Tissue Reactions (ALTRs) is a term that includes a broad spectrum of pathological changes associated with the presence of hip implants. It was used in the 1970s and 1980s to describe the pathology in the tissues surrounding hip implants (Forest et al., 1985), and was reintroduced to describe the failure of the second-generation MoM hip prosthesis in a literature review by Carli et al. (2011). It is currently the most frequently used term to define the aseptic periprosthetic lesions (Carli et al., 2011).

Histological Characteristics of ALTRs

ALTRs are described as solid masses or cystic cavities, in which the ulceration of the synovial surface with or without fibrin deposition, is accompanied by sub superficial necrosis, mononuclear cell infiltration and variable number of eosinophils and giant multinucleated cells, in a thickened synovial membrane composed of dense connective tissue (**Figure 5**; Mahendra et al., 2009; Natu et al., 2012; Perino et al., 2014).

It is accepted that, as in most foreign body reactions, the immune system plays a critical role in the development of ALTRs. This is supported by the histological observations of macrophages and T cells in the tissue, occasionally with giant multinucleated cells and eosinophils (Mahendra et al., 2009). Generally, lesions with a large number of macrophages presenting a low lymphocyte infiltration and highly lymphocyte-infiltrated lesions do not exhibit large number of macrophages (**Figure 6**) (Campbell et al., 2010; Ricciardi et al., 2016). The T-cell infiltration varies from the diffuse presence of T cells that has been found to have an equivalent number of CD4+ and CD8+, to the presence of large perivascular mononuclear aggregates composed of T (CD3+) and B (CD20+) cells, which has been defined as a characteristic of high-grade ALTRs (Natu et al., 2012). By use of immunohistochemistry, a high level of organization has been observed in the perivascular aggregates in which the B cells are located in the central zones (follicles) surrounded by T cells (Mittal et al., 2013). Because of this organization, and the molecular interactions between cells have been proposed corresponding to tertiary lymphoid organs, similar to those observed in peripheral organs with chronic inflammation (Natu et al., 2012; Neyt et al., 2012; Mittal et al., 2013). The phagocytic role of macrophages in ALTRs has also been reported, and the presence of metal particles inside the macrophage has been confirmed by optical microscopy (**Figure 6C**) or transmission electron microscopy (TEM) (Huber et al., 2009; Xia et al., 2011). There is an association between the amount of wear on implant surfaces and the number of macrophages in the tissues (Campbell et al., 2010). TEM observations of living macrophages within the tissues have shown that the particles were inside the phagosomes. But when the cells died, the membranes disintegrated, and the particles were released (Xia et al., 2011).

Etiology of ALTRs: Role of the Immune System, Hypersensitivity Hypothesis

The products of material degradation (both metal ions and solid particles) released from the implants as a consequence of corrosion or wear, have been accepted as the main etiological factor of ALTRs (Langton et al., 2011b). Nevertheless, studies have failed to correlate the amount of wear or corrosion in the implants with the severity of the lesions and clinical observations (Schmalzried, 2009; Campbell et al., 2010). These results, together

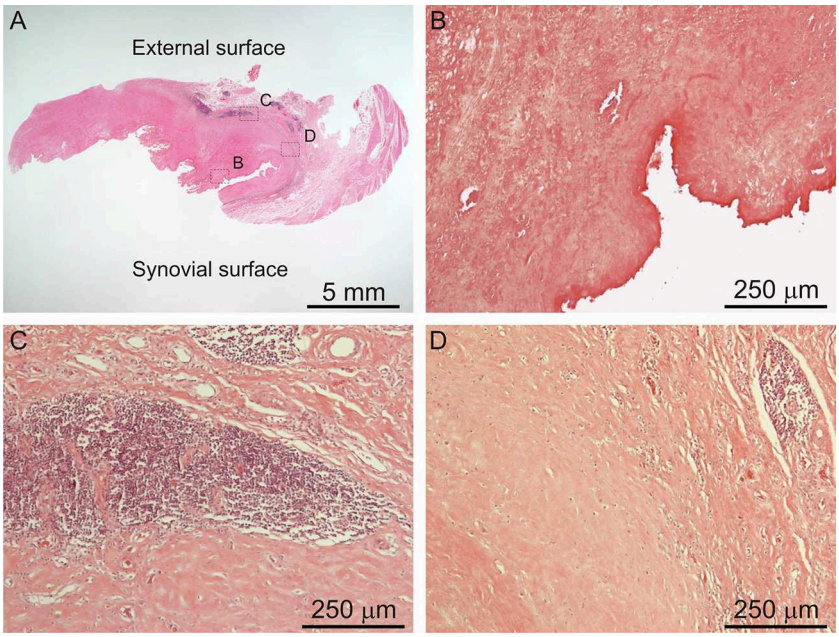

FIGURE 5 | Histological images of ALTR. Low magnification of biopsied lesions **(A)**, characterized by synovial ulceration and sub superficial necrosis **(B)**, mononuclear cell infiltration **(C)**, and macrophages **(D)**.

with histological descriptions support the hypersensitivity theory that ALTRs correspond to a type IV or delayed hypersensitivity reaction triggered by metals (Huber et al., 2009; Mahendra et al., 2009; Thomas et al., 2009). Type IV hypersensitivity corresponds to the harmful effects of the cell-mediated immune response, in which the damage generated by the immune system is exaggerated in comparison to the damage that the etiological agent may produce (Abbas et al., 2015). Activated perivascular T-cells trigger cell death and secrete cytokines that induce macrophages to fuse forming giant multinucleated cells around the damaged area (granuloma), and also stimulate the proliferation of fibroblasts leading to tissue fibrosis (Kumar et al., 2012). All these features (T-cell infiltration, vasculitis, giant multinucleated cells, cell death, granuloma, and fibrosis) are found in ALTRs (**Figure 7**), providing strong support to this theory (Natu et al., 2012; Perino et al., 2014; Ricciardi et al., 2016).

The possible evidence of the interaction between metal species and T-cell is the decrease in the total number of circulating T lymphocytes observed in patients with MoM implants (Granchi et al., 2003; Catelas et al., 2015), and the CD8+ T-cell lymphopenia associated with high concentration of cobalt and chromium ions in plasma (Hart et al., 2009). It is thought that Co^{2+} interferes with antigen presentation, inhibiting T-cell expansion. However, this decrease in circulating T-cells could also be due to the local sequestration that occurs in periprosthetic tissues.

It is not clear how metals can induce hypersensitivity, but a molecular mechanism by which metals ions induce T-cell mediated hypersensitivity (type IV) has been recently described for beryllium (Be). The Be^{2+} ion conjugates with part of the HLA-peptide complex (HLA-DP2) and generates structural changes in the molecule. This modified-HLA molecule is recognized by the T-cell receptor, triggering the immune reaction responsible for severe lung destruction due to chronic inflammation in 1–15% of people exposed to beryllium (Clayton et al., 2014; Kugelberg, 2014; Fontenot et al., 2016). A similar pathway involving T-cell receptor activation may also be part of the mechanisms of immunogenicity triggered by the metals from the implants. Quite a few researchers have proposed that metal ions or nanoparticles can act as haptens or "incomplete antigens," that combine with host proteins to generate a "neoantigen" (a new antigen that the immune system has not been exposed before) that activates T cell receptors (Hallab and Jacobs, 2009; Athanasou, 2016). Nevertheless, a study of lymphocyte activation in the presence of cobalt and chromium showed no differences between the lymphocytes obtained from patients with failed MoM implants and the control group, which suggests that metal hypersensitivity may not be the main mechanism in the development of ALTRs (Kwon et al., 2010). Clinical studies have also shown no association between metal allergy and implant failure (Thyssen et al., 2009). Further analyses demonstrate that the frequency of positive metal sensitivity test increases in patients who receive a hip replacement, and the increase is even higher in patients with failed implants; however, the test is not predictive for ALTRs (Granchi et al., 2012). Currently in most surgical centers all patients who are receiving hip implants are tested for metal allergy before surgery. And CoCrMo alloys are not used in patients with allergy. Nevertheless, a high rate of ALTRs is still observed in patients with MoM implants. These observations, together with the higher risk on patients with elevated Co^{2+} and Cr^{3+} ions in blood, suggest that a complex process involving multiple mechanisms such as cellular damage

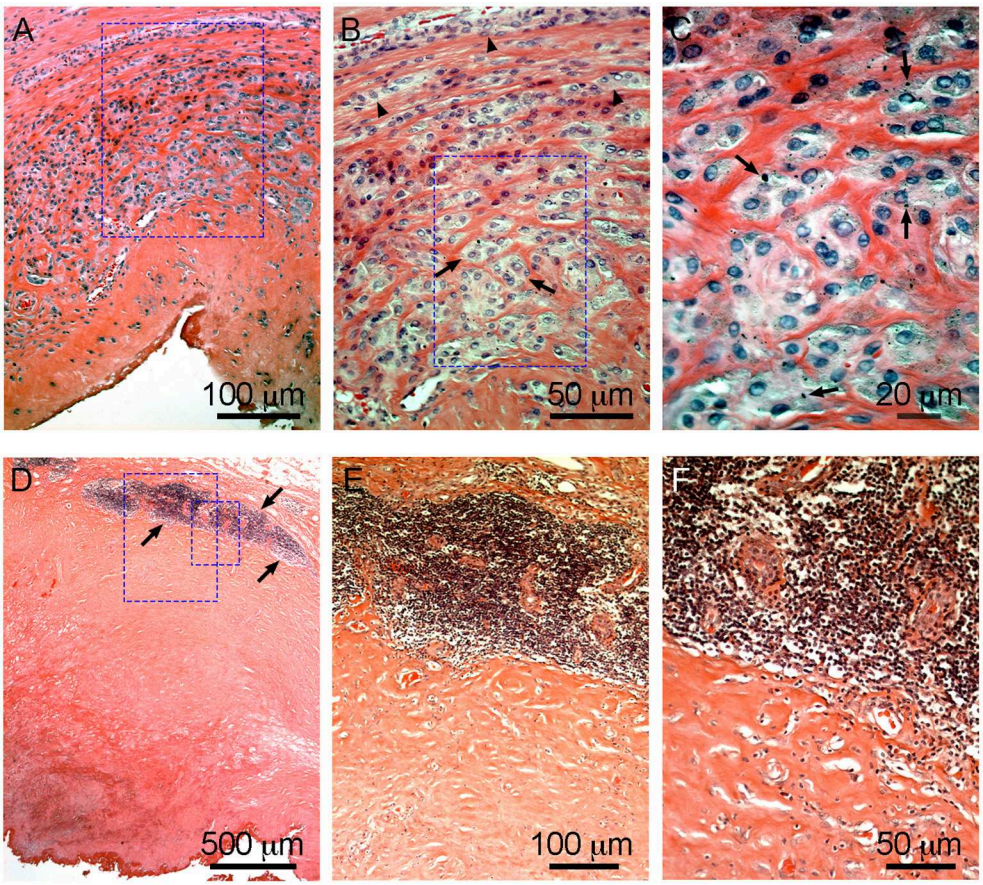

FIGURE 6 | Characteristic macrophage-dominated ALTR **(A–C)** and ALTR with lymphocyte infiltration and hypersensitivity features **(D–F)**. Macrophage dominated lesions are associated with evidence of high wear, corrosion, and elevated Co and Cr in serum (53 and 48 μg/L, respectively, in the case shown). ALTRs with predominant lymphocyte infiltrate and hypersensitivity features usually are not associated with elevated wear or corrosion and may be present with lower Co and Cr in serum (6.2 μg/L and 1.2 μg/L in the case in **D–F**). Low extension of sub superficial necrosis is observed in macrophage-dominated lesion with macrophages that infiltrate the whole synovium **(A)**, forming clusters (arrows) or epithelioid cells (arrowheads) in **(B)**, and multiple micron/sub-micron particles (arrows) are observed in macrophages cytoplasm **(C)**. Hypersensitivity feature ALTRs usually present with large extension of sub superficial necrosis **(D)**, with perivascular lymphocyte infiltration that form large aggregates (over 1 mm) and may constitute tertiary lymphoid organs (arrows in **D,E**), with low (or none) number of particles observed in the tissues **(F)**.

induced by metal ions, cell death, and immunogenicity of metal ions (Harinderjit et al., 2012).

Etiology of ALTRs: Hypothesis of Cellular Hypoxic Stress

The roles of cobalt and chromium products in triggering the cellular phenomena observed in ALTRs such as inflammation, cell death and fibrosis, have been partially demonstrated *"in vitro."* Studies carried out at the Rizzolli Orthopedic Institute had shown that high concentrations of Co^{2+} ions generated necrosis in human peripheral mononuclear cells, while lower concentrations induced apoptosis in the same cell population. On the other hand, Cr^{3+} ions at high concentrations induced apoptosis in the cells and no effects were observed in lower concentrations (Granchi et al., 1998a). Another study in macrophage-type cells (J774), showed that after 24 h of exposure to elevated cobalt and chromium concentrations the cell death was due to apoptosis. But after 48 h of exposure, the cells experienced necrosis (Huk et al., 2004). The same group, in a later report by Catelas et al. (2005) showed that chromium need higher ion concentrations than cobalt (250 vs. 8 ppm) to generate similar effects in J774 cells, suggesting that elevated concentration of these ions *"in vivo"* could be responsible of the cell death in the tissues (Catelas et al., 2005).

Cobalt and chromium particles also have toxic effects on human cells. Studies in keratinocytes (HaCaT cells), cultured with different concentration of nanoparticles of Cr_2O_3 showed the increased cell death due to apoptosis with the increased number of particles (Horie et al., 2013). It was later demonstrated that the cell death induced in a macrophage cell line (J774) by nanoparticles of chromium oxide corresponded to apoptosis (VanOs et al., 2014). A study using dermal fibroblast showed that nanoparticles of CoCrMo alloy produced a higher rate of cell death than a similar volume of micron-size particles; The authors then proposed that the higher surface area of the nano-sized particles generated a higher ion release (Papageorgiou et al.,

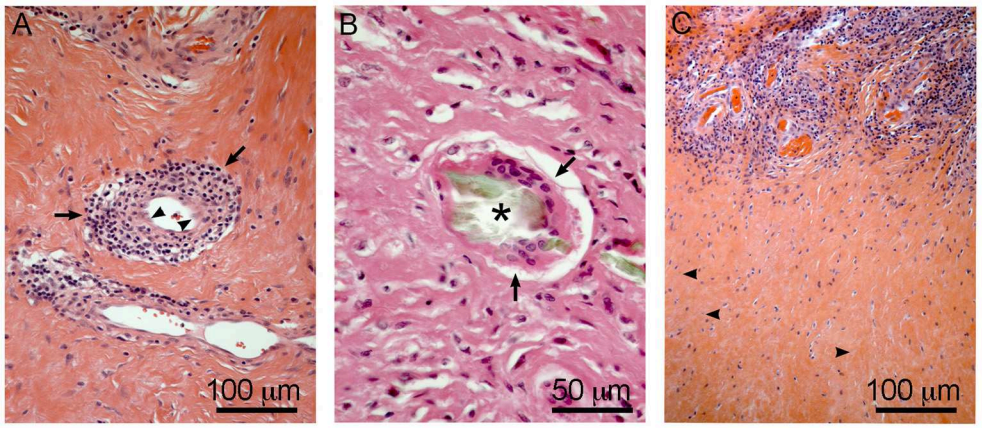

FIGURE 7 | Hypersensitivity features in ALTRs. Perivascular T cell infiltration/vasculitis (arrows) observed in **(A)**, note the changes in the morphology of the endothelial cells to rounded or prismatic (arrowheads). Giant multinucleated cell (arrows) in **(B)**, frequently they are associated with large corrosion-product (Cr rich, no Co) particles (asterisk). T cell infiltration zones are usually surrounded by necrotic areas with low vascularity and evidence of cell degeneration (arrowheads) **(C)**.

2007). These effects of metal particles on cell viability are thought to be associated with release of metal ions that have direct effects on cells. It has been demonstrated that cobalt ions produce significantly higher cytotoxicity than cobalt particles in lung fibroblasts (Smith et al., 2014), and the generation of reactive oxygen species (ROS) in T-cells is induced by Co ions but not by nano- and micron sized particles (Chamaon et al., 2019).

The described difference in toxicity of cobalt and chromium may be attributed to their difference in solubility and the capability to penetrate the plasma membrane. It was explained previously that chromium tends to precipitate in the presence of phosphate ions, the common species present in human tissues, decreasing the concentration of "free ions" able to penetrate the cells and cause deleterious effects. Chromium usually exists in the form of Cr^{3+} in synovial tissues and fluids, which differs from the carcinogenic Cr^{6+} that is soluble and uses phosphate channels to penetrate the cell membranes (Jobby et al., 2018). Cobalt in tissues is in the form of Co^{2+}, which is mostly soluble and is an important cofactor for vitamin B12 (Cobalamin); it can penetrate cells, and interact with organelles and proteins (Czarnek et al., 2015).

As previously explained, the elevated concentration of cobalt ions can have cytotoxic effects on several cell types (Granchi et al., 1998b; Huk et al., 2004; Catelas et al., 2005; Fleury et al., 2006; Posada et al., 2015), produce necrosis and apoptosis (Granchi et al., 1998a; Huk et al., 2004), and increase the production of ROS (Salloum et al., 2018; Chamaon et al., 2019). It has also been demonstrated that human macrophages exposed to Co^{2+} and Cr^{3+} ions have an increased expression of apoptotic proteins Bax-2, caspase 3 and caspase 8 and a decreased expression of the antiapoptotic protein BCL-2 (Petit et al., 2004). However, a recent study using primary synovial fibroblasts showed no induction of apoptosis even at high concentrations (1 mM), but evident metabolic stress and cytokine secretion even at low concentrations (0.1 mM) (Eltit et al., submitted). One limitation in the analyses is that most of the described results were obtained "*in vitro*" by using concentrations of cobalt of 0.5 mM, which is higher than the values observed "*in vivo*." At lower and more "physiopathological" concentrations (1–10 μM), ATP synthesis has shown to be inhibited by cobalt in a dose-dependent manner. This happens not as the result of the inhibition of ATP synthase or the respiratory chain, but as consequence of the opening of the mitochondrial permeability transition pore (MPT), which allows the H^+ to migrate from the intermembrane space to the mitochondria matrix, thus decreasing the electromotive force that activates the ATP synthase (**Figure 8A**) (Bragadin et al., 2007). As a consequence of this aerobic respiration failure, the production of ATP is decreased, and the anaerobic pathway for ATP generation is stimulated (Kurhaluk et al., 2019). This opening of MPT pore induced by cobalt also decreases the pool of NADH and NADPH in rat liver mitochondria, and may "leak" antioxidant proteins from the mitochondrial matrix (Battaglia et al., 2009). The compositions and functions of MPT in normally functioning mitochondria are unknown. But it is known that they constitute pore structures with a cut-off of 1.5 kDa that alter the permeability of the internal membrane, resulting in massive flux of protons to the internal chamber and the release of calcium and metabolites, with a consequent loss of function and swelling of the mitochondria (Baines and Gutiérrez-Aguilar, 2018). This mechanism has been recently proposed to be responsible for cell damage in the traumatic injury of central nervous system (Springer et al., 2018).

The presence of cobalt ions has also been associated with the stabilization of the α-subunit of hypoxia-inducible factor−1 (HIF-1α), and an increased expression of the HIF-1α regulated genes (Karovic et al., 2007). The activation of HIF-1α normally occurs in response to hypoxia conditions, activating a survival program, and promoting vascularization and hematopoiesis (Lukyanova and Kirova, 2015). The mechanisms by which the MPT activation would lead to HIF-1α stabilization in the presence of cobalt are still not fully understood, but as

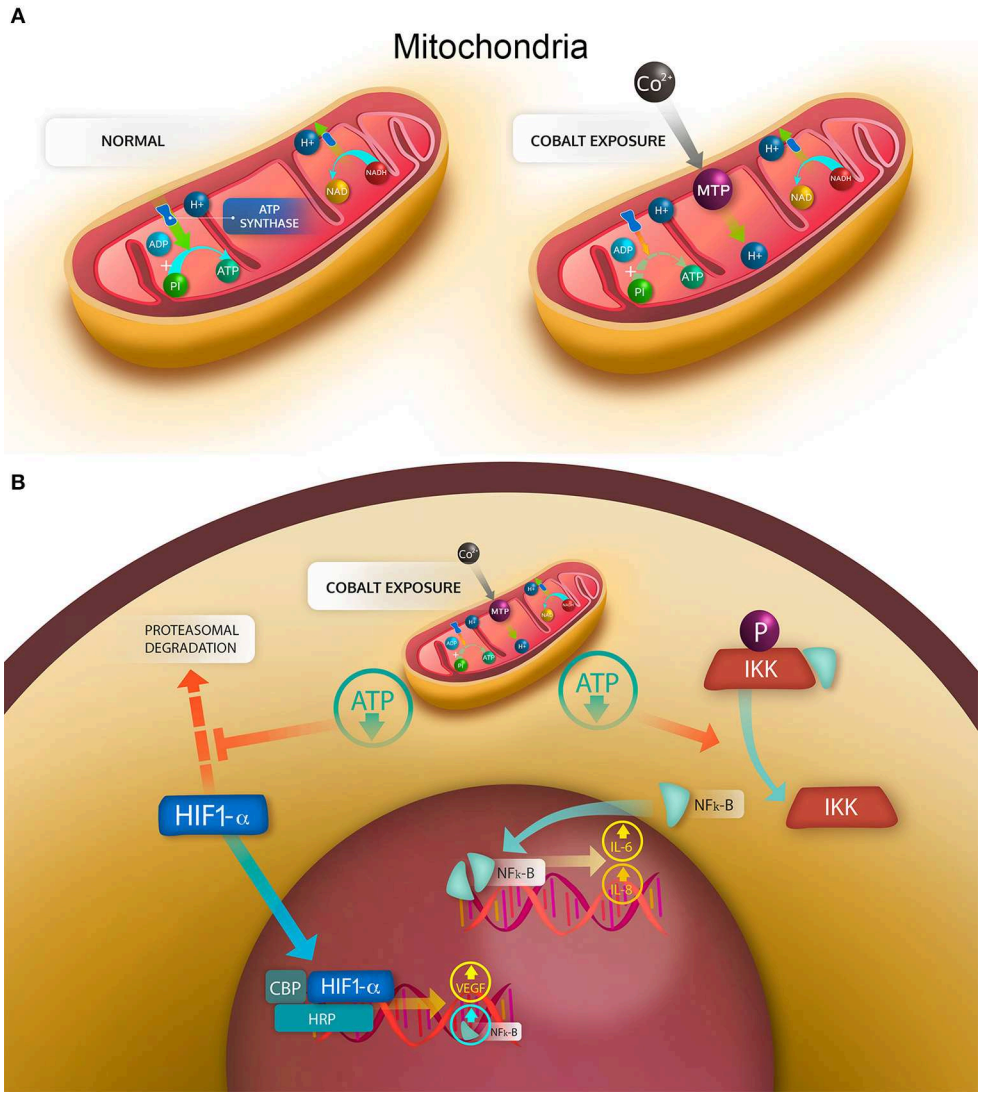

FIGURE 8 | Mechanisms of cell damage induced by cobalt ions. **(A)** mitochondrial stress generated by the cobalt-induced opening of the mitochondrial transition pore (MTP). Under normal conditions in aerobic respiration, the H^+ generated during the tricarboxylic acid cycle in the form of NADH and NAPH are transferred to the intermembrane space by the electron transport chain, generating an electrochemical gradient, in which a high concentration of H^+ is found in the intermembrane space. By use of this electrochemical gradient, the ATP synthase can phosphorylate ADP into ATP. With the opening of MTP, the electrochemical gradient is lost, then the synthesis of ATP is decreased. **(B)** cellular effects of the mitochondrial stress. Under normal conditions, the hypoxia induced factor HIF-1α is degraded by the proteasome; similarly, phosphorylated IKK bound in the cytoplasm NF-κB. With a drop in ATP, the degradation of HIF-1α is decreased, allowing HIF-1α to translocate into the nucleus and bind CBP and HRP to enhance transcription of target genes, such as NF-κB and VEGF. The decrease in ATP also reverses the phosphorylation of IKK that in a non-phosphorylated state releases NF-κB, which dimerizes and translocates to the nucleus, binding DNA and enhancing the transcription of target genes, such as IL-6 and IL-8.

consequence of HIF-1α stabilization cells release cytokines that would promote neovascularization, inflammation and hematopoiesis (Seeber et al., 2011). Furthermore, recently HIF pathway has been demonstrated to be activated in a macrophage cell line after being exposure to cobalt alloy nanoparticles, and this activation was associated with an increase in the secretion of the cytokines transforming growth factor alpha (TNF-α), interleukin 1 beta (IL-1β) and vascular endothelial growth factor (VEGF) (Nyga et al., 2015). Taken together these data suggest that the inflammation and cell death observed in the ALTRs could be explained by the hypoxic stress induced by cobalt, which is capable of eliciting the synthesis and secretion of pro-inflammatory cytokines that recruit cells of the immune system. However, this hypothesis could not explain the presence of highly destructive ALTRs in MoP implants with minimum wear or corrosion and low cobalt ions in synovial fluid and blood. Neither could it explain the fact that some patients with elevated levels of cobalt and chromium due to wear or corrosion do not develop a necrotic reaction and do not present a lymphocytic infiltrate.

A MIXED MODEL IN THE ETIOLOGY OF ALTRs

In one of the early studies in hip pathology associated with MoM hip implants, Campbell et al. (2010) observed that most of the lesions could be explained by excessive wear of the articulating surfaces and subsequent presence of metals in the tissues, but some lesions were also present in low wear implants. The authors then proposed that those reactions in low wear implants could be due to a type IV (delayed) hypersensitivity reaction (Campbell et al., 2010). Six years later, in a thorough histological analysis of ALTRs, Ricciardi et al. (2016) classified the lesions into four groups: macrophage-dominated, mixed macrophage-lymphocytic with or without hypersensitivity features, and granulomatous pattern. They reported that ALTRs with a mixed infiltrate and hypersensitivity features were more frequent in non-MoM ALTRs and were associated with a shorter revision time (Ricciardi et al., 2016). Similarly, a study including ALTRs in MoM and MoP implants showed a shorter revision time, higher lymphocyte infiltration, higher necrosis and ALVAL score in the MoP group, which also had lower concentration of metals in serum (Eltit et al., 2017).

The observations explained above suggest that there are two main events that explain two types of possibly interrelated reactions. The first is the a physiopathological event of metal-induced inflammation of the hip joints, which affects a larger number of patients, mostly with MoM implants. The second event is associated with hypersensitivity reaction, which is less prevalent in MoM ALTRs, but correspond to most of ALTRs in MoP ALTRs and low wear MoM.

As described previously, cobalt ions can induce MPT, which is not a constitutional structure of the mitochondria, but is stabilized under pathologic conditions. The increased permeability of the mitochondrial internal membrane decreases the electrochemical gradient between the intermembrane space and the mitochondrial matrix. Subsequently the proton-motive force is reduced, and the generation of ATP is impaired (**Figure 8**). The reduced ATP provokes the activation of hypoxia response, characterized by the HIF-1α stabilization and the production of cytokines associated with this factor. There is an evidence that HIF-1α also increases the expression of NFκB, a transcription factor that elicits the synthesis and secretion of inflammatory cytokines (Mukandala et al., 2016) (**Figure 8B**). The cytokine secretion is also accompanied by an increase in the reactive oxygen species (ROS) in the cell, which is enhanced by the MPT stabilization, which allows antioxidant molecules such as glutathione to leave the mitochondria, reducing their protective capability. The intracellular increase in ROS can also trigger the secretion of proinflammatory cytokines and is known to activate endothelium and cells of the immune system (Mittal et al., 2014). The proinflammatory effects of the secreted cytokines has been demonstrated to induce migration in monocytes and activation of endothelial cells, thus generating inflammatory changes in the synovium (Eltit et al., submitted). This synovial inflammation has been observed in most of the patients with hip replacements and is especially frequent in patients with MoM hip implants, which also present with high levels of Co and Cr in synovial fluid and serum. It is thought to be the mechanism that trigger the macrophage-dominated lesions that are mostly observed in MoM ALTRs and are associated with high wear and elevated metal ions in plasma (**Figures 7A–C**).

Some patients develop a hypersensitivity reaction, initiated by the activation of T-cells, driving to a predominant Th1 reaction (Catelas et al., 2015). The specific antigen that triggers hypersensitivity in ALTRs has not been described, but the presence of tertiary lymphoid structures needs the specific activation of T-cell receptors that are highly specific. Because of this specificity and the traditionally accepted model for metal allergies (Saito et al., 2016), the presence of an hapten-carrier complex, in which metal elements combined with host proteins became a new antigen for T-cell receptors has been proposed for ALTRs. Similarly, chronic inflammation or necrosis can expose intracellular antigens that can activate T-cells triggering hypersensitivity reactions, as is observed in lupus (Kubota, 1998); thus the presence of hypersensitivity could also be secondary to the pre-existing chronic inflammation of the hip joints. The open question then is whether these two events (mitochondrial stress-induced inflammation and delayed hypersensitivity) are related or they are different pathologies that affect patients with different characteristics? It seems that cytotoxicity-associated ALTRs affect patients with elevated levels of Co and Cr while hypersensitivity ALTRs affect patients with genetic predisposition independent of the metal levels or cell damage. However, the evidence of hypersensitivity reactions as a consequence of chronic inflammation, together with the existence of ALTRs with mixed characteristics (metal particles and macrophage infiltrate, and also hypersensitivity-like features), supports the hypothesis of a combined pathogenesis. In this model, both etiological elements are related, and the development of hypersensitivity is a consequence of the pre-existing cell damage-driven chronic inflammation. In consequence, ALTRs should be considered as a single pathology with two pathogenic variances.

CONCLUSION REMARKS

It is accepted that CoCrMo over release from either tribocorrosion at the articular surfaces or fretting corrosion at the modular junctions of hip implants trigger adverse local tissue reactions. These mechanisms of degradation results in elevated metals ions in the periprosthetic tissues and fluids, which are the most likely species to induce cell damage. The generation of particles has an important role in metal ion release by re-passivating exposed surfaces, increasing the exposed surface, and inducing phagocytosis that expose the particles to an oxidative environment. Metal ions, mainly cobalt, induces mitochondrial stress, by opening transition pores in the mitochondrial internal membrane. The presence of pores in the membrane decrease the electrochemical potential reducing the ATP synthesis generating a hypoxia-like condition in the cells. Subsequently the transcription factors HIF-1α and NFκB trigger the synthesis and secretion of cytokines that elicit the inflammation in the periprosthetic tissues. The mechanisms of hypersensitivity are not clear, but activation of T-cell is highly specific, thus the presence of specific antigens that activates the

lymphocyte response is needed. In summary, ALTRs are complex pathology, in which two major physiopathological events are involved: the mitochondrial stress induced by metal ions, and the development of hypersensitivity in a pre-existing chronic inflammation setting.

AUTHOR CONTRIBUTIONS

All authors contributed to reviewing the relevant literature and drafting the manuscript. Figures were obtained and processed by QW and FE.

FUNDING

This work has been partially funded by a grant of Orthopedic Research Excellence Fund (OREF), and the Collaborative Health Research Projects jointly funded by the Natural Sciences and Engineering Research Council of Canada (NSERC), and the Canadian Institutes of Health Research (CIHR).

ACKNOWLEDGMENTS

Graphic design in **Figure 8** by estudiokbza.cl.

REFERENCES

Abbas, A. K., Lichtman, A. H., Pillai, S. (2015). *Basic Immunology Functions and Disorders of the Immune System.* Philadelphia, PA: Elsevier; Saunders.

Albrektsson, T., Brånemark, P. I., Hansson, H. A., and Lindström, J. (1981). Osseointegrated titanium implants. Requirements for ensuring a long-lasting, direct bone-to-implant anchorage in man. *Acta Orthop. Scand.* 52, 155–170. doi: 10.3109/17453678108991776

Al-Hajjar, M., Fisher, J., Williams, S., Tipper, J. L., and Jennings, L. M. (2013). Effect of femoral head size on the wear of metal on metal bearings in total hip replacements under adverse edge-loading conditions. *J. Biomed. Mater. Res. B.* 101, 213–222. doi: 10.1002/jbm.b.32824

Almousa, S., Greidanus, N., Masri, B., Duncan, C., and Garbuz, D. (2013). The natural history of inflammatory pseudotumors in asymptomatic patients after metal-on-metal hip arthroplasty. *Clin. Orthop. Relat. Res.* 471, 3814–3821. doi: 10.1007/s11999-013-2944-4

Amstutz, H. C., and Le Duff, M. J. (2017). Correlation between serum metal ion levels and adverse local tissue reactions after conserve® plus hip resurfacing arthroplasty. *Hip. Int.* 27, 336–342. doi: 10.5301/hipint.5000481

Anissian, L., Stark, A., Gustafson, A., Good, V., and Clarke, I. (1999). Metal-on-metal bearing in hip prosthesis generates 100-fold less wear debris than metal-on-polyethylene. *Acta Orthop Scand.* 70, 578–582. doi: 10.3109/17453679908997845

Ardaugh, B. M., Graves, S. E., and Redberg, R. F. (2013). The 510(k) ancestry of a metal-on-metal hip implant. *N. Engl. J. Med.* 368, 97–100. doi: 10.1056/NEJMp1211581

Athanasou, N. A. (2016). The pathobiology and pathology of aseptic implant failure. *Bone Joint Res.* 5, 162–168. doi: 10.1302/2046-3758.55.BJR-2016-0086

Baines, C. P., and Gutiérrez-Aguilar, M. (2018). The still uncertain identity of the channel-forming unit(s) of the mitochondrial permeability transition pore. *Cell Calcium.* 73, 121–130. doi: 10.1016/j.ceca.2018.05.003

Baleani, M., Erani, P., Bordini, B., Zuccheri, F., Makosa, M. K., De Pasquale, D., et al. (2017). *In vivo* damage of the head-neck junction in hard-on-hard total hip replacements: effect of femoral head size, metal combination, and 12/14 taper design. *Materials.* 10:733. doi: 10.3390/ma10070733

Battaglia, V., Compagnone, A., Bandino, A., Bragadin, M., Rossi, C. A., Zanetti, F., et al. (2009). Cobalt induces oxidative stress in isolated liver mitochondria responsible for permeability transition and intrinsic apoptosis in hepatocyte primary cultures. *Int. J. Biochem. Cell Biol.* 41, 586–594. doi: 10.1016/j.biocel.2008.07.012

Billi, F., and Campbell, P. (2010). Nanotoxicology of metal wear particles in total joint arthroplasty: a review of current concepts. *J. Appl. Biomater. Biomech.* 8, 1–6. doi: 10.1177/228080001000800101

Bitounis, D., Pourchez, J., Forest, V., Boudard, D., Cottier, M., and Klein, J.-P. (2016). Detection and analysis of nanoparticles in patients: A critical review of the status quo of clinical nanotoxicology. *Biomaterials.* 76, 302–312. doi: 10.1016/j.biomaterials.2015.10.061

Brånemark, P. I. (1983). Osseointegration and its experimental background. *J. Prosthet. Dent.* 50, 399–410. doi: 10.1016/S0022-3913(83)80101-2

Bragadin, M., Toninello, A., Mancon, M., and Manente, S. (2007). The interactions of cobalt(II) with mitochondria from rat liver. *J. Biol. Inorg. Chem.* 12, 631–635. doi: 10.1007/s00775-007-0222-1

Brown, S., Flemming, C., Kawalec, J., Placko, H., Vassaux, C., Merrit, K., et al. (1995). Fretting corrosion accelerates crevice corrosion of modular hip tapers. *J. Appl. Biomater.* 6, 19–26. doi: 10.1002/jab.770060104

Cadosch, D., Chan, E., Gautschi, O. P., and Filgueira, L. (2009). *Metal is not inert* : role of metal ions released by biocorrosion in aseptic loosening-Current concepts. *J. Biomed. Mater. Res. A.* 91, 1252–1262. doi: 10.1002/jbm.a.32625

Campbell, P., Beaulé, P., Ebramzadeh, E., LeDuff, M., De Smet, K., Lu, Z. et al. (2006). The john charnley award: a study of implant failure in metal-on-metal surface arthroplasties. *Clin. Orthop. Relat. Res.* 453, 35–46. doi: 10.1097/01.blo.0000238777.34939.82

Campbell, P., Ebramzadeh, E., Nelson, S., Takamura, K., De Smet, K., et al. (2010). Histological features of pseudotumor-like tissues from metal-on-metal hips. *Clin. Orthop. Relat. Res.* 468, 2321–2327. doi: 10.1007/s11999-010-1372-y

Carli, A., Reuven, A., Zukor, D. J., and Antoniou, J. (2011). Adverse soft-tissue reactions around non-metal-on-metal total hip arthroplasty - a systematic review of the literature. *Bull. N. Y. U. Hosp.* 69(Suppl. 1), S47–51.

Catelas, I., Bobyn, D., MEdley, J., Kryngier, J., Zukor, D., and Huk, O. (2003). Size, shape, and composition of wear particles from metal-metal hip simulator testing: effects of alloy and number of loading cycles. *J. Biomed. Mater. Res. A.* 67, 312–327. doi: 10.1002/jbm.a.10088

Catelas, I., Campbell, P. A., Bobyn, J. D., Medley, J. B., and Huk, O. L. (2006). Wear particles from metal-on-metal total hip replacements: effects of implant design and implantation time. *Proc. Inst. Mech. Eng. Part H.* 220, 195–208. doi: 10.1243/09544119JEIM112

Catelas, I., Lehoux, E. A., Hurda, I., Baskey, S. J., Gala, L., Foster, R., et al. (2015). Do patients with a failed metal-on-metal hip implant with a pseudotumor present differences in their peripheral blood lymphocyte subpopulations? *Clin. Orthop. Relat. Res.* 473, 3903–3914. doi: 10.1007/s11999-015-4466-8

Catelas, I., Medley, J. B., Campbell, P. A., Huk, O. L., and Bobyn, J. D. (2004). Comparison of in vitro with *in vivo* characteristics of wear particles from metal-metal hip implants. *J. Biomed. Mater. Res. B.* 70, 167–178. doi: 10.1002/jbm.b.20036

Catelas, I., Petit, A., Vali, H., Fragiskatos, C., Meilleur, R., Zukor, D. J., et al. (2005). Quantitative analysis of macrophage apoptosis vs. necrosis induced by cobalt and chromium ions *in vitro*. *Biomaterials.* 26, 2441–2453. doi: 10.1016/j.biomaterials.2004.08.004

Chamaon, K., Schönfeld, P., Awiszus, F., Bertrand, J., and Lohmann, C. H. (2019). Ionic cobalt but not metal particles induces ROS generation in immune cells *in vitro*. *J. Biomed. Mater. Res. B.* 107, 1246–1253. doi: 10.1002/jbm.b.34217

Chana, R., Esposito, C., Campbell, P. A., Walter, W. K., and Walter, W. L. (2012). Mixing and matching causing taper wear: corrosion associated with pseudotumour formation. *J. Bone Joint Surg. Br.* 94, 281–286. doi: 10.1302/0301-620X.94B2.27247

Clarke, I. C., Good, V., Williams, P. A., Schroeder, D., Anissian, L., Stark, A., et al. (2000). Ultra-low wear rates for rigid-on-rigid bearings in total hip replacements. *Proc. Inst. Mech. Eng. Part H J. Eng. Med.* 214, 331–347. doi: 10.1243/0954411001535381

Clarke, M. T., Lee, P. T. H., Arora, A., and Villar, R. N. (2003). Levels of metal ions after small- and large-diameter metal-on-metal hip arthroplasty. *J. Bone Joint Surg. Br*. 85, 913–917. doi: 10.1302/0301-620X.85B6.14166

Clayton, G. M., Wang, Y., Crawford, F., Novikov, A., Wimberly, B. T., Kieft, J. S., et al. (2014). Structural basis of chronic beryllium disease: linking allergic hypersensitivity and autoimmunity. *Cell*. 158, 132–142. doi: 10.1016/j.cell.2014.04.048

Cobb, A. G., and Schmalzreid, T. P. (2006). The clinical significance of metal ion release from cobalt-chromium metal-on-metal hip joint arthroplasty. *Proc. Inst. Mech. Eng. H.* 220, 385–398. doi: 10.1243/09544119JEIM78

Cohen, D. (2011). Out of joint: the story of the ASR. *BMJ*. 342:d2905. doi: 10.1136/bmj.d2905

Collier, J., Supernant, V., Jensen, R., and Mayor, M. (1990). Corrosion at the interface of cobalt-Alloy heads on titanium-alloys stems. *Clin. Orthop. Relat. Res*. 271, 305–312. doi: 10.1097/00003086-199110000-00042

Collier, J., Supernant, V., Jensen, R., Mayor, M., and Supernant, H. (1992). Corrosion between the components of modular femoral hip prostheses. *J. Bone Joint Surg. Br*. 74, 511–517. doi: 10.1302/0301-620X.74B4.1624507

Cooper, H. J., Urban, R. M., Wixson, R. L., Meneghini, R. M., Jacobs, J. J., Archibeck, M., et al. (2013). Adverse local tissue reaction arising from corrosion at the femoral neck-body junction in a dual-taper stem with a cobalt-chromium modular neck. *J. Bone Joint Surg. Am*. 95, 865–72. doi: 10.2106/JBJS.L.01042

Czarnek, K., Terpiłowska, S., and Siwicki, A. K. (2015). Review paper Selected aspects of the action of cobalt ions in the human body. *Cent. Eur. J. Immunol*. 2, 236–242. doi: 10.5114/ceji.2015.52837

Dargel, J., Oppermann, J., Brüggemann, G.-P., and Eysel, P. (2014). Dislocation following total hip replacement. *Dtsch. Arztebl. Int*. 111, 884–90. doi: 10.3238/arztebl.2014.0884

Davda, K., Lali, F. V., Sampson, B., Skinner, J. A., and Hart, A. J. (2011). An analysis of metal ion levels in the joint fluid of symptomatic patients with metal-on-metal hip replacements. *J. Bone Joint Surg. Br*. 93, 738–745. doi: 10.1302/0301-620X.93B6.25804

De Smet, K., De Haan, R., Calistri, A., Campbell, P. A., Ebramzadeh, E., Pattyn, C., et al. (2008). Metal ion measurement as a diagnostic tool to identify problems with metal-on-metal hip resurfacing. *J. Bone Joint Surg. Am*. 90 (S4), 202–208. doi: 10.2106/JBJS.H.00672

Doorn, P. F., Campbell, P. A., Worrall, J., Benya, P. D., McKellop, H. A., and Amstutz, H. C. (1998). Metal wear particle characterization from metal on metal total hip replacements: transmission electron microscopy study of periprosthetic tissues and isolated particles. *J. Biomed. Mater. Res*. 42, 103–111. doi: 10.1002/(SICI)1097-4636(199810)42:1<103::AID-JBM13>3.0.CO;2-M

Doorn, P. F., Mirra, J. M., Campbell, P. A, and Amstutz, H. C. (1996). Tissue reaction to metal on metal total hip prostheses. *Clin. Orthop. Relat. Res*. 329 (Suppl), S187–205. doi: 10.1097/00003086-199608001-00017

Dowson, D. (2006). Tribological principles in metal-on-metal hip joint design. *Proc. Inst. Mech. Eng. Part H J. Eng. Med*. 220, 161–171. doi: 10.1243/095441105X63255

Eltit, F., Assiri, A., Garbuz, D., Duncan, C., Masri, B., Greidanus, N., et al. (2017). Adverse reactions to metal on polyethylene implants: highly destructive lesions related to elevated concentration of cobalt and chromium in synovial fluid. *J. Biomed. Mater. Res. A*. 105, 1876–1886 doi: 10.1002/jbm.a.36057

Fillingham, Y. A., Della Valle, C. J., Bohl, D. D., Kelly, M. P., Hall, D. J., Pourzal, R., et al. (2017). Serum metal levels for diagnosis of adverse local tissue reactions secondary to corrosion in metal-on-polyethylene total hip arthroplasty. *J. Arthroplasty*. 32, S272–S277. doi: 10.1016/j.arth.2017.04.016

Firkins, P. J., Tipper, J. L., Saadatzadeh, M. R., Ingham, E., Stone, M. H., Farrar, R., et al. (2001). Quantitative analysis of wear and wear debris from metal-on-metal hip prostheses tested in a physiological hip joint simulator. *Biomed. Mater. Eng*. 11, 143–157.

Fleury, C., Petit, A., Mwale, F., Antoniou, J., Zukor, D. J., Tabrizian, M., et al. (2006). Effect of cobalt and chromium ions on human MG-63 osteoblasts *in vitro*: morphology, cytotoxicity, and oxidative stress. *Biomaterials*. 27, 3351–3360. doi: 10.1016/j.biomaterials.2006.01.035

Fontenot, A. P., Falta, M. T., Kappler, J. W., Dai, S., and McKee, A. S. (2016). Beryllium-induced hypersensitivity: genetic susceptibility and neoantigen generation. *J. Immunol*. 196, 22–27. doi: 10.4049/jimmunol.1502011

Foote, H. W. (1923). Equilibrium in the systems, nickel chloride, cobalt chloride, cupric chloride—hydrochloric acid-water. *J. Am. Chem. Soc*. 45, 663–667. doi: 10.1021/ja01656a014

Forest, M., Courpied, J. P., Lefloch, P., Carlioz, A., Abelanet, R., and Postel, M. (1985). Hip surgery: local tissue reactions. *Ann. Pathol*. 5, 3–18.

Fricker, D., and Shivanatil, R. (1990). Fretting corrosion studies of universal femoral head prostheses and cone taper spigots. *Biomaterials*. 11, 495–500. doi: 10.1016/0142-9612(90)90064-W

Garbuz, D. S., Tanzer, M., Greidanus, N. V., Masri, B. A., and Duncan, C. P. (2010). MEtal-on-metal hip resurfacing versus large head metal-on-metal hip arthroplasty. *Clin. Orthop. Relat. Res*. 468, 318–325. doi: 10.1007/s11999-009-1029-x

Gilbert, J., Bucley, C., and Jacobs, J. (1993). *In vivo* corrosion of modular hip prosthesis components in mixed and similar metal combinations. The effect of crevice, stress, motion, and alloy coupling. *J. Biomed. Mater. Res*. 27, 1533–1544. doi: 10.1002/jbm.820271210

Gilbert, J. L., Sivan, S., Liu, Y., Kocagöz, S. B., Arnholt, C. M., and Kurtz, S. M. (2015). Direct *in vivo* inflammatory cell-induced corrosion of CoCrMo alloy orthopedic implant surfaces. *J. Biomed. Mater. Res. A*. 103, 211–223. doi: 10.1002/jbm.a.35165

Goldberg, J. R., and Gilbert, J. L. (1997). Electrochemical response of CoCrMo to high-speed fracture of its metal oxide using an electrochemical scratch test method. *J. Biomed. Mater. Res*. 37, 421–431. doi: 10.1002/(SICI)1097-4636(19971205)37:3<421::AID-JBM13>3.0.CO;2-E

Goldsmith, A. A. J., Dowson, D., Isaac, G. H., and Lancaster, J. G. (2000). A comparative joint simulator study of the wear of metal-on-metal and alternative material combinations in hip replacements. *Proc. Inst. Mech. Eng. H*. 214, 39–47. doi: 10.1243/0954411001535228

Goode, A. E., Perkins, J. M., Sandison, A., Karunakaran, C., Cheng, H., Wall, D., et al. (2012). Chemical speciation of nanoparticles surrounding metal-on-metal hips. *Chem. Commun*. 48, 8335–8337. doi: 10.1039/c2cc33016d

Granchi, D., Cenni, E., Ciapetti, G., Savarino, L., Stea, S., Gamberini, S., et al. (1998b). Cell death induced by metal ions: Necrosis or apoptosis? *J. Mater. Sci. Mater. Med*. 9, 31–37. doi: 10.1023/A:1008878527233

Granchi, D., Cenni, E., Giunti, A., and Baldini, N. (2012). Metal hypersensitivity testing in patients undergoing joint replacement a systematic review. *J. Bone Jt. Surg. Br*. 94-B, 1126–1134. doi: 10.1302/0301-620X.94B8.28135

Granchi, D., Savarino, L., Ciapetti, G., Cenni, E., Rotini, R., Mieti, M., et al. (2003). Immunological changes in patients with primary osteoarthritis of the hip after total joint replacement. *J. Bone Joint. Surg. Br*. 85, 758–764. doi: 10.1302/0301-620X.85B5.13729

Granchi, D., Verri, E., Ciapetti, G., and Savarino, L. (1998a). Effects of chromium extract on cytokine release by mononuclear cells. *Biomaterials*. 19, 283–91. doi: 10.1016/S0142-9612(97)00148-8

Griffin, C., Buchanan, R., and Lemons, J. E. (1983). *In vitro* electrochemical corrosion study of coupled surgical implant materials. *J. Biomed. Mater. Res*. 17, 489–500. doi: 10.1002/jbm.820170308

Griffiths, H., Burke, J., and Bonfiglio, T. (1987). Granulomatous pseudotumors in total joint replacement. *Skeletal. Radiol*. 16, 146–152. doi: 10.1007/BF00367764

Hallab, N. J., and Jacobs, J. J. (2009). Biologic effects of implant debris. *Bull. N. Y. U. Hosp*. 67, 182–188.

Hallab, N. J., Skipor, A., and Jacobs, J. J. (2003). Interfacial kinetics of titanium- and cobalt-based implant alloys in human serum: metal release and biofilm formation. *J. Biomed. Mater. Res. A*. 65, 311–318. doi: 10.1002/jbm.a.10429

Hanawa, T. (2004). Metal ion release from metal implants. *Mater. Sci. Eng. C*. 12, 745–752. doi: 10.1016/j.msec.2004.08.018

Harinderjit, S. G., Grammatopoulos, G., Adshead, S., Tsialogiannis, E., and Tsiridis, E. (2012). Molecular and immune toxicity of CoCr nanoparticles in MoM hip arthroplasty. *Trends Mol. Med*. 18, 145–155. doi: 10.1016/j.molmed.2011.12.002

Hart, A. J., Quinn, P. D., Lali, F., Sampson, B., Skinner, J. A., Powell, J. J., et al. (2012). Cobalt from metal-on-metal hip replacements may be the clinically relevant active agent responsible for periprosthetic tissue reactions. *Acta Biomater*. 8, 3865–3873. doi: 10.1016/j.actbio.2012.05.003

Hart, A. J., Quinn, P. D., Sampson, B., Sandison, A., Atkinson, K. D., Skinner, J. A., et al. (2010). The chemical form of metallic debris in tissues surrounding metal-on-metal hips with unexplained failure. *Acta Biomater*. 6, 4439–4446. doi: 10.1016/j.actbio.2010.06.006

Hart, A. J., Skinner, J. A., Winship, P., Faria, N., Kulinskaya, E., Webster, D., et al. (2009). Circulating levels of cobalt and chromium from metal-on-metal hip replacement are associated with CD8 $^{+}$ T-cell lymphopenia. *J. Bone Joint. Surg. Br*. 91, 835–842. doi: 10.1302/0301-620X.91B6.21844

Hedberg, Y., and Odnevall Wallinder, I. (2014). Metal release and speciation of released chromium from a biomedical CoCrMo alloy into simulated physiologically relevant solutions. *J. Biomed. Mater. Res. B*. 102, 693–699. doi: 10.1002/jbm.b.33048

Horie, M., Nishio, K., Endoh, S., Kato, H., Fujita, K., Miyauchi, A., et al. (2013). Chromium(III) oxide nanoparticles induced remarkable oxidative stress and apoptosis on culture cells. *Environ. Toxicol*. 28, 61–75. doi: 10.1002/tox.20695

Huber, M., Reinisch, G., Trettenhahn, G., Zweymüller, K., and Lintner, F. (2009). Presence of corrosion products and hypersensitivity-associated reactions in periprosthetic tissue after aseptic loosening of total hip replacements with metal bearing surfaces. *Acta Biomater*. 5, 172–180. doi: 10.1016/j.actbio.2008.07.032

Huk, O. L., Catelas, I., Mwale, F., Antoniou, J., Zukor, D. J., and Petit, A. (2004). Induction of apoptosis and necrosis by metal ions *in vitro*. *J. Arthroplasty*. 19, 84–87. doi: 10.1016/j.arth.2004.09.011

Igual Munoz, A., Schwiesau, J., Jolles, B. M., and Mischler, S. (2015). *In vivo* electrochemical corrosion study of a CoCrMo biomedical alloy in human synovial fluids. *Acta Biomater*. 21, 228–236. doi: 10.1016/j.actbio.2015.03.008

Illgen, R. L., Forsythe, T. M., Pike, J. W., Laurent, M. P., and Blanchard, C. R. (2008). Highly crosslinked vs conventional polyethylene particles–an *in vitro* comparison of biologic activities. *J. Arthroplasty*. 23, 721–731. doi: 10.1016/j.arth.2007.05.043

Jacobs, J. J., Gilbert, J. L., and Urban, R. M. (1998). Corrosion of metal orthopaedic implants. *J. Bone Joint Surg. Am*. 80, 268–282. doi: 10.2106/00004623-199802000-00015

Jacobs, J. J., Urban, R. M., Gilbert, J. L., Skipor, A. K., Black, J., Jasty, M., et al. (1995). Local and distant products from modularity. *Clin Orthop Relat Res*. 94–105. doi: 10.1097/00003086-199510000-00010

Jameson, S., Kyle, J., Baker, P., Mason, J., Deechan, D., McMurtry, I., et al. (2012). Patient and implant survival following 4323 total hip replacements for acute femoral neck fracture: a retrospective cohort study using National Joint Registry data. *J. Bone Joint Surg. Br*. 94, 1557–1566. doi: 10.1302/0301-620X.94B11.29689

Jobby, R., Jha, P., Yadav, A. K., and Desai, N. (2018). Biosorption and biotransformation of hexavalent chromium: A comprehensive review. *Chemosphere*. 207, 255–266. doi: 10.1016/j.chemosphere.2018.05.050

Karovic, O., Tonazzini, I., Rebola, N., Edström, E., Lövdahl, C., Fredholm, B. B., et al. (2007). Toxic effects of cobalt in primary cultures of mouse astrocytes: similarities with hypoxia and role of HIF-1α. *Biochem. Pharmacol*. 73, 694–708. doi: 10.1016/j.bcp.2006.11.008

Kawalec, J., Brown, S., Payer, J., and Merrit, K. (1995). Mixed-metal fretting corrosion of Ti6Al4V and wrought cobalt alloy. *J. Biomed. Mater. Res*. 29, 867–873. doi: 10.1002/jbm.820290712

Keegan, G. M., Learmonth, I. D., and Case, C. (2008). A systematic comparison of the actual, potential, and theoretical health effects of cobalt and chromium exposures from industry and surgical implants. *Crit. Rev. Toxicol*. 38, 645–674. doi: 10.1080/10408440701845534

Konan, S., Duncan, C. P., Masri, B. S., and Garbuz, D. S. (2017). What is the natural history of asymptomatic pseudotumors in metal-on-metal thas at mid-term followup? *Clin. Orthop. Relat. Res*. 475, 433–441. doi: 10.1007/s11999-016-4981-2

Kop, A., Keogh, C., and Swarts, E. (2012). Proximal component modularity in THA—at what cost? an implant retrieval study. *Clin. Orthop. Relat. Res*. 470, 1885–1894. doi: 10.1007/s11999-011-2155-9

Kostensalo, I., Seppänen, M., Makela, K. T., Mokka, J., Virolainen, P., and Hirviniemi, J. (2012). Early results of large head metal-on-metal hip arthroplasties. *Scand. J. Surg*. 101, 62–65. doi: 10.1177/145749691210100112

Kovochich, M., Fung, E. S., Donovan, E., Unice, K. M., Paustenbach, D. J., and Finley, B. L. (2018). Characterization of wear debris from metal-on-metal hip implants during normal wear versus edge-loading conditions. *J. Biomed. Mater. Res. B*. 106, 986–996. doi: 10.1002/jbm.b.33902

Kubota, T. (1998). What is the primary antigen in systemic lupus erythematosus? *Japns. J. Rheumatol*. 8, 93–104. doi: 10.3109/BF03041333

Kugelberg, E. (2014). T cell recognition: a hidden heavy metal. *Nat. Rev. Immunol*. 14:518. doi: 10.1038/nri3724

Kumar, V., Abbas, A. K., and Aster, J. C. (2012). *Robbins Basic Pathology*. Philadelphia, PA: Elsevier; Saunders.

Kurhaluk, N., Lukash, O., Nosar, V., Portnychenko, A. G., Portnychenko, V., Wszedybyl-Winklewska, M., et al. (2019). Liver mitochondrial respiratory plasticity and oxygen uptake evoked by cobalt chloride in rats with low and high resistance to extreme hypobaric hypoxia. *Can. J. Physiol. Pharmacol*. 97, 392–399. doi: 10.1139/cjpp-2018-0642

Kwon, Y., Ostlere, S., McLardy-Smith, P., Athanasou, N., Harinderjit, S. G., and MUrray, D. (2011). Asymptomatic pseudotumors after metal-on-metal hip resurfacing arthroplasty prevalence and metal ion study. *J. Arthroplasty*. 26, 511–518. doi: 10.1016/j.arth.2010.05.030

Kwon, Y., Thomas, P., Summer, B., Pandit, H., Taylor, D., MUrray, D., et al. (2010). Lymphocyte proliferation responses in patients with pseudotumors following metal-on-metal hip resurfacing arthroplasty. *J. Orthop. Res*. 28, 444–450. doi: 10.1002/jor.21015

Kwon, Y.-M., Lombardi, A. V., Jacobs, J. J., Fehring, T. K., Lewis, C. G., and Cabanela, M. E. (2014). Risk stratification algorithm for management of patients with metal-on-metal hip arthroplasty. *J. Bone Joint Surg*. 96:e4. doi: 10.2106/JBJS.M.00160

Lalmohamed, A., MacGregor, A. J., de Vries, F., Leufkens, H. G. M., and van Staa, T. P. (2013). Patterns of risk of cancer in patients with metal-on-metal hip replacements versus other bearing surface types: a record linkage study between a prospective joint registry and general practice electronic health records in England. *PLoS ONE*. 8:e65891. doi: 10.1371/journal.pone.0065891

Langton, D. J., Jameson, S. S., Joyce, T. J., Gandhi, J., Sidaginamale, R. P., Mereddy, P., et al. (2011b). Accelerating failure rate of the ASR total hip replacement. *J. Bone Joint Surg. Br*.93, 1011–1016. doi: 10.1302/0301-620X.93B8.26040

Langton, D. J., Jameson, S. S., Joyce, T. J., Hallab, N. J., Natu, S., and Nargol, A. V. F. (2010). Early failure of metal-on-metal bearings in hip resurfacing and large-diameter total hip replacement-a consequence of excess wear. *Bone Joint J*. 92, 38–46. doi: 10.1302/0301-620X.92B1.22770

Langton, D. J., Joyce, T. J., Jameson, S., Lord, J., Orsouw, V., Holland, J., et al. (2011a). Adverse reaction to metal debris following hip resurfacing. *J. Bone Joint Surg. Br*. 93, 164–171. doi: 10.1302/0301-620X.93B2.25099

Langton, D. J., Sprowson, A. P., Joyce, T. J., Reed, M., Carluke, I., Partington, P., et al. (2009). Blood metal ion concentrations after hip resurfacing arthroplasty. *J. Bone Joint Surg. Br*. 91, 1287–1295. doi: 10.1302/0301-620X.91B10.22308

Lass, R., Grübl, A., Kolb, A., Stelzeneder, D., Pilger, A., Kubista, B., et al. (2014). Comparison of synovial fluid, urine, and serum ion levels in metal-on-metal total hip arthroplasty at a minimum follow-up of 18 years. *J. Orthop. Res*. 32, 1234–1240. doi: 10.1002/jor.22652

Lhotka, C., Szekeres, T., Steffan, I., Zhuber, K., and Zweymüller, K. (2003). Four-year study of cobalt and chromium blood levels in patients managed with two different metal-on-metal total hip replacements. *J. Orthop. Res*. 21, 189–195. doi: 10.1016/S0736-0266(02)00152-3

Li, Y.-S., Wang, K., He, P., Huang, B. X., and Kovacs, P. (1999). Surface-enhanced Raman spectroelectrochemical studies of corrosion films on implant Co-Cr-Mo alloy in biosimulating solutions. *J. Raman Spectrosc*. 30, 97–103. doi: 10.1002/(SICI)1097-4555(199902)30:23.0.CO;2-X

Liao, Y., Hoffman, E., Wimmer, M., Fischer, A., Jacobs, J., and Marks, L. (2013). CoCrMo metal-on-metal hip replacements. *Phys. Chem. Chem. Phys*. 15, 746–756. doi: 10.1039/C2CP42968C

Liu, Y., and Gilbert, J. L. (2017). The effect of simulated inflammatory conditions on the corrosion and fretting corrosion of CoCrMo alloy. *Wear*. 390, 302–311. doi: 10.1016/j.wear.2017.08.011

Lucas, L., Buchanan, R., and Lemons, J. (1981). Investigations on the galvanic corrosion of multialloy total hip prostheses. *J. Biomed. Mater. Res*. 15, 731–747. doi: 10.1002/jbm.820150509

Lukyanova, L. D., and Kirova, Y. I. (2015). Mitochondria-controlled signaling mechanisms of brain protection in hypoxia. *Front. Neurosci*. 9:320. doi: 10.3389/fnins.2015.00320

Mahendra, G., Pandit, H., Kliskey, K., Murray, D., Gill, H. S., and Athanasou, N. (2009). Necrotic and inflammatory changes in metal-on-metal resurfacing hip arthroplasties. *Acta Orthop*. 80, 653–659. doi: 10.3109/17453670903473016

Makela, K. T., Visuri, T., Pulkkinen, P., Eskelinen, A., Remes, V., Virolainen, P., et al. (2012). Risk of cancer with metal-on-metal hip replacements: population based study. *Br. Med. J.* 345:e4646. doi: 10.1136/bmj.e4646

Malek, I. A., King, A., Sharma, H., Malek, S., Lyons, K., Jones, S., et al. (2012). The sensitivity, specificity and predictive values of raised plasma metal ion levels in the diagnosis of adverse reaction to metal debris in symptomatic patients with a metal-on-metal arthroplasty of the hip. *J. Bone Joint Surg. Br.* 94, 1045–1050. doi: 10.1302/0301-620X.94B8.27626

Martin, E. J., Pourzal, R., Mathew, M. T., and Shull, K. R. (2013). Dominant role of molybdenum in the electrochemical deposition of biological macromolecules on metallic surfaces. *Langmuir.* 29, 4813–4822. doi: 10.1021/la304046q

Matharu, G. S., Berryman, F., Brash, L., Pynsent, P. B., Treacy, R. B. C., Dunlop, D. J., et al. (2016b). The effectiveness of blood metal ions in identifying patients with unilateral birmingham hip resurfacing and corail-pinnacle metal-on-metal hip implants at risk of adverse reactions to metal debris. *J. Bone Joint Surg. Am.* 98, 617–626. doi: 10.2106/JBJS.15.00340

Matharu, G. S., Berryman, F., Judge, A., Reito, A., McConnell, J., Lainiala, O., et al. (2017). Blood metal ion thresholds to identify patients with metal-on-metal hip implants at risk of adverse reactions to metal debris. *J. Bone Joint Surg.* 99, 1532–1539. doi: 10.2106/JBJS.16.01568

Matharu, G. S., Pandit, H. G., Murray, D. W., and Judge, A. (2016a). Adverse reactions to metal debris occur with all types of hip replacement not just metal-on-metal hips: a retrospective observational study of 3340 revisions for adverse reactions to metal debris from the National Joint Registry. *BMC Musculoskelet Disord.* 17:495. doi: 10.1186/s12891-016-1329-8

Mathiesen, E., Ahlbom, A., Bermann, G., and Lindgren, U. (1995). Total hip replacement and cancer. *A cohort study. J Bone Joint Surg Br.* 77, 345–350. doi: 10.1302/0301-620X.77B3.7744912

Mathiesen, E. B., Lindgren, J. U., Blomgren, G., and Reinholt, F. P. (1991). Corrosion of modular hip prostheses. *J. Bone Joint Surg. Br.* 73, 569–575. doi: 10.1302/0301-620X.73B4.2071637

Matthies, A., Underwood, R., Cann, P., Ilo, K., Nawaz, Z., Skinner, J., et al. (2011). Retrieval analysis of 240 metal-on-metal hip components, comparing modular total hip replacement with hip resurfacing. *J. Bone Joint Surg. Br.* 93, 307–314. doi: 10.1302/0301-620X.93B3.25551

Maurer-Ertl, W., Friesenbichler, J., Liegl-Atzwanger, B., Kuerzl, G., Windhager, R., and Leithner, A. (2011). Noninflammatory pseudotumor simulating venous thrombosis after metal-on-metal hip resurfacing. *Orthopedics.* 34, e678–e681. doi: 10.3928/01477447-20110826-32

McGrory, B. J., Payson, A. M., and MacKenzie, J. A. (2017). Elevated intra-articular cobalt and chromium levels in mechanically assisted crevice corrosion in metal-on-polyethylene total hip arthroplasty. *J. Arthroplasty.* 32, 1654–1658. doi: 10.1016/j.arth.2016.11.056

Medicines and Healthcare products Regulatory Agency (2015). *Metal-on-Metal (MoM) Hip Replacements - Guidance on Implantation and Patient Management Medical Safety Alert - GOV.UK.* Available online at: https://www.gov.uk/drug-device-alerts/metal-on-metal-mom-hip-replacements-guidance-on-implantation-and-patient-management (accessed May 16, 2019).

Meier, B. (2010, March 3). Concerns over 'metal on metal' hip implants. *New York Times.*

Metikos-Huković, M., Pilić, Z., Babić, R., and Omanović, D. (2006). Influence of alloying elements on the corrosion stability of CoCrMo implant alloy in Hank's solution. *Acta Biomater.* 2, 693–700. doi: 10.1016/j.actbio.2006.06.002

Milošev, I., and Strehblow, H.-H. (2003). The composition of the surface passive film formed on CoCrMo alloy in simulated physiological solution. *Electrochim. Acta.* 48, 2767–2774. doi: 10.1016/S0013-4686(03)00396-7

Mittal, M., Siddiqui, M. R., Tran, K., Reddy, S. P., and Malik, A. B. (2014). Reactive oxygen species in inflammation and tissue injury. *Antioxid. Redox. Signal.* 20, 1126–1167. doi: 10.1089/ars.2012.5149

Mittal, S., Revell, M., Barone, F., Hardie, D. L., Matharu, G. S., Davenport, A. J., et al. (2013). Lymphoid aggregates that resemble tertiary lymphoid organs define a specific pathological subset in metal-on-metal hip replacements. *PLoS ONE.* 8:e63470. doi: 10.1371/journal.pone.0063470

Mukandala, G., Tynan, R., Lanigan, S., O'Connor, J., Mukandala, G., Tynan, R., et al. (2016). The effects of hypoxia and inflammation on synaptic signaling in the CNS. *Brain Sci.* 6:6. doi: 10.3390/brainsci6010006

Natu, S., Sidaginamale, R. P., Gandhi, J., Langton, D. J., and Nargol, A. V. F. (2012). Adverse reactions to metal debris: histopathological features of periprosthetic soft tissue reactions seen in association with failed metal on metal hip arthroplasties. *J. Clin. Pathol.* 65, 409–18. doi: 10.1136/jclinpath-2011-200398

Ness, A. T., Smith, R. E., and Evans, R. L. (1952). The preparation and some properties of chromic phosphate. *J. Am. Chem. Soc.* 74, 4685–4688. doi: 10.1021/ja01138a070

Neyt, K., Perros, F., GeurtsvanKessel, C. H., Hammad, H., and Lambrecht, B. (2012). Tertiary lymphoid organs in infection and autoimmunity. *Trends Immunol.* 33, 297–305. doi: 10.1016/j.it.2012.04.006

Nyga, A., Hart, A., and Tetley, T. D. (2015). Importance of the HIF pathway in cobalt nanoparticle-induced cytotoxicity and inflammation in human macrophages. *Nanotoxicology.* 9, 905–917. doi: 10.3109/17435390.2014.991430

Okazaki, Y., and Gotoh, E. (2005). Comparison of metal release from various metallic biomaterials *in vitro*. *Biomaterials.* 26, 11–21. doi: 10.1016/j.biomaterials.2004.02.005

Ormsby, R. T., Solomon, L. B., Yang, D., Crotti, T. N., Haynes, D. R., Findlay, D. M., et al. (2019). Osteocytes respond to particles of clinically-relevant conventional and cross-linked polyethylene and metal alloys by up-regulation of resorptive and inflammatory pathways. *Acta Biomater.* 87, 296–306. doi: 10.1016/j.actbio.2019.01.047

Pandit, H., Glyn-Jones, S., McLardy-Smith, P., Gundle, R., Whitwell, D., Gibbons, C. L. M., et al. (2008). Pseudotumours associated with metal-on-metal hip resurfacings. *J. Bone Joint Surg. Br.* 90, 847–851. doi: 10.1302/0301-620X.90B7.20213

Papageorgiou, I., Brown, C., Schins, R., Singh, S., Newson, R., Davis, S., et al. (2007). The effect of nano- and micron-sized particles of cobalt-chromium alloy on human fibroblasts *in vitro*. *Biomaterials.* 28, 2946–2958. doi: 10.1016/j.biomaterials.2007.02.034

Park, J.-B. (2003). Phagocytosis induces superoxide formation and apoptosis in macrophages. *Exp. Mol. Med.* 35, 325–335. doi: 10.1038/emm.2003.44

Perino, G., Ricciardi, B. F., Jerabek, S. A., Martignoni, G., Wilner, G., Maass, D., et al. (2014). Implant based differences in adverse local tissue reaction in failed total hip arthroplasties: a morphological and immunohistochemical study. *BMC Clin. Pathol.* 14:39. doi: 10.1186/1472-6890-14-39

Petit, A., Mwale, F., Zukor, D. J., Catelas, I., Antoniou, J., and Huk, O. L. (2004). Effect of cobalt and chromium ions on bcl-2, bax, caspase-3, and caspase-8 expression in human U937 macrophages. *Biomaterials.* 25, 2013–2018. doi: 10.1016/j.biomaterials.2003.08.040

Posada, O. M., Tate, R. J., and Grant, M. H. (2015). Toxicity of cobalt-chromium nanoparticles released from a resurfacing hip implant and cobalt ions on primary human lymphocytes *in vitro*. *J. Appl. Toxicol.* 35, 614–622. doi: 10.1002/jat.3100

Rai, D., Sass, B. M., and Moore, D. A. (1987). Chromium(III) hydrolysis constants and solubility of chromium(III) hydroxide. *Inorg. Chem.* 26, 345–349. doi: 10.1021/ic00250a002

Ricciardi, B. F., Nocon, A. A., Jerabek, S. A., Wilner, G., Kaplowitz, E., Goldring, S. R., et al. (2016). Histopathological characterization of corrosion product associated adverse local tissue reaction in hip implants: a study of 285 cases. *BMC Clin. Pathol.* 16:3. doi: 10.1186/s12907-016-0025-9

Rieker, C. B., Schön, R., Konrad, R., Liebentritt, G., Gnepf, P., Shen, M., et al. (2005). Influence of the clearance on in-vitro tribology of large diameter metal-on-metal articulations pertaining to resurfacing hip implants. *Orthop. Clin. North Am.* 36, 135–42. doi: 10.1016/j.ocl.2005.02.004

RIPO (2014). *Regional Register of Orthopedic Prosthetic Implantology.* Annual Report. Bologna.

Saito, M., Arakaki, R., Yamada, A., Tsunematsu, T., Kudo, Y., and Ishimaru, N. (2016). Molecular mechanisms of nickel allergy. *Int. J. Mol. Sci.* 17:E202. doi: 10.3390/ijms17020202

Salloum, Z., Lehoux, E. A., Harper, M.-E., and Catelas, I. (2018). Effects of cobalt and chromium ions on oxidative stress and energy metabolism in macrophages *in vitro*. *J. Orthop. Res.* 36, 3178–3187. doi: 10.1002/jor.24130

Savarino, L., Granchi, D., Cenni, E., Pantoli, N., Rotini, R., Veronesi, C., et al. (2002). Ion release in patients with metal-on-metal hip bearings in total joint replacement: a comparison with metal-on-polyethylene bearings. *J. Biomed. Mater. Res.* 63, 467–474. doi: 10.1002/jbm.10299

Schmalzried, T. P. (2009). Metal-metal bearing surfaces in hip arthroplasty. *Orthopedics* 32. doi: 10.3928/01477447-20090728-06

Schmidt, M., Weber, H., and Schön, R. (1996). Cobalt chromium molybdenum metal combination for modular hip prostheses. *Clin. Orthop. Relat. Res.* 329 (Suppl.):S35–47. doi: 10.1097/00003086-199608001-00004

Seeber, L. M. S., Horrée, N., Vooijs, M. A., Heintz, A. P. M., van der Wall, E., Verheijen, R. H. M., et al. (2011). The role of hypoxia inducible factor-1alpha in gynecological cancer. *Crit. Rev. Oncol. Hematol.* 78, 173–184. doi: 10.1016/j.critrevonc.2010.05.003

Shahgaldi, B. F., Heatley, F. W., Dewar, A., and Corrin, B. (1995). *In vivo* corrosion of cobalt-chromium and titanium wear particles. *J. Bone Joint Surg. Br.* 77, 962–966. doi: 10.1302/0301-620X.77B6.7593115

Simoes, T. A., Bryant, M. G., Brown, A. P., Milne, S. J., Ryan, M., Neville, A., et al. (2016). Evidence for the dissolution of molybdenum during tribocorrosion of CoCrMo hip implants in the presence of serum protein. *Acta Biomater.* 45, 410–418. doi: 10.1016/j.actbio.2016.08.051

Smith, A., Dieppe, P., Vernon, K., and Porter, M. (2012). Failure rates of stemmed metal-on-metal hip replacements: analysis of data from the National Joint Registry of England and Wales. *Lancet* 379, 1199–1204. doi: 10.1016/S0140-6736(12)60353-5

Smith, L. J., Holmes, A. L., Kandpal, S. K., Mason, M. D., Zheng, T., and Wise, J. P. (2014). The cytotoxicity and genotoxicity of soluble and particulate cobalt in human lung fibroblast cells. *Toxicol. Appl. Pharmacol.* 278, 259–265. doi: 10.1016/j.taap.2014.05.002

Springer, J. E., Prajapati, P., and Sullivan, P. G. (2018). Targeting the mitochondrial permeability transition pore in traumatic central nervous system injury. *Neural. Regen. Res.* 13, 1338–1341. doi: 10.4103/1673-5374.235218

Srinivasan, A., Jung, E., and Levine, B. R. (2012). Modularity of the femoral component in total hip arthroplasty. *J. Am. Acad. Orthop. Surg.* 20, 214–222. doi: 10.5435/JAAOS-20-04-214

Svensson, O., and Mathiesen, E. (1988). Formation of a fulminant soft-tissue pseudotumor after uncemented hip arthroplasty. *J. Bone Joint Surg.* 70, 1238–1242 doi: 10.2106/00004623-198870080-00017

Swaminathan, V., and Gilbert, J. L. (2012). Fretting corrosion of CoCrMo and Ti6Al4V interfaces. *Biomaterials.* 33, 5487–5503. doi: 10.1016/j.biomaterials.2012.04.015

Talha, M., Ma, Y., Kumar, P., Lin, Y., and Singh, A. (2019). Role of protein adsorption in the bio corrosion of metallic implants. *Colloids Surf. B.* 176, 494–506. doi: 10.1016/j.colsurfb.2019.01.038

The Canadian Joint Replacement Registry (2015). *Hip and Knee Replacements in Canada: Canadian Joint Replacement Registry 2015.* Annual Report.

Thomas, P., Braathen, L., Dörig, M., and Auböck, J. (2009). Increased metal allergy in patients with failed metal-on-metal hip arthroplasty and peri-implant T-lymphocytic inflammation. *Allergy.* 64, 1157–1165. doi: 10.1111/j.1398-9995.2009.01966.x

Thyssen, J. P., Jakobsen, S. S., Engkilde, K., Johansen, J. D., Søballe, K., and Menné, T. (2009). The association between metal allergy, total hip arthroplasty, and revision. *Acta Orthop.* 80, 646–652. doi: 10.3109/17453670903487008

Tipper, J., Firkins, P., Besong, A., Barbour, P. S., Nevelos, J., Stone, M., et al. (2001). Characterisation of wear debris from UHMWPE on zirconia ceramic, metal-on-metal and alumina ceramic-on-ceramic hip prostheses generated in a physiological anatomical hip joint simulator. *Wear* 250, 120–128. doi: 10.1016/S0043-1648(01)00653-6

Topolovec, M., Milošev, I., Cör, A., and Bloebaum, R. D. (2013). Wear debris from hip prostheses characterized by electron imaging. *Cent. Eur. J. Med.* 8, 476–484. doi: 10.2478/s11536-013-0156-7

Urban, R., Jacobs, J., Gilbert, J., Rice, S., Jasty, M., Bragdon, C., et al. (1997). "Characterization of solid products of corrosion generated by modular-head femoral stems of different designs and materials," in *Modularity of Orthopedic Implants*, eds D. Marlowe, J. Parr, and M. Mayor (West Conshohocken, PA: ASTM International), 33–44. doi: 10.1520/STP12019S

Urban, R. M., Jacobs, J. J., Gilbert, J. L., and Galante, J. O. (1994). Migration of corrosion products from modular hip prostheses. Particle microanalysis and histopathological findings. *J. Bone Joint Surg. Am.* 76, 1345–1359. doi: 10.2106/00004623-199409000-00009

Urban, R. M., Jacobs, J. J., Tomlinson, M. J., Gavrilovic, J., Black, J., and Peoc'h, M. (2000). Dissemination of wear particles to the liver, spleen, and abdominal lymph nodes of patients with hip or knee replacement. *J. Bone Joint Surg. Am.* 82, 457–76. doi: 10.2106/00004623-200004000-00002

Valero Vidal, C., Olmo Juan, A., and Igual Muñoz, A. (2010). Adsorption of bovine serum albumin on CoCrMo surface: effect of temperature and protein concentration. *Colloids Surf. B.* 80, 1–11. doi: 10.1016/j.colsurfb.2010.05.005

van der Bracht, H., vander eecken, S., Vyncke, D., van Dooren, J., and Jansegers, E. (2011). Clinical and functional outcome of the Birmingham Hip Resurfacing. *Acta Orthop. Belg.* 77, 771–6.

VanOs, R., Lildhar, L. L., Lehoux, E. A., Beaulé, P. E., and Catelas, I. (2014). *In vitro* macrophage response to nanometer-size chromium oxide particles. *J. Biomed. Mater. Res. B.* 102, 149–159. doi: 10.1002/jbm.b.32991

Wang, Q., Parry, M., Masri, B. A., Duncan, C., and Wang, R. (2016). Failure mechanisms in CoCrMo modular femoral stems for revision total hip arthroplasty. *J. Biomed. Mater. Res. B. Appl. Biomater.* 105, 1525–1535. doi: 10.1002/jbm.b.33693

Ward, M. B., Brown, A. P., Cox, A., Curry, A., and Denton, J. (2010). Microscopical analysis of synovial fluid wear debris from failing CoCr hip prostheses. *J. Phys. Conf. Ser.* 241:012022. doi: 10.1088/1742-6596/241/1/012022

Ward, W., Carter, C., Barone, M., and Jinnah, R. (2011). Primary total hip replacement versus hip resurfacing: hospital considerations. *Bull. N. Y. U Hosp. Jt. Dis.* 69, S95–S97.

Willert, H. G., Gottfried, H. B., Fayyazi, A., Flury, R., Windler, M., Koster, G., et al. (2005). Metal-on-Metal bearings and hypersensitivity in patients with artificial hip joints. *J. Bone Jt. Surg. Am.* 87, 28–36. doi: 10.2106/JBJS.A.02039pp

Williams, D. H., Greidanus, N. V., Masri, B. A., Duncan, C. P., and Garbuz, D. S. (2011). Prevalence of Pseudotumor in asymptomatic patients. *J. Bone Joint Surg. Inc.* 93, 2164–2171. doi: 10.2106/JBJS.J.01884

Xia, Z., Kwon, Y.-M., Mehmood, S., Downing, C., Jurkschat, K., and Murray, D. W. (2011). Characterization of metal-wear nanoparticles in pseudotumor following metal-on-metal hip resurfacing. *Nanomedicine.* 7, 674–681. doi: 10.1016/j.nano.2011.08.002

Xia, Z., Ricciardi, B. F., Liu, Z., von Ruhland, C., Ward, M., Lord, A., et al. (2017). Nano-analyses of wear particles from metal-on-metal and non-metal-on-metal dual modular neck hip arthroplasty. *Nanomed. Nanotechnol. Biol. Med.* 13, 1205–1217. doi: 10.1016/j.nano.2016.11.003

Conflict of Interest Statement: The authors declare that the research was conducted in the absence of any commercial or financial relationships that could be construed as a potential conflict of interest.

frontiers in Bioengineering and Biotechnology

REVIEW
published: 23 August 2019
doi: 10.3389/fbioe.2019.00205

Peptide-Based Functional Biomaterials for Soft-Tissue Repair

Katsuhiro Hosoyama[1], *Caitlin Lazurko*[1,2], *Marcelo Muñoz*[1], *Christopher D. McTiernan*[1] *and Emilio I. Alarcon*[1,2]*

[1] Division of Cardiac Surgery Research, University of Ottawa Heart Institute, Ottawa, ON, Canada, [2] Biochemistry, Microbiology and Immunology Department, Faculty of Medicine, University of Ottawa, Ottawa, ON, Canada

Synthetically derived peptide-based biomaterials are in many instances capable of mimicking the structure and function of their full-length endogenous counterparts. Combine this with the fact that short mimetic peptides are easier to produce when compared to full length proteins, show enhanced processability and ease of modification, and have the ability to be prepared under well-defined and controlled conditions; it becomes obvious why there has been a recent push to develop regenerative biomaterials from these molecules. There is increasing evidence that the incorporation of peptides within regenerative scaffolds can result in the generation of structural recognition motifs that can enhance cell attachment or induce cell signaling pathways, improving cell infiltration or promote a variety of other modulatory biochemical responses. By highlighting the current approaches in the design and application of short mimetic peptides, we hope to demonstrate their potential in soft-tissue healing while at the same time drawing attention to the advances made to date and the problems which need to be overcome to advance these materials to the clinic for applications in heart, skin, and cornea repair.

Keywords: peptides, biomaterials, tissue engineering, functional materials, synthetic polymers

OPEN ACCESS

Edited by:
Hasan Uludag,
University of Alberta, Canada

Reviewed by:
Oscar Castano,
University of Barcelona, Spain
Jennifer Patterson,
KU Leuven, Belgium

***Correspondence:**
Emilio I. Alarcon
ealarcon@ottawaheart.ca

Specialty section:
This article was submitted to Biomaterials, a section of the journal Frontiers in Bioengineering and Biotechnology

Received: *06 May 2019*
Accepted: *09 August 2019*
Published: *23 August 2019*

Citation:
Hosoyama K, Lazurko C, Muñoz M, McTiernan CD and Alarcon EI (2019) Peptide-Based Functional Biomaterials for Soft-Tissue Repair. Front. Bioeng. Biotechnol. 7:205. doi: 10.3389/fbioe.2019.00205

INTRODUCTION

Bioinspired materials for tissue repair have been amongst the most exhaustively explored fields in biomaterials research, yet mimicry of native extra cellular matrix (ECM), remains one of the most challenging tasks in tissue engineering. Further, while remarkable progress in recombinant protein expression has been made, there remains a gap as these processes are still relatively expensive particularly for heteromeric proteins; thus limiting scientists to the use animal origin (e.g., extracted from tissues) proteins including collagen and elastin for engineering translatable biomaterials. This limitation has severely halted clinical translation of functional biomaterials to the clinic. It is well-known that proteins take on an important role in almost all biological processes. While they have well-defined roles in the structural integrity of cells, organs, and tissues; their roles in other processes such as cell motility, signal transduction, immunological response, and enzymatic reactions are much more dynamic (Ouzounis et al., 2003). As such, many of the important findings regarding wound healing and tissue repair have come through the study of protein-protein and protein-ligand interactions. One such finding is that molecules which present binding sites for proteins, typically associated with either disease or wound healing, are excellent targets for the development of therapeutic solutions (Webber et al., 2010b). Given recent advancements in both chemical peptide

synthesis and the recombinant production of full length proteins and peptides, generating and studying the interactions of mimetic molecules has been greatly simplified. Whether it is the production of exact copies of full-length or fragments of proteins, the incorporation of non-coded amino acids, or modification of the peptide backbone to enhance its proteolytic stability or the inclusion of tethers for further functionalization; one can generally find a suitable method to produce the desired molecule. For these reasons peptides, which are the small building blocks of proteins, have rapidly emerged as a cost-effective alternative for developing functional materials for tissue repair.

While the design options are almost limitless, these mimics usually interact with their target through the presentation of a specific amino acid sequence, a functional structure, or a combination of both. In this review, we will focus on peptides structures prepared using solid-phase peptide synthesis (SPPS), which for most systems nowadays takes place in cyclically automated synthetic equipment where each amino acid of the peptide structure is sequentially incorporated. Readers interested in learning more on peptide synthesis using transgenic organisms are encouraged to seek out reviews on this specific topic (Structural Genomics et al., 2008).

SPPS was conceptualized in 1959 and first reported on in the early 1960's by the Nobel awardee Robert Bruce Merrifield, its popularity and mainstream adoption grew in the 1970's and 1980's as technological advances in peptide chemistry made the process more robust (Merrifield, 1963). The concept of extending a peptide chain through the α-Nitrogen of an amino acid (*a.a.*) by coupling it with the carboxyl terminal of the next sequential *a.a.* whose other functional groups are protected, truly revolutionized the way peptides chains were produced. These protecting groups serve to prevent both oxidations and unspecific reactions of the *a.a.* side chains (Isidro-Llobet et al., 2009). Decades of intense synthetic research have yielded a number of versatile protecting groups such as the archetypical Fluorenylmethyloxycarbonyl (Fmoc) group. Single *a.a.*'s bearing Fmoc group are readily available on the market (Sigma-Aldrich, 2019). Technological improvement in SPPS, such as the use of microwave reactors and advanced temperature control systems, has allowed for the synthesis of peptides containing hundreds of *a.a.*'s in improved yield and reaction time in comparison to room temperature and convectional heating methods (Bacsa et al., 2006; Loffredo et al., 2009; Pedersen et al., 2012; Thapa et al., 2014). These technological advances have also contributed to the expedited synthesis of so-called difficult peptide sequences. Difficult peptide sequences refer to peptide sequences that agglomerate forming insoluble products during synthesis or after removal of the protective groups, a process that results in reduced yields or deactivation of the peptide preventing further modifications (Tickler and Wade, 2007). In most instance these problems arise due to introduction of functionalities capable a participating in non-covalent interactions, such as hydrogen bonds and dipole-dipole interactions (Paradis-Bas et al., 2016). Thus, when designing peptides for SPPS, both the individual *a.a.* and the resulting coupling products (on the resin) should be screened for the potential formation of self-assembled structures, side reactions, and tendency to fold onto the resin. The following parameters have been demonstrated to aid in the synthesis of difficult peptide sequences: (i) high temperatures (e.g., 95°C for microwave-assisted synthesis), (ii) presence of salt or detergents for improving solubility, (iii) protecting groups at the amide group to avoid potential hydrogen-bond interactions, (iv) incorporation of amino acids with unreactive side chains to prevent undesired interactions, and (v) glycosylation or pegylation to improve peptide solubility.

BIOACTIVE PEPTIDE SEQUENCE MIMICS

Structural mimics developed using peptide sequences are in fact epitopes of bioactive sites, where in many instances the recognition site of the mimic is defined by both the amino acid sequence and three-dimensional conformation. In the following sections, we will discuss a number of bioactive short peptide sequences that have been identified, synthesized, and/or incorporated into structures to impart some type of biological response which could be exploited in tissue engineering or the development of regenerative biomaterials. The peptide sequences which will be discussed correspond to a representative set of examples, which we believe fall into one of the following three categories which we deemed most important in the development of functional biomaterials for the regeneration of heart, skin, and corneal tissue, namely, (i) pro-angiogenic sequences, (ii) anti-inflammatory, and (iii) pro-adherence sequences. **Table 1** contains some representative peptide sequences that have been identified and used in the fabrication of functional materials. **Scheme 1** depicts a representative summary for the concepts revised in this review. While we have limited this review to our expertise in soft tissue targets such as the heart, skin, and cornea, it is important to mention that peptide based materials have also found applications in the regeneration of hard-tissues such as bone and teeth, and that further information regarding these applications and recent advancements can be found in more specialized reviews (Pountos et al., 2016; Wang et al., 2017).

Pro-Angiogenic Sequences

Angiogenesis is a process which involves the proliferation and migration of endothelial cells as well as the concurrent remodeling of the extracellular matrix, which drives the development of new blood vessels from exiting vasculature (Potente et al., 2011). The principal regulator of angiogenesis in both physiological and diseased state is vascular endothelial growth factor (VEGF). VEGF and its many isoforms induce physiological responses through interaction with three well-described tyrosine kinase receptors (Simons et al., 2016). To date the most promising pro-angiogenic peptides are VEGF mimics. Of the available VEGF-mimics the most well-characterized is peptide QK, which was designed to imitate the binding of VEGF to its receptor through a N-terminal α-helix mimic comprised of the amino acid sequence, KLTWQELYQLKYKGI (Andrea et al., 2005). The angiogenic properties of peptide QK have been demonstrated both *in vitro* and *in vivo*, with evident endothelial cell activation and increases in VEGF related cellular functions such as chemotaxis, invasion, sprouting of new capillaries, and enhanced organization (Andrea et al., 2005; Finetti et al., 2012).

TABLE 1 | Representative peptide sequences of potential interest in the development of functional biomaterials for tissue engineering.

	Peptide Sequence	Reference(s)	Main findings	Limitations	Portion of protein extracted	Receptors involved
ECM PROTEINS						
Collagen	GFOGER	Knight et al., 2000; Wojtowicz et al., 2010	Authors demonstrate the utility of coating grafts and improvement in bone growth with the peptide	Used an original sequence that included a GGYGG sequence that does not demonstrate utility in the self-assemble process and was added originally for radiolabeling (Reyes and Garcia, 2003)	Residues 502–507 of the αI(I)-CB3 fragment of type I collagen	α2β1 integrin receptor
	DGEA	Mehta et al., 2015	DGEA induced osteogenesis only when encapsulated with cells in a 3D network. The peptide does not provide any advantages when used in 2D cell culture	The authors do not provide details regarding the nature of peptide attachment to the polymer or whether it formed dimers through the carboxylic acids of the peptides	Residues 435–438 of the αI(I)-CB3 fragment of type I collagen	α2β1 integrin receptor
	FPGERGVEGPGP	Gelain et al., 2006; Bradshaw et al., 2014	Authors demonstrated the ability of the peptide to induce migration of fibroblast in hydrogels	The peptide itself does not induce cell proliferation	–	–
Laminin	IKVAV	Tashiro et al., 1989; Yamada et al., 2002	Authors demonstrate that the peptide promotes cell attachment	The peptide sequence does not produce the same response as laminin	From the α-helix A chain segment of fragment E8 starts at amino acid position 1886	–
	YIGSR	Graf et al., 1987b; Yoshida et al., 1999; Boateng et al., 2005	They demonstrated the ability of the peptide to attach cardiomyocytes onto a silica treated surface	The peptide sequence does not produce the same response as laminin	β1 chain amino acid residues 929–933 on the of Laminin-1	–
	PDGSR	Kleinman et al., 1989; Huettner et al., 2018	They demonstrated an improvement in the adhesion of tumoral cells in the presence of the peptide	They compared the peptide with a cyclic YIGSR peptide, but did not provide information if the cyclic PDGSR could be improved too	β1 chain amino acid residues 902–906 on the of Laminin-1	–
	LRE	Hunter et al., 1991	They assessed the active protein recognition of the peptide for neurite outgrowth and its correlation with salts in the solution	No direct assessment of antibody interaction to identify the specific receptor involved in the interaction	The A-subunit of laminin and synaptic basal lamina	–
	IKLLI	Tashiro et al., 1999	They demonstrated attachment of cells is similar to that seen with IKVAV peptide. Also demonstrate that conformation of the peptide in a secondary structure affects adhesion	They did not use other highly charged positive peptides to compare the affinity of the heparin	α1 chain of laminin, between amino acids residues 2080–2095	Integrin receptor α3β1 and a cell surface heparan sulfate proteoglycan
Fibronectin	RGDS	(Ruoslahti, 1988; D'souza et al., 1991; Leahy et al., 1996)	One of the most used sequences for cell attachment	It is not the only site involved in cell attachment and recognition, other molecules could be also key, as an example proteoglycans.	Domain 10, from amino acid sequence 1493 to 1496	More than 10 RGD dependent receptors, as an example: α3β1, α5β1, αvβ1, etc…
	KQAGDV	Hautanen et al., 1989; Calvete et al., 1992	They provide well-documented information of attachment sectors of the peptide to the receptor	The authors did not show inhibition studies with the peptides under study	γ chain in the fibronectin protein	αIIbβ3, αVβ3

(Continued)

TABLE 1 | Continued

	Peptide Sequence	Reference(s)	Main findings	Limitations	Portion of protein extracted	Receptors involved
	REDV	Hubbell et al., 1991; Massia and Hubbell, 1992	Demonstrate similarities between this peptide and RGD peptide, also selectivity for vessel forming endothelial cells	–	Within the spliced type III connecting segment (III CS) domain of human plasma fibronectin	α4β1
	PHSRN	Feng and Mrksich, 2004	Demonstrate that this fragment is also recognized by integrin receptor, competitive with RGD, but with less strength than RGD	–	Within the 9th type III domain	α5β1
REMODELING ENZYMES						
Collagenase	GPQGIWGQ GPQGYIAGQ GPQGYILGQ	Nagase and Fields, 1996; Lutolf et al., 2003; Patterson and Hubbell, 2010	Substrates containing the sequence are cleaved under the conditions tested and can induce release of specific molecules after proteolytic effects	The sequence is not specific for one type of enzyme	Sequence presented in position 775 of αI fibril of the collagen	GPQG↓ (↓ = Enzyme proteolytic effect)
Matrix metalloproteinases (MMPs)	CPENYFFWGGGG	Salinas and Anseth, 2008	Demonstrate that biomaterials performance depends on the presence and dynamic concentration of the receptor in the hydrogel	In hydrogels, the enzyme degradation rate is fast for surface and slow for deeper cues	Cleaved by MMP-13	CPEN↓
	APGL	West and Hubbell, 1999	The sequence is selective for collagenase, but not for plasmin.	The authors do not provide proof the sequence could be cleaved through cell culture	Cleaved by collagenase	APG↓
	LGPA	Patel et al., 2005	The sequence is attached to a photo responsive material, that can control hydrogel formation with light and degradation by the peptide sequence.	The sequence by itself does not induce cell attachment and survival in the long term	Collagenase-sensitive degradable sequence	–
	GTAGLIGQ	Jun et al., 2005; Kim et al., 2009	The sequence is used to release other drugs, in this case cis-platin	The sequence is attached with an RGD sequence. This could affect enzymatic degradation rates (not evaluated without the RGD sequence)	MMP-2 specific cleavage	GTAG↓
Plasmin	YKNRD	Pratt et al., 2004; Raeber et al., 2005	The sequence induces bone regeneration and cell attachment. Selective to plasmin	–	Plasmin sensitive sequence that is enhanced at the carboxylic side of the lysine amino acid	YK↓
	ELAPLRAP FPLRMRDW EGTKKGHK KKGHKLHL HPVGLLAR	Patterson and Hubbell, 2011; Singh et al., 2012	Depending on the sequence selected, the hydrogel degradation rate can be tuned with respect to its sensibility toward plasmin	Sequences have shared activity with other MMPs	–	ELAP↓ FPLR↓ EGTKKGHK↓ KKGHK↓ HPVG↓
TARGET PROTEIN/RECEPTOR						
Vascular endothelial growth factor	KLTWQELYQLKYKGI	Diana et al., 2011; Liu et al., 2012	Demonstrated ability to promote angiogenesis		VEGF mimetic peptide agonist from amino acid sequence 87 to 100	VEGF receptor 1-D2

(Continued)

TABLE 1 | Continued

	Peptide Sequence	Reference(s)	Main findings	Limitations	Portion of protein extracted	Receptors involved
	LRK_2LGKA	Webber et al., 2010a	Cationic amino acids are used to bind heparin binding factors to a self-assembling sequence	The attachment of the heparin binding is ionic and is not compared with covalent bonding, which could increase long term release of the factors	–	–
Glycosaminoglycans	PNDRRR	Gilmore et al., 2013	Heparin binding through the sequence RRR (or KKK) is used for increasing angiogenic properties	The attachment of heparin is ionic, thus reducing the long-term stability of the aminoglycan	–	–
SUPRAMOLECULAR STRUCTURE						
Vesicle/Micelle	G_4D_2 G_6D_2 G_8D_2 $G_{10}D_2$	Santoso et al., 2002	Length of the peptide glycine chain, dictated the formation of nanovesicles or nanotubes	Lack of homogeneous structures	–	–
	V_6K_2 L_6K_2 A_6K V_6H V_6K H_2V_6 KV_6	Von Maltzahn et al., 2003	The peptides have the ability to self-assemble in different macro-structures. One of the main advantages, is that they dissemble above their pI	Lack of homogeneous structures	–	–
Fiber	$(PKG)_4(POG)_4(DOG)_4$	O'leary et al., 2011	Stable formation of a hydrogel that has similar characteristics to collagen	Lack of D periodicity	–	–
	$PRG)_4(POG)_4(EOG)_4$	Rele et al., 2007	Stable formation of a hydrogel that has similar characteristics to collagen	Lack of strength when compared to collagen bundles	–	–
	$(RADA)_4$ $(RARADADA)_2$ $(FKFE)_2$ $(KLDL)_3$	Sieminski et al., 2008	Fibers are formed by β-sheet interactions. RADA incorporation leads to better attachment of cells	Ability to control fiber dimensions could improve comparison of the system	–	–
MULTI-DOMAIN PEPTIDES						
Double function peptide	$E_2(SL)_6E_2$-G-RGDS	Bakota et al., 2011	Left sequence used for self-assembly as a β-sheet [$E_2(SL)_6E_2$]. Right sequence to be sensed as fibronectin receptor [RGDS]	–	–	–
	$C_{12}H_{25}O$-YGAAKKAAKAAKKAAKAA	Chu-Kung et al., 2004	Left sequence: lipid portion to interact with lipidic membranes [$C_{12}H_{25}O$]. Right sequence: cationic sequence to facilitate interaction with bacteria wall as an anti-microbial peptide [YGAAKKAAKAAKKAAKAA]	Lipid attachment could result in toxicity toward eukaryotic cells	–	–
Quadruple function peptide	$KS(LS)_2$-LRG-$(SL)_3$KG-KLTWQELYQLKYKGI	Kumar et al., 2015	Left sequence [$KS(LS)_2$] used for self-assembly as a β-sheet Center left sequence (LRG) MMP-2 substrate. Center Right sequence [$(SL)_3KG$]: used for self-assembly as a β-sheet Right sequence [KLTWQELYQLKYKGI] is a vascular endothelial growth factor	–	–	–

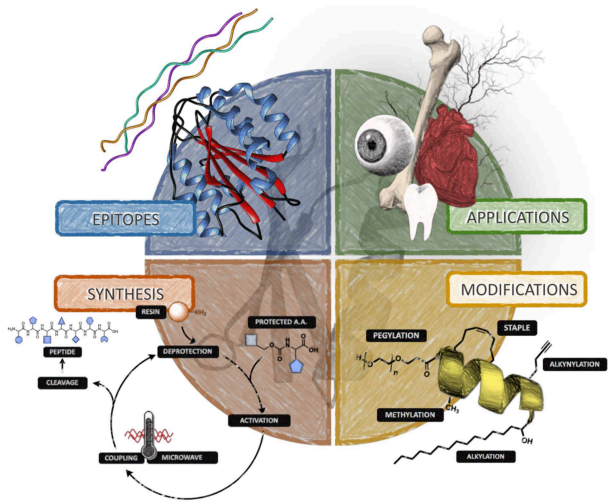

SCHEME 1 | Diagram summarizing the main concepts revised in this review for the use of peptide-based materials in tissue and organ repair.

A self-assembling β-sheet peptide hydrogel encompassing the QK sequence has also shown to promote cell infiltration and vascularization when injected subcutaneously in a rat model as shown in **Figure 1** (Kumar et al., 2015).

It may also be interesting to explore the ability of these VEGF mimics to bind heparin as there is much literature regarding the propensity of different isoforms of VEGF to bind heparin and the necessity of this binding to promote endothelial cell growth and proliferation (Ferrara et al., 2003). Furthermore the incorporation of VEGF within oxygen generating or hypoxia inducing hydrogels or matrices could potentially influence hypoxia inducible factors which are important in the expression and function of VEGF (Krock et al., 2011).

Other peptides which have shown promise in regulating angiogenesis are targets of growth factor receptors which typically work in conjunction with VEGF. For example, fibroblast growth factor as well as neural cell adhesion molecules (NCAMs), which have been shown to bind to fibroblast growth factor receptors can also promote angiogenesis (Elfenbein et al., 2007). Peptide mimics of both FGF2 and NCAM have been prepared synthetically and while they may act in either a canonical or non-canonical fashion, there is strong evidence that they influence angiogenesis (Elfenbein et al., 2007; Rubert Pérez et al., 2017). There are also a number of angiopoietin-1 mimics which have shown promise in regulating angiogenesis via interaction with a tyrosine kinase receptor (Tie2) which is found primarily on vascular endothelial cells and hematopoietic cells (Cho et al., 2004; Miklas et al., 2013). Other peptides one may want to incorporate within materials destined for vascularized tissue are those capable of mimicking transforming growth factors (TGFα and TGFβ) (Ferrari et al., 2009), tumor necrosis factor (TNFα) (Sainson et al., 2008), Angiogenin (Hu et al., 1997), Interleukin 8 (IL8) (Li et al., 2008), or hepatocyte growth factor (HGF) (Xin et al., 2001) as these mitogens and chemokines have been demonstrated to promote angiogenesis through control of endothelial cell growth and/or interaction with VEGF mediated pathways. Considering the effect these factors can have on the expression and efficacy of VEGF and that they are typically targets of surface bound receptors, their incorporation into soft materials may need to be done in such a way that their interaction with the target receptor is not hindered, which may limit covalent attachment within the matrix.

Anti-inflammatory Sequences

In the design of scaffolds and biomaterials for tissue engineering and regeneration, the host immune system is one of the largest barriers to overcome. However, this does not mean that immune response is to be completely avoided; in fact in order to maximize the therapeutic efficacy of implants it is necessary for them to modulate the resulting immune response. Furthermore, inflammation promotes angiogenesis and the formation of new blood vessels can lead to further inflammation. For this reason it is important to understand that inflammation is a complex process which eventually brings homeostasis to the effected tissue through the promotion of cell infiltration, proliferation, and subsequent polarization. While there are many players involved in immune response, macrophages are considered amongst the most important and as such the current section will focus on the ways peptide mimetics can or could be used in their regulation. Macrophages are dynamic cells whose phenotype is subject to polarization from the extracellular environment as well as active signaling molecules (Taraballi et al., 2018). Classically, when discussing the phenotype of macrophages, there is said to be two distinct subsets (i) M1 (pro-inflammatory) and (ii) M2 (anti-inflammatory/pro healing). However, this is a highly simplified view considering the polarization toward either phenotype is actually more of a continuum with the difference between M1 and M2 not being discrete (Martinez and Gordon, 2014). Through the design of short peptides that interact with immunogenic receptors of M2 macrophages like TGF-bR, IL-4R, IL-6R, IL-10R, and MCSFR it is possible to modulate the immunological response associated with tissue damage and repair as well as the introduction of foreign materials (Taraballi et al., 2018). Upon acting on the expression of both pro- and anti-inflammatory cytokines such IL 6 and TNF-α as well as the production of reactive oxygen species one could develop materials which can reduce inflammation, recruit cells via chemotaxis, and ultimately improve wound healing (Boersema et al., 2016). While most inflammation related to foreign material response can be eliminated or reduced through the use of recombinant or autologous proteins or protein/peptide mimics, it may be possible to include small peptide mimetics to activate and polarize macrophages toward a type 2 phenotype. However, due to the complexity of the activation process it is difficult to pin down a sequence or multiple sequences which could bring about the desired response; and for this reason there are not many sequences known to modulate immune response in ways which are beneficial to tissue regeneration and the design of regenerative biomaterials. There are also a number of sequences defined as being anti-bacterial and as such anti-inflammatory (Rotem and Mor, 2009).

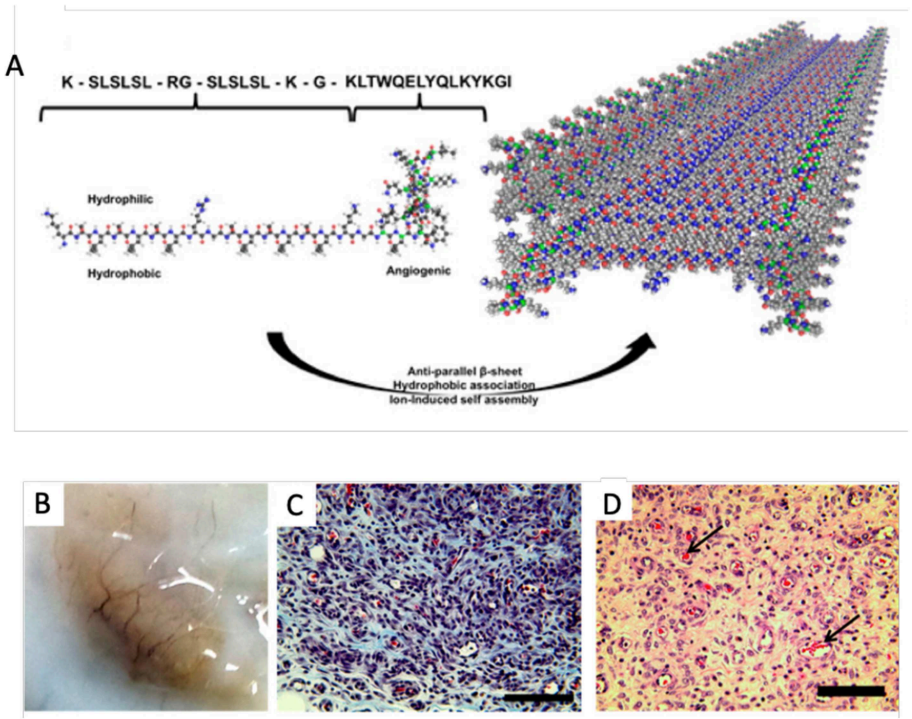

FIGURE 1 | Self-assembling angiogenic peptide hydrogel. **(A)** Schematic illustrating the structure of the the multi-domain peptide comprising the VEGF mimic QK sequence and its assembly into a β-sheet. **(B)** Visible macroscale vessels apparent within the explant materal 7 days post injection. **(C)** Massons's Trichrome and **(D)** HandE staining showing infiltration of scaffolds and presence of blood vessels with red blood cells [arrows] at 1 week post injection; scale bar 100 μm. Adapted with permission from Kumar et al. (2015). Copyright 2015 American Chemical Society.

One class of peptides which have shown promise in modulating immune responses are innate defense regulator (IDR) peptides (Niyonsaba et al., 2013). These cationic antimicrobial peptides are synthetic cationic analogs of naturally occurring host defense peptides or proteins (HDP). They are relatively short peptides (10–50 *a.a.*), with no specific consensus sequence. While they have some ability to directly kill microbes, they are also capable of modulating immune and inflammatory responses. For example, they are capable of influencing chemotaxis, stimulating the production of chemokines, directing macrophage polarization, and modulating the expression of neutrophil adhesion and activation markers (Niyonsaba et al., 2013). IDR-1018, is a peptide of this class consisting of 12 *a.a.* (VRLIVAVRIWRR-NH_2) and has been shown to enhance the anti-inflammatory response while maintaining key pro-inflammatory processes important in fighting off infection, an ability made possible by the fact that this peptide drives macrophage polarization toward an intermediate M1-M2 state (Pena et al., 2013). Other members of this class of peptide include IDR-HH2 and IDR-1002, both of which have similar immunomodulatory abilities. Antimicrobial peptides LL-37 and SET-M33 have also been shown to mediate inflammation through the reduction of pro-inflammatory cytokines, enzymes, and transduction factors (Kahlenberg and Kaplan, 2013; Brunetti et al., 2016).

One of the ways in which macrophage activation controls the immune response is through the expression/production of matrix metalloproteinases (MMPs). MMPs are a family of proteolytic enzymes which themselves are capable of modulating immune responses through the regulation of cytokines and chemokines. There are a handful of different types of MMPs all of which are capable of degrading extracellular matrix proteins and activating bioactive molecules via proteolytic cleavage or other modifications. Through the inclusion of MMP binding and cleavage sequences within the peptides that comprise a material it is possible to increase its local concentration while enhancing the proteolytic degradation of the material which can allow for its replacement with endogenous matrix and the release of small peptide fragments which can in turn modulate other cellular responses. An example, of an MMP epitope found in Type I collagen is the amino acid sequence GPQGIAG (Turk et al., 2001). The presence of such a sequence in collagen-PEG conjugates has been shown to enhance proteolytic degradation by both MMP-1 and MMP-2 (Turk et al., 2001; Patterson and Hubbell, 2010).

Pro-Adherence Sequences

One of the key requirements of regenerative biomaterials is that they support the in-growth, attachment, and proliferation of endogenous cells. One way to ensure that cells attach to a material is to modify the material in such a way to incorporate a peptide that displays a specific binding sequence. One of the most ubiquitous and simple binding sequences are the RGD

and RGDS motifs, which are prominent in adhesion proteins like fibronectin and fibrinogen but also structural proteins such as collagen and laminin (Yamada, 1991). They act as an anchoring site for a number of different α and β integrin binding receptors. The RGDS sequence has also been shown to inhibit platelet aggregation and as such displays some anti-thrombolytic activity (Samanen et al., 1991). As a polar opposite to RGD, KGD sequences have been found to disrupt cell attachment by inhibiting integrin binding (Scarborough et al., 1991). Another pro-adherence sequence derived from the adhesion protein fibronectin is PHSRN. PHSRN like RGD is an integrin cell adhesion motif, however it differs from many of the other linear cell attachment sequences in that the spatial organization of this sequence must mimic that found in fibronectin for it to be beneficial (Mardilovich et al., 2006). Also coming from fibronectin are the REDV, LDV, and KQAGDV integrin binding motifs, which have been shown to help in the anchoring of human umbilical vein endothelial cells (HUVECs) as wells as promote smooth muscle cell adhesion (Hubbell et al., 1991; Mould et al., 1991; Shin et al., 2003). Laminin derived sequences such as IKVAV and YIGSR are also important as integrin binding ligands. While YIGSR also displays some anti-cancer properties, both YIGSR and IKVAV sequences have been shown to stimulate neurite growth and have found use in the design of several therapeutic materials (Graf et al., 1987a; Tashiro et al., 1989). Structural proteins such as collagen also display some cell adhesion sequences, with the most well-described ones being derived from collagen type I and IV. As is the case with the previously mentioned pro-adherence sequences, the short DGEA, GFOGER (where O is hydroxyproline), and GFPGER sequences play a key role in integrin recognition and as such have been incorporated in a number of tissue repair strategies (Staatz et al., 1991; Knight et al., 2000).

Also important to mention is that some peptide sequences can self-assemble due to intra or inter molecular interactions to form supramolecular structures driven by Van-Der-Waals, electrostatic, hydrogen bonding, hydrophobic, and π-π stacking (see **Table 1**). Different kinds of self-assembly structures can be generated from the peptides depending on their structure at the nanometer scale. Peptides can assemble as (i) α-coil, (ii) β-sheet, (iii) β-hairpins, and (iv) poly-proline helix. Depending on the supramolecular structure of the peptide assembly a variety of configurations can be achieved, which include vesicles, rods, or fibers. In addition, advancements in peptide synthesis have allowed for the fabrication of peptides bearing more than one property in their sequences. Thus, for example, in **Table 2**, some peptide sequences contain a self-assembly portion and a second portion which acts as a bio-recognition sequences for receptors, or a lipid-like portion for vesicle formation (see **Table 1**).

APPLICATIONS OF PEPTIDES IN TISSUE ENGINEERING AND BIOMATERIALS

The modification of materials through bioengineering techniques has given rise to a promising route for the generation of synthetic and hybrid materials which not only display biological function and compatibility, but are also capable of controlling cellular microenvironment. The field of tissue engineering is continuously evolving and improving, changing the way scientists and engineers treat damaged tissues (Chen and Liu, 2016). One of the most important aspects of tissue engineering is the design of materials that are biocompatible and capable of interacting with cells and the host environment to promote healing (Girotti et al., 2004; Chen and Liu, 2016). To this end, a number of matrices have been developed for applications that range from tissue replacement and repair to drug delivery (Girotti et al., 2004; Chow et al., 2011; Chen and Liu, 2016). Peptides are increasingly being incorporated or self-assembled into matrices to enhance cell signaling and the bioactivity, improve drug delivery, and provide antibacterial properties amongst many other applications (Girotti et al., 2004; Chow et al., 2011; Miotto et al., 2015). In this section, we will briefly review some representative examples of peptide-based approaches for regenerative therapies in heart, skin, and cornea (Girotti et al., 2004; Chattopadhyay and Raines, 2014; Rodríguez-Cabello et al., 2018). In selecting literature, we have limited our search to articles that contain *in vivo* assessments for the materials, see **Table 2**.

Peptides Sequences in Cornea and Skin Therapeutics

Collagen- and elastin-like peptides are commonly used peptides in skin and cornea tissue repair (Chattopadhyay and Raines, 2014; Rodríguez-Cabello et al., 2018). Collagen is the most abundant protein in the extracellular matrix and commonly used in biomaterials (Chattopadhyay and Raines, 2014; Tanrikulu et al., 2016). Full-length human collagen is complicated to synthesize, as it requires significant post-transcriptional modifications and it is not soluble in most buffers, making it difficult to study (Koide, 2005; Tanrikulu et al., 2016). However, short collagen-mimetic peptide sequences are being used to mimic full-length collagen, by incorporating important peptide sequences at a fraction of the length (Tanrikulu et al., 2016). These collagen mimetic sequences typically require a glycine residue present in every third position and contain many proline and hydroxyproline repeats (Chattopadhyay and Raines, 2014; Tanrikulu et al., 2016). These sequences form left-handed polyProline II helix chains, which then self-assemble in groups of three to produce a right-handed superhelix (Fields, 2010; Chattopadhyay and Raines, 2014; Tanrikulu et al., 2016). The peptide sequence $(PKG)_4(POG)_4(DOG)_4$ has also been designed to self-assemble as a collagen mimetic peptide (O'leary et al., 2011). The N-terminus of this self-assembling peptide was then modified to contain a glycine spacer and terminal cysteine (CG-linker). The addition of a terminal cysteine allowed for the attachment of the peptide to an 8-arm PEG polymer via maleimide chemistry. The application of this new collagen mimetic peptide-hybrid polymer as solid implant resulted in transparent and well-shaped corneas with the deposition of new collagen and the infiltration of stromal cells after 12 months of implantation in porcine model (Islam et al., 2016). An improvement in the

TABLE 2 | Peptide-containing biomaterials as therapeutic agents for tissue and organ repair of cornea, skin, and heart tissues.

Peptide sequence	Tissue/Organ	Functional effect	Specific cell receptor	Delivery System	*In vitro* or *In vivo test*	Main findings	References
$CG(PKG)_4(POG)_4(DOG)_4$, *with O being hydroxyproline*	Cornea	Corneal implant promoting cell and nerve regeneration	–	Self-assembly	Collagenase Cell proliferation *In vivo* biocompatibility by subcutaneous implantation Corneal implantation (pigs) *In vitro* toxicology, biocompatibility, metabolic activity, live/dead, DSC	Corneal implant was compatible for transplantation showing cell and nerve regeneration	Islam et al., 2016 Jangamreddy et al., 2018
YIGSR		Promotes epithelial cell growth and neurite extension	Epithelial cells	Hydrogel	*In vitro* characterization (cell layers and thickness, nerve density, IR spectroscopy), immunohistochemistry, regeneration, corneal touch sensitivity	Overall corneal regeneration including nerve regeneration	Li et al., 2003
Q11 (Ac-QQKFQFQFEQQ-Am)	Skin	Wound healing in strong immune response		dermal	Wound closure, type of cell recruitment in mice with strong immune response	Immunogenic peptides do not delay healing, even in mice with heightened immune response	Vigneswaran et al., 2016
KGF–ELP		Chronic wound healing	KGF receptor	Fibrin hydrogel vehicle	Characterization (DLS, TEM), cell proliferation, full thickness wound healing	Enhanced granulation and reepithelialization	Koria et al., 2011
Pexiganan Acetate GIGKFLKKAKKFGKAFVKILKK		Antibacterial properties	Disturbs membrane permeability	Topical	MIC against gram-negative and positive bacteria, anaerobes, *in vivo* antibacterial activity, short term tolerability tests	Indication: infected diabetic foot ulcers, similar efficacy to ofloxacin	Lamb and Wiseman, 1998
HBPA (palmitoyl–AAAAGGGLRKKLGKA)		Increased angiogenesis	VEGF and FGF-2	Gel administered subcutaneously	Subcutaneous implantation, histological and morphological analysis of wound site, skinfold chamber model, *in vivo* microscopy, microcirculatory analysis	Increased angiogenesis, including *de novo* angiogenesis	Ghanaati et al., 2009
RADA16-I, [COCH3]-RADARADARADARADA-[CONH2] with EGF		Improved would healing	Keratinocytes and fibroblasts	Topical	*In vitro* human skin equivalent wound healing model, proliferation assay, apoptosis assay, Histological analysis	Epithelialization and wound healing are accelerated with EGF and RADA-16, as opposed to RADA-16 alone	Schneider et al., 2008
RADA16-GG-RGDS and RADA16-GG-FPGERGVEGPGP		Improved cell migration	Keratinocytes and fibroblasts	Hydrogel	*In vivo* analysis, including SEM of cells with SAP, cell proliferation, cell migration	Improved cellular migration	Bradshaw et al., 2014
$(RADA)_4$	Heart	Self-assembling		Nanofiber	Rat MI model	Improved Angiogenesis	Dubois et al., 2008
$(RADA)_4$-LRKKLGKA		Self-assembling heparin-binding sequence		Nanofiber with VEGF	Rat MI model	Improved Angiogenesis Improved Left ventricle contraction Decrease Fibrosis and Left ventricle remodeling	Guo et al., 2012

(Continued)

TABLE 2 | Continued

Peptide sequence	Tissue/Organ	Functional effect	Specific cell receptor	Delivery System	*In vitro* or *In vivo test*	Main findings	References
$(RARADADA)_2$		Self-assembling		IFG-1 bound nanofiber with CMs	Rat MI model	Improved Cell survival Improved Left ventricle contraction Decrease cardiac remodeling	Davis et al., 2006
		Self-assembling		Dissolved in solution with MNCs	Porcine MI model	Improved Angiogenesis, Cell survival, and Left ventricle contraction. Reduced ventricular remodeling	Lin et al., 2010, 2015
		Self-assembling		Nanofiber with VEGF	Rat MI model Porcine MI model	Improved Angiogenesis Left ventricle contraction. Reduced ventricular remodeling	Lin et al., 2012
		Self-assembling		PDGF bound nanofiber	Rat MI model	Improved Angiogenesis, Cell survival and Left ventricle contraction. Reduced ventricular remodeling	Hsieh et al., 2006a,b
		Self-assembling		Dissolved in solution with ADSCs	Rat MI model	Improved Angiogenesis, Cell survival and Left ventricle contraction. Reduced ventricular remodeling	Kim et al., 2017
		Self-assembling		SDF-1 bound nanofiber	Rat MI model	Increases EPC recruitment, Angiogenesis and Left ventricle contraction	Segers et al., 2007
		Self-assembling heparin-binding sequence		Nanofiber with MSCs	Rat MI model	Increases cell survival, Angiogenesis and Left ventricle contraction	Cui et al., 2010
$(RARADADA)_2$-CDDYYYGFGCNKFCRPR(Notch ligand Jagged-1)		Self-assembling Cell adhesion sequence		Hydrogel with CACs	Rat MI model	Increases cell survival and Left ventricle contraction. Decreases ventricular remodeling	Boopathy et al., 2014
AAAAGGGEIKVAV(peptide amphiphile)-YIGSR AAAAGGGEIKVAV(peptide amphiphile)-KKKKK		Self-assembling EC adhesive ligand NO producing donor		Nanofiber	N/A	Increases EPC viability and differentiation	Andukuri et al., 2013
Heparin-AAAAGGGEIKVAV(peptide amphiphile)		Self-assembling		VEGF/bFGF bound nanofiber	Mouse MI model	Increases Angiogenesis and Left ventricle contraction	Webber et al., 2010a
VVAGEGDKS		Glycosaminoglycan mimetic		Nanofiber	Rat MI model	Increases Angiogenesis and Left ventricle contraction	Rufaihah et al., 2017
AcSDKP(Thymosinβ4)		Angiogenic		Collagen-chitosan hydrogel	Rat MI model	Increases Angiogenesis and cell survival. Reduces ventricular remodeling	Chiu et al., 2012
KAFDITYVRLKF-AcSDKP(Thymosinβ4)		Proangiogenic Anti-inflammatory		Collagen hydrogel	Mouse subcutaneous implant	Increases Angiogenesis. Reduces Inflammation	Zachman et al., 2013

(Continued)

TABLE 2 | Continued

Peptide sequence	Tissue/Organ	Functional effect	Specific cell receptor	Delivery System	*In vitro* or *In vivo test*	Main findings	References
RGD		Cell adhesion sequence		Alginate microsphere with MSCs	Rat MI model	Improved Angiogenesis, Cell survival, and Left ventricle contraction. Reduced ventricular remodeling	Yu et al., 2010
RGD		Cell adhesion sequence		Alginate scaffold	Rat MI model	Improved Angiogenesis and Left ventricle function	Yu et al., 2009
RGDfK		Cell adhesion sequence		Alginate scaffold with MSCs	Rat MI model	Improved Angiogenesis and Left ventricle contraction	Sondermeijer et al., 2017
RGDS-AAAAGGGEIKVAV(peptide amphiphile)		Cell adhesion sequence Self-assembling		Subcutaneous injection with MNCs	Mouse	Improved Cell survival	Webber et al., 2010c
RGDSP-$(RADA)_4$		Cell adhesion sequence Self-assembling		Dissolved in solution with MCSCs	Rat MI model	Improved Cell survival and Left ventricle contraction. Reduced fibrosis	Guo et al., 2010
GGGGRGDY		Cell adhesion sequence		Alginate scaffold	N/A	Improved NRVM contractility and viability	Shachar et al., 2011
GRGDS		Cell adhesion sequence		Collagen hydrogel	N/A	Improved NRVM contractility and viability	Schussler et al., 2009
QHREDGS		Cell adhesion sequence		Collagen-chitosan scaffold	N/A	Improved EC survival and tube formation	Miklas et al., 2013
		Cell adhesion sequence		Collagen-chitosan scaffold	N/A	Improved NRVM survival	Reis et al., 2012
		Cell adhesion sequence		Azidobenzoic acid-chitosan scaffold	N/A	Improved NRVM survival	Rask et al., 2010
		Cell adhesion sequence		Collagen-chitosan hydrogel	Rat MI model	Improved Cell survival and Left ventricle contraction. Reduced ventricular remodeling	Reis et al., 2015
WKYMVm		Formyl peptide receptor 2 agonist		Dissolved in solution	Mouse MI model	Improved Angiogenesis and Left ventricle contraction. Reduced fibrosis	Heo et al., 2017
KPVSLSYRCPCRFFESH PPLKWIQEYLEKALN		SDF-1a analog		Dissolved in solution	Mouse MI model	Improved Angiogenesis and Left ventricle contraction	Hiesinger et al., 2011
YPHIDSLGHWRR		78kDa Glucose-regulated protein receptor's ligand		Chitosan hydrogel	Rat MI model	Improved, Cell survival, Angiogenesis and Left ventricle contraction. Reduced ventricular remodeling	Shu et al., 2015
MHSPGAD		Stem cell recruitment		Collagen hydrogel	Mouse MI model	Improved Angiogenesis and Left ventricle contraction. Reduced fibrosis and ventricular remodeling	Zhang et al., 2019

formulation was achieved through the addition of the molecule 2-methacryloyloxyethyl phosphorylcholine (MPC), which has been shown to reduce inflammation and improve hydrogel biocompatibility (Jangamreddy et al., 2018). In terms of recovery after 12 months, the same epithelium, stromal and nerve recovery was found between the improved formulation and a cornea model graft made from Type III Recombinant Human Collagen.

The laminin adhesion pentapeptide motif, YIGSR, has also been grafted onto biosynthetic corneas comprised of hydrated collagen and *N*-isopropylacrylamide copolymers, and tested in Yucatan micropigs (Li et al., 2003). The materials were 5.5 mm in diameter and 200 μm think and implanted via lamellar keratoplasty. After 6 weeks, the implants were able to demonstrate successful regeneration of the host corneal epithelium, stroma, and nerves. In contrast, no nerve regeneration was observed in control eyes which received allografts, during the experimental period (Li et al., 2003).

Peptides have also been functionalized in ways which allow them to be tethered to nanoparticles to generate biomimetic platforms, alter physical properties and cellular interactions, or allow for their incorporation into fibrils or hydrogels for various application (Chattopadhyay and Raines, 2014; Chen and Liu, 2016; Rodríguez-Cabello et al., 2018).

Elastin-like peptides (ELPs) have shown to be extremely useful in tissue engineering, due to their elastic properties, which help them mimic the physical properties of a number of different tissues and organs (Rodríguez-Cabello et al., 2018). While the abundance of elastin in the human body is low (2–4% of dry weight of skin) it plays an important part in the mechanical strength and support of skin and has also been demonstrated to be involved in cell signaling (Rodríguez-Cabello et al., 2018). ELPs are typically derived from the pentapeptide sequence of elastin (VPGXG), where X can be any amino acid (Urry et al., 1981; Urry, 1988; Girotti et al., 2004; Rodríguez-Cabello et al., 2018). This sequence maintains its elastomeric properties when it is crosslinked (Urry et al., 1981; Girotti et al., 2004). It has been suggested that the human body cannot discern ELPs from endogenous elastin and ELP matrices show similar mechanical properties as endogenous elastin, which allows the body to use the scaffold to rebuild the natural ECM (Girotti et al., 2004).

Peptides such as Q11 and RADA-16, have also been incorporated into biomaterials and used in tissue engineering (Vigneswaran et al., 2016). RADA-16 with EGF has shown to improve cell mobility in the skin, which can result in improved wound healing, especially in non-healing wounds (Schneider et al., 2008; Bradshaw et al., 2014). Lastly, wound healing antimicrobial peptides (AMPs) have also been used in applications of non-healing infected wounds, such as diabetic foot ulcers. These peptides prevent infection, reduce inflammatory response, and promote cell proliferation and migration (Mangoni et al., 2016; Gomes et al., 2017). AMPs have a wide range of amino acid sequences, however they are generally composed of an amphipathic structure, which contains a high prevalence of basic residues (Mangoni et al., 2016). In human skin, AMPs are synthesized and stored by keratinocytes in the granular layer (Mangoni et al., 2016).

Applications in the Heart

Myocardial infarction (MI) is a leading cause of death globally, and can ultimately lead to heart failure (World Health Organization, 2017). In order to be effective peptide-based therapeutics need to be resistant to local proteases and retained long enough to exert the desired effect in the myocardium. The employed self-assembling peptides are typically comprised of alternating hydrophilic and hydrophobic amino acids (Zhang, 2003), which on exposure to physiological osmolality and pH, rapidly assemble into nanofibrous structures that can be injected into the myocardium to form 3D microenvironments (Zhang et al., 1993; Davis et al., 2005). Such therapy has shown promise in the treatment of infarcted myocardium. The RADA class of ionic self-complementary peptide is one of the first generations of self-assembling peptide and the most intensively studied for applications in MI, as it is commercially available (Dubois et al., 2008). When delivered with platelet-derived growth factor (PDGF), the self-assembling nanofibers fabricated from the RADA sequence decreased infarct size and improved cardiac function in a rat MI model (Hsieh et al., 2006a,b). Despite cardiac-specific overexpression of several members of the PDGF family and the fact that it has been reported to induce fibroblast overgrowth and cardiac fibrosis (Ponten et al., 2005), this study demonstrated that PDGF conjugated to the self-assembling nanofibers actually reduced cardiac fibrosis, suggesting a well-controlled release of PDGF. When combined with VEGF, the RADA-derived nanofibrous hydrogels were also shown to improve angiogenesis and cardiac performance in rat and porcine MI models (Lin et al., 2012). The RADA sequence has also been used in combination with cell therapies. For example, injection of a RADA derived hydrogel into a porcine MI model with bone marrow mononuclear cells (MNCs) increased cell retention about 8-fold and improve the cardiac function at 1 month post-MI (Lin et al., 2010, 2015). Similarly, human adipose-derived stromal cells (ADSCs) with fibroblast growth factor (FGF)-immobilized within a RADA hydrogel were injected into a rat MI heart, and demonstrated to promote angiogenesis and improve cardiac contraction (Kim et al., 2017). Likewise, tethering of insulin-like growth factor-1 (IGF-1) to self-assembling peptides increased survival of transplanted neonatal rat cardiomyocytes in a rat MI model (Davis et al., 2006). Cell mediated therapies are also enhanced by well-controlled release of some types of chemokines. Stromal cell-derived factor-1 (SDF-1) was combined to RADA nanofibers, and was demonstrated to improve cardiac function via recruitment of endothelial progenitor cells (EPCs) (Segers et al., 2007). Of note, is the fact that the SDF-1 has also been attached to a 6-amino acid sequence susceptible to MMP-2 cleavage to achieve "smart release" of the chemokine at the site of infarction, albeit showing no additional effect *in vivo* (Segers et al., 2007).

Self-assembled peptide amphiphiles have emerged as versatile biomaterials (Beniash et al., 2005). The amphiphilicity of the peptides allows for self-assembly in aqueous media, eliminating the necessity of organic solvents and as such broadens their applicability. To improve cell retention, a peptide amphiphile scaffold was combined with RGDS, and delivered with MNCs

subcutaneously (Webber et al., 2010c). The incorporation of RGDS improved retention and proliferation of the cells *in vivo*, along with enhancing endothelial marker expression *in vitro*. Likewise, heparin-binding peptide amphiphile (HBPA) was developed and assessed as a biomaterial for MI therapies, which was designed to mimic natural heparin-binding proteins and enable binding to a variety of proteins, increasing cellular recognition of these factors (Rajangam et al., 2006). When combined with VEGF or FGF, HBPA demonstrated improved angiogenesis and heart contractility in mouse (Webber et al., 2010a). Heparin is known to preserve growth factors in their active form by protecting them from proteolysis, and enhancing the affinity to their respective receptors, enabling consistent release of growth factors (Zhou et al., 2004); however, the use of heparin could trigger immune reactions due to its animal origin. To overcome this limitation, synthetic glycosaminoglycan (GAG) mimetic peptide nanofiber scaffolds were developed and assessed *in vivo* (Rufaihah et al., 2017). The GAG scaffolds induced neovascularization in the infarcted myocardium, along with increased VEGF expression and recruitment of vascular cells, which lead to significant improvements in cardiac performance.

Given the "hostile" environment within the infarcted heart, another approach has been to deliver soluble peptides within polymeric scaffolds to mimic extracellular matrix degradation products, which can act in a cytokine fashion (Zachman et al., 2013). The pro-angiogenic laminin-derived C16 and the anti-inflammatory thymosin β4-derived Ac-SDKP loaded in collagen hydrogels of scaffolds has shown to up-regulate the angiogenic response in subcutaneous implantation, while down-regulating inflammation, thus holding promise as a strategy for addressing ischemia and inflammation post-MI. Thymosin β4 has also been successfully incorporated into collagen-chitosan hydrogels for release in the heart post-MI, resulting in superior vascular growth and myocardial repair compared to unmodified hydrogels (Chiu et al., 2012).

Modification for Combination Therapies With Cells

Some large extracellular matrix (ECM) molecules, such as collagen and fibronectin, have multiple peptide sequences that are recognized by cells and induce multiple regenerative responses. To tackle the issue of poor retention and survival of reparative cellular components for MI, mimics of the nanotopographical cues of native ECM have been used to improve integration, proliferation and differentiation. The RGD sequence has been identified as the major cell-binding domain in fibronectin (Ruoslahti and Pierschbacher, 1987), and is able to act as ligands for the integrins αvβ5, αvβ3, and α5β1, which are expressed by cardiomyocytes (Ross Robert and Borg Thomas, 2001; Brancaccio et al., 2006). Functionalization of materials with the RGD motif may exert advantageous properties to the regenerating myocardium via better adhesion and cell integration. RGD incorporation into collagen and alginate scaffolds has been shown to improve cardiomyocyte contractility and viability (Schussler et al., 2009; Shachar et al., 2011). An RGD-alginate system was also able to improve vascular endothelial cell adhesion and proliferation, and increase blood vessel formation *in vivo* (Yu et al., 2009). When applied as microspheres encapsulating mesenchymal stem cells (MSCs); the RGD-alginate combination improved cell retention at the site of injection, in addition to enhanced arteriole formation in a rat MI model (Yu et al., 2010). Similarly, alginate scaffolds modified with a cyclic RGDfK-peptide, which is protease resistant and displays high affinity to cellular integrins, improved survival of transplanted MSCs and promoted angiogenesis in a rat MI model (Sondermeijer et al., 2017). RGDSP is also an adhesion sequence, which promotes cell adhesion and stimulates integrins relevant to early cardiac development (Kraehenbuehl et al., 2008). When combined with self-assembling peptide RADA16, the RGDSP scaffolds elicited protective effects for marrow-derived cardiac stem cells, which were isolated from MSCs and identified as c-kit, Nkx2.5, and GATA4 positive populations, and improved the cardiac function of post-MI rats via enhanced cardiac differentiation (Guo et al., 2010). RGDSP showed fibrous structure with nanometer diameters when assembled with RADA16, providing 3-dimensional scaffolds and presumably being beneficial to the microenvironment for the growth of transplanted cells. The YIGSR sequence (laminin-derived) is another example of ECM-derived peptide that has been investigated as functional additive to enhance cell therapies (Boateng et al., 2005). In one study, YIGSR was immobilized into a self-assembled peptide amphiphile in combination with a nitric oxide donor polylysine sequence (KKKKK) (Andukuri et al., 2013). The combination of these peptides was superior in capturing EPCs and inducing their differentiation into endothelial cells. QHREDGS is also a type of ECM-derived peptide, based on the fibrinogen-like domain of angiopoietin-1 (Rask et al., 2010; Miklas et al., 2013). Due to the homologous nature of the integrin ligands, QHREDGS sequence reportedly has a dual protective effect for both cardiomyocytes and endothelial cells *in vitro* (Reis et al., 2012). In rat MI model, QHREDGS incorporated within a collagen-chitosan hydrogel was demonstrated to improve cardiac function along with cardiac cell recruitment via β1-integrin (Reis et al., 2015). Although this data is promising in terms of cell recruitment to the site of treatment, the provoked downstream signaling may not be the same as that of native matrix possibly due to the other components contained within ECM proteins or structural differences. In an *in vitro* study, myocytes cultured with RGD and YIGSR peptides showed lower expression of focal adhesion kinase (FAK), a part of mechano-transduction pathways, even though the adhesion of the cells was comparable to the native proteins, fibronectin and laminin, and the β1-integrin expression levels were unchanged (Boateng et al., 2005).

Other peptide ligands which are fundamental to specific cell types have also been investigated. For instance, due to the fact that Notch signaling has been shown to promote cardiac progenitor cell (CPC) mediated cardiac repair (Boni et al., 2008), RADA self-assembling peptides have been functionalized with a peptide mimic of the Notch1 ligand Jagged1 and demonstrated to have therapeutic benefit when transplanted with CPCs by improving acute retention and ameliorating the cardiac remodeling in a rat MI model (Boopathy et al., 2014). Development of biomaterials which are capable of modulating signaling pathways

critical for endogenous cell types such as NOTCH1 is of great importance as these cells are endogenously present in niches of defined composition and exert reparative effects depending on environmental cues following injury, aging or disease (Sanada et al., 2014). Circulating angiogenic cells (CACs) are another promising candidate of cell therapy for MI, playing essential roles in angiogenesis and myocardial regeneration. Formyl peptide receptor 2 (FPR2), belonging to the G protein-coupled receptor family, has been suggested to stimulate and promote chemotaxis of monocytic cell lines, neutrophils, and B lymphocytes (Gavins, 2010). WKYMVm, a synthetic hexapeptide with strong affinity to FRP2 was injected to post-MI mice, and demonstrated to enhance the mobilization of CACs from the bone marrow, this resulted in myocardial protection from apoptosis with increased vascular density and preservation of cardiac function (Heo et al., 2017). Likewise, stromal cell–derived factor-1 (SDF-1) is one of the key regulators of hematopoietic stem cells, and shown to effect proliferation and mobilization of EPCs, one of the major population of CACs, to induce vasculogenesis and to be significantly upregulated in myocardial ischemia (Pillarisetti and Gupta, 2001). However, exogenous SDF is quickly degraded by multiple proteases (Sierra et al., 2004). To overcome this limitation, a polypeptide analog was engineered and demonstrated enhanced physiological ability to induce EPC migration and improved ventricular performance compared with native SDF (Hiesinger et al., 2011). In another study, RoY, a 12 amino-acid synthetic peptide specifically binding to the 78 kDa glucose-regulated protein (GRP78) receptor, which is largely expressed on vascular endothelial cells under hypoxia, was conjugated to a thermosensitive chitosan chloride hydrogel. The material induced angiogenic activity and attenuated myocardial injury in a rat MI model (Shu et al., 2015). Histone deacetylase 7 (HDAC7)-derived- phosphorylated 7-amino-acid peptide has also been successfully incorporated into collagen hydrogels for release in the heart post-MI, resulting in superior vascular growth and myocardial repair via enhanced stem cell antigen-1 (Sca-1) positive stem cell recruitment and differentiation (Zhang et al., 2019). Although peptide-based strategies allow for control over cell adhesion, signal localization and cytokine release, the peptides are often highly ubiquitous and not specific to particular cell types or signaling pathways. Further investigations are required before these therapeutic materials are ready for clinical application.

CONCLUSIONS AND OUTLOOK

As the field looks to develop clinically translatable biomimetic materials for tissue regeneration, it is evident that peptide-based biomaterials have the ability to give rise to therapies which will not only provide improved quality of life, but also solve current problems associated with the xenogeneic nature of animal derived materials and the high cost of recombinantly prepared proteins. Due to recent advancements in SPPS and a better understanding of the structure-function relationship of peptides and proteins in complex biological settings, it is becoming more feasible to design targeted biomaterials capable of eliciting a desired response or enhanced biocompatibility. These short mimetic peptides are also typically more processable than their full length analogs and as such simpler to modify with a variety of different functionalities which could impart beneficial properties such as enhanced solubility, simple one step tethering to polymeric backbones, or stimuli responsiveness (pH, light, temperature, etc.). Given the complexity of the wound healing process, as we learn more about the factors determining tissue regeneration, it is likely that we will begin to see an increase in the development of combinatorial approaches and the design of materials consisting of numerous different structural and sequence based peptide mimics. While such complex materials are currently difficult to design, as predictive models improve and large bioactive peptide databases become available this task will be greatly simplified.

AUTHOR CONTRIBUTIONS

All authors listed have made a substantial, direct and intellectual contribution to the work, and approved it for publication.

FUNDING

This work was made possible by funding from the Natural Sciences and Engineering Research Council of Canada (NSERC) Discovery Grant No. RGPIN-2015-0632 to EA. EA would also like to thank the Canadian Institutes of Health Research (CIHR) for a Project Grant No. 375854. CM thanks the University of Ottawa Cardiac Endowment Fund at the Heart Institute for a postdoctoral fellowship. CL was thankful for the Queen Elizabeth II Graduate Scholarship in Science and Technology.

ACKNOWLEDGMENTS

The authors would like to thank all the authors cited in this work.

REFERENCES

Andrea, L. D., Iaccarino, G., Fattorusso, R., Sorriento, D., Carannante, C., Capasso, D., et al. (2005). Targeting angiogenesis: structural characterization and biological properties of a *de novo* engineered VEGF mimicking peptide. *PNAS* 102, 14215–14220. doi: 10.1073/pnas.0505047102

Andukuri, A., Sohn, Y. D., Anakwenze, C. P., Lim, D. J., Brott, B. C., Yoon, Y. S., et al. (2013). Enhanced human endothelial progenitor cell adhesion and differentiation by a bioinspired multifunctional nanomatrix. *Tissue Eng. Part C Met.* 19, 375–385. doi: 10.1089/ten.tec.2012.0312

Bacsa, B., Desai, B., Dibo, G., and Kappe, C. O. (2006). Rapid solid-phase peptide synthesis using thermal and controlled microwave irradiation. *J. Pept. Sci.* 12, 633–638. doi: 10.1002/psc.771

Bakota, E. L., Wang, Y., Danesh, F. R., and Hartgerink, J. D. (2011). Injectable multidomain peptide nanofiber hydrogel as a delivery agent for stem cell secretome. *Biomacromolecules* 12, 1651–1657. doi: 10.1021/bm200035r

Beniash, E., Hartgerink, J. D., Storrie, H., Stendahl, J. C., and Stupp, S. I. (2005). Self-assembling peptide amphiphile nanofiber matrices for cell entrapment. *Acta Biomater.* 1, 387–397. doi: 10.1016/j.actbio.2005.04.002

Boateng, S. Y., Lateef, S. S., Mosley, W., Hartman, T. J., Hanley, L., and Russell, B. (2005). RGD and YIGSR synthetic peptides facilitate cellular adhesion identical to that of laminin and fibronectin but alter the physiology of neonatal cardiac myocytes. *Am. J. Physiol. Cell Physiol.* 288, C30–C38. doi: 10.1152/ajpcell.00199.2004

Boersema, G. S. A., Grotenhuis, N., Bayon, Y., Lange, J. F., and Bastiaansen-Jenniskens, Y. M. (2016). The effect of biomaterials used for tissue regeneration purposes on polarization of macrophages. *BioResearch* 5, 6–14. doi: 10.1089/biores.2015.0041

Boni, A., Urbanek, K., Nascimbene, A., Hosoda, T., Zheng, H., Delucchi, F., et al. (2008). Notch1 regulates the fate of cardiac progenitor cells. *PNAS* 105, 15529–15534. doi: 10.1073/pnas.0808357105

Boopathy, A. V., Che, P. L., Somasuntharam, I., Fiore, V. F., Cabigas, E. B., Ban, K., et al. (2014). The modulation of cardiac progenitor cell function by hydrogel-dependent Notch1 activation. *Biomaterials* 35, 8103–8112. doi: 10.1016/j.biomaterials.2014.05.082

Bradshaw, M., Ho, D., Fear, M. W., Gelain, F., Wood, F. M., and Iyer, K. S. (2014). Designer self-assembling hydrogel scaffolds can impact skin cell proliferation and migration. *Sci. Rep.* 4:6903. doi: 10.1038/srep06903

Brancaccio, M., Hirsch, E., Notte, A., Selvetella, G., Lembo, G., and Tarone, G. (2006). Integrin signalling: the tug-of-war in heart hypertrophy. *Cardiovasc. Res.* 70, 422–433. doi: 10.1016/j.cardiores.2005.12.015

Brunetti, J., Roscia, G., Lampronti, I., Gambari, R., Quercini, L., Falciani, C., et al. (2016). Immunomodulatory and anti-inflammatory activity *in vitro* and *in vivo* of a novel antimicrobial candidate. *J. Biol. Chem.* 291, 25742–25748. doi: 10.1074/jbc.M116.750257

Calvete, J. J., Schafer, W., Mann, K., Henschen, A., and Gonzalez-Rodriguez, J. (1992). Localization of the cross-linking sites of RGD and KQAGDV peptides to the isolated fibrinogen receptor, the human platelet integrin glicoprotein IIb/IIIa. Influence of peptide length. *Eur. J. Biochem.* 206, 759–765. doi: 10.1111/j.1432-1033.1992.tb16982.x

Chattopadhyay, S., and Raines, R. T. (2014). Review collagen-based biomaterials for wound healing. *Biopolymers* 101, 821–833. doi: 10.1002/bip.22486

Chen, F.-M., and Liu, X. (2016). Advancing biomaterials of human origin for tissue engineering. *Prog. Pol. Sci.* 53, 86–168. doi: 10.1016/j.progpolymsci.2015.02.004

Chiu, L. L., Reis, L. A., Momen, A., and Radisic, M. (2012). Controlled release of thymosin beta4 from injected collagen-chitosan hydrogels promotes angiogenesis and prevents tissue loss after myocardial infarction. *Regen. Med.* 7, 523–533. doi: 10.2217/rme.12.35

Cho, C.-H., Kammerer, R. A., Lee, H. J., Steinmetz, M. O., Ryu, Y. S., Lee, S. H., et al. (2004). COMP-Ang1: a designed angiopoietin-1 variant with nonleaky angiogenic activity. *PNAS* 101, 5547–5552. doi: 10.1073/pnas.0307574101

Chow, L. W., Bitton, R., Webber, M. J., Carvajal, D., Shull, K. R., Sharma, A. K., et al. (2011). A bioactive self-assembled membrane to promote angiogenesis. *Biomaterials* 32, 1574–1582. doi: 10.1016/j.biomaterials.2010.10.048

Chu-Kung, A. F., Bozzelli, K. N., Lockwood, N. A., Haseman, J. R., Mayo, K. H., and Tirrell, M. V. (2004). Promotion of peptide antimicrobial activity by fatty acid conjugation. *Bioconjug. Chem.* 15, 530–535. doi: 10.1021/bc0341573

Cui, X.-J., Xie, H., Wang, H.-J., Guo, H.-D., Zhang, J.-K., Wang, C., et al. (2010). Transplantation of mesenchymal stem cells with self-assembling polypeptide scaffolds is conducive to treating myocardial infarction in rats. *Tohoku J. Exp. Med.* 222, 281–289. doi: 10.1620/tjem.222.281

Davis, M. E., Hsieh, P. C., Takahashi, T., Song, Q., Zhang, S., Kamm, R. D., et al. (2006). Local myocardial insulin-like growth factor 1 (IGF-1) delivery with biotinylated peptide nanofibers improves cell therapy for myocardial infarction. *PNAS* 103, 8155–8160. doi: 10.1073/pnas.0602877103

Davis, M. E., Motion, J. P., Narmoneva, D. A., Takahashi, T., Hakuno, D., Kamm, R. D., et al. (2005). Injectable self-assembling peptide nanofibers create intramyocardial microenvironments for endothelial cells. *Circulation* 111, 442–450. doi: 10.1161/01.CIR.0000153847.47301.80

Diana, D., Basile, A., De Rosa, L., Di Stasi, R., Auriemma, S., Arra, C., et al. (2011). beta-hairpin peptide that targets vascular endothelial growth factor (VEGF) receptors: design, NMR characterization, and biological activity. *J. Biol. Chem.* 286, 41680–41691. doi: 10.1074/jbc.M111.257402

D'souza, S. E., Ginsberg, M. H., and Plow, E. F. (1991). Arginyl-glycyl-aspartic acid (RGD): a cell adhesion motif. *Trends Biochem. Sci.* 16, 246–250. doi: 10.1016/0968-0004(91)90096-E

Dubois, G., Segers, V. F., Bellamy, V., Sabbah, L., Peyrard, S., Bruneval, P., et al. (2008). Self-assembling peptide nanofibers and skeletal myoblast transplantation in infarcted myocardium. *J. Biomed. Mater. Res. B* 87, 222–228. doi: 10.1002/jbm.b.31099

Elfenbein, A., Simons, M., and Murakami, M. (2007). Non-canonical fibroblast growth factor signalling in angiogenesis. *Cardiovasc. Res.* 78, 223–231. doi: 10.1093/cvr/cvm086

Feng, Y., and Mrksich, M. (2004). The synergy peptide PHSRN and the adhesion peptide RGD mediate cell adhesion through a common mechanism. *Biochemistry* 43, 15811–15821. doi: 10.1021/bi049174

Ferrara, N., Gerber, H.-P., and Lecouter, J. (2003). The biology of VEGF and its receptors. *Nat. Med.* 9, 669–676. doi: 10.1038/nm0603-669

Ferrari, G., Cook, B. D., Terushkin, V., Pintucci, G., and Mignatti, P. (2009). Transforming growth factor-beta 1 (TGF-beta1) induces angiogenesis through vascular endothelial growth factor (VEGF)-mediated apoptosis. *J. Cell. Physiol.* 219, 449–458. doi: 10.1002/jcp.21706

Fields, G. B. (2010). Synthesis and biological applications of collagen-model triple-helical peptides. *Org. Biomol. Chem.* 8, 1237–1258. doi: 10.1039/b920670a

Finetti, F., Basile, A., Capasso, D., Di Gaetano, S., Di Stasi, R., Pascale, M., et al. (2012). Functional and pharmacological characterization of a VEGF mimetic peptide on reparative angiogenesis. *Biochem. Pharm.* 84, 303–311. doi: 10.1016/j.bcp.2012.04.011

Gavins, F. N. (2010). Are formyl peptide receptors novel targets for therapeutic intervention in ischaemia–reperfusion injury? *Trends Pharm. Sci.* 31, 266–276. doi: 10.1016/j.tips.2010.04.001

Gelain, F., Bottai, D., Vescovi, A., and Zhang, S. (2006). Designer self-assembling peptide nanofiber scaffolds for adult mouse neural stem cell 3-dimensional cultures. *PLoS ONE* 1:e119. doi: 10.1371/journal.pone.0000119

Ghanaati, S., Webber, M. J., Unger, R. E., Orth, C., Hulvat, J. F., Kiehna, S. E., et al. (2009). Dynamic *in vivo* biocompatibility of angiogenic peptide amphiphile nanofibers. *Biomaterials* 30, 6202–6212. doi: 10.1016/j.biomaterials.2009.07.063

Gilmore, L., Rimmer, S., Mcarthur, S. L., Mittar, S., Sun, D., and Macneil, S. (2013). Arginine functionalization of hydrogels for heparin binding–a supramolecular approach to developing a pro-angiogenic biomaterial. *Biotechnol. Bioeng.* 110, 296–317. doi: 10.1002/bit.24598

Girotti, A., Reguera, J., Rodríguez-Cabello, J. C., Arias, F. J., Alonso, M., and Testera, A. M. (2004). Design and bioproduction of a recombinant multi(bio)functional elastin-like protein polymer containing cell adhesion sequences for tissue engineering purposes. *J. Mat. Sci.* 15, 479–484. doi: 10.1023/B:JMSM.0000021124.58688.7a

Gomes, A., Teixeira, C., Ferraz, R., Prudêncio, C., and Gomes, P. (2017). Wound-healing peptides for treatment of chronic diabetic foot ulcers and other infected skin injuries. *Molecules* 22:1743. doi: 10.3390/molecules22101743

Graf, J., Iwamoto, Y., Sasaki, M., Martin, G. R., Kleinman, H. K., Robey, F. A., et al. (1987a). Identification of an amino acid sequence in laminin mediating cell attachment, chemotaxis, and receptor binding. *Cell* 48, 989–996. doi: 10.1016/0092-8674(87)90707-0

Graf, J., Ogle, R. C., Robey, F. A., Sasaki, M., Martin, G. R., Yamada, Y., et al. (1987b). A pentapeptide from the laminin B1 chain mediates cell adhesion and binds the 67,000 laminin receptor. *Biochemistry* 26, 6896–6900. doi: 10.1021/bi00396a004

Guo, H. D., Cui, G. H., Wang, H. J., and Tan, Y. Z. (2010). Transplantation of marrow-derived cardiac stem cells carried in designer self-assembling peptide nanofibers improves cardiac function after myocardial infarction. *Biochem. Biophys. Res. Commun.* 399, 42–48. doi: 10.1016/j.bbrc.2010.07.031

Guo, H. D., Cui, G. H., Yang, J. J., Wang, C., Zhu, J., Zhang, L. S., et al. (2012). Sustained delivery of VEGF from designer self-assembling peptides improves cardiac function after myocardial infarction. *Biochem. Biophys. Res. Commun.* 424, 105–111. doi: 10.1016/j.bbrc.2012.06.080

Hautanen, A., Gailit, J., Mann, D. M., and Ruoslahti, E. (1989). Effects of modifications of the RGD sequence and its context on recognition by the fibronectin receptor. *J. Biol. Chem.* 264, 1437–1442.

Heo, S. C., Kwon, Y. W., Jang, I. H., Jeong, G. O., Lee, T. W., Yoon, J. W., et al. (2017). Formyl peptide receptor 2 is involved in cardiac repair after myocardial

infarction through mobilization of circulating angiogenic cells. *Stem Cells* 35, 654–665. doi: 10.1002/stem.2535

Hiesinger, W., Perez-Aguilar, J. M., Atluri, P., Marotta, N. A., Frederick, J. R., Fitzpatrick, J. R. III, Mccormick, R. C., et al. (2011). Computational protein design to reengineer stromal cell-derived factor-1alpha generates an effective and translatable angiogenic polypeptide analog. *Circulation* 124, S18–S26. doi: 10.1161/CIRCULATIONAHA.110.009431

Hsieh, P. C., Davis, M. E., Gannon, J., Macgillivray, C., and Lee, R. T. (2006a). Controlled delivery of PDGF-BB for myocardial protection using injectable self-assembling peptide nanofibers. *J. Clin. Invest.* 116, 237–248. doi: 10.1172/JCI25878

Hsieh, P. C., Macgillivray, C., Gannon, J., Cruz, F. U., and Lee, R. T. (2006b). Local controlled intramyocardial delivery of platelet-derived growth factor improves postinfarction ventricular function without pulmonary toxicity. *Circulation* 114, 637–644. doi: 10.1161/CIRCULATIONAHA.106.639831

Hu, G. F., Riordan, J. F., and Vallee, B. L. (1997). A putative angiogenin receptor in angiogenin-responsive human endothelial cells. *Proc. Natl. Acad. Sci. U.S.A.* 94, 2204–2209. doi: 10.1073/pnas.94.6.2204

Hubbell, J. A., Massia, S. P., Desai, N. P., and Drumheller, P. D. (1991). Endothelial cell-selective materials for tissue engineering in the vascular graft via a new receptor. *Nat. Biotechnol.* 9, 568–572. doi: 10.1038/nbt0691-568

Huettner, N., Dargaville, T. R., and Forget, A. (2018). Discovering cell-adhesion peptides in tissue engineering: beyond RGD. *Trends Biotechnol.* 36, 372–383. doi: 10.1016/j.tibtech.2018.01.008

Hunter, D. D., Cashman, N., Morris-Valero, R., Bulock, J. W., Adams, S. P., and Sanes, J. R. (1991). An LRE (leucine-arginine-glutamate)-dependent mechanism for adhesion of neurons to S-laminin. *J. Neurosci.* 11, 3960–3971. doi: 10.1523/JNEUROSCI.11-12-03960.1991

Isidro-Llobet, A., Alvarez, M., and Albericio, F. (2009). Amino acid-protecting groups. *Chem. Rev.* 109, 2455–2504. doi: 10.1021/cr800323s

Islam, M. M., Ravichandran, R., Olsen, D., Ljunggren, M. K., Fagerholm, P., Lee, C. J., et al. (2016). Self-assembled collagen-like-peptide implants as alternatives to human donor corneal transplantation. *RSC Adv.* 6, 55745–55749. doi: 10.1039/C6RA08895C

Jangamreddy, J. R., Haagdorens, M. K. C., Mirazul Islam, M., Lewis, P., Samanta, A., Fagerholm, P., et al. (2018). Short peptide analogs as alternatives to collagen in pro-regenerative corneal implants. *Acta Biomater.* 69, 120–130. doi: 10.1016/j.actbio.2018.01.011

Jun, H. W., Yuwono, V., Paramonov, S. E., and Hartgerink, J. D. (2005). Enzyme-mediated degradation of peptide-amphiphile nanofiber networks. *Adv. Mater.* 17, 2612–2617. doi: 10.1002/adma.200500855

Kahlenberg, J. M., and Kaplan, M. J. (2013). Little peptide, big effects: the role of LL-37 in inflammation and autoimmune disease. *J. Immunol.* 191, 4895–4901. doi: 10.4049/jimmunol.1302005

Kim, J. H., Park, Y., Jung, Y., Kim, S. H., and Kim, S. H. (2017). Combinatorial therapy with three-dimensionally cultured adipose-derived stromal cells and self-assembling peptides to enhance angiogenesis and preserve cardiac function in infarcted hearts. *J. Tissue Eng. Regen. Med.* 11, 2816–2827. doi: 10.1002/term.2181

Kim, J. K., Anderson, J., Jun, H. W., Repka, M. A., and Jo, S. (2009). Self-assembling peptide amphiphile-based nanofiber gel for bioresponsive cisplatin delivery. *Mol. Pharm.* 6, 978–985. doi: 10.1021/mp900009n

Kleinman, H. K., Graf, J., Iwamoto, Y., Sasaki, M., Schasteen, C. S., Yamada, Y., et al. (1989). Identification of a second active site in laminin for promotion of cell adhesion and migration and inhibition of *in vivo* melanoma lung colonization. *Arch. Biochem. Biophys.* 272, 39–45. doi: 10.1016/0003-9861(89)90192-6

Knight, C. G., Morton, L. F., Peachey, A. R., Tuckwell, D. S., Farndale, R. W., and Barnes, M. J. (2000). The collagen-binding A-domains of integrins alpha(1)beta(1) and alpha(2)beta(1) recognize the same specific amino acid sequence, GFOGER, in native (triple-helical) collagens. *J. Biol. Chem.* 275, 35–40. doi: 10.1074/jbc.275.1.35

Koide, T. (2005). Triple helical collagen-like peptides: engineering and applications in matrix biology. *Connect. Tissue Res.* 46, 131–141. doi: 10.1080/03008200591008518

Koria, P., Yagi, H., Kitagawa, Y., Megeed, Z., Nahmias, Y., Sheridan, R., et al. (2011). Self-assembling elastin-like peptides growth factor chimeric nanoparticles for the treatment of chronic wounds. *PNAS* 108, 1034–1039. doi: 10.1073/pnas.1009881108

Kraehenbuehl, T. P., Zammaretti, P., Van Der Vlies, A. J., Schoenmakers, R. G., Lutolf, M. P., Jaconi, M. E., et al. (2008). Three-dimensional extracellular matrix-directed cardioprogenitor differentiation: systematic modulation of a synthetic cell-responsive PEG-hydrogel. *Biomaterials* 29, 2757–2766. doi: 10.1016/j.biomaterials.2008.03.016

Krock, B. L., Skuli, N., and Simon, M. C. (2011). Hypoxia-induced angiogenesis: good and evil. *Genes Cancer* 2, 1117–1133. doi: 10.1177/1947601911423654

Kumar, V. A., Taylor, N. L., Shi, S., Wang, B. K., Jalan, A. A., Kang, M. K., et al. (2015). Highly angiogenic peptide nanofibers. *ACS Nano* 9, 860–868. doi: 10.1021/nn506544b

Lamb, H. M., and Wiseman, L. R. (1998). Pexiganan acetate. *Drugs* 56, 1047–1052. doi: 10.2165/00003495-199856060-00011

Leahy, D. J., Aukhil, I., and Erickson, H. P. (1996). 2.0 Å crystal structure of a four-domain segment of human fibronectin encompassing the RGD loop and synergy region. *Cell* 84, 155–164. doi: 10.1016/S0092-8674(00)81002-8

Li, F., Carlsson, D., Lohmann, C., Suuronen, E., Vascotto, S., Kobuch, K., et al. (2003). Cellular and nerve regeneration within a biosynthetic extracellular matrix for corneal transplantation. *PNAS* 100, 15346–15351. doi: 10.1073/pnas.2536767100

Li, M., Zhang, Y., Feurino, L. W., Wang, H., Fisher, W. E., Brunicardi, F. C., et al. (2008). Interleukin-8 increases vascular endothelial growth factor and neuropilin expression and stimulates ERK activation in human pancreatic cancer. *Cancer Sci.* 99, 733–737. doi: 10.1111/j.1349-7006.2008.00740.x

Lin, Y. D., Chang, M. Y., Cheng, B., Liu, Y. W., Lin, L. C., Chen, J. H., et al. (2015). Injection of Peptide nanogels preserves postinfarct diastolic function and prolongs efficacy of cell therapy in pigs. *Tissue Eng. Part A* 21, 1662–1671. doi: 10.1089/ten.tea.2014.0581

Lin, Y. D., Luo, C. Y., Hu, Y. N., Yeh, M. L., Hsueh, Y. C., Chang, M. Y., et al. (2012). Instructive nanofiber scaffolds with VEGF create a microenvironment for arteriogenesis and cardiac repair. *Sci. Transl. Med.* 4:146ra109. doi: 10.1126/scitranslmed.3003841

Lin, Y. D., Yeh, M. L., Yang, Y. J., Tsai, D. C., Chu, T. Y., Shih, Y. Y., et al. (2010). Intramyocardial peptide nanofiber injection improves postinfarction ventricular remodeling and efficacy of bone marrow cell therapy in pigs. *Circulation* 122, S132–S141. doi: 10.1161/CIRCULATIONAHA.110.939512

Liu, X., Wang, X., Horii, A., Wang, X., Qiao, L., Zhang, S., et al. (2012). *In vivo* studies on angiogenic activity of two designer self-assembling peptide scaffold hydrogels in the chicken embryo chorioallantoic membrane. *Nanoscale* 4, 2720–2727. doi: 10.1039/c2nr00001f

Loffredo, C., Assuncao, N. A., Gerhardt, J., and Miranda, M. T. (2009). Microwave-assisted solid-phase peptide synthesis at 60 degrees C: alternative conditions with low enantiomerization. *J. Pept. Sci.* 15, 808–817. doi: 10.1002/psc.1178

Lutolf, M. P., Weber, F. E., Schmoekel, H. G., Schense, J. C., Kohler, T., Muller, R., et al. (2003). Repair of bone defects using synthetic mimetics of collagenous extracellular matrices. *Nat. Biotechnol.* 21, 513–518. doi: 10.1038/nbt818

Mangoni, M. L., Mcdermott, A. M., and Zasloff, M. (2016). Antimicrobial peptides and wound healing: biological and therapeutic considerations. *Exp. Dermatol.* 25, 167–173. doi: 10.1111/exd.12929

Mardilovich, A., Craig, J. A., Mccammon, M. Q., Garg, A., and Kokkoli, E. (2006). Design of a novel fibronectin-mimetic peptide–amphiphile for functionalized biomaterials. *Langmuir* 22, 3259–3264. doi: 10.1021/la052756n

Martinez, F. O., and Gordon, S. (2014). The M1 and M2 paradigm of macrophage activation: time for reassessment. *F1000Prime Rep.* 6, 13–13. doi: 10.12703/P6-13

Massia, S. P., and Hubbell, J. A. (1992). Vascular endothelial cell adhesion and spreading promoted by the peptide REDV of the IIICS region of plasma fibronectin is mediated by integrin alpha 4 beta 1. 267, 14019–14026.

Mehta, M., Madl, C. M., Lee, S., Duda, G. N., and Mooney, D. J. (2015). The collagen I mimetic peptide DGEA enhances an osteogenic phenotype in mesenchymal stem cells when presented from cell-encapsulating hydrogels. *J. Biomed. Mater. Res. A* 103, 3516–3525. doi: 10.1002/jbm.a.35497

Merrifield, R. B. (1963). Solid phase peptide synthesis. I. The synthesis of a tetrapeptide. *J. Am. Chem. Soc.* 85, 2149–2154. doi: 10.1021/ja00897a025

Miklas, J. W., Dallabrida, S. M., Reis, L. A., Ismail, N., Rupnick, M., and Radisic, M. (2013). QHREDGS enhances tube formation, metabolism and survival

of endothelial cells in collagen-chitosan hydrogels. *PLoS ONE* 8:e72956. doi: 10.1371/journal.pone.0072956

Miotto, M., Gouveia, R. M., and Connon, C. J. (2015). Peptide amphiphiles in corneal tissue engineering. *J. Funct. Biomater.* 6, 687–707. doi: 10.3390/jfb6030687

Mould, A. P., Komoriya, A., Yamada, K. M., and Humphries, M. J. (1991). The CS5 peptide is a second site in the IIICS region of fibronectin recognized by the integrin alpha 4 beta 1. Inhibition of alpha 4 beta 1 function by RGD peptide homologues. *J. Biol. Chem.* 266, 3579–3585.

Nagase, H., and Fields, G. B. (1996). Human matrix metalloproteinase specificity studies using collagen sequence-based synthetic peptides. *Biopolymers* 40, 399–416.

Niyonsaba, F., Madera, L., Afacan, N., Okumura, K., Ogawa, H., and Hancock, R. E. (2013). The innate defense regulator peptides IDR-HH2, IDR-1002, and IDR-1018 modulate human neutrophil functions. *J. Leukoc. Biol.* 94, 159–170. doi: 10.1189/jlb.1012497

O'leary, L. E., Fallas, J. A., Bakota, E. L., Kang, M. K., and Hartgerink, J. D. (2011). Multi-hierarchical self-assembly of a collagen mimetic peptide from triple helix to nanofibre and hydrogel. *Nat. Chem.* 3, 821–828. doi: 10.1038/nchem.1123

Ouzounis, C. A., Coulson, R. M. R., Enright, A. J., Kunin, V., and Pereira-Leal, J. B. (2003). Classification schemes for protein structure and function. *Nat. Rev. Gen.* 4:508. doi: 10.1038/nrg1113

Paradis-Bas, M., Tulla-Puche, J., and Albericio, F. (2016). The road to the synthesis of "difficult peptides". *Chem. Soc. Rev.* 45, 631–654. doi: 10.1039/C5CS00680E

Patel, P. N., Gobin, A. S., West, J. L., and Patrick, C. W. Jr. (2005). Poly(ethylene glycol) hydrogel system supports preadipocyte viability, adhesion, and proliferation. *Tissue Eng.* 11, 1498–1505. doi: 10.1089/ten.2005.11.1498

Patterson, J., and Hubbell, J. A. (2010). Enhanced proteolytic degradation of molecularly engineered PEG hydrogels in response to MMP-1 and MMP-2. *Biomaterials* 31, 7836–7845. doi: 10.1016/j.biomaterials.2010.06.061

Patterson, J., and Hubbell, J. A. (2011). SPARC-derived protease substrates to enhance the plasmin sensitivity of molecularly engineered PEG hydrogels. *Biomaterials* 32, 1301–1310. doi: 10.1016/j.biomaterials.2010.10.016

Pedersen, S. L., Tofteng, A. P., Malik, L., and Jensen, K. J. (2012). Microwave heating in solid-phase peptide synthesis. *Chem. Soc. Rev.* 41, 1826–1844. doi: 10.1039/C1CS15214A

Pena, O. M., Afacan, N., Pistolic, J., Chen, C., Madera, L., Falsafi, R., et al. (2013). Synthetic cationic peptide IDR-1018 modulates human macrophage differentiation. *PLoS ONE* 8:e52449. doi: 10.1371/journal.pone.0052449

Pillarisetti, K., and Gupta, S. K. (2001). Cloning and relative expression analysis of rat stromal cell derived factor-1 (SDF-1): SDF-1 α mRNA is selectively induced in rat model of myocardial infarction. *Inflammation* 25, 293–300. doi: 10.1023/A:1012808525370

Ponten, A., Folestad, E. B., Pietras, K., and Eriksson, U. (2005). Platelet-derived growth factor D induces cardiac fibrosis and proliferation of vascular smooth muscle cells in heart-specific transgenic mice. *Circ. Res.* 97, 1036–1045. doi: 10.1161/01.RES.0000190590.31545.d4

Potente, M., Gerhardt, H., and Carmeliet, P. (2011). Basic and therapeutic aspects of angiogenesis. *Cell* 146, 873–887. doi: 10.1016/j.cell.2011.08.039

Pountos, I., Panteli, M., Lampropoulos, A., Jones, E., Calori, G. M., and Giannoudis, P. V. (2016). The role of peptides in bone healing and regeneration: a systematic review. *BMC Med.* 14:103. doi: 10.1186/s12916-016-0646-y

Pratt, A. B., Weber, F. E., Schmoekel, H. G., Muller, R., and Hubbell, J. A. (2004). Synthetic extracellular matrices for *in situ* tissue engineering. *Biotechnol. Bioeng.* 86, 27–36. doi: 10.1002/bit.10897

Raeber, G. P., Lutolf, M. P., and Hubbell, J. A. (2005). Molecularly engineered PEG hydrogels: a novel model system for proteolytically mediated cell migration. *Biophys. J.* 89, 1374–1388. doi: 10.1529/biophysj.104.050682

Rajangam, K., Behanna, H. A., Hui, M. J., Han, X., Hulvat, J. F., Lomasney, J. W., et al. (2006). Heparin binding nanostructures to promote growth of blood vessels. *Nano Lett.* 6, 2086–2090. doi: 10.1021/nl0613555

Rask, F., Dallabrida, S. M., Ismail, N. S., Amoozgar, Z., Yeo, Y., Rupnick, M. A., et al. (2010). Photocrosslinkable chitosan modified with angiopoietin-1 peptide, QHREDGS, promotes survival of neonatal rat heart cells. *J. Biomed. Mater. Res. A* 95, 105–117. doi: 10.1002/jbm.a.32808

Reis, L. A., Chiu, L. L., Liang, Y., Hyunh, K., Momen, A., and Radisic, M. (2012). A peptide-modified chitosan-collagen hydrogel for cardiac cell culture and delivery. *Acta Biomater.* 8, 1022–1036. doi: 10.1016/j.actbio.2011.11.030

Reis, L. A., Chiu, L. L., Wu, J., Feric, N., Laschinger, C., Momen, A., et al. (2015). Hydrogels with integrin-binding angiopoietin-1-derived peptide, QHREDGS, for treatment of acute myocardial infarction. *Circ. Heart Fail.* 8, 333–341. doi: 10.1161/CIRCHEARTFAILURE.114.001881

Rele, S., Song, Y., Apkarian, R. P., Qu, Z., Conticello, V. P., and Chaikof, E. L. (2007). D-periodic collagen-mimetic microfibers. *J. Am. Chem. Soc.* 129, 14780–14787. doi: 10.1021/ja0758990

Reyes, C. D., and Garcia, A. J. (2003). Engineering integrin-specific surfaces with a triple-helical collagen-mimetic peptide. *J. Biomed. Mater. Res. A* 65, 511–523. doi: 10.1002/jbm.a.10550

Rodríguez-Cabello, J. C., González De Torre, I., Ibañez-Fonseca, A., and Alonso, M. (2018). Bioactive scaffolds based on elastin-like materials for wound healing. *Adv. Drug Deliv. Rev.* 129, 118–133. doi: 10.1016/j.addr.2018.03.003

Ross Robert, S., and Borg Thomas, K. (2001). Integrins and the Myocardium. *Circul. Res.* 88, 1112–1119. doi: 10.1161/hh1101.091862

Rotem, S., and Mor, A. (2009). Antimicrobial peptide mimics for improved therapeutic properties. *Biochim. Biophys. Acta* 1788, 1582–1592. doi: 10.1016/j.bbamem.2008.10.020

Rubert Pérez, C. M., Álvarez, Z., Chen, F., Aytun, T., and Stupp, S.I. (2017). Mimicking the bioactivity of fibroblast growth factor-2 using supramolecular nanoribbons. *ACS Biomater. Sci. Eng.* 3, 2166–2175. doi: 10.1021/acsbiomaterials.7b00347

Rufaihah, A. J., Yasa, I. C., Ramanujam, V. S., Arularasu, S. C., Kofidis, T., Guler, M. O., et al. (2017). Angiogenic peptide nanofibers repair cardiac tissue defect after myocardial infarction. *Acta Biomater.* 58, 102–112. doi: 10.1016/j.actbio.2017.06.009

Ruoslahti, E. (1988). Fibronectin and its receptors. *Annu. Rev. Biochem.* 57, 375–413. doi: 10.1146/annurev.bi.57.070188.002111

Ruoslahti, E., and Pierschbacher, M. D. (1987). New perspectives in cell adhesion: RGD and integrins. *Science* 238, 491–497. doi: 10.1126/science.2821619

Sainson, R. C., Johnston, D. A., Chu, H. C., Holderfield, M. T., Nakatsu, M. N., Crampton, S. P., et al. (2008). TNF primes endothelial cells for angiogenic sprouting by inducing a tip cell phenotype. *Blood* 111, 4997–5007. doi: 10.1182/blood-2007-08-108597

Salinas, C. N., and Anseth, K. S. (2008). The enhancement of chondrogenic differentiation of human mesenchymal stem cells by enzymatically regulated RGD functionalities. *Biomaterials* 29, 2370–2377. doi: 10.1016/j.biomaterials.2008.01.035

Samanen, J., Ali, F., Romoff, T., Calvo, R., Sorenson, E., Vasko, J., et al. (1991). Development of a small RGD peptide fibrinogen receptor antagonist with potent antiaggregatory activity *in vitro*. *J. Med. Chem.* 34, 3114–3125. doi: 10.1021/jm00114a022

Sanada, F., Kim, J., Czarna, A., Chan, N. Y.-K., Signore, S., Ogórek, B., et al. (2014). c-Kit–positive cardiac stem cells nested in hypoxic niches are activated by stem cell factor reversing the aging myopathy. *Circul. Res.* 114, 41–55. doi: 10.1161/CIRCRESAHA.114.302500

Santoso, S., Hwang, W., Hartman, H., and Zhang, S. (2002). Self-assembly of surfactant-like peptides with variable glycine tails to form nanotubes and nanovesicles. *Nano Lett.* 2, 687–691. doi: 10.1021/nl025563i

Scarborough, R. M., Rose, J. W., Hsu, M. A., Phillips, D. R., Fried, V. A., Campbell, A. M., et al. (1991). Barbourin. A GPIIb-IIIa-specific integrin antagonist from the venom of Sistrurus m. barbouri. *J. Biol. Chem.* 266, 9359–9362.

Schneider, A., Garlick, J. A., and Egles, C. (2008). Self-assembling peptide nanofiber scaffolds accelerate wound healing. *PLoS ONE* 3:e1410. doi: 10.1371/journal.pone.0001410

Schussler, O., Coirault, C., Louis-Tisserand, M., Al-Chare, W., Oliviero, P., Menard, C., et al. (2009). Use of arginine-glycine-aspartic acid adhesion peptides coupled with a new collagen scaffold to engineer a myocardium-like tissue graft. *Nat. Clin. Pract. Cardiovasc. Med.* 6, 240–249. doi: 10.1038/ncpcardio1451

Segers, V. F., Tokunou, T., Higgins, L. J., Macgillivray, C., Gannon, J., and Lee, R. T. (2007). Local delivery of protease-resistant stromal cell derived factor-1 for stem cell recruitment after myocardial infarction. *Circulation* 116, 1683–1692. doi: 10.1161/CIRCULATIONAHA.107.718718

Shachar, M., Tsur-Gang, O., Dvir, T., Leor, J., and Cohen, S. (2011). The effect of immobilized RGD peptide in alginate scaffolds on cardiac tissue engineering. *Acta Biomater.* 7, 152–162. doi: 10.1016/j.actbio.2010.07.034

Shin, H., Jo, S., and Mikos, A. G. (2003). Biomimetic materials for tissue engineering. *Biomaterials* 24, 4353–4364. doi: 10.1016/S0142-9612(03)00339-9

Shu, Y., Hao, T., Yao, F., Qian, Y., Wang, Y., Yang, B., et al. (2015). RoY peptide-modified chitosan-based hydrogel to improve angiogenesis and cardiac repair under hypoxia. *ACS Appl. Mater. Interfaces* 7, 6505–6517. doi: 10.1021/acsami.5b01234

Sieminski, A. L., Semino, C. E., Gong, H., and Kamm, R. D. (2008). Primary sequence of ionic self-assembling peptide gels affects endothelial cell adhesion and capillary morphogenesis. *J. Biomed. Mater. Res. A* 87, 494–504. doi: 10.1002/jbm.a.31785

Sierra, M. D. L. L., Yang, F., Narazaki, M., Salvucci, O., Davis, D., Yarchoan, R., et al. (2004). Differential processing of stromal-derived factor-1α and stromal-derived factor-1β explains functional diversity. *Blood* 103, 2452–2459. doi: 10.1182/blood-2003-08-2857

Sigma-Aldrich (2019). *Standard Fmoc Amino Acids*. Available online at: https://www.sigmaaldrich.com/chemistry/chemistry-products.html?TablePage=111084330

Simons, M., Gordon, E., and Claesson-Welsh, L. (2016). Mechanisms and regulation of endothelial VEGF receptor signalling. *Nat. Rev. Mol. Cell Biol.* 17, 611–625. doi: 10.1038/nrm.2016.87

Singh, H. D., Bushnak, I., and Unsworth, L. D. (2012). Engineered peptides with enzymatically cleavable domains for controlling the release of model protein drug from "soft" nanoparticles. *Acta Biomater.* 8, 636–645. doi: 10.1016/j.actbio.2011.10.028

Sondermeijer, H., Witkowski, P., Seki, T., Van Der Laarse, A., Itescu, S., and Hardy, M. A. (2017). RGDfK-peptide modified alginate scaffold for cell transplantation and cardiac neovascularization. *Tissue Eng. Part A* 24, 740–751. doi: 10.1089/ten.tea.2017.0221

Staatz, W. D., Fok, K. F., Zutter, M. M., Adams, S. P., Rodriguez, B. A., and Santoro, S. A. (1991). Identification of a tetrapeptide recognition sequence for the alpha 2 beta 1 integrin in collagen. *J. Biol. Chem.* 266, 7363–7367.

Structural Genomics, C., China Structural Genomics, C., Northeast Structural Genomics, C., Graslund, S., Nordlund, P., Weigelt, J., et al. (2008). Protein production and purification. *Nat. Methods* 5, 135–146. doi: 10.1038/nmeth.f.202

Tanrikulu, I. C., Forticaux, A., Jin, S., and Raines, R. T. (2016). Peptide tessellation yields micrometre-scale collagen triple helices. *Nat. Chem.* 8:1008. doi: 10.1038/nchem.2556

Taraballi, F., Sushnitha, M., Tsao, C., Bauza, G., Liverani, C., Shi, A., et al. (2018). Biomimetic tissue engineering: tuning the immune and inflammatory response to implantable biomaterials. *Adv. Healthcare Mater.* 7:1800490. doi: 10.1002/adhm.201800490

Tashiro, K., Sephel, G. C., Weeks, B., Sasaki, M., Martin, G. R., Kleinman, H. K., et al. (1989). A synthetic peptide containing the IKVAV sequence from the A chain of laminin mediates cell attachment, migration, and neurite outgrowth. *J. Biol. Chem.* 264, 16174–16182.

Tashiro, K.-I., Monji, A., Yoshida, I., Hayashi, Y., Matsuda, K., Tashiro, N., et al. (1999). An IKLLI-containing peptide derived from the laminin α1 chain mediating heparin-binding, cell adhesion, neurite outgrowth and proliferation, represents a binding site for integrin α3β1 and heparan sulphate proteoglycan. *Biochem. J.* 340, 119–126. doi: 10.1042/bj3400119

Thapa, P., Zhang, R. Y., Menon, V., and Bingham, J. P. (2014). Native chemical ligation: a boon to peptide chemistry. *Molecules* 19, 14461–14483. doi: 10.3390/molecules190914461

Tickler, A. K., and Wade, J. D. (2007). Overview of solid phase synthesis of "difficult peptide" sequences. *Curr. Protoc. Protein Sci.* 50, 18.8.1–18.8.6. doi: 10.1002/0471140864.ps1808s50

Turk, B. E., Huang, L. L., Piro, E. T., and Cantley, L. C. (2001). Determination of protease cleavage site motifs using mixture-based oriented peptide libraries. *Nat. Biotechnol.* 19, 661–667. doi: 10.1038/90273

Urry, D. W. (1988). Entropic elastic processes in protein mechanisms. I. Elastic structure due to an inverse temperature transition and elasticity due to internal chain dynamics. *J. Protein Chem.* 7, 1–34. doi: 10.1007/BF01025411

Urry, D. W., Harris, R. D., and Long, M. M. (1981). Compounding of elastin polypentapeptide to collagen analogue: a potential elastomeric prosthetic material. *Biomater. Med. Dev. Art Organs* 9, 181–194. doi: 10.3109/10731198109118999

Vigneswaran, Y., Han, H., De Loera, R., Wen, Y., Zhang, X., Sun, T., et al. (2016). Winner of the student award in the hospital intern category, 10th World Biomaterials Congress, May 17–22, 2016, Montreal QC, Canada: peptide biomaterials raising adaptive immune responses in wound healing contexts. *J. Biomed. Mat. Res. A* 104, 1853–1862. doi: 10.1002/jbm.a.35767

Von Maltzahn, G., Vauthey, S., Santoso, S., and Zhang, S. (2003). Positively charged surfactant-like peptides self-assemble into nanostructures. *Langmuir* 19, 4332–4337. doi: 10.1021/la026526

Wang, C., Liu, Y., Fan, Y., and Li, X. (2017). The use of bioactive peptides to modify materials for bone tissue repair. *Regen. Biomater.* 4, 191–206. doi: 10.1093/rb/rbx011

Webber, M. J., Han, X., Prasanna Murthy, S. N., Rajangam, K., Stupp, S. I., and Lomasney, J. W. (2010a). Capturing the stem cell paracrine effect using heparin-presenting nanofibres to treat cardiovascular diseases. *J. Tissue Eng. Reg. Med.* 4, 600–610. doi: 10.1002/term.273

Webber, M. J., Kessler, J. A., and Stupp, S. I. (2010b). Emerging peptide nanomedicine to regenerate tissues and organs. *J. Int. Med.* 267, 71–88. doi: 10.1111/j.1365-2796.2009.02184.x

Webber, M. J., Tongers, J., Renault, M.-A., Roncalli, J. G., Losordo, D. W., and Stupp, S. I. (2010c). Development of bioactive peptide amphiphiles for therapeutic cell delivery. *Acta Biomater.* 6, 3–11. doi: 10.1016/j.actbio.2009.07.031

West, J. L., and Hubbell, J. A. (1999). Polymeric biomaterials with degradation sites for proteases involved in cell migration. *Macromolecules* 32, 241–244. doi: 10.1021/ma981296k

Wojtowicz, A. M., Shekaran, A., Oest, M. E., Dupont, K. M., Templeman, K. L., Hutmacher, D. W., et al. (2010). Coating of biomaterial scaffolds with the collagen-mimetic peptide GFOGER for bone defect repair. *Biomaterials* 31, 2574–2582. doi: 10.1016/j.biomaterials.2009.12.008

World Health Organization (2017). *The Top 10 Causes of Death*. Available online at: http://www.who.int/mediacentre/factsheets/fs310/en/ (accessed March 2019).

Xin, X., Yang, S., Ingle, G., Zlot, C., Rangell, L., Kowalski, J., et al. (2001). Hepatocyte growth factor enhances vascular endothelial growth factor-induced angiogenesis *in vitro* and *in vivo*. *Am. J. Pathol.* 158, 1111–1120. doi: 10.1016/S0002-9440(10)64058-8

Yamada, K. M. (1991). Adhesive recognition sequences. *J. Biol. Chem.* 266, 12809–12812.

Yamada, M., Kadoya, Y., Kasai, S., Kato, K., Mochizuki, M., Nishi, N., et al. (2002). Ile-Lys-Val-Ala-Val (IKVAV)-containing laminin α1 chain peptides form amyloid-like fibrils. *FEBS Lett.* 530, 48–52. doi: 10.1016/S0014-5793(02)03393-8

Yoshida, N., Ishii, E., Nomizu, M., Yamada, Y., Mohri, S., Kinukawa, N., et al. (1999). The laminin-derived peptide YIGSR (Tyr-Ile-Gly-Ser-Arg) inhibits human pre-B leukaemic cell growth and dissemination to organs in SCID mice. *Br. J. Cancer* 80, 1898–1904. doi: 10.1038/sj.bjc.6690618

Yu, J., Du, K. T., Fang, Q., Gu, Y., Mihardja, S. S., Sievers, R. E., et al. (2010). The use of human mesenchymal stem cells encapsulated in RGD modified alginate microspheres in the repair of myocardial infarction in the rat. *Biomaterials* 31, 7012–7020. doi: 10.1016/j.biomaterials.2010.05.078

Yu, J., Gu, Y., Du, K. T., Mihardja, S., Sievers, R. E., and Lee, R. J. (2009). The effect of injected RGD modified alginate on angiogenesis and left ventricular function in a chronic rat infarct model. *Biomaterials* 30, 751–756. doi: 10.1016/j.biomaterials.2008.09.059

Zachman, A. L., Crowder, S. W., Ortiz, O., Zienkiewicz, K. J., Bronikowski, C. M., Yu, S. S., et al. (2013). Pro-angiogenic and anti-inflammatory regulation by functional peptides loaded in polymeric implants for soft tissue regeneration. *Tissue Eng. Part A* 19, 437–447. doi: 10.1089/ten.tea.2012.0158

Zhang, S. (2003). Fabrication of novel biomaterials through molecular self-assembly. *Nat. Biotechnol.* 21, 1171–1178. doi: 10.1038/nbt874

Zhang, S., Holmes, T., Lockshin, C., and Rich, A. (1993). Spontaneous assembly of a self-complementary oligopeptide to form a stable macroscopic membrane. *PNAS* 90, 3334–3338. doi: 10.1073/pnas.90.8.3334

Zhang, Y., Zhu, D., Wei, Y., Wu, Y., Cui, W., Liuqin, L., et al. (2019). A collagen hydrogel loaded with HDAC7-derived peptide promotes the regeneration of infarcted myocardium with functional improvement in a rodent model. *Acta Biomater.* 86, 223–234. doi: 10.1016/j.actbio.2019.01.022

Zhou, Z., Wang, J., Cao, R., Morita, H., Soininen, R., Chan, K. M., et al. (2004). Impaired angiogenesis, delayed wound healing and retarded tumor growth in perlecan heparan sulfate-deficient mice. *Cancer Res.* 64, 4699–4702. doi: 10.1158/0008-5472.CAN-04-0810

Conflict of Interest Statement: The authors declare that the research was conducted in the absence of any commercial or financial relationships that could be construed as a potential conflict of interest.

frontiers in Bioengineering and Biotechnology

REVIEW
published: 12 September 2019
doi: 10.3389/fbioe.2019.00217

Addressing Patient Specificity in the Engineering of Tumor Models

Laura J. Bray[1,2,3†], *Dietmar W. Hutmacher*[1,2,3,4,5] *and Nathalie Bock*[2,3,4*†]

[1] School of Chemistry, Physics and Mechanical Engineering, Science and Engineering Faculty, Institute of Health and Biomedical Innovation, Queensland University of Technology, Brisbane, QLD, Australia, [2] Centre in Regenerative Medicine, Institute of Health and Biomedical Innovation (IHBI), Queensland University of Technology (QUT), Kelvin Grove, QLD, Australia, [3] Translational Research Institute, Queensland University of Technology (QUT), Brisbane, QLD, Australia, [4] School of Biomedical Sciences, Faculty of Health and Australian Prostate Cancer Research Centre (APCRC-Q), Brisbane, QLD, Australia, [5] Australian Research Council (ARC) Industrial Transformation Training Centre in Additive Biomanufacturing, Queensland University of Technology (QUT), Kelvin Grove, QLD, Australia

Cancer treatment is challenged by the heterogeneous nature of cancer, where prognosis depends on tumor type and disease stage, as well as previous treatments. Optimal patient stratification is critical for the development and validation of effective treatments, yet pre-clinical model systems are lacking in the delivery of effective individualized platforms that reflect distinct patient-specific clinical situations. Advances in cancer cell biology, biofabrication, and microengineering technologies have led to the development of more complex *in vitro* three-dimensional (3D) models to act as drug testing platforms and to elucidate novel cancer mechanisms. Mostly, these strategies have enabled researchers to account for the tumor microenvironment context including tumor-stroma interactions, a key factor of heterogeneity that affects both progression and therapeutic resistance. This is aided by state-of-the-art biomaterials and tissue engineering technologies, coupled with reproducible and high-throughput platforms that enable modeling of relevant physical and chemical factors. Yet, the translation of these models and technologies has been impaired by neglecting to incorporate patient-derived cells or tissues, and largely focusing on immortalized cell lines instead, contributing to drug failure rates. While this is a necessary step to establish and validate new models, a paradigm shift is needed to enable the systematic inclusion of patient-derived materials in the design and use of such models. In this review, we first present an overview of the components responsible for heterogeneity in different tumor microenvironments. Next, we introduce the state-of-the-art of current *in vitro* 3D cancer models employing patient-derived materials in traditional scaffold-free approaches, followed by novel bioengineered scaffold-based approaches, and further supported by dynamic systems such as bioreactors, microfluidics, and tumor-on-a-chip devices. We critically discuss the challenges and clinical prospects of models that have succeeded in providing clinical relevance and impact, and present emerging concepts of novel cancer model systems that are addressing patient specificity, the next frontier to be tackled by the field.

Keywords: tumor heterogeneity, tumor microenvironment, 3D tumor models, primary cells, patient-derived, tissue engineering, hydrogels, microfluidics

OPEN ACCESS

Edited by:
Hasan Uludag,
University of Alberta, Canada

Reviewed by:
Francesco Pampaloni,
Goethe University Frankfurt, Germany
Stephanie Michelle Willerth,
University of Victoria, Canada

***Correspondence:**
Nathalie Bock
n.bock@qut.edu.au

[†]These authors have contributed equally to this work

Specialty section:
This article was submitted to Biomaterials, a section of the journal Frontiers in Bioengineering and Biotechnology

Received: *30 May 2019*
Accepted: *27 August 2019*
Published: *12 September 2019*

Citation:
Bray LJ, Hutmacher DW and Bock N (2019) Addressing Patient Specificity in the Engineering of Tumor Models. Front. Bioeng. Biotechnol. 7:217. doi: 10.3389/fbioe.2019.00217

THE HETEROGENEITY OF CANCER

The multi-faceted nature of cancer as a dynamic disease makes it complex to fully capture the traits of individual tumors at specific points in time (Dagogo-Jack and Shaw, 2017). With a high number of different cancer types and sub-types, interpatient heterogeneity arises due to unique genetics and epigenetics, as well as dynamic factors such as age, environment, lifestyle, and medical history (Alizadeh et al., 2015). Intertumoral and intratumoral heterogeneity further increase during the course of the disease (**Figure 1**), upon degree, stage, and treatment history which, ultimately, lead to therapeutic resistance and treatment failures in patients (Fisher et al., 2013). With the continual biotechnological advances that enable in-depth sequencing, specific tumor subclones may be isolated and used in tumor models of heterogeneity, representing the next roadblock to tackle in order to develop more effective personalized medicine (Lawson et al., 2018).

At the tumor level, heterogeneity arises from two key players; the genetic/epigenetic intrinsic factor and the extrinsic stromal factor (Lawson et al., 2018). Intrinsically, variations in clonal growth, functional properties, metabolic state, and expression markers are commonly found within the same tumor clones (Burrell et al., 2013; Sabaawy, 2013). The clonal evolution model is the most accepted cause of intratumoral heterogeneity, where genetic/epigenetic alterations lead to novel clones with better advantages compared to ancestral clones (Burrell et al., 2013). Although debated, cancer stem cells may further increase heterogeneity through epigenetic variations, which give rise to small subpopulations within tumors (Shackleton et al., 2009). Extrinsically, the tumor microenvironment comprises stromal components in various differentiation states, pro/anti-tumor immune products, and the expression of organ-specific extracellular matrix (ECM) (Junttila and de Sauvage, 2013). While tumor cells initially modulate the local tumor microenvironment, activated stromal cells, in turn, generate a feedback loop that contributes to oncogenic phenotypes of the tumor cells, synergistically fueling intrinsic/extrinsic crosstalk (Plava et al., 2019). Anti-neoplastic drug treatment is the most common route to improve overall survival of cancer patients, yet disease heterogeneity often results in unsuitable or ineffective treatments, and may lead to unnecessary toxic side-effects. In the future, advanced sequencing techniques will enable individual molecular characterization, forming the basis of better therapy selection or personalized medicine (Meijer et al., 2017; Senft et al., 2017). Yet, this undertaking requires the validation of biomarkers prior to their implementation in the clinic using patient-specific models that account for both intrinsic and extrinsic heterogeneity factors, in spatial and temporal contexts (Dagogo-Jack and Shaw, 2017).

In this review, we present an overview of the key heterogeneity components of various microenvironments, followed by a discussion of the current patient-specific culture systems that are addressing tumor heterogeneity by using patient-derived cells arising from both tumor and stroma. Finally, we present an outlook for the future, predicting what technology platforms will be able to address patient specificity and accurate disease modeling in order to progress basic research and clinical studies alike.

OVERVIEW OF THE KEY HETEROGENEITY COMPONENTS IN TUMOR MICROENVIRONMENTS

The tumor microenvironment is key to cancer progression and tumors cannot survive without the appropriate support of microenvironment-derived factors (Risbridger et al., 2018). To date, the profiling of clinical specimens has identified gene dysregulations, not only in cancer cells, but also in the adjacent stroma (Planche et al., 2011). Tumor identity is dynamically shaped by physical and chemical parameters arising from cancer/stroma interactions and strongly dictate clonal reprogramming leading to heterogeneous adaptive cellular responses in both tumor and stromal cells (**Figure 1B**). Hereafter we introduce the key components of heterogeneity, providing background for efficient tumor modeling of patient-specific microenvironments.

Key Cellular Components

Tumors commonly consist of heterogeneous cell populations that encompass both genetically mutated and unmutated sub-populations (Burrell et al., 2013). Broadly, the cellular stroma contains epithelial cells (Thiery and Chopin, 1999), normal and cancer-associated fibroblasts (CAFs) (Kalluri, 2016), endothelial cells (Hida et al., 2018), adipocyte cells (Cozzo et al., 2017), infiltrating immune cells (Smith and Kang, 2013), and pericytes (Paiva et al., 2018), which assist cancer progression in various ways (Junttila and de Sauvage, 2013). Critical to tumor growth and dissemination, induced angiogenesis is the key component that transcends all cancers (Hanahan and Weinberg, 2011). Metabolic stresses on tumor cells signal for the recruitment of endothelial cells and fibroblasts and the establishment of new microvessels around the tumor stroma, known as the angiogenic switch (Qiao and Tang, 2018). When tumor angiogenesis occurs through this mechanism, the vessels are often irregular, leaky and do not form organized capillaries (Shchors and Evan, 2007). Variability also arises among different organs, where organ-specific endothelial cells influence tumor progression to different extents (Peela et al., 2017).

CAFs are another key stromal component highly responsible for tumor heterogeneity (Ochiai and Neri, 2016). CAFs arise from the secretion of pro-fibrotic cues, such as growth factors, cytokines, and metabolites, following cancer-stroma crosstalk, where myofibroblasts develop from stromal fibroblasts, ultimately leading to a CAF phenotype (LeBleu and Kalluri, 2018). CAFs can also arise from vascular smooth muscle cells, pericytes, circulating fibrocytes and bone marrow derived cells (Ochiai and Neri, 2016). Highly proliferative, CAFs are the largest contributor to ECM remodeling and the main source of collagen production, providing cancer cells with the mechanical support needed for progression (Ochiai and Neri, 2016). The biological properties of CAFs are heterogeneous and different types of CAFs make distinct functional contributions (Junttila and de Sauvage,

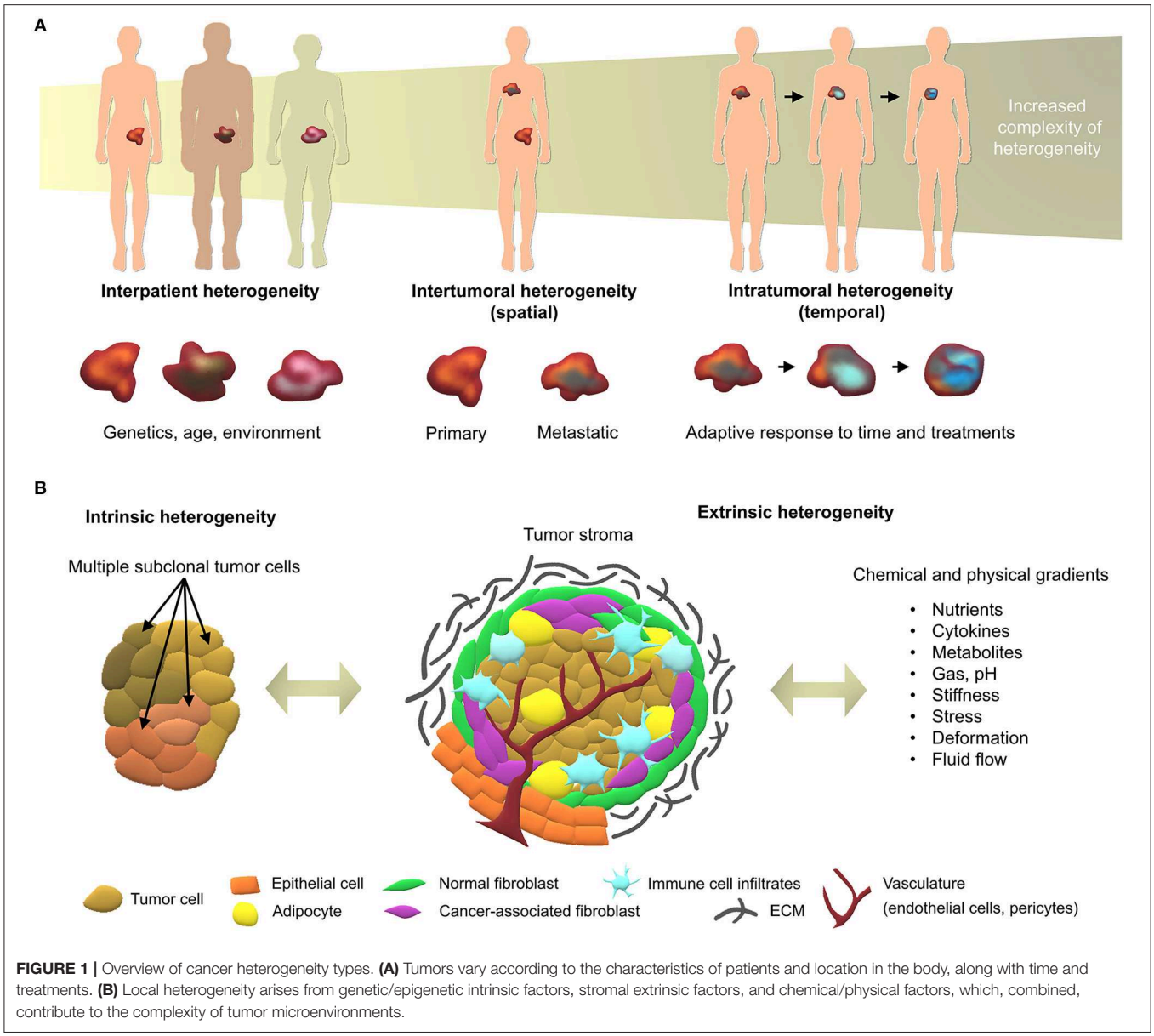

FIGURE 1 | Overview of cancer heterogeneity types. **(A)** Tumors vary according to the characteristics of patients and location in the body, along with time and treatments. **(B)** Local heterogeneity arises from genetic/epigenetic intrinsic factors, stromal extrinsic factors, and chemical/physical factors, which, combined, contribute to the complexity of tumor microenvironments.

2013). CAFs are also key to metastasis success and a fraction can disseminate along with cancer cells, helping to prepare the secondary microenvironment for cancer cell homing and survival and overall contribute to high levels of heterogeneity (LeBleu and Kalluri, 2018).

During progression of the primary tumor, cancer cells may disseminate throughout the body using blood or lymphatic vessels, or may advance via direct invasion of surrounding microenvironments (Stacker et al., 2002). Cell-cell and cell-matrix interactions, and paracrine signaling are key to these activities (Lu et al., 2012). Cancer cell migration itself is controlled through a paracrine loop involving colony stimulating factor 1 (CSF1), epidermal growth factor (EGF), and their receptors, which are differentially expressed on carcinoma cells and macrophages, resulting in movement of cancer cells toward macrophages (Smith and Kang, 2013). Additional paracrine loops exist between cancer cells expressing C-X-C chemokine receptor 4 (CXCR4) and stromal cells, such as fibroblasts and pericytes, producing the stromal cell-derived factor 1, also known as C-X-C motif chemokine 12 (CXCL12), which contribute to directional cancer cell migration (Kucia et al., 2005). Cancer cell intravasation into the blood circulation is directly associated with the presence of perivascular macrophages and tumor associated macrophages (Jeffrey et al., 2004; Wyckoff et al., 2007). The macrophages, along with the cancer cells themselves, mediate disruption in the vascular basement membrane (Bissell and Radisky, 2001). Entry of cancer cells into the lymphatic system is due to a lack or disruption in the basement membrane, as well as help from factors secreted by neighboring pericytes, among other influences (Saharinen et al., 2004). Intrinsic to tumor

cells, epithelial-to-mesenchymal transition (EMT), and reverse EMT, are the key cellular processes for tumor progression and survival in the secondary microenvironment, by modulation of E-cadherins (Yao et al., 2011; Banyard and Bielenberg, 2015; Paduch, 2016).

The formation of a pre-metastatic niche is required to facilitate tumor cell engraftment and is formed due to the secretion of factors from the tumor itself (Kaplan et al., 2005; Hiratsuka et al., 2006; Psaila and Lyden, 2009). Pre-metastatic niches are intrinsic to each cancer and are proposed as a key determinant to the site of extravasation (Chen et al., 2018). Attracted by local factors, hematopoietic progenitor cells, stromal cells, endothelial cells, and macrophages aggregate at the pre-metastatic niche (Kaplan et al., 2005; Hiratsuka et al., 2006). After surviving in the circulatory microenvironment, only around 0.01% of extravasated tumor cells home to the pre-metastatic niche (Chambers et al., 2002; Kaplan et al., 2006). While some cells will remain dormant or die shortly after homing, surviving cells start to heavily modify the ECM, forming micrometastases (de Boer et al., 2009), which are too small to be captured by current detection methods. The growth and maintenance of metastatic tumors is due to tumor cell clonal adaptation to the new environment and help from the local cellular populations, ECM produces and dynamic paracrine signaling (Psaila and Lyden, 2009). While there may be some level of genomic concordance between primary tumors and metastatic tumors in some cancers (e.g., colorectal; Urosevic and Gomis, 2018), heterogeneity is, overall, highest in metastatic tumors (Fidler, 1978). This is due to having resided longest in the patient, leading to a high number of subclonal evolutions and exposure to multiple microenvironments, further altering cellular programs to better-fit each site specifically (Dagogo-Jack and Shaw, 2017). Importantly, as cellular heterogeneity increases steadily as a tumor progresses, cellular/non-cellular interactions and their variable physicochemical gradients further contribute to heterogeneity, progression, and therapy response (Burrell et al., 2013).

Key Non-cellular Components

The ECM is a key player in regulating cancer cell behavior by offering both biophysical and biochemical cues that influence cancer cell proliferation, invasion, migration, differentiation, metastasis, therapy response, and apoptosis (Griffith and Swartz, 2006). The ECM is highly dynamic and heterogeneous, structurally and biochemically, hence heavily contributing to the heterogeneity of cancer microenvironments (Seewaldt, 2014). The ECM comprises several hundreds of macromolecule types (Filipe et al., 2018), such as collagens, proteoglycans, elastin, fibronectin, laminin, hyaluronan, and is remodeled by enzymes such as matrix metalloproteinases (MMPs) (Lu et al., 2012). Inflammation involves high ECM remodeling with large ECM protein deposition, which are crosslinked by increased levels of lysyl oxidase (LOX) (Barker et al., 2012), contributing to solid stresses (Kalli and Stylianopoulos, 2018), tumor ECM stiffening (Gkretsi and Stylianopoulos, 2018), and drug resistance (Erler et al., 2006). The increased deposition of ECM proteins promotes cancer progression by altering cell-cell adhesion, cell polarity and growth factor signaling (Walker et al., 2018). A review by Poltavets et al. describes the role of each cell type in directing ECM change and how this influences cancer cells and their plasticity (Poltavets et al., 2018). The ECM organization is different for each tumor microenvironment, including large variations in stiffness, topography, and biochemical composition (Filipe et al., 2018). Highly aligned fiber networks are found in connective tissues such as bone, while amorphous substrates are found in disorganized structures, as seen in the brain, resulting in higher and less stiff microenvironments, respectively (Malandrino et al., 2018). As an example, brain is in the 100–2,000 Pa range (Cox and Erler, 2011; Barney et al., 2015) and glioblastoma-associated ECM is mostly composed of collagen IV, procollagen III, laminins, fibronectin, and hyaluronan (HA)-fibrillar collagens (Gkretsi et al., 2015). Conversely, the normal glandular tissue of breast is in the 1–45 kPa range (Cox and Erler, 2011; Ramião et al., 2016) and tumor ECM involves collagen I, IV, V, fibronectin, laminins, entactin, proteoglycans, and glycosaminoglycans (Gkretsi et al., 2015). Tumor ECM has a unique protein composition which, when isolated, has been shown to enhance the growth of cancer cells *in vitro*, compared to normal ECM (Romero-López et al., 2017). Stiffness increases dramatically during cancer, for example a 13-fold increase in stiffness was observed from fibroglandular breast tissue to high-grade invasive ductal carcinoma (Samani et al., 2007). In turn, increased stiffness reciprocally forces tumor progression (Boyd et al., 2014). Increasing ECM stiffness in breast cancer tissues in particular is a prominent indicator for cancer aggressiveness, metastatic potential, response to therapy, and overall prognosis (Acerbi et al., 2015). This is linked to ECM changes in both tissue organization and composition with matrix proteins such as increasingly crosslinked fibrillar collagens, fibronectin, laminins, proteoglycans, as well as remodeling enzymes (Insua-Rodríguez and Oskarsson, 2016).

Cancer invasion is critically prompted by the tumor ECM, which deposition is increased compared to normal stroma, resulting in higher matrix stiffness and cancer cell migration by durotaxis (Friedl and Alexander, 2011). A disruption in intercellular adhesion results in the detachment of certain tumor cells from the primary mass. These cells then migrate through the ECM, invading surrounding tissue and leading to the degradation of natural ECM. Collagen fibers are often used by cancer cells for this purpose, via microtrack formation (Paul et al., 2017). As these fibers are often attached to the local blood vessels, cancer cells can collect at these sites (Condeelis and Segall, 2003). Initially, the collagen fibers found in primary tumors progressively align themselves perpendicularly to the tumor boundaries, facilitating dissemination from the primary site (Belgodere et al., 2018). When cancer cells eventually detach from the primary tumor and become motile, they undertake migration by heterogeneous modes, namely mesenchymal or amoeboid (Malandrino et al., 2018). Recent studies suggest that while migration starts as a collective of tumor cells, eventually cell migration becomes an individual process facilitated more by the actin cytoskeleton and less by their arrangement along the collagen fibers (Ilina et al., 2018). In other cases, even though a degree of porosity at the micrometer scale exists within

anatomical structures, cancer cells need to degrade surrounding ECM when the pore size is <7 μm^2 (Wolf et al., 2013). The tumor cells may then intravasate into blood or lymphatic vessels entering the circulation, which can happen both actively or passively (Diab et al., 2009). Intravasation is usually favored chemically by chemokine gradients that actively lead cancer cells toward circulatory vessels, yet it can also take place due to high local stresses and a fragile vascular network that ultimately passively collapses (Peela et al., 2017). There is a definite role for protein assembly from the stromal compartment in influencing tumor cell colonization, including fibronectin, collagen IV, tenascin, and periostin, which are deposited by fibroblasts and endothelial cells (Barkan et al., 2010; Oskarsson, 2013). These proteins promote cell adhesion and growth at the metastatic sites. It has also been hypothesized that integrin expression is an important factor in the targeting of an organ by a tumor cell. Integrin β1, α2, and α6 are expressed in the brain, liver, and lung ECM, and overall have control over cell adhesion in these sites (Barney et al., 2015). Moreover, a role for exosomes, also known as extracellular vesicles which carry signaling molecules, has been defined in the formation of the pre-metastatic niche by preparing the tissue for extravasated tumor cell propagation (Costa-Silva et al., 2015; Hoshino et al., 2015). The exosomes derived from tumor cells show integrin expression that promotes binding to organ-specific cells (Hoshino et al., 2015). Once the tumor cells arrive, they are then maintained in a fibronectin and growth factor rich pre-metastatic niche. The remodeling of local tissue after tumor cell arrival is essential to manage invasion and metastatic outgrowth (Paget, 1989). Therefore, expression of MMPs are also upregulated in the pre-metastatic niche (Kaplan et al., 2005). ECM composition and mechanical stiffness are equally remodeled heavily around metastatic tumors. Metastases usually have more aggressive features compared to primary tumors, with more active paracrine signaling for more rapid growth at the secondary site (Urosevic and Gomis, 2018). Various cancer types and subtypes preferentially metastasize to different organs, suggesting that each cancer is more inclined to home to and grow in a distinct microenvironment (Minn et al., 2005; Bos et al., 2009; Peinado et al., 2017). As a result, the identification of major ECM components for each tumor microenvironment, their biochemical composition, spatial organization, and resulting stiffness provide a relevant foundation to engineer more physiologically-relevant matrices, in turn better addressing tumor ECM heterogeneity.

ENGINEERING PATIENT-SPECIFIC TUMOR MICROENVIRONMENT MODELS

Traditional three-dimensional (3D) tumor culture systems have relied on immortalized cell lines. While cell lines are essential to validate the efficiency of novel culture systems and provide important insight in tumor behavior when grown in 3D, they lack power as tumor models for personalized medicine. For instance, even if cancer cell lines retain driver mutations, several studies revealed a drift at the transcriptomic level where cancer cell lines bore more resemblance to each other, regardless of the tissue origin, than to the clinical samples they were modeling (Gillet et al., 2013). Hence, the use of cell lines, even in *in vivo* preclinical 3D settings, has failed to be an efficient therapy platform for patients. This has correlated with high drug failure rates in phase II and III clinical trials (Colditz and Peterson, 2018), calling out for a paradigm shift toward the use of patient-derived cells. Yet, the culture of such cells *in vitro* is challenging due to difficulties in isolation, low isolated numbers, and limited proliferative capacity due to being highly dependent on the supportive surrounding stroma. Where successful two-dimensional (2D) culture of these cells allows rapid diagnostic testing at low passages, extended culture is impossible, and whereas they are more relevant than cancer cell lines, they are not suited to the wide testing span required to be an effective predictive model. Yet drug efficacy prediction is not always the goal and an important consideration lies in a model's purpose, where model complexity is largely dependent on the objectives (Katt et al., 2016). While some of the simpler systems are most suited for drug screening, the more complex and physiologically relevant models are necessary for validation purposes (Meijer et al., 2017). Primary culture systems in 2D have so far remained optimal for drug screening, as they provide high-throughput possibility. However, the local penetration of drugs in a real tumor is influenced by interstitial fluid flow, hypoxia, pH, and ECM composition (Vilanova et al., 2018) that are missing in the 2D setting, leading to less therapeutic efficacy correlation and a reduced ability to serve as drug efficacy predictors *in vivo*. The development of more advanced 3D systems is tackling some of these issues, yet to date, there are no pre-clinical models that fully recapitulate the patient-specific stromal, immune, structural, chemical, and molecular aspects of the heterogeneous microenvironments that cancer cells are sequentially exposed to in the course of the disease (Belgodere et al., 2018). This concept also needs to be balanced with over-engineering considerations, where a complex model may not be as easily translated for routine pre-clinical use, but may serve as a relevant mechanistic platform. Nevertheless, current advances have started to recapitulate more complex stages of cancer progression, integrating advanced biomaterials, and technologies, which current state-of-the-art will be discussed hereafter. We will describe how patient-derived microenvironments are more traditionally modeled by scaffold-free approaches, followed by novel biomaterials and tissue engineering techniques that have allowed more complexity. Finally we will discuss the system-based technologies that employ dynamic culture approaches (**Figure 2**).

Scaffold-Free Approaches

To date, a large proportion of patient-derived cultures have been used for drug testing purposes, rather than for the recapitulation and study of cancer processes, which are predominantly performed using cell lines. Other than very limited material availability, one of the critical hurdles when dealing with patient-derived materials, resides indeed in maintaining the tissue for a period sufficient to enable drug testing and biological assessment. As such, simple and short-term strategies have been used traditionally and are described hereafter.

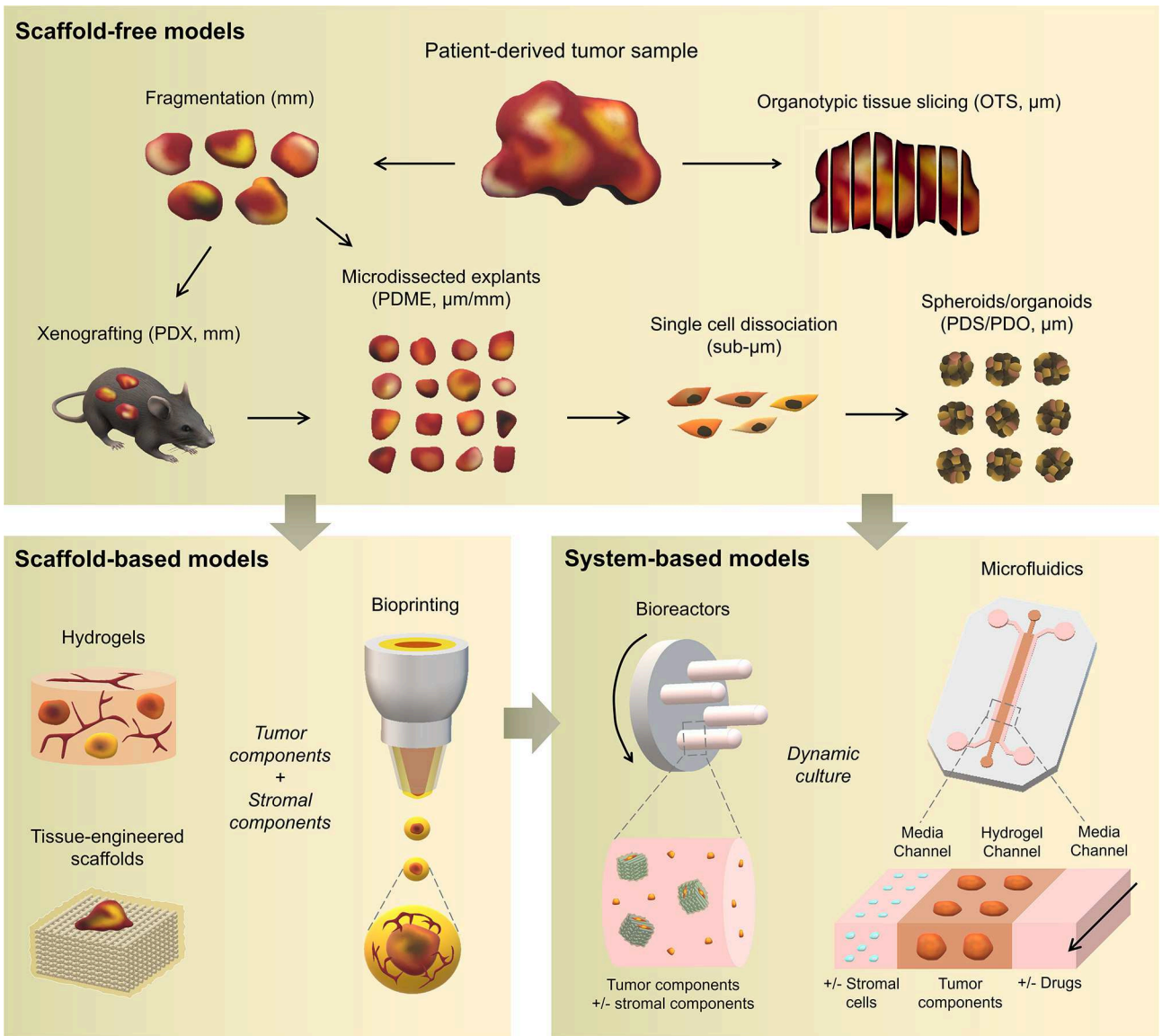

FIGURE 2 | Overview of patient-specific tumor models. Traditionally used with no matrix or simple natural matrices, and mainly for drug testing purposes, patient-derived materials are now used in combination with scaffold-based biomaterials, allowing the incorporation of stromal components to better mimic the native microenvironment or to study a specific process (angiogenesis, metastasis). Both approaches are also being used with dynamic systems to; further mimic/test physical and chemical gradients, better control the addition of stromal components, increase viability, and enable multiple drug testing.

Patient-Derived Xenografts (PDXs)

PDXs have been standard practice for target validation, proposing, to date, the most advanced preclinical models that can overcome issues from *in vitro* settings. PDXs involve the propagation of a fresh patient tumor biopsy in immunocompromised mice (NOD/SCID, Nude, NSG) in either ectopic or orthotopic sites, including intact stroma and ECM architecture. In some cases, dissociated tumor cells are regrown in organoids using Matrigel® (Kondo et al., 2018) or other gels [fibrin (Liu et al., 2012), gelatin (Kondo et al., 2011)] prior to implantation. The presence of the mouse circulatory system allows the testing of chemotherapeutics, while also monitoring the downstream effects on various organs. The tumors of many cancers have been used for PDXs and while some metastatic tumors are increasingly used for PDXs [pancreatic ductal adenocarcinoma (Roife et al., 2016), uveal melanoma (Nemati et al., 2010), colorectal cancer (Bertotti et al., 2011; Julien et al., 2012), breast cancer (Whittle et al., 2015), prostate cancer (McCulloch et al., 2005; Nguyen et al., 2017; Beshiri et al., 2018; Risbridger et al., 2018)], a large focus has been on primary tumors. Some of the latest studies include xenografting of primary breast cancer (Matossian et al., 2019), glioblastoma (Hribar et al., 2019), head and neck cancer (Majumder et al., 2015; Ghosh et al., 2019), prostate cancer (Fong et al., 2014),

pancreatic ductal adenocarcinoma (Roife et al., 2016), and colorectal cancer (Kondo et al., 2011). So far, they have been used for biomarker screening and testing, pre-clinical drug evaluation, and personalized medicine strategies (Hidalgo et al., 2014).

Within the native stroma and architecture, PDXs retain the global biological and genetic characteristics of the native tumor and remain relatively stable over multiple passages. Yet, PDXs present limitations with engraftment rates in mice and cross-species contamination which alter ECM composition, ultimately an important factor altering tumor cells in this long-term incubation setting. Some excised tumors also present with a lack of viable human stroma, which may be rapidly overcome by mouse stroma and can be influenced by the xenograft sites. This is critical for tumor tissues that have low proliferation rates, enabling further colonization by host cells (Risbridger et al., 2018). Depending on the site of implantation and type of tumor (primary, metastatic), some PDXs can be established relatively rapidly [1–3 weeks for glioblastoma PDX (Tentler et al., 2012)] whereas some PDXs require months of culture [up to 22 months for prostate cancer (Risbridger et al., 2018)]. Those significant culture times are problematic as it increases genetic alterations, in turn lengthening drug screening times, altering responses and reducing predictive power. For example, Daniel et al. showed that PDX models of small cell lung cancer (SCLC) retained a gene expression signature similar to primary tumor tissue, yet irreversible changes occurred when brought back in culture and re-established as secondary xenografts (Daniel et al., 2009). As PDXs do not fully account for non-cell autonomous heterogeneity of the tumor microenvironment (Cassidy et al., 2015), various strategies have been used. Specific to the stroma, CAFs, and mesenchymal stem cells (MSCs) confer bulk tumor heterogeneity and these could be implanted alongside the PDX (Augsten, 2014). Using matched patient stromal components provide a more relevant humanized microenvironment, yet it may not be possible to isolate and expand cells quickly enough to ensure viability and engraftment success of the original tumor. Immune infiltration is another important aspect, yet for PDXs, immunodeficient mice need to be used, with strains such as NSG, lacking functional lymphocytes, and macrophages (Choi et al., 2018). This has been addressed by implantation of human CD34+ hematopoietic stem cells which can differentiate into T and B cells. The final consideration is ECM which is tissue-specific, while in PDX models, the commonly used method to increase engraftment efficiency is the murine-basement membrane Matrigel, due to its inherent rich composition of growth factors. Moreover, the models used are often ectopic, and hence comprise altered ECM components. These limitations could be addressed by synthetic hydrogel alternatives with ECM components similar to the target microenvironment, and by using orthotopic sites where possible.

Another way to limit material-induced heterogeneity is to limit the time of PDX culture (which are typically in the range of several months). This was recently addressed (2018) by introducing a new PDX variant referred to as "mini-PDXs," as a rapid drug sensitivity assay so that patients receive personalized chemotherapy in a clinically relevant time frame. In this model, the tumors were dissociated into single cells and inserted in hollow fiber capsules (OncoVee®, Biotech) before implantation in nu/nu mice and cultured for 7 days under various drug treatments, prior to extraction, tumor cell viability, and tumor cell growth inhibition measurements. Little details about the biocompatible capsules were mentioned in these studies, other than that the pore size allowed the passage of molecules <500 kDa. The mini-PDXs were used with patient-derived tumor cells from gastric, lung, pancreatic cancer tissues (Zhang et al., 2018a), metastatic duodenal carcinoma (Zhao et al., 2018), and gallbladder carcinoma (Zhan et al., 2018). Significant differences in drug responsiveness were observed, yet overall survival was longer in patients in the PDX-guided chemotherapy compared to the conventional chemotherapy group of 12 patients with gallbladder carcinoma patients (18.6 vs. 13.9 months) and so was disease free survival (17.6 vs. 12 months) (Zhan et al., 2018). While encouraging, it is important to note that the cell dissociation and short timeframe prohibited any native stromal structure and no proper 3D structure recapitulation (Zhang et al., 2018a) as seen in traditional PDXs. There are also some ethical concerns about using animals for such short-term experiments, when an *in vitro* explant model could lead to the same results. In the future, a comparative study of the mini-PDXs should be done either with explants or organoids, to prove that the method is more predictive.

Ultimately, PDXs are the most widely accepted pre-clinical platforms that address both the heterogeneity and complexity of the original tumor. However it has been shown that PDXs may also eventually falsely recapitulate original tumor traits, since engraftment and propagation can lead to selective maintenance of cancer cells with the most aggressive phenotypes (Hidalgo et al., 2014). Coupled with the lack of an immune system, a high cost for maintenance and ethical considerations, PDXs may not be the most sensible system to use for drug testing.

Patient-Derived Organoids (PDOs) and Spheroids (PDS)

PDOs and PDS can arise from dissociated single cells that arrange themselves into a self-directed organizational structure *in vitro* that better retain the characteristics of an original patient tumor compared to 2D monocultures or PDXs (Yuhas et al., 1977; Fischbach et al., 2007). Here, we define PDS as matrix-free 3D cell aggregates and PDOs as 3D cultures supported by naturally-derived matrices. By far the most utilized method of culturing PDOs is using naturally-derived hydrogel matrices, such as Matrigel (Sato et al., 2011; Cheung et al., 2013; Gao et al., 2014; van de Wetering et al., 2015; Weeber et al., 2015; Beshiri et al., 2018; Orditura et al., 2018; Tanaka et al., 2018; Vlachogiannis et al., 2018; Kijima et al., 2019; Mousavi et al., 2019; Schnalzger et al., 2019) or Collagen I (Cheung et al., 2013; Neal et al., 2018), while PDS are often formed using non-adhesive/agarose-coated plates (Bansal et al., 2014; Halfter et al., 2015; Hagemann et al., 2017; Linxweiler et al., 2018) (**Table 1**), all requiring minimal engineering strategies (**Figures 3A–D**). PDO cultures using natural hydrogels have long-term culture potential and are unique due to the heterogeneous nature of the tissue from which it is derived. However, challenges arise in the success rate of organoid formation, as PDOs often lack

key cellular components that direct intratumoral heterogeneity, such as fibroblasts, immune cells, and other various supporting cell types that contribute to the tumor microenvironment. Nonetheless, compared to cell-line-derived organoids, PDOs have been demonstrated to more accurately maintain the genetic diversity of *in vivo* tumors, more closely recapitulate native histopathology; and can predict *in vivo* drug sensitivity, in turn providing robust pre-clinical models (Nagle et al., 2018).

Matrix-free PDS formation

PDS formation without matrix support is most often performed using the Hanging Drop method (Hagemann et al., 2017) and ultra-low-adherent plates/coatings (Bansal et al., 2014, 2016; Halfter et al., 2015; Hagemann et al., 2017; Linxweiler et al., 2018) (**Figures 3A,B**), and more rarely Aggrewell plates (Hribar et al., 2019). The hanging drop method relies on the gravity-mediated self-assembly of tumor cells, using suspension culture, while ultra-low attachment (ULA) culture plates have surfaces that are not conducive to cell attachment, therefore leading to cellular aggregation. The Aggrewell plates are especially beneficial to obtain highly uniform 3D spheroid cultures. Hagemann et al. (2017) compared the two techniques and found that ULA plates led to more consistent spheroid formation from head and neck squamous cell carcinomas (HNSCCs) than the hanging drop method. A similar protocol using ULA plates was developed for prostate cancer PDS growth using 109 patient samples (Linxweiler et al., 2018). Higher grade Gleason scores led to less spheroid formation than lower Gleason scored tumor tissues. Moreover, tumors of $>100\,\mu m$ often displayed necrosis in their center, mimicking hypoxia, and nutrient deprivation in the early stages of tumor development. PDS were also found to contain and support both prostate epithelial and stromal cells. The models were used to test various drug treatments with results dependent upon individual patient samples. Similarly, Plummer et al. (2019) used a co-culture approach to generate PDS from glioblastoma tissue, first differentiating induced pluripotent stem cells (iPSCs) into neural progenitor cells, and then co-culturing with patient-derived glioblastoma cells, plated on top. After 24 h, both cell types were scraped and re-seeded, prior to exposure to chemotherapeutics or fixed/embedded to create tissue microarrays for high-throughput analyses.

Halfter et al. (2015) reported on a larger scale breast cancer study on the biopsies of 78 patients. PDS were formed using non-treated dishes coated with agar, to prevent cell attachment, leading to cell aggregation. Inter-PDS heterogeneity was noted. Interestingly, the PDS formed were less compact if the tissue was derived from high grade tumors when compared with low grade tumor tissue. The model was able to predict the outcome for various treatments received by individual patients in the clinic. Also using agarose-coated plates, Bansal et al. formed spheroids from both prostate cancer tissues (Bansal et al., 2014, 2016). The authors studied the inhibition of a B-cell-specific insertion site, affecting cell survival, clonogenicity, and motility. Interpatient heterogeneity was observed. Overall, while PDS culture is relatively easy and cost-effective to perform, the biomechanical and biochemical cues provided by a surrounding tissue microenvironment not only affects the development of a tumor, but also the infiltration and effects of various chemotherapeutics. These factors are missing in a matrix-free spheroid model.

PDO formation supported by natural matrices

Matrigel, or basement membrane extract, is the most studied matrix to date used to culture PDOs, despite presenting with batch-to-batch variability in manufacturing, and complexity in composition, making it difficult to link matrix signals to cell function (Fang and Eglen, 2017). Hereafter are presented recent or key PDO studies which have used Matrigel. A key paper by Sato et al. (2011) reported the culture of intestinal crypts from 20 patients with colon cancer in Matrigel. The human organoids could be cultured for at least 1 month, after which their morphology changed, and proliferation decreased. The length of PDO culture can be extended with passaging (usually every 1–2 weeks), up to 6 months with the addition of essential growth factors and inhibitors. Subsequently, similar protocols were developed for the culture of pancreatic (Boj et al., 2015), colorectal (van de Wetering et al., 2015; Weeber et al., 2015; Schnalzger et al., 2019), prostate (Bansal et al., 2014; Gao et al., 2014), gastrointestinal (Vlachogiannis et al., 2018), breast (Orditura et al., 2018), and HNSCC (Tanaka et al., 2018; Kijima et al., 2019). PDOs have become a regular tool to expand our knowledge of cancer biology (Matano et al., 2015; Drost et al., 2016). For example, Sato's group later published a report using CRISPR-Cas9 genome-editing to create tumor suppressor and oncogene mutations in normal intestinal PDOs (Matano et al., 2015). These engineered organoids highlighted that these mutations alone were not sufficient to induce cancer progression. Additional studies have sought to apply PDO cultures to drug testing and predictive clinical medicine (Pauli et al., 2017; Kondo et al., 2018; Orditura et al., 2018; Vlachogiannis et al., 2018; Hribar et al., 2019; Kijima et al., 2019) or as biobanks of PDOs for future research (van de Wetering et al., 2015; Beshiri et al., 2018).

Various success rates can be achieved with PDO grown in Matrigel. In pancreatic PDOs (80% success rate), while healthy pancreatic organoids stopped proliferating after 6 months in culture, the tumor samples could be propagated "indefinitely" and survived cryopreservation (Boj et al., 2015). Following orthotopic PDO transplantation into mice, normal ductal architecture within the mouse pancreas was observed and the entire process of tumor development was mimicked. The heterogeneity of the tumor changed over time and tumor progression. Whether these changes were instigated by the organoid itself, the murine microenvironment, or by the Matrigel matrix remains to be determined (Boj et al., 2015). One impressive study characterized a biobank collection of 20 matched patient healthy and malignant colorectal organoids (van de Wetering et al., 2015). Overall, success rate and survival upon freeze-thawing were both $\geq$80%.

While PDOs are predominantly made of primary tumors, metastatic PDOs remain limited. In metastatic colorectal cancer (Weeber et al., 2015), Matrigel-cultured PDOs (71% success rate) from 14 patients retained 90% of the somatic mutations compared to the original tumors. Kijima et al. successfully

TABLE 1 | Overview of spheroid models.

Main cancer type	Purpose and application	Patient numbers	Method	Maximum culture time	References
Brain cancer	Drug response; preparation of spheroid tissue mircroarray	Not stated	Non-coated well	49 days	Plummer et al., 2019
Breast cancer	Biological studies into the indentification of invasive cancer cells	10	Matrigel and Collagen I Hydrogels	4 days	Cheung et al., 2013
Breast cancer	Drug response in parallel with the clinic	78	Agar-coated plate	5 days	Halfter et al., 2015
Breast cancer	Drug response; biological studies into tumor mutations	27	Matrigel	30 days	Orditura et al., 2018
Esophageal and Oropharyngeal cancer	Biological studies	21	Matrigel	21 days	Kijima et al., 2019
Gastrointestinal cancer	High-throughput drug screening	32	Matrigel	7 days	Kondo et al., 2018
Gastrointestinal cancer	Drug response; mass spectrometry	4	Basement membrane extract	10 days	Liu et al., 2018
Gastrointestinal cancer	Biological studies into tumor mutations	11	Matrigel	10 days	Matano et al., 2015
Gastrointestinal cancer	Biological studies into tumor mutations	26	Matrigel	11 days	Mousavi et al., 2019
Gastrointestinal cancer	Biological studies	20	Matrigel	90 days	Sato et al., 2011
Gastrointestinal cancer	Biological studies	Not stated	Matrigel	As per Sato et al. (2011)	Schnalzger et al., 2019
Gastrointestinal cancer	Biobank establishment; high-throughput drug screening; biological studies into tumor mutations	20	Basement membrane extract	6 days	van de Wetering et al., 2015
Gastrointestinal cancer	Drug response in parallel with the clinic; biological studies	71	Agarose-coated plate and Matrigel	12 days	Vlachogiannis et al., 2018
Gastrointestinal cancer	Biological studies into tumor mutations	14	Matrigel	90 days	Weeber et al., 2015
Head and neck cancer	Drug and radiotherapy response	Not stated	ULA and Hanging-Drop	7 days	Hagemann et al., 2017
Head and neck cancer	Drug response; biological studies	10	Matrigel	30 days	Tanaka et al., 2018
Pancreatic cancer	Biological studies	10	Matrigel	6 months	Boj et al., 2015
Prostate cancer	Biological studies	24	Agarose-coated plate	14 days	Bansal et al., 2016
Prostate cancer	Biological studies	24	Matrigel	3–6 months	Bartucci et al., 2015, 2016
Prostate cancer	Biobank establishment; biological studies	3	Matrigel	14 days	Beshiri et al., 2018
Prostate cancer	Biological studies; establishment of new organoid lines	7	Matrigel	60 days	Gao et al., 2014
Prostate cancer	Drug response	109	ULA plates	Several months	Linxweiler et al., 2018
Prostate cancer	High-throughput drug screening; biological studies	34	Matrigel	12 months	Puca et al., 2018

developed PDOs from oropharyngeal and esophageal squamous cell carcinomas, highly heterogeneous and therapy resistant cancers (71.4% success rate) (Kijima et al., 2019). Over 3 weeks, the PDOs established mimicry of the original tumor through expression of p53, CD44, proliferation, and autophagy. The PDOs allowed the authors to mimic 5-fluorouracil therapy resistance in those patients associated with high CD44 expression and autophagy. Another study had a high establishment rate of >90% for breast cancer, however this rate dropped during 30 days expansion to ∼72% (Orditura et al., 2018). The authors found significant correlation between patients with PI3KA mutations and sensitivity to those inhibitory agents, elegantly addressing interpatient heterogeneity. Perhaps one of the most groundbreaking PDO studies displaying predictive clinical potential, is with PDOs form 110 patients with metastatic gastrointestinal cancer (70% success rate) (Vlachogiannis et al., 2018). Histological evaluations of the PDO and original tissue were similar, and in addition, there was a 96% similarity between the mutational spectrum of the original tumor and the PDO model. Spatiotemporal heterogeneity, and tumor evolution/resistance to treatments, was upheld in the model, with 88% positive predictive value in the clinic (**Figures 3E–H**) (Vlachogiannis et al., 2018).

Interestingly, prostate cancer has quite a low success rate for PDO propagation. In a long-term prostate PDO cultivation study, the authors compared metastatic tumors, PDX tumors, and PDO models derived from the same patient. Seven PDOs could be maintained for up to 2 months for ∼70% of soft

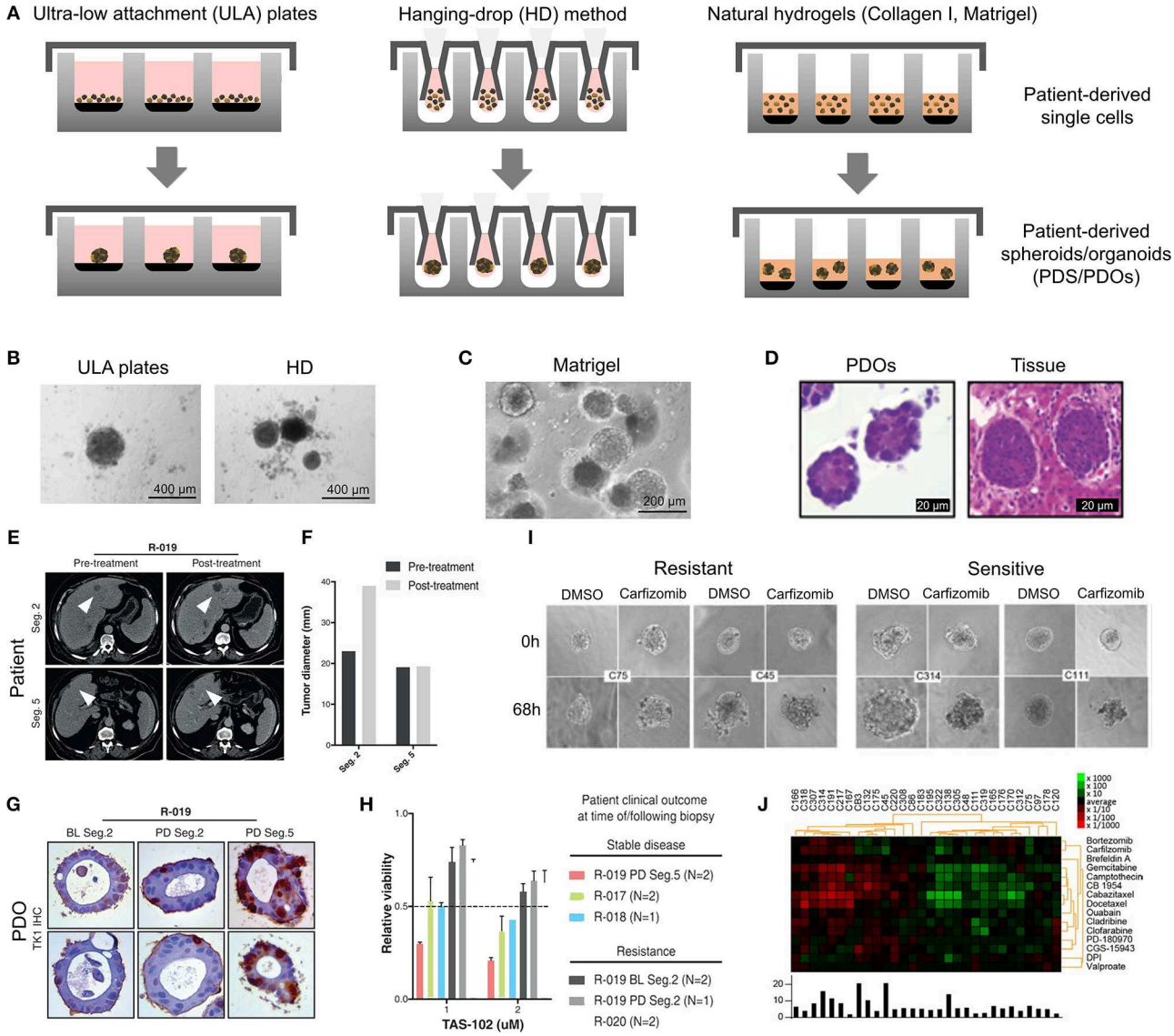

FIGURE 3 | Patient-derived organoids/spheroids (PDO/PDS). **(A)** Schematic diagram displaying the key techniques utilized in current literature for the culture of PDO and PDS. Left, ultra-low attachment (ULA) plates; Center, hanging drop method; Right, natural hydrogels. **(B)** Primary head and neck cancer cells can form consistent spheroids in ULA plates (left), but are not as reproducible in hanging drop culture (right) as visualized using phase contrast microscopy. **(C)** Phase contrast image of a colorectal cancer PDO cultured in Matrigel, and **(D)** hematoxylin and eosin staining comparing PDOs to their matching patient biopsy sample. **(E–H)** PDOs recapitulate intra- and interpatient heterogeneity in response to chemotherapeutics (TAS-102). **(E)** Spheroids were established from a patient with mixed response to TAS-102 with multiple metastases. **(F)** While the segment 2 metastasis rapidly progressed, the segment 5 metastasis remained stable upon TAS-102 treatment. **(G)** Thymidine kinase 1 (TK1) IHC expression is stronger in TAS-102-, compared to sensitive (segment 5) PDOs TAS-102-refractory (segment 2). BL, Core biopsy (baseline); PD, post-treatment (progressive disease). **(H)** There was no significant decrease in cell viability in PDOs in response to TAS-102 in resistant patients. **(I,J)** Diversity of sensitivities for drugs among colorectal cancer tissue-PDX spheroids assessed via high throughput screening. **(I)** Morphological changes after treatment with 100 nmol/L of carfilzomib. **(J)** Heat map and clustering analysis of the average IC50 of 15 drugs in the panel. **(B,C–J)** reproduced with permission from Hagemann et al. (2017), Vlachogiannis et al. (2018), and Kondo et al. (2018), respectively.

metastatic tumor biopsies and ∼30% of bone biopsies. However, efficiency of establishing "continuously" proliferative organoid cultures (>6 months) was ∼18%. The 3D organoid cultures mimicked the histological structures and marker expression present in the primary patient biopsy specimens, maintaining interpatient heterogeneity (Gao et al., 2014). Another study of HNSCC (Tanaka et al., 2018) also found low (30%) success rates using Matrigel, however the successful PDOs showed similar drug responses as displayed *in vivo*.

PDOs provide a valuable resource in the personalized medicine space and have the potential to model various cancer types. Most crucial when using patient-derived tissues, low tissue

quantities can still result in large numbers of testable organoids. The renewable resource that they offer as cryopreserved or live biobanks and the high correlations achieved between treatment response in the clinic and in the organoid model offers a highly accessible tool for drug screening. A key biotechnology development for the application of PDOs for pharmaceutical drug testing is the development of automated pipetting tools that can both create the organoid cultures and apply the drug panel (Kondo et al., 2018), screening thousands of drugs across spheroids (**Figures 3I,J**). While the variations that occur between batches of Matrigel hinder the reproducibility of the organoid cultures (Postovit, 2016), the engineering of various semi-synthetic and synthetic matrices (Bray et al., 2017, 2018; Romero-López et al., 2017; Wang et al., 2019) may be able to build a new platform from the bottom-up rather than starting with a complex microenvironment such as Matrigel. Moreover, the morphological and phenotypic differences in PDO behavior between Matrigel and collagen hydrogels (Cheung et al., 2013) reiterates that the microenvironmental cues are directing cell response, warranting careful consideration of matrices used. The lack of blood supply is a limitation in the growth potential of the PDO, however this could be brought together and integrated through novel multi-PDO chip-based platforms (Maschmeyer et al., 2015), or through the co-culture of organoid microenvironments (Birey et al., 2017).

Patient-Derived Explants

While PDOs exploit cells regrown in 3D, another patient-specific approach consists of culturing the tumor tissue collected upon surgery, either as organotypic explants or as tissue slice cultures. Advantageously, the 3D structure of the tumor remains intact with only macroscopic dissociation. Patient-derived microdissected explants (PDMEs) are usually minced into pieces prior to gentle dissociation into tissue fragments, while patient-derived organotypic tissue slices (OTS) are either sliced manually using a scalpel or using a specialized slicing instrument, such as a vibratome. The morphology, cell proliferation, and viability of tissues can be maintained using these techniques, although for a relatively short time (Davies et al., 2015; Koerfer et al., 2016; Naipal et al., 2016).

Patient-derived microdissected explants (PDMEs)

PDMEs are widely used for drug testing purposes. The primary tissue isolated from surgical specimens is mechanically disaggregated and mildly processed using enzymatic and collagenase digestion. Density centrifugation or sieving may then allow the isolation of micro- to milli-sizes fragments [40–100 μm fractions (Aref et al., 2018; Jenkins et al., 2018; Wang et al., 2018a), 300 μm (Holton et al., 2017), 1 mm^3 (Moore et al., 2018), 3 mm^3 (Carr et al., 2014; Cheah et al., 2017)]. A major benefit is that PDMEs do not require days or weeks of tissue manipulation, which is critical to rapid drug screening capabilities. Contrary to PDOs, which may be equally used for drug testing as well as mechanistic investigation, PDMEs have low proliferation indexes and cannot be cultured for more than several days, hence are usually not used for mechanistic investigation. Yet, because of ease of manipulation, their viability can be improved by systems such as microfluidics or bioreactors, pushing culturing times up to 7–10 days (Holton et al., 2017; Aref et al., 2018).

Overall, PDMEs offer a highly representative platform to be used to predict response to clinical therapy when taking the tumor microenvironment into account. Some examples include when it has been used to select chemotherapy in untreated, advanced or metastatic non-small cell lung cancer (NSCLC) (Nagourney et al., 2012). This strategy allowed a 2-fold improvement over historical control of 30%. PDMEs were also used successfully in prostate (Centenera et al., 2018; Risbridger et al., 2018) and breast cancer (Carranza-Torres et al., 2015), with 100% survival after 96 h. In some studies, the PDMEs were not simply immersed in media but sometimes placed on substrates such as titanium or stainless grids, or gelatin sponges (Geller et al., 1997; Centenera et al., 2012, 2013, 2018; Schiewer et al., 2012; Risbridger et al., 2018). This prevented cell outgrowth from tumor tissues, which may often occur, as seen in prostate cancer PDMEs for example, maintaining viability for up to one week of culture (Centenera et al., 2013). Importantly, unlike PDXs and PDOs, PDMEs still maintain stromal and immune cells, which enable drug screening in immuno-oncology, such as the immune checkpoint blockade (ICB), which is impossible for any other 3D approach that lack an immune compartment. This has been heavily investigated using microfluidic devices (Aref et al., 2018; Jenkins et al., 2018; Moore et al., 2018; Wang et al., 2018a).

The most significant disadvantage in PDMEs is the poor control of sizes used for experiments. Often, there is little control over dimensions and pieces are grossly cut. Even when the fragments are sieved, fractions still include large variations (with often more than 2-fold size differences) resulting in increased degrees of heterogeneity, which unnecessarily increases variability in drug responses, in a context where it should be kept to a minimum. In this respect, organotypic slices represent a much more reproducible way to culture explants for drug testing purposes.

Organotypic tissue slices (OTS)

OTS are thin sections prepared from whole tumor tissue, which are cultured either as floating pieces or on a supporting structure. Currently, OTS are best at taking into consideration intratumoral heterogeneity and the tumor-stromal interactions of *in vivo* tumors (Meijer et al., 2017). OTS are able to retain the complexity of the tissue environment, unlike the dissociation of tissue required for organoid culture, however only for a short amount of time. OTS contain the native cells that support heterogeneous phenotypes. Although OTS have many advantages, they have become less utilized in modern research. This is mostly due to a low number of samples that can be generated from biopsy tissue, their inability to be passaged, and the limited timeframe available to study the samples during culture.

OTS have mainly been used for the study of chemotherapeutic response to various cancer tissues (Holliday et al., 2013; Merz et al., 2013; Gerlach et al., 2014; Koerfer et al., 2016; Naipal et al., 2016). Automated slicing, via tissue slicers and vibratomes, has enabled the maintainance of tissue integrity and minimal handling of the tissue pieces, ensuring higher viability (Krumdieck et al., 1980). The thickness of slices needs

to allow for appropriate media perfusion but also maintain tissue architecture, most often this occurs around 300 μm (Risbridger et al., 2018). Some reports suggested that smaller tumors may need to be embedded in agarose gel prior to sectioning (Davies et al., 2015). Tumor texture also relates to its ease of slicing as soft, mucinous or fibrous tumor sections could not be sliced into sections <500 μm (Holliday et al., 2013; Gerlach et al., 2014; Naipal et al., 2016). Automated slicing has been used extensively in the preparation of OTS for NSCLC (Vaira et al., 2010; Davies et al., 2015), brain (van der Kuip et al., 2006; Holliday et al., 2013; Merz et al., 2013; Carranza-Torres et al., 2015; Davies et al., 2015; Naipal et al., 2016), colon (Vaira et al., 2010), prostate (Hällström et al., 2007; Vaira et al., 2010; Zhang et al., 2018b), HNSCC (Gerlach et al., 2014), and pancreatic tumor tissues (Lim et al., 2018; Misra et al., 2019).

OTS can be cultured in various ways, most often as floating in medium or supported by a membrane. The use of a supporting structure has been a key feature of OTS cultures for some time. In earlier publications this was served by titanium or stainless steel grids (Parrish et al., 2002; Hällström et al., 2007), and in more recent publications, by the Millipore cell culture inserts (Vaira et al., 2010; Merz et al., 2013; Gerlach et al., 2014; Koerfer et al., 2016; Misra et al., 2019). Some research groups also use gelatin sponges to support OTS cultures (Papini et al., 2007), to prevent an unrelated inflammatory response at the surface of each slice. As a comparison, Davies et al. (2015) maintained cultures for 72 h either floating in medium, or on a Millipore cell culture insert, before fixation and histological sectioning. OTS as floating pieces displayed alterations in their stress pathways and also a loss of tissue integrity, while these changes were not apparent for slices cultured on membranes. A local microenvironment was established at the point where the air and filter met, mimicking oxygen gradients as present in tumors *in situ*. For static floating cultures, it is suggested that a lack of oxygen and nutrient perfusion is most likely the reasoning behind short tissue viability (Davies et al., 2015). Floating cultures are often sustained for a longer time by using a rotating device to ensure perfusion (Pretlow et al., 1995; Naipal et al., 2016). Well-defined media supplementation (Naipal et al., 2016), or the use of autologous serum (Majumder et al., 2015), can also lead to longer culture durations or improved clinical relatability. Autologous serum, while highly relevant to interpatient heterogeneity, also contains a degree of variability arising from the patients' past clinical history (Majumder et al., 2015). The longest OTS culture durations we found to be published was by Merz et al. (2013) who prepared primary glioblastoma tissue slices to a thickness of 350 μm, on Millipore cell culture inserts. Twelve patient samples were able to maintain the original tumor structure and phenotype for a minimum of 16 days.

When incorporated into preclinical studies, OTS enable the quantitative evaluation of clinically relevant endpoints. Undoubtedly, the ability to visualize the effect of treatments on the tissue as an entire structure (undigested), including native tumor heterogeneity, provides a broader overview than with those techniques involving tissue digestion and reformation, albeit for a short duration. Additionally, the opportunity to culture tumor tissue alongside adjacent normal tissue allows for the testing of therapeutics that target malignant cells while not affecting the healthy surrounding cells. In future, to fully leverage the value of OTS, users may need to consider high-throughput live spinning disc and light-sheet confocal microscopy, which, when performed on entire OTS, will provide a significant advantage compared to static analysis. Such a technique will enable to observe temporal responses to drug treatments according to various spatial zones. This approach may report live cellular mechanisms according to drug responses to hopefully an even greater degree than seen with intravital microscopy on animals.

Scaffold-Based Approaches

Scaffolds-based systems provide a toolkit where both tumor and stroma-derived materials can be cultured. Using natural or synthetic matrices with tailorable chemical and physical cues, the influence of various microenvironmental factors may be studied. While innovative and more relevant strategies are constantly being reported, Matrigel is still today the gold standard in 3D cell culture of patient-derived materials, despite lack of tenability, and despite being derived from a mouse tumor ECM. Hereafter, we will focus on all other scaffold-based alternatives, with a focus on synthetic/semi-synthetic hydrogels and tissue-engineered scaffolds, or combination of the above (**Table 2**).

Hydrogels and Tissue-Engineered Scaffolds

Hydrogels

PDOs represent a significant improvement in the biomimetic culture of primary tumor cells. Yet one issue lies in the lack of malleable surrounding matrix that prohibits spatial control and controlled additions of multiple cell layers (Fong et al., 2016b). Semi-synthetic and synthetic materials offer inertness and therefore an ability for cells to deposit their own ECM rather than being cued to develop a specific phenotype or morphology. This means that decreased biomaterial heterogeneity is achievable when using synthetic materials, while Matrigel compounds patient heterogeneity with its own interscaffold and interbatch heterogeneity (Postovit, 2016). The state-of-the-art in 3D bioengineered models, pre-dominantly polyethylene glycol (PEG)-derived with a glycoprotein component, allows for control over added ECM proteins while supporting the development of natural matrix deposition. These approaches are being constantly improved and have resulted in the generation of novel materials, however applications toward primary patient-derived tumor cell cultures has been more rare (Li and Kumacheva, 2018).

Hribar et al. (2019) demonstrated the culture of glioblastoma and renal cell carcinoma within a photocrosslinkable hydrogel called VersaGel, a growth factor free platform with integrin binding sites and MMP degradability. VersaGel was demonstrated to support the growth of dissociated cells and tumor fragments from PDX samples or patient tissue. Prior culture in ULA flasks promoted spheroid formation before being plated and into VersaGel. Gels incubated in conditioned media from the original ULA spheroid cultures resulted in an invasive phenotype of the renal cancer PDX tissue while fresh media resulted in more tightly packed spheroids. Five patient samples of glioblastoma were also cultured within the VersaGel

TABLE 2 | Overview of scaffold-based tumor models from patient-derived materials.

Main cancer type	Purpose and application	Patient numbers	Method	Stromal cell components	Maximum culture time	References
HYDROGEL-BASED						
Acute myeloid leukemia	Drug response; biological studies	3	PEG-Heparin hydrogels	HUVECs and MSCs	14 days	Bray et al., 2017
Appendiceal cancer	Drug response; immunotherapy testing	12	HA-Collagen hydrogels	Lymph node cells	11 days	Votanopoulos et al., 2018
Brain cancer and kidney cancer	Drug response in parallel with the clinic	5	VersaGel	–	15 days	Hribar et al., 2019
Breast cancer	Biological studies into matrix deposition	Not stated	Gelatin porous microbeads cultured in a spinning flask	CAFs and normal fibroblasts	12 days	Brancato et al., 2017
Breast cancer and brain metastasis	Biological studies into cancer cell migration	15	Cells were pre-grown in 2D, cell aggregation using nucleo-pore filters membrane; PEG-HA-Collagen hydrogels	CAFs from normal, primary, and brain metastatic samples	4 weeks	Chung et al., 2017
Breast cancer	Biological studies	Not stated	Gelatin cryogels (GelMA)	CAFs	3 days	Zhang et al., 2017
Liver cancer	Drug response; biological studies	16 PDX tumor samples	MA-HPC sponges	–	20 days	Fong et al., 2018
Lung cancer	Drug response	2	Collagen-HA hydrogels	–	5 weeks	Mazzocchi et al., 2019
Multiple Myeloma	Biological studies	Not stated	Fibrinogen gels, PLGA microspheres, Aligimatrix, and Matrigel	HUVECs and stromal cells from MM patients	7 days	de la Puente et al., 2015
Prostate cancer	Drug response	2 PDX tumor samples	PEG-HA hydrogels	–	14 days	Fong et al., 2014
TISSUE-ENGINEERED SCAFFOLDS						
Breast cancer	Drug response; biological studies	4	PCL porous scaffold	Immortalized CAFs were pre-cultured on PCL scaffolds and then decellularized	10 days	Nayak et al., 2019
Prostate cancer	Biological studies	3	PCL scaffolds and Matrigel	Osteoblasts	3 weeks	Shokoohmand et al., 2019
Prostate cancer	Drug response; biological studies	2 PDX tumor samples	PCL scaffolds	Osteoblasts	30 days	Paindelli et al., 2019
Prostate cancer	Biological studies in ECM remodeling	14 matched fibroblast samples	PCL scaffolds	CAFs and mast cells	2 days of co-culture	Pereira et al., 2019

CAFs, cancer-associated fibroblasts; ECM, extracellular matrix; HA, hyaluronan; HUVEC, human umbilical vein endothelial cells; PEG, polyethylene glycol; PCL, polycaprolactone; PDX, patient-derived xenograft; PLGA, poly(lactic-co-glycolic acid); MA-HPC, methacrylate-hydroxypropylcellulose; MSCs, mesenchymal stem cells.

and exposed to temozolomide, a first-line chemotherapy treatment for glioblastoma. The response was compared with Matrigel, finding that while VersaGel therapeutic response correlated with all five patient clinical responses, Matrigel culture correlated with only three out of the five patients. A combinatory hydrogel approach was used by others (Mazzocchi et al., 2019) to culture two lung cancer samples, isolated from pleural effusion, the excess fluid found between the pleura and lungs. The hydrogels were composed of methacrylated collagen I and thiolated HA, using UV polymerization. Cultures were maintained for 6 weeks and preserved the heterogeneity of the cell populations, and chemotherapeutic treatment was less effective on gels compared to 2D cultures. In another combined hydrogel approach, HA-collagen hydrogel models were created from 12 patients with appendiceal cancer (Votanopoulos et al., 2018). In some cultures, the researchers added cells derived from the patient's lymph nodes in addition to the tumor samples from the same patient to "immune enhance" the culture. From the 12 patients, 75% of the cultures could be established. The high-grade tumors demonstrated tissue-like structures within the hydrogels, whereas the low-grade tumors showed more spread out cells/organoids. Interestingly, the low-grade tumors did not respond to chemotherapy, while the high-grade tumors had a variable response. In the tumors co-cultured with lymph node cells, increased mitochondrial metabolic activity was demonstrated in organoids treated with immunotherapeutics, 24 h after first exposure. However, 96 h after exposure, decreased mitochondrial metabolism was seen in the treatment groups. These interactions with immune cells are a key part of recapitulating the tumor microenvironment, especially in immunotherapy research. Tam et al. (2018) developed a metastatic lung cancer model using a biomimetic

hydrogel platform also containing HA (**Figures 4A–C**). To mimic the viscoelastic features of lung tissue, methylcellulose was added to the 3D model. MMP-mediated cell migration and invasion was accounted for by including collagen-I-derived peptide crosslinkers that could be enzymatically degraded by cell-secreted MMPs. The researchers modified their culture platform to develop a 384-well format in order to enable high-throughput drug screening, a key priority for the future of patient-specific *ex vivo* models.

A fusion of PDX samples and tissue engineering was performed by Fong et al. (2014). Immediately after the PDX prostate tumor dissociation, the cell pellets were resuspended in HA-PEG hydrogels, where the PEG component had been modified with the tripeptide Arg-Gly-Asp (RGD) and MMP-cleavable sequences. In some cases, the PDX samples were co-encapsulated with MC3T3-E1 osteoblastic cells. In the model, the osteoblastic cells spread over time, while the PDX prostate cancer samples remained as aggregates. The co-culture resulted in higher proliferation than the individual mono-cultures, demonstrating effective cell-cell signaling within the model. Moreover, this study demonstrated strong structural and phenotypic similarities between the original patient tumor, the murine PDX model and the *in vitro* hydrogel model. Fong et al. later published a novel microporous hydrogel sponge derived from hydroxypropylcellulose methacrylate to culture 16 liver cancer PDX samples. Of those 16 samples, two were not viable within the system, suggesting tumor diversity amongst the samples (Fong et al., 2018). In our own work, we have previously used semi-synthetic PEG-heparin hydrogels for the culture of patient-derived samples (Chwalek et al., 2014; Bray et al., 2015, 2018; Taubenberger et al., 2016).

Most recently, we published a study investigating the growth of human acute myeloid leukemia (AML) cells within these hydrogels and treated them with first-line chemotherapy (**Figures 4I–K**) (Bray et al., 2017). Cell lines and primary AML cells derived from the peripheral blood of three patients displayed a tendency to grow along the vascular network derived from human umbilical vein endothelial cells (HUVECs) and MSCs. However, while the cell lines proliferated throughout the culture, the primary AML cells were maintained but not propagated. Cultures were maintained for 7 days before chemotherapy treatment, with varied results between donors. A study from de la Puente et al. (2015) developed a multi-cellular culture of multiple myeloma cells, stromal cells (derived from multiple myeloma patients), and HUVECs using fibrinogen hydrogels. The fibrinogen was compared with poly(lactic-co-glycolic acid) (PLGA) microspheres, AlgiMatrix, and Matrigel. Using the fibrinogen model, the authors found that the co-culture of patient-derived multiple myeloma (MM) cells with stromal cells resulted in increased proliferation of MM cells, this further increased when the endothelial cells were also added, showing the importance of adding supporting cell types to tumor microenvironment models. This is an interesting finding, as MM cells are notoriously difficult to cultivate using 2D conditions, and most often do not grow at all *ex vivo*. When looking at other matrix types, PLGA microspheres did not support patient-derived MM proliferation, AlgiMatrix, and Matrigel supported a small amount of MM proliferation, while the fibrinogen scaffolds supported a 250% increase in the proliferation of three patient MM samples, perhaps due to it being a natural component of blood and marrow plasma. These scaffolds also created oxygen gradients, whereby higher levels of hypoxia-inducible factor 1-alpha (HIF1α) and pimonidazole were found in the lower layer of the scaffold, while drug penetration was reversely correlated with scaffold depth.

In the glioblastoma research field, progress in 3D tumor modeling has occurred using synthetic PEG hydrogels combined with alginate microfibers (**Figures 4D–H**) (Wang et al., 2019). The researchers utilized a patient-derived adult glioblastoma xenograft cell line (D-270 MG) combined with a mouse brain microvascular endothelial cell line. The tumor cells were resuspended in a PEG-HA hydrogel precursor solution with MMP cleavable and RGD peptides. These tumor cells were then either co-cultured with acellular alginate microfibers (formed via photocrosslinking) or with the endothelial cell line pre-suspended in the alginate solution. These endothelial monolayers were well-formed in monoculture, however were disorganized and cells became rounded in co-cultures with tumor cells. After 14 days, glioblastoma tumors near the endothelial channels were more spherical, while those tumors in monoculture were more migratory. However, the use of mouse endothelial cells with human glioblastoma cells will not provide a realistic response. It is also worthwhile to note that the microfiber channels created did not allow for perfusion or flow. Nonetheless, the spatial organization of the capillary structures with the combination of hydrogel materials allows for the reconstruction of a useful *in vitro* model. Future studies with perfusable capillaries would enable analysis from the perspective of nutrient and oxygen delivery to the tumor.

The recapitulation of the tumor microenvironment goes beyond the culture of tumor cells. A recent study used gelatin porous microbeads to create either microtissue constructs or produce spheroids (Brancato et al., 2017). CAFs or normal fibroblasts were loaded together with the microbeads into a spinning flask or seeded into round bottom, non-treated 96-well plates in methylcellulose solution and maintained for up to 12 days. The biophysical properties of the methylcellulose models were relatively similar between CAFs and normal fibroblasts, however marked differences were apparent when cultured on the microbeads, highlighting the importance of structural considerations in model development. There was an increase in matrix deposition by the CAFs, a higher proliferation rate and a higher stiffness of microtissue compared to that created by the normal fibroblasts. Additionally, cryogels can be created by forming hydrogels below the melting point of a solvent. Cryogels formed from PEG-heparin have been reported by our group (Bray et al., 2018), where they were used to create a bone microenvironment using mineralized primary human osteoblasts for co-culture with breast cancer cells lines. Another study utilized a gelatin-based cryogel modified with methacrylate groups (GelMA) (Zhang et al., 2017). The authors used the cryogels to create a tumor stromal microenvironment using CAFs derived from breast cancer patients, showing increased cancer cell migration compared to their mono-cultures. CAFs

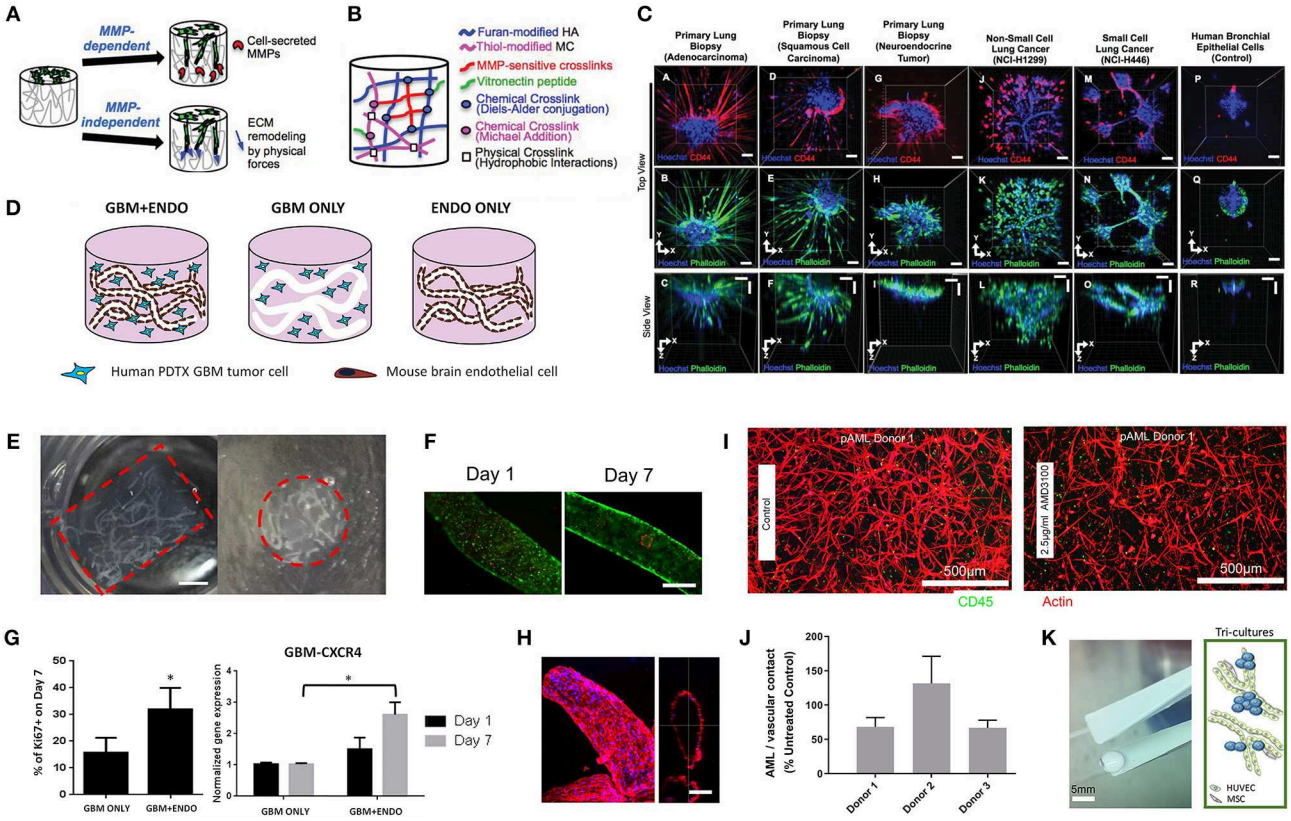

FIGURE 4 | Hydrogel culture approaches. **(A–C)** Rationally designed 3D hydrogels model normal and malignant lung tissue. **(A)** Schematic of potential cell invasion mechanisms. **(B)** Schematic of the composition of biomimetic stimuli-responsive 3D hyaluronan (HA) hydrogels. **(C)** Lung cancer cells express CD44 and show varying invasiveness into 3D HA hydrogels. (A–I) Primary cells isolated and cultured from three separate lung carcinoma biopsies identified as (A–C) adenocarcinoma, (D–F) squamous cell carcinoma, and (G–I) neuroendocrine tumor. (J–L) Non-small cell lung cancer and (M–O) small cell lung cancer cells. (P–R) Healthy human bronchial epithelial control cells do not invade into 3D hydrogels. (A,D,G,J,M) Lung cancer cells express CD44, while (P) healthy bronchial epithelial cells do not. (D–H) Combination approach to mimicking glioblastoma using PDX derived cell lines. **(D)** Schematic of hydrogel/microfiber structure and cellular combinations. **(E)** Cross-sectional views of encapsulated alginate microfibers in 3D hydrogels. Left = side view. Right = top view. Red = hydrogel edge. Scale bar = 2 mm. **(F)** Live (green) and dead (red) staining of endothelial cells after 7 days in cultures. **(G)** Co-culture with mouse endothelial cells increased glioblastoma proliferation via Ki67 staining ($n = 150$) (left), and increased expression of CXCR4 in glioblastoma tumor cells (right). $^*p < 0.05$. **(H)** Confocal image demonstrating CD31 expression from HUVECs within alginate microfibres. **(I–K)** 3D culture of acute myeloid leukemia using starPEG-heparin hydrogels. **(I)** AML cells from a patient with AML untreated (left) or treated with 2.5 μg/mL AMD3100 (right), co-cultured with HUVECs and MSCs. **(J)** Percentage of AML contact with HUVECs and MSCs decreased after AMD3100 treatment in two out of three donors, compared with the untreated control sample. Means ± SD (variability within experiment, $n = 1$). **(K)** A biohybrid starPEG-heparin hydrogel for the culture of AML mono-cultures and tri-cultures with HUVECs and bone marrow-derived MSCs. Scale bar = 5 mm. **(A–K)** reproduced with permission from Tam et al. (2018), Wang et al. (2019), and Bray et al. (2017), respectively.

were also utilized by others (Chung et al., 2017) to study their effects on breast cancer primary and brain metastatic cell migration. Using a PEG-HA-Collagen hydrogel, they found that significantly higher numbers of patient-derived tumor cells migrated toward CAFs derived from brain metastatic samples, supporting the theory of the pre-metastatic niche and highlighting the effectiveness of such cytokine gradients in cancer cell attraction.

The creation of these microenvironmental changes that a local tissue undergoes during malignant transformation is an important and often overlooked aspect of tumor engineering, which needs to be incorporated in cancer modeling. Nonetheless, it should be noted that despite what a researcher may gain in reproducibility using semi-synthetic and synthetic hydrogel matrices, including decreased material interference, there is a loss of rich ECM components that are found in Matrigel. Therefore, it must be ensured that these synthetic models are fully characterized to determine that interpatient and intertumoral heterogeneities are maintained similarly to Matrigel-based models. The most suitable ECM recapitulation *in vitro* depends on the tissue of choice. Collagen would be the most significant component of many tumor tissues, including breast, prostate and colorectal regions. Aside from collagens, ECM contributions also arise from proteoglycans, laminins, and fibronectin, all significant in the context of tumor progression. Applications for heparin and HA-derived hydrogels were described above, however further work could be performed to include other glycosaminoglycans such as chondroitin sulfate

in the engineering of semi-synthetic hydrogel materials. In the tissue engineering space, it has also been possible to integrate peptide motifs into synthetic materials to mimic collagen I (GFOGER), laminin-111 (IKVAV), and fibronectin (RGD) for ECM mimicry (Taubenberger et al., 2016), however these were not tested using patient-derived tissues. In some cases, the incorporation of ECM components into synthetic hydrogels may not be necessary if included supporting cells are able to deposit their own matrix readily.

Tissue-engineered scaffolds

Scaffolds applied to the engineering of tumor microenvironments are based on natural or synthetic polymers which offer a high degree of tailorability for a targeted microenvironment. Constructs made from natural polymers (alginate, chitosan) offer low toxicity with components similar to natural ECM, yet have weak mechanical properties and limited options for fine-tuning of degradability or chemistry. Synthetic constructs can be made from medical-grade polymers (polycaprolactone (PCL) and PLGA-based) that offer more reproducibility and tailoring options in terms of chemical and mechanical properties.

While hydrogels are more relevant to mimic soft tumors, hard scaffolds may suit better tumor sites with higher stiffness, such as hard bone, which stiffness range from 2 to 10 GPa (Qiao and Tang, 2018). Medical grade PCL (mPCL) has been widely used for bone tissue engineering applications due to suitable viscoelastic properties and low melting temperature enabling easy processing into various scaffold architectures (Woodruff and Hutmacher, 2010). While this has been heavily investigated for *in vivo* applications, mPCL is now also used in *in vitro* cancer models, mostly printed as microfiber 3D architectures enabling seeding and culture of bone cells. In our work (Shokoohmand et al., 2016, 2019; Bock et al., 2019), we have used melt electrospinning combined with additive manufacturing ("melt electrowriting") to print mPCL microfibers into linear or tubular porous scaffolds populated with primary osteoprogenitors isolated from human bone tissue (**Figures 5A–C**). By coating the fibers with calcium phosphate and using osteogenic differentiation media, the resulting osteoblast-derived microtissues contained osteoblastic and osteocytic cells with abundant key ECM deposition. The patient-derived microtissues were used as an *in vitro* mineralized model platform to study prostate cancer growth in bone, by co-culturing cancer lines (Bock et al., 2019) and PDXs (Shokoohmand et al., 2019). In the PDX study (**Figures 5D–I**), prostate cancer PDX models were used; from lymph node metastasis (LuCaP35) and bone metastasis (BM18). PDXs were supported by Matrigel in the center of the tubular osteoblast-derived microtissues and cultured for 3 weeks. The co-culture generated bone mimicry of both PDXs at the gene, protein and mineralization levels. Interestingly, while the PDX co-cultures were done with microtissues made from the osteoprogenitor cells from only one donor, the study reported that the microtissues were initially made with cells from three different donors. While reproducible for cells from one patient, the bone microtissues showed donor heterogeneity, with one patient displaying poor mineralization of the construct, which was explained by a severely obese BMI. These results spoke of the importance of using primary cells in 3D culture system models to ensure tissue engineering of a relevant patient-specific context. In future, Matrigel could be replaced by attractive synthetic options such GelMA, to avoid a murine component in this otherwise fully human model. Using a similar scaffold design as in Bock et al. (2019), melt mPCL electrowritten scaffolds were used to create a osteoblast-like microenvironment, although using differentiated immortalized human MSCs (**Figures 5J–M**). Two patient-derived PDX samples were dissociated and cultured on top of the mineralized microtissue up to 50 days for 1 patient and 30 days for the other. PDX cells from neither donor survived when the construct was stroma-free. This indicates the need for stromal context to support longer term cultures of patient-derived components (Paindelli et al., 2019).

Melt electrowritten mPCL scaffolds were also used to culture prostate CAFs and normal fibroblasts and facilitate ECM deposition to create a microtissue construct with stromal context (Pereira et al., 2019). It was reported that BPH-1 benign prostate hyperplasia epithelial cells altered their sphericity, orientation and cell length when cultured on the CAF microtissues when compared with normal prostate fibroblasts. Similarly, Nayak et al. (2019) utilized a PCL porous scaffold, created via a salt leaching technique, to culture two patient-derived breast cancer specimens with an ECM matrix deposited by immortalized CAFs. In this instance, the PCL scaffold with CAFs was decellularized after ECM deposition. The presence of the CAF ECM increased the breast cancer epithelial cells viability and cell-matrix interactions when compared with bare PCL scaffolds. The drug response of the breast cancer cells varied between patients, indicating maintained interpatient heterogeneity (Pereira et al., 2019).

Additive Biomanufacturing/3D Bioprinting

Most scaffold-based or scaffold-free approaches to design 3D *in vitro* tumor models present limitations such as limited control over cellular and matrix patterning, limited simultaneous deposition of multiple cell populations and/or ECM types, low throughput, manual production, and batch-to-batch variability. Additive biomanufacturing, or bioprinting, is a versatile alternative that allows the reproducible manufacturing of complex, spatially-defined 3D biostructures (Li et al., 2018a). Traditionally, 3D bioprinting can be achieved by extrusion, inkjet or laser assisted (Albritton and Miller, 2017; Tsai et al., 2017). Comprising multiple cell types or tissues, bioprinted multicellular models can more truthfully recreate specific microenvironments for modeling of both normal and diseased tissues (Ma et al., 2018). Most recently, this versatile technology has enabled the generation of more reproducible and complex *in vitro* cancer models (Knowlton et al., 2015; Zhang et al., 2016; Albritton and Miller, 2017; Ma et al., 2018), by simultaneously printing multicellular cancer and stromal compartments. Initially though and still currently, bioprinted systems are heavily composed of cell lines. Yet, a small portion of studies are starting to display patient-specific components, found either in the cancer (Langer et al., 2019) (rarer) or stromal (Zhou et al., 2016; Wang et al., 2018b) compartments and has enabled the assessment of

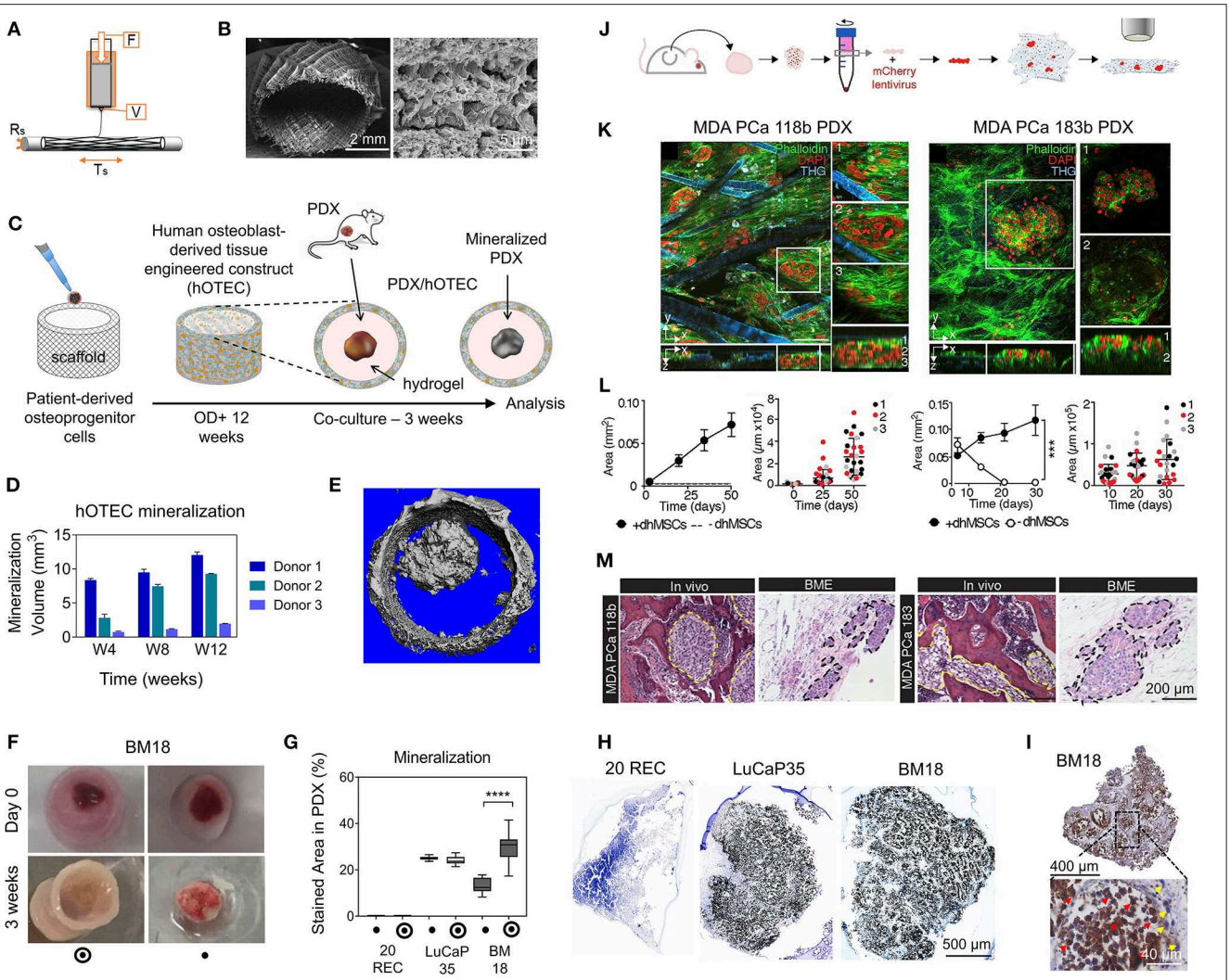

FIGURE 5 | Tissue-engineered model approaches combining scaffolds, patient-derived materials, and primary cells. **(A–I)** prostate cancer (PCa) PDX osteomimicry when co-cultured with a patient-derived mineralized microtissue scaffold. **(A)** Schematic of melt electrowriting of medical grade polycaprolactone (mPCL) into a porous tubular microfiber scaffold. **(B)** SEM images of mPCL scaffold after calcium phosphate treatment to induce osteogenic properties. **(C)** Scaffold seeding with patient-derived osteoprogenitor cells, cultured for 12 weeks under osteogenic differentiation leading to a human osteoblast-derived tissue engineered construct (hOTEC), followed by co-culture with PDX for 3 weeks. **(D)** Mineralization differences in hOTECs according to patients. **(E)** Micro-computed tomography image of bone metastasis-derived PCa PDX (BM18) in co-culture with hOTEC shows high mineralization of both hOTEC and PDX mass after 3 weeks (Mean ± SE). **(F)** Photographs of BM18 PDX, cultured either alone or co-cultured with hOTEC at day 0 and after 3 weeks of culture. **(G)** Mineralization quantification from von Kossa staining inside PDX, shows that BM18 became more mineralized than lymph node-derived PCa PDX (LuCaP35) and endometrial cancer metastasis-derived PDX (20REC), in the presence of hOTEC. **(H)** Von Kossa staining shows strong mineralization in PCa PDXs (BM18 and LuCaP35) but no mineralization in the control endometrial PDX (20REC). **(I)** NuMA staining in BM18 PDX shows a majority of human cells (>75%, red arrows = human, yellow arrows = mouse). **(J–M)** PCa PDX-derived cells growth in a bone mimetic environment (BME). **(J)** Process schematic; PCa PDX (MDA PCa 118b and 183) were extracted from mice, dissociated in single cells, and transfected with mCherry lentivirus prior to co-culture on an osteoblast-derived microtissue made from melt electrowritten mPCL porous scaffolds populated with immortalized human MSCs differentiated into osteoblasts (dhMSCs) for 30 days prior to co-culture. **(K)** Multiphoton microscopy of tumor cells co-cultured with dhMSC scaffolds. **(L)** Growth areas of tumor cells on scaffolds ± dhMSCs shows no survival without dhMSCs and increase in the presence of dhMSCs. **(M)** Histology of MDA PCa 118b and MDA PCa 183 in bone and BME. Yellow and black dashed lines outline the tumor areas. **(A–M)** reproduced with permission from Shokoohmand et al. (2019) and Paindelli et al. (2019), respectively. ****$P < 0.0001$.

patient specificity and microenvironment heterogeneity better than previously simplified 3D systems.

In a 2019 key study in the field (**Figures 6A–G**), Langer et al. used a Organovo's Novogen MMX bioprinter platform to print millimeter-size scaffold-free structures composed of a cancer core surrounded by patient-derived stromal cell types (**Figures 6A–D**) (Langer et al., 2019). A pancreatic cancer PDX cell line (OPTR3099C) and two primary patient tumor (OPTR) tissues were used for the inner core. The stromal component, comprising the outer core, was half primary with

a composition of HUVECs mixed with primary pancreatic stellate cells (PSCs). The hydrogel was made of an alginate-containing gelatin hydrogel, and designed to dissolve after 48 h in culture at 37°C. The OPTR/stromal bioprints recapitulated the morphological structures of the corresponding PDX analog and primary tissue. Signal heterogeneity was also recapitulated by assessing pS6 staining, a readout of mTOR signaling. However, the tumor tissue and original PDX showed clear pS6 staining not only in the cancer cells, but also in the surrounding stroma, but was not seen in the bioprints (**Figure 6E**). Heterogeneous staining within cancer cell areas was similar between bioprints, PDX, and primary tissue. Overall, all bioprinted tumor models displayed low (<10%) levels of proliferative cells (assessed by Ki67+, **Figures 6F,G**), similar to native tissues. While viability was not assessed, the addition of various cells or different drug treatments showed quantifiable effects more akin to the clinical scenario. For example, the use of PSCs in the stromal mixture showed a more reactive ECM-rich tumor microenvironment, and the efficacy of drugs such as dactolisib (a PI3K inhibitor) was reduced with the addition of fibroblast conditioned-media. This was anticipated as it has been suggested in the past that paracrine factors from fibroblasts may contribute to dactolisib therapeutic resistance, which was recapitulated in the bioprints. In summary, this "vitrine" study suggested the possibility to capture heterogeneity in therapeutic response, migration, and signaling using a combination of patient-derived materials and supportive cell lines (Langer et al., 2019).

Other bioprinted systems have used cancer cell lines but have used bioprinted stromal compartments with primary cells. This strategy is relevant when the focus is the study of cancer/stroma interactions. This was adopted in a breast cancer bone metastasis model with bone marrow (BM)-MSCs printed in various photocurable GelMA bioinks (**Figure 6H**) (Zhou et al., 2016). In co-culture, the BM-MSCs increased the proliferation of cancer cells and vascular endothelial growth factor expression, while reciprocal effects involved reduction of alkaline phosphatase activity in BM-MSCs. Similar results were seen in both MSCs and an osteoblast cell line (hFOB 1.19). However, when comparing the viability between the osteoblast cell line bioprint vs. primary BM-MSCs, the latter were significantly damaged by the process, with >75% of dead cells upon bioprinting in all GelMA bioink variants (**Figure 6I**), which was less for the osteoblast cell line (Zhou et al., 2016). This result suggested that primary cells may be more sensitive than cell lines for bioprinting, warranting a thorough viability assessment for bioprinted models.

In another breast cancer study (**Figures 6J,K**), dual hydrogel-based bioinks were extruded to have a cancer cell line core and a stroma shell made of primary adipose-derived MSCs (ADMSCs) with various layer sizes (Wang et al., 2018b). Both compartments were printed successively, and with different biomaterials properties. Overall, the bioinks contained HA and gelatin, that were methacrylated or not. A softer mixture (leading to ∼400 Pa) was used for the cancer cells while a higher concentration of the components (leading to ∼1,000 Pa) was used for the ADMSC gels to promote cell spreading. Overall, HA and gelatin, without modification, were used to increase the viscosity and printability and maintain the softness of the bioprinted constructs for cell migration. Heterogeneity here was addressed from the structural point of view by varying the thickness of the stromal layer (thin: 0.4, moderate: 0.8, thick: 1.2 mm) mimicking obesity status. After culturing for 21 days, doxorubicin (DOX) and LOX inhibitor responses were assessed for 3 days. Apoptosis rates were lower for the moderate and thick ADMSC layers. Interestingly, LOX, which drives the cross-linking of collagen and elastin and is negatively associated to breast cancer progression, was expressed regardless of changes in the ADMSC layer thickness or DOX administration. However, qPCR results showed that a thicker ADMSC layer upregulated multidrug resistance-related genes such as ABCC1, ABCB1, and ABCG1, which were accordingly reduced in the presence of the LOX inhibitor but only significantly in the moderate ADMSC layer (**Figure 6K**). Finally, the researchers showed that ADMSCs rather than hypoxia (as measured by HIF1α) was the major contributor to drug resistance (Wang et al., 2018b).

In a recent glioblastoma study, dissociated tumor-initiating cells (TICs) mixed with 2% HA were extruded in macroscopic alginate tubes (400 μm, **Figures 6L,M**) (Li et al., 2018b). The cells filled the tubes within 7 days (**Figure 6N**) with over 30-fold expansion and high viability (**Figure 6O**). The elegance of this simple system enabled to expand and culture the TICs up to 10 passages with neither viability issues (>95% live), nor phenotypic changes. Upon growth factor removal, the TICs successfully differentiated into neuron and glial cells, expressing Tuj1+ and GFAP+, respectively (**Figure 6P**). This study highlights how the combination of a simple extrusion system and the appropriate choice of biomaterials were able to relevantly support the expansion, phenotype, and differentiation of primary-derived tumor stem cells (Li et al., 2018b).

While still in its infancy, 3D bioprinting warrants significant advances in the field by enabling both heterogeneity and complexity. With the ability to print multiscale ECM-like biomaterials, heterogeneous and more comprehensive tumor microenvironments that include gradients can be reproducibly recreated (Albritton and Miller, 2017). Ideally, bioinks that present a high degree of physicochemical functionalization may be preferred for the printing of patient-derived tissues, so that stiffness and additional tumor ECM may be tailored to more closely mimic native microenvironments.

System-Based Approaches

One of the challenges in the culture of 3D culture models resides in static systems. In fact, while 3D tumors initially resemble *in vivo* samples, the lack of a dynamic microenvironment rapidly impacts cell proliferation due to mass transport limitations (Hirt et al., 2015). Dynamic systems such as rotary cell culture system (RCCS) bioreactors have been widely used in the general field of tissue engineering (Martin et al., 2004) and offer improved mass transfer and shear stress. In tumor engineering, such parameters are critical to recapitulate the native microenvironment that experiences local mechanical stresses. Similarly, this can be achieved by microfluidic systems (Sung and Beebe, 2014). With perfusion, the system provides continuous nutrient supply and waste removal, in turn maintaining a more stable culture environment, and enables to quantify transport parameters more

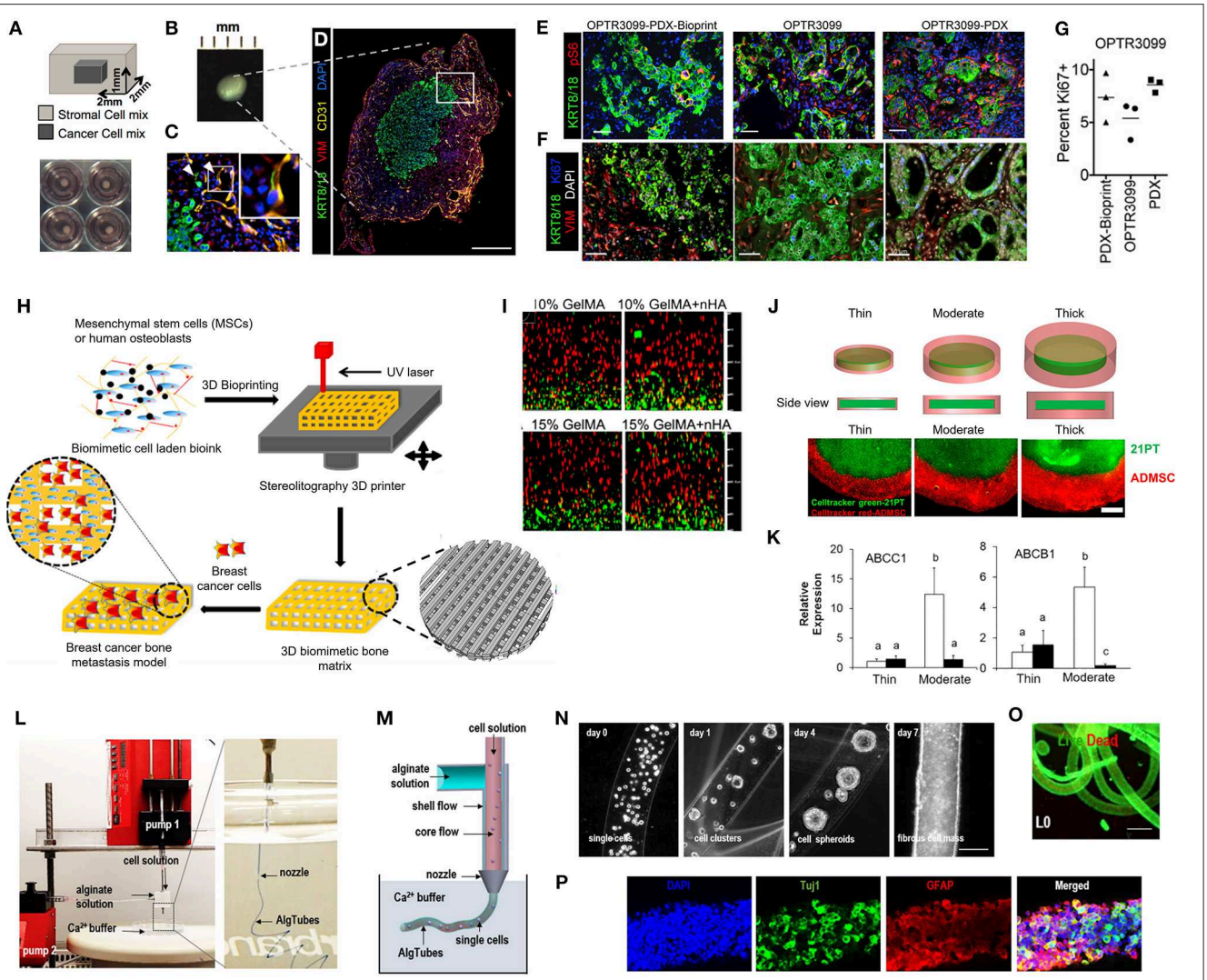

FIGURE 6 | Bioprinting with patient-derived materials and primary cells. **(A–G)** Bioprinted tissues from pancreatic patient-derived xenograft PDX-derived materials surrounding by a mixture of primary stellate cells (PSCs) and human umbilical vein endothelial cells (HUVECs) and comparison with original tissue. **(A)** Schematic of bioprint structure and photographs of bioprints in normal tissue culture plates. **(B)** Photograph of individual bioprint. **(C,D)** Low and high magnification of immunofluorescence (IF) images of bioprints from PDX-derived cell line after 7 days in culture, showing KRT8/18 (cancer cells) in green, vimentin (VIM, stroma) in red and CD31 (vasculature) in yellow, and DAPI (nuclei) in blue. **(E)** IF for KRT8/18 (green), pS6 (red), and DAPI (blue) of OPTR3099-PDX-Bioprint tissue (PSCs and HUVECs in the stromal compartment with disassociated PDX tumor tissue generated from OPTR3099 in the cancer compartment), primary patient tissue from OPTR3099, and PDX tumor tissue generated from OPTR3099 (OPTR3099-PDX). **(F)** Similar tissue to **(E)**, except that IF is for KRT8/18 (green), VIM (red), Ki67 (blue), and DAPI (gray). **(G)** Ki67+ quantification of the percentage of Ki67+/KRT8/18+ dual positive cells shown in **(F)**, $n = 3$ random fields of view, $N = 1$ PDX bioprint. **(H,I)** Bioprinted breast cancer bone metastasis model. **(H)** Schematic of primary mesenchymal or osteoblast cell line-laden GelMa-based 3D bioprint from stereolithography and further co-culture with breast cancer cell lines. Four groups were used, containing either 10 or 15% GelMA ± nanohydroxyapatite powder (nHA). Insert shows CAD model of the 3D matrix (gray) and 3D surface plot of the bioprinted matrix (colored image). **(I)** Confocal micrographs of mesenchymal stem cells (MSCs)-laden 3D bioprints 1 day post printing (cross-sectional views) for each bioprint group. Live (green) and dead (red) cells. Over 75% of cells were dead after bioprinting. **(J,K)** Bioprinted primary breast cancer model. **(J)** 21PT breast cancer line cells were first bioprinted in a photocrosslinkable gel followed by printing hydrogels of primary adipose derived MSCs (ADMSCs) around the cancer cell gel, with various thicknesses. ADMSCs in the edge region were labeled by cell tracker red, and 21PT in the middle region were labeled by cell tracker green (fluorescence images). **(K)** qPCR analysis of adenosine triphosphate (ATP)-binding cassette transporter gene expression of the bioprinted constructs with and without the lysyl oxidase (LOX) inhibitor, $n = 3$. **(L–P)** Glioblastoma tumor-initiating cells (TICs) culture in alginate hydrogel tubes (AlgTubes). **(L)** Images of extrusion system. **(M)** Schematic of AlgTubes production. **(N)** TIC growth in AlgTubes. Scale bar: 200 μm. **(O)** Live/dead staining of day 7 cells in AlgTubes. Scale bar: 400 μm. **(P)** *In vitro* differentiation of TICs after 10 passages. Scale bar: 100 μm. **(A–P)** reproduced with permission from Zhou et al. (2016), Wang et al. (2018b), Langer et al. (2019) and Li et al. (2018b), respectively.

readily (Avendano et al., 2019). With advanced microfluidic systems, such as organs-on-a-chip (Bhatia and Ingber, 2014), such properties can be combined with additional stromal components enabling the study of drug responses in dynamic contexts that incorporate spatiotemporal and biochemical heterogeneities (**Table 3**).

TABLE 3 | Overview of microfluidic-based tumor models using patient-derived materials.

Main cancer type	Purpose and application	Tumor model used	Patient numbers	Supporting matrix	Stromal cell components	Device	Maximum culture time	References
Glioblastoma	Drug response	PDS	3	PEGDA	–	Custom built (glass)	14 days	Akay et al., 2018
Head and neck cancer	Radiation response	PDMEs	18	–	–	Custom built (PEEK)	68 h	Kennedy et al., 2019
Head and neck cancer	Radiation response	PDMEs	5 (3 primary, 2 metastasis)	–	–	Custom built (PDMS)	48 h	Cheah et al., 2017
Head and neck cancer	Radiation response	PDMEs	35	–	–	Custom built (glass)	72 h	Carr et al., 2014
Intestinal cancer	ICB profiling	PDMEs	1	Rat tail collagen-I	–	DAX-1, AIM BIOTECH	9 days	Aref et al., 2018
Liver cancer	Immunoresponse	HepG2 organoids (cell line)	–	Rat tail collagen-I	Monocytes and HBV-specific T cells	Custom built (PDMS)	24 h	Lee et al., 2018
Lung cancer	Immunoresponse	PDMEs	1	–	Tumor matched primary TILs	Custom built (COC)	4 days	Moore et al., 2018
Lung cancer	Biological studies, drug response	H1975 2D cells (cell line)	–	–	Primary airway and alveolar epithelial cells, primary lung microsvaculature endothelial cells	Custom built (PDMS)—wells coated with ECM (laminin, fibronectin, collagen-I)	28 days	Hassell et al., 2017
Lung cancer	Chemotherapy response	Single cell suspensions	8	Culturex BME	–	Custom built (PDMS)	48 h	Xu et al., 2013
Lung and squamous cancers	Chemotherapy response	Epithelial PDS	3	–	Primary pericytes	Custom built (PDMS)	3 days	Ruppen et al., 2015
Lung cancer	Chemotherapy response	PDMEs after xenografting	1	–	–	Custom built (PDMS)	10 days	Holton et al., 2017
Melanoma	ICB profiling	PDMEs	>20	Rat tail collagen-I	–	DAX-1, AIM BIOTECH	3 days	Jenkins et al., 2018
Mesothelioma	Chemotherapy response	PDOs (variable sizes)	2	HA/Gelatin	–	Custom built (PS, glass)	14 days	Mazzocchi et al., 2018
Multiple Myeloma	Chemotherapy response	MM single cells	7	Bovine collagen-I	Mesenchymal cells	μ-slide Chemotaxis 3D Ibitreat, IBIDI, LLC	7 days	Khin et al., 2014
Multiple Myeloma	Biological studies	MM single cells	3	–	Osteoblast cell line (hFOB 1.19)	Custom built (PDMS)	21 days	Zhang et al., 2014
Multiple Myeloma	Biological studies	MM single cells	9	–	Osteoblast cell line (hFOB 1.19)	Custom built (PDMS)	21 days	Zhang et al., 2015
Multiple Myeloma	Drug response	MM single cells	17	–	CD138- bone marrow stromal cells	Custom built (PDMS)	3 days	Pak et al., 2015
Ovarian cancer	Chemotherapy response	PDMEs after xenografting	2	–	–	Custom built (PDMS)	8 days	Astolfi et al., 2016
Pancreatic cancer	Immunoresponse	PDMEs	5–10	Rat tail collagen-I	–	DAX-1, AIM BIOTECH	24 h	Wang et al., 2018a

BME, basement extract membrane; COC, cyclic olefin copolymer; ECM, extracellular matrix; HA, hyaluronan; ICB, immune checkpoint blockade; MM, multiple myeloma; PDME, patient-derived microdissected explants; PDMS, polydimethylsiloxane; PDOs, patient-derived organoids; PDS, patient-derived spheroid; PDX, patient-derived xenograft; PEGDA, poly-(ethylene glycol) diacrylate; PEEK, polyether ether ketone; PS, polystyrene.

Bioreactors

RCCS bioreactors have been widely used primarily to facilitate the self-assembly and culture of scaffold-free spheroids (Ferreira et al., 2018). Yet, bioreactors have been most often used *post* production for patient-derived tumor models to prolong the life and predictive power of 3D tumor models, in the context of drug screening. Physical bioreactors include roller tuber, spinner flask, gyratory shakes, and microgravity bioreactors (Saglam-Metiner et al., 2019) or obtain shear via perfusion systems, with the general purpose of increasing fluid transfer by convection, ultimately improving mass transfer (Selden et al., 2018). In the context of patient-derived 3D models, both RCCS and perfusion systems were used in the field of multiple myeloma (Ferrarini et al., 2013; Belloni et al., 2018), breast cancer (Muraro et al., 2017), colorectal cancer (Manfredonia et al., 2019), and glioblastoma (Li et al., 2018b), overall enhancing the viability of the culture systems.

Specifically, in a study by Ferrarini et al. (2013), a RCCS^{TM} bioreactor was used to culture various multiple myeloma PDMEs (2–3 mm^3 in size) from various metastatic sites. Histological examination demonstrated conservation of viable myeloma cells within their native microenvironment, with a well-conserved histological architecture that included bone lamellae (when relevant) and vessels. The use of dynamic culture for 7 days was particularly important to the maintenance of the vessels, which overall architecture was otherwise disrupted and disappeared in static culture. A further 3-day treatment with bortezomib, a standard anti-myeloma drug, showed that the drug-treated samples displayed an overall concordance in the response to the drug *ex vivo* and *in vivo*. Notably, *in vivo* drug resistance seen for one of the patients treated was also observed for the corresponding explant in the bioreactor system (Ferrarini et al., 2013). In a follow-up study by the same group (Belloni et al., 2018), the authors focused on isolated MM cells. But here, the authors used a scaffold-based approach, Spongostan sheets, a sponge derived from porcine gelatin (Ethicon, Inc.), pre-loaded with patient-matched BM-MSCs and HUVECs. The co-culture promoted the survival of isolated primary MM cells for up to 7 days in the bioreactor (**Figure 7A**). The pool of allogeneic BM-MSCs, HUVECs and MM cells retrieved from the scaffolds at the end of culture matched the input number, indicating that the cells survived but did not proliferate. IHC showed uniform distribution of MM cells and CD73+ stroma. For 6 patients used in culture in the bioreactor, both MM cells and stroma retained their specialized functions and relevant chemotherapeutic responses. Overall, the *ex vivo* 3D co-culture model in bioreactor met the requirements of recapitulated MM-BM dialogue, permanence, and survival of primary MM cells for an extended time period, thereby also incorporating a temporal dimension rarely seen in 2D and static systems of MM. This achievement allowed the dissection of clonal dynamics during MM progression and in response to therapy, a central issue in MM investigations. The combination of allogeneic BM-MSCs to match the patient multiple myeloma cells was another strength of this study, as it allowed for the recapitulation of the patient's bone marrow niche specificity (Belloni et al., 2018).

In breast cancer, Muraro et al. used a custom perfusion bioreactor to maintain breast cancer explants for up to 14 days (27 patients) (Muraro et al., 2017). Upon manual fragmentation of tumor specimens into 2 × 2 × 2 mm pieces, two 8 mm-scaffold discs made of collagen type I were used in a sandwich culture system to induce homogeneous tissue perfusion by the medium. The authors used next generation sequencing to validate a close match between clinical samples and the bioreactor-cultured explants. As a comparison, the tumor fragments from static cultures displayed significantly lower percentages of viable tumor cells. The maintenance of explants for up to 2 weeks enabled the assessment of anti-estrogen treatments and other antibody treatments. Subsequently, the same perfusion bioreactor concept (**Figure 7B**) was used to culture tumor fragments from colorectal cancer specimens, a cancer known to be more difficult to culture *in vitro* (Manfredonia et al., 2019). Contrary to the breast cancer study, the colorectal samples were cultured for only 3 days with the bioreactor. Compared to static cultures, the bioreactor-cultured specimen preserved tissue mass, higher tissue cellularity, and overall initial architecture, whereas it was lost in non-perfused cultures (**Figure 7C**). For instance, the epithelial component and immune cell subsets in perfused cultures were similar to fresh tissue but reduced in static tissues. Critically, highly heterogeneous responses were observed between patients (**Figure 7D**). Overall, these studies strongly demonstrated how bioreactor systems combined with scaffold systems have clear benefits for the maintenance and longer culture of primary tissue samples with the capacity to address heterogeneity (Cassidy et al., 2015; Dagogo-Jack and Shaw, 2017; Bocci et al., 2019). An important consideration is however the likelihood of different biomaterials surviving in a bioreactor microenvironment, where softer materials such as hydrogels may be torn a part in rotary well-culture systems. In this context, perfusion on a static system may be recommended.

In glioblastoma, a prototype bioreactor was developed for the scalable manufacturing of patient-derived glioblastoma cells, after extrusion in alginate hydrogel tubes (**Figure 7E**) (Li et al., 2018b). A mechanical stage enabled to compress the compartment containing the media, resulting in cyclic flow in the compartment containing the tubes. Compared to low expansion in static 2D/3D and dynamic free suspension in 3D, the cells within the alginate tubes were able to be expanded up to 14 days with a 710-fold expansion (**Figures 7F,G**) and high volumetric yield when placed in the bioreactor. This study represents a key advance in the rapid, cost-effective and scalable expansion of patient-derived cells, with significant impact for personalized high throughput drug screening, which require high cell numbers (Li et al., 2018b).

Microfluidics

Microfluidic 3D cell culture represents an optimum strategy to deliver more complex cancer microenvironments and investigate cancer dynamics. The concept of microfluidics allows researchers to culture and study cellular processes and drug responses in a miniaturized, yet well-defined and more biologically relevant culture environment (Holton et al., 2017). Suitable to study an array of cancer hallmarks, such as cancer

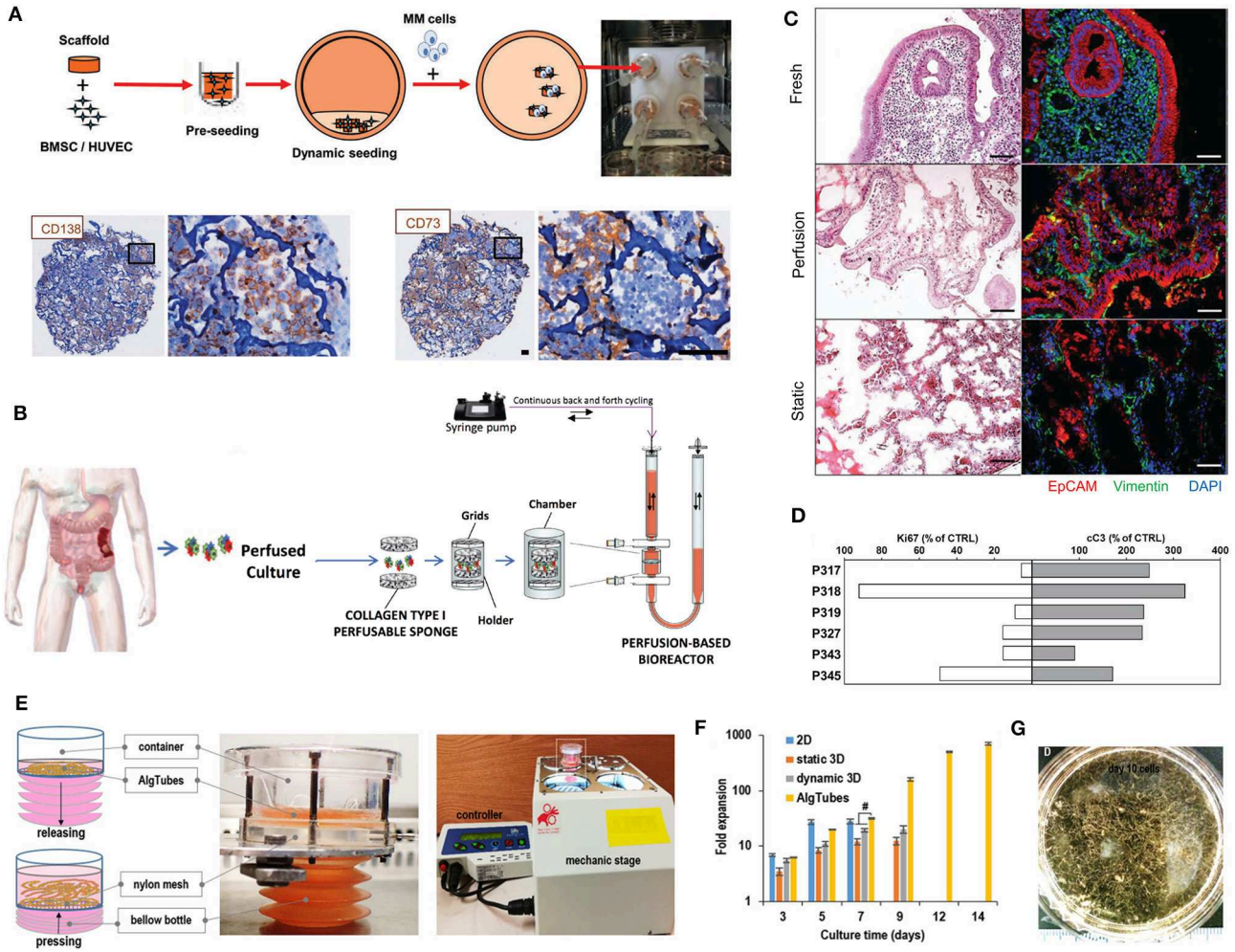

FIGURE 7 | Bioreactor systems with patient-derived materials and/or primary cells. **(A)** Generation of a 3D multiple myeloma (MM) microenvironment in a rotary cell culture system (RCCS^{TM}) bioreactor; scaffold is pre-seeded *in vitro* with bone marrow stromal cells (BM-MSCs)/endothelial cells (HUVECs) and transferred to the RCCS bioreactor. MM cells are then added and cultured dynamically up to 7 days. IHC shows uniform distribution of CD138+ MM cells and CD73+ stroma. Scale = 100 μm. **(B)** Schematic representation of the experimental design. For perfused cultures, colorectal cancer specimens (n = 3/bioreactor) were placed between two collagen type I discs within a ring-shaped holder, restrained by two grids on the top and bottom. The holder was then inserted in the bioreactor chamber and subjected to continuous alternate perfusion. **(C)** Immunostaining shows architectures and protein expression in perfused tissues similar to fresh tissues [EpCAM (red), vimentin (green), DAPI (blue)]. **(D)** Percentages of proliferative (Ki67+) and apoptotic (cC3+) cells in perfused cultures supplemented with 5-FU relative to untreated tissues for tissues from 6 individual patients, showing high heterogeneity in response. **(E–G)** A prototype bioreactor for scalable glioblastoma tumor-initiating cells (TIC) production in alginate tubes (AlgTubes). **(E)** The bioreactor contains a cylindrical container and a plastic bellow bottle, which are separated by a nylon mesh. AlgTubes with TICs are suspended in the cylindrical container and the medium is stored in the plastic bellow bottle that can be pressed to flow the medium into, or released to withdraw the medium from the container. The mechanic stage is used to press and release the bellow bottle. The controller can be programmed for the pressing and releasing speed, as well as the duration of the interval between the pressing and releasing. **(F)** Fold-expansion of glioblastoma TICs cultured in AlgTubes, 2D, static 3D, and dynamic 3D suspension. **(G)** Image of glioblastoma TICs harvested from the bioreactor on day 10. **(A–G)** reproduced with permission from Belloni et al. (2018), Manfredonia et al. (2019) and Li et al. (2018b), respectively. $^{\#}P < 0.05$.

proliferation, angiogenesis, migration, invasion, microfluidic devices enable multiple spatiotemporal layers of complexity. Numerous applications have used microfluidics to measure the response of tumor cells to quantifiable concentration of chemokine gradients (Xu et al., 2014). Both tumor and stromal cells indeed exhibit directional migration toward a chemokine source during growth and dissemination, which can be achieved by microfluidic platforms. Compared to the highly complex models used with cancer cell lines, patient-specific microfluidic models are relatively more modest, mainly using scaffold-free PDME/PDS/PDO approaches or simple co-culture models, used mostly for cytokine profiling or treatment assessment, and up to 28 days culture, and are presented hereafter.

Immunotherapy

One specific patient-derived application using microfluidic devices is the modeling of the dynamic response to ICB in immuno-oncology. Immune checkpoint pathways can indeed

be co-opted by cancer to evade immune response and drugs, while interrupting immune checkpoints can be an effective way to boost anti-tumor immunity and prompt cancer regression (Topalian et al., 2015). Microfluidic devices are an elegant option to assess the response of PDMEs against various ICB-related inhibitors, due to the presence of native immune cells. In a study by Aref et al. for example, using enzymatic digestion, tumor specimens from various tumors were dissociated into single cells, PDS, and macroscopic PDMEs (>100 μm). The spheroid fraction was mixed with collagen-I and used for culture in a cyclic olefin co-polymer (COC)-based 3D microfluidic device (DAX-1, AIM BIOTECH) (Aref et al., 2018). In that study, a small intestinal neuroendocrine tumor was cultured up to 9 days for RNA-sequencing and cytokine profiling. This study was a follow-up by the same group, who used a similar microfluidic approach to culture melanoma PDMEs from a higher number of patients (>20) (Jenkins et al., 2018). Lymphoid and myeloid cell populations were maintained in organoids from various cancer types and the PDS adequately responded to ICB. One of the limitations of these systems resides in the inability to recapitulate T-cell priming or recruitment of naïve immune cells to the tumor microenvironment. This could be addressed in the future by designing more complex tumor-on-a-chip platforms that provide a source of immune cells for interactions with the PDMEs. Additionally, traditional microfluidic devices usually employ polydimethylsiloxane (PDMS) which adsorbs small hydrophobic molecules, likely influencing drug testing. In this context, the use of COC-derived microfluidic devices may be more suitable. The COC-derived microfluidic device was also recently used for PDME from pancreatic ductal adenocarcinoma (PDA) (Wang et al., 2018a) prepared similar to Jenkins et al. (2018) and Aref et al. (2018) (**Figure 8H**) ICB studies. After mincing of the explant and resuspending the PDMEs in collagen, the mixture was inserted into the DAX-1 microfluidic device before assessing a novel inhibitor molecule (RIP1i) (**Figure 8I**). The use of the microfluidic device for the PDA-derived PDMEs enabled the assessment of reproducible treatment with RIP1i, and the profiling of a spectrum of immunogenic cytokines of up to 10 patients, which corroborated the results from animal model experiments.

Chemotherapy

Microfluidic chambers often allow a high number of replicates that are tested on several fragments of specimens from the same tumor piece, with the overall possibility to extend explant viability due to perfusion. In a study by Astolfi et al. (**Figures 8A–D**), large PDMEs extracted from ovarian (2 patients) and prostate (1 patient) cancer were successfully cultured inside a PDMS microfluidic device for up to 8 days, with no decreased of viability over time (Astolfi et al., 2016). Four PDME types displayed heterogeneous staining patterns with the non-cancerous tissue being the least viable of all 4, possibly due to reduced metabolism (**Figures 8B,D**). Subsequently, one of the ovarian PDMEs was treated with carboplatin after 24 and 48 h inside the device, at a dose equivalent to the maximum theoretical blood concentration of the drug in a normal patient treated. Due to tissue availability and the high number of microfluidic chambers, a total of 25 PDME replicates were loaded in the device to ensure that intratumoral heterogeneity could be addressed. Specifically, high variability between PDMEs was observed (**Figures 8C,D**), which the authors attributed to a variable chemoresponse of different cell subpopulations within the tumor tissue, as ovarian tumors are known to exhibit high intratumoral heterogeneity. Ultimately, despite high variance, the patient response to the treatment corroborated the *in vitro* results. In some cancers, the use of PDMEs is impractical due to tumors that are either not stiff enough or too dependent on the microenvironment for survival. In this case, xenografting may be used to expand the tumor mass prior to excision, fragmentation, and culture in a microfluidic device. Holton et al. used this strategy for lung, bladder, and melanoma explants (Holton et al., 2017). After mouse excision, the PDXs were dissociated by fine needle aspiration and cultured in a continuous perfusion microfluidic device for up to 10 days. In this study, the lung-derived patient PDXs were dissociated in 18 PDME samples and used for treatment with staurosporine (a broad protein kinase inhibitor) for 5 days. The PDMEs showed significantly reduced viability compared to non-treated controls, and displayed only slight intratumoral heterogeneity, providing more chance of success when clinically translated (Holton et al., 2017).

It is known that cancer cell lines respond differently than primary tumor cells to chemotherapeutic agents. This was evidenced in lung cancer using a microfluidic chip-based 3D co-culture device (Xu et al., 2013). After isolation of primary tumor cells from fresh lung tumor specimens, the cells were co-cultured for 24 h with cell-basement membrane extract and submitted to drug testing. When cancer cell lines were used instead of the primary cells for co-culture, the IC50 of gefitinib was much larger for primary cancer cells. Overall the apoptosis rates were similar between the 8 patients tested. However, it must be noted that this study was looking at individual cells, with some cell aggregates (Xu et al., 2013). In a study by Mazzocchi et al. (2018) (**Figures 8E–G**), tumor cells were derived from mesothelioma (2 patients), which were grown *in situ* into organoids of high cellular viability in HA-gelatin hydrogels. Organoids were observed after 1 and 7 days for each patient, upon which two different doses of chemotherapeutic mixtures carboplatin/pemetrexed or cisplatin/pemetrexed were injected. Different responses were observed for each patient after a further 7 and 14 days according to the cocktails of drugs and doses selected, highlighting the intrinsic patient differences in response to similar treatments. A non-traditional microfluidic device was also recently presented by Akay et al. (2018), where various drug concentrations were able to be tested simultaneously (7 channels containing up to 11 microwells) on glioblastoma PDS and effectiveness was measured by spheroid size and viability. From the three patients tested, large interpatient heterogeneity was observed, although the same decreasing trend was observed for 4 out of the 7 channels tested. This method offers high-throughput testing, as it allows researchers to simultaneously treat organoids with various drug concentrations.

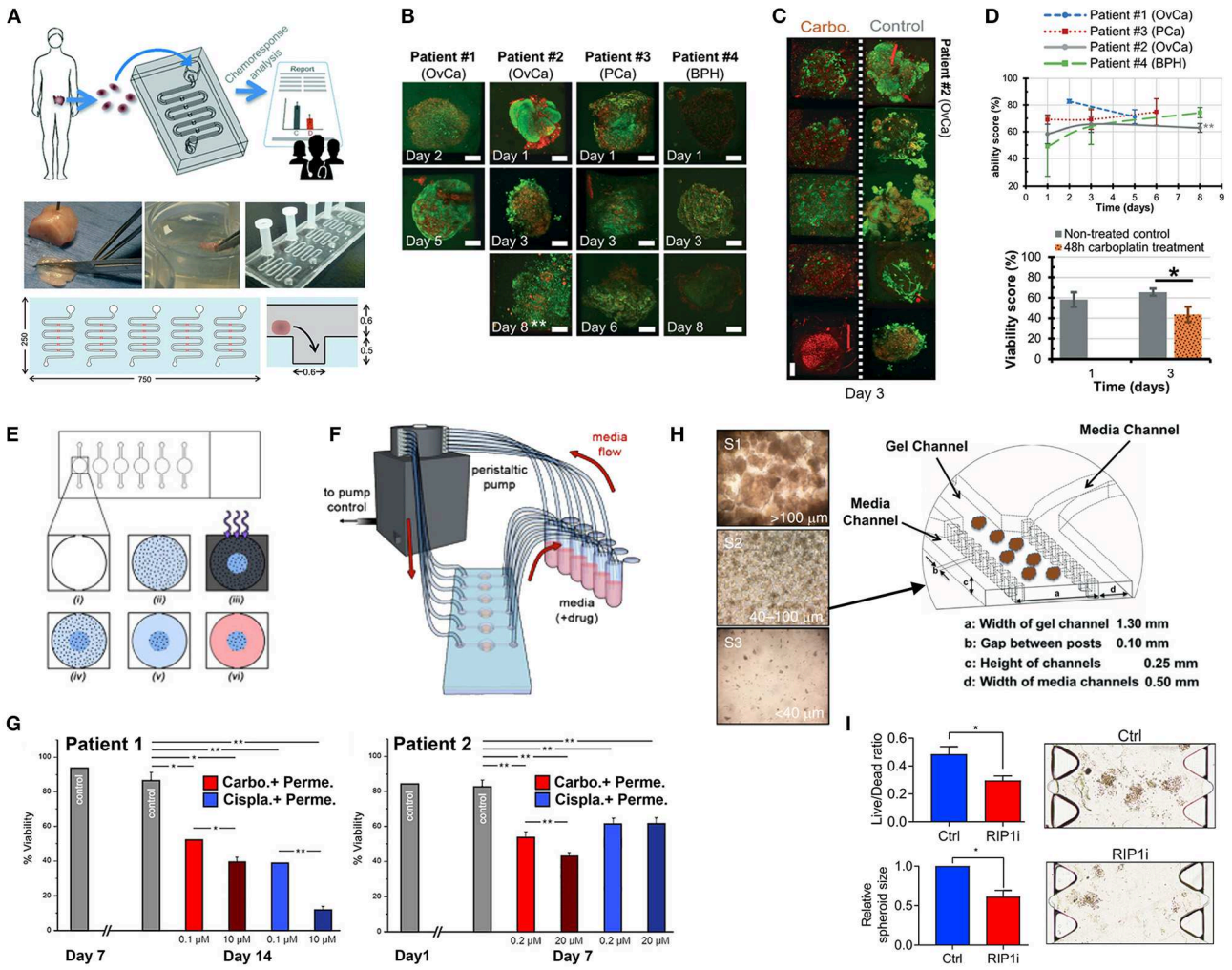

FIGURE 8 | Microfluidic systems using patient-derived materials for chemotherapy **(A–G)** and immunotherapy **(H,I)**. **(A)** Top: schematic of a patient-derived tumor explant, microdissected, loaded in a microfluidic device and injected with various drugs. Results are then interpreted to identify non-responders to treatment for a personalized treatment strategy. Bottom: photograph of tumor prior and after microdissection in 500 µm-PDMEs and design of the microfluidic device containing up to 5 chambers for PDME entrapment and drug testing. **(B)** PDMEs from various patients and different cancers are analyzed by live/dead cell assay using confocal microscopy (green = live, red = dead), showing various PDME architectures and viability patterns. **(C)** PDMEs from an ovarian tumor treated with carboplatin shows high heterogeneity in PDME structure and viability response for PDME originating from the same tumor. **(D)** Corresponding graphs of viability data from **(B)** (top) and **(C)** (bottom) compared to non-treated controls show inter-cancer tumor heterogeneity and drug efficacy on PDMEs from one tumor, despite intra-tumor heterogeneity observed in **(C)**. **(E)** Microfluidic device enabling *in situ* spheroid patterning technique: a microfluidic chamber (i) is filled with a mixture (blue) containing hydrogel precursors, photoinitiator, and patient-derived tumor cells (ii) and then illuminated with UV light through a photomask (gray) (iii). Exposed precursor is crosslinked into a hydrogel (dark blue), detaining cells within the region (iv), and non-crosslinked gel is flushed form the chamber with clean saline from the chamber (v). Finally, saline is replaced with media (red) (vi) for incubation. **(F)** Schematic of system that offers low volumes and closed loop fluidic circuit controlled by a computer-controlled peristatic pump to treated individual organoids. **(G)** *In vitro* chemotherapy assessment of organoids derived from two patients with mesothelioma treated with various drug doses and combinations shows different response between patients, although treatment occurred at different times between patients (viability measured from live/dead confocal microscopy on organoids). **(H)** Schematic of PDMEs obtained after dissection and sieving. Fraction 2 (40–100 µm) is usually used in microfluidic devices such as the 3D cell culture chip from AIM Biotech shown, which contains a center gel region. Gel loading port and media ports labeled **(B)**, along with center and side channels **(C)**. **(I)** The AIM Biotech microfluidic device was used by Wang et al. to test a selective RIP1 inhibitor on pancreatic ductal adenocarcinoma PDMEs. After RIP1i treatment ($n = 5$ patients shown), PDME live/dead ratio, and size decreased. **(A–I)** reproduced with permission from Astolfi et al. (2016), Aref et al. (2018), Mazzocchi et al. (2018), and Wang et al. (2018a), respectively. **(D) Top:** **Result for PDMEs stained and imaged a second time; **Bottom:** *p-value = 0.014. **(G)** *$p < 0.05$, **$p < 0.01$. **(I)** *$p < 0.05$.

In a study by Ruppen et al. PDS were formed using primary lung adenocarcinoma cells from two patients, using a cell gravity microwell-entrapment system (Ruppen et al., 2015). After the first 24 h of spheroid formation, their size decreased due to compaction. In a variant, the epithelial cells were injected with primary pericytes at a 5:1 ratio, as to assess the known drug barrier effect from pericytes. Spheroids again formed homogeneously and

when treated with various cisplatin concentrations, the tumor/pericytes spheroids were significantly less chemosensitive, validating the known effect of pericytes using this microfluidic device.

Radiotherapy

In some cancers such as HNSCC, the standard treatment strategy involves gamma irradiation. As a result, microfluidic devices have been developed not only to maintain the viability of tumor specimens but also to sustain irradiation. The microfluidic devices used for the irradiation of HNSCC PDME samples have consisted of mostly PDMS (Cheah et al., 2017), but also glass (Carr et al., 2014) or more recently, polyether ether ketone (PEEK) (Kennedy et al., 2019). In the study with the largest number of patients (Carr et al., 2014), the specimens of 35 patients were sectioned into 3 mm^3 PDME samples and loaded in the microfluidic device for 72 h of culture. The study showed increased apoptotic index with increasing Gy dose, but when clinical doses were used, cell death decreased after 22 h. In a subsequent study (Cheah et al., 2017), the PDMEs from 5 HNSCC patients (3 primary and 2 metastatic) were tested from 0 to 20 Gy but only left in culture for 24 h following irradiation. Interestingly, whereas metastatic samples were expected to be more resistant to irradiation, two out of three of the metastatic PDMEs had higher responses following a 15 Gy dose compared to non-metastatic samples. Overall, the PDMEs from the 5 patients displayed very variable responses to irradiation from none to mild, confirming intertumoral, and intratumoral heterogeneity. These results emphasize the value of individual analysis of tumors, combined with a high number of technical replicates per patient, to truly determine patient specific response (Cheah et al., 2017). In a recent study by Kennedy et al. a PEEK-derived microfluidic device was used to load freshly excised samples from 18 patients (Kennedy et al., 2019). The specimens were cut using vibratome slicing and cultured for 68 h with 2 h interval perfusions. The specimens were further submitted to 2 Gy irradiation ± Cisplatin, which denotated increased apoptotic staining compared to the controls. Intratumoral heterogeneity was evident in all of the immunohistochemistry markers before and after irradiation treatments. While the advantage of this PEEK system resides in an easy-to-use setup with the possibility to assess irradiation-related effects, the microfluidic device comprised only 4 chambers, limiting the number of replicates being investigated simultaneously (Kennedy et al., 2019).

Tumor-on-a-Chip

In the last decade, numerous tumor-on-a-chip systems, deriving from organ-on-a-chip systems, have shown great potential in providing the complexity of various dynamic aspects of the cancer while also incorporating high-throughput techniques (Caballero et al., 2017). These systems rely on microfluidics approaches and combine the advantages of individual tumor models, by offering multicellular architecture, tissue-tissue interface, and a biomimetic physical microenvironment that can sustain vascular perfusion (Sontheimer-Phelps et al., 2019). Yet, dynamic cancer processes such as invasion, migration, intravasation, extravasation, and metastasis models have been developed mostly using cell lines. Only recently have studies combined patient-derived tumor materials and stroma toward the development of more complex "personalized tumor-on-a-chip" systems, yet often combining cell lines in the process. Compared to the previous section which reported simple microfluidic systems used mostly to assess cytokine profiling/therapy on single-cell-type-derived spheroids or explants, the following section reports more complex systems (mimicking the immune system and metastasis) that combine various cell types for therapy response as well as biological studies.

Immune-system-on-a-chip

It is generally acknowledged that in the arena of cancer modeling, the immune response has been relatively neglected, due to the complexities of recapitulating it *in vitro* (Polini et al., 2019). Yet, tumors-on-a-chip provide a relevant technology that can pave the way toward this direction, as they can possibly offer a mean to overly study inflammation (Han et al., 2012) and immune cells-tumor interactions by combining patient-derived materials with cell lines. For instance, Moore et al. developed a COC-derived microfluidic model termed EVIDENT (*ex vivo* immuno-oncology dynamic environment for tumor biopsies) enabling the accommodation of 12 separate biopsy fragments for interaction with patient-matched flowing tumor-infiltrating lymphocytes (TILs) (**Figures 9A,B**) (Moore et al., 2018). The EVIDENT microfluidic system displayed quantifiable levels of TIL infiltration and tumor death, mimicking *in vivo* tumor response to ICB treatment of flowing TILs. Innovatively, the system used a material with high optical transparency and was loadable onto the stage of high resolution confocal microscope enabling real-time image acquisition and analysis (Moore et al., 2018). While the method was established with cell lines, the study also assessed one NSCLC patient sample. At 24 h post TIL administration, the treated NSCLC tumor fragment displayed substantial TIL infiltration with proximal cellular apoptosis and was time-dependent. Other studies have focused on recreating cell line tumor organoids and used a microfluidic device to test the response upon addition of differentiated patient-derived immune cells. For example, Lee et al. developed an intrahepatic tumor microenvironment model to investigate the immunosuppressive potential of monocytes toward Hepatite B virus-specific T cells (differentiated from peripheral blood mononuclear cells) and the role of ICB signaling using a static 3D microfluidic model (**Figures 9C,D**) (Lee et al., 2018). The benefit of using the microfluidic device, beyond the 3D micro-chamber, was to allow sequential injection, with first HepG2 cell lines aggregates and patient-derived monocytes, then followed by the patient-derived T cells. It was shown that functional differences existed among differently produced T cells, where monocytes suppressed only retrovirally transduced T cell cytotoxicity toward cancer cells while cytotoxicity was not affected by the presence of monocytes. This result was only observed in the microfluidic device (dynamic 3D) (**Figure 9E**) and not in a static 2D setting.

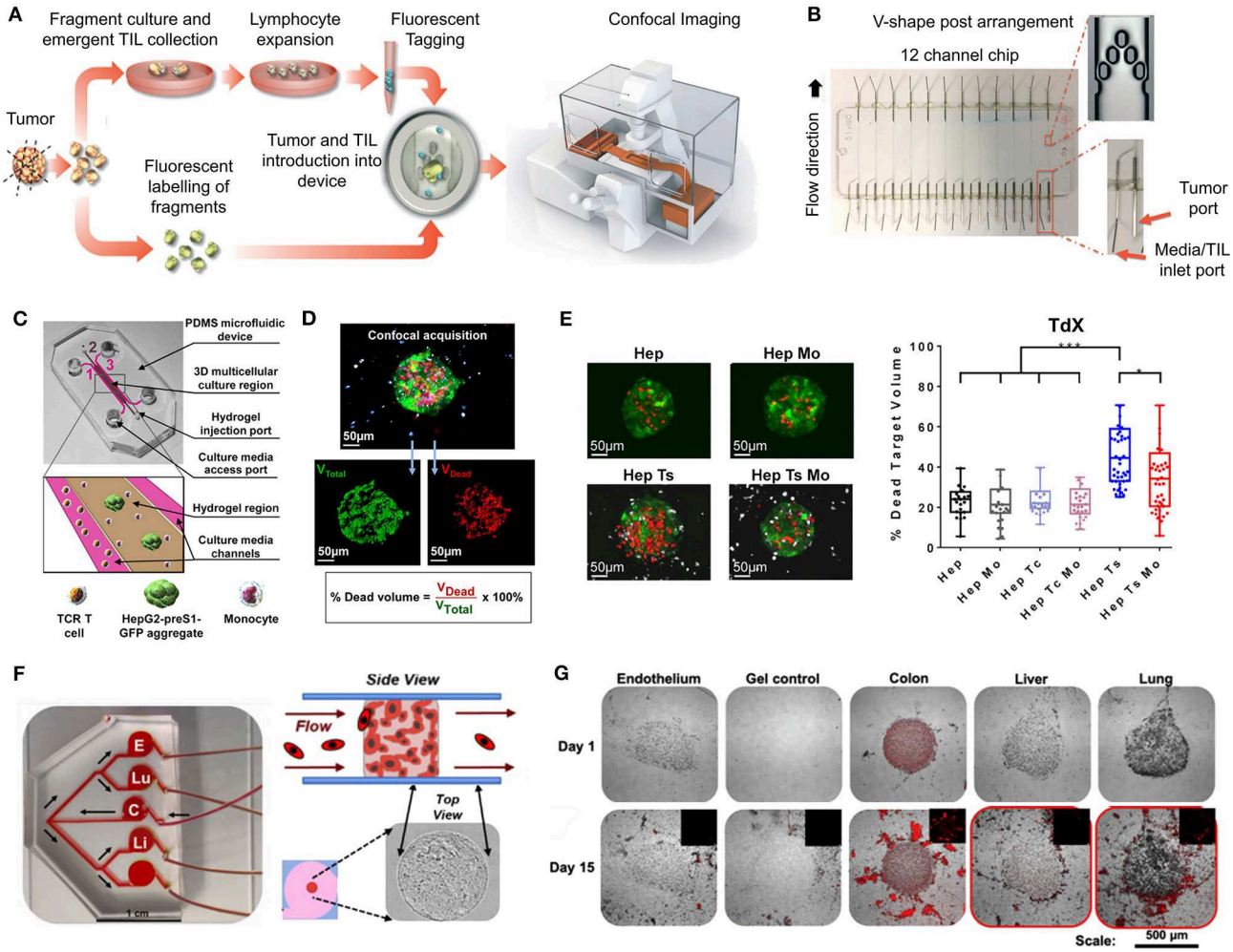

FIGURE 9 | Tumor-on-chip systems. **(A)** Diagram illustrating the processing steps involved in the preparation of patient-derived tumor cells and tumor-infiltrating lymphocytes (TILs) from the same tumor sample, and live imaging by confocal microscope. **(B)** 12-channel multiplexed cyclic-olefin-copolymer (COC)-based microfluidic device with V-trap design for capturing tumor sample in flow stream and dual port entry for TILs. **(C)** A 3D multicellular tumor microenvironment microfluidic model consisting of a middle hydrogel channel (2) surrounded by two media channels (1, 3) for the mechanistic study of the effect of monocytes on T cell receptor-redirected T cell (TCR T cell) killing of tumor cell aggregates. Human monocytes were inserted together with target HepG2-preS1-GFP cell organoids in collagen gel in the central hydrogel region (2), while hepatitis B virus (HBV)-specific TCR T cells were added into one fluidic channel (1) to mimic the intrahepatic carcinoma environment. **(D)** Representative confocal image of a target cell organoid (in green) surrounded by monocytes (in blue) and HBV-specific TCR T cells (in white), in which the presence of dead target cells is DRAQ7+. **(E)** Left: Representative target cell HepG2 cell organoids (Hep) cultured with monocytes (Mo) and/or HBV-specific T cell (Ts), in which the presence of dead target cells is DRAQ7+(in red). HBV-specific TCR T cells are labeled with Cell tracker violet dye (in white), while monocytes are unlabeled. Right: Box plot of the percentage of dead target volume after 24 h of co-culture with retrovirally transduced (Tdx) HBV-specific TCR T cells (Tc = control T cell). **(F)** Metastasis-on-a-chip device and *in situ* tumor and tissue construct biofabrication. Arrows show fluid flow (E, endothelium; Lu, Lung; C, colorectal cancer organoids made of RFP tagged HCT116 cells; Li, liver; blank, control). Constructs comprised of cells in ECM hydrogels exist under fluid flow and have the capability to experience circulating cells either interact or pass by. **(G)** Metastasis tracking at day 1 and day 15 showing HCT116 cells colonizing other organs, using phase and epifluorescence microscopy **(A–G)** reproduced with permission from Lee et al. (2018), Moore et al. (2018), and Aleman and Skardal (2019), respectively. $^{*}P \leq 0.05$, $^{***}P \leq 0.001$.

Metastasis-on-a-chip

The dynamic process of metastasis is highly suitable for study using microfluidic platforms (Caballero et al., 2017), and was largely investigated for bone metastasis. This was investigated heavily for MM since primary MM cells are easily accessible and could be injected easily in microfluidic devices comprising bone-like tissues. Zhang et al. exploited this strategy by creating what the authors referred to as a "3D ossified" tissue (Zhang et al., 2014). This study is highly cited in the field of microfluidics, as reported in many reviews (Bhatia and Ingber, 2014; Carvalho et al., 2015; Fong et al., 2016a; Arrigoni et al., 2017; Peela et al., 2017; Rothbauer et al., 2019; Sakthivel et al., 2019; Sontheimer-Phelps et al., 2019), yet the limitations of the study escaped most of them. The "3D ossified" "tissue" appellation was merely disproportionate; the "tissue" consisted simply of a monolayer of human osteoblasts (hFOB 1.19 cell line) cultured on the

flat surface of microfluidic chambers for 4 days prior to the pumping of bone marrow mononuclear cells from MM patients for 4 h, followed by perfused culture for 21 days. Due to the improper "scaffold" terminology used in the paper, it was often wrongly assumed that a physical 3D scaffold was employed to grow the tissue. Structurally, the osteoblast-derived tissue was $<60\,\mu m$ (i.e., actually 2D). Additionally, no characterization of bone ECM markers, critical to bone metastasis, was performed, although CD138+ and CD38+ CD56+ populations were capable of proliferating for 7 days on top of the osteoblast layer before stopping proliferation and forming colonies in the 7–21 days range. The authors stated that less mineralization took place in the presence of MM cells, but this arose from basic visual inspection, without quantitative measure (Zhang et al., 2014). A follow-up study by the same group sought to provide more mechanistic discussion regarding the osteoblasts/MM cells interactions and showed how N-cadherin from osteoblasts contributed to the homing and retention of MM cells onto the osteoblast layer. In this study, the authors described how to maximize long-term maintenance of co-cultured primary MM (Zhang et al., 2015). Further work interrogated bone stroma/MM cells interactions and drug responses in microfluidic devices (Khin et al., 2014; Pak et al., 2015), using solely primary cells, yet the bone marrow microenvironment reflected simple 2D co-culture models aided by microfluidic technologies, rather than "tumors-on-a-chip" systems. Interestingly, in one study investigating 17 patients (Pak et al., 2015), response to the proteasome inhibitor bortezomib was clinically matched with the response from the *in vitro* model, but only when the MM cells were co-cultured with CD138- bone marrow stromal cells present. This achievement questions the necessity of having complex structural 3D microenvironments.

Recently, ingenious multi-site metastasis-on-a-chips, deriving from multi-organ-on-a-chip technologies (Skardal et al., 2017), have combined photopatterning of HA-gelatin hydrogels and microfluidics, to recreate various types of organoids in individual chambers, including endothelium, lung, and liver (**Figure 9F**) (Aleman and Skardal, 2019). By culturing upstream organoids of colorectal cancer under recirculating fluid flow for up to 15 days, fluorescently-tagged tumor cells were tracked when they detached from the colorectal cancer organoids and metastasized in the organs from other chambers, homing preferentially to liver and lung (**Figure 9G**), as seen clinically. While this study was entirely performed with cell lines (HCT116), the use of similar systems with patient-derived primary tumor cells hold potential for a more holistic approach to assess individual metastatic prevalence and personalized therapy selection.

PERSPECTIVE

Advances in 3D cell culture have led to novel discoveries, including specific details that occur during cancer development and progression that had previously remained unknown. Each 3D model comes with its own advantages and limitations (**Figure 10**), although typically, no model can answer all questions, thereby, a multi-model approach seems most sensible to study cancer heterogeneity. The inability to provide representative preclinical platforms that are patient-specific is, today, one of the key frontiers impairing personalized and effective cancer treatment. Encouragingly, 3D tumor modeling has made significant progress in this direction by combining advanced modeling technologies with innovative biomaterials that can partly mimic the heterogeneous context of real tumors (Fong et al., 2016a; Peela et al., 2017). Unfortunately, these systems have reduced translational power by failing to systematically use patient-derived materials as these present with limited tissue access, tissue quantity and viability *ex vivo*. In the arena of *ex vivo* culture of patient-derived tumors, efforts are still today largely focused on the use of scaffold-free/Matrigel approaches using predominantly PDOs and PDS (Nagle et al., 2018), that allow minimal processing/engineering and rapid drug assessment. While this strategy offers advantages in terms of simplicity, yield, minimal labor, and are relatively high-throughput, all of which appealing to pharmaceutical companies, these models suffer from batch-to-batch heterogeneity and moreover lack the supportive 3D stromal network that is critical in enabling heterogeneity considerations.

First, it is necessary to delineate the purpose of each system, and the key components related to the research questions. For example, vascularized networks in the assessment of metastasis, increased viability in the case of long-term drug testing or multiple stroma components in the assessment of drug resistance. The determinants of tumor growth highly depend on tumor type, hence it is imperative to use specific tools that mimic individual contexts (Thoma et al., 2014), in terms of cellular and non-cellular components, as well as physical/chemical cues. Innovative biomaterials and tissue engineering strategies, coupled with manufacturing technologies such as bioprinting, currently enable researchers to adequately mimic disease-specific contexts by providing stiffness, architectures, and chemical compositions specific to local organs. Yet, the full potential of these techniques has not been sufficiently exploited in the context of patient-derived components, requiring the adoption of a new mindset that allows heterogeneity to be an intrinsic part of tumor models. Biomaterial-based models allow for the effective support of heterogeneous cultures, bringing forth a degree of complexity in 3D cultures that was previously unachievable. However, due to a lack of inherent factors, scaffold design is key to sustaining patient-derived samples.

Synthetic and semi-synthetic hydrogels for instance have the power to be tuned to replicate local ECM libraries, with the possibility to incorporate growth factors, MMPs, and RGD motifs specific to each microenvironment, and hold promise to mimic a high spectrum of heterogeneities. For instance in our own work, we have shown how PEG-Heparin hydrogels represent a modular platform for systematic angiogenesis modeling by incorporating a variety of growth factors, ligands, and cleavable peptide linkers for prostate and breast cancer modeling (Bray et al., 2015). Similarly, semi-synthetic gelatin-methacryloyl (GelMA)-derived hydrogels are attractive photocrosslinkable hydrogels that offer a high degree of physicochemical functionalization and properties (Yue et al., 2015; Loessner et al., 2016; Meinert et al., 2018). In the Hutmacher group, Kaemmerer et al. have

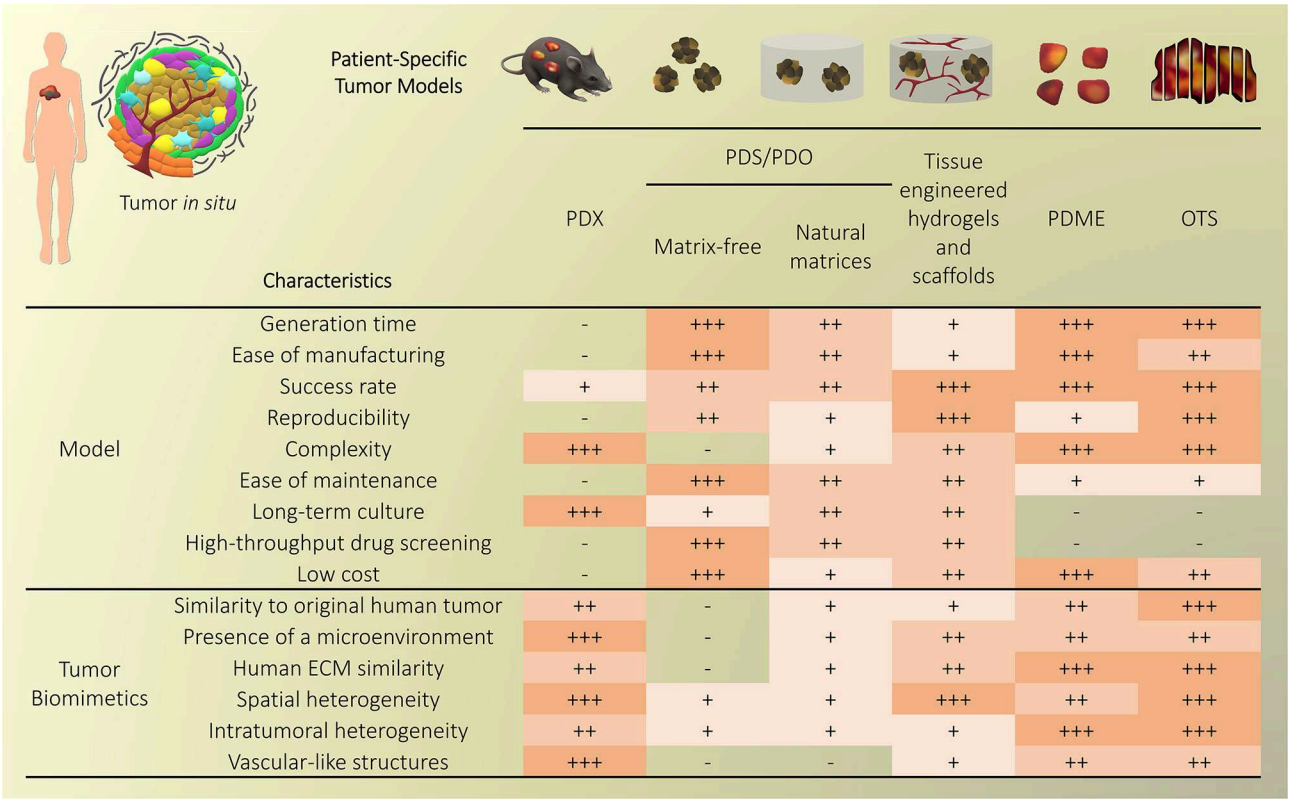

Characteristics		PDX	PDS/PDO: Matrix-free	PDS/PDO: Natural matrices	Tissue engineered hydrogels and scaffolds	PDME	OTS
Model	Generation time	-	+++	++	+	+++	+++
	Ease of manufacturing	-	+++	++	+	+++	++
	Success rate	+	++	++	+++	+++	+++
	Reproducibility	-	++	+	+++	+	+++
	Complexity	+++	-	+	++	+++	+++
	Ease of maintenance	-	+++	++	++	+	+
	Long-term culture	+++	+	++	++	-	-
	High-throughput drug screening	-	+++	++	++	-	-
	Low cost	-	+++	+	++	+++	++
Tumor Biomimetics	Similarity to original human tumor	++	-	+	+	++	+++
	Presence of a microenvironment	+++	-	+	++	++	++
	Human ECM similarity	++	-	+	++	+++	+++
	Spatial heterogeneity	+++	+	+	+++	++	+++
	Intratumoral heterogeneity	++	+	+	+	+++	+++
	Vascular-like structures	+++	-	-	+	++	++

FIGURE 10 | Advantages and disadvantages of current patient-specific tumor models.

indeed shown how they could be a suitable platform for the growth of ovarian cancer spheroids, investigating the effects of key tumor ECM components (laminin and hyaluronan) and matrix stiffness (ranging from 0.5 to 9 kPa) which both revealed significant responses in growth and treatments of organoids (Kaemmerer et al., 2014). Subsequently, GelMA gels were successfully used to model breast cancer invasion and chemoresponse *in vitro* with cell lines (Donaldson et al., 2018). Recently GelMA gels were also able to modulate the production of pro-inflammatory cytokines, TNF-α, by human mononuclear cells (Donaldson et al., 2018). Such property is of high interest when addressing immunoresponse *in vitro*. The ease of use with GelMA gels is also attractive to bioprinting, as specific patterns with different compartments, could be bioprinted followed by simple UV or light crosslinking (Pepelanova et al., 2018). Ultimately, using such hybrid biomaterial systems provides a versatile tissue culture platform that addresses the limited bioactivity of synthetic matrices while controlling batch-to-batch physical properties that critically influence each tumor microenvironment. Combining the physicochemical versatility of GelMA with the tailorability of bioprinting (multiple components printed simultaneously; Ke and Murphy, 2019; Meng et al., 2019), will offer tremendous opportunities to recreate complex biomaterial composite platforms that account for heterogeneous tissue level organization without losing control over relevant biochemical and biophysical cues, as seen in explants. 3D bioprinting is further advantageous as it can reconstruct complex structures from digital designs that can be patient-specific and has upscaling potential (Ma et al., 2018). Yet, it must be noted that the viability of patient-derived materials may be compromised by the printing process and so manufacturing systems that are rapid, mild, and cell-friendly should be chosen in this context. The incorporation of decellularized tumor matrices may be another option that enables heterogeneity recapitulation. To date, many studies have shown how such matrices led to very useful 3D tumor models for breast (Jin et al., 2019; Liu et al., 2019), skin (Brancato et al., 2018), and colon cancer (Hoshiba and Tanaka, 2016; Pinto et al., 2017; Romero-López et al., 2017), yet they are still to be used in co-culture with patient-derived tumor cells.

So where do we go from here? In order to mimic an organ or tissue, a combination of expertise from chemists, biologists, and biomedical engineers will be required to manufacture a more *in vivo*-like tumor microenvironment to give context to the spheroids, and/or to support the culture of multiple supporting cell types derived from the original organoids (Foley, 2017). In this context, the use of CAFs is one important component which can be relatively easily incorporated to models, but efficiently raise the heterogeneity profile of tumor models (Augsten, 2014). More problematically, tissue-specific endothelial cells and vessel-supporting cells are critical to establish patient and organ-specific vascularization, which has considerable downstream effects on

tumor cell survival and metastasis, with implications on access to nutrients and therapeutics. Such primary cells are however difficult to collect, expand and maintain in a 3D setting and the community has traded this aspect of heterogeneity for well-characterized HUVECs.

Finally, biotechnologies, such as bioreactors (Selden et al., 2018), microfluidics (Shang et al., 2019), and tumor-on-chip (Rothbauer et al., 2019; Sun et al., 2019) approaches represent exciting options to raise heterogeneity by offering integrative platforms for controlled dynamic co-cultures, including relevant physical and chemical gradients specific to individual microenvironments. The use of patient-derived components, either tumor or stromal derived, combined with supportive scaffold biomaterials integrated into such dynamic platforms may offer the highest degree of heterogeneity, and hence relevance, in tumor models (Esch et al., 2015). In the specific context of metastasis, the multi-site organs-on-chips are relevant candidates for increased complexity (Skardal et al., 2016a,b, 2017; Aleman and Skardal, 2019), although it may be impossible to recreate fully patient-specific micro-organs with this strategy. In this case, a mixture of organ-specific cell-lines derived organoids with a primary patient-derived tumor still hold great potential for metastasis assessment and personalized chemotherapeutic guidance. In addition, in the event of multi-cellular or multi-organ model development, a question as to how to enlarge the models remains. Due to nutrient and oxygen deprivation as researchers develop real-sized tumors and their matrix *in vitro*, cell/tissue death and necrosis will inevitably occur. The need for the implementation of blood vessels and other structures are required to be a part of the tumor model, leading to additional issues including perfusion, functionality, endothelial cell origin and phenotype, and their co-culture with tumor cells. While these goals may seem distant, in fact, they are closer than we realize. Novel techniques involving the separate 3D culture and then combination of nerves (Workman et al., 2017) or neurons (Birey et al., 2017) has led to the connection of cell types and tissue structures previously unattainable. On top of this, automated pipetting, imaging and other robotic strategies will allow for the high-throughput and reproducible output of the model of choice (Kondo et al., 2018).

The final considerations in the engineering of patient-specific microenvironments are to leverage the emerging engineering technologies with relevant characterization technologies. At the cellular level, this includes the identification of intratumoral subclones using next-generation sequencing and combined multi-omics techniques (Chakraborty et al., 2018). Such techniques are key to uncover molecular signatures underlying heterogeneous phenotypes, yet are faced with bioinformatics challenges such as data analysis, interpretation, and multi-technique integration into comprehensive stratifications (Halfter and Mayer, 2017). Such an undertaking will be critical to match tumor subcategories into representatively stratified tumor models for clinical implementation. Next, the characterization of 3D models are often faced with limited high content characterization that prohibit rapid and in-depth analysis in live settings. Again, this will need to be addressed by increasing the capacity of *in situ* localized detection combined with more powerful computational modeling to enable more effective quantification of mechanistic and drug responses in heterogeneous microenvironments (Xu et al., 2014). Ultimately, it is only when combining heterogeneity considerations and working toward the development of comprehensively integrated technologies that we will have a decent chance to reconstitute the complex tumor microenvironment, which is key to understanding individual cancer progression and realistically enable personalized medicine.

AUTHOR CONTRIBUTIONS

NB delineated the topic and outline. LB and NB reviewed and evaluated the literature, designed, and wrote the article. DH provided feedback and edited the final article.

FUNDING

LB and NB acknowledge funding from Lush UK, in the form of two Young Investigators awards supporting non-animal testing alternatives. LB was supported by a grant from the National Breast Cancer Foundation (PF-16-004) and acknowledges the support of grant 1159637 awarded through the 2018 Priority-driven Collaborative Cancer Research Scheme and co-funded by Cancer Australia and Leukemia Foundation of Australia. DH acknowledges the Humboldt Foundation and the Australian Research Council for funding of an ARC Industrial Transformation Training Centre in Additive Biomanufacturing (IC160100026). NB was supported by a John Mills Young Investigator Award (YI0715) from the Prostate Cancer Foundation of Australia (PCFA) and acknowledges funding from the Australian National Health and Medical Research Council (NHMRC) in the form of an ECR Peter Doherty fellowship (APP1091734) and J.J. Richards & Sons Pty Ltd., via an *in vitro* Excellence Research grant.

ACKNOWLEDGMENTS

The authors thank Dr. Christoph Meinert for proofreading the manuscript and Maxime Le Mounier for help with figures.

REFERENCES

Acerbi, I., Cassereau, L., Dean, I., Shi, Q., Au, A., Park, C., et al. (2015). Human breast cancer invasion and aggression correlates with ECM stiffening and immune cell infiltration. *Integr. Biol.* 7, 1120–1134. doi: 10.1039/c5ib00040h

Akay, M., Hite, J., Avci, N. G., Fan, Y., Akay, Y., Lu, G., et al. (2018). Drug screening of human GBM spheroids in brain cancer chip. *Sci. Rep.* 8:15423. doi: 10.1038/s41598-018-33641-2

Albritton, J. L., and Miller, J. S. (2017). 3D bioprinting: improving *in vitro* models of metastasis with heterogeneous tumor microenvironments. *Dis. Model. Mech.* 10, 3–14. doi: 10.1242/dmm.025049

Aleman, J., and Skardal, A. (2019). A multi-site metastasis-on-a-chip microphysiological system for assessing metastatic preference of cancer cells. *Biotechnol. Bioeng.* 116, 936–944. doi: 10.1002/bit.26871

Alizadeh, A. A., Aranda, V., Bardelli, A., Blanpain, C., Bock, C., Borowski, C., et al. (2015). Toward understanding and exploiting tumor heterogeneity. *Nat. Med.* 21, 846–853. doi: 10.1038/nm.3915

Aref, A. R., Campisi, M., Ivanova, E., Portell, A., Larios, D., Piel, B. P., et al. (2018). 3D microfluidic *ex vivo* culture of organotypic tumor spheroids to model immune checkpoint blockade. *Lab Chip* 18, 3129–3143. doi: 10.1039/C8LC00322J

Arrigoni, C., Gilardi, M., Bersini, S., Candrian, C., and Moretti, M. (2017). Bioprinting and organ-on-chip applications towards personalized medicine for bone diseases. *Stem Cell Rev. Rep.* 13, 407–417. doi: 10.1007/s12015-017-9741-5

Astolfi, M., Péant, B., Lateef, M. A., Rousset, N., Kendall-Dupont, J., Carmona, E., et al. (2016). Micro-dissected tumor tissues on chip: an *ex vivo* method for drug testing and personalized therapy. *Lab Chip* 16, 312–325. doi: 10.1039/C5LC01108F

Augsten, M. (2014). Cancer-associated fibroblasts as another polarized cell type of the tumor microenvironment. *Front. Oncol.* 4:62. doi: 10.3389/fonc.2014.00062

Avendano, A., Cortes-Medina, M., and Song, J. W. (2019). Application of 3-D microfluidic models for studying mass transport properties of the tumor interstitial matrix. *Front. Bioeng. Biotechnol.* 7:6. doi: 10.3389/fbioe.2019.00006

Bansal, N., Bartucci, M., Yusuff, S., Davis, S., Flaherty, K., Huselid, E., et al. (2016). BMI-1 targeting interferes with patient-derived tumor-initiating cell survival and tumor growth in prostate cancer. *Clin. Cancer Res.* 22, 6176–6191. doi: 10.1158/1078-0432.CCR-15-3107

Bansal, N., Davis, S., Tereshchenko, I., Budak-alpdogan, T., Zhong, H., Stein, M. N., et al. (2014). Enrichment of human prostate cancer cells with tumor initiating properties in mouse and zebrafish xenografts by differential adhesion. *Prostate* 74, 187–200. doi: 10.1002/pros.22740

Banyard, J., and Bielenberg, D. R. (2015). The role of EMT and MET in cancer dissemination. *Connect. Tissue Res.* 56, 403–413. doi: 10.3109/03008207.2015.1060970

Barkan, D., Green, J. E., and Chambers, A. F. (2010). Extracellular matrix: a gatekeeper in the transition from dormancy to metastatic growth. *Eur. J. Cancer* 46, 1181–1188. doi: 10.1016/j.ejca.2010.02.027

Barker, H. E., Cox, T. R., and Erler, J. T. (2012). The rationale for targeting the LOX family in cancer. *Nat. Rev. Cancer* 12, 540–552. doi: 10.1038/nrc3319

Barney, L. E., Dandley, E. C., Jansen, L. E., Reich, N. G., Mercurio, A. M., and Peyton, S. R. (2015). A cell-ECM screening method to predict breast cancer metastasis. *Integr. Biol.* 7, 198–212. doi: 10.1039/c4ib00218k

Bartucci, M., Ferrari, A. C., Kim, I. Y., Ploss, A., Yarmush, M., and Sabaawy, H. E. (2016). Personalized medicine approaches in prostate cancer employing patient derived 3D organoids and humanized mice. *Front. Cell Dev. Biol.* 4:64. doi: 10.3389/fcell.2016.00064

Bartucci, M., Patrizii, M., Huselid, E., Yussuf, S., Bansal, N., Flaherty, K., et al. (2015). Abstract 223: generation of single cell-derived normal, benign and cancer mini-prostates from primary patient-derived tissues. *Cancer Res.* 75, 223–223. doi: 10.1158/1538-7445.AM2015-223

Belgodere, J. A., King, C. T., Bursavich, J. B., Burow, M. E., Martin, E. C., and Jung, J. P. (2018). Engineering breast cancer microenvironments and 3D bioprinting. *Front. Bioeng. Biotechnol.* 6:66. doi: 10.3389/fbioe.2018.00066

Belloni, D., Heltai, S., Ponzoni, M., Villa, A., Vergani, B., Pecciarini, L., et al. (2018). Modeling multiple myeloma-bone marrow interactions and response to drugs in a 3d surrogate microenvironment. *Haematologica*. 2018:167486. doi: 10.3324/haematol.2017.167486

Bertotti, A., Migliardi, G., Galimi, F., Sassi, F., Torti, D., Isella, C., et al. (2011). A molecularly annotated platform of patient-derived xenografts (andquot;xenopatientsandquot;) identifies HER2 as an effective therapeutic target in cetuximab-resistant colorectal cancer. *Cancer Discov.* 1, 508–523. doi: 10.1158/2159-8290.CD-11-0109

Beshiri, M. L., Tice, C. M., Tran, C., Nguyen, H. M., Sowalsky, A. G., Agarwal, S., et al. (2018). A PDX/organoid biobank of advanced prostate cancers captures genomic and phenotypic heterogeneity for disease modeling and therapeutic screening. *Clin. Cancer Res.* 24, 4332–4345. doi: 10.1158/1078-0432.CCR-18-0409

Bhatia, S. N., and Ingber, D. E. (2014). Microfluidic organs-on-chips. *Nat. Biotechnol.* 32, 760–772. doi: 10.1038/nbt.2989

Birey, F., Andersen, J., Makinson, C. D., Islam, S., Wei, W., Huber, N., et al. (2017). Assembly of functionally integrated human forebrain spheroids. *Nature* 545, 54–59. doi: 10.1038/nature22330

Bissell, M. J., and Radisky, D. (2001). Putting tumours in context. *Nat. Rev. Cancer* 1, 46–54. doi: 10.1038/35094059

Bocci, F., Gearhart-Serna, L., Boareto, M., Ribeiro, M., Ben-Jacob, E., Devi, G. R., et al. (2019). Toward understanding cancer stem cell heterogeneity in the tumor microenvironment. *Proc. Natl. Acad. Sci. U.S.A.* 116, 148–157. doi: 10.1073/pnas.1815345116

Bock, N., Shokoohmand, A., Kryza, T., Röhl, J., Meijer, J., Tran, P. A., et al. (2019). Engineering osteoblastic metastases to delineate the adaptive response of androgen-deprived prostate cancer in the bone metastatic microenvironment. *Bone Res.* 7:13. doi: 10.1038/s41413-019-0049-8

Boj, S. F., Hwang, C.-I., Baker, L. A., Chio, I. I. C., Engle, D. D., Corbo, V., et al. (2015). Organoid models of human and mouse ductal pancreatic cancer. *Cell* 160, 324–338. doi: 10.1016/J.CELL.2014.12.021

Bos, P. D., Zhang, X. H. F., Nadal, C., Shu, W., Gomis, R. R., Nguyen, D. X., et al. (2009). Genes that mediate breast cancer metastasis to the brain. *Nature* 459, 1005–1009. doi: 10.1038/nature08021

Boyd, N. F., Li, Q., Melnichouk, O., Huszti, E., Martin, L. J., Gunasekara, A., et al. (2014). Evidence that breast tissue stiffness is associated with risk of breast cancer. *PLoS ONE* 9:e100937. doi: 10.1371/journal.pone.0100937

Brancato, V., Garziano, A., Gioiella, F., Urciuolo, F., Imparato, G., Panzetta, V., et al. (2017). 3D is not enough: building up a cell instructive microenvironment for tumoral stroma microtissues. *Acta Biomater.* 47, 1–13. doi: 10.1016/J.ACTBIO.2016.10.007

Brancato, V., Ventre, M., Imparato, G., Urciuolo, F., Meo, C., and Netti, P. A. (2018). A straightforward method to produce decellularized dermis-based matrices for tumour cell cultures. *J. Tissue Eng. Regen. Med.* 12, e71–e81. doi: 10.1002/term.2350

Bray, L. J., Binner, M., Holzheu, A., Friedrichs, J., Freudenberg, U., Hutmacher, D. W., et al. (2015). Multi-parametric hydrogels support 3D *in vitro* bioengineered microenvironment models of tumour angiogenesis. *Biomaterials* 53, 609–620. doi: 10.1016/j.biomaterials.2015.02.124

Bray, L. J., Binner, M., Körner, Y., Von Bonin, M., Bornhäuser, M., and Werner, C. (2017). A three-dimensional *ex vivo* tri-culture model mimics cell-cell interactions between acute myeloid leukemia and the vascular niche. *Haematologica* 102, 1215–1226. doi: 10.3324/haematol.2016.157883

Bray, L. J., Secker, C., Murekatete, B., Sievers, J., Binner, M., Welzel, P. B., et al. (2018). Three-dimensional *in vitro* hydro-and cryogel-based cell-culture models for the study of breast-cancer metastasis to bone. *Cancers* 10, 1–25. doi: 10.3390/cancers10090292

Burrell, R. A., McGranahan, N., Bartek, J., and Swanton, C. (2013). The causes and consequences of genetic heterogeneity in cancer evolution. *Nature* 501, 338–345. doi: 10.1038/nature12625

Caballero, D., Kaushik, S., Correlo, V. M., Oliveira, J. M., Reis, R. L., and Kundu, S. C. (2017). Organ-on-chip models of cancer metastasis for future personalized medicine: from chip to the patient. *Biomaterials* 149, 98–115. doi: 10.1016/J.biomaterials.2017.10.005

Carr, S. D., Green, V. L., Stafford, N. D., and Greenman, J. (2014). Analysis of radiation-induced cell death in head and neck squamous cell carcinoma and rat liver maintained in microfluidic devices. *Otolaryngol. Neck Surg.* 150, 73–80. doi: 10.1177/0194599813507427

Carranza-Torres, I. E., Guzmán-Delgado, N. E., Coronado-Martínez, C., Bañuelos-García, J. I., Viveros-Valdez, E., Morán-Martínez, J., et al. (2015). Organotypic culture of breast tumor explants as a multicellular system for the screening of natural compounds with antineoplastic potential. *Biomed Res. Int.* 2015:618021. doi: 10.1155/2015/618021

Carvalho, M. R., Lima, D., Reis, R. L., Correlo, V. M., and Oliveira, J. M. (2015). Evaluating biomaterial- and microfluidic-based 3D tumor models. *Trends Biotechnol.* 33, 667–678. doi: 10.1016/J.TIBTECH.2015.09.009

Cassidy, J. W., Caldas, C., and Bruna, A. (2015). Maintaining tumor heterogeneity in patient-derived tumor xenografts. *Cancer Res.* 75, 2963–2968. doi: 10.1158/0008-5472.CAN-15-0727

Centenera, M. M., Gillis, J. L., Hanson, A. R., Jindal, S., Taylor, R. A., Risbridger, G. P., et al. (2012). Evidence for efficacy of new hsp90 inhibitors revealed by

ex vivo culture of human prostate tumors. *Clin. Cancer Res.* 18, 3562–3570. doi: 10.1158/1078-0432.CCR-12-0782

Centenera, M. M., Hickey, T. E., Jindal, S., Ryan, N. K., Ravindranathan, P., Mohammed, H., et al. (2018). A patient-derived explant (PDE) model of hormone-dependent cancer. *Mol. Oncol.* 12, 1608–1622. doi: 10.1002/1878-0261.12354

Centenera, M. M., Raj, G. V., Knudsen, K. E., Tilley, W. D., and Butler, L. M. (2013). *Ex vivo* culture of human prostate tissue and drug development. *Nat. Rev. Urol.* 10, 483–487. doi: 10.1038/nrurol.2013.126

Chakraborty, S., Hosen, M. I., Ahmed, M., and Shekhar, H. U. (2018). Onco-multi-OMICS approach: a new frontier in cancer research. *Biomed Res. Int.* 2018, 1–14. doi: 10.1155/2018/9836256

Chambers, A. F., Groom, A. C., and MacDonald, I. C. (2002). Dissemination and growth of cancer cells in metastatic sites. *Nat. Rev. Cancer* 2:563. doi: 10.1038/nrc865

Cheah, R., Srivastava, R., Stafford, N. D., Beavis, A. W., Green, V., and Greenman, J. (2017). Measuring the response of human head and neck squamous cell carcinoma to irradiation in a microfluidic model allowing customized therapy. *Int. J. Oncol.* 51, 1227–1238. doi: 10.3892/ijo.2017.4118

Chen, W., Hoffmann, A. D., Liu, H., and Liu, X. (2018). Organotropism: new insights into molecular mechanisms of breast cancer metastasis. *NPJ Precis. Oncol.* 2:4. doi: 10.1038/s41698-018-0047-0

Cheung, K. J., Gabrielson, E., Werb, Z., and Ewald, A. J. (2013). Collective invasion in breast cancer requires a conserved basal epithelial program. *Cell* 155, 1639–1651. doi: 10.1016/j.cell.2013.11.029

Choi, Y., Lee, S., Kim, K., Kim, S.-H., Chung, Y.-J., and Lee, C. (2018). Studying cancer immunotherapy using patient-derived xenografts (PDXs) in humanized mice. *Exp. Mol. Med.* 50:99. doi: 10.1038/s12276-018-0115-0

Chung, B., Esmaeili, A. A., Gopalakrishna-Pillai, S., Murad, J. P., Andersen, E. S., Reddy, N. K., et al. (2017). Human brain metastatic stroma attracts breast cancer cells via chemokines CXCL16 and CXCL12. *NPJ Breast Cancer* 3, 1–8. doi: 10.1038/s41523-017-0008-8

Chwalek, K., Tsurkan, M. V., Freudenberg, U., and Werner, C. (2014). Glycosaminoglycan-based hydrogels to modulate heterocellular communication in *in vitro* angiogenesis models. *Sci. Rep.* 4:4414. doi: 10.1038/srep04414

Colditz, G. A., and Peterson, L. L. (2018). Obesity and cancer: evidence, impact, and future directions. *Clin. Chem.* 64, 154–162. doi: 10.1373/clinchem.2017.277376

Condeelis, J., and Segall, J. E. (2003). Intravital imaging of cell movement in tumours. *Nat. Rev. Cancer* 3, 921–930. doi: 10.1038/nrc1231

Costa-Silva, B., Aiello, N. M., Ocean, A. J., Singh, S., Zhang, H., Thakur, B. K., et al. (2015). Pancreatic cancer exosomes initiate pre-metastatic niche formation in the liver. *Nat. Cell Biol.* 17, 816–826. doi: 10.1038/ncb3169

Cox, T. R., and Erler, J. T. (2011). Remodeling and homeostasis of the extracellular matrix: implications for fibrotic diseases and cancer. *Dis. Model. Mech.* 4, 165–178. doi: 10.1242/dmm.004077

Cozzo, A. J., Fuller, A. M., and Makowski, L. (2017). Contribution of adipose tissue to development of cancer. *Compr. Physiol.* 8:237. doi: 10.1002/CPHY.C170008

Dagogo-Jack, I., and Shaw, A. T. (2017). Tumour heterogeneity and resistance to cancer therapies. *Nat. Rev. Clin. Oncol.* 15, 81–94. doi: 10.1038/nrclinonc.2017.166

Daniel, V. C., Marchionni, L., Hierman, J. S., Rhodes, J. T., Devereux, W. L., Rudin, C. M., et al. (2009). A primary xenograft model of small-cell lung cancer reveals irreversible changes in gene expression imposed by culture *in vitro*. *Cancer Res.* 69, 3364–3373. doi: 10.1158/0008-5472.CAN-08-4210

Davies, E. J., Dong, M., Gutekunst, M., Närhi, K., van Zoggel, H. J. A. A., Blom, S., et al. (2015). Capturing complex tumour biology *in vitro*: histological and molecular characterisation of precision cut slices. *Sci. Rep.* 5:17187. doi: 10.1038/srep17187

de Boer, M., van Deurzen, C. H. M., van Dijck, J. A. A. M., Borm, G. F., van Diest, P. J., Adang, E. M. M., et al. (2009). Micrometastases or isolated tumor cells and the outcome of breast cancer. *N. Engl. J. Med.* 361, 653–663. doi: 10.1056/NEJMoa0904832

de la Puente, P., Muz, B., Gilson, R. C., Azab, F., Luderer, M., King, J., et al. (2015). 3D tissue-engineered bone marrow as a novel model to study pathophysiology and drug resistance in multiple myeloma. *Biomaterials* 73, 70–84. doi: 10.1016/J.biomaterials.2015.09.017

Diab, D. L., Yerian, L., Schauer, P., Kashyap, S. R., Lopez, R., Hazen, L., et al. (2009). Cytokeratin 18 fragment levels as a noninvasive biomarker for nonalcoholic steatohepatitis in bariatric surgery patients. *Clin. Gastroenterol. Hepatol.* 6, 1249–1254. doi: 10.1016/j.cgh.2008.07.016

Donaldson, A. R., Tanase, C. E., Awuah, D., Vasanthi Bathrinarayanan, P., Hall, L., Nikkhah, M., et al. (2018). Photocrosslinkable gelatin hydrogels modulate the production of the major pro-inflammatory cytokine, TNF-α, by human mononuclear cells. *Front. Bioeng. Biotechnol.* 6:116. doi: 10.3389/fbioe.2018.00116

Drost, J., Karthaus, W. R., Gao, D., Driehuis, E., Sawyers, C. L., Chen, Y., et al. (2016). Organoid culture systems for prostate epithelial and cancer tissue. *Nat. Protoc.* 11, 347–358. doi: 10.1038/nprot.2016.006

Erler, J. T., Bennewith, K. L., Nicolau, M., Dornhöfer, N., Kong, C., Le, Q.-T., et al. (2006). Lysyl oxidase is essential for hypoxia-induced metastasis. *Nature* 440, 1222–1226. doi: 10.1038/nature04695

Esch, E. W., Bahinski, A., and Huh, D. (2015). Organs-on-chips at the frontiers of drug discovery. *Nat. Rev. Drug Discov.* 14, 248–260. doi: 10.1038/nrd4539

Fang, Y., and Eglen, R. M. (2017). Three-dimensional cell cultures in drug discovery and development. *SLAS Discov. Adv. life Sci. R D* 22, 456–472. doi: 10.1177/1087057117696795

Ferrarini, M., Steimberg, N., Ponzoni, M., Belloni, D., Berenzi, A., Girlanda, S., et al. (2013). *Ex-vivo* dynamic 3-D culture of human tissues in the RCCS^{TM} bioreactor allows the study of multiple myeloma biology and response to therapy. *PLoS ONE* 8:e71613. doi: 10.1371/journal.pone.0071613

Ferreira, L. P., Gaspar, V. M., and Mano, J. F. (2018). Design of spherically structured 3D *in vitro* tumor models -advances and prospects. *Acta Biomater.* 75, 11–34. doi: 10.1016/j.actbio.2018.05.034

Fidler, I. J. (1978). Tumor heterogeneity and the biology of cancer invasion and metastasis. *Cancer Res.* 38, 2651–60.

Filipe, E. C., Chitty, J. L., and Cox, T. R. (2018). Charting the unexplored extracellular matrix in cancer. *Int. J. Exp. Pathol.* 99, 58–76. doi: 10.1111/iep.12269

Fischbach, C., Chen, R., Matsumoto, T., Schmelzle, T., Brugge, J. S., Polverini, P. J., et al. (2007). Engineering tumors with 3D scaffolds. *Nat. Methods* 4, 855–860. doi: 10.1038/nmeth1085

Fisher, R., Pusztai, L., and Swanton, C. (2013). Cancer heterogeneity: implications for targeted therapeutics. *Br. J. Cancer* 108, 479–485. doi: 10.1038/bjc.2012.581

Foley, K. E. (2017). Organoids: a better *in vitro* model. *Nat. Methods* 14, 559–562. doi: 10.1038/nmeth.4307

Fong, E. L. S., Harrington, D. A., Farach-Carson, M. C., and Yu, H. (2016a). Heralding a new paradigm in 3D tumor modeling. *Biomaterials* 108, 197–213. doi: 10.1016/J.biomaterials.2016.08.052

Fong, E. L. S., Martinez, M., Yang, J., Mikos, A. G., Navone, N. M., Harrington, D. A., et al. (2014). Hydrogel-based 3D model of patient-derived prostate xenograft tumors suitable for drug screening. *Mol. Pharm.* 11, 2040–2050. doi: 10.1021/mp500085p

Fong, E. L. S., Toh, T. B., Lin, Q. X. X., Liu, Z., Hooi, L., Mohd Abdul Rashid, M. B., et al. (2018). Generation of matched patient-derived xenograft *in vitro-in vivo* models using 3D macroporous hydrogels for the study of liver cancer. *Biomaterials* 159, 229–240. doi: 10.1016/J.biomaterials.2017.12.026

Fong, E. L. S., Wan, X., Yang, J., Morgado, M., Mikos, A. G., Harrington, D. A., et al. (2016b). A 3D *in vitro* model of patient-derived prostate cancer xenograft for controlled interrogation of *in vivo* tumor-stromal interactions. *Biomaterials.* 2016:59. doi: 10.1016/j.biomaterials.2015.10.059

Friedl, P., and Alexander, S. (2011). Cancer invasion and the microenvironment: plasticity and reciprocity. *Cell* 147, 992–1009. doi: 10.1016/j.cell.2011.11.016

Gao, D., Vela, I., Sboner, A., Iaquinta, P. J., Karthaus, W. R., Gopalan, A., et al. (2014). Organoid cultures derived from patients with advanced prostate cancer. *Cell.* 2014:16. doi: 10.1016/j.cell.2014.08.016

Geller, J., Partido, C., Sionit, L., Youngkin, T., Nachtsheim, D., Espanol, M., et al. (1997). Comparison of androgen-independent growth and androgen-dependent growth in BPH and cancer tissue from the same radical prostatectomies in sponge-gel matrix histoculture. *Prostate* 31, 250–254. doi: 10.1002/(SICI)1097-0045(19970601)31:4<250::AID-PROS6>3.0.CO;2-O

Gerlach, M. M., Merz, F., Wichmann, G., Kubick, C., Wittekind, C., Lordick, F., et al. (2014). Slice cultures from head and neck squamous cell carcinoma: a novel test system for drug susceptibility and mechanisms of resistance. *Br. J. Cancer* 110, 479–488. doi: 10.1038/bjc.2013.700

Ghosh, S., Prasad, M., Kundu, K., Cohen, L., Yegodayev, K. M., Zorea, J., et al. (2019). Tumor tissue explant culture of patient-derived xenograft as potential prioritization tool for targeted therapy. *Front. Oncol.* 9:17. doi: 10.3389/FONC.2019.00017

Gillet, J.-P., Varma, S., and Gottesman, M. M. (2013). The clinical relevance of cancer cell lines. *JNCI J. Natl. Cancer Inst.* 105, 452–458. doi: 10.1093/jnci/djt007

Gkretsi, V., and Stylianopoulos, T. (2018). Cell adhesion and matrix stiffness: coordinating cancer cell invasion and metastasis. *Front. Oncol.* 8:145. doi: 10.3389/fonc.2018.00145

Gkretsi, V., Stylianou, A., Papageorgis, P., Polydorou, C., and Stylianopoulos, T. (2015). Remodeling components of the tumor microenvironment to enhance cancer therapy. *Front. Oncol.* 5:214. doi: 10.3389/fonc.2015.00214

Griffith, L. G., and Swartz, M. A. (2006). Capturing complex 3D tissue physiology *in vitro*. *Nat. Rev. Mol. Cell Biol.* 7, 211–224. doi: 10.1038/nrm1858

Hagemann, J., Jacobi, C., Hahn, M., Schmid, V., Welz, C., Schwenk-Zieger, S., et al. (2017). Spheroid-based 3D cell cultures enable personalized therapy testing and drug discovery in head and neck cancer. *Anticancer Res.* 37, 2201–2210. doi: 10.21873/anticanres.11555

Halfter, K., Ditsch, N., Kolberg, H.-C., Fischer, H., Hauzenberger, T., von Koch, F. E., et al. (2015). Prospective cohort study using the breast cancer spheroid model as a predictor for response to neoadjuvant therapy–the SpheroNEO study. *BMC Cancer* 15:519. doi: 10.1186/s12885-015-1491-7

Halfter, K., and Mayer, B. (2017). Bringing 3D tumor models to the clinic – predictive value for personalized medicine. *Biotechnol. J.* 2017:295. doi: 10.1002/biot.201600295

Hällström, T. M. K., Jäämaa, S., Mönkkönen, M., Peltonen, K., Andersson, L. C., Medema, R. H., et al. (2007). Human prostate epithelium lacks Wee1A-mediated DNA damage-induced checkpoint enforcement. *Proc. Natl. Acad. Sci. U.S.A.* 104, 7211–7216. doi: 10.1073/PNAS.0609299104

Han, S., Yan, J.-J., Shin, Y., Jeon, J. J., Won, J., Eun Jeong, H., et al. (2012). A versatile assay for monitoring *in vivo*-like transendothelial migration of neutrophils. *Lab Chip* 12:3861. doi: 10.1039/c2lc40445a

Hanahan, D., and Weinberg, R. A. (2011). Hallmarks of cancer: the next generation. *Cell* 144, 646–674. doi: 10.1016/J.CELL.2011.02.013

Hassell, B. A., Goyal, G., Lee, E., Sontheimer-Phelps, A., Levy, O., Chen, C. S., et al. (2017). Human organ chip models recapitulate orthotopic lung cancer growth, therapeutic responses, and tumor dormancy *in vitro*. *Cell Rep.* 21, 508–516. doi: 10.1016/J.CELREP.2017.09.043

Hida, K., Maishi, N., Annan, D. A., and Hida, Y. (2018). Contribution of tumor endothelial cells in cancer progression. *Int. J. Mol. Sci.* 19:1272. doi: 10.3390/ijms19051272

Hidalgo, M., Amant, F., Biankin, A. V., Budinská, E., Byrne, A. T., Caldas, C., et al. (2014). Patient-derived xenograft models: an emerging platform for translational cancer research. *Cancer Discov.* 4, 998–1013. doi: 10.1158/2159-8290.CD-14-0001

Hiratsuka, S., Watanabe, A., Aburatani, H., and Maru, Y. (2006). Tumour-mediated upregulation of chemoattractants and recruitment of myeloid cells predetermines lung metastasis. *Nat. Cell Biol.* 8, 1369–1375. doi: 10.1038/ncb1507

Hirt, C., Papadimitropoulos, A., Muraro, M. G., Mele, V., Panopoulos, E., Cremonesi, E., et al. (2015). Bioreactor-engineered cancer tissue-like structures mimic phenotypes, gene expression profiles and drug resistance patterns observed "*in vivo*." *Biomaterials* 62, 138–146. doi: 10.1016/J.biomaterials.2015.05.037

Holliday, D. L., Moss, M. A., Pollock, S., Lane, S., Shaaban, A. M., Millican-Slater, R., et al. (2013). The practicalities of using tissue slices as preclinical organotypic breast cancer models. *J. Clin. Pathol.* 66, 253–255. doi: 10.1136/JCLINPATH-2012-201147

Holton, A. B., Sinatra, F. L., Kreahling, J., Conway, A. J., Landis, D. A., and Altiok, S. (2017). Microfluidic biopsy trapping device for the real-time monitoring of tumor microenvironment. *PLoS ONE* 12:e0169797. doi: 10.1371/journal.pone.0169797

Hoshiba, T., and Tanaka, M. (2016). Decellularized matrices as *in vitro* models of extracellular matrix in tumor tissues at different malignant levels: mechanism of 5-fluorouracil resistance in colorectal tumor cells. *Biochim. Biophys. Acta - Mol. Cell Res.* 1863, 2749–2757. doi: 10.1016/J.BBAMCR.2016.08.009

Hoshino, A., Costa-Silva, B., Shen, T. L., Rodrigues, G., Hashimoto, A., Tesic Mark, M., et al. (2015). Tumour exosome integrins determine organotropic metastasis. *Nature* 527, 329–335. doi: 10.1038/nature15756

Hribar, K. C., Wheeler, C. J., Bazarov, A., Varshneya, K., Yamada, R., Buckley, P., et al. (2019). A simple three-dimensional hydrogel platform enables *ex vivo* cell culture of patient and PDX tumors for assaying their response to clinically relevant therapies. *Mol. Cancer Ther.* 18:molcanther.0359.2018. doi: 10.1158/1535-7163.MCT-18-0359

Ilina, O., Campanello, L., Gritsenko, P. G., Vullings, M., Wang, C., Bult, P., et al. (2018). Intravital microscopy of collective invasion plasticity in breast cancer. *Dis. Model. Mech.* 11:dmm034330. doi: 10.1242/dmm.034330

Insua-Rodríguez, J., and Oskarsson, T. (2016). The extracellular matrix in breast cancer. *Adv. Drug Deliv. Rev.* 97, 41–55. doi: 10.1016/J.ADDR.2015.12.017

Jeffrey, W., Weigang, W., Elaine, Y. L., Yarong, W., Fiona, P., Stanley, E. R., et al. (2004). A paracrine loop between tumor cells and macrophages is required for tumor cell migration in mammary tumors. *Cancer Res.* 64, 7022–7029. doi: 10.1158/0008-5472.CAN-04-1449

Jenkins, R. W., Aref, A. R., Lizotte, P. H., Ivanova, E., Stinson, S., Zhou, C. W., et al. (2018). *Ex vivo* profiling of PD-1 blockade using organotypic tumor spheroids. *Cancer Discov.* 8, 196–215. doi: 10.1158/2159-8290.CD-17-0833

Jin, Q., Liu, G., Li, S., Yuan, H., Yun, Z., Zhang, W., et al. (2019). Decellularized breast matrix as bioactive microenvironment for *in vitro* three-dimensional cancer culture. *J. Cell. Physiol.* 234, 3425–3435. doi: 10.1002/jcp.26782

Julien, S., Merino-Trigo, A., Lacroix, L., Pocard, M., Goere, D., Mariani, P., et al. (2012). Characterization of a large panel of patient-derived tumor xenografts representing the clinical heterogeneity of human colorectal cancer. *Clin. Cancer Res.* 18, 5314–5328. doi: 10.1158/1078-0432.CCR-12-0372

Junttila, M. R., and de Sauvage, F. J. (2013). Influence of tumour micro-environment heterogeneity on therapeutic response. *Nature* 501, 346–354. doi: 10.1038/nature12626

Kaemmerer, E., Melchels, F. P. W., Holzapfel, B. M., Meckel, T., Hutmacher, D. W., and Loessner, D. (2014). Gelatine methacrylamide-based hydrogels: an alternative three-dimensional cancer cell culture system. *Acta Biomater.* 10, 2551–2562. doi: 10.1016/j.actbio.2014.02.035

Kalli, M., and Stylianopoulos, T. (2018). Defining the role of solid stress and matrix stiffness in cancer cell proliferation and metastasis. *Front. Oncol.* 8:55. doi: 10.3389/fonc.2018.00055

Kalluri, R. (2016). The biology and function of fibroblasts in cancer. *Nat. Rev. Cancer* 16, 582–598. doi: 10.1038/nrc.2016.73

Kaplan, R. N., Rafii, S., and Lyden, D. (2006). Preparing the "soil": The premetastatic niche. *Cancer Res.* 66, 11089–11093. doi: 10.1158/0008-5472.CAN-06-2407

Kaplan, R. N., Riba, R. D., Zacharoulis, S., Bramley, A. H., Vincent, L., Costa, C., et al. (2005). VEGFR1-positive haematopoietic bone marrow progenitors initiate the pre-metastatic niche. *Nature* 438, 820–827. doi: 10.1038/nature04186

Katt, M. E., Placone, A. L., Wong, A. D., Xu, Z. S., and Searson, P. C. (2016). *In vitro* tumor models: advantages, disadvantages, variables, and selecting the right platform. *Front. Bioeng. Biotechnol.* 4:12. doi: 10.3389/fbioe.2016.00012

Ke, D., and Murphy, S. V. (2019). Current challenges of bioprinted tissues toward clinical translation. *Tissue Eng. Part B Rev.* 25, 1–13. doi: 10.1089/ten.teb.2018.0132

Kennedy, R., Kuvshinov, D., Sdrolia, A., Kuvshinova, E., Hilton, K., Crank, S., et al. (2019). A patient tumour-on-a-chip system for personalised investigation of radiotherapy based treatment regimens. *Sci. Rep.* 9:6327. doi: 10.1038/s41598-019-42745-2

Khin, Z. P., Ribeiro, M. L. C., Jacobson, T., Hazlehurst, L., Perez, L., Baz, R., et al. (2014). A preclinical assay for chemosensitivity in multiple myeloma. *Cancer Res.* 74, 56–67. doi: 10.1158/0008-5472.CAN-13-2397

Kijima, T., Nakagawa, H., Shimonosono, M., Chandramouleeswaran, P. M., Hara, T., Sahu, V., et al. (2019). Three-dimensional organoids reveal therapy resistance of esophageal and oropharyngeal squamous cell carcinoma cells. *Cmgh* 7, 73–91. doi: 10.1016/j.jcmgh.2018.09.003

Knowlton, S., Onal, S., Yu, C. H., Zhao, J. J., and Tasoglu, S. (2015). Bioprinting for cancer research. *Trends Biotechnol.* 33, 504–513. doi: 10.1016/J.TIBTECH.2015.06.007

Koerfer, J., Kallendrusch, S., Merz, F., Wittekind, C., Kubick, C., Kassahun, W. T., et al. (2016). Organotypic slice cultures of human gastric and esophagogastric junction cancer. *Cancer Med.* 5, 1444–1453. doi: 10.1002/cam4.720

Kondo, J., Ekawa, T., Endo, H., Yamazaki, K., Tanaka, N., Kukita, Y., et al. (2018). High-throughput screening in colorectal cancer tissue-originated spheroids. *Cancer Sci.* 345–355. doi: 10.1111/cas.13843

Kondo, J., Endo, H., Okuyama, H., Ishikawa, O., Iishi, H., Tsujii, M., et al. (2011). Retaining cell-cell contact enables preparation and culture of spheroids composed of pure primary cancer cells from colorectal cancer. *Proc. Natl. Acad. Sci. U.S.A.* 108, 6235–6240. doi: 10.1073/pnas.1015938108

Krumdieck, C. L., Santos, J. E., and Ho, K. (1980). A new instrument for the rapid preparation of tissue slices. *Anal. Biochem*. 104, 118–123

Kucia, M., Reca, R., Miekus, K., Wanzeck, J., Wojakowski, W., Janowska-Wieczorek, A., et al. (2005). Trafficking of normal stem cells and metastasis of cancer stem cells involve similar mechanisms: pivotal role of the SDF-1-CXCR4 axis. *Stem Cells* 23, 879–894. doi: 10.1634/stemcells.2004-0342

Langer, E. M., Allen-Petersen, B. L., King, S. M., Kendsersky, N. D., Turnidge, M. A., Kuziel, G. M., et al. (2019). Modeling tumor phenotypes *in vitro* with three-dimensional bioprinting. *Cell Rep.* 26:608-623.e6. doi: 10.1016/J.CELREP.2018.12.090

Lawson, D. A., Kessenbrock, K., Davis, R. T., Pervolarakis, N., and Werb, Z. (2018). Tumour heterogeneity and metastasis at single-cell resolution. *Nat. Cell Biol.* 20, 1349–1360. doi: 10.1038/s41556-018-0236-7

LeBleu, V. S., and Kalluri, R. (2018). A peek into cancer-associated fibroblasts: origins, functions and translational impact. *Dis. Model. Mech.* 11:dmm029447. doi: 10.1242/dmm.029447

Lee, S. W. L., Adriani, G., Ceccarello, E., Pavesi, A., Tan, A. T., Bertoletti, A., et al. (2018). Characterizing the role of monocytes in T cell cancer immunotherapy using a 3D microfluidic model. *Front. Immunol.* 9:416. doi: 10.3389/fimmu.2018.00416

Li, H., Tan, C., and Li, L. (2018a). Review of 3D printable hydrogels and constructs. *Mater. Des.* 159, 20–38. doi: 10.1016/J.MATDES.2018.08.023

Li, Q., Lin, H., Rauch, J., Deleyrolle, L. P., Reynolds, B. A., Viljoen, H. J., et al. (2018b). Scalable culturing of primary human glioblastoma tumor-initiating cells with a cell-friendly culture system. *Sci. Rep.* 8:3531. doi: 10.1038/s41598-018-21927-4

Li, Y. F., and Kumacheva, E. (2018). Hydrogel microenvironments for cancer spheroid growth and drug screening. *Sci. Adv.* 4:8998. doi: 10.1126/sciadv.aas8998

Lim, C. Y., Chang, J. H., Lee, W. S., Lee, K. M., Yoon, Y. C., Kim, J., et al. (2018). Organotypic slice cultures of pancreatic ductal adenocarcinoma preserve the tumor microenvironment and provide a platform for drug response. *Pancreatology* 18, 913–927. doi: 10.1016/j.pan.2018.09.009

Linxweiler, J., Hammer, M., Muhs, S., Kohn, M., Pryalukhin, A., Veith, C., et al. (2018). Patient-derived, three-dimensional spheroid cultures provide a versatile translational model for the study of organ-confined prostate cancer. *J. Cancer Res. Clin. Oncol.* 2018, 1–9. doi: 10.1007/s00432-018-2803-5

Liu, G., Wang, B., Li, S., Jin, Q., and Dai, Y. (2019). Human breast cancer decellularized scaffolds promote epithelial-to-mesenchymal transitions and stemness of breast cancer cells *in vitro*. *J. Cell. Physiol.* 234, 9447–9456. doi: 10.1002/jcp.27630

Liu, J., Tan, Y., Zhang, H., Zhang, Y., Xu, P., Chen, J., et al. (2012). Soft fibrin gels promote selection and growth of tumorigenic cells. *Nat. Mater.* 11, 734–741. doi: 10.1038/nmat3361

Liu, X., Lukowski, J. K., Flinders, C., Kim, S., Georgiadis, R. A., Mumenthaler, S. M., et al. (2018). MALDI-MSI of immunotherapy: mapping the EGFR-targeting antibody cetuximab in 3D colon-cancer cell cultures. *Anal. Chem.* 90, 14156–14164. doi: 10.1021/acs.analchem.8b02151

Loessner, D., Meinert, C., Kaemmerer, E., Martine, L. C., Yue, K., Levett, P. A., et al. (2016). Functionalization, preparation and use of cell-laden gelatin methacryloyl-based hydrogels as modular tissue culture platforms. *Nat. Protoc.* 11, 727–746. doi: 10.1038/nprot.2016.037

Lu, P., Weaver, V. M., and Werb, Z. (2012). The extracellular matrix: a dynamic niche in cancer progression. *J. Cell Biol.* 196, 395–406. doi: 10.1083/jcb.201102147

Ma, X., Liu, J., Zhu, W., Tang, M., Lawrence, N., Yu, C., et al. (2018). 3D bioprinting of functional tissue models for personalized drug screening and *in vitro* disease modeling. *Adv. Drug Deliv. Rev.* 132, 235–251. doi: 10.1016/J.ADDR.2018.06.011

Majumder, B., Baraneedharan, U., Thiyagarajan, S., Radhakrishnan, P., Narasimhan, H., Dhandapani, M., et al. (2015). Predicting clinical response to anticancer drugs using an *ex vivo* platform that captures tumour heterogeneity. *Nat. Commun.* 6:6169. doi: 10.1038/ncomms7169

Malandrino, A., Mak, M., Kamm, R. D., and Moeendarbary, E. (2018). Complex mechanics of the heterogeneous extracellular matrix in cancer. *Extrem. Mech. Lett.* 21, 25–34. doi: 10.1016/J.EML.2018.02.003

Manfredonia, C., Muraro, M. G., Hirt, C., Mele, V., Governa, V., Papadimitropoulos, A., et al. (2019). Maintenance of primary human colorectal cancer microenvironment using a perfusion bioreactor-based 3D culture system. *Adv. Biosyst.* 3:1800300. doi: 10.1002/adbi.201800300

Martin, I., Wendt, D., and Heberer, M. (2004). The role of bioreactors in tissue engineering. *Trends Biotechnol.* 22, 80–86. doi: 10.1016/J.TIBTECH.2003.12.001

Maschmeyer, I., Hasenberg, T., Jaenicke, A., Lindner, M., Lorenz, A. K., Zech, J., et al. (2015). Chip-based human liver-intestine and liver-skin co-cultures–A first step toward systemic repeated dose substance testing *in vitro*. *Eur. J. Pharm. Biopharm.* 95, 77–87. doi: 10.1016/j.ejpb.2015.03.002

Matano, M., Date, S., Shimokawa, M., Takano, A., Fujii, M., Ohta, Y., et al. (2015). Modeling colorectal cancer using CRISPR-Cas9 – mediated engineering of human intestinal organoids. *Nat. Med.* 21, 256–262. doi: 10.1038/nm.3802

Matossian, M. D., Burks, H. E., Elliott, S., Hoang, V. T., Bowles, A. C., Sabol, R. A., et al. (2019). Drug resistance profiling of a new triple negative breast cancer patient-derived xenograft model. *BMC Cancer* 19:205. doi: 10.1186/s12885-019-5401-2

Mazzocchi, A., Devarasetty, M., Herberg, S., Petty, W. J., Marini, F., Miller, L., et al. (2019). Pleural effusion aspirate for use in 3D lung cancer modeling and chemotherapy screening. *ACS Biomater. Sci. Eng.* 5, 1937–1943. doi: 10.1021/acsbiomaterials.8b01356

Mazzocchi, A. R., Rajan, S. A. P., Votanopoulos, K. I., Hall, A. R., and Skardal, A. (2018). *In vitro* patient-derived 3D mesothelioma tumor organoids facilitate patient-centric therapeutic screening. *Sci. Rep.* 8:2886. doi: 10.1038/s41598-018-21200-8

McCulloch, D. R., Opeskin, K., Thompson, E. W., and Williams, E. D. (2005). BM18: a novel androgen-dependent human prostate cancer xenograft model derived from a bone metastasis. *Prostate* 65, 35–43. doi: 10.1002/pros.20255

Meijer, T. G., Naipal, K. A., Jager, A., and van Gent, D. C. (2017). *Ex vivo* tumor culture systems for functional drug testing and therapy response prediction. *Futur. Sci. OA*. 2017:3. doi: 10.4155/fsoa-2017-0003

Meinert, C., Theodoropoulos, C., Klein, T. J., Hutmacher, D. W., and Loessner, D. (2018). "A method for prostate and breast cancer cell spheroid cultures using gelatin methacryloyl-based hydrogels," in *Methods in Molecular Biology*, ed Z. Culig (New York, NY: Humana Press), 175–194. doi: 10.1007/978-1-4939-7845-8_10

Meng, F., Meyer, C. M., Joung, D., Vallera, D. A., McAlpine, M. C., and Panoskaltsis-Mortari, A. (2019). 3D bioprinted *in vitro* metastatic models via reconstruction of tumor microenvironments. *Adv. Mater.* 2019:1806899. doi: 10.1002/adma.201806899

Merz, F., Gaunitz, F., Dehghani, F., Renner, C., Meixensberger, J., Gutenberg, A., et al. (2013). Organotypic slice cultures of human glioblastoma reveal different susceptibilities to treatments. *Neuro. Oncol.* 15, 670–681. doi: 10.1093/neuonc/not003

Minn, A. J., Gupta, G. P., Siegel, P. M., Bos, P. D., Shu, W., Giri, D. D., et al. (2005). Genes that mediate breast cancer metastasis to lung. *Nature* 436, 518–524. doi: 10.1038/nature03799

Misra, S., Moro, C. F., Del Chiaro, M., Pouso, S., Sebestyén, A., Löhr, M., et al. (2019). *Ex vivo* organotypic culture system of precision-cut slices of human pancreatic ductal adenocarcinoma. *Sci. Rep.* 9:2133. doi: 10.1038/s41598-019-38603-w

Moore, N., Doty, D., Zielstorff, M., Kariv, I., Moy, L. Y., Gimbel, A., et al. (2018). A multiplexed microfluidic system for evaluation of dynamics of immune–tumor interactions. *Lab Chip* 18, 1844–1858. doi: 10.1039/C8LC00256H

Mousavi, N., Truelsen, S. L. B., Hagel, G., Jorgensen, L. N., Harling, H., Timmermans, V., et al. (2019). *KRAS* mutations in the parental tumour accelerate *in vitro* growth of tumoroids established from colorectal adenocarcinoma. *Int. J. Exp. Pathol.* 2019:12308. doi: 10.1111/iep.12308

Muraro, M. G., Muenst, S., Mele, V., Quagliata, L., Iezzi, G., Tzankov, A., et al. (2017). *Ex-vivo* assessment of drug response on breast cancer primary tissue with preserved microenvironments. *Oncoimmunology* 2017:e1331798. doi: 10.1080/2162402X.2017.1331798

Nagle, P. W., Plukker, J. T. M., Muijs, C. T., van Luijk, P., and Coppes, R. P. (2018). Patient-derived tumor organoids for prediction of cancer treatment response. *Semin. Cancer Biol.* 53, 258–264. doi: 10.1016/J.SEMCANCER.2018.06.005

Nagourney, R. A., Blitzer, J. B., Shuman, R. L., Asciuto, T. J., Deo, E. A., Paulsen, M., et al. (2012). Functional profiling to select chemotherapy in untreated, advanced or metastatic non-small cell lung cancer. *Anticancer Res.* 32, 4453–60.

Naipal, K. A. T., Verkaik, N. S., Sánchez, H., van Deurzen, C. H. M., den Bakker, M. A., Hoeijmakers, J. H. J., et al. (2016). Tumor slice culture system to assess drug response of primary breast cancer. *BMC Cancer* 16:78. doi: 10.1186/s12885-016-2119-2

Nayak, B., Manohari, G., and Manjunath, S. (2019). Colloids and Surfaces B : Biointerfaces Tissue mimetic 3D sca ff old for breast tumor-derived organoid culture toward personalized chemotherapy. *Colloids Surf. B Biointerfaces* 180, 334–343. doi: 10.1016/j.colsurfb.2019.04.056

Neal, J. T., Li, X., Zhu, J., Giangarra, V., Grzeskowiak, C. L., Ju, J., et al. (2018). Organoid modeling of the tumor immune microenvironment. *Cell* 175, 1972–1988.e16. doi: 10.1016/J.CELL.2018.11.021

Nemati, F., Sastre-Garau, X., Laurent, C., Couturier, J., Mariani, P., Desjardins, L., et al. (2010). Establishment and characterization of a panel of human uveal melanoma xenografts derived from primary and/or metastatic tumors. *Clin. Cancer Res.* 16, 2352–2362. doi: 10.1158/1078-0432.CCR-09-3066

Nguyen, H. M., Vessella, R. L., Morrissey, C., Brown, L. G., Coleman, I. M., Higano, C. S., et al. (2017). LuCaP prostate cancer patient-derived xenografts reflect the molecular heterogeneity of advanced disease an–d serve as models for evaluating cancer therapeutics. *Prostate* 77, 654–671. doi: 10.1002/pros.23313

Ochiai, A., and Neri, S. (2016). Phenotypic and functional heterogeneity of cancer-associated fibroblast within the tumor microenvironment. *Adv. Drug Deliv. Rev.* 99, 186–196. doi: 10.1016/J.ADDR.2015.07.007

Orditura, M., Della Corte, C. M., Diana, A., Ciaramella, V., Franzese, E., Famiglietti, V., et al. (2018). Three dimensional primary cultures for selecting human breast cancers that are sensitive to the anti-tumor activity of ipatasertib or taselisib in combination with anti-microtubule cytotoxic drugs. *Breast* 41, 165–171. doi: 10.1016/j.breast.2018.08.002

Oskarsson, T. (2013). Extracellular matrix components in breast cancer progression and metastasis. *Breast* 22, S66–S72. doi: 10.1016/j.breast.2013.07.012

Paduch, R. (2016). The role of lymphangiogenesis and angiogenesis in tumor metastasis. *Cell. Oncol.* 39, 397–410. doi: 10.1007/s13402-016-0281-9

Paget, S. (1989). The distribution of secondary growths in cancer of the breast. 1889. *Cancer Metastasis Rev.* 8, 98–101.

Paindelli, C., Navone, N., Logothetis, C. J., Friedl, P., and Dondossola, E. (2019). Engineered bone for probing organotypic growth and therapy response of prostate cancer tumoroids *in vitro*. *Biomaterials* 197, 296–304. doi: 10.1016/j.biomaterials.2019.01.027

Paiva, A. E., Lousado, L., Guerra, D. A. P., Azevedo, P. O., Sena, I. F. G., Andreotti, J. P., et al. (2018). Pericytes in the premetastatic niche. *Cancer Res.* 78, 2779–2786. doi: 10.1158/0008-5472.CAN-17-3883

Pak, C., Callander, N. S., Young, E. W. K., Titz, B., Kim, K., Saha, S., et al. (2015). MicroC(3): an *ex vivo* microfluidic cis-coculture assay to test chemosensitivity and resistance of patient multiple myeloma cells. *Integr. Biol.* 7, 643–654. doi: 10.1039/c5ib00071h

Papini, S., Rosellini, A., De Matteis, A., Campani, D., Selli, C., Caporali, A., et al. (2007). Establishment of an organotypic *in vitro* culture system and its relevance to the characterization of human prostate epithelial cancer cells and their stromal interactions. *Pathol. Res. Pract.* 203, 209–216. doi: 10.1016/j.prp.2007.02.004

Parrish, A. R., Sallam, K., Nyman, D. W., Orozco, J., Cress, A. E., Dalkin, B. L., et al. (2002). Culturing precision-cut human prostate slices as an *in vitro* model of prostate pathobiology. *Cell Biol. Toxicol.* 18, 205–19.

Paul, C. D., Mistriotis, P., and Konstantopoulos, K. (2017). Cancer cell motility: lessons from migration in confined spaces. *Nat. Rev. Cancer* 17, 131–140. doi: 10.1038/nrc.2016.123

Pauli, C., Hopkins, B. D., Prandi, D., Shaw, R., Fedrizzi, T., Sboner, A., et al. (2017). Personalized *in vitro* and *in vivo* cancer models to guide precision medicine. 7:462–77. doi: 10.1158/2159-8290.CD-16-1154

Peela, N., Truong, D., Saini, H., Chu, H., Mashaghi, S., Ham, S. L., et al. (2017). Advanced biomaterials and microengineering technologies to recapitulate the stepwise process of cancer metastasis. *Biomaterials* 133, 176–207. doi: 10.1016/J.biomaterials.2017.04.017

Peinado, H., Zhang, H., Matei, I. R., Costa-Silva, B., Hoshino, A., Rodrigues, G., et al. (2017). Pre-metastatic niches: organ-specific homes for metastases. *Nat. Rev. Cancer* 17, 302–317. doi: 10.1038/nrc.2017.6

Pepelanova, I., Kruppa, K., Scheper, T., and Lavrentieva, A. (2018). Gelatin-methacryloyl (GelMA) hydrogels with defined degree of functionalization as a versatile toolkit for 3D cell culture and extrusion bioprinting. *Bioengineering* 5:55. doi: 10.3390/bioengineering5030055

Pereira, B. A., Lister, N. L., Hashimoto, K., Teng, L., Flandes-Iparraguirre, M., Eder, A., et al. (2019). Tissue engineered human prostate microtissues reveal key role of mast cell-derived tryptase in potentiating cancer-associated fibroblast (CAF)-induced morphometric transition *in vitro*. *Biomaterials* 197, 72–85. doi: 10.1016/J.biomaterials.2018.12.030

Pinto, M. L., Rios, E., Silva, A. C., Neves, S. C., Caires, H. R., Pinto, A. T., et al. (2017). Decellularized human colorectal cancer matrices polarize macrophages towards an anti-inflammatory phenotype promoting cancer cell invasion via CCL18. *Biomaterials* 124, 211–224. doi: 10.1016/J.biomaterials.2017.02.004

Planche, A., Bacac, M., Provero, P., Fusco, C., Delorenzi, M., Stehle, J.-C., et al. (2011). Identification of prognostic molecular features in the reactive stroma of human breast and prostate cancer. *PLoS ONE* 6:e18640. doi: 10.1371/journal.pone.0018640

Plava, J., Cihova, M., Burikova, M., Matuskova, M., Kucerova, L., and Miklikova, S. (2019). Recent advances in understanding tumor stroma-mediated chemoresistance in breast cancer. *Mol. Cancer* 18:67. doi: 10.1186/s12943-019-0960-z

Plummer, S., Wallace, S., Ball, G., Lloyd, R., Schiapparelli, P., Quiñones-Hinojosa, A., et al. (2019). A Human iPSC-derived 3D platform using primary brain cancer cells to study drug development and personalized medicine. *Sci. Rep.* 9:1407. doi: 10.1038/s41598-018-38130-0

Polini, A., del Mercato, L. L., Barra, A., Zhang, Y. S., Calabi, F., and Gigli, G. (2019). Towards the development of human immune-system-on-a-chip platforms. *Drug Discov. Today* 24, 517–525. doi: 10.1016/J.DRUDIS.2018.10.003

Poltavets, V., Kochetkova, M., Pitson, S. M., and Samuel, M. S. (2018). The role of the extracellular matrix and its molecular and cellular regulators in cancer cell plasticity. *Front. Oncol.* 8:431. doi: 10.3389/fonc.2018.00431

Postovit, L. (2016). Matrigel : a complex protein mixture required for optimal growth of cell Matrigel : a complex protein mixture required for optimal growth of cell culture. Proteomics 10:1886–90. doi: 10.1002/pmic.200900758

Pretlow, T. G., Yang, B., and Pretlow, T. P. (1995). Organ culture of benign, aging, and hyperplastic human prostate. *Microsc. Res. Tech.* 30, 271–281. doi: 10.1002/jemt.1070300403

Psaila, B., and Lyden, D. (2009). The metastatic niche: adapting the foreign soil. *Nat. Rev. Cancer* 9, 285–293. doi: 10.1038/nrc2621

Puca, L., Bareja, R., Prandi, D., Shaw, R., Benelli, M., Karthaus, W. R., et al. (2018). Patient derived organoids to model rare prostate cancer phenotypes. *Nat. Commun.* 9, 1–10. doi: 10.1038/s41467-018-04495-z

Qiao, H., and Tang, T. (2018). Engineering 3D approaches to model the dynamic microenvironments of cancer bone metastasis. *Bone Res.* 6:3. doi: 10.1038/s41413-018-0008-9

Ramião, N. G., Martins, P. S., Rynkevic, R., Fernandes, A. A., Barroso, M., and Santos, D. C. (2016). Biomechanical properties of breast tissue, a state-of-the-art review. *Biomech. Model. Mechanobiol.* 15, 1307–1323. doi: 10.1007/s10237-016-0763-8

Risbridger, G. P., Toivanen, R., and Taylor, R. A. (2018). Preclinical models of prostate cancer: patient-derived xenografts, organoids, and other explant models. *Cold Spring Harb. Perspect. Med.* 8:a030536. doi: 10.1101/cshperspect.a030536

Roife, D., Dai, B., Kang, Y., Rios Perez, M. V., Pratt, M., Li, X., et al. (2016). *Ex vivo* testing of patient-derived xenografts mirrors the clinical outcome of patients

with pancreatic ductal adenocarcinoma. *Clin. Cancer Res.* 22, 6021–6030. doi: 10.1158/1078-0432.CCR-15-2936

Romero-López, M., Trinh, A. L., Sobrino, A., Hatch, M. M. S., Keating, M. T., Fimbres, C., et al. (2017). Recapitulating the human tumor microenvironment: colon tumor-derived extracellular matrix promotes angiogenesis and tumor cell growth. *Biomaterials* 116, 118–129. doi: 10.1016/J.biomaterials.2016.11.034

Rothbauer, M., Rosser, J. M., Zirath, H., and Ertl, P. (2019). Tomorrow today: organ-on-a-chip advances towards clinically relevant pharmaceutical and medical *in vitro* models. *Curr. Opin. Biotechnol.* 55, 81–86. doi: 10.1016/J.COPBIO.2018.08.009

Ruppen, J., Wildhaber, F. D., Strub, C., Hall, S. R. R., Schmid, R. A., Geiser, T., et al. (2015). Towards personalized medicine: chemosensitivity assays of patient lung cancer cell spheroids in a perfused microfluidic platform. *Lab Chip* 15, 3076–3085. doi: 10.1039/C5LC00454C

Sabaawy, H. E. (2013). Genetic heterogeneity and clonal evolution of tumor cells and their impact on precision cancer medicine. *J. Leuk.* 1:1000124. doi: 10.4172/2329-6917.1000124

Saglam-Metiner, P., Gulce-Iz, S., and Biray-Avci, C. (2019). Bioengineering-inspired three-dimensional culture systems: organoids to create tumor microenvironment. *Gene* 686, 203–212. doi: 10.1016/j.gene.2018.11.058

Saharinen, P., Tammela, T., Karkkainen, M. J., and Alitalo, K. (2004). Lymphatic vasculature: development, molecular regulation and role in tumor metastasis and inflammation. *Trends Immunol.* 25, 387–395. doi: 10.1016/j.it.2004.05.003

Sakthivel, K., O'Brien, A., Kim, K., and Hoorfar, M. (2019). Microfluidic analysis of heterotypic cellular interactions: a review of techniques and applications. *TrAC Trends Anal. Chem.* 2019:26. doi: 10.1016/J.TRAC.2019.03.026

Samani, A., Zubovits, J., and Plewes, D. (2007). Elastic moduli of normal and pathological human breast tissues: an inversion-technique-based investigation of 169 samples. *Phys. Med. Biol.* 52, 1565–1576. doi: 10.1088/0031-9155/52/6/002

Sato, T., Stange, D. E., Ferrante, M., Vries, R. G. J., Van Es, J. H., Van Den Brink, S., et al. (2011). Long-term expansion of epithelial organoids from human colon, adenoma, adenocarcinoma, and Barrett's epithelium. *Gastroenterology* 141, 1762–1772. doi: 10.1053/j.gastro.2011.07.050

Schiewer, M. J., Goodwin, J. F., Han, S., Brenner, J. C., Augello, M. A., Dean, J. L., et al. (2012). Dual roles of PARP-1 promote cancer growth and progression. *Cancer Discov.* 2, 1134–1149. doi: 10.1158/2159-8290.CD-12-0120

Schnalzger, T. E., de Groot, M. H., Zhang, C., Mosa, M. H., Michels, B. E., Röder, J., et al. (2019). 3D model for CAR-mediated cytotoxicity using patient-derived colorectal cancer organoids. *EMBO J.* 2019:e100928. doi: 10.15252/embj.2018100928

Seewaldt, V. (2014). ECM stiffness paves the way for tumor cells. *Nat. Med.* 20, 332–333. doi: 10.1038/nm.3523

Selden, C., Fuller, B., Selden, C., and Fuller, B. (2018). Role of bioreactor technology in tissue engineering for clinical use and therapeutic target design. *Bioengineering* 5:32. doi: 10.3390/bioengineering5020032

Senft, D., Leiserson, M. D. M., Ruppin, E., and Ronai, Z. A. (2017). Precision oncology: the road ahead. *Trends Mol. Med.* 23, 874–898. doi: 10.1016/j.molmed.2017.08.003

Shackleton, M., Quintana, E., Fearon, E. R., and Morrison, S. J. (2009). Heterogeneity in cancer: cancer stem cells versus clonal evolution. *Cell* 138, 822–829. doi: 10.1016/J.CELL.2009.08.017

Shang, M., Soon, R. H., Lim, C. T., Khoo, B. L., and Han, J. (2019). Microfluidic modelling of the tumor microenvironment for anti-cancer drug development. *Lab Chip* 19, 369–386. doi: 10.1039/C8LC00970H

Shchors, K., and Evan, G. (2007). Tumor angiogenesis: cause or consequence of cancer? *Cancer Res.* 67, 7059–7061. doi: 10.1158/0008-5472.CAN-07-2053

Shokoohmand, A., Bock, N., Clements, J. A., and Hutmacher, D. W. (2016). An advanced bioengineered 3D model mimicking prostate cancer-induced bone metastasis microenvironment. *Front. Bioeng. Biotechnol.* 4:3011. doi: 10.3389/conf.FBIOE.2016.01.03011

Shokoohmand, A., Ren, J., Baldwin, J., Atack, A., Shafiee, A., Theodoropoulos, C., et al. (2019). Microenvironment engineering of osteoblastic bone metastases reveals osteomimicry of patient-derived prostate cancer xenografts. *Biomaterials* 220:119402. doi: 10.1016/J.biomaterials.2019.119402

Skardal, A., Devarasetty, M., Forsythe, S., Atala, A., and Soker, S. (2016a). A reductionist metastasis-on-a-chip platform for *in vitro* tumor progression modeling and drug screening. *Biotechnol. Bioeng.* 113, 2020–2032. doi: 10.1002/bit.25950

Skardal, A., Murphy, S. V., Devarasetty, M., Mead, I., Kang, H.-W., Seol, Y.-J., et al. (2017). Multi-tissue interactions in an integrated three-tissue organ-on-a-chip platform. *Sci. Rep.* 7:8837. doi: 10.1038/s41598-017-08879-x

Skardal, A., Shupe, T., and Atala, A. (2016b). Organoid-on-a-chip and body-on-a-chip systems for drug screening and disease modeling. *Drug Discov. Today* 21, 1399–1411. doi: 10.1016/J.DRUDIS.2016.07.003

Smith, H. A., and Kang, Y. (2013). The metastasis-promoting roles of tumor-associated immune cells. *J. Mol. Med.* 91, 411–429. doi: 10.1007/s00109-013-1021-5

Sontheimer-Phelps, A., Hassell, B. A., and Ingber, D. E. (2019). Modelling cancer in microfluidic human organs-on-chips. *Nat. Rev. Cancer* 19, 65–81. doi: 10.1038/s41568-018-0104-6

Stacker, S. A., Baldwin, M. E., and Achen, M. G. (2002). The role of tumor lymphangiogenesis in metastatic spread. *FASEB J.* 16, 922–934. doi: 10.1096/fj.01-0945rev

Sun, W., Luo, Z., Lee, J., Kim, H.-J., Lee, K., Tebon, P., et al. (2019). Organ-on-a-chip for cancer and immune organs modeling. *Adv. Healthc. Mater.* 2019:1801363. doi: 10.1002/adhm.201801363

Sung, K. E., and Beebe, D. J. (2014). Microfluidic 3D models of cancer. *Adv. Drug Deliv. Rev.* 79–80, 68–78. doi: 10.1016/J.ADDR.2014.07.002

Tam, R. Y., Yockell-Lelievre, J., Smith, L. J., Julian, L. M., Baker, A. E. G., Choey, C., et al. (2018). Rationally designed 3D hydrogels model invasive lung diseases enabling high-content drug screening. *Adv. Mater.* 1806214:e1806214. doi: 10.1002/adma.201806214

Tanaka, N., Osman, A. A., Takahashi, Y., Lindemann, A., Patel, A. A., Zhao, M., et al. (2018). Head and neck cancer organoids established by modification of the CTOS method can be used to predict *in vivo* drug sensitivity. *Oral Oncol.* 87, 49–57. doi: 10.1016/j.oraloncology.2018.10.018

Taubenberger, A. V., Bray, L. J., Haller, B., Shaposhnykov, A., Binner, M., Freudenberg, U., et al. (2016). 3D extracellular matrix interactions modulate tumour cell growth, invasion and angiogenesis in engineered tumour microenvironments. *Acta Biomater.* 36, 73–85. doi: 10.1016/j.actbio.2016.03.017

Tentler, J. J., Tan, A. C., Weekes, C. D., Jimeno, A., Leong, S., Pitts, T. M., et al. (2012). Patient-derived tumour xenografts as models for oncology drug development. *Nat. Rev. Clin. Oncol.* 9, 338–350. doi: 10.1038/nrclinonc.2012.61

Thiery, J. P., and Chopin, D. (1999). Epithelial cell plasticity in development and tumor progression. *Cancer Metastasis Rev.* 18, 31–42.

Thoma, C. R., Zimmermann, M., Agarkova, I., Kelm, J. M., and Krek, W. (2014). 3D cell culture systems modeling tumor growth determinants in cancer target discovery. *Adv. Drug Deliv. Rev.* 69–70, 29–41. doi: 10.1016/J.ADDR.2014.03.001

Topalian, S. L., Drake, C. G., and Pardoll, D. M. (2015). Immune checkpoint blockade: a common denominator approach to cancer therapy. *Cancer Cell* 27, 450–461. doi: 10.1016/J.CCELL.2015.03.001

Tsai, H.-F., Trubelja, A., Shen, A. Q., and Bao, G. (2017). Tumour-on-a-chip: microfluidic models of tumour morphology, growth and microenvironment. *J. R. Soc. Interface* 14:20170137. doi: 10.1098/rsif.2017.0137

Urosevic, J., and Gomis, R. R. (2018). Organ-specific metastases. *Nat. Biomed. Eng.* 2, 347–348. doi: 10.1038/s41551-018-0249-3

Vaira, V., Fedele, G., Pyne, S., Fasoli, E., Zadra, G., Bailey, D., et al. (2010). Preclinical model of organotypic culture for pharmacodynamic profiling of human tumors. *Proc. Natl. Acad. Sci. U.S.A.* 107, 8352–8356. doi: 10.1073/pnas.0907676107

van de Wetering, M., Francies, H. E., Francis, J. M., Bounova, G., Iorio, F., Pronk, A., et al. (2015). Prospective derivation of a living organoid biobank of colorectal cancer patients. *Cell* 161, 933–945. doi: 10.1016/J.CELL.2015.03.053

van der Kuip, H., Mürdter, T. E., Sonnenberg, M., McClellan, M., Gutzeit, S., Gerteis, A., et al. (2006). Short term culture of breast cancer tissues to study the activity of the anticancer drug taxol in an intact tumor environment. *BMC Cancer* 6:86. doi: 10.1186/1471-2407-6-86

Vilanova, G., Burés, M., Colominas, I., and Gomez, H. (2018). Computational modelling suggests complex interactions between interstitial flow and tumour angiogenesis. *J. R. Soc. Interface* 15:20180415. doi: 10.1098/rsif.2018.0415

Vlachogiannis, G., Hedayat, S., Vatsiou, A., Jamin, Y., Fernández-Mateos, J., Khan, K., et al. (2018). Patient-derived organoids model treatment response of metastatic gastrointestinal cancers. *Science* 359, 920–926. doi: 10.1126/science.aao2774

Votanopoulos, K. I., Mazzocchi, A., Sivakumar, H., Forsythe, S., Aleman, J., Levine, E. A., et al. (2018). Appendiceal cancer patient-specific tumor organoid model for predicting chemotherapy efficacy prior to initiation of treatment: a feasibility study. *Ann. Surg. Oncol.* 2018, 1–9. doi: 10.1245/s10434-018-7008-2

Walker, C., Mojares, E., and Del Río Hernández, A. (2018). Role of extracellular matrix in development and cancer progression. *Int. J. Mol. Sci.* 19:3028. doi: 10.3390/ijms19103028

Wang, C., Li, J., Sinha, S., Peterson, A., Grant, G. A., and Yang, F. (2019). Mimicking brain tumor-vasculature microanatomical architecture via co-culture of brain tumor and endothelial cells in 3D hydrogels. *Biomaterials* 202, 35–44. doi: 10.1016/j.biomaterials.2019.02.024

Wang, W., Marinis, J. M., Beal, A. M., Savadkar, S., Wu, Y., Khan, M., et al. (2018a). RIP1 kinase drives macrophage-mediated adaptive immune tolerance in pancreatic cancer. *Cancer Cell 34*, 757–774.e7. doi: 10.1016/J.CCELL.2018.10.006

Wang, Y., Shi, W., Kuss, M., Mirza, S., Qi, D., Krasnoslobodtsev, A., et al. (2018b). 3D bioprinting of breast cancer models for drug resistance study. *ACS Biomater. Sci. Eng.* 4, 4401–4411. doi: 10.1021/acsbiomaterials.8b01277

Weeber, F., Wetering, M., van de, Hoogstraat, M., Dijkstra, K. K., Krijgsman, O., Kuilman, T., et al. (2015). Preserved genetic diversity in organoids cultured from biopsies of human colorectal cancer metastases. *Proc. Natl. Acad. Sci. U.S.A.* 112, 13308–13311. doi: 10.1073/PNAS.1516689112

Whittle, J. R., Lewis, M. T., Lindeman, G. J., and Visvader, J. E. (2015). Patient-derived xenograft models of breast cancer and their predictive power. *Breast Cancer Res.* 17:17. doi: 10.1186/s13058-015-0523-1

Wolf, K., Te Lindert, M., Krause, M., Alexander, S., Te Riet, J., Willis, A. L., et al. (2013). Physical limits of cell migration: control by ECM space and nuclear deformation and tuning by proteolysis and traction force. *J. Cell Biol.* 201, 1069–1084. doi: 10.1083/jcb.201210152

Woodruff, M. A., and Hutmacher, D. W. (2010). The return of a forgotten polymer—Polycaprolactone. *Prog. Polym. Sci.* 2010:2. doi: 10.1016/j.progpolymsci.2010.04.002

Workman, M. J., Mahe, M. M., Trisno, S., Poling, H. M., Watson, C. L., Sundaram, N., et al. (2017). Engineered human pluripotent-stem-cell-derived intestinal tissues with a functional enteric nervous system. *Nat. Med.* 23, 49–59. doi: 10.1038/nm.4233

Wyckoff, J. B., Wang, Y., Lin, E. Y., Li, J. F., Goswami, S., Stanley, E. R., et al. (2007). Direct visualization of macrophage-assisted tumor cell intravasation in mammary tumors. *Cancer Res.* 67, 2649–2656. doi: 10.1158/0008-5472.CAN-06-1823

Xu, X., Farach-Carson, M. C., and Jia, X. (2014). Three-dimensional *in vitro* tumor models for cancer research and drug evaluation. *Biotechnol. Adv.* 32, 1256–1268. doi: 10.1016/j.biotechadv.2014.07.009

Xu, Z., Gao, Y., Hao, Y., Li, E., Wang, Y., Zhang, J., et al. (2013). Application of a microfluidic chip-based 3D co-culture to test drug sensitivity for individualized treatment of lung cancer. *Biomaterials* 34, 4109–4117. doi: 10.1016/J.biomaterials.2013.02.045

Yao, D., Dai, C., and Peng, S. (2011). Mechanism of the mesenchymal-epithelial transition and its relationship with metastatic tumor formation. *Mol. Cancer Res.* 9, 1608–1620. doi: 10.1158/1541-7786.mcr-10-0568

Yue, K., Trujillo-de Santiago, G., Alvarez, M. M., Tamayol, A., Annabi, N., and Khademhosseini, A. (2015). Synthesis, properties, and biomedical applications of gelatin methacryloyl (GelMA) hydrogels. *Biomaterials* 73, 254–271. doi: 10.1016/J.biomaterials.2015.08.045

Yuhas, J. M., Li, A. P., Martinez, A., and Ladman, A. J. (1977). A simplified method for production and growth of multicellular tumor spheroids. *Cancer Res.* 37:3639–43.

Zhan, M., Yang, R., Wang, H., He, M., Chen, W., Xu, S., et al. (2018). Guided chemotherapy based on patient-derived mini-xenograft models improves survival of gallbladder carcinoma patients. *Cancer Commun.* 38:48. doi: 10.1186/s40880-018-0318-8

Zhang, F., Wang, W., Long, Y., Liu, H., Cheng, J., Guo, L., et al. (2018a). Characterization of drug responses of mini patient-derived xenografts in mice for predicting cancer patient clinical therapeutic response. *Cancer Commun.* 38:60. doi: 10.1186/s40880-018-0329-5

Zhang, G., Song, X., Mei, J., Ye, G., Wang, L., Yu, L., et al. (2017). A simple 3D cryogel co-culture system used to study the role of CAFs in EMT of MDA-MB-231 cells. *RSC Adv.* 7:17208–16. doi: 10.1039/C6RA28721B

Zhang, W., Gu, Y., Sun, Q., Siegel, D. S., Tolias, P., Yang, Z., et al. (2015). *Ex vivo* maintenance of primary human multiple myeloma cells through the optimization of the osteoblastic niche. *PLoS ONE* 10:e0125995. doi: 10.1371/journal.pone.0125995

Zhang, W., Lee, W. Y., Siegel, D. S., Tolias, P., and Zilberberg, J. (2014). Patient-specific 3D microfluidic tissue model for multiple myeloma. *Tissue Eng. Part C Methods* 20:663–70. doi: 10.1089/ten.tec.2013.0490

Zhang, W., van Weerden, W., de Ridder, C. A., Erkens-Schulze, S., Schönfeld, E., Meijer, T., et al. (2018b). *Ex vivo* treatment of prostate tumor tissue recapitulates *in vivo* therapy response. *Prostate* 2018, 1–13. doi: 10.1002/pros.23745

Zhang, Y. S., Duchamp, M., Oklu, R., Ellisen, L. W., Langer, R., and Khademhosseini, A. (2016). Bioprinting the cancer microenvironment. *ACS Biomater. Sci. Eng.* 2, 1710–1721. doi: 10.1021/acsbiomaterials.6b00246

Zhao, P., Chen, H., Wen, D., Mou, S., Zhang, F., and Zheng, S. (2018). Personalized treatment based on mini patient-derived xenografts and WES/RNA sequencing in a patient with metastatic duodenal adenocarcinoma. *Cancer Commun.* 38:54. doi: 10.1186/s40880-018-0323-y

Zhou, X., Zhu, W., Nowicki, M., Miao, S., Cui, H., Holmes, B., et al. (2016). 3D Bioprinting a cell-laden bone matrix for breast cancer metastasis study. *ACS Appl. Mater. Interfaces* 8, 30017–30026. doi: 10.1021/acsami.6b10673

Conflict of Interest Statement: The authors declare that the research was conducted in the absence of any commercial or financial relationships that could be construed as a potential conflict of interest.

frontiers in Bioengineering and Biotechnology

HYPOTHESIS AND THEORY
published: 09 October 2019
doi: 10.3389/fbioe.2019.00255

Specifications for Innovative, Enabling Biomaterials Based on the Principles of Biocompatibility Mechanisms

David F. Williams[1,2]*

[1] Wake Forest Institute of Regenerative Medicine, Winston-Salem, NC, United States, [2] Strait Access Technologies, Cape Town, South Africa

In any engineering discipline, whenever products are designed, manufactured and ultimately utilized for the benefits of society, a series of specifications for the product are defined, and maybe refined, in order that they perform as effectively as possible, with due attention being paid to the safety, and economic aspects. These specifications are established with respect to all of the relevant properties, including those determined by mechanical, physical, chemical, manufacturing and environmental conditions, and the resulting design and materials selection reflects the optimal balance. In areas of medical technology, these specifications should be based on both functionality, which determines whether a device can actually perform as intended, and biocompatibility, which determines how the device interacts, both acutely and chronically, with the body. Unfortunately, whilst so much progress has been made with the development of superior functionality for the treatment and diagnosis of so many disease states, this is not the same for biocompatibility, where the single most-important currently adopted specification is that the device should do no harm, which falls far short of the ideal requirement. This paper addresses the profound need for biomaterials specifications to be based on the mechanisms of biocompatibility.

Keywords: host response, inflammation, mechanotransduction, implant, template

OPEN ACCESS

Edited by:
Hasan Uludag,
University of Alberta, Canada

Reviewed by:
Sergey V. Dorozhkin,
Independent Researcher,
Moscow, Russia
Jose Mauro Granjeiro,
National Institute of Metrology, Quality and Technology, Brazil
James Morley Anderson,
Case Western Reserve University, United States

***Correspondence:**
David F. Williams
dfwillia@wakehealth.edu

Specialty section:
This article was submitted to Biomaterials, a section of the journal Frontiers in Bioengineering and Biotechnology

Received: *06 August 2019*
Accepted: *23 September 2019*
Published: *09 October 2019*

Citation:
Williams DF (2019) Specifications for Innovative, Enabling Biomaterials Based on the Principles of Biocompatibility Mechanisms. Front. Bioeng. Biotechnol. 7:255. doi: 10.3389/fbioe.2019.00255

INTRODUCTION

We have recently re-defined the term biomaterial as "*a material designed to take a form that can direct, through interactions with living systems, the course of any therapeutic or diagnostic procedure*" (Zhang and Williams, 2018). The two critical parts of this definition relate to the objectives of the systems in which a biomaterial is used and the fact that the material has to interact with living systems, in most cases parts of the human body, in order for these objectives to be realized. This definition, and indeed, the whole concept of biomaterials science, applies equally to situations involving implantable devices, artificial organs, tissue engineering templates, non-viral gene vectors, drug delivery systems and contrast agents. When determining the specifications for the biomaterials used in every application, it is natural that the functional requirements are considered first; after all, there is no point in using an opaque material for an intraocular lens, a rigid metallic scaffold for tissue-engineered cartilage or an unresponsive elastomer for an MRI contrast agent. In the majority of situations, there are predicates that give some idea of the functional

characteristics that are likely to be appropriate, and a variety of laboratory and pre-clinical tests allow designers and manufacturers to refine materials selection parameters and, hopefully, optimize the final choice. These procedures are facilitated by lists of materials known to have previously received regulatory approval in similar types of situations, and international standards that advise on the tests that could or should be performed.

So far, so good. But what about the ability to control the function through interactions with living systems. These interactions are generally considered within the phenomena related to biocompatibility. This term has also been recently reconsidered (Zhang and Williams, 2018), when the original definition agreed in 1986 (Williams, 1986), was confirmed as still correct, being "*the ability of a material to perform with an appropriate host response in a specific application*."This is important since it mandates that the performance of a biomaterial is dependent on the host response, as now indicated in the definition of biomaterial, and especially that this response will vary from one application to another. This is an excellent contextual definition but it does not, indeed cannot, tell us how to design a material with good, or even appropriate, biocompatibility.

The main problem with this situation, as implied with reference to the dependence of biocompatibility on the application, is that biocompatibility is not a property of a biomaterial, but of a biomaterial-host system. As emphasized in several recent publications, the biocompatibility characteristics of a material will vary depending on specific biological and clinical factors. No material can be described as a generic "biocompatible" material (Williams, 2008; Williams and Williams, 2014). It is unfortunate that even today, major journals include papers that refer to biocompatible materials, as do documents from the FDA and other regulators, and also those of the most widely used medical device standards.

The theme of the present paper is that in order to design better biomaterials for future clinical therapies, we need to identify specifications for biocompatibility as well as functionality, and this will have to take into account the need to define the precise material-host system and not just the material. The discussion will focus on the pathways involved in the host response, using three scenarios within implantable devices, tissue engineering, and contrast agents to reinforce the arguments.

BIOCOMPATIBILITY AND TOXICITY

For a long time, and indeed before the term biocompatibility became recognized, the ideal characteristic of a biomaterial was considered to involve a lack of any effect on the body (Williams and Roaf, 1973; Scales and Winter, 1975), often couched in terms of having no adverse effect, but in reality this equated with having no effect on, or no interaction with, the tissues of the body. This became obvious from discussions in the literature that described the ideal biomaterial as one that had no effect on blood clotting, or on inflammation and the immune system, and generically was non-cytotoxic. As long as the applications were within simple implantable devices, there was some sense in this, especially when it was appreciated that most materials are modified to some extent by the fluids within the body so that the preferred scenario was one in which there was minimal degradation and minimal response to the material and its degradation products. Over half a century ago, the surgeon's biomaterials armamentarium consisted of a group of such substances. Even then, it soon became appreciated that this was not quite good enough so that the accepted list of biomaterials for long-term implantation was narrowed in order to include only the most degradation resistant materials that the engineering professions could supply, including just a few alloys, based on titanium (Williams, 1977), cobalt-chromium (Metikos-Hukovic et al., 2006) or platinum-palladium (Woodward, 2012), a few oxide ceramics, especially alumina (Webster et al., 1999) and zirconia (Siddiqi et al., 2017), and some thermoplastic or elastomeric materials such as ePTFE (Cassady et al., 2014), acrylics (Frazer et al., 2005), high density polyethylene (Gomez-Barrena et al., 2008), and silicones (Colas and Curtis, 2013).

There is nothing intuitively wrong with this list; it is pragmatic and based on aspects of clinical experience. It could be argued that there was just one biocompatibility specification, and that was the appropriate host response should be no response. The difficulty, which lies at the heart of this paper, is how this empirical list can lead to the development of specifications for the biomaterials of the future. If we take metallic systems as an example, the biocompatibility will be dependent on corrosion rates, which for each alloy system will be dependent on variables such as pH, electrode potential, oxygen potential, galvanic couples and mechanical stress, and on the biological effect of the corrosion products, which will depend on speciation, morphology, stoichiometry, and so on. It is impossible, at this stage, to quantify the risk of adverse host responses in any conceivable system when there are so many independent variables. The same principle applies with all types of biomaterial.

For many years, this problem has been addressed by using surrogates for host responses, and by analogy, biocompatibility. These surrogates largely concern toxicity. As more devices were being developed, regulators became anxious about their decision-making algorithms that had to be based on crude estimates on how biomaterials would perform in the body. This scenario was taken up by standards organizations, to whom regulators looked for guidance on testing procedures. Accordingly, the overarching standards body, ISO, the International Standards Organization, started to produce a series of standard test protocols for the assessment of the biological safety of medical devices, the so-called ISO-10993 series[1]. It is not surprising that this series, now numbering 20 or so parts, in various stages of drafting and revision, has concentrated on this surrogacy, with sections on cytotoxicity, systemic toxicity, genotoxicity, reproductive toxicity, and toxicokinetics of degradation products, included in the recommended tests.

[1]International Standards Organization, ISO 10993-1 Biological Evaluation of Medical Devices—Part 1: Evaluation and Testing Within a Risk Management System, Revised 2018.

There is some logic to this approach, as manufacturers, clinicians, and regulators should be aware of any toxicological concerns. However, these tests do nothing to further our understanding of biocompatibility pathways and specifications, and should not be considered as the critical determinants of whether specific biomaterials should be used in specific situations.

Most of these tests rely on the effect that extracts derived from the material have on cells in culture. Thus, for cytotoxicity, the material in question is incubated with one of a group of standard extraction media, for example, cotton-seed oil or isotonic saline solution, typically for 72 h at 37°C, and the resulting solution is then incubated with the designated cells, typically fibroblasts, for a further time, again typically 72 h at 37°C, and the effects on the cells noted. With other toxicity and sensitization-type tests, the same type of extraction solution is evaluated either *in vitro* or in a small animal model for short-term effects under standard conditions. In the majority of situations, the results with the text extract are compared to extracts derived from standard, reference, materials.

It will be obvious that such tests have been designed to detect whether any components of a biomaterial that can be leached or extracted from the material in a short space of time can have any negative effect in a designated test system. If there is any component that is not extracted during this 72-h period, its potential effects, either positive of negative, will not be detected. The implications of this are discussed in the next sections. It should be borne in mind that the substances most likely to be extracted will be residual monomers, oligomers, catalysts, and impurities in polymer systems, processing substances in animal tissue-derived biomaterials (such as cross-linking, anti-calcification, and decellularization agents) and surface treatment residues on metallic, and ceramic systems. These are not the substances that control biocompatibility within real-life medical technology situations.

IMPLANTABLE MEDICAL DEVICES

Without doubt, implantable medical devices have played an immense role, over many years, in therapies for a wide spectrum of conditions. Ranging from mechanical support systems for musculoskeletal diseases and trauma, to electronic systems for the control of Parkinson's symptoms and cardiac arrhythmias and to meshes for assisting in complex wound healing processes, millions of patients have been successfully treated with the assistance of such devices. As implied above, the materials used in these devices have predominantly been those of maximal inertness and, generally, provide good long-term performance. However, over several decades there have been many well-publicized situations where devices have not, or appear to have not, provided satisfaction in a significant minority of patients[2]. Of profound importance here is the fact that the materials used in most of these devices will have had previous successful use in implantable devices and will have passed all of the relevant tests for biological safety of the device in question.

It is worth considering briefly what biocompatibility issues have arisen here:

- Silicone breast implants; claims of systemic effects associated with components of the silicone gel, including claims that such components initiate autoimmune conditions such as scleroderma, lupus or rheumatoid arthritis and more recently, anaplastic large-cell lymphoma.
- Silver coated textile sewing rings on mechanical heart valves, with claims of adverse effects on local wound healing,
- Polypropylene urogynecological meshes used for treatment of stress urinary incontinence and pelvic organ prolapse, with claims of degradation-induced adverse local responses, and enhanced susceptibility to infection,
- Metal-on-metal hip replacements, with claims of poor tribological performance, and lymphocytic responses to wear debris,
- Hernia meshes, with claims of adverse host responses to several forms of mesh, either synthetic polymers, or biologically-derived materials.

Since all of these examples have resulted in significant litigation procedures, from which it is difficult to determine the precise details of mechanisms by which the materials could possibly have a role in the causation of adverse host responses, very little unequivocal scientific evidence emerges. This is hugely important since very beneficial, potentially life-saving, or certainly life enhancing, devices may be taken off the market on the basis of a small number of real or imaginary adverse effects that can rarely be proved to be device or material related.

The case of the silver coated heart valves mentioned above is worthy of discussion. For several years, especially in the 1990s, St. Jude Medical (SJM) manufactured several series of mechanical heart valves. In order to try to reduce the risk of bacterial endocarditis with the valves, a design was introduced, on the sewing ring of which was deposited an ultrathin layer of the anti-bacterial metal silver. After undergoing standard preclinical tests, including those for biological safety, the so-called "Silzone" device received regulatory approval in several jurisdictions, including the USA, Canada and Europe, and over 35,000 of the valves were implanted in patients worldwide. After the widely publicized deaths of a few patients in Canada and Wales (UK), claims were made that the silver was implicated in either or both thrombus formation or delayed healing. The concerns of the regulators ensured that the valve was taken-off the market, even though there was no evidence of any causation between silver and such events and in spite of the fact that there were many other potential causes of clinical failure. It was later shown that patients who survived the first few months of implantation (i.e., the vast majority) had equivalent of better long-term performance than similar non-silver coated valves (Grunkenmeier et al., 2006) and that from an actuarial perspective patients who received silver coated SJM valves had survival rates no different to those who had received non-silver valves before the Silzone era or those who received non-silver

[2]17 Food and Drugs Administration: Statement from FDA Commissioner Scott Gottlieb MD and Jeff Shuren MD, Director of the Center for Devices and Radiological Health, on efforts to evaluate materials in medical devices to address potential safety issues. March 15th 2019.

valves after the Silzone era (Brennan et al., 2015). The one class-action legal case that was resolved, in Toronto, Canada, found in favor of SJM, i.e., there was no proof of causation[3].

The significance of this in relation to the present paper is that no definitive evidence could be provided to show whether silver could or could not have caused the claimed adverse events. On the one hand it is known that silver does have biological activity (i.e., it is not chemically or biologically "inert" in the context of the definition of biocompatibility discussed above) and the question arises as to whether silver ions were released from the Silzone coating in such a way as to present a risk to mammalian cells in or near the heart. On the other hand, there are many potential causes of heart valve related thrombus formation and delayed healing sufficient to cause a paravalvular leak other than the valve material.

In other words, although the device could, and did, pass standard tests to confirm a low biological safety risk, insufficient was known about the biocompatibility pathways involved with the interaction between silver-coated textiles and the human body so that the risk could be quantified; more importantly, the tests we rely on with respect to biological safety were inadequate to assist in our understanding of these pathways before clinical use was started. This conclusion is valid for any equivalent situation where biological risk is eventually determined to be either positive or negative during clinical use.

In order to assess this conundrum in even more stark terms, it is appropriate to consider the situations with silicone breast implants and autoimmunity and with metal-on-metal hip replacements. In the former example, the major controversy about silicone implants that had such an effect on the implantable device arena in the 1990s eventually centered on the claims that components of silicone gel caused autoimmune diseases. If this were true, it would be of major consequence since these diseases, especially lupus and scleroderma, are clinically very serious. There had never been any previous proof that autoimmunity was caused by any chemical agent but, on the grounds that "absence of proof of harm does not mean that there is no harm" it was initially very difficult to deny that the biocompatibility of silicones could have some autoimmunity-causation component. It was only when several large and very authoritative epidemiological studies showed there was no such link (Janowsky et al., 2000) did the controversy appear to subside (Bondurant et al., 1999). The fact remained, however, that there was no substantial scientific evidence, one way or the other, about the molecular biological characteristics of potential interactions between silicone gel oligomers and the signaling pathways of, for example, scleroderma induction (Al Aranji et al., 2014). There is still no valid test for assessing the risk of biomaterials-induced autoimmunity such that the medical device industry has no definitive answer to the recent resurgence of emotive claims that silicone breast implants have devastating effects on large numbers of women through autoimmunity (Watad et al., 2018). We cannot always hide behind statements that our biomaterials are safe because they pass industry-standard biological safety tests when we do not have clear evidence of the potential biocompatibility pathways. There are no specifications for silicone-based biomaterials that are based on biocompatibility pathways.

There are several differences with respect to metal-on-metal (MOM) hip replacements, but ultimately the problems also arose from a lack of understanding of the relevant biocompatibility pathways. The introduction of new MOM hip prostheses in the early 2000s was based on the perceived need to reduce wear rates in hips in view of the well-documented effect of micron-sized wear particles of acetabular polyethylene components on the macrophage—osteoclast interactions and resulting bone lysis, which caused device loosening (Gallo et al., 2013). It was believed that the significant reduction in the volume of wear particles that would arise if the interface was derived from acetabular and femoral components both made from the same hard alloy would minimize this osteolysis (Allen et al., 2008). While a number of controversial engineering and tribological features contributed to some difficulties that arose (Underwood et al., 2012), the main clinically relevant outcome was a different biocompatibility pathway scenario that was seen with the metal debris. Instead of a preponderance of micron-size particles, which are normally dealt with by macrophage phagocytosis, the bulk of the metal particles were substantially sub-micron (often 10–100 nm) in size (Gill et al., 2012), which could be internalized within lymphocytes, giving, in susceptible patients, an idiosyncratic response of the immune system (Gustafson et al., 2014), often with rapid-onset failure of the device. This was not anticipated on the basis of known metal biocompatibility mechanisms at that time, and could not have been picked up by the standard biological safety tests. Once again, the specifications for these alloys were based on functional characteristics and not on biocompatibility pathways or biological activity.

It should be emphasized that millions of patients, world-wide, are implanted with medical devices, with successful outcomes and no biocompatibility-oriented problems. However, the three scenarios discussed in the previous paragraphs are not unique, and regulatory agencies and manufacturers alike are frequently faced with difficult decisions about whether to allow or keep devices on the market on the basis of a limited number of less-than perfect outcomes that are putatively considered to be caused by poor material selection and resulting toxicity or adverse biological reactions but which could well be due to significant co-morbidities (such as diabetes or obesity) or clinician inexperience.

TISSUE ENGINEERING PRODUCTS

Tissue engineering has been described as "*the creation of new tissue for the therapeutic reconstruction of the human body, by the deliberate and controlled stimulation of selected target cells through a systematic combination of molecular and mechanical signals*" (Williams, 2006). Clearly these molecular and mechanical signals cannot be effective in a vacuum and some construct will commonly be required to control the relevant processes. These constructs have usually been described as

[3]Andersen v. St. Jude Medical, Inc. (2012). ONSC 3660 COURT FILE NO.: 00-CV-195906CV, Toronto, CA.

scaffolds. However, the term "template" is preferable since as this implies a different concept; this is so crucial in the next phase of tissue engineering development.

In the area of implantable devices, discussed above, there is already a hint that, without additional agents, biomaterials may not necessarily produce the best results in every situations. Vascular grafts may require endothelial cells in order to generate superior neointima (Meinhart et al., 2005), intravascular stents are assisted by anti-proliferative drugs in the control of in-stent restenosis (Kastrati et al., 2005), spinal fusion devices may be assisted by locally released bone morphogenetic proteins (Lo et al., 2012) and thrombosis of heart valves is inhibited by systemic anticoagulation (Iung et al., 2014). Although the fundamental requirements of the biomaterials remain the same, the achievement of the optimal and appropriate host response is seen to be influenced by biological and pharmacological factors, entirely consistent with the basic tenets of biocompatibility (Williams, 2017).

Taking this argument a little further, if inertness facilitates the biocompatibility of implantable biomaterials, which involves minimal biological activity, how can this be translated into tissue engineering applications where, by definition, the biomaterials have to take part in mechanisms of cell stimulation? A different paradigm is clearly required.

It is of no surprise that the majority of the early group of tissue engineering products to be developed and used in clinical practice incorporated biodegradable polymeric materials that had formed parts of medical devices such as surgical sutures; previous FDA approval in the context of devices constituted the first specification for the new tissue engineering scaffolds. However, a surgical suture was not intended to play a biological role in wound healing; it was simply used to hold tissues together mechanically during healing and then resorb with minimal host response. This was far from the main requirement of a tissue engineering biomaterial, which has to take part in the active process of tissue regeneration.

Considering this from a slightly different perspective, microphotographs of polymeric or ceramic tissue engineering scaffolds usually show that they have been produced by techniques such as solid free form fabrication. The question arises as to whether those microscale porous structures, which should be intended to facilitate the delivery of the "systematic combination of molecular and mechanical signals," mentioned before, to the target cells, can actually replicate the natural environment of those target cells? In other words, do these structures resemble the niche of the target cells? Furthermore, the niche of these target cells, including stem cells, changes during extracellular matrix expression. If the biomaterial were undergoing degradation and resorption, would its degradation profile be consistent with the profile of cell niche maturation? The answer to these questions is almost certainly no.

It may well be that some tissue engineering processes that involve classical degradable polymers such as poly(glycolic acid) and polycaprolactone do allow the generation of some functional tissue, but this happens in spite of rather than because of the choice of material. More specifically, the tissue-engineering field has progressed in the absence of any clearly delineated specifications for tissue engineering biomaterials or tissue engineering templates. It is now necessary to define these specifications (Williams, 2017); some may be associated with the mechanical characteristics, including those of elasticity (stiffness, compliance etc.), that control the delivery of the necessary mechanical stimuli. Others relate to the delivery of molecular signals and nutrients to the target cells. The majority, however, are concerned with the biocompatibility of these templates, which inevitably will not involve the characteristics of inertness. Essentially, the template has to recapitulate the morphology of the target cell niche and should adapt to the changing microenvironment.

Thus, the tissue engineering biomaterial should have mechanical properties, particularly stiffness, that favor mechanical signaling in order to optimize differentiation, proliferation, and gene expression in the target cells. The material should have surface characteristics that enhance cell adhesion and function and should enable the orchestration of molecular signaling to the relevant cells, through the direction of endogenous molecules and delivery of exogenous molecules. The template should usually be degradable, with relevant degradation kinetics and suitable morphological, and chemical degradation profiles. The material should have a physical form that provides relevant shape to the regenerating tissue and its architecture should optimize the transport of nutrients, gas and biomolecules, either or both *ex vivo* or *in vivo*, and facilitate nerve and blood vessel development. Naturally, the material should be non-cytotoxic, non-immunogenic, and minimally pro-inflammatory.

The concept of replicating the cell niche introduced above is consistent with the trend of recent years. The architecture of tissue engineering templates has been changing, with a move toward hybrid macro- and nano-scale structures and toward hydrogels based on tissues, tissue-derived, or tissue-mimicking components. These include injectable peptide based hydrogels (Greenfield et al., 2010), biomimetic hydrogels (Green et al., 2016), and decellularized tissues (Yu et al., 2016). In such materials, great care has to be taken to avoid undesirable host responses, again consistent with the basic principles of biocompatibility, for example through immunological responses with xenogeneic-derived substances, but this is not the main driving force or specification for their development. Here, the appropriate host response (Williams, 2014) is not no response, but that which is optimal for the stimulation of those target cells within a recognizable, niche-mimicking, microenvironment. Without a clear understanding of the mechanisms of biocompatibility pathways within the tissue engineering context, which may be different to those for long-term implantable devices, there is little chance of designing new functional biomaterials for regenerative medicine.

CONTRAST AGENTS

It is worth mentioning briefly the situation with contrast agents. Anatomical and functional imaging techniques, especially MRI and CT modalities, have been in clinical use for decades, but

their utility has been significantly enhanced in recent years through the use of highly specific contrast agents. These are able, for example to accelerate the relaxation times of protons from bulk water in MRI (Peng et al., 2016) or improve targeting ability so that imaging can be used intraoperatively in tumor therapy (McHugh et al., 2018). These contrast agents have typically involved metallic or ceramic nanoparticles or semiconductor quantum dots where issues of *in vivo* distribution, residence time, and toxicity were raised at an early stage.

Until recently, the toxicity of contrast agents has been treated on a case-by-case basis, which has not provided an overall perspective of the potential pathophysiology of conditions that arise from their use. This is perhaps not surprising since they are based on many different chemical structures and morphologies. The situation is made more complex by significant variations in the development of agent-related diseases on the basis of the patient's condition and co-morbidities. For example several gadolinium-based agents have good records of incident free use in MRI but prove remarkably toxic when used in patients with existing renal insufficiency (Ramalho et al., 2016). Individual toxicity profiles exist for contrast agents based on iron oxide (Schmid et al., 2017), gold nanoparticles (Arami et al., 2015), manganese oxides (Pernia Leal et al., 2015), and so on and databases are gradually evolving.

Fortunately, the language of contrast agent biological safety is now turning to concepts of biocompatibility rather than conventional toxicity. This move has been driven by the considerable potential of quantum dots in tumor imaging. Many quantum dot preparations used in non-healthcare applications are based on cadmium compounds, but their recognized cytotoxicity means that clinical applications are highly unlikely (Hardman, 2006). This has provided the opportunity to design quantum dots utilizing metals such as silver or copper, or even carbon, where biocompatibility pathways can be examined and specifications derived from this can be placed alongside functionality specifications in the overall design.

BIOCOMPATIBILITY PATHWAYS

As noted earlier, the present author has recently discussed mechanisms of biocompatibility in terms of biocompatibility pathways (Williams, 2017). This comprehensive analysis, based on experimental and, especially, clinical evidence, established that the classical views of the development of the host response required reassessment of factors such as the role of protein adsorption on subsequent tissue responses and the temporal sequence of events in inflammation and fibrosis. In particular, in the majority of circumstances the role of protein behavior at biomaterials surfaces is minimal, as is that of surface microtopography; for reviews of the effects of proteins in blood compatibility, see Sefton et al. (2019).

Two major types of mechanism dominate the events in tissues adjacent to biomaterials (which are likely to act synergistically); these are mechanotransduction and sterile inflammation. "Mechanotransduction" describes the processes at the cellular and molecular levels that are involved with the transduction of mechanical stimuli into biochemical signals. Implantable devices do not perform in a stress-free environment, and both structural and hemodynamic forces are likely to be encountered at interfaces. There will, almost inevitably be a mismatch of elastic moduli between tissues and engineering materials; this will result in differential stresses and strains between these components. When forces are applied in normal or abnormal physiological systems, pathways of mechanotransduction which involve sensing and signaling processes, lead to modulation of gene and protein expression profiles, that control sequence of changes in biocompatibility. The timescale will typically be milliseconds/seconds for mechanosensor stretching, hours for modified gene expression and days or weeks with cell function and tissue regeneration. Mechanical forces are inevitably involved in the formation of the response to orthopedic bone and joint replacements, breast implants, vascular grafts, intravascular stents, and many other forms of implanted device. Any discussion of biochemical processes taking place within the host response to a biomaterial has to be superimposed on the effects of mechanical force. Moreover, it does not make sense to assess biocompatibility in a stress-free *in vitro* environment.

Alongside the effects of the mechanical environment are those of the changes of the chemical characteristics associated with the presence of a biomaterial. There are two factors here, the chemical nature of the surface and of any components released from it, and the processes of inflammation, immunity, and fibrosis in the tissues.

It may be possible to demonstrate the effects of modifications to surface chemistries on the release of biological factors from cells *in vitro* but this is rarely relevant to clinical biocompatibility. This is important as literature reviews of biocompatibility may contain citations to this type of *in vitro* study, and these often form the basis of regulatory submissions.

However, some substances are released from these surfaces during contact with tissues by leaching, diffusion, degradation or erosion processes, and when the material is presented to the physiological environment in a labile form. In metallic materials, these may be impurities, metal ions, corrosion products and retained manufacturing, and surface treatment agents. With polymers, they are likely to include monomers and oligomers, catalysts, antioxidants and processing additives, and degradation products. Following decades of clinical experience, the choice of the main biomaterial component in a device has had to be refined; the portfolio of widely accepted engineering materials is now much smaller and is confined to those which are very inert, both biologically and chemically.

When assessing biocompatibility under conditions relevant to *in vivo* applications, we have to take into account these interactions within the context of existing knowledge about mechanisms of sterile inflammation, fibrosis and the response to stress, however they originate. This is based on the immune system; however, the biomaterials community has not been comfortable with the implications of immune system involvement in the host response since the materials are

normally considered to be associated with host—non-pathogen interactions, whereas the immune system does address host-pathogen interactions. It is now known that there is a commonalty in the immunological response to danger signals whatever the nature of the stressor. This has given rise to phenomena described as Damage Associated Molecular Patterns (DAMPs), the understanding of which originated with the work of Matzinger (2002) who described the concept of the danger model, replacing the standard self and non-self paradigm. Sterile inflammation was described as inflammation that results from trauma or chemically-induced injury without the involvement of any microorganism. It is associated with the recruitment of cells such as neutrophils and macrophages and the generation of pro-inflammatory chemokines and cytokines, especially IL-1 and TNF. With respect to biomaterials, including those used in devices that have an extended residence time in the body, the progress of biomaterial-induced sterile inflammation throughout this period has to be considered; it is helpful to note that this involves mechanisms similar to sterile inflammatory diseases, which may be associated with both endogenous and exogenous substances; examples include gout and pneumoconiosis.

There are several processes that are mechanistically involved in the sterile inflammatory process (Chen and Nunez, 2010). Importantly, pattern recognition receptors (PRRs) on inflammatory cells, which can sense conserved structural entities in microorganisms, also sense some exogenous molecules. The released intracellular cytokines and chemokines activate common pathways downstream, where innate multiprotein complexes, the inflammasomes, induce inflammation in response to both pathogens and molecules derived from the proteins of the host. It is also noted that in all types of fibrosis, whatever the cause, inflammatory-immunologic reactions take place that upregulate pro-fibrotic processes; fibrosis around an implant occurs simultaneously with inflammation and is not a separate event.

It should be obvious here that the characteristics of the stress environment control those features of the inflammation-fibrosis response, which influence the eventual outcome and identification of the pathways that are associated with both sterile inflammation and mechanotransduction will facilitate this understanding. This approach to the host response also subsumes the role of macrophages, where evidence now points to processes whereby these cells undergo time-dependent phenotypic and functional alterations according to the stress factors. These lead to either pro-inflammatory or anti-inflammatory situations (Wynn and Vannella, 2016), that are dependent on the DAMP profiles.

This discussion has focused on the innate immune response. However, other components of immune responses, and also other forms of toxicity, may be involved, possibly explaining some of the difficult clinical biocompatibility events, especially those of idiosyncratic feature, including adaptive immune responses (especially hypersensitivity), autoimmune effects, and genotoxicity. It could also be instructive to use models of adverse outcomes pathways that have recently been developed within general toxicology, for example as used by Zhang et al. with respect to the comparative toxicity of contrast agents (Zhang et al., 2018).

CONTROL OF BIOCOMPATIBILITY THROUGH MODULATION OF BIOCOMPATIBILITY PATHWAYS

The above analysis shows that it should be possible to influence biocompatibility characteristics through a modulation of biocompatibility pathways, possibly by locally delivered pharmaceutical agents or by control of biomaterial architecture or morphology. There is little consistent data on these possibilities and it is not yet possible to create generic paradigms. However, a few examples of the way forward can be quoted.

With respect to mechanotransduction, several recent studies have pointed to some key pathways. For example, Janson and Putnam (2015) have highlighted the signaling pathways that have been implicated in mechanotransduction through the effects of topographical cues; cells share common mechanisms to respond to physical and chemical topography and to matrix elasticity, potentially leading to changes in gene transcription. Molecular components here include integrins, focal adhesion-associated proteins such as FAK, and the RhoA/ROCK/MAPK axis. Lee et al. have similarly demonstrated the role of nuclear mechanosensitivity in determining cellular responses, such as the way in which matrix stiffness alters laminin A/C expression in mesenchymal stem cells, which ultimately determines the lineage specification (Lee et al., 2019).

With respect to inflammatory responses, Liu et al. have shown that the size of graphene oxide particles influences phagocytosis processes through modulation of interactions with toll-like receptors and activation of NF- κB pathways (Ma et al., 2015). Inflammatory responses to cobalt-chromium dental alloys have been shown to be due to upregulation of pro-inflammatory cytokines such as TNF- α, IL-1 β, IL-6, and IL-8. The alloys activate the NRF2 pathway, up-regulate antioxidant enzymes including heme oxidase-1 and activate JAK2/STAT3, p38/ERK/JNK MAPKs, and NF- κB pathways (Kim et al., 2016).

The classical foreign body response may now be seen as a process regulated by specific biochemical pathways, the nature of which will depend on the local circumstances. Liao et al. have shown that the response to the widely used implant material polyetheretherketone is controlled by the miR-29ab1-mediated SLT3 upregulation, and that this may be influenced by the local delivery of pravastatin (Liao et al., 2014). With degradable magnesium alloys, the stimulation of osteogenesis may be achieved *via* the upregulation of transcription factors in the ERK signaling pathway through the effects of released metal ions such as calcium and strontium (Li et al., 2016); the overall effects of magnesium on the fate of mesenchymal stem cells mediated *via* different pathways has been reviewed by Luthringer and Willumeit-Romer (2016). Huang et al. have recently shown that silicon, magnesium and calcium ions released from silicate bioceramics inhibit macrophage inflammatory responses by suppressing the activated inflammatory MAPK and NF- κB pathways (Huang et al., 2018), while Pang et al. have similarly reported the effects of different modified hydroxyapatite structures on the expression of both inflammatory and anti-inflammatory cytokines (Pang et al., 2019). The possibility of modifying the

activation of the ERK1/2 signaling pathway during osteogenic differentiation of mesenchymal stem cells through various functional groups including -OH, -COOH, $-NH_2$, and $-CH_3$ has been shown by Bai et al. (2013). Wang et al. have shown that chitosan-collagen composite films can regulate the expression of osteoblastic marker genes, and specifically that osteoblast differentiation of mesenchymal stem cells can be promoted through an ERK1/2 activated Runx2 pathway (Wang et al., 2016).

With nanoparticles, the macrophage inflammatory activity of titania nanotubes is attenuated if he MAPK and NF-κB pathways are inhibited (Neacsu et al., 2015) and gold nanoparticles promote the differentiation of embryonic stem cells into dopaminergic neurons *via* the mTOR/p70S6K pathway (Wei et al., 2017) or the osteogenic differentiation of periodontal ligament cells *via* the p38 MAPK pathway (Niu et al., 2018). Poly(lactic acid) nanoparticles are internalized in lung epithelial cells through clathrin-coated pits and lipid rafts (Da Luz et al., 2017) while the effect of PAMAM dendrimers on the activation of pro-inflammatory signaling pathways, especially involving NF-κB transduction may be influenced by pyrrolidone modification (Janaszewska et al., 2017). Pathways for nanoparticle-induced apoptosis with cerium oxide (Khan et al., 2017) and autophagy with silver (Mao et al., 2016) have been identified.

The examples given in the preceding paragraphs merely give a hint of how the identification of pathways associated with biocompatibility phenomena, ranging from fibrotic and inflammatory responses to implanted materials to stem cell differentiation associated with biomaterial templates and nanoparticle toxicity, can lead to the modulation of these phenomena and the potential optimization of biocompatibility performance.

CONCLUSIONS

The principal conclusion of this perspectives paper on the fundamental characteristics of biocompatibility is that, through a far better understanding of the precise mechanisms of biocompatibility phenomena, and especially the biological pathways that are involved, it should be possible to influence these phenomena, such modulation improving the clinical outcomes associated with biomaterials. During recent years, significant progress has been made with identifying the specific mechanisms, especially those of mechanotransduction and sterile inflammation, that should now profoundly modify the classical concepts of the foreign body response, allowing, through very different objectives, the optimization of biocompatibility outcomes with implanted devices, tissue engineering templates, imaging contrast agents, and other biomaterials-based technologies. The control of biocompatibility, rather than the simple subjective observation of events, should significantly improve biomaterials performance.

AUTHOR CONTRIBUTIONS

The author confirms being the sole contributor of this work and has approved it for publication.

REFERENCES

Al Aranji, G., White, D., Solanki, K., Al Aranji, G., White, D., and Solanki, K. (2014). Scleroderma renal crisis following silicone breast implant rupture: a case report and review of the literature. *Clin. Exp. Rheumatol.* 32, 262–266.

Allen, D. J., Beaulé, P. E., Allen, D. J., and Beaule, P. E. (2008). Rationale for metal-on-metal total hip replacement. *J. Surg. Orthop. Adv.* 17, 6–11. doi: 10.1097/01.blo.0000193809.85587.f8

Arami, H., Khandhar, A., Liggitt, D., and Krishnan, K. M. (2015). *In vivo* delivery, pharmacogenetics, biodistribution and toxicity of iron oxide nanoparticles. *Chem. Soc. Rev.* 44, 8856–8607. doi: 10.1039/C5CS00541H

Bai, B., He, J., Li, Y.-S., Yang, X.-M., Ai, H.-J., and Cui, F.-Z. (2013). Activation of the ERK1/2 signaling pathway during the osteogenic differentiation of mesenchymal stem cells cultures on substrates modified with various chemical groups. *Bio. Med. Res. Int.* 2013:361906. doi: 10.1155/2013/361906

Bondurant, S., Ernster, V., and Herdman, R. (1999). *Safety of Silicne Breast Implants*. Washington, DC: Institute of Medicine, Committee on the Safety of Breast Implants, National Academies Press.

Brennan, J. M., Zhao, Y., Williams, J., O'Brien, S., Dokholyan, R., Gammie, J., et al. (2015). Long-term clinical outcomes of Silzone era St. Jude Medical mechanical heart valves. *J. Heart Valve Dis.* 24, 66–73.

Cassady, A. I., Hidzir, N. M., and Grondahl, L. (2014). Enhancing expanded poly(tetrafluoroethylene) (ePTFE) for biomaterials applications. *J. Appl. Poly. Sci.* 131:40533. doi: 10.1002/app.40533

Chen, G. Y., and Nunez, G. (2010). Sterile inflammation: sensing and reacting to damage. *Nat. Rev. Immunol.* 10, 826–37. doi: 10.1038/nri2873

Colas, A., and Curtis, J. (2013). "Silicones," in *Biomaterials Science, 3rd Edn*, eds B. Ratner, et al. (Oxford: Elsevier), 82–91. doi: 10.1016/B978-0-08-087780-8.00010-3

Da Luz, C. M., Boyles, M. S. O., Falagan-Lotsch, P., Pereira, M. R., Tutumi, H. R., de Oliveira Santos, E., et al. (2017). Polylactic acid nanoparticles (PLA-NP) promote physiological modifications in lung epithelial cells and are internalized by clathrin-coated lipid rafts. *J. Nanobiotech.* 15, 11–6. doi: 10.1186/s12951-016-0238-1

Frazer, R. Q., Byron, R. T., Osborne, P. B., and West, K. P. (2005). PMMA: an essential material in medicine and dentistry. *J. Long Term Effect Med. Implants* 15, 629–639. doi: 10.1615/JLongTermEffMedImplants.v15.i6.60

Gallo, J., Goodman, S. B., Konttinen, Y. T. Wimmer, M. A., and Holinka, M. (2013). Osteolysis around total knee arthroplasty: a review of pathogenic mechanisms. *Acta Biomater.* 9, 8046–8058. doi: 10.1016/j.actbio.2013.05.005

Gill, H. S., Grammatopoulos, G., Adshead, S., Tsialogiannis, E., and Tsiridis, E. (2012). Molecular and immune toxicity of CoCr nanoparticles in MoM hip arthroplasty. *Trends Mol. Med.* 18, 145–152. doi: 10.1016/j.molmed.2011.12.002

Gomez-Barrena, E., Puertolas, J. A., Munuera, L., and Konttinen, Y. T. (2008). Update on UHMWPE research; from the bench to the bedside. *Acta Orthop.* 79, 832–840. doi: 10.1080/17453670810016939

Green, J. J., Elisseeff, J. H.,Green, J. J., and Eiisseeff, J. H. (2016). Mimicking biological functionality with polymers for biomedical applications. *Nature* 540, 386–394. doi: 10.1038/nature21005

Greenfield, M. A., Hoffman, J. R., de la Cruz, M. O., and Stupp, S. I. (2010). Tunable mechanics of peptide nanofiber gels. *Langmuir.* 26, 3641–3647. doi: 10.1021/la9030969

Grunkenmeier, G. L., Jin, R., Im, K., Holubkov, R., Kennard, E. D., and Schaff, H. V. (2006). Time-related risk of the St. Jude Silzone heart valve. *Eur. J. Cardio-thorac. Surg.* 30, 20–27. doi: 10.1016/j.ejcts.2006.04.012

Gustafson, K., Jakobsen, S. S., Lorenzen, N. D., Thyssen, J. P., Johansen, J. D., Bonefeld, C. M., et al. (2014). Metal release and metal allergy after total

hip replacement with resurfacing versus conventional hybrid prosthesis. *Acta Orthop*. 85, 348–354. doi: 10.3109/17453674.2014.922730

Hardman, R. (2006). A toxicological review of quantum dots: Toxicity depends on physicochemical and environmental factors. *Environ. Health Perspect*. 114, 165–172. doi: 10.1289/ehp.8284

Huang, Y., Wu, C., Zhang, X., Chang, J., and Dai, K. (2018). Regulation of immune response by bioactive ions released from silicate bioceramics for bone regeneration. *Acta Biomater*. 66, 81–92. doi: 10.1016/j.actbio.2017.08.044

Iung, B., Rodés-Cabau, J.,Iung, B., and Rodes-Cabau, J. (2014). The optimal management of anti-thrombotic therapy after valve replacement: certainties and uncertainties. *Europ. Heart J*. 35, 2942–2949. doi: 10.1093/eurheartj/ehu365

Janaszewska, A., Gorzkiewicz, M., Ficker, M., Petersen, J. F., Paolucci, V., Christensen, J. B., et al. (2017). Pyrrolidone modification prevents PAMAM dendrimers from activation of pro-inflammatory signaling pathways in human monocytes. *Mol. Pharmaceut*. 15, 12–20. doi: 10.1021/acs.molpharmaceut.7b00515

Janowsky, E. C., Kupper, L. L., Hulka, B. S.,Janowsky, E. C., Kupper, L. L., and Hulka, B. S. (2000). Meta-analyses of the relation between silicone breast implants and the risk of connective-tissue diseases. *N. Engl. J. Med*. 342, 781–790. doi: 10.1056/NEJM200003163421105

Janson, I. A., Putnam, A. J. (2015). Extracellular matrix elasticity and topography: material-based cues that affect cell function via conserved mechanisms. *J. Biomed. Mater. Res. Part A*. 103, 1246–58. doi: 10.1002/jbm.a.35254

Kastrati, A., Mehilli, J., von Beckerath, N., Dibra, A., Hausleiter, J., Pache, J., et al. (2005). Sirolimus-eluting stent or paclitaxel-eluting stent vs balloon angioplasty for prevention of recurrences in patients with coronary in-stent restenosis. *JAMA* 293, 165–171. doi: 10.1001/jama.293.2.165

Khan, S., Ansari, A. A., Rolfo, C., Coelho, A., Abdulla, M., Al-Khayal, K., et al. (2017). Evaluation of *in vitro* cytotoxicity. biocompatibility, and changes in the expression of apoptosis regulatory proteins induced by cerium oxide nanocrystals. *Sci. Tech. Adv. Mater*. 18, 364–373. doi: 10.1080/14686996.2017.1319731

Kim, E. C., Kim, M. K., Leesungbok, R., Lee, S. W., and Ahn, S. J. (2016). Co-Cr dental alloys induces cytotoxicity and inflammatory responses via activation of Nrf2 antioxidant signaling pathways in human gingival fibroblasts and osteoblasts. *Dental Mater*. 32, 1394–1405. doi: 10.1016/j.dental.2016.09.017

Lee, J. H., Kim, D. H., Lee, H. H., and Kim, H. W. (2019). Role of nuclear mechanosensitivity in determining cellular responses to forces and biomaterials. *Biomaterials* 197, 60–71. doi: 10.1016/j.biomaterials.2019.01.010

Li, M., He, P., Wu, Y., Zhang, Y., Xia, H., Zheng, Y., et al. (2016). Stimulatory effects of the degradation products from Mg-Ca-Sr alloy on the osteogenesis through regulating ERK signaling pathway. *Sci. Rep*. 6:32323. doi: 10.1038/srep32323

Liao, Y., Ouyang, L., Ci, L., Chen, B., Lv, D., Li, Q., et al. (2014). Pravastatin regulates host foreign-body reaction to polyetheretherketone implants via miR-29ab1-mediated SLIT# upregulation. *Biomaterials* 203, 12–22. doi: 10.1016/j.biomaterials.2019.02.027

Lo, K. W., Ulery, B. D., Ashe, K. M., and Laurencin, C. T. (2012). Studies of bone morphogenetic protein-based surgical repair. *Adv. Drug Del. Rev*. 64, 1277–1291. doi: 10.1016/j.addr.2012.03.014

Luthringer, B. J. C., and Willumeit-Romer, R. (2016). Effects of magnesium degradation products on mesenchymal stem cell fate and osteoblastogenesis. *Gene* 575, 9–20. doi: 10.1016/j.gene.2015.08.028

Ma, J., Liu, R., Wang, Z., Liu, Q., Chen, Y., Valle, R. P., et al. (2015). Crucial role of lateral size for graphene oxide in activating macrophages and stimulating pro-inflammatory responses in cell and animals. *ACS Nano*. 9, 10498–10515. doi: 10.1021/acsnano.5b04751

Mao, B.-H., Tsai, J.-C., Chen, C.-W., Yan, S. J., and Wang, Y. J. (2016). Mechanisms of silver particle induced toxicity and important role of autophagy. *Nanotoxicology* 10, 1021–1040. doi: 10.1080/17435390.2016.1189614

Matzinger, P. (2002). The danger model: a renewed sense of self. *Science* 296, 301–5. doi: 10.1126/science.1071059

McHugh, K. J., Jing, L., Behrens, A. M., Jayawardena, S., Tang, W., Gao, M., et al. (2018). Biocompatible semiconductor quantum dots as cancer imaging agents. *Adv. Mater*. 30:1706356. doi: 10.1002/adma.201706356

Meinhart, J. G., Schense, J. C., Schima, H., Gorlitzer, M., Hubbell, J. A., Deutsch, M., et al. (2005). Enhanced endothelial cell retention on shear-stresses synthetic vascular grafts precoated with RGD-cross linked fibrin. *Tissue Eng*. 11, 887–895. doi: 10.1089/ten.2005.11.887

Metikos-Hukovic, M., Pilac, Z., Babic, R., and Omanovićc, D. (2006). Influence of alloying elements on the corrosion stability of CoCrNo implants in Hanks solution. *Acta Biomater*. 2, 693–700. doi: 10.1016/j.actbio.2006.06.002

Neacsu, P., Mazare, A., Schmuki, P., and Cimpean, A. (2015). Attenuation of the macrophage inflammatory activity by TiO2 nanotubes via inhibition of MAPK and NF- κB pathways. *Int. J. Nanomed*. 10, 6455–6467. doi: 10.2147/IJN.S92019

Niu, C., Yuan, K., Ma, R., Gao, L., Jiang, W., Hu, X., et al. (2018). Gold nanoparticles promote the osteogenic differentiation of human periodontal ligament stem cells via the p38 MAPK signaling pathway. *Mol. Med. Rep*. 2017, 4879–4886. doi: 10.3892/mmr.2017.7170

Pang, S., Li, X., Wu, D., Li, H., and Wang, X. (2019). Tuning inflammation response via adjusting microstructure of hydroxyapatite and biomolecule modification. *Coll. Surf. B Biointerfaces*. 177, 496–505. doi: 10.1016/j.colsurfb.2019.02.026

Peng, Y.-K., Tsang, S. C. E., and Chou, P.-T. (2016). Chemical design of nanoprobes for T1-weighted magnetic resonance imaging. *Mater. Today* 19, 336–348. doi: 10.1016/j.mattod.2015.11.006

Pernia Leal, M., Rivera-Fernández, S., Franco, J. M., Pozo, D., de la Fuente, J. M., and García-Martín, M. L. (2015). Long-circulating PEGylated manganese ferrite nanoparticles for MRI-based molecular imaging. *Nanoscale* 7, 2050–2059. doi: 10.1039/C4NR05781C

Ramalho, J., Semelka, R. C., Ramalho, M., Nunes, R. H., AlObaidy, M., and Castillo, M. (2016). Gadolinium-based contrast agent accumulation and toxicity: an update. *Am. J. Neuroradiol*. 37, 1192–1198. doi: 10.3174/ajnr.A4615

Scales, J. T., and Winter, G. D. (1975). Clinical considerations in the choice of materials for orthopaedic internal prostheses. *J. Biomed. Mater. Res. Symp*. 6, 176–186. doi: 10.1002/jbm.820090420

Schmid, G., Kreyling, W. G., Simon, U., Schmid, G., Kreyling, W. G., and Simon, U. (2017). Toxic effects and biodistribution of ultrasmall gold nanoparticles. *Arch. Toxicol*. 91, 3011–3037. doi: 10.1007/s00204-017-2016-8

Sefton, M. V., Sperling, C., Maitz, M. F., and Werner, C. (2019). The blood compatibility challenge; Editorial introduction. *Acta Biomater*. 94:1. doi: 10.1016/j.actbio.2019.06.041

Siddiqi, A., Khan, A. S., Zafar, S.,Siddiqi, A., Khan, A. S., and Zafar, S. (2017). Thirty years of translational research in zirconia dental implants: a systematic review of the literature. *J. Oral. Implantol*. 43, 314–325. doi: 10.1563/aaid-joi-D-17-00016

Underwood, R. J., Zografos, A., Sayles, R. S., Hart, A., and Cann, P. (2012). Edge loading in metal-on-metal hips: low clearance is a new risk factor. *Proc. Inst. J. Eng. Med*. 26, 217–226. doi: 10.1177/0954411911431397

Wang, X., Wang, G., Liu, L., and Zhang, D. (2016). The mechanism of a chitosan-collagen composite film used as a biomaterial support for MC3T3-E1 cell differentiation. *Sci. Rep*. 6:39322. doi: 10.1038/srep39322

Watad, A., Rosenberg, V., Tiosano, S., Cohen Tervaert, J. W., Yavne, Y., Shoenfeld, Y., et al. (2018). Silicone breast implants and the risk of autoimmune/rheumatic disorders: a real world analysis. *Int. J. Epidemiol*. 47, 1846–54. doi: 10.1093/ije/dyy217

Webster, T. J., Siegel, R. W., and Bizios, R. (1999). Design and evaluation of nanophase alumina for orthopedic/dental applications. *Nano. Struct. Mater*. 12, 983–986. doi: 10.1016/S0965-9773(99)00283-4

Wei, M., Li, S., Yang, Z., Zheng, W., and Le, W. (2017). Gold nanoparticles enhance the differentiation of embryonic stem cells into dopaminergic neurons via mTOR/p70S6K. *Nanomedicine* 12:1305–1317. doi: 10.2217/nnm-2017-0001

Williams, D. F. (1977). Titanium as a metal for implantation II. Biological properties and clinical uses. *J. Med. Eng. Tech*. 1, 266–9. doi: 10.3109/03091907709162192

Williams, D. F. (1986). "*Definitions in Biomaterials*," in *Proceedings of a Consensus Conference of the European Society for Biomaterials* (Chester: Elsevier).

Williams, D. F. (2006). To engineer is to create; the link between engineering and regeneration. *Trends Biotech*. 24, 4–8. doi: 10.1016/j.tibtech.2005.10.006

Williams, D. F. (2008). On the mechanisms of biocompatibility. *Biomaterials* 29, 2941–2953. doi: 10.1016/j.biomaterials.2008.04.023

Williams, D. F. (2014). The biomaterials conundrum in tissue engineering. *Tissue Eng.* 20, 1129–1131. doi: 10.1089/ten.tea.2013.0769

Williams, D. F. (2017). Biocompatibility pathways: biomaterials-induced sterile inflammation, mechanotransduction, and principles of biocompatibility control. *ACS Biomater. Sci. Eng.* 3, 2–35. doi: 10.1021/acsbiomaterials.6b00607

Williams, D. F., and Roaf, R. (1973). *Implants in Surgery*. London: WB Saunders.

Williams, D. F., and Williams, D. F. (2014). There is no such thing as a biocompatible material. *Biomaterials* 35, 10009–10014. doi: 10.1016/j.biomaterials.2014.08.035

Woodward, B. (2012). Palladium in temporary and permanently implantable medical devices. *Plat Metals Rev.* 56, 213–217. doi: 10.1595/147106712X651748

Wynn, T. A., and Vannella, K. M. (2016). Macrophages in tissue repair, regeneration and fibrosis. *Immunity* 44, 450–60. doi: 10.1016/j.immuni.2016.02.015

Yu, Y., Alkhawaji, A., Ding, Y., and Mei, J. (2016). Decellularized scaffolds in regenerative medicine. *Oncotarget* 7:58671. doi: 10.18632/oncotarget.10945

Zhang, H., Wang, T., Zheng, Y., Yan, C., Gu, W., and Ye, L. (2018). Comparative toxicity and contrast enhancing assessments of Gd_2O_3@BSA and MnO_2@BSA nanoparticles for MR imaging in brain glioma. *Biochem. Biophys. Res. Comm.* 499, 488–492. doi: 10.1016/j.bbrc.2018.03.175

Zhang, X. D., and Williams, D. F. (2018). Definitions of biomaterials for the twenty-first century," in *Proceedings of Conference* (Chengdu: Elsevier).

Conflict of Interest: The author declares that the research was conducted in the absence of any commercial or financial relationships that could be construed as a potential conflict of interest.

frontiers in Bioengineering and Biotechnology

ORIGINAL RESEARCH
published: 08 November 2019
doi: 10.3389/fbioe.2019.00315

Migration and Differentiation of Neural Stem Cells Diverted From the Subventricular Zone by an Injectable Self-Assembling β-Peptide Hydrogel

Sepideh Motamed[1,2], Mark P. Del Borgo[2], Kun Zhou[1], Ketav Kulkarni[2], Peter J. Crack[3], Tobias D. Merson[4], Marie-Isabel Aguilar[2], David I. Finkelstein[5]* and John S. Forsythe[1]**

[1] Department of Materials Science and Engineering, Monash Institute of Medical Engineering, Monash University, Clayton, VIC, Australia, [2] Department of Biochemistry and Molecular Biology, Biomedicine Discovery Institute, Monash University, Clayton, VIC, Australia, [3] Department of Pharmacology, The University of Melbourne, Parkville, VIC, Australia, [4] Australian Regenerative Medicine Institute, Monash University, Clayton, VIC, Australia, [5] Florey Institute of Neuroscience and Mental Health, The University of Melbourne, Parkville, VIC, Australia

OPEN ACCESS

Edited by:
Evelyn K. F. Yim,
University of Waterloo, Canada

Reviewed by:
Eyleen L. Goh,
National Neuroscience Institute (NNI), Singapore
Mayara Vieira Mundim,
Federal University of São Paulo, Brazil

***Correspondence:**
Marie-Isabel Aguilar
mibel.aguilar@monash.edu
David I. Finkelstein
david.finkelstein@florey.edu.au
John S. Forsythe
john.forsythe@monash.edu

Specialty section:
This article was submitted to Biomaterials, a section of the journal Frontiers in Bioengineering and Biotechnology

Received: 03 February 2019
Accepted: 24 October 2019
Published: 08 November 2019

Citation:
Motamed S, Del Borgo MP, Zhou K, Kulkarni K, Crack PJ, Merson TD, Aguilar M-I, Finkelstein DI and Forsythe JS (2019) Migration and Differentiation of Neural Stem Cells Diverted From the Subventricular Zone by an Injectable Self-Assembling β-Peptide Hydrogel. Front. Bioeng. Biotechnol. 7:315. doi: 10.3389/fbioe.2019.00315

Neural stem cells, which are confined in localised niches are unable to repair large brain lesions because of an inability to migrate long distances and engraft. To overcome these problems, previous research has demonstrated the use of biomaterial implants to redirect increased numbers of endogenous neural stem cell populations. However, the fate of the diverted neural stem cells and their progeny remains unknown. Here we show that neural stem cells originating from the subventricular zone can migrate to the cortex with the aid of a long-lasting injectable hydrogel within a mouse brain. Specifically, large numbers of neuroblasts were diverted to the cortex through a self-assembling β-peptide hydrogel that acted as a tract from the subventricular zone to the cortex of transgenic mice (NestinCreER^{T2}:R26eYFP) in which neuroblasts and their progeny are permanently fluorescently labelled. Moreover, neuroblasts differentiated into neurons and astrocytes 35 days post implantation, and the neuroblast-derived neurons were Syn1 positive suggesting integration into existing neural circuitry. In addition, astrocytes co-localised with neuroblasts along the hydrogel tract, suggesting that they assisted migration and simulated pathways similar to the native rostral migratory stream. Lower levels of astrocytes were found at the boundary of hydrogels with encapsulated brain-derived neurotrophic factor, comparing with hydrogel implants alone.

Keywords: brain repair, neural stem cells, peptide hydrogels, self-assembly, neural tissue engineering

INTRODUCTION

Brain lesions are a consequence of physical injury, stroke and neurodegeneration (Lindvall et al., 2004; Hyder et al., 2007; Eltzschig and Eckle, 2011; Hernández-Ortega et al., 2011) resulting in severe neurological disabilities (Orive et al., 2009). Current treatments are associated with preserving healthy neural tissue and there are no clinical treatments that promote regeneration and fully restore lost function (Pettikiriarachchi et al., 2010). While cell transplantation is an important strategy to replace lost neural tissue, issues with immune rejection, poor engraftment, ethical issues

of embryonic cell sources and teratoma formation must first be resolved (Kondziolka et al., 2000; Master et al., 2007; Li et al., 2008; Hwang et al., 2010; Yasuda et al., 2010; Wang et al., 2012; Kang et al., 2014). Harnessing the regenerative power of the brain by using endogenous cells is therefore highly attractive.

Neural progenitor cells are continuously being produced in the adult brain, but their genesis is confined to the subgranular zone and the subventricular zone (SVZ) (Ma et al., 2009). Following brain injury, neural progenitor cells migrate into the injured region where they attempt differentiation and repair (Rennert et al., 2012). However, the brain's intrinsic repair mechanisms are largely ineffective, especially in the case of large lesions. The implications for the patient are therefore serious, manifesting in drastic and permanent disabilities.

In the healthy adult brain, neural stem cells (NSCs) residing in the SVZ divide and transit into amplifying cells which consequently differentiate into neuroblasts. The neuroblasts slide as neuronal chains along the rostral migratory stream (RMS) toward the olfactory bulb, where they differentiate into neurons and integrate in the granule and periglomerular layers into neural networks (Doetsch et al., 1999; Alvarez-Buylla and Lim, 2004; Ghashghaei et al., 2007; Whitman and Greer, 2009). Directed neuroblast migration through the RMS proceeds without dispersing into the surrounding tissue, however, this is a complicated process requiring a combination of cellular structures, signals, and cues (Lalli, 2014). Neuroblast migration from the SVZ is mediated by insulin-like growth factor I and fibroblast growth factor 2 (Hurtado-Chong et al., 2009). In addition, the chain of migrating neuroblasts use blood vessels, which are located in high density and aligned along the RMS, as a physical support to move forward (Bovetti et al., 2007). Vascular endothelial growth factor (VEGF), secreted by astrocytes surrounding the RMS, induces blood vessel generation and therefore indirectly regulates neuroblast motility (Bozoyan et al., 2012). Inhibition of brain-derived neurotrophic factor (BDNF) causes disruption of neuroblast migration throughout the RMS (Zhou et al., 2015). BDNF, secreted by blood vessels (Snapyan et al., 2009), promotes neuroblast movement via the $p75^{NTR}$ receptor and increases the number of migratory cells (Chiaramello et al., 2007). It has also been shown that BDNF increases the displacement distance of neuroblasts by promoting neuroblasts to switch from a mitotic phase to a motile phase (Snapyan et al., 2009). Migrating neuroblasts are isolated from the surrounding tissue via glial tubes made by astrocytes, preventing the dispersion of cells from the stream and guiding them in the direction of the RMS (Ghashghaei et al., 2007).

In response to injury, the brain initiates a glial response (Fitch and Silver, 2008) and subsequently, the SVZ proliferates new neuroblasts, some of which re-direct from the SVZ toward the injured area to replace lost neurons and glia (Kernie and Parent, 2010; Saha et al., 2012), using signals such as stromal-cell-derived factor-1α (SDF1α) and metalloproteinases (MMP9) released from the local neurons and glia at the site of injury (Miller et al., 2005; Ghashghaei et al., 2007). Infusion of epidermal growth factor (EGF) and fibroblast growth factor 2 in a Parkinson's disease animal model elevated neural stem cell proliferation in the SVZ and enhancement of dopaminergic neurogenesis in the olfactory bulb (Winner et al., 2008). Neuroblasts migrating toward ischemia utilize a similar mechanism as used in the RMS to migrate, using blood vessels as physical guidance. Neuroblasts migrating toward ischemia have longer stationary phases in comparison to cells migrating through the RMS (Grade et al., 2013), which could be attributed to the low levels of endogenous BDNF. Low levels of endogenous BDNF after spinal cord injury is one of the important reasons for the hindrance of regeneration (Song et al., 2008). Therefore, by injecting exogenous BDNF into mouse injury models, neuroblast displacement toward ischemia doubled per hour by reducing the cell stationary phase periods (Grade et al., 2013).

We have previously investigated the feasibility of using scaffolds to promote neuroblast migration, which include the use of injectable gelatin-based hydrogels consisting of glial cell line-derived neurotrophic factor, electrospun poly-ε-caprolactone nanofibers releasing a BDNF mimetic, and graphene coated electrospun poly-ε-caprolactone fibres from the SVZ (Fon et al., 2014a,b; Zhou et al., 2016). The scaffolds were implanted into the brain in a way to impinge on the SVZ, and promoted neuroblast migration in all studies in comparison to injury only controls. Other studies have also demonstrated the possibility to redirect neuroblasts from RMS and SVZ by implanted scaffolds with specific signal cues such as β1 integrin, N-cadherin, VEGF, and nerve growth factor (Clark et al., 2016; Fujioka et al., 2017; Jinnou et al., 2018) being incorporated. However, to develop viable therapies to treat brain injuries, it is important to develop new injectable scaffolds that dramatically increase: (1) the number of migrating neuroblasts, (2) the migration distance, and (3) the persistency of migration over time. It is also important to determine the fate of the diverted neuroblasts, which the previous studies have not fully addressed.

Previously, we introduced a new self-assembling peptide hydrogel composed exclusively of β-amino acids and a C_{14} hydrophobic acyl tail (C_{14}-peptide hydrogel). The peptide self-assembled to form a stable and long-lasting hydrogel which was biocompatible with neuronal cells (Motamed et al., 2016). A dual-functionalized peptide hydrogel with an integrin binding arginylglycylaspartic acid (RGD) was also used to enhance cell attachment (RGD-peptide hydrogel). By mixing the C_{14}- and RGD-peptides, the matrix was optimised to achieve high cell attachment *in vitro* (Kulkarni et al., 2016). In the present study, C_{14}- and RGD-peptide (Kulkarni et al., 2016; Motamed et al., 2016) was used to encapsulate BDNF, and was implanted into the SVZ of tamoxifen inducible Nes-$CreER^{T2}$: R26eYFP transgenic mice. NSCs residing in the SVZ of Nes-$CreER^{T2}$:R26eYFP transgenic mice are permanently labelled when administered with tamoxifen, enabling tracking of these cells, throughout all developmental stages (Imayoshi et al., 2006, 2008). By using this transgenic animal, neuroblast migration along the implanted hydrogel tract was investigated in the brain and the fate of the migrating neuroblasts determined following differentiation. Our approach is summarised in **Figure 1**.

MATERIALS AND METHODS

Peptide Synthesis

Detailed peptide synthesis was reported in our previous papers (Del Borgo et al., 2013; Kulkarni et al., 2016; Motamed et al.,

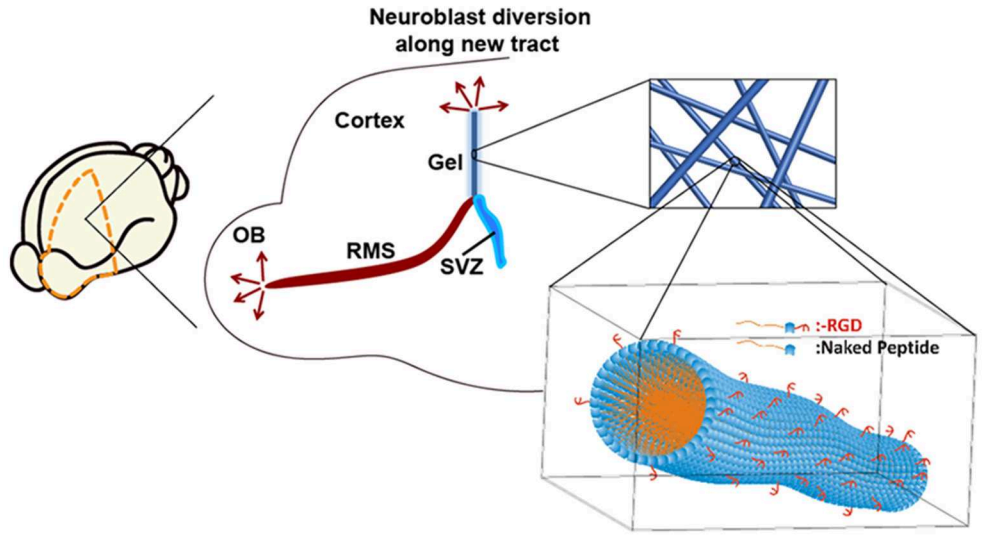

FIGURE 1 | Neuroblasts originating from the SVZ migrate along the rostral migratory stream (RMS) to the olfactory bulb (OB). An implantable matrix composed of self-assembling β-peptide hydrogel forms a matrix tract between the SVZ and the cortex allowing diversion of neuroblast migration. Inset: Schematic of supramolecular self-assembly of N-acetylated β3-peptide functionalised with the integrin binding RGD epitope.

2016). Briefly, the hydrogel consists of 90% tri-peptide (Ac-β A*(C_{14})-β K-β A-OH), where C_{14} alkyl chain was attached to the first amino acid by reducing azide (Motamed et al., 2016), and 10% RGD peptide (Ac-β A*(C_{14})-β A# (RGD)-β K-OH (Kulkarni et al., 2016).

BDNF Release From the Hydrogel

Ten microliters of BDNF full protein (13.5 kDa) stock (R&D Systems) with a concentration of 25 μg mL^{-1} was dissolved in 20 μL phosphate-buffered saline (PBS) to reach a final concentration of ∼0.0083 mg mL^{-1}. 0.3 mg of the optimized peptide containing 10% RGD peptide and 90% peptide was added to the BDNF solution to reach a final concentration of 10 mg mL^{-1} to form a hydrogel (Hook et al., 2004). The formed hydrogel was then incubated overnight. Three hundred microliters PBS was added on top of the hydrogel and the samples were incubated at 37°C. BDNF release was determined by taking 30 μL aliquots of PBS on top of the hydrogel at different time points and the solution was topped up to keep the volume constant over the course of the assay. Samples were analysed by analytical HPLC (Agilent HP1100), fitted with an Agilent 1100 variable wavelength UV detector. All samples were injected into the HPLC and were run in a system using gradient of solution A (0.1% trifluoroacetic acid (TFA) in water) to solution B (0.1% TFA in acetonitrile), using the method 5% B to 95% B in 20 min. BDNF was monitored by absorbance at 254 nm. All conditions were repeated in triplicate. The amount of released BDNF was quantified by integrating the area under the peak at the retention time of 8.2 min. The released BDNF from the hydrogels at each time point was determined by converting the relevant HPLC peak area to concentration, using a calibration curve (Fon et al., 2014b).

Nestin-CreER^{T2}:R26eYFP Transgenic Mice

In this study Nes-CreERT2 line 5.1: Rosa26-eYFP transgenic mice were used to track the migration of NSCs residing in the SVZ (Imayoshi et al., 2006, 2008; Xing et al., 2014). All animal experiments, approved by the ethics committee of the Florey Institute of Neuroscience (Parkville, VIC, Australia), were performed in accordance with the National Health and Medical Research Council guidelines. To induce recombination, tamoxifen (40 mg mL^{-1} in corn oil) was induced by oral gavage at a dosage of 300 mg/kg. Gavaging was repeated for 4 consecutive days (Xing et al., 2014).

Hydrogel Preparation

Hydrogels were formed in a sterile environment with UV sterilized peptide powder and sterile PBS and BDNF. Optimized peptide containing 10% RGD-peptide and 90% C14-peptide was dissolved in PBS to reach a concentration of 10 mg mL^{-1}. Optimisation was carried out using a cell attachment assay using SN4741 cells (**Figure S1**). The optimised hydrogel was characterised using and Anton Paar rheometer (**Figure S2**). For BDNF-loaded hydrogel, BDNF protein (0.0083 mg mL^{-1}) was also added to the hydrogel. With reference to mouse atlas (AP 1.1 mm), the hydrogel should be 2.3 mm long to be able to hit the SVZ. Since a 23 g needle with inner diameter of 0.337 mm was used, the required volume of hydrogel considering the density of hydrogel was calculated to be 2.4 μL. To ensure that the formed hydrogel is sufficient to cover the whole area from the SVZ to the cortex a final volume of 3 μL was used. Prior to implantation, 3 μL of hydrogel was loaded into a modified 23-gauge needle. The loaded hydrogels were implanted 5 min after loading to ensure stable hydrogel formation. To ensure that the needle tip did not cause additional injury to the brain, the needle

tip was cut and the needle was polished to yield a round and smooth edge.

Hydrogel Implantation

Implantation of hydrogel was performed 3 days after the final gavaging. Sixteen adult male transgenic mice (average age of 13 weeks) were divided into four mice per experimental condition. They were used to study the change of astrocyte and microglia in response to hydrogel implants/shame injections and also to investigate neuroblast migration along the hydrogel with and without loaded BDNF. Pre-anaesthesia injection was performed intraperitoneally using 0.1 mL atropine (Pfizer) and 0.2 mL xylazine (Troy Laboratories) in 0.7 mL saline (Baxter); 0.001 mL g^{-1} of mouse. Anaesthesia was then induced with the inhalation of 1% isoflurane followed by reducing to 0.5%, which was maintained during the surgery. In order to disrupt the SVZ, the hydrogel implantation was performed at 1.0 mm anterior of bregma, 2.0 mm laterally from the midline of the skull at an injection angle of 25 degrees, with the needle being tilted toward the midline in the coronal plane into the left hemisphere. A needle injury only (sham injection) was created following the same procedure as the hydrogel implantation method. The sham injection served as a control to investigate the cellular response following injury at the same coordinate into the right hemisphere of the animals.

To determine cellular responses, mice were culled 7 days and 35 days after the implantation with 0.1 mL Lethabarb (sodium pentobarbitone) in 0.9 mL saline; 0.006 mL g^{-1} of animal and perfused first with PBS (0.2 M) and then with 4% PFA (paraformaldehyde) in PBS. The brains were removed and fixed in 4% PFA for 2 h and then transferred to a 30% sucrose solution until the brains sank to the bottom of the tube. Brains were then frozen with dry ice and stored at −80°C. The brains were serially sectioned in the coronal plane using a cryostat (Leica) with a thickness of 30 μm (micron) and then the sections were air dried for 1 h prior to storage (Zhou et al., 2016). In total 60 sections were collected on 10 slides per each mouse to cover the whole thickness of implant.

Immunohistochemistry

Brain sections were fixed with 4% paraformaldehyde (Sigma-Aldrich) for 1 min at room temperature and then rinsed with PBS for 3 × 5 min. The brain sections were then permeabilised in 0.3% Triton-X100 for 5 min and washed in PBS for 3 × 5 min. The non-specific antibody binding was blocked with 10% NGS (Normal goat serum) (Vector Laboratories) including 1% BSA (Bovine serum albumin) (Sigma) and 0.2% Tween20 in PBS for 1 h at room temperature followed by a PBS wash. Brain sections were then stained with several antibodies: rabbit anti-Iba1 (1:250) (Wako Pure Chemical Industries) (microglia marker), rabbit anti-GFAP (1:1000) (Dako) (astrocyte marker), chicken anti-GFP (1:200) (Abcam), rabbit doublecortin (1:400) (Cell Signalling) (DCX; neuroblast and immature neurons marker), mouse anti-NeuN (1:100) (mature neuron marker) (Abcam), and rabbit anti-synapsin 1 (1:100) (Thermofisher) in 1% BSA in PBS at 4°C overnight. The sections were rinsed thoroughly with 0.2% Tween 20 in PBS on the following day (3 × 5 min) and incubated in anti-rabbit Alexa Flour 568 (1:1000), anti-chicken Alexa Flour 488 (1:000) or anti-mouse Alexa Flour 488 (1:000) (Thermo Fisher Scientific) in 0.05% Tween 20 in PBS at 37°C for 1 h. After thorough washing with 0.2% Tween 20 in PBS (2 × 5 min), the sections were counterstained with DAPI (1 μg/ml) (Thermo Fisher Scientific) for 5 min and after additional thorough washing (1 × 5 min) the slides were mounted by coverslip and prepared for fluorescent imaging using a Leica microscope. Images were captured with three fluorescence channels and were merged using ImageJ software (NIH). The boundaries of hydrogel and sham injection were estimated via the accumulation of cells using DAPI staining, due to high levels of brain tissue response to sham injuries and implants. This was revealed by high density of cells (e.g., microglia, astrocytes) with DAPI staining at these boundaries. For cell quantification, the whole length of the hydrogel from SVZ to the top of the brain was taken into consideration. Microglia cells per 10^4 μm were counted within the hydrogel and compared to the sham injection. The centre of the material tracts was estimated and 100 μm by 100 μm grids were put along the centre line on both sides for quantification (**Figures S4e,f**). Cells quantification occurred in the same position relative to the needle track in all animals. Astrocyte quantification was performed using the fluorescence intensity from the implant boundary outwards in comparison to a region of the brain away from the implant. The neuroblast migration distance was determined to investigate the ability of the hydrogel to re-direct the neuroblasts from the ventricles. Co-expression of GFP and GFAP was studied by using ImageJ software (NIH). Briefly, a stack image was created by composite GFP and GFAP channel images. A 5 μm wide straight line was drawn across cells of interest. An intensity plot was then generated by the region of interest to study the colocalisation of fluorescence intensity from different channels.

Statistical Analysis

Statistical analysis was performed on 9 sections for each cell type quantifications. Cell quantifications were expressed as mean ± standard deviation. Equal variances in different groups were confirmed by Levene's Median Test. The groups were then compared using one-way ANOVA with Tukey's *post hoc* testing (GraphPad Prism Version 6.01). $P < 0.05$ was used to determine statistical significance.

RESULTS AND DISCUSSION

β-Peptide Hydrogel Is Biocompatible in the Brain

The change of astrocyte and microglia level in response to the β-peptide hydrogel was assessed by quantifying the astrocyte and microglial responses. A 23 g stainless steel hypodermic needle was injected into the brain as a control to determine the cellular response to injury caused by the injection of the material with the same sized needle. The change of astrocyte and microglia level was examined at 7 d which corresponds to the time period of peak acute activation (Nisbet et al., 2009) and also at 35 d. Sham injection (needle injury) is commonly used as one of the

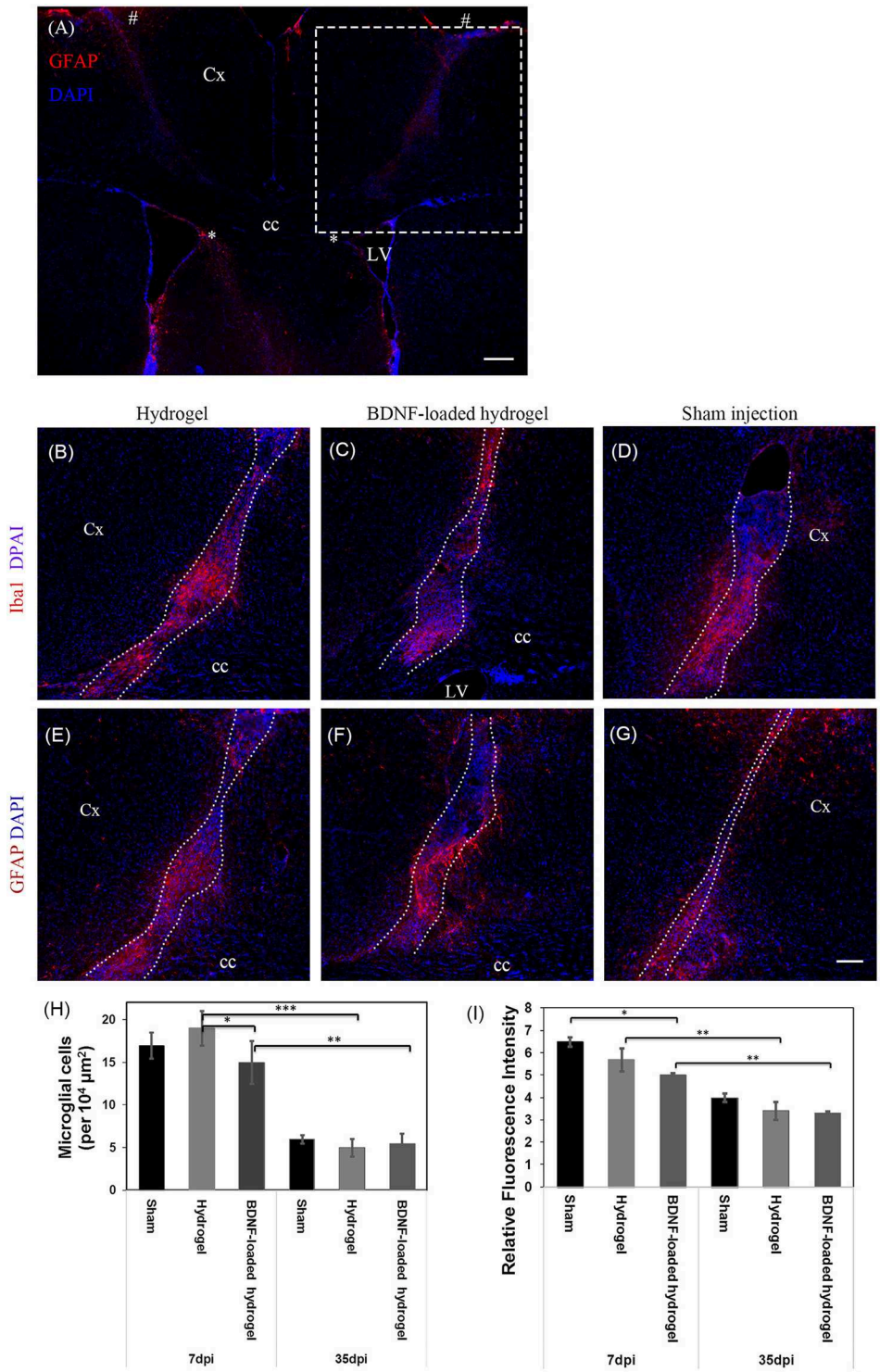

FIGURE 2 | Astrocyte and microglia response to implants and sham injections. **(A)** Low magnification image showing the full track of sham injection (left hemisphere) and hydrogel implantation (right hemisphere). * and # indicate the start and end point of the tract. The dash box indicates the imaging region for **(B–G)**. Dash box not shown in the symmetric left hemisphere. Iba1 positive microglial cells at 7 d, **(B)** Hydrogel; **(C)** BDNF-loaded hydrogel; **(D)** Sham injection; The sections were counter stained with DAPI (blue) to stain all cell nuclei. Astrocyte cells at 7 d, **(E)** hydrogel; **(F)** BDNF-loaded hydrogel; **(G)** sham injection; Cells were stained with GFAP (red) as astrocyte marker and DAPI (blue) for all cell nuclei. **(H)** Number of microglia per 10^4 μm^2 around the center of the injection site and infiltrated into the hydrogels. **(D,G)** have been rotated horizontally for comparison purposes. **(I)** Relative GFAP intensity to the uninjured part of the brain (*$P \leq 0.05$, **$P \leq 0.01$, and ***$P \leq 0.001$). Error bars represent standard deviation. Cx, cortex; cc, corpus callosum; LV, lateral ventrical. Scale bar = 200 μm for **(A)** and 100 μm for **(B–G)**. Dotted line indicates the boundary of hydrogel/sham injection tracks. $n = 4$ animals.

methods to study brain injury (Bjugstad et al., 2010; Nagamoto-Combs et al., 2010; Kishimoto et al., 2012; Rasouli et al., 2012; Xia et al., 2015). **Figure 2A** shows the location of the full tract of the sham injection (left hemisphere) and hydrogel implantation (right hemisphere). **Figures 2B–D** are representative images of the cellular response to injury for β-peptide and the sham

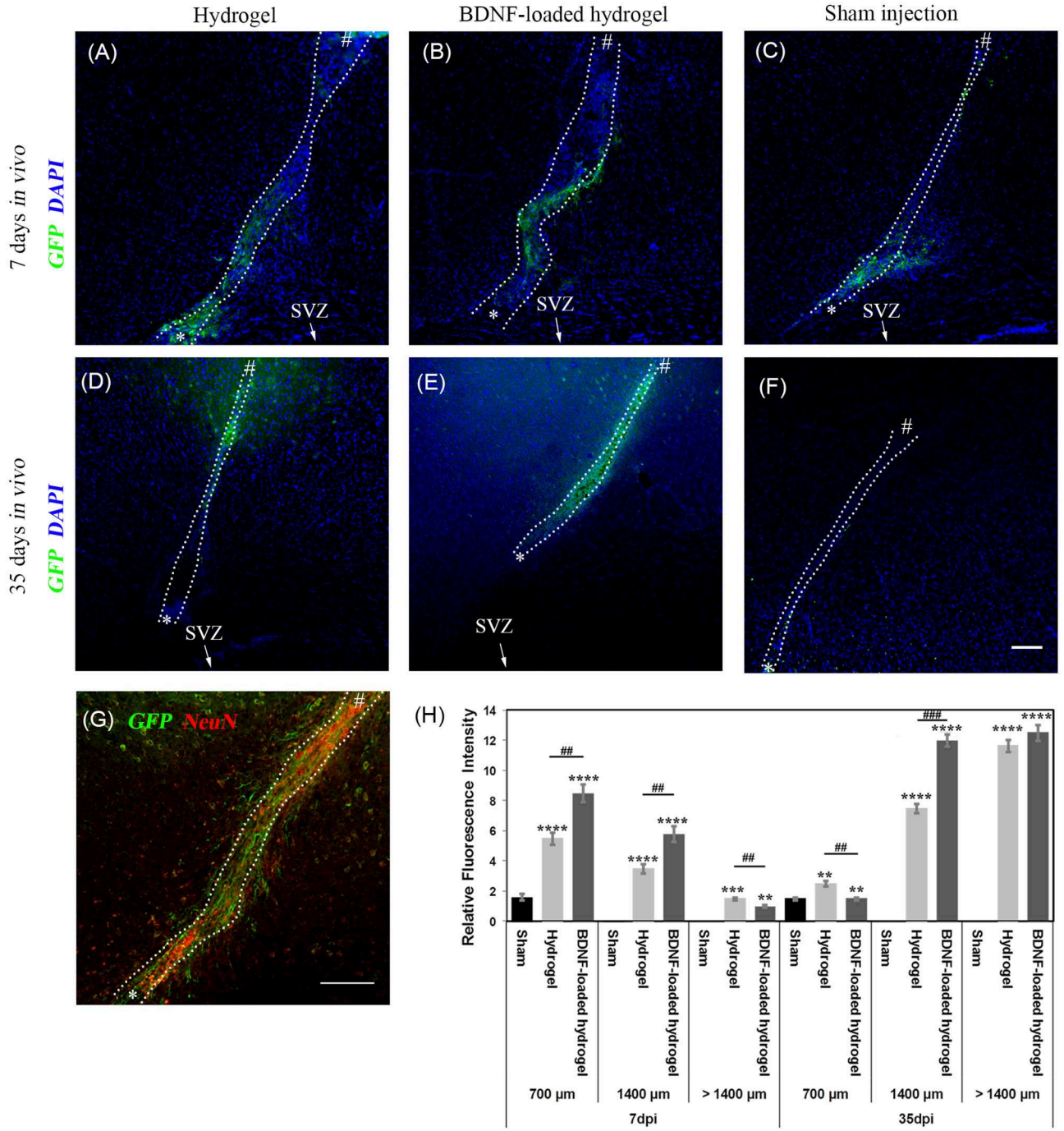

FIGURE 3 | Neuroblast migration within the cortex in response to injury. **(A)** hydrogel at 7 d; **(B)** BDNF-loaded hydrogel at 7 d; **(C)** sham injection at 7 d; **(D)** hydrogel at 35 d; **(E)** BDNF-loaded hydrogel at 35 d; **(F)** sham injection at 35 d; **(G)** high magnification image of neuroblasts at 35 d for the BDNF-loaded hydrogel. GFP positive (green) and DAPI stained nuclei (blue) are shown. Scale bar = 100 μm for A-F. "*" and "#" indicate the start and end points of hydrogel/sham injection tracks, respectively in **(A–G)**. **(H)** Relative GFP fluorescence intensity to the uninjured part of the brain for different distances from the SVZ. *indicate significant difference between sham and hydrogel with or without loaded BDNF groups. # indicate significant difference between hydrogel and BDNF-loaded hydrogel groups. $^{*}P \leq 0.05$, ** and $^{\#\#}P \leq 0.01$, *** and $^{\#\#\#}P \leq 0.001$, $^{****}P \leq 0.0001$. Error bars represent standard deviation. $n = 4$ animals. **(C,F)** were horizontally rotated for easy comparison. Dotted line indicates the boundary of hydrogel/sham injection tracks.

injection at 7 d. Microglia cells were observed within 150 μm of the boundary. The number of microglia around the injection and inside the β-peptide hydrogel was counted and the average number of cells per 10^4 μm presented in **Figure 2H.** There was a significant increase in microglia at the site of injury at 7 d, where the microglia cell number was almost similar for both the hydrogel and sham injection. Microglial response around the BDNF-loaded hydrogel was significantly lower than the response around the hydrogel and sham injection, which can be attributed to the anti-inflammatory properties of BDNF (Joosten and Houweling, 2004; Fon et al., 2014b), reducing the number of microglia. The number of microglia cells decreased dramatically from 7 to 35 d, most of which were accumulated inside the hydrogel (**Figures S4a,b**).

The number of astrocytes was determined by relative glial fibrillary acidic protein (GFAP) fluorescence intensity to the uninjured parts of the brain (**Figures 2E–G**). Astrogliosis was seen within 100 μm of the boundary of sham injection (injury)/implant at both 7 and 35 days which slightly decreased as a function of Htime and distance from the lesion (**Figure 2I**, **Figures S4c,d**). Astrocyte cell number within 100 μm of the centre of the lesion was similar for both sham injection and hydrogel. Astrocytes were present along the hydrogel tract, which increased as a function of time, similar to a previous study (Fon et al., 2014a), and there was no evidence of glial scar formation. From observation of the section, the incorporation of BDNF in the hydrogel appeared to reduce the numbers of actrocytes, with the number of astrocytes decreased as a function of distance from the centre of the lesion. An *in vitro* BDNF release study (**Figure S3**) showed that all the added BDNF was released by 5 days, however we expect this to be more rapid *in vivo* due to the higher surface area of the injected hydrogel tract. There was an increased number of astrocytes toward the centre the BDNF-loaded hydrogel tract which could ultimately play key roles for the survival and migration of neuroblasts (Theodosis et al., 2008).

Overall, the number of microglia and astrocyte found in this study suggest that the hydrogel is biocompatible and integrates well with the parenchyma. While the exogenous BDNF released from the hydrogel is expected to be rapidly released *in vivo*, it suppressed the tissue response and subsequently improving tissue-scaffold integration.

Neuroblasts Migrate Through the Entire Length of Implanted β-Peptide Hydrogel

NSCs that originate from the SVZ in Nes-CreER^{T2}:R26eYFP transgenic mice are permanently labelled as GFP+ve cells, regardless of the different developmental stages. Therefore, it is possible to identify the migrating cells and their progeny

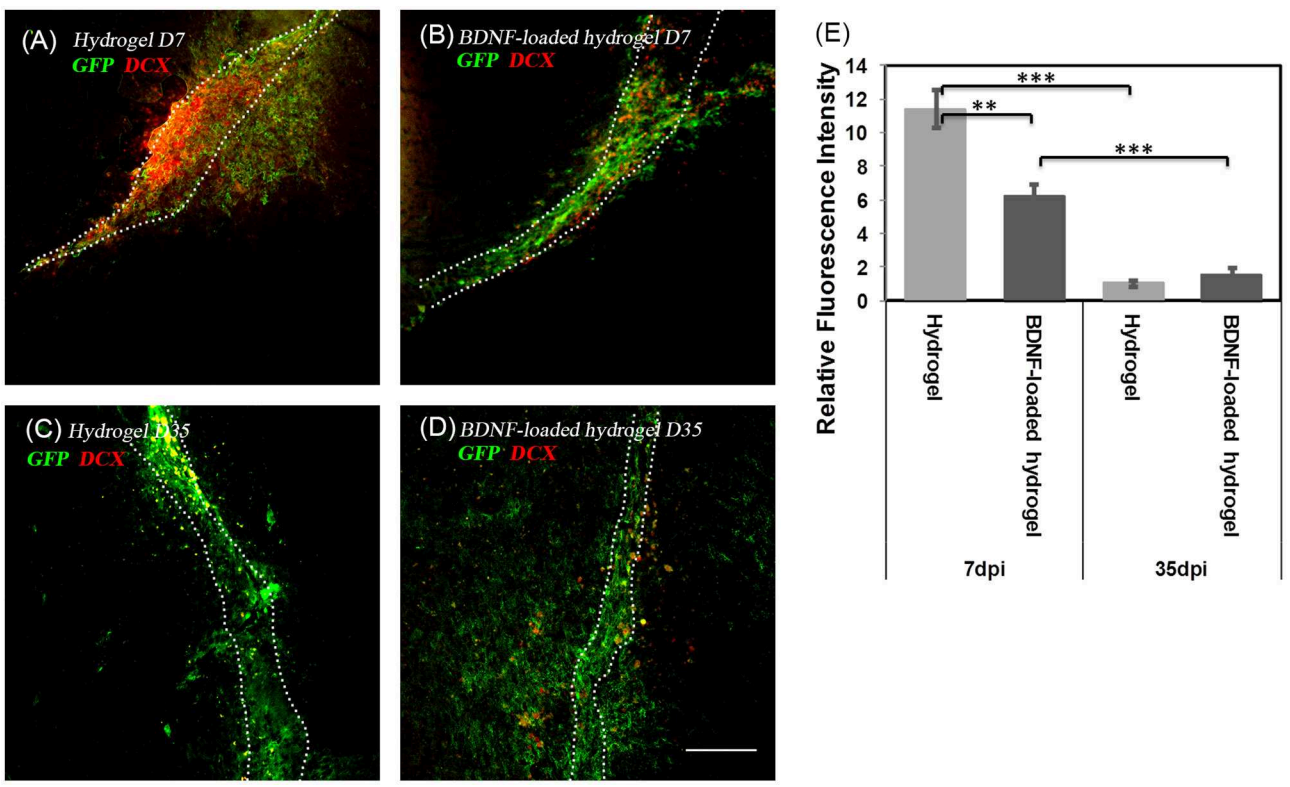

FIGURE 4 | The co-localization of GFP+ve cells and immature neuroblasts at two time points; **(A)** hydrogel at 7 d; **(B)** BDNF-loaded hydrogel at 7 d; **(C)** hydrogel at 35 d; **(D)** BDNF-loaded hydrogel at 35 d. Cells were stained with GFP (green) and DCX (red). Scale bar = 100 μm for all images. **(E)** Relative DCX intensity to the uninjured part of the brain (**$P \leq 0.01$ and ***$P \leq 0.001$). Error bars represent standard deviation. $n = 4$ animals. Dotted line indicates the boundary of hydrogel/sham injection tracks.

(Imayoshi et al., 2006; Xing et al., 2014; Kulkarni et al., 2016). GFP+ve cell migration was observed in response to injury at 7 d for all studied conditions, where the number of migrating cells and the distance of migration were significantly lower ($P \leq 0.01$) for the sham injection (**Figure 3**). GFP+ve cells migrated for a short distance from the SVZ around the lesion due to the injury caused by the sham injection (**Figure 3C**). In contrast, GFP+ve cells migrated away from the SVZ through the implanted β-peptide hydrogels and were quantified in terms of relative fluorescence intensity as a function of distance from the SVZ at 7 days and 35 days (**Figure 3H**).

GFP+ve cells were observed along the hydrogel tract. At 7 days, the number of migrating cells along both the hydrogel tracts decreased as a function of distance from the SVZ and the migration was confined along the hydrogel (**Figures 3A,B**). At 35 days, the migration was uniform (**Figure 3E**) with greater numbers of cells for the BDNF-loaded hydrogels (**Figure 3G**). This is reminiscent of neuroblast migration through the RMS (Ghashghaei et al., 2007). After 35 days, GFP+ve cells reached the end of the hydrogel tract at the cortex and migrated to the surrounding tissue, forming clusters. **Figure 3E** shows that the migration along the BDNF-loaded hydrogel was more abundant and cells migrated in greater numbers.

Neuroblasts Differentiate Into Neurons and Astrocytes

NSCs differentiate into various types of cells through their developmental stages. NSCs residing in the SVZ initially express GFAP. They then differentiate into migrating neuroblasts and can be detected as immature DCX+ve neuroblasts. At the end of the migration, they either differentiate into cells expressing GFAP, oligodendrocytes or mature into neurons, expressing the mature neuron marker, NeuN (Ming and Song, 2011; Faiz et al., 2015). In order to understand the stage of maturation of the GFP+ve cells along the β-peptide hydrogel, brain sections were stained with different markers at 7 and 35 d.

To investigate the fate of NSCs, DCX staining, a marker for migrating and immature neurons was performed. At 7 d, the majority of migrating cells along the hydrogel expressed DCX, showing that the GFP+ve cells are in their immature migrating state (**Figures 4A,B**). However, after 35 d, the population of DCX+ve cells significantly decreased (**Figures 4C–E**).

Most GFP+ve cells are co-localized with NeuN+ve cells (**Figures 5A,B**), indicating that the neuroblasts differentiated into neurons by 35 d. This co-localization is more abundant at the end of the hydrogel tract than the start (**Figures 5C,D**), where most of the GFP+ve cells are not stained with NeuN+ve, showing that they are most likely immature neurons or differentiated into astrocytes or oligodendrocytes. The migration stream was narrow for the hydrogel and most of the cells migrated toward the surrounding tissue at the end of their migration. From observation, large numbers of migrating cells remained along the BDNF-loaded hydrogel, suggesting that this matrix was more permissive for substantial neuroblast migration. Significantly, most of the newly generated neurons were Syn1 positive suggesting the formation of synapses (**Figure S5**).

While a number of previous studies have utilised matrices to promote neuroblast migration, the length of migration has been limited to the first quarter of the implant length (Fon et al., 2014a; Clark et al., 2016). Our previous work using injectable gelatin hydrogels was degraded quickly and was cleared after 3 weeks, and therefore was unable to promote neuroblast migration over longer periods. The number of neuroblasts around the gelatin matrix decreased from 7 to 21 d, while at the same time the number of neurons increased, which may be due to differentiation of migrated neuroblasts to neurons (Fon et al., 2014a). However, there was no conclusive evidence of this, because of the inability to conclusively map neuroblast progeny.

Migrating Neuroblasts Are Co-localised With Astrocytes

Astrocytes play a pivotal role in neuroblast migration through the RMS (Gengatharan et al., 2016). At the early postnatal stages, they are located at the border of the RMS, secreting VEGF to induce vasculature, which is required for neuroblast direction toward the olfactory bulb (Ma et al., 2009). Later on, their branches are elongated along blood vessels and in close proximity to migrating neuroblasts (Bovetti et al., 2007; Whitman et al., 2009), enveloping the migrating cells and blood vessels and forming a glial tube to isolate the neuroblast migration from the surrounding tissue (Snapyan et al., 2009).

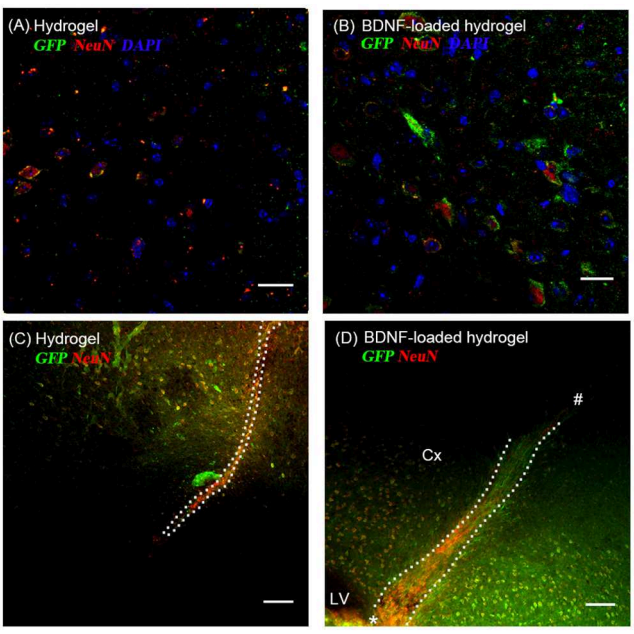

FIGURE 5 | The co-localization of GFP+ve cells originated from the SVZ and mature neurons at 35 d; **(A,C)** hydrogel; **(B,D)** BDNF-loaded hydrogel. Cells were stained with GFP (green), NeuN (red), and DAPI (blue). **(D)** "*" and "#" indicate the start and end point of hydrogel track, respectively. Scale bar for **(A,B)** = 25 μm. Scale bar for **(C,D)** = 100 μm. Dotted line indicates the boundary of hydrogel/sham injection tracks. Cx, cortex; LV, lateral ventrical. $n = 4$ animals.

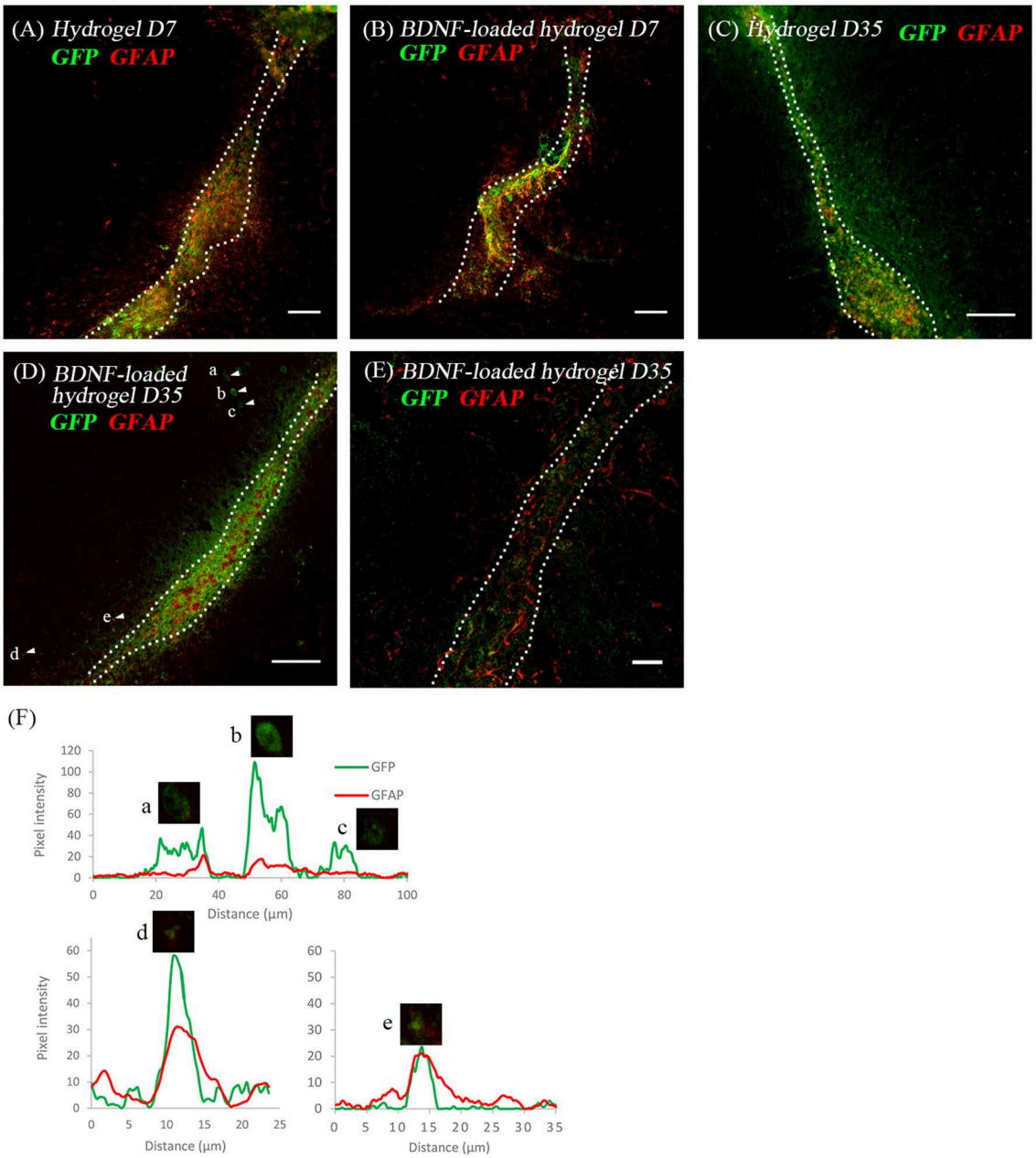

FIGURE 6 | The co-location of GFP+ve cells and astrocytes at two time points; **(A)** hydrogel at 7 d; **(B)** BDNF-loaded hydrogel at 7 d; **(C)** hydrogel at 35 d; **(D)** BDNF-loaded hydrogel at 35 d; **(E)** high magnification image showing the co-existence of GFP+ve cells with astrocytes. Scale bar = 20 μm. Cell were stained with GFP (green) and GFAP (red). Scale bar = 100 μm for **(A–D)**. **(F)** Fluorescence intensity map shows examples of cells that expressed GFP only (Cells a, b, and c) and those that co-expressed GFP and GFAP (Cells d and e). Intensity is presented as a function of moving through the cells (distance). Dotted line indicates the boundary of hydrogel/sham injection tracks. $n = 4$ animals.

They also release EGF, soluble melanoma inhibitory activity (MIA) protein and glutamate, which are crucial for neuroblasts to exit from the SVZ, neuroblast migration and survival of neuroblasts (Mason et al., 2001; Caldwell et al., 2004; Platel et al., 2010). In addition, astrocytes trap BDNF through high affinity tropomyosin receptor kinase B receptors, inducing the neuroblast stationary phase, thus regulating the migration process (Snapyan et al., 2009). Previous studies have shown astrocytes distribute at the scaffold boundary and use the scaffold orientation to assist the guidance of neurite extension (Deumens et al., 2004; Schnell et al., 2007; Yucel et al., 2010).

Considering the critical role of astrocytes in the RMS, we investigated the astrocyte-neuroblast co-location along the implanted β-peptide hydrogel tract. **Figures 6A,B** shows the

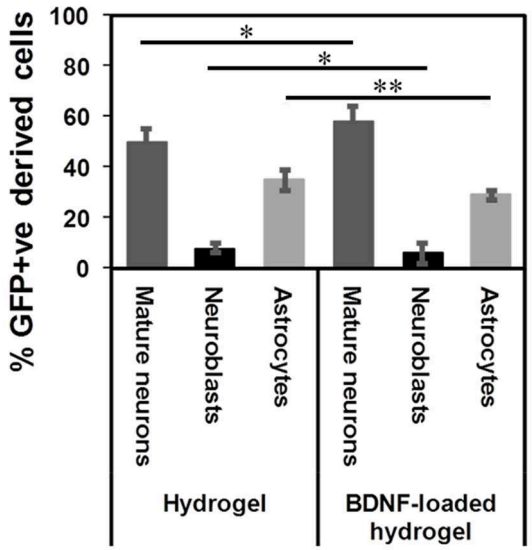

FIGURE 7 | GFP+ve cells differentiated into different cells at 35 d: mature neurons (dark grey), neuroblasts (black), and astrocytes (light grey) (*$P \leq 0.05$, **$P \leq 0.01$). $n = 4$ animals.

presence of astrocytes and GFP+ve cells along the hydrogel tract at 7 days. After 35 days some of the neuroblasts differentiated into astrocytes (**Figures 6C,D**). There is a mixture of GFP+ve cells co-localised with GFAP+ve cells (**Figures 6D,F**) and some GFP+ve cells in close proximity to the GFAP+ve cell processes (**Figure 6E**). After 35 days, a mixture of astrocytes including both GFP+ve astrocytes and local astrocytes were present along the hydrogel tract (**Figures 6C,D**). Astrocytes formed a pathway along the direction of the BDNF-loaded hydrogel tract, leading to a greater number of migratory cells (**Figure 3G**). At day 35, it was also evident that endogenous BDNF was localised along the hydrogel tract which would also act to facilitate migration of the neuroblasts (**Figure S6**).

Hydrogel Persisted in the Brain at 35 Days

β-peptides are proteolytically stable providing long-term support for cell migration and differentiation (Aguilar et al., 2007; Kulkarni et al., 2016; Motamed et al., 2016). In contrast, more commonly used self-assembling α-peptide hydrogels are degraded by 14 d (Fon et al., 2014a; Li et al., 2014). **Figure S7** shows that the β-peptide hydrogel remained intact in the brain. The tract contained numerous types of cells at 35 d. 50 ± 5% of GFP+ve cells differentiated into mature neurons along the hydrogel tract, while 8 ± 2% of cells still had a migrating DCX+ phenotype and 35 ± 4% had differentiated into astrocytes (**Figure 7**). Although the proportion of differentiation was independent of the presence of BDNF, the number of migrating cells and consequently the number of mature neurons were significantly higher for the BDNF-loaded hydrogel. This may be attributed to the initial effect of released BDNF in suppressing the tissue response.

CONCLUSIONS

Utilising *NestinCreER^{T2}:R26eYFP* transgenic mice for the indelible labelling of neuroblasts originating in the SVZ, the impact of a long-lasting β-peptide hydrogel on the migration of neuroblasts and their progenies in a healthy brain was determined. After 7 days, the number of migrating neuroblasts along the hydrogel tract decreased as a function of distance from the SVZ and the migration was confined along the hydrogel tract. The addition of exogenous BDNF did not affect the number of migrating neuroblasts along the hydrogel tract. However, exogenous BDNF attenuated the tissue response and the neuroblasts migrated in a more uniform pattern. After 35 days neuroblasts migrated along the hydrogel tract for some distance and then left the hydrogel tract. However, in the BDNF-loaded hydrogel, the neuroblasts tended to remain along the hydrogel tract. Fate mapping showed that the neuroblasts differentiated into Syn1-positive neurons and astrocytes.

DATA AVAILABILITY STATEMENT

The raw data supporting the conclusions of this manuscript will be made available by the authors, without undue reservation, to any qualified researcher.

ETHICS STATEMENT

All animal experiments, approved by the ethics committee of the Florey Institute of Neuroscience (Parkville, VIC, Australia), were performed in accordance with the National Health and Medical Research Council guidelines.

AUTHOR CONTRIBUTIONS

JF, DF, M-IA, MD, PC, and TM conceptualised the ideas. SM, MD, KK, and KZ performed the experiments. SM wrote the first draft of the manuscript. All authors provided revisions, designed the experiments, and analysed the data.

FUNDING

The Florey Institute of Neuroscience and Mental Health acknowledge the strong support from the Victorian Government and in particular funding from the Operational Infrastructure Support Grant. We gratefully acknowledge the support of the Melbourne Neuroscience Institute Interdisciplinary Seed Funding Scheme and National Health and Medical Research Council Project Grant (APP1156744 to PC, JF, M-IA, and DF). PC and TM are recipients of Australian Research Council Future Fellowships, FT110100218 and FT150100207, respectively.

SUPPLEMENTARY MATERIAL

The Supplementary Material for this article can be found online at: https://www.frontiersin.org/articles/10.3389/fbioe.2019.00315/full#supplementary-material

REFERENCES

Aguilar, M.-I., Purcell, A. W., Devi, R., Lew, R., Rossjohn, J., Smith, A. I., et al. (2007). β-Amino acid-containing hybrid peptides—new opportunities in peptidomimetics. *Org. Biomol. Chem.* 5, 2884–2890. doi: 10.1039/b708507a

Alvarez-Buylla, A., and Lim, D. A. (2004). For the long run. *Neuron* 41, 683–686. doi: 10.1016/S0896-6273(04)00111-4

Bjugstad, K. B., Lampe, K., Kern, D. S., and Mahoney, M. (2010). Biocompatibility of poly(ethylene glycol)-based hydrogels in the brain: an analysis of the glial response across space and time. *J. Biomed. Mater. Res. Part A* 95A, 79–91. doi: 10.1002/jbm.a.32809

Bovetti, S., Hsieh, Y.-C., Bovolin, P., Perroteau, I., Kazunori, T., and Puche, A. C. (2007). Blood vessels form a scaffold for neuroblast migration in the adult olfactory bulb. *J. Neurosci.* 27, 5976–5980. doi: 10.1523/JNEUROSCI.0678-07.2007

Bozoyan, L., Khlghatyan, J., and Saghatelyan, A. (2012). Astrocytes control the development of the migration-promoting vasculature scaffold in the postnatal brain via VEGF signaling. *J. Neurosci.* 32, 1687–1704. doi: 10.1523/JNEUROSCI.5531-11.2012

Caldwell, M. A., Garcion, E., terBorg, M. G., He, X., and Svendsen, C. N. (2004). Heparin stabilizes FGF-2 and modulates striatal precursor cell behavior in response to EGF. *Exp. Neurol.* 188, 408–420. doi: 10.1016/j.expneurol.2004.05.007

Chiaramello, S., Dalmasso, G., Bezin, L., Marcel, D., Jourdan, F., Peretto, P., et al. (2007). BDNF/ TrkB interaction regulates migration of SVZ precursor cells via PI3-K and MAP-K signalling pathways. *Eur. J. Neurosci.* 26, 1780–1790. doi: 10.1111/j.1460-9568.2007.05818.x

Clark, A. R., Carter, A. B., Hager, L. E., and Price, E. M. (2016). *In vivo* neural tissue engineering: cylindrical biocompatible hydrogels that create new neural tracts in the adult mammalian brain. *Stem Cells Dev.* 25, 1109–1118. doi: 10.1089/scd.2016.0069

Del Borgo, M. P., Mechler, A. I., Traore, D., Forsyth, C., Wilce, J. A., Wilce, M. C. J., et al. (2013). Supramolecular self-assembly of N-Acetyl-Capped β-peptides leads to nano- to macroscale fiber formation. *Angew. Chem. Int. Edn.* 52, 8266–8270. doi: 10.1002/anie.201303175

Deumens, R., Koopmans, G. C., den Bakker, C. G. J., Maquet, V., Blacher, S., Honig, W. M. M., et al. (2004). Alignment of glial cells stimulates directional neurite growth of CNS neurons *in vitro*. *Neuroscience* 125, 591–604. doi: 10.1016/j.neuroscience.2004.02.010

Doetsch, F., Caillé, I., Lim, D. A., García-Verdugo, J. M., and Alvarez-Buylla, A. (1999). Subventricular zone astrocytes are neural stem cells in the adult mammalian brain. *Cell* 97, 703–716. doi: 10.1016/S0092-8674(00)80783-7

Eltzschig, H. K., and Eckle, T. (2011). Ischemia and reperfusion—from mechanism to translation. *Nat. Med.* 17, 1391–401. doi: 10.1038/nm.2507

Faiz, M., Sachewsky, N., Gascon, S., Bang, K. W. A., Morshead, C. M., and Nagy, A. (2015). Adult neural stem cells from the subventricular zone give rise to reactive astrocytes in the cortex after stroke. *Cell Stem Cell* 17, 624–634. doi: 10.1016/j.stem.2015.08.002

Fitch, M. T., and Silver, J. (2008). CNS injury, glial scars, and inflammation: inhibitory extracellular matrices and regeneration failure. *Exp. Neurol.* 209, 294–301. doi: 10.1016/j.expneurol.2007.05.014

Fon, D., Al-Abboodi, A., Chan, P. P. Y., Zhou, K., Crack, P., Finkelstein, D. I., et al. (2014a). Effects of GDNF-loaded injectable gelatin-based hydrogels on endogenous neural progenitor cell migration. *Adv. Healthcare Mater.* 3, 761–774. doi: 10.1002/adhm.201300287

Fon, D., Zhou, K., Ercole, F., Fehr, F., Marchesan, S., Minter, M. R., et al. (2014b). Nanofibrous scaffolds releasing a small molecule BDNF-mimetic for the re-direction of endogenous neuroblast migration in the brain. *Biomaterials* 35, 2692–2712. doi: 10.1016/j.biomaterials.2013.12.016

Fujioka, T., Kaneko, N., Ajioka, I., Nakaguchi, K., Omata, T., Ohba, H., et al. (2017). β1 integrin signaling promotes neuronal migration along vascular scaffolds in the post-stroke brain. *EBioMedicine* 16, 195–203. doi: 10.1016/j.ebiom.2017.01.005

Gengatharan, A., Bammann, R. R., and Saghatelyan, A. (2016). The role of astrocytes in the generation, migration, and integration of new neurons in the adult olfactory bulb. *Front. Neurosci.* 10:149. doi: 10.3389/fnins.2016.00149

Ghashghaei, H. T., Lai, C., and Anton, E. S. (2007). Neuronal migration in the adult brain: are we there yet? *Nat. Rev. Neurosci.* 8, 141–151. doi: 10.1038/nrn2074

Grade, S., Weng, Y. C., Snapyan, M., Kriz, J., Malva, J. O., and Saghatelyan, A. (2013). Brain-derived neurotrophic factor promotes vasculature-associated migration of neuronal precursors toward the ischemic striatum. *PLoS ONE* 8:e55039. doi: 10.1371/journal.pone.0055039

Hernández-Ortega, K., Quiroz-Baez, R., and Arias, C. (2011). Cell cycle reactivation in mature neurons: a link with brain plasticity, neuronal injury and neurodegenerative diseases? *Neurosci. Bull.* 27, 185–196. doi: 10.1007/s12264-011-1002-z

Hook, D. F., Gessier, F., Noti, C., Kast, P., and Seebach, D. (2004). Probing the proteolytic stability of β-peptides containing α-fluoro- and α-hydroxy-β-amino acids. *ChemBioChem* 5, 691–706. doi: 10.1002/cbic.200300827

Hurtado-Chong, A., Yusta-Boyo, M. J., Vergaño-Vera, E., Bulfone, A., De Pablo, F., and Vicario-Abejón, C. (2009). IGF-I promotes neuronal migration and positioning in the olfactory bulb and the exit of neuroblasts from the subventricular zone. *Eur. J. Neurosci.* 30, 742–755. doi: 10.1111/j.1460-9568.2009.06870.x

Hwang, D.-Y., Kim, D.-S., and Kim, D.-W. (2010). Human ES and iPS cells as cell sources for the treatment of Parkinson's disease: current state and problems. *J. Cell. Biochem.* 109, 292–301. doi: 10.1002/jcb.22411

Hyder, A. A., Wunderlich, C. A., Puvanachandra, P., Gururaj, G., and Kobusingye, O. C. (2007). The impact of traumatic brain injuries: a global perspective. *NeuroRehabilitation* 22, 341–353.

Imayoshi, I., Ohtsuka, T., Metzger, D., Chambon, P., and Kageyama, R. (2006). Temporal regulation of Cre recombinase activity in neural stem cells. *Genesis* 44, 233–238. doi: 10.1002/dvg.20212

Imayoshi, I., Sakamoto, M., Ohtsuka, T., Takao, K., Miyakawa, T., Yamaguchi, M., et al. (2008). Roles of continuous neurogenesis in the structural and functional integrity of the adult forebrain. *Nat. Neurosci.* 11, 1153–1161. doi: 10.1038/nn.2185

Jinnou, H., Sawada, M., Kawase, K., Kaneko, N., Herranz-Pérez, V., Miyamoto, T., et al. (2018). Radial glial fibers promote neuronal migration and functional recovery after neonatal brain injury. *Cell Stem Cell* 22, 128–137.e129. doi: 10.1016/j.stem.2017.11.005

Joosten, E. A. J., and Houweling, D. A. (2004). Local acute application of BDNF in the lesioned spinal cord anti-inflammatory and anti-oxidant effects. *NeuroReport* 15, 1163–1166. doi: 10.1097/00001756-200405190-00016

Kang, X., Xu, H., Teng, S., Zhang, X., Deng, Z., Zhou, L., et al. (2014). Dopamine release from transplanted neural stem cells in Parkinsonian rat striatum *in vivo*. *Proc. Natl. Acad. Sci. U.S.A.* 111, 15804–15809. doi: 10.1073/pnas.1408484111

Kernie, S. G., and Parent, J. M. (2010). Forebrain neurogenesis after focal Ischemic and traumatic brain injury. *Neurobiol. Dis.* 37, 267–274. doi: 10.1016/j.nbd.2009.11.002

Kishimoto, N., Shimizu, K., and Sawamoto, K. (2012). Neuronal regeneration in a zebrafish model of adult brain injury. *Dis. Models Mech.* 5, 200–209. doi: 10.1242/dmm.007336

Kondziolka, D., Wechsler, L., Goldstein, S., Meltzer, C., Thulborn, K. R., Gebel, J., et al. (2000). Transplantation of cultured human neuronal cells for patients with stroke. *Neurology* 55, 565–569. doi: 10.1212/WNL.55.4.565

Kulkarni, K., Motamed, S., Habila, N., Perlmutter, P., Forsythe, J. S., Aguilar, M.-I., et al. (2016). Orthogonal strategy for the synthesis of dual-functionalised β3-peptide based hydrogels. *Chem. Commun.* 52, 5844–5847. doi: 10.1039/C6CC00624H

Lalli, G. (2014). "Extracellular signals controlling neuroblast migration in the postnatal brain," in *Cellular and Molecular Control of Neuronal Migration,* eds. L. Nguyen and S. Hippenmeyer (Dordrecht: Springer Netherlands), 149–180. doi: 10.1007/978-94-007-7687-6_9

Li, A., Hokugo, A., Yalom, A., Berns, E. J., Stephanopoulos, N., McClendon, M. T., et al. (2014). A bioengineered peripheral nerve construct using aligned peptide amphiphile nanofibers. *Biomaterials* 35, 8780–8790. doi: 10.1016/j.biomaterials.2014.06.049

Li, J.-Y., Christophersen, N. S., Hall, V., Soulet, D., and Brundin, P. (2008). Critical issues of clinical human embryonic stem cell therapy for brain repair. *Trends Neurosci.* 31, 146–153. doi: 10.1016/j.tins.2007.12.001

Lindvall, O., Kokaia, Z., and Martinez-Serrano, A. (2004). Stem cell therapy for human neurodegenerative disorders–how to make it work. *Nat. Med.* 10, S42–S50. doi: 10.1038/nm1064

Ma, D. K., Bonaguidi, M. A., Ming, G. L., and Song, H. (2009). Adult neural stem cells in the mammalian central nervous system. *Cell Res.* 19, 672–82. doi: 10.1038/cr.2009.56

Mason, H. A., Ito, S., and Corfas, G. (2001). Extracellular signals that regulate the tangential migration of olfactory bulb neuronal precursors: inducers, inhibitors, and repellents. *J. Neurosci.* 21, 7654–7663. doi: 10.1523/JNEUROSCI.21-19-07654.2001

Master, Z., McLeod, M., and Mendez, I. (2007). Benefits, risks and ethical considerations in translation of stem cell research to clinical applications in Parkinson's disease. *J. Med. Ethics* 33, 169–173. doi: 10.1136/jme.2005.013169

Miller, J. T., Bartley, J. H., Wimborne, H. J., Walker, A. L., Hess, D. C., Hill, W. D., et al. (2005). The neuroblast and angioblast chemotaxic factor SDF-1 (CXCL12) expression is briefly up regulated by reactive astrocytes in brain following neonatal hypoxic-ischemic injury. *BMC Neurosci.* 6:63. doi: 10.1186/1471-2202-6-63

Ming, G.-,l., and Song, H. (2011). Adult neurogenesis in the mammalian brain: significant answers and significant questions. *Neuron* 70, 687–702. doi: 10.1016/j.neuron.2011.05.001

Motamed, S., Del Borgo, M. P., Kulkarni, K., Habila, N., Zhou, K., Perlmutter, P., et al. (2016). A self-assembling β-peptide hydrogel for neural tissue engineering. *Soft Matter* 12, 2243–2246. doi: 10.1039/C5SM02902C

Nagamoto-Combs, K., Morecraft, R. J., Darling, W. G., and Combs, C. K. (2010). Long-term gliosis and molecular changes in the cervical spinal cord of the rhesus monkey after traumatic brain injury. *J. Neurotrauma* 27, 565–585. doi: 10.1089/neu.2009.0966

Nisbet, D. R., Rodda, A. E., Horne, M. K., Forsythe, J. S., and Finkelstein, D. I. (2009). Neurite infiltration and cellular response to electrospun polycaprolactone scaffolds implanted into the brain. *Biomaterials* 30, 4573–4580. doi: 10.1016/j.biomaterials.2009.05.011

Orive, G., Anitua, E., Pedraz, J. L., and Emerich, D. F. (2009). Biomaterials for promoting brain protection, repair and regeneration. *Nat. Rev. Neuroscience* 10, 682–692. doi: 10.1038/nrn2685

Pettikiriarachchi, J. T. S., Parish, C. L., Shoichet, M. S., Forsythe, J. S., and Nisbet, D. R. (2010). Biomaterials for brain tissue engineering. *Austr. J. Chem.* 63, 1143–1154. doi: 10.1071/CH10159

Platel, J.-C., Dave, K. A., Gordon, V., Lacar, B., Rubio, M. E., and Bordey, A. (2010). NMDA receptors activated by subventricular zone astrocytic glutamate are critical for neuroblast survival prior to entering a synaptic network. *Neuron* 65, 859–872. doi: 10.1016/j.neuron.2010.03.009

Rasouli, J., Lekhraj, R., White, N. M., Flamm, E. S., Pilla, A. A., Strauch, B., et al. (2012). Attenuation of interleukin-1beta by pulsed electromagnetic fields after traumatic brain injury. *Neurosci. Lett.* 519, 4–8. doi: 10.1016/j.neulet.2012.03.089

Rennert, R. C., Sorkin, M., Garg, R. K., and Gurtner, G. C. (2012). Stem cell recruitment after injury: lessons for regenerative medicine. *Regen. Med.* 7, 833–850. doi: 10.2217/rme.12.82

Saha, B., Jaber, M., and Gaillard, A. (2012). Potentials of endogenous neural stem cells in cortical repair. *Front. Cell. Neurosci.* 6, 14–14. doi: 10.3389/fncel.2012.00014

Schnell, E., Klinkhammer, K., Balzer, S., Brook, G., Klee, D., Dalton, P., et al. (2007). Guidance of glial cell migration and axonal growth on electrospun nanofibers of poly-ε-caprolactone and a collagen/poly-ε-caprolactone blend. *Biomaterials* 28, 3012–3025. doi: 10.1016/j.biomaterials.2007.03.009

Snapyan, M., Lemasson, M., Brill, M. S., Blais, M., Massouh, M., Ninkovic, J., et al. (2009). Vasculature guides migrating neuronal precursors in the adult mammalian forebrain via brain-derived neurotrophic factor signaling. *J. Neurosci.* 29, 4172–4188. doi: 10.1523/JNEUROSCI.4956-08.2009

Song, X.-Y., Li, F., Zhang, F.-H., Zhong, J.-H., and Zhou, X.-F. (2008). Peripherally-derived BDNF promotes regeneration of ascending sensory neurons after spinal cord injury. *PLoS ONE* 3:e1707. doi: 10.1371/journal.pone.0001707

Theodosis, D. T., Poulain, D. A., and Oliet, S. H. R. (2008). Activity-dependent structural and functional plasticity of astrocyte-neuron interactions. *Physiol. Rev.* 88, 983–1008. doi: 10.1152/physrev.00036.2007

Wang, T.-Y., Forsythe, J. S., Nisbet, D. R., and Parish, C. L. (2012). Promoting engraftment of transplanted neural stem cells/progenitors using biofunctionalised electrospun scaffolds. *Biomaterials* 33, 9188–9197. doi: 10.1016/j.biomaterials.2012.09.013

Whitman, M. C., Fan, W., Rela, L., Rodriguez-Gil, D. J., and Greer, C. A. (2009). Blood vessels form a migratory scaffold in the rostral migratory stream. *J. Comp. Neurol.* 516, 94–104. doi: 10.1002/cne.22093

Whitman, M. C., and Greer, C. A. (2009). Adult neurogenesis and the olfactory system. *Prog. Neurobiol.* 89, 162–175. doi: 10.1016/j.pneurobio.2009.07.003

Winner, B., Couillard-Despres, S., Geyer, M., Aigner, R., Bogdahn, U., Aigner, L., et al. (2008). Dopaminergic lesion enhances growth factor-induced striatal neuroblast migration. *J. Neuropathol. Exp. Neurol.* 67, 105–116. doi: 10.1097/nen.0b013e3181630cff

Xia, Y., Kong, L., Yao, Y., Jiao, Y., Song, J., Tao, Z., et al. (2015). Osthole confers neuroprotection against cortical stab wound injury and attenuates secondary brain injury. *J. Neuroinflammation* 12:155. doi: 10.1186/s12974-015-0373-x

Xing, Y. L., Röth, P. T., Stratton, J. A. S., Chuang, B. H. A., Danne, J., Ellis, S. L., et al. (2014). Adult neural precursor cells from the subventricular zone contribute significantly to oligodendrocyte regeneration and remyelination. *J. Neurosci.* 34, 14128–14146. doi: 10.1523/JNEUROSCI.3491-13.2014

Yasuda, H., Kuroda, S., Shichinohe, H., Kamei, S., Kawamura, R., and Iwasaki, Y. (2010). Effect of biodegradable fibrin scaffold on survival, migration, and differentiation of transplanted bone marrow stromal cells after cortical injury in rats. *J. Neurosurg.* 112, 336–344. doi: 10.3171/2009.2.JNS08495

Yucel, D., Kose, G. T., and Hasirci, V. (2010). Tissue engineered, guided nerve tube consisting of aligned neural stem cells and astrocytes. *Biomacromolecules* 11, 3584–3591. doi: 10.1021/bm1010323

Zhou, K., Motamed, S., Thouas, G. A., Bernard, C. C., Li, D., Parkington, H. C., et al. (2016). Graphene functionalized scaffolds reduce the inflammatory response and supports endogenous neuroblast migration when implanted in the adult brain. *PLoS ONE* 11:e0151589. doi: 10.1371/journal.pone.0151589

Zhou, Y., Oudin, M. J., Gajendra, S., Sonego, M., Falenta, K., Williams, G., et al. (2015). Regional effects of endocannabinoid, BDNF and FGF receptor signalling on neuroblast motility and guidance along the rostral migratory stream. *Mol. Cell. Neurosci.* 64, 32–43. doi: 10.1016/j.mcn.2014.12.001

Conflict of Interest: The authors declare that the research was conducted in the absence of any commercial or financial relationships that could be construed as a potential conflict of interest.

frontiers in Bioengineering and Biotechnology

REVIEW
published: 15 November 2019
doi: 10.3389/fbioe.2019.00317

Biomaterials and Scaffold Design Strategies for Regenerative Endodontic Therapy

Gavin Raddall[1], *Isabel Mello*[2] *and Brendan M. Leung*[3,4]*

[1] Faculty of Dentistry, Dalhousie University, Halifax, NS, Canada, [2] Department of Dental Clinical Sciences, Faculty of Dentistry, Dalhousie University, Halifax, NS, Canada, [3] Department of Applied Oral Sciences, Faculty of Dentistry, Dalhousie University, Halifax, NS, Canada, [4] School of Biomedical Engineering, Faculties of Medicine and Engineering, Dalhousie University, Halifax, NS, Canada

Challenges with traditional endodontic treatment for immature permanent teeth exhibiting pulp necrosis have prompted interest in tissue engineering approaches to regenerate the pulp-dentin complex and allow root development to continue. These procedures are known as regenerative endodontic therapies. A fundamental component of the regenerative endodontic process is the presence of a scaffold for stem cells from the apical papilla to adhere to, multiply and differentiate. The aim of this review is to provide an overview of the biomaterial scaffolds that have been investigated to support stem cells from the apical papilla in regenerative endodontic therapy and to identify potential biomaterials for future research. An electronic search was conducted using Pubmed and Novanet databases for published studies on biomaterial scaffolds for regenerative endodontic therapies, as well as promising biomaterial candidates for future research. Using keywords "regenerative endodontics," "scaffold," "stem cells" and "apical papilla," 203 articles were identified after duplicate articles were removed. A second search using "dental pulp stem cells" instead of "apical papilla" yielded 244 articles. Inclusion criteria included the use of stem cells from the apical papilla or dental pulp stem cells in combination with a biomaterial scaffold; articles using other dental stem cells or no scaffolds were excluded. The investigated scaffolds were organized in host-derived, naturally-derived and synthetic material categories. It was found that the biomaterial scaffolds investigated to date possess both desirable characteristics and issues that limit their clinical applications. Future research investigating the scaffolds presented in this article may, ultimately, point to a protocol for a consistent, clinically-successful regenerative endodontic therapy.

Keywords: biomaterials, bone, regenerative medicine, instructive scaffolds, endodontic therapy, stem cells, clinical considerations, blood-biomaterials interactions

OPEN ACCESS

Edited by:
Hasan Uludag,
University of Alberta, Canada

Reviewed by:
Sahng Kim,
Columbia University, United States
Lauren Flynn,
University of Western Ontario, Canada
Xin Xu,
Sichuan University, China

***Correspondence:**
Brendan M. Leung
bleung@dal.ca

Specialty section:
This article was submitted to Biomaterials, a section of the journal Frontiers in Bioengineering and Biotechnology

Received: *16 July 2019*
Accepted: *25 October 2019*
Published: *15 November 2019*

Citation:
Raddall G, Mello I and Leung BM (2019) Biomaterials and Scaffold Design Strategies for Regenerative Endodontic Therapy. Front. Bioeng. Biotechnol. 7:317. doi: 10.3389/fbioe.2019.00317

INTRODUCTION

Traditional Root Canal Treatment in the Context of Regenerative Endodontic Therapy

Major challenges are associated with current endodontic treatment of permanent teeth with pulpal necrosis and immature root development, found primarily in children and adolescent patients. Developing roots have open apices and thin dentinal walls resulting in fragility, which complicate the use of mechanical means to disinfect the root canal system (Friedlander et al., 2009; Lovelace et al., 2011). Consequently, endodontic therapies involving these teeth often rely on

irrigation and intracanal medications to disinfect the canal space. Immature teeth that require endodontic treatment have been traditionally treated with long-term calcium hydroxide ($Ca(OH)_2$). After initial disinfection of the pulp space, a calcium hydroxide paste is left in the canal to induce the deposition of a hard tissue barrier at the apical area. This barrier helps contain the filling materials in the canal without great risk of extravasation to the periapical tissues. This can be a lengthy process as it may take several months for the tissue barrier to form (Raldi et al., 2009). Alternatively, a more novel approach is the use of calcium silicate-based cements (MTA-like cements) to form an artificial apical plug with clinical outcomes superior to induced apexification by $Ca(OH)_2$.

Both apexification techniques form a barrier on which permanent root canal filling material can be compacted against and promote healing of apical tissues. Apexification procedures do not promote further root development and the tooth will continue to have thin, fragile root canal walls that makes these teeth susceptible to cervical fracture from normal mastication forces or trauma (Wilkinson et al., 2007; Cotti et al., 2008). A clinical study conducted by Cvek (1992) demonstrated that the incidence of cervical root fracture ranged from 28 to 77% in immature teeth that had been treated with $Ca(OH)_2$; teeth in earlier stages of development occupied the highest percentiles and were significantly more likely to fracture than mature teeth. Consequently, an alternative treatment protocol that can potentially reinforce the root and strengthen the root against fracture would help preserve the integrity of the afflicted tooth and maintain desirable function for patients.

Regenerative endodontic therapy (RET) employs principles of bioengineering and is a contemporary alternative to conventional apexification procedures (**Figure 1**). It consists of irrigating the root canal space with low-concentration sodium hypochlorite (NaOCl) to dissolve necrotic tissue and disinfect the canal space, followed by the placement of $Ca(OH)_2$ or an antibiotic mixture in the canal at the conclusion of the first appointment to further disinfect the dentinal tissue and protect the tooth from reinfection (Lee et al., 2015). In a subsequent appointment, the $Ca(OH)_2$ or antibiotic mixture is removed, and a hand file is extended approximately 3 mm beyond the apical foramen to induce bleeding (Lee et al., 2015). Real-time reverse transcription polymerase chain reaction (rtPCR) and histologic evaluation of intracanal blood samples by Lovelace et al. demonstrated that mesenchymal stem cells (MSCs) are delivered to the root canal space after the induction of bleeding based on the expression of MSC markers CD105 and STRO-1; they speculated that these cells are ultimately responsible for deposition of both connective and hard tissues (Lovelace et al., 2011). After clot formation, a collagen matrix is placed at the cervical portion of the canal which is then sealed with MTA, followed by the placement of a bonded restoration (Lee et al., 2015). Over the ensuing 2 years, radiographic evidence is used to monitor root development along with a clinical examination (Lee et al., 2015). Although this is a viable, less complicated treatment alternative to traditional procedures, the outcomes of current revascularization strategies are often difficult to predict and an optimized protocol remains to be developed (Lee et al., 2015).

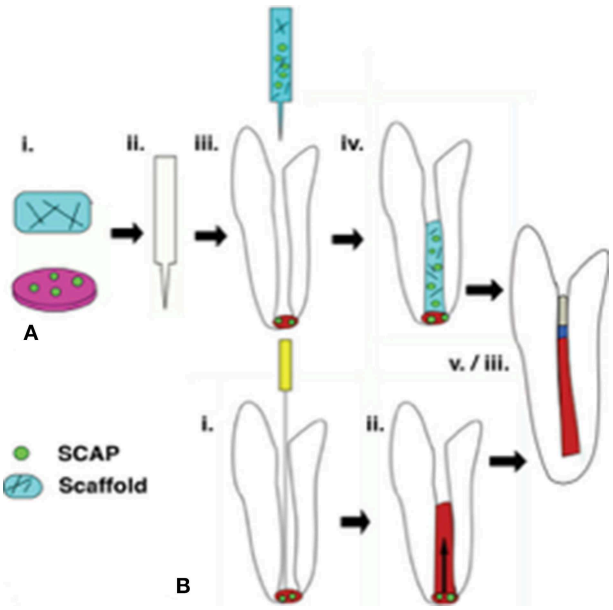

FIGURE 1 | Regenerative endodontic therapies employ SCAP in achieving revascularization of the root canal and continued root development. **(A)** Following conservative preparation of the root canal and disinfection, cultured SCAP maybe combined with an injectable scaffold and inserted into the canal space. **(B)** The current clinical standard for regenerative therapies involves over instrumentation with and endodontic file to induce blood flow from the apical region into the canal space, forming a blood clot. SCAP migrate into the root canal as a result of this process. In a successful retreatment pathway. **(A,B)** both lead to root lengthening and dentinal wall thickening, as well as pulpal revascularization beneath an MTA seal and restoration material.

Stem Cells From the Apical Papilla

Within the past decade, a population of postnatal mesenchymal stem cells from the apical papilla (SCAP) has been identified by Sonoyama et al. (2006) immediately adjacent to the root apex of immature teeth. Given the proximity of SCAP to the apical foramen, it has been suggested that these are the cells that enter the root canal space in current regenerative procedures (Lovelace et al., 2011). Importantly, the apical location of SCAP enables these cells to be supplied with collateral blood circulation, allowing them to survive during pulpal infection and necrosis (Huang et al., 2008). In both *in vitro* and *in vivo* analyses, it has been consistently observed that SCAP have the ability to differentiate into odontoblast-like cells that produce dentin in the root canal (Huang et al., 2009) While it has been determined that SCAP also have the capacity to undergo adipogenic and neurogenic differentiation *in vitro*, the same observations have not been made *in vivo* and it has been concluded that SCAP differentiate to only dentinogenic cells under *in vivo* conditions (Huang et al., 2009). Numerous biologically-active growth factors are trapped in the dentinal matrix during dentinogenesis, namely transforming growth factor-beta 1 (TGF- β1) and bone morphogenetic protein 2 (BMP-2), which are key in driving the odontogenic differentiation of SCAP, as well as vasoendothelial growth factor (VEGF), platelet-derived growth factor (PDGF) and other angiogenic factors that drive vascularization and pulpal regeneration (Zein et al., 2019).

Compared to other dental stem cells, SCAP are more capable of surviving infections such as apical periodontitis and abscesses, and have a superior ability to differentiate into dentin-forming cells (Huang et al., 2009). SCAP have been observed to have elevated telomerase activity, increased ability to survive infection, a higher rate of population doubling, and superior migratory behavior within the canal space (Sonoyama et al., 2006; Huang et al., 2010). Therefore, SCAP serve as suitable candidates for the regeneration of the pulp-dentin complex.

Design Criteria for Endodontic Biomaterials

The variable clinical success associated with traditional apexification procedures in teeth with immature roots has recently driven a shift toward the regeneration of the pulp-dentin complex in the field of endodontics research. RET is the process of delivering dental stem cells to the root canal space and aims to reform the pulp-dentin complex to replace compromised dental tissues and allow root development to continue. A clinically-effective regenerative protocol using functional biomaterials would promote further root development and consistently result in the formation of new dentin by the deposition of calcified tissue to increase both root thickness and length, strengthening the tooth against fracture and improving its stability in the dental alveolus.

Multiple clinical, biological and physical factors must be considered when developing biomaterials for endodontic applications. Importantly, clinical compatibility is a fundamental requirement for all materials used in dental procedures. For a biomaterial to be of practical use in endodontic therapies, it should be endogenous or prefabricated and ready-to-use, stored in sterile packaging, adaptable to the eccentric shapes and sizes of root canals, easily manipulated in operatory settings and involve minimal patient discomfort. Short setting times, together with cervical sealability with MTA and antiseptic properties to help ensure and maintain canal sterility are also desirable attributes.

From a biological viewpoint, a suitable scaffold that can support the survival and differentiation of SCAP should mimic the physical and biochemical microenvironment of the root canal. These include growth factors and other bioactive molecules being presented in a spatial-temporally appropriate manner. It should also contain the appropriate extracellular matrix that promotes SCAP adhesion and migration thus serving as a template for tissue regeneration (O'Brien, 2011). Scaffolds that incorporate growth factors, such as TGF- β1, BMP-2, VEGF, and PDGF, further support odontogenic differentiation and drive pulpal revascularization (Zein et al., 2019). Numerous requirements must be considered when selecting an appropriate scaffold to support SCAP survival and proliferation, including: (i) biocompatibility; that is, the material supports SCAP viability and odontogenic differentiation and biodegrades to products that do not cause harm to the host; (ii) architecture with adequate, controllable porosity to permit cell migration, vascularization, as well as the diffusion of nutrients and waste; (iii) mechanical strength suited to the location and anatomy of the afflicted tooth; and (iv) biodegradability such that mature cells may completely replace the scaffold (O'Brien, 2011; Chang et al., 2017). Although hard tissue formation is a goal of RET, the formation of dentin is preferable to cementum due to dentin's higher mineral content and superior physical properties that enhance resistance against fracture. Lastly, to be clinically feasible, an endodontic biomaterials should not be cost prohibitive to patients nor oral health professionals.

Endodontic biomaterials may also be developed in pre-formed or injectable varieties. Pre-formed scaffolds have definite conformations that remain constant when fixed in the target location, while the compliant nature of injectable scaffolds permits their molding to exactly match the unique anatomy of the scaffold's destination. The fluidity of injectable scaffolds offers a number of advantages over pre-formed scaffolds in the context of pulp-dentin regeneration, including their critical ability to occupy and adapt to the irregular topology of the root canal space, their ease of application which reduces patient discomfort, and their capacity to be mixed with SCAP prior to being injected which facilitates exposure to signaling molecules, cell adhesion and the initiation of other downstream processes (Chang et al., 2017). However, cell-free endodontic biomaterials that recruit endogenous cells into the canal space remain more clinically practical, as they avoid clinical hurdles such as regenerative cell isolation, banking and insertion in the root canal that are yet to be routine in dental practice.

SCAP Scaffolds

The relatively unpredictable clinical outcomes associated with regenerative endodontic procedures have largely been attributed to individual variations in intracanal blood clot formation due to variable sizes of the apical foramen and inconsistencies in the extent of blood influx into the root canal space, which may be compromised by the use of vasoconstrictor-containing local anesthetic (Lenzi and Trope, 2012; Jadhav et al., 2013). Furthermore, varying levels of growth factors and stem cells trapped in the blood clot may influence cell proliferation and odontogenic differentiation, ultimately impacting the degree of root lengthening and thickening in the endodontically treated tooth. Consequently, there has been a recent push to develop strategies to improve the success and predictability of dental tissue regeneration. As with other tissue engineering protocols, the regeneration of the pulp-dentin complex requires a triad of stem cells, growth factors, and a scaffold biomaterial (O'Brien, 2011). Due to the superior tissue-forming properties of SCAP, these cells have recently become a popular focus for regenerative endodontics research endeavors. The interaction of SCAP with highly-porous scaffolds designed to serve as templates for the regeneration of pulpal tissues strongly influences critical stages of reconstruction, including cell adhesion, migration, and proliferation. The recent surge in research investigating intracanal scaffolds and their effects on SCAP specifically has warranted a review of the literature pertaining to this ever-evolving topic. This paper will review the strengths and limitations of various forms of host-derived, naturally-derived, and synthetic scaffolds that have been investigated for pulp-dentin tissue regeneration from SCAP, and will discuss possibilities for future study in scaffold development.

PREVIOUSLY INVESTIGATED SCAFFOLDS FOR SCAP

Several studies have determined that the introduction of SCAP into the root canal system in the absence of a scaffold inhibits the attachment of viable cells to the canal walls, and thus fails to regenerate the pulp-dentin complex (Trevino et al., 2011; Jadhav et al., 2012). This clearly demonstrates the necessity for a SCAP scaffold to serve as a template for tissue growth in order to have a successful RET. Numerous host-derived, naturally-derived and synthetic scaffolds have been studied for the delivery and growth of SCAP in the root canal space (**Table 1**). However, a biomaterial that can successfully support guided regeneration of the pulp-dentin complex has yet to be identified.

Current regenerative endodontic procedures typically utilize intracanal blood clots, as previously described, or platelet-rich plasma (PRP) to form host-derived scaffolds (Chrepa et al., 2017). While these scaffolds supply the necessary signaling molecules and growth factors for tissue regeneration, their use has been complicated by the unpredictable nature of clot formation and challenges in acquiring PRP, as well as limited efficacy (He et al., 2009; Chrepa et al., 2017). To provide a more predictable alternative to host-derived scaffolds, numerous naturally-derived biomaterials have been developed for the delivery of SCAP to the root canal space and tissue regeneration (Chang et al., 2017). These scaffolds include alginate, hyaluronic acid and its derivates, and chitosan. Naturally-derived scaffolds offer several advantages, such as signaling molecules that aid in cell recognition and adhesion (Chang et al., 2017). However, the use of natural-derived products is limited by the possibility of pathogen transmission, foreign body response, poor mechanical properties, and product variability (O'Brien, 2011; Chang et al., 2017).

Several synthetic scaffolds have been studied as potential candidates for the regeneration of the dentin-pulp tissue from SCAP, and are primarily in the form of hydrogels (Chrepa et al., 2017). Synthetic scaffolds that have been investigated for SCAP delivery include nano-fibrous microspheres, hydrogels and PLGA-PEG nanoparticles. These biomaterials avoid the risk of transmitting pathogens, induce a desirable immune response, and can have a consistent production processes that ensure properties such as mechanical strength, porosity, and rate of biodegradation are uniform (Chang et al., 2017; Chrepa et al., 2017). However, synthetic scaffolds lack the intrinsic signaling abilities of naturally-derived scaffolds and have high costs resulting from their complex production (Chang et al., 2017). This section will identify and discuss the advantages and limitations of the host-derived, naturally-derived, and synthetic scaffolds in pre-formed or injectable designs for SCAP delivery and growth that have been investigated to date.

Host-Derived Scaffolds

Intracanal Blood Clot

As previously described, the induction of bleeding and formation of an intracanal blood clot is a current procedure used in regenerative endodontics to provide a scaffold for pulp-dentin regeneration, presumably from SCAP (Chrepa et al., 2017). In immature teeth with open apices, induced bleeding results in the delivery of SCAP from the periradicular tissues of the tooth into the root canal space through the apical foramen, thus eliminating the need to inject foreign stem cells (Trevino et al., 2011). Induced bleeding also allows endogenous hemostatic factors to enter the canal space and form a fibrin clot that supports processes required for SCAP survival and growth. The advantages of an intracanal blood clot are that it provides an autologous scaffold consisting of cross-linked fibrin that contains the growth factors necessary to support SCAP migration, differentiation, vascularization and tissue regeneration, and does not induce a foreign body response (Jadhav et al., 2012; Chrepa et al., 2017; Dianat et al., 2017). These qualities, in addition to the low cost, clinical simplicity, short setting time and cervical sealability with MTA provide an attractive treatment option for both patients and dental practitioners.

Challenges that complicate the use of intracanal blot clots include their instability and unpredictable clinical outcomes as a consequence of unregulated stem cell entry into the canal space, as well as difficulties in invoking bleeding and hemostasis in some patients (Dianat et al., 2017). These obstacles are major limitations of the use of blot clots in regenerative endodontics, and have driven research efforts for more consistent, effective scaffolds. However, given the extremely favorable and clinically-feasible properties of the intracanal blot clot, investigating strategies to improve its reliability may secure this scaffold as the gold standard for RET.

Platelet-Rich Plasma-Based Therapeutics

Platelet-rich plasma (PRP) represents an autologous injectable scaffold that has been used in numerous *in vitro* and clinical studies, in both regenerative endodontics and other surgical tissue regeneration procedures (Torabinejad and Turman, 2011; Trevino et al., 2011; Jadhav et al., 2012; Bezgin et al., 2015). A volume of peripheral blood can be obtained from the patient undergoing the endodontic procedure and is mixed with anticoagulants in a test tube. The tube is then spun in a centrifuge to separate the platelets and leukocytes from erythrocytes, which collect at the bottom more rapidly due to their higher density (Saucedo et al., 2012). The PRP is then separated from platelet-poor plasma, and is further processed to increase the platelet concentration up to 1 million/μL, which is approximately 5 times higher than the physiologic platelet concentration (Trevino et al., 2011; Jadhav et al., 2012; Saucedo et al., 2012). The final volume of PRP and platelet concentration varies with the type of preparation system used. Coagulation may be achieved by combining the PRP with saline solution, calcium chloride and bovine thrombin and injecting the mixture into the canal space, waiting 10 min for clot formation. Alternatively, PRP can be carried to the canal space in a collagen sponge, which activates the platelets and enables degranulation (Trevino et al., 2011).

An elevated number of platelets results in a larger overall quantity of growth factors release by degranulation increasing SCAP growth and proliferation rates and expediting the tissue regeneration process (Jadhav et al., 2012; Bezgin et al., 2015). These growth factors include PDGF, TGF-β, insulin-like growth factor (IGF), VEGF, epidermal growth factor (EGF), and

TABLE 1 | Summary of SCAP scaffolds used for regenerative endodontic therapies investigated to date.

Scaffold	Pros	Cons	References
Intracanal blood clot	Host compatibility Autologous growth factors Inexpensive Clinical simplicity	Unstable Inconsistent outcomes Bleeding challenges Inadequate mechanical strength	Jadhav et al., 2012 Chrepa et al., 2017 Dianat et al., 2017
Platelet-rich plasma	Host compatibility Autologous growth factor abundance Elevated revascularization rates Inexpensive	Blood collection difficulties Composition variability Rapid growth factor reduction Inadequate mechanical strength Complexity in clinical formation	Trevino et al., 2011 Jadhav et al., 2012 Bezgin et al., 2015 Fernandes and Yang, 2016
Alginate	Biocornpatibility Low immunogenicity Mild gelation requirements Inexpensive Optimal structure for nutrient exchange	Reduced SCAP viability Inadequate mechanical strength Potential pathogen transmission Product variability	Lambricht et al., 2014 Zhang et al., 2013
Hyaluronic acid	Promotes odontogenic differentiation Biocompatibility Biodegradable Bioactive Porous architecture Adapts to canal morphology Pro-angiogenic degradation factors Fast setting	Inadequate mechanical strength Exogenous growth factors Hypersensitivity to bacterial impurities Reduced SCAP viability Formation of reparative dentin only	Ferroni et al., 2015 Pardue et al., 2014 Friedman et al., 2002
Chitosan	Improved SCAP viability Improved odontogenic differentiation Biocompatibility Biodegradable Low cytotoxicity break Low immunogenicity Broad-spectrum antibacterial properties Mechanical strength	Complex gelation scheme and controlled degradation profile	Chang et al., 2017 Shrestha et al., 2016 Souto et al., 2016
PLLA NF-MS with BMP-2	Adapts to canal morphology Biodegradable Exogenous growth factor incorporation Drug incorporation Optimal structure for nutrient exchange Improved odontogenic differentiation Minimally invasive	Disorganized tissue formation Lack intrinsic signaling abilities Prohibitive cost	Wang et al., 2016 Horst et al., 2012 Ceccarelli et al., 2017
PLGA- PEG nanoparticles	Biodegradable Fast setting Low toxicity Biocompatibility Low immunogenicity Anti-fouling Accelerates bone repair	Prohibitive cost Lack intrinsic signaling abilities	Shiehzadeh et al., 2014 Chang et al., 2017
VitroGel 3D with SDF-lα and BMP-2	Biodegradable Adapts to canal morphology Low immunogenicity Low cytotoxicity Improved odontogenic differentiation Mimics pulp ECM Exogenous growth factor incorporation	Prohibitive cost Lack intrinsic signaling abilities	Xiao et al., 2019

epithelial cell growth factor (ECGF), which all aid in the stimulation of revascularization and increase cell proliferation (Trevino et al., 2011). These are critical elements of tissue regeneration and contribute to the appeal of the PRP scaffold. Importantly, it has been hypothesized that the clinical success observed with PRP scaffolds is due to the role these growth factors play in attracting stem cells located in the periapical region, such as SCAP, and facilitating their migration to the root canal space (Torabinejad and Turman, 2011).

Benefits of PRP include elevated rates of angiogenesis and revascularization, which are fundamental for a successful RET. Furthermore, PRP is an attractive scaffold because of its avoidance of a foreign body response and pathogen transmission, and its cost-effective application relative to synthetic scaffolds as well as cervical sealability (Jadhav et al., 2012; Bezgin et al., 2015). A recent clinical study by Ulusoy et al. (2019) evaluated radiographic changes in root dimensions in 88 necrotic human incisors following the treatment using blood clots, PRP, platelet-rich fibrin and a platelet pellet. The study found similar outcomes among all treatment groups, with all teeth scoring high treatment success score in periapical healing, radiographic root development and positive responses to sensitivity tests

after an average of 28.25 months. Minor differences in linear measurements of radiographic canal area and radiographic root area were observed when follow-up time was not used as a factor. An important finding in this study is that the injection of a PRP scaffold yields similar clinical outcomes as intracanal blood clots, while presenting less of a risk of root canal obliteration by avoiding the induction of an apical bleed. However, use of the PRP scaffold is limited by the necessity of obtaining blood from pediatric patients who may not comply with the blood collection process, the additional equipment and reagents required to process PRP in-clinic, variability in its composition, and the failure of this scaffold to guide complete, long-term pulp-dentin regeneration, as growth factors are rapidly released upon degranulation and levels significantly decline as the regeneration process proceeds (Trevino et al., 2011; Bezgin et al., 2015; Fernandes and Yang, 2016).

Naturally-Derived Polymeric Scaffolds

Alginate

Alginate is a natural polysaccharide that is purified from the cell walls and intracellular spaces of brown seaweed, and has been extensively used in biomaterial applications (Venkatesan et al., 2014). Alginate hydrogels are formed by crosslinking the polysaccharides with divalent cations to form ionic bridges in a water-insoluble network (Lambricht et al., 2014). Stem cells may be seeded into the gels during this process, which are then injected into the canal space where the gelation process occurs. This rapid gelation feature as well as good mixing properties with other biopolymers have also contributed to the widespread use of alginate as a component and many 3-D printed scaffolds. For example, alginate can be mixed with dentin matrix extracts in equal mass ratio has been fashioned into bioink with high dimensional stability and supports odontoblast-like cells viability (>80%) over a period of 5 days in culture (Athirasala et al., 2018).

The popularity of alginate scaffolds in tissue engineering endeavors can be attributed to its biocompatibility, favorable immunogenicity, low cost, and mild gelation requirements (Zhang et al., 2013). Furthermore, the highly organized, macroporous form of the alginate scaffold permits nutrient/waste exchange and solute diffusion. However, in addition to general complications of natural biomaterials such as potential pathogen transmission, product variability and inadequate mechanical strength, a study conducted by Lambricht et al. (2014) determined that SCAP viability was markedly reduced when exposed to an alginate hydrogel relative to other naturally-derived hydrogels *in vitro*, and the highest levels of apoptosis *in vivo*. Therefore, scaffolds containing only alginate may have limited potential in regenerative endodontic procedures with SCAP. Careful design and blending with other bioactive polymers and growth factors should be considered to extend the usefulness of alginate.

Hyaluronic Acid and Derivatives

Several recent studies have investigated the use of hyaluronic acid (HA) as a potential scaffold for SCAP delivery and growth in the root canal space (Lambricht et al., 2014; Chrepa et al., 2017). HA is a glycosaminoglycan consisting of alternating D-glucuronic acid and N-acetyl-D-glucosamine units, which are natural components of the extracellular matrix (ECM) that can interact with SCAP membrane receptors such as CD44, activating signaling pathways that drive cellular migration which could be critical to SCAP recruitment to the root canal space (Lambricht et al., 2014). In the ECM, HA maintains extracellular spacing and, thus, preserves the matrix's morphology (Inuyama et al., 2010). Furthermore, HA has been found in the dental pulp and decreases as teeth develop during odontogenesis, suggesting that HA may have a role in the initial formation of the dentin matrix and pulp (Ferroni et al., 2015). These properties, together with HA's potential to be structurally and chemically modified for a wide range of applications, are of particular interest in the field of dental tissue engineering (Neilson et al., 2015).

HA and its derivatives have numerous advantages, including their biocompatibility, biodegradability, and bioactivity, and their porous architecture that resembles the native pulp-dentin ECM (Chang et al., 2017). HA is often in the form of an injectable fluid that undergoes gelation *in situ*. As such, HA-based scaffolds are able to adapt to the morphology of the root canal and have a relatively fast setting time, which are clinically-attractive features (Ferroni et al., 2015). An analysis completed by Pardue et al. (2014) also suggested that HA degradation products may include pro-angiogenic growth factors, which are instrumental in the revascularization of the regenerated dental tissues (Pardue et al., 2014). Limitations of HA-based scaffolds include their relatively low mechanical strength their requirement to be combined with growth factors such as BMP-2 and TGF-β1 for desirable regeneration of the pulp-dentin complex. Hypersensitivity reactions due to bacterial impurities is another potential complication of HA scaffolds (Friedman et al., 2002).

Several HA derivatives, including HA-based hydrogels like Corgel™ and Restylane, have been investigated as candidates for SCAP delivery and growth (Lambricht et al., 2014; Chang et al., 2017; Chrepa et al., 2017). An *in vitro* study investigating the effects of increasing concentrations of NaOCl on SCAP survival and differentiation in organotype root canal models employed a HA hydrogel as the scaffold, and found that HA alone supported SCAP viability and odontogenic differentiation, both of which were further promoted by the addition of 17% EDTA (Martin et al., 2014). As observed by Chrepa et al. (2017), the HA-based hydrogel Restylane has the ability to increase SCAP mineralization and odontogenic differentiation based on significantly increased alkaline phosphatase activity after seven days in an *in vitro* 3D transwell system compared to scaffold-free controls, and elevated expression of odontoblastic differention markers dentin sialophosphoprotein (DSPP), dentin matrix acidic phosphoprotein 1 (DMP-1) and matrix extracellular phophoglycoprotein (MEPE) after 14 days. However, this scaffold induced the formation of reparative dentin instead of tubule-forming dentin, and significantly compromises a cell viability relative to scaffold-free controls. Lambricht et al. (2014)

investigated another HA-based hydrogel, Corgel™, and observed that this scaffold positively impacted SCAP proliferation and metabolism *in vitro*, while increased collagen production and decreased rates of apoptosis were observed *in vivo* when hydrogel and SCAP mixtures were injected into peritoneal pockets in mice. However, similar to Restylane, Corgel™ significantly reduced the degree of SCAP viability after 7 days. As such, HA scaffolds and their derivates serve as possible candidates for regenerative endodontic procedures, however, further investigation is required to improve SCAP viability with this scaffold.

Chitosan Derivatives

Chitosan is a linear, cationic aminopolysaccharide biopolymer that is similar to components of the ECM and is produced through *N*-deacetylation of chitin, the main component of the exoskeleton of crustaceans such as crabs and shrimp (Feng et al., 2014; Shrestha et al., 2016). Chitosan also possess reactive amine groups that can aid in the functionalization of bioactive molecules, and can be degraded through enzymatic and hydrolytic reactions to non-cytotoxic metabolites (Jung et al., 2015; Shrestha et al., 2015). Chitosan can be easily molded into a highly-porous structure at a low cost, facilitating processes such as cell migration. Alternatively, chitosan can be prepared in the form of nanoparticles for tissue regeneration through ionotropic gelation (Souto et al., 2016). For the purpose of tissue regeneration, the geometric features of nanoparticles are generally desirable due to the increased surface area for cell adhesion and biological activity compared to other biomaterials formats. Their mass transport properties can be tuned and developed into controlled-release platform of essential growth factors such as TGF-β1, which is critical to support and regulate stem cell differentiation in tissue regeneration procedures (Shrestha et al., 2014). As such, nanoparticles have become an attractive delivery system for bioactive molecules in recent years (Lee et al., 2011).

Advantages of chitosan include its biocompatibility, biodegradability, low cytotoxicity, low immunogenicity, and its broad-spectrum antibacterial properties (Shrestha et al., 2016; Souto et al., 2016; Chang et al., 2017). Furthermore, chitosan nanoparticles are mechanically strong, are resistant to degradation by bacterial enzymes, and have been shown to improve SCAP adhesion, viability, and differentiation, even in environments that have been exposed the powerful root canal antimicrobial agent, NaOCl (Shrestha et al., 2016). However, chitosan use is complicated by its complex gelation and degradation scheme due to its unusual polycationic chain and highly-crystalline structure, thus limiting the range of its potential applications as an injectable scaffold in its naturally-occurring form (Chang et al., 2017).

The usefulness of chitosan nanoparticle as a bioactive, controlled-release scaffold has been demonstrated by Shrestha et al. (2014) where they evaluated SCAP mineralization by measuring alkaline phosphatase (ALP) activity in the presence of chitosan nanoparticles loaded with bovine serum albumin (BSA), a model protein for drug delivery, *in vitro*. Two forms of chitosan nanoparticles were synthesized for use in this study, including BSA-encapsulated (BSA-CSnpI) and BSA-absorbed nanoparticles (BSA-CSnpII). The individual effects of chitosan nanoparticles and BSA on SCAP were simultaneously evaluated. It was observed that BSA-CSnpI showed a 10% release within 10 days, while BSA-CSnpII demonstrated a rapid 40% release within the same time period. At the end of a 3-week trial, BSA-CSnpI demonstrated significantly higher ALP activity than both BSA-CSnpII and CSnp, suggesting that nanoparticles encapsulating BSA best supported SCAP differentiation to hard tissue-forming cells. Researchers speculated that this phenomenon may have been due to the prolonged release of BSA by BSA-CSnpII over the 3-week period, demonstrating the critical importance of the controlled-release of bioactive molecules in SCAP differentiation.

A subsequent *in vitro* study conducted by the same team investigated the same forms of chitosan nanoparticles in dexamethasone-encapsulated (DEX-CSnpI) and dexamethasone-absorbed (DEX-CSnpII) varieties (Shrestha et al., 2015). Unlike the above described BSA-loaded nanoparticle system, rapidly-releasing DEX-CSnpII significantly enhanced odontogenic differentiation compared to slow-releasing DEX-CSnpI and chitosan nanoparticles alone over a 3-week period, based on alizarin red staining for mineralization and real-time reverse-transcription polymerase chain reaction for alkaline phosphatase, DSPP and DMP-1. Shrestha et al. then studied human dentin slabs conditioned with slowly-releasing and rapidly-releasing variants of dexamethasone-releasing chitosan nanoparticles. It was found that rapid-releasing DEX-CSnpII further improved SCAP adhesion and viability relative to unconditioned controls based on calcein-AM staining, and expression of odontogenic differentiation markers DSPP and DMP-1 was markedly increased in DEX-CSnpII conditions compared to DEX-CSnpI as well as unconditioned and CSnp controls after 2 weeks in an immunofluorescent analysis (Shrestha et al., 2016). Importantly, this study determined that CSnp, DEX-CSnpI, and DEX-CSnpII may have the ability to minimize the loss of SCAP viability and adherence in root canal systems that have been disinfected with NaOCl (Trevino et al., 2011; Shrestha et al., 2016).

A carboxymethyl chitosan-based scaffold (CMCS) with TGF-β1-releasing chitosan nanoparticles (TGF-β1-CSnp) was investigated by Bellamy et al. *in vitro*, and significantly enhanced SCAP migration through transwell membranes in 24 h, as well as expression of odontogenic differentiation markers DSPP and DMP-1 compared to scaffolds with TGF-β1 or CSnp alone (Bellamy et al., 2016). Although the definite role of TGF-β1 requires further investigation, several studies have indicated that TGF-β1induces the cytological and functional differentiation of odontoblasts in animal dental papillae cultures, and plays an important role in the secretion of the dentin matrix (Begue-Kirn et al., 1994; Li et al., 2011). The CMCS scaffold is water soluble, compatible with SCAP, and modifies the surface of the dentin matrix such that its antibacterial properties are improved and its ultrastructure is stabilized, hence its use in the Bellamy et al. study (Bellamy et al., 2016). The research team concluded that

the CMCS scaffold containing TGF-β1-CSnp enhanced SCAP viability, migration and odontogenic differentiation, suggesting that this system may be yet another promising chitosan-based scaffold for SCAP in RET.

Synthetic Scaffolds

PLLA Nanofibrous Microspheres

The use of poly (L-lactic acid) (PLLA) nanofibrous microspheres (NF-MS) has recently been studied by Wang et al. (2016) as a novel injectable scaffold for SCAP growth. The PLLA NF-MS was evaluated as a SCAP carrier for delivery in combination with poly (lactic-co-glycolic acid, PLGA) microspheres for controlled bone morphogenic protein 2 (BMP-2) release to promote SCAP differentiation into odontoblast-like cells. A chiral isoform of polylactic acid (PLA), PLLA-based scaffolds maintain their integrity for a 42-day period and are, therefore, well-suited for tissue regeneration procedures (Horst et al., 2012). The morphogenic factor BMP-2 had been shown to induce odontogenic differentiation of other dental stem cells *in vitro* and *in vivo* prior to the study by Wang et al., and therefore, was considered a promising candidate for the induction of human SCAP odontogenesis. PGLA is a copolymer formed through the union of polylactic acid (PLA) and polyglycolic acid (PGA) through ester bonds (Ceccarelli et al., 2017). The 12:13 combination of PLA and PGA results in a biomaterial that has an extended half-life relative to both acids individually, increasing the degradation time of the PLGA microspheres and prolonging the exposure of SCAP to BMP-2 (Ceccarelli et al., 2017).

Advantages of PLLA NF-MS with controlled BMP-2 release include their injectability and ability adapt to root canal morphology, biodegradability, and potential for growth factor and drug incorporation. With similar architecture to collagen, high porosity and a large surface area, NF-MS facilitate cell adhesion, growth, as well as nutrient and waste exchange (Wang et al., 2016). The controlled release BMP-2 from PLGA microspheres has been observed to increase SCAP odontogenic differentiation and dentin-like tissue production *in vivo*. Clinically, this would minimize the need to reapply BMP-2 and would thus, reduce the invasiveness of the scaffold's application and minimize the need for complex manipulations (Wang et al., 2016). Like other synthetic scaffolds used in tissue engineering, the PLLA NF-MS system allows for consistency in properties such as the morphology and diameter of the pores and surface features, as well as a low likelihood of inducing a foreign body response (Ceccarelli et al., 2017). However, Wang et al. noted several limitations of the NF-MS scaffold that may comprise its clinical success, such as the disorganized formation of dentin-like tissues because the architecture of the scaffold did not guide the formation of the desired dentinal tubules found in the natural state of the tooth. The cost associated with the complex production of the NF-MS material that incorporates BMP-2 may also be clinically prohibitive, compared to endogenous or naturally-derived scaffolds with innate bioactive capacities. It should also be noted that the degradation of PLLA as well as PLGA release acidic residues into the surrounding microenvironment which may be reduce local cell viability. For this reason, careful control of hydrolytic degradation rate is necessary for i*n vivo* applications.

PLGA-PEG Nanoparticles

Recently, Poly (lactide-co gylcolide)-polyethylene glycol (PLGA-PEG) nanoparticles have been clinically investigated as a scaffold for SCAP by Shiehzadeh et al. (2014). PEG is an absorption-resistant polyether with a high molecular weight (Ceccarelli et al., 2017). Together with PLGA, this scaffold has been found to be more conducive to dental pulp fibroblast proliferation and development of dental tissues compared to hydrogel and alginate scaffolds (Shiehzadeh et al., 2014). To determine if PLGA-PEG nanoparticles had similar effects on SCAP, Shiehzadeh et al. seeded this scaffold with autologous SCAP from banked teeth in this study prior to injecting the mixture into patients' root canal system (Shiehzadeh et al., 2014). Periapical healing and was monitored radiographically for 18–24 months postoperatively for each patient.

Compared to many biomaterials, PLGA-PEG nanoparticles have numerous advantages in SCAP scaffold applications. The nanoparticles biodegrade within clinically-feasible time periods (weeks/months) to carbon dioxide and water, and they are in a transparent fluid-form at room temperature that is quickly converted to an opaque gel at 37°C (Shiehzadeh et al., 2014). PLGA-PEG nanoparticles also have a low toxicity, excellent biocompatibility and are minimally immunogenic (Chang et al., 2017). Additionally, the PEG component has an anti-fouling property that inhibits the adherence of residual bacteria to the biomaterial's surface (Chang et al., 2017). In the study conducted by Shiehzadeh et al. (2014), the PLGA-PEG scaffold did not have adverse effects on the tissues surrounding the afflicted tooth, and accelerated periapical bone repair within 6 months while the tooth remained functional. However, like other synthetic scaffolds employed in tissue engineering, the use of the PLGA-PEG nanoparticles scaffold is limited by the clinically-prohibitive costs of production and standardization, as well as the necessity to bank and pre-mix autologous SCAP with scaffolds prior to injection. Furthermore, there was minimal radiographic evidence of continued root formation in length and canal wall thickness in the cases presented by Shiehzadeh et al., suggesting that the injectable PLGA-PEG scaffold may induce apexification while facilitating periapical healing.

VitroGel 3D®

The synthetic polysaccharide hydrogel, VitroGel 3D, was recently evaluated as a potential injectable SCAP scaffold by Xiao et al. (2019) *in vitro* and *in vivo*. The synergistic effects of stromal cell-derived factor-1α (SDF-1α) and BMP-2 together with the VitroGel 3D solution on SCAP was also investigated. In this study, VitroGel 3D solution was diluted 1:2 with dionized water before being mixed with SCAP suspension. Hydrogel experimental groups consisted of VitroGel 3D alone and supplemented with SDF-1α and/or BMP-2, each at concentrations of 100 ng/ml. SCAP viability and proliferation were evaluated *in vitro* after 4 days using

live/dead staining and cell counting kit (CCK)-8 assays, while odontogenic differentiation was evaluated at three, seven and 14 days using real time RT-PCR, ALP activity and western blot assays. Target genes and proteins included DMP-1 and DSPP, among several other markers of odontogenic/osteogenic differentiation. Finally, the odontogenic differentiation was assessed *in vivo* through ectopic subcutaneous injection in mice after 8 weeks using the same experimental groups.

The results of the study showed that the VitroGel 3D hydrogel did not significantly impact SCAP viability or proliferation compared to 2D controls. Furthermore, SDF-1α and BMP-2 synergistically enhanced the expression of odontogenic genes and proteins *in vitro*, with significantly greater DMP-1 and DSPP expression after 14 days in hydrogels supplemented with both SDF-1α and BMP-2, as well as hydrogels with BMP-2 alone. Histologic and immunohistochemical evaluations of specimens cultured *in vivo* echoed the *in vitro* results, with elevated levels of DSPP expression, osteoid dentin and vascularization in VitroGel 3D with both SDF-1α and BMP-2, as well as with BMP-2 alone, compared to control groups and SDF-1α alone. These results suggest that VitroGel 3D injectable scaffolds may hold promise in supporting intracanal hard tissue deposition and continued root development in RET. Like other injectable scaffolds, however, VitroGel 3D maintains practical issues such as the necessity to bank SCAP and associated expenses currently impede the clinical feasibility of this scaffold.

POTENTIAL SCAFFOLDS FOR FUTURE STUDIES

Scaffold Properties for SCAP Delivery

Existing literature suggests that the type of scaffold selected presents profound influences on critical aspects of the regeneration of the pulp-dentin complex, including SCAP viability, migration, adhesion, differentiation, and mature structural form (Zhang et al., 2013; Wang et al., 2016; Chang et al., 2017). The physical form of the scaffold, as an endogenous substance, pre-formed material, or injectable foam or gel also influences SCAP development pathways and the morphogenesis of the mature dental tissues (Zhang et al., 2013; Wang et al., 2016; Chang et al., 2017). A clinically-relevant scaffold for pulp-dentin tissue regeneration must enable angiogenesis and the vascularization of the regenerated tissue; the organized formation of odontoblast-like cells on existing dentin structures in the root canal; and the coordinated addition of dentin produced by these cells to existing dentin tubules (Huang et al., 2010). Further research is required to develop an effective biomaterial for SCAP delivery and growth in the root canal system. Investigating the application of biomaterials and their derivatives that have been used in other bone regenerative procedures and in protocols that utilize other forms of dental stem cells may prove to be constructive.

Scaffolds in Other Tissue Regeneration Procedures

As a consequence of the relatively recent identification of SCAP, a more extensive spectrum of scaffolds has been researched for dental pulp stem cells (DPSC), another type of dental stem cell capable of regenerating the pulp-dentin complex *in vivo* (Huang et al., 2009). Although SCAP comprise a post-natal stem cell population that is distinct from DPSC and have a superior dentin regeneration potential, the two stem cell varieties have displayed comparable trends in viability, migration and differentiation potentials when exposed to identical conditions (Sonoyama et al., 2006; Huang et al., 2010; Bakopoulou et al., 2011). Therefore, investigating biomaterials that have successfully guided dentin formation from DPSC progenitors may be worthwhile in future SCAP scaffold research.

Scaffolds that have been studied for DPSC delivery and growth but have yet to be investigated for SCAP applications include collagen type-I, collagen type-III, gelatin, silk protein, and peptide scaffolds including self-assembling peptides and peptide amphiphiles (Zhang et al., 2013; Gong et al., 2016). Of these, collagen, self-assembling peptide scaffolds such as Puramatrix™, and calcium polyphosphate have experienced significant success and will be discussed (Cavalcanti et al., 2013; Gong et al., 2016).

Collagen

Collagen is a natural biomaterial that is widely-used in tissue regeneration applications as a result of its architectural resemblance of many tissues' extracellular matrix and its ability to adapt to the morphology of the target (Zhang et al., 2013). Type I collagen is the most abundantly used, and best promotes DPSC proliferation and mineralization capacity compared to other collagen types (Gong et al., 2016; Chang et al., 2017). A pre-formed collagen sponge scaffold has been studied with success for the delivery of DPSC to the root canal system *in vivo* (Sumita et al., 2006). Additionally, a recent clinical study completed by Nosrat et al. (2019) evaluated the use of SynOss™ putty, a bovine type I collagen and synthetic carbonate apatite material, as an intracanal scaffold in three human patients with non-infected immature first premolars scheduled for extraction. After 2.5–7 months, teeth treated with SynOss™ putty together with an intracanal blood clot displayed histologic evidence of mineralized, cementum-like tissues on dentinal walls, while teeth treated with SynOss™ putty alone displayed asymptomatic periapical lesions radiographically with no new intracanal tissue, and intracanal blood clots alone resulted in the formation of fibrotic connective tissue with malformed cementum in the canal space, along with reparative cementum on dentinal walls. These findings suggest that type I collagen-based scaffolds together with dental stem cell-containing blood clots may promote intracanal hard tissue formation compared to blood clots alone.

Advantages of collagen include its biocompatibility and bioactivity, owing to its motifs that can be recognized by DPSC which facilitate adhesion and downstream signaling pathways for proliferation and differentiation, as well as its extracellular

matrix that is structurally comparable to that of the pulp-dentin complex (Kim et al., 2009; Zhang et al., 2013; Chang et al., 2017). The porous structure of collagen also facilitates its colonization by seeded stem cells (Sumita et al., 2006). However, the difficulties encountered in collagen scaffold studies pertaining to regenerative endodontics are its low mechanical strength, irregular biodegradation and the generation of tissues that resemble connective tissue instead of dentin *in vivo* (Kim et al., 2009). Furthermore, like other naturally-derived scaffolds, product variability and risk of immunogenicity and pathogen transmission complicate the clinical applicability of collagen scaffolds.

Self-Assembling Peptide Hydrogel: Puramatrix™

Puramatrix™ is a synthetic, self-assembling peptide hydrogel that creates a 3D environment that is biocompatible, biodegradable, and non-toxic to cells (Aligholi et al., 2016). The hydrogel exists as an aqueous solution, however, polymerizes to form a solid gel instantly when exposed to physiologic salt conditions and is, thus, a clinically-practical scaffold (Nune et al., 2013).

In a study of DPSC seeded in a Puramatrix™ scaffold conducted by Cavalcanti et al. (2013), it was observed that Puramatrix™ enabled DPSC viability and proliferation *in vitro*, as well as odontoblastic differentiation over a 3-week period when DPSC and Puramatrix™ were seeded on tooth slices. Contrary to other primary cell types, varying concentrations of Puramatrix™ did not significantly affect DPSC proliferation; a 0.2% gel was, therefore, employed because of its increased rigidity and stability. It was speculated in this study that the soluble factors responsible for odontogenic differentiation diffused from existing dentin in the tooth slice models that were employed in the study, since odontogenic differentiation was not observed in DPSC cultured with Puramatrix™ in the absence of tooth slices. An additional *in vitro* and *in vivo* study by Dissanayaka et al. (2015) investigated Puramatrix™ together with DPSC alone and co-cultured with human umbilical vein endothelial cells (HUVEC). Similar to Cavalcanti et al. (2013) and Dissanayaka et al. (2015) found that the Puramatrix™ scaffold supported DPSC survival, while DPSC/HUVEC co-cultures demonstrated significantly higher viability than either monoculture. Furthermore, significantly elevated ALP expression and greater mineralization was observed in DSPC/HUVEC co-cultures compared to DSPC monocultures after seven days. Histological evaluation of human tooth root segments loaded with each cell group and Puramatrix™ after 4 weeks *in vivo* in mice revealed similar patterns, with osteodentin formation adjacent to dentin in DPSC/HUVEC co-cultures together with dentin sialoprotein (DSP) expression, as well as significantly greater vascularization an extracellular matrix deposition in the co-culture compared to other groups. Based on these promising findings, it can be speculated that Puramatrix™ may also prove to be a suitable scaffold for SCAP in regenerative endodontic applications.

Calcium Polyphosphate/Calcium Phosphate Cement

Calcium polyphosphate (CPP) scaffolds have been extensively studied in bone repair and regenerative applications due to their biocompatibility, controllable degradability, mechanical strength and similarity to naturally-occurring bone (Xie et al., 2016). As with other inorganic polyphosphates, CPP serves as a source of phosphate that induces bone differentiation in osteoblasts (Ozeki et al., 2015). The scaffold also has a chain-like structure with oxygen atoms connecting monomeric subunits that provide easily-accessible sites for hydrolysis to naturally-occurring, readily-metabolized calcium orthophosphate products (Comeau et al., 2012). As the CPP scaffold degrades, released calcium, and phosphorous components contribute to the formation of calcified tissues, such as dentin (Maruyama et al., 2016).

A study completed by Wang et al. (2006) investigated the viability of human DPSC when exposed to a porous CPP scaffold *ex vivo*. The scaffold was fabricated from a mixture of porous agent and amorphous powder, which was seeded with DPSC. The porous CPP scaffold allowed for effective nutrient/waste exchange, had no cytotoxic effect on the DPSC, improved cell adhesion and migration, and had no adverse effects on proliferation. A subsequent study conducted by Ozeki et al. (2015) observed that polyphosphate induced matrix metalloproteinase (MMP)-3 expression in purified odontoblast-like cells derived from pluripotent stem cells from mice. The MMP-3 expression increased cell proliferation and resulted in increased expression mature odontoblastic phenotype markings, including DMP-1 and DSPP. It can be speculated that CPP may exhibit similar effects on SCAP differentiation to odontoblasts-like cells. Because of the comparable behaviors of DPSC and SCAP, a CPP scaffold may exert similar influences on SCAP and could be an effective biomaterial in RET.

Calcium phosphate cement (CPC) has also been investigated as a scaffold for human DPSC (Qin et al., 2018). Although CPC alone has relatively weak strength properties, the incorporation of chitosan has been shown to increase flexural strength of CPC-based scaffolds (Weir and Xu, 2010). Qin et al. (2018) loaded CPC with 15% liquid chitosan and 50 μg of metformin, and evaluated DPSC viability and proliferation after 7 days, as well as odontogenic differentiation, ALP activity and mineralization after 14–21 days when combined with the scaffolds *in vitro*. Live/Dead and CCK-8 assays demonstrated that the CPC scaffold supports DPSC viability and proliferation, while ALP activity and mineralization were significantly increased in CPC with both chitosan and metformin, as was expression of odontoblastic gene markers, including DSPP, DMP-1, Runt-related transcription factor 2 (RUNX2), and OCN (osteocalcin) mRNA determined by quantitative RT-PCR. These findings suggest that, like CPP, CPC may also support SCAP growth and differentiation based on this material's effects on DPSC.

CONCLUSIONS

Current research relating to SCAP delivery, growth, and differentiation shows a great deal of promise for future clinical applications of these cells in regenerative endodontic procedures. Although a variety of scaffolds have been developed for SCAP delivery and growth in the root canal space, a candidate

that meets all the requirements for an functional scaffold in dental tissue regeneration remains to be identified. Scaffolds derived from host, natural and synthetic source each possess desirable features as well as disadvantages that limit their clinical feasibility. This paper has outlined the beneficial properties and limitations of biomaterials that have been previously developed as SCAP scaffolds, and has described potential scaffolds for future investigation based on their performance with DPSC in aspiration of drawing nearer to a consistent, clinically-successful RET.

AUTHOR CONTRIBUTIONS

GR, IM, and BL contributed to the writing and editing of this manuscript.

FUNDING

This research was funded by the Dalhousie University Faculty of Dentistry Research Funds. GR was supported by the Faculty of Dentistry Summer Student Fellowship.

REFERENCES

Aligholi, H., Rezayat, S. M., Azari, H., Ejtemaei Mehr, S., Akbari, M., Modarres Mousavi, S. M., et al. (2016). Preparing neural stem/progenitor cells in PuraMatrix hydrogel for transplantation after brain injury in rats: a comparative methodological study. *Brain Res.* 1642, 197–208. doi: 10.1016/j.brainres.2016.03.043

Athirasala, A., Tahayeri, A., Thrivikraman, G., Franca, C. M., Monteiro, N., Tran, V., et al. (2018). A dentin-derived hydrogel bioink for 3D bioprinting of cell laden scaffolds for regenerative dentistry. *Biofabrication* 10:024101. doi: 10.1088/1758-5090/aa9b4e

Bakopoulou, A., Leyhausen, G., Volk, J., Tsiftsoglou, A., Garefis, P., Koidis, P., et al. (2011). Comparative analysis of *in vitro* osteo/odontogenic differentiation potential of human dental pulp stem cells (DPSCs) and stem cells from the apical papilla (SCAP). *Arch. Oral Biol.* 56, 709–721. doi: 10.1016/j.archoralbio.2010.12.008

Begue-Kirn, C., Smith, A. J., Loriot, M., Kupferle, C., Ruch, J. V., and Lesot, H. (1994). Comparative analysis of TGF beta s, BMPs, IGF1, msxs, fibronectin, osteonectin and bone sialoprotein gene expression during normal and *in vitro*-induced odontoblast differentiation. *Int. J. Dev. Biol.* 38, 405–420.

Bellamy, C., Shrestha, S., Torneck, C., and Kishen, A. (2016). Effects of a bioactive scaffold containing a sustained transforming growth factor-beta1-releasing nanoparticle system on the migration and differentiation of stem cells from the apical papilla. *J. Endod.* 42, 1385–1392. doi: 10.1016/j.joen.2016.06.017

Bezgin, T., Yilmaz, A. D., Celik, B. N., Kolsuz, M. E., and Sonmez, H. (2015). Efficacy of platelet-rich plasma as a scaffold in regenerative endodontic treatment. *J. Endod.* 41, 36–44. doi: 10.1016/j.joen.2014.10.004

Cavalcanti, B. N., Zeitlin, B. D., and Nor, J. E. (2013). A hydrogel scaffold that maintains viability and supports differentiation of dental pulp stem cells. *Dent. Mater.* 29, 97–102. doi: 10.1016/j.dental.2012.08.002

Ceccarelli, G., Presta, R., Benedetti, L., Cusella De Angelis, M. G., Lupi, S. M., and, Y., et al. (2017). Emerging perspectives in scaffold for tissue engineering in oral surgery. *Stem Cells Int.* 2017:4585401. doi: 10.1155/2017/4585401

Chang, B., Ahuja, N., Ma, C., and Liu, X. (2017). Injectable scaffolds: Preparation and application in dental and craniofacial regeneration. *Mater. Sci. Eng.* 111, 1–26. doi: 10.1016/j.mser.2016.11.001

Chrepa, V., Austah, O., and Diogenes, A. (2017). Evaluation of a commercially available hyaluronic acid hydrogel (Restylane) as injectable scaffold for dental pulp regeneration: an *in vitro* evaluation. *J. Endod.* 43, 257–262. doi: 10.1016/j.joen.2016.10.026

Comeau, P. A., Frei, H., Yang, C., Fernlund, G., and Rossi, F. M. (2012). *In vivo* evaluation of calcium polyphosphate for bone regeneration. *J. Biomater. Appl.* 27, 267–275. doi: 10.1177/0885328211401933

Cotti, E., Mereu, M., and Lusso, D. (2008). Regenerative treatment of an immature, traumatized tooth with apical periodontitis: report of a case. *J. Endod.* 34, 611–616. doi: 10.1016/j.joen.2008.02.029

Cvek, M. (1992). Prognosis of luxated non-vital maxillary incisors treated with calcium hydroxide and filled with gutta-percha. A retrospective clinical study. *Endod. Dent. Traumatol.* 8, 45–55. doi: 10.1111/j.1600-9657.1992.tb00228.x

Dianat, O., Mashhadi Abas, F., Paymanpour, P., Eghbal, M. J., Haddadpour, S., and Bahrololumi, N. (2017). Endodontic repair in immature dogs' teeth with apical periodontitis: blood clot vs plasma rich in growth factors scaffold. *Dent. Traumatol.* 33, 84–90. doi: 10.1111/edt.12306

Dissanayaka, W. L., Hargreaves, K. M., Jin, L., Samaranayake, L. P., and Zhang, C. (2015). The interplay of dental pulp stem cells and endothelial cells in an injectable peptide hydrogel on angiogenesis and pulp regeneration *in vivo*. *Tissue Eng. A* 21, 550–563. doi: 10.1089/ten.tea.2014.0154

Feng, X., Lu, X., Huang, D., Xing, J., Feng, G., Jin, G., et al. (2014). 3D porous chitosan scaffolds suit survival and neural differentiation of dental pulp stem cells. *Cell. Mol. Neurobiol.* 34, 859–870. doi: 10.1007/s10571-014-0063-8

Fernandes, G., and Yang, S. (2016). Application of platelet-rich plasma with stem cells in bone and periodontal tissue engineering. *Bone Res.* 4:16036. doi: 10.1038/boneres.2016.36

Ferroni, L., Gardin, C., Sivolella, S., Brunello, G., Berengo, M., Piattelli, A., et al. (2015). A hyaluronan-based scaffold for the *in vitro* construction of dental pulp-like tissue. *Int. J. Mol. Sci.* 16, 4666–4681. doi: 10.3390/ijms16034666

Friedlander, L. T., Cullinan, M. P., and Love, R. M. (2009). Dental stem cells and their potential role in apexogenesis and apexification. *Int. Endod. J.* 42, 955–962. doi: 10.1111/j.1365-2591.2009.01622.x

Friedman, P. M., Mafong, E. A., Kauvar, A. N., and Geronemus, R. G. (2002). Safety data of injectable nonanimal stabilized hyaluronic acid gel for soft tissue augmentation. *Dermatol. Surg.* 28, 491–494. doi: 10.1046/j.1524-4725.2002.01251.x

Gong, T., Heng, B. C., Lo, E. C., and Zhang, C. (2016). Current advance and future prospects of tissue engineering approach to dentin/pulp regenerative therapy. *Stem Cells Int.* 2016:9204574. doi: 10.1155/2016/9204574

He, L., Lin, Y., Hu, X., Zhang, Y., and Wu, H. (2009). A comparative study of platelet-rich fibrin (PRF) and platelet-rich plasma (PRP) on the effect of proliferation and differentiation of rat osteoblasts *in vitro*. *Oral Surg. Oral Med. Oral Pathol. Oral Radiol. Endod.* 108, 707–713. doi: 10.1016/j.tripleo.2009.06.044

Horst, O. V., Chavez, M. G., Jheon, A. H., Desai, T., and Klein, O. D. (2012). Stem cell and biomaterials research in dental tissue engineering and regeneration. *Dent. Clin. North Am.* 56, 495–520. doi: 10.1016/j.cden.2012.05.009

Huang, G. T., Gronthos, S., and Shi, S. (2009). Mesenchymal stem cells derived from dental tissues vs. those from other sources: their biology and role in regenerative medicine. *J. Dent. Res.* 88, 792–806. doi: 10.1177/0022034509340867

Huang, G. T., Sonoyama, W., Liu, Y., Liu, H., Wang, S., and Shi, S. (2008). The hidden treasure in apical papilla: the potential role in pulp/dentin regeneration and bioroot engineering. *J. Endod.* 34, 645–651. doi: 10.1016/j.joen.2008.03.001

Huang, G. T., Yamaza, T., Shea, L. D., Djouad, F., Kuhn, N. Z., Tuan, R. S., et al. (2010). Stem/progenitor cell-mediated de novo regeneration of dental pulp with newly deposited continuous layer of dentin in an *in vivo* model. *Tissue Eng. Part A* 16, 605–615. doi: 10.1089/ten.tea.2009.0518

Inuyama, Y., Kitamura, C., Nishihara, T., Morotomi, T., Nagayoshi, M., Tabata, Y., et al. (2010). Effects of hyaluronic acid sponge as a scaffold on odontoblastic cell

line and amputated dental pulp. *J. Biomed. Mater. Res. Part B Appl. Biomater.* 92, 120–128. doi: 10.1002/jbm.b.31497

Jadhav, G., Shah, N., and Logani, A. (2012). Revascularization with and without platelet-rich plasma in nonvital, immature, anterior teeth: a pilot clinical study. *J. Endod.* 38, 1581–1587. doi: 10.1016/j.joen.2012.09.010

Jadhav, G. R., Shah, N., and Logani, A. (2013). Comparative outcome of revascularization in bilateral, non-vital, immature maxillary anterior teeth supplemented with or without platelet rich plasma: a case series. *J. Conserv. Dent.* 16, 568–572. doi: 10.4103/0972-0707.120932

Jung, S. M., Yoon, G. H., Lee, H. C., and Shin, H. S. (2015). Chitosan nanoparticle/PCL nanofiber composite for wound dressing and drug delivery. *J. Biomater. Sci. Polym. Ed.* 26, 252–263. doi: 10.1080/09205063.2014.996699

Kim, N. R., Lee, D. H., Chung, P. H., and Yang, H. C. (2009). Distinct differentiation properties of human dental pulp cells on collagen, gelatin, and chitosan scaffolds. *Oral Surg. Oral Med. Oral Pathol. Oral Radiol. Endod.* 108, e94–e100. doi: 10.1016/j.tripleo.2009.07.031

Lambricht, L., De Berdt, P., Vanacker, J., Leprince, J., Diogenes, A., Goldansaz, H., et al. (2014). The type and composition of alginate and hyaluronic-based hydrogels influence the viability of stem cells of the apical papilla. *Dent. Mater.* 30, e349–e361. doi: 10.1016/j.dental.2014.08.369

Lee, B. N., Moon, J. W., Chang, H. S., Hwang, I. N., Oh, W. M., and Hwang, Y. C. (2015). A review of the regenerative endodontic treatment procedure. *Restor. Dent. Endod.* 40, 179–187. doi: 10.5395/rde.2015.40.3.179

Lee, K., Silva, E. A., and Mooney, D. J. (2011). Growth factor delivery-based tissue engineering: general approaches and a review of recent developments. *J. R. Soc. Interface* 8, 153–170. doi: 10.1098/rsif.2010.0223

Lenzi, R., and Trope, M. (2012). Revitalization procedures in two traumatized incisors with different biological outcomes. *J. Endod.* 38, 411–414. doi: 10.1016/j.joen.2011.12.003

Li, Y., Lu, X., Sun, X., Bai, S., Li, S., and Shi, J. (2011). Odontoblast-like cell differentiation and dentin formation induced with TGF-beta1. *Arch. Oral Biol.* 56, 1221–1229. doi: 10.1016/j.archoralbio.2011.05.002

Lovelace, T. W., Henry, M. A., Hargreaves, K. M., and Diogenes, A. (2011). Evaluation of the delivery of mesenchymal stem cells into the root canal space of necrotic immature teeth after clinical regenerative endodontic procedure. *J. Endod.* 37, 133–138. doi: 10.1016/j.joen.2010.10.009

Martin, D. E., De Almeida, J. F., Henry, M. A., Khaing, Z. Z., Schmidt, C. E., Teixeira, F. B., et al. (2014). Concentration-dependent effect of sodium hypochlorite on stem cells of apical papilla survival and differentiation. *J. Endod.* 40, 51–55. doi: 10.1016/j.joen.2013.07.026

Maruyama, K., Henmi, A., Okata, H., and Sasano, Y. (2016). Analysis of calcium, phosphorus, and carbon concentrations during developmental calcification of dentin and enamel in rat incisors using scanning electron microscopy with energy dispersive X-ray spectroscopy (SEM-EDX). *J. Oral Biosci.* 58, 173–179. doi: 10.1016/j.job.2016.08.003

Neilson, L., Mankus, C., Thorne, D., Jackson, G., DeBay, J., and Meredith, C. (2015). Development of an *in vitro* cytotoxicity model for aerosol exposure using 3D reconstructed human airway tissue; application for assessment of e-cigarette aerosol. *Toxicol. In Vitro* 29, 1952–1962. doi: 10.1016/j.tiv.2015.05.018

Nosrat, A., Kolahdouzan, A., Khatibi, A. H., Verma, P., Jamshidi, D., Nevins, A. J., et al. (2019). Clinical, radiographic, and histologic outcome of regenerative endodontic treatment in human teeth using a novel collagen-hydroxyapatite scaffold. *J. Endodontics* 45, 136–143. doi: 10.1016/j.joen.2018.10.012

Nune, M., Kumaraswamy, P., Krishnan, U. M., and Sethuraman, S. (2013). Self-assembling peptide nanofibrous scaffolds for tissue engineering: novel approaches and strategies for effective functional regeneration. *Curr. Protein Pept. Sci.* 14, 70–84. doi: 10.2174/1389203711314010010

O'Brien, F. J. (2011). Biomaterials and scaffolds for tissue engineering. *Mater. Today* 14, 88–95. doi: 10.1016/S1369-7021(11)70058-X

Ozeki, N., Hase, N., Yamaguchi, H., Hiyama, T., Kawai, R., Kondo, A., et al. (2015). Polyphosphate induces matrix metalloproteinase-3-mediated proliferation of odontoblast-like cells derived from induced pluripotent stem cells. *Exp. Cell Res.* 333, 303–315. doi: 10.1016/j.yexcr.2015.01.007

Pardue, E. L., Ibrahim, S., and Ramamurthi, A. (2014). Role of hyaluronan in angiogenesis and its utility to angiogenic tissue engineering. *Organogenesis* 4, 203–214. doi: 10.4161/org.4.4.6926

Qin, W., Chen, J.-Y., Guo, J., Ma, T., Weir, M. D., Guo, D., et al. (2018). Novel calcium phosphate cement with metformin-loaded chitosan for odontogenic differentiation of human dental pulp cells. *Stem Cells Int.* 2018, 1–10. doi: 10.1155/2018/7173481

Raldi, D. P., Mello, I., Habitante, S. M., Lage-Marques, J. L., and Coil, J. (2009). Treatment options for teeth with open apices and apical periodontitis. *J. Can. Dent. Assoc.* 75, 591–596.

Saucedo, J. M., Yaffe, M. A., Berschback, J. C., Hsu, W. K., and Kalainov, D. M. (2012). Platelet-rich plasma. *J. Hand. Surg. Am.* 37, 587–9; quiz 590. doi: 10.1016/j.jhsa.2011.12.026

Shiehzadeh, V., Aghmasheh, F., Shiehzadeh, F., Joulae, M., Kosarieh, E., and Shiehzadeh, F. (2014). Healing of large periapical lesions following delivery of dental stem cells with an injectable scaffold: new method and three case reports. *Indian J. Dent. Res.* 25, 248–253. doi: 10.4103/0970-9290.135937

Shrestha, S., Diogenes, A., and Kishen, A. (2014). Temporal-controlled release of bovine serum albumin from chitosan nanoparticles: effect on the regulation of alkaline phosphatase activity in stem cells from apical papilla. *J. Endod.* 40, 1349–1354. doi: 10.1016/j.joen.2014.02.018

Shrestha, S., Diogenes, A., and Kishen, A. (2015). Temporal-controlled dexamethasone releasing chitosan nanoparticle system enhances odontogenic differentiation of stem cells from apical papilla. *J. Endod.* 41, 1253–1258. doi: 10.1016/j.joen.2015.03.024

Shrestha, S., Torneck, C. D., and Kishen, A. (2016). Dentin conditioning with bioactive molecule releasing nanoparticle system enhances adherence, viability, and differentiation of stem cells from apical papilla. *J. Endod.* 42, 717–723. doi: 10.1016/j.joen.2016.01.026

Sonoyama, W., Liu, Y., Fang, D., Yamaza, T., Seo, B. M., Zhang, C., et al. (2006). Mesenchymal stem cell-mediated functional tooth regeneration in swine. *PLoS ONE* 1:e79. doi: 10.1371/journal.pone.0000079

Souto, G. D., Farhane, Z., Casey, A., Efeoglu, E., McIntyre, J., and Byrne, H. J. (2016). Evaluation of cytotoxicity profile and intracellular localisation of doxorubicin-loaded chitosan nanoparticles. *Anal. Bioanal. Chem.* 408, 5443–5455. doi: 10.1007/s00216-016-9641-6

Sumita, Y., Honda, M. J., Ohara, T., Tsuchiya, S., Sagara, H., Kagami, H., et al. (2006). Performance of collagen sponge as a 3-D scaffold for tooth-tissue engineering. *Biomaterials* 27, 3238–3248. doi: 10.1016/j.biomaterials.2006.01.055

Torabinejad, M., and Turman, M. (2011). Revitalization of tooth with necrotic pulp and open apex by using platelet-rich plasma: a case report. *J. Endod.* 37, 265–268. doi: 10.1016/j.joen.2010.11.004

Trevino, E. G., Patwardhan, A. N., Henry, M. A., Perry, G., Dybdal-Hargreaves, N., Hargreaves, K. M., et al. (2011). Effect of irrigants on the survival of human stem cells of the apical papilla in a platelet-rich plasma scaffold in human root tips. *J. Endod.* 37, 1109–1115. doi: 10.1016/j.joen.2011.05.013

Ulusoy, A. T., Turedi, I., Cimen, M., and Cehreli, Z. C. (2019). Evaluation of blood clot, platelet-rich plasma, platelet-rich fibrin, and platelet pellet as scaffolds in regenerative endodontic treatment: a prospective randomized trial. *J. Endodontics* 45, 560–566. doi: 10.1016/j.joen.2019.02.002

Venkatesan, J., Nithya, R., Sudha, P. N., and Kim, S. K. (2014). Role of alginate in bone tissue engineering. *Adv. Food Nutr. Res.* 73, 45–57. doi: 10.1016/B978-0-12-800268-1.00004-4

Wang, F.-M., Qiu, K., Hu, T., Wan, C.-X., Zhou, X.-D., and Gutmann, J. L. (2006). Biodegradable porous calcium polyphosphate scaffolds for the three-dimensional culture of dental pulp cells. *Int. Endodontic J.* 39, 477–483. doi: 10.1111/j.1365-2591.2006.01114.x

Wang, W., Dang, M., Zhang, Z., Hu, J., Eyster, T. W., Ni, L., et al. (2016). Dentin regeneration by stem cells of apical papilla on injectable nanofibrous microspheres and stimulated by controlled BMP-2 release. *Acta Biomater.* 36, 63–72. doi: 10.1016/j.actbio.2016.03.015

Weir, M. D., and Xu, H. H. K. (2010). Culture human mesenchymal stem cells with calcium phosphate cement scaffolds for bone repair. *J. Biomed. Mater. Res. B Appl. Biomater.* 93, 93–105. doi: 10.1002/jbm.b.31563

Wilkinson, K. L., Beeson, T. J., and Kirkpatrick, T. C. (2007). Fracture resistance of simulated immature teeth filled with resilon, gutta-percha, or composite. *J. Endod.* 33, 480–483. doi: 10.1016/j.joen.2006.11.014

Xiao, M., Qiu, J., Kuang, R., Zhang, B., Wang, W., and Yu, Q. (2019). Synergistic effects of stromal cell-derived factor-1α and bone morphogenetic protein-2 treatment on odontogenic differentiation of human stem cells from apical papilla cultured in the VitroGel 3D system. *Cell Tissue Res.* 378, 207–220. doi: 10.1007/s00441-019-03045-3

Xie, H., Gu, Z., Li, C., Franco, C., Wang, J., Li, L., et al. (2016). A novel bioceramic scaffold integrating silk fibroin in calcium polyphosphate for bone tissue-engineering. *Ceramics Int.* 42, 2386–2392. doi: 10.1016/j.ceramint.2015.10.036

Zein, N., Harmouch, E., Lutz, J.-C., Grado, G. F. D., Kuchler-Bopp, S., Clauss, F., et al. (2019). Polymer-based instructive scaffolds for endodontic regeneration. *Materials* 12:2347. doi: 10.3390/ma12152347

Zhang, L., Morsi, Y., Wang, Y., Li, Y., and Ramakrishna, S. (2013). Review scaffold design and stem cells for tooth regeneration. *Jpn. Dental Sci. Rev.* 49, 14–26. doi: 10.1016/j.jdsr.2012.09.001

Conflict of Interest: The authors declare that the research was conducted in the absence of any commercial or financial relationships that could be construed as a potential conflict of interest.

Advantages of publishing in Frontiers

OPEN ACCESS
Articles are free to read for greatest visibility and readership

FAST PUBLICATION
Around 90 days from submission to decision

HIGH QUALITY PEER-REVIEW
Rigorous, collaborative, and constructive peer-review

TRANSPARENT PEER-REVIEW
Editors and reviewers acknowledged by name on published articles

Frontiers
Avenue du Tribunal-Fédéral 34
1005 Lausanne | Switzerland

Visit us: www.frontiersin.org
Contact us: info@frontiersin.org | +41 21 510 17 00

REPRODUCIBILITY OF RESEARCH
Support open data and methods to enhance research reproducibility

DIGITAL PUBLISHING
Articles designed for optimal readership across devices

FOLLOW US
@frontiersin

IMPACT METRICS
Advanced article metrics track visibility across digital media

EXTENSIVE PROMOTION
Marketing and promotion of impactful research

LOOP RESEARCH NETWORK
Our network increases your article's readership